FEB - FRESENIUS ENVIRONMENTAL BULLETIN
Founded jointly by F. Korte and F. Coulston
Production by PSP - Vimy Str. 1e, 85354 Freising, Germany in
cooperation with PRT-Parlar Research & Technology
Vimy Str 1e, 85354 Freising

Printed in Germany-ISSN 1018-4619

Fresenius Environmental Bulletin is abstracted/indexed in:
Biology & Environmental Sciences, BIOSIS, CAB International, Cambridge Scientific abstracts, Chemical Abstracts, Current Awareness, Current Contents/Agriculture, CSA Civil Engineering Abstracts, CSA Mechanical & Transportation Engineering, IBIDS database, Information Ventures, NISC, Research Alert, Science Citation Index (SCI), Scisearch, Selected Water Resources Abstracts

CONTENTS

ORIGINAL PAPERS

© by PSP Volume 29 – No. 05/2020 pages 3329-3337 Fresenius Environmental Bulletin

MARKETING STRUCTURES OF CARROT PRODUCTION AND CHALLENGES AND RECOMMENDATIONS: THE CASE OF KONYA PROVINCE, TURKEY

Musa Acar[1,*], Mevlut Gul[2]

[1] Aksaray University, Eskil Vocational School, Aksaray, Turkey
[2]Isparta University of Applied Sciences, Faculty of Agriculture, Department of Agricultural Economics, 32260, Isparta, Turkey

ABSTRACT

The main objective of the study was to determine the structure of marketing, problems in marketing and to suggest solutions to the problems of carrot marketing. Primary data used in the research were gathered through personal interviews with the help of well-designed questionnaires from 73 carrot producer farms, 30 marketing channels' actors (broker/merchants) and 10 cold storage firms in Konya, Turkey. The surveyed samples were selected randomly. The data covered 2011 production season. Carrot marketing cost was calculated to be US$0.40 per kg; distributed as 69.39% of raw materials, 11.7% broker commission, 8.89% transport costs, 7.04% packing, 3.39% labour and 0.22% other cost. For the carrot production, high input costs, difficulties in finding new markets, climatic conditions and delays or even failure in payment for product, were identified as the main problems. Regarding exports, to eliminate the complications at custom offices will ensure the sustainability of existing markets; and it should help to create new markets. National or international funds to support organizations and institutions involved could be provided for improvement of the sectors.

KEYWORDS:
Carrot, Marketing channels, Konya, Turkey

INTRODUCTION

People have given an increasing importance for the health and healthy foods. Vegetables play a major role in healthy diets. Besides the vegetable production, its marketing has been a vital issue in order to provide the required amount of vegetables for the increasing population.

Turkey produces 26 million ton of vegetables annually, it is the fourth largest vegetable producer after China, India and USA and 20% of this production in Turkey takes place under green-houses [1].

Turkey is diverse in vegetable production. The carrot is a key ingredient in Turkish meals because it is healthy and delicious. Turkey carrot production constitutes 1.6% of world production. Konya province accounts for an important share in the production and export of carrot. There are not many studies on the marketing structure of carrot in the region. However, marketing depends on and in other cases, help to define the carrot production chain.

The consumer markets are the markets where the producers sell their own products. On the other hand, wholesale food markets are markets where the products obtained by the gatherers were sold to the processing facilities and other retailers. The market which provides the consumer access to products bought from wholesalers or other middlemen is retail market. There are generally merchants, affairs, processing firms and retailers between the producer and the last consumer in fruit and vegetable marketing in Turkey and merchant and commissioners are highly effective in the pricing [2].

Fertő and Szabó [3] aimed to examine the choice among various supply channels in the fruit and vegetable business in Hungary. Their analysis was based on a survey within fruit and vegetable producers in Csongrád County exploring their choice of marketing channels. They used a multinomial logit model to reveal the determinants influencing the choice among various supply channels. In their findings, producers that sold their product to a wholesale market were strongly and negatively affected by the farmer's age, information costs, and negatively by the bargaining power and monitoring costs [3].

On the other hand, Sakurai et al. [4] investigated the fruit and vegetable marketing channel by considering the "commissioner-producer" relationships in Khon Kaen. They stated that, there was a multi-stage fruit and vegetable marketing channel in which the farmer sells his products directly to the commissioner in North East Thailand. They detected an important difference between the producer prices and the retail prices in their studies [4].

Adhikari [5] compared the yield and economics of organic and inorganic carrot production and its profit in Chitwan district of Nepal. He found that inorganic production system got higher cost and higher revenue, but organic production system had higher benefit cost ratio. Ahmad et al., [6] also determined the factors causing yield variation in carrot cultivation and its profitability in two dis-

tricts of the Punjab province by Cobb Douglas type production function. They found great potential exists in improving the carrot yield per acre by farmers' access to certified seed, better land preparation, recommended dose of seed and fertilizer and availability of credit [6].

The main objective of this study was to determine the marketing structure of the local enterprises and the role of the middlemen involved in carrot production in Konya, Turkey; as well as to detect some marketing problems in order to bring out some solutions.

MATERIALS AND METHODS

Konya province, which provides the 69% of carrot production in Turkey, was selected as the research region. The data of the study was acquired from the farms involved in carrot production and actors (commissioner, merchant, cold storage house enterprises) involved in the marketing channel in Konya. The information acquired from these shareholders constitutes the primary data of the study. The acquired data represents the 2011 production season.

The population was applied the layered sampling Neyman method and the number of the carrot producer farms was determined as 73. In the interviews with the middlemen, it was found that there were above 300 middlemen in the region; thus, 30 middlemen/merchants were taken as a 10% representative figure of the total to be interviewed. Additionally, 10 cold storage house managers were surveyed in the region.

The data gathering techniques used in the studies of agricultural economy is generally survey, monitoring and focus group interviews. The most common used one is the survey method. The data used in this study was obtained through surveys conducted with the farms, middlemen and cold storage house owners involved in the carrot production. The main data gathering tools, which were used in the survey method, change, as well. Data gathering tools are personal meeting, through phone and mails. Considering the detailed survey used in this study, face to face meeting method was used.

The questionnaires which were well designed accordingly to the structure of marketing and problems were applied. The farms involved in carrot production were divided into carrot cultivated fields groups (I. group 0-2.49 ha, II. group 2.50-4.99 ha, III. group 5.00-9.99 ha, IV. group 10.0+ ha) and the data was interpreted by creating crosstabs with the variables.

RESULTS AND DISCUSSION

Findings Obtained from the Carrot Producers. The average farm size was 12.62 ha in the surveyed carrot producers. 8.61% of the average farm size of the surveyed farms was the cereal cultivation fields, 10.58% was industrial plant cultivated fields, 69.67% was vegetable fields and 11.14% was fallow fields. 26.13-61.90% of the total production fields were allocated to the carrot production in the farm size classes of the surveyed carrot producers. This ratio was 50.71% in the average of farms. The results indicated that the surveyed farms were mostly focused on the carrot production.

When the carrot producers were asked about the reason why they chose carrot, 56.16% of the farms stated because of its high profitability, 31.51% because of no other mainstay, 12.33% because carrot was the regional main crop.

The methods to determine the carrot harvest time of the surveyed farms were searched. 19.67% of the carrot producers stated that they decided the harvest time of the carrot according to its colour, 32.79% according to its ripeness, 13.11% according to its hardness, 20.77% according to the market conditions and 13.66% according to the climate conditions.

In the surveyed farms, it was found out that, the total yield loss 82.19% occurred during the harvest or transportation. The scale of the yield loss was between 5-10% in many farms, but it reached up to 20% in some farms.

The categorization of the products was an important marketing activity. Categorization was dividing the different products with their similar ones in terms of height, size, shape, colour, etc. Categorization enables the consumers to select the products according to their tastes and income levels. It makes purchase and sale of the products easier. It prevents the purchase of undesired products. It facilitates assigning prices to the products [7].

There were three classes of carrots according to Turkish Standard Institute 1193 and farms take this categorization into consideration. These are; extra, first class, second class. The carrots were sold according to the market conditions and those carrots which do not meet the demand of the market were preferred by the fruit juice enterprises. As the producer obtains more money, he attempts to produce extra class product. Considering the average of the farms, extra class has the highest ratio with 73.80%. 1st class products follow with 17.33% and the 2nd class products with 8.86% (Table 1).

The 71.23% of the farms stated that they divided the carrots into classes according to hardness, 36.99% according to colour and 32.88% according to the size. Producers sale first, second and third quality products and this situation provides

TABLE 1
Categorization of the Carrot Production in the Farms

Farm groups (ha)	Extra-Class	I. Class	II. Class	Total
	The average of farms (kg)			
I	83628	18798	11441	113867
II	255853	52653	21654	330160
III	428055	106534	42036	576625
IV	1050643	249430	142683	1442667
Average	393209	92356	47213	532778
	The share in the total production (%)			
I	73.44	16.51	10.05	100.00
II	77.49	15.95	6.56	100.00
III	74.23	18.48	7.29	100.00
IV	72.83	17.28	9.89	100.00
Average	73.80	17.33	8.86	100.00

marketing diversity for the producer and causes disadvantage for the producer in terms of the prices in some cases.

When the farms were asked where was the categorization process take place, 94.52% stated in the facilities. The reasons of this situation were the facts that facilities have the tools to process, wash, sort and categorize, they enable the consumers to select personally and it was obligatory to make the categorization in the facilities.

When the farms were asked where they learnt the required information for categorization from, 79.45% stated the demand of the buyers. 15.07% stated the demands of the exporter company, 4.11% stated the producers of the region and 1.37% stated the required informing of technical staff.

Ok [8] stated that 65.06% of the producers involved in categorization learned the required information from the buyer and company staff as the buyer and company preferred the categorized products, 20.48% learned from the other regional producers, 14.46% learned from the technical staff.

Packaging was the process of covering the product in order to protect from external factors, to keep the product clean, to make loading, unloading and storage easier, to increase the demand and to enable the consumer select personally [9].

Considering the package types used for the sale of product by the farms; 45.54% uses wooden cases and 41.58% uses plastic bags. 11.88% of the surveyed farms market the carrot in bulk.

The surveyed farms involved in the carrot production stated that 72.60% of the payment was made on credit, 1.37% was paid in cash and 26.03% was partial in cash and partial on credit.

The 50.51% of the surveyed farms stated that they got the information about the carrot market on their own. The facts that the research field was the region providing the carrot potential in Turkey and the farms were experienced in carrot farming affected this answer.

The 21.21% of the farms stated that they got the information from other farms, 11.11% stated that they got the information from the exporter company. Approximately 15% stated that they got the information from the chamber of agriculture and cooperative.

When the marketing activities of the farms were investigated, it was found out that 26.03% worked with a commissioner. As the carrot cultivated areas increase in the surveyed farms, the possibility to work with commissioner increases.

Agricultural marketing was a department investigating and regulating the journey of the agricultural products from the producer or the fields to the last stage of the consumption or to the meals of the consumers [10]. The main purpose of the marketing was the satisfaction of the consumer and building confidence at the consumers in the long run. Today's marketing understanding and concept aim to serve the interests of the consumer by getting away from the sales understanding [11].

The products produced either in the agriculture business or production business follows different ways to the last consumer. The ways and places that the products pass through after the production were called "distribution channels" [11]. The distribution channels of the products changes from product to product. The distribution channels used in the fruit and vegetable marketing in Turkey were given below [11].

The Distribution Channels of the Fruit and Vegetable in Turkey.

- Producer – Agriculture Cooperative – Retailer - Consumer .
- Producer – Wholesaler – Commissioner – Retailer – Consumer. Producer – Commissioner – Wholesaler – Retailer – Consumer
- Producer – Middleman – Commissioner (at the production place) – Wholesaler – Commissioner (at the consumption place) – Retailer – Consumer.

The fruit and vegetables were marketed in wholesale affairs in Turkey. Daily prices of fruit and vegetables were determined at the affairs according to the supply and demand. Affairs were the places where fruits and vegetables were constantly

marketed and built at the producer and consumer centres. A large part of the produced fruits and vegetables were marketed outside the wholesaler food markets in spite of the obligatory legal responsibilities [12]. Kaptangil [13] states that 85% of the sales was made outside the wholesale food markets and it was very common that commissioners buy and sell on their own. Similar findings were found in the studies of Güneş et al. [14] and Erkal and Şafak [15] and Gül [16].

Wholesale food markets law which was put into force in 1960 could not respond to today's economic conditions and changing market conditions. Therefore, 552 numbered Vegetable and Fruit Trade Regulation and Wholesale Food Markets Statutory Decree was put into force on 27 June 1995. After this decree and notification and legal regulations which were put into force in 2000, 5957 numbered "Law on the Trade of Vegetable and Fruits and Other Goods which have enough Demand and Supply" Food Markets law passed into law on 11.03.2010. A regulation about the Vegetable and Fruit Trade and Wholesale Food Markets was put into force on 7.08.2012. In this context, no product can be sold before entering to the Food markets. The audits were planned to be made easier and more effective. Therefore, it was aimed with law and regulations to achieve the trade of vegetable and fruit under free competition conditions which were of good quality and comply with the standards and food security, to have a modern structure of wholesale food markets, to keep observe and announce the information of traded vegetable and fruits inside food markets on electronic media, to keep the record of members of the profession and those concerned, to create a data base for them, to provide the common information sharing and communication among wholesale food markets, to protect the rights and interests of the producers and consumers and to regulate the activities of the members of the profession [17].

As a result of the meetings in region, some inadequacies were detected related to the entrance to the food markets and registry of the carrot.

As the producers were not organized while the commissioner and merchants were organized under associations and cooperatives, the producers were not very effective at the prices [18].

The amount of money that the producer gets from the money paid by the consumer was different and low for the fruit and vegetables. For example, Güneş et al. [14] stated in their study that 14.47%-64.76% of the consumer payment returned to the producer.

According to the findings of this study, 22.33%-35.19% of consumer payment returned to the carrot producers.

Dastagiri et al. [19] found that the producer share in consumer payment varied from 46% to 74% in Andhra Pradesh, 26% to 60% in West Bengal, 33% to 60% in Rajasthan, 85% to 88% in Manipur 91% to 95% in Tamil Nadu and 100% in Punjab in India. Al [20] calculated this share for carrot 44% in Sri Lanka.

In investigated region, the first two distribution channels choices of the farms involved in the carrot production for marketing their products; (32.88% of the farms) Producer => Sender Merchant => Commissioner of the Consumption Centre =>Retailer => Consumer distribution channel and (30.14% of the farms) Producer => Commissioner of the Production Centre => Retailer => Consumer distribution channel. Other distribution channels stated by the farms; 16.44% of the farms, Producer =>Commissioner of the Production Centre =>Commissioner of the Consumption Centre => Retailer = Consumer distribution channel, 9.59% of the farms, Producer => Consumer distribution channel, 5.48% of the farms Producer => Direct Export distribution channel, 4.11% of the farms, Producer => Cooperative => Commissioner of the Consumption Centre => Retailer => Consumer distribution channel, 1.37% of the farms, Producer => Commissioner of the Production Centre => Exporter Firm => Consumer distribution channel (Table 2).

Dastagiri et al. [19] found that the most common marketing channel for majority of the crops is that Producer-Wholesaler-Retailer-Consumer in India. They found that producer to consumer channel was the highest marketing efficiency. Marketing channels differ from country to country. For instance, marketing channel of USA starts from the producers through retailers to shippers up to grocery. Retailers' concentration is at the increasing rate [21]. In general, the world trend of fresh products corroborate the following trends; the large multinational companies becoming increasingly involved; increased attention of food safety; overproduction of fruit and vegetables; electronic fresh produce markets are increasing; large production in terms of packing is shifting towards mass individuation to cater for specific needs of consumers [22]; [23].

The middlemen used by the farms involved in the carrot production for marketing the products were given at Table 3. Accordingly, 67.12% of the surveyed farms give the products to the middleman, 20.55% to the regional commissioners, 12.33% to the regional producer traders. The provinces to which carrots were sent by the farms were determined according to the customer demands. The surveyed farms stated that carrots were transported to all the cities of Turkey. But they stated that Konya, İstanbul, Bursa, Kayseri, İzmir, Ankara, Adana, Mersin, Antalya, Erzurum provinces were important trade cities.

The problems at the carrot production were evaluated in the 5 point likert scale. The producers stated the important problems as the high prices of

TABLE 2
Marketing Channels of the Carrot Producers

Farm groups	1	2	3	4	5	6	7	Total
				N				
I	3	7	4	0	11	0	2	27
II	2	5	2	0	4	0	2	15
III	0	5	3	1	6	1	0	16
IV	2	5	3	2	3	0	0	15
Total	7	22	12	3	24	1	4	73
				Percentage (%)				
I	11.11	25.93	14.81	0.00	40.74	0.00	7.41	100.00
II	13.33	33.33	13.33	0.00	26.67	0.00	13.33	100.00
III	0.00	31.25	18.75	6.25	37.50	6.25	0.00	100.00
IV	13.33	33.33	20.00	13.33	20.00	0.00	0.00	100.00
Total	9.59	30.14	16.44	4.11	32.88	1.37	5.48	100.00

(1). Producer/Farmer => Consumer
(2). Producer/Farmer => Production Centre Broker => Retailer => Consumer
(3). Producer/Farmer =>Production Centre Broker =>Consumer Centre Broker => Retailer = Consumer
(4). Producer/Farmer => Cooperative => Consumer Centre Broker => Retailer => Consumer
(5). Producer/Farmer => Middleman => Consumer Centre Broker =>Retailer => Consumer
(6). Producer/Farmer => Production Centre Broker => Exporter Firm => Consumer
(7). Producer/Farmer => Exporter Firm

TABLE 3
Buyer of Carrot Production in Investigated Farms

Farm groups	Producer trader in investigated area		Middleman		Commissioners in investigated area		Total	
	N	%	N	%	N	%	N	%
I	5	18.52	20	74.07	2	7.41	27	100.00
II	0	0.00	9	60.00	6	40.00	15	100.00
III	0	0.00	12	75.00	4	25.00	16	100.00
IV	4	26.67	8	53.33	3	20.00	15	100.00
Total	9	12.33	49	67.12	15	20.55	73	100.00

inputs in the carrot production, low prices of the product, insufficient market and buyer.

In the farm groups, I. farm group complained the most about the high prices of inputs and low price of the product. In the II. farm group, supply of water and irrigation, supply of high quality seed, fertilizer, pesticide, procurement of equipment, high prices of inputs, low prices of the product, insufficient market and buyer were listed as the important problems. In the III. farm group, fight against the illness and pests, high prices of inputs, low prices of the product, insufficient market and buyer were listed as the important problems. In the IV. farm group, fight against the illness and pests, high prices of inputs, fertilizer and fertilization, low prices of the product, insufficient market and buyer, lack of organization and cooperation among producers were listed as the important problems (Table 4).

Findings Obtained from the Middlemen. When the legal status of the firms of the 30 surveyed carrot middlemen in the research region were examined, it was found out that 20 enterprises were individual-family firm, 8 enterprises were individual partnership and the other 2 enterprises were limited companies.

It was found out that 12 of those employed at the managing positions in the surveyed contractor enterprises were graduates of the primary school, 10 were graduates of secondary school, 4 graduated from high school and 4 had their bachelor degree.

When the fields activity of the surveyed contractor enterprises was investigated, it was found out that 11 enterprises were operating as carrot producer-exporter-domestic marketer, 9 enterprises were operating as carrot producer-exporter, 9 enterprises were operating as carrot producer-domestic marketer.

The carrots produced in the region were sent to all provinces of Turkey. The enterprises surveyed face to face stated that the carrots produced in the region were exported mainly to Romania, Bulgaria, Italy, Serbia, Georgia, Kazakhstan, Moldova, Germany, Jordan, Iraq and Saudi Arabia. The amount of exported carrots from the region was stated to be approximately 30 thousand tons. 23 (76.67%) of the surveyed middlemen buy the carrots directly from the producer. 23.33% buy the carrots through the middlemen.

17 (56.70%) of the surveyed commissioner-merchant-firms have the infrastructure facility for carrot processing. 13 (43.30%) of the surveyed commissioner-merchant-firms do not have the infrastructure facility for carrot processing. The enterprises which own the infrastructure facilities avoided from giving information about the capacity of the facilities.

TABLE 4
The Problems of Carrot Production in Farmers' Level

Problems	I	II	III	IV	Average
The prices of inputs are high	4.07	4.40	4.25	4.20	4.21
Product prices are low	4.26	4.13	3.88	4.47	4.19
Insufficient market/trader	3.85	4.07	4.38	4.27	4.10
Supply of equipment	3.70	4.13	3.75	4.27	3.92
Supply of water and irrigation	3.85	4.33	3.56	3.87	3.89
The lack of cooperation between farmers	3.78	3.80	3.75	4.27	3.88
Supply of high quality seeds, fertilizer, pesticide	3.70	4.27	3.94	3.67	3.86
Disease and pest	3.41	3.67	4.19	4.33	3.82
Auditing of input vendors	3.74	3.73	3.44	4.20	3.77
Cultivation	3.22	3.80	4.00	4.40	3.75
Appropriate credit	3.89	3.40	3.19	3.67	3.59
Machinery	3.78	3.27	3.38	3.40	3.51
Fertilization	3.15	3.27	3.56	4.00	3.44

SCALE	No problem at all	No problem	Less important	Important	Very important
	1	2	3	4	5

27 (90%) of the contractor enterprises made research about the carrots that they market. It was found out that 10% (3 enterprises) did not make market research.

The distribution channels for the marketing of the carrot were also examined. When the carrot marketing distribution channels of the contractor/merchant were examined; 30% of the middlemen uses the following channel, Producer => (THE SURVEYED FIRM) => Commissioner of the Production Centre => Retailer => Consumer, another 30% uses this channel, Producer => (THE SURVEYED FIRM) => Commissioner of the Consumption Centre => Retailer => Consumer. 26.7% of the middlemen use the following channel, Producer => (THE SURVEYED FIRM) => Commissioner of the Production Centre => Commissioner of the Consumption Centre => Retailer => Consumer. The other two distribution channels were; (Producer => (THE SURVEYED FIRM) => Consumer) channel used by the 6.7% of the middlemen and (Producer => (THE SURVEYED COMPANY) => Sender Merchant => Commissioner of the Consumption Centre => Retailer => Consumer) channel used by the 6.7%.

Carrot marketing cost was found US$0.40 through the data obtained from the 30 surveyed middlemen. The carrot prices changes between US$0.24 and US$0.90 in some wholesale affairs in the researched period. The merchants who have cold storage house were advantageous in the price fluctuations.

The 69.39% of the cost items emerging at the contractor level were raw material, 11.07% was commission, 8.89% was transportation and 7.04% was cost of package (Figure 1).

When the problems encountered in the carrot sales were examined in the survey with the middlemen, 21 middlemen (70%) referred to the competition problem. They proposed such a solution like the establishment of the institutional structures which provides a common price policy. The problems with the procurement of the product, package, transportation, problems arising from the legislation of the importing country and problems from the export legislation follows the competition problems respectively.

Concerning the findings obtained from intermediaries; the weak sides of the carrot production were gathered under three titles. 50% of the enterprises stated about the weak sides that being no incentives for the carrot production by the state, 33.3% stated the climate conditions (frost, hail). 16.7% stated that the current market was not enough for the products and therefore there occurred problems in the carrot marketing.

In the meeting with the carrot middlemen at the region, 43.3% stated about the strong sides in the carrot production that carrot was an important product as it both contributed to the agricultural value added and created value added in the processing and service business. 23.3% referred the increased quality and the fact that as the carrot needs plenty of irrigation, the region will not have a problem compared to the other regions thanks to the new irrigation projects. The employed labour force was also considered important as it created employment.

The surveyed carrot merchants showed the good tonnage of the carrot as an opportunity when the opportunities were examined. The decreases of carrot production in other regions due to various reasons, the expected increase in the demand of carrot thanks to the advertisement and promotion, execution of becoming a cooperative professionally can be considered as the opportunities of the carrot production.

The first threat (56.7%) referred by the surveyed middlemen was diseases and the second threat (50%) was frost and cold weather. Lack of

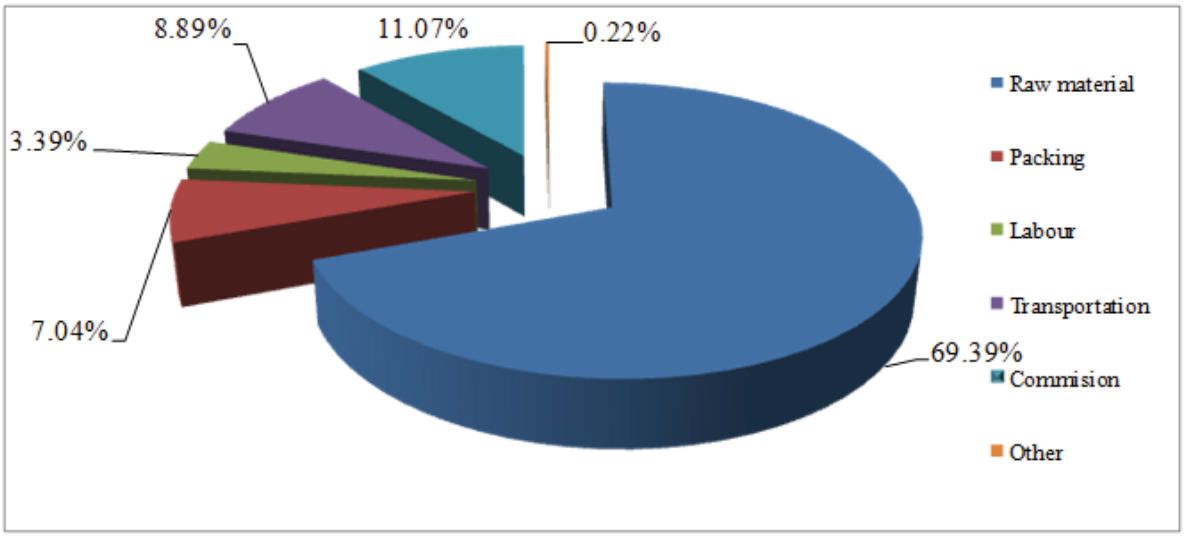

FIGURE 1
Carrot Expense Items Components at the Middlemen Level

competition and becoming a cooperative, consumer resistance, lack of marketing and bad checks were referred respectively.

Findings Obtained from the Cold Storage Houses. When the way that the temperature was determined for the products in the cold storage houses was examined, it was found that the enterprises adjusted the temperature according to the need of the product and it was an important factor to be experienced in the cold storage enterprise which was one of the methods to store carrot.

When the way of determining prices was examined, it was found that producers or some merchants built the cold storage houses on their own and used them in marketing channel of private enterprises. It was stated that the prices of renting the cold storage house to another producer or merchant changed between US$20.96 and US$23.95 per day. It was emphasized that the main determining factor of the cost was the amount of electricity used.

Carrot storage in the enterprises starts in the August and continues until the February. Carrot storage was highly made in September, October, November and December. October and November were the busiest months. The reasons behind this situation were high supply and low demand of carrot during these months.

The weak sides of carrot production according to the cold storage house enterprises were absence of a standard marketing understanding and state incentives. However, the strong sides were a better income compared to other products and producing a lot more compared to the other regions in Turkey. The opportunity in the carrot production was that, the market can be dominated in case of a good tonnage and high quality. The threats in the carrot production were the competition between the producer and merchants, problems arising from the climate, high costs, problems with the receipt of the marketed goods and no redemption of the debt, arbitrary cuts in the amount to be paid, not paying for the perished goods during transportation and default of payment. The reason behind this situation was that enterprises worked on the basis of credit account according to the mutual trust and reference.

CONCLUSIONS

Konya province (Turkey) has an important vegetable potential because of its convenient climate conditions and soil structure, developing production technologies, intense labour force, experienced carrot producers. However, there was no producer union associated specifically with the carrot farming in the region. But, the precise assessment of the production potential of the region are limited depend on the uncertainties in input prices, the inadequacy of the budget allocated to research and development activities in marketing matters, the weak structure of producer organizations.

Farmers need to be informed and guided from time to time on specific issues. For this reason, education and counselling services should be increased.

Compared with the world market, high cost (seed, diesel, land lease, customs costs, etc.), competition, lack of promotion, and lack of branding can be expressed as important problems in national markets.

Activities to be carried out at the point of cooperativeness, institutionalization and promotion can be a step towards branding.

Carrot production is an important activity in terms of ensuring the livelihood of the people of the region. Sustainability of production depends on the good income of the producers, in order to achieve

this, the import and export of carrots should be continued and increased. It is imperative that the production is carried out in accordance with certain standards in order for the exports to continue and the products to be marketed well in the domestic market.

In the agricultural product marketing chain, intermediaries receive a large share of profit from the product. Packaging and cold storage facilities requiring large capital investment cannot be installed by producers due to economic and structural reasons. Measures to facilitate the use of grant - project support in these areas may be important for carrot producers.

Today, the conflicts in the Middle East countries affects exports negatively to these markets. The problems that may arise in the export to these countries should be forecasted, precautions should be taken and alternative market searches should be expedited.

ACKNOWLEDGEMENTS

We would like to thank Süleyman Demirel University Scientific Research and Projects Coordination Unit (Project number: SDÜ BAP 3148-YL-12) for their financial support of this project.

REFERENCES

[1] Abak, K., Düzyaman, E., Şeniz, V., Gülen, H., Pekşen, A. and Kaymak, H.C. (2010) Development Methods and Objectives of Vegetable Production VII. Agricultural Engineering Technical Conference Proceedings AETCP No. 1. Ankara, (Turkey). 477-492. (in Turkish)

[2] Emeksiz, F., Albayrak, M., Güneş, E., Özçelik, A., Özer, O.O. and Taşdan, K. (2005) Marketing Channels and Evaluation of Tools of Agricultural Products in Turkey Turkey Chamber of Agricultural Engineers' Publication, Ankara, (Turkey), 20. (in Turkish)

[3] Fertő, I. and Szabó, G.G. (2002) The Choice of Supply Channels in Hungarian Fruit and Vegetable Sector. Paper Presented at the Annual Meeting of the American Agricultural Economics Association in Long Beach, July 5-8, 15.

[4] Sakurai, S., Ando, M. and Piansak, P. (2004) Marketing of Fruits and Vegetables in Northeastern Thailand. Agricultural Marketing J. of Japan. 60, 115-118.

[5] Adhikari, R.K. (2009) Economics of Organic Vs Inorganic Carrot Production in Nepal. Journal of Agriculture and Environment. 10 (Jun. 2009), 23-28.

[6] Ahmad, Z., Ali, N., Ahmad, M. and Ahmad, S. (2005) Yield and Economics of Carrot Production in Organic Farming. Sarhad Journal of Agriculture. 21(3),357-364.

[7] Güneş, T. (1996) Agricultural Marketing Ankara University Publication, Ankara, Turkey. 297. (in Turkish)

[8] Ok, Ü. (2009) Production and Marketing of Stake-tomato in Central villages of Tokat Province. Msc Thesis, Department of Agricultural Economics, Gaziosmanpasa University, Institute of Natural and Applied Sciences, Tokat, 132 (in Turkish).

[9] Gülten, S. (1985) Agricultural Marketing Atatürk University, Publication Number 631, Erzurum, Turkey. 114. (in Turkish)

[10] Açıl, A.F. (1980) Agricultural Economy Ankara University, Agriculture Faculty Publication Number 721, Ankara, Turkey. 611. (in Turkish)

[11] Yurdakul, O. (1998) Marketing of Agricultural Products. Cukurova University, Faculty of Agriculture Publication No 127, Adana, (Turkey), 240. (in Turkish)

[12] Özkan, B., Yılmaz, S. and Yılmaz, İ. (1999) Fresh Fruit and Vegetable Marketing in Turkey: Problems and Proposed Solutions. Akdeniz University, Journal of the Faculty of Agriculture. 12, 157-168. (in Turkish)

[13] Kaptangil, M.K. (1980) Wholesalers Fruits, Vegetables and Cooperative Journal of Agricultural Economics. 30-31, 21-22. (in Turkish)

[14] Güneş, T., Arikan, R., Erdem, H., Vural, H., Ergenoğlu, F., Gezerel, Ö., Kaplankiran, M. and Çetin, B. (1986) Regulation of Marketing of Fruits and Vegetables and Reducing the Costs Which Produced Adana and Içel Province and Transportation to Ankara TÜBİTAK Project Number: TOAG-550, Ankara. (in Turkish)

[15] Erkal, S. and Şafak, A. (1991) Fresh Fruit and Vegetable Marketing in Turkey Journal of TOK, 59. (in Turkish)

[16] Gül, M. (2005) Economic Analysis of Apple Farming in the Trans Taurus Mountains Region Ph.D. Thesis, Department of Agricultural Economics, Çukurova University, Institute of Natural and Applied Sciences, Adana. 378. (in Turkish)

[17] Anonymous. (2013) Official Gazette. 6 May 1960 No.10605, 27 June 1995 No. 22326, 14 June 1998 No.23372, 01 December 2004 No. 5262, 23 May 2007 No.23372, 11 March 2010 No.5957, 07 July 2012 No. 28346, Ankara. (in Turkish)

[18] Hatirli, S.A. and Yurdakul, O. (1992) Marketing Structure and Problems of Protected Cultivation in Mersin. Journal of the Faculty of Agriculture, Cukurova University. 7(2), 159-172. (in Turkish)

[19] Dastagiri, M.B., Chand, R., Immanuelraj, T.K., Hanumanthaiah, C.V., Paramsivam, P., Sidhu, R.S., Sudha, M., Mandal, S., Singh, B., Chand, K. and Kumar, B.G. (2013) Indian Vegetables: Production Trends, Marketing Efficiency and Export Competitiveness. American Journal of Agriculture and Forestry. 1(1), 1-11.
[20] Al, S. (2011) Impact of Middlemen on Vegetable Marketing Channels in Sri Lanka. Tropical Agricultural Research and Extension. 14(3), 58-62.
[21] Calvin, L., Cook, R., Denbaly, M., Dimitri, C., Glaser, L., Handy, C., Jekanowski, M., Kaufman, P., Krissoff, B., Thompson, G. and Thornsbury, S. (2001) U.S. Fresh Fruit and Vegetable Marketing: Emerging Trade Practices, Trends, and Issues. U.S. Dept. Agr., Econ. Res. Serv., Agricultural Economic Report Number 795, 52.
[22] Van Heerden, J. and Willemse J. (2000) Agricultural economic, trade and policy issues for 2000. Agricultural Outlook Conference held in Nelspruit, 1 March 2000. (in German)
[23] Blomkamp, E. (2000) Outlook for the International Marketing of Fruit and Vegetables. Agricultural Outlook Conference held in Nelspruit, 1 March 2000.

Received: **17.10.2017**
Accepted: **02.03.2020**

CORRESPONDING AUTHOR

Musa Acar
Aksaray University, Eskil Vocational School,
Aksaray University
Aksaray – Turkey

e-mail: musaacar@aksaray.edu.tr

© by PSP Volume 29 – No. 05/2020 pages 3338-3343 Fresenius Environmental Bulletin

THE UTILIZATION OF THE PRECONCENTRATION FOR THE ARTIFICIAL WASTEWATER BY FREEZE–CONCENTRATING TECHNIQUE WITH MIXING NON-AQUEOUS PHASE LIQUID- NOVEC 7300

Chunhong Shao[1], Yao Cheng[2], Xiandong Zhang[2], Tingliang Yan[2], Yingjie Dai[3,*]

[1]College of Civil and Architectural Engineering, Heilongjiang Institute of Technology, Daowai District, Harbin, China
[2]College of Chemical and Environmental Engineering, Harbin University of Science and Technology, Harbin, China
[3]Laboratory of Environmental Remediation, College of Resources and Environment, Northeast Agricultural University, Xiangfang District, Harbin, China

ABSTRACT

This study was carried out to determine the removal of COD from aqueous solution using layer crystallization method. In this study, the influence of several parameters, such as adding as not-aqueous phase liquid, 3M Novec 7300 (FN), freezing temperature, initial COD concentration, and the stirring speed upon removal ratio of COD were carried out. Results showed that the removal ratios of COD in the ice with FN adding were higher than that of no FN adding. When the freezing temperatures of the solution were decreased from –5 to –25 °C, the removal ratios of COD in the ice were decreased. The values of removal ratios of COD for the wastewater concentrations of 250 mg/L, 500 mg/L and 1000 mg/L with FN adding ratio of 10% were 93.36%, 91.52% and 89.91%, respectively. The driven force of concentration poor, water molecules in liquid was diffused to the interface of solid and liquid, while the pollutants near the interface of solid and liquid was diffused to liquid.

KEYWORDS:
Freeze–concentration, FN, Separation efficiency, Wastewater

INTRODUCTION

Freezing is an ancient method. The earliest record of freezing method for desalination was appeared in the mid-seventeenth century [1]. However, this method has not been widely promoted because of the technical problems. In 1945, Vacino and Visintin wrote a paper, which meant that freezing technology entered a phase of laboratory research and extension process [2]. In 1955, a variety of refrigeration processes have emerged, the scope of application of refrigeration has also been greatly expanded [3]. Since then, the freezing method was mainly used for the concentration of beer and orange juice, frozen wine concentration and seawater desalination [3-5].

According to the different sources of frozen, freezing concentration could be divided into natural freezing and artificial freezing [6]. And the natural freezing method is divided into suspended freezing method and progressive freezing method [6]. Researchers found that there were many advantages about freeze-concentration throughout the long-term research. First of all, the energy required for freezing and concentrating mainly came from the cold energy in nature [7]. Cold energy was a green energy and it would not produce pollution. Therefore, compared with other methods of concentration, the energy of freezing concentration would be greatly reduced. Freeze concentration only needs 420 kJ/kg of energy to fully freeze water of 293K, it is six times lower than that fully vaporized water in the same temperature [8]. Moreover, the corrosion of the material during freeze concentration is very light, equivalent to one-thousandth of the distillation. So it is possible to use inexpensive structural materials such as mild steel, plastic and aluminum alloy. Afterwards, the elimination of corrosion products are greatly reduced, freezing concentration needn't to add any chemicals. Because of these advantages above, the use of application of freeze-concentration has been further expanded to the food, pharmaceutical, chemical and other fields. In recent years, freeze-concentration technology has also played a role in wastewater treatment. Freezing-concentration was used to treat the wastewater in paper mills, chemical plants, pharmaceutical factories in Canada, the United Kingdom, Japan and Singapore [9]. Wakisaka et al. replaced the wastewater with dextrose and imitated the actual wastewater treatment [10]. Freezing-concentration can also be combined with other processes, Ma et al. used the frozen and reverse osmosis technology for urea wastewater research [11].

However, because of the washing of ice crystals and separation was difficult, freeze-concentration technology was difficult to enter the

industrialization. Cold energy has not yet been introduced as a new energy source according to the Global New Energy Development Report in 2016. While many of the continents were in the cold zone, which has the advantages of developing cold energy sources. At present, the development of new energy is valued by all countries in the world. Cold energy is a clean energy source after wind energy and light energy. Therefore, the use of freeze-concentration has a high research value in wastewater treatment and other fields.

MATERIALS AND METHODS

Materials. Novec 7300 (3M Novec 7300, FN) is a colorless clarified, slightly odorous liquid substance as not-aqueous phase liquid was used in this work. The nonvolatile component is less than 2.0pmm and is specifically used to replace Freon and other " Ozone layer destructive "substances. Environmentally friendly solvents that do not affect the environment. Features of FN: colorless, tasteless, non-toxic, non-burning, ODP value is zero; low surface tension, low viscosity, low latent heat of evaporation. Effective substance content :100 (%). Chemical formula of FN is $C_6F_{13}OH_3$, and it is liquid phase at room temperature, with ether bond, excellent thermal stability and chemical stability (recyclable), and a fluorine liquid which has moderate solubility. The physical properties of FN are as follows: boiling point: 98 °C; freezing point: -38 °C; absolute viscosity: 0.0012 Pa seconds.

TABLE 1
Composition of artificial wastewater

Sample	Concentration (g/L)
(D)+Glucose	10
Sodium Hydrogen L-Glutamate Monohydrate	10
Ammonium Sulfate	10
Sodium Chloride	0.2
Calcium Chloride, Anhydrous	0.1
Magnesium Sulfate, Anhydrous	0.06
Dipotassium Hydrogenphosphate	1.3
Potassium Dihydrogenphosphate	0.3
Sodium Hydrogen Carbonate	13

The artificial wastewater were prepared by COD:T-N:T-P=30:10:1. The target concentration of COD_{cr} was set at 1000 mg/L and the composition of artificial wastewater are shown in Table 1. The artificial wastewater was diluted 250 mg/L and 500 mg/L, respectively using deionized and distilled water. The freeze–concentrating technique was used to preconcentrate the artificial wastewater. The artificial wastewater solution was stored at 4 ± 0.5 °C.

Experimental apparatus and procedure. A equipment of freezing concentration that incluing stirrer HTY8S25N–1(Japan Servo Co., Ltd.), stationary vessels (acrylic resin, diameter 120 mm, depth 180 mm), a pump, and a tank is shown in Figure 1. The artificial wastewater solution was supplied into the stationary vessels by a pump from the tank. The artificial wastewater solution (1 L) in the stationary vessels was frozen with the different stirring speed that was located in a low temperature laboratory. The temperature of the low temperature laboratory was set at –5 °C, –15 °C and –25 °C, respectively. When most of the artificial wastewater solution from the surrounding of stationary vessels was frozen, the ice was separated with concentrated solution of the artificial wastewater solution. The concentration of wastewater in the sample solutions and the melted ice layer formed in the sample solutions were measured using a COD meter (HC–407, Central Kagaku Corp., Japan). The parameters in Eq. (1), which were determined from freezing experiment, The removal ratio (R) was calculated by dividing the concentration of COD in the solution and in the ice by the initial concentration of COD in the solution.

$$R = \frac{C_0 - C}{C_0} \times 100\% \qquad (1)$$

Here, R is the COD removal ratio (%); C_0, the initial COD concentration in the solution (mg/L); C, the COD concentration in the ice (mg/L). Three replicate runs were carried out for each experimental treatment.

RESULTS

Effect of adding FN. Five hundred milliliter mixtures of wastewater (500 mg/L) and FN (adding ratio: 0-20%) was frozen at the freezing temperature of –15 °C with the stirring speed of 200 rpm in the 1L beaker in a refrigerator. The removal ratios of COD in the ice is shown in Figure 2. The values of removal ratios of COD of FN adding ratio of 0, 10% and 20% were 84.43%, 91.52% and 92.01%, respectively. It has found that the removal ratios of COD in the ice with FN adding were higher than that of no FN adding. However, that of with FN adding ratio of 10% and 20% were not significantly affected. So the FN adding ratio of 10% was selected in other run. The addition of FN in the ice mixture results in the increase of liquid ratio in the ice-liquid mixture, it will reduce the shearing force of the ice-crystal-bonded concentrate and the residual concentrate between ice crystals.

Effect of the freezing temperature. Five hundred milliliter mixtures of wastewater (500

mg/L) and FN (adding ratio: 10%) was frozen at –5°C, –15 °C, and –25 °C with the stirring speed of 200 rpm in the 1L beaker in a refrigerator. After freezing most of the wastewater solution, the ice samples were melted and the concentration of COD in the ice samples were measured. Figure 3 shows that the removal ratios of COD in the ice with different freezing temperatures (from –5 to –25 °C) at COD concentration of 500 mg/L. It shows that the removal ratios of COD in the ice were decreased with the freezing temperatures decreased. The values of removal ratios for COD in the ice for the freezing temperatures of –5°C, –15°C and –25°C were 94.15%, 91.52% and 87.19%, respectively. Under the rapid freezing conditions (such as –25 °C), there appears ice crystals with tree branches and needle–like crystals at the solid–liquid interface [12]. Much more ice crystals were obtained by caging pollutant molecules, lead to decrease the removal ratio of COD, because the speed of freezing for water molecule was faster than that of exceed for pollutant from wastewater solution[13]

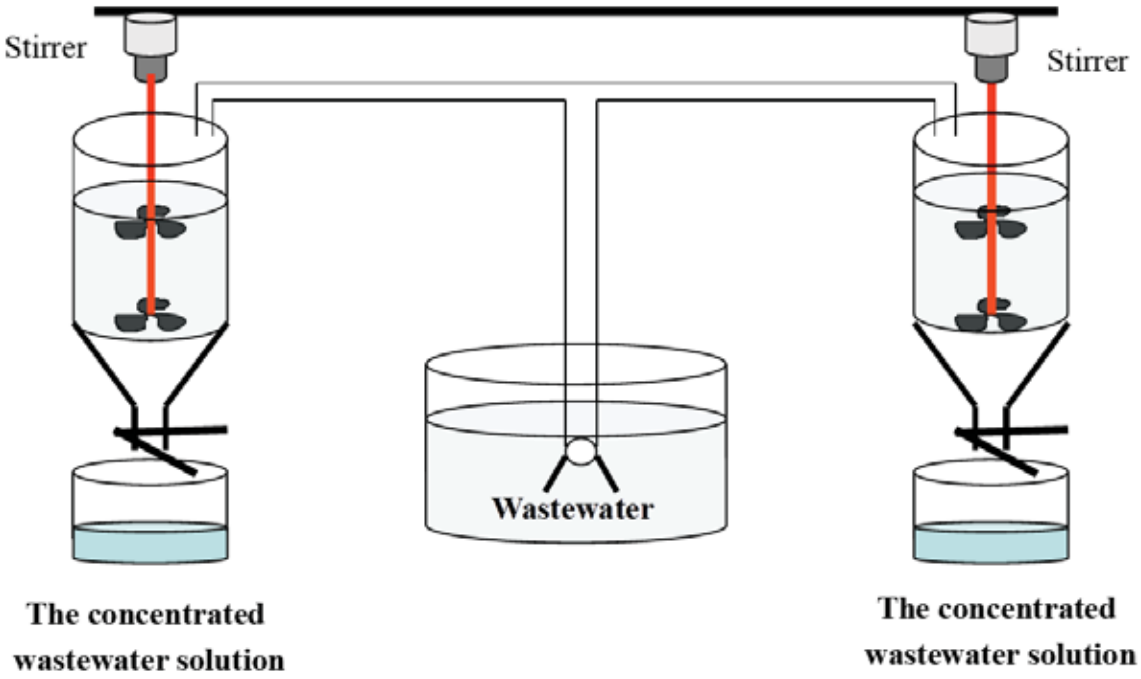

FIGURE 1
Schematic of freezing concentration equipment

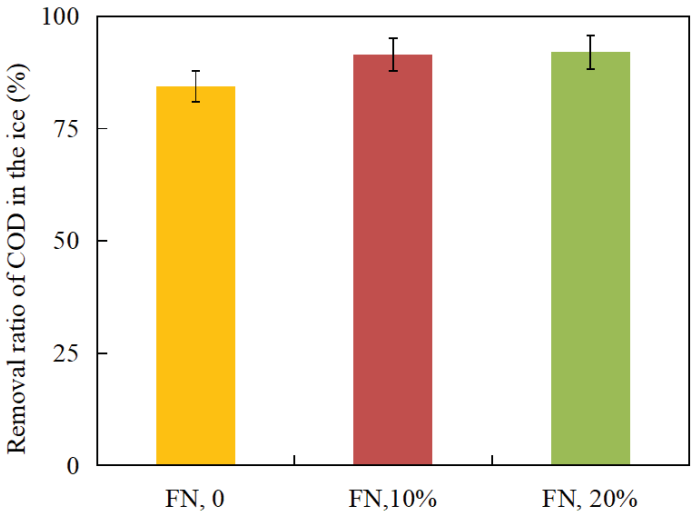

FIGURE 2
Removal ratios of COD in the ice with different adding ratio of FN at the COD concentration of 500 mg/L

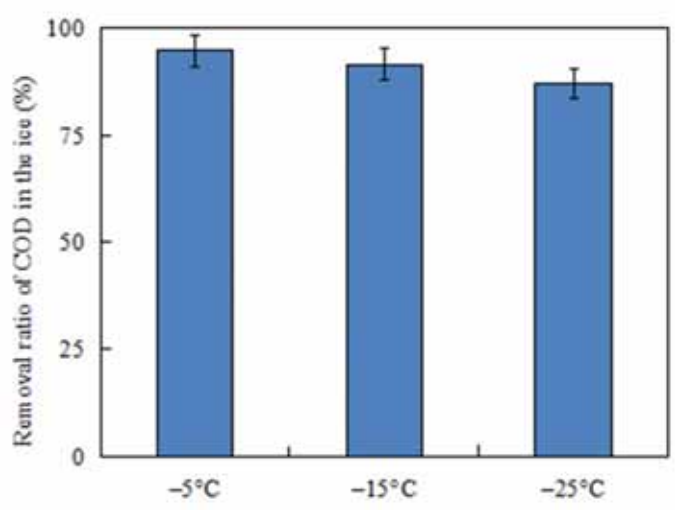

FIGURE 3
Removal ratios of COD with different freezing temperatures at the COD concentration of 500 Mg/L

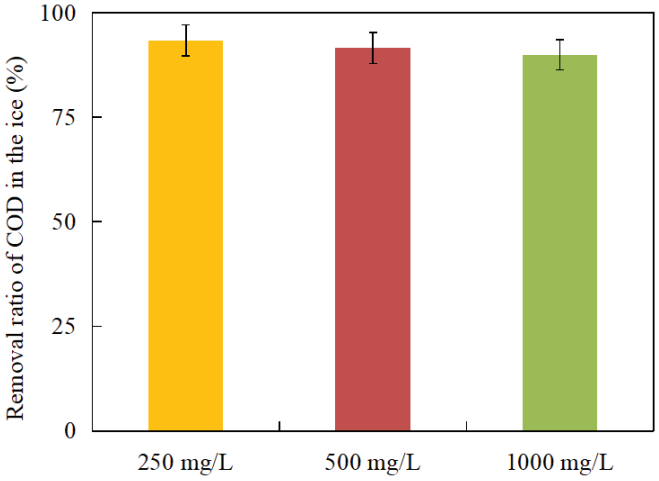

FIGURE 4
Removal ratios of COD with different COD concentrations at the freezing temperature of –15 °C

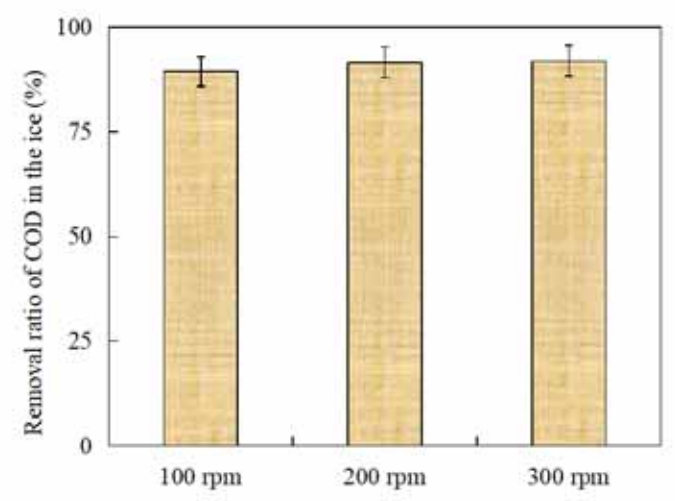

FIGURE 5
Removal ratios of COD in the ice with different stirring speed at the freezing temperature of –15 °C

Effect of the COD concentration. Five hundred milliliter mixtures of wastewater (250 mg/L, 500 mg/L and 1000 mg/L) and FN (adding ratio: 10%) was frozen with the stirring speed of 200 rpm at the freezing temperature of –15 °C. The removal ratios of COD in the ice is shown in Figure 4. The values of removal ratios of COD for the wastewater concentrations of 250 mg/L, 500 mg/L and 1000 mg/L were 93.36%, 91.52% and 89.91%, respectively. The results (see Figure 4) show that the removal ratios of COD in the ice were significantly varied among the different concentrations (250 mg/L, 500 mg/L and 1000 mg/L) of the wastewater solution.

Effect of the stirring speed. Five hundred milliliter mixtures of wastewater (500 mg/L) and FN (adding ratio: 10%) was frozen at the freezing temperature of –15 °C with the stirring speed of 100 rpm, 200 rpm, and 300 rpm. The removal ratios of COD in the ice is shown in Figure 5. The values of removal ratios of COD for the wastewater concentrations of 100 rpm, 200 rpm, and 300 rpm were 89.39%, 91.52% and 91.86%, respectively. It has found that the removal ratios of COD in the ice were not significantly affected for the different stirring speed. So the stirring speed of 200 rpm was selected in other run.

DISCUSSION

The system in the aquatic solution begin generate ice crystals when the temperature of the solution decreases to a freezing point [14]. Then part of the pollutants of the solution was precipitated rapidly, it increase the formation possibility for critical dimensions of ice nuclear, prompted water out-of-phase nuclear and accelerate the formation of ice [15]. So water molecules of the solution was crystallized slowly and it take shape the clean ice layer [12]. The growth rate of crystal was relevant to water molecules added to the rate that water molecules go up to crystals nucleus and state of the interface of solid and liquid, the nucleation near the interface can be attached to the nucleation surface only through the interface warp [16]. Nearby the interface of solid and liquid, water molecules was crystallized under the hydrogen bonding interaction, adhere to the ice surface, and pollutants will be squeezed from ice to the solution, the concentration of water molecules near the interface of solid and liquid are much less that in the whole liquid, the concentration of the pollutants near the interface of solid and liquid is much more than that entire liquid [17]. The driven force of concentration poor, water molecules in liquid was diffused to the interface of solid and liquid, while the pollutants near the interface of solid and liquid was diffused to liquid [18].

CONCLUSIONS

The removal of COD from the artificial wastewater solution using layer crystallization method was to investigate the influence of several parameters, such as adding FN, freezing temperature, initial concentration of COD, and the stirring speed for the removal ratio of COD. The removal ratios of COD in the ice with FN adding were higher than that of without FN. When the freezing temperatures of the solution were decreased from –5 to –25 °C, the removal ratios of COD in the ice were decreased. The removal ratios of COD in the ice were significantly affected by the different concentrations of the COD solution, and the values of removal ratios of COD for the wastewater concentrations of 250 mg/L, 500 mg/L and 1000 mg/L were 93.36%, 91.52% and 89.91%, respectively. It has found that the removal ratios of COD in the ice were not significantly affected for the different stirring speed. The driven force of concentration was poor, water molecules in liquid was diffused to the interface of solid and liquid, while the pollutants molecule near the interface of the solid and liquid was diffused to liquid. In general, the removal ratios of COD in the ice was increased by adding FN into the mixture of ice and wastewater solution comparing with that of without FN. This study introduced a method with improved simpleness, lower costs and higher removal ratio.

REFERENCES

[1] Lu, Z., Xu, L.C. (1994) The current status and prospect of freezing desalination technology, Technol. Water Treat. 20 (3), 140-145.
[2] Sanin, F., Vesilind, P., Martel, C., (1994) Pathogen reduction capabilities of freezing/thawing sludge conditioning. Water Res. 28, 2393-2398.
[3] Muller M., Sekoulov I. (1992) Waste water reuse by freeze concentration with falling film reactor, Water Sci, Technol. 26, 7-8.
[4] Rubenstein, S.H., Orbach, H.G., Shuber, N., King E., Zackler J. (1971) Freeze concentration of viral agents from large volumes of water, J. - Am. Water Works Assoc. 63, 301-302.
[5] Holt, S. (1999) The role of freeze concentration in waste water disposal, Filtration. 36, 34-35.
[6] Zhang, Y., Zhang, C.J., Zhou, Q. (2013) Research and application of freezing process in wastewater treatment, Technol. Water Treat. 7 (39), 6-10.
[7] Wang, L.P. (2017) Boron removal and its concentration in aqueous solution through progressive freeze concentration, Environ. Technol. 38, 2224-2232.

[8] Attia, A.A.A. (2010) New proposed system for freeze water desalination using auto reversed R-22 vapor compression heat pump, Desalination. 254, 179-184.
[9] Yu, T., Ma, J. (2005) Study on influence factors of ice crystal purity during freeze concentration process, J. Harbin University Commerce (Natural Sciences Edition). 21 (5), 572-578.
[10] Wakisaka, M., Shirai, Y., Sakashita, S. (2001) Ice crystallization in a pilot-scale freeze wastewater treatment system, Chem. Eng. Process. 40, 201-208.
[11] Yu, T., Ma, J., Zhang, L.Q., Zhang, J.L. (2006) Urine treatment by the combined freeze-concentration and reverse osmosis in space station, J. Harbin Institute of Technology. 38 (4), 567-570.
[12] Lorain, O., Thiebaud, P., Badorc, E., Aurelle, Y. (2001) Potential of freezing in wastewater treatment: soluble pollutant applications, Water Res. 35, 541-547.
[13] Jiang, Y., Fei, X., Wang, X., Du, G. (2011) Study on the treatment of the refractory organic waste water by freezing separation, Environ. Sci. Manag. 4, 72-75.
[14] Kobayashi, A., Shirai, Y., Nakanishi, K. (1996) A method for making large agglomerated ice crystals for freeze concentration, J.Food Eng. 27, 1-15.
[15] Gao, W., Smith, D.W., Sego, D.C. (2004) Release of contaminants from melting spray ice of industrial wastewater, Cold Reg. Sci. Technol. 18, 35-51.
[16] Halde, R. (1980) Concentration of impurities by progressive freezing, Water Res. 14, 575-580.
[17] Gao, W., Smith, D.W., Habib, M. (2008) Petroleum refinery secondary effluent polishing using freezing processes–toxicity and organic contaminant removal, Water Environ. Res. 80, 517-523.
[18] Gao, W., Smith, D.W., Li, Y. (2006) Natural freezing as a wastewater treatment method: E. coli inactivation capacity. Water Res. 40, 2321–2326.

Received: **04.12.2017**
Accepted: **04.03.2020**

CORRESPONDING AUTHOR

Yingjie Dai
Laboratory of Environmental Remediation,
College of Resources and Environment,
Northeast Agricultural University,
No.600 Changjiang Road,
Xiangfang District, Harbin 150030,China

e-mail: dai5188@hotmail.com

© by PSP Volume 29 – No. 05/2020 pages 3344-3353 Fresenius Environmental Bulletin

THE PROTECTIVE EFFECTS OF GOLDENBERRY (*PHYSALIS PERUVIANA* L.) EXTRACT AGAINST TO THE OXIDATIVE AND DESTRUCTIVE EFFECTS OF TYPE I DIABETES IN RATS

Fazilet Erman[1], Tubay Kaya[2], Sevinc Aydin[3,*], Orhan Erman[2], Okkes Yilmaz[2]

[1]Firat University, Faculty of Health Sciences, Elazig, Turkey
[2]Firat University, Faculty of Science, Biology Department, Elazig, Turkey
[3]Munzur University, Cemişgezek Vocational School, Tunceli, Turkey

ABSTRACT

Type I diabetes is known as insulin-dependent diabetes mellitus, and the most important factor playing role in its formation is the genetic predisposition. *Physalis peruviana* L. (Goldenberry) is a plant, which has strong antioxidant properties, from Solanaceae family and, because of its fructose content, plays regulatory role in blood glucose level of diabetics. In this study, it has been investigated the effects of goldenberry on the malondialdehyde (MDA), reduced glutathione (GSH), total protein, vitamins A, D, E, and K, and cholesterol levels which are the indicators of antioxidant defense and the oxidative damages in serum, muscle, kidney, liver and brain tissues of the rats, on which type I diabetes was induced by STZ.

According to the obtained results, among the rats with STZ-induced type I diabetes, it was observed that the level of glutathione (GSH) increased and the level of malondialdehyde (MDA) decreased in all of the tissues of rats given goldenberry extract, while significant decreases were determined in the levels of vitamins K-1, K-2, D-2 and D-3 in all of tissues (except serum), and there were also decreases in the levels of α-tocopherol and cholesterol in tissues of muscle, liver and kidney.

In this study, it was shown that the goldenberry decreased the destructive effects of type-I diabetes by decreasing the serum glucose and lipid peroxidation and increasing the level of glutathione. It is believed that the obtained results would be used in follow-up of diabetic patients and in early diagnosis of the disease in future.

KEYWORDS:
Goldenberry (*Physalis peruviana* L.), lipid peroxidation (LPO), MDA, GSH, vitamin

INTRODUCTION

As in entire world, diabetes is a disease that is widely seen in Turkey as well. Despite the fact that the incidence of type 2 diabetes has been increased significantly because of the increasing obesity and sedentary lifestyle, and the dietary habits in both developed and developing countries, type-I diabetes has been found to be rarer. Even though the diabetes' effects on lipid peroxidation and fatty acids were comprehensively investigated, the studies on the subjects such as antioxidant enzymes, lipid phase transition, lipid mechanism and dynamics, protein structure, lipid-protein ratio, and relationship between lipid peroxidation and membrane dynamics are very limited.

Physalis peruviana is a very strong antioxidant herb from Solanaceae family, and it plays regulatory role in blood glucose levels of diabetics under favor of its fructose content. It is colloquially known as cape gooseberry or groundcherries. Some of the goldenberry species in Turkey are *P. alkekengi, P. philadelphica, P. angulate,* and *P. pubescens.*

The studies carried out on *P. peruviana* fruits are revealed the high level of beta carotene (0.32% PO) content, anti-carcinogenic effects of which have been proven in epidemiological studies, in the peels. Goldenberry also contains fatty acids, phytosterol, carotene, and fat-soluble vitamins [1].

Some researchers are emphasized the positive relationship between the increasing in consumption of goldenberry and decreasing in hyperglycemia because of its fibrous structure [2-4]. In this study, we aimed to investigate the protective and positive effects of *P. peruviana* fruits on possible effects of oxidative stress increasing in tissues along type-I diabetes.

MATERIALS AND METHODS

Preparation of Plant Extracts in Solution Form. Goldenberry fruits (50g) were oven-dried, and then separately powdered in blender. Following

the decomposition in 3/2 hexane isopropanol alcohol mixture, they were left in rotary evaporator for evaporation. The preparations were mixed with DMSO solution, and became ready for injection after filtering using filter paper.

Extraction and Analysis Of ADEK and Phytosterols of Fruit Extract. *P. peruviana* (Goldenberry) fruit samples were weighed and homogenized with n-hexane/isopropyl at 3/2 (v/v) ratio [5] and after the hydrolysis with 5% KOH at 85°C, extraction of phytosterols were performed with n-hexane [6]. The amounts of ADEK vitamins and phytosterols were analysed at 202 nm and 326 nm using a UV detector on a HPLC device [6-8].

Animal Experiment. The experimental study were provided by the Experimental Research Center at Fırat University School of Medicine (FUDAM) with no: FF.11.40 ethics committee permits (30.06.2011). In this study 27 wistar albino male rats were used (200-250 g. bw). Rats were divided into three groups. These groups and the concentrations of substance given to them were as follows:

Study Groups:

1. Control Group (Group C) (n=7): The rats in this group were not administered a STZ injection, and they were fed with standard feed and water.

2. Diabetes Group (Group D) (n=10): The rats in this group were administered 65 mg/kg STZ injection (in citrate buffer, p 4.5) intraperitoneally for establishing the type-I diabetes groups. They were fed with standard feed and water throughout the study period.

3. Diabetes Group+Goldenberry (Group D+G) (n=10): One week after inducing type-I diabetes by STZ injection, the goldenberry extract injection was performed twice a week (1 ml/kg) intraperitoneally. Throughout the study period, the rats were fed with standard feed and water added with 2g extracts (in powder form).

The procedure was executed for 2 months.

The rats in all of the groups were weighed weekly throughout the study period, and their blood glucose levels and changes in their weights were recorded. The blood glucose levels were measured using a glucometer. At the end of the experiments, the rats in all of the groups were decapitated. The tissue samples were taken from blood, liver, brain, kidney, and muscles, and MDA, GSH, total protein, and vitamin analyses were performed.

Sampling. After the end of the experiment, procedures were performed according to the following rules and tissues were taken. According to the ethics committee report, the animals were given anesthesia and sacrificed by withdrawing blood from the heart, then they were decapitated. Promptly after decapitation, blood, liver, kidney, brain and striat muscle tissues were taken. These tissue samples were promptly rinsed with 0.9% serum physiologic, so that, the samples were cleaned from the blood and were stored at -86°C until biochemical analyses. The blood taken from experimental animals were placed into tubes containig EDTA. And immediately centrifuged at 5000 rpm for 5 min, and the supernatant segments were taken into different tubes and kept at -86°C until the analyses.

Determination of GSH and Total Protein Levels. To quantify the glutathione and total protein levels in the tissues, 1g tissue sample taken from the animals were homogenized in 5 mL Tris (Tris base+Tris HCl+EDTA (pH:7.4) buffer, then separated from tissue pellet after the centrifugation at 9072 rcf for 20 min at +4°C. After centrifugation, the supernatant were divided into three aliquots, one of which was used for GSH analysis. For this purpose, the proteins in the supernatant were precipitated by adding 1 ml of 10% trichloroacetic acid reactive. This mixture was centrifuged at 2268 rcf for 5 min, so that the pellet was precipitated and the supernatant was removed into another tube. The supernatant was added in 1 mL DTNB,2 mL of 0.3 M Na_2HPO_4 solution and 1mL citrate, the color changed to yellow was read at 412 nm against blank [9]. The aliquot of supernatant remaining from the glutathione analysis was used for total protein analysis. For this purpose, the supernatant was separated and subjected to Lowry method [10]. The same method was applied for serum samples.

Measuring the Lipid Peroxidation Levels in Tissues (TBARS- MDA). By taking 1ml of tissue homogenate resting from the GSH and total protein measurements, the samples were added in with 0.5ml of 8.1% SDS, 0.5ml 0.8% TBA, 1ml 10% TCA, 1ml 20% acetic acid, and 50µl 4% BHT. And then this mixture was vortexed. Then the preparation was kept in boiling water bath at 85ºC for 1 hour. After removing them, they were added with 3ml pyridine, and then centrifuged. 2ml sample was taken from supernatant part, and the measurements were made at 532 nm in spectrophotometer. The results were separately recorded. The same procedure was executed for the serum samples [11].

Analysis of ADEK Vitamins and Cholesterol Levels in Tissues by HPLC Device. Remaining tissue sample underneath of the supernatant phase were homogenized with 10 mL n-hexane/ isopropyl at 3/2 (v/v) ratio [5] and centrifuged in +4°C at the 2800 rcf. To analysis of unsaponifiable lipophilic molecules, 5 mL of supernatant was put into 25-mL test tubes with caps, then the tubes were added 5% KOH solution. After vortexing, the tubes were kept at 85°C for 15 minutes. The tubes were removed and cooled to room temperature; then, the tubes were added 5 mL of distilled water and stirred. The unsaponifiable lipophilic molecules were extracted with

2x5 mL of hexane. The hexane phase was evaporated by nitrogen stream; then it was dissolved in 1 mL of acetonitrile/methanol (60%+40%, v/v) mixture, put into auto-sampler vials and analyzed [6-8]. The analysis was done on Shimadzu HPLC device. Calculations were done using Class *VP 6.27* program (Shimadzu, Kyota Japan). 326nm of detection wavelength was used for vitamin-A, 202nm for vitamin E, and 265 nm for vitamin D and vitamin K [12, 7].

Statistical Analysis. SPSS 15.0 program was used for statistical analysis. Comparison between the control group and experimental groups was done with the analysis of variance (ANOVA) and LSD tests. The results were given as mean±SEM. For determining the differences between the groups, $p>0.05$, $p<0.05$, $p<0.01$, and $p<0.001$ values were used (d: p<0.001; c: p<0.01; b: p<0.05; a: p>0.05 and a: There are no statistical differences between the groups, b: there is a partial difference between the groups, c: there is a significant difference between the groups, d: the difference between groups is much more pronounced. First P values: Comparison of D+G and D groups with group C, The second P values: Comparison of D+G with group D). Statistical interpretations were made according to control and diabetes groups.

RESULTS

The Contents of Vitamins and Sterols in Goldenberry. Table 1 shows the vitamins and sterols levels in the goldenberry. The level of α-tocopherol (Vitamin E), which is known to act as chain-breaking antioxidant by preventing the propagation of free radical reactions, was found to be the highest.

Body Weight Changing in Type I Diabetes. Table 2 shows body weights level of rats all the groups. Throughout the study, in weight measurements made in 1st (after STZ), 4th, and 8th weeks, a regular increase was observed in control group (C), while a decrease was determined in diabetes group (D) (p<0.01). Values similar to those of the control group were obtained in Diabetes + Goldenberry group (D+G), while a increase was determined in weight on the contrary D group (Table 2).

Fasting Glucose Levels in Type I Diabetes. Table 3 shows fasting glucose levels of the rats in all the groups. The fasting glucose levels were measured in 1st, 4th and 8th weeks were within the normal limits in group C, while increases in groups D and D+G. Furthermore, in the end of 8th week, the blood glucose level was found to be slightly lower then 4th week in group D+G (Table 3).

Muscle Tissue Values in Type I Diabetes. Table 4 shows MDA, GSH, and total protein values in muscle tissue. D and D+G groups compared to C group, also the D and D+G groups were compared with each other. When compared to control group, MDA level was observed to be significantly higher in group D (p<0.001). When comparing groups D and D+G, the level of MDA was seen to be slightly lower in group D+G (p<0.05). While the levels of GSH and protein were significantly lower in group D in proportion to the levels in group C (p<0.001, p<0.01, respectively), the level of GSH were observed to significantly increase in group D+G when compared to group D (p<0.01) (Table 4).

TABLE 1
The Contents of Vitamins and Sterols in 1g Of Goldenberry

Vitamin	K1	α-Toc	δ-Toc	D3	Cholesterol	Retinol	Ergosterol	Stigmasterol	βsitosterol
µg/g	6,35	125,55	1,05	0,95	51,00	0,2	46,3	59,15	32,05

TABLE 2
Body Weight Levels in All Groups (g)

Fasting Weight	C	D	D+G
After STZ Injection	212,20±5,36	213,15±5,78	201,75±8,28
4th week	221,00±4,52	204,31±8,30	210,70±14,42
8th week	226,60±4,60	202,36±7,18	236,36±7,18

TABLE 3
Fasting Glucose Levels of The Rats in All Groups (mg/dL)

Blood Glucose	C	D	D+G
After STZ Injection	90,40±9,50	316,15±117,72	263,08±44,16
4th week	111,40±3,94	466,31±35,04	334,50±39,18

TABLE 4
MDA, GSH, and Total Protein Values in The Muscle Tissue of The Rats In All Groups

Groups	MDA (nmol/g)	GSH (µg/g)	Total Protein (µg/g)
C	18,16±0,49	155,69±0,17	8,18±0,12
D	23,05±1,55[d]	140,77±2,60[d]	7,79±0,11[c]
D+G	19,92±0,95[a,a]	152,94±2,12[a,c]	8,46±0,26[a,a]

d: p<0.001; c: p<0.01; b: p<0.05; a: p>0.05

TABLE 5
Vitamin (µg/g) and Cholesterol Levels (µmol/g) in the Muscle Tissue of the Rats in All Groups

Vitamins	C	D	D+G
K-1	0,33±0,06	1,18±0,13[d]	0,48±0,18[b]
α-Tocopherol	2,73±0,28	4,36±1,22[c]	3,17±0,34[d,d]
δ- Tocopherol	0,50±0,10	2,67±0,14[c]	2,15±8,05[d]
D-3	0,40±0,12	0,83±0,19[d]	0,23±0,13[c,d]
Cholesterol (µmol/g)	0,63±0,50	6,98±0,08[d]	1,12±0,03[c,d]
Retinol	1,62±0,37	1,77±0,15[b]	0,63±0,16[c,c]

d: p<0.001; c: p<0.01; b: p<0.05; a: p>0.05

TABLE 6
MDA, GSH, and total protein levels of the liver tissue of the rats in all groups

Groups	MDA (nmol/g)	GSH (µg/g)	Total Protein (µg/g)
C	32,24±0,95	780,98±22,61	16,03±0,19
D	40,94±0,28[c]	364,76±14,19[d]	13,10±0,61[d]
D+G	31,71±0,41[a,c]	469,54±30,72[c,b]	18,54±0,81[b,d]

d: p<0.001; c: p<0.01; b: p<0.05; a: p>0.05

TABLE 7
Vitamin (µg/g) and Cholesterol Values (µmol/g) in the Liver Tissue of the Rats in All Groups

Vitamins	C	D	D+G
K-1	2,38±0,08	7,77±0,51[d]	1,83±0,11[b,d]
K-2	2,38±0,21	5,45±0,30[d]	2,70±0,17[b]
α- Tocopherol	17,88±2,34	26,72±2,04[d]	19,15±0,89[a,d]
D-2	0,75±0,19	0,58±0,08[a]	0,45±0,05 [b]
Cholesterol (µmol/g)	1,76±0,05	2,98±0,15[d]	1,63±0,02[b,c]
Retinol	641,22±35,14	1214,01±69,44[d]	747,66±41,44 [b,c]

d: p<0.001; c: p<0.01; b: p<0.05; a: p>0.05

Table 5 shows the vitamin and cholesterol levels in the muscle tissue**.** D and D+G groups compared to C group, also the D and D+G groups were compared with each other. When compared to group C, the group D was found to have significantly higher levels of K-1, D-3 and cholesterol (p<0.001), α-tocopherol and δ-tocopherol (p<0.01), while the levels of α-tocopherol and δ-tocopherol significantly increased (p<0.001) and D-3 and retinol levels significantly decreased in group D+G (p<0.01).When compared to group D, the levels of α-tocopherol and cholesterol significantly increased (p<0.001) and the levels of D-3 and retinol significantly decreased in group D+G (p<0.001, p<0.01, respectively) (Table 5).

Liver Tissue Values in Type I Diabetes. Table 6 shows MDA, GSH, and total protein levels in the liver tissue**.** D and D+G groups compared to C group, also the D and D+G groups were compared with each other. When compared to group C, MDA level significantly increased in group D (p<0.01), while it significantly decreased in group D+G in proportion to group D (p<0.01). When compared to group C, the level of GSH significantly decreased in group D (p<0.001), while the same parameter partially increased in group D+G in proportion to group D (p<0.05). On the other hand, the level of total protein, significantly increased in group D+G when compared to group D (p<0.001) (Table 6).

Table 7 shows the vitamin and cholesterol levels in the liver tissue**.** D and D+G groups compared to C group, also the D and D+G groups were compared with each other. When compared to group C, the levels of K-1, K-2, α-tocopherol, cholesterol and retinol significantly increased in group D (p<0.001), while the levels of K-1, α-tocopherol (p<0.001), cholesterol and retinol (p<0.01) decreased in group D+G in proportion to group D (Table 7).

Kidney Tissue Values in Type I Diabetes. Table 8 shows MDA, GSH, and total protein levels in kidney tissue**.** D and D+G groups compared to C group, also the D and D+G groups were compared with each other. When compared to group C, MDA

level was found significantly increased in group D ($p<0.01$), while it significantly decreased in group D+G in proportion to group D ($p<0.001$). When compared to group C, the level of GSH significantly decreased in group D and group D+G ($p<0.001$, $p<0.01$, respectively), while the same parameter significantly increased in group D+G when compared to group D ($p<0.01$). On the other hand, the level of total protein, significantly decreased in group D+G when compared to group D ($p<0.001$) (Table 8).

Table 9 shows the vitamins and cholesterol levels in the kidney tissue**.** D and D+G groups compared to C group, also the D and D+G groups were compared with each other. When compared to group C, the levels of α-tocopherol, D3, cholesterol, retinol ($p<0.001$), K-1 and D-2 ($p<0.01$) significantly increased in group D. On the other hand, K-2 level significantly decreased in group D ($p<0.01$). In group D+G, significant decreases were observed in levels of K-1, K-2 ($p<0.001$), cholesterol, and retinol ($p<0.01$). When compared to group D, the levels of K-1, α-tocopherol, D-3, retinol ($p<0.001$), K-2, and cholesterol ($p<0.01$) decreased in group D+G (Table 9).

Brain Tissue Values in Type I Diabetes. Table 10 shows MDA, GSH, and total protein levels in the brain tissue**.** D and D+G groups compared to C group, also the D and D+G groups were compared with each other. When compared to group C, the level of MDA significantly increased in group D ($p<0.001$), while its level significantly decreased between the groups D and D+G ($p<0.01$). When compared to group C, the level of GSH significantly decreased in group D ($p<0.001$), while it increased in group D+G in proportion to group D ($p<0.01$). The level of total protein significantly increased in group D when compared to group C ($p<0.001$), while it decreased in group D+G in proportion to group D ($p<0.001$) (Table 10).

Table 11 shows the vitamins and cholesterol levels in the brain tissue**.** D and D+G groups compared to C group, also the D and D+G groups were compared with each other. When compared to group C, the levels of K-1, K-2, D-3, retinol ($p<0.001$) and δ-tocopherol and cholesterol ($p<0.01$) significantly increased while the level of α-tocopherol significantly decreased in group D ($p<0.001$). In Group D+G, significant increase was observed in level of K-2 ($p<0.01$), while decreases were seen in levels of α-tocopherol and D-3 ($p<0.01$). When compared to group D, the levels of K-1, δ-tocopherol, retinol ($P<0.001$) and K-2 ($P<0.01$) significantly decreased while significantly increased α-tocopherol level ($P<0.01$) in group D+G (Table 11).

Serum Values in Type I Diabetes. Table 12 shows MDA and total protein levels in the serum**.** D and D+G groups compared to C group, also the D and D+G groups were compared with each other. When compared to group C, the level of total protein was showed a small difference in groups D and D+G ($p<0.05$), while the level of MDA significantly increased in group D ($p<0.001$), and MDA level was found significantly decreased in group D+G in proportion to group D ($p<0.01$) (Table 12).

TABLE 8
MDA, GSH, and Total Protein Levels of The Kidney Tissue of The Rats in All Groups

Groups	MDA (nmol/g)	GSH (µg/g)	Total Protein (µg/g)
C	40,64±0,11	480,36±8,02	18,09±0,65
D	54,78±0,64^{c}	221,90±18,79^{d}	20,32±0,92^{b}
D+G	39,46±0,87^{a,d}	293,83±20,91^{c,c}	15,74±0,82^{c,d}

d: $p<0.001$; c: $p<0.01$; b: $p<0.05$; a: $p>0.05$

TABLE 9
Vitamins (µg/g) and Cholesterol Values (µmol/g) in the Kidney Tissue of The Rats in All Groups

Vitamins	C	D	D+G
K-1	1,55±0,15	2,06±0,12^{c}	0,91±0,09^{d,d}
K-2	13,88±0,99	5,94±0,32^{c}	3,51±0,09^{d,c}
α- Tocopherol	23,87±1,38	95,88±3,86^{d}	20,62±0,23^{b,d}
D-2	0,19±0,06	0,22±0,04^{c}	0,18±0,04^{a}
D-3	0,14±0,03	0,28±0,02^{d}	0,13±0,02^{a,d}
Cholesterol (µmol/g)	3,70±0,38	4,29±0,11^{d}	3,33±0,12^{c,c}
Retinol	3,11±0,46	6,81±0,20^{d}	2,26±0,15^{c,d}

d: $p<0.001$; c: $p<0.01$; b: $p<0.05$; a: $p>0.05$

TABLE 10
MDA, GSH, and Total Protein Levels of The Brain Tissue of The Rats in All Groups

Groups	MDA (nmol/g)	GSH (µg/g)	Total Protein (µg/g)
C	11,83±0,37	261,49±0,49	4,68±0,33
D	16,24±0,36^{d}	235,08±0,56^{d}	6,39±0,17^{d}
D+G	11,81±0,56^{a,c}	254,94±0,72^{b,c}	4,87±0,16^{a,d}

d: $p<0.001$; c: $p<0.01$; b: $p<0.05$; a: $p>0.05$

TABLE 11
Vitamins (µg/g) and Cholesterol Values (µmol/g) in the Brain Tissue of The Rats in All Groups

Vitamins	C	D	D+G
K-1	2,35±0,32	8,66±0,57[d]	2,83±0,60[b,d]
K-2	2,60±0,21	18,33±0,88[d]	10,17±0,18[c,c]
α-Tocopherol	107,31±0,12	59,82±1,79[d]	72,59±2,98[c,c]
δ-Tocopherol	0,20±0,10	0,35±0,05[c]	0,18±0,15[a,d]
D-3	0,26±0,07	1,63±0,20[d]	0,16±0,04[c]
Cholesterol(µmol/g)	7,04±0,62	6,25±0,08[c]	6,62±0,23[b]
Retinol	0,15±0,02	0,74±0,12[d]	0,20±0,02[b,d]

d: p<0.001; c: p<0.01; b: p<0.05; a: p>0.05

TABLE 12
MDA and Total Protein Levels of the Serum of the Rats in All Groups

Groups	MDA (nmol/mL)	Total Protein (µg/mL)
C	4,43±0,19	4,26±0,07
D	7,70±0,14[d]	4,19±0,15[b]
D+G	5,37±0,52[a,d]	4,40±0,07[b]

d: p<0.001; c: p<0.01; b: p<0.05; a: p>0.05

TABLE 13
Vitamins (µg/g) and Cholesterol Values (µmol/g) in the Serum of The Rats in All Groups

Vitamins	C	D	D+G
K-1	0,33±0,06	0,15±0,02[d]	0,19±0,08[c]
K-2	0,43±0,13	0,76±0,10[c]	0,87±0,17[d]
α-Tocopherol	11,50±0,19	12,76±0,27[b]	13,09±0,33[c]
D-2	0,14±0,07	0,18±0,03[a]	0,13±0,03[a]
D-3	0,21±0,03	0,18±0,07[a]	0,54±0,10[d,d]
Cholesterol	491,27±27,14	365,49±9,23[b]	342,26±13,84[c]
Retinol	0,28±0,04	0,47±0,14[c]	0,22±0,04[b]

d: p<0.001; c: p<0.01; b: p<0.05; a: p>0.05

Table 13 shows the vitamins and cholesterol levels in the serum. D and D+G groups compared to C group, also the D and D+G groups were compared with each other. When compared to group C, the level of K-1 found significantly decreased in group D and D+G (p<0.001, p<0.01, respectively), while the level of K-2 and retinol significantly increased (p<0.01) in group D. On the other hand, in group D+G, the levels of K-2 and D-3 were observed to significantly increased (p<0.001). When compared to group D, the level of D-3 was found significantly increased in group D+G (p<0.01) (Table 13).

DISCUSSION

Diabetes mellitus, which affects the lives of millions of people throughout the world, has led people to die or have low quality of live for many years because the insulin started to be used in 1900s.The herbal treatment methods gain importance in literature as the alternative studies on diabetes and its complications [13, 14].

Horn et al. [13], investigated the effects of aqueous extract of *P. peruviana* and shown that this extract decreased the levels of TBARS (MDA) and GSH and had effect on antioxidant system of organism. The results of the study show that it is an increase of the thiobarbituric acid reactive substances (TBARS-MDA) after the exposure to the 2,4-dichlorophenoxyacetic (2,4-D). On the other hand, after the treatment of the samples there was a decrease of the lipid peroxidation levels on the groups that were exposed to the extract on the concentrations of 1 and 10g/L. The results show that the *P. Peruviana* owns an effect on the antioxidant system of the organism, it was able to fix damages in lipids specially on the concentrations of 1 and 10 g/L. The results of our study are similar to MDA results of this study [13].

Hassan and Ghoneim [14], to investigate the potential antidiabetic, hypolipidemic, and antioxidant effects of *P. pubescens* L., to the diabetic rats were given 1ml of *P. pubescens* extract once a day for 21 days. In diabetic rats, the levels of blood glucose, serum insulin and pancreatic insulin, troponin, effect on tumor, necrosis factor (TNF), interleukin6 (IL-6), vascular endothelial, growth factor (VEGF), serotonin, dopamine, and malondialdehyde (MDA) were measured. The study on the effects of pancreas beta cells on anti-free radicals is the study, where *P. pubescens* showed its effects for the first time [14].

Diabetes mellitus is a metabolic disease that is related with the oxidative stress. In another study, the hypoglycemic and antioxidant effects of *P. peruviana* fruit's extract on Wistar rats, which were made diabetic using STZ, were examined. It was concluded that *P. peruviana* had positive effects on diabetes. They observed that the blood glucose levels

were reduced further than 30 %, and the lipid peroxidation and protein oxidation levels were reduced after the extract administered. The results of our study are similar to this study [15].

The structural proteins have important effects on the body weight, and the weight losses were observed in diabetes due to the deteriorations seen in structural proteins. In studies on this subject, it was determined that, at the end of 4-6 week of experiments with rats made diabetic by giving STZ, decreases were observed in body weights [16,17]. Many studies were carried out on the subject that STZ plays role in deformation of Langerhans islets of pancreas and pathogenesis of diabetes [18]. In parallelly with those studies, it was determined in our study that the groups, which were exposed to rapid losses of weight under the effect of STZ, started to re-gain weight under favor of injected goldenberry extract.

In a study of herbal products, it was reported that the passage of monosaccharides into blood was prevented since the enzymes playing role in carbohydrate digestion such as α-amylase and α-glucosidase were blocked by certain active molecules, and thus the postprandial glucose levels decreased. In 3rd and 6th weeks following the injection of STZ, increases in glucose concentration in brain cortex and hipotalamus and decreases in glycolytic enzyme activities were observed in rats [19]. In a similar study on goldenberry, it was reported that it controlled the level of glucose by absorbing the carbohydrates under favor or its fibrous structure [20]. In our study, similar to that study, it was found that the level of blood glucose increased in diabetic groups, but it normalized again under favor of goldenberry extract injection.

MDA is a determinant of membrane lipid peroxidation originating from the interaction with reactive oxygen species with the cell membrane [21]. In many studies, the presence of relationship between lipid peroxidation and diabetic complications were put forth [22-24]. Furthermore, it was also reported that the chronic hyperglycemia contributed to the increase in level of free radicals as a result of affection antioxidant defense system in diabetic rats. It was reported that, even if there is a low level of metabolic decomposition in diabetic adults, the level of lipid peroxidation increased as a result of the oxidative stress [25, 26]. For this reason, the lipid peroxidation should be taken under control. In a study related with goldenberry, the malondialdehyde (MDA) levels of diabetic persons were examined and positive outcomes were observed following the treatment [14]. In our results, similar to the mentioned studies, MDA level was found to significantly increased in diabetic groups when compared to control group, while the post-treatment MDA level of group D+G was found to be similar to the level in control group but lower than the level in group D.

GSH is known to be an important intracellular antioxidant. In a previous study, it was reported that, when compared to control group the level of GSH decreased in rats made diabetic using STZ, while it increased following the use of vitamin E [27]. Başaraner [28] reported that the use of vitamins C and E and selenium in diabetic rats decreased the GSH level, which has decreased in diabetics. In our study, low level of GSH in all of the groups made diabetic by using STZ might have occurred as a result of decrease in level of NADPG originating from the decrease in activity of pentose phosphate path, because NADPH is used in synthesis of GSH. But, after the treatment using antioxidant goldenberry, the level of GSH increased and closed to the level in control group. Our findings are in corroboration with those of similar studies.

Proteins are an important target of oxidative damage. In previous studies, the level of carbonyl was seen to increase in both of type-I and type-2 diabetes [29, 30]. In present study, the level of protein was seen to be high in kidney and brain tissues and low in other tissues. After the treatment, group D+G was found to have similar level of protein with control group. Vitamin E is known to act as chain-breaking antioxidant by preventing the propagation of free radical reactions [31]. In previous studies, goldenberry was reported to contain vitamins B, C, and E [1, 32]. In our study, the level of vitamin E was found to be high in muscle, liver, and kidney tissues in group D. The level of vitamin E was found to decrease in group D+G as a result of treatment. These findings are in corroboration with the literature.

It was reported that, as a result of stimulating the beta cells in pancreas via glucose, vitamin D was activated but vitamin D was found to not influence the basal insulin secretion. The increase in level of vitamin D was reported to be related with increase in blood pressure, excessive thirst, deterioration in renal functions, and loss of protein via the urine [33]. Almost all of these symptoms are clinic events related with the diabetes. In present study, when compared to control group, D-2 levels were observed to increase in serum, muscle, and kidney tissues.

Vitamin K is necessary to establish the balance in activation of blood coagulation and anticoagulation factors (carboxylation). But, the intake of vitamin K can be ensured only through a healthy diet. Goldenberry was reported to contain high level of K-1. Also, α-tocopherol, δ- tocopherol, ergosterol, stigmasterol and βsitosterol contents were determined [1]. In our study, these contents were observed at certain levels in goldenberry extract, and the level of K-1 in serum of group D and the level of K-2 in kidney tissues of group D were observed to decrease.

Zanardo et al. [34], reported that the cholesterol levels increased in various tissues of diabetic rats and this increase was contributed by the increase in cholesterogenesis. In our study, the cholesterol levels were found to be high in muscle, liver, and kidney

tissues in diabetes groups. Moreover, the level of cholesterol in group D+G was found to be similar to the value of control group and lower than group D. This change might be attributed to the lack of insulin, since insulin hormone is an important regulator of cholesterol biosynthesis. The decrease in insulin among the diabetic patients affects other metabolic mechanisms and thus it deteriorates the cholesterol level.

It was determined that, in rats that were experimentally made diabetic, the level of vitamin A (Retinol) increased in liver tissue but decreased in plasma. It was shown that the irregularities in retinol metabolism were treated via insulin treatment. In previous studies, it was revealed that the levels of retinol-carrier proteins in tissues and blood circulation of diabetic subjects were affected. It was found in our study that the retinol concentration in plasmas of rats, which were made diabetic by using STZ, increased in proportion to the rats in control group. The deterioration of the system conveying vitamin A from the liver, where it is stored, to other parts of body and the insufficient intake of vitamin A were shown to cause deterioration of vitamin A metabolism in diabetes [35, 36]. The serum retinol concentration of patients having type-I diabetes was found to be similar to the concentrations of rats, which were made diabetic by using STZ, but, in type 2 diabetes that is insulin-independent, no change was found in plasma retinol levels [33]. In our study, the level of retinol was observed to be high in serum, muscle, liver, and kidney tissues in diabetes groups in corroboration with the literature.

CONCLUSION

In our study, the potential effects of diabetes on various tissues and the protective and therapeutic effects of goldenberry on those tissues were investigated. It can be stated that goldenberry increases the level of glutathione and decreases the levels of blood glucose and lipid peroxidation. But, at the molecular level, it was seen to be ineffective on especially the enzyme activities. In conclusion, it was determined that these plants can be used in follow-up and healing periods of diabetic patients.

ACKNOWLEDGEMENTS

This study was supported by Firat University, FUBAP with the project no. FF.11.40.

The authors report no conflicts of interest. The authors alone are responsible for the content and writing of this paper.

A part of this study was presented as oral presentation in International Science Symposium (ISS2016), on 1-4 September 2016, Istanbul, Turkey, and as both oral and poster presentation in International Conference on Computational Mathematics and Engineering Sciences (CMES2017), May 20 to 22, 2017 in Istanbul, Turkey.

REFERENCES

[1] Ramadan, M.F. (2011) Bioactive phytochemicals, nutritional value and functional properties of cape gooseberry (*Physalis peruviana*): An overview. Food Res. Int. 44, 1830-1836.

[2] Nishimune, T., Yakushiji, T., Sumimoto, T., Taguchi, S., Konishi, Y., Nakahara, S., Ichikawa, T., Kunita, N. (1991) Glycemic response and fiber content of some food. Am. J. Clin. Nutr. 54, 414-419.

[3] Berger, M., Venhaus, A. (1992) Dietary fibre in the prevention and treatment of diabetes mellitus. In: Schweizer, T.F., Edwards, C.A. (Ed.) Dietary Fibre - A component of food. Springer Verlag, N.Y., 279-293.

[4] Flourie, B. (1992) The influence of dietary fiber on carbohydrate digestion and absorption. In: Schweizer, T.F., Edwards, C.A. (Ed.) Dietary Fibre -A component of food nutritional function in health and disease. Springer, London, 181-196.

[5] Hara, A., Radin, N.S. (1978) Lipid extraction of tissues with a low-toxicity solvent. Anal. Biochem. 90, 420-6.

[6] Katsanidis, E., Addis, P.B. (1999) Novel HPLC analysis of tocopherols, tocotrienols and cholesterol in tissue. Free Radical Bio. Med. 27, 1137-40.

[7] Lopez-Cervantes, J., Sanchez-Machado, D.I., Rios-Vazquez, N.J. (2006) High-performance liquid chromatography method for the simultaneous quantification of retinol, alpha-tocopherol and cholesterol in shrimp waste hydrolysate. J. Chromatogr A. 1105, 135-139.

[8] Karpińska, J., Mikołuć, B., Motkowski, R., Piotrowska-Jastrzebska, J. (2006) HPLC method for simultaneous determination of retinol, alpha-tocopherol and coenzyme Q10 in human plasma. J. Pharmaceut. Biomed. 42, 232-6.

[9] Elman, G.I. (1959) Tissue Sulfhydryl Groups. Arch. Biochem. Biophys. 82, 70-77.

[10] Lowry, O.H., Rosenbrough, N.J., Farr, A.L., Randall, R.J. (1951) Protein measurement with the Folin-phenol reagent. T. J. of Biochem. 193, 265-277.

[11] Ohkawa, H., Ohishi, N., Yagi, K. (1979) Assay for lipid peroxides in animal tissues by thiobarbituric acid reaction. Anal. Biochem. 95, 351-358.

[12] Sánchez-Machado, D.I., López-Hernández. J., Paseiro-Losada, P. (2002) High performance liquid chromatographic determination of alpha-tocopherol in macro algae. J. Chromatogr. A. 976, 277-284.
[13] Horn, R.C., Soares, J.C., Mori, N.C., Gelatti, G.T., Manfio, C.E., Golle, D.P., Koefender, J., Deuschle, R.A., Oliveira, C. (2015) Antioxidant effect of *Physalis peruviana* fruit aqueous extract−The antioxidant effect of *Physalis*. J. Agr. Sci. 7, 137-143.
[14] Hassan, A.I., Ghoneim, M.A.M. (2013) A possible inhibitory effect of *Physalis (Physalis pubescens* L.*)* on diabetes in male rats. World App. Sci. J. 21(5), 681-688.
[15] Mora, Á.C., Aragon, D.M., Ospina, L.F. (2010) Effects of *Physalis peruviana* fruit extract on stress oxidative parameters in streptozotocin-diabetic rats. Lat. Am. J Pharm. 29(7), 1132-6.
[16] Cam, M., Yavuz, O., Güven, A. (2003) Protective effects of chronic melatonin treatment against renal injury in streptozotocin-induced diabetic rats. J Pineal Res. 35, 212-220.
[17] Aksoy, N., Vural, H., Sabuncu, T., Aksoy, S. (2003) Effects of melatonin on oxidative-antioxidative status of tissues in streptozotocin-induced diabetic rats. Cell Biochem. Funct. 21, 121-125.
[18] Heineke, E.W., Johnson, M.B., Dilbergen, J.E. (1993) Antioxidant MDL29, 311 prevents diabetes in nonobese diabetic and multiple low-dose STZ-injected mice. Diabetes. 42, 1721-30.
[19] Plaschke, K., Hoyer, S. (1993) Action of the diabetogenic drug streptozotocin on glycolytic and glycogenolytic metabolism in adult rat brain cortex and hippocampus. Int. J. Dev. Neurosci. 11(4), 477-483.
[20] Bornet, F.R.J., Billaux, M.S., Messing, B. (1997) Glycemic index concept and metabolic diseases. Int. J. Biol. Macromol. 21, 207-219.
[21] Bachowski, S., Kolaja, K.L., Xu, Y., Ketcham, C.A., Stevenson, D.E., Walborg Jr, E.F., Klaunig, J.E. (1997) Role of oxidative stress in the mechanism of dieldrin's hepatotoxicity. Ann. Clin. Lab. Sci. 27, 196-208.
[22] Vincent, A.M., Russell, J.W., Low, P., Feldman, E.L. (2004) Oxidative stress in pathogenesis of Diabetic Neuropathy. Endocr. Rev. 25, 612-628.
[23] Memisogullari, R., Bakan, E. (2004) Levels of ceruloplasmin, transferin and lipid peroxidation in the serum of patients with type 2 diabetes mellitus. J. Diabetes Complicat. 18, 193-197.
[24] Sekeroglu, M.R., Sahin, H., Dulger, H., Algun, E. (2000) The effect of dietary treatment on erytrocyte lipid peroxidation, superoxide dismutase, glutathione peroxidase and serum lipid peroxidation in patients with type 2 diabetes mellitus. Clin. Biochem. 33, 669-674.
[25] Faure, P., Corticelli, P., Richard, M.J., Arnaud, J., Coudray, C., Halimi, S., Favie, A., Roussel, A.M. (1993) Lipid peroxidation and trace element status in diabetic ketotic patients: influence of insulin therapy. Clin. Biochem. 39, 789-793.
[26] Vantyghem, M.C., Balduyck, M., Zerimech, F., Martin, A., Douillard, C., Bans, S., Degand, P.M., Lefebvre, J. (2000) Oxidative markers in diabetic ketoacidosis. J. Endocrinol Invest. 23, 732-6.
[27] Garg, M., Singh, K., Bansal, D. (1996) Effect of vitamin E supplementation on antioxidant status of diabetic rats. J. Res. Med. Sci. 24, 325-326.
[28] Başaraner, H. (1999) The effect of vitamin E, vitamin C and selenium on the various tissue antioxidant systems of STZ induced diabetic rats. Graduate Thesis. Istanbul University, Institute of Science and Technology, Istanbul, Turkey.
[29] Telci, A., Cakatay, U., Salman, S., Satman, L., Sivas, A. (2000) Oxidative protein damage in early stage Type I diabetic patients. Diabetes Res. Clin. Pr. 50, 213-223.
[30] Cakatay, U., Telci, A., Salman, S., Satman, L., Sivas, A. (2000) Oxidative protein damage in Type I diabetic patients with and without complication. Endocr. Res. 26, 365-379.
[31] Stocker, A., Baumann, U. (2003) Supernatant protein factor in complex with RRR tocopherylquinone: a link between oxidized vitamin E and cholesterol biosynthesis. J. Mol. Biol. 332, 59-765.
[32] Yanartaş, Ö., Yılmaz, Y., Baykaran, M.B., Saygılı, İ., Bozkurt, Zincir, S. (2012) A manic episode induced by herbal preparate golden berry (cape gooseberry) (*Physalis peruviana* L.). J. Mood Disor. 2(1), 12-14.
[33] Basu, T.K., Basualdo, C. (1997) Vitamin A, homeostasis and diabetes mellitus. Nutrition. 13(9), 804 - 806.
[34] Zanardo, R.C., Costa Cruz, J.W., Oliveira, M.A., Fortes, Z.B. (2004) Ascorbic acid supplementation restores defective leukocyte-endothelial interaction in alloxan-diabetic rats. Diabetes Metab. Res. 19, 60-68.
[35] Marshall, S.M., Alberti, K.G.M.M. (1989) Comparison of the prevalence and associated features of abnormal albumin excretion in insulin-dependent and non-insulin dependent diabetes. QJM-Int. J. Med. 70, 61-71.
[36] Tuitoek, P.J., Ritter, S.J., Smith, J.E., Basu, T.K. (1996) Streptozotocin-induced diabetes lowers retinol-binding protein and transthyretin concentrations in rats. Brit. J. Nut. R. 76(6), 891-897.

Received: **13.07.2019**
Accepted: **19.01.2020**

CORRESPONDING AUTHOR

Sevinc Aydin
Munzur University,
Çemişgezek Vocational School,
Tunceli – Turkey

e-mail: sevincaydin2380@gmail.com

© by PSP Volume 29 – No. 05/2020 pages 3354-3361 Fresenius Environmental Bulletin

ENZYMATIC BIOMARKER RESPONSES OF FRESHWATER PLANARIANS EXPOSED TO ENDOCRINE DISRUPTING COMPOUNDS

Mei-Hui Li*

Environmental Toxicology Laboratory, Department of Geography, National Taiwan University, Taipei, 106, Taiwan

ABSTRACT

Endocrine disrupting compounds (EDCs) are commonly detected in aquatic environments and can endanger aquatic life. The responses of enzymatic biomarkers in asexual freshwater planarians (lactate dehydrogenase, glutathione S-transferase, glucose-6-phosphate dehydrogenase, and isocitric dehydrogenase) were evaluated after 7-day exposure to endocrine disruptors (bisphenol A [BPA], diethylstilbestrol [DES], 17α-ethinylestradiol [EE2], and 17β-estradiol [E2]). These biomarkers are ubiquitous enzymes and play crucial physiological roles in living organisms. In this study, EDCs influenced the nonspecific enzyme activities of asexual planarians. However, the effects of EDCs on enzymatic biomarkers did not correspond with the order of their estrogenic potencies. Furthermore, exposure to EDCs for 7 days mostly slightly or significantly reduced the enzyme activities of planarians compared with those of their respective controls. Alterations in enzyme activities can affect the energy metabolism and health status of organisms. The environmental levels of E2, EE2, and DES can range from lower than their detectable limits to tens of ng L^{-1}, and BPA levels in river water can be several μg L^{-1}. These findings suggest that some aquatic animals might be affected by the current levels of BPA in hotspot pollution scenarios.

KEYWORDS:
Freshwater invertebrate, aquatic toxicity, non-specific biomarker, endocrine disrupter, *Dugesia japonica*

INTRODUCTION

Many pharmaceuticals and personal care products containing various endocrine disrupting compounds (EDCs) are used in daily life and continually discharged into domestic wastewater systems and surface water bodies. EDCs are commonly detected in aquatic environments and can endanger aquatic ecosystems [1]. Vitellogenin and zona radiata have been suggested as useful specific biomarkers of exposure to EDCs, not only in fish but also in aquatic invertebrates [2-5]. However, studies have reported conflicting results [6-8]. Compared with aquatic vertebrates, biomarker responses to EDCs and their effects on aquatic invertebrates remain relatively unclear. Therefore, investigating the effects of EDCs in aquatic vertebrates and invertebrates could facilitate the accurate assessment of the ecological risk of these compounds in aquatic ecosystems.

Biomarkers, signaling physiological responses of individual organisms to pollutants, can be considered early indicators of environmental pollution. In the past three decades, enzymatic biomarkers have been commonly used for environmental monitoring to demonstrate stress in aquatic fauna following exposure to pollutants [9]. In the present study, the responses of four enzymatic biomarkers in freshwater planarian were measured after exposure to different EDCs. The selected biomarkers lactate dehydrogenase (LDH), glutathione S-transferase (GST), glucose-6-phosphate dehydrogenase (G6PD), and isocitric dehydrogenase (IDH) are metabolic enzymes with crucial physiological functions in organisms and are frequently used as nonspecific biomarkers of aquatic pollution.

LDH is a key enzyme in anaerobic metabolism and is typically considered an indicator of cell injury and tissue damage in humans and animals [10]. IDH is a major enzyme in the tricarboxylic acid cycle central to aerobic metabolism, and G6PD is the first enzyme in the pentose phosphate pathway [11]. IDH and G6PH are established estrogen-sensitive enzymes in mammals [12, 13]. A main physiological function of both IDH and G6PD is to produce nicotinamide adenine dinucleotide phosphate (NADPH), which is essential for reductive biosynthesis and protecting cells from oxidative stress [11]. GST is a phase II biotransformation enzyme that catalyzes the conjugation of electrophilic compounds [14]. Moreover, IDH, G6PD, and GST play major roles in protecting cells from oxidative stress [11, 14].

Freshwater invertebrates, a biologically diverse group of animals, face serious challenges in freshwater biodiversity conservation because of freshwater scarcity, climate change, and water pollution [15, 16]. Few studies have investigated the effects of EDCs on freshwater invertebrates except for some annelids, molluscs, and arthropods [17]. The present study investigated the effects of 7-day exposure to

bisphenol A (BPA), diethylstilbestrol (DES), 17α-ethinylestradiol (EE2), and 17β-estradiol (E2) on enzymatic biomarkers in asexual freshwater planarians (*Dugesia japonica [D. japonica]).*

MATERIALS AND METHODS

Chemicals. All test chemicals were obtained from Sigma–Aldrich (St. Louis, MO, USA), except BPA (Fluka, Sigma–Aldrich). The chemical purity of the test compounds was >99%. Test media were reconstituted with water purified using a Barnstead Nanopure Diamond system (Dubuque, IA, USA) by adding 2.5 mM $CaCl_2$, 0.4 mM $MgSO_4$, 0.8 mM $NaHCO_3$, and 77 μM KCl. The test stock solution was prepared by dissolving E2, EE2, and DES in dimethyl sulfoxide (DMSO), and DMSO solvent controls were used in the tests for the three chemicals. The BPA test stock solution was directly prepared in test media. All biochemical agents for enzyme assays were purchased from Sigma–Aldrich.

Experimental Animals and Conditions. Freshwater planarians, *D. japonica*, were obtained from Taikong Corporation (New Taipei City, Taiwan). The planarians were fed raw chicken liver once a week and maintained asexually in dechlorinated tap water at room temperature (25 ± 3°C). The animals were not fed for at least 4 days before the experiments.

Treatments for Metabolic Enzyme Measurements. The effects of three concentrations (10, 50, and 250 μg L^{-1}) of each chemical on the enzyme activities of planarians were examined. In all cases, two independent experiments were conducted for each chemical and each treatment group was replicated four times in each experiment. For each concentration, six animals were maintained in 50 mL of test solution at 25 ± 1 °C with a 12-h dark–light cycle for 7 days. To restore the nominal concentration in the test solution, the test medium was replaced at 48 and 96 h after initial exposure. The test animals were not fed during the entire experimental period, and no animals died during the study.

Metabolic Enzyme Measurements. At the end of each experiment, the planarians were gently rinsed with distilled water at least three times. Six animals were homogenized with 150 μL of 0.3 M sucrose in 0.1 M Tris buffer with 1 mM ethylenediaminetetraacetic acid (pH 7.4). The homogenate was centrifuged at 12,000 g at 4 °C for 20 min and the supernatant was immediately used to determine the enzyme activities.

The GST activity was determined according to the method described by Habig et al. [18]. Ten microliters of the supernatant was transferred to each well in a 96-well ultraviolet (UV) microplate containing 1 mM 1-chloro-2,4-dinitrobenzene (CDNB) in 0.1 M potassium phosphate buffer (pH 6.5). The plate was incubated for 5 min at room temperature. Furthermore, 10 μL of 150 mM reduced glutathione (GSH) was added to each well in a total volume of 300 μL per well to initiate the reaction. The GST activity was then measured by following the formation of the GSH–CDNB conjugate at 340 nm for 2 min in a FLUOstar Omega microplate reader.

The G6PD activity was determined using the method described by Noltmann et al. [19]. Twenty microliters of the planarian supernatant was transferred to each well in a 96-well UV microplate containing 5 mM G6P in 0.05 M Tris-HCl buffer with 0.003 M $MgCl_2$ (pH 7.4). The plate was incubated for 5 min at room temperature. Furthermore, 10 μL of 10 mM $NADP^+$ was added to each well in a total volume of 200 μL per well to initiate the reaction. The G6PD activity was subsequently measured by following the formation of NADPH at 340 nm for 5 min in the FLUOstar Omega microplate reader.

The IDH activity was measured as described by Ernt and Bergmeyer [20]. Ten microliters of the planarian supernatant was transferred to each well in a 96-well UV microplate containing 5 mM isocitric acid in 0.05 M Tris-HCl buffer with 0.003 M $MgCl_2$ (pH 7.4). The plate was incubated for 5 min at room temperature. Moreover, 10 μL of 10 mM $NADP^+$ was added to each well in a total volume of 200 μL per well to initiate the reaction. The IDH activity was subsequently measured by following the formation of NADPH at 340 nm for 5 min in the FLUOstar Omega microplate reader.

The LDH activity was assayed based on the method described by Vassault [21]. Ten microliters of the planarian supernatant was transferred to each well in a 96-well UV microplate containing 3.33 mM NADH in 0.05 M Tris-HCl buffer (pH 7.4). The plate was incubated for 5 min at room temperature. Furthermore, 10 μL of 30 mM sodium pyruvate was added to each well in a total volume of 300 μL per well to start the reaction. The LDH activity was then measured by following the rate of oxidation of reduced nicotinamide adenine dinucleotide (NADH) to NAD^+ at 340 nm for 2 min in the FLUOstar Omega microplate reader.

All enzyme activities were measured in duplicate. One unit of metabolic enzyme activity is the amount of enzyme that produces 1 μmol of NADPH/min/mg protein at an extinction coefficient of 6220 $M^{-1}cm^{-1}$. The specific activity of GST was expressed as μmol GSH–CDNB conjugate formed/min/mg protein at an extinction coefficient of 9.6 $mM^{-1}cm^{-1}$. Protein estimation was performed in triplicate by using the Bradford method [22].

Data Analysis. All statistical analyses were performed using Minitab (Version 17). For each test

chemical, the enzyme activity data were first examined for normality by using the Kolmogorov–Smirnoff test, and all data were matched with a normal distribution. Furthermore, the homogeneity of variances was determined using Bartlett's test. Because most data met the assumptions of the homogeneity of variance, all statistical analyses were performed using parametric tests. Two independent experiments were performed at different time points for each chemical in this study. Therefore, an analysis of covariance (ANCOVA) was performed by treating the experiment as a categorical factor with two levels and the exposure concentration as a continuous variable to determine whether both experimental data could be combined for further statistical analyses. The ANCOVA revealed that except BPA, all chemicals have significant experiment effect on the activities of all enzymes. Thereafter, the results from two independent experiments were analyzed separately using analysis of variances (ANOVAs). In the case of a significant result, Dunnett's multiple comparison was applied to determine which treatment group was significantly different from the controls.

RESULTS

Enzyme Activities after 7-day Exposure to BPA. The effects of BPA on the enzyme activities of planarians are shown in Figure 1. In experiment one, the GST activity was significantly lower in the 250 μg L^{-1} treatment group compared with the control group. However, the activities of all other enzymes did not significantly differ between the control and treatment groups. In experiment two, the LDH activity was significantly lower in the 10 and 250 μg L^{-1} treatment groups compared with the control group. Moreover, the IDH activity was markedly lower in the 250 μg L^{-1} treatment group.

Enzyme Activities after 7-day Exposure to DES. The effects of DES on the enzyme activities of planarians are shown in Figure 2. In experiment one, only the IDH activity was significantly lower in the 250 μg L^{-1} DES treatment group compared with the control group. However, the activities of all other enzymes were not significantly different between the control and treatment groups. In experiment two, the LDH activity was significantly lower in the 10 and 250 μg L^{-1} treatment groups compared with the control group.

Enzyme Activity after 7-day Exposure to E2. The effects of E2 on the enzyme activities of planarians are shown in Figure 3. In experiment one, the LDH activity was significantly lower in the 10 and 250 μg L^{-1} treatment groups compared with the control group. Moreover, the GST activity was significantly lower in the 250 μg L^{-1} treatment group compared with the control groups. In experiment two, the LDH activity was significantly lower in the 10 μg L^{-1} treatment group compared with the control group. However, the activities of other enzymes showed no significant differences between the control and treatment groups.

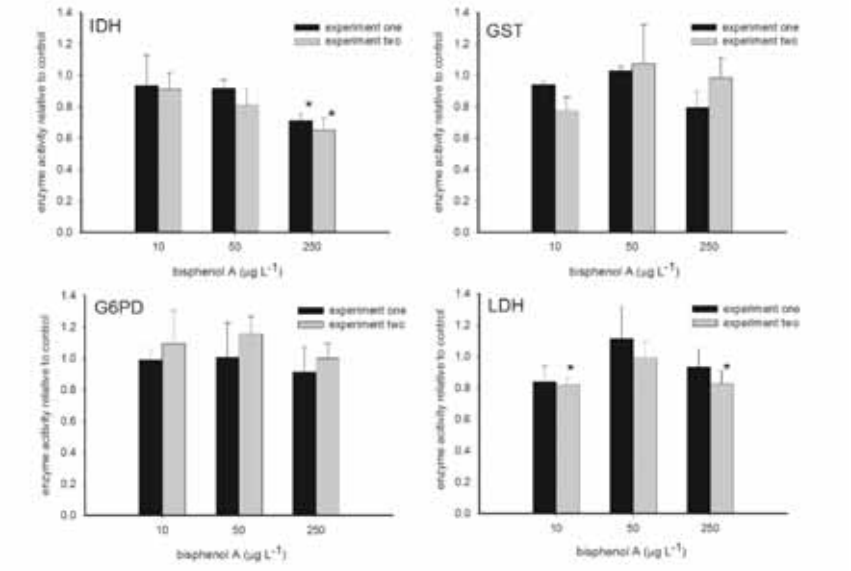

FIGURE 1
Enzyme activities of isocitric dehydrogenase (IDH), glucose-6-phosphate dehydrogenase (G6PD), glutathione S-transferase (GST) lactate dehydrogenase (LDH) in planarians in two independent experiments after 7-day exposure to bisphenol A (BPA).
Bars represent mean ± standard deviation (n = 4). Asterisks denote significant differences from the controls; *, $p \leq 0.05$.

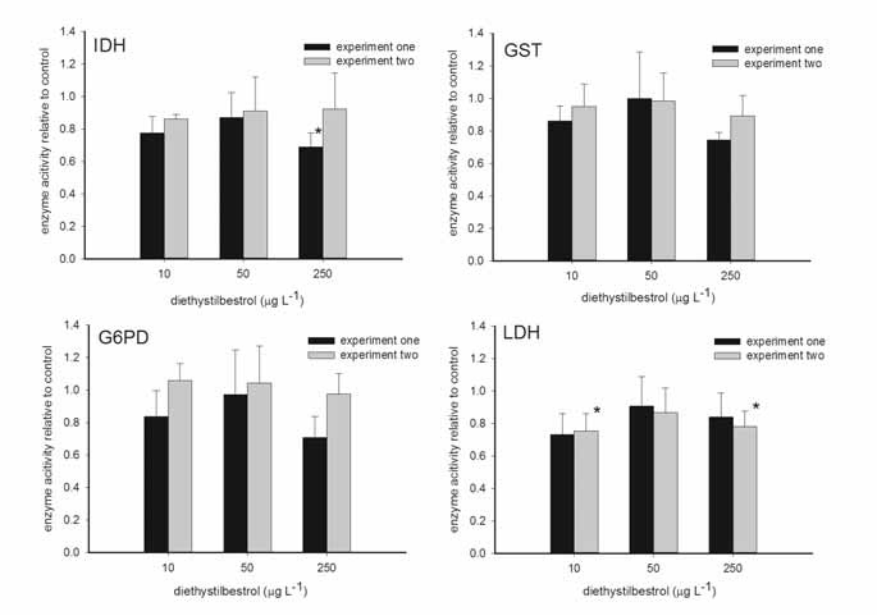

FIGURE 2
Enzyme activities of isocitric dehydrogenase (IDH), glucose-6-phosphate dehydrogenase (G6PD), glutathione S-transferase (GST) lactate dehydrogenase (LDH) in planarians in two independent experiments after 7-day exposure to diethylstilbestrol (DES).
Bars represent mean ± standard deviation (n = 4). Asterisks denote significant differences from the controls; *, $p \leq 0.05$.

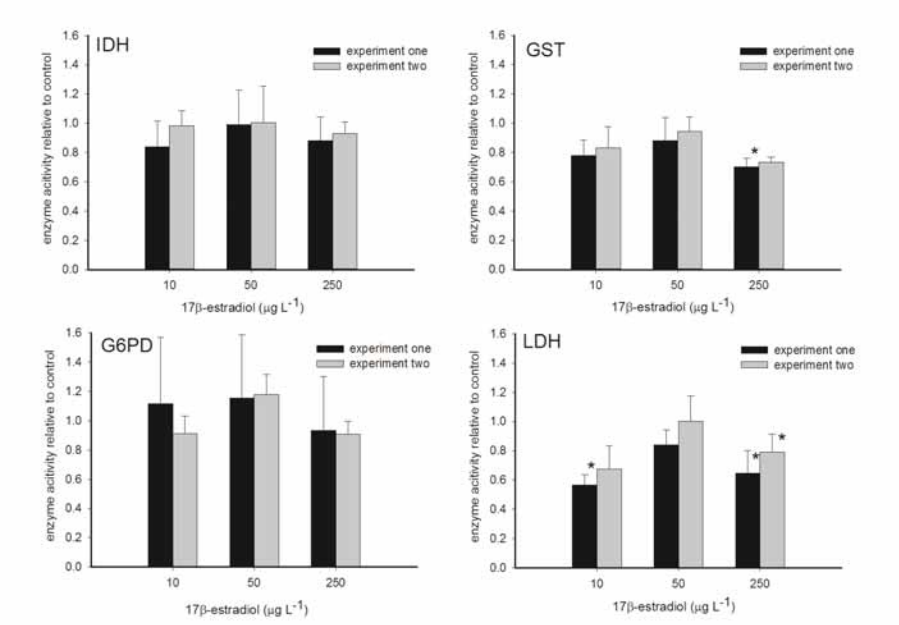

FIGURE 3
Enzyme activities of isocitric dehydrogenase (IDH), glucose-6-phosphate dehydrogenase (G6PD), glutathione S-transferase (GST) lactate dehydrogenase (LDH) in planarians in two independent experiments after 7-day exposure to 17β-estradiol (E2).
Bars represent mean ± standard deviation (n = 4). Asterisks denote significant differences from the controls; *, $p \leq 0.05$.

Enzyme activities after 7-day exposure to EE2. The effects of EE2 on the enzyme activities of planarians are shown in Figure 4. In experiment one, the G6PD activity was significantly higher in the 50 µg L^{-1} treatment group and significantly lower in the 10 µg L^{-1} treatment group compared with the control group. The IDH activity was significantly lower in the control and treatment groups. Moreover, GST and LDH activities were markedly decreased in the 250 µg L^{-1} treatment groups compared with the control group. In experiment two, only the LDH activity was significantly lower in the 250 µg L^{-1} treatment

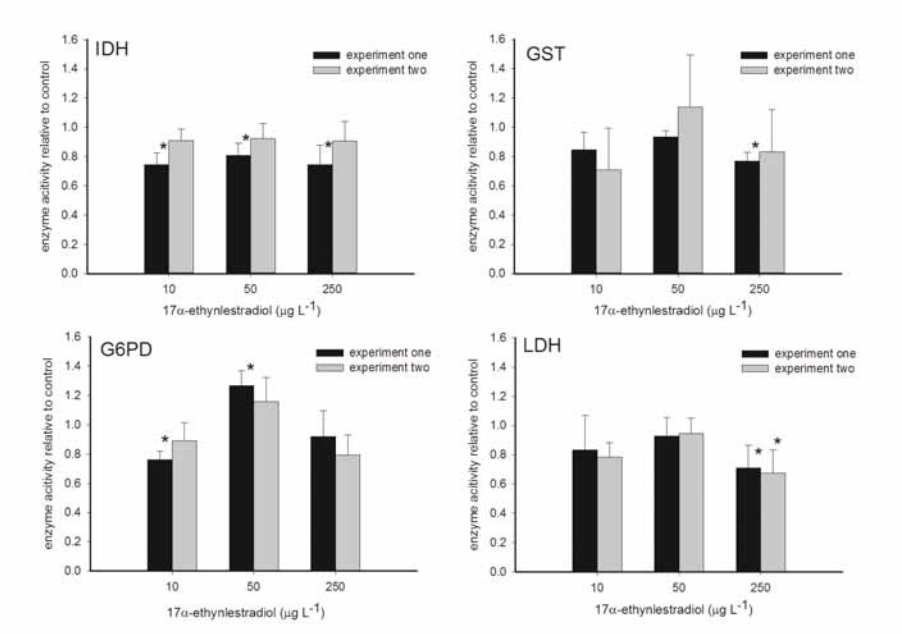

FIGURE 4
Enzyme activities of isocitric dehydrogenase (IDH), glucose-6-phosphate dehydrogenase (G6PD), glutathione S-transferase (GST) lactate dehydrogenase (LDH) in planarians in two independent experiments after 7-day exposure to 17α-ethnylestradiol (EE2).
Bars represent mean ± standard deviation (n = 4). Asterisks denote significant differences from the controls; *, $p \leq 0.05$.

group compared with the control group. However, the activities of all other enzymes did not significantly differ between the control and treatment groups.

DISCUSSION

The activities of all four enzymes in this study are commonly considered environmental biomarkers that are responsive to a large number of environmental contaminants in field and laboratory studies [23-26]. Environmental pollutants have been reported to induce and inhibit the activities of these biomarkers [27, 28]. Enzymatic biomarker responses can follow an expected dose–response trend or nonmonotonic dose–response pattern. Moreover, the enzyme responses to environmental pollutants typically show an inverted U-shaped trend, with an initial increase due to the activation of enzyme synthesis followed by a decrease in enzyme activities due to enhancing the catabolic rate or inhibiting the action of toxic chemicals on the enzyme molecules [29].

In the present study, statistical analysis did not yield consistently significant results in either experiment for each EDC. This may be partially because of large variations among individuals in the treatment groups or interassay variations under both experimental conditions. However, the activities of the four enzymes measured from two independent experiments did show similar concentration–response trends among the test chemicals. The responses of the enzymatic biomarkers in EDC-treated planarians were slightly or significantly lower than those of their respective controls after 7-day exposure.

Both LDH and G6PD have been suggested as indicators of environmental stress in invertebrates [30-33]. In the present study, the LDH activity showed significant decreases in planarians exposed to all four EDCs for 7 days. Notably, the G6PD activity was only affected by EE2 in one experiment, with a significant decrease after 10 μg L^{-1} treatment and a marked increase after 50 μg L^{-1} treatment. However, no significant changes were induced by the remaining EDCs. The results of LDH and G6PD activities in planarians exposed to EDCs are in concordance with those of previous studies, where immature fish exhibited an inhibition of LDH and no change in G6PD after E2 exposure. Both immature *Epinephelus akaara* [34] and *Chrysophrys major* [35] treated with E2 showed significant decreases in LDH but no changes in G6PD. By contrast, these studies have revealed marked increases in IDH in both fish. However, in the present study, no increase was observed in the IDH activity of planarians exposed to EDCs. By contrast, the IDH activity showed significant decreases after treatment with 250 μg L^{-1} BPA, DES, or EE2 exposure.

GSTs are a family of enzymes that play crucial roles in xenobiotic biotransformation [36]. The induction of GST was suggested as a biomarker of xenoestrogen exposure in *Nereis succinea* (Polychaeta) [37]. However, no consistent results are available on GST activity in aquatic animals after EDC exposure. For example, the GST activity increased after 24-h exposure to 0.01, 1, and 10 μg

BPA L^{-1} and after 24-h exposure to 0.1, 10, and 100 μg E2 L^{-1} [28]. An injection of 500 μg kg^{-1} E2 yielded no changes in the hepatic GST activity of carps *(Cyprinus carpio)* compared with that of controls [38]. Conversely, freshwater male fish *(Rhamdia quelen)* injected with a single dose of 0.1, 1, and 10 mg kg^{-1} E2 exhibited lower GST activity at a similar magnitude in all exposed groups compared with male and female controls after 11 days of injection [39]. The GST activity was significantly decreased in the polychaete *(Perinereis aibuhitensis)* after chronic exposure (205 days) to 0.1, 1, 10, 100, and 1000 μg E2 L^{-1} [40]. In the present study, the GST activity showed significant decreases after treatment with 250 μg L^{-1} BPA, E2, or EE2 exposure.

Enzymatic biomarkers have been considered sensitive indicators of environmental pollutants [9, 29], and the present findings are in accordance with this observation. For example, the 96-h nominal LC_{50} values of DES, EE2, E2, and BPA to this species of planarians were found to be 0.5–6.0 mg L^{-1} [41]. The 7-day no-observed-effect levels of planarian head regeneration were 50 μg L^{-1} for BPA and DES and 1 mg L^{-1} for EE2 and E2 [42]. In the present study, the activities of LDH showed significant changes after exposure to 250 μg L^{-1} all four EDCs compared with their respective controls. In addition, the activities of LDH showed significant changes after exposure to 10 μg L^{-1} BPA, DES or E2 compared with their respective controls. The environmental levels of E2, EE2, and DES can range from lower than the detectable limits to tens of ng L^{-1} [43]. Conversely, the level of BPA in river water can be several μg L^{-1} [44]. These findings suggest that some aquatic animals might be adversely affected by the current levels of BPA in some hotspot pollution scenarios.

This study found that EDCs influenced the nonspecific enzyme activities of asexual planarians. However, the effects of EDCs on enzymatic biomarkers did not correspond with the order of their estrogenic potencies. Testosterone was detected in sexually reproductive individuals in the freshwater planarian *Bdellocephala brunnea* [45]. Estradiol or testosterone has not been detected in the freshwater planarian D. japonica and no estrogen-related receptor genes have been found in the Planarian EST database for this organism. The findings suggest that the enzymatic responses to EDCs were caused by general toxicity rather than the estrogen-mediated mechanisms of these chemicals in the present study.

All four enzymatic biomarkers are ubiquitous enzymes present in bacteria, fungi, plants, and animals [46, 47] and play crucial physiological roles in living organisms. Alterations in these enzyme activities can affect the energy metabolism and growth of organisms. Both NADPH-generating enzymes, IDH and G6PH, were inhibited by EE2, and the low supply of NADPH in organisms can reduce the efficiency of NADPH-related metabolic processes and nonenzymatic defense systems. In summary, reduction of these enzyme activities after exposure to EDCs potentially reduces an organism's ability to defend itself against oxidative stress.

ACKNOWLEDGEMENTS

This study was supported by the Ministry of Science and Technology (Taiwan) under grant NSC 100-2313-B-002-009-MY3 and MOST-103-2313-B-002-028-MY3. The author would like to thank Ms. Chun-Yuan Huang for her assistance on planarian enzyme assays.

REFERENCES

[1] Brausch, J.M., Rand, G.M. (2011) A review of personal care products in the aquatic environment: environmental concentrations and toxicity. Chemosphere. 82, 1518-1532.

[2] Arukwe, A., Knudsen, F.R., Goksøyr, A. (1997) Fish zona radiata (eggshell) protein: a sensitive biomarker for environmental estrogens. Environmental Health Perspectives. 105, 418-422.

[3] Segner, H., Caroll, K., Fenske, M., Janssen, C.R., Maack, G., Pascoe, D., Schafers, C., Vandenbergh, G.F., Wenzel, A. (2003) Identification of endocrine-disrupting effects in aquatic vertebrates and invertebrates: report from the European IDEA project. Ecotoxicology and Environmental Safety. 54, 302-314.

[4] Matozzo, V., Gagné, F., Marin, M.G., Ricciardi, F., Blaise, C. (2008) Vitellogenin as a biomarker of exposure to estrogenic compounds in aquatic invertebrates: a review. Environment International. 34, 531-545.

[5] Dang, Z. (2016) Interpretation of fish biomarker data for identification, classification, risk assessment and testing of endocrine disrupting chemicals. Environment International. 92, 422-441.

[6] Riffeser, M., Hock, B. (2002) Vitellogenin levels in mussel hemolymph—a suitable biomarker for the exposure to estrogens?. Comparative Biochemistry and Physiology Part C: Toxicology and Pharmacology. 132, 75-84.

[7] Puinean, A.M., Labadie, P., Hill, E.M., Osada, M., Kishida, M., Nakao, R., Novillo, A., Callard, I.P., Rotchell, J.M. (2006) Laboratory exposure to 17β-estradiol fails to induce vitellogenin and estrogen receptor gene expression in the marine invertebrate *Mytilus edulis*. Aquatic Toxicology. 79, 376-383.

[8] Short, S., Yang, G., Kille, P., Ford, A.F. (2014) Vitellogenin is not an appropriate biomarker of feminisation in a Crustacean. Aquatic Toxicology. 153, 89-97.

[9] Roméo, M., Giambérini, L. (2013) History of biomarkers. In: Ecological Biomarkers: Indicators of Ecotoxicological Effects. CRC Press Boca Raton, USA, 15-44.
[10] Almeida, J.R., Oliveira, C., Gravato, C., Guilhermino, L. (2010) Linking behavioural alterations with biomarkers responses in the European seabass *Dicentrarchus labrax* L. exposed to the organophosphate pesticide fenitrothion. Ecotoxicology. 19, 1369-1381.
[11] Lee, S.M., Koh, H.J., Park, D.C., Song, B.J., Huh, T.L., Park, J.W. (2002) Cytosolic NADP+-dependent isocitrate dehydrogenase status modulates oxidative damage to cells. Free Radical Biology and Medicine. 32, 1185-1196.
[12] Lerner, L.J., Hilf, R., Turkheimer, A.R., Michel, I., Engel, J. (1966) Effects of hormone antagonists on morphological and biochemical changes induced by hormonal steroids in the immature rat uterus. Endocrinology. 78, 111-124.
[13] Max, S.R., Knudsen, J.F. (1980) Effect of sex hormones on glucose-6-phosphate dehydrogenase in rat levator ani muscle. Molecular and Cellular Endocrinology. 17, 111-118.
[14] Board, P.G., Menon, D. (2013) Glutathione transferases, regulators of cellular metabolism and physiology. Biochimica et Biophysica Acta (BBA)-General Subjects. 1830, 3267-3288.
[15] Strayer, D.L. (2006) Challenges for freshwater invertebrate conservation. Journal of the North American Benthological Society. 25, 271-287.
[16] Collen, B., Whitton, F., Dyer, E.E., Baillie, J.E., Cumberlidge, N., Darwall, W.R., Pollock, C., Richman, N.I., Soulsby, A.M., Böhm, M. (2014) Global patterns of freshwater species diversity, threat and endemism. Global Ecology and Biogeography. 23, 40-51.
[17] Oetken, M., Bachmann, J., Schulte-Oehlmann, U., Oehlmann, J. (2004) Evidence for endocrine disruption in invertebrates. International Review of Cytology. 236, 1-44.
[18] Habig, W.H., Pabst, M.J., Jakoby, W.B. (1974) Glutathione S-transferase. The first enzymatic step in mercapturic acid formation. Journal of Biology Chemistry. 249, 7130-7139.
[19] Noltmann, E.A., Gubler, C.J., Kuby. S.A. (1961) Glucose-6-phosphate dehydrogenase. Journal of Biological Chemistry. 236, 1225-1230.
[20] Ernt, E., Bergmeyer, H.U. (1974) Isocitrate dehydrogenase - UV assay. In: Bergmeyer, H.U. (ed.) Methods of Enzymatic Analysis. Vol. 2, 624-627.
[21] Vassault, A. (1983) Lactate dehydrogenase. In: Bergmeyer, H.U. (ed.) Methods in Enzymatic Analysis. Academic Press, London, U.K. 118–126.
[22] Bradford, M.M. (1976) A rapid and sensitive method for the quantitation of microgram quantities of protein utilizing the principle of protein-dye binding. Analytical Biochemistry. 72, 248-254.
[23] Oliva, M., Perales, J.A., Gravato, C., Guilhermino, L., Galindo-Riaño, M.D. (2012) Biomarkers responses in muscle of Senegal sole (*Solea senegalensis*) from a heavy metals and PAHs polluted estuary. Marine Pollution Bulletin. 64, 2097-2108.
[24] Rodrigues, A.P., Santos, L.H., Oliva-Teles, M.T., Delerue-Matos, C., Guimarães, L. (2014) Joint effects of salinity and the antidepressant sertraline on the estuarine decapod *Carcinus maenas*. Aquatic Toxicology. 156, 169-178.
[25] Alves, L.M., Nunes, M., Marchand, P., Le Bizec, B., Mendes, S., Correia, J.P., Lemos, M.F., Novais, S.C. (2016) Blue sharks *(Prionace glauca*) as bioindicators of pollution and health in the Atlantic Ocean: Contamination levels and biochemical stress responses. Science of the Total Environment. 563, 282-292.
[26] Caron, A., Pannetier, P., Rosabal, M., Budzinski, H., Lauzent, M., Labadie, P., Nasri, B., Pierron, F., Baudrimont, M., Couture, P. (2016) Organic and inorganic contamination impacts on metabolic capacities in American and European yellow eels. Canadian Journal of Fisheries and Aquatic Sciences. 73, 1557-1566.
[27] Correia, A.D., Gonçalves, R., Scholze, M., Ferreira, M., Henriques, M.A.R. (2007). Biochemical and behavioral responses in gilthead seabream (*Sparus aurata*) to phenanthrene. Journal of Experimental Marine Biology and Ecology. 347, 109-122.
[28] Lee, S.B., Choi, J. (2007) Effects of bisphenol A and ethynyl estradiol exposure on enzyme activities, growth and development in the fourth instar larvae of *Chironomus riparius* (Diptera, Chironomidae). Ecotoxicology and Environmental Safety. 68, 84-90.
[29] Viarengo, A., Lowe, D., Bolognesi, C., Fabbri, E., Koehler, A. (2007) The use of biomarkers in biomonitoring: a 2-tier approach assessing the level of pollutant-induced stress syndrome in sentinel organisms. Comparative Biochemistry and Physiology Part C: Toxicology and Pharmacology. 146, 281-300.
[30] Augenfeld, J.M. (1966) Lactic dehydrogenase activities in invertebrates in relation to environment and mode of gas exchange. Comparative Biochemistry and Physiology. 18, 983-985.
[31] Wu, R.S., Lam, P.K. (1997) Glucose-6-phosphate dehydrogenase and lactate dehydrogenase in the green-lipped mussel (*Perna viridis*): Possible biomarkers for hypoxia in the marine environment. Water Research. 31, 2797-2801.

[32] Diamantino, T.C., Almeida, E., Soares, A.M., Guilhermino, L. (2001) Lactate dehydrogenase activity as an effect criterion in toxicity tests with *Daphnia magna* straus. Chemosphere. 45, 553-560.
[33] Nathan, S.S., Kalaivani, K., Murugan. K. (2006) Effect of biopesticides on the lactate dehydrogenase (LDH) of the rice leaffolder, *Cnaphalocrocis medinalis* (Guenée) (Insecta: Lepidoptera: Pyralidae). Ecotoxicology and Environmental Safety. 65, 102-107.
[34] Ng, T.B., Woo, N.Y., Tam, P.P., Au, C.Y. (1984) Changes in metabolism and hepatic ultrastructure induced by estradiol and testosterone in immature female *Epinephelus akaara* (Teleostei, Serranidae). Cell and Tissue Research. 236, 651-659.
[35] Woo, N.Y.S., Chung, A.S.B., Ng, T.B. (1993) Influence of oral administration of estradiol-17β and testosterone on growth, digestion, food conversion and metabolism in the underyearling red sea bream, *Chrysophrys major*. Fish Physiology and Biochemistry. 10, 377-387.
[36] Rushmore, T.H., Pickett, C.B. (1993) Glutathione S-transferases, structure, regulation therapeutic implications. Journal of Biological Chemistry. 268, 11475-11475.
[37] Ayoola, J. A., García-Alonso, J., Hardege, J.D. (2011) Glutathione-S-transferase in *Nereis succinea* (Polychaeta) and its induction by xeno-estrogen. Environmental Toxicology. 26, 559-565.
[38] Sol, M., Porte, C., Barcel, D. (2000) Vitellogenin induction and other biochemical responses in carp, *Cyprinus carpio*, after experimental injection with 17-ethynylestradiol. Archives of Environmental Contamination and Toxicology. 4, 494-500.
[39] Costa, D.M., Neto, F.F., Costa, M.D.M., Morais, R.N., Garcia, J.R.E., Esquivel, B.M., Ribeiro, C.O. (2010) Vitellogenesis and other physiological responses induced by 17-β-estradiol in males of freshwater fish Rhamdia quelen. Comparative Biochemistry and Physiology Part C: Toxicology and Pharmacology. 151, 248-257.
[40] Lv, L., Dong, X., Lv, F., Yu, Y., Zhao, W., Liu, F. (2016) Antioxidant enzymes responses of polychaete *Perinereis aibuhitensis* following chronic exposure to 17β-estradiol. Italian Journal of Animal Science. 15, 552-557.
[41] Li, M.-H. (2013) Acute toxicity of industrial endocrine-disrupting chemicals, natural and synthetic sex hormones to the freshwater planarians, *Dugesia japonica*. Toxicological and Environmental Chemistry. 95, 984-991.
[42] Li, M.-H. (2014) Effects of bisphenol A, two synthetic and a natural estrogens on head regeneration of the freshwater planarians, *Dugesia japonica*. Toxicological and Environmental Chemistry. 96, 1174-1184.
[43] Rocha, M.J., Cruzeiro, C., Reis, M., Pardal, M.Â., Rocha, E. (2014) Spatial and seasonal distribution of 17 endocrine disruptor compounds in an urban estuary (Mondego River, Portugal): evaluation of the estrogenic load of the area. Environmental Monitoring and Assessment. 186(6), 3337-3350.
[44] Huang, G.Y., Liu, Y.S., Chen, X.W., Liang, Y.Q., Liu, S.S., Yang, Y.Y., Hu, L.X., Shi, W.J., Tian, F., Zhao, J.L., Chen, J. (2016) Feminization and masculinization of western mosquitofish (*Gambusia affinis*) observed in rivers impacted by municipal wastewaters. Scientific Reports. 6, 20884.
[45] Fukushima, M., Funabiki, I., Hashizume, T., Osada, K., Yoshida, W., Ishida, S. (2008) Detection and changes in levels of testosterone during spermatogenesis in the freshwater planarian *Bdellocephala brunnea*. Zoological Science. 25, 760-765.
[46] Doolittle, R.F., Feng, D.F., Tsang, S., Cho, G., Little, E. (1996) Determining divergence times of the major kingdoms of living organisms with a protein clock. Science. 271, 470-476.
[47] Sheehan, D., Meade, G., Foley, V.M. (2001) Structure, function and evolution of glutathione transferases: implications for classification of non-mammalian members of an ancient enzyme superfamily. Biochemical Journal. 360, 1-16.

Received: **01.02.2018**
Accepted: **19.02.2020**

CORRESPONDING AUTHOR

Mei-Hui Li
Environmental Toxicology Lab,
Dep. of Geography
National Taiwan University,
Taipei 106 – Taiwan

e-mail: meihuili@ntu.edu.tw

© by PSP Volume 29 – No. 05/2020 pages 3362-3369 Fresenius Environmental Bulletin

PLANARIAN MOBILITY ASSAY AS A SIMPLE ALTERNATIVE FOR RAPID SCREENING AQUATIC ACUTE TOXICITY OF PERSONAL CARE PRODUCTS

Mei-Hui Li*

Environmental Toxicology Lab, Department of Geography, National Taiwan University, Taipei, Taiwan

ABSTRACT

The effects of 25 chemicals used in personal care products, including benzophenone-type UV filters, paraben preservatives, and surfactants, on freshwater planarian locomotion were examined using an automated video tracking system during the second 5-min period exposure. The slope of the linear regression for second 5-min EC_{50} and 24-h median lethal concentration (LC_{50}) was 0.9904. The second 5-min EC_{50} values of planarian mobility were similar to their corresponding 24-h LC_{50} values. The results suggest that changes in mobility velocity in planarians can serve as a rapid acute aquatic toxicity indicator. Moreover, planarian mobility assay can be a useful tool in preliminary evaluation of water samples and in deciding the timely precautionary measures required to prevent episodic water pollution, even in the absence of acute aquatic toxicity information. Based on the result of this study, planarian mobility assay provides great advantages to promote 3Rs principle in toxicology study, by replacing vertebrates to invertebrates, reducing numbers of experimental animals used, and refining animals by greatly increased survival and recovery.

KEYWORDS:
Episodic pollution, real-time warming, UV filter, paraben preservatives, surfactant, 3Rs principle

INTRODUCTION

During major urban stormwater runoff events and accident spills, rapid evaluation of the potential toxicity of water *in situ* or of that collected in the field is necessary to determine the optimal immediate course of action. Episodic pollution discharges can be acutely toxic to aquatic organisms or exert sublethal toxic effects on aquatic invertebrates and fishes [1]. Several *in situ* water quality sensors that can determine common physical and chemical characteristics of water in a timely manner have been recently developed [2]. However, rapid determination of toxicological characteristics of water samples to provide an early warning remains a challenge to environmental toxicologists and ecotoxicologists [3]. In particular, standardized toxicity tests are labor and time intensive. The experimental time required for measuring acute aquatic toxicity to aquatic animals is at least 1–4 d. To effectively prevent the hazardous effects of water pollution, providing near real-time information regarding water toxicity is crucial for environmental decision makers.

Animal behaviors are usually considered rapid and sensitive responses to environmental pollution [4-8]. In particular, locomotion is an essential function in animals and represents the general physical status of most organisms. Compared with other animal behaviors, motor activities and patterns in various aquatic invertebrates are considered sensitive indicators of different environmental pollutants. Locomotory function in animals is an indicator of their health, fecundity and survival [9]. In ecotoxicological tests, changes in the locomotory function in animals is often used as an indicator of sublethal toxicity [10-12].

Freshwater planarians have been used as animal models for behavioral studies on the effects of pharmacological drugs or toxicants [13-17]. The median effective concentration (EC_{50}) of planarian mobility during the second 5-min exposure period was reported to be in the same range of the 24-h median lethal concentration (LC_{50}) of planarians exposed to various surfactants [18]. Further investigation of planarian mobility responses as alternative acute toxicity responses after exposure to environmental pollutants for a short period should be conducted. In addition, compared with other commonly used aquatic animal models for behavioral studies, such as daphnia or zebrafish, maintaining freshwater planarians is easier and cheaper.

A substantially high number of chemicals in such personal care products as sun screens, preservatives, disinfectants, and surfactants are commonly found in urban discharge or surface waters worldwide [19]. Acute toxicities of several chemicals in personal care products, including benzophenone-type UV filters, paraben preservatives, and surfactants, were determined in freshwater planarians [20, 21]. In this study, the effects of similar chemicals on freshwater planarian

mobility were examined. In addition, whether planarian mobility responses after a very short period exposure can be reliably used in screening for the acute toxicity of chemicals (i.e.; reported 24-h LC_{50}) in personal care products were evaluated and discussed.

MATERIALS AND METHODS

Chemicals. 4-Nonylphenol (94%) was purchased from Riedel-de Haën (St Louis, MO, USA) and 2,3,4-trihydroxybenzophenone (2,3,4-THBP, >98%) was purchased from Alfa Aesar (Ward Hill, MA, USA). Perfluorooctane sulfonate (>98%) and sulisobenzone (98.9%) were obtained from Fluka (Sigma-Aldrich, Steinheim, Germany). Sodium dodecylbenzene sulfonate (80%) was purchased from Sigma-Aldrich (St Louis, MO, USA). All other test chemicals were also purchased from Sigma-Aldrich (St Louis, MO, USA) and their purities were > 99%. All test stock solutions were prepared in reconstituted water [22]. The 25 test chemicals and the nominal test concentration ranges for each compound are listed in Table 1. Test media were reconstituted using purified water produced by the NANO pure Diamond system (Barnstead, Dubuque, USA) by adding 2.5 mmol L^{-1} $CaCl_2$, 0.4 mmol $L^{-1}MgSO_4$, 0.8 mmol L^{-1} $NaHCO_3$, and 77 µmol L^{-1} KCl. Test media had a hardness of 136.5 ± 2.0 mg L^{-1} as $CaCO_3$, a conductivity of 0.73 ± 0.6 µS cm^{-1}, and a pH of 7.8 ± 0.1.

TABLE 1
Test chemicals and their concentration ranges used in planarian mobility assay

Chemicals	CAS No.	Test concentration (mg/L)
benzophenone-type UV filters		
benzophenone	119-61-9	0, 2.5, 5, 10, 25
2,4-dihydroxybenzophenone	131-56-6	0, 1, 2.5, 10, 20
2,2',4,4'-tetrahydroxybenzophenone	131-55-5	0, 5, 10, 20, 40
oxybenzone	131-57-7	0, 0.5, 1, 5, 10
sulisobenzone	4065-45-6	0, 50, 100, 200, 400
2,2'-dihydroxy-4,4'-dimethoxybenzophenone	131-54-4	0, 5, 12.5, 25, 50
5-chloro-2-hydroxybenzophenone	85-19-8	0, 1, 2.5, 5, 10
dioxybenzone	131-53-3	0, 1, 2.5, 5, 10
mexenone	1641-17-4	0, 1, 2.5, 5, 10
4,4'-dihydroxybenzophenone	611-99-4	0, 5, 10, 25, 50
2-hydroxybenzophenone	117-99-7	0, 1, 2.5, 5, 10
3-hydroxybenzophenone	13020-57-0	0, 5, 10, 25, 50
4-hydroxybenzophenone	1137-42-4	0, 2.5, 5, 10, 25
2,3,4-trihydroxybenzophenone	1143-72-2	0, 2.5, 5, 10, 25
paraben preservatives		
butylparaben	94-26-8	0, 1, 10, 25, 50
ethylparaben	120-47-8	0, 50, 100, 200, 400
methylparaben	99-76-3	0, 6.25, 12.5, 25, 50
propylparaben	94-13-3	0, 1, 5, 10, 25
surfactants		
benzethonium chloride	121-54-0	0, 2.5, 5, 10, 20
cetyltrimethylammonium bromide	57-09-0	0, 1, 2.5, 5, 10
dodecylbenzene sulfonate	25155-30-0	0, 1, 2.5, 5, 10
lauryl sulfate	151-21-3	0, 0.25, 0.5, 1, 2.5
4-nonylphenol	104-40-5	0, 0.5, 1, 2.5, 5
octylphenol ethoxylate	9002-93-1	0, 5, 10, 20, 40
perfluorooctane sulfonate	2795-39-3	0, 25, 50, 100, 200

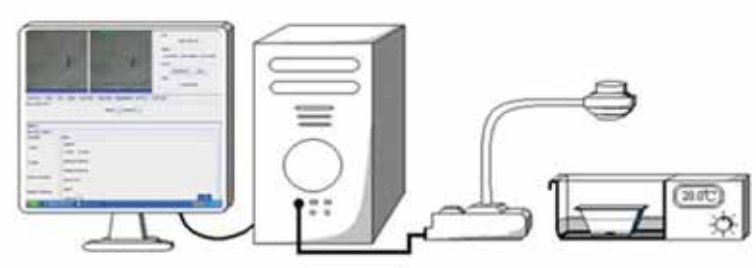

FIGURE 1
Automated video tracking device and measurement setup

Test organisms. Freshwater planarian, *Dugesia japonica* was collected from the Nanshi stream located in Wulai, Taiwan. The animals were maintained asexually in dechlorinated tap water at ambient room temperature (28 ± 3°C). The planarians fed raw chicken liver once a week followed by immediate transfer to new culture water. The animals were not fed for at least 4 d prior to the mobility assays.

Mobility assay. The effects of different chemicals in personal care products on freshwater planarian mobility were determined as previously described in Li's study [18]. Figure 1 depicts the observation device and measurement setup. Two independent mobility assays for each test chemical were performed on different days. On the basis of previous acute toxicity results [20, 21], 4 different concentrations for the test chemical and a control were analyzed in triplicate in each mobility assay. After 5 min of exposure, mobility was recorded and quantified for the next 5-min period in the same exposure solution using a FiexCam video camera (NTSC, version 3; Videolabs Inc, Minneapolis, USA) and a video tracking recording system (Singa Technology Corporation, Taipei, Taiwan) at 28 ± 1 °C.

Data analysis. The EC_{50} of planarian mobility as 50% of the control velocity in the second 5-min exposure period was computed through a nonlinear regressions (lognormal model) by using the Excel macro REGTOX software (version EV7.0.4) [23]. Linear regression, t test, and correlation analysis between acute toxicity (24-h LC_{50}) and mobility (second 5-min EC_{50}) were determined using Minitab (Version 17).

RESULTS AND DISCUSSION

Exposure to test chemicals for a short period produced a concentration-dependent reduction in freshwater planarian locomotor velocities. The traced trajectories of planarian movements ranged from spatially complex patterns at low concentrations to almost completely immobile at high concentrations, as recorded for the second 5-min exposure period after the first 5-min exposure to paraben preservatives (Figure 2), surfactants (Figure 3) and benzophenone-type UV filters (data not shown). These concentration-dependent changes in movement patterns are consistent with those in our previous study, where we observed movement patterns ranging from total mobility to immobility in planarians exposed to natural and synthetic surfactants [18].

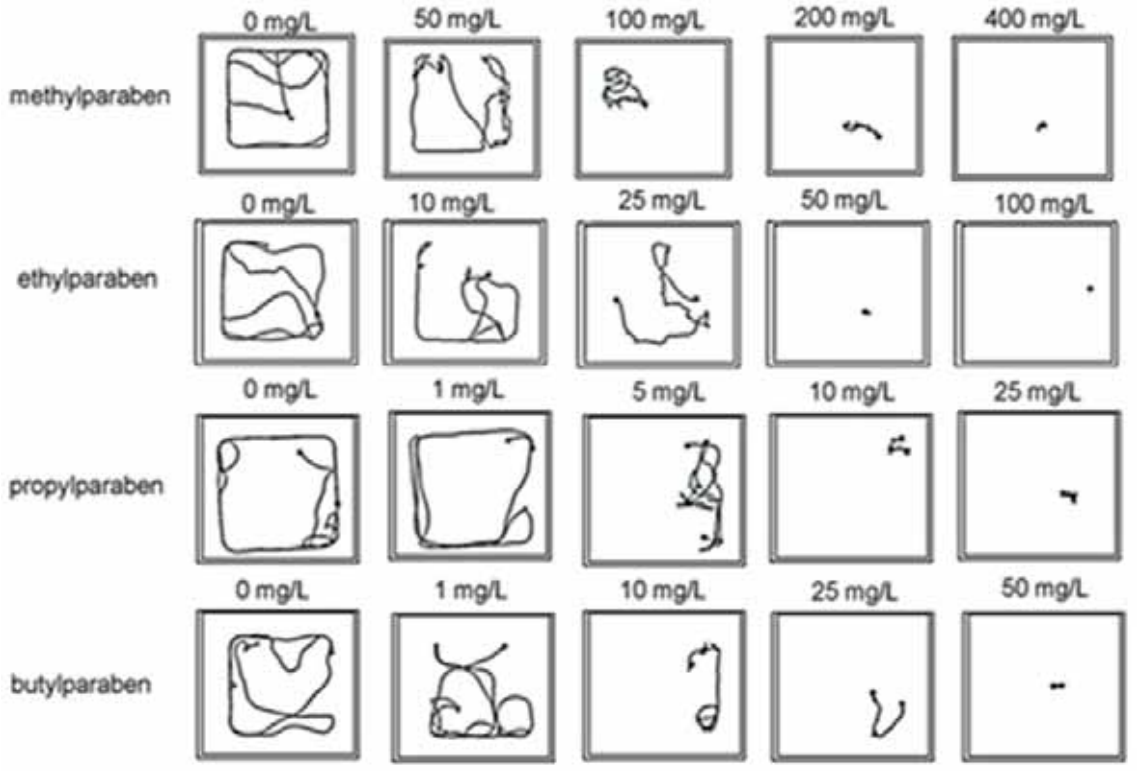

FIGURE 2
Locomotion movement patterns of planarians after the first 5-min exposure to paraben preservatives and their subsequent locomotion monitoring for the second 5 min in the same test solution.

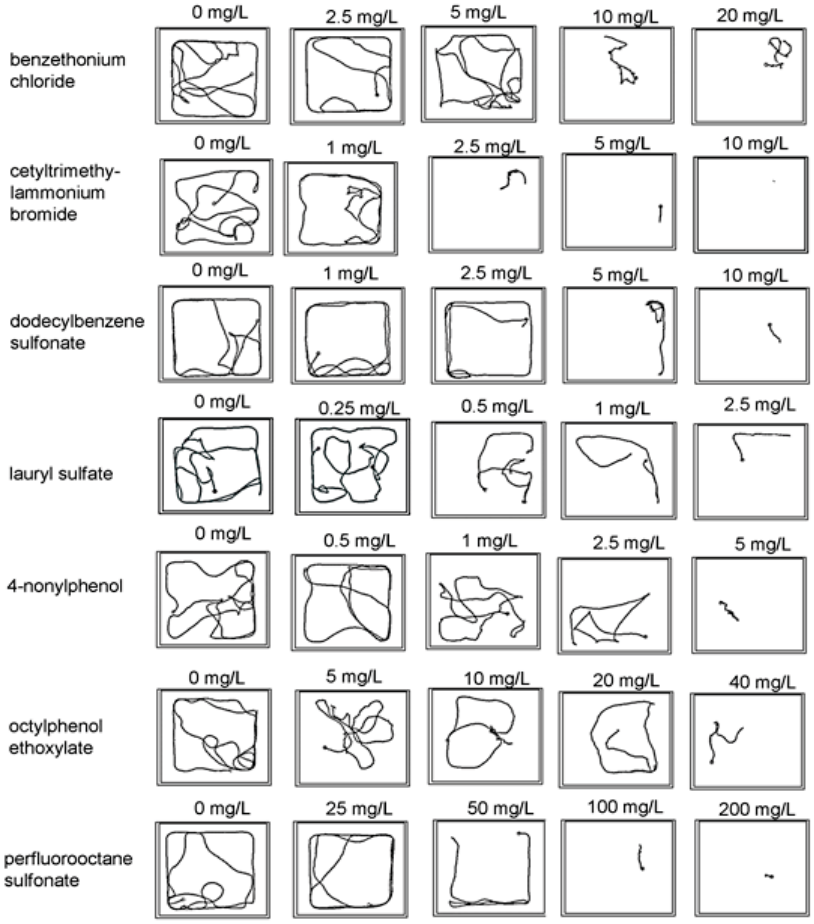

FIGURE 3
Locomotion movement patterns of planarians after the first 5-min exposure to surfactants and their subsequent locomotion monitoring for the second 5 min in the same test solution.

The published 24-h LC_{50} [20, 21] and the second 5-min EC_{50} of planarian mobility estimated through the lognormal model are shown in Table 2. A comparison of the 24-h LC_{50} and the corresponding second 5-min EC_{50} by using the t test revealed that LC_{50} did not differ significantly from the corresponding EC_{50}. The Pearson correlation coefficients between 24-h LC_{50} and second 5-min EC_{50} values were 0.911 ($P < 0.001$), suggesting that the second 5-min EC_{50} of planarian mobility is a useful indicator of LC_{50} toxicity in planarians exposed to the test chemicals.

Three linear regression models were used to analyze the relationship between 24-h LC_{50} and second 5-min EC_{50}, and all linear, quadratic, and cubic regression models exhibited a strong positive association between 24-h LC_{50} and second 5-min EC_{50} ($P < 0.0001$; Figure 4). Among the 3 linear regression models, the cubic regression yielded the strongest coefficient of determination (r^2): r^2 was 0.946 for second 5-min EC_{50}. In addition, the slope of the linear regression model for second 5-min EC_{50} and 24-h LC_{50} was 0.9904 (Figure 4). These results show that the second 5-min EC_{50} values of planarian mobility are similar to their corresponding 24-h LC_{50} values.

Compared with traditional aquatic toxicity tests, the planarian mobility assays are relatively quicker in screening the chemicals of interest. The time required to complete a computerized video tracking measurement of planarian movements for 5 concentrations in triplicate was 2–2.5 h for each test chemical. Automated video tracking systems and techniques have been widely used by various investigators in planarians [17, 24-25] and other aquatic animal models [26-29] to study the effects of different chemicals; furthermore, these systems provide several advantages, including consistency, reliability, productivity, and standardized determination of locomotion. By using those commercial available video tracking systems, the planarian mobility assay can be completed within in 1 hr by simultaneous tracing 6 animals in 6-well microplate.

TABLE 2
Published 24-h LC_{50} of planarians exposed to different chemicals of personal care products and second 5-min locomotion EC_{50} (mg/L) for *Dugesia japonica* after 5-min exposure to test chemicals and their subsequent locomotion monitoring for next 5 min in the same test solution in this study.

Chemicals	Reported 24-h LC_{50} (mg/L)	The second 5-min locomotion EC_{50} (mg/L)
benzophenone-type UV filters		
benzophenone	15.8[a]	6.3
2,4-dihydroxybenzophenone	4.5[a]	6.3
2,2',4,4'-tetrahydroxybenzophenone	8.3[a]	28.7
oxybenzone	2.2[a]	2.4
sulisobenzone	158.0[a]	115.9
2,2'-dihydroxy-4,4'-dimethoxybenzophenone	35.0[a]	31.8
5-chloro-2-hydroxybenzophenone	3.5[a]	4.1
dioxybenzone	5.3[a]	3.1
mexenone	1.5[a]	2.3
4,4'-dihydroxybenzophenone	17.0[a]	21.9
2-hydroxybenzophenone	4.9[a]	5.2
3-hydroxybenzophenone	15.8[a]	9.0
4-hydroxybenzophenone	15.8[a]	9.5
2,3,4-trihydroxybenzophenone	34.6[a]	53.2
paraben preservatives		
butylparaben	8.7[a]	4.4
ethylparaben	39.0[a]	84.3
methylparaben	97.0[a]	96.7
propylparaben	14.7[a]	7.4
surfactants		
benzethonium chloride	7.6[b]	8.7
cetyltrimethylammonium bromide	3.2[b]	1.2
dodecylbenzene sulfonate	6.8[b]	4.6
lauryl sulfate	0.4[b]	0.6
4-nonylphenol	1.0[b]	1.9
octylphenol ethoxylate	11.8[b]	26.8
perfluorooctane sulfonate	53.0[b]	57.8

[a][21]
[b][18]

In general, most standard acute toxicity tests will require at least 150 animals (6 concentrations with 5 replicates; 5 animals for each replicate) and 2-4 days performing acute toxicity test. Planarian mobility assay used in this study only require a minimum of 30 planarians (a total of 6 animals for each concentration and at least 5 concentrations conducted) for each chemical toxicity testing. Furthermore, most exposed planarians will be replaced to clean culture media after 10-minute experiment and survive and recover health after mobility tracking studies. Based on the result of this study, planarian mobility assay provides great advantages to promote 3R principles in toxicology study, by replacing vertebrates to invertebrates, reducing numbers of experimental animals used, and refining animals by greatly increased survival and recovery.

Behavioral observations can be cumbersome, and standardizing behavioral endpoints for different animal species and quantifying and interpreting the behavioral results are difficult. Compared with other behavioral responses and patterns, locomotion is easy to record and quantify for most animals under toxicological experiments. Planarian mobility EC_{50} obtained in this study support the conclusions of other investigators that motor activities and patterns in various aquatic invertebrates are sensitive indicators of environmental pollutants [30-34]. In addition, the significant association between the second 5-min EC_{50} and their corresponding 24-h LC_{50} can be used in deciding the timely precautionary measures required to prevent episodic water pollution, even in the absence of acute aquatic toxicity information.

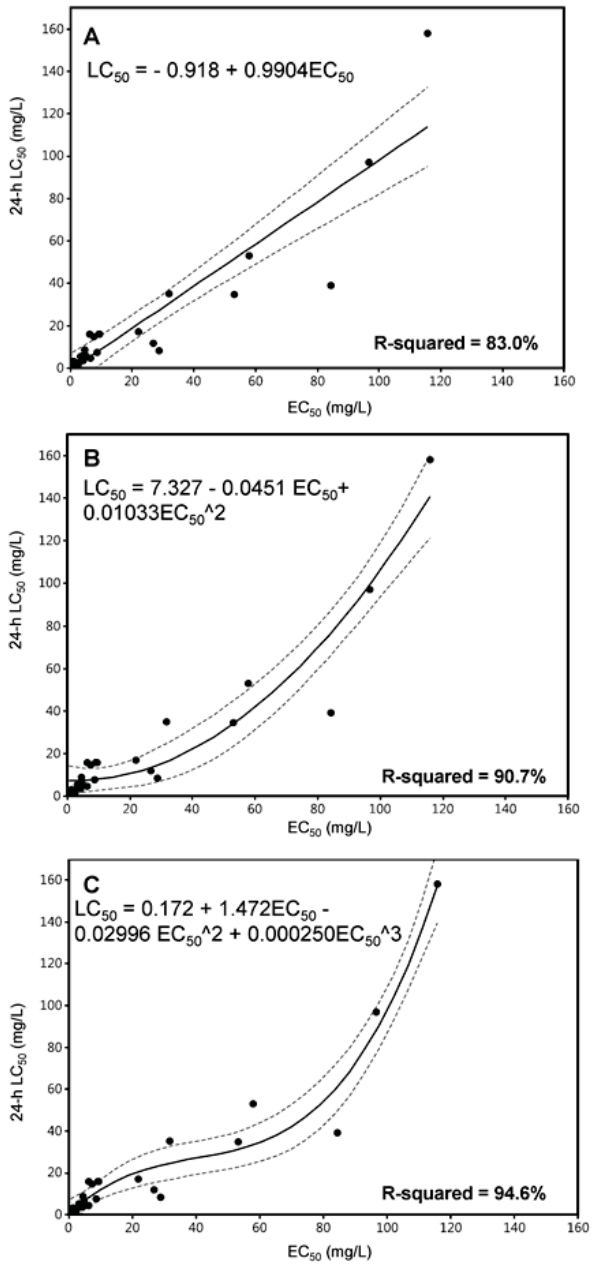

FIGURE 4

24-h LC_{50} of planarians exposed to 25 chemicals in personal care products as a function of the second 5-min EC_{50} (lognormal model) of planarian mobility for 3 linear regressions: (a) linear, (b) quadratic, and (c) cubic regression. Solid lines show the linear regression lines, and dashed lines show the 95% confidence interval for the mean regression line.

CONCLUSIONS

While discussing alternative acute toxicity testing models, it is crucial to consider that multiple sublethal endpoints for different species should be determined for effectively assessing the ecological risk for aquatic ecosystems. In this study, I examined the effects of 25 chemicals found in personal care products on freshwater planarian locomotion during the second 5-min exposure period. The second 5-min EC_{50} values of planarian mobility corresponded significantly with their 24-h LC_{50}. Before the application of planarian mobility assays in preliminary evaluation of water samples, additional studies should be conducted to link the acute toxicity of various environmental pollutants in freshwater planarians with other potential effects on other aquatic species.

ACKNOWLEDGEMENTS

The author thanks Ms. Yen-Ling Lin and Mr. Wei-Chien-Benny Chin for their assistance in

planarian behavioral study. The author is grateful for the funding support under grant MOST 103-2313-B-002-028-MY3 and NSC 97-2313-B-002-026-MY3 from the Ministry of Science and Technology, Taiwan.

REFERENCES

[1] Rueda, J., Camacho, A., Mezquita, F., Hernández, R., Roca J.R. (2002) Effect of episodic and regular sewage discharges on the water chemistry and macroinvertebrate fauna of a Mediterranean stream. Water, Air, & Soil Pollution. 140, 425-444.

[2] Etheridge, J.R., Birgand, F., Osborne, J.A., Osburn, C.L., Burchell, M.R., Irving, J. (2014) Using *in situ* ultraviolet-visual spectroscopy to measure nitrogen, carbon, phosphorus, and suspended solids concentrations at a high frequency in a brackish tidal marsh. Limnology and Oceanography Methods. 12, 10-22.

[3] Bae, M.J., Park, Y.S. (2014) Biological early warning system based on the responses of aquatic organisms to disturbances, a review. Science of the Total Environment. 466, 635-649.

[4] Zala, S.M., Penn, D.J. (2004) Abnormal behaviours induced by chemical pollution, a review of the evidence and new challenges. Animal Behavior. 68, 649-664.

[5] Hellou, J. (2011) Behavioural ecotoxicology, an early warning signal to assess environmental quality. Environmental Science and Pollution Research. 18, 1-11.

[6] Marentette, J.R., Tong, S., Wang, G., Sopinka, N.M., Taves, M.D., Koops, M.A., Balshine, S. (2012) Behavior as biomarker? Laboratory versus field movement in round goby (*Neogobius melanostomus*) from highly contaminated habitats. Ecotoxicology. 21, 1003-1012.

[7] Melvin, S.D., Wilson, S.P. (2013) The utility of behavioral studies for aquatic txicology testing, a meta-analysis. Chemosphere. 93, 2217-2223.

[8] Chevalier, J., Harscoët, E., Keller, M., Pandard, P., Cachot, J., Grote, M. (2015) Exploration of daphnia behavioral effect profiles induced by a broad range of toxicants with different modes of action. Environmental Toxicology and Chemistry. 34, 1760-1769.

[9] Baatrup, E., Bayley, M. (1998) Animal locomotor behaviour as a health biomarker of chemical stress. Archives of Toxicology. Supplement. 20, 164-178.

[10] Bayley, M. (2002) Basic behavior, the use of animal locomotion in behavioural ecotoxicology. In Behavioural Ecotoxicology (*ed.* G. Dell'Omo), pp. 211-230. Chichester, UK, John Wiley & Sons.

[11] Kane, A.S., Salierno, J.D., Gipson, G.T., Molteno, T.C.A., Hunter, C. (2004) A video-based movement analysis system to quantify behavioral stress responses of fish. Water Research. 38, 3993-4001.

[12] Mills, C.L., Shukla, D.H., Compton, G.J. (2006) Development of a new low cost high sensitivity system for behavioural ecotoxicity testing. Aquatic Toxicology. 77, 197-201.

[13] Buttarelli, F.R., Pellicano, C., Pontieri, F.E. (2008) Neuropharmacology and behavior in planarians, translations to mammals. Comparative Biochemistry and Physiology. - Part C 147, 399-408.

[14] Rowlands, A.L., Pagán, O.R. (2008) Parthenolide prevents the expression of cocaine-induced withdrawal behavior in planarians. European Journal of Pharmacology. 583, 170-172.

[15] Alonso, Á., Camargo, J.A. (2011) The freshwater planarian *Polycelis felina* as a sensitive species to assess the long-term toxicity of ammonia. Chemosphere. 84, 533-537.

[16] Hagstrom, D., Cochet-Escartin, O., Zhang, S., Khuu, C., Collins, E.M.S. (2015) Freshwater planarians as an alternative animal model for neurotoxicology. Toxicological Science. 147, 270-285.

[17] Rodrigues, A.C., Henriques, J.F., Domingues, I., Golovko, O., Žlábek, V., Barata, C., Soares, A.M., Pestana, J.L. (2016) Behavioural responses of freshwater planarians after short-term exposure to the insecticide chlorantraniliprole. Aquatic Toxicology. 170, 371-376

[18] Li, M.H. (2012) Survival, mobility, and membrane-bound enzyme activities of freshwater planarians, *Dugesia japonica*, exposed to synthetic and natural surfactants. Environmental Toxicology and Chemistry. 31, 843-850.

[19] Tijani, J.O., Fatoba, O.O., Babajide, O.O., Petrik, L.F. (2015) Pharmaceuticals, endocrine disruptors, personal care products, nanomaterials and perfluorinated pollutants, a review. Environmental Chemistry Letter. 14, 27–49.

[20] Li, M.H. (2008) Effects of nonionic and ionic surfactants on survival, oxidative stress, and cholinesterase activity of planarian. Chemosphere. 70, 1796-1803.

[21] Li, M.H. (2012) Acute toxicity of benzophenone-type UV filters and paraben preservatives to freshwater planarians, *Dugesia japonica*. Toxicological and Environmental Chemistry. 94, 566-573.

[22] ISO. (2012) Water Quality - Determination of the Inhibition of the Mobility of Daphnia Magna Straus (Cladocera, Crustacea) ISO 6341. 22 pp. Geneva, Switzerland: International Organization for Standardization.
[23] Vindimian, E. (2005) MSExcel macro REGTOX_EV7.0.5.xls, 2005. http://eric.vindimian.9online.fr/.
[24] Hicks, C., Sorocco, D., Levin, M. (2006) Automated analysis of behavior, a computer-controlled system for drug screening and the investigation of learning. Journal of Neurobiology. 66, 977-990.
[25] Talbot, J., Schötz, E.M. (2011) Quantitative characterization of planarian wild-type behavior as a platform for screening loco-motion phenotypes. Journal of Experimental Biology. 214, 1063-1067.
[26] Kokkali, V., Katramados, I., Newman, J.D. (2011) Monitoring the effect of metal ions on the mobility of *Artemia salina nauplii*. Biosensors. 1, 36-45.
[27] Zhang, Y., Wang, X., Yin, X., Shi, M., Dahlgren, R.A., Wang, H. (2016) Toxicity assessment of combined fluoroquinolone and tetracycline exposure in zebrafish (*Danio rerio*) Environmental Toxicology. 31, 736-750.
[28] Zhao, J., Xu, T., Yin, D.Q. (2014) Locomotor activity changes on zebrafish larvae with different 2, 2′, 4, 4′-tetrabromodiphenyl ether (PBDE-47) embryonic exposure modes. Chemosphere. 94, 53-61.
[29] Chevalier, J., Grote, M., Keller, M., Pandard, P., Cachot, J. (2014) A new multi-cell exposure system for continuous tracking of daphnia behavior for toxicity assessments. Journal of Environmental & Analytical Toxicology. 5, 246.
[30] Anderson, G.L., Cole, R.D., Williams, P.L. (2004) Assessing behavioral toxicity with *Caenorhabditis elegans*. Environmental Toxicology and Chemistry. 23, 1235-1240.
[31] Faimali, M., Garaventa, F., Piazza, V., Greco, G., Corrà, C., Magillo, F., Pittore, M., Giacco, E., Gallus, L., Falugi, C., Tagliafierro, G. (2006) Swimming speed alteration of larvae of *Balanus amphitrite* as a behavioural end-point for laboratory toxicological bioassays. Marine Biology. 149, 87-96.
[32] Duquesne, S., Küster, E. (2010) Biochemical, metabolic, and behavioural responses and recovery of *Daphnia magna* after exposure to an organophosphate. Ecotoxicology and Environmental Safety. 73, 353-359.
[33] Garaventa, F., Gambardella, C., Di Fino, A., Pittore, M., Faimali, M. (2010) Swimming speed alteration of *Artemia* sp. and *Brachionus plicatilis* as a sub-lethal behavioural end-point for ecotoxicological surveys. Ecotoxicology. 19, 512-519.
[34] Michalec, F.G., Holzner, M., Menu, D., Hwang, J.S., Souissi, S. (2013) Behavioral responses of the estuarine calanoid copepod *Eurytemora affinis* to sub-lethal concentrations of waterborne pollutants. Aquatic Toxicology. 138-139, 129-138.

Received: **18.02.2018**
Accepted: **19.02.2020**

CORRESPONDING AUTHOR

Mei-Hui Li
Environmental Toxicology Lab.,
Department of Geography,
National Taiwan University,
1, Section 4, Roosevelt Road,
Taipei 106 – Taiwan

e-mail: meihuili@ntu.edu.tw

© by PSP Volume 29 – No. 05/2020 pages 3370-3379 Fresenius Environmental Bulletin

A PRELIMINARY STUDY ON RADON CONCENTRATIONS AND HEALTH RISK ASSESSMENT OF DRINKING WATER SAMPLES IN KILIS PROVINCE, TURKEY

Cumhur Canbazoglu[1,*], Ayse Gundogan[2], Sultan Sahin Bal[3], Mahmut Dogru[4]

[1]Department of Physics, Faculty of Arts and Sciences, Kilis 7 Aralik University, Kilis, Turkey
[2]Graduate School of Natural and Applied Sciences, Kilis 7 Aralik University, Kilis, Turkey
[3]Department of Physics, Faculty of Arts and Sciences, Bitlis Eren University, Bitlis, Turkey
[4]Department of Physics, Faculty of Science, Firat University, Elazig, Turkey

ABSTRACT

Determination of radon concentration in drinking water is very important to assessment whether it poses a health risk in terms of public health or not. For this purpose, radon (^{222}Rn) concentration of forty nine drinking water samples collected from Kilis province were determined by using CR-39 passive nuclear track detectors with closed-can technique in this study. The radon concentrations for drinking water samples were found between 0.69 and 6.93 Bq L^{-1} with average of 1.86 Bq L^{-1}. All obtained values for radon concentrations were below 11.1 Bq L^{-1} that recommended as maximum contaminant level (MCL) by the United States Environmental Protection Agency (USEPA). In addition, effective dose and population weighted fatal cancer risk due to ^{222}Rn in drinking waters were estimated. Average effective dose values were calculated to be 4.75 µSv y^{-1}, 4.69 µSv y^{-1}, 0.57 µSv y^{-1} and 0.56 µSv y^{-1} for ingestion, inhalation, stomach and lungs, respectively. All obtained effective dose values were well below the reference level that suggested as 0.1 mSv y^{-1} by Word Health Organization (WHO). Population weighted fatal cancer risk varied from 2.62E-06 to 2.54E-04 and average value was found to be 3.07E-05 for Kilis province. In addition, per caput risk was estimated 1.99E-08 due to radon in drinking water samples. Investigated water samples for Kilis province were well below the permissible limits and have no risk to public health.

KEYWORDS:
Radon, Drinking water, Annual effective dose, Cancer risk, Nuclear track detectors, Closed-can technique, Kilis

INTRODUCTION

Human beings have been constantly exposed to cosmic and terrestrial ionizing radiation since the world has existed. Cosmic rays come from outer space and from the sun's surface. Terrestrial radionuclides are present in the earth's crust, building materials, air, water and foods, and even within the human body. External and internal exposure doses from these natural radiation sources are approximately 2.4 mSv. External exposures are due to cosmic rays and terrestrial gamma radiation. Internal exposures occur by inhalation and ingestion of radionuclides into the body and are mainly from inhaled radon (1.2 mSv) [1].

Radon is a colorless, tasteless, odorless and alpha emitting radioactive noble gas with high water solubility, which is found in soil, rock and groundwater. Radon (^{222}Rn), thoron (^{220}Rn) and actinon (^{219}Rn) are the three natural isotopes of radon, with a half-life of 3.824 day, 55 second and 3.96 second, respectively. The most important of the radon isotopes is ^{222}Rn, which is the most abundant in nature. It is decay product of ^{226}Ra and belongs to ^{238}U decay chain [2, 3]. Radon that emanates from soil substantially accumulates in dwellings and causes to radiation exposure of humans through inhalation. In addition, radon in water leads to exposures due to ingestion of drinking water and inhalation of radon that released from drinking water to air when water is used. Contribution of radon dissolved in water to exposure dose depends on radon concentration of water used for showering, laundry etc., and sometimes it can be important. In UNSCEAR 1993 publication, it has been reported that the concentrations of radon in well water, groundwater and surface water are generally being at the highest, intermediate and lowest, respectively [1, 2].

Exposure of humans to high ^{222}Rn concentrations and its decay products for a long time through inhalation can lead to health problem such as occurrence lung cancer. In addition, a very high radon level in drinking water can also pose a significant risk for stomach cancer. In addition to that the radon (^{222}Rn) dissolved in the water is transferred to the bloodstream via molecular diffusion and can radiological affect other organs [4-6]. Because of its potential health hazard, the monitoring of radon (^{222}Rn) concentration in the water is a necessary and important in terms of public health. Many studies have

been conducted worldwide to estimate radon concentration in water and its health effect for human beings [7-12]. However, such a study has not been carried out so far for the Kilis province of Turkey. The aim of this study is to determine radon concentration of tap waters that is generally used drinking purpose in Kilis province and estimate radiation dose that people are exposed through ingestion and inhalation due to radon in water. This study is significant for the public health because the radon concentrations and health risk assessment of drinking water samples in Kilis province are performed and reported for the first time.

MATERIALS AND METHODS

Study Area. The province of Kilis, which is in the southeastern part of the Turkey and border with Syria, is located between latitude 36° 38′ - 37° 32′ N and longitude 36° 50′ - 37° 56′ E. The surface area of Kilis province is 1,521 km^2 and is divided into four administrative regions (Figure 1). Its population is 130,825 and eighty percent of the population lives in the city center. The province of Kilis is under the influence of Mediterranean climate with an annual temperature of 16.8 ^{0}C. Average temperature is above 25 ^{0}C for summer season whilst varied from 3.5 ^{0}C to 6.5 ^{0}C for winter season. Kilis province has both surface and underground water resources although it is one of the low precipitation areas in Turkey. Municipal waters of Kilis province have being supplied by Seve Dam Lake, which covers 2.38 km^2, in the region. However, main water resources for Kilis province are originating from underground. Underground waters are often used in most of the houses in Kilis due to surface waters inadequacy [13].

Sample Collection and Preparation. Investigated drinking water samples were collected from the houses in the Kilis province. The water faucets were opened for about 4-5 minutes before sampling

FIGURE 1
Map of the Turkey Showing to Kilis Province.

and then drinking water samples were taken in 1 liter polyethylene cylindrical containers of radius 5 cm, length 12.7 cm. Their caps of cylindrical containers were tightly sealed to prevent radon escaping. Collected samples were carefully transferred to the laboratory without allowing the water samples to be shaken as much as possible. Water samples were completely covered with aluminum foil to prevent of external influences such as sunlight. The samples were then stored 1 month in the laboratory for radioactive equilibrium. At the end of the waiting period, the covers of the cylindrical containers were opened carefully and the square-shaped CR-39 passive nuclear track detectors in dimension of 1 cm^2 were vertically placed under the cover. Afterwards, the covers were serially closed. The detectors were exposed to the alpha particles emitted from the water samples, for 30 days. CR-39 detectors were then carefully collected and wrapped in aluminum foil. CR-39 detectors were labeled and sent to Bitlis Eren University Nuclear Physics Research Laboratory for analysis [14-16].

Chemical Etching of CR-39 Radon Detectors. Cr-39 Radon detectors were analyzed by using RADOSYS radon analyzer at nuclear physics research laboratory in Bitlis Eren University. The RADOSYS device is shown in Figure 2. Chemical etching process was performed using 25% NaOH solution at 90 °C for 4.5 hours. Etched detectors were washed with 4 liters of purified water and dried for 12 hours outside the RADOSYS device. Finally, alpha particle tracks formed on each CR-39 detector due to radon were counted automatically with an optical microscope [14-16]. The tracks formed on CR-39 film due to alpha particle are shown in Figure 3.

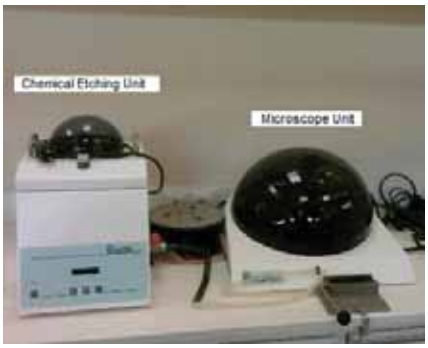

FIGURE 2
RADOSYS device.

Calculation of ^{222}Rn Activity Concentration in Water Samples Using by Closed-Can Technique. Radon concentrations of water samples were determined using by CR-39 passive nuclear track detectors with closed-can technique. Chemical etching process was performed to CR-39 detectors which exposed alpha radiation in the closed-can. Then, track density (track cm^{-2}) on the each detector was counted using by optical microscope. Configuration of closed-can used in experiment is shown in Figure 4 [14].

^{222}Rn activity concentration in air and water in the closed-can were calculated using Equation (1) and Equation (2), respectively [14, 15].

$$A_{air} = \frac{C_0 T_0 \rho}{\rho_0 T} \quad (1)$$

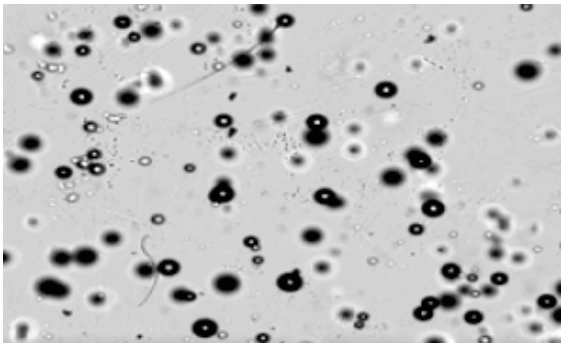

FIGURE 3
The tracks formed on CR-39 film due to alpha particle.

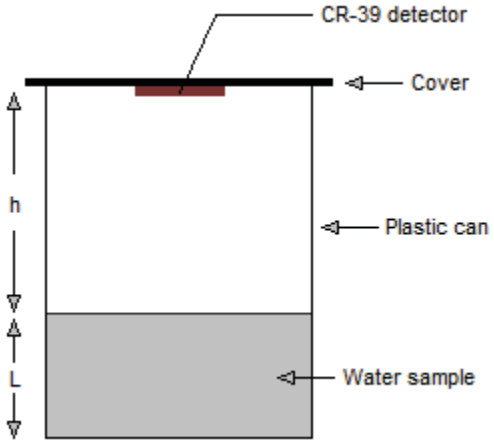

FIGURE 4
Configuration of closed-can.

Where, A_{air} is radon activity concentration in air above the surface of water sample, C_0 is radon activity concentration of calibration chamber, T_0 is exposure time to calibration, ρ_0 is surface density of tracks on calibrated detectors, ρ is the measured surface density of tracks on the detectors which exposed to alpha particle in the closed-can, and T is exposure time (720 h) of the sample.

$$A_{water} = \frac{\lambda A_{air} h T}{L} \quad (2)$$

Where, A_{water} is radon activity concentration in the water sample, λ is radioactive decay constant of ^{222}Rn, h is the distance from the water in the sample vessel to the detector, T is exposure time of sample, L is the depth of the water sample.

Effective Dose Estimation in Water Samples. Internal radiation exposure due to radon in the waters

arises from not only consumption of waters by humans but also radon transfer from water into the air in the house. Estimating exposure radiation dose due to ingestion and inhalation of radon in the water is very important for the assessment of possible health risks. For this reason, both the ingestion and inhalation situations must be considered to calculate the total dose estimate. Ingestion dose largely depends on the amount of water consumption that can vary considerably because of physical activities and climate. However the greatest contribution to the inhalation dose is due to the amount of radon transferred to the domestic environment because of the use of the water in the bath and kitchen. In this study, both ingestion dose and inhalation dose for radon in the water samples were estimated.

Annual effective dose due to consumption of drinking water by humans was calculated using Equation (3) [1, 17].

$$D_{ing} = A_w \times V_w \times F_{ing} \quad (3)$$

Where, D_{ing} is annual effective dose rate (mSv y^{-1}), A_w is radionuclide activity concentration in water sample (Bq L^{-1}), V_w is the water consumption rate (730 L y^{-1}), F_{ing} is dose conversion factor for ingestion (3.5 x 10^{-6} mSv Bq^{-1}).

Annual effective dose due to radon transfer from water into the air was calculated using Equation (4) [1, 17].

$$D_{inh} = A_w \times TF \times F \times F_{inh} \times T \quad (4)$$

Where, D_{inh} is annual effective dose rate (mSv y^{-1}), A_w is the radionuclide activity concentration of water sample (Bq L^{-1}), TF is transfer factor which is related to increment of airborne radon concentration per unit radon concentration in water and its value is 10^{-4}, F is radon equilibrium factor between radon and its decay products (0.4), F_{inh} is the effective dose coefficient for inhalation (9 x 10^{-6} mSv$h^{-1}Bq^{-1}m^3$) and T is the exposure time (0.8 x 24h x 365 = 7000 h y^{-1}).

Cancer Risk Estimation due to Inhaled Radon. Mean population risk, PR, is calculated by using Equation (5) according to United States Environmental Protection Agency (USEPA) report [6, 18]:

$$PR = (UD) \times (RF) \times (C_{mean}) \times (N) \quad (5)$$

Where, PR is population risk of fatal cancer per year due to inhalation of radon in water, UD is unit dose (pCi inhaled per year per pCi L^{-1} of radon in water), RF is risk factor that described as lifetime cancer risk per person per pCi inhaled per year and its value is $1.1x10^{-12}$, C_{mean} is population-weighted mean radon concentration (pCi L^{-1}) in water, N is the number of people in the population.

Unit dose that given in Equation (5) depends on three factors and is given in Equation (6) [6, 18]:

$$UD = (TF) \times (BR) \times (OF) \times (365\ d\ y^{-1}) \quad (6)$$

Where, TF is transfer factor that represents increase in airborne radon concentration per unit radon concentration in water and its value is 10^{-4}, BR is breathing rate (13000 L d^{-1}), OF is occupancy factor (fraction of time spent in indoors) and taken as 80%.

C_{mean} given in Equation (5) is calculated by using Equation (7):

$$C_{mean} = (\Sigma A_i P_i)/(\Sigma P_i) \quad (7)$$

Where, A_i is the radon concentration in water (pCi L^{-1}) and P_i is the number of people in population using water supply.

RESULTS AND DISCUSSION

In this study, radon concentration in the number of 49 drinking water samples from Kilis province of Turkey were determined by using closed-can technique. In addition, fatal cancer risk and effective doses due to radon in drinking water were estimated. Radon concentrations of drinking waters and estimated effective dose values (for ingestion, inhalation, stomach and lung) were comparatively given in Figure 5 and Table 1. The lowest and highest radon.

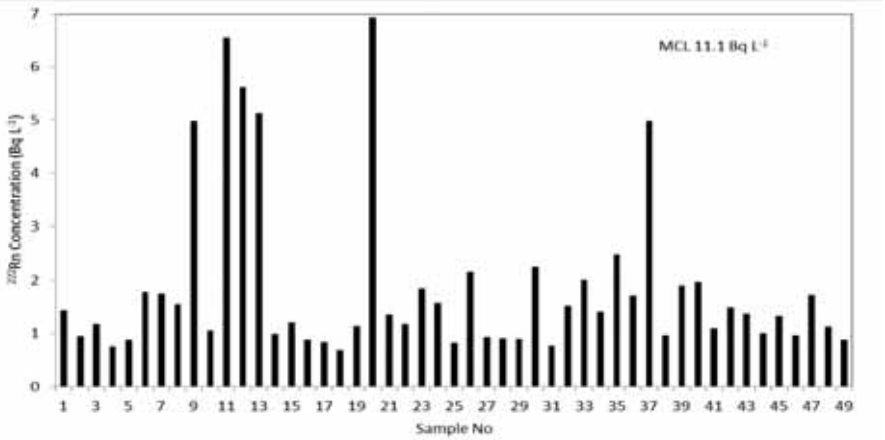

FIGURE 5
Radon concentrations in drinking water samples for Kilis province.

TABLE 1
Radon concentrations of drinking waters and estimated effective dose values for Kilis province.

Sample No	Neighborhood	Population (N)	^{222}Rn (Bq L^{-1})	Ingestion Dose (μSv y^{-1})	Inhalation Dose (μSv y^{-1})	Stomach Dose (μSv y^{-1})	Lung Dose (μSv y^{-1})
1	Mehmet Sanlı	4463	1.44	3.68	3.63	0.44	0.44
2	Bölük	475	0.95	2.44	2.41	0.29	0.29
3	Tekye	234	1.18	3.02	2.98	0.36	0.36
4	Şehitler	432	0.76	1.94	1.92	0.23	0.23
5	İslambey	333	0.88	2.26	2.23	0.27	0.27
6	Aslan	220	1.79	4.58	4.52	0.55	0.54
7	Vaiz	398	1.75	4.46	4.40	0.54	0.53
8	Yeni	409	1.55	3.97	3.91	0.48	0.47
9	Çaylak	299	4.99	12.74	12.57	1.53	1.51
10	Yedi Aralık	862	1.06	2.71	2.67	0.33	0.32
11	Abdioymağı	325	6.55	16.74	16.51	2.01	1.98
12	Tırıklı	235	5.62	14.35	14.16	1.72	1.70
13	Müslümanbey	756	5.14	13.14	12.96	1.58	1.56
14	Demirciler	911	0.99	2.52	2.49	0.30	0.30
15	Hakverdi	392	1.21	3.09	3.04	0.37	0.37
16	Helvacıoğlu	2296	0.88	2.24	2.21	0.27	0.27
17	Bilalhabeşi	1794	0.85	2.17	2.14	0.26	0.26
18	Okçular	540	0.69	1.76	1.74	0.21	0.21
19	Mehmet Çavuş	1282	1.14	2.92	2.88	0.35	0.35
20	M. Rıfat Bilge	921	6.93	17.71	17.46	2.13	2.10
21	Atatürk	4454	1.36	3.47	3.42	0.42	0.41
22	TOKİ	4463	1.19	3.04	3.00	0.37	0.36
23	Çengel	1246	1.85	4.73	4.66	0.57	0.56
24	İsmet Paşa	3784	1.58	4.03	3.98	0.48	0.48
25	Hürriyet	1029	0.83	2.11	2.08	0.25	0.25
26	Ekrem Çetin	12800	2.17	5.54	5.47	0.67	0.66
27	Barış	1217	0.94	2.39	2.36	0.29	0.28
28	Altınüzüm	484	0.91	2.32	2.29	0.28	0.28
29	İzzettin İyigün	950	0.90	2.31	2.28	0.28	0.27
30	Nedim Ökmen	1569	2.26	5.77	5.70	0.69	0.68
31	Şıhahmet	398	0.77	1.98	1.95	0.24	0.23
32	Doğan Güreş Paşa	2347	1.53	3.90	3.85	0.47	0.46
33	A İ Karaoğlanoğlu	4807	2.02	5.16	5.09	0,62	0.61
34	M.R Kazancıoğlu	6384	1.41	3.60	3.55	0.43	0.43
35	Kazım Karabekir	5048	2.49	6.36	6.27	0.76	0.75
36	Kartalbey	932	1.71	4.36	4.30	0.52	0.52
37	Mullahamit	404	4.99	12.74	12.57	1.53	1.51
38	Şehit Sakıp	939	0.97	2.49	2.46	0.30	0.30
39	Namık Kemal	1005	1.91	4.88	4.81	0.59	0.58
40	Cumhuriyet	206	1.97	5.03	4.96	0.60	0.60
41	İnönü/Elbeyli	704	1.10	2.80	2.77	0.34	0.33
42	Hürriyet/Elbeyli	590	1.50	3.83	3.78	0.46	0.45
43	Akyüz/Elbeyli	294	1.37	3.50	3.45	0.42	0.41
44	Şehitler/Elbeyli	299	1.01	2.59	2.55	0.31	0.31
45	Cumhuriyet/Mus.	994	1.33	3.40	3.35	0.41	0.40
46	Pınar/Musabeyli	288	0.96	2.46	2.42	0.30	0.29
47	Akyüz/Musabeyli	132	1.73	4.43	4.37	0.53	0.52
48	Şehit Ali/Polateli	193	1.13	2.89	2.85	0.35	0.34
49	Atatürk/Polateli	233	0.88	2.26	2.23	0.27	0.27

concentrations were found to be 0.69 Bq L^{-1} and 6.93 Bq L^{-1} in *Okçular* and *Muallim Rıfat Bilge* neighborhoods, respectively. The values of ingestion dose, inhalation dose, stomach dose and lung dose were calculated 1.76, 1.74, 0.21 and 0.21 μSv y^{-1} for *Okçular* neighborhood and 17.71, 17.46, 2.13 and 2.10 μSv y^{-1} for Muallim Rıfat Bilge neighborhood, respectively. Maximum contaminant level (MCL) of radon in public drinking water has recommended as 11.1

TABLE 2
Statistical Results for Radon Concentrations of Drinking Water Samples from Kilis Province.

Statistics	^{222}Rn (Bq L^{-1})	Ingestion Dose (μSv y^{-1})	Inhalation Dose (μSv y^{-1})	Stomach Dose	Lung Dose (μSv y^{-1})
Mean	1.8595	4.7512	4.6859	0.5708	0.5633
Std. Error of Mean	0.21957	0.56094	0.55332	0.06736	0.06644
Median	1.3572	3.4700	3.4201	0.4200	0.4100
Std. Deviation	1.53701	3.92657	3.87325	0.47155	0.46508
Variance	2.362	15.418	15.002	0.222	0.216
Skewness	2.185	2.186	2.185	2.187	2.187
Std. Error of Skewness	0.340	0.340	0.340	0.340	0.340
Kurtosis	3.870	3.873	3.870	3.884	3.875
Std. Error of Kurtosis	0.668	0.668	0.668	0.668	0.668
Range	6.24	15.95	15.73	1.92	1.89
Minimum	0.69	1.76	1.74	0.21	0.21
Maximum	6.93	17.71	17.46	2.13	2.10

Bq L^{-1} (300 pCi L^{-1}) by the United States Environmental Protection Agency (USEPA) [19-21]. World Health Organization (WHO) has proposed that a reference level for annual effective dose received from drinking water consumption is 0.1 mSv. Besides, The World Health Organization has indicated that if the annual effective dose received from drinking water is less than 0.1 mSv, the water is suitable for drinking purpose but if it is high, corrective measures are necessary to reduce the received dose [22, 23]. UNSCEAR has reported that average radon concentration in water is 10 Bq L^{-1} [1]. Average values of inhalation and ingestion dose due to radon in water were also calculated to be 0.025 mSv and 0.002 mSv (for 60 L y^{-1} water consumption) in UNSCEAR 2000 report, respectively [1]. In addition, the World Health Organization has proposed that action level of radon concentration in drinking waters for public water resources to be 100 Bq L^{-1} and stated that necessary precautions should be taken to reduce the radon concentration if the radon activity in drinking water exceeds 100 Bq L^{-1} [22, 23]. All values that were reported for Kilis province due to radon in drinking water are well below the permissible limits recommended by USEPA, WHO, and UNSCEAR. It can be summarized from the obtained data that all water samples that investigated in this study are suitable for drinking purpose and not pose threat to public health

Statistical results for obtained data from this study were analyzed using statistical packed program (SPSS version 20) and given in Table 2. Radon concentration in drinking waters varied between 0.69 and 6.93 Bq L^{-1} with an average value of 1.86 Bq L^{-1}. Ingestion and inhalation dose values ranged from 1.76 to 17.71 μSv y^{-1} and 1.74 to 17.46 μSv y^{-1} with an average value of 4.75 μSv y^{-1} and 4.69 μSv y^{-1}, respectively. Radiation exposure to the lungs and stomach due to radon in drinking water is calculated by multiplying the inhalation and ingestion dose by the tissue weighting factor for the lungs and stomach, respectively.

The tissue weighting factor is reported as 0.12 for both lungs and stomach in ICRP Publication 103 [24]. As seen in Table 2, stomach and lung tissue doses varied from 0.21 to 2.13 μSv y^{-1} and 0.21 to 2.10 μSv y^{-1}, respectively. Average value for stomach and lung dose are 0.57 μSv y^{-1} and 0.56 μSv y^{-1}, respectively. Median, Skewness and Kurtosis values were found to be 1.36, 2.19 and 3.87 Bq L^{-1} for radon concentration of water samples; 3.47, 2.19 and 3.87 μSv y^{-1} for ingestion dose; 3.42, 2.19 and 3.87 μSv y^{-1} for inhalation dose; 0.42, 2.19 and 3.88 μSv y^{-1} for stomach dose; and 0.41, 2.19 and 3.88 μSv y^{-1} for lung dose, respectively.

Population risk of fatal cancer (PR) per year due to the inhaled radon for each neighborhood in Kilis province was estimated by using Equation (5) and given in Table 3. Unit dose (UD) was found to be 380 according to Equation (6). Population-weighted average radon concentration (C_{mean}) was calculated to be 47.52 pCi L^{-1} by using Equation (7). Per caput risk within the exposed population due to radon in drinking water samples was estimated to be 1,99E-08 by using N=1 and UD=380 values in Equation (5). This value is low compared with the mean individual risk of 6.2E-07 reported by USEPA [6]. It summarizes that the individual fatal cancer risk faced by a person in the Kilis province due to radon in drinking water is lower than the average. It can be seen from the Table 3 that population-weighted fatal cancer risk varied from 2.62E-06 to 2.54E-04 with an average value of 3.07E-05. In addition, as seen in Table 3, the lowest and highest fatal cancer risk values were observed in Akyüz (2.62E-06) and Ekrem Çetin (2.54E-04) neighborhoods, respectively. However, in Okçular and Muallim Rıfat Bilge neighborhoods where the lowest and highest

TABLE 3
Population Weighted Cancer Risk Due to Inhaled Radon in Drinking Water Samples for Neighborhoods in Kilis Province

Sample No	Neighborhood	Population (N)	^{222}Rn (Bq L^{-1})	^{222}Rn (pCi L^{-1})	Cancer risk (PR)
1	Mehmet Sanlı	4463	1.44	38.97	8.87E-05
2	Bölük	475	0.95	25.80	9.44E-06
3	Tekye	234	1.18	31.95	4.65E-06
4	Şehitler	432	0.76	20.54	8.58E-06
5	İslambey	333	0.88	23.87	6.62E-06
6	Aslan	220	1.79	48.45	4.37E-06
7	Vaiz	398	1.75	47.21	7.91E-06
8	Yeni	409	1.55	41.96	8.12E-06
9	Çaylak	299	4.99	134.80	5.94E-06
10	Yedi Aralık	862	1.06	28.62	1.71E-05
11	Abdioymağı	325	6.55	177.10	6.46E-06
12	Tırıklı	235	5.62	151.82	4.67E-06
13	Müslümanbey	756	5.14	139.01	1.50E-05
14	Demirciler	911	0.99	26.68	1.81E-05
15	Hakverdi	392	1.21	32.64	7.79E-06
16	Helvacıoğlu	2296	0.88	23.70	4.56E-05
17	Bilalhabeşi	1794	0.85	22.99	3.56E-05
18	Okçular	540	0.69	18.61	1.07E-05
19	Mehmet Çavuş	1282	1.14	30.89	2.55E-05
20	Muallim Rıfat Bilge	921	6.93	187.28	1.83E-05
21	Atatürk	4454	1.36	36.68	8.85E-05
22	TOKİ	4463	1.19	32.13	8.87E-05
23	Çengel	1246	1.85	50.02	2.48E-05
24	İsmet Paşa	3784	1.58	42.66	7.52E-05
25	Hürriyet	1029	0.83	22.30	2.04E-05
26	Ekrem Çetin	12800	2.17	58.63	2.54E-04
27	Barış	1217	0.94	25.28	2.42E-05
28	Altınüzüm	484	0.91	24.58	9.61E-06
29	İzzettin İyigün Paşa	950	0.90	24.40	1.89E-05
30	Nedim Ökmen	1569	2.26	61.08	3.12E-05
31	Şıhahmet	398	0.77	20.89	7.91E-06
32	Doğan Güreş Paşa	2347	1.53	41.25	4.66E-05
33	Albay İbrahim Karaoğlanoğlu	4807	2.02	54.59	9.55E-05
34	Mehmet Rıfat Kazancıoğlu	6384	1.41	38.09	1.27E-04
35	Kazım Karabekir	5048	2.49	67.22	1.00E-04
36	Kartalbey	932	1.71	46.16	1.85E-05
37	Mullahamit	404	4.99	134.80	8.03E-06
38	Şehit Sakıp	939	0.97	26.32	1.87E-05
39	Namık Kemal	1005	1.91	51.61	2.00E-05
40	Cumhuriyet	206	1.97	53.18	4.09E-06
41	İnönü/Elbeyli	704	1.10	29.66	1.40E-05
42	Hürriyet/Elbeyli	590	1.50	40.54	1.17E-05
43	Akyüz/Elbeyli	294	1.37	37.03	5.84E-06
44	Şehitler/Elbeyli	299	1.01	27.38	5.94E-06
45	Cumhuriyet/Musabeyli	994	1.33	35.98	1.97E-05
46	Pınar/Musabeyli	288	0.96	25.97	5.72E-06
47	Akyüz/Musabeyli	132	1.73	46.86	2.62E-06
48	Şehit Ali/Polateli	193	1.13	30.54	3.83E-06
49	Atatürk/Polateli	233	0.88	23.87	4.63E-06
	Population-weighted average cancer risk				3.07E-05

TABLE 4
Reported Radon Concentrations in Drinking Waters from Different Countries of the World and Other Parts of Turkey.

Region	Radon concentrations in drinking water (Bq L^{-1})		References
	Range	Average	
Northern Rajasthan, India	0.50-22	4.42	[25]
Shimoga district, Kartanaka, India	3.10-38.5	13.60	[4]
Hasan district, Karnata, India	0.85-60.74	26.50	[5]
West Bengal, India	1.9-9.0	5.0	[26]
Karak district, Pakistan	1.1-25.1	9.4	[3]
Southern Greater Polan Region, Poland	0.43-10.52	2.67	[27]
Ramsar region, Iran	11.42-83.36	25.34	[28]
Eskişehir, Turkey	1.6-230	-----	[17]
	(wet season)		
	3.7-251	-----	
	(dry season)		
Osmaniye, Turkey	0.16-0.99	0.44	[29]
Kastamonu, Turkey	0.50-19.21	5.78	[30]
	(spring water in summer)		
	0.39-12.73	5.04	
	(spring water in spring)		
	0.31-13.14	3.24	
	(Tap water in summer)		
	0.36-9.29	2.73	
	(tap water in spring)		
Bursa, Turkey	1.46-53.64	----	[31]
	(for well water)		
	0.91-12.58	----	
	(for tap water)		
Kütahya, Turkey	0.1-48.6	----	[32]
Kilis, Turkey	0.69-6.93	1.86	This study

radon concentrations were observed, the fatal cancer risks were estimated 1.07E-05 and 1.83E-05 due to the fact that low population, respectively.

Reported radon concentrations in drinking waters for different countries of the world and other parts of the Turkey have been compared with obtained results for Kilis province and are shown in Table 4 [3-5, 17, 25-32]. Radon concentration of drinking water samples in this study lies in the range from 0.69 to 6.93 Bq L^{-1}. Average value of radon concentration (1.86 Bq L^{-1}) obtained for Kilis province is lower than average values reported for other regions (except Osmaniye, Turkey) in Table 4. It can be seen from the Table 4 that the range of radon concentration in the drinking water samples in this study is largely consistent with other regions that has an average radon concentration of less than 10 Bq L^{-1} suggested by UNSCEAR. It can be concluded that the results obtained from this study are compatible with the literature.

CONCLUSIONS

In this study, Radon concentrations of drinking water samples in Kilis province were determined using by CR-39 passive nuclear track detectors with closed-can technique. In addition, population-weighted fatal cancer risk and effective dose estimation were also performed. Average radon concentration of drinking water samples were calculated as 1.86 Bq L^{-1}. The highest and lowest radon concentration were observed in Muallim Rıfat Bilge (6.93 Bq L^{-1}) and Okçular (0.69 Bq L^{-1}) neighborhoods, respectively. Radon concentrations of all water samples were below the maximum contaminant level (MCL) that recommended as 11.1 Bq L^{-1} by USEPA. Average effective dose values were estimated to be 4.75 µSv y^{-1}, 4.69 µSv y^{-1}, 0.57 µSv y^{-1} and 0.56 µSv y^{-1} for ingestion, inhalation, stomach and lungs, respectively. All effective dose values obtained from this study were well below the reference level of 0.1

mSv y^{-1} that suggested by WHO. In addition, per caput risk within the exposed population for Kilis province due to radon in drinking water samples was estimated to be 1.99E-08. This value is lower than mean individual risk of 6.2E-07 reported by USEPA**.** Besides that, population-weighted average fatal cancer risk was found to be 3.07E-05 for Kilis province. The lowest and highest fatal cancer risk were observed in Akyüz/Musabeyli (2.62E-06) and Ekrem Çetin (2.54E-04) neighborhoods, respectively. Finally, it can be concluded that drinking water samples in Kilis province are well below the permissible limits and has no risk to public health.

ACKNOWLEDGEMENTS

This study was supported by the Scientific Research Projects Department (Project no: 2013/02/LTP/02) at Kilis 7 Aralik University.

REFERENCES

[1] UNSCEAR (2000) Sources and Effects of Ionizing radiation. Report of the United Nations Scientific Committee on the Effects of Atomic Radiation to the General Assembly, with Scientific Annexes, United Nations, New York.

[2] UNSCEAR (1993) Sources and Effects of ionizing radiation. Report of the United Nations Scientific Committee on the Effects of Atomic Radiation to the General Assembly, with Scientific Annexes, United Nations, New York.

[3] Khattak, N.U., Khan, M.A., Shah, M.T. and Ali, N. (2014) Radon Concentration in Drinking Water Sources of the Region Adjacent to a Tectonically Active Karak Thrust, Southern Kohat Plateau, Khyber Pakhtunkhwa, Pakistan, J Radioanal Nucl Chem. 302, 315-329.

[4] Rangaswamy, D.R., Srinivasa, E., Srilatha, M.C. and Sannappa, J. (2016) Measurement of Radon Concentration in Drinking Water of Shimoga District, Karnataka, India. J Radioanal Nucl Chem. 307, 907-916.

[5] Srinivasa, E., Rangaswamy, D.R. and Sannappa, J. (2015) Determination of Radon Activity Concentration in Drinking Water and Evaluation of the Annual Effective Dose in Hassan District, Karnataka State, India. J Radioanal Nucl Chem. 305, 665-673.

[6] National Research Council NRC (1999) Risk Asessment of Radon in Drinking Water. National Academy Press, Washington, D.C.

[7] Gurler, O., Akar, U., Kahraman, A., Yalcin, S., Kaynak, G. and Gundogdu, O. (2010) Measurements of Radon Levels in Thermal Waters of Bursa, Turkey. Fresen. Environ. Bull. 19, 3013-3017.

[8] Pirsaheb, M., Sharafi, K., Hemati, L. and Fazlzadehdavil, M. (2015) Radon measurement in drinking water and assessment of average annual effective dose in the west region of Iran. Fresen. Environ. Bull. 24, 3515-3519.

[9] Gurler, O., Akar Tarim, U. and Yalcin, S. (2013) Estimation of Mean ^{222}Rn Concentration in Water and in Indoor air of Karacabey, Bursa (Turkey). Fresen. Environ. Bull. 22, 247-251.

[10] Todorovic, N., Nikolov, J., Forkapic, S., Bikit, I., Mrdja, D., Krmar, M. and Veskovic, M. (2012) Public Exposure to Radon in Drinking Water in SERBIA. Appl Radiat Isot. 70, 543-549.

[11] Nandakumaran, P., Vinayachandran, N., Anitha Shyam, T.S., Jose, B., Sreehari Sarangan, M.S. and Santhana Subramani, M. (2016) Radon in Groundwater in Parts of Coastal Tracts of Southern Kerala, India. J Radioanal Nucl Chem. 308, 99-104.

[12] Ravikumar, P. and Somashekar, R.K. (2018) Distribution of ^{222}Rn in Groundwater and Estimation of Resulting Radiation Dose to Different Age Groups: A Case Study from Bangalore City. Hum Ecol Risk Assess. 24, 174-185.

[13] Strategic Plan of Municipality of Kilis (2014) Municipality of Kilis, Kilis, Turkey.

[14] Al-Bataina, B.A., Ismail, A.M., Kullab, M.K., Abumurad, K.M. and Mustafa, H. (1997) Radon Measurements in Different Types of Natural Waters in Jordan. Radiat Meas. 28, 591-594.

[15] Baykara, O. and Doğru, M. (2006) Measurements of Radon and Uranium Concentration in Water and Soil Samples from East Anatolian Active Fault Systems (Turkey). Radiat Meas. 41, 362-367.

[16] Lima Marques, A., dos Santos, W. and Paulo Geraldo, L. (2004) Direct Measurements of Radon Activity in Water from Various Natural Sources Using Nuclear Track Detectors. Appl Radiat Isot. 60, 801-804.

[17] Yüce, G. and Gasparon, M. (2013) Preliminary Risk Assessment of Radon in Groundwater: a Case Study from Eskisehir, Turkey. Isotopes Environ Health Stud. 49, 163-179.

[18] US Environmental Protection Agency US EPA (1995) Uncertainty Analysis of Risks Associated with Exposure to Radon in Drinking Water. US EPA, Office of Water, EPA-822-R-96-005, Washington, D.C.

[19] US Environmental Protection Agency US EPA (1991) National Primary Drinking Water Regulations; Radionuclides; Proposed Rule. Federal Register. 56, 33050.

[20] US Environmental Protection Agency US EPA (1994) Report to the United States Congress on Radon in Drinking Water: Multimedia Risk and Cost Assessment of Radon. US EPA, Office of Water, 4601, EPA 811-R-94-001, Washington, D.C.
[21] US Environmental Protection Agency US EPA (1999) Radon in Drinking Water Health Risk Reduction and Cost Analysis; Notice, Federal Register. 64, 9559-9599.
[22] World Health Organization WHO (2004) Guidelines for Drinking-water Ouality. In: Radiological Aspects, vol 1, 3rd ed., World Health Organization, Geneva.
[23] World Health Organization WHO (2008) Guidelines for Drinking-water Ouality. In: Radiological aspects, vol 1, 3rd ed., World Health Organization, Geneva.
[24] International Commission on Radiological Protection ICRP (2007) The 2007 Recommendations of the International Commission on Radiological Protection. ICRP Pubication 103, Ann. ICRP 37 (2-4), Elsevier, UK.
[25] Mittal, S., Rani, A. and Mehra, R. (2016) Estimation of Radon Concentration in Soil and Groundwater Samples of Northern Rajasthan, India. J Radiat Res Appl Sci. 9, 125-130.
[26] Krishan, G., Rao, M.S., Kumar, C.P. and Semwal, P. (2015) Radon Concentration in Groundwater of East Coast of West Bengal, India. J. Radioanal Nucl. Chem. 303, 2221-2225.
[27] Bem, H., Plota, U., Staniszewska, M., Bem, E.M. and Mazurek, D. (2014) Radon (^{222}Rn) in Underground Drinking Water Supplies of the Southern Greater Poland Region. J Radioanal Nucl Chem. 299, 1307-1312.
[28] Mowlavi, A.A., Shahbahrami, A. and Binesh, A. (2009) Dose Evaluation and Measurement of Radon Concentration in Some Drinking Water Sources of the Ramsar Region in Iran. Isotopes Environ Health Stud. 45, 269-272.
[29] Erdogdu, M., Damla, N., Kara, A., Sahan, H., Isik, U., Tel, E. and Sahan, M. (2016) Spatial Distribution of ^{222}Rn Concentrations and Dose Estimations in Various Waters. Hum Ecol Risk Assess. 22, 927-940.
[30] Yalcin, S., Gurler, O., Akar Tarim, U., Incirci, F., Kaynak, G. and Gundogdu, O. (2011) Measurements of Radon Concentration in Drinking Water Samples from Kastamonu (Turkey). Isotopes Environ Health Stud. 47, 438-445.
[31] Akar Tarim, U., Gurler, O., Akkaya, G., Kilic, N., Yalcin, S., Kaynak, G. and Gundogdu, O. (2012) Evaluation of Radon Concentration in Well and Tap Waters in Bursa, Turkey. Radiat Prot Dosim. 150, 207-212.
[32] Sahin, L., Çetinkaya, H., Saç, M.M. and Içhedef, M. (2013) Determination of Radon and Radium Concentrations in Drinking Water Samples Around the City of Kutahya. Radiat Prot Dosim. 155, 474-482.

Received: **23.07.2018**
Accepted: **21.02.2020**

CORRESPONDING AUTHOR

Cumhur Canbazoglu
Department of Physics,
Faculty of Arts and Sciences,
Kilis 7 Aralik University,
79000 Kilis, Turkey

e-mail:cumhurcanbazoglu@gmail.com

© by PSP Volume 29 – No. 05/2020 pages 3380-3387 Fresenius Environmental Bulletin

TILLAGE, NUTRIENTS AND WEED CONTROL AFFECTS YIELD OF SUGAR BEET

Tasneem ur Rehman[1], Muhammad Azim Khan[1], Haroon Khan[1], Wajid Ali Shah[2], Volkan Altay[3], Munir Ozturk[4,*]

[1]Department of Weed Science, The University of Agriculture Peshawar, Pakistan
[2]Bacha Khan University Charsadda, KP, Pakistan
[3]Biology Department, Faculty of Science and Arts, Hatay Mustafa Kemal University, Hatay, Turkey
[4]Botany Department and Centre for Environmental Studies, Ege University, Izmir, Turkey

ABSTRACT

Field trials were conducted to study the effectiveness of tillage, nutrients and weed management on the yield related variables of sugar beet at two locations (Mardan and D.I. Khan) of Pakistan during 2015 and repeated in 2016. Data of first year reveals that tillage and nutrient sources have no effect on weed related variables at both locations. However, during the second year tillage sources had no effect while nutrient sources had significant effect on the weed density and fresh biomass at both locations. Weed management differently affected weed density and fresh biomass that ultimately increased sugar beet related variables. In both the years, broadleaf weeds were dominant in the experimental fields. Highest sugar beet yield was found in year 1 at Mardan (67.87 tons ha^{-1}) in Dual gold treated plots. While highest sugar quantity was produced during year 2 at Mardan (11.44 tons ha^{-1}) in two time hand weeded plots. By comparing the data of both locations, it was concluded that performance of sugar beet was better at Mardan as compared to D.I Khan. This difference may be due to soil and climatic conditions. Net income has shown that Dual gold proved profitable than the rest of the treatments. Intercropping increased the income and decreased weed density but it can also increase the extra cost. It was concluded that weeds are major threat to sugar beet and being a root crop it can be severely affected due to infestation of weeds and thus can greatly decrease the sugar beet yield. Application of Dual gold effectively controls weeds and as a result ultimate increase occurs in the sugar beet yield and net income.

KEYWORDS:
Fresh biomass, FYM, NPK, sugar beet yield, weed density, dual gold

INTRODUCTION

Sugar beet (*Beta vulgaris* L.) is a member of the family Chenopodiaceae and is considered second important crop in terms of global sugar production [1]. Around forty percent of world sugar on annual basis is met by sugar beet [2]. In Pakistan sugar beet is grown successfully in several regions. The sugar beet is a temperate region crop but some of its varieties are also grown in subtropical areas. Proper attention has been given to agronomic practices for achieving higher yield and stable growth of sugar beet which is rich in sucrose. The yield of this crop is determined by the nutrient management and production technology [3]. The kinetic energy of sun is converted to organic matter energy in sugar beet crop. Therefore production technology is very important for the yield of sugar beet [4]. In Khyber Pakhtunkhwa region of Pakistan both the sugar beet as well as sugarcane are cultivated. Later is commercially grown on more than 100 thousand hectares as compared to sugar beet cultivated on 7000 hectares annually in Pakistan. Several sugar industries are well operational with cutting facilities and in this way sugarcane and sugar beet are successfully grown [5]. Due to suitability of climatic conditions in the Sindh region of Pakistan sugar beet is grown in various provinces. The climate of this region is like the Nile delta valley in Egypt which is a popular area for growing sugar beet since decades [6].

The concept of intercropping results in more number of plants per unit area that can ultimately affect the underground yield of sugar beet. The intercropping increases the net income, depending on the location and species grown. In view of this many scientists recommend to grow sugar beet as a companion crop. Usmanikhail et al. [7] have reported that growing wheat either with sunflower or sugar beet is a popular and profitable cropping system. In sugar beet cultivation, weed management plays a vital role. This root crop is negatively influenced by the presence of weeds for example, if weed management is not performed well, there are chances of crop yield losses up to 100% due to crop weed competition [8]. However, the herbicidal dose is critical for weed control in this crop. For complete weed execution, the rate of individual herbicide needs to be increased to get desirable outcomes in terms of weed management [9]. Suitable tillage

operations at proper time result in desirable soil properties that favour the growth of this crop. On the other hand, unnecessary and improper tillage lead to several undesirable effects [10].

In Pakistan, conventional tillage (already in practice) are the popular tillage operations that are used for growing sugar beet. The sugar beet as a root crop is directly affected by the fertilizer applications as well as soil structure and texture. Therefore these two factors are important for getting better yield. Previously it was claimed that soil natural carbon content and the biomass of microbes was increased by farmyard manure (FYM) and is thought to be eco-friendly approach to enhance soil structure and richness. No undesirable effect was found on the environment although it increased yield and growth of many crops [11]. Due to heavy infestation of weeds and imbalanced fertilizers that are applied to sugar beet and improper use of tillage, present experiments were designed to decipher the combination of all these for better weed management and higher yield of sugar beet in Khyber Pakhtunkhwa region of Pakistan.

MATERIALS AND METHODS

Sugar beet is commercially grown in two provinces of Khyber Pakhtunkhwa (Mardan and D.I. Khan) in Pakistan. The field experiments were conducted in the above two provinces in October 2015/2016 and repeated in 2016/2017. The latitude of Mardan is 34.2001° N and longitude is 72.0508° E with an elevation of 315 m. The latitude and longitude of D.I. Khan are 31.8424° N, 70.8952° E with an elevation of 165 m. Fields, previously infested with weeds were selected for experiments in the two provinces. The experimental field was divided into two main plots. Deep tillage and conventional tillage were given to main plots. While two nutrients sources nitrogen, phosphorus and potassium (NPK) and farm yard manure (FYM) were allotted to sub plots. NPK is a commercial fertilizer containing nitrogen, phosphorus and potassium at the ratio of 20:10:10. NPK was applied at the rate of 120 kg ha^{-1}. Well rotten and decomposed FYM was applied at the rate of 7.5 tons ha^{-1}. There were eight treatments, assigned to sub-sub plots. Seeds of sugar beet (California) were sown as a single row on the ridges, 45 cm apart. While the plant to plant distance was kept 6-7 inches. A pre-emergence (Pendimethalin) was applied to the soil at proper moisture level at the rate of 0.66 kg active ingredients ha^{-1}. While S-metolachlor was sprayed at the rate of 0.8 kg active ingredients ha^{-1} at pre-emergence. Cauliflower seedlings were transplanted as intercrop in the selected treatments, and pea seeds were sown in the respective treatments. Both sugar beet and pea were transplanted on the same day. The herbicides were applied soon after sowing the seeds. Variety of sugar beet, cauliflower, pea, dose of fertilizers and herbicides were the same at both the locations. Sowing at Mardan was done earlier than D.I Khan because sowing of sugar beet starts earlier at Mardan due to difference in temperature. Experimental field was irrigated as per requirement.

Weeds related variables. A quadrate of 50 x 50 cm size was randomly thrown in each treatment and the weeds inside the quadrate were counted. Average of the quadrates was calculated and the data was converted to the density m^{-2}. Weed density m^{-2} was recorded for comparing the treatments with the control.

Fresh and dry weed biomass (kg ha^{-1}): The above mentioned quadrats were randomly placed in all experimental units and then weeds inside the quadrate were collected from each treatment and finally biomass was recorded by using digital balance to record fresh biomass. The samples collected were dried in an oven and dry weight was recorded. Average of fresh and dry biomass was calculated and recorded in kg ha^{-1}.

Weed identification: All the major weeds considered as potential threat to sugar beet were carefully identified and recorded.

Sugar beet related variables. The root yield of the sugar beet (kg ha^{-1}) was recorded in each plot separately during harvesting and average was calculated to get root yield per hectare.

Sugar yield (ton/ha) was determined by using the following formula:

Sugar yield (tons/ha) = Pol % beet yield (tons/ha) / 100

Statistical analysis. The data recorded for different variables of sugar beet and weeds was converted to the units mentioned in the tables. The data recorded for each location was statistically analyzed separately by using the software (Statistics, version 8). LSD was applied where treatments were significant at p value of 0.05.

RESULTS AND DISCUSSION

Weed density m^{-2}. In all weed management plans weed density is considered as an important factor because higher weed density causes more yield losses, depending on the weed species infesting the crop. The objective of all weed management is to reduce the density of weeds which will ultimately increase the yield of the crop. Our results showed that weed density m^{-2} was not affected by the tillage. In the first year, deep tillage and conventional tillage produced numerically similar values of 35.50, 38.33 weeds m^{-2} at Mardan; 28.92 m^{-2} and 33.17 weeds m^{-2} at D.I Khan. During the sec-

ond year, the values in deep tillage and conventional tillage showed that the weed density at Mardan was 26.95, 33.02 m^{-2} and at D.I Khan 32.52, 37.83 m^{-2}, these were statistically similar (Table 1); although there is a reduction in weed density in deep tillage as compared to conventional tillage. In an analogous study, Ali et al. [12] state that deep tillage system reduces the weed density as compared to conventional tillage system. Data further depicted that like tillage, the nutrients also insignificantly affected the weed density. It was observed that during the first year in Mardan weed density was 36.92 m^{-2} and in the second year it was 31.12 m^{-2} and 28.85 m^{-2} at farmyard manure and NPK treated plots. In D.I Khan during the first year weed density was 30.33 as observed in FYM and 31.75 m^{-2} at places where NPK was used. In the second year, numerical values recorded were 38.64 m^{-2} and 31.70 m^{-2} under FYM and NPK respectively. Our data reveals that the nutrients have significant effect on weed density during the second year.

The weed management treatments have significant effects on the weed density m^{-2} as shown in Table 1. The highest density of weeds was recorded in weedy check plot. At both the locations the highest weed densities of 57.33 m^{-2} and 54.17 m^{-2} were recorded during the first year. In the second year 50.50 m^{-2} and 53.08 m^{-2} densities were recorded in weedy check plots. Similarly, minimum weed density in the first year (22.50 m^{-2}) and (18.67 m^{-2}) was found in Dual gold treated plot. Unlike first year, during the second year lowest weed density was found in two hand weeded plots (15.25 m^{-2}) at Mardan. At D.I Khan the lowest weed density was recorded in Dual gold plots (20.25 m^{-2}) which was statistically close to the treatment where 2 hand weeding was done (25.67 weeds m^{-2}). Similarly in weed control studies Khan et al. [13] have stated that weed density and fresh weed biomass significantly decreases by hand weeding. The herbicide application like hand weeding also effectively controls weed density and biomass [14]. Intercropping of cauliflower and pea produced weed density of 37.50 m^{-2} and 38.17 m^{-2} during the first year and 32.08 m^{-2} and 36.33 m^{-2} in second year at Mardan. While at D.I Khan during the first year weed density recorded was 32.33 m^{-2}, (31.67 m^{-2}) and in second year (37 m^{-2}), (41.91 m^{-2}) at both locations. These values were statistically lower than control and higher than weed density in herbicide and hand weeded treated plots. These results depict that herbicide application is more effective in controlling weeds as compared to intercropping. While intercropping of cauliflower and pea did not control weeds to an acceptable limit.

Fresh weed biomass (kg ha^{-1}). Our data shows that fresh weed biomass was not affected by the tillage during the first year. This feature in deep tillage at Mardan (360.33 kg ha^{-1}) was statistically similar to mean value recorded in conventional tillage (324.33 kg ha^{-1}). While in D.I Khan the mean value recorded for deep tillage was (361.39 kg ha^{-1}) and for conventional tillage (356.67 kg ha^{-1}). However, during the second year tillage had significant effect on fresh weed biomass at Mardan as is clear from the data recorded in deep tillage (317.41 kg^{-1}) and in conventional tillage (357.92 kg^{-1}). The non-significant effects on weed fresh biomass at D.I Khan reveals that values recorded are 318.44 kg ha^{-1} and 341.48 kg ha^{-1} in deep tillage and conventional tillage respectively. Similar results have been reported by Ali et al. [15] who concluded that deep tillage disturbs weed seed bank buried deep in the soil or exposes seeds to the sun. Most of these did not germinate, therefore in deep tillage fresh biomass was less than conventional tillage. Data further reveals that nutrients FYM and NPK applied during the first year also did not affect fresh weed biomass. The mean values recorded at Mardan and D.I Khan for FYM are 327 kg ha^{-1} and 385 kg ha^{-1}; while the same parameter for NPK are 357.67 kg ha^{-1} and 333.06 kg ha^{-1}. It could be inferred from these results that during the first year both the nutrient sources (FYM, NPK) equally supported the weeds and their growth which ultimately produced similar biomass. In the second year nutrients had significant effect on fresh weed biomass at both locations. The mean values of fresh weed biomass recorded at Mardan in farm yard manure and NPK treated plots were 358.24 kg^{-1} and 317.10 kg^{-1}; while at D.I Khan these were 346.33 kg ha^{-1} and 313.58 kg ha^{-1}. Farm yard manure supports weeds as a nutrient source reported by Bajwa et al. [16].

The efficacy of weed control methods was different, depending on the nature of the treatment (Table 1). Our data depicted that weed control treatments significantly affected the fresh weed biomass during both years (Table 1). The mean values of Mardan and D.I Khan Field data in the first year indicated a highest weed biomass (498.67 kg ha^{-1}) and (568.89 kg ha^{-1}), recorded in the control plot (weedy check). During the second year maximum weed density was recorded at Mardan 549.11 kg ha^{-1} followed by D.I Khan 544.33 kg ha^{-1} in control treatments. Our findings are similar to Yaseen et al. [17] who reported that weed check gave the highest values for fresh weed biomass. In first year the lowest fresh weed biomass (229 kg ha^{-1}, 291.11 kg ha^{-1}) was observed in the Dual gold treated plots at Mardan and D.I Khan. During the second year minimum fresh weed biomass was recorded at Mardan (236.92 kg ha^{-1}) in two hand weeded treated plots; whereas at D.I Khan 200.50 kg ha^{-1} values were recorded in Dual gold application plot. Some claim that *S*-metolachlor is effective for weed management in sugar beet. Chikoye et al. [14] who stated that biomass and density of weeds was lowered by herbicide application. Khan et al. [13] report that like herbicides, the weed density and fresh biomass also successfully decrease by

hand weeding. Overall our results show that weed management lowers the fresh weed biomass as compared to control (weedy check). Mean data of the intercropping plots reveals that in both years there is decrease in the fresh weed biomass but it is not significant.

Weed identification. In both seasons the weeds present in the fields belonging to different species and families (Tables 2 and 3) were observed, most of these were broadleaf forms. In both experimental fields perennial as well as annual weeds were recorded. The weeds found in sugar beet field are highly competitive with this crop. Thus weed management in sugar beet crop is an important part of sugar beet crop production. It can be concluded that to avoid losses in sugar beet crop all types of weeds should be controlled. As the sugar beet fields are free of weeds which ultimately give us good return.

TABLE 1
Effect of tillage, nutrients and weed control on weed density and fresh weed biomass

Factors/Treatment	Weed density m^{-2}				Fresh biomass of weeds (kg ha^{-1})			
	First Year		Second Year		First Year		Second Year	
Location	Mardan	D.I Khan	Mardan	D.I Khan	Mardan	D.I Khan	Mardan	D.I Khan
Tillage								
Deep	35.5	28.92	26.95	32.52	360.33	361.39	317.41b	318.44
Conventional	38.33	33.17	33.02	37.83	324.33	356.67	357.92a	341.48
$LSD_{0.05}$	NS	NS	NS	NS	NS	NS	19.73	NS
Nutrients								
FYM	36.92	30.33	31.12a	38.64a	327	385.00a	358.24a	346.33a
NPK	36.92	31.75	28.85b	31.70b	357.67	333.06b	317.10b	313.58b
$LSD_{0.05}$	NS	NS	1.77	6.83	NS	15.2	31.87	26.77
Weed control								
Sugar beet (control)	57.33a	54.17a	50.50a	53.08a	498.67a	568.89a	549.11a	544.33a
Sugar beet + 1 hand weeding	55.50a	45.67b	42.91b	45.75b	484.00a	481.11b	464.22b	484.58b
Sugar beet + 2 hand wedding	25.67cd	24.83c	15.25g	23.75g	273.33c	268.89f	236.92f	205.17f
Sugar beet + Pendimethalin	29.00cd	21.33de	23.41e	31.41e	274.67c	295.56e	272.72e	286.58d
Sugar beet + Cauliflower	37.50b	32.33c	32.08d	37.00d	345.33b	353.33d	332.31d	321.25c
Sugar Beet + Pendimethalin + S-metolachlor	29.67c	19.67de	21.75e	28.25f	272.00c	241.11g	245.78f	244.83e
Sugar beet + Pea	38.17b	31.67c	36.33c	41.91c	361.33b	372.22c	358.83c	352.42c
Sugar beet + S-metolachlor	22.50d	18.67e	17.67f	20.25h	229.33d	291.11e	241.44f	200.50f
$LSD_{0.05}$	6.537	5.626	2.32	2.46	18.104	91.021	21.12	32.99

Values with dissimilar lower-case letters are significantly different at $p<0.05$.

TABLE 2
Major weeds identified in the sugar beet field during the first year

Botanical name	Common name	Family	Life Cycle
Chenopodium album	Lamb's Quarters	Amaranthaceae	Annual
Cirsium arvense	Creeping Thistle	Asteraceae	Perennial
Convolvulus arvensis	Field bind weed	Convolvulaceae	Perennial
Coronopus didymus	Swinecress	Brassicaceae	Annual
Cynodon dactylon	Bermuda grass	Poaceae	Perennial
Euphorbia helioscopia	Sun spurge	Euphorbiaceae	Annual
Fumaria indica	Indian Fumitory	Fumariaceae	Annual
Medicago polymorpha	Burclover	Fabaceae	Annual
Phalaris minor	Canary grass	Poaceae	Annual

TABLE 3
Major weeds identified in the sugar beet fields during the second year

Botanical name	Common name	Family	Life cycle
Anagallis arvensis	Scarlet Pimpernel	Primulaceae	Annual
Chenopodium album	Lamb's Quarters	Amaranthaceae	Annual
Cirsium arvense	Creeping Thistle	Asteraceae	Perennial
Convolvulus arvensis	Field bind weed	Convolvulaceae	Perennial
Coronopus didymus	Swinecress	Brassicaceae	Annual
Cynodon dactylon	Bermuda grass	Poaceae	Perennial
Euphorbia helioscopia	Sun spurge	Euphorbiaceae	Annual
Fumaria indica	Indian Fumitory	Fumariaceae	Annual
Melilotus indica	Sweet clover	Fabaceae	Annual

TABLE 4
Effect of tillage, nutrients and weed control on sugar beet root yield and sugar yield

Factors/ Treatment	Sugar beet yield (ton ha^{-1})				Sugar yield (ton ha^{-1})			
	First Year		Second Year		First Year		Second Year	
Location	Mardan	D.I Khan	Mardan	D.I Khan	Mardan	D.I Khan	Mardan	D.I Khan
Tillage								
Deep tillage	49.95	47.70	54.06a	50.66	7.25	5.69	8.00a	7.50
Conventional	48.34	49.05	48.00b	45.87	7.08	6.28	6.87b	6.62
$LSD_{0.05}$	NS	NS	4.84	NS	NS	NS	0.75	NS
Nutrients								
FYM	48.29	45.51	48.25b	44.68b	7.04	5.47	6.92a	6.41b
NPK	50.01	51.24	53.81a	51.85a	7.29	6.50	7.93b	7.71a
$LSD_{0.05}$	NS	NS	3.77	3.86	NS	NS	0.64	0.68
Weed control								
Sugar beet (control)	29.54e	31.52d	35.83e	31.66f	4.12d	2.93e	4.64g	4.26e
Sugar beet + 1 hand weeding	47.66cd	45.93c	46.41c	45.00c	7.23c	5.30cd	6.42e	6.32c
Sugar beet + 2 hand weedings	63.08ab	57.97a	65.66a	59.75a	8.95ab	8.28ab	10.56a	9.17a
Sugar beet + Pendimethalin	56.00bc	48.52bc	57.08b	53.00b	8.16bc	5.84c	8.15d	7.70b
Sugar beet + Cauliflower	38.08de	42.86c	40.58d	41.33d	5.50d	4.63cd	5.49f	5.86c
Sugar Beet + Pendimethalin + S-metolachlor	53.71bc	56.55ab	59.33b	55.91b	7.85bc	7.40b	8.87c	8.22b
Sugar beet + pea	37.25e	40.50c	39.16d	37.41e	5.24d	4.27de	5.16f	5.26d
Sugar beet + S-metolachlor	67.87a	63.16a	64.16a	62.08a	10.26a	9.22a	10.09b	9.68a
$LSD_{0.05}$	50.201	40.337	2.42	3.30	0.8054	0.7043	0.41	0.55

Values with dissimilar lower-case letters are significantly different at $p<0.05$.

Sugar beet yield (ton ha^{-1}). Root yield is the economic yield and thus is a major concern of the sugar beet growers, higher yield of beet roots gives higher net return to them. The numerical data (Table 4) shows that in the first year deep tillage and conventional tillage both produce statistically similar yield of sugar beet roots both in Mardan as well as D.I Khan, the values are 49.95 tons ha^{-1}, 48.34 tons ha^{-1} and 47.70 tons ha^{-1}, 49.05 tons ha^{-1} respectively. During the first year root production in deep tillage and conventional tillage shows that the soil of the experimental fields was favourable for the growth of sugar beet. During the second year, the tillage had significant effect on root yield at Mardan location as per data recorded- 54.06 tons ha^{-1} for deep tillage, but only 48.00 tons ha^{-1} for conventional tillage. These results comply with those of Schneider et al. [18]. According to these authors the yield of sugar beet increases in deep tillage, it loosens the soil and decreases the penetration resistance. At D.I Khan tillage has nonsignificant effect on sugar beet yield as compared to the values recorded in deep tillage (50.66 tons ha^{-1}), in conventional tillage it was 45.86 tons ha^{-1}. These findings are similar with those of Koch et al. [19]. These workers report that tillage has nonsignificant effect on sugar beet yield.

Like tillage, the nutrient sources (FYM and NPK) also do not affect the sugar beet yield in the first year (Table 4). The values recorded are; 48.29 and 50.01 tons ha^{-1} in FYM and NPK at Mardan, while in D.I Khan the mean values recorded in FYM are 45.51 tons ha^{-1} and in NPK 51.24 tons ha^{-1} respectively. During the second year nutrient sources FYM and NPK also have a nonsignificant effect on sugar beet yield (48.25 tons ha^{-1}) and (53.81 ton ha^{-1}) at Mardan, whereas at D.I Khan nutrient sources have significant effect on root yield (44.68 tons ha^{-1}) and (51.85 tons ha^{-1}) in FYM and NPK respectively. Our results show that the combination of NPK are effective in making the soil suitable for the growth of sugar beet, as such the farmers should use any of these available fertilizers for sugar beet production. An analysis of data shows that different treatments have significant effect on sugar beet yield in both years (Table 4). Higher values of sugar beet root yield in the first year was recorded at both locations in Dual gold treated plots, 67.87 tons ha^{-1} at Mardan and 63.16 tons ha^{-1} at D.I Khan. In the second year maximum root yield is recorded in two hand weeded plots (65.66 ton ha^{-1}) at Mardan and at D.I Khan, same maximum root yield was recorded for dual gold application plots 62.08 tons ha^{-1}. Similarly during both years minimum root yield of 29.5452 tons ha^{-1}, 31.52 tons ha^{-1} and 35.83 ton ha^{-1}, 31.66 tons ha^{-1} was observed in control plots at Mardan and D.I Khan. Root yield is one of the vital characters of sugar beet, which is responsible for determining the total sugar yield per hectare. In an analogous study Bezhin et al. [9] have reported that control of weeds is significantly higher than sugar beet yield. The weed management is an important part for production of sugar beet. In a similar study Vasel et al. [20] state that it is important to control competitive weed species for better sugar beet yield. It was mentioned that in the experimental filed competitive weed species found significantly decrease the sugar beet yield, in view of this in sugar beet weed management is suggested. It was observed that intercropping can suppress the weeds to a minimum level but on the other hand, the beet root yield is

also decreased, therefore farmers may be interested in intercropping but, the industries might be unhappy with intercropping due to decrease in the total production of beet in the area.

Sugar yield (ton ha^{-1}). Getting higher yield of sugar is the major concern of all industries. The climatic condition and environmental factors like different type of varieties, sowing time and cultural practices can affect the sugar content. Like all other studied variables, sugar yield is insignificantly affected by tillage. The mean values presented in Table 4 show that during the first year sugar yield at Mardan location is 7.25 tons ha^{-1} in deep tillage and 7.08 tons ha^{-1} in conventional tillage, at D.I Khan mean values in deep tillage is 5.69 tons ha^{-1} and in conventional tillage 6.28 tons ha^{-1}. In the second year the statistical analysis of the data shows that effect of tillage on sugar yield was significant, mean values recorded at Mardan under deep tillage are 8.00 ton ha^{-1} and under conventional tillage 6.87 ton ha^{-1}. At D.I Khan sugar yield was nonsignificant, mean value of 7.50 tons ha^{-1} was recorded in deep tillage and 6.62 tons ha^{-1} in conventional tillage. Similar results were observed by Niari et al. [24] who concluded that, application of different tillage methods does not affect sugar beet yield and sugar yield. Our results also show that most of the sugar yield was not affected by tillage systems. The nutrient sources in the first year also did not affect sugar yield in sugar beet. The values presented for this variable are statistically similar at both locations, whereas in the second year nutrient sources did affect the sugar yield at both the locations. At Mardan the values recorded for FYM and NPK are 6.92 ton ha^{-1} and 7.93 ton ha^{-1}, at D.I Khan values are 6.41 tons ha^{-1} and 7.71 tons ha^{-1} respectively. In another study Amin et al. [21] concluded that sugar beet yield is higher with the application of nitrogen fertilizer. It can be concluded that plants can easily uptake nitrogen from NPK as a result rapid cell division and cell elongation occurred which leads to increased root yield and also sugar yield.

The weed control methods significantly affect the sugar yield during both years. In the first year highest sugar yield is observed in dual gold application plots. The values recorded in this treatment are 10.26 tons ha^{-1} and 9.22 tons ha^{-1} at Mardan and D.I Khan respectively. In the second year at Mardan the values show that maximum sugar yield for two hand weeded treated plots was 10.56 ton ha^{-1}, but at D.I Khan the highest sugar yield was observed in dual gold application plots 9.68 tons ha^{-1}. Sugar yield obtained during the first year from control plots at Mardan (4.12 tons ha^{-1}) and at D.I Khan (2.93 tons ha^{-1}). Similarly during second year the values recorded for control plots at Mardan are 4.64 ton ha^{-1} and for D.I Khan it was 4.26 tons ha^{-1}. These values are the least among all other treatments. Intercropping is not an effective method to control weeds, if monetary return is not considered. But intercropping of cauliflower and pea does not control the weeds up to that limit in which it did not cause the economic losses. According to Deveikyte et al. [22] sugar beet yield and sugar yield is higher when we control broad leaf weeds effectively in the field. The infestation of weeds in a field of sugar beet crop can greatly decrease sugar yield and root yield. Similarly, Cioni and Maines [23] suggest that weed control and nutrients are integral culture practices and these should be used for growing sugar beet. They suggest that culture practices should be done in sugar beet for controlling weeds which can ultimately lead to an increased root yield and sugar yield.

CONCLUSIONS

In the light of our studies it can be concluded that mostly tillage has nonsignificant effect on sugar beet, however in deep tillage the yield of sugar beet increases because it loosens the soil and decreases penetration resistance. Better growth of sugar beet is found at the plots where NPK is applied as compared to FYM. Herbicide (Dual gold) application proves effective for weed control that consequently leads to better root yield. While hand weeding seems to be laborious and difficult for growers having large area under sugar beet, in intercropping cauliflower and pea in sugar beet can be popularized in the areas where farmers have small land holdings. However, more research is needed for exploring the best possible combinations of the factors. The soil structure and texture are at two different locations. While the efficacy of Dual gold was similar at both these locations, our findings show that this application works effectively in different types of soils. The data related to net income reveals that application of herbicide is economical as compared to other weed management practices. Therefore application of these herbicides and balanced dose of fertilizers are recommended for proper weed management and higher net income in sugar beet.

ACKNOWLEDGEMENTS

The financial support of Higher Education Commission of Pakistan to conduct these studies under research grant No: 4047 is greatly acknowledged. Our thanks also go to the Universities in Pakistan and Turkey for supporting our collaborative efforts towards the completion of this project.

REFERENCES

[1] El-Beltagi, H.S., Mohamed, H.I., Megahed, B.M.H., Gamal, M. and Gehan S.G. (2018) Evaluation of some chemical constituents, antioxidant, antibacterial and anticancer activities of *Beta vulgaris* L. root. Fresen. Environ. Bull. 27, 6369-6378.

[2] Abo-Shady, K.A., Samia, M., Hilal, M.M., El-Sheref and Ibrahim, M.F.M. (2010) Yield and quality of sugar beet crop as affected by irrigation interval, cultivars and potassium fertilization in north delta. Journal of Agriculture Research Kafer El-Sheikh University. 36(4), 361-376.

[3] Ferdous, H.M., Khaliq, Q.A. and Karim, A. (2015) Effect of sowing dates on growth and yield of tropical sugar beet. International Journal of Agronomy and Agriculture Research. 7(1), 53-60.

[4] Marinkovic, B., Crnobarac, J., Jacimovic, G., Latkovic, D., Marinkovic, D., Mirkov, D.V. and Petrovic, C.A. (2015) Sugar beet yield and quality dependence on fertilizing with NPK nutrients. Research Journal of Agricultural Science. 47(1), 90-95.

[5] Iqbal, M.A. and Saleem, A.M. (2015) Sugar beet potential to beat sugarcane as a sugar crop in Pakistan. Americ. Euras. Journal of Agriculture and Environmental Science. 15(1), 36-44.

[6] Kaloi, G.M., Mari, A.H., Zubair, M., Panhwar, R.N., Bughio, N., Junejo, S., Unar, G.S. and Bhutto, M.A. (2014) Performance of exotic sugar beet varieties under agro-climatic conditions of lower Sindh. Journal of Animal and Plant Science. 24(1), 1135-1140.

[7] Usmanikhail, M.U., Tunio, S.D., Jamro, G.H., Oad, F.C., Hassan, S.W., Chachar, Q.D. and Khanzada, M.A. (2013) Effect of intercropping cereals and lentil in sugar beet on yield and monetary benefits. Pakistan Journal of Botany. 45(2), 401-406.

[8] Jalali, A.H. and Salehi, F. (2013) Sugar beet yield as affected by seed priming and weed control. Archives of Agronomy and Soil Science. 59(2), 281-288.

[9] Bezhin, K., Santel, H.J. and Gerhards, R. (2015) Evaluation of two chemical weed control systems in sugar beet in Germany and the Russian Federation. Plant Soil Environment. 61, 489-495.

[10] Rashidi, M. and Abbasi, S. (2011) Influence of different tillage methods on root yield, yield components and some quality characteristics of sugar beet (Beta vulgaris). International Journal of Agriculture and Biology. 13(5), 796-800.

[11] Suthar, S. (2009) Impact of vermicompost and composted farmyard manure on growth and yield of garlic (*Allium sativum* L.) field crop. International Journal of Plant Production. 3(1), 27-38.

[12] Ali, K., Khalil, S.K., Hussain, Z., Munsif, F., Din, I., Waqas, M. and Wagma (2011) Effect of various tillage methods and nitrogen management on weeds and maize performance. Pakistan Journal of Weed Science Research. 17(3), 253-262.

[13] Khan, I., Khan, M.A., Khan, M.I., Saeed, M., Hanif, Z., Khan, S.M. and Ali, M. (2016) Weed management in maize (*Zea mays* L.) through different control strategies. Pakistan Journal of Weed Science Research. 22(1), 25-35.

[14] Chikoye, D., Abaidoo, R. and Fontem, L.A. (2014) Response of weeds and soil microorganisms to imazaquin and pendimethalin in cowpea and soybean. Crop Protection. 65, 168-172.

[15] Ali, K., Munsif, F., Uddin, I., Khan, A. and Khan, N. (2012) Maize penology as affected by tillage practices and nitrogen sources. Agriculture Sciences Research Journal. 2(8), 453-458.

[16] Bajwa, A.A., Anjum, S.A., Nafees, W., Tanveer, M. and Saeed, H.S. (2014) Impact of fertilizer use on weed management in conservation agriculture - A review. Pakistan Journal of Agriculture Research. 27(1), 69-78.

[17] Yaseen, Y., Ullah, W., Ahmad, M., Ali, N.K., Abdullah and Amin, M. (2015) Effect of tillage and weed control methods on weeds density and tomato (*Lycopersicon esculentum*) productivity. Pakistan Journal of Weed Science Research. 21(2), 153-161.

[18] Schneider, F., Don, A., Hennings, I., Schmittmann, O. and Seidel, S.J. (2017) The effect of deep tillage on crop yield-What do we really know? Soil and Tillage Research. 174, 193-204.

[19] Koch, H.J., Dieckmann, J., Büchse, A. and Märländer, B. (2009) Yield decrease in sugar beet caused by reduced tillage and direct drilling. European Journal of Agronomy. 30(2), 101-109.

[20] Vasel, E.H., Ladewig, E. and Marlander, B. (2012) Weed composition and herbicide use strategies in sugar beet cultivation in Germany. Journal of fur Kulturpflan. 64, 112-125.

[21] Amin, G.A., Badr, E.A. and Afifi, M.H.M. (2013) Root yield and quality of sugar beet (Beta vulgaris L.) in response to biofertilizer and foliar application with micronutrients. World Applied Science Journal. 27, 1385-1389.

[22] Deveikyte, I., Seibutis, V., Feiza, V. and Feiziene, D. (2015) Control of annual broadleaf weeds by combinations of herbicides in sugar beet. Zemdirbyste-Agriculture. 102(2), 147-152.
[23] Cioni, F. and Maines, G. (2010) Weed control in sugar beet. Sugar Tech. 12(3), 243-255.
[24] Niari, S.M., Rashidi, M., Mousavi, S.M. and Nazari, M. (2012) Effect of different tillage methods on yield and quality of sugar beet. Middle-East Journal of Science and Research. 12(6), 859-863.

Received: **05.10.2018**
Accepted: **28.01.2020**

CORRESPONDING AUTHOR

Munir Ozturk
Botany Department and
Centre for Environmental Studies,
Ege University,
Izmir – Turkey

e-mail: munirozturk@gmail.com

© by PSP Volume 29 – No. 05/2020 pages 3388-3395 Fresenius Environmental Bulletin

BIOLOGICAL ACTIVITIES OF *URGINEA MARITIMA* L. BAKER

Gulten Okmen*

Department of Biology, Faculty of Science, Mugla Sitki Kocman University, Mugla, Turkey

ABSTRACT

Food-spoilage pathogens threaten human health. Moreover, these pathogens are resistant to antibiotics. Scientists are in search of a new path against these pathogens. In this study, biological activities of plant known as the "ada soğanı" in Turkey was studied and made a contribution to the literature. There are less studies on biological activities of *Urginea maritima* collected from Mugla province. The aim of this study is to determine the antimicrobial, antioxidant and antimutagenic activities of *U. maritima*. *Urginea maritima* from Mugla province were collected for antimicrobial, antioxidant and antimutagenic studies. The antimicrobial activities have been analyzed with the disc diffusion method. A total of eight microorganisms were used in the study, seven of them were bacteria and the other was yeast. Non-enzymatic antioxidant activity tests have been done with the 1,1-diphenyl-2-picrylhydrazyl (DPPH) method. For the antimutagenic activity studies an Ames Test was used. The antimicrobial activity of plant was found effective against food pathogens. The radical scavenging activity of plant was determined as 80 %. In addition, the antimutagenic activities of *U. maritima* were found to be 58.2% for *Salmonella* Typhimurium TA98 and 32.9% for *Salmonella* Typhimurium TA100. These values are high and important. As a result, it can be told that *Urginea maritima* has antimicrobial, antioxidant and antimutagenic capacities. This plant is thought to be a good candidate for new agent searches.

KEYWORDS:
Antimicrobial activity, Antimutagenic activity, Antioxidant activity, Food pathogen, *Urginea*

INTRODUCTION

Increasing antibiotic resistance among human pathogenic bacteria and fungi is becoming a serious challenge and a cause for global concern. Emergence of multidrug-resistant pathogenic strains of bacteria and fungi has caused a high rate of morbidity and mortality among patients. Therefore, there is a need to explore new sources for discovering novel classes of active secondary metabolites that have biological activities against multidrug-resistant bacteria and fungi.

Therefore, this study is intending to explore the potential antimicrobial, antioxidant and antimutagenic activities of the selected medicinal plant *Urginea maritima* (L.) Baker. The plant *U. maritima* is classified as a herb of the Liliaceae family and it is indigenous to the Mediterranean region including Turkey [1]. *Urginea maritima* is known as "ada soğanı" in Koycegiz province in Turkey. *Urginea maritima* is a perennial bulbous geophyte (a herbaceous plant with an underground storage organ) [2], native to the Mediterranean basin and well-adapted to its type of climate [3]. It generally occurs in the slopes of hills, the sandy grounds near the Mediterranean Sea and in certain regions of Northern Africa [4], Middle East and Europe. From the phytochemical point of view, it has been reported that the major constituents of *U. maritima* bulbs are glycosides [5], anthocyanins [6], flavonoids [7], fatty acids, polysaccharides [8] and calcium oxalate [9]. The cardiac glycosides (scillaren and scillarenin) are used in Europe as a cardiotonic diuretic for the treatment of cardiac marasmus and edema [10]. It was expected that this plant inhibited Na+/K+ adenosine triphosphatase [11]. Furthermore, Bayazit and Konar [12] showed that Squill bulb scillioside can reduce the musculoskeletal pains. This plant is traditionally used for treatment of asthma, cancer and cardiac failure [13]. *U. maritima* showed a strong cytotoxic effect against human cervical cell lines [14].

It has been well-known as a medicinal herb for a long time. This plant is known to exert diuretic, cardiotonic properties, treat edema and has been used as a cough syrup [15]. On the other hand, the medicinal and poisonous activities of this plant are indicators for the presence of active phytochemicals. Analyzes of *U. maritima* lead to the identification of many active compounds, such as cardiac steroids, anthocyanins, flavonoids, polysaccharides, and calcium oxalate [16]. It was reported that the bulb and leaf extracts of *U. maritima* have some potential antifungal activity [17, 18]. However, the antibacterial, antioxidant and antimutagenic activities of this plant are still largely unexplored.

Reactive Oxygen Species (ROS) are highly reactive and potentially damaging transient chemical species, created in all cells through various physiological and biochemical processes, as undesirable

metabolic by-products of normal aerobic metabolism [19, 20, 21]. Most ROS, such as superoxide radical ($O^{\bullet -}$), hydroxyl radical ($OH^{\bullet}$), peroxyl radical ($ROO^{\bullet}$), and nitric oxide radical ($NO^{\bullet}$), attack biological molecules, such as proteins, lipids, DNA and RNA leading to cell or tissue damage and injury associated with many diseases, from malignancy to cardiovascular disease and dementia [22]. Antioxidant compounds must be present in biological systems in sufficient concentrations to prevent an accumulation of pro-oxidant molecules, a state known as oxidative stress [23]. Currently used synthetic antioxidants have been suspected to cause or promote negative health effects [24]; hence stronger restrictions have been placed on their application. Therefore, there is a trend to substitute synthetic antioxidants with naturally occurring antioxidants. Recent studies have reported that natural antioxidants [25, 26], obtained from medicinal plants, are protecting against toxic and harmful effects of free radicals [27], and have a wide range of antimicrobial [28, 29, 30], antimutagenic [31], and antiallergic [32], antioxidant [33, 34], radical scavenging activity [35], and anticarcenogenic effects [36].

In this study, a screening of *U. maritima* extracts was conducted with seven test bacteria and one fungus (*Candida albicans*), in order to determine the antimicrobial and antimutagenicity activities of the extracts. Moreover, there is relatively little knowledge and information available concerning the antimicrobial, antioxidant and antimutagenic potential of the plant in general, and in Mugla plants in particular. The objective of this research was to study extracts of *U. maritima*. The evaluation of antioxidant, antimutagenic activities and antibacterial effects of the extracts was also carried out.

MATERIALS AND METHODS

Plant Material. *Urginea maritima* bulb and seeds were picked up from different locations of Koycegiz, Mugla region, Turkey in 2016. Taxonomical identification of the plant was performed by Dr. Neslihan Balpinar (voucher number: 1600) from Burdur Mehmet Akif Ersoy University, Turkey and a specimen was stored in the herbarium. The identity of these specimen was applied by the Flora of Turkey [37]. The bulbs and seeds were cleaned thoroughly two to three times with flowing and sterile distilled water. These materials were dried by air. The plant parts pulverized in a disruptive mill. All of samples were stocked at room temperature. Then the plant parts were stocked at 4 °C until needed for assay.

Plant Extraction. The dried materials (26 g of bulb or seed) were extracted with organic solvent (250 ml of methanol, water) with the Soxhlet apparatus. These materials were evaporated. Then materials were stored in mat bottles. These vials were stored and refrigerated until use (200 mg/mL).

Microorganisms and Cultivation. In this work, *Urginea maritima* extracts were singly tested against food pathogens such as *Bacillus subtilis* RSKK245, *Staphylococcus aureus* RSKK2392, *Salmonella* Typhimurium RSKK19, *Enterococcus faecalis* ATCC8093, *Escherichia coli* ATCC11229, *Listeria monocytogenes* ATCC7644, *Yersinia enterocolitica* NCTC11174 and *Candida albicans* RSKK02029. The bacteria were grown for 24 hours, at 37 °C in Mueller- Hinton Broth (Merck). *C. albicans* was grown for 24 - 48 hours, at 30 °C in Sabouraud Dextrose Broth (Merck). These pathogens were provided from different culture collections. These strains of bacteria and *C. albicans* were obtained from ATCC (American Type Culture Collection, USA), RSKK (Refik Saydam National Type Culture Collection, Turkey) or NCTC (National Collection of Type Cultures).

Antimicrobial Activity Assay. In this study, Kirby-Bauer assay was applied for antibacterial activities. The bacteria were preserved on MHA plates at 37 °C [38]. Bacterial cultures adjusted to 0.5 McFarland. Incubations of bacteria were at 37 °C for 24 hours. The assessment of antibacterial activity was based on measurement of the diameter of the inhibition zones around the discs after 24 hours. We have used methanol and chloramphenicol (30 µg) and nystatin (100 µg) as control in our study. All tests were performed in triplicate and the mean values were given.

Minimum Inhibitory Concentration Assay (MIC). The MICs of plant extracts were measured by broth dilution assay. The MIC values were given as the lowest concentration of plant extracts. The broth dilution assay was done according to CLSI standards [39, 40]. We have used final concentrations of the extract in our work. These concentrations were from 6500 µg/ml to 406.25 µg/ml (6500; 3250; 1625, 812.5, and 406.25 µg/ml).

Determination of Non-Enzymatic Antioxidant Activity. The non-enzymatic antioxidant activity was analyzed using DPPH free radical. The stable DPPH was used for determination of free radical-scavenging activities of the extracts. The extract (0.1 mL) was added to methanol DPPH mixture (0.1 mM). This solution was incubated for 30 minutes and afterwards the absorbance of the solution was measured spectrophotometrically. Methanol was blank. The methanol with DPPH solution was used as a control variable [41]. Additionally, trolox was used as a reference. The free radical scavenging capacity expressed in percentage (%), was calculated from formula.

Antimutagenic Activity Assay. Antimutagenic activities of extracts were done by the *Salmonella*-microsome assay. In this study, *Salmonella* Typhimurium tester strains were used for antimutagenic activity tests. These bacteria were provided from previous studies by Dr. B. N. Ames [42]. In our study, two tester strains were utilized to test the antimutagenicity of *Urginea maritima* extract. These bacteria are *Salmonella* Typhimurium TA98 and TA100. The calculation percentage of antimutagenic activity was done according to [43]. Sodium azide was used as a positive control and methanol as a negative control. Concurrently, a positive control (with mutagen, but no extract was added) and a negative control (no mutagen was added) were also set. The test sample was dissolved in methanol, but the mutagen was dissolved in distilled water. In cytotoxicity experiments, concentrations of the plant extracts were studied as 50000, 25000, 12500 ve 6250 µg/plate. At the end of this study, non-toxic concentrations of the test sample used for investigating were 12500 and 25000 µg /plate. These concentrations were categorized as non-toxic because they showed a well-developed lawn, almost similar size of colonies and no statistical difference in the number of spontaneous revertants in test and control plates.

RESULTS AND DISCUSSION

The antimicrobial activities of water and methanol extracts of *Urginea maritima* were evaluated *in vitro* against eight microorganisms test species, which are known to cause some diseases in foods. Results of antimicrobial activities of used plant extracts against the test bacteria are shown in Table 1. Besides, the inhibition zone diameters of the reference antibiotics and the test microorganisms are shown in Table 1. The results of antibacterial activities were recorded as zone of inhibition in mm, for all the materials used as follows. Results show that all of the extracts have antimicrobial activity. The highest antimicrobial activity was found for the water extract of bulb, in which the inhibition zone was 8 mm. In addition, the aqueous and methanolic extracts of this plant did not determine any anticandidal effects against used yeast. Chloramphenicol and nystatin antibiotics were used as a positive control. Chloramphenicol very strongly inhibited the bacterial growths (Table 1).

Table 2. shows MICs of *Urginea maritima* extracts, obtained by the broth dilution method. Three bacteria showed the lowest sensitivity to extracts of *Urginea maritima* (3250 µg/ml).

The non-enzymatic antioxidant activities of plant extracts were evaluated by the DPHH radical scavenging capacity. Table 3 shows the percent of DPPH radical scavenging capacity with trolox as reference. The aqueous extract showed 80% inhibition at 150 mg/ml concentration. Trolox equivalent value was 2.1 mM/g DW (Table 3).

TABLE 1
Antimicrobial Activities of *Urginea maritima* Extracts against Food Pathogens (200 mg/ml)

Microorganisms	Inhibition zon diameters (mm)					
	Bulb/ methanol	Bulb/ aqueous	Seed/ methanol	Seed/ aqueous	C	N
Bacillus subtilis RSKK245	-	5	-	-	12	nt
Staphylococcus aureus RSKK2392	4	6	4	4	15	nt
Listeria monocytogenes ATCC7644	5	8	6	4	22	nt
Enterococcus faecalis ATCC8093	4	-	-	-	22	nt
Escherichia coli ATCC 1122	-	-	4	4	21	nt
Yersinia enterocolitica NCTC 11174	-	4	-	-	20	nt
Salmonella Typhimurium RSKK19	-	-	3	4	22	nt
Candida albicans RSKK 02029	-	-	-	-	nt	7

C: Chloramphenicol, N: Nystatin, AE: Aqueous Extract, ME: Methanol Extract, nt: not tested, (-): No inhibition

TABLE 2
Minimum Inhibitory Concentrations of *Urginea maritima* Extracts

Bacteria	AE (µg/ml)	ME (µg/ml)
Bacillus subtilis RSKK245 (bulb)	3250	nt
Staphylococcus aureus RSKK2392 (bulb)	3250	3250
Listeria monocytogenes ATCC7644 (bulb)	3250	3250
Yersinia enterocolitica NCTC 11174 (bulb)	3250	3250

AE: Aqueous Extract, ME: Methanol Extract

TABLE 3
DPPH Radical Scavenging Activity of *Urginea maritima* Extracts (150 mg/ml)

Plant part	Extracts					
	EE		ME		AE	
	Scavenging activity (%)	TE	Scavenging activity (%)	TE	Scavenging activity (%)	TE
U. maritima (bulb)	-	-	18.85	0.66	21.8	0.7
U. maritima (seed)	21.07	1.21	1.81	0.3	80.3	2.14

TE: Troloks equivalent (mM/g DW) EE: Ethanol Extract ME: Methanol Extract, AE: Aqueous Extract, DW: Dry weight

The antimutagenic activities of the extracts were evaluated by the "against sodium azide by Ames test" in absence of rat microsomal liver enzyme (-S9). Table 4 and Table 5 show the percent of inhibition. The extract of *Urginea maritima* (25000 µg/plate) was found to have its strongest antimutagenic activity for *Salmonella* Typhimurium TA98. This inhibition value is 58%. *Urginea maritima* extract (12500 µg/plate) showed the highest positive inhibitory effect (46%) for *Salmonella* Typhimurium TA98. The extracts of *Urginea maritima* (at both doses) were found to have its moderate positive inhibitory effect for *Salmonella* Typhimurium TA100 (Table 4 and Table 5).

Medicinal and aromatic plants have proved to be abundant sources of biologically active compounds, many of which have been used as compounds to develop new pharmaceuticals [44]. Microbial resistance to conventional antibiotics has become a major healthcare problem [45]. There are considerable alternative sources of natural antimicrobials derived from medicinal plants with different mode of actions. Medicinal plants are rich in secondary metabolites [46, 47]. Many clinically useful antibiotics are derived from plants [48]. Therefore, there is an urgent need to discover new antimicrobial agents from unexplored plants which may produce secondary metabolites that can control serious bacterial and fungal infections. *Urginea maritima* bulbs and seeds were selected based on their relevant ethnomedical use. In this study, extracts of the plant were tested against eight microorganisms.

Results of antimicrobial activity tests show that the extracts of the plants inhibited the growths of microorganisms and the highest inhibition zone is 8 mm. The aqueous extract of this plant had shown the highest antibacterial activity against *Listeria monocytogenes* (Table 1). Obeidat and Sharab [1] reported that the different extracts of *Urginea maritima* were inhibited by *Staphylococcus aureus*, *Escherichia coli* and *Candida albicans*. These values are high (respectively 28, 25 and 15 mm). In this study, plant extracts were not inhibited by the growth of *Candida albicans* (Table 1). On the other hand, researchers had reported that the bulbs extract of *U. maritima* has some potential antifungal activity [18], and the

TABLE 4
Antimutagenic Activity of *Urginea maritima* Extract (25000 µg/plate)

Test substances	*Salmonella* Typhimurium TA98		*Salmonella* Typhimurium TA100	
	Revertant	% Inhibition	Revertant	% Inhibition
Control	48		121	
Negative control	47		123	
Pozitive control	91		152	
Urginea maritima	38	58.2	102	32.9

TABLE 5
Antimutagenic Activity of *Urginea maritima* Extract (12500 µg/plate)

Test substances	*Salmonella* Typhimurium TA98		*Salmonella* Typhimurium TA100	
	Revertant	% Inhibition	Revertant	% Inhibition
Control	48		121	
Negative control	47		123	
Pozitive control	91		152	
Urginea maritima	49	46.2	112	26.3

leaves extract exhibited moderate to low antifungal activity [17]. Ivancheva et al., [49] attributed these activities to the presence of secoiridoid glucosides, phenylethanoids and flavonoids, contained in the extract. The presence of compounds, such as tannins, flavonoids, proanthocyanidins and phenols in *Urginea maritima* extract, may give credibility to its local use for the management of oxidant related pains. Tannins have been found to have antiviral, antibacterial, anti-parasitic effects, anti-inflammatory, antiulcer and antioxidant property for possible therapeutic applications [50, 51]. Flavonoids, the major group of phenolic compounds, are reported for their antimicrobial, antiviral and spasmolytic activity.

The DPPH˙ system is a stable radical generating procedure. It can be used to assay a large number of samples in a short period of time and is sensitive enough to detect active compounds, even at low concentrations. In the DPPH˙ assay, hydrogen–donating ability is an index of the primary chain-breaking antioxidant. These antioxidants donate hydrogen to free radicals which are then converted to non-radical species and thus inhibit the propagation phase of lipid peroxidation [52, 53]. Consequently, the extracts that showed strong or remarkable activity against DPPH˙ free radical scavenging could have substances, rich in available hydroxyl groups such as flavonoids.

Table 3 shows the percent of DPPH radical scavenging capacity with trolox as reference. The aqueous extract showed 80% inhibition. Jamous et al. [54] reported that antioxidant activity index of this plant was at 0.02. In another study, Mammadov et al. [55] reported that the antioxidant activity of *U. maritima* tuber methanol extract was 66.9%. Raj et al., [56] reported that *Urginea* has flavonoids, it has been confirmed that pharmacological effect of flavonoids is correlating with their antioxidant activities [57, 58, 59]. The result of this study is better than the results obtained from literature. The difference between the results, shown in this study and reports in the literature, could be explained by the difference in the procedure of the assays used. There are many investigations of antioxidant activity of medicinal plant extracts [60, 61, 62, 63, 64, 65]. However, it is difficult to compare the results of these studies unless they are based on the same assay and extraction procedures. A number of factors affect the antioxidant activities in plants. Factors, such as the phase the plant is in (such as blooming, seeding etc.), the extraction technique, the polarity of the solvents, the dryness or freshness of the plant material affect the plant's activity.

In this study, the extract of *Urginea maritima* (25000 µg/plate) was found to have its strongest antimutagenic activity for *Salmonella* Typhimurium TA98. This inhibition value is 58% (Table 4). In determining the antimutagenic potential of a sample, a value smaller than 25% inhibition of the mutagen activity indicates a weak or non-antimutagenic effect, a moderate effect when the value is between 25 and 40% and a strong antimutagenicity when the value is greater than 40% [66]. Bayrak et al. [67] reported that the flower extract of *Lavandula stoechas* (12500 µg/plate) was found to have its highest antimutagenic activity for *Salmonella* Typhimurium TA98 and its inhibition value is 42 %. Different resources have reported that *Urginea maritima* (squill) showed antioxidant and free radical scavenging activities [55], and strong cytotoxic effect against cultured melanoma cell line [68].

CONCLUSION

In conclusion, all of the extracts of *Urginea maritima* tested in the study, was determined to have potential antibacterial activities against food pathogens. Our findings show that *Urginea maritima* has antibacterial activity. We believe that it could be very beneficial in the field of new antibacterial agents of plant origin. Furthermore, aqueous extracts of the plant have a high importance for antioxidant activities. The results obtained in this study show that the extract obtained with various solvents from the *U. maritima* plant is a convenient, natural source of antioxidants and that it can be used in medicine. Additionally, this plant showed antimutagenic properties, which is of high importance. The study suggests that *Urginea maritima*, owing to its antimutagenic property, can be beneficial for prevention of cancer. Further research is required to determine the best antioxidant, antimutagenic and antibacterial agents. So, further investigations of total extracts and their active compounds *in vivo* studies, toxicological and clinical studies are needed to confirm these activities and the safety of them.

ACKNOWLEDGEMENTS

The diagnosis of this plant was done by Dr. Neslihan Balpinar (Burdur Mehmet Akif Ersoy University, Turkey). The author thanks her.

This study was presented as an oral presentation at the International Conference on Science and Technology (ICONST-2018) hold from September 5 to 9, 2018, in Prizren, Kosovo. It was published as an abstract paper in proceedings and abstracts book of the ICONST-2018.

REFERENCES

[1] Obeidat, M., Sharab, A. (2018) Antimicrobial and Anticancer Activities of Extracts from *Urginea maritima* Fruits. African Journal of Traditional, Complementary and Alternative Medicines. 15(1), 74-84.

[2] Bruneton, J. (1996) Poisonous Plants - Plants Dangerous to Humans and Animals. Tec & Doc Lavoisier, Paris. (In French)
[3] Kopp, B., Krenn, L., Draxler, M., Hoyer, A., Terkola, R, Vallaster, P., and Robien, W. (1996) Bufadienolides from *Urginea maritima* from Egypt. Phytochemistry. 42, 513-522.
[4] Bellakhdar, J. (1997) Traditional Pharmacopeia of Morocco. Ibis Press. Paris. (In French).
[5] Krenn, L., Jelovina, M., and Kopp, B. (2000) New Bufadienolides from *Urginea maritima* sensu strictu. Fitoterapia. 71, 126-129.
[6] Vega, F.A., Jalon, G.I., Fernandez, M., and Renedo, J. (1972) Anthocyanins of red squill, *Urginea maritima.* Phytochemistry. 11(9), 2657-2896.
[7] Fernandez, M., Vega, F.A., Arrupe, T., and Renedo, J. (1972) Monocotyledonae Liliaceae Flavonoids of Squill, *Urginea maritima*. Phytochemistry. 11, 1534.
[8] Spies, T., Praznik, W., Hofinger, A., Altmann, F., Nitsch, E., and Wutka, R. (1992) The Structure of the Fructan Sinistrin from *Urginea maritima*. Carbohydrate Research. 235, 221- 230.
[9] Cogne, A.L., Marston, A., Mavi, S., and Hostettmann, K. (2001) Study of Two Plants Used in Traditional Medicine in Zimbabwe for Skin Problems and Rheumatism: *Dioscora sylvatica* and *Urginea altissima*. Journal of Ethnopharmacology. 75, 51-53.
[10] Mitsuhashi, H., Tanaka, O., Nozoe, S., and Nagai, M. (1994) Chemistry of Organic Natural Products. Nankoudou Press. Tokyo, Japan.
[11] Schonfeld, W., Weiland, J., Lindig, C., Masnyk, M., Kabat, M.M., Kurek, A., Wicha, J., and Repke, K.R. (1985) The Lead Structure in Cardiac Glycosides Is 5β, 14β- androstane-3β 14-diol. Naunyn Schmiedeberg's Archives of Pharmacology. 329(4), 414-426.
[12] Bayazit, V. and Konar, V. (2010) Analgesic Effects of Scilliroside, Proscillaridin-A and Taxifolin from Squill Bulb (*Urginea maritima*) on Pains. Digest Journal of Nanomaterials and Biostructures. 5(2), 457-465.
[13] Duke, J.A., Bogenshutz-Godwin, M.J., duCellier, J., and Duke, P.A.K. (2002) Handbook of Medicinal Herbs. Second edition, CRC Press, Boca Raton, USA. 896 pages (in: 693-694).
[14] Merghoub, N., Benbacer, L., Amzazi, S., Morjani, H., El-Mzibri, M. (2009) Cytotoxic Effect of Some Moroccan Medicinal Plant Extracts on Human Cervical Cell Lines. Journal of Medicinal Plants Research. 3(12), 1045-1050.
[15] Bozcuk, H., Özdoğan, M., Aykurt, O., Topcuoglu, F., Özturk, H., Ekinci, D., Karadeniz, A., Mutlu, A., and Burgucu, D. (2011) *Urginea maritima* (L.) Baker (Liliaceae) Extract Induces More Cytotoxicity than Standard Chemotherapeutics in the A549 Non-Small Cell Lung Cancer (NSCLC) Cell Line. Turkish Journal of Medical Sciences. 41, 101-108.
[16] Al-Tardeh, S., Sawidis, T., Diannelidis, B.E., and Delivopoulos, S. (2006) Anatomical Studies on the Adventitious Roots of the Geophytes *Urginea maritima* (L.) Baker. Journal of Biological Research. 5, 61-70.
[17] Abou-Jawdah, Y., Wardan, R., Sobh, H. and Salameh, A. (2004) Antifungal Activities of Extracts from Selected Lebanese Wild Plants against Plant Pathogenic Fungi. Phytopathologia Mediterranea. 43, 377-386.
[18] Khan, I.A. and Abourashed, E.A. (2010) Leung's Encyclopedia of Common Natural Ingredients Used in Food, Drugs, and Cosmetics. John Wiley and Sons. New Jersey, USA.
[19] Smith, M.A., Richey, Harris, P.L., Sayre, L.M., Beckman, J.S., Perry, G. (1997) Widespread peroxynitrite-mediated Damage in Alzheimer's Disease. The Journal of Neuroscience. 17(8), 2653-2657.
[20] Rice-Evans, C. and Miller, N.J. (1994) Total Antioxidant Status in Plasma and Body Fluids. Methods in Enzymology. 234, 279-93.
[21] Rice-Evans, C. (2000) Measurement of Total Antioxidant Activity as a Marker of Antioxidant Staus *in vivo*: Precedures and Limitations. Free Radical Research. 33, 59-66.
[22] Hashim, M.S., Lincy, S., Remya, V., Teena, M. and Anila, L. (2005) Effect of Polyphenolic Compounds from *Coriandrum sativum* on H_2O_2-Induced Oxidative Stress in Human Lymphocytes. Food Chemistry. 92(4), 653-660.
[23] Buettner, G.R. and Schafer, F.Q. (2000) Free Radicals, Oxidants, and Antioxidants. Teratology. 62(4), 234.
[24] Amarowicz, R., Pegg, R.B., Rahhimi-Moghaddam, P., Barl, B. and Weil, J.A. (2004) Free Radical Scavenging Capacity and Antioxidant Activity of Selected Plant Species from Canadian Prairies. Food Chemistry. 84, 551-562.
[25] Balpinar, N., Okmen, G., Vurkun, M. (2019) Antibacterial and Antioxidant Activities of *Vitex agnus-castus* L. against Mastitis Pathogens. Fresen. Environ. Bull. 28(12A), 9731-9737.
[26] Gidik, B., Akar, Z., Can, Z., Sefali, A., Erturk, O. (2019) Determination of Antioxidant, Antimicrobial Activities, Phenolic Compounds of Wild *Rosa* L. Species Bayburt, Turkey. Fresen. Environ. Bull. 28(12A), 9973-9982.
[27] Lobo, V., Patil, A., Phatak, A. and Chandra, N. (2010) Free Radicals, Antioxidants and Functional Foods: Impact on Human Health. Pharmacognosy Reviews. 4(8), 118-126.

[28] Celik, A., Mercan, N., Arslan, İ., Davran, H. (2008) Chemical Composition and Antimicrobial Activities of Essential Oils from *Nepeta cadmea.* Chemistry Natural Compounds. 44, 119.
[29] Celik, A., Herken, E.N., Arslan, I., Özel, M.Z., Mercan, N. (2010) Screening of the Constituents, Antimicrobial and Antioxidant Activity of Endemic *Origanum hypericifolium* O. Schwartz and P.H. Davis. Natural Product Research. 24, 1568.
[30] Sevindik, E., Aydın, S., Apaydın, E., Okan, K., Efe, F. (2019) Antibacterial and Antifungal Activities of Essential Oils from *Laurus nobilis* L. Flowers and Leaves Grown in the West Anatolia Area. Fresen. Environ. Bull. 28(9), 6555-6559.
[31] İkken, Y., Morales, P., Martínez, A., Marín, M.L., Haza, A.I., Cambero, M.I. (1999) Antimutagenic Effect of Fruit and Vegetable Ethanolic Extract against Nitrosamines Evaluated by the Ames Test. Journal of Agricultural and Food Chemistry. 47(8), 3257-3264.
[32] Noguchi, Y., Fukuda, K., Matsushima, A., Haishi, D., Hiroto, M., Kodera, Y., Nishimura, H., Inada, Y. (1999) Inhibition of Df-protease Associated with Allergic Diseases by Polyphenol. Journal of Agricultural and Food Chemistry. 47(8), 2969-2972.
[33] Makasci, A., Mammadov, R., Dusen, O., Isik, H. (2010) Antimicrobial and Antioxidant Activities of Medicinal Plant Species *Ornithogalum alpigenum* Stapf. from Turkey. Journal of Medicinal Plants Research. 4(16), 1637-1642.
[34] Mammadov, R., Düsen, O., Uysal, D., Köse, E. (2009) Antioxidant and Antimicrobial Activities of Extracts from Tubers and Leaves of *Colchicum balansae* Planchon. Journal of Medicinal Plants Research. 3(10), 767-770.
[35] Arslan, I., Celik, A. (2010) Free Radical Scavenging Activities and Essential Oil Analysis of *Salvia cedronella* Boiss. and *Salvia fruticosa* Miller. Journal of Essential Oil Bearing Plants. 13, 545.
[36] Przemysław, S.H., Zbigniew, J., Zastosowanie, R.R. (2003) Liliaceae Farmakoterapi: Application of Plants from Liliaceae family in Pharmacotherapy. Farm Polska. 59, 785.
[37] Davis, P.H. (1965-1988) Flora of Turkey and East Aegean Islands. University Press. Edinburgh, Scotland.
[38] Bauer, A.W., Kirby, W.M., Sherris, J.C. and Turck, M. (1966) Antibiotic Susceptibility Testing by a Standardized Single Disk Method. American Journal of Clinical Pathology. 45(4), 493.
[39] C.L.S.I. (2003) Clinical and Laboratory Standarts Institute: Methods for Dilution Antimicrobial Susceptibility Test for Bacteria that Grow Aerobically- 6th Edition. Approved Standard M7-A. Wayne, Philadelphia, USA.
[40] C.L.S.I. (2006) Clinical and Laboratory Standarts Institute: Performance Standards for Antimicrobial Susceptibility Testing -16th Edition. Informational Supplement, M100-S16. Wayne, Philadelphia, USA.
[41] Brand-Williams, W., Cuvelier, M.E. and Berset, C.L.W.T. (1995) Use of a Free Radical Method to Evaluate Antioxidant Activity. LWT-Food Science and Technology. 28(1), 25-30.
[42] Maron, D.M. and Ames, B.N. (1983) Revised Methods for the *Salmonella* Mutagenicity Test. Mutation Research. 113(3-4), 173-215.
[43] Ong, T.M., Whong, W.Z., Stewart, J. and Brockman, H.E. (1986) Chlorophyllin: a Potent Antimutagen against Environmental and Dietary Complex Mixtures. Mutation Research. 173(2), 111-115.
[44] Gao, X., Xu, Y.X., Divine, G., Janakiraman, N., Chapman, R.A., Gautam, S.C. (2002) Disparate *in vitro* and *in vivo* Antileukemic Effects of Resveratrol, a Natural Polyphenolic Compound Found in Grapes. Journal of Nutrition. 132, 2076-2081.
[45] Alanis, A.J. (2005) Resistance to Antibiotics: Are We in the Post-Antibiotic Era? Archives of Medical Research. 36, 697-705.
[46] Tiwari, S. and Singh, A. (2004) Toxic and Sub-Lethal Effects of Oleadrin on Biochemical Parameters of Freshwater Air Breathing Murrel, *Chant punctatus* (Bloch.). Indian Journal of Experimental Biology. 42, 413-418.
[47] Lewis, K. and Ausubel, F.M. (2006) Prospects of Plant Derived Antibacterials. Nature Biotechnology. 24, 1504-1507.
[48] Gilani, A.H. and Atta-ur, R. (2005) Trends in Ethnopharmacology. Journal of Ethnopharmacology. 100, 43-49.
[49] Ivancheva, S., Nikolova, M. and Tsvetkova, R. (2006) Pharmacological Activities and Biologically Active Compounds of Bulgarian Medicinal Plants. Imperato, F. (Ed.) Research Signpost. Fort, P.O.
[50] Akiyama, H., Fujii, K., Yamasaki, O., Oono, T. and Iwatsuki, K. (2001) Antibacterial Action of Several Tannins against *Staphylococcus aureus*. Journal of Antimicrobial Chemotherapy. 48(4), 487-491.
[51] Ly, L., Liu, S.W., Jiang, S.B. and Wu, S.G. (2004) Tannin Inhibits HIV-1 Entry by Targeting gp41. Acta Pharmacologica Sinica. 25(2), 213-218.
[52] Koleva, I., Van Beek, T., Linssen, J., Groot, A. and Evstatieva, L. (2002) Screening of Plant Extracts for Antioxidant Activity: A Comparative Study on Three Testing Methods. Phytochemical Analysis. 13, 8-17.

[53] Apati, P., Szentmihalyi, K., Kristo, S.T., Papp, I., Vinkler, P., Szoke, E. and Kery, A. (2003) Herbal Remedies of Solidago-Correlation of Phytochemical Characteristics and Antioxi-dative Properties. Journal of Pharmaceutical Biomedical Analysis Drug Analysis. 32(4-5), 1045-1053.

[54] Jamous, R.M., Ebu Zaitoun, S.Y., Husein, A.I., Qasem, I. and Ali-Shtayeh M.S. (2015) Screening for Biological Activities of Medicinal Plants Used in Traditional Arabic Palestinian Herbal Medicine. European Journal of Medicinal Plants. 9(1), 1-13.

[55] Mammadov, R., Makasçı-Afacan, A., Uysal-Demir, D., Görk, Ç. (2010) Determination of Antioxidant Activities of Different *Urginea maritima* (L.) Baker Plant Extracts. Iranian Journal of Chemistry and Chemical Engineering. 29(3), 47-53.

[56] Raj, M.S., Shiva Kameshwari, M.N., Tharasaraswathi, K.J. and Shubharani, R. (2017) Qualitative and Quantitative Analysis of Phytochemicals in Two Different Species of *Urginea*. International Journal of Pharmaceutical and Life Sciences. 8(2), 5433-5438.

[57] Boumerfeg, S., Baghiani, A., Messaoudi, D., Khennouf, S. and Arrar, L. (2009) Antioxidant Properties and Xanthine Oxidase Inhibitory Effects of *Tamus communis* L. Root Extracts. Phytotherapy Research. 23, 283-288.

[58] Adithya E.S., Lakshmi, M.S. and Hephzibah, P. (2013) *In vitro* antioxidant, anti-lipid peroxidation activities and HPLC analysis of methanol extracts from bark and stem of *Mahonia leschenaultia* takeda. Asian Journal of Plant Science and Research. 3(2), 116-126.

[59] Ibraheem, Z.O., Satar, M., Abdullah, N.A., Rathore, H., Tan, Y.C., Uldin, F., Basri, R., Abdullah, M.H. and Edward, J.E. (2014) Antioxidant and Cardio Protective Effect of Palm Oil Leaves Extract (Standardized Ethanolic Fraction) in Rats' Model of Saturated Fats Induced Metabolic Disorders. Pakistan Journal of Pharmaceutical Sciences. 27(1), 1-9.

[60] Chanwitheesuk, A., Teerawutgulrag, A. and Rakariyatham, N. (2005) Screening of Antioxidant Activity and Antioxidant Compounds of Some Edible Plants of Thailand. Food Chemistry. 92(3), 491-497.

[61] Ivanova, D., Gerova, D., Chervenkov, T. and Yankova, T. (2005) Polyphenols and Antioxidant Capacity of Bulgarian Medicinal Plants. Journal of Ethnopharmacology. 96, 145-150.

[62] Tepe, B., Sokmen, M., Akpulat, H.A. and Sokmen, A. (2005a) *In vitro* Antioxidant Activities of the Methanol Extracts of Five *Allium* Species from Turkey. Food Chemistry. 92(1), 89-92.

[63] Tepe, B., Sokmen, M., Akpulat, H.A., Daferera, D., Polissiou, M. and Sokmen, A. (2005b) Antioxidative Activity of Essential Oils of *Thymus sipyleus* subsp. *sipyleus* var. *sipyleus* and *Thymus sipyleus* subsp. *sipyleus* var. *rosulans*. Journal of Food Engineering. 66, 447-454.

[64] Katalinic, V., Milos, M., Kulisic, T. and Jukic, M. (2006) Screening of 70 Medicinal Plant Extracts for Antioxidant Capacity and Total Phenols. Food Chemistry. 94(4), 550-557.

[65] Tepe, B., Akpulat, H.A., Sokmen, M., Daferera, D., Yumrutas, O., Aydin, E., Polissiou, M. and Sokmen, A. (2006) Screening of the Antioxidative and Antimicrobial Properties of The Essential Oils of *Pimpinella anisetum* and *Pimpinella flabellifolia* from Turkey. Food Chemistry. 97(4), 719-724.

[66] Negi, P.S., Jayaprakasha, G.K. and Jena, B.S. (2003) Antioxidant and Antimutagenic Activities of Pomegranate Peel Extracts. Food Chemistry. 80(3), 393-397.

[67] Bayrak, D., Okmen, G., Arslan, A. (2017) The Biological Activities of *Lavandula stoechas* L. against Food Pathogens. International Journal of Secondary Metabolite. 4(3), 270-279.

[68] Sathiyamoorthy, P., Lugasi-Evgi, H., Schlesinger, P., Kedar, I., Gopas, J., Pollack, Y., Golan-Goldhirsh A. (1999) Screening for Cytotoxic and Antimalarial Activities in Desert Plants of the Negev and Bedouin Market Plant Products. Pharmaceutical Biology. 37(3), 188-195.

Received: **12.11.2018**
Accepted: **04.03.2020**

CORRESPONDING AUTHOR

Gulten Okmen
Department of Biology
Faculty of Science
Mugla Sitki Kocman University
Mugla 48000 – Turkey

e-mail: gultenokmen@gmail.com

© by PSP Volume 29 – No. 05/2020 pages 3396-3408 Fresenius Environmental Bulletin

DETERMINATION OF ACC DEAMINASE, NITROGENASE AND ANTAGONISTIC ACTIVITIES OF GRAM NEGATIVE BACTERIA ISOLATED FROM WHEAT FIELDS AND THEIR SALT TOLERANCE

Sukran Kardas, Gulten Okmen*

Mugla Sitki Kocman University, Faculty of Science, Department of Biology, Mugla, Turkey

ABSTRACT

1-aminocyclopropane-1-carboxylate (ACC) deaminase activity is an important marker for bacteria to support plant growth by lowering ethylene levels in plants. The enzyme has been found in limited numbers of bacteria and plays an important role in supporting plant growth and development under environmental stress conditions, by reducing stress induced ethylene production in plants. The aim of this study is to investigate strains with ACC deaminase, nitrogenase and antagonistic activities.

In the present study, bacteria isolated from rhizosphere soils and wheat seedlings from Canakkale were screened for ACC deaminase activity, and eight isolates were determined to be ACC deaminase positive. The results of traditional methods showed that eight bacteria were identified as *Pseudomonas*, *Enterobacter* and *Serratia* strains. ACC deaminase activity was determined by measuring the production of α-ketobutyrate. Nitrogenase activity was analyzed by Acetylene Reduction Assay (ARA).

According to the results, there are some differences in ACC deaminase activities among all strains isolated from wheat fields. ACC deaminase activity was analyzed on eight bacteria. The highest ACC deaminase activity was found on *Pseudomonas* sp. CKB55 (2833 nmol α-ketobutyrate.mg^{-1}.h^{-1}). The highest nitrogenase activity was determined on *Pseudomonas* sp. CKB10 (808 nmol ethylene/ mg.h). In antagonistic activity studies, *Pseudomonas* sp. CKB52 has shown an maximum inhibition zone against *Erwinia caratovora* ECC100, and the zone was 11 mm. Most of the isolates have shown tolerance to 1000 mM NaCl concentration.

It can be said that ACC deaminase- contaning bacteria could be an environment-friendly and promising potential strategy to promote plant growth, alleviate biotic and abiotic stresses and provide sustainable agriculture, especially for ethylene-sensitive plants production. As a conclusion, Gram negative bacteria, isolated from wheat fields, have high ACC deaminase, nitrogenase and antagonistic activities. Additionally, these bacteria have a high salt tolerance.

KEYWORDS:
Bacteria, ACC Deaminase Activity, Nitrogenase Activity, Antagonistic Activity, Salt Tolerance

INTRODUCTION

Today's world population is increasing, and new researches are still going on, in order to obtain higher yields from the unit area in order to ensure the feeding of this population. The purpose of agricultural production is to produce efficient, quality and reliable products. Many commercially produced chemicals are used to increase plant yield and to combat plant diseases. Microorganisms gain resistance against these chemicals and the chemicals cause environmental pollution, therefore negatively affect the plant, animal and human health [1]. Therefore, there is a need for agricultural practices, which do not disrupt the ecological balance of the environment [2].

In our country, which has a rich variety of agricultural products, due to its geographical features and climatic characteristics, the predominant agricultural crops are composed of cereals. Wheat, which is 40% in the field of field crops and is the most cultivated grain, has 225 million hectares of cultivation area in the world, 685 million tons of production and 3038 kg / ha of average yield [3]. There are biotic and non-biotic factors that cause significant losses in wheat yield. Non-biotic stress factors cause an avergage loss of yield of more than 50% of the plant, and the primary cause of loss of agricultural crops in the world [4].

One of the effects of these factors is the accumulation of ions, such as Na^+ and Cl^- in the soil, resulting in salt stress, which negatively affects the growth of the plant. Often salt stress is stimulating the production of ethylene, known to be a stress hormone [5,6]. In recent studies, it has been suggested that normal growth may occur under salt stress in plants, vaccinated with plant growth promoting rhizobacteria (PGPR) which contain ACC deaminase. Ethylene is an important growth hormone that is produced in most plants, expressed as mediators of different reactions and developmental

processes in plants [7, 8]. Ethylene can have both limiting and stimulating effects [7].

PGPRs in the rhizosphere region that stimulate the growth of the plant, because of the presence of ACC deaminase activity and the wide range of domains, such as the application of the chemical is more accurate [9, 10, 11, 12, 13]. These features make the selection of PGPR that exhibit ACC deaminase activity more reliable than other alternatives. ACC deaminase catalyzes the conversion of ACC to α-ketobutyrate and ammonia, by controlling the production of ethylene in the plant [14]. ACC deaminase has been identified in many microbial species, such as Gram-negative bacteria [15, 16], Gram-positive bacteria [17, 18], endophytic bacteria [19, 20], *Rhizobium* [21, 22, 23] and fungi [24, 25]. The researchers first studied ACC deaminase on *Pseudomonas* spp. and, in particular, these studies are based on the aim of reducing the negative effects of stress, by promoting plant growth under stress conditions [26, 27, 28, 29]. Several studies have shown that rhizobacteria exhibiting ACC deaminase activity have an antagonistic effect against microbial pathogens. In these studies, it is a widely used strategy to treat plant seeds and roots with bacteria that stimulate plant growth with ACC deaminase activity and can be used as biocontrols. For example, the damage caused by *Pythium ultimum* in cucumber and *Erwinia carotovora* in potatoes was prevented by the use of biocontrol agents with ACC deaminase activity [15]. Similarly, Yuquan et al. [30] reported that, ACC deaminase activity strains showed strong antagonistic effect against the *Fusarium oxysporum* pathogen [31, 32, 33, 34].

Nitrogen cannot be used directly by biological systems and therefore it is involved in soil and plant systems by biological and chemical fixation [35]. Some microorganisms convert the atmospheric nitrogen (N_2), which cannot be used by plants by biological nitrogen fixation, into the form of NH_4 which can be used with the help of nitrogenase enzyme [36, 37]. The conversion of free nitrogen in the air to ammonia by microorganisms is referred to as nitrogen fixation. Nitrogen, the enzyme that catalyses nitrogen fixation, was first obtained in 1966 by purification from the *Azotobacter vinelandii* by Bulen and Le-Comte [38]. *Clostridium*, *Alcaligenes*, *Pseudomonas*, *Rhizobium*, *Azospirillum*, *Serratia*, *Agrobacterium*, *Xanthomonas*, *Bacillus*, *Enterobacter*, *Klebsiellla*, *Sinorhizobium*, *Acinetobacter*, *Mesorhizobium*, *Bradyrhizobium*, *Azorhizobium*, *Phosphobacteria*, *Glucanacetobacter*, *Burkholderia* species are among the bacteria with high biofertilizer potential [39, 40, 41, 42, 43, 44, 45, 46, 47, 48].

Recent studies show that microbiological factors are the sources that meet the nutrients, needed by the plant as biological fertilizers and plant stimulants. The production of these microorganisms and their metabolites in industrial terms and their use in agriculture is regarded as an environmentally friendly approach in terms of the sustainability of the ecosystem [2]. Therefore, the aim of this study was to determine ACC deaminase, nitrogenase and antagonistic activities of Gram negative bacteria, isolated from wheat fields and to investigate salt tolerances.

MATERIALS AND METHODS

Organisms. The bacteria with ACC deaminase activity were isolated from the samples of wheat seedlings and rhizosphere soil (about 15 cm depth) from Çanakkale / Biga Koruoba Village. The organisms used in the antagonistic activity studies were five microorganisms. These bacteria were *Pseudomonas tomato* Pt52-a, *Agrobacterium vitis*, *Rathayibacter tritici* DSMZ7486, *Rathayibacter iranicus* DSMZ7484, *Erwinia caratovora* subsp. *caratavora* ECC100. All species were obtained from Deutsche Sammlung von Mikroorganismen und Zellkulturen (DSMZ) (Germany) and Plant Protection Central Research Institute (Ankara). The bacteria used in antagonistic activity studies were cultured in Nutrient Broth (NB) (Merck) medium at 37 °C for 24 hours [49]. In this study, *Pseudomonas putida* DSMZ291, which is also used as a positive control, was obtained from the Deutsche Sammlung von Mikroorganismen und Zellkulturen (DSMZ) Culture Collection (Germany). This bacterium was cultured for 24 hours at 37 °C in King B medium.

Sterilization of Plant Surface. All root and leaf samples of the wheat plant were kept in 95% ethyl alcohol for two minutes and kept in 1% sodium hypochlorite (NaOCl) for one minute. It was then rinsed six times with sterile distilled water and prepared for the work [50].

Isolation and Identification of Organisms. After the roots of the wheat seedlings were shaken, 1 g of soil was taken from the soil and the appropriate dilutions were made. Then 100 µl from dilutions was taken to Nutrient Agar (NA) and the inoculations were made by spread plate method and the plates were incubated at 37 °C for 24 hours. Random selections were made from different colonies that developed at the end of the incubation period and after a series of passages, were inoculated into Nutrient agar (NA) medium and stored in refrigerator conditions. Furthermore, the wheat roots and leaves which were subjected to surface sterilization were crushed with the help of mortar and shaken into sterile water. The obtained solution was inoculated into the NA medium and used for isolation. All cultures were examined according to cell morphology and Gram staining characteristics and Gram-negative bacteria were used for the study.

Biochemical tests (Oxidase test, motility test, Glucose fermentation test, H_2S production, lactose fermentation, gelatinase activity, etc.) have been applied on these cultures and identification of these bacteria on the basis of morphological and biochemical assays was performed by Assoc. Prof. Dr. Gulten Okmen [51].

Qualitative Determination of ACC Deaminase Activities of Bacterial Cultures. Gram-negative bacteria, selected for use in the study, were inoculated into the Dwork-Foster medium (DF) and improved in this medium, containing ACC as a single nitrogen source [52, 53, 54]. Cultures were incubated for 24 hours at 37 °C in media containing ACC and, at the end of the incubation period, grown cultures were considered ACC positive.

Optimization of Cultures with ACC Deaminase Activity. Different temperature, pH, shaking speed and time studies were conducted to determine the environmental conditions essential for the best growth of eight bacteria, with ACC deaminase activity.

Effect of Temperature on the Growth of Cultures. All cultures were inoculated into NB media to determine the effect of temperature on bacterial growth. In this study, 25 ml serum bottles that contain 10 ml NB medium have been used. 100 µl of active cultures were inoculated into these flasks at different temperature values (28, 37 and 45° C), followed by incubation for 18 hours (Nüve EN500, Binder USA, Stuart Scientifica UK). At the end of the incubation period, growth was recorded as dry weight (mg/ml). All trials were conducted independently and three parallel.

Effect of pH on the Growth of Cultures. 100 µl active cultures were inoculated into serum flasks, containing 10 ml NB at different pH values (6, 7 and 8). Cultures were allowed to incubate at their optimum temperature for 18 hours. At the end of the incubation period, bacterial growth was determined as dry weight (mg/ml). The pH of the media was adjusted with the aid of pH meter (Thermo, USA) using 1N NaOH and 1N HCl. All trials were conducted independently and three of them parallel.

Effect of Agitation Speed on the Growth of Cultures. All of the isolates were inoculated into NB media at optimal temperature and pH values to determine the effects of shaking speed on the growth of cultures. 100 µl of active cultures were inoculated to the media prepared to be 10 ml of NB in 25 ml serum flasks at different agitation speeds (100, 200 and 300 rpm), and were incubated for 18 hours. At the end of the incubation period, bacterial growth was determined as dry weight (mg/ml). All trials were performed independently and simultaneously.

Effect of Incubation Period on the Growth of Cultures. All cultures were inoculated into NB media at optimal temperature, pH and agitation speed in order to determine the best growth time of bacteria. 100 µl of active cultures were inoculated to the NB medium, which had been prepared as 10 ml NB in 25 ml serum bottles at different time intervals (from one to five days). At the end of the incubation period, the time-dependent growth of the cultures was followed and dry weights (mg/ml) were recorded. All experiments were carried out independently and simultaneously.

Quantitative Determination of ACC Deaminase Activity. 100 µl of active cultures with ACC deaminase activity were inoculated into NB media (10 ml), and the cultures were centrifuged after 24 hours of incubation, under optimum conditions. The pellet was washed two times with physiological saline, then suspended into JNFB (7.5 ml) medium containing 5 mM 1-aminocyclopropane-1-carboxylate (ACC), and the next steps were performed according to [55]. The amount of alpha-ketobutyrate was recorded by measuring the absorbance values at 540 nm. Alpha-ketobutyrate concentrations were calculated from the standard curve. Enzyme activity was expressed in nmol alpha-ketobutyrate/dry weight x hours. *Pseudomonas putida* DSMZ291, known to have ACC deaminase activity, was included in the trial as a positive control.

Effect of Salt Stress on the Growth of Cultures. In this study, to determine the salt tolerance of cultures, all cultures were exposed to different NaCl concentrations (10, 25, 50, 100, 200, 300, 400, 800 and 1000 mM). 100 µl of active cultures were inoculated into the 10 ml of NB medium, with different NaCl concentrations. Cultures were incubated under optimal growth conditions. At the end of the incubation period, the growth of all cultures was determined as dry weight (mg/ml). The experiments were carried out in three parallel ways. In addition, the experiments were performed with positive control organism, *Pseudomonas putida* DSMZ291. At the end of this study, cultures with a high salt tolerance have been included in the next experiments.

Determination of Antagonistic Activity as *in Vitro.* The antagonistic activities of cultures were determined against yield spoilage pathogens, such as *Pseudomonas tomato* Pt52- a (30 °C), *Agrobacterium vitis* (30 °C), *Rathayibacter tritici* DSMZ7486 (30 °C), *Rathayibacter iranicus* DSMZ7484 (30 °C), *Erwinia caratovora* subsp. *carotavora* ECC100 (30 °C). The strains used in the

study were obtained from cultural collections of DSMZ and Central Research Institute of Plant Protection. Cultures used in antagonistic activity studies were activated in NB (Merck) medium at 37 °C for 18 hours and their density was adjusted to 0.5 McFarland. The inoculum ratio of the cultures was set to 100 µl. The active cultures (100 µl) with ACC deaminase activity were inoculated to plates containing Mueller Hinton Agar (MHA). The cultures have been inoculated toward the center from the edge of plate, then the plates were allowed to diffuse for 10 minutes. At the end of this period, the yield spoilage pathogen cultures were inoculated against bacteria with ACC deaminase activity with a 90-degree angle. All of the plates were incubated at 30 °C for 24 hours, and microbial interaction was examined. The antagonistic activity was recorded as an inhibition zone (mm) [56].

Determination of Dry Weight. All cultures developed at the medium for 37 °C for 24 hours were harvested in logarithmic phase. The harvested pellet was filtered through Whatman GF/C filters, with a diameter of 0.45 µm and dried for 24 hours at 50 °C [57].

Determination of Nitrogenase Activity. Nitrogenase activities have been measured to determine the biofertilizer potentials of cultures, known to have ACC deaminase activity. The amount of ethylene was calculated by applying acetylene reduction technique to all cultures [58]. Cultures were developed under optimal environmental conditions, afterwards the vials were closed with plastic plugs and covered with parafilm. 1 ml of acetylene gas was injected into the medium and the cultures were incubated again under the experimental conditions and afterwards 10 µl gas samples were injected to the gas chromatography and its data was read. The results were calculated as nmol ethylene/dry weight x hour (nmol ethylene/mg.h). The gas chromatography (Agilent J6W GC) used during the analyzes was set to following values: DB-1 column and flame ionized detector (FID), the column temperature to 100 °C, the temperature of the injection room to 100 °C and the detector temperature to 120 °C. The pure ethylene gas (99.9%) was used as the standard and the flow rate of the helium gas was adjusted to 1.4 ml / min.

RESULTS

Soil samples from wheat fields were used for the isolation of bacteria with ACC deaminase activity. Cultures grown in suitable media were examined, and colonies, which were developed in different morphological structure and color, were purified by passaging under aseptic conditions. The number of isolates obtained was 61 and 24 of them were Gram-negative and 37 were Gram-positive bacteria. The studies were carried out on Gram-negative bacteria. To determine qualitatively the ACC deaminase activity of the 24 Gram-negative bacteria isolated from wheat fields, a salt medium containing ACC (DF) was used as the only nitrogen source. The ACC deaminase activities of all cultures were determined by inoculation to this medium. The bacteria which showed growth at the end of the incubation period, was evaluated as ACC deaminase positive (Figure 1).

FIGURE 1
Qualitative ACC Deaminase Activities of Gram Negative Bacteria

Considering the results obtained in this study, qualitative ACC deaminase activities of 24 Gram-negative bacteria were investigated and only eight bacteria were found to be ACC positive (Table 1). Biochemical tests were applied to the cultures, in order to identify the eight Gram-negative and bacil bacteria which were determined to be positive for ACC deaminase activity. These tests were applied to the cultures, which include a motility test, IMVIC test, oxidase test, nitrate reduction test, glucose fermentation, fluorescent diffused blue pigment, H_2S production, lactose fermentation, gelatinase activity and urease activity. These cultures were identified after the tests (data not shown).

TABLE 1
Qualitative Results of ACC Deaminase Activities at Gram Negative Bacteria

Isolates	CKB2	CKB5	CKB8	CKB9	CKB10	CKB11	CKB16	CKB13
ACC deaminase activity	-	-	-	+	+	-	-	-
Isolates	CKB17	CKB18	CKB22	CKB25	CKB32	CKB33	CKB37	CKB44
ACC deaminase activity	+	-	-	-	-	+	-	-
Isolates	CKB45	CKB46	CKB49	CKB50	CKB52	CKB55	CKB56	CKB58
ACC deaminase activity	-	+	-	-	+	+	-	+

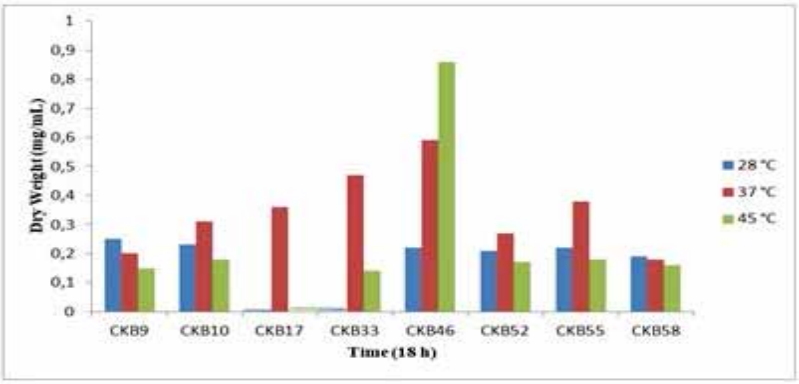

FIGURE 2
Effect of Temperature on the Growth of Cultures with ACC Deaminase Activity

The effects of different environmental factors were investigated, in order to determine the best growth conditions for the eight Gram-negative bacteria with ACC deaminase activity. These are different temperature, pH, agitation speed and time (Figures 2, 3, 4, and 5). The effects of different temperature values (28, 37 and 45 °C) on the growth of eight Gram-negative isolates were investigated. Considering the data obtained at the end of the study, only one isolate was optimally produced at 28 °C, and this bacterium is *Pseudomonas* sp. CKB9. Isolates showing optimum improvement at 37 °C were in total six, which are *Pseudomonas* sp. CKB10, *Enterobacter* sp. CKB17, *Serratia* sp. CKB33, *Pseudomonas* sp. CKB52, *Pseudomonas* sp. CKB55 and *Pseudomonas* sp. CKB58. At 45 °C, only *Pseudomonas aeruginosa* CKB46 could be developed optimally. According to this study, the optimum temperature for 75% of the isolates, was determined as 37 °C (Figure 2).

The effects of different pH values (pH 6, 7, 8) on the growth of isolates were investigated. Considering the data obtained from this study, the number of bacteria showing optimum growth in the application of pH 6 is one, and this bacterium is *Pseudomonas* sp. CKB52. In the application of pH 7, three bacteria showed optimum growth. These are *Serratia* sp. CKB33, *Pseudomonas aeruginosa* CKB46 and *Pseudomonas* sp. CKB58. When the values, obtained as a result of pH 8 application were taken into consideration, it was determined that four bacteria showed optimum growth. These are *Pseudomonas* sp. CKB9, *Pseudomonas* sp. CKB10, *Enterobacter* sp. CKB17 and *Pseudomonas* sp. CKB55. When different pH values were examined, the optimum pH for 50% of the isolates was determined as 8 (Figure 3).

Considering the studies on the effect of different agitation speeds on growth, eight Gram-negative bacteria, with ACC deaminase activity were found to be affected differently. According to this study, the growth of all strains was inhibited at 300 rpm. The highest growth of 200 rpm belongs to *Pseudomonas aeruginosa* CKB46 (2.16 mg/ml). The best growing cultures at 100 rpm were *Pseudomonas* sp. CKB9 (0.41 mg/ml) and *Serratia* sp. CKB33 (0.56 mg/ml). Six of the cultures showed a high growth of 200 rpm applications. Among these, the highest growth belongs to *Pseudomonas aeruginosa* CKB46 with 2.16 mg/ml. Other cultures that showed the best growth of 200 rpm, were *Pseudomonas* sp. CKB10, *Enterobacter* sp. CKB17, *Pseudomonas* sp. CKB52, *Pseudomonas* sp. CKB55 ve *Pseudomonas* sp. CKB58 (Figure 4).

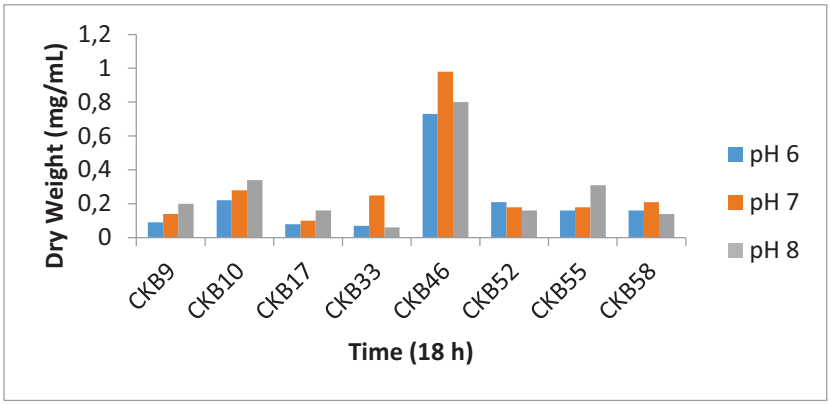

FIGURE 3
Effect of pH on the Growth of Cultures with ACC Deaminase Activity

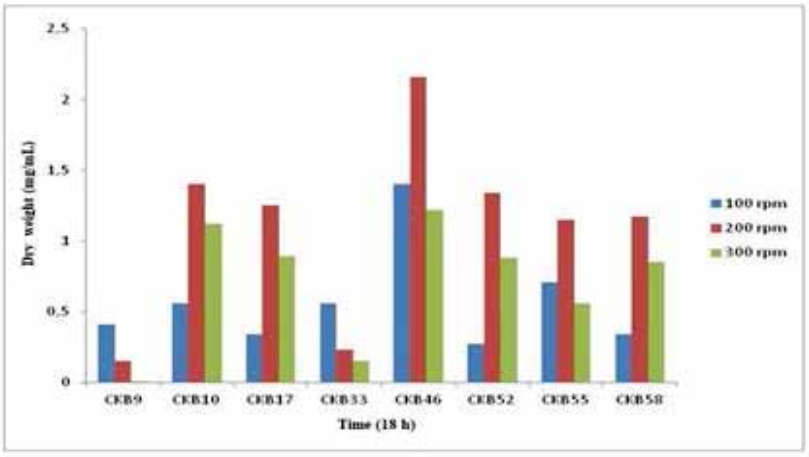

FIGURE 4
Effect of Agitation on the Growth of Cultures with ACC Deaminase Activity

In this study, eight Gram-negative bacteria, isolated from wheat fields and known to have ACC deaminase activity, were allowed to incubate under their optimal conditions (temperature, pH, rpm). The active cultures (100 µl) were inoculated to the prepared media under optimum conditions, and incubated at different time intervals (1, 2, 3, 4, 5 days). At the end of the incubation period, cultures were recorded as dry weight (mg/ml). Considering the data obtained from the study, 63% of the cultures showed optimum growth at the end of the first day, and 12% of the cultures showed the optimum growth at the end of the 4th day. At the end of the first day, the best growth showing cultures were *Pseudomonas* sp. CKB10, *Enterobacter* sp. CKB17, *Pseudomonas aeruginosa* CKB46, *Pseudomonas* sp. CKB52 ve *Pseudomonas* sp. CKB58. Subsequent studies were continued at the optimum growth times and conditions of their cultures (Figure 5).

The active cultures with ACC deaminase activity were inoculated into the NB medium, and these cultures were incubated under their optimal conditions for 24 hours. Then cultures were harvested, and pellets were put into the JNFB medium, that contain 1-aminocyclopropane-1-carboxylate (ACC), and the amount of alpha-ketobutyrate was calculated. The amount of ACC deaminase activity was recorded as nmol α-ketobutyrate.mg^{-1}.h^{-1}. In this study, *Pseudomonas putida* DSMZ291 known to have ACC deaminase activity, was used as a positive control. Considering the data obtained from this study, the highest ACC deaminase activity was determined from *Pseudomonas* sp. CKB55 (2833 nmol α-ketobutyrate.mg^{-1}.h^{-1}). The activity obtained from this culture is higher than *P. putida* DSMZ291 (1975 nmol α-ketobutyrate.mg^{-1}.h^{-1}), which is a positive control. Only 25% of the cultures had high ACC deaminase activity, while 75% of the cultures had less than the control value (Figure 6).

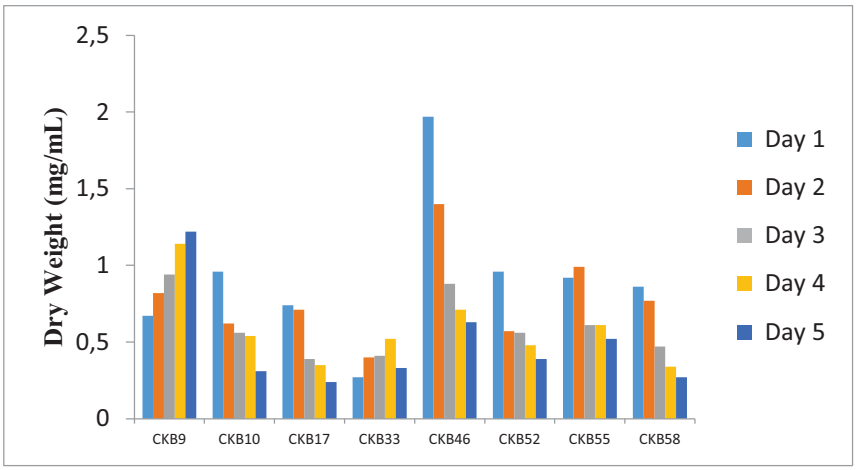

FIGURE 5
Effect of Incubation Period on the Growth of Cultures with ACC Deaminase Activity

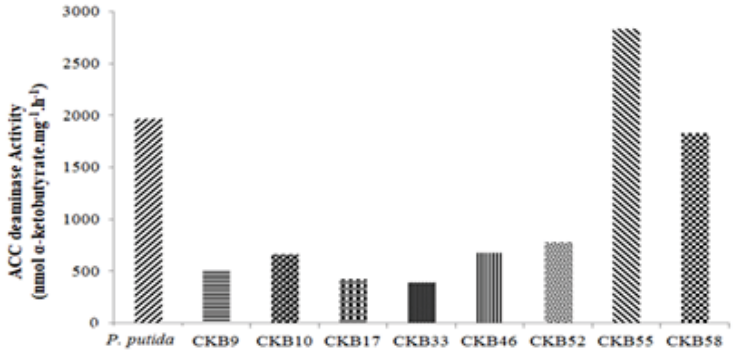

FIGURE 6
Quantitative ACC Deaminase Activities of Cultures

Considering the effects of salt concentrations on the growth of Gram-negative cultures which had ACC deaminase activity, 75% of the isolates were tolerant up to 1000 mM NaCl concentration. The highest amount of biomass was obtained from *Pseudomonas aeruginosa* CKB46 at 400 mM NaCl trial (7.4 mg/ml). It was found out that one culture has evolved up to 800 mM, which is *Serratia* sp. CKB33 (Figure 7). The growth of *Pseudomonas* sp. CKB9 was influenced as suppression at 400 mM salt concentration, although it was initially stimulated from low salt concentrations. On the other hand, growth of *Pseudomonas* sp. CKB10 was stimulated in all salt concentrations, and it was grown at 1000 mM salt concentration. Although the growth of *Enterobacter* sp. CKB17 was stimulated up to the 400 mM salt concentration, its growth was severely suppressed at 800 mM salt. The growth of *Serratia* sp. CKB33 was partially stimulated from the beginning, and this growth was continued up to 300 mM salt concentration, but was severely suppressed at 400 mM. *Pseudomonas aeruginosa* CKB46 is a culture with high adaptation to salt concentrations. The growth up to 400 mM salt concentration had increased in this culture, and the highest biomass was obtained from this bacterium at 400 mM salt concentration (7.4 mg/ml). Also, the culture was increased with high biomass at 800 mM (6.8 mg/ml), but it was suppressed at 1000 mM (4.5 mg/ml). Another tolerant culture is *Pseudomonas* sp. CKB52. The bacterium was partially stimulated up to 800 mM salt concentration, but it was suppressed at 1000 mM salt. Other cultures that can develop at 1000 mM salt concentrations are *Pseudomonas* sp. CKB55 and *Pseudomonas* sp. CKB58 (Figure 7).

As a result of the analyzes on the effect of salt concentrations on growth of the eight Gram-negative bacteria, five cultures for further studies have been selected. These cultures have a high salt tolerance. These cultures were incubated at their optimum conditions, then nitrogenase enzyme activity assays were carried out to investigate the biofertilizer potentials. At the end of study, the highest nitrogenase activity was obtained from *Pseudomonas* sp. CKB10 (808 nmol/mg.h). Furthermore, other cultures with high nitrogenase activity were *Pseudomonas* sp. CKB52 and *Pseudomonas* sp. CKB55. The lowest nitrogenase enzyme activity belongs to *Pseudomonas aeruginosa* CKB46 (Figure 8).

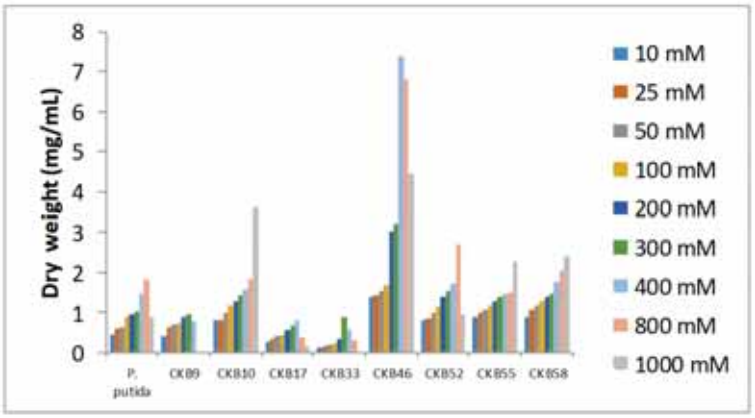

FIGURE 7
Effect of Salt Stress on the Growth of Cultures with ACC Deaminase Activity

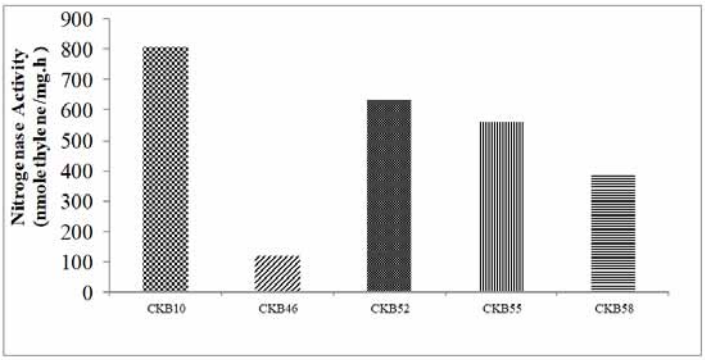

FIGURE 8
Nitrogenase Activities of Cultures

Five Gram-negative bacteria with high salt tolerance were investigated against five yield-spoilage pathogens for antagonistic activity. In this study, *Pseudomonas* sp. CKB52 had the highest antagonistic activity against *Erwinia caratovora* subsp. *caratovora* ECC100 (11 mm). The other high antagonistic activity belongs to *Pseudomonas* sp. This inhibition zone against *Agrobacterium vitis* was 10 mm. Only *Pseudomonas* sp. CKB58 isolate showed low activity against *Pseudomonas tomato* Pt52-a (3 mm). *Pseudomonas tomato* Pt52-a, which breaks the yield, has shown resistance to most cultures. The antagonistic activities of cultures against *Rathayibacter tritici* DSMZ7486 were found to be low. The highest antagonistic activity against *Rathayibacter iranicus* DSMZ7484 was found in *Pseudomonas* sp. CKB52 as 9 mm (Table 2). In another antibacterial activity study, standard antibiotics were used against yield pathogens. In this study, two antibiotics were used as a positive control, being penicillin and gentamicin. The inhibition zone of penicillin was determined against *Rathayibacter tritici* DSMZ7486 and *Rathayibacter iranicus* DSMZ7484, respectively as 28, 26 mm. As a result of the studies using the gentamicin antibiotic, the highest inhibition zone was found against *Erwinia caratovora* subsp. *caratovora* ECC100. This inhibition zone was 21 mm (Table 3).

TABLE 2
Antagonistic Activities of Bacterial Cultures with ACC Deaminase Activity Against Yield-Spoilage Pathogens

Bacteria	Inhibiton zone diameters (mm)				
	R. tritici DSMZ7486	*R. iranicus* DSMZ7484	*A. vitis*	*E. caratovora* ECC100	*P. tomato* Pt52-a
Pseudomonas sp. CKB10	4	-	10	5	-
Pseudomonas aeruginosa CKB46	4	-	3	4	-
Pseudomonas sp. CKB52	5	9	8	11	-
Pseudomonas sp. CKB55	2	2	-	-	-
Pseudomonas sp. CKB58	3	-	-	-	3

TABLE 3
Antibiotic resistance profiles of yield spoilage pathogens

Pathogens	Inhibiton zone diameters (mm)	
	P	GE
R. tritici DSMZ7486	28	nt
R. iranicus DSMZ7484	26	nt
A. vitis	nt	21
E. caratovora ECC100	nt	19
P. tomato Pt52-a	nt	19

P: Penicillin (10μg); GE: Gentamicin (10 μg); nt: not tested

DISCUSSIONS

The growth of plants and agricultural demands are severely affected from non-biotic stress. The regulation of ethylene levels in plants by bacterially produced ACC deaminase, is an important feature that can affect the physiology of the host plant. In soils with drought stress, drought-tolerant ACC deaminase-producing microorganisms can reduce stress on plants by reducing ethylene production, thus facilitating growth and development of plants [59]. Wang et al., [60] reported that soil microbial community structure varies under different tillage managements, especially in the 0-10 cm layer.

As a result of our studies, *Pseudomonas aeruginosa* CKB46 has showed an optimum growth at 45 °C (Figure 2), pH 7 (Figure 3), 200 rpm (Figure 4). Sivaprakasam et al. [61] reported that *Pseudomonas aeruginosa* has shown optimum growth at pH 7.5 and 160 rpm. In another study, it was reported that *Pseudomonas aeruginosa* UD-5 isolates showed optimum growth at 40 ˚C [62]. These results are similar with our work.

The highest ACC deaminase activity was determined from *Pseudomonas* sp. CKB55 (2833 nmol α-ketobutyrate.mg^{-1}.h^{-1}), and this value is higher than the value of *Pseudomonas putida* (Figure 6). Li et al. [63] have reported that *Pseudomonas* species have ACC deaminase activity. Ghyselinck et al. [64] stated that the ACC deaminase activity of *Pseudomonas* sp. R43582 was 310 nmol α-ketobutyrate.mg^{-1}.h^{-1}. In another study, ACC deaminase activity for *Pseudomonas* strains were given differently [55]. A similar study was conducted by Grichko and Glick [65]. In their study, *P. putida* ATCC17399 have ACC deaminase activity, and the value was 3.8 μmol.mg^{-1} protein.h^{-1}. In another research, the ACC deaminase activity of *Bacillus subtilis* HYT-12-1 was reported as 112 nmol α-ketobutyrate.mg^{-1}.h^{-1} [66]. The results obtained from our study were found to be higher than the data obtained from the literature, and the studies in the literature support our results.

As a result of our studies, *Pseudomonas aeruginosa* CKB46 was found to be tolerant to high salt concentrations (Figure 7). Different researchers reported that *Pseudomonas aeruginosa* was tolerant to high salt concentrations, too [61, 62]. These studies support our results.

As a result of nitrogenase activity studies, the highest nitrogenase activity was found at *Pseudomonas* sp. CKB10 (808 nmol/mg.h) (Figure 8). Han et al. [67] reported that the nitrogenase activity of *Pseudomonas stutzeri* was at 1400 nmol ethylene/mg protein/h. Borowiak et al. [68] reported that soil bacteria have various enzyme activities. Our findings are similar to these results.

The analysis of the antagonistic activities of cultures, isolated from wheat fields, that have ACC deaminase activity showed the following results. The highest antagonistic activity of *Pseudomonas* sp. CKB52 was found against *Erwinia caratovora* ECC 100 (11 mm) (Table 2). Weller [69] reported that fluorescent *Pseudomonas* strains were among the most effective root bacteria against soil pathogens. Algeblawi and Adam's study [70] reported that all of the bacteria (*Pseudomonas fluorescens, Bacillus thuringiensis, Bacillus subtilis*) showed antagonistic activity against *Erwinia caratovora*. In many studies, researchers reported that different bacteria shown antagonistic activity against various crop pathogens [71, 72].

CONCLUSIONS

Pseudomonas species are known to be microorganisms capable of metabolizing natural and synthetic organic compounds. These bacteria show a very wide spread at the plants and animals. They are valuable for plant growth because they have a lot of ecological diversity, have simple nutrient requirements and are capable of metabolizing a wide range of organic compounds. Therefore, it is thought that *Pseudomonas* will play an important role in the growth of plants in stressed soils.

As a result, *Pseudomonas aeruginosa* CKB46 had the highest tolerance to all NaCl concentrations and also showed other biological activities. We suggest that this bacterium can be used for sustainability in agriculture in all saline areas up to 1000 mM NaCl concentration. We believe that this bacterium contributes to sustainable agriculture because of its potential to reduce stress of the plant, its biofertilizer potential and its antagonistic activity against product pathogens. In future studies, it is necessary to analyze the growth of these bacteria, isolated from wheat fields under conditions of various organic pollutants, also to investigate the genome structures of isolates, with high activity and consequently, after the determination of gene expression of tolerant genera, studies are needed to transfer the gene of the plants.

ACKNOWLEDGEMENTS

This work was supported by Mugla Sitki Kocman University Scientific Research Project (BAP /2015-034). Authors thank Mugla Sitki Kocman University.

This study was presented as an oral presentation at the International Conference on Science and Technology (ICONST-2018) hold from September 5 to 9, 2018, in Prizren, Kosovo. It was published as an abstract paper in proceedings and abstracts book of the ICONST-2018.

This study is a part of Master Science thesis.

REFERENCES

[1] Avis, T.J., Gravel, V., Antoun, H. and Tweddell, R.J. (2008) Multifaceted Beneficial Effects of Rhizosphere Microorganisms on Plant Health and Productivity. Soil Biol Biochem. 40, 1733-1740.

[2] Küçük, Ç. and Güler, İ. (2009) Some Biocontrol Microorganisms That Promote Plant Growth. Electronic Journal of Microbiology TR. 7(1), 30-42. (In Turkish)

[3] FAO, (2012) FAO Statistical Yearbook, 2012. World Food and Agriculture. http://www.fao.org/3/i2490e/i2490e03a.pdf. Access Date: 18.03.2020.

[4] Bray, E.A., Bailey-Serres, J. and Weretilnyk, E. (2000) Responses to Abiotic Stresses. In: Buchanan, B., Gruissem, W. and Jones, R., (eds.) Biochemistry and Molecular Biology of Plants. Rockville, MD: ASPB.

[5] Cuartero, J. and Fernandez-Munoz, R. (1999) Tomato and Salinity. Sci. Hortic. 78, 83-125.

[6] Blumwald, E. (2000) Sodium Transport and Salt Tolerance in Plants. Curr Opin Cell Biol. 12, 431-434.

[7] Arshad, M. and Frankenberger, W.T. (2002) Ethylene: Agricultural Sources and Applications. Kluwer Academic Publisher, New York.

[8] Belimov, A.A., Safronova, V.I. and Mimura, T. (2002) Response of Spring Rape (*Brassica napus* var. *oleifera* L.) to Inoculation with Plant Growth Promoting Rhizobacteria Containing 1-aminocyclopropane-1-carboxylate Deaminase Depends on Nutrient Status of the Plant. Can. J. Microbiol. /Rev. Can. Microbiol. 48, 189-199.

[9] Tabor, C.W. and Tabor, H. (1985) Polyamines in Microorganisms. Microbiol Rev. 49, 81-99.

[10] Frankenberger, W.T. and Arshad, M. (1995) Phytohormones in Soil: Microbial Production and Function. Marcel Dekker, New York.

[11] Patten, C.L. and Glick, B.R. (2002) Role of *Pseudomonas putida* Indole-acetic Acid in Development of the Host Plant Root System. Appl. Environ. Microbiol. 68, 3795-3801.

[12] Zahir, Z.A., Arshad, M. and Frankenberger, W.T. (2004) Plant Growth Promoting *Rhizobacteria*: Applications and Perspectives in Agriculture. Adv. Agron. 81, 97-168.

[13] Çakmakçı, R., Dönmez, M.F. and Erdoğan, Ü. (2007) The Effect of Plant Growth Promoting Rhizobacteria on Barley Seedling Growth, Nutrient Uptake, Some Soil Properties, and Bacterial Counts. Turkish J. Agric. For. 31, 189-199.

[14] Honma, M. and Shimomura, T. (1978) Metabolism of 1-aminocyclopropane-1-carboxylic Acid. Agric. Biol. Chem. 42, 1825-1831.

[15] Wang, C.K.E., Glick, B.R. and Defago G. (2000) Effect of Transferring 1-aminocyclopropane-1-carboxylic Acid (ACC) Deaminase Genes into *Pseudomonas fluorescens* Strain CHA0 and Its gacA Derivative CHA96 on their Growth-promoting and Disease-suppressive Capacities. Can. J. Microbiol. 46, 898-907.

[16] Babalola, O.O., Osir, E.O., Sanni, A.I., Odhaimbo, G.D. and Bulimo, W.D. (2003) Ampliflacation of 1-aminocyclopropane-1-carboxylic (ACC) Deaminase from Plant Growth Promoting Rhizobacteria in Striga-infested Soils. Afr. J. Biotechnol. 2, 157-160.

[17] Belimov, A.A., Safronova, V.I., Sergeyeva, T.A., Egorova, T.N., Matveyeva, V.A., Tsyganov, V.E., Borisov, A.Y., Tikhonovich, I.A., Kluge, C., Preisfeld, A., Dietz, K.J. and Stepanok, V.V. (2001) Characterization of Plant Growth Promoting *Rhizobacteria* Isolated from Polluted Soils and Containing 1-aminocyclopropane-1-carboxylate Deaminase. Can. J. Microbiol. 47, 242-252.

[18] Ghosh, S., Penterman, J.N., Little, R.D., Chavez, R. and Glick, B.R. (2003) Three Newly Isolated Plant Growth-Promoting Bacilli Facilitate the Seedling Growth of Canola, *Brassica campestris*. Plant Physiol. Biochem. 41, 277-281.

[19] Pandey, P., Kang, S.C. and Maheshwari, D.K. (2005) Isolation of Endophytic Plant Growth Promoting *Burkholderia* sp. MSSP from Root Nodules of *Mimosa pudica*. Curr. Sci. 89, 170-180.

[20] Sessitsch, A., Coenye, T., Sturz, A.V., Vandamme, P., Barka, E., Wang- Pruski, G., Faure, D., Reiter, B., Glick, B.R. and Nowak, J. (2005) *Burkholderia phytoflrmins* sp. nov., a Novel Plant-associated Bacterium with Plant Beneficial Properties. Int. J. Syst. Evol. Microbiol. 55, 1187-1192.

[21] Ma, W., Sebestianova, S., Sebestian, J., Burd, G.I., Guinel, F. and Glick, B.R. (2003) Prevalence of 1-aminocyclopropaqne-1-carboxylate in Deaminase in *Rhizobia* spp. Antonie Van Leeuwenhoek. 83, 285-291.

[22] Uchiumi, T., Oowada, T., Itakura, M., Mitsui, H., Nukui, N., Dawadi, P., Kaneko, T., Tabata, S., Yokoyama, T., Tejima, T., Saeki, K., Oomor, H., Hayashi, M., Maekawa, T., Sriprang, R., Murooka, Y., Tajima, S., Simomura, K., Nomura, M., Suzuki, A., Shimoda, S., Sioya, K., Abe, M. and Minamisawa, K. (2004) Expression Islands Clustered on Symbiosis Island of *Mesorhizobium loti* Genome. J. Bacteriol. 186, 2439-2448.

[23] Stiens, M., Schneiker, S., Keller, M., Kuhn, S., Pühler, A. and Schlüter, A. (2006) Sequence Analysis of the 144-kilobase Accessory Plasmid Psmesm11a, Isolated from a Dominant *Sinorhizobium meliloti* Strain Identified during a Long-term Weld Release Experiment. Appl. Environ. Microbiol. 72, 3662-3672.

[24] Minami, R., Uchiyama, K., Murakami, T., Kawai, J., Mikami, K., Yamada, T., Yokoi, D., Ito, H., Matsui, H. and Honma, M. (1998) Properties, Sequence, and Synthesis in *Escherichia coli* of 1-aminocyclopropane- 1-carboxylate Deaminase from *Hansenula saturnus.* J. Biochem. (Tokyo). 123, 1112-1118.

[25] Jia, Y.J., Kakuta, Y., Sugawara, M., Igarashi, T., Oki, N., Kisaki, M., Shoji, T., Kanetuna, Y., Horita, T., Matsui, H. and Honma, M. (1999) Synthesis and Degradation of 1-aminocyclopropane-1-carboxylic Acid by *Penicillium citrinum*. Biosci. Biotechnol. Biochem. 63, 542-549.

[26] Belimov, A.A., Hontzeas, N., Safronova, V.I., Demchinskaya, S.V., Piluzza, G., Bullitta, S. and Glick, B.R. (2005) Cadmium-tolerant plant Growth-promoting Bacteria Associated with the Roots of Indian Mustard (*Brassica juncea* L. Czern.). Soil. Biol. Biochem. 37, 241-250.

[27] Hontzeas, N., Richardson, A.O., Belimov, A.A., Safranova, V.I., Abu-Omar, M.M. and Glick, B.R. (2005) Evidence for Horizontal Gene Transfer (HGT) of ACC Deaminase Genes. App Environ Microbiol. 71, 7556-7558.

[28] Blaha, D., Prigent-Combaret, C., Mirza, M.S. and Moënne-Loccoz, Y. (2006) Phylogeny of the 1-aminocyclopropane-1- Carboxylic Acid Deaminase-encoding Gene acdS in Phytobeneficial and Pathogenic Proteobacteria and Relation with Strain Biogeography. FEMS Microbiol. Ecol. 56, 455-470.

[29] Madhaiyan, M., Poonguzhali, S., Ryu, J. and Sa, T. (2006) Regulation of ethylene levels in canola (*Brassica campestris*) by 1-aminocyclopropane- 1-carboxylate Deaminase-containing *Methylobacterium fujisawaense*. Planta. 224, 268-78.

[30] Yuquan, X., Rong, S. and Zhixing, L. (1999) Quickly Screening a Strain of *Pseudomonas* B8 with both ACC Deaminase Activity and Antagonism against *Fusarium oxysporum*. Journal of Shanghai Jiaotong University. 33(2), 206-209.

[31] Liang, Y., Di, Y., Zhao, J. and Ma, D. (1990) A biotype 3 strain of *Agrobacterium radiobacter* Inhibits Crown Gall Formation on Grapevine. Acta Microbiologica Sinica. 30, 165-171.

[32] Bell, C.R., Dickie, G.A. and Chan, J.W.Y.F. (1995) Variable Response of Bacteria Isolated from Grapevine Xylem to Control Grape Crown Gall Disease in Planta. Am. J. Enol. Vitic. 46, 499-508.

[33] Chen, Y., Mei, R., Lu, S., Lui, L. and Kloepper, J.W. (1996) The Use of Yield Increasing Bacteria (YIB) as Plant Growth-promoting Rhizobacteria in Chinese Agriculture. In: Utkhede, R.S. and Grupta, V.K. (eds.) Kalyani Publishers, New Delhi, India.

[34] Kawaguchi, A., Inoue, K. and Nasu, H. (2005) Inhibition of Crown Gall Formation by *Agrobacterium radiobacter* Biovar 3 Strains Isolated from Grapevine. J. Gen. Plant. Pathol. 71, 422-430.

[35] Jensen, E.S. and Nielsen, H.H. (2003) How Can Increased Use of Biological N_2 Fixation in Agriculture Benefit the Environment. Plant. Soil. 252, 177-186.

[36] Glick, B.R. (1995) The Enhancement of Plant Growth by Fee-living Bacteria. Can. J. Microbiol. 41, 109-117.

[37] Lucy, M., Reed, E. and Glick, B.R. (2004) Aplications of Free Living Plant Growth-Promoting Rhizobacteria. Antonie van Leeuwenhoek. 86, 1-25.

[38] Bulen, W.A. and Le Comte, J.R. (1966) Proceedings of the National Academy of Science of the United States of America. 56, 979.

[39] Rodriguez, H. and Fraga, R. (1999) Phosphate solubilizing Bacteria and their Role in Plant Growth. Biotechnology Advances. 17, 319-339.

[40] Sturz, A.V. and Nowak, J. (2000) Endophytic Communities of *Rhizobacteria* and the Strategies Required to Create Yield Enhancing Associations with Crops. Applied Soil Ecology. 15, 183-190.

[41] Bloemberg, G.V., Lugtenberg, B.J.J. (2001) Molecular Basis of Plant Growth Promotion and Biocontrol by *Rhizobacteria*. Curr. Opin. Plant Biotech. 4, 343-350.

[42] Eşitken, A., Karlıdağ, H., Erçişli, S., Turan, M. and Şahin, F. (2003) The Effect of Spraying a Growth Promoting Bacterium on the Yield, Growth and Nutrient Element Composition of Leaves of Apricot (*Prunus armeniaca* L. cv. Hacıhaliloğlu). Aust J Agric Res. 54, 377-380.

[43] Khalid, A., Arshad, M. and Zahir, Z.A. (2003) Growth and Yield Response of Wheat to Inoculation with Auxin Producing Plant Growth Promoting Rhizobacteria. Pakistan J. Bot. 35(4), 483-498.

[44] Çakmakçı, R. and Erdoğan, Ü.G. (2005) Organic Farming. Ataturk Univ. Ispir Hamza Polat Vocational School. Erzurum, Turkey. (In Turkish)

[45] Samuel, S. and Muthukkaruppan, S.M. (2011) Caharacterization of Plant Growth Promoting Rhizobacteria and Fungi Associated with Rice, Mangrove and Effluent Contaminated soil. Current Botany. 2(3), 22-25.

[46] Çakmakçı, R., Ertürk, Y., Dönmez, M.F., Erat, M., Kutlu, M., Sekban, R. and Haznedar, A. (2012) The effect of N_2-fixing and P-solubilizing Bacteria on Turkish Tea Clone Muradiye 10 Growth, Yield and Nutrient Uptake. TABAD. (2), 176-181. (In Turkish)

[47] Neiverth, A., Delai, S., Garcia, D.M., Saatkamp K., deSouza, E.M., Pedrosa, F.O., Guimaraes, V.F., dosSantos, M.F., Vendruscolo, E.C.G. and daCosta, A.C.T. (2014) Performance of Different Wheat Genotypes Inoculated with the Plant Growth Promoting Bacterium *Herbaspirillum seropedicae.* Eur. J. Soil Biol. 64, 1-5.

[48] Bhattacharya, C. and Pandey B. (2015) Isolation and Characterization of *Rhizobium* Species and Its Effect on Growth on Monocot Plant Used as Biofertilizer Chitra. International Journal of Research. 2(1), 597-604.

[49] Altundağ, Ş., Karahan, A., Aksu, P., ve Kılınç, A.O. (2010) Investigation of Antibacterial Effect of *Satureja cuneifolia* Ten. Essential Oil on Some Wheat Pathogenic Bacteria under in *invitro* Conditions. Plant Protection Bulletin. 50, 25-33. (In Turkish)

[50] Öğüt, M., Er, F. and Kandemir N. (2008) Morphological Properties of the *Azospirillum* Strains Isolated from Tokat Region's Soils. Journal of Selcuk University Faculty of Agriculture. 22(45), 66-73. (In Turkish)

[51] Raj, A., Khess, N., Pujari, N., Bhattacharya, S., Das, A. and Rajan, S.S. (2012) Enhancement of Protease Production by *Pseudomonas aeruginosa* Isolated from Dairy Effluent Sludge and Determination of its Fibrinolytic Potential. Asian Pac. J. Trop. Biomed. 2(3), 1845-1851.

[52] Dworkin, M. and Foster, J.W. (1958) Experiments with Some Microorganisms Which Utilize Ethane and Hydrogen. J. Bacteriol. 75(5), 592-603.

[53] Brown, C.M. and Dilworth, M.J. (1975) Ammonia Assimilation by *Rhizobium* Cultures and Bacteroids. J. Gen. Microbiol. 86, 39-48.

[54] Opelt, K., Chobot, V., Hadacek, F., Schönmann, S., Eberl, L. and Berg, G. (2007) Investigations of the Structure and Function of Bacterial Communities Associated with *Sphagnum mosses*. Environ. Microbiol. 9(11), 2795-2809.

[55] Shrivastava, U.P. and Kumar, A. (2013) Characterization and Optimization of 1-aminocyclopropane-1-carboxylate Deaminase (ACCD) Activity in Different Rhizospheric PGPR along with *Microbacterium* sp. Strain ECI-12A. Int J Appl Sci Biotechnol. 1(1), 11-15.

[56] Madigan, M.T., Martinko, J.M. and Parker, J. (1997) Brock Biology of Microorganisms. Prentice-All Int. Ltd., London.

[57] Cappuccino, J.G. and Sherman, N. (2001) Microbiology a Laboratory Manual. Benjamin Cummings, Francisco.

[58] Burlage, R.S., Atlas, R., Stahl, D., Geesey, G. and Sayler, G. (1998) Techniques in Microbial Ecology. Oxford University Press, America.

[59] Glick, B.R., Penrose, D.M. and Li, J. (1998) A Model for the Lowering of Plant Ethylene Concentrations by Plant Growth-promoting bacteria. J Theor Biol. 190, 63-68.

[60] Wang, Y., Hu, C., Dong, W. (2011) Relationship between Soil Nutrients and Soil Microbial Biomass, Structure and Diversity under Different Tillage Management in Wheat-corn Double-cropping System. Fresen. Environ. Bull. 20(7), 1721-1728.

[61] Sivaprakasam, S., Surianarayanan, M., Sudharshan, S. and Susheela, R. (2008) Biological Treatment of Tannery Wastewater by Using Salt-Tolerant Bacterial Strains. Microbial Cell Factories. 7(15), 1-7.

[62] Ulhas, P. and Ambalal, C. (2011) Optimal Production of Alkaline Protease from Solvent-tolerant Alkalophilic *Pseudomonas aeruginosa* MTCC7926. Indian Journal of Biotechnology. 10, 329-339.

[63] Li, Z., Chang, S., Lin, L., Li, Y. and An, Q. (2011) A Colorimetric Assay of 1-aminocyclopropane-1-carboxylate (ACC) Based on Ninhydrin Reaction for Rapid Screening of Bacteria Containing ACC Deaminase. Letters in Applied Microbiology. 53, 178-185.

[64] Ghyselincka, J., Siva, L.S., Velivelli, B., Heylena, K., O'Herlihyb, E., Francod, J., Rojase, M., De Vosac, P. and Prestwichb, B.D. (2013) Bioprospecting in Potato Fields in the Central Andean Highlands: Screening of Rhizobacteria for Plant Growth-promoting Properties. Systematic and Applied Microbiology. 36, 116-127.

[65] Grichko, V.P. and Glick, B.R. (2001) Amelioration of Flooding Stress by ACC Deaminase-containing Plant Growth-promoting Bacteria. Plant Physiol. Biochem. 39, 11-17.

[66] Xu, M., Sheng, J., Chen, L., Men, Y., Gan, L., Guo, S. and Shen, L. (2014) Bacterial Community Compositions of Tomato (*Lycopersicum esculentum* Mill.) Seeds and Plant Growth Promoting Activity of ACC Deaminase Producing *Bacillus subtilis* (HYT-12-1) on Tomato Seedlings. World J. Microbiol. Biotechnol. 30, 835-845.

[67] Han, Y., Wang, R., Yang, Z., Zhan, Y., Ma, Y., Ping, S., Zhang, L., Lin, M. and Yan, Y. (2015). 1-aminocyclopropane-1-carboxylate Deaminase from *Pseudomonas stutzeri* A1501 Facilitates the Growth of Rice in the Presence of Salt or Heavy Metals. J. Microbiol. Biotechnol. 25(7), 1119-1128.

[68] Borowiak, K., Niewiadomska A., Sulewska H., Szymanska G., Gluchowska K., Maruwka, A.W. (2016) Effect of PRP SOL and PRP EBV Nutrition on Yield, Photosynthesis Activity and Soil Microbial Activity of Three Cereal Species. Fresen. Environ. Bull. 25(6), 2020-2035.
[69] Weller, D.M. (1988) Biological Control of Soil-borne Plant Pathogens in the Rhizosphere with Bacteria. Annu. Rev. Phytopathol. 26, 379-407.
[70] Algeblawi, A. and Adam, F. (2013) Biological Control of *Erwinia carotovora* subsp. *carotovora* by *Pseudomonas fluorescens*, *Bacillus subtilis* and *Bacillus thuringiensis*. International Journal of Chemical, Environmental and Biological Sciences. 1(5), 771-774.
[71] Liao, C.H. (1989) Antagonism of *Pseudomonas putida* Strain PP22 to Phytopathogenic Bacteria and Its Potantial Use as a Biocontrol Agent. Plant Disease. 73, 223-226.
[72] Rashid, M., Chowdhury, M.S.M. and Sultana, N. (2013) *In vitro* Screening of Some Chemicals and Biocontrol Agents Against *Erwinia carotovora* subsp. *carotovora*, the Causal Agent of Soft Rot of Potato (*Solanum tuberosum*). The Agriculturists. 11(2), 1-9.

Received: **12.11.2018**
Accepted: **27.02.2020**

CORRESPONDING AUTHOR

Gulten Okmen
Department of Biology
Faculty of Science
Mugla Sitki Kocman University
48000, Mugla, TURKEY

e-mail: gultenokmen@gmail.com

© by PSP Volume 29 – No. 05/2020 pages 3409-3414 Fresenius Environmental Bulletin

ANALYSIS OF IRRIGATION PERFORMANCE IN WATER RESOURCES PLANNING AND MANAGEMENT: A CASE STUDY

Mahmut Cetin[1], Harun Kaman[2,*], Cevat Kirda[1], Sertan Sesveren[3]

[1]Cukurova University, Faculty of Agriculture, Department of Agricultural Structures and Irrigation, Balcali, Adana, Turkey
[2]Akdeniz University, Faculty of Agriculture, Department of Agricultural Structures and Irrigation, Campus, Antalya, Turkey
[3]Kahramanmaras Sutcu Imam University, Faculty of Agriculture, Department of Biosystem Engineering, Kahramanmaras, Turkey

ABSTRACT

In this research, it was aimed to create a model on monitoring and evaluation of irrigation schemes in large areas where several plant species and cultivars were grown in an irrigation season. In the study, the flow gauging stations (*FGSs*) were installed on drainage and irrigation canals to measure incoming and outgoing flows to evaluate irrigation management practices in a large-scale irrigation scheme. The amount of irrigation waters diverted to the area was measured with the *FGSs* on the irrigation canals, concurrently with the measurements of outgoing drainage waters, i.e. irrigation return flows (*IRFs*). In this regard, water depths at the canal cross-sections were firstly recorded at ten-minute intervals, then measured water depths (*h*) were converted to flow rates (*Q*) by utilizing stage-discharge rating curves ($Q=f(h)$) developed exclusively at each *FGS*. Assessing *IRF* hydrographs by time revealed that irrigation was mostly done during daytime in the catchment although the irrigation scheme was planned and designed for continuous irrigation. Inappropriate irrigation management technique caused to waste recklessly precious fresh water source to the drainage. Excessive and unconscious water use in the irrigation scheme may be prevented by taking basic measures such as obeying planning principles of the irrigation scheme and being aware of the fact that water should be saved for the sake of other water demanding sectors.

KEYWORDS:
Crop water use, Irrigation, Drainage, Irrigation district.

INTRODUCTION

As a result of climate change, temperatures are increasing and water resources are decreasing in the world [1]. Efficient use of water resources is one of the most important problems to be solved [2]. The important factor limiting the plant growth is lack of water beneficial to the crop [3]. Moreover, the distribution of water resources on the earth is not well balanced both spatially and temporally. For example, while some places are in sufficient condition in terms of water resources, in some other places the demand for water is at the highest level. As all sectors need water to some extent, there is also a significant increase in the need for water in agriculture. On the other hand, agriculture is the sector which uses almost 74% of water withdrawals in Turkey [4]. Especially in arid and semi-arid regions where water resources are scarce, the most efficient use of irrigation water has become a very important issue. Problems such as demand for good quality water, climate change, drought, contamination of underground and surface water resources, the high cost of irrigation services, low efficiency in irrigation management and household purposes negatively affect the sustainability of irrigated agriculture [5]. Despite the fact that the water resources of the world have not changed much from year to year, it has been requested from the agricultural sector to reduce remarkable water amounts used for irrigation purposes in the near future.

Today, perhaps one of the most important research areas of humanity has been the sustainable use of freshwater resources. Improvements in irrigation management as well as development of soil and water resources help authorities to increase agricultural production to the desired levels. In Turkey, agriculture is the sector that demands majority of fresh water resources [6, 7, 8]. However, it is an important issue to highlight that irrigation efficiencies have not been increased to the desired levels since the introduction of irrigation in Turkey. In dry periods, i.e., in irrigation season, if the water table rises to the plant root zone and reaches at the critical levels (<0.90 m), it can be concluded that the groundwater is fed by irrigation and consequently, the rate of irrigation is low and irrigation management is also problematic [9, 10]. In order to refrain from water logging and salinity problems related to the poor water management, more efficient use of water in the agricultural sector should be achieved for the sake of meeting water demands of other sectors [11,

12]. Under no circumstances, this is necessary for sustainable water management so as to meet additional water demand of other sectors. On the other hand, it has been experienced lately that farmers in the Lower Seyhan Plain (ASO) have incontrovertibly faced irrigation water shortages due to the increasing demand for irrigation water.

The *ASO*, one of the largest irrigation area in Turkey, has been partially irrigated since the construction of the Seyhan Dam in 1956 [6]. As a result of irrigation applications in the region, problems related to irrigation, drainage, salinity and alkalinity have begun to come to exist in irrigated areas [6]. This research was aimed at investigating irrigation performance in a large-scale irrigation catchment located in the Lower Seyhan Plain.

MATERIALS AND METHODS

The research was conducted on the command area of Akarsu Irrigation Association, located in the south of Adana province, Turkey. Within the Lower Seyhan Plain (*ASO*), Akarsu Irrigation Association (*AID*) has a potentially significant agricultural land of 9495 ha. In the research area, irrigation has been practiced for more than 60 years. Irrigation management was transferred to *AID* in 1994 by the State Hydraulic Works (DSI) which is a state agency and uniquely responsible for the development of soil and water resources of Turkey.

In the research area, the Mediterranean climate is dominant. Summers are hot and dry; winters are moderately warm and rainy. Long-term (about 60 years) mean temperature was recorded as 18.8 °C in the region. August is the hottest month with 28.1 °C. However, the coldest month is January by 9.9 °C. All of the precipitation nearly falls during the winter months in the form of rain. The average annual precipitation is 649.5 mm, and the distribution of precipitation during the year is not homogeneous. Notably, relative humidity is usually high (>80%) in summer months, but low in wet season (<50).

A field survey was performed to determine subsurface lateral flows from the Ceyhan river, located on the east of study area, and vice versa. In this regard, 8 piezometer batteries (*Pi*'s in Figure 1) were installed along the east borderline of the study area. Flow rate monitoring stations (*FGSs*) were installed on irrigation and drainage channels to measure incoming and outgoing waters in the study area (Figure 1). The incoming irrigation waters were measured at L3, L6, L7 and L9 points. L9 is a pumping station to divert irrigation water from Ceyhan River to the *AID* in the peak irrigation season. L2 and L4 are drainage flow gauging statins for conducting water balance work. In addition, irrigation water measurement was done through *FGS* in L5 to quantify the amount of water leaving the *AID* area.

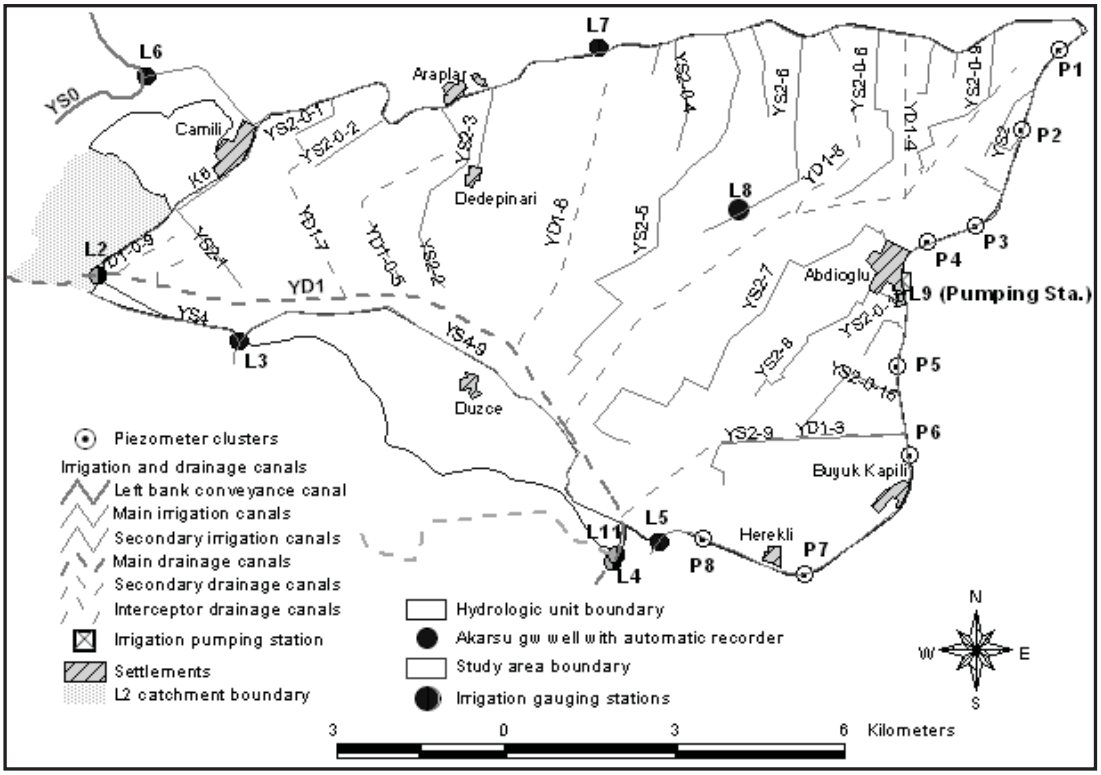

FIGURE 1
Water Sampling Locations in the Study Area

The basic equation for water balance calculations [13], based on the model illustrated in Figure 2, is given as;

$$P+(I_{in}-I_{out})+(D_{si}-D_{so})-(Q_{out}-Q_{in})-ETc=\pm 10\eta\Delta h\pm\Delta S$$

where P is rainfall (mm), $(I_{in}-I_{out})$ the net irrigation water (mm) diverted into the area, $(Q_{out}-Q_{in})$ net drainage water outflow (mm), $(D_{si}-D_{so})$ net subsurface lateral flow (seepage in mm), ETc crop water use (mm), Δh "*areal mean change*" in groundwater table depth (m) in tree meters soil depth, η average porosity (%) of the soils in the study area. Additionally, ΔS (mm) stands for the "*areal mean change*" in soil water storage in the rooting depth of 0.9 m. In this study, for the sake of simplicity, it was assumed that there was no deep percolation and capillary rise in the study area.

In order to carry out the mass balance studies for the water elements in Figure 2, it was necessary to measure or estimate the main inputs and outputs in the study area. In terms of water balance, the primary inputs were considered as precipitation (P), irrigation inflows (I_{in}), drainage inflows (Q_{in}) originated from outside areas, likely lateral seepage (D_{si}) along Ceyhan River flood levee; and outputs were crop evapotranspiration (ET_c), irrigation outflows (I_{out}) discharging from *YS2* main irrigation canal, drainage outflows, i.e., *IRFs* (Q_{out}) at the outlet of the study area (L4), and possible lateral seepage (D_{so}) through Ceyhan River flood levee. All the inputs and outputs for water balance model were depicted in Figure 2.

Precipitation data and other climatic variables were obtained from automatic weather station - installed almost in the center of the study area- next to *L8* in Figure 1. Irrigation and drainage in- and out-flows were measured regularly using electronic limnigraphs installed on the inputs and outputs of drainage and irrigation canals -*L3*, *L6*, *L7* and *L9* are on irrigation inputs, *L5* on irrigation output; *L2* and *L11* on drainage inputs and *L4* on drainage output- as seen in Figure 1. Limnigraphs were set up such that flow rates were recorded on hourly base by averaging 6 readings with ten minutes intervals in an hour.

Likely subsurface lateral flows (seepage) in- and out-flows along right-hand bank of Ceyhan River were assessed once a week, at each cluster/batteries of piezometers which were installed at eight critical points along Ceyhan River flood levee (Figure 1 and Figure 2). In situ horizontal hydraulic conductivities of the soil profile along Ceyhan River were determined by auger-hole technique, following the principles given in Oosterbaan and Nijland [14]. Then, the subsurface seepage along the Ceyhan River was estimated through using Darcy's law [15].

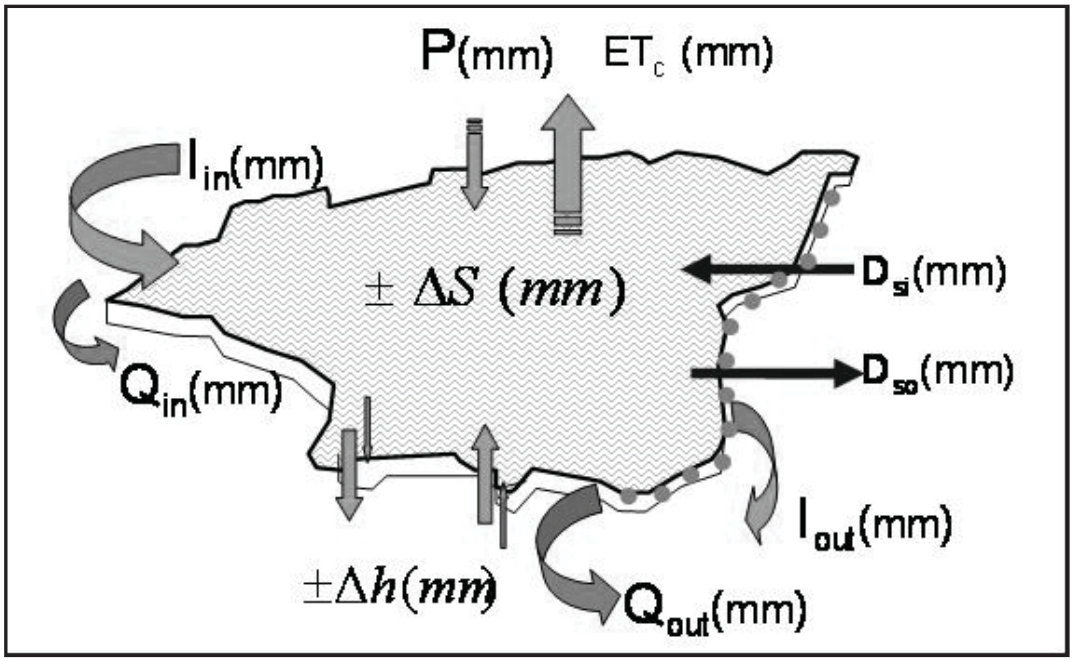

FIGURE 2
Model Used for Mass Balance Study in the Study Area.

RESULTS AND DISCUSSION

In the study area, the largest acre-age of plant was winter wheat [16]. Corn was the dominant irrigated field crop in summer, planted either as a first crop or as a second crop following winter wheat. The areal coverage of citrus orchards (around 20% in the study years) follows the first crop corn. Assessing cropping pattern data led us to conclude that there was a gradual increase in citrus-planted areas.

During the study period which the survey was conducted (1 October 2006- 30 September 2007), the limnigraph devices were set up in such a way that average water depths at the canal cross-sections should be recorded at ten-minute intervals at each *FGS*. Assessing limnigraph data showed that total amount of irrigation water diverted into the study area was around 1014 mm, while a total of 676 mm precipitation was recorded throughout the year. The district's irrigation efficiency (*IE*) was only 47.7% in the irrigation season (*IS*) (Table 1). It implies that the irrigation water diverted for the study area was recklessly wasted as drainage outflows during the irrigation season. This was due to the fact that farmers did not irrigate at night. However, irrigation canals should have been operated based on the continuous flow conditions. Ignoring this rule resulted in wasting considerable amount of irrigation water. Inevitably, drainage coefficient (*DF*) was as high as 46.7% [16]. Although *DF* is high, it remained constant during irrigation season (*IS*) and non-irrigation season (*NIS*).

In the Lower Seyhan Irrigation area, water user associations as well as the farmers imitates each other. Given those realities in the region, growers generally irrigate their fields during daytime and therefore irrigation water in the system is simply lost as drainage outflow during the night. Because district *IE* is low and *DF* is high at the catchment level, irrigation management authorities should undertake some measures immediately [16] in order to save fresh water for other water demanding sectors.

The relationship between water level and discharge at each discharge observation station were determined exclusively. It was found that flow rates increased parallel with the increase of water depths at the canal cross-sections. This, as expected, reveals that the flow process was a function of water-level change. During the study period, the terms of water budget model in Figure 2 were calculated by means of observation measurements and related formulas. Irrigation operation in the research area is based on the "c*ontinuous flow system*" method. According to the continuous flow method, irrigation water is always available in secondary and tertiary irrigation canals, i.e. canalettes. For this reason, the farmers in the study area are supposed to irrigate their fields at all times, i.e. by day and by night. Contrary to all expectations, the farmers on the area usually irrigate their lands during the day. Because of the irrigation made during the day, the waters in the irrigation channels go down the drains during nights. When the plant pattern of the research area was examined by considering the past years, it was found that cotton planted area reached to the peak (96%) in 1964. In a study conducted by Cetin and Ozcan [6] in the Lower Seyhan Plain (*ASO*) revealed that monoculture cotton cultivation was carried out until 1978, and at the beginning of the 1980's, changes in the crop pattern were triggered by the commencement of the second crop corn, soybean, groundnut and sesame. Monoculture cropping pattern development affects adversely irrigation performance in the district even if there is nocturnal irrigation in the area. There is no doubt that introduction of nocturnal irrigations will increase district irrigation efficiencies and decrease drainage fractions. In our case, diurnal irrigation practice was not well enough to increase irrigation management performance due to the fact that field crops, in particular, have been irrigated by surface irrigation methods. Therefore, almost 50% of the water diverted to the study area has been wasted by drainage. Isidoro *et al.* [18] conducted a study in Spain. It was determined that almost 73% of the diverted irrigation waters were squandered away by drainage. High drainage fraction is an important indicator for low district irrigation efficiency in large-scale irrigation districts as such in this case study. Likewise, the average irrigation efficiency was found to be between 35-40% in a study conducted by Cetin and Ozcan [6]. Cakmak and Akuzum [19] reported that the irrigation ratios, district irrigation efficiencies and water use efficiencies were generally very low in the irrigation schemes of Turkey. In parallel with the findings of Cetin and Ozcan [6], Cakmak and Akuzum [19] pointed out that the most important problem that caused to reduce irrigation efficiency was excessive water use in agriculture. In our study conducted at the catchment level, it was found that producers irrigated during daytime and that the available water in the irrigation channels disappeared through drainage at night. This indirectly caused excessive and unconscious water use in large irrigation schemes. A shift from surface irrigation (furrow and border) to modern irrigation techniques such as drip and sprinkler irrigation will help agricultural water managers to increase irrigation efficiencies and decrease drainage fractions at the district level, indicating remarkable water savings in favor of other water demanding sectors.

TABLE 1
Irrigation System Management Parameters (%) in the Study Area.

Irrigation management quality parameters	Irrigation Season (*IS*)	N*IS*
District's irrigation efficiency (*DIE*)	47.7	-
DIE=[(ETc - Pef[1]) / I]×100		
Water use efficiency (*WUE*)	47.5	31.2
WUE=[ETc / (I + P)] ×100		

[1] Pef is effective rainfall, which was calculated based on the method described in Brouwer and Heibloem [17].

CONCLUSIONS

Surface irrigation methods were common in the catchment, and this kind of irrigation technique under Mediterranean climate caused an adverse effect and reduced irrigation efficiency against high drainage fraction. Therefore, sprinkler and drip irrigation methods -which are considered as the water saving methods- must be promoted to replace traditional surface methods.

Adaptation of sprinkler and drip irrigation methods will help irrigation management to save notably irrigation water in the district by rendering both diurnal and nocturnal irrigation practices in the region. This type of changes in the irrigation methods over the district will decrease pressure on water demand from the irrigation system, and help to increase service quality of irrigation management. Additionally, deficit irrigation methods should also be considered as means of increasing crop water use efficiency as well as district level irrigation efficiency. In this regard, our suggestion is that, in the short term, partial-root-zone drying (*PRD*) irrigation technique is worth trying to adopt in the region for saving irrigation water and increasing both crop water use efficiency and district irrigation efficiency. However, fully adaptation of irrigation management and farmers to pressurized irrigation system as well as modern irrigation techniques will be a remedy for the water authorities to overcome existing problems related to irrigation.

ACKNOWLEDGEMENTS

Authors gratefully acknowledge that this work was funded by the European Union QUALIWATER project (INCO-CT-2005-015031) and partial support received from Cukurova University Research Fund (Project #: ZF2006KAP1 & ZF2009KAP1). The authors also would like to thank the Research Fund of Akdeniz University for its partial support.

REFERENCES

[1] Ucak, A.B., Bagdatli, M.C. (2017) Effects of deficit irrigation treatments on seed yield, oil ratio and water use efficiency of sunflower (*Helianthus annuus* L.). Fresen. Environ. Bull. 26(4), 2983-1991.

[2] Sen, F., Sekerci, I. (2019) A study on water quality of Karasu Stream (Van, Turkey) and assessment of usage in drinking, irrigation and fisheries. Fresen. Environ. Bull. 28, 1676-1682.

[3] Demir, Y., Demir, A.D., Surucu, A., Meral, R., Demirkiran, A.R., Yuksel, A., Meral, A. (2019) The effect of organic wastes on the horizontal and vertical wetting distance in soil. Fresen. Environ. Bull. 28, 6858-6864.

[4] Cetin, M., Kirda, C., Ibrikci, H., Topcu, S., Karaca, O.F., Karnez, E., Efe, H., Sesveren, S., Oztekin, E., Dingil, M., Kaman, H. (2008) Using geographic information systems (GIS) media to determine water, salt and nitrate budget elements in areas of irrigated agriculture: A case study in the Lower Seyhan Plain. The Fifth World Water Forum, DSI Domestic Regional Water Meetings: Proceedings Book of Irrigation-Drainage Conference, April 10–11, 2008, Adana, Turkey, 173–183 (in Turkish with English abstract).

[5] Buyukcangaz, H., Degirmenci, H. (2002) Reuse of drainage effluents in irrigation. Symposium on Conservation of Soil and Water Resources, their Development and Management in River Basins, September 18–20, 2002, Antakya, Turkey, Proceedings Book, 614–617 (in Turkish).

[6] Cetin, M., Ozcan, H. (1999) Problems encountered in the irrigated and non-irrigated areas of the Lower Seyhan Plain and recommendations for solution: A case study. Tr. J. of Agr. and For. 23(1), 207–217 (in Turkish with English abstract).

[7] Gundogdu, K.S. (2004) Evaluation of groundwater depth in irrigation project areas by using geostatistical methods. Journal of Agricultural Faculty of Uludag University, 18(2), 85-95 (in Turkish with English abstract).

[8] Cetin, M., Kirda, C., Efe, H., Topcu, S. (2007) Evaluation of relationship between groundwater depth and irrigation management using geographic information systems in the Lower Seyhan Plain. The Fifth National Hydrology Congress, Middle East Technical University, September 5-7, 2007, Ankara, Turkey, Proceedings Book, 419-428 (in Turkish with extended English abstract).

[9] DSI (1982) The Lower Seyhan Plain (ASO)-planning drainage report for the Fourth Stage Project Area. DSI Printing Office, Ankara, Turkey, 1-155 (in Turkish).

[10] Cetin, M., Diker, K. (2003) Assessing drainage problem areas by GIS: A case study in the Eastern Mediterranean Region of Turkey. Irrig. and Drainage, 52, 343-353.

[11] FAO (2001) Drainage and sustainability. IPTRID Issues Paper No. 3, Food and Agriculture Organization of the United Nations, Rome, Italy, 1-28.

[12] FAO (2002) Crops and drops: Making the best use of water for agriculture. Food and Agriculture Organization of the United Nations, Rome, Italy, 1-24.

[13] Loucks, D.P., Van Beek, E. (2005) Water resources systems planning and management. Studies and Reports in Hydrology, UNESCO, 1-680.
[14] Oosterbaan, R.J., Nijland, H.J. (1994) Determining the saturated hydraulic conductivity. In: Drainage Principles and Applications by H. P. Ritzema (editor-in-chief), ILRI Publication 16, The Netherlands, 1-1125.
[15] USBR (1984) Drainage manual. A Water Resources Technical Publication, Second Printing, U.S. Government Printing Office, Denver, Colorado, 1-286.
[16] Kaman, H., Cetin, M., Kirda, C. (2017) Monitoring and assessment of irrigation management in a large irrigation project area. Fresen. Environ. Bull. 26(6), 3986-3994.
[17] Brouwer, C., Heibloem, M. (1986) Irrigation water management: Irrigation water needs. FAO Training Manuel 3, The International Support Programme for Irrigation Water Management, Land and Water Development Division FAO, Via delle Terme di Caracalla 00100 Rome, 1-42.
[18] Isidoro, D., Quilez, D., Aragues, R. (2004) Water balance and irrigation performance analysis: La Violada Irrigation District (Spain) as a case study. Agricultural Water Management, 64, 23-142.
[19] Cakmak, B., Akuzum, T. (2006) Problems and solution proposals for water management issues in agriculture, Turkey. Union of Chambers of Turkish Engineers and Architects (TMMOB), Chamber of Civil Engineers (IMO), Congress on Water Politics, Ankara, Turkey, Book of Proceedings, Volume 2, 349-359 (in Turkish with English abstract).

Received: **29.11.2018**
Accepted: **07.03.2020**

CORRESPONDING AUTHOR

Harun Kaman
Department of Agricultural Structures and Irrigation
Faculty of Agriculture
Akdeniz University
Antalya 07058 – Turkey

e-mail: hkaman@akdeniz.edu.tr

© by PSP Volume 29 – No. 05/2020 pages 3415-3421 Fresenius Environmental Bulletin

EVALUATION OF TURKISH RICE VARIETIES (*ORYZA SATIVA* L.) FOR REPRODUCTIVE STAGE COLD ENVIRONMENTAL CONDITIONS TOLERANCE IN AFRICA

Negussie Zenna[1], Fanomezantsoa Rasoazany[1], Rehema Kwayu[2], Martin Ndomondo[2], Halil Surek[3], Necmi Beser[4,*]

[1]Madagascar Substation, Africa Rice Center, Madagascar
[2]Tanzania Sub station, Africa Rice Center, Tanzania
[3]Trakya Agricultural Research Institute, Edirne, Turkey
[4]Department of Genetics and Bioengineering, Engineering Faculty, Trakya University, Edirne, Turkey

ABSTRACT

Low-temperature-induced crop loss is one of a major threat in rice production; introduction of cold tolerant trait from cultivars that are well adapted to cooler climates is considered a vital strategy to mitigate the crop loss. In this study, twenty genotypes obtained from Trakya Agricutural Research Institute, in Turkey were evaluated for their reproductive stage cold tolerance in order to identify best performers for African cold-prone rice growing ecologies. The genotypes were first screened in temperature regulated screen house at AfricaRice research station in Tanzania, then field evaluated in Madagascar at the elevation of 1650 meter above sea level in rainfed lowland ecology. The genotypes showed range of reactions for the cold stress from highly susceptible to highly tolerant level. The susceptible genotypes showed consistent delay in flowering date up to 20 days, height reduction up to 40% and spikelet sterility up to 100% and consequently yield loss up to 100%. Nevertheless, in the field trial six genotypes; namely: Meric, Surek-95, Serhat-92, Duragan, Negis and Halilbey were identified to have superior performance compared to the local cold tolerant checks, with the yield potential of more than 5 t/ha. These candidate genotypes can be used to expand rice production in cold prone areas and contribute to food security in Africa.

KEYWORDS:
Food security, low-temperature, reproductive stage, rice, tolerance

INTRODUCTION

Rice in Africa has been transformed in a short period from a holiday meal to a daily dish in many countries; consequently, this has created a huge demand for rice in the continent. Recently, through active intervention from the national and international organizations, there has been a sharp increase in rice production in Africa; nevertheless, to satisfy the ever growing demand countries are still importing about 40% of the total rice consumed from international market [1]. To achieve food security, Africa needs to increase productivity per unit area as well as per unit time. Unfortunately, at field level, it has been observed that both biotic and abiotic stresses are major challenges for rice productivity. Consequently, rice growth and yield are very much affected by climate conditions, in particular temperature and moisture status. Rice has been cultivated in a vast tract of land at high elevation ecologies in Eastern and Southern Africa, the productivity however is highly constrained by low temperature stress, while another millions of hectare land is lying idle for the lack of better cold tolerant varieties to be grown [2].

Among the rice growing stages, reproductive development is the most sensitive stage to low temperature, resulting in high spikelet sterility and hence massive yield loss [3,4]. Furthermore, delay in heading and flowering dates, which could also be affected of both the pre-tillering and pre-productive phases cold stress, also contributes to spikelet sterility and low seed setting, or immature grains. Low temperatures affect not only heading but also panicle exertion by preventing normal elongation of internodes and panicle emergence [5]. The panicles may emerge partially and remain partly covered by the sheath of the flag leaf. Incomplete exertion increases the incidence of sheath rot, and causes considerable damage even to cold-tolerant varieties [6]. These symptoms have been typical of highland rice growing ecology in Africa [7]. Cold tolerant varieties introduction and development are crucial steps to increase rice production for cold prone ecologies [8] as well as contributing to food security in Africa. Consequently, the objective of this study is to characterize of rice genotypes obtained from Turkey for cold environmental conditions tolerance in a representative location of African Highlands, with the aim to identify useful genotypes.

MATERIAL AND METHODS

Materials. Eighteen Turkish, two Italian (Rocca, Europa) totally twenty rice genotypes were obtained from Trakya Agricultural Research Institute, Turkey; through the collaborative network of Temperate Rice Research Consortium (TRRC) that is initiated and coordinated by the International Rice Research Institute (IRRI) in order to address the problems faced by rice growing countries in temperate regions and tropical highlands. These genotypes together with checks were evaluated in this study.

Methods. Screenhouse evaluation. The cold tolerance screening in temperature controlled screenhouse was carried out at Sokoine University of Agriculture, Tanzania in 2014. The University is located at 100 masl and in a warm climate. The screening chamber was designed in order to mimic the actual field condition in high elevation ecologies (>1500 masl) of the tropics and serve as a preliminary screening facility. The high elevation ecologies have stable cool weather throughout the rice growing season, hence it was ecessary to control both water and air temperature for the screening protocol. Accordingly, water temperature of 12ºC was maintained following the procedure by [9], while air temperature of 17ºC was imposed through the application of air conditioner as described by [10]. Data loggers (TynTag Ultra 2,TGU-4500, UK) were used to monitor and record the water and air temperature throughout the experiment. Seedlings were grown on a tray with 5cmx5cm spacing and at active tillering stage all the tillers were removed leaving the main tiller. Each variety was replicated five times, with each replication having 10 plants per entry. Then one month old seedlings from the three replications were introduced to the cold screening chamber leaving two of the replications to continue growing outside the chamber in the warm environment as a control. In order to capture all relevant reproductive developmental stages, the test genotypes were exposed to cold treatment for the period of 60 days. The mean air and water temperature throughout the experiment were 17.3±0.5 and 12.7±1.0 respectively. All the necessary agronomic data such as: 50% flowering date, plant height, panicle number, rate of sterility and yield, were recorded from both the treated and the control sets for final statistical analysis.

Field evaluation. The field trial was conducted in Antsirabe, Madagascar in cropping season of 2015. The site is located at 1650 masl in rainfed low land ecology. Three weeks old seedlings were transplanted in lowland rice field with RCBD and three replications. The field management was done according to the local recommendations for lowland rice cultivation. The average night temperature was 15ºC with the range of 12-17ºC while the day temperature was 25ºC ranging from 22-28ºC. Data on agronomic traits of: 50% flowering date, tiller number, plant height, panicle exertion, panicle length and maturity date was collected for both treated and control plants. Post-harvest data on filled and unfilled grains was collected to determine the rate of sterility and final yield. The R-statistical program was used to analyze the data.

RESULTS

Screen house evaluation. Different reaction were observed among the cold treated and control groups for the five agronomic parameters measured in the temperature regulated screenhouse trial (Table 1). As compared to the non-stressed genotypes, cold stressed genotypes showed delay in flowering date up to one month for susceptible test genotypes. One of the prominent phenotypic reactions to cold stress is height reduction. Height of the cold treated genotypes was in general reduced by an average of 15 cm (Table 1). The striking differences were observed in the rate of sterility and yield. There was a very high sterility in the stressed genotypes that some entries did not produce any seeds while they have similar fertility level with local checks in the non-treated group, except for one entry, Demir, which seems to have high sterility even in normal growing conditions.

TABLE 1
Performance of cold stressed and non-stressed genotypes for different agronomic traits

Parameters	Cold stressed		Non-stressed	
	Mean ± SE*	Range	Mean ± SE	Range
Days to Flowering	86.5 ± 1.6	74–120	65.8 ± 0.45	55-78
Sterility (%)	73.5 ± 3.0	27–100	11 ± 0.9	1-34
Yield (g)	4.2 ± 0.5	0–20	17.1 ± 0.7	6-28
Height (cm)	74.5 ± 1.9	43–116	81.5 ± 1.6	54-120
Panicle-Length (cm)	11.4 ± 0.3	6-18	14.8 ± 0.31	10-21

Results are means ± standard error

We have also compared the stress imposed penalty on yield for the cold treated genotypes as a result of sterility caused by the low temperature and we noticed that yield was as low as zero for susceptible genotypes, nevertheless, five of the entries from Turkey showed higher yield and lower sterility as compared to the local checks (Figure 1). Although the genotypes seem to have higher sterility than the check, Kunming, they also showed higher yield potential.

We also analyzed the correlation among the five agronomic parameters under cold treatment. Table 2 shows that there was a negative but highly significant correlation between yield and rate of sterility, -0.92, but significant and positive correlation between yield and height as well as panicle length, 0.57 and 0.79 respectively. We also noticed highly significant and positive correlation between plant height and panicle length, 0.78.

Field evaluation. In the field experiment in cold prone site at Antsirabe the test genotypes have shown variable performance from less than 1 t/ha to 5 t/ha productivity (Figure 2). We also noticed rate of sterility ranging 15% - 75% and an inverse relationship between yield and sterility. Six of the test entries showed higher yield and lower sterility as compared to the local checks (Figure 2). Yavuz has shown a high level of tolerance with low sterility rate comparable to the checks but with significantly low yield potential. On the other hand variety Meric seems to show very high tolerance to cold and the highest yield in this trial followed by the other five tolerant varieties.

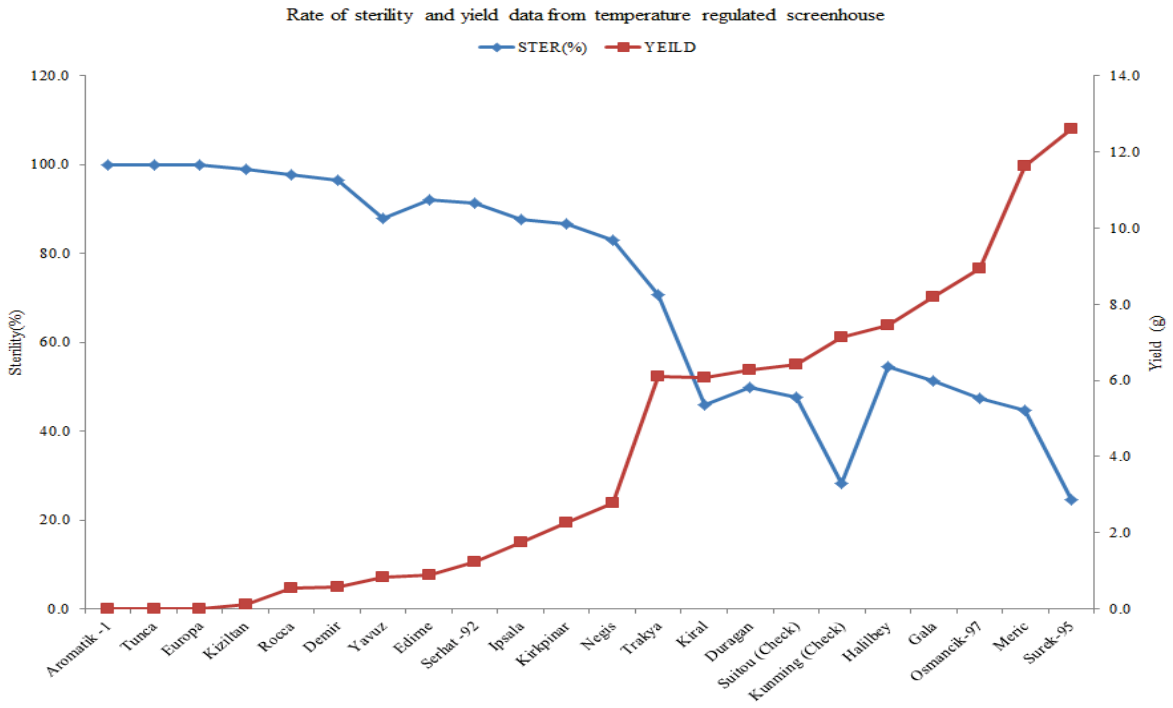

FIGURE 1
Data for rate of sterility and yield showing the diverse reactions of the tested genotypes exposed to low temperature stress treatment at temperature regulated screen house

TABLE 2
Correlation coefficients among five agronomic parameters measured under cold treatment

	Days to flowering	Sterility (%)	Yield	Plant height	Panicle length
Days to flowering	1.00				
Sterility (%)	0.78	1.00			
Yield	-0.76	-0.92	1.00		
Plant height	-0.66	-0.59	0.57	1.00	
Panicle length	-0.79	-0.73	0.79	0.78	1.00

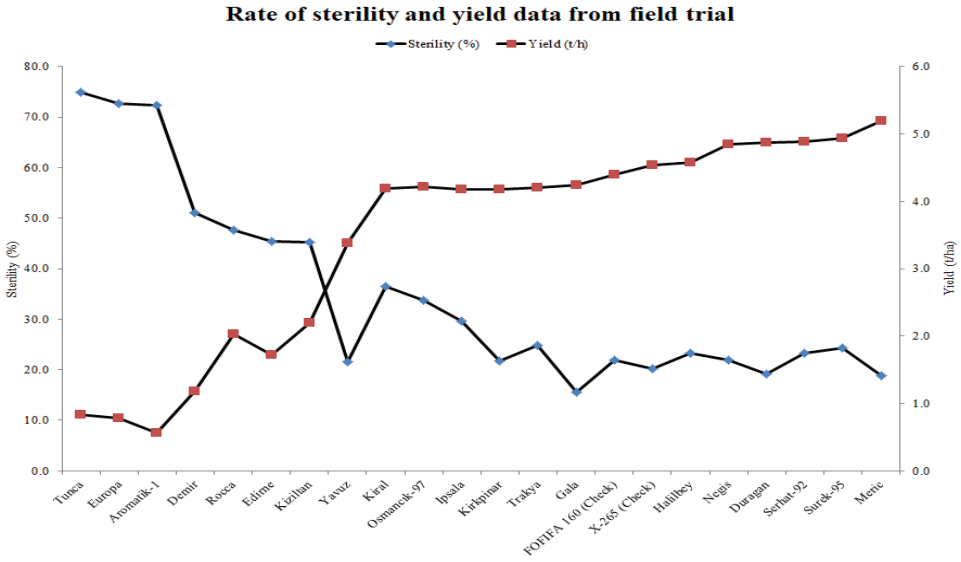

FIGURE 2
Data for rate of sterility and yield showing the diverse reactions of the tested genotypes to low temperature stress in a field screening

Correlation analysis among the five agronomic parameters in the field evaluation shows a negative but highly significant correlation between yield and percent sterility, -0.93, while there was some positive correlation between yield and height as well as panicle length, 0.43 and 0.29 respectively (Table 3). Tiller number also had a positive correlation with yield, 0.25. We also noticed highly significant and positive correlation between plant height and panicle length, 0.86.

The cluster analysis using the five agronomic parameters measured from the field trial seem to clearly classified the susceptible genotypes (> 40 % sterility) from moderately tolerant and highly tolerant groups (<40% sterility) at the primary node. Meric seem to be outlier with highly tolerant trait and clustered close to other tolerant varieties, while Halilbey seem to have similar performance with the local checks and hence cluster group with the checks. On the other hand Yavuz is established in separate but tolerant groups (Figure 3).

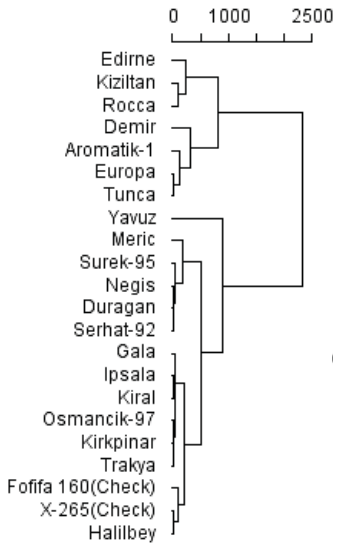

FIGURE 3
Cluster analysis considering all the agronomic parameters measured in the field trial under cold stress condition

TABLE 3
Correlation coefficients among five agronomic parameters measured under field evaluation in cold prone environment

	Days to flowering	*Sterility (%)*	*Yield*	*Panicle length*	*Plant height*	*Tiller number*
Days to flowering	1.00					
Sterility (%)	0.15	1.00				
Yield	-0.17	-0.93	1.00			
Panicle length	0.56	-0.29	0.29	1.00		
Plant height	0.40	-0.38	0.43	0.88	1.00	
Tiller number	0.22	-0.31	0.25	0.32	0.26	1.00

DISCUSSION

The screenhouse experiment data was a good indicator for identifying tolerant varieties and had a high correlation with the field evaluation data; 71% for yield and 61% for sterility. In both screenhouse and field experiments Meric, Surek-95 and Halilbey had higher yield than the local checks, while Negis, Duragan and Gala were comparable to the checks.

In the trials we recorded sever cold triggered stunting more than 40% by three of the susceptible varieties, this is similar to the observation by different researchers that low temperature prevents normal elongation of internodes and panicle emergence, [9,11,12] meanwhile low temperature seems also to delay the physiological growth of the plants as noticed by the average 20 days delay to flower by the varieties, in fact five of them were late by more than 30 days similar observation was reported by [13].

We also noticed a positive and significant correlation between height and panicle length that also seem to influence yield of a genotype as shown by positive correlation between height and yield. This result was consistent with observations made by [14] and [15].

Screening for cold tolerance at the reproductive stage can be well characterized based on one major parameter, spikelet fertility, due to the observed highly significant but negative correlation between sterility and yield. This finding was also well elucidated by [10], that low temperature has negative effect on microsporogenesis, resulting under developed pollen grains.

The slight variations in the performance among the genotypes in the different trials (screenhouse and field) can be explained due to the ability or inability to regulate the temperature in the growing environment. In the screenhouse test we imposed both cold air and water stress to ensure no escapes, genotypes were under severe stress, while in the field trials where there could be a better chance of adaptation to the stress as well as some escapes due to the daily temperature fluctuation. The average temperature during the field trial was 15^{o}C although sometimes it was below 12^{o}C.

We also noticed that there were some genotypes with superior yielding ability in control condition, in the screen house experiment, this yield potential, however, was not translated with corresponding higher yield under cold stress, while the moderate performers in normal environment have shown a better yielding ability under cold stress. The result shows that there is no correlation between yielding ability at normal state and when subjected to cold stress, a similar finding as reflected by [13].

Based on the field trial the six genotypes; namely: Meric, Surek-95, Serhat-92, Duragan, Negis and Halilbey were identified with a potential for cultivation at high elevation ecologies in East and Southern Africa and also they can serve as donors for the trait in a breeding program. These varieties were indicated to have yield potential of 8-10 t/ha in Edirne, Turkey, under irrigated lowland condition (unpublished data), however the observed lower yield in our location (5t/ha) in Antsirabe, Madagascar could be attributed to the variable growing condition as well as the huge altitudinal and latitudinal differences. We have evaluated the genotypes in Antsirabe under the rainfed lowland condition and at an altitude of 1650 masl and latitude of 19°52'22.83"S and 47°1'44.82"E, while in Turkey the genotypes were developed and grown in Edirne-at about 50 masl and latitude of 41° 40' 29.8740" N and 26° 35' 0.5316" E. The effect of altitude and latitude on the plant growth has also been reported by [16] and [17] for rice as well as tea crops respectively. Nevertheless, the yield we obtained is still acceptable in high altitude ecology in Africa where limited high yielding varieties exist. Further study on genetic characterization of the candidate varieties specially for the identification of chromosomal segment and development of genetic markers for the trait could useful to speed up the introgression of cold tolerant trait into popular varieties through marker assisted breeding programs. In the meantime in order to facilitate the quick delivery of these genotypes for the farmers, the candidate genotypes can be validated in on-farm trials through farmers' participatory approach while conducting consumer preference and cooking quality test for wider acceptability and hence adoption of the preferred varieties.

Food security has a paramount importance in Sub Saharan Africa. However, taking into account the huge impact agricultural activities are imposing in the ecology, farming need to be sustainable and environmentally sound [18]. Having improved varieties that are climate stress resilient and high yielding per unit area could be one of the ways to sustainable food production and reduce the environmental foot print. Therefore such exchange of useful germplasm can contribute towards the sustainable rice production in the developing countries while contributing towards achieving food security.

CONCLUSIONS

In screen house evaluation**,** as compared to the non-stressed genotypes, cold stressed genotypes showed delay in flowering date up to one month for susceptible test genotypes. One of the prominent phenotypic reactions to cold stress is height reduction. Height of the cold treated genotypes was in general reduced by an average of 15 cm. Yield was as low as zero for susceptible genotypes, nevertheless, five of the entries from Turkey; namely Halilbey, Gala, Osmancik-97, Meric, Surek-95

showed higher yield and lower sterility as compared to the local checks.

In field screening six of the Turkish varieties (Halilbey, Negis, Duragan, Serhat-92, Surek-95, Meric) showed higher yield and lower sterility as compared to the local checks at low temperature environmental conditions in field screening.

In both screenhouse and field experiments Meric, Surek-95 and Halilbey had higher yield than the local checks.

Based on the field trial the six genotypes; namely: Meric, Surek-95, Serhat-92, Duragan, Negis and Halilbey were identified with a potential for cultivation at high elevation, cold environmental conditions in East and Southern Africa and also they can serve as donors for the trait in a breeding program.

ACKNOWLEDGEMENTS

This work was supported in part by grants from Bill and Melinda Gates Foundation through the Stress Tolerant Rice for Africa and South Asia project, while the germplasm was obtained through the Temperate Rice Research Consortium.

REFERENCES

[1] AfricaRice (2008). Annual report. Africa Rice Center. Cotounou Benin. 4-6 pp.

[2] Zenna, N., Luzi-Kihupi, A., Manneh, B., Raymond, R., Gasore, E.R., Traore, K. (2010). Weathering the cold. Rice Today, 9(1), 26-27.

[3] Satake, T., Hayase, H. (1970). Male sterility caused by cooling treatment at the young microspore stage in rice plants. V. Estimation of pollen developmental stage and the most sensitive stage to coolness. Proc. Crop Sci. Soc. Jpn. 39, 468-473.

[4] Farrell, T.C., Fox, K.M., Williams, R.L., Fukai, S. (2006). Genotypic variation for cold tolerance during reproductive development in rice: Screening with cold air and cold water. Field Crop Res. 98, 178-194.

[5] Li, T.G., Visperas, R.M., Vergara, B.S. (1981). Correlation of cold tolerance at different growth stages in rice. Acta Bot. Sin. 23, 203-207.

[6] Hamdani, A.R. (1979). Low temperature problems and cold tolerance research activities for rice in India. In: Report of a Rice Cold Tolerance Workshop. Int. Rice Res. Ins., Los Baños, Laguna, Philippines 39-48 pp.

[7] Zenna, N., Senthilkumar, K., Sie, M. (2017). Rice production in Africa. In: G. Mahajan, K. Jabran, B. S. Chauhan (eds). Rice Production Worldwide. Switzerland. Springer International AG. p.117-136.

[8] Mackill, D.J., Lei, X. (1997). Genetic variation for traits related to temperate adaptation of rice cultivars. Crop Sci. 37, 1340-1346.

[9] Andaya, V.C. and Tai, T.H. (2006). Fine mapping of *qCTS12* locus, a major QTL for seedling cold tolerance in rice. Theor. Appl. Genet. 113, 467-475.

[10] Cruz, R.P., Milach, S.C.K., Federizzi, L.C. (2006). Rice cold tolerance at the reproductive stage in a controlled environment. Sci. Agric. (Piracicaba, Braz.), 63(3), 255-261.

[11] Imin, N., Kerim, T., Weinman, J.J., Rolfe, B.G. (2006). 'Low Temperature Treatment at the Young Microspore Stage Induces Protein Changes in Rice Anthers', Molecular and Cellular Proteomics. 5(2), 274-292.

[12] Sthapit, B.R., Witcombe, J.R. (1998). Inheritance of tolerance to chilling stress in rice during germination and plumule greening. Crop Sci. 38, 660–665.

[13] Wang, J., Lin, X., Sun, Q., Jena, K.K. (2013). Evaluation of Cold Tolerance for Japonica Rice Varieties from Different Country. Adv. J. Food Sci. and Tech. 5(1), 54-56.

[14] Lee, J.H. (1979).Screening methods for cold tolerance at Crop Experiment Station Phytotron and at Chuncheon. In: Rice Cold Tolerance Workshop, Los Baños, 1979. Report. Los Baños: Int. Rice Res. Ins. p.77-90.

[15] Takeuchi, Y., Hayasaka, H., Chiba, B., Tanaka, I., Shimano, T., Yamagishi, M., Nagano, K., Sasaki, T., Yano, M. (2001). Mapping quantitative trait loci controlling cool- temperature tolerance at booting stage in temperate Japonica rice. Breed. Sci. 51, 191-197.

[16] Xiong, Z.Y., Zhang, S.J., Ford-Lloyd, B.V., Jin, X., Wu, Y., Yan, H.X., Liu, P., Yang, X., Lu, B.R. (2011). Latitudinal Distribution and Differentiation of Rice Germplasm: Its Implications in Breeding. Crop Science. 51, 1050-1058.

[17] Özdemir, F., Şahin, N.H., Akdoğan, A., Dinçer, C., Topuz, A. (2018). Effect of altitude, shooting period, and tea grade on the catechins, caffeine, theaflavin, and thearubigin of Turkish black tea. Turkish J. of Agric. and Forestry. 42(5), 334-339.

[18] FAO (2015) FAO and 17 Sustainable Development Goals. Rome, Italy pp.8 http://www.fao.org/3/a-i4997e.pdf

Received: **14.02.2019**
Accepted: **07.10.2019**

CORRESPONDING AUTHOR

Necmi Beser
Trakya University
Engineering Faculty
Department of Genetics and Bioengineering
Edirne, Turkey

e-mail: necmibeser@trakya.edu.tr

© by PSP Volume 29 – No. 05/2020 pages 3422-3427 Fresenius Environmental Bulletin

EFFECTS OF *BEAUVERIA BASSIANA* ISOLATES ON *SITOPHILUS ORYZAE* L. UNDER IN VITRO CONDITIONS

Yusuf Yanar*, Durdane Yanar, Dogan Sahin Budak

Gaziosmanpasa University, Agricultural Faculty, Plant Protection Department, Tokat,Turkey

ABSTRACT

Stored grain insect pests can reduce weight, quality, seed viability and commercial value of stored grains. Management of these pests mainly rely on synthetic insecticides and fumigants. Negative effects of these pesticides have urged the researchers to develop alternative and environmentally friendly management strategies such as microbial control. Microbial control strategy uses living organisms called microbial control agents and entomopathogenic fungi are one of these agents. The objective of the current study was to assess the efficacy of entomopathogenic *Beauveria bassiana* isolates (F-52, F-53 and F-56) against rice weevil (*Sitophilus oryzae*) and the damage they cause to stored wheat grains. Morphological analysis of the isolated fungi and molecular identification was determined using PCR technique. The efficacy of fungal isolates against *S. oryzae* was tested by wheat grain dipping method. Wheat grains were dipped into different conidial concertation (1×10^3, 1×10^5, 1×10^7, 1×10^8, 1×10^9 conidia/ml) for 1 hour. The seeds were then dried and transferred to glass vial containing ten adult insects. The vials were incubated at 25±1 ^{0}C temperature and 75% relative humidity for 11 days. Thereafter, the treated adult insects were checked for mortality after 1st, 3rd, 5th, 7th, and 9th days of incubation. Dead insects were transferred to moist sterile 90 mm glass Petri dishes to determine the mycosis rate. The cumulative mortality in adults 9 days after exposure to isolates of *B. bassiana* ranged between 22% and 94%, 31% and 100%, and 14% and 86% for different concentrations of F-52, F-53, and F-56, respectively. The highest mortality rate (100%) was obtained after 9 days incubation period with F-53 isolate at 1×10^8 conidia/ml concentration. The highest mycosis rate (95%) was obtained at the end of the 14th day with F-52 isolate in 1×10^9 conidia/ml, which was followed by F-53 (93%) and F-56 (82%) isolates. The results indicated that these isolates caused high mortality and exhibited higher mycosis rate. Further storage trial should be conducted, particularly with these isolates to see their in vivo performances.

KEYWORDS:
Entomopathogen, fungi, biological control, storage

INTRODUCTION

Rice weevil (*Sitophilus oryzae* L.) is one of the most destructive pests of stored grains. The weevil can cause significant losses to stored grains, especially cereals under favorable conditions (25–35 0C and low relative humidity). Integrated management of *S. oryzae* is considered as the most effective approach for its control. The adult weevils feeding on the endosperm cause reduction in the carbohydrate content, while feeding of larvae on grains resulted in the removal of the large percentage of the protein and vitamins. The control of arthropod pests on stored products has been primarily relied on the use of fumigants and residual chemical insecticides [1]. The excessive and miss-use of synthetic chemical insecticides have resulted in insecticide resistance, negative effects on non-target insects, environmental pollutions, toxicity to humans and wildlife as well as increase in production cost [2]. Keeping in view the negative impacts of insecticides, alternative products or reduced use of fumigants is needed for the control of stored-grain pests [3, 4, 5]. The negative effects of insecticides have forced the development of more environmentally friendly alternative management strategies, such as microbial control relying on living organisms named as microbial control agents. One of these microbial control agents are entomopathogenic fungi. Several studies have shown the effectiveness of entomopathogenic fungi against stored products' pests [6, 7]. The ability of entomopathogenic fungi to manage stored-grains' pests, particularly, coleopterans has been confirmed in many studies in recent years [8, 9]. *Beauveria bassiana* (Balsamo) Vuillemin (Ascomycota: Hypocreales) has gained considerable importance in the integrated management of stored products' insects [10]. The objective of present study was to assess the efficacy of different isolates of entomopathogenic *B. bassiana* in controling rice weevil and the damage they cause to stored wheat grains.

MATERIALS AND METHODS

Source and Rearing of the Insect. The initial stock of *Sitophilus oryzae* L. adults was taken from the culture kept in Entomology laboratory, Depart-

ment of Plant Protection, Gaziosmanpasa University, Tokat, Turkey. Insects were mass produced in an incubater at 27 ºC and 75% relative humidity with 12 h photoperiod. Insects were maintained in glass jars (1 l capacity) with 500 g of healthy wheat grains. The jars were covered with a muslin cloth and after 2 weeks the original adults were removed by sieving. Once new adult weevils started to emerge, each jar was observed daily to collect the progeny which were kept in separate jars, according to their age group.

Fungal Isolates. Three Turkish isolates of *Beauveria bassiana* were obtained from the collection maintained at the Phytopathology Laboratory, Gaziosmanpasa University, Tokat, Turkey. All fungal isolates were cultured on Potato Dextrose Agar (PDA) in 9 cm diameter plastic sterile Petri dishes and incubated at 25±1 ºC and 75±5% relative humidity for 4 weeks for complete sporulation. After this period, conidia were harvested by flooding the Petri dishes with sterile distilled water containing 0.02% (v/v) Tween 80. Conidial suspensions were filtered through four layers of cheese clothes to remove the debris. The suspensions were vortexed for 2 min to break up the conidial clumps. The number of conidia were estimated with a hemocytometer. Five different spore concentrations of each isolates (1×10^3, 1×10^5, 1×10^7, 1×10^8, 1×10^9 conidia/ml) were prepared and used in bioassays.

Identification of Fungal Isolates. The entomopathogenic fungal isolates were morphologically identified based on colony morphology, conidia, and conidiogenous cell shapes obtained from monosporic cultures [11] and confirmed by molecular characterization, using amplified ITS sequences. The genomic DNA of fungal isolates were extracted using a DNA extraction mini-kit (Gene-jet, Thermo Scientific, Lithuania). The fungal ITS region was amplified using the primers ITS1 and ITS4 [12]. The standard PCR cycling protocol used here included the following steps: an rDNA-ITS amplification procedure consisting of pre-degeneration at 94°C for 3 min, degeneration at 94°C for 30 s, annealing at 55°C for 30 s, and extension at 72°C for 1 min; this protocol was repeated for 35 cycles with a 72°Cextension for 10 min. The following mixture was then subjected to PCR in a reaction system (50µL): 22 µL ddH2O, 25µL 2×Power Tag PCR MasterMix 1 µL ITS1 primer 1, 1 µL ITS4 primer 1, and 1µl DNA template. Finally, the resulting PCR products were subjected to electrophoresis on a 1% agarose gel using Gold view I dye (3–10µL were loaded and run at 100 volts and 220 MA). The PCR products were sequenced by MedSanTek on an ABI-PRISM3730 automated sequencer (Molecular Diagnostics, Istanbul,TURKEY). The obtained rDNA-ITS sequences were analyzed and compared with similar sequences through the BLAST on GenBank of NCBI and MEGA 5.0 software (IGE Biotechnology,Guangzhou).

Bioassays. Grain dipping method was used for the assays. Randomly selected fifty healthy wheat grains were dipped in spore solution of each isolates for 1 h, dried and transferred to the glass vial containing ten adult insects. Each vial was sealed using muslin cloth and a perforated lid and incubated at 75% relative humidity, 25±1 ºC for 11 days. Mortalities were recorded on the 1st 3rd, 5th, 7th, and 9th days after inoculation. The dead adults collected in the indicated periods were immediately submerged in 95% ethanol for 1 min, washed in sterile distilled water for 5 min, allowed to dry and then transferred to the moist chamber for mycosis. Experiment was repeated twice with 5 replications. Sterile distilled water containing 0.02% (v/v) Tween 80 was used for control treatment.

Data Analysis. The data were analyzed using one-way ANOVA and Tukey's post-hoc test was used to determine the differences among concentrations using SPSS statistical software [13]. The data obtained from dose-mortality experiment were subjected to Probit analysis [14] to estimate LC_{50} values and 95% confidence limits.

RESULTS AND DISCUSSION

Insect pathology have witnessed rapid development in the field of insect pest management, and the knowledge on microbial diseases of insects is progressing rapidly [3,15]. Moreover, studies during the past decade have proved that microbial control, or the use of microbial pest control agents, is an integral part of applied insect control. Microbial control is of special value when other methods have been found inadequate, for example, when insecticidal residues are toxic to human beings, insect parasites, and predators. Although some insect pathogens may replace certain insecticides, parasites and predators, most of the successful applications of pathogens in the future will probably be made in conjunction with these and other control agents [16, 17]. This study demonstrated a different degree of susceptibility of *Sitophilus oryzae* to various entomopathogenic isolates of *Beauveria bassiana*. Although all isolates tested caused mortality in *S. oryzae*, fungal isolates showed variability in virulence against the insects. All fungal isolates used in the present study were able to infect and cause mortality in the adults of S. oryzae at all concentrations ranging from 1×10^3 to 1×10^9 conidia/ml but no mortality was observed after 1-day post inoculation for all isolates and concentrations used. However, the degree of infection varied greatly with the concentration used. Mortality caused by the isolates was confirmed by external sporulating of

mycelial insects cadavers and 84-96% of all dead insects showed mycosis of the respective isolates. The level of mortality increased with increasing spore concentration of *B. bassiana* isolates at all observations (Table 1, 2, and 3). Starting from fifth day of post-inoculation mortality rates of $1x10^8$ and $1x10^9$ conidia/ml concetrations of F52 was significantly higher than the other concentrations and the control. Also mortality rates of $1x10^9$ was significantly higher than that of $1x10^8$ conidia/ml concentration ($F= 104.26$, $p\leq0.0001$) (Table 1). Similar results were obtained with isolate F53 but mortality rates at $1x10^8$ and $1x10^9$ conidia/ml concentration were not significantly different ($F=216.38$, $p\leq0.0001$) after nine day post-inoculation. Differences between mortality rates of F56 at $1x10^7$, 10^8, and 10^9 conida/ml concentrations were statistically significant at the end of seven and nine day incubation period ($F=117.88$ and $F= 130.29$, $p\leq0.0001$) (Table 3). Other researchers have reported that treating stored grain pests with entomopathogenic *B. bassiana* and *Metarhizium anisopliae* isolates can suppress the population of them. Obtained results are in a good agreement with their results [9,18, 19]. Shams et al. (2011) [20] pointed out that increase in concentrations of B. bassiana isolates resulted in increase in mortality of S. granaries. Kavallieratos et al. (2014) [21] also reported that mortality of *S. oryzea* increased with increase in spore concentration of *B. bassiana* isolates. The cumulative mortality in adults exposed to isolates of *B. bassiana* ranged between 22 and 94%, 31 and 100%, and 14 and 86% for different concentrations of F-52, F-53, and F-56, respectively at 9 days of post incubation (Table 1, 2, and 3).

The highest mortality rate of 100% was obtained at the end of 9 days incubation period with 1×10^8 spore concentration of F-53 isolate (Table 2). Mortality rate caused by the isolates increased after 5 days of post-incubation. The increased mortality percentage after 5 days might be due to the latent effect of the *B. bassiana* fungal conidia which takes time to penetrate through the cuticle of the insect.

TABLE 1

Percent mortality of *Sitophilus oryzae* exposed to different concentrations of *Beauveria bassiana* isolate F-52

Treatments	Mean mortality %				
	1st day	3rd day	5th day	7th day	9th day
Control	0.0±0.00 a*	0.0±0.00 a	0.0±0.00 a	6.0±2.45 a	6.0±2.45 a
1×10^3	0.0±0.00 a	0.0±0.00 a	4.0±2.45 a	16.0±2.45 ab	22,0±3.74 b
1×10^5	0.0±0.00 a	4.0±2.33 a	5.7±2.33 a	26.0±2.45 bc	34,0±2.45 bc
1×10^7	0.0±0.00 a	5.7±2.40 a	6.0±2.45 a	35.3±2.25 cd	44,0±2.45 cd
1×10^8	0.0±0.00 a	5.8±2.45 a	16.0±2.45 b	46.0±2.45 d	56,0±2.45 d
1×109	**0.0±0.00 a**	**6.0±2.45 a**	**54.5±2.82 c**	**88.0±3.74 e**	**94,0±4.5 e**

*Means followed by the same letter in each column are not significantly different ($P < 0.05$)

TABLE 2

Percent mortality of *Sitophilus oryzae* exposed to different concentrations of *Beauveria bassiana* isolate F-53

Treatments	Mean mortality %				
	1st day	3rd day	5th day	7th day	9th day
Control	0.0±0.00 a*	0.0±0.00 a	0.0±0.00 a	6.0±2.45 a	6.0±2.45 a
1×10^3	0.0±0.00 a	0.0±0.00 a	8.4±2.13 b	19.1±2.37 b	31.3±3.90 b
1×10^5	0.0±0.00 a	3.8±2.34 ab	11.8±2.05 b	23.6±2.62 b	33,6±4.32 b
1×10^7	0.0±0.00 a	4.2±2.59 ab	14.2±2.37 bc	68.9±2.88 c	78,2±2.24 c
1×10^8	0.0±0.00 a	8.0±2.00 b	22.0±2.00 c	94.0±4.00 d	100,0±0.0 d
1×10^9	0.0±0.00 a	10.0±0.00 b	42.0±2.00 d	98.0±2.00 d	100,0±0.0 d

*Means followed by the same letter in each column are not significantly different ($P < 0.05$)

TABLE 3

Percent mortality of *Sitophilus oryzae* exposed to different concentrations of *Beauveria bassiana* isolate F-56

Treatments	Mean mortality %				
	1st day	3rd day	5th day	7th day	9th day
Control	0.0±0.00 a*	0.0±0.00 a	0.0±0.00 a	6.0±2.45 a	6.0±2.45 a
$1x10^3$	0.0±0.00 a	2.0±2.00 a	11.6±2.1 ab	13.6±2.60 ab	13,6±2.60 ab
$1x10^5$	0.0±0.00 a	2.0±2.00 a	10.0±0.00 b	22.0±2.00 b	22,0±2.00 b
$1x10^7$	0.0±0.00 a	4.0±2.45 ab	40.0±0.00 c	52.0±3.74 c	52,0±3.74 c
$1x10^8$	0.0±0.00 a	6.0±2.45 ab	47.0±3.70 c	66.0±2.45 d	72,0±3.74 d
$1x10^9$	2.0±2.00 a	10.0±0.00 b	62.0±2.00 d	80.0±3.16 e	86,0±2.45 e

*Means followed by the same letter in each column are not significantly different ($P < 0.05$)

TABLE 4
The LC_{50} and LC_{90} values (with 95% confidence limit) and probit analysis parameters for adults of *S. oryzae* inoculated with conidial suspension of *Beauveria bassiana* isolates

Isolate No	Slope (±SE)[a]	LC_{50} (95% confidence intervals)	LC_{90} (95% confidence intervals)	χ^{2b}
F-52	0.282±0.02	6.6×10^6 (5.4×10^5 – 1.4×10^7)	6.3×10^7(4.8×10^7-9.1×10^7)	134.8
F-53	0.490±0.02	1.8×10^5 (6.9×10^4 – 2.9×10^5)	1.3×10^5 (1.1×10^6-1.6×10^7)	55.0
F-56	0.338±0.02	4×10^6 (4.5×10^5 – 1.7×10^7)	8.6×10^8 (5.8×10^7-1.7×10^8)	114.0

[a]Slope of the concentration (± standard error) response of S. oryzae to Beauveria bassiana isolates.
[b]Pearson chi-square goodness-of-fit test on the probit model ($\alpha = 0.05$).

TABLE 5
GenBank accession number of local entomopathogenic fungal isolates F-53,F-52 and F-56.

	Accesion number	Isolate	Organism
SeqID1	MK411541	F-53	Beauveria bassiana
SeqID2	MK411542	F-52	Beauveria bassiana
SeqID3	MK411543	F-56	Beauveria bassiana

The current results are in line with Samodra and Ibrahim (2006) [22], who cleared that the application of *B. bassiana* had a great impact on the adult of *S. oryzae* that achieved a significantly high cumulative-mortality percentage of 90%.The highest mycosis rate (95%) was obtained at the end of the 14th day with 1×10^9 conidia/ml concentration of F-52 isolate, which was followed by F-53 (93%) and F-56 (82%) isolates. The results indicated that these isolates also exhibited higher mycosis rate.

Probit analysis showed that the concentration for the isolate F-53 to cause 50% mortality (LC_{50}) in *S. oryzae* was 1.8×10^5 spore/ml, followed by isolate F-56 with 4×10^6 spore/ml (Table 4). The LC_{90} values for isolates F-53, F-52 and F-56 were 1.3×10^5, 6.3. $\times10^7$ and 8.6×10^8 spores/ml, respectively. Therefore, the isolates F-53 was more virulent than the other two isolates (Table 4). *S. oryzae* LC50 and LC90 values confirmed that *S. oryzae* was more susceptible to the isolate F-53 than the other isolates tested. The mortality concentration curve of the F-53 presented the steepest slope (0.49), while the slopes of the other isolates (0.282 and 0.338) were not as steep as F-53 (Table 4).

Blast analysis revealed that the fungal isolates are Beauveria bassiana. The DNA sequences obtained from this study were deposited in NCBI GenBank database. For B. bassiana isolates (F-52, F-53 and F-56), accession numbers are MK411542, MK411541 and MK411543 (Table 5).

CONCLUSIONS

In conclusion, the activities of the three tested *B. bassiana* isolates on adult mortality of *S. oryzae* were reported in this paper are valuable. These activities suggest that the isolates, particularly F-53 (MK411541), have the potential to be an effective and alternative biocontrol agent for managing S. oryzae after confirmation of its efficacy in storage conditions.

ACKNOWLEDGEMENTS

This Project was funded by Tokat Gaziosmanpasa University Research Council with a Project number 2012/25. The results of this study was presented as an oral presentation in Ecology Congress held during 19-23 June 2018, Kastamonu, Turkey and abstract was published in congress proceedings book. I would like to thank to Dr. Serife Topkaya (Department of Plant Protection, Gaziosmanpasa University, Tokat, TURKEY) for her help on molecular characterisation of the fungal isolates.

REFERENCES

[1] Adane, K., Moore, D., Archer, S.A. (1996) Preliminary studies on the use of *Beauveria bassiana* to control *Sitophilus zeamais* (Coleoptera: Curculionidae) in the laboratory. J. Stored Prod. Res. 32, 105-113.

[2] Khan, A.R., Selman, B.J. (1989) Nosema spp. (Microspora: Microsporida:Noesematidae) of stored product Coleoptera and their potential as microbial control agents. Agricultural Zoology Reviews. 3, 193-223.

[3] Dal-Bello, G., Padin, S., Lopez-Lastra, C., Fabrizio, M. (2001) Laboratory evaluation of chemical–biological control of the rice weevil (*Sitophilus oryzae* L.) in stored grains. Journal of Stored Products Research. 37 (1), 77–84.

[4] Stathers, T., Zd'arkova, E., Wakefield, M., Lukas, J., Hubert, J. (2002) Entomopathogenic fungi in grain storage: biological control of pest insects and mites with special reference to entomophthorales. In: Zd'arkova, E., Lukas, J., Hubert, J. (Eds.), Proceedings of the Second Meeting of Working Group-4: Biocontrol of Arthropod Pests in the Stored-Products, Prague, Czech Republic, 30–31 May, 100-109

[5] Wakefield, M., Cox, P.D., Wildey, K.B., Price, N.R., Moore D., Bell, B.A., Zd'-arkova, E., Lukas, J., Hubert, J. (2002) The use of entomopathogenic fungi for stored-product insect and mite control: biological control of pest insects and mites with special reference to entomophthorales. In: Zd'arkova, E., Lukas, J., Hubert, J. (Eds.), Proceedings of the Second Meeting of Working Groupe-4: Biocontrol of Arthropod Pests in the Stored-Products, Prague, Czech Republic. 30–31 May, 110-115

[6] Padin, S.B., Dal-Bello, G.M., Fabrizio, M. (2002) Grain losses caused by *Tribolium castaneum, Sitophilus oryzae* and Acanthoscelides obtectus in stored durum wheat and beans treated with *Beauveria bassiana*. Journal of Stored Product Research. 38, 69-74.

[7] Akbar, W., Lord, J.C., Nechols, J.R., Howard, R.W. (2004) Diatomaceous earth increases the efficacy of *Beauveria bassiana* against Tribolium castaneum larvae and increase conidia attachment. Journal of Economic Entomology. 97, 273-280.

[8] Bourassa C., Vincent C., Lomer C.J., Borgemeister C., Mauffette Y. (2001) Effects of entomopathogenic Hyphomycetes against the larger grain borer, *Prostephanus truncatus* (Horn) (Coleoptera: Bostrichidae), and its predator, *Teretriosoma nigrescens* Lewis (Coleoptera: Histeridae). Journal of Invertebrate Pathology. 77, 75-77.

[9] Kassa, A., Zimmermann, G., Stephan, D., Vidal, S. (2002) Susceptibility of *Sitophilus zeamais* (Motsch.) (Coleoptera: Curculionidae) and *Prostephanus truncatus* (Horn) (Coleoptera: Bostrichidae) to entomopathogenic fungi from Ethiopia. Biocontrol Sci. Technol. 12, 727-736.

[10] Michalaki, M.P., Athanassiou, C.G., Kavallieratos, N.G., Batta, Y.A., Balotis, G.N. (2006) Effectiveness of *Metarhizium anisopliae* (Metschinkoff) Sorokin applied alone or in combination with diatomaceous earth against *Tribolium confusum* Du Val larvae: Influence of temperature, relative humidity and type of commodity. Crop Protection. (2006) 25, 418-425.

[11] Humber, R.A. (1997). Fungi-Identification In: Manual of Techniques in Insect Pathology (L. Lacey, ed.), 153-185. Academic Press, London.

[12] Tanaka, K., Hirayama, K., Yonezawa, H., Hatakeyama, S., Harada, Y., Sano, T. (2009) Molecular taxonomy of bambusicolous fungi: Tetraplosphaeriaceae, a new pleosporalean family with Tetraploa-like anamorphs. Stud Mycol. 64(64), 175–209.

[13] SPSS (2008) SPSS 17 for windows user's guide release. Chicago Spss Inc.

[14] Finney, D.J. (1971) Probit Analysis. 3rd edn.- Cambridge University Press, London.

[15] Sindhu, S.S., Rakshiya, Y.S., Verna, M.K. (2011) Biological control of termites by antagonistic soil microorganisms. In: Singh A, Parmar N, Kuhad RC, editors. Bioaugmentation, Biostimulation and Biocontrol. Berlin, Springer. 261-309.

[16] Butt, T.M., Jackson, C.W., Magan, N. (2001) Fungi as biocontrol Agents-Progress, problems and potential. CABI publishing. United Kingdom London. pp 26.

[17] Ekesi, S., Egwurube, E.A., Akpa, A.D., Onu, I. (2001) Laboratory evaluation of the entomopathogenic fungus, *Metarhizium anisopliae* for the control of the groundnut bruchid, Caryedon serratus on groundnut. Journal of Stored Product Research. 37, 313-321.

[18] Khashaveh, A., Safaralizade, M.H., Ghosta, Y. (2008) Pathogenicity of three Iranian isolates of fungus *Metarhizium anisopliae* against Granary Weevil *Sitophilus granaries*. Journal of Biological Sci. 8(4), 804-808.

[19] Batta, Y.A. (2005) Control of the lesser grain borer (Rhyzopertha *dominica* Fab., Coleoptera: Bostrychidae) by treatments with residual formulations of *Metarhizium anisopliae* (Metsch.) Sorokin. J. Stored Prod. Res. 41, 221-229.

[20] Shams, G., Safaralizadeh, M.H., Imani, S., Shojai, M., Aramideh, S. (2011) A laboratory assessment of the potential of the entomopathogenic fungi *Beauveria bassiana* (Beauvarin®) to control *Callosobruchus maculatus* (F.) (Coleoptera: Bruchidae) and *Sitophilus granarius* (L.) (Coleoptera: Curculionidae). African J. Microbiol. Res. 5 (10), 1192-1196.

[21] Kavallieratos, N.G., Athanassiou, C.G., Aountala, M.M., Kontodimas, D.C. (2014) Evaluation of the entomopathogenic fungi *Beauveria bassiana, Metarhizium anisopliae*, and *Isaria fumosorosea* for control of Sitophilus oryzae. J Food Prot. 1, 4-17.

[22] Samodra, H., Ibrahim, Y. (2006) Effects of dust formulations of three entomophatogenic fungal isolates against *Sitophilus oryzae* (coleoptera: curculionidae) in rice grain. Journal Biosains. 17(1), 1-7.

Received: **02.03.2019**
Accepted: **25.01.2020**

CORRESPONDING AUTHOR

Yusuf Yanar
Gaziosmanpasa University,
Agricultural Faculty,
Plant Protection Department
Tokat – Turkey

e-mail: yusuf.yanar@gop.edu.tr

© by PSP Volume 29 – No. 05/2020 pages 3428-3432 Fresenius Environmental Bulletin

ANTIOXIDATIVE AND ANTIMICROBIAL ACTIVITIES OF *PHELLINUS IGNIARIUS* AND *PHELLINUS RIMOSUS*

Celal Bal*

Gaziantep University, Oguzeli Vocational School, Gaziantep, Turkey

ABSTRACT

This study aims to determine the antimicrobial activities, total antioxidant status (TAS), total oxidant status (TOS) and oxidative stress index (OSI) of the medicinal mushroom *Phellinus igniarius* (L.) Quél. and *P. rimosus* (Berk.). Within this scope, mushroom samples were subjected to extraction in a Soxhlet extractor. Antimicrobial activity were tested using the agar dilution method against *Staphylococcus aureus* ATCC 29213, *S. aureus* MRSA ATCC 43300, *Enterococcus faecalis* ATCC 29212, *Escherichia coli* ATCC 25922, *Pseudomonas aeruginosa* ATCC 27853, *Acinetobacter baumannii* ATCC 19606, *Candida albicans* ATCC 10231, *C. krusei* ATCC 34135 ATCC 13803, and *C. glabrata*. TAS, TOS and OSI values were determined using Rel Assay kits. As a result of the study, it was found that extracts of *P. igniarius* and *P. rimosus* had antimicrobial effect at 50-400 (µg/mL) concentrations. Moreover, it was found that *P. igniarius* had a higher TAS value. *P. rimosus* also had higher TOS and OSI values. Consequently, it is thought that *P. igniarius* and *P. rimosus* have antioxidant and antimicrobial potential, and these mushrooms can be used as natural sources in pharmacological research.

KEYWORDS:
Antimicrobial, Antioxidant, *Phellinus igniarius, Phellinus rimosus,* Oxidative stress

INTRODUCTION

The earth hosts many plant, mushroom, animal and microorganism species that can be found in various faunas and floras that contain secondary metabolites and cannot be used in pharmaceutical research [1-5]. Mushrooms exhibit a cosmopolitan distribution and have nearly 140.000 species [6,7]. It is possible to classify mushrooms as edible, non-edible and poisonous mushrooms. The mushroom species that will be used in this study, i.e. *P. igniarius* and *P. rimosus*, are included in the non-edible group due to their hard structure. However, non-edible mushrooms include some mushrooms that are important from a medical aspect. Previous studies have shown that mushrooms are rich in secondary metabolites and exhibit a good lipid peroxidation inhibition activity and radical scavenging activity [8, 9]. Moreover, mushrooms spread and grow in different habitats and environmental conditions since they are generally saprophytic. Therefore, they are a potent and natural antimicrobial source due to the secondary metabolites that they produce.

Members of the Hymenochaetaceae family go through development and reproduction as wood destroyers. A member of the Hymenochaetaceae family, i.e. *Phellinus* species causes wood decay, root decay in living trees and leads to cancerous diseases. *Phellinus* species are parasitic and/or saprophytic, which causes a white rot in which both the lignin and cellulose are degraded. Phellinus species have crusty fructification organs, they are rarely pale, dark brown to black on the crust, glabrous and hairless, radially cracked in older basidiocarps with variable pores [10].

TAS, TOS and OSI values, as well as antimicrobial activities against test fungus and bacterium strains of *Phellinus igniarius* (L.) Quél. and *P. rimosus* (Berk.) mushrooms were determined in this study.

EXPERIMENTAL

Laboratory Studies. Samples of *P. igniarius* and *P. rimosus* used in this study were collected from Gaziantep. Collected mushroom samples were dried at 40 °C in the desiccator. 30 g of the pulverized material was weighed and placed in a cartridge followed by ethanol (EtOH) extraction in a Soxhlet apparatus (BUCHI Extraction System Model B-811). The extracts were concentrated under pressure using a rotary evaporator and kept at 4 ^{0}C until testing (BUCHI Rotavapor Model R-144).

Determination of TAS, TOS and OSI. TAS and TOS values of mushroom samples were determined using Rel Assay brand commercial kits (Rel Assay Diagnostics Kits, Turkey). Trolox was used as a calibrator in determining the TAS value and the results were expressed in mmol Trolox equiv./L. Hydrogen peroxide was used as a calibrator in determining the TOS value and the results were expressed in µmol H_2O_2 equiv./L [11,12]. The following formula was used in calculating the OSI value, which

indicates how much oxidant compounds are tolerated by antioxidant compounds in percentage: TOS/(TASx10) [12].

Antimicrobial Activity Tests. Antimicrobial activity tests of the ethanol extracts of mushrooms were conducted using the agar dilution method recommended by the Clinical and Laboratory Standards Institute (CLSI) and European Committee on Antimicrobial Susceptibility Testing (EUCAST). The minimum inhibitory concentration (MIC) of each mushroom extract was determined against standard bacterium and fungus strains. *Staphylococcus aureus* ATCC 29213, *S. aureus* MRSA ATCC 43300, *Enterococcus faecalis* ATCC 29212, *Escherichia coli* ATCC 25922, *Pseudomonas aeruginosa* ATCC 27853, *Acinetobacter baumannii* ATCC 19606, *Candida albicans* ATCC 10231, *Candida krusei* ATCC 34135 ATCC 13803, and *Candida glabrata* ATCC 90030 were used as testing microorganisms. Bacterium strains were precultured in a Mueller Hinton Broth and fungus strains were precultured in a RPMI 1640 Broth. The turbidity of the bacteria and mushrooms was prepared in accordance with the 0.5 McFarland standard, in order to obtain a standard inoculum. All extracts were tested at 800, 400, 200, 100, 50, 25 and 12.5 µg/mL concentrations and all dilutions were performed using distilled water. Solvents used for the extracts were also tested for antimicrobial activity separately. Fluconazole and Amphotericin B were used as reference drugs for fungi, and Amikacin, Ampicillin and Ciprofloxacin were used as reference drugs for bacteria. The lowest dilution that prevents bacteria and fungi growth was determined as the minimum inhibitory concentration (MIC) [13-18].

RESULTS AND DISCUSSIONS

TAS, TOS and OSI Values. Oxidative stress occurs as a result of the imbalance between endogenous antioxidants and free radicals. Antioxidant supplements can be taken in order to reduce the effects of oxidative stress when endogenous antioxidants fail to suffice. In this study, TAS (mmol/L), TOS (µmol/L) and OSI values of the mushroom *P. igniarius* and *P. rimosus* were determined using Rel Assay kits and the results are shown in Table 1.

As a result of this study, it was found that the TAS of *P. igniarius* was higher than that of *P. rimosus*. Moreover, it was observed that the TOS and OSI values of *P. rimosus* were higher, compared to the mushroom *P. igniarius*. There are no previous studies concerning the TAS, TOS and OSI values of *P. igniarius* and *P. rimosus*. In studies conducted on different mushroom species, it was reported that the TAS, TOS and OSI values of *Cyclocybe cylindracea* were 4.325 mmol/L, 21.109 µmol/L and 0.488, respectively [19]. In another study, it was reported that the TAS, TOS and OSI values of *Lentinus tigrinus* were 1.748 mmol/L, 19.294 µmol/L and 1.106, respectively [20]. Moreover, the TAS, TOS and OSI values of the mushroom *Clavariadelphus truncatus* were reported as 2.415 mmol/L, 3.367 µmol/L and 0.140, respectively [21]. In comparison to these studies, *P. igniarius* was found to have a higher TAS value compared to *P. rimosus, C. cylindracea, L. tigrinus* and *C. truncatus* in this current study. It was also observed that the TAS value of *P. rimosus* was lower than that of *P. igniarius* and *C. cylindracea* and higher than that of *L. tigrinus* and *C. truncatus*. This difference between the TAS values stems from different antioxidant production capacities of the mushrooms.

Moreover, previous studies reported that *P. igniarius* and *P. rimosus* have antioxidant potential [22-25]. In this current study, the antioxidant activities of mushrooms *P. igniarius* and *P. rimosus* were studied for the first time using Rel Assay kits and it was determined that they have antioxidant potential.

Concerning the TOS values, it was observed that the mushroom *P. igniarius* had lower values compared to the mushroom *P. rimosus* and *C. cylindracea* and higher values compared to the mushroom *L. tigrinus* and *C. truncatus*. Moreover, the mushroom *P. rimosus* had higher TOS values compared to the mushroom *P. igniarius, C. cylindracea, L. tigrinus* and *C. truncatus*. It is thought that this difference between the TOS values stems from the fact that mushrooms were collected from different regions and from the different oxidant compound production capacities of the mushrooms.

Regarding the OSI value, which indicates how much TAS values suppress TOS values in percentage, it was observed that the mushroom *P. igniarius* had higher values compared to the mushroom *C. truncatus* and lower values compared to the mushroom *P. rimosus, L. tigrinus* and *C. cylindracea*. Furthermore, it was seen that *P. rimosus* had lower values compared to L. tigrinus and higher values

TABLE 1
TAS, TOS and OSI Values

	TAS	TOS	OSI
P. igniarius	5.364±0.097	20.854±0.130	0.389±0.008
P. rimosus	3.772±0.073	24.323±0.074	0.645±0.014

Values are presented as mean±S.D.; n=6 (Experiments were made as 5 parallel)

TABLE 2
Antimicrobial Activity of Mushroom Extracts

	1	2	3	4	5	6	7	8	9
P. igniarius	100	100	200	400	200	100	50	50	50
P. rimosus	100	400	200	400	100	100	50	50	50
Ampicillin	1.56	3.12	1.56	3.12	3.12	-	-	-	-
Amikacin	-	-	-	1.56	3.12	3.12	-	-	-
Ciprofloksasin	1.56	3.12	1.56	1.56	3.12	3.12	-	-	-
Flukanazol	-	-	-	-	-	-	3.12	3.12	-
Amfoterisin B	-	-	-	-	-	-	3.12	3.12	3.12

The MIC values are presented in units of µg/mL
1: *S. aureus*, 2: *S. aureus* MRSA, 3: *E. faecalis*, 4: *E. coli*, 5: *P. aeruginosa*, 6: *A. baumannii*, 7: *C. albicans*, 8: *C. glabrata*, 9: *C. krusei*

compared to *P. igniarius*, *C. truncatus* and *C. cylindracea*. Consequently, although the mushrooms used in this study had high TAS values, they also had high OSI values due to the high amount of oxidant compounds they produce as a result of the environmental and inherent effects.

Antimicrobial Activity. Drugs with antimicrobial properties have caused a striking change not only in the treatment of contagious diseases but also in the fate of the humankind. Significant progress has been made in antimicrobial treatment. However, organisms resistant to antimicrobial drugs started to emerge and infections have become and still is an important and challenging problem in clinical practice. In addition, the selection of agents for antimicrobial treatment can be significantly limited when multiple organisms resistant to antimicrobial drugs emerge in a widespread manner. Currently, the number of new antimicrobial agents introduced to the pharmaceutical market is low. Considering this situation, there is a very limited selection of antimicrobial agents with the increasing awareness of drug safety [26,27]. In this current study conducted within this scope, the researchers used ethanol extracts of the mushroom *P. igniarius* and *P. rimosus* and investigated their antimicrobial effects on 9 microorganisms. The findings are shown in Table 2.

It was found that *P. igniarius* and *P. rimosus* extracts used in this study had an effect on the microorganisms at 50-400 µg/mL concentrations. Moreover, it was determined that both mushroom extracts were more effective against the tested fungus strains. It was reported in previous antimicrobial activity studies that *P. igniarius* had antimicrobial effects on *Bacillus subtilis, B. pumilus, Staphylococcus aureus, Sarcina lutea, Pseudomonas aeruginosa, Escherichia coli* and *Penicilium* spp. [28, 29]. Moreover, previous studies have also reported that *P. rimosus* showed antimicrobial effects on *E. coli, P. aeruginosa, S. aureus, Salmonella typhimurium* and *B. subtilis* [30]. According to this current study, ethanol extracts of the mushroom *P. igniarius* were effective against the test microorganisms used in this study at different concentrations. Consequently, it was found that the mushroom *P. igniarius* and *P. rimosus* could be potential antimicrobial agents against the tested microorganisms.

CONCLUSIONS

In this study, the researchers aimed to determine the antioxidant and antimicrobial activities of the medicinal mushroom *P. igniarius* and *P. rimosus*. It was determined that the mushrooms have a high antioxidant activity. It was also found that they can be natural antimicrobial agents against the tested microorganisms. In conclusion, it was found that the mushrooms *P. igniarius* and *P. rimosus* could be used as antioxidant and antimicrobial agents in pharmacological designs.

ACKNOWLEDGEMENT

I would like to express our gratitude to Dr. Hasan AKGUL and Dr. Mustafa SEVİNDİK for their contributions to the present study.

Author declare no conflict of interest.

REFERENCES

[1] Colegate, S.M., Molyneux, R.J. (2008) Bioactive natural products: Detection, isolation and structure determination. CRC Press, Boca Raton
[2] Dewick, P.M. (2009) Medicinal natural products: A Biosynthentic Approach, 3rd Edn. Wiley, Great Britain.
[3] Mishra, B.B., Tiwari, V.K. (2011) Natural products: an evolving role in future drug discovery. Euro J. Med. Chem. 46, 4769–4807

[4] Sevindik, M., Akgul, H., Akata, I., Alli, H., Selamoglu, Z. (2017) *Fomitopsis pinicola* in healthful dietary approach and their therapeutic potentials. Acta Alimentaria. 46(4), 464-469.
[5] Bal, C., Sevindik, M., Akgul, H., Selamoglu, Z. (2019) Oxidative Stress Index and Antioxidant Capacity of *Lepista nuda* Collected From Gaziantep/Turkey. Sigma. 37(1), 1-5.
[6] Lima, A.D., Costa Fortes, R., Garbi Novaes, M.R.C., Percário, S. (2012) Poisonous mushrooms; a review of the most common intoxications. Nutricion Hospitalaria. 27(2).
[7] Bal, C., Akgul, H., Sevindik, M., Akata, I., Yumrutas, O. (2017). Determination of the antioxidative activities of six mushrooms. Fresen. Environ. Bull. 26(10), 6246-6252.
[8] Cheung, L.M., Cheung, P.C., Ooi, V.E. (2003) Antioxidant activity and total phenolics of edible mushroom extracts. Food Chemistry. 81(2), 249-255.
[9] Sevindik, M., Akgul, H., Dogan, M., Akata, I., Selamoglu, Z. (2018). Determination of antioxidant, antimicrobial, DNA protective activity and heavy metals content of Laetiporus sulphureus. Fresen. Environ. Bull. 27(3), 1946-1952.
[10] Ranadive, K., Jagtap, N., Vaidya, J. (2012) Host diversity of genus Phellinus from world. Elixir Appl. Botany. 52, 11402-11408.
[11] Erel, O. (2004) A novel automated direct measurement method for total antioxidant capacity using a new generation, more stable ABTS radical cation. Clinical Biochemistry. 37(4), 277-285.
[12] Erel, O. (2005) A new automated colorimetric method for measuring total oxidant status. Clinical Biochemistry. 38(12), 1103-1111.
[13] Bauer, W.A., Kirby, W.M., Sherris, J.C., Turck, M. (1966) Antibiotic susceptibility testing by a standardized single disk method. Am J Clin Pathol. 45, 493-496.
[14] Hindler, J., Hochstein, L., Howell, A. (1992) Preparation of routine media and reagents used in antimicrobial susceptibility testing. Part 1. McFarland standards, p. 5.19.1-5.19.6. In H. D. Isenberg (ed) Clinical microbiology procedures handbook, vol. 1. American Society for Microbiology, Washington, D.C.
[15] CLSI (The Clinical and Laboratory Standards Institute) (2012) Antimicrobial Susceptibility Testing of Anaerobic Bacteria. Approved Standard-Eighth Edition (M11-A8).
[16] EUCAST (European Committee on Antimicrobial Susceptibility Testing) (2014) Breakpoint tables Fungal Isolate for Interpretation of MICs. 2014; Version 7.0
[17] Matuschek, E., Brown, D.F., Kahlmeter, G. (2014) Development of the EUCAST disk diffusion antimicrobial susceptibility testing method and its implementation in routine microbiology laboratories. Clin. Microbiol. Infect. 20, 255-266.
[18] EUCAST (European Committee on Antimicrobial Susceptibility Testing) (2015) Breakpoint tables for Bacteria interpretation of MICs and Zone Diameters 2015. Version 5.0
[19] Sevindik, M., Akgul, H., Bal, C., Selamoglu, Z. (2018) Phenolic Contents, Oxidant/Antioxidant Potential and Heavy Metal Levels in *Cyclocybe cylindracea*. Indian Journal of Pharmaceutical Education and Research. 52(3), 437-441.
[20] Sevindik, M. (2018) Investigation of Antioxidant/Oxidant Status and Antimicrobial Activities of *Lentinus tigrinus*. Advances in Pharmacological Sciences. 2018
[21] Sevindik, M. (2018) Investigation of Oxidant and Antioxidant Status of Edible Mushroom *Clavariadelphus truncatus*. Mantar Dergisi. 9 (2), 165-168.
[22] Ajith, T.A., Janardhanan, K.K. (2002) Antioxidant and antihepatotoxic activities of *Phellinus rimosus* (Berk) Pilat. Journal of Ethnopharmacology. 81(3), 387-391.
[23] Lung, M.Y., Tsai, J.C., Huang, P.C. (2010) Antioxidant properties of edible basidiomycete Phellinus igniarius in submerged cultures. Journal of Food Science. 75(1), E18-E24.
[24] Li, S.C., Yang, X.M., Ma, H.L., Yan, J.K., Guo, D.Z. (2015) Purification, characterization and antitumor activity of polysaccharides extracted from Phellinus igniarius mycelia. Carbohydrate Polymers. 133, 24-30.
[25] Shou, D., Dong, Y., Wang, N., Li, H., Zhang, Y., Zhu, Y. (2016) Simultaneous Quantification of Antioxidant Compounds in Phellinus igniarius Using Ultra Performance Liquid Chromatography-Photodiode Array Detection-Electrospray Ionization Tandem Mass Spectrometry. PloS One. 11(9), e0163797.
[26] Saga, T., Yamaguchi, K. (2009) History of Antimicrobial Agents and Resistant Bacteria. JMAJ. 52(2), 103–108,
[27] Gurgen, A., Yildiz, S., Can, Z., Tabbouche, S., Kilic, A. O. (2018). Antioxidant, antimicrobial and anti-quorum sensing activities of some wild and cultivated mushroom species collected from Trabzon, Turkey. Fresen. Environ. Bull. 27(6), 4120-4131.
[28] Sittiwet, C., Puangpronpitag, D. (2008) Anüstaphytococcus aureus Activity of *Phellinus igniarius* Aqueous Extract. International Journal of Pharmacology. 4(6), 503-505.

[29] Nedelkoska, D.N., Pančevska, N.A., Amedi, H., Veleska, D., Ivanova, E., Karadele, M., Kungulovsk, D. (2013). Screening of antibacterial and antifungal activities of selected macedonian wild mushrooms. Jour. Nat. Sci, Matica Srpska Novi Sad. 124, 333–340.
[30] Sheena, N., Ajith, T. A., Mathew, A., Janardhanan, K. K. (2003) Antibacterial activity of three macrofungi, *Ganoderma lucidum*, Navesporus floccosa and *Phellinus rimosus* occurring in South India. Pharmaceutical Biology. 41(8), 564-567.

Received: **05.04.2019**
Accepted: **12.07.2019**

CORRESPONDING AUTHOR

Celal Bal
Gaziantep University,
Oguzeli Vocational School,
Gaziantep – Turkey

e-mail: bal@gantep.edu.tr

© by PSP Volume 29 – No. 05/2020 pages 3433-3445 Fresenius Environmental Bulletin

DIFFERENT ADSORPTION PATTERN OF MERCURY AND ARSENIC ON PRISTINE AND MnO_x LOADED BIOCHAR

Dilixiati Abulizi[1,4], Rehemanjiang Wufuer[1,2,4], Wenfeng Li[1,2,4], Jinglong Fan[1,2,4], Xiangliang Pan[1,3,*]

[1] Xinjiang Key Laboratory of Environmental Pollution and Bioremediation, Xinjiang Institute of Ecology and Geography, Chinese Academy of Sciences, Urumqi, China
[2]State Key Laboratory of Desert and Oasis Ecology, Xinjiang Institute of Ecology and Geography, Chinese Academy of Sciences, Urumqi, China
[3] Key Laboratory of Microbial Technology for Industrial Pollution Control of Zhejiang Province, College of Environment, Zhejiang University of Technology, Hangzhou, China
[4] University of Chinese Academy of Sciences, Beijing, China

ABSTRACT

Biochar (BC) and its manganese oxidation complex (MnBC) were synthesized by a simple method and used as a new, low-cost adsorbent to remove As (III) and Hg (II). The surface characteristics of the adsorbents before and after adsorption of As (III) and Hg (II) were characterized by Scanning Electron Microscopy/Energy Dispersive Spectroscopy (SEM/EDS), X-ray Diffraction (XRD) and Fourier Transform Infrared Spectroscopy (FTIR). The adsorption equilibrium isotherms were investigated in batch experiments to determine the adsorption capacity of the biochars for As(III) and Hg(II) in a single component system. The adsorption data were fitted to the Langmuir model. The maximum adsorption capacity of (q_m) of MnBC was higher than BC for As(III). The q_m of BC and MnBC for Hg(II) was 95.24 mg g^{-1} and 67.11 mg g^{-1}, respectively. Loading MnO_x on the biochar surface decreased the adsorption capacity of BC for Hg(II). The q_m of BC and MnBC for As(III) was 62.11 mg g^{-1} and 102.04 mg g^{-1}, respectively. MnBC had higher adsorption capacity for As(III) than BC, suggesting that oxygen-contaning functional groups, zeta potentials and amount of functional groups and surface area were important in determining As(III) and Hg(II) adsorption by these biochars. The surface modification of biochar and adsorption of metal ions were confirmed by EDS data. The results show that BC and MnBC are low-cost adsorbents that can be used to remove arsenic and mercury from waste water.

KEYWORDS:
Adsorption, mercury, arsenic, biochar, manganese oxide

INTRODUCTION

Heavy metal pollution of groundwater has been recognized as a global environmental threat, mainly due to increased wastewater emissions from mining and electroplating industries.[1]. These wastewater contain large amounts of cadmium, mercury, copper, arsenic, and lead. Among them, arsenic (As) and mercury (Hg) are examples of heavy metals, which are classified as priority pollutants because of its significant impact on human life and the environment, even at low concentrations.[2].

Arsenic and mercury can be present in the water and soil environment [3]. The toxicity of these heavy metals to aquatic organisms and consequently to mankind has been established for many years. Researchers have adopted a variety of methods, including physical, chemical, and biotechnology, to treat heavy metals in aqueous solutions. Conventional methods applied to remove heavy metals from wastewater include ion-exchange[4], membrane filtration[5], electrolysis[6], coagulation[7], flotation[8], adsorption[1,2,9-11]. Among these methods, adsorption technology is frequently applied due to its high efficiency, low cost, easy operation, and insensitivity to toxic substances. [12-13]. In recent years, a particular emphasis has been given to low cost adsorbents from highly available natural sources[5].

Biochar (BC) is a pyrolytic carbon-rich material derived from the thermal decomposition of biomass in a closed system with little or no oxygen [14]. Recent studies [15-18] have confirmed that biochar has many advantages in removing pollutants due to surface functional groups and higher adsorption potential.

Xinjiang is China's major high-quality cotton production base, cotton industry has a pivotal position in Xinjiang, where cotton planting area has reached 1.978 million hm^2 in 2014, and the output reached 4.5 million t. However, recycling of agricultural waste are becoming an issue of importance due to lack of bio-residue management practices, which resulting in arbitrary discard or even direct incineration of these agricultural resources[19]. Thus, if biochar can be applied to the removal of

As(III) and Hg(II) from wastewater, these agricultural wastes will provide additional benefits.

However, there are few studies on the adsorption properties of cotton stalk biochar and its modified products. The purpose of this paper is to study the adsorption capacity of cotton stalk biochar and its MnO_x modified form on As (III) and Hg (II), to explore the adsorption mechanism of heavy metals, and to evaluate its application potential.

MATERIALS AND METHODS

Chemicals. Distilled deionized water (DDW) with a resistivity of 18MΩ cm (Millipore, Milford, MA) was used for all procedures in this study. Stock solution (1000 mg L^{-1}) of metal ions was prepared by analytical grade compounds in DDW. All other chemicals used were of analytical grade and all solutions were prepared using DDW. Control experiments were carried out to correct for any adsorption metal ions on the container walls.

Preparation of biochars. Biochars (BC) produced from cotton stalks were obtained from Xinjinag Academy of Agricultural Sciences and were treated by the following procedure. Briefly, the obtained BC samples were ground and sieved to 60 meshes and 5g of the BC sample was soaked with 40 mL of $KMnO_4$ solution. The weight ratio of $KMnO_4$ to BC was selected as 1:10 (10%) [20]. Suspension was mixed ultrasonically for 2h and was then oven dried at 80°C for 24h. The mixture of BC and $KMnO_4$ was heated at 600°C for 0.5 h to produce MnO_x-loaded biochar (MnBC). The obtained samples were rinsed thoroughly with deionized water to remove impurities and dried at 80°C for 24h. Untreated BC was also included as adsorbent for comparison.

The effects of initial pH on As(III) and Hg(II) adsorption. The adsorption of As(III) and Hg(II) was studied at different pHs separately. The pH was adjusted within the pH 2.0±0.1–10.0±0.1, using either 0.1 M NaOH or 0.1 M HCl. The adsorption procedure is similar to the procedure used for the batch equilibrium adsorption which is described in the batch equilibrium adsorption section, except that in this study only one concentration of As(III) or Hg(II) was used, 10 mg/L.The concentration of the remaining As(III) and Hg(II) in the solution was measured after 24 h of equilibration.

Batch equilibrium adsorption. Batch experiments were conducted in duplicate using polypropylene centrifuge tubes (50mL) mixing 50 mg of biochar sample with 30 ml of either As(III) and Hg(II) solution, at concentration range of 10–100 mg L^{-1}, with a pH of 3.0±0.1 and 6.0±0.1 for As(III) and Hg(II), respectively. The background electrolyte was 0.01 M $NaNO_3$ and pH of all test solutions was adjusted using 0.01 M NaOH or HCl. Reactors were then shake at 40 rpm for 24 h at a temperature of 30°C. Afterward, the mixture was centrifuged at 6000g for 10 min and the metal ion concentrations in the supernatant were determined via hydride generation atomic florescence spectroscopy (HG-AFS) (AFS-810, Jitian, Beijing, China). Prior to analysis, the sample was first acidified with 2% HNO_3. All experiments were conducted in duplicate. The amount of metal ions adsorbed was determined by difference between initial and final metal concentrations in the solution.

The adsorption capacity of As(III) and Hg(II) were calculated from:

$$q_e = \frac{(C_0 - C_e)V}{W}$$

where q_e (mg g^{-1}) is the metal ion adsorption capacity at equilibrium, V (L) is the volume of the aqueous solution, W (g) is the mass of dry adsorbent added in the solution (g), and C_0 and C_e (mg L^{-1}) are the initial and equilibrium metal ion concentrations, respectively.

Characterization and analytical techniques. Raw material analysis. According to the researches, the proximate analysis of cotton stalk indicated that this raw material contained 44.47 % of fixed carbon, 5.60 % of hydrogen, 0.53 % of nitrogen, and 49.47 % of oxygen, which shows that the carbon content of cotton stalk is higher than the other biomass resources [21].Cotton stalk had the following chemical composition: cellulose 43.1%, hemicelluloses 26.9%, lignin 27.3%, ash 1.3%, and ethanol-benzene extractives 5.6%[22].

XRD analysis. X-ray powder diffraction (XRD) patterns of BC and MnBC were obtained on an X'Pert PRO X-ray diffractometer (PANalytical, Holland) at 40 kV/40 mA using CuKa radiation (k=0.154 nm). XRD patterns were recorded by step scanning from 10°C to 80°Cwith the sample spinning at 2 r/s[23].

Zeta potential analysis. The zeta potential of the BC and MnBC were determined in triplicate by placing a 0.02 g sample in a 250-mL conical flask and then adding 100 mL of 0.1 M NaCl solution. The suspension pH was adjusted within the range of 2.0±0.1–10.0±0.1, using 0.1 M NaOH or 0.1 M HCl. The suspensions were ultrasonically dispersed in a bath-type sonicator for 2 h at 30°C[24]. The suspensions were kept standing at room temperature for 24 h, after which electrophoresis mobility was measured using Malvern Zetasizer Nano analyzer. (Malvern, UK).

Scanning electron microscopy analysis. The surface morphology of the BC and MnBC before

and after adsorption of As(III) and Hg(II), was analyzed by scanning electron microscopy (SEM) (Zeiss Super 55VP, Germany)-energy dispersive spectroscopy (EDS) (Bruker XFlash 5010, Germany).

FTIR analysis. Fourier transform infrared (FTIR) spectroscopy analysis was carried out to determine the surface functional groups of the BC and MnBC before and after the adsorption of As(III) and Hg(II), using a FTIR spectrometer (Vertex 70, Bruker, Germany).

RESULTS AND DISCUSSION

X-ray diffraction analysis. In order to prove whether MnO_x was successfully loaded on MnBC, we tested the original biochar and MnO_x modified biochar using XRD technology.The XRD patterns of BC and MnBC samples are presented in Figure 1. The wide diffraction peak at a small angle could be attributed to the amorphous phase of the biochar that was apparent in all samples [25]. The XRD patterns of all biochars are quite similar and are characterized by the more or less elevated background between 2 theta of 16 and 26, due to the presence of organic matter [26]. However, some slight differences were noted in the samples. Compared with Power Diffraction and Standards (PDF), sharp peaks in the biochars indicate the presence of inorganic components such as SiO_2, $CaCO_3$ and $CaSi_2$. According to the study, the content of SiO_2 in cotton stalk chars reaches up to 18.21% [27], which explains high Si content in biochar samples.

Compared with BC, MnBC exhibited major characteristic peaks of 2 Theta at 12.5, 25.2, 37.4, 46.7 and 66.3 which were attributed to the existence of MnO_x crystal and amorphous MnO_x [28-30]. Thus, it can be concluded that MnO_x was successfully loaded on MnBC.

Zeta potential of the BC and MnBC. The zeta potentials of BC and MnBC at different pHs are shown in Figure 2.In the pH range of 3.0±0.1–10.0±0.1, the zeta potentials of both biochars were negative, while at pH of 2.0±0.1 the zeta potential of unmodified biochar shows positive. The zeta potential of the BC and MnBC at pH 2.0±0.1 was 5.34 mV and 6.4 mV, respectively, and became negative with increasing pH. The zeta potential of the BC after pH 2.0±0.1 became drastically more negative with increasing pH, reaching -28.1 mV at a pH of 5.0±0.1. However, the negative value of the zeta potential of MnBC reached -18.4mV at pH of 4.0±0.1, and thereafter, the zeta potentials was not significantly affected by the increasing pH.

The Zeta potential of MnBC was higher than that of BC at all pH values. The negative values of the zeta potential of the two biochars at all pH indicate that the surfaces of the two biochars are negatively charged, and the number of negative charges increases with increasing pH. [24].

The effect of initial pH on As(III) and Hg(II) adsorption. Solution pH plays an important role in controlling heavy metal adsorption mechanism [25,31].The adsorption of heavy metals depends on the surface properties of the adsorbent and the distribution of metal ions in the solution, which mainly depends on the pH value of the system [32]. Figure 3 shows the effect of variation of initial solution pH (3.0– 10.0) on the adsorption of As(III) and Hg(II), which revealed that the removal efficiency of Hg(II) of BC and MnBC were higher than that of As(III).

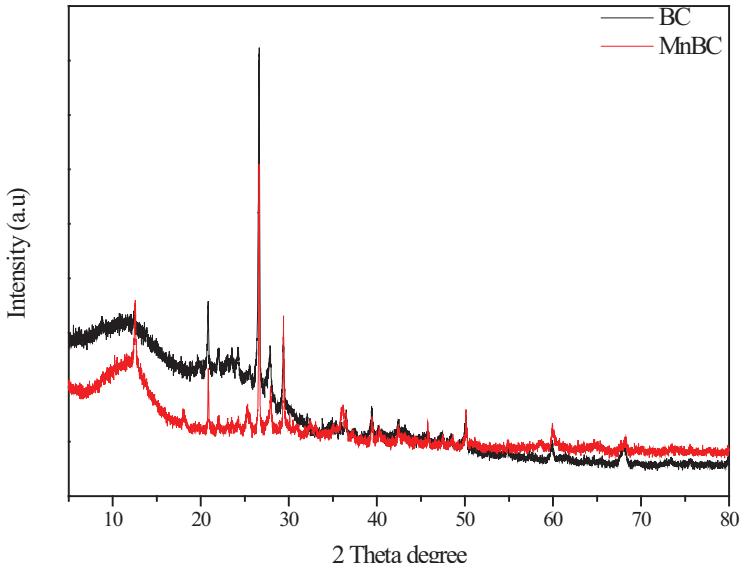

FIGURE 1
XRD intensity patterns for BC and MnBC

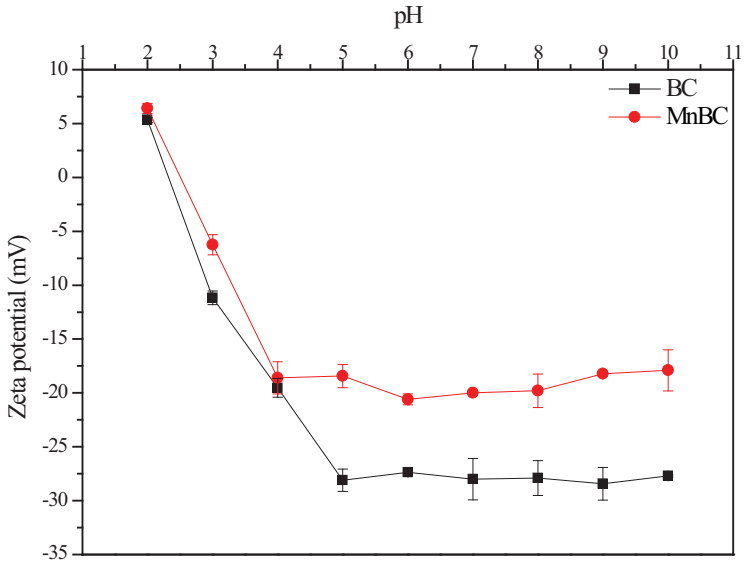

FIGURE 2
Zeta potential of the BC and MnBC at different pHs are displayed as the mean of triplicates with error bars of 1 standard deviation

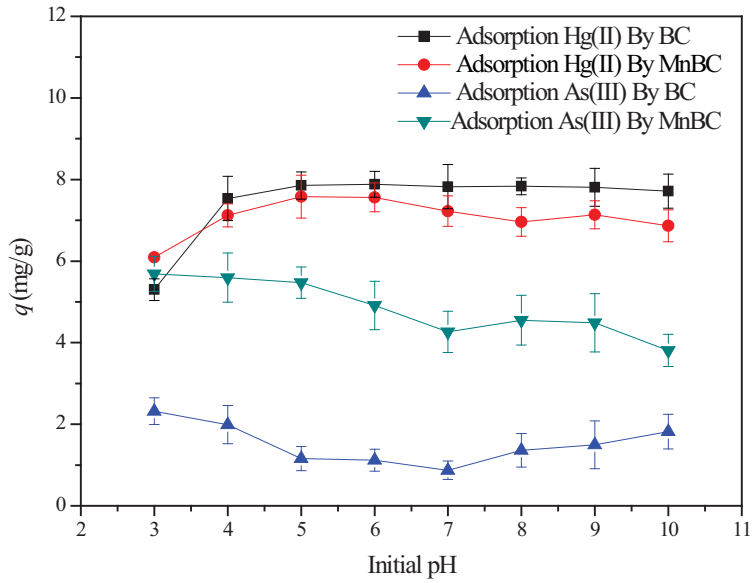

FIGURE 3
The amounts of As(III) and Hg(II) adsorbed by the BC and MnBC at different pHs are displayed as the mean of duplicates with error bars of 1 standard deviation

Adsorption of Hg (II). As can be seen from Figure 3, the amount of Hg(II) adsorbed increased with increasing initial pH and maximum adsorption occurred around pH 6.0±0.1. This is close to the value reported by Kadirvelu et al [33] and Namasivayam et al [34], who used activated carbon as a sorbent. The amount of Hg(II) adsorbed by BC increased with increasing pH (from 3.0±0.1 to 6.0±0.1) and then remained constant up to a pH value of 10±0.1, while by MnBC it deceased after pH from 6.0±0.1 to 10.0±0.1.

Adsorption of As (III). Figure 3 indicates that with modified BC, the amount of As(III) adsorbed decreases with an increase in pH from 3.0±0.1 to 7.0±0.1, and then increased up to pH of 10.0±0.1. Maximum adsorption capacity of As(III) was observed in the pH range of 3.0±0.1-4.0±0.1 for both raw and MnO_x-loaded biochars followed by a decrease with increase in the pH from 4.0±0.1 to 7.0±0.1. However, our result is in contrast with result of Gupta et al[35] who reported removal of As(III) increases with an increase in pH from 4.5 to 7.5 and remains almost constant on further increase in pH up to 10.5. But our data also have similar

results with that of Mohan and Pittman [36], who reported maximum As(III) adsorption onto the biochar derived from oak bark, oak wood, pine bark, and pine wood in the pH range 2.0 to 4.0. It can be seen from the data that the modification of biochar with MnO_x improves the adsorption capacity of biochar to As(III).

Adsorption equilibrium analysis. The effects of initial concentrations on the absorption of As(III) and Hg(II) by BC and MnBC were studied at initial metal concentrations of 10-100 mg L^{-1}.The results are reported as the functions of the equilibrium adsorption capacities of the As(III) and Hg(II) (qe) versus the equilibrium concentration of the As(III) and Hg(II) in the testing solutions (Ce).

In order to evaluate the adsorption capacity and predict the adsorption mechanism, the Langmuir isotherm model was used to analyze the adsorption equilibrium data.

The following equations represent the Langmuir isotherms:

$$\frac{C_e}{q_e} = \frac{C_e}{q_m} + \frac{1}{bq_m}$$

Where q_e and C_e are the adsorption capacity (mg g^{-1}) and equilibrium metal ion concentrations (mg L^{-1}) respectively. q_m and b represent the maximum monolayer adsorption capacity of adsorbents (mg g^{-1}) and the Langmuir adsorption constant related to the energy of adsorption (mg L^{-1}), respectively. A linearized plot of C_e/q_e against Ce gives a q_m and b.

The results of data fitting to the Langmuir isotherms are given in Table 1. They suggest that Langmuir isotherms show a good fit to the experimental data, as indicated by the high R^2 values.

The maximum adsorption capacity (q_m) of BC and MnBC for Hg(II) was 95.24 mg g^{-1} and 67.11 mg g^{-1}, respectively. Loading MnO_x on the biochar decreased the q_m of BC for Hg(II) to 67.11 mg g^{-1}. The q_m of BC and MnBC for As(III) was 62.11 mg g^{-1} and 102.04 mg g^{-1}, respectively. Modifying the biochar surface with MnO_x increased its adsorption capacity for As(III). However, the Langmuir affinity values (b) of BC and MnBC for Hg(II) higher than As(III). The adsorption capacity of the both biochar for Hg(II) and As(III) higher than the values reported in the litireature for other bichars [27, 37].

The results show that cotton stalk biochar has good adsorption performance and can be used as an effective adsorbent to remove mercury and arsenic from aqueous solution. In addition, after loading MnO_x, the adsorption capacity of biochar for As (III) was increased.

SEM-EDS. In order to further study the surface properties of biochar and verify the adsorption of As(III) and Hg(II), SEM-EDS analysis was performed on the samples.The SEM images for surface morphology of BC and MnBC before and after adsorption of As(III) and Hg(II) were shown in Figure 4 and Figure 5, respectively. The structures of BC and MnBC are shown in Figure 4b and 5b.

As can be seen from Figures 4 and 5, due to the different surface area and pore volume of biochar, the surface of biochar exhibits irregular porosity, including different sizes and shapes. SEM images show that the surface of BC is composed of a porous structure, which is smoother than MnBC (Figure 4b and Figure 5b). The EDS is used to determine the chemical composition of the sample [31].As shown in Figures 5a-5c, EDS of MnBC showed strong signals for Mn and O atoms, which confirms the existence of manganese oxides on $KMnO_4$ treated BC.

The EDS analysis spectrum before adsorption of the Hg(II) and As(III) (Figure 4a and Figure 5a) showed the absence of the Hg and As while the success of adsorption could be observed by EDS spectrum after adsorption of Hg(II) (Figure 4b and Figure 5b) and As(III) (Figure 4c and Figure 5c). It can be attributed to the Hg(II) and As(III) adsorption onto the BC and MnBC surfaces.

TABLE 1
Parameters of the isotherms for Hg(II) and As(III) adsorption onto adsorbents

Biochar		Langmuir's model		
		q_m (mg g^{-1})	b	R^2
BC	Hg(II)	95.24	0.0692	0.9902
MnBC	Hg(II)	67.11	0.0748	0.9957
BC	As(III)	62.11	0.0087	0.9844
MnBC	As(III)	102.04	0.0089	0.9899

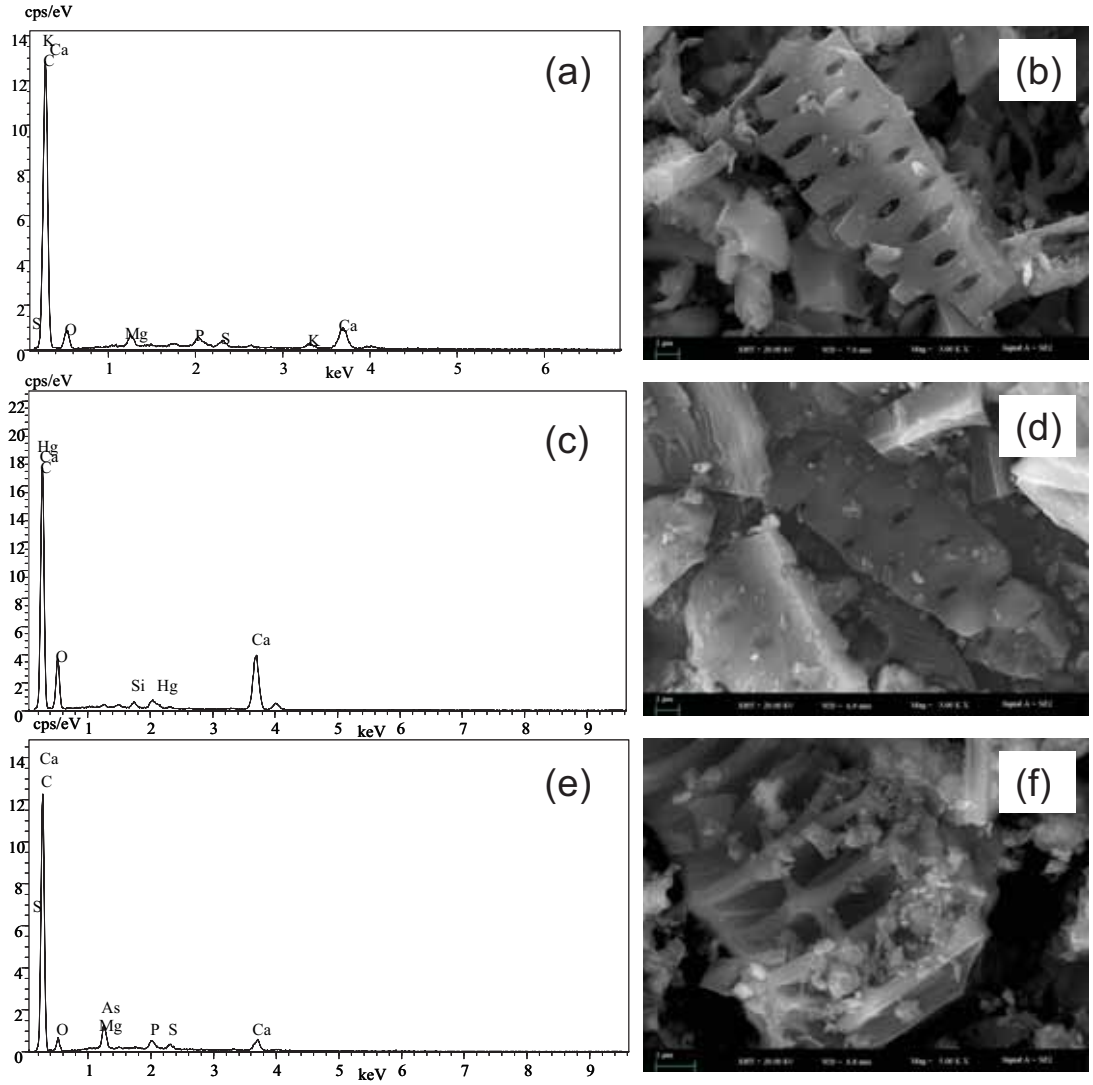

FIGURE 4
The SEM images for the BC: (a) EDS spectrum of the BC before adsorption; (b) Surface of BC before adsorption; (c) EDS spectrum of the BC after adsorption of Hg(II); (d) Surface of BC after adsorption of Hg(II); (e) EDS spectrum of the BC after adsorption of As(III); (f) Surface of BC after adsorption of As(III);

FTIR spectra analysis of BC and MnBC before and after adsorption of As(III). The FTIR spectra of the BC and MnBC before and after adsorption of As(III) are shown in Figure 6 (A-B), respectively.

The broad and weak band observed at 3435 and 3431 cm^{-1} could be assigned to the stretching vibration of hydroxyl functional groups in BC and MnBC, respectively [38]. New peaks appeared after adsorption of arsenic at 1635 cm^{-1} in MnBC, which can be attributed to amide C=O stretching, as observed mainly in proteins [39]. The peaks at 1581cm^{-1} in BC before and after adsorption of metal was attributed to C=C ring or COO–group stretching [40].The peak around 1440cm^{-1} in both biochars was attributed to aromatic C=C stretching. Bands appearing around 1400 to 1425cm^{-1} in MnBC correspond to the C=O stretching vibration [38]. Bands around 1140-1000cm^{-1} were attributed to C-O-C stretching vibrations and Si–O–Si in-plane vibration [41].Peaks at 875 and 775cm^{-1} representing aromatic C−H groups. It was reported that the characteristic absorption bands of adsorbed arsenate was 650-1050cm^{-1} for As-OH or As-O stretching vibration [42]. Buciuman et al. [43] assigned the 510 and 580 cm^{-1} peaks to be the characteristic features of MnO_2, while the peak around 650 cm^{-1} is attributed to β-MnO_2 by.

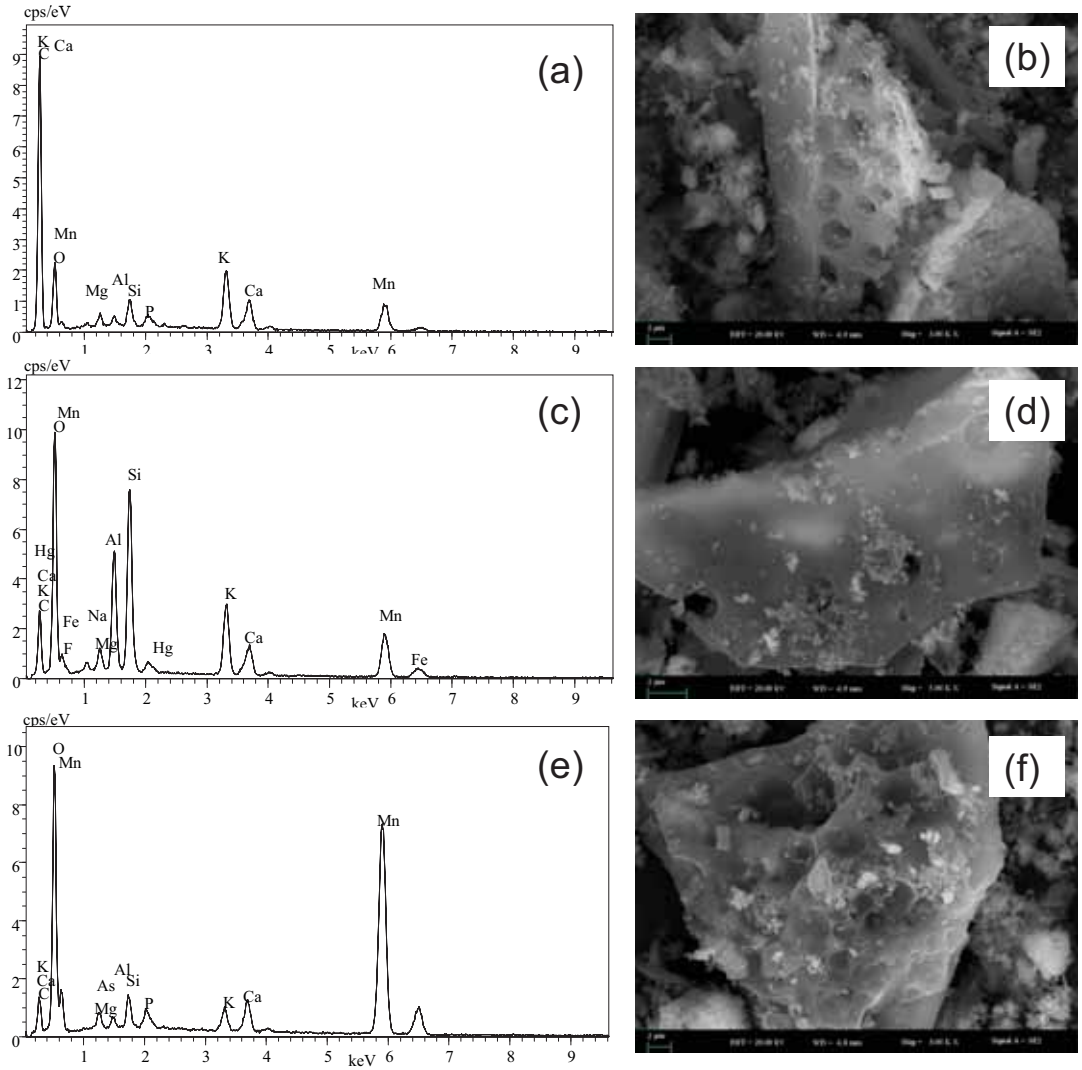

FIGURE 5
The SEM images for the MnBC: : (a) EDS spectrum of the MnBC before adsorption; (b) Surface of MnBC before adsorption; (c) EDS spectrum of the MnBC after adsorption of Hg(II); (d) Surface of MnBC after adsorption of Hg(II); (e) EDS spectrum of the MnBC after adsorption of As(III); (f) Surface of MnBC after adsorption of As(III);

FTIR spectra analysis of BC and MnBC before and after adsorption of Hg(II). The FTIR spectra of the BC and MnBC before and after adsorption of Hg(II) are shown in Figure 7. The broad and weak band observed at 3278 cm^{-1} and 3430 cm^{-1} could be assigned to the stretching vibration of hydroxyl functional groups [38]. The metal loaded adsorbents showed a shift in the absorption frequencies of OH group indicating the probability of binding of mercury to the -OH groups present in BC and MnBC by complex formation [44]. The strong bands at 1581 cm^{-1} in BC before and after the adsorption of Hg(II) were attributed to the C=O stretching vibration of aromatic rings, which became weaker in MnBC. The peaks at 1430 cm^{-1} in both BC and MnBC was attributed to aromatic C=C stretching [45]. Bands around 1110-1040 cm^{-1} were attributed to C-O-C stretching vibrations in cellulose and hemicelluloses [41].Peaks between 885 and 750cm^{-1} representing aromatic C−H groups was consistent with condensation of biochar structure [46]. The sharp adsorption bands at 520 cm^{-1} and 609 cm^{-1} can be attributed to Mn–O stretching vibration and bending, which indicates that the BC was successfully treated with MnO_x [47]. Noticeably, modification with $KMnO_4$ increased the contents of O-containing groups of BC, reflected by the enhanced band intensities such as 1110-1040 cm^{-1}.

Reig et al [48] assigned the 712 cm^{-1} peak to be calcium carbonate ($CaCO_3$), an inorganic compound found in biochars from different types of feed stocks [49]. The 1030cm^{-1} peak is correlated with the SiO stretching and an indication of SiO_2 [50].

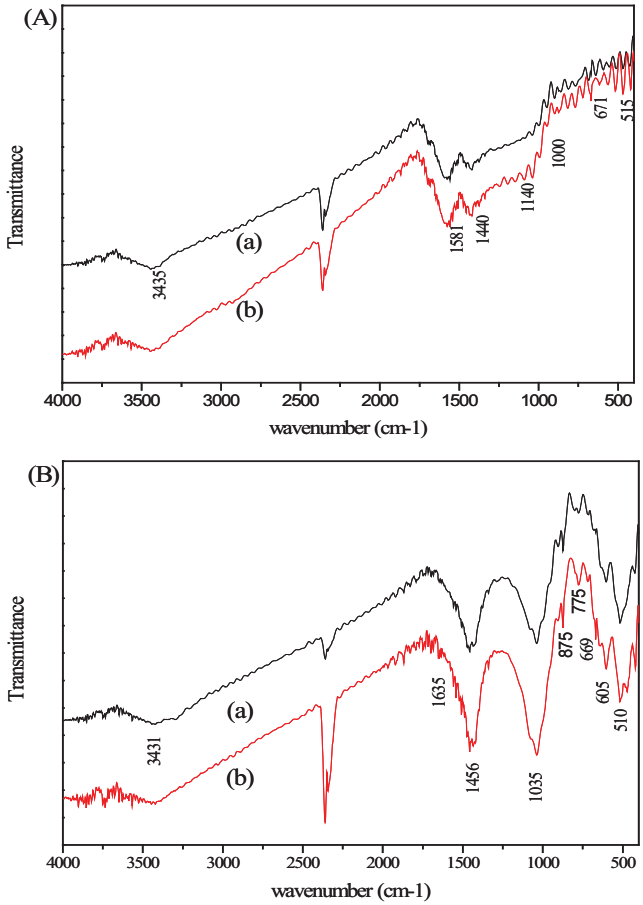

FIGURE 6
The FTIR spectra of BC (A) and MnBC (B) : (A) before adsorption of As(III); (B) after adsorption of As(III)

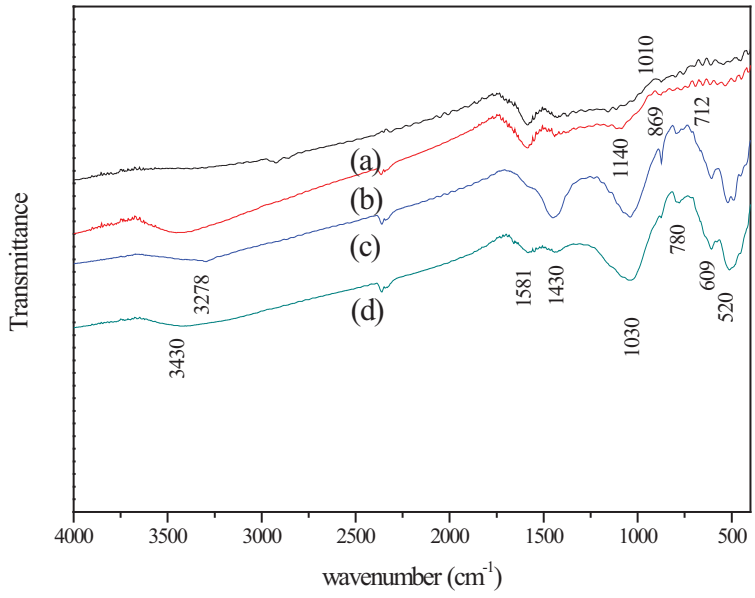

FIGURE 7
The FTIR spectra for (a) BC before adsorption; (b) MnBC before adsorption; (c) BC after adsorption of Hg(II); (d) MnBC after adsorption of Hg(II);

Analysis of possible mechanism. Absorption of metal ions from aqueous solutions is generally controlled by surface chemistry and the surface area of the absorbent[51]. Studies [20,39,52] suggested that manganese oxides and impurities from the decomposition of $KMnO_4$ at high temperature could heavily block the micro pores and reduce the surface area and pore volume of biochar. On the other hand, the strong oxidization of $KMnO_4$ on MnBC may lead to the destruction of some nanopores and deformation from nanopores to mesopores/macropores.[20], similar result was obtained with carbon nanotubes activated by KOH etching [53].The findings of our study indicate that the Hg sorption capacity of BC was higher than those of MnBC while As sorption capacity of MnBC was much higher than BC **(Table 1**), this shows that biochar has different adsorption modes for mercury and arsenic. The adsorption of mercury by BC or MnBC is controlled by its surface area, while the adsorption of arsenic has little relationship with biochar's surface area.

In addition, from zeta potential analysis, it can be seen that at pH values of 3 to 10, both BC and MnBC surfaces are negatively charged (**Figure 2**), which is conducive to the adsorption of Hg cations through electrostatic interactions [54]. However, the zeta potential of MnBC (**Figure 2)** is higher than that of BC at each pH, indicating that the negative charge on the surface of MnBC is less than that of BC, which may be the reason why MnBC has a lower adsorption capacity for Hg (II) than BC **(Table 1**). Meanwhile, compared with BC, MnBC's surface charge is more favorable for the adsorption of As(III), which also explains why MnBC has a stronger adsorption capacity for As(III) than Hg(II)(**Table 1**).

Sorption mechanism of Hg(II) on biochars. It was proposed that Hg(II) can be bound to the surface of adsorbents by complexing with functional groups, electrostatic interaction [55] or ion exchange [56]. Precipitation and reduction reactions were other two important mechanisms for Hg(II) sorption[54].

The predominant removal mechanisms appear to be chemical binding of Hg to functional groups (e.g., thiol, hydroxyl, carboxylic, chloride) on the surface of and within the biochars [57]. Based on the XRD,SEM and FTIR analyses, and published studies [57-58], the following Hg removal mechanisms are proposed:

$$2—Cl+Hg^{2+}\rightarrow—Cl—Hg—Cl— \quad (1)$$

$$2Cl^{-}+Hg^{2+}=HgCl_2 \quad (2)$$

$$—OH+Hg^{2+}=—OHg^{+}+H^{+} \quad (3)$$

$$—COOH+Hg^{2+}=—COOHg^{+}+H^{+} \quad (4)$$

Based on the FTIR and SEM analyses, MnBC contains surface active sites (e.g., –OH) which can adsorb mercury. Furthermore, the Mn–O or Mn–OH in MnO_2 or MnOOH likely plays a significant role in the complexation between MnO_2 or MnOOH and Hg(II)[59]. The type of mercury species may also be an important role in mercury removal efficiency.

Sorption mechanism of As(III) on biochars. Véronique et al [60] reported that manganese-based materials are very effective for the removal and oxidation of arsenic. Yu et al [39] found the O content increased from 5.16 to 10.90% after impregnation BC with manganese oxides, which may reflect an increased number of oxygen containing functional groups in MnO_x coated biochar, indicating its potential for oxidation performance. Adsorption isotherm and FTIR analyses indicated that the adsorption of As(III) occurred on the surface of the adsorbent, where Mn-O/As bonds and other oxygenated function groups were formed during the adsorption process on BC and MnBC surface. Based on our XRD, SEM-EDS and FTIR analyses, As(III) removal was achieved through partial oxidation of As(III) to As(V) by Mn oxides. Then, As(V) and As(III) are adsorbed on the surface via interactions with functional groups, diffuse into the interior, and finally, achieve equilibrium in the absorbent [61], and the strong oxidative property of $KMnO_4$ on MnBC [20] could be attributed to higher adsorption capacity of MnBC for As(III). The possible adsorption mechanism of As(III) onto the MnBC is an oxidation coupled with adsorption behavior of biochars, which can be briefly represented by following equations:

$$As(III)+(–S_{Mn-O})\rightarrow As(III)–S_{Mn-O} \quad (5)$$

$$As(III)–S_{Mn-O}+MnO_2 + 2H^{+}\rightarrow As(V)+ Mn^{2+}+H_2O \quad (6)$$

$$As(V)+As(III)–S_{Mn-O}\rightarrow As(V)–S_{Mn-O}+As(III) \quad (7)$$

Where $(–S_{Mn-O})$ represents an adsorption site on the MnOx adsorbent surface. $As(III)–S_{Mn-O}$ represents the As(III) surface species and $As(V)–S_{Mn-O}$ represents the As(V) surface species [62]. This oxidation and sorption mechanism could explain the As(III) adsorption by MnBC in our study.

CONCLUSION

This study investigated the adsorption capacity of cotton stalk biochar and its modified products on As (III) and Hg (II). Changes in solution initial pH dramatically affected the adsorption processes.The adsorption isotherm experiment showed that cotton stalk biochar and its manganese oxide composite had good adsorption properties and could be used as effective adsorbents to remove mercury and arsenic. The Langmuir model is consistent with the adsorption process of As (III) and Hg (II). The adsorption parameters reveal that loading MnO_x can increase the adsorption capacity of biochar to As (III). The XRD test verified that MnO_x was successfully loaded on MnBC. The adsorption mechanism

of biochar to As(III) and Hg(II) was discussed based on the results of SEM-EDS and FTIR analysis. The results show that cotton stalk biochar is a promising adsorbent for removing As (III) and Hg (II) from wastewater. Loading MnO_x on the surface of biochar effectively improves its ability to adsorb arsenic.

ACKNOWLEDGEMENTS

This work was supported by Science and Technology Department of Xinjiang Uyghur Autonomous Region (2016D03003, 2017B03014), the West Light Foundation of Chinese Academy of Sciences (2016-QNXZ-B-15), the National Natural Science Foundation of China (U1120302 and 21177127).

REFERENCES

[1] Van Vinh, N., Zafar, M., Behera, S.K., Park, H.S. (2015) Arsenic(III) removal from aqueous solution by raw and zinc-loaded pine cone biochar: equilibrium, kinetics, and thermodynamics studies. International Journal of Environmental Science and Technology. 12(4), 1283-1294.

[2] Sulaymon, A.H., Yousif, S.A., Alfaize, M.M. (2014) Competitive biosorption of lead mercury chromium and arsenic ions onto activated sludge in fixed bed adsorber. Journal of the Taiwan Institute of Chemical Engineers. 45(2), 325-337.

[3] Nriagu, J.O. (1996) A History of Global Metal Pollution. Science. 272(5259), 223-0.

[4] Bilge, A., Veli, S. (2009) Kinetics and equilibrium studies for the removal of nickel and zinc from aqueous solutions by ion exchange resins. Journal of Hazardous Materials. 167(1-3), 482-488.

[5] Shaalan, H.F., Sorour, M.H., Tewfik, S.R. (2001) Simulation and optimization of a membrane system for chromium recovery from tanning wastes. Desalination. 141(3), 315-324.

[6] Abou-Shady, A., Peng, C.S., Bi,J.J., Xu, H.J. (2012) Recovery of Pb (II) and removal of NO_3^- from aqueous solutions using integrated electrodialysis, electrolysis, and adsorption process. Desalination. 286(none), 304-315.

[7] Song, S., Lopez-Valdivieso, A., Hernandez-Campos, D.J., Peng, C., Monroy-Fernandez, M.G., Razo-Soto, I. (2006) Arsenic removal from high-arsenic water by enhanced coagulation with ferric ions and coarse calcite. Water Research. 40(2), 0-372.

[8] Mavrov, V., Erwe,T., Blöcher, C., Chmiel,H. (2003) Study of new integrated processes combining adsorption, membrane separation and flotation for heavy metal removal from wastewater. Desalination. 157(1), 97-104.

[9] Ngah, W.S.W., Hanafiah, M.A.K.M. (2008) Removal of heavy metal ions from wastewater by chemically modified plant wastes as adsorbents: A review. Bioresource Technology. 99(10), 3935-3948.

[10] Martins, A.E., Pereira, M.S., Jorgetto, A.O., Martines, M.A.U., Silva, R.I.V., Saeki, M.J., Castroa, G.R. (2013) The reactive surface of Castor leaf [*Ricinus communis L.*] powder as a green adsorbent for the removal of heavy metals from natural river water. Applied Surface Science. 276(Complete), 24-30.

[11] Zhu, N., Yan, T., Qiao,J., Cao, H. (2016) Adsorption of arsenic, phosphorus and chromium by bismuth impregnated biochar: Adsorption mechanism and depleted adsorbent utilization. Chemosphere. 164, 32-40.

[12] Aydın, H., Bulut,Y., Yerlikaya, C. (2008) Removal of copper (II) from aqueous solution by adsorption onto low-cost adsorbents. Journal of Environmental Management. 87(1), 37-45.

[13] Liu, Z., Chen, B., Wang, L.A., Li, X. (2019) Screening of adsorbents in the Phytoremediation of mercury-contaminated soil. Fresen. Environ. Bull. 28, 4357-4362.

[14] Inyang, M., Gao, B., Yao, Y., Xue, Y., Zimmerman, A.R., Pullammanappallil, P. (2012) Removal of heavy metals from aqueous solution by biochars derived from anaerobically digested biomass. Bioresour. Technol. 110(none), 50-56.

[15] Chen, Y.N., Chai, L.Y., Shu, Y.D. (2008) Study of arsenic(V) adsorption on bone char from aqueous solution. Journal of Hazardous Materials. 160(1), 168-172.

[16] Mohan, D., Pittman, C.U., Bricka, M., Smith, F., Yancey, B., Mohammad, J. (2007) Sorption of arsenic, cadmium, and lead by chars produced from fast pyrolysis of wood and bark during bio-oil production. Journal of Colloid & Interface Science. 310(1), 57-73.

[17] Ahmad, M., Lee, S.S., Dou, X., Mohan, D., Sung, J.K., Yang, J.E., Yong, S.O. (2012) Effects of pyrolysis temperature on soybean stover-and peanut shell-derived biochar properties and TCE adsorption in water. Bioresource Technology. 118(none), 536-544.

[18] Zhang, J., Fu, H., Lv, X., Tang, J., Xu, X. (2011) Removal of Cu(II) from aqueous solution using the rice husk carbons prepared by the physical activation process. Biomass & Bioenergy. 35(1), 464-472.

[19] Ying, M.(2016) Analysis of influencing factors of treatment methods of cotton planting's productive waste disposal in Xinjiang. Chinese Journal of Agricultural Resources & Regional Planning. 37(1),23-29.

[20] Song, Z., Lian, F., Yu, Z., Zhu, L., Xing, B., Qiu, W. (2014) Synthesis and characterization of a novel MnO_x-loaded biochar and its adsorption properties for Cu^{2+} in aqueous solution. Chemical Engineering Journal. 242, 36-42.

[21] Chen, M., Kang, X., Wumaier, T., Dou, J., Gao, B., Han, Y. (2013) Preparation of activated carbon from cotton stalk and its application in supercapacitor. Journal of Solid State Electrochemistry. 17(4), 1005-1012.

[22] Nada, A.M.A., El-Wakil, N.A., Hassan, M.L., Adel, A.M. (2006) Differential adsorption of heavy metal ions by cotton stalk cation-exchangers containing multiple functional groups. Journal of Applied Polymer Science. 101(6), 4124-4132.

[23] Wang, M.C., Sheng, G.D., Qiu, Y.P. (2015) A novel manganese-oxide/biochar composite for efficient removal of lead(II) from aqueous solutions. International Journal of Environmental Science and Technology. 12(5), 1719-1726.

[24] Samsuri, A.W., Sadegh-Zadeh, F., Seh-Bardan, B.J. (2013) Adsorption of As(III) and As(V) by Fe coated biochars and biochars produced from empty fruit bunch and rice husk. Journal of Environmental Chemical Engineering. 1(4), 981-988.

[25] Tan, Z., Wang, Y., Alfreda Kasiulienė, Huang, C., Ai, P. (2017) Cadmium removal potential by rice straw-derived magnetic biochar. Clean Technologies and Environmental Policy. 19(3), 761-774.

[26] Cao, X., Harris, W. (2010) Properties of dairy-manure-derived biochar pertinent to its potential use in remediation. Bioresource Technology. 101(14), 5222-5228.

[27] Ye, F., Tie, M., Xiong, Z., Haiping, Y., Xianhua, W., Shihong, Z. (2014) Influence of silica on physicochemical characteristic of modified bio-chars. Transactions of the Chinese Society of Agricultural Engineering. 30(24), 259-265.

[28] Fathy, N.A., El-Shafey, S.E., El-Shafey, O.I., Mohamed, W.S. (2013) Oxidative degradation of RB19 dye by a novel γ-MnO_2/MWCNT nanocomposite catalyst with H_2O_2. Journal of Environmental Chemical Engineering. 1(4), 858-864.

[29] Szlachta, M., Gerda, V., Chubar, N. (2012) Adsorption of arsenite and selenite using an inorganic ion exchanger based on Fe–Mn hydrous oxide. Journal of Colloid & Interface Science. 365(1), 213-221.

[30] Mckenzie, R.M. (1989) Manganese oxides and hydroxides. In: Minerals in Soil Environments. CSIRO Division of soils, Glen Osmond, South Australia, 371-425.

[31] Deng, H., Zhu, Z., Zhu, Y., Huang, B., Li, Y., Liang, Y., Jiang, Y. (2018) Preparation of a hierarchical porous hydroxyapatite-carbon composite with Luffa sponge bio-template and its use for the removal of Pb(II) ions from aqueous solution. Fresen. Environ. Bull. 27, 8747-8764.

[32] Kadirvelu, K., Kanmani, P., Senthilkumar, P., Subburam, V. (2004) Separation of Mercury(II) from Aqueous Solution by Adsorption onto an Activated Carbon Prepared from Eichhornia crassipes. Adsorption Science & Technology. 22(3), 207-222.

[33] Kadirvelu, K., Kavipriya, M., Karthika, C., Vennilamani, N., Pattabhi, S. (2004) Mercury (II) adsorption by activated carbon made from sago waste. Carbon. 42(4), 745-752.

[34] Namasivayam, C., Kadirvelu, K. (1999) Uptake of mercury (II) from wastewater by activated carbon from an unwanted agricultural solid by-product: coirpith. Carbon. 37(1), 79-84.

[35] Gupta, V.K., Saini, V.K., Jain, N. (2005) Adsorption of As(III) from aqueous solutions by iron oxide-coated sand. Journal of Colloid & Interface Science. 288(1), 55-60.

[36] Mohan, D., Pittman, C.U.(2007) Arsenic removal from water/wastewater using adsorbents—A critical review. Journal of Hazardous Materials. 142(1-2), 1-53.

[37] Somayajula, A., Aziz, A.A., Saravanan, P., Matheswaran, M. (2013) Adsorption of mercury (II) ion from aqueous solution using low-cost activated carbon prepared from mango kernel. Asia-Pacific Journal of Chemical Engineering. 8(1), 1-10.

[38] Faheem, Yu, H., Liu, J., Shen, J., Sun, X., Li, J. (2016) Preparation of MnO_x-loaded biochar for Pb^{2+} removal: Adsorption performance and possible mechanism. Journal of the Taiwan Institute of Chemical Engineers. S1876107016302279.

[39] Yu, Z.H., Zhou, L., Huang, Y.F., Song, Z.G., Qiu, W.W.(2015) Effects of a manganese oxide-modified biochar composite on adsorption of arsenic in red soil. Journal of Environmental Management. 163, 155-162.

[40] Han, X., Liang, C.F., Li, T.Q., Wang, K., Huang, H.G., Yang, X.E. (2013) Simultaneous removal of cadmium and sulfamethoxazole from aqueous solution by rice straw biochar. Journal of Zhejiang University Science B.14(7), 640-649.

[41] Wu, W.X., Yang, M., Feng, Q.B., McGrouther, K., Wang, H.L., Lu, H.B., Chen, Y.X. (2012) Chemical characterization of rice straw-derived biochar for soil amendment. Biomass & Bioenergy. 47(4), 268-276.
[42] Kang, L.P., Zhang, M.M., Liu, Z.H., Ooi, K. (2007) IR spectra of manganese oxides with either layered or tunnel structures. Spectrochimica Acta Part A: Molecular and Biomolecular Spectroscopy. 67(3-4), 864-869.
[43] Buciuman, F., Patcas, F., Craciun, R., Zahn, D.R.T. (1999) Vibrational spectroscopy of bulk and supported manganese oxides. Physical Chemistry Chemical Physics. 1(1), 185-190.
[44] Kushwaha, S., Sreedhar, B., Sudhakar, P.P. (2012) Adsorption of Hg^{2+} onto Borassus Flabellifer: A redox mechanism. Chemical Engineering Journal. 193-194(none), 0-0.
[45] Keiluweit, M., Nico, P.S., Johnson, M.G., Kleber, M. (2010) Dynamic Molecular Structure of Plant Biomass-Derived Black Carbon (Biochar). Environmental Science & Technology. 44(4), 1247-1253.
[46] Dong, X., Ma, L.Q., Zhu, Y., Li, Y., Gu, B. (2013) Mechanistic Investigation of Mercury Sorption by Brazilian Pepper Biochars of Different Pyrolytic Temperatures Based on X-ray Photoelectron Spectroscopy and Flow Calorimetry. Environmental Science & Technology. 47(21), 12156-12164.
[47] Parikh, S.J., Chorover, J. (2005) Spectroscopic Study of Biogenic Mn-Oxide Formation by Pseudomonas putida GB-1. Geomicrobiology Journal. 22(5), 207-218.
[48] Reig, F.B., Adelantado, J.V., Moya Moreno. M.C. (2002) FTIR quantitative analysis of calcium carbonate (calcite) and silica (quartz) mixtures using the constant ratio method. Application to geological samples Talanta. 58(4), 811-821.
[49] Yuan, J.H., Xu, R.K., Zhang, H. (2011) The forms of alkalis in the biochar produced from crop residues at different temperatures. Bioresour Technol. 102(3), 3488-3497.
[50] Plácido, Jersson, Capareda, S. (2015) Production of silicon compounds and fulvic acids from cotton wastes biochar using chemical depolymerization. Industrial Crops and Products. 67, 270-280.
[51] Zhou, J.H., Sui, Z.J., Zhu, J., Li, P., Chen, D., Dai, Y.C., Yuan, W.K. (2007) Characterization of surface oxygen complexes on carbon nanofibers by TPD, XPS and FT-IR.Carbon. 45(4), 785-796.
[52] Herbstein, F.H., Kapon, M., Weissman, A. (1994) Old and new studies of the thermal decomposition of potassium permanganate. Journal of Thermal Analysis. 25(41), 303-322.
[53] Ji, L., Shao, Y., Xu, Z., Zheng, S., Zhu, D. (2010) Adsorption of Monoaromatic Compounds and Pharmaceutical Antibiotics on Carbon Nanotubes Activated by KOH Etching. Environmental Science & Technology. 44(16), 6429-6436.
[54] Xu, X.Y., Schierz, A., Xu, N., Cao, X.D. (2016) Comparison of the characteristics and mechanisms of Hg(II) sorption by biochars and activated carbon. Journal of Colloid and Interface Science. 463, 55-60.
[55] Das, S.K., Das, A.R., Guha, A.K. (2007) A Study on the Adsorption Mechanism of Mercury on Aspergillus versicolor Biomass. Environmental Science & Technology. 41(24), 8281-8287.
[56] Kiliç, M., Keskin, M.E., Süleyman Mazlum, Mazlum, N. (2008) Hg(II) and Pb(II) adsorption on activated sludge biomass: Effective biosorption mechanism. International Journal of Mineral Processing. 87(1-2), 1-8.
[57] Liu, P., Ptacek, C.J., Blowes, D.W., Landis, R.C. (2016) Mechanisms of mercury removal by biochars produced from different feedstocks determined using X-ray absorption spectroscopy. Journal of Hazardous Materials. 308, 233-242.
[58] Gibson, B.D., Ptacek, C.J., Lindsay, M.B.J., Blowes, D.W. (2011) Examining Mechanisms of Groundwater Hg(II) Treatment by Reactive Materials: An EXAFS Study. Environmental Science & Technology. 45(24), 10415-10421.
[59] Lu, X.X, Huangfu X.L., Ma, J. (2014) Removal of trace mercury(II) from aqueous solution by in situ formed Mn–Fe (hydr)oxides. Journal of Hazardous Materials. 280, 71-78.
[60] Véronique Lenoble., Laclautre, C., Serpaud, B., Véronique Deluchat, Bollinger, J.C. (2004) As(V) retention and As(III) simultaneous oxidation and removal on a MnO_2-loaded polystyrene resin. Science of the Total Environment. 326(1-3), 197-207.
[61] Nesbitt, H.W., Canning, G.W., Bancroft, G.M. (1998) XPS study of reductive dissolution of 7Å-birnessite by H_3AsO_3, with constraints on reaction mechanism. Geochimica et Cosmochimica Acta. 62, 2097-2110.
[62] Zhang, G.S., Qu, J.H., Liu, H.J., Liu, R.P., Li, G.T. (2007) Removal Mechanism of As(III) by a Novel Fe-Mn Binary Oxide Adsorbent: Oxidation and Sorption. Environmental Science & Technology. 41(13), 4613-4619.

Received: **05.04.2019**
Accepted: **10.02.2020**

CORRESPONDING AUTHOR

Xiangliang Pan
College of Environment,
Zhejiang University of Technology,
Hangzhou 310014, China

e-mail: xiangliangpan@163.com

© by PSP Volume 29 – No. 05/2020 pages 3446-3457 Fresenius Environmental Bulletin

DETERMINATION OF INORGANIC PHOSPHATE-SOLUBILIZING BACTERIA IN SEDIMENT SAMPLES COLLECTED FROM LAKE VAN, TURKEY

Erdal Ogun*

Van Yuzuncu Yil University, Faculty of Science, Department of Molecular Biology and Genetics, Van, Turkey

ABSTRACT

In this study, it was aimed to determine the bacteria species of inorganic phosphate-solubilizing bacteria (IPSB) isolated from sediment samples collected from Lake Van, Turkey. The National Botanical Research Institute's phosphate (NBRIP)-bromophenol blue (BPB) growth medium was used to screen the IPSB. An alkalotolerant isolate was determined in the soluble tricalcium phosphate in the NBRIP-BPB medium. This isolate, called the S1 isolate, had a wide tolerance, ranging from pH 5.0 to 10.0. As a result of the spectrophotometric measurements, it was determined that the S1 isolate dissolved a maximum amount of PO_4^{-3} (109.6 mg/L) at pH 6.0, 30 °C, and 120 h. In addition, phenotypic and molecular identification of the S1 isolate that dissolved in the inorganic phosphate was performed. Within the scope of molecular identification, the 16S ribosomal RNA region was amplified by polymerase chain reaction using appropriate universal primers. It was determined that this isolate belonged to the *Bacillus pumilus* species, based on the phylogenetic analysis of the 16S rRNA gene, using the maximum-likelihood method.

KEYWORDS:
Bacillus pumilus S1, phosphate-solubilizing bacteria, Lake Van

INTRODUCTION

Soda lakes are saline and alkaline ecosystems that are thought to have existed throughout the Earth's geological record. They are commonly spread throughout the world, but abundant in terrestrial biomes, such as deserts and steppes, and in geologically interesting areas, such as the East African Rift Valley [1].

These lakes are extremely alkaline extreme environments that form after subjection to elevated evaporation rates in closed drainage basins. Due to the scarcity of Mg^{2+} and Ca^{2+} in their water chemistry, these lakes are enhanced with CO_3^{2-} and Cl^-, with a pH ranging from 8 to >12 [2].

Lake Van is located in Turkey's central Anatolian plateau at 38°38′N, 42°49′E. It is the world's fourth largest lake, covering an area of 3522 km^2, at an altitude of 1648 m, with a volume of 576 km^3, and a maximum depth of 451 m. It is also the world's largest soda lake, with a pH of 9.7–9.8 and salinity of 2.17‰, which is comprised of sodium chloride (NaCl) and sodium carbonates, with minor sulfate, potassium, and magnesium contributions in equal shares. The level of calcium is very low (4.6 mg/L^{-1}) [3].

Lake Van fish (*Alburnus tarichi* Güldenstädt, 1814) is the only vertebrate species in Lake Van to have adapted, via osmoregulation, to its alkaline conditions. These fish are a group of anadromic fish that migrate for reproduction to fresh water [4]. It has been reported that the Lake Van basin has the potential for moderate to high-nature tourism growth [5]. Moreover, the Van Lake basin is essential for the ornithological elements in the area. The basin is situated on many bird species migration paths. Thus far, 177 bird species have been recognized in the basin through ornithological research [6]. Phosphorous rocks are transported by sedimentation to rivers, and then to lakes and seas, as shown in Figure 1, showing the global phosphorus cycle [7]. Heterotrophic microbes convert the organic P and polyphosphate (polyP) retained in the organic residue material to orthophosphate under anaerobic conditions. The soluble phosphorus in the sediments enters the food chain via bacteria, phytoplankton, and zooplankton, and then through macrophytes and macro-invertebrates, and ultimately, in fish [8].

Microorganisms undergo a biochemical transformation of various essential elements that make up their cells, such as carbon, nitrogen, phosphorus, and sulfur [12]. In lakes, phosphate-solubilising bacteria cause the release of phosphorus [13]. While the number of phosphate-solubilising bacteria is low in winter, it is at its highest level in autumn [14].

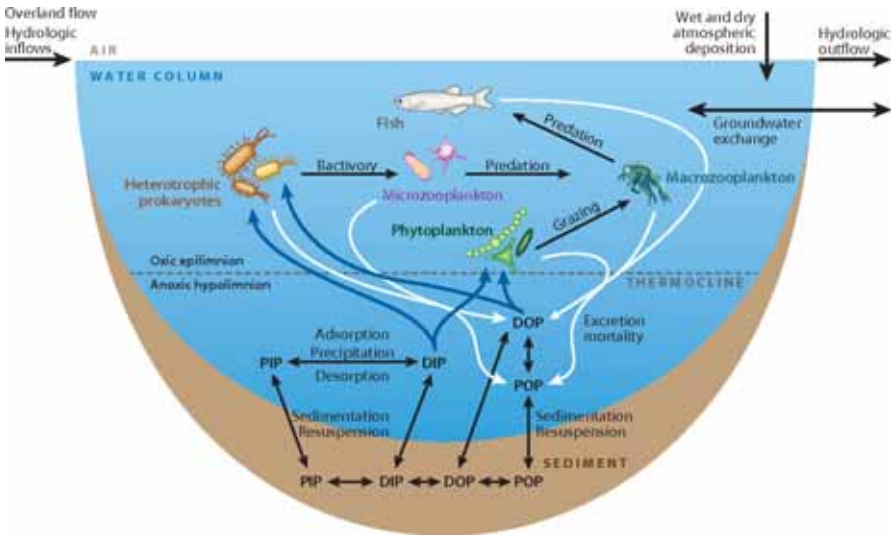

FIGURE 1
Phosphorus (P) cycle in eutrophic lakes [8]

The literature comprises research about the screening of phosphate-solubilising bacteria in different lakes (Table 1). In this study, it was aimed to determine phosphate-dissolving bacteria in sediment samples collected from Lake Van, Turkey.

MATERIALS AND METHODS

Chemicals Used in The Research. All of the chemicals and microbiological media used in used in this study were purchased commercially from Sigma-Aldrich (St. Louis, MO, USA) at local medical companies.

Collection of Sediment Samples. Samples of the sediments were collected from the shoreline near the Van Yüzüncü Yil University in July 2019, as outlined in Figure 2, from 38°33′07.7″ N, 43°16′56.2″ E. Using an Ekman-Birge sampler, the sediment samples were drawn at a depth of 100 m and transported in sterile sample containers (Figures 3A and 3B).

TABLE 1
Phosphate-dissolving bacteria species isolated from different lakes

Bacteria	Source
Achromobacter sp. *Acinetobacter* sp. *Aeromonas* sp. *Alcaligenes* sp. *Bacillus* sp. *Beneckea* sp. *Brevibactcrium* sp. *Enterobacter* sp. *Flavobacterium* sp. *Microbacterium* sp. *Micrococcus* sp. *Pseudomonas* sp. *Serratia* sp. *Xanthomonas* sp. *Zymomonas* sp.	[15]
Bacillus sp., *Micrococcus* sp. *Pseudomonas* sp.	[16]

Acinetobacter haemolyticus *Agrobacterium* sp. *Azospirillum* sp. *B. megaterium* *Blastobacter aggregatus* *Enterobacter aerogenes* *E. asburiae* *Janthinobacterium lividum* *Staph. epidermidis* *Staphylococcus caprae* *Terrabacter tumescens*	[17]
Acinetobacter sp. *Burkholderia* sp. *Citrobacter freundii* *Cupriavidus basilensis* *Enterobacter* sp. *Pantoea agglomerans* *Pseudomonas* sp.	[13]
B. cereus *Pseudomonas* sp. *Stenotrophomonas maltophilia* *Stenotrophomonas* sp. *Xanthomonas* sp.	[18]
Aeromonas sp. *Pseudomonas* sp. *P. fluorescens* *P. mandelii*	[19]
Bacillus sp. *B. selenatarsenatis* *Halobacillus* sp. *Salicola marasensis* *Sediminibacillus halophilus* *Thalassobacillus* sp.	[20]
Acinetobacter sp. *Agrobacterium* sp. *Bacillus* sp. *Brevibacillus* sp. *Curtobacterium* sp. *Enterobacter* sp. *Microbacterium* sp. *Novosphingobium* sp. *Pseudomonas* sp. *Stenotrophomonas* sp.	[21]
Agrobacterium sp. *B. pumilus* *Novosphingobium* sp. *Pseudomonas koreensis* *Rhodobacter* sp.	[22]
Bacillus marisflavi FA7 *Chromohalobacter israelensis* WA3	[23]
Bacillus SWSI1728 *Bacillus* SWSI1734 Micromonosporaceae SWSI1719	[24]
Acinetobacter sp. *Bacillus* sp. *Enterobacter* sp. *Klebsiella* sp. *Proteus* sp. *Pseudomonas* sp. *Staphylococcus* sp.	[25]

FIGURE 2
Sampling area in Lake Van

FIGURE 3A
Sediment taken with the Ekman-Birge sampler

FIGURE 3B
Sediment sample

Isolation of Alkalophilic Bacteria from the Sediment Samples. Serial dilutions were prepared for the isolation of alkalophilic bacteria from the water and sediment samples. Next, as was recommended by Horikoshi and Akiba [26], a 100-µL L-shaped spreader was used to spread these dilutions onto the surface of the media. The contents of the media comprised 1% glucose, 0.5% polypeptone, 0.5% yeast extract, 0.1% K_2HPO_4, 0.02% $MgSO_4$ $7H_2O$, 2% agar, and pH 10.5. A Na_2CO_3 solution was autoclaved separately and added to the media. The Petri plates were then left to incubate for 48 h at 30 °C. Following incubation, reproducible colonies were evaluated as probable alkaliphilic bacterial colonies. The isolates were maintained in liquid media containing 20% glycerol at –20 °C for later use [27].

Plate Assay Used in Screening of the Phosphate-Solublizing Bacteria. The National Botanical Research Institute's phosphate (NBRIP)-bromophenol blue (BPB) growth medium was used for screening of phosphate-soluble bacteria. Each liter of NBRIP-BPB media comprised 10 g of glucose, 2.5 g of $Ca_3(PO_4)_2$, 5 g of $MgCl_2.6H_2O$, 0.25 g of $MgSO_4.7H_2O$, 0.2 g of KCl, 0.1 g of ammonium sulfate, 0.025 g of bromophenol blue, and 15 g of agar. The pH of the medium was adjusted to 7.0 [28]. The Petri plates were incubated at 30 °C for 4 days. The formation of a clear zone around the biomass after incubation was considered positive for phosphatase enzyme production.

Determination of Phosphate Release Rates of the Isolates for Different Parameters. For the production of phosphate-dissolving bacteria, submerged culture method was used. For the cultivation of these isolates, 250-mL flasks containing 100 mL of sterile NBRIP broth medium were used. Adolescents were inoculated with 100 µL of 24-h culture of the phosphate-dissolving isolates. The flasks were placed into a shaker for different time intervals (24, 48, 72, 96, and 120 h), pH levels (5.0, 6.0, 7.0, 8.0, and 9.0) and temperatures (25, 30, 35,

40, 45, and 50 °C), and then incubated at 150 rpm [29].

Cultures developed under different physiological conditions were saturated at 8000 rpm for 10 min and diluted to 1/20. Dissolved phosphorus and phosphate analysis in the cultures was performed via the PhosVer 3 (ascorbic acid) – (0.02–2.50 mg/L PO_4^{-3}) method using PhosVer 3 phosphate Powder Pillow phosphor reagent in a HACH DR 5000 spectrophotometer (Hach Company, Loveland, CO, USA) and the results were calculated in mg/L [30].

Phenotypic Identification of the Phosphate-Solubilizing Isolate. The morphological, physiological, and biochemical properties of the phosphatase-producing isolates were based on Section B in the Firmicutes of Bergey's Manual of Systematic Bacteriology, including proteobacteria phylum and gammaproteobacteria [31].

16S Rrna Gene Sequencing and Phylogenetic Analysis. Genomic DNA was isolated using a bacterial genomic DNA purification kit (DP02-150; GeneMark Technology) and the 16S rRNA gene was sequenced and analyzed as described previously by Chen et al. [32]. Genomic DNA was isolated using a bacterial genomic DNA purifcation kit (DP02-150, GeneMark). Primers 27F (5′- AGAGTTTGATCCTGGCTCAG-3′) and 1541R (5′-AAG GAGGTGATCCAGCC-3′) were used for amplification of the bacterial 16S rRNA genes by polymerase chain reaction [33, 34].

The read sequences were opened in the CodonCode Aligner v.6.02 program, and their chromatograms were checked visually, and the incorrectly read head and end sections were manually removed. The 16S rRNA gene sequence of the S1 isolate was aligned with the sequnces of 15 other organisims retrieved from GenBank (See Figure 9 for assesion numbers) using ClustalW implemented in MegaX [35]. Ambigiously aligned regions were masked using Gblocks v.0.91b, allowing a gap position in the final blocks [36, 37]. Phylogenetic analyses of the concatenated sequences were performed using the maximum-likelihood (ML) method implemented in IQ-TREE v.1.6.6 [38]. According to the optimal substitution models under the rapid bootstrap algorithm (1000 replicates), the best fitting substitution model for the data set was estimated in the program ModelFinder [39]. According to the Akaike information criterion, model TPM3u+F+I+G4 was chosen as the most suitable model.

RESULTS AND DISCUSSION

$Ca_3(PO_4)_2$ is practically insoluble in water, but soluble in dilute hydrochloric and nitric acid [40]. The transformation of phosphorus (P) is a major factor of lake eutrophication and phosphate-releasing bacteria play an important role in the release process [13]. Inorganic phosphate-solubilizing bacteria (IPSB) are an important component of microbial populations in lake sediments [24].

Phosphorus plays a major role in plant growth, but due to insoluble complex formation in soil, it is mainly unavailable for plants. Phosphate-solubilizing bacteria dissolve phosphate, and hence are regarded as a biofertilizer. These bacteria are present in different habitats and screening of such habitats could introduce potent phosphate-solubilizing bacteria as biologic fertilizers [41].

Findings from Screening of the Phosphate-Solubilising Bacteria Via Plaque Test. In this study, it was determined that the S1 isolate isolated from sediment samples obtained from Van Lake dissolved ticalcium phosphate in NBRIP-BPB medium (Figure 4).

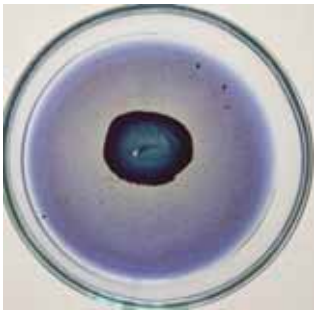

FIGURE 4
Phosphate-solubilising S1 isolate in NBRIP-BPB medium

PO_4^{-3} Release Rates of S1 Isolate. It was determined that the S1 isolate, which dissolved inorganic phosphate, dissolved the maximum amount (109.6 mg/L PO_4^{-3}) at pH 6.0, 30 °C, and in 120 h (Figure 5). Phosphate release rates of this isolate at different temperatures and time intervals at pH 6.0 are given in Table 2.

It was determined that the S1 isolate dissolved the maximum amount of phosphate (109.6 mg/L) at pH 6.0, while it dissolved the minimum amount (6 mg/L) at pH 9.0 (Figure 6).

It was determined that the S1 isolate dissolved the maximum amount of phosphate (109.6 mg/L) in 120 h, while it dissolved the minimum amount (24.9 mg/L) in 24 h (Figure 7).

It was determined that the S1 isolate dissolved the maximum amount of phosphate (109.6 mg/L) at

pH5.0 pH 6.0 pH 7.0 pH 8.0 pH 9.0 pH 10.0

FIGURE 5
Reaction of supernatants of the isolates at different pH levels with the phosphorus reagent

TABLE 2
Phosphate release rate of the S1 isolate for different parameters

Parameters	PO_4^{-3} (mg/L)
Different pH levels	
pH 5.0	32
pH 6.0	109.6
pH 7.0	34.8
pH 8.0	16.8
pH 9.0	6.0
pH 10.0	12.8
Different time intervals	
24 h	24.9
48 h	39.8
72 h	54.6
96 h	79.8
120 h	109.6
Different temperatures	
25 °C	87.3
30 °C	109.6
35 °C	95.4
40 °C	70.3
45 °C	5.6
50 °C	1.8

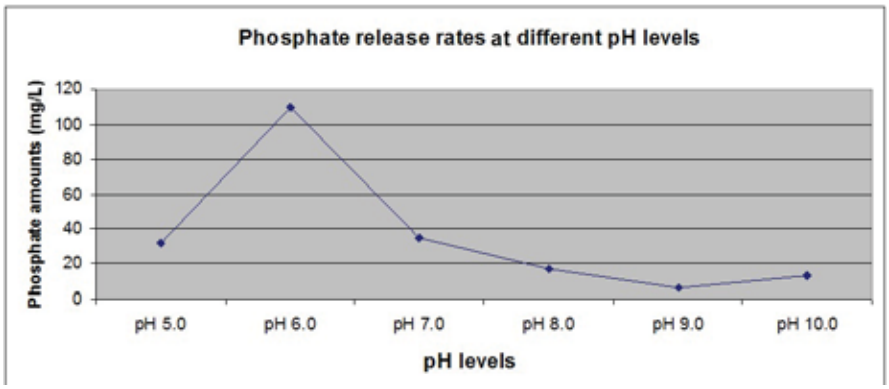

FIGURE 6
Phosphate release rate of the S1 isolate at different pH levels

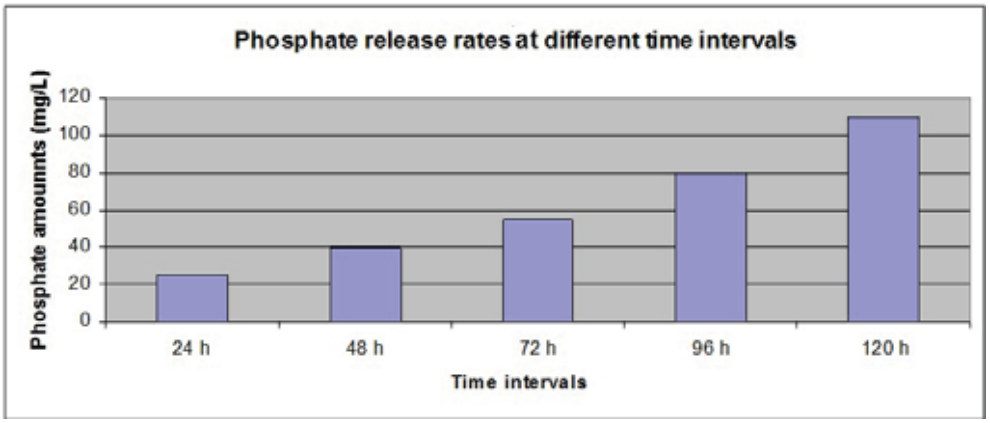

FIGURE 7
Phosphate release rate of the S1 isolate at different time intervals

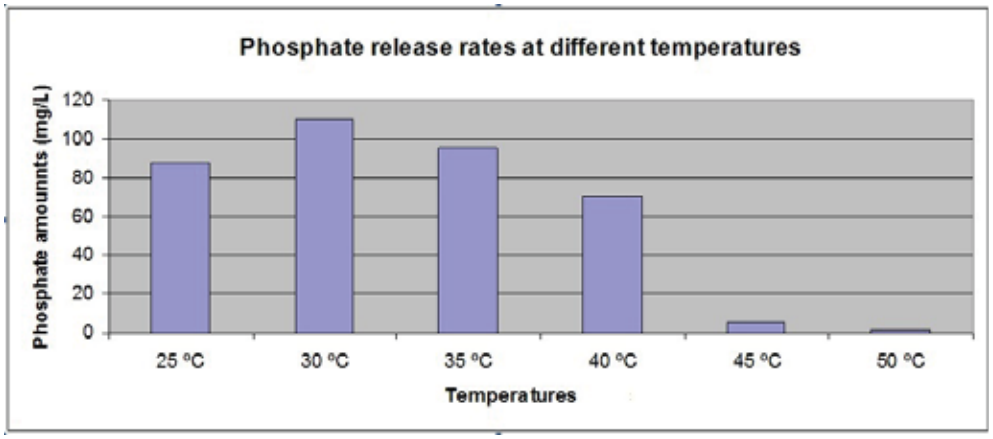

FIGURE 8
Phosphate release rate of the S1 isolate at different temperatures

30 °C, while it dissolved the minimum amount (1.6 mg/L) at 50 °C (Figure 8).

Phosphate-dissolving bacteria in samples from various sources have been screened by different researchers. These bacteria were isolated from samples of soil, lake water, and lake sediments. In addition, researchers have also tested the phosphate solubility of the phosphate-dissolving bacteria.

The strain *B. megaterium* var. *phosphaticum* was reported to be soluble in 39.03 mg of P_2O_5/100 mL, showing maximum activity at pH 7.0 [42]. It was reported that the population structure of phosphate-dissolving bacteria in Donghu Lake in Wuhan, China, was examined. According to the morphological, physiological, and biochemical characteristics of bacterial strains that were reported to have dissolved phosphate in water and sediment samples taken from 3 stations, the following genera were determined: *Bacillus*, *Micrococcus*, *Aeromonas*, *Achromobacter*, *Acinetobacter*, *Alcaligenes*, *Brevibacterium*, *Beneckea*, *Enterobacter*, *Flavobacterium*, *Microbacterium, Pseudomonas*, *Xanthomonas*, and *Zymomonas*. [15]. In research conducted on the detection of phosphate-dissolving bacteria in East Lake in Haikou, Hainan, China, it was reported that the dominant species were among *Bacillus*, *Micrococcus*, and *Pseudomonas* genus [16]. In eastern China, the characterization of bacteria that released phosphorus was reported in a small eutrophic shallow lake. It was demonstrated that these inorganic phosphorus-dissolving bacteria belonged to *Bacillus megaterium*, *Terrabacter tumescens*, and *Janthinobacterium lividum* species [17]. It was also reported that the most efficient strain among phosphate-dissolving bacteria from a shallow eutrophic lake and a wetland, isolated from sediment samples, released 170 mg/L^{-1} of orthophosphate [13]. According to the 16S rDNA sequence analysis of organic phosphorus-dissolving bacteria isolated from the sediment of Lake Taihu, a large shallow eutrophic lake in China, the species belonged to *Bacillus cereus*, *Stenotrophomonas maltophilia*, *Stenotrophomonas* sp., *Xanthomonas* sp., and *Pseudomonas* sp. [18]. The *Rhizobium* sp. C50 strain was reported to dissolve 107.2 mg/L^{-1} of phosphorus after a 12-day fermentation process. [43]. It was demonstrated that the T-K6 isolate of phosphate-dissolving bacteria isolated from sugarcane waste released P_2O_5 at a rate of 0.74 mg/L. [44]. Phosphorus release rates by *Pseudomonas*

species isolated from various agricultural ecosystems in India were reported to be between 2.11–15.19 mg/L^{-1} [45]. In a study conducted on the isolation of phosphate-dissolving bacteria from Oxbow Lakes in West Bengal, India, it was reported that the isolates had dissolved between 6.3–68.8 mg. In addition, it was assumed that these phosphate-dissolving strains belonged to species of the following genera: *Bacillus*, *Brevibacillus*, *Enterobacter*, *Agrobacterium*, *Pseudomonas*, *Acinetobacter*, *Microbacterium*, *Curtobacterium*, *Stenotrophomonas*, and *Novosphingobium*. [21]. In studies conducted on bacteria that released phosphorus isolated from Lake Wabu, a shallow lake, in China, it was reported by researchers that a strain of *B. pumilus* dissolved phosphorus at a rate of 0.20 mg/L^{-1}, which was similar to that reported in the current study. [22]. Offering a positive contribution to the growth of tomato plants, a *Pantoea* sp. Pot1 shunt was observed to have dissolved phosphate at a rate of 966 mg/L^{-1} [46]. It was reported that the *Pseudomonas knackmussii* R10 strain, isolated from the rhizosphere of natural wetlands, dissolved 125.88 mg/L^{-1} of phosphorus in tricalcium phosphate medium. [47]. The *Pseudomonas prosekii* YLYP6 strain, isolated from sewage sludge, was reported to have dissolved 716 mg/L^{-1} of phosphate under optimal culture conditions [48]. *Staphylococcus* and *Enterobacter* strains isolated from the Renuka Lake Ecosystem in the Lesser Himalayas were reported to have dissolved phosphorus at a rate of 7.976 ± 0.01 µg/L and 6.322 ± 0.01 µg/L, respectively. [25]. In a study related to the screening of inorganic phosphate-dissolving bacteria in Eutrophic Sancha Lake in the Tianfu New District of Sichuan Province, China, it was reported that the SWSI1725 strain of the genus *Bacillus* dissolved phosphate at a rate of 103.57 mg/L. [24].

Phenotypic Characteristics of Phosphate Solubilising Positive Isolate. It was determined that the inorganic phosphate-dissolving S1 isolate was included in the phenotypic properties of the genus *Bacillus*. This isolate was found to have Gram-positive rod morphology with aerobic endospores. It was determined that this isolate grew within a pH range of 5.0–10.0 and was saturated by 10% sodium chloride. It was determined to be positive in terms of Voges-Proskauer, oxidase, and catalase tests. It was found to be negative for indole and hydrogen sulfide. It was observed that Tween 80 did not hydrolyze esculin and starch while hydrolyzing casein and gelatin. It was determined that the isolate used citrate as a carbon source and was unable to reduce nitrate. While using cellobiose, D-fructose, D-glucose, D-mannitol, D-mannose, L-arabinose, and sucrose as carbon sources, D-galactose, D-maltose, D-trehalose, D-xylose, and lactose sugar were not observed to have been oxidized. Moreover, L-asparagine used amino acids L-ornithine and L-proline as nitrogen sources, however, L-arginine, L-cysteine, L-glutamine, L-glysine, L-lysine, L-methionine, L-tryptophan, L-tyrosine, and phenylalanine were found to have been unable to decarboxylate amino acids. The morphological, physiological, and biochemical properties of the isolates are given in Table 3.

TABLE 3
Phenotypic properties of the inorganic phosphorus dissolving S1 isolate

Characteristic	Test results
Gram stain	+
Endospore	+
Anaerobic growth	-
Motility	+
Catalase	+
Oxidase	+
NaCl tolerance	2.5% –10%
Temperature tolerance	5 °C–50 °C
pH tolerance	5.0–10.0
Acid production from carbohydrates	
Cellobiose	+
D-fructose	+
D-galactose	-
D-glucose	+
D-maltose	-
D-mannitol	+
D-mannose	+

D-trehalose	-
D-xylose	-
Lactose	-
L-arabinose	+
Sucrose	+
Amino acid decarboxylation	
L-arginine	-
L-asparagine	+
L-cysteine	-
L-glutamine	-
L-glysine	-
L-lysine	-
L-methionine	-
L-ornithine	+
L-proline	+
L-tryptophan	-
L-tyrosine	-
Phenylalanine	-
Hydrolysis	
Aesculin	-
Casein	+
Gelatin	+
Starch	-
Tween 80	-
Urea	+
Citrate	-
H_2S	-
Indole	-
Voges-Proskauer	+
Nitrate	-

The *B. pumilus* S1 strain was similar to the type strain of the *B..pumilus* species in Bergey's Manual Systematic Bacteriology in terms of its phenotypic properties [31]. However, in various studies of the identification of *B. pumilus* species, it was observed that this species had variability in phenotypic properties [49, 50, 51, 52, 53]. A 16S rDNA sequence analysis was performed to make a definitive diagnosis of this sheath in the genus *Bacillus*.

16S rDNA Sequence Analysis and Phylogenetic Tree. As a result of the BLAST analysis, it was determined that the S1 isolate was 100% similar to the sequins of *B. pumilus* strains from the National Biotechnology Information Center. According to different gap selection criteria in Gblocks, the alignment of the combined dataset comprised 1377 (allowed gap positions = all) positions. In the phylogenetic tree modeling created with the ML approach, this strain was found to be in the cluster formed by *B pumilus* strains. In addition, *B. safensis* strains were found to be located closely with the *B. pumilus* cluster. As seen in the ML phylogenetic tree, it was determined that it forms a cluster within the genus *Bacillus* (Figure 9). The 16S rDNA gene region (1.377 nt) of the *B. pumilus* S1 isolate, which dissolved inorganic phosphate, was registered in GenBank under access number MN988851.

CONCLUSIONS

The phosphorus cycle is undoubtedly an extremely important cycle in the food chain in aquatic ecosystems. In this study, the presence of bacteria that dissolved inorganic phosphate in the Lake Van phosphorus cycle was determined. These isolates possess the potential to be used as phosphate solvent microorganisms in agricultural soils with an acidic soil profile. Plankton, which is located at the beginning of the food chain, cannot use phosphate directly. Organic and inorganic phosphate must be released into aquatic habitats in the form of phosphorus. However, the concentration of phosphorus must be at a certain level in bodies of water. The World Health Organization has recommended that the phosphorus content in bodies of water should be between 0.01 and 0.03 mg/L in order to prevent health risks and algae blooms, which are derived from toxic algae [54]. From this point of view, the most important measure is the balanced use of phosphate-containing fertilizers in agricultural areas.

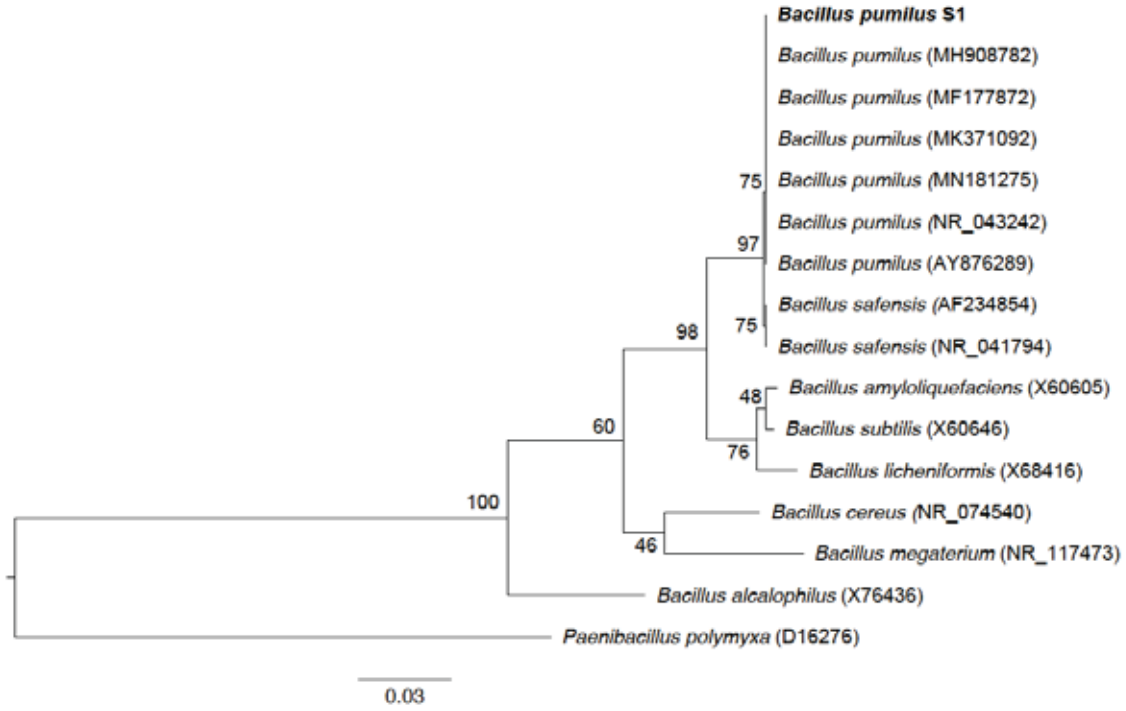

FIGURE 9

ML phylogenetic tree based on the 16S rDNA gene sequences showing relationships between the S1 strain and members of the genus *Bacillus*. The sequence of *Paenibacillus polymyxa* (D16276) was used as an outgroup. The percentage of trees in which the associated taxa clustered together is shown next to the branches. Bar, 0.03 substitutions per nucleotide position.

ACKNOWLEDGEMENTS

No potential conflict of interest was reported by the authors.

REFERENCES

[1] [1] Antony, C.P., Kumaresan, D., Hunger, S., Drake, H.L., Murrell, J.C, Shouche, Y.S (2013) Microbiology of Lonar Lake and other soda lakes. Int Soc Microb Ecol J. 7, 468.

[2] Jones, B.E., Grant, W.D., Duckworth, A.W., Owenson, G.G. (1998) Microbial diversity of soda lakes. Extremophiles. 2, 191-200.

[3] Kempe, S., Kaźmierczak, J., Landmann, G., Konuk, T., Reimer, A., Lipp, A. (1991) Largest known microbialites discovered in Lake Van, Turkey. Nature. 349, 605-608.

[4] Danulat, E., Selçuk, B. (1992) Life history and environmental conditions of the anadromous Chalcalburnus tarichi (Cyprinidae) in the highly alkaline Lake Van, Eastern Anatolia, Turkey. Arch Hydrobiol. 126, 105-125.

[5] Alaeddinoglu, F, Can, A.S. (2011) Identification and classification of nature-based tourism resources: western Lake Van basin, Turkey. Procedia Soc Behav Sci. 19, 198-207.

[6] Adızel, Ö., Durmuş, A. (2009) A study on bird species under threat and avifauna of Erçek Lake (Van-Turkey). Sci Res Essay. 4, 1006-1011.

[7] Ruttenberg, K.C. (2003) The global phosphorus cycle. Treatise Geochem. 8, 585-643.

[8] McMahon, K.D., Read, E.K. (2013) Microbial contributions to phosphorus cycling in eutrophic lakes and wastewater. Annu Rev Microbiol. 67, 199-219.

[9] Stewart JWB, Mckercher, RB (1982) Phosphorus cycle. In: Burns, R.G., Slater, J.H. (Eds.) Experimental Microbial Ecology. Blackwell, Oxford, UK. 221-238.

[10] Kremser, U., Schnug, E. (2002) Impact of fertilizers on aquatic ecosystems and protection of water bodies from mineral nutrients. Landbauforsch Volk. 52, 81-90.

[11] Savci, S. (2012) An agricultural pollutant: Chemical fertilizer. Int J Environ Sci Dev. 3, 77-80.

[12] Stout, L.M., Joshi, S.R., Kana, T.M., Jaisi, D.P. (2014) Microbial activities and phosphorus cycling: An application of oxygen isotope ratios in phosphate. Geochim Cosmochim Ac. 138, 101-116.

[13] Qian, Y., Shi, J., Chen, Y., Lou, L., Cui, X., Cao, R., Li, P., Tang, J. (2010). Characterization of phosphate solubilizing bacteria in sediments from a shallow eutrophic lake and a wetland: Isolation, molecular identification and phosphorus release ability determination. Molecules. 15, 8518-8533.
[14] Song, W., Yuan, L.N., Xiao, L., Zhan, Z., Yang, L.Y., Jiang, L.J. (2007) ALPase activity and the distribution of phosphate solubilizing bacteria and the relationship between them in sediments of Lake Taihu. Huanjing Kexue. 28, 2355-2360.
[15] Qinsheng, L., Li, H. (1989) [Population structure of the phosphate dissolving bacteria in Donghu Lake, Wuhan]. Acta Hydrochim. 4. (Article in Chinese)
[16] Wang, R., Chen, Y. (2001) The preliminary report of studies on phosphate bacteria from east lake in Haikou. J Hainan Nor Univ (Nat Sci). 14, 84-88.
[17] Gen-Fu, W., Xue-Ping, Z. (2005) Characterization of phosphorus-releasing bacteria in a small eutrophic shallow lake, eastern China. Water Res. 39, 4623-4632.
[18] Zhou, C., Song, C., Huang, D., Liu, Y., Cao, X., Zhou, Y. (2011) Isolation and characterization of organic phosphorus-mineralizing bacteria in sediment of a Chinese large shallow eutrophic lake (Lake Taihu). Geomicrobiol J. 28, 660-666.
[19] Qu, J.H., Wang, F.F., Yan, J.Z., Hu, Y.S., Zhao, J. (2012) [Screening and identification of several phosphate-solubilizing bacteria from the interfacial sediment of Xiliu Lake].J He nan Agric. 5. (Article in Chinese)
[20] Sahay, H., Mahfooz, S., Singh, A.K., Singh, S., Kaushik, R., Saxena, A.K., Arora, D.K. (2012) Exploration and characterization of agriculturally and industrially important haloalkaliphilic bacteria from environmental samples of hypersaline Sambhar lake, India. World J Microbiol Biotechnol. 28, 3207-3217.
[21] Maitra, N., Bandopadhyay, C., Samanta, S., Sarkar, K., Sharma, A.P., Manna, S.K. (2015) Isolation, identification and efficacy of inorganic phosphate-solubilizing bacteria from Oxbow lakes of west Bengal, India. Geomicrobiol. 32, 751-758.
[22] Li, H., Liu, Y., Cao, X., Song, C., Zhou, Y. (2016) Functions of calcium-bound phosphorus in relation to characteristics of phosphorus releasing bacteria in sediment of a Chinese shallow lake (Lake Wabu). Geomicrobiol. 33, 751-757.
[23] Prabhu, N., Borkar, S., Garg, S. (2016) Alkaliphilic and haloalkaliphilic phosphate solubilizing bacteria from coastal ecosystems of Goa. Int J Adv Biotechnol Res. 7, 2015-2027.
[24] Li, Y., Zhang, J., Zhang, J., Xu, W., Mou, Z. (2019). Characteristics of inorganic phosphate-solubilizing bacteria from the sediments of a eutrophic Lake. Int J Environ Res Public Health. 16, 2141.
[25] Kour, D., Rana, K.L., Yadav, N., Yadav, A.N. (2019). Bioprospecting of phosphorus solubilizing bacteria from Renuka Lake ecosystems, Lesser Himalayas. J Appl Biol Biotechnol. 7, 1-6.
[26] Horikoshi, K. (1999) Alkaliphiles: Some applications of their products for biotechnology. Microbiol Mol Biol Rev. 63, 735-750.
[27] Kirsop, B.E., Doyle, A. (Eds.) (1991) Maintenance of Microorganisms and Cultured Cells: A Manual of Laboratory Methods. Academic Press, London, UK.
[28] Khan, M.S., Zaidi, A., Musarrat, J. (Eds.). (2014) Phosphate Solubilizing Microorganisms: Principles and Application of Microphos Technology. Springer, Switzerland, 8.
[29] Bisswanger, H. Enzyme assays. Perspectives in Science, 2014; 1(1-6), 41-55.
[30] Hach Inc. (2008) DR 5000 Spectrophotometer Procedures Manual. 2nd Edition. HachCompany, Colorado, USA.
[31] Vos, P., Garrity, G., Jones, D., Krieg, N.R., Ludwi, W., Rainey, F.A., Whitman WB (Eds.). (2011) Bergey's Manual of Systematic Bacteriology: Volume 3: The Firmicutes. Springer Science and Business Media, Berlin, Germany.
[32] Chen, W.M., Laevens, S., Lee, T.M., Coenye, T., De Vos, P., Mergeay, M. Vandamme, P. (2001) Ralstonia taiwanensis sp. nov., isolated from root nodules of Mimosa species and sputum of a cystic fibrosis patient. Int J Syst Evol Microbiol. 51, 1729-1735.
[33] Weisburg, W.G., Barns, S.M., Pelletier, D.A., Lane, D.J. (1991) 16S ribosomal DNA amplification for phylogenetic study. J Bacteriol. 173, 697-703.
[34] Anzai, Y., Kudo, Y., Oyaizu, H. (1997) The phylogeny of the genera Chryseomonas, Flavimonas, and Pseudomonas supports synonymy of these three genera. Int J Syst Evol Microbiol. 47, 249-251.
[35] Kumar, S., Stecher, G., Li, M., Knyaz, C., Tamura, K. (2018) MEGA X: molecular evolutionary genetics analysis across computing platforms. Mol Biol Evol. 35, 1547-1549.
[36] Castresana, J. (2000) Selection of conserved blocks from multiple alignments for their use in phylogenetic analysis. Mol Biol Evol. 17(4), 540-552.
[37] Talavera, G., Castresana, J. (2007) Improvement of phylogenies after removing divergent and ambiguously aligned blocks from protein sequence alignments. Sys Biol. 56, 564-577.

[38] Nguyen, L.T., Schmidt, H.A., von Haeseler, A., Minh, B.Q. (2015) IQ TREE: A fast and effective stochastic algorithm for estimating maximum likelihood phylogenies. Mol Biol Evol. 32, 268-274.
[39] Kalyaanamoorthy, S., Minh, B.Q., Wong, T.K.F., von Haeseler A, Jermiin L.S. (2017) ModelFinder: fast model selection for accurate phylogenetic estimates. Nat Methods. 14, 587-589.
[40] Lewis, R.A. (2016). Hawley's Condensed Chemical Dictionary. Wiley, NJ, USA, 246.
[41] Motamedi, H., Aalivand, S., Varzi, H.N., Mohammadi, M. (2016) Screening cabbage rhizosphere as a habitat for isolation of phosphate-solubilizing bacteria. Environ Exp Biol. 14, 173-181.
[42] Bajpai, P.D., Rao, W.S. (1971) Phosphate solubilising bacteria: PART I. Solubilisation of phosphate in liquid culture by selected bacteria as affected by different pH values. Soil Sci Plant Nutr. 17, 41-43.
[43] López-Ortega, M.D.P., Criollo-Campos, P.J., Gómez-Vargas, R.M., Camelo-Rusinque, M., Estrada-Bonilla, G., Garrido-Rubiano, M.F., Bonilla-Buitrago, R. (2013) Characterization of diazotrophic phosphate solubilizing bacteria as growth promoters of maize plants. Rev Colomb Biotecnol. 15, 115-123.
[44] Atekan, A., Nuraini, Y., Handayanto, E., Syekhfani, S. (2014) The potential of phosphate solubilizing bacteria isolated from sugarcane wastes for solubilizing phosphate. J Degrade Min Land Manage. 1, 175-182.
[45] Goteti, P.K., Desai, S., Emmanuel, L.D.A., Taduri, M., Sultana, U. (2014) Phosphate solubilization potential of fluorescent Pseudomonas spp. isolated from diverse agro-ecosystems of India. Int J Soil Sci. 9, 101-10.
[46] Sharon, J.A., Hathwaik, L.T., Glenn, G.M., Imam, S.H., Lee, C.C. (2016). Isolation of efficient phosphate solubilizing bacteria capable of enhancing tomato plant growth. J Soil Sci Plant Nutr. 16, 525-536.
[47] Cao, Y., Fu, D., Liu, T., Guo, G., Hu, Z. (2018) Phosphorus solubilizing and releasing bacteria screening from the rhizosphere in a natural wetland. Water. 10, 195.
[48] Yu, L.Y., Huang, H.B., Wang, X.H., Li, S., Feng, N.X., Zhao, H.M., Huang, X.P., Li, Y.W., Li, H., Cai, Q.Y., Mo, C.H. (2019) Novel phosphate-solubilising bacteria isolated from sewage sludge and the mechanism of phosphate solubilisation. Sci Total Environ. 658, 474-484.
[49] O'donnell, A.G., Norris, J.R., Berkeley, R.C.W., Claus, D., Kaneko, T., Logan, N.A., Nozaki, R. (1980) Characterization of Bacillus subtilis, Bacillus pumilus, Bacillus licheniformis, and Bacillus amyloliquefaciens by pyrolysis gas-liquid chromatography, deoxyribonucleic acid-deoxyribonucleic acid hybridization, biochemical tests, and API systems. Int J Syst Evol Microbiol. 30, 448-459.
[50] Parvathi, A., Krishna, K., Jose, J., Joseph, N., Nair, S. (2009) Biochemical and molecular characterization of Bacillus pumilus isolated from coastal environment in Cochin, India. Brazilian J Microbiol. 40, 269-275.
[51] Kimouli, M., Vrioni, G., Papadopoulou, M., Koumaki, V., Petropoulou, D., Gounaris, A.K., Friedrich, A.W., Tsakris, A. (2012) Two cases of severe sepsis caused by Bacillus pumilus in neonatal infants. J Med Microbiol. 61, 596-599.
[52] Zaghian, S., Shokri, D., Emtiazi, G. (2012) Co-production of a uv-stable bacteriocin-like inhibitory substance (BLIS) and indole-3-acetic acid hormone (IAA) and their optimization by Taguchi design in Bacillus pumilus. Ann Microbiol. 62, 1189-1197.
[53] Surendra, S.V., Mahalingam, B.L., Velan, M. (2017) Degradation of monoaromatics by Bacillus pumilus MVSV3. Braz Arch Biol Technol. 60, e17160319.
[54] WHO (2003) Guidelines for safe recreational water environments: Coastal and fresh waters (Vol. 1). World Health Organization.

Received: **26.01.2020**
Accepted: **19.02.2020**

CORRESPONDING AUTHOR

Erdal Ogun
Van Yüzüncü Yıl University,
Faculty of Science,
Department of Molecular Biology and Genetics,
Van,65080 – Turkey

e-mail: eogun@yyu.edu.tr

© by PSP Volume 29 – No. 05/2020 pages 3458-3464 Fresenius Environmental Bulletin

AN EVALUATION OF PESTS LYONETIIDAE, TORTRICIDAE AND YPONOMEUTIDAE (LEPIDOPTERA) SPECIES ON FRUIT TREES IN IGDIR PROVINCE OF TURKEY

Yesim Bulak Korkmaz*, Erol Yildirim

Atatürk University, Faculty of Agriculture, Department of Plant Protection, Erzurum, Turkey

ABSTRACT

This study was carried out to determine of *Prunus* spp. (stone fruit), *Malus* spp. and *Pyrus* spp. (Pome fruit) trees moth pests species in Igdır provinces during the seasons of spring, summer and autumn of 2013 and 2016. The result of this study, five pests species are recorded. At these; ***Lyonetia clerkella*** (Linnaeus, 1758), ***Cydia pomonella*** (Linnaeus, 1758), ***Grapholita janthinana*** (Duponchel, 1843), ***Yponomeuta padella*** (Linnaeus, 1758) and ***Ypsolopha persicella*** (Fabricius, 1787). ***Cydia pomonella*** (Linnaeus, 1758), which is economically important and the main pest species in Igdır. Codling moth under natural climatic conditions gives two or three generation year in Igdır province. Codling moth adults are active in nature for about five months from the second week of April to the second week of September.

KEYWORDS:
Lyonetiidae, Tortricidae, Yponomeutidae, *Cydia pomonella*, Codling moth, Igdır

INTRODUCTION

Turkey has an important place in the production and export of different fruits in the world [1,2,3,4,5]. It is possible for commercial cultivation of many fruit species except for tropical and subtropical species in Igdir. The climate of Igdir is known as "Cukurova of the East", which enables the cultivation of many agricultural products thanks to its microklima property and soil structure. According to 2017 data, 82,163 tons of fruit production was made in Iğdir province. The production of apple, apricot and peach are more dominant than the other fruits [6]. In other words, in the valley of Aras, fruit growing increases towards Igdır [7].

The codling moth [*Cydia pomonella* (L.) (Lep. Tortricidae)] is an important cosmopolitan pest of apple growing areas throughout the world [8,9,10,11]. Apart from apple, codling moth attack pear, walnut, and quince [12].

Damage is done by larvae, which feed on the fruit skin and bore deeply into the fruit. Larvae can cause up to 100% damage in untreated orchards [13]. Codling moth management mainly relies on chemical control. Two to three cover sprays are commonly used to target hatching eggs and larvae of the first-generation codling moth [14]. In Turkey, growers begin to spray insecticides sprayer at 150 degree-days after the biofix in pheromone traps. Likewise, second-generation codling moth larvae are also treated with at least two insecticide sprays at 800 degree-days [12].

Lyonetiidae is small moths with very narrow wings. Ocelli and maxillary palps are usually lacking. The larvae are leaf miners or live in webs between the leaves [8]. The pest is particularly destructive and has the potential to destroy entire leaves and cause heavy defoliation before harvest if not controlled [15,16].

The Yponomeutidae (Ermine Moths) are small and usually brightly patterned moths with rather narrow wings. The moths in the genus *Yponomeuta* have front wings white dotted with black; the larvae of *Y. padella* (L) feed in a common web on apple and cherry [8].

The present research aimed to determine the present conditions of the fruit trees in Igdır region in terms of pest. Investigate the biology of codling moth, which using the sexually attractive pheromone traps of *Cydia pomonella* (Linnaeus, 1758), which is economically important and the main pest species in this area, the first adult emergence time, population changes and active periods in nature have been determined.

MATERIALS AND METHODS

Surveys were conducted in the years 2013 and 2016 to determine the pest species in Igdır. Surveys were periodically carried out (weekly between March and October). The method was used for the determination of other species except for *C. pomonella*.

Sampling method. Samples were randomly collected as shown in Table 1 [17]. The samples were taken from leaves and fruits of the trees from the four cardinal directions.

TABLE 1
The number of trees controlled in the sampled fields

Number of total trees	Number of control trees samples
1-20	All trees
21-70	10-30
71-150	31-40
151-500	41-80
501-1000	15% of all trees
More than 1000	5% of all trees

Pheromone trap method. In this study, delta type pheromone traps were used to monitor the population change of *C. pomonella*. Besides, the study was carried out in apple orchards that selected common areas of apple growing Igdır (Center 1, Center 2), Melekli and Tuzluca (Eğrekdere) locations of the province during vegetation periods. The traps were hanged in four orchards where only apple varieties were made intensively in Igdır. Traps were more than 250 meters away from each other. Four pheromone traps were installed at a height of 1,5-2 meters above the ground level within the tree in April 2016. Pheromone containing capsules was changed every 4-6 weeks according to the manufacturer's instructions, and the roof and adhesive tabs were changed as needed. It was checked every day until the first adult exit time was determined. Then the first adult exit time was determined and controlled once a week. Trapped codling moths were being removed with forceps and recorded in each inspection. This observation continued from late April to late September when no more moths were trapped. Finally, the mean of trapped adults of codling moths were calculated for everyday and plotted against time to determine generation numbers, flight peaks, the first adult emergence time, population changes and active periods in nature have been determined.

RESULT AND DISCUSSION

In this study, ***Lyonetia clerkella*** (Linnaeus, 1758), ***Cydia pomonella*** (Linnaeus, 1758), ***Grapholita janthinana*** (Duponchel, 1843), ***Yponomeuta padella*** (Linnaeus, 1758) and ***Ypsolopha persicella*** (Fabricius, 1787) were determined pests on ***Prunus*** spp. (stone fruit), ***Malus*** spp. and ***Pyrus*** spp. (Pome fruit) trees in Igdır province.

Family. Lyonetiidae. ***Lyonetia clerkella*** (Linnaeus, 1758). During the study, it was found to be very low density and no damage to the leaves was observed.

Hosts. *Prunus armeniaca* and *Prunus avium* were detected in the study area.

Material examined. Igdır. Akyumak, K 39°58.109', D 044°03.545', 866 m, 19.VIII.2014, 4 exs., (*P. armeniaca*), 5 exs., (*P. avium*), Çalpala, K 40°00.738', D 043°53.389', 896 m, 05.VII.2015, 12 exs., (*P. armeniaca*), Melekli, K 39°57.140', D 044°05.576', 859 m, 05.VIII.2015, 18 exs., (*P. armeniaca*), K 39°57.457', D 044°07.668', 860 m, 19.VII.2016, 2 exs., (*P. armeniaca*), K 39°56.819', D 044°06.869', 857 m, 28.VII.2016, 4 exs., (*P. armeniaca*), Oba, K 39°56.963', D 043°59.812', 870 m, 26.VII.2016, 5 exs., (*P. armeniaca*), K 39°57.400', D 043°59.782', 902 m, 26.VII.2016, 11 exs., (*P. armeniaca*), Tuzluca, Eğrekdere, K 39°69.619', D 043°38.802', 1380 m, 09.VIII.2014, 3 exs., *(P. armeniaca),* K 39°59.622', D 043°39.207', 1490 m, 23.VIII.2014, 5 exs., (*P. armeniaca*), K 40°00.599', D 043°38.637', 1216 m, 03.VII.2015, 4 exs., (*P. armeniaca*), 04.VII.2015, 2 exs., (*P. armeniaca*), 13.VII.2015, 2 exs., (*P. armeniaca*), K 39°59.614', D 043°038.803', 1373 m, 19.VIII.2015, 4 exs., (*P. armeniaca*), Üçkaya, K 39°95.896', D 043°326.915', 1505 m, 04.VII.2015, 2 exs., (*P. armeniaca*), 5 exs., (*P. avium*), (Figure 1a).

Family. Yponomeutidae. ***Yponomeuta padella*** (Linnaeus, 1758). Only adults in the branches of apricot and peach trees in the nearby gardens found only in Melekli were found in the last year of the study.

Hosts. *Prunus armeniaca* was detected in the study area.

Material examined. Igdır. Melekli, K 39°56.417', D 044°05.769', 856 m, 05.VIII.2015, 2 exs., (*P. armeniaca*), K 39°57.140', D 044°05.576', 859 m, 05.VIII.2015, 8 exs., (*P. armeniaca*), K 39°57.301', D 044°07.382', 861 m, 05.VIII.2015, 1 ex., (*P. armeniaca*), K 39°56.475', D 044°06.272', 850 m, 19.VII.2016, 180 exs., (*P. armeniaca*), 2 exs., (*P. persica*), K 39°57.308', D 044°07.386', 861 m, 19.VII.2016, 6 exs., (*P. armeniaca*), K 39°56.798', D 044°06.931', 862 m, 19.VII.2016, 2 exs., (*P. armeniaca*), K 39°56.318', D 044°05.301', 862 m, 19.VII.2016, 1 ex., (*P. armeniaca*), K 39°57.308', D 044°07.386', 861 m, 19.VII.2016, 1 ex., (*P. armeniaca*), K 39°56.819', D 044°06.869', 857 m, 28.VII.2016, 23 exs., (*P. armeniaca*), Eğrekdere, K 39°58.490', D 043°39.236', 1479 m, 19.VIII.2015, 1 ex., (*P. armeniaca*), (Figure 1b).

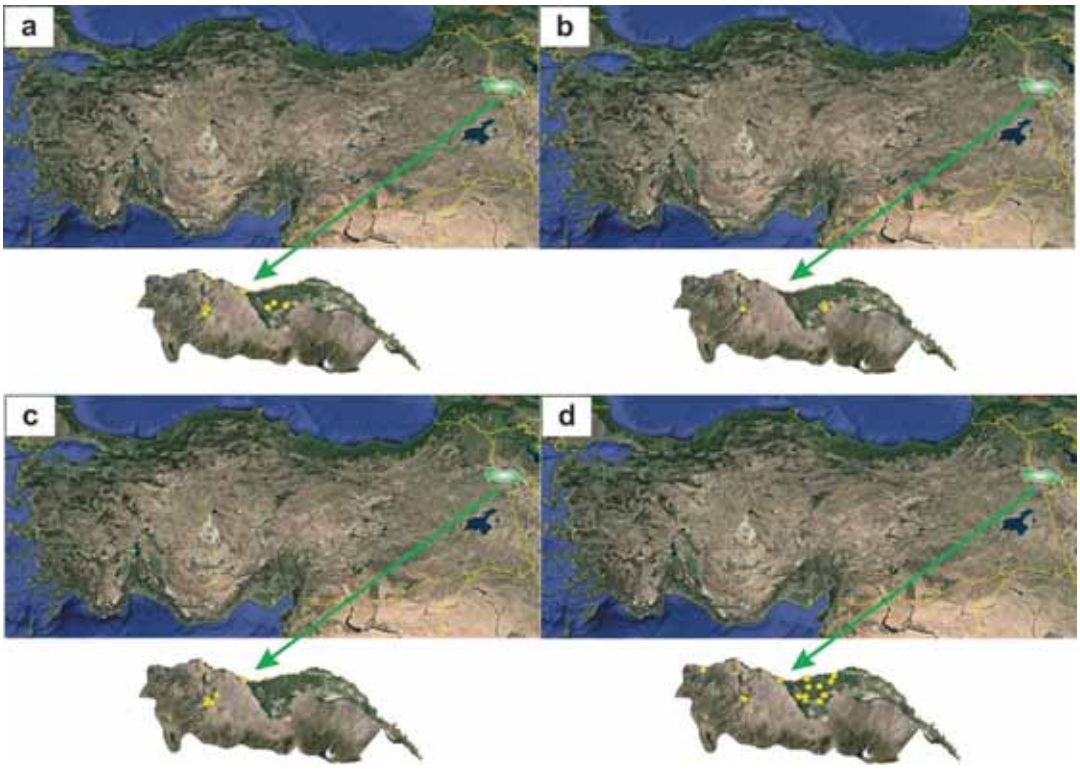

FIGURE 1
Distribution in Igdır of species: a) *Lyonetia clerkella*; b) *Yponomeuta padella*; c) *Ypsolopha persicella*; d) *Grapholita janthinana*.

Ypsolopha persicella (Fabricius, 1787). In the study area, it was found that only apricots were found in low density in Tuzluca district.

Hosts. *Prunus armeniaca* was detected in the study area.

Remarks. The presence of *Y. persicella* in Igdır province was the first recorded in this study.

Material examined. Igdır. Çalpala, K 40°00.738', D 043°53.389', 896 m, 05.VII.2015, 12 exs., (*P. armeniaca*), Tuzluca, Eğrekdere, K 39°58.486', D 043°39.237', 1475 m, 15.IX.2014, 1 ex., (*P. armeniaca*), Karabulak, K 39°59.246', D 043°42.973', 1364 m, 14.IX.2014, 1 ex., (*P. armeniaca*), Küçükova, K 39°56.941', D 043°40.661', 1624 m, 14.IX.2014, 2 exs., Üçkaya, K 39°95.896', D 043°3265.915', 1505 m, 08.VIII.2013, 5 exs., (*P. armeniaca*), 09.VIII.2013, 5 exs., (*P. armeniaca*), 10.VIII.2013, 4 exs., (*P. armeniaca*), 31.VIII.16, 2 exs., (*P. armeniaca*), (Figure 1c).

Family. Tortricidae. *Cydia pomonella* (Linnaeus, 1758). Biological observations were made in apple orchards. As a result of observations, the *Cydia pomonella* larvae (Figure 2a,2b) enter from the flower pit, especially in the elbow near the stalk, and proceed by opening the gallery towards the core house and larvae are nourished in the core house (Figure 2a). Only one larva was found in each apple. This feature is striking. Mature larvae overwintering in the white cocoons under the bark of apple trees and in other protected places (Figure 2c). As a result of observations made in the apple orchards the average infestation (100 apple fruit) of 32% were larvae, 21% were larvae damage but larvae were leaving fruit and 47% were healthy. *Cydia pomonella* (Linnaeus, 1758), which is economically important and the main pest species in this area.

Sexual attractive pheromone traps are used for monitoring the development of the population. The study followed the biological periods of codling moth.

The study was carried out in four apple orchard that located in the districts of Igdır (Center 1, Center 2), Melekli and Tuzluca (Eğrekdere) locations of the province during vegetation periods in 2016.

The population development curves of *C. pomonella* according to the numbers of butterflies captured in the pheromone traps given in Figure 3. Figure 3a represents Melekli town. The first Figure 3a is examined, the first adult output of *C. pomonella* on April 17 and it is seen that there are three peaks of codling moth. These peak points are; on May 11, on June 23 and July 5, respectively. The last adult was seen in the trap on 02 October 2016. Figures 3b and 3c represent Igdır province.

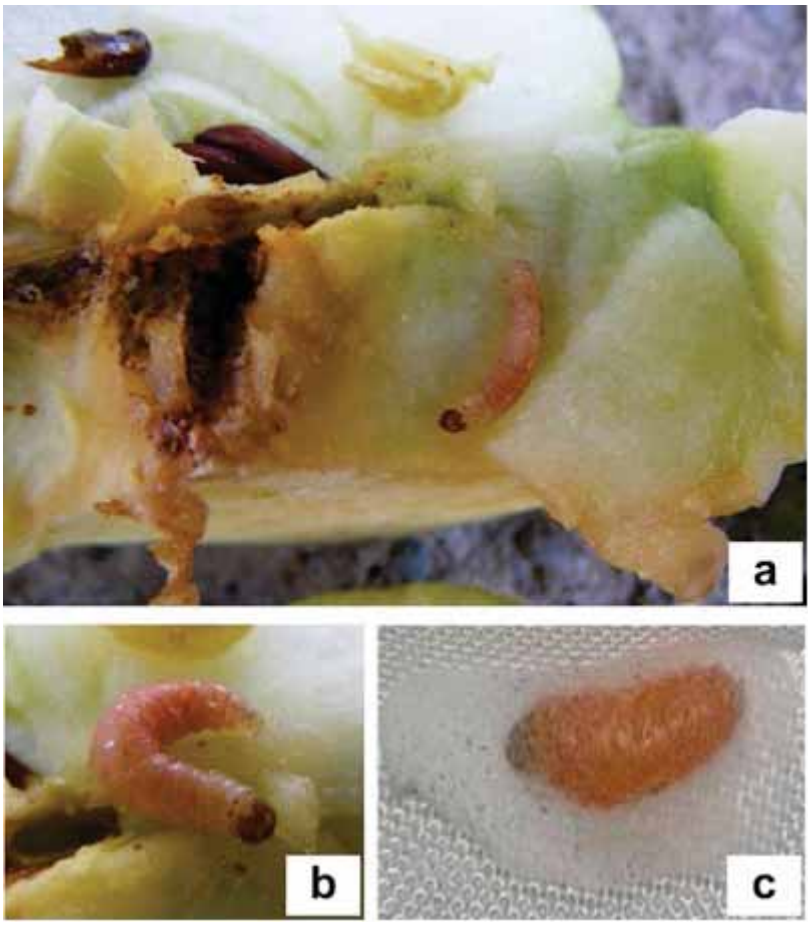

FIGURE 2
***Cydia pomonella* (Linnaeus, 1758) in apple, a-damage b- larva c- mature larva**

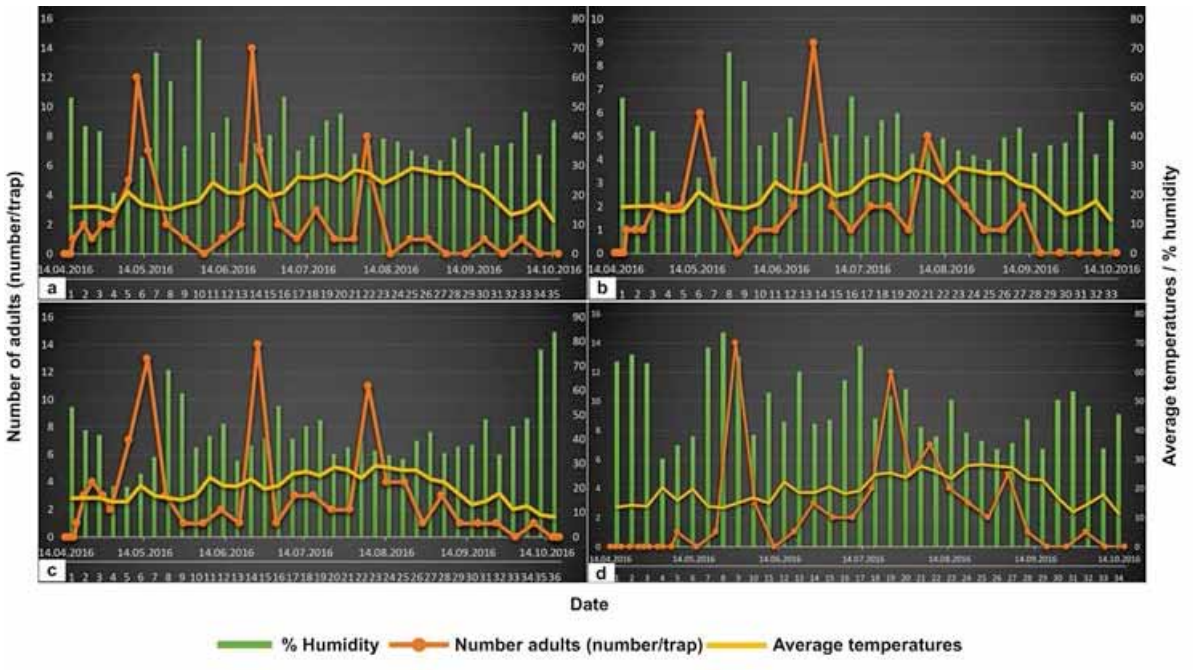

FIGURE 3
Population fluctuation of *Cydia pomonella* a- Melekli town b,c- Igdır (Center 1, Center 2) d- Tuzluca (Eğrekdere) village

Figures 3b and 3c represent Igdır (Center 1, Center 2). When Figure 3b and figure 3c are examined, the first adult output of *C. pomonella* on April 18 and it is seen that there are three peaks of codling moth. These peak points are; on May 15, on June 26 and Augst 7, respectively When Figure 3b is examined, the last adult was seen in the trap on 09 October 2016. However, When Figure 3c is examined, the last adult was seen in the trap on 03 September 2016.

Figure 3d represents Tuzluca town. The last Figure 3d is examined, the first adult output of *C. pomonella* on May 8 and it is seen that there are two peaks of codling moth. These peak points are; on May 29, and July 24, respectively. The last adult was seen in the trap on 25 September 2016.

As a result of research, it was determined that *Cydia pomonella* (Linnaeus, 1758), which is economically important and the main pest species in this area. Codling moth under natural climatic conditions gives two or three generation years in Igdır province. Codling moth adults are active in nature for about five months from the second week of April to the second week of September. Different researchers said that codling moth adults are active in nature for about five months [18,19,20]

Hosts. *Malus Domestica* and *Prunus persica* were detected in the study area

Grapholita janthinana (Duponchel, 1843). The larvae were seen in the period when the apples began to mature and adults were obtained from culture. It is similar to ***C. pomonella*** in terms of damage and even manufacturers think that this species is ***C. pomonella***. In this study, the differences between the two species were revealed. ***G. janthinana*** larvae are dark brown and smaller than ***C. pomonella*** larvae. Larvae are usually fed in the fruit by entering the fruit from the cheek.

Hosts. *Malus domestica* was detected in the study area.

Remarks. The presence of *Y. persicella* in Igdır province was the first recorded in this study.

Material examined. Igdır. K 39°56.278', D 044°00.454', 873 m, 05.VIII.2015, 2 exs., (*M. domestica*), Şemsettin Uzun, K 39°56.831', D 043°58.949', 866 m, 19.VIII.2015, 5 exs., (*M. domestica*), Ağaver, K 40°01.096', D 044°00.655', 864 m, 19.VIII.2014, 1 ex., (*M. domestica*), Akyumak, K 39°58.109', D 044°03.545', 866 m, 19.VIII.2014, 3 exs., (*M. domestica*), Alikamerli, K 39°59.528', D 044°00.768', 832 m, 19.VII.2016, 3 exs., (*M. domestica*), Çalpala, K 39°59.767', D 043°54.538', 890 m, 31.VIII.2014, 2 exs., (*M. domestica*), Kadıkışlak, K 40°01.414', D 044°03.749', 874 m, 19.VIII.2014, 3 exs., (*M. domestica*), Kazancı, K 40°00.120', D 044°01.710', 881 m, 19.VIII.2014, 1 ex., (*M. domestica*), Melekli, K 39°57.529', D 044°05.448', 847 m, 13.VIII.2014, 2 exs., (*M. domestica*), 18.VIII.2014, 3 exs., (*M. domestica*), K 39°56.389', D 044°05.768', 847 m, 14.VIII.2014, 2 exs., (*M. domestica*), Oba, K 39°56.844', D 043°59.864', 854 m, 26.VIII.2016, 1 ex., (*M. domestica*), Yaycı, K 39°56.805', D 043°48.953', 867 m, 23.VIII.2014, 2 exs., (*M. domestica*), 15.IX.2015, 1 ex., (*M. domestica*), 14.IX.2014, 2 exs., (*M. domestica*), 27.VIII.2014, 3 exs., (*M. domestica*), Karakoyunlu, Zülfikar, K 39°50.239', D 044°36.718', 843 m, 23.IX.2014, 2 exs., (*M. domestica*), Tuzluca, Eğrekdere, K 39°58.498', D 043°39.234', 1485 m, 09.VIII.2014, 1 exs., (*M. domestica*), K 39°58.296', D 043°39.109', 1057 m, 07.IX.2014, 1 ex., (*M. domestica*), Gaziler, K 40°06.129', D 043°28.624', 1027 m, 07.IX.2014, 5 exs., (*M. domestica*), (Figure 1d).

CONCLUSION

In this study, pest enemy fauna of fruit orchards in Igdır was studied Lyonetiidae, Tortricidae and Yponomeutidae for the first time.

As a result, ***Lyonetia clerkella*** (Linnaeus, 1758), ***Cydia pomonella*** (Linnaeus, 1758), ***Grapholita janthinana*** (Duponchel, 1843), ***Yponomeuta padella*** (Linnaeus, 1758) and ***Ypsolopha persicella*** (Fabricius, 1787) were determined pests on fruit trees in Igdır province. ***Cydia pomonella*** (Linnaeus, 1758), which is economically important and the main pest species on fruit trees in Igdır.

It is important to note that ***Grapholita janthinana*** and ***Ypsolopha persicella*** were recorded for the first time in Igdır during this study.

Additionally, codling moth under natural climatic conditions gives two or three generation years in Igdır province. It is thought that this situation is caused by the differences in the climatic characteristics of the cultivated areas. Codling moth adults are active in nature for about five months from the second week of April to the second week of September.

Besides, it is known that producers in the region sprayed *C. pomonella* between 7-14 during the production season. In spite of such intensive treatments, the damage of *C. pomonella* was determined in 53% of the fruits. These data may serve as a useful resource for integrated pest management (IPM) programs in a fruit orchard.

ACKNOWLEDGEMENTS

We deeply thank Dr. Mustafa Özdemir (Plant Protection Central Research Institute, Ankara, Turkey) for identifying Lyonetiidae, Tortricidae and Yponomeutidae.

*A partial summary of Yeşim Bulak Korkmaz's Ph.D. thesis (Atatürk University, Institute of Science, Department of Plant Protection) and II. International Igdır Symposium (09-11 October 2017) is presented as a poster and printed as a summary.

REFERENCES

[1] Elekcioglu, N.Z. and Olculu, M. (2017). Pest, predator and parasitoid species in persimmon orchards in the eastern Mediterranean region of Turkey, with new records. Fresen. Environ. Bull. 26, 5170-5176.

[2] Kaplan, M. and Alaserhat, İ. (2019). Investigation on Mass-Trapping of *Archips rosanus* L. (Lepidoptera: Tortricidae), Pest of Cherry Trees. Fresen. Environ. Bull. 28, 1308-1311.

[3] Demirel, N. (2019). Trapping Genders of *Ceratitis capitata* (Diptera: Tephritidae) and other Dipteran with Various Attractants On Pomegranate Fruits in Turkey. Fresen. Environ. Bull. 28, 2937-2941.

[4] Kaplan, M. (2019). Determining The Criterion and Biotechnical Struggle Methods Against *Forficula auricularia* L.(Dermaptera: Forficulidae) Harming in Apricot Orchards In Turkey. Fresen. Environ. Bull. 28, 6701-6706.

[5] Elekcioglu, N.Z., Artun, O. and Kavur, H. (2019). Predicting The Potential Geographic Distribution And Seasonality of *Ceratitis capitata* Wiedemann (Diptera, Tephritidae) in the Mediterranean Region of Turkey. Fresen. Environ. Bull. 28, 10164-10173.

[6] Şimşek, M., Gülsoy, E. and. Karadaş, K. (2018). Fruit Production Potential and Its Contribution to the Local Economy in Igdır Province. Igdır Univ. J. Inst. Sci. & Tech. 8(3), 39-44. (In Turkish).

[7] Koday, Z. (2004). Fruit-Growing In the Town of Kağızman. Eastern Geographical Review. 9(12), 189-206. (In Turkish).

[8] Borror, J.D., De Long, M.D. and Triplehorn, A.C. (1981). An introduction to the study of insects. New York. Saunders College Publishing, Philadelphia.516-517.

[9] Bariola, L.A., and Lingren, P.D. (1984). Comparative toxicities of selected insecticides against pink bollworm (Lepidoptera: Gelechiidae) moths. Journal of Economic Entomology. 77(1), 207-210.

[10] Reuveny, H. and Cohen, E. (2004). Resistance of the codling moth *Cydia pomonella* (L.) (Lep., Tortricidae) to pesticides in Israel. Journal of Applied Entomology. 128(9-10), 645-651.

[11] Mota-Sanchez, D., Wise, J.C., Poppen, R.V., Gut, L.J. and Hollingworth, R.M. (2008). Resistance of codling moth, *Cydia pomonella* (L.) (Lepidoptera: Tortricidae), larvae in Michigan to insecticides with different modes of action and the impact on field residual activity. Pest Management Science. 64(9), 881-890.

[12] Kovanci, O.B. (2017). Comparıson of the Costs of Mating Disruption with Traditional Insecticide Applications for Control of Codling Moth in Apple Orchards in Turkey. Scientific Papers-Series B-Horticulture. LXI (61), 455-460.

[13] Elkins R.B., Klonsky K.M. and De Moura R.L. (2005). Cost of production for transitioning from conventional codling moth control to aerosol-released mating disruption ("puffers") in pears. Proceedings of the 9th International Pear Symposium. (671), 559-563.

[14] Kovanci, O.B. (2015). Co-application of microencapsulated pear ester and codlemone for mating disruption of *Cydia pomonella*. Journal of Pest Science. 88(2), 311-319.

[15] Wang, H., Jia, J., Yu, X., Feng, J. and Chen, F. (1999). Studies on occurrence and control techniques of *Lyonetia clerkella* Linnaeus. Plant Protection Technology and Extension. 19(4), 22-24.

[16] Yang, Y., Huang, Q., Sun, X. and Xu, W. (2000). The effect of four toadstools on peachminer. Chinese Journal of Biological Control. 16(4), 188-189.

[17] Lazarov, A. and Grigorov, P. (1961). Karantinana Rastenijata. Zemizdat, Sofia, 258.

[18] Özpınar, A., Şahin, A.K. and Polat, B. (2009). Determination of Dispersal Area and Population Density of Codling Moth (*Cydia pomonella* (L) (Lepidoptera: Tortricidae)) in Canakkale Province. Proceedıngs of the Third Plant Protection Congress of Turkey. 15-18 July, Van, Turkey, 100.

[19] Mamay, M. and Yanık., E. (2013). Determination of Population Development and Infestation Rates of Codling Moth [*Cydia pomonella* (L.) (Lepidoptera: Tortricidae)] by Using Different Sampling Methods in Şanlıurfa Province. Journal of Agricultural Sciences. 19(2), 113-120. (In Turkish).

[20] Çelik, H. and Ünlü, L. (2016). Determination of the Population Development and Infestation Ratio of Coldling Moth [*Cydia pomonella* (L.) (Lep.: Tortricidae)] in Apple Orchards in Beyşehir (Konya). Turkey 6th Plant Protection Congress with International Participation. 5-8 September, Konya, Turkey, 289.

Received: **08.05.2019**
Accepted: **10.02.2020**

CORRESPONDING AUTHOR

Yesim Bulak Korkmaz
Atatürk University,
Faculty of Agriculture,
Department of Plant Protection,
25240, Erzurum-Turkey

e-mail: yesim.bulak@atauni.edu.tr

© by PSP Volume 29 – No. 05/2020 pages 3465-3472 Fresenius Environmental Bulletin

ALLELOPATHIC ACTIVITIES OF *SPATHIPHYLLUM WALLISII* ROOT EXTRACT ON BLOOM-FORMING CYANOBACTERIUM "*MICROCYSTIS AERUGINOSA*"

Jingsi Gao[1], Wenyi Dong[2], Xiaoxiong Wang[1,*], Yim Tong Szeto[3], Jia Zhu[1], Jiacheng Zhu[4]

[1]School of Civil and Environmental Engineering, Shenzhen Polytechnic, Shenzhen 518055, China
[2]Shenzhen Key Laboratory of Water Resource Utilization and Environmental Pollution Control, Harbin Institute of Technology, Shenzhen, 518055, PR China
[3]Diagnostix Medical Centre, Room 601, 6/F, China Insurance Group Building, 141 Des Voeux Road Central, Hong Kong SAR, China
[4]Wuxi Children's Hospital, Road Qingyang 299-1 214023, Wuxi, China

ABSTRACT

Harmful algae blooms (HABs) contribute to economic loss as well as the threat to human and animal health. Among various technologies developed, allelopathic algicides are considered a promising technology to control excessive algal growth. In this study, the effect on *Microcystis aeruginosa* with different concentrations of *Spathiphyllum wallisii* root extract (SWRE) was tested. Results suggested that the SWRE doses from 0.5 to 4.0 g L^{-1} suppressed the growth of algae in a concentration-dependent manner. After 18 days of treatment, the highest inhibition rate was up to 99.2% and the chlorophyll-a (Chl-*a*) concentration in *M. aeruginosa* was 2.7 μg L^{-1} only. Inhibition of photosynthetic activity was reflected by changing photosynthesis efficiency (alpha) and relative electron transport rate (rETRs) of *M. aeruginosa* cells. Results also showed the activity of antioxidant enzyme Peroxidase in *M. aeruginos*a cells was inhibited by allelochemicals from SWRE. This resulted to the reaction between highly reactive and toxic intracellular free radicals reacting with the macromolecules in the algae.

KEYWORDS:
Esterase activity, Flow cytometry, *Microcystis aeruginosa*, Phyto-PAM, *Spathiphyllum wallisii*

INTRODUCTION

Water bloom refers to lake, pond response to excess organic and mineral nutrients which enhance rapid cyanobacteria growth [1]. This contributes to serious environmental, social, and economical impacts globally [2]. The negative influences of cyanobacterial harmful algal blooms (CHABs) affect various aspects, including the changes in odour, colour, taste, depleting oxygen level and suppressing aquatic animal survival in water bodies [3]. Furthermore, metabolites produced by both eukaryotic algae and cyanobacteria are highly toxic, exemplified by the secondary metabolites namely microcystins, which is a threat to ecosystem and human health [4]. Therefore, the control of CHABs in fresh water bodies is an important issue in eutrophic water body management.

Although physical, chemical and biological technologies are available to control and mitigate cyanobacterial growth, most of them are difficult to implement [5]. Hurdles include high costs, low effectiveness and secondary pollution problem [6]. Some biological methods lack of reproducibility and may bear biological invasion risks. Recent researches show that allelopathy is an effective and environmentally friendly method to control CHABs, which can minimise the use of chemical herbicides and hence reducing chance of secondary pollution [7]. Nevertheless, plants being used were mainly aquatic origin, including *Sagittaria trifolia*, *Myriophyllum verticillatum* and *Hydrilla verticillata* [8-10]. Information for the application of allelochemicals from dry plants and terrestrial plants in aquatic environment is limited [6]. Thus exploring the algistatic effects and the associated mechanism of terrestrial plants on CHAB deserve further study.

Inhibition of *M. aeruginosa* growth involves at least four major mechanisms, such as destruction of algal cell structure as well as inhibiting photosynthesis, respiration and enzymatic activities of algae [6]. Cyanobacteria have been in aquatic environments for 3.5 billion years and demonstrating the universal feature of photosynthetic process with high nutrient utilization efficiency [11]. Physiological and biochemical parameters such as the algal biomass content of chlorophyll-a (Chl-*a*), malondialdehyde (MDA) and antioxidative enzymes such as peroxidase (POD) [12] are frequently used parameters to evaluate the *M. aeruginosa* physiological response to some allelopathic plants or algal inhibition chemicals.

The current study aimed to investigate the algistatic effect of the root extract from a popular plant *Spathiphyllum wallisii* (SWRE) on *M. aeruginosa* for harmful algae blooms (HABs) control-

ling [13]. The mechanisms of SWRE on *M. aeruginosa* were also studied.

MATERIALS AND METHODS

The Roots Extract Preparation of *S. wallisii* and Culture of *M. Aeruginosa*. *S. wallisii* was collected from Shenzhen, Guangdong Province, China, which fresh plant roots was cut into pieces at about 5 mm in length after soak in tap water for 24 hours and in BG-11 medium for 2 days. It was dried at 50 °C for 2 days in oven. Fifty grams of grinded root was mixed with 500 mL BG-11 medium and incubated for 2 days at 26±1°C. The mixture was then filtered through the 0.22 μm membrane and kept at 4°C.

The *M. aeruginosa* FACHB-915 strain was obtained from the freshwater algae culture of hydrobiology (China). Algae grew for about 10 days in 250 mL conical flasks in BG-11 medium. The 14:10 h light/dark cycle under light of 30 μmol photons m^{-2} s^{-1} at 25±1 °C was applied [14]. Two mL of each algal suspension was sub-cultured to 1000 mL BG-11 medium and the initial content of chlorophyll-*a* (Chl-*a*) was about 2.0 μg L^{-1}. The extract of roots was added to microalgae cultures at the final concentrations of 0.5, 1.0, 2.0, 3.0, 4.0 g L^{-1}.

PAM Fluorometry Measurements. Samples were taken and measured on day 1, 4, 7, 10, 13 and 18 after SWRE exposure. *M. aeruginosa* growth was determined by measuring Chl-*a* content using pulse amplitude-modulated fluorescence phytoplankton analyzer (Phyto-PAM, Walz, Germany). Calibration was done with chlorophyll dissolved in acetone. Four mL algal samples were measured automatically and the light frequency was set to 32 (after chlorophyll calibration). Data acquisition and analysis was performed using PhytoWin v2.13. The inhibitory effect of the extract on the growth of algae was estimated by percentage inhibition:

$$\text{Percentage inhibition}\,(\%) = (1 - C/C_0) \times 100$$

Where C and C_0 are Chl-*a* content in the extract-treated and control cultures, respectively.

The F_v/F_m parameter was obtained from Phyto-PAM which reflect the maximal photochemical efficiency of PS II. All samples were measured after 5 min incubation in dark. The YII were measured firstly, then the F_v/F_m, and followed by the rapid light curves (RLCs). Detailed procedures are described previously [15].

The RLCs shows the relative electron transport rate (rETR) compared to the incident photosynthetic active radiation (PAR). Each of the Sat-Pulse length was 30 seconds and the total of light emitted during the Sat-Pulse was 300 seconds. The range of PAR from 16 to 1664 μmol $m^{-2}s^{-1}$ and 30 second exposure of each actinic light were used. Ten pulses were applied for each curve. Detailed procedures are described previously [15]. A nonlinear curve fit procedure using the Platt equation was constructed to estimate the photosynthesis efficiency (initial slope, alpha), and maximal relative electron transport rate (rETRmax) of *M. aeruginosa* [16].

Malondialdehyde (MDA) and Peroxidase (POD) Content Measurements. Lipid peroxidation was measured in term of malondialdehyde (MDA) concentration. MDA content was determined as described by [17, 18]. Peroxidase (POD) activity was measured according to [19].

Statistical Analysis. All experiments were run in triplicate. Data were presented as mean ± one standard deviation. One-way Analysis of Variance (ANOVA) followed by Tukey's multiple comparison test were used with the SPSS analytic package 16.0 (SPSS Inc., Chicago, IL, USA).

RESULTS AND DISCUSSION

Extract of *S. wallisii* Root on the Growth of *M. Aeruginosa*. The Chl-*a* concentration is closely related to the growth and photosynthetic activity of *M. aeruginosa*. The effect of SWRE on the Chl-*a* concentration of *M. aeruginosa* was shown in Figure 1. The Chl-*a* concentration remained low from day 1 to day 10 in all treatment groups, which was only 2.5 μg L^{-1} at a root extract dose of 4.0 g L^{-1}, while 69.7 μg L^{-1} for the control on day 10. The Chl-*a* concentrations increased slowly at high dose of root extract treatment (3.0 g L^{-1} and 4.0 g L^{-1}) after day 10 which were 4.1 μg L^{-1} and 2.7 μg L^{-1}on day 18, respectively. However, it was about 538.8 μg L^{-1} in the control at the end of experiment. The growth of *M. aeruginosa* was substantially inhibited within the 18-day period (P<0.01, ANOVA).

The growth inhibition on *M. aeruginosa* by different doses of SWRE was measured. Results showed that a range of SWRE concentrations ranging from 2.0 to 4.0 g L^{-1} effectively inhibited the growth of *M. aeruginosa*. Highest dose at 4.0 g L^{-1} could inhibit the growth up to 99% (Figure 2).

In the experiment, effectiveness of the crude extract of *S. Wallisii* root on controlling the growth of *M. aeruginosa* were tested. The significant decreases of Chl-*a* concentrations following addition of the SWRE indicated that the extract had antialgal activity. The result was in accordance with other plant extracts, such as crops straw [6, 20] as well as some terrestrial plants leaf litter [21-23] which could decrease growth of *M. aeruginosa*. However, previous crops straw studies required high extract

concentrations (about 10.0 g L^{-1}) [20, 24] added might aggravate eutrophication [25] which make application not feasible. In this study, lower concentration (4.0 g L^{-1}) the extract of *S. wallisii* root was able to produce significant suppressing effect compared to crops straw (8.0~10.0 g L^{-1}). Nevertheless, our data also suggested that 2-day decomposition of *S. wallisii* roots was also effective in inhibiting the growth of *M. aeruginosa*.

SWRE on the rETRmax and Alpha of *M. aeruginosa*. The photosynthesis efficiency alpha and rETRmax were about 0.03 to 0.15 µmol electrons m^{-2} s^{-1}/µmol photons m^{-2} s^{-1} and 33 to 96 µmol electrons m^{-2} s^{-1} respectively on day 1. Both parameters declined sharply in the presence of extract and increased gradually over 9-day period (Figure 3). A 64% dropped of alpha value was observed at 2.0 g L^{-1} extract after 9-day treatment (Figure 3a). The rETRmax at the level of 2.0 g L^{-1} was 2.6 µmol electrons m^{-2} s^{-1}, which was only 1.7% of the control sample (150.4 µmol electrons m^{-2} s^{-1}) on day 9 (Figure 3b). It is worth to note both alpha and rETRmax parameters did not return to the level of control at high dose (≥2.0 g L^{-1}) of treatment condition over 9-day experiment.

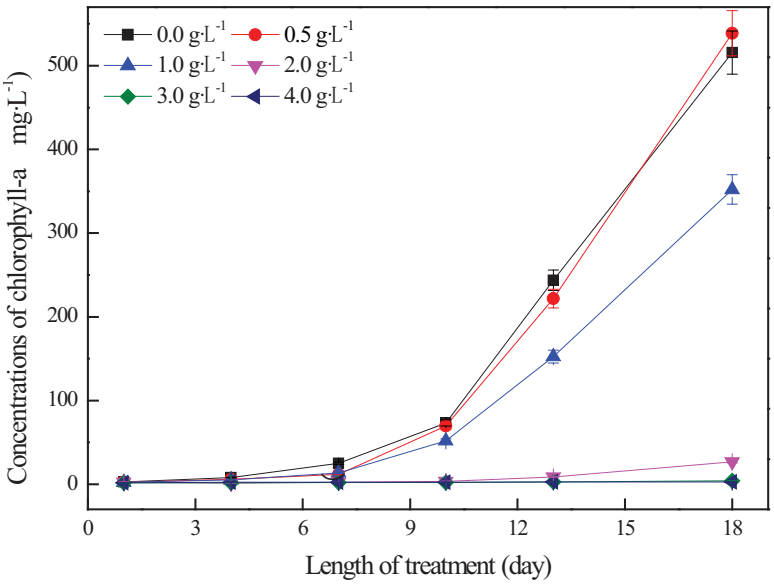

FIGURE 1
Chl-*a* concentrations in *M. aeruginosa* culture with 1, 4, 7, 10, 13, and 18 days of exposure to SWRE

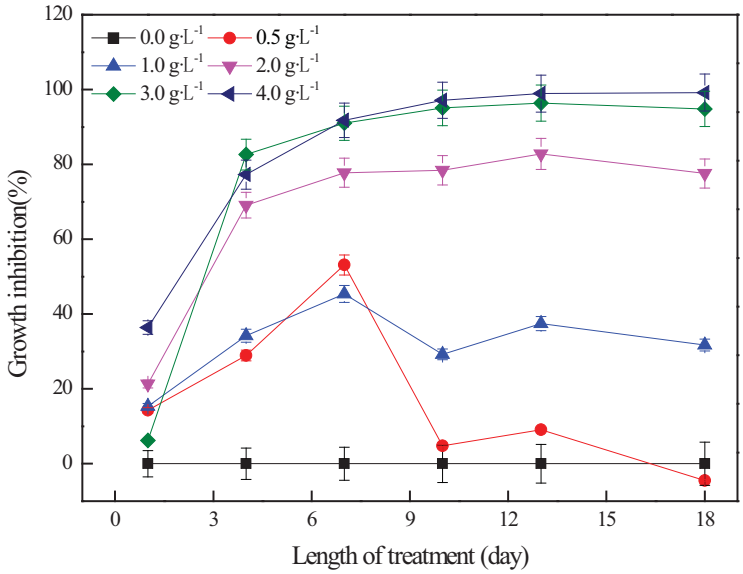

FIGURE 2
Inhibition of *M. aeruginosa* culture growth after1, 4, 7, 10, 13, and 18 days of exposure to SCRE

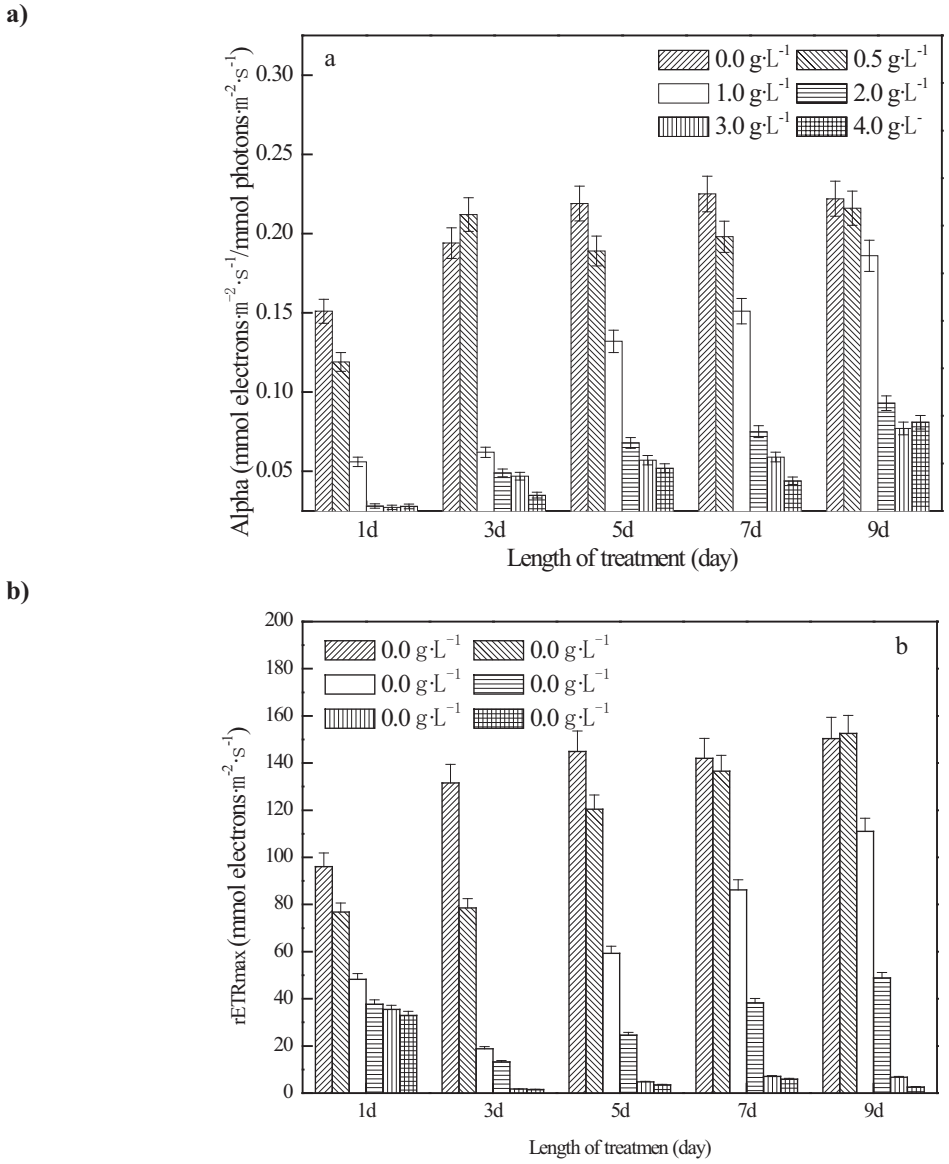

FIGURE 3
Photosynthesis efficiency (alpha) and maximal relative electron transport rate of *M. aeruginosa* exposure to root extract over 9-day period. a) the photosynthesis efficiency (alpha); b) the maximal relative electron transport rate (rETRmax).

Photosynthetic activities of *M. aeruginosa* were evaluated by alpha and rETRmax in this study. The two photosynthetic parameters are often used as the indexes of the photo-acclimation of algal vegetal state which associate with growth. Our results showed that the SCRE could decrease both alpha and rETRmax, suggesting damage to the PS II reaction center. The reduction showed that both the energy transfer and capacity of electron transport chain had been inhibited, which aligned with previous study [26]. The efficiency resumed from stress after about 3 days at low doses of treatment (0.5 and 1.0 g L^{-1}), which was not significantly difference with the control (p>0.05). However, alpha and rETRmax remained at low level from higher concentration (2.0, - 4.0 g L^{-1}) treatments on day 9 (p<0.05). Generally, the photosynthetic parameters decreased with the increasing dose of some allelochemicals, implying a dose-dependent nature in impairing algae photosynthetic system [27]. This observation indicated that the impairment of alpha and rETRmax was temporary and reversible at lower concentration treatment.

SWRE on the Maximal Efficiency and Effective Quantum Yield of *M. Aeruginosa*. The inhibition of capacity of the electron transport chain often results to the decline of photochemical efficiency for PSII. The effect of *S. wallisii* root extract on the Chl-*a* concentration of *M. aeruginosa* was shown in Figure 3. On day 1, the F_v/F_m of *M.*

aeruginosa reduced to 0 at the 4.0 g L^{-1} extract treatment while the control was about 0.32 in the experiment. Statistical significant growth inhibition of *M. aeruginosa* growth was seen in concentration-dependent manner (P<0.01, ANOVA). During the experiment, the values of F_v/F_m were kept at low level (0.08-0.2) at high doses SWRE treatment (2.0 - 4.0 g L^{-1}) while the control was about 0.32 to 0.51. On day 9, the F_v/F_m value was about 0.2 at the highest dose of extract (4.0 g L^{-1}), while it was 0.5 in the control (Figure 3a). Generally, changes in YII at different extract concentrations were consistent with F_v/F_m changes. However, YII increased when the cultures were treated at low SWRE concentration (0.5 g L^{-1}) and in control group. While the value of YII were 0.18 and 0.19 at the highest extract concentration on day 7 and day 9, which was only about 40% the value under control treatment (Figure 3b).

In the present study, the variation in F_v/F_m and YII exhibited a pattern similar to that of alpha and rETRmax parameters. F_v/F_m and YII are key indicators of the light absorbed by PSII and can be inhibited to a low degree by some kinds of allelochemicals, such as luteolin [11]; garlic and diallyl trisulfide [27]; aquatic extract of plant leaf litter [28]; or crops straw [24, 29]. In the current study, results suggested that SWRE could inhibit F_v/F_m and YII from 1 to 9 day treatment especially at high dose. During the experiment, F_v/F_m and YII demonstrated upward trend. However, the two parameters were also about 0.2 when exposed to higher dose of SWRE (3.0 and 4.0 g L^{-1}) on day 9 (Figure 4). Previous report showed that the F_v/F_m value of algae above about 0.5 indicate healthy state while below 0.3 is in regarded as poor condition [30], which also implied the impairment of photosynthetic system was temporary. However, the Chl-*a* concentration parameter haven't exhibited until about day 10. So, these findings also indicated that it was comprehensive to utilize photosynthetic parameters than Chl-*a* concentration to assess the growth state of *M. aeruginosa*.

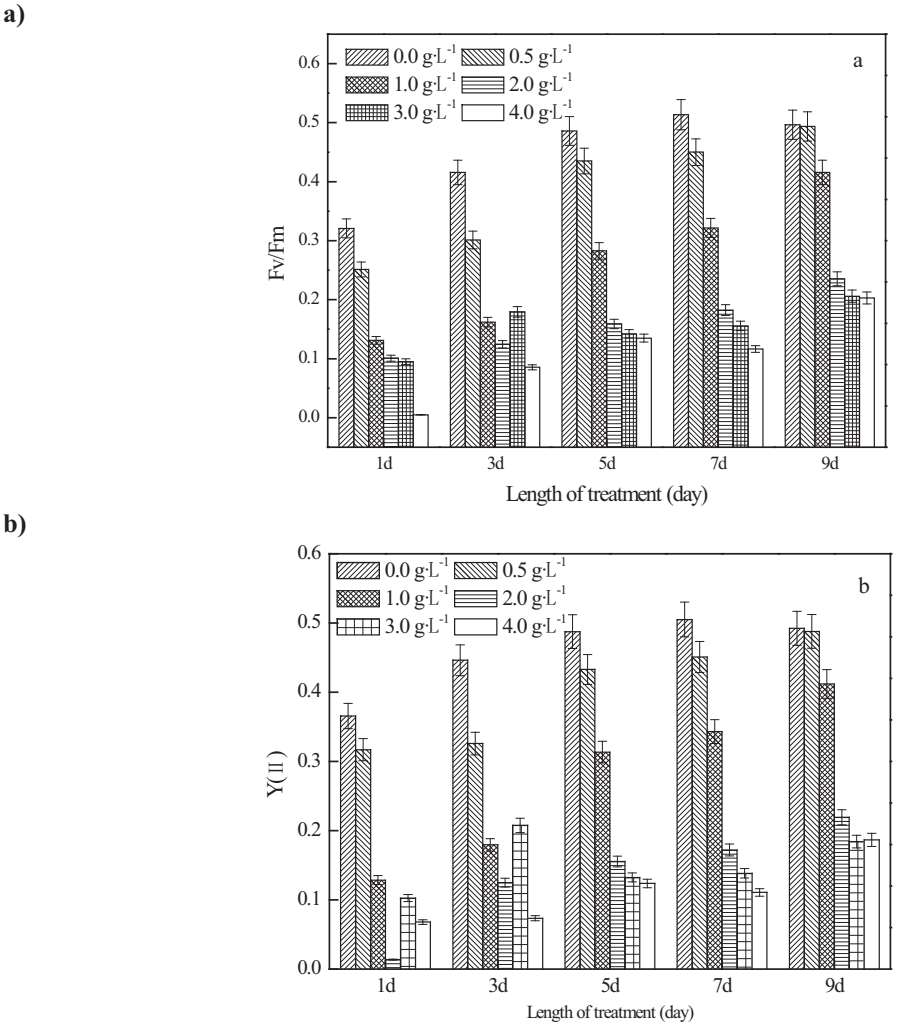

FIGURE 4

The maximal efficiency and effective quantum yield of *M. aeruginosa* in different extract treatments over 9-day period. a) the maximal efficiency (F_v/F_m); b) the effective quantum yield (YII).

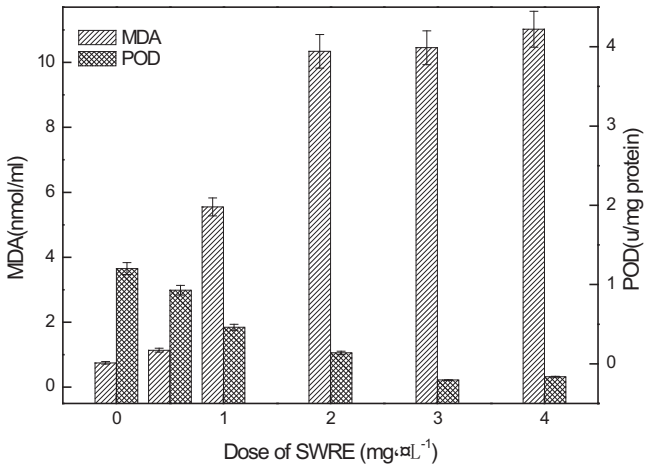

FIGURE 5
The MDA and POD in *M. aeruginosa* with different concentrations of SWRE on the day 5

SWRE on the MDA and POD Histogram in *M. aeruginosa*. The effect of SWRE on the MDA and POD of *M. aeruginosa* was shown in Figure 3. The content of MDA increased markedly with dose of SWRE on day 5. The MDA values were over 10 nmoL L^{-1} at the concentration of 2.0-4.0 g L^{-1}, which was over 14 times than the control group (0.75 nmoL L^{-1}) (Figure 5). The POD values decreased to 6.0% and 8.8% of the control at the treatment groups of 3.0 and 4.0 g L^{-1} respectively (Figure5).

Algal membrane lipid peroxidation status reflected the oxidative stress on algal cells. MDA is a decomposition product and has been employed as a biomarker to estimate oxidative damage in cells of *M. aeruginosa* [31]. Previous study showed that reactive oxygen radicals could cause severe oxidative stress and damage to cytomembrane polyunsaturated fatty acid of *M. aeruginosa* induced by rice straw aqueous extract [6]. The activities of POD at the low initial cell density of *Scenedesmus obliquus* were stimulated, and the contents of MDA increased in *Potamogeton malaianus* treatments [32]. In the present study, SWRE stimulated MDA and POD activities at high doses of extract. When exposed to SWRE, the MDA and POD content in the algal cells changed significantly in *M. aeruginos*a cells exposed to high doses of SWRE (3.0 and 4.0 g L^{-1}). The allelochemicals lowered POD activity and was the potential cause of the increased MDA content in *M. aeruginos*a which finally cause the death of algae.

CONCLUSIONS

Through the analysis of above growth and physiological indexes, the inhibition mechanism of *S. wallisii* root aqueous extract on *M. aeruginosa* growth was explored. The results demonstrated that the Chl-*a* concentration decreasing was directly related to the activity of photosynthetic activities and antioxidant system of algal cells. Allelochemicals secreted from *S. wallisii* root aqueous extract could restrict photosynthetic and antioxidant enzyme system activity. They reduced both photosynthesis efficiency and relative electron transport rate, and resulted to the decline of photochemical efficiency of PSII. In addition, allelochemicals from *S. wallisii* root affected antioxidant system in *M. aeruginos*a cells, which further weakened the system of algae. Therefore, the research provided an alternative technology to suppress HABs, could also decrease the use of chemical herbicides and reduce to harm the environment. Further studies are needed to identify of allelochemicals in *S. wallisii* roots and allelopathic mechanisms on growth and physiological processes of algae.

ACKNOWLEDGEMENTS

This work was supported by the National Natural Science Foundation (NSFC) of China, Grant No. 51978415 for their financial support.

REFERENCES

[1] Zhu, Z., Liu, Y., Zhang, P., Zeng, G., Hu, X., Li, H., Guo, Y., Guo, X. (2014) Co-culture with *Cyperus alternifolius* induces physiological and biochemical inhibitory effects in *Microcystis aeruginosa*. Biochem. Syst. Ecol. 56, 118-124.

[2] Paerl, H.W., Otten, T.G. (2013) Harmful cyanobacterial blooms: causes, consequences, and controls. Microb. Ecol. 65, 995-1010.

[3] Paerl, H.W., Huisman, J. (2009) Climate change: A catalyst for global expansion of harmful cyanobacterial blooms. Environmental Microbiology Reports.1, 27-37.
[4] Conley, D.J., Paerl, H.W., Howarth, R.W., Howarth, R.W., Boesch, D.F., Seitzinger, S.P., Havens, K.E., Lancelot, C., Likens, G.E. (2009) Controlling eutrophication: nitrogenand phosphorus. Science. 323 (5917), 1014-1015.
[5] Jančula, D., Maršálek, B. (2011) Critical review of actually available chemical compoundsfor prevention and management of cyanobacterial blooms. Chemosphere. 85 (9), 1415-1422.
[6] Hua, Q., Liu, Y.G., Yan, Z.L., Zeng, G.M., Liu, S.B., Wang, W.J., Tan, X.F., Deng, J.Q., Tang, X., Wang, Q.P. (2018) Allelopathic effect of the rice straw aqueous extract on the growth of *Microcystis aeruginosa*. Ecotox. Environ. Safe. 148, 953-959.
[7] Huang, H.M., Xiao, X., Lin, F., Grossart, H.P., Nie, Z.Y., Sun, L.J., Xu, C., Shi, J.Y. (2016) Continuous-release beads of natural allele-chemicals for the long-term control of cyano-bacterial growth: Preparation, release dynamics and inhibitory effects. Water Res. 95, 113-123.
[8] Hilt, N.K.S., Beutler, E., Bauer, N. (2012) Comparison of methods to detect allelopathic effects of submerged macrophytes on green al-gae. J. Phycol. 48 (1), 40-44.
[9] Mulderij, G., Mau, B., de Senerpont Domis, L., Smolders, A., Van Donk, E. (2009) Interaction between the macrophyte *Stratiotes aloides* and filamentous algae: does it indicate allelopathy? Aquat. Ecol. 43 (2), 305-312.
[10] Zhang, S., Cheng, S., Sun, P., Wang, H., Wu, Z. (2011) Isolation and identification of antialgal compounds from *Potamogeton maackianus* by activity-guided fractionation. Allelopathy J. 28 (1), 95-104.
[11] Huang, H.M., Xiao, X., Ghadouani, A., Wu, J.P., Nie, Z.Y., Peng, C., Xu, X.H., Shi, J.Y. (2015) Effects of natural flavonoids on photo-synthetic activity and cell integrity in *Micro-cystis aeruginosa*. Toxins. 7 (1), 66-80.
[12] Mallick, N., Mohn, F.H. (2000) Reactive oxygen species: response of algal cells. J. Plant Physiol. 157 (2),183-193.
[13] Parseh, I., Teiri, H., Hajizadeh, Y., Ebra-himpour, K. (2018) Phytoremediation of ben-zene vapors from indoor air by *Schefflera ar-boricola* and *Spathiphyllum wallisii* plants. Atmospheric Pollution Research. 9 (6), 1083-1087.
[14] Rippka, R., Deruelles, J., Waterbury, J.B., Herdman, M., Stanier, R.Y. (1979) Genetic assignments, stain histories and properties of pure culture of cyanobacteria. J. Gen. Microbiol. 111, 1-61.
[15] Suggett, D.J., Borowitzka, M.A., Prášil, O. (2010) Chlorophyll a Fluorescence in Aquatic Sciences: Methods and applications, Springer, London.
[16] Platt, T., Gallegos, C.L., Harrison, W.G. (1980) Photoinhibition of photosynthesis in natural assemblages of marine phytoplankton. J. Mar. Res. 38 (4), 687-701.
[17] Health, R.L., Packer, G. (1968) Photo-peroxidation in isolated chloroplasts. I. Kinetics and stoichiometry of fatty acid peroxidation. Arch. Biochem. Biophys. 125 (1), 189-198.
[18] Shiu, C.T., Lee, T.M. (2005) Ultraviolet-B-induced oxidative stress and responses of the ascorbate-glutathione cycle in a marine macroalga *Ulva fasciata*. J. Exp. Bot. 56 (421), 2851-2865.
[19] Andrews, J., Malone, M., Thompson, D.S., Ho, L.C., Burton, K.S. (2000) Peroxidase isozyme patterns in the skin of maturing tomato fruit. Plant Cell Environ. 23 (4), 415-422.
[20] Xiao, X., Chen, Y.X., Liang, X.Q., Lou, L.P., Tang, X.J. (2010) Effects of Tibetan hulless barley efficiently inhibited bloom-Forming cyanobacterium *Microcystis aeruginosa*. Chemosphere. 81 (9), 1118-1123.
[21] Ni, L.X., Hao, X.Y., Li, S.Y.,, Chen, S.J., Ren, G.X., Zhu, L. (2011) Inhibitory effects of the extracts with different solvents from three compositae plants on cyanobacterium *Microcystis aeruginosa*. Sci. China. Chem. 54 (7), 1123-1129.
[22] Wang, X.X., Jiang, C.C., Szeto, Y.T., Li, H.K., Yam, K.L., Wang, X.J. (2016) Effects of *Dracontomelon duperreanum* defoliation extract on *Microcystis aeruginosa*: physio-logical and morphological aspects. Environ. Sci. Pollut. Res. 23, 8731-8740.
[23] Wang, X.X., Szeto, Y.T., Jiang, C.C., Wang, X.J. (2018) Effects of *Litchi chinensis* leaf litter extract on the growth, photosynthesis and metabolic activity in *Microcystis aeruginosa*. Allelopathy J. 45 (1), 65-76.
[24] Su, W., Johannes, A.H., Jia, Y.H., Lu, Y.P., Kong, F.X. (2014) Effects of rice straw on the cell viability, photosynthesis, and growth of *Microcystis aeruginosa*. Chin. J. Oceanol. Limn. 32 (1), 120-129.
[25] Lürling, M., Beekman, W. (2010) Anti-cyanobacterial activity of *Moringa oleifera* seeds. J. Appl. Phycol. 22 (4), 503-510.
[26] Ralph, P.J., Gademann, R. (2005) Rapid light curves: a powerful tool to assess photosynthetic activity. Aquatic Botany. 82 (3), 222-237.

[27] Wang, S.B., Wang, Y.N., Ma, X.X., Xu Z.R. (2016) Effects of garlic and diallyl trisulfide on the growth, photosynthesis, and alkaline phosphatase activity of the toxic cyanobacterium *Microcystis aeruginosa*. Environ. Sci. Pollut. Res. 23 (6), 5712-5720.

[28] Wang, X.X., Szeto, Y.T., Jiang, C.C., Wang, X.J., Tao, Y., Tu, J.G., Chen, J. (2018) Effects of *Dracontomelon duperreanum* Leaf Litter on the Growth and Photosynthesis of *Microcystis aeruginosa.* B. Environ. Contam. Tox. 100 (5), 690-694.

[29] Daniel, E.T., Ferrier, M.D., Armbrester, E.A., Anlauf, K.A. (2002) Inhibition of dinoflagellate growth by extracts of barley straw (*Hordeum vulgare*). J. Appl. Phycol. 14 (4), 275-280.

[30] Zhou, S.Q., Shao, Y.S., Gao, N.Y., Deng, Y., Qiao, J.L., Ou, H.S., Deng, J. (2013) Effects of different algaecides on the photosynthetic capacity, cell integrity and microcystin-LR release of *Microcystis aeruginosa*. *Sci*. Total. Environt. 463-464, 111-119.

[31] Shao, J., Xu, Y., Wang, Z., Jiang, Y., Yu, G., Peng, X., Li, R. (2011) Elucidating the toxicity targets of β-ionone on photosynthetic system of *Microcystis aeruginosa* NIES-843 (Cyanobacteria). Aquat. Toxicol. 104 (1-2), 48-55.

[32] Wu, Z.B., Deng, P., Wu, X.H., Luo, S., Gao, Y.N. (2007) Allelopathic effects of the submerged macrophyte *Potamogeton malaianus* on *Scenedesmus obliquus.* Hydrobiologia. 592 (1), 465-474.

Received: **10.05.2019**
Accepted: **19.02.2020**

CORRESPONDING AUTHOR

Xiaoxiong Wang
School of Civil and Environmental Engineering,
Shenzhen Polytechnic,
Shenzhen 518055, China

e-mail: wangxiaoxiong20@szpt.edu.cn

© by PSP Volume 29 – No. 05/2020 pages 3473-3481 Fresenius Environmental Bulletin

ASSESSMENT OF POLLUTION IN AGRICULTURAL FIELDS AROUND CORLU DUMPSITE THROUGH GIS

Orhan Yuksel, Huseyin Sari*

Department of Soil Science and Plant Nutrition, Faculty of Agriculture, Tekirdag Namik Kemal University, Tekirdag, Turkey

ABSTRACT

This study aims to reveal the effects of hazardous waste storage sites on environment over the analyses performed on soils and plants. To this end, the hazardous waste storage site (dump site) in Çorlu town of Tekirdag province, which has the largest area and volume in the region, was chosen as the study area. Çorlu is among the important industrial centers of the region (Thrace). In addition, present dump site collects the waste of surrounding districts, especially the industrially developed districts such as Çerkezkoy. Therefore, it may be expected that the dump site had excessive quantities of polluted materials and thus exerted greater threats of pollution on environment. Moreover, the preliminary surveys carried out indicated that existence of agricultural fields around the dumpsite led this area to be selected as the study area. In this sense, heavy metal, macro and micro element analyses were performed on 66 soil samples taken from 22 different points and on 14 plant samples taken from the points where agricultural activities (wheat farming) were practiced. Present findings were not able to reveal any significant correlations between the distance from the dump site and soil-plant heavy metal contents. However, there were significant positive correlations between the heavy metal and clay contents of the sampling sites. It can be stated that sloping nature of the research site reduced heavy metal concentrations of seepage water through the soil profile. It was believed that Çorlu stream located at the furthest position to dump site at the end of slope served as a drainage canal for the sampling sites and heavy metals leached through soil profile by precipitations drained into Çorlu stream.

KEYWORDS:
Dumpsite, Pollution, GIS, Tekirdağ, Waste, Soil

INTRODUCTION

Open landfill sites (irregular storage), also known as dumpsites, in which municipal wastes are haphazardly stored, generate visual and odor pollution and have various negative impacts on environment, groundwater and soils. Although majority of the municipalities has already turned irregular dump sites into regular waste storage sites (sanitary landfills), several municipalities are still dumping municipal wastes into dumpsites. According to 2016 statistics, 1390 of 1397 municipalities in Turkey provide waste services. With these services, municipalities collect annually 31.6 million tons of waste. While about 63% of collected waste are sent to sanitary landfills, about 30% is still dumped into irregular storage sites (dumpsites) [1]. In Turkey, solid wastes have long been haphazardly dumped and stored in various sites and they are still being dumped so. Such dumpsites generate significant environmental pollution, especially in soil and water resources. Seepage water is among the most significant problems in open storage sites. They seep into soil and groundwater and ultimately generate serious pollution in soil and groundwater [2]. Seepage water seeps through wastes and thus subjected to various physical, chemical and biological processes and holds high quantities of organic and inorganic pollutants. Seepage water moves along the slope gravitationally, seeps deep into soil profile and ultimately discharge into groundwater. Such a movement of seepage water carries various organic and inorganic pollutants into surrounding agricultural fields [3].

In Thrace region (especially in Çorlu) of Turkey, solid and liquid wastes of industrial activities generate significant environmental problems. Considering potential seepage of wastewaters into soils through irrigations or into drinking waters through deep percolations, it is quite evident that these wastes should meticulously be stored. Regular/irregular storages are the most common methods of disposal for municipal wastes. In both methods, a polluted wastewater is generated through seepages from stored wastes or seepage of precipitations through stored wastes. This uncontrolled seepage water generates significant threats on soil and water resources [4].

In Thrace region, Çorlu has the greatest industrialization and population increase. Population of Çorlu is around 250.000 people and about 300 tons waste are transported to Çorlu waste storage facility. The facility is constructed over 60 da (decares) land area and irregular storage is practiced in this

FIGURE 1
Image of the Research Site

facility [5]. Wastes of Çorlu and industrial wastes of neighboring Çerkezköy town with a developed industry are dumped into this facility. Such haphazard dumps generate serious threats of pollution on surrounding agricultural fields and groundwaters.

This study was conducted to put forth potential pollutant effects of Çorlu dumpsite on surrounding soils and plants grown in these soils. Soil samples were taken from increasing distances from the dumpsite and from increasing depths of soil profile and changes in heavy metal contents of the soil samples were analyzed. In addition, these changes are shown on maps made using Geographic Information Systems (GIS). GIS methods are widely used in agriculture for different purposes [6, 7, 8]. Plant samples were also taken from the same soil sampling locations and plant heavy metal contents were determined. Finally, soil and plant heavy metal contents were compared.

MATERIALS AND METHODS

Materials. This study was conducted in Çorlu town located in Northwestern part of Turkey (Thrace). The town is located right at the center of Thrace region. Surface area of the town is about 949 km² and altitude is between 150-180 m. Çorlu is located over a fill site in which sediments transported from Yıldız Mountains and dragged from the rivers were deposited. The study was mainly conducted in agricultural fields (41°11.071' N-27°48.447' E) adjacent to irregular waste storage facility (dumpsite) of Çorlu (Figure 1).

Çorlu has a land size of 950.000 ha. of these lands, 702.290 da are agricultural lands, 39.300 da are pasture-meadow lands, 8.000 da are forest lands. Fine-textured forest soils and red-brown colored soils are dominant in Çorlu. These soils are around 30-40 cm thick and are quite fertile. It was indicated in historical documents that forest cover of Ergene Basin has destroyed through invasions and turned into agricultural fields. Current tree populations are mostly generated through recent afforestation works [9].

Çorlu has a dominant terrestrial climate with hot and dry summers and cold and precipitated winters. The town has the least precipitations in Thrace. Annual total precipitation is 545 mm. of these precipitations, 20% is received in spring, 105 in summer, 30% in autumn and 40% in winter. Since Çorlu is located between Black Sea and Mediterranean, the town is mostly influenced by these two climate zones. Cold air masses coming from the north, mild and humid air flows from the South, Mediterranean and Aegean dominate the climate pattern of the region [10].

Methods. Sampling Locations and Samplings. A grid system was applied to determine sampling locations. Samplings were performed through formation of 100x200 m grids. Soil samples were taken from 3 different depths (0-30/30-60 /60-90 cm) in April 2017 with a shovel and

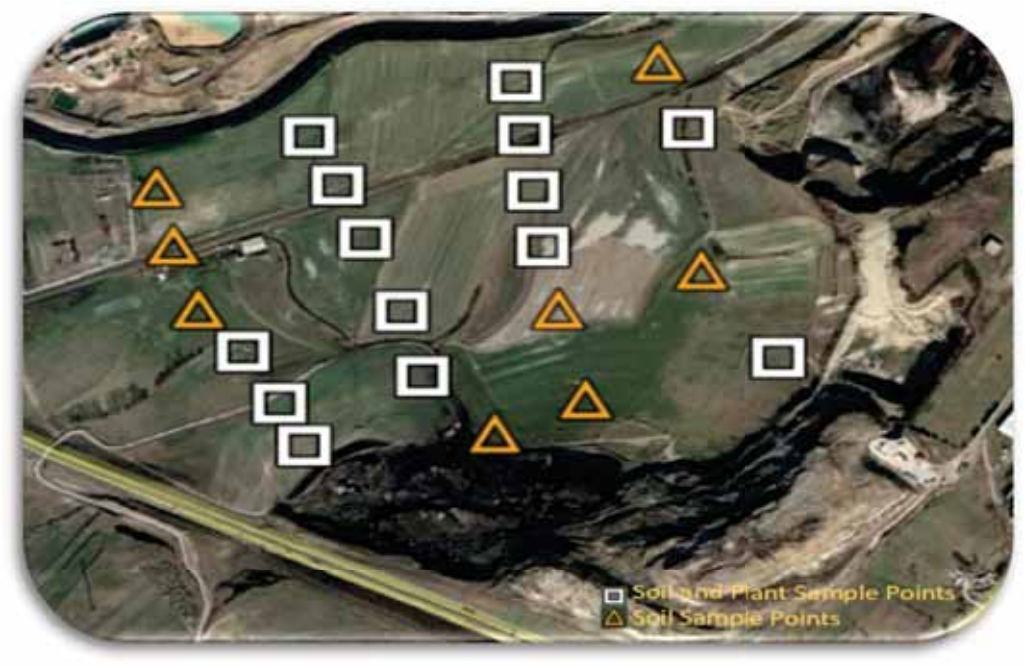

FIGURE 2
Soil and Plant Sampling Sites

semi-bucket soil auger [11]. Plant samples were also taken from the same locations at full-mature period of the plants in May [12]. Since plant production was not practiced in all soil sampling sites, plant samples were not taken these locations. While soil samples were taken from 22 different locations, plant samples were taken from 14 different locations. Soil and plant sampling sites are presented in Figure 2.

Soil samples were air-dried in laboratory, ground, sieved and made ready for analyses. Plant samples were separated into leaves and grains and air-dried under laboratory conditions. Plant samples were then dried in a drying cabin at 70 ºC until a constant weight, they were ground in a mill and made ready for analyses [12].

Analysis Methods. Soil reaction (pH) was measured in 1:2.5 soil:water suspension with a glass-electrode pH meter [13]; EC was measured again in 1:2.5 soil:water suspension with Wheatstone Bridge conductivity device [14]; grain size distribution (texture) was analyzed with the aid of Bouyoucos hydrometer method [15]; soil heavy metal analyses were performed with the aid of wet digestion method in nitric-perchloric acid mixture [12]. Plant total heavy metal analyses were performed through readings on microwave-digested samples in an ICP-OES device [12]. Limit values for soil heavy metals are provided in Table 1 [16]. Inverse Distance Weighting (IDW) method was used to estimate the values of intermediate locations and present spatial distribution of soil heavy metals in geographical information systems. The method primarily depends on greater weights of closer points and lesser weights of further points in estimation of unknown sampling points. Spatial distribution maps were generated with the aid of IDW method of ArcMap version 10.1 [17].

Research results were assessed through TARIST statistical software. Distance-dependent variations in soil heavy metal contents were determined with the aid of t-test. Correlation analyses

TABLE 1
Limit Values for Soil Heavy Metals [16]

Heavy Metals (Total)	Limit Value (6≤pH <7) (mg kg^{-1} dry matter soil)
Lead (Pb)	70
Cadmium (Cd)	1
Chrome (Cr)	60
Copper (Cu)	50
Nickel (Ni)	50
Zinc (Zn)	150

were performed to determine the relationships between heavy metal and clay contents and between EC and clay [18]. For distance-dependent analysis of soil heavy metals, research site was divided into 6 sections based on distance from the dump site (100 m, 200 m, 300 m, 400 m, 500 m, 600 m). Average of 3 points in each section was taken and used in statistical analyses (for instance, sampling sites 1, 12 and 13 for 100 m section; sampling sites 6, 7 and 18 for 600 m section).

RESULTS AND DISCUSSION

EC values of the soil samples varied between the lowest 25 µS cm^{-1} (30-60 cm of sampling site 22) and the greatest 690 µS cm^{-1} (60-90 cm of sampling site 9). In general, EC values varied between 50-200 µS cm^{-1} (with an average of 126,45 µS cm^{-1}). Since soil samples were taken in April, it can be stated that winter and spring precipitations significantly reduced soil salt contents. Similar soil EC values were also reported in a previous study conducted in Çorlu region [19]. Soil EC values exhibited differences in close sampling sites and even at different depths of the same sampling site. Such differences were mainly attributed to soil texture. Some sampling sites with high EC values (10, 11, 14, 15, 18) had high clay contents. Also, the sampling sites with the lowest EC values had high sand contents. Such a case revealed that salt in sites with high clay contents was relatively less leached. In sampling sites with high clay contents (sampling sites 10 and 11), there were significant positive correlations between the clay and EC (r^2: 0731) at 5% significance level.

Soil pH values varied between 4.20-7.28 with an average value of 5.87. Soil samples were slightly acidic based on these values. Soil pH values were <5 in 5 sampling sites (5, 6, 9, 15, 20) and >7 in 2 sampling sites (9, 14).

Soil grain size distribution analysis revealed that research site soils mostly had sandy-clay-loam (SCL) texture and partially had clay (C) and sandy-loam (SL) textures. Soil sand, silt and clay contents exhibited differences in close distances and different depths.

Soil cobalt (Co) contents varied between 3.10-16.70 ppm with the lowest value in sampling site 22 (60-90 cm) and the greatest value in sampling site 18 (60-90 cm). Soil Co contents generally varied with the soil textures. For instance, the sampling sites with the greatest Co contents (11, 14, 10, 15, 16, 18 (60-90 cm)) generally had high clay contents. There were significant positive correlations between Co and clay in sampling sites 11 and 14 (r^2: 0.731); in sampling sites 10 and 15 (r^2: 0.940) and in sampling site 18 (r^2: 0.858). The lowest Co contents were observed in SL and LS-like light-textured soils. There were significant positive correlations between the distances of sampling sites from the dumpsite and Co contents of the sampling sites 1 and 3 and sampling sites 1 and 4 at 1% significance level.

Soil lead (Pb) contents varied between 41.90 ppm (sampling site 22) and 277.10 ppm (sampling site 16). Soil Pb contents varied with the distances from dumpsite in some sampling sites. Such differences were found to be significant only between 100 m and 500 m sections. Distance-dependent differences were not found to be significant in the other sampling sites. Soil Pb contents were mostly related to soil clay contents. For instance, sampling sites with high Pb contents (sampling sites 11, 15, 16, 18) generally had high clay contents. There were significant positive correlations between Pb and clay contents in sampling sites 10 and 15 (r^2: 0.843) and in sampling site 18 (r^2: 0.932) at 1% significance level.

Soil nickel (Ni) contents varied between 9.50-89.30 ppm with the lowest value in sampling site 22 and the greatest value in sampling site 1. Soil Ni contents varied with the distance from the dumpsite. However, there were significant positive correlations between the distance from the dumpsite and Ni contents in 200 and 500 m sections and in 300 and 500 m sections. The correlations between distance from the dumpsite and Ni contents were not found to be significant in the other sections. The sampling sites with high Ni contents (sampling sites 3, 4 and 11 and especially the sampling sites 10, 15 and 18) had high clay contents. However, there were significant positive correlations between Ni and clay contents only of sampling site 18 at 1% significance level.

Soil chrome (Cr) contents varied between 11.70-58.50 ppm with the lowest value in sampling site 22 (0-30 cm) and the greatest value in sampling site 1 (0-30 cm). Despite the spatial differences, significant distance-dependent differences were observed only in Cr contents of 150 m and 250 m sections. There were significant positive correlations between clay and Cr contents of sampling site 18.

Soil cadmium (Cd) contents varied between 0.20-1.70 ppm with the lowest value in sampling site 22 (0-30 cm) as it was in the other metals and the greatest value in sampling site 16 (0-30 cm) as it was in Pb and Co. Soil Cd contents varied with the distance from the dumpsite. There were significant positive correlations between the distance from the dumpsite and Cd contents only in 150 and 250 m sections.

Soil iron (Fe) contents varied between 4028-27671 ppm with the lowest value in sampling site 22 and the greatest value in sampling site 16 (0-30 cm). The sampling sites 11 and 18 had the greatest Fe contents. While sampling site 11 was located at the closest position to dumpsite, sampling site 18 was located at the furthest position to dumpsite. These sites had high clay contents, thus had clay (C) soil texture. The sampling sites 21 and 22 had the lowest clay contents. These sites were the closest sites to dumpsite, but they still had low Fe contents. Soil tex-

ture of these sites were LS and SL. There were significant correlations between the distance from the dumpsite and Fe contents only in 150 and 250 m sections. There were significant positive correlations between the clay and Fe contents of the sampling sites 12, 11, 15 and 18.

Soil manganese (Mn) contents varied between 205.40-802.90 ppm with the lowest value in sampling site 7 (0-30 cm) and the greatest value in sampling site 15 (30-60 cm). Mn contents varied with the sampling sites and depths. The distance from the dumpsite had remarkable effects on such differences. There were significant positive correlations between the distance from the dumpsite and Mn contents in 100 and 500 m sections, in 200 and 400 m sections and in 400 and 600 m sections. Clay contents had direct impacts on soil Mn contents. For instance, the sampling site 15 with a high clay content had the greatest Mn content and the sampling sites 1, 2, 21 and 22 with low clay contents had the lowest Mn contents. There were significant positive correlations between the clay and Mn contents of the sampling site 15 (r^2: 0,895).

The greatest soil zinc (Zn) content (112.70 ppm) was observed in sampling site 1 and the lowest Zn content (21.40 ppm) was observed in sampling site 21. Sampling distances did not have significant effects on soil Zn contents. There were significant correlations between Zn and clay contents in sampling sites 3, 10, 15 (r^2: 0,787) and in sampling site 18 (r^2: 0,866). The sampling sites 11, 15 and 18 with high clay contents had relatively high Zn contents and the sampling sites 1, 2, 7, 21, 22 with low clay contents had relatively low Zn contents.

The greatest soil copper (Cu) content was observed in sampling site 18 (60-90 cm) and the lowest Cu content (2.90 ppm) was observed in sampling site 22. As it was in Zn, variations of soil Cu contents with the distances from the dumpsite were not found to be significant. As it was in the other metals, soil Cu contents mostly varied with the soil texture. The sampling sites 11, 15 and 18 with the greatest Cu contents had high clay contents. The sampling sites 2, 7, 13, 21 and 22 with low Cu contents also had remarkably low clay contents. There were significant positive correlations between the Cu and clay contents in sampling site 11 (r^2: 0,727), 15 (r^2: 0,915) and 18 (r^2: 0,916).

According to plant heavy metal analyses, the greatest leaf Cr content (27.80 ppm) was observed in sampling site 7, the greatest Pb (2.90 ppm) and Ni (2.30 ppm) contents were observed in sampling site 9 and the greatest Co content (2.019 ppm) was observed in sampling site 11. The lowest leaf Cr content (3.0 ppm) was observed in sampling site 8, the lowest Pb content (0.5 ppm) was observed in sampling site 4, the lowest Ni content (0.4 ppm) was observed in sampling site 11 and the lowest Co content (0.29 ppm) was observed in sampling site 9. For heavy metal contents of the grains, the greatest grain Cr content (17.6 ppm) was observed in sampling site 5, the greatest Pb content (1.8 ppm) was observed in sampling site 8, the greatest Ni content (7.9 ppm) was observed in sampling site 3 and the greatest Co content (1.71 ppm) was observed in sampling site 5.

Leaf heavy metal contents (Cr, Pb, Ni, Co) were parallel to soil heavy metal contents in some sampling sites, but in general, there were not distinctive similarities. For instance, while the sampling sites 11 and 15 with the greatest soil heavy metal contents had relatively high plant heavy metal contents (plant sampling sites 7 and 10) and plant sampling site 10 had relatively lower heavy metal contents. While there were similarities in soil and plant micro element (Zn, Fe, Mn and Cu) contents in some sampling sites, similarities were not observed in several other sampling sites. For instance, plant sampling site 6 generally had high micro element contents, but the same soil sampling site (sampling site 10) had relatively low micro element contents. On the other hand, the soil sampling sites 1, 11 and 18 with relatively high micro element contents also had high plant micro element contents in plant sampling sites 1, 8 and 12.

Inverse Distance Weighting (IDW) method was used to estimate soil and plant heavy metal contents of non-sampled points and resultant maps are comparatively illustrated in Figure 3 and 4.

CONCLUSION

Present findings on soil heavy metals revealed that heavy metals generally concentrated within the upper zone (0-30 cm) of sampling sites 1 and 16, within 30-60 cm soil profile of the sampling site 3 and within the entire horizons of the sampling sites 11 and 15. The sampling sites 1 (0-30 cm), 11 and 15 with high soil heavy metal contents also had high EC values within the entire horizons. Such a case proved the existence of an accumulation in these sites. Results of t-test, conducted to put forth the relations of soil heavy metal contents with the distance from the dumpsite, were not able to put forth any significant relationships. There were significant differences between some sampling sites, but such differences were mainly attributed to high clay contents of those sites rather than the distance from the dumpsite. There were significant positive correlations between heavy metal and clay contents of some sampling sites. The sampling sites with high clay contents generally had high heavy metal

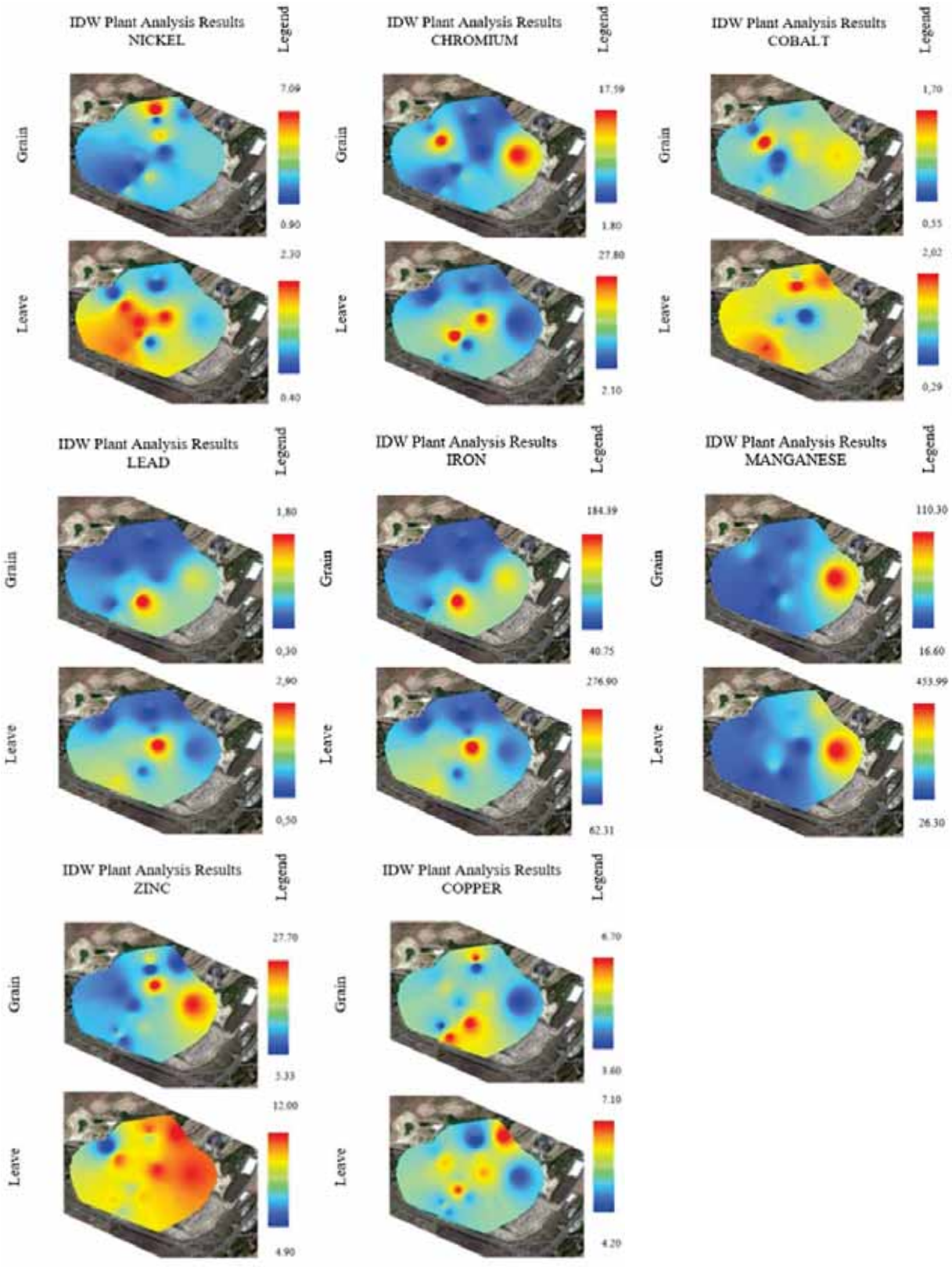

FIGURE 3
Heavy Metal Contents of Research Plants

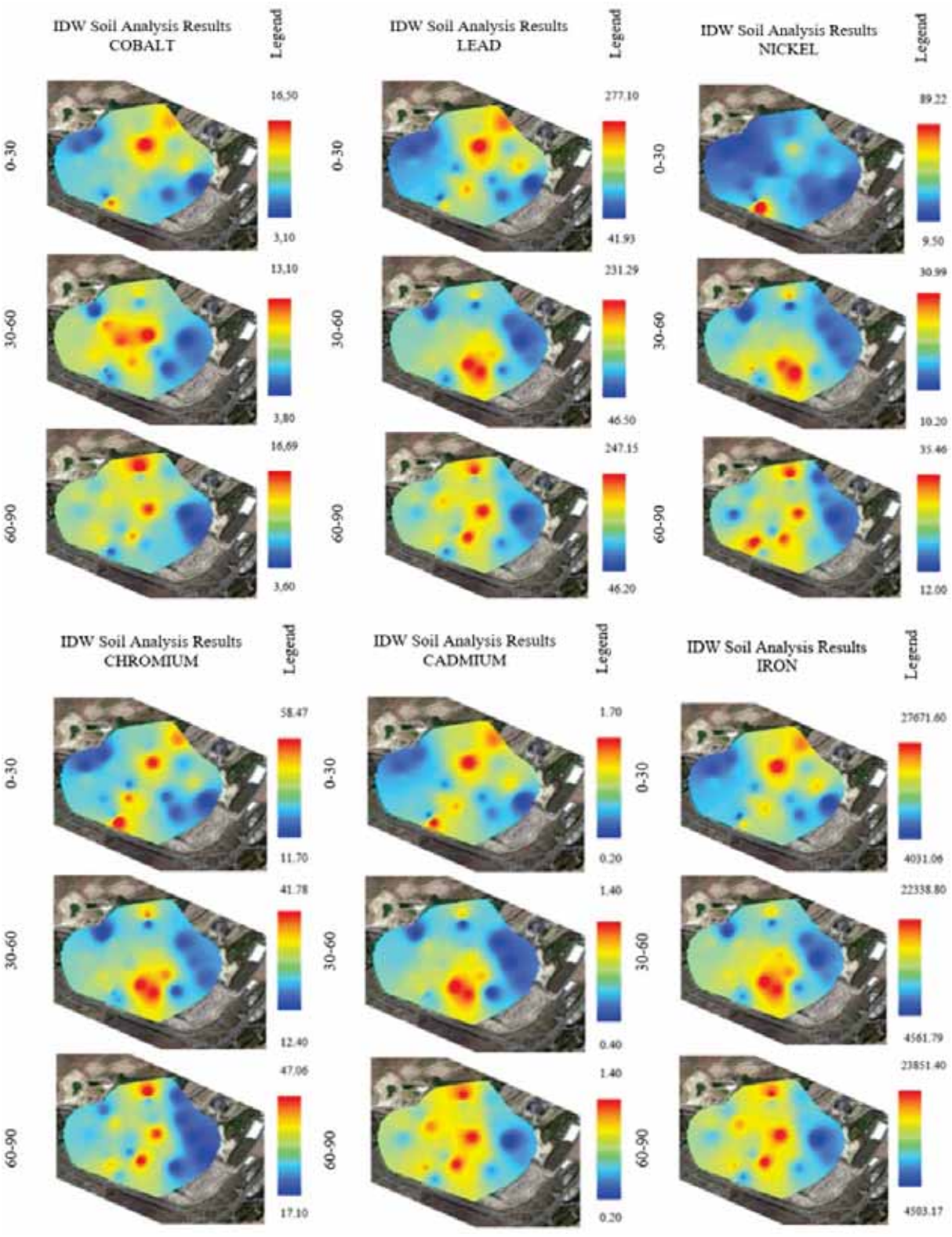

FIGURE 4
Heavy Metal Contents of Research Area

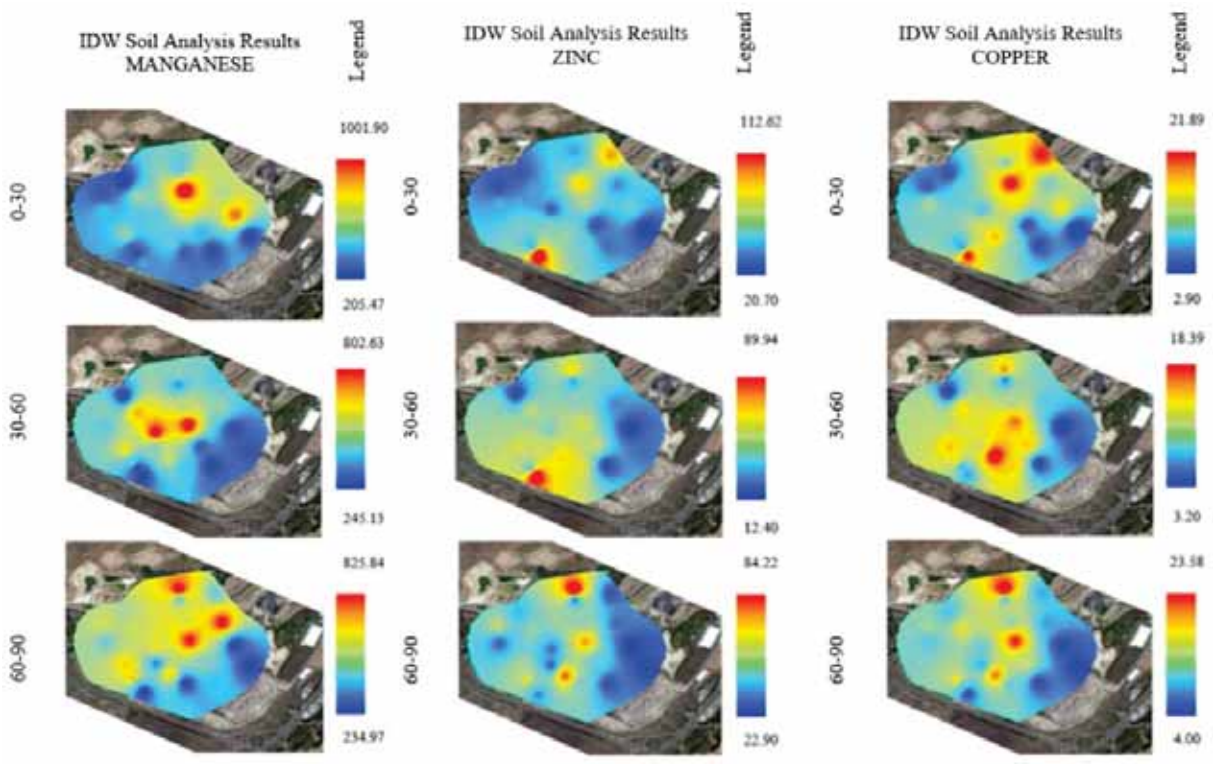

FIGURE 4
Heavy Metal Contents of Research Area (Continued)

contents. For instance, the sampling sites 11, 14 and 15 with high heavy metal contents had clay (C) soil texture and the sampling sites 6, 7, 13, 21 and 22 with a light soil textures (SL and LS) generally had low heavy metal contents. Such a case indicated active role of clay in heavy metal accumulation. The present research site has a sloppy terrain. The elevation difference between the dumpsite and the furthest sampling point is 80 m. The dump site had the highest altitude (450 m) within the sampling sites. The initial slope is 20%, slope decreases towards the mid-sections and vary between 3-5% at the end of the sampling area. Therefore, both the quantity of water leached through soil profile and the motion and concentration of heavy metals varied from site to site. Çorlu stream located at the furthest position to dumpsite at the end of slope served as a drainage canal for the sampling sites and it was through that heavy metals leached through soil profile by precipitations drained into Çorlu stream. However, some soil heavy metals still exceeded the limits specified by Turkish Standards (Table 1). Cd contents of sampling sites 1, 3, 8, 10, 11, 12, 14 15, 18 and 19; Ni contents of sampling site 1 and Pb contents of sampling sites 2, 6, 7, 21 and 22 at different depths exceeded the limit values. Cr, Zn and Cu contents did not exceed the limit values in any sites.

ACKNOWLEDGEMENTS

This study was supported by Tekirdağ Namık Kemal University with NKUBAP.03.GA.17.097 project number.

REFERENCES

[1] TUIK (Turkish Statistical Institute) (2017) Municipal Solid Waste Statistics. http://www.tuik.gov.tr/HbPrint.do?id=24876. Access: 30.03.2019 (In Turkish).

[2] Özel, S. (2018) Studying of Environmental Effects of a Disposal Area Leachates with Geophysical and the Water Analyses Methods. Çukurova University Journal of the Faculty of Engineering and Architecture. 33(2), 113-124.

[3] Öztürk, İ., Onay, T.T., Çallı, B., Mertoğlu, B., Yıldız, Ş. (2010) Leachate Management Specialization Commission Draft Working Report. Ministry of Environment and Urbanization, General Directorate of Environmental Management. https://webdosya.csb.gov.tr/db/cygm/editordosya/sizintisuyuyontaslak.pdf. Access: 12.09.2019 (In Turkish).

[4] Abacı, Ş. (1997) Evaluation of Solid Waste Storage Areas as Hydrogeological. https://mmo.org.tr/sites/default/files/eac43aceba42c87_ek.pdf Access: 05.09.2019 (In Turkish).

[5] Anonymous (2016) Status of Solid Waste Disposal Facilities and Operation Unions. Ministry of Environment and Urbanization, Tekirdağ Directorate of Environment and Urbanization, Research Report. https://tekirdag.tarimorman.gov.tr/Sayfalar/EN/AnaSayfa.aspx. Access: 05.09.2019 (In Turkish).
[6] Erdogan, O., Bagdatli, M.C., Zeybek, A. (2016) Spatial Analysis with GIS Mapping of Fungicide Consumption in Agricultural Areas. Fresen. Environ. Bull. 25, 2676-2681.
[7] Gokdogan, O., Bagdatli, M.C., Erdogan, O. (2018) The Determination with Geographic Information Systems (GIS) Mapping of The Energy Use Efficiency of Potato Production Areas in Turkey: A Study in Nevsehir Province. Fresen. Environ. Bull. 27, 8917-8927.
[8] Gulcin, D. (2019) The Influence of Urban Growth on Surroundıng Mediterranean Landscapes with Particular Reference to Degradation of Olive Orchards. Fresen. Environ. Bull. 28, 3854-3864.
[9] Anonymous (2015) Çorlu Strategic Plan (2015-2019). https://www.corlu.bel.tr/yayin/4/0/1/stratejik-plan-20152019. Accessed 15. 03. 2019 (In Turkish).
[10] Anonymous (2014) Agricultural Report, 2014. Tekirdağ Directorate of Provincial Agriculture and Forestry. https://tekirdag.tarimorman.gov.tr/Sayfalar/EN/AnaSayfa.aspx. Accessed 03. 04. 2019 (In Turkish).
[11] Anonymous (1993) Soil Survey Laboratory Methods and Procedures for Collecting Soil Samples. Soil Survey Investigation Report No:1 USDA. Washington DC., USA.
[12] Kacar, B., İnal, A. (2008) Plant Analyses. Nobel press, Ankara-Turkey (In Turkish)
[13] Jackson, M.L. (1958). Soil Chemical Analysis. Prentice Hall, London
[14] Richards, L.A. (1954) Diagnosis and Improvement of Saline and Alkali Soils. USDA Agric. Handbook 60. Washington, D. C.
[15] Gee, G.W., Bauder. J.W. (1986) Particle-Size Analysis. In: Klute, A. (Ed.) Methods of soil analysis. ASA and SSSA, Madison. 383-411
[15] Anonymous (2019) ArcGIS Geostatistical Analyst. http://downloads2.esri.com/support/documentation/ao_/Using_ArcGIS_Geostatistical_Analyst.pdf
[16] Anonymous (2010) The Regulation for Use of Household and Urban Sewage Sludge in Soils. Official Gazette of Turkish Repuclic. Date: 03.08.2010, No: 27661. http://www.resmi gazete. gov.tr. Accessed April 2019 (In Turkish).
[17] Düzgüneş, O., Kesici, T., Kavuncu, O., Gürbüz, F. (1987) Research and Experiment Methods (Statistical Methods II). AU Faculty of Agriculture Publications: 1021. (In Turkish).
[18] Sarı, H. (2017) The Effect of Some Soil Characteristics on the Hydraulic Conductivity of Soil in Tekirdağ Province. Alınteri Journal of Agriculture Sciences. 32(2), 95-103.

Received: **13.05.2019**
Accepted: **07.03.2020**

CORRESPONDING AUTHOR

Huseyin Sarı
Department of Soil Science and Plant Nutrition
Faculty of Agriculture
Namik Kemal University
Tekirdag – Turkey

e-mail: hsari@nku.edu.tr

© by PSP Volume 29 – No. 05/2020 pages 3482-3490 Fresenius Environmental Bulletin

A QUANTITATIVE METHOD FOR RISK ANALYSIS OF WATER RIGHTS TRANSACTION BASED ON HWHI PREDICTION

Jiarui Ren[1], Deshan Tang[2], Guangxiong Mao[1,*], Chuanming Liu[1], Fei Zhang[1], Hongbo Zhang[1], Lin Chen[1], Xuan Fei[1], Ming Li[1]

[1]School of Urban and Environmental Sciences, Huaiyin Normal University, Huai'an,223300 , China
[2]College of Water Conservancy and Hydropower Engineering, Hohai University, Nanjing, 210098, China

ABSTRACT

With the unbalanced development of social economies, regional water shortage is becoming more and more serious. Some countries alleviate this water shortage to a certain extent by implementing water rights trading. However, the sustainable development of the transfer of water rights can easily be affected by carrying out excessive water rights transaction in arid areas. Because of the uncertainty of natural water inflow and the regional comprehensive development level, there are certain risks in water rights trading. In this paper, a human water harmony index (HWHI) is introduced into the quantitative analysis of water rights transaction risk, which can effectively predict the possible risk degree of a water rights transaction, contributing to the healthy development of the water rights transaction market and restoration of ecological environment. In this study, we applied the quantitative model for risk analysis of water rights transaction to the northwest arid region of China. The calculation results show that the overall risk of water rights trading is below 0.16, and that the overall water rights trading belongs to a lower risk level, which shows that the water rights trading market has great potential for development.

KEYWORDS:
HWHI,water rights,transaction,risk analysis

INTRODUCTION

China is a country with a serious water shortage. Although the total amount of freshwater resources is approximately 280 billion cubic meters, the per capita water resources in China are 2300 cubic meters, which is only one-fourth of the world average level. It is one of the countries with the poorest per capita water resources in the world. The arid and semi-arid areas account for 47% of the land area, and the lives of about 400 million people are closely related to this area. With the impact of human activities and the gradual deterioration of the environment, land desertification occurs frequently in arid and semi-arid areas. Water rights trading in arid areas presents as a means to improve the efficiency of water use. In order to ensure the healthy development of water rights trading market, however, it is necessary to carry out risk analysis of water rights trading.

Many scholars have carried out extensive research on the water resources allocation and water rights. At the present time, many mathematical allocation models of water rights and influence factors have been established [1–5]. A multi-agent and multi-objective optimal allocation model was introduced to direct the distribution of water resources in the Shiyang River Basin [6]. Water right transaction is gradually transferred from bilateral transaction to multi-objective transaction[7]. Water resource rights holders are faced with the uncertainty of rights distribution value, and take agricultural economy as an example[8]. The risk analysis method is used to study water safety[9-12]. The research shows that by reducing the transaction cost of water rights, the trade income can be improved[13]. The influencing factors of water right price were studied [14]. The evaluation of water rights trading activities by using network analysis method is being researched [15].At the same time, the study of human-water harmony has been one of the major areas of focus in water resource management research. Human–water relationships have been quantitatively researched[16-18]. With the development of water rights trading, transaction costs, modes, and scales from agricultural to industrial water rights trading were studied [19], the sustainable development of water rights trading is being researched [20], and studies of risk analysis in water rights trading and water resources management have been performed [21–25]. The above methods only solve the problem of the optimal allocation of water resources and qualitative risk analysis; they neglect the quantitative and sustainable development of water rights transaction risk analysis.

Risk analysis and the human water harmony index (HWHI) are current research hotspots. Many scholars have gained important insights into water rights allocation and risk analysis. However, there

are few studies on the quantification of water rights transaction risk and its practical application at present, especially the application of the HWHI to the water rights transaction risk. This paper realizes the risk prediction of a water rights transaction based on the predicted HWHI. To this end, Firstly, we explain the calculation method of the HWHI; secondly, we establish the risk analysis model of water rights transaction based on the HWHI; finally, we validate the risk analysis model of water rights transaction with an example.

MATERIALS AND METHODS

Study Area. The Tarim River Basin is located in the northwest arid region of China, with a total area of 1.02 million km^2 and a total length of 1321 km. At present, only the Akesu River, Yarkant River and Hotan River are connected with the main stream of the Tarim River. The Kaidu–Kongque river pumps water from Bosten Lake to the irrigation area in the lower reaches of Tarim River through a water pumping station, thus forming a pattern of "four sources and one main stream". The Tarim River Basin location map is shown in Figure 1.

Formula Expression of Water Rights Transaction Risk. In order to measure the degree of risk, combined with the actual water rights trading in arid areas, this paper adopts the concept of risk degree as follows: The ratio of mathematical expectations of square error between actual loss and predicted loss to the mathematical expectation of predicted loss under specific objective conditions and in a given time. Risk degree is a dimensionless quantity.

The risk degree of a water rights transaction is defined as the ratio of mathematical expectations of A to B, where A is the mean square error between the predicted water shortage in water rights transaction and the water shortage in water rights transaction settled at the end of the year. B is the prediction of water shortage in water rights trading during the year.

The risk degree of water rights transaction is computed as shown in Equation (1).

$$\delta = \frac{\sqrt{\sum_{m=1}^{12}(WY(t)^y - WS(t)^y)^2 / 12}}{\sum_{m=1}^{12} WY(t)^y / 12} \quad (1)$$

where δ is the risk degree of water rights transaction in the y year. $WY(t)^y$ is the water shortage in the water rights transaction in the t month of the y year based on the HWHI prediction. $WS(t)^y$ is the water shortage in the water rights transaction in the t month of the y year.

The Calculation Process of Water Rights Transaction Risk. According to Equation (1), the predictive accuracy of water shortage in water rights trading during the year directly affects the risk degree of water rights trading. Therefore, it is a prerequisite to establish a risk analysis model for water rights trading by establishing a method to calculate the predicted water shortage during the year.

There are many predicting methods at present. By comparing and selecting the advantages and disadvantages of each predicting method, a Grey–Markov model GM–M(1,1) is formed, which utilizes the advantages of the Grey model GM(1,1) [26] and the Markov model [27], respectively. The model is applied to the HWHI value prediction to improve the accuracy of prediction results.

Therefore, the key points in establishing the risk analysis model of water rights trading are to establish the predicting model of the HWHI value based on the GM–M(1,1) and to study the relationship between the HWHI value and water rights tradable quantity. The risk analysis model map for water rights trading based on the HWHI can be seen in Figure 2.

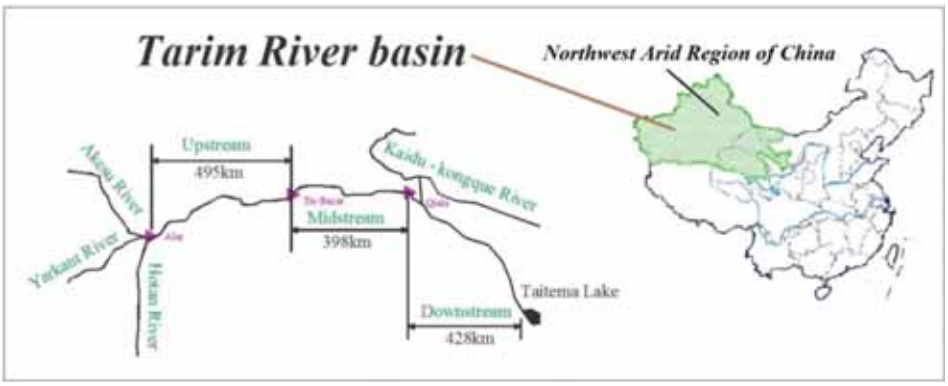

FIGURE 1
***Tarim River basin* location map.**

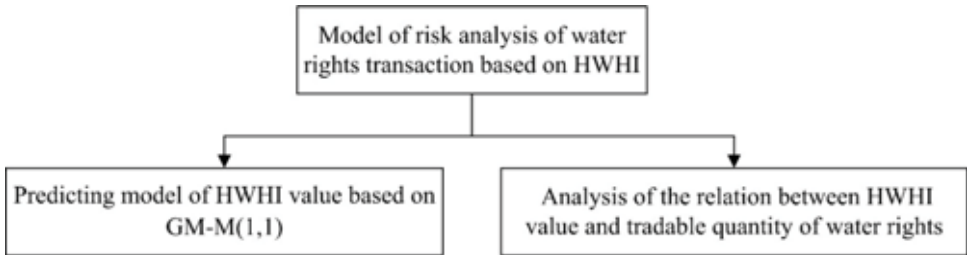

FIGURE 2
Model map of risk analysis of water rights transaction based on the human water harmony index (HWHI).

Predicting Model of HWHI Value Based on GM–M(1,1). (1)The Mathematical Expression of HWHI.HWHI is a function of health, development, harmony and ecology [18]. HWHI is computed as shown in Equation (2).

$$HWHI_{(T)} = f(H_{1(T)}, D_{(T)}, H_{2(T)}, E_{(T)}) = H_{1(T)} \bullet \beta_1 + D_{(T)} \bullet \beta_2 + H_{2(T)} \bullet \beta_3 + E_{(T)} \bullet \beta_4 \quad (2)$$

The constraint conditions are:

$$0 < HWHI_{(T)} < 1 \quad , \quad 0 < H_{1(T)} < 1 \quad , \quad 0 < D_{(T)} < 1 \quad ,$$

$$0 < H_{2(T)} < 1, 0 < E_{(T)} < 1,$$

where T is the time, e.g., year; $HWHI_{(T)}$ is the human water harmony index value at T, $H_{1(T)}$ is the health index value at T, $D_{(T)}$ is the development index value at T, $H_{2(T)}$ is the harmony index value at T, and $E_{(T)}$ is the ecology index value at T. β_1 is the weight value of the health index, β_2 is the weight value of the development index, β_3 is the weight value of the harmony index, and β_4 is the weight value of the ecology index.

(2)HWHI Value Prediction Based on GM–M(1,1).

①GM(1,1) model formula.

Suppose the original HWHI data are as follows:

$$X^{(0)} = [X^{(0)}(1), X^{(0)}(2), \cdots, X^{(0)}(n)]$$

where $X^{(0)}(n)$ represents the actual value for the n year. GM(1,1) model is established based on the above data.

The above data are accumulated once to form the following data.

$$X^{(1)}(k) = \sum_{i=1}^{k} X^{(0)}(i) \qquad (k = 1, 2, \cdots, n)$$

The data series is as follows:

$$X^{(1)} = [X^{(1)}(1), X^{(1)}(2), \cdots, X^{(1)}(n)]$$

$Z^{(1)}$ is the nearest mean series of $X^{(1)}$.

$$Z^{(1)} = [Z^{(1)}(1), Z^{(1)}(2), \cdots, Z^{(1)}(n)]$$

$$Z^{(1)}(k) = \frac{1}{2}[X^{(1)}(k) + X^{(1)}(k-1)]$$

The differential equation of model GM(1,1) is as follows:

$$X^{(0)}(\mathrm{k}) = b - aZ^{(1)}(k), \quad (3)$$

where a is the coefficient of development, b is ash action.

The solutions of the above discrete equations are as follows:

$$\hat{X}^{(1)}(\mathrm{t}+1) = [X^{(0)}(1) - \frac{b}{a}]\mathrm{e}^{(-at)} + \frac{b}{a}$$

$$(t = 0, 1, 2, \cdots, n-1) \quad (4)$$

The grey prediction model of the original data series is obtained by restoring the data.

$$\hat{X}^{(0)}(i) = \hat{X}^{(1)}(i) - \hat{X}^{(1)}(i-1) \qquad (i = 1, 2, \cdots, n) \quad (5)$$

②The GM(1,1) model accuracy test.

$$E = [\mathrm{e}(1), \mathrm{e}(2), \cdots, \mathrm{e}(\mathrm{i})] = \mathrm{X}^{(0)} - \hat{X}^{(0)}$$

$$e(i) = x^{(0)}(i) - \hat{x}^{(0)}(i)$$

$$S_1^2 = \frac{1}{n}\sum_{i=1}^{n}[x^{(0)}(i) - \overline{x}]^2 , \quad (6)$$

$$S_2^2 = \frac{1}{n}\sum_{i=1}^{n}[e(i) - \overline{e}]^2 \quad (7)$$

$$\overline{x} = \frac{1}{n}\sum_{i=1}^{n} x^{(0)}(i) \ \overline{e} = \frac{1}{n}\sum_{i=1}^{n} e(i).$$

Using posterior difference C and small error probability p to judge the accuracy level of prediction,

$$C = \frac{S_2}{S_1} \quad (8)$$

where S_1^2 is the residual variance of the predicted value (Equation (6)) and S_2^2 is the residual variance of the actual value (Equation (7)).

The formula for calculating the probability of small error is as follows:

$$p = P\left\{\left|e(i) - \overline{e}\right| < 0.6745S_1\right\} \quad (9)$$

The reference table for the accuracy inspection level can be seen in Table 1.

TABLE 1
Inspection grade standard.

Serial Number	*C*	*p*	Level
1	$C \le 0.35$	$0.95 \le p$	I (excellent)
2	$0.35 < C \le 0.50$	$0.80 \le C < 0.95$	II (good)
3	$0.50 < C \le 0.65$	$0.70 \le C < 0.80$	III (qualified)
4	$0.65 < C$	$p < 0.70$	IV (Unqualified)

Note: *C* is the posterior difference. *p* is the small error probability.

The accuracy level of the model is Max {*C* level, *P* level}.

③The mathematical model of GM–M(1,1)

Set $E_1, E_2, \cdots, E_n$ to N states with HWHI values, where E_i is the current state and E_j is the next state adjacent.

The Markov chain representation is as follows:

$$P\left\{Y_{n+1} = E_j \middle| Y_n = E_i, Y_{n-1} = E_{i-1}, \cdots, Y_1 = E_1, Y_0 = E_0\right\} = P_{ij}$$

P_{ij} is expressed as a state transition probability (E_i transferred to E_j).

$$P_{\mathrm{ij}} = \frac{M_{\mathrm{ij}}}{M_{\mathrm{i}}} \tag{10}$$

where M_{ij} is the number of state transitions, and M_{i} represents the total number of times in state E_{i}.

Analysis of the Relation between HWHI Value and Tradable Quantity of Water Rights.

(1)The Concept and Characteristics of Tradable Quantity of Water Rights.

①The concept of tradable quantity of water rights.

The tradable quantity of water rights is the difference between the allocation of a water right and the amount of water used to satisfy one's life, production and ecology. The indication of the water rights tradable quantity is shown in Figure 3.

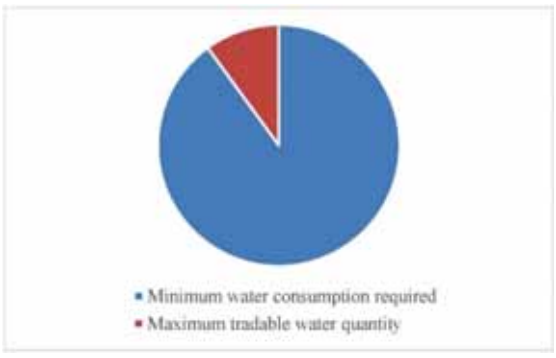

FIGURE 3
Tradable quantity map of water rights.

②Characteristics of tradable quantity of water rights

Tradable water rights are obtained through legal channels, and water rights allocation plans of relevant departments should be adopted. There should be a perfect trading place in the region where water users can trade surplus water rights. Water users must retain the amount of water rights suitable for local development. The range of the water rights tradable quantity is [0, maximum water rights tradable quantity].

(2)Research on Regression Equation between HWHI Value and Tradable Quantity of Water Rights Based on Excel. According to research on the relationship between the HWHI and the tradable quantity of water rights, there are many factors affecting the relationship. The premise of this study is that the revenue from the transfer of water rights can also be used for water saving in science and technology. The impact of the revenue and the transfer of water rights on the value of the HWHI is basically the same.

Because the tradable quantity of water rights is different in different regions, the concept of a tradable water rights proportion is introduced in order to more intuitively reflect the relationship between the HWHI value and the tradable quantity of water rights.

The proportion of tradable water rights is the ratio of the tradable water rights to the maximum tradable water rights.

$$H^{(0)} = [H^{(0)}(1), H^{(0)}(2), \cdots, H^{(0)}(n)]$$

$$S^{(0)} = [S^{(0)}(1), S^{(0)}(2), \cdots, S^{(0)}(n)]$$

where $H^{(0)}(n)$ represents the HWHI value for the *n* year, and $S^{(0)}(n)$ represents the proportion of tradable water rights for the *n* year.

Excel software is used to fit a polynomial equi regression curve of $H^{(0)}(n)$ and $S^{(0)}(n)$ data, and a calibration R^2 method is used to optimize the selection. The polynomial regression curve formula is as follows:

$$Y = a_{(1)}X^{(n)} + a_{(2)}X^{(n-1)} + \cdots + a_{(n)}X^{(1)} + a_{(n+1)} \qquad (n = 1, 2, 3, 4) \tag{11}$$

The range of R^2 is [0, 1]. When R^2 is close to 1, the better the linear correlation between the two variables, and the better the fitting of the formula.

When R^2 is close to 0, the worse the linear correlation between the two variables and the worse the fitting of the formula.

The relationship between the HWHI value and the tradable water rights can be deduced by the relationship curve between the HWHI value and the proportion of tradable water rights.

Risk Level Criteria for Water Rights Transaction. According to the different risk degree value and the actual situation in arid area, the risk level of water right transaction is divided. The risk levels of water rights transaction are based on different risk values are shown in Table 2.

As shown in Table 2, when the value of risk degree is within the range of (0, 0.25], water right transaction is considered to be in the lower risk level, which indicates that the water right transaction has great potential for development; when the value of the risk degree is within the range of (0.25, 0.50], the risk of water right transaction is in the low risk level, and the amount of the water right transaction can be increased appropriately according to the actual situation; when the value of risk degree is within the range of (0.50, 0.75], the risk of water right transaction is in the high level, and the quantity of water rights transaction should be reduced appropriately; when the risk degree value is greater than 0.75, the water right transaction belongs to the higher risk level. At this time, the risk of implementing a water rights transaction is higher, and the risk aversion measures should be considered in advance to reduce the possible losses.

RESULTS

Risk Calculation of Water Rights Transaction Based on HWHI. (1)Prediction of the HWHI Value Based on GM–M(1,1). According to HWHI and GM–M(1,1) model, the predicted values of HWHI in the Tarim River Basin from 2004 to 2017 are calculated in Table 3.

(2)Analysis of the Relationship between HWHI Value and the Proportion of Transactable Water Rights.

By studying the relationship between the HWHI value and the proportion of transactable water rights in the Tarim River Basin, investigating the basin institutions and local governments, and combining it with the actual situation of the Tarim River Basin, the relationship between the HWHI value and the proportion of transactable water rights is preliminarily given. After fitting with Excel regression curves in different forms, it is showed that the polynomial curve fits well. Figure 4 shows the relation curve between the HWHI value and the proportion of transactable water rights.

The correlation formulas between the HWHI value and the proportion of transactable water rights are shown in Equation (12).

$$Y=\begin{cases}0 & (0\le X<0.5)\\ 41.667X^4\text{-}141.67X^3\text{+}174.58X^2\text{-}90.083X\text{+}16.5 & (0.5\le X<1.0)\end{cases} \quad (12)$$

TABLE 2
Classifications of water rights transaction based on risk degree values.

Serial Number	Risk Degree Value	Risk Level
1	$0<\delta\le 0.25$	Lower risk
2	$0.25<\delta\le 0.50$	Low risk
3	$0.50<\delta\le 0.75$	High risk
4	$0.75<\delta<1.00$	Higher risk

TABLE 3
The predicted values of HWHI in Tarim river basin (2004–2017).

Year	HWHI(a)	HWHI(p)	Residual Value	Relative Error (%)
2004	0.5827	0.5631	0.0196	3.36
2005	0.5833	0.5826	0.0007	0.12
2006	0.5973	0.5935	0.0038	0.64
2007	0.5986	0.6121	−0.0135	−2.26
2008	0.6027	0.6158	−0.0131	−2.17
2009	0.6032	0.5899	0.0133	2.20
2010	0.6172	0.6041	0.0131	2.12
2011	0.64	0.6332	0.0068	1.06
2012	0.6503	0.6449	0.0054	0.83
2013	0.6603	0.6626	−0.0023	−0.35
2014	0.6612	0.6598	0.0014	0.21
2015	0.6656	0.6586	0.007	1.05
2016	0.6673	0.6659	0.0014	0.21
2017	0.6685	0.6665	0.002	0.30

Note: HWHI(a) is HWHI actual value. HWHI(p) is HWH predicted value.

According to Equation (1), the calculation process of the water rights transaction risk degree from 2004 to 2017 is as follows:①According to the correlation formula between the HWHI value and the proportion of transactable water rights, the actual proportion of tradable water rights and the predicted proportion of tradable water rights are calculated respectively.② The actual demand for water rights ranges from 0% to 100% (0 to 1.0). After investigation, the risk degree was calculated as 40% (0.4).

The risk degrees of the Tarim River Basin from 2004 to 2017 are calculated in Table 4. Figure 5 shows the water rights transaction risk degree based on the HWHI prediction.

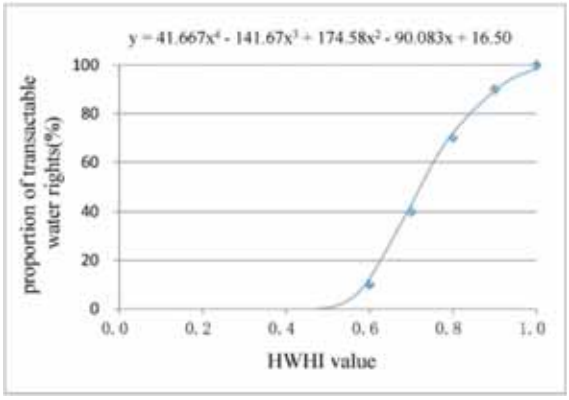

FIGURE 4
Relation curve between the HWHI value and the proportion of transactable water rights.

TABLE 4
Degrees of Tarim River Basin from 2004 to 2017.

Year	H(a)	H(p)	P(a)	P(p)	P(d)	δ
2004	0.5827	0.5631	0.0597	0.0246	0.4	0.1
2005	0.5833	0.5826	0.0609	0.0595	0.4	0.01
2006	0.5973	0.5935	0.0919	0.0831	0.4	0.03
2007	0.5986	0.6121	0.0950	0.1288	0.4	0.12
2008	0.6027	0.6158	0.1049	0.1386	0.4	0.13
2009	0.6032	0.5899	0.1061	0.0750	0.4	0.1
2010	0.6172	0.6041	0.1424	0.1084	0.4	0.12
2011	0.64	0.6332	0.2075	0.1874	0.4	0.09
2012	0.6503	0.6449	0.2387	0.2222	0.4	0.09
2013	0.6603	0.6626	0.2699	0.2771	0.4	0.06
2014	0.6612	0.6598	0.2727	0.2683	0.4	0.03
2015	0.6656	0.6586	0.2866	0.2645	0.4	0.16
2016	0.6673	0.6659	0.2921	0.2876	0.4	0.04
2017	0.6685	0.6665	0.2958	0.2895	0.4	0.06

Note: HWHI(a) is HWHI actual value. HWHI(p) is the HWHI predicted value. P(a) is the proportion of actual water rights transaction quantity. P(p) is the proportion of predicted water rights transaction quantity. P(d) is the proportion of actual water right demand. δ is the water rights transaction risk degree.

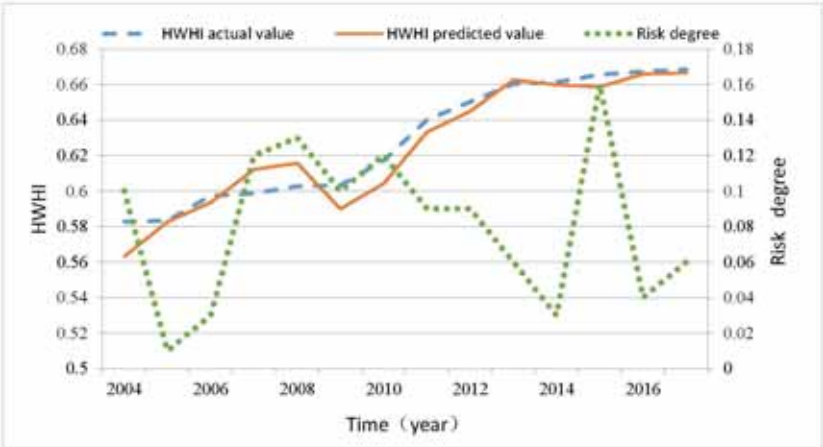

FIGURE 5
Risk degree of water rights transaction based on the HWHI prediction.

DISCUSSION AND CONCLUSIONS

Accuracy Analysis of HWHI Prediction Model. According to Equations (5)–(8), S_1^2 and S_2^2 are calculated, C = 0.33, and p = 1.00. According to the Table 1, the model accuracy level is I (excellent). R^2 = 1, which shows that HWHI and the proportion of transactable water rights have a good linear correlation.

Trend Analysis of Water Rights Transaction Risk. According to Table 4 and Figure 5, the risk values of water rights trading are below 0.16 between 2004 and 2017. According to Table 2, water rights trading generally belongs to a lower risk level.

Quantitative Scientificality of Water Rights Transaction Risk. As the HWHI system contains natural factors such as river inflow, HWHI also reflects the comprehensive development level of the region. Therefore, carrying out a risk analysis of water rights trading based on the HWHI can effectively predict the possible risk level of water rights trading, thus contributing to the healthy development of the water rights trading market.

The GM(1,1) model is mainly based on Grey theory, which processes the original data in an orderly way and generates a series with certain regularity. It is mainly applicable to the prediction problems with less data and shorter time. As a long-term prediction, the prediction accuracy of the results is low due to the poor fitting of the series. In order to remedy this defect, the Markov method is introduced into the GM(1,1) model prediction, which solves the prediction problem of long-term data random fluctuations. The above two models are optimized to form a Grey–Markov model GM–M(1,1).

Through scientific HWHI predictions, water rights transaction risks are quantified. This not only helps to provide data support for government decision-making departments, but it also provides a direct basis for local water users to make water rights trading decisions.

The research on the risk of water rights transaction is generally embodied in qualitative research. This paper quantifies the analysis results of water rights transaction risk, establishes the risk analysis model of water rights transaction based on the HWHI, and applies the model to the Tarim River Basin for case study. The results conform to the current situation regarding water rights transaction. It is suggested that the river basin should properly develop water rights trade and promote the optimal allocation of water resources.

There is a positive correlation between the water rights transaction risk and the tradable quantity of water rights. Therefore, the water rights transaction risk value can be used as the basis for the government to approve a water rights transaction initially, and to also further provide some theoretical support for the optimal allocation of water resources.

Many countries and regions in the world are involved in water rights trading. Due to changing conditions, water rights transaction risk levels are also different. We hope that the quantitative method for risk analysis of water rights transaction based on HWHI prediction will contribute to the optimal allocation of water resources and restoration of ecological environment in other arid regions of the world.

ACKNOWLEDGEMENTS

This research was funded by Humanities and Social Sciences Foundation of the Chinese Ministry of Education（No.18YJA790061）, Social Science Foundation of Jiangsu Province（No.18EYB008）and Foundation of the research institute of grand canal cultural belt construction (No. DYH19YB01).

REFERENCES

[1] Wu, D. (2012) Research progress of initial allocation of water rights in river basins. Advances in Science and Technology of Water Resources. 32(2), 89–94.

[2] Zhao, P., Dou, M., Hong, M., Li, P., Wang, Y. (2016) Two levels water rights trading model of river basin under the most strict water resources management system. China Rural Water and Hydropower. 1, 21–25.

[3] Vaghefi, S.A., Mousavi, S.J., Abbaspour, K.C., Srinivasan, R., Arnold, J.R. (2015)Integration of hydrologic and water allocation models in basin-scale water resources management considering crop pattern and climate change: Karkheh River Basin in Iran. Regional Environmental Change. 15(3), 475–484.

[4] Bekchanov, M., Bhaduri, A., Ringler, C. (2015) Potential gains from water rights trading in the Aral Sea Basin. Agricultural Water Management. 152, 41–56.

[5] Null, S.E., Prudencio, L. (2016)Climate change effects on water allocations with season dependent water rights. Science of the Total Environment. 571, 943–954.

[6] Wang, L.Z., Zhao, Y., Huang, Y.F., Wang, J.H., Li, H.H., Zhai, J.Q., Zhu, Y.N., Wang, Q.M., Jiang, S. (2019) Optimal Water Allocation Based on Water Rights Transaction Models with Administered and Market-Based Systems: A Case Study of Shiyang River Basin, China. Water. 11(3), 577.

[7] Kendy, E., Aylward, B., Ziemer, L.S., Richter, B.D., Colby, B.G., Grantham, T.E., Sanchez, L., Dicharry, W.B., Powell, E.M., Martin, S. (Martin, Season)., Culp, P.W., Szeptycki, L.F., Kappel, C.V. (2018) Water Transactions for Streamflow Restoration, Water Supply Reliability, and Rural Economic Vitality in the Western United States. Journal of The American Water Resources Association. 54(2),487-504.

[8] Delorit, J.D., Parker, D.P., Block, P.J. (2019) An agro-economic approach to framing perennial farm-scale water resources demand management for water rights markets. Agricultural Water Management. 218,68-81.

[9] Hall, J., Borgomeo, E. (2013) Risk-based principles for defining and managing water security. Philosophical Transactions Of The Royal Society A-Mathematical Physical and Engineering Sciences. 371, 20120407.

[10] Baig, S., Begum, F., Khan, M.Z., Mumtaz, S., Shedayi, AA., Wafee, S., Ali, K., Ali, H. (2019) A Human Health Risk Assessment Of Heavy Metals In Drinking Water Systems Of Central-Hunza, Gilgit-Baltistan, Pakistan. Fresen. Environ. Bull. 28, 2269-2277.

[11] Cosic, D., Popovic, L., Popov,S., Zivkovic, S. (2019)Hydrological Conflicts Risk Estimation In Vojvodina, Serbia. Fresen. Environ. Bull. 28, 6580-6588.

[12] Li, L., Sun, Y., Cao, J., Guo, Y. (2019) Study On Emergency Mechanism Of Sudden Environmental Pollution Events In Danjiangkou Section. Fresen. Environ. Bull. 28, 9359–9365.

[13] Bekchanov, M., Bhaduri, A., Ringler, C. (2015) Potential gains from water rights trading in the Aral Sea Basin. Agricultural Water Management. 152, 41-56.

[14] Payne, M.T., Smith, M.G. (2013) Price determination and efficiency in the market for water rights in New Mexico's Middle Rio Grande Basin. International Journal Of Water Resources Development. 29(4),588-604.

[15] Xu, T.T., Zheng, H., Liu, Y.C., Wang, Z.J. (2016) Assessment of the water market in the xiying irrigation district, shiyang river basin, China. Journal Of Water Resources Planning And Management. 142(8), 04016021.

[16] Ding, Y.F., Tang, D.S., Dai, H.C., Wei, Y.H. (2014) Human water harmony index: A New Approach to Assess the Human Water Relationship. Water Resources Management. 28(4), 1061-1077.

[17] Zuo, Q.T., Zhao, H., Mao, C.C., Ma, J.X., Cui, G.T. (2015) Quantitative Analysis of Human-Water Relationships and Harmony-Based Regulation in the Tarim River Basin. Journal Of Hydrologic Engineering. 20(8), 05014030.

[18] Ren, J.R., Tang, D.S., Wang, M., Ding, Y.F., Zhang, J.X. (2017) An optimization model for water resources allocation based on the concept of human water harmony index. Fresen. Environ. Bull. 26(5), 3257-3267.

[19] Deng, X.H., Song, X.Y., Xu, Z.M. (2018) Transaction Costs, Modes, and Scales from Agricultural to Industrial Water Rights Trading in an Inland River Basin, Northwest China. Water. 10(11), 1598.

[20] Xu, ZW., Yao, L.M., Zhou, X.Y., Moudi, M., Zhang, L.W. (2019) Optimal irrigation for sustainable development considering water rights transaction: A Stackelberg-Nash-Cournot equilibrium model. Journal Of Hydrology. 575, 628-637.

[21] Chen, J.M., Li, J., Wang, X.J., Zheng G.N. (2015) Tradable Water Rights Analysis and Risk Prevention of Water Rights Transaction. China Water Resource. 5, 9-12.

[22] Fang, G.H., Yang, Y., Yuan, Y., Huang, X.F., Wen, X. (2017) Risk decision analysis of floodwater resource utilization based on adjusting flood limited water level of reservoir. Fresen. Environ. Bull. 26, 5745–5753.

[23] Yue, W.C., Cai, Y.P., Xu, L.Y., Yang, Z.F., Yin, X.A., Su, M.R. (2017)Industrial water resources management based on violation risk analysis of the total allowable target on wastewater discharge. Scientific Reports. 7, 5055.

[24] Chen, C., Huang, G.H., Li, Y.P., Zhou, Y. (2013) A robust risk analysis method for water resources allocation under uncertainty. Stochastic Environmental Research and Risk Assessment. 27(3), 713 -723.

[25] Sen Gupta, A., Jain, S., Kim, J.S. (2011 Past climate, future perspective: An exploratory analysis using climate proxies and drought risk assessment to inform water resources management and policy in Maine, USA. Journal Of Environmental Management. 92(3), 941 -947.

[26] Zhao, Y., Sun, J.X., Han, H.L. (2014) Application of Grey Prediction GM(1,1) Model in Zhangjiakou water demand forecasting. Water Resources and Power. 32(7), 40 -43.

[27] Zhao, Y., Zhang, X.Q., Xin, L. (2017)Study of water exchange between regions based on the Markov method. Chinese Journal of Hydrodynamics. 32(5), 623 -629.

Received: **18.05.2019**
Accepted: **12.02.2020**

CORRESPONDING AUTHOR

Guangxiong Mao
School of Urban and Environmental Sciences,
Huaiyin Normal University,
Huai'an, Jiangsu, 223300 – China

e-mail: mao@hytc.edu.cn
jshysfxy@126.com

© by PSP Volume 29 – No. 05/2020 pages 3491-3504 Fresenius Environmental Bulletin

COMPREHENSIVE EVALUATION OF FOREST ECOSYSTEM SERVICES VALUE IN CASE OF JILIN FOREST INDUSTRY GROUP

Xiaoliang Shi[1], Chen Ke[1], Chenxi Lu[2], Li Chen[3], He Dan[1], Xianlei Cao[4], Weina Duan[5], Lyu Jie[1,*]

[1]College of Economics and Management, Shenyang Agricultural University, Shenyang, 110866, China
[2]Department of Earth System Science, Tsinghua University, MengMinwei Science Building, Qinghuayuan 1, Beijing 100084, China
[3]School of Sociology, Beijing Normal University,Beijing,100875,China
[4]School of International Trade, Shanxi University of Finance and Economics, Taiyuan,030060, China
[5]Social Affairs Division, Shenyang Municipal Development and Reform Commission, Shenyang, 110866, China

ABSTRACT

The study considered on research of forest ecosystem services value accounting only focused on a single service content evaluation and simple sum in past. Previous research did not consider difference between research methods and theory of forest ecosystem services value use and follow it. Different content have different vector, it was necessary to make comprehensive evaluation process before direct additive, to remove repetitive accumulation and synergy between various services value, etc. Research comprehensive evaluated forest ecosystem services value calculation results in case of Jilin Forest Industry Group, in order to make the results more objective and reasonable, and provide the basis for forest ecosystem management. There has certain innovation. Research designed forest ecosystem services value evaluation model with factor analysis method. It used the model to evaluate forest ecosystem services value of Jilin Forest Industry Group from 2009 to 2013. The results showed that forest ecosystem service value was 55.757 billion Yuan of Jilin Forest Industry Group in 2013 after adjustment. The order of forest ecosystem services value was purify the atmosphere environment (46.552 billion Yuan, accounting for 83.49% of the total service value); value of water conservation (3.423 billion Yuan, accounting for 6.14%); value of biodiversity maintenance (2.334 billion Yuan, accounting for 4.19%); value of farmland/pasture protection (2.048 billion Yuan, accounting for 3.67%); value of conservation of soil (1.393 billion Yuan, accounting for 2.5%); value of carbon release oxygen (8 million Yuan, accounting for 0.01%). The study, which defined the forest ecosystem service content, and established the corresponding evaluation index system, corrected the disadvantage of the evaluation method, laid the basis for evaluation of forest ecosystem services.

KEYWORDS:
Jilin Forest Industry Group, Forest Ecosystem Services, Service Value, Comprehensive Evaluation, Factor Analysis, Politics

INTRODUCTION

The natural ecological environment and socio-economic activities have close and complex linkages. However, the value of forest system services in daily production and life is often overlooked. Instead, the economy is developed at the cost of excessive consumption of forest resources, which severely damages the forest system and ecology. The environment continues to deteriorate, and the basic living conditions of human beings are seriously threatened, hindering the sustainable development of society [1]. Forests are the natural ecosystems with the largest area, the most complex compositional structure, the highest total biomass, the most complete functions, and the strongest adaptability among terrestrial ecosystems, and have a decisive influence on the terrestrial ecosystem. The forest system is an important source of providing ecological services, and it is a unified link between environment and development [2-4]. It can not only provide various production and living materials such as timber and under store economic by-products, but also has water conservation and conservation of soil. Various direct and indirect services, such as purifying the atmospheric environment and maintaining regional ecological balance, are the most comprehensive gene banks and resource banks in nature [5–10].

In the report of the 18th CPC National Congress, the first single discussion of the "ecological civilization" construction. Closely focused on promoting resource conservation, increasing natural ecological systems and environmental protection efforts, and strengthening the building of an ecological civilization system, we have made a comprehensive deployment of ecological civilization under the new situation. Afterwards, at the Third Plenary Session of the 18th CPC Central Committee, the

Central Committee of the Communist Party of China deliberated and adopted the "Decision of the CPC Central Committee on Several Major Issues Concerning Comprehensively Deepening the Reform." It pointed out that we must accurately grasp the core issues that restrict the development of the current environmental protection industry in the country and push the industry into a new phase. Focus on accelerating the establishment of an ecological civilization system. It can be seen that the current prominent status of ecological civilization construction in China is given as the largest ecosystem on the land, the forest ecosystem.

In recent years, with the deterioration of the global environment and the continuous development of social economy, people have gradually realized that forest ecosystem services have various values. After Costanza et al. [11] evaluated the economic value of the world's major ecosystem services, people have more clearly recognized the value of forest ecosystem services, and more scholars have begun to engage in ecosystem service value evaluation research. However, there are many problems in the study of the value of forest ecosystem services, such as misuse of "functions" and "services". The largest and most common mistakes occurred in the UN Millennium Ecosystem Assessment Report completed by 1,360 scholars in 95 countries. Ecosystem Assessment Chinese translation of "Ecosystems and Human Welfare: Assessment Framework (Abstract), in the MA [12] translation, a total of 103 "transportation of ecosystem services" traffic concept, translated into "ecosystem services functions", assets Confused with the production concept. For example, translate "support services" into "support functions" and "regulate services" into "adjustment functions". The Chinese translation of MA made confusion in our country's academia. After retrieving the paper that quoted this translation, we found that over 90% of the articles were misleading. Many scholars in China have confused the value of forest ecosystems as assets, the value of products and services they produce, and even added the value of asset stocks when they are conducting national, provincial, municipal, and even forestry-level ecological value assessments. Product and service flow value, and will publish the wrong "green GDP" society. The translation of MA even misled the Ministry of Forestry's Forestry Industry Standard (LY/T1721-2008) issued by the State Forestry Administration on April 28, 2008. "Specifications for Assessment of Forest Ecosystem Services in China". The English translation should be translated as "forest ecosystem services" but translated as "forest ecosystem service functions." Judging from the forestry industry standard's interpretation of the "forest ecosystem service function," it is more systematic to confuse "functionality" with "service." According to this "standard" assessment of forest ecosystem service value, inevitably assets and service values are not separated, and if the GDP is calculated, the result can be imagined.

Due to the influence of previous Chinese translations of Chinese translation of MA, most forest ecosystem service evaluations have been misused with "functionality" and "services". This has erroneously defined the content of forest ecosystem services evaluation, such as the forestry industry standard LY/T1721-2008. The "Code for Assessment of Service Functions of Forest Ecosystem Services" [13] divides forest ecosystem services into conservation water resources, conservation of soil, carbon fixation and oxygen release, accumulation of nutrients, purification of atmospheric environment, protection of forests, maintenance of biodiversity, and forest recreation. In eight aspects, the accumulation of nutrients and the conservation of soil are double counting. Therefore, determining the concept of forest ecosystem services and studying the boundary is the premise of accurate accounting of value, otherwise it will result in serious problems such as content omission, duplication, or inconsistent calibre. The standardization of forest ecosystem service classification and indicator systems is also directly related to the comparability of evaluation results. The research is based on a clear distinction between "functionality" and "services," and clearly defines the content of forest ecosystem services. It also considers that the services of forest ecosystems should be evaluated separately, and that simply summing up total values is unscientific. The reason is that there are differences between the research methods adopted in different forest ecosystem service evaluations and the basic theories followed, and there are different vectors between different service contents, and direct summation may cause problems such as repetitive accumulation or synergy. Therefore, the study establishes and improves the forest ecosystem service evaluation index system and measurement method, and firstly calculates each service value one by one, and then adopts a factor analysis method to comprehensively evaluate the service value, so as to make the result more objective and reasonable, and to be the forest ecology. System management provides the basis for innovation.

RESEARCH AREA

As a major forestry province in China and an important timber production base in Jilin Province, the forest coverage rate has reached 43.8% by 2013, with 8.288 million hm^2 of forest land and 956.13 million m^3 of standing timber (Jilin Provincial Department of Forestry, 2012). Jilin Forest Industry Group Co., Ltd. (hereinafter referred to as "Jilin Forest Industry Group") construction area is located in the Changbaishan Forest District of Jilin Province. It is one of the four major forestry industry

groups in China, and it is also an extremely important timber production base and natural ecological barrier in China. Jilin Forest Industry Group is a diversified enterprise group based on the management of forest resources. The forest coverage rate of the group is 90.9%, the total operating area is 1,347,500 hm^2, the forest area is 1,224,800 hm^2, the standing timber volume is 179,781,200 m^3, and the trees the unit of hectare of forest is 151.95 m^3/hm^2, which ranks first among the developed forest areas in China. Among them, the forest carbon storage amounted to 77.8 million tons, and the forest ecosystem service value was about 65.1 billion Yuan (Jilin Forest Industry Group 2013 Forest Resources Analysis Report, 2013). The value of this service accounted for the total GDP of Jilin Province in 2013 (1,298.146 billion Yuan) for 5%, the significance of the value of forest ecosystem services is more prominent, how to better integrate the value of forest ecosystem services into the socio-economic value, and has a very strong impact on the sustainable development and management of forests in Jilin Forest Industry Group. Important practical significance.

MATERIALS AND METHODS

Research content. Forest ecosystem services come from forest ecosystem functions, and different services come from different functions [14-17]. "Feature" and "service" are the concept of stock and traffic, respectively, and they have essential differences. At present, international consensus recognizes that forest ecosystem services refer to those functions that are available to humans. They can only be evaluated if they are used by humans. Therefore, forest ecosystem services refer to various benefits that can be obtained directly or indirectly from the functions of forest ecosystems. However, currently the classification of forest ecosystem services has not been unified. For example, the United Nations and other five departments jointly issued Integrated Environmental-Economic Accounting System - Core Framework, ie SEEA-2012 divides forest environmental services into soil and water conservation, biodiversity conservation, carbon sequestration and forest recreation (United Nations et al., 2012); World Food and Agriculture Organization (FAO) to forest environment services are divided into soil and water conservation, biodiversity conservation, carbon sequestration, forest tourism, noise reduction, crop pollination, wind protection and spiritual values in the “Forest Environment and Economic Accounts Guide” (FAO Forestry Department, 2004). The division of forest ecosystem services in China is also inconsistent, such as the division of soil erosion, water conservation, wildlife protection, and supply of oxygen, forest recreation, noise reduction and forest health care [18]. The study follows the mainstream practice of our country, and integrates the previous research results, especially with reference to the literature on China's Sustainable Development Strategy Research 2: Re-recognition of Forest Functions and China's Forest Resources and Sustainable Development. It is mainly divided into four services: support, supply, regulation, and culture. This is consistent with MA's research results [12], but considering that some of these services (MA called “support services”) cannot be directly used by humans, and humans benefit from the system. Are all final products, so "support/autotrophic services" should not be valued as non-final products (Jean-Lucpeyron, 2005). In addition, forest ecosystem services generally include three aspects of economic, ecological, and social assessments: Economic services refer to the benefits of forest systems that directly serve economic output, such as the understory economy (collection, aquaculture, forest tourism, etc.) Eco-service refers to purely ecological services provided based on the functions of the forest system itself, such as conservation of soil and conservation of water resources. Social services refer to benefits (material and spiritual) directly served by society, which can eliminate fatigue and pleasure. Such as forest recreation, forest health care and providing employment opportunities. In summary, the forest ecosystem services of this study are divided into conservation water, soil conservation, purification of atmospheric environment, farmland/pasture protection, biodiversity maintenance, and carbon fixation and oxygen release [19], and six types of 16 indicators are constructed. Fig. 1.

Sources of data. The data used in the research mainly originated from the forestry management plans of the eight forestry bureaus prepared by the Jilin Provincial Forestry Survey and Planning Institute; it also originated from the data published in the 2009-2013 China Forestry Statistical Yearbook and Jilin Province Statistical Yearbook. There are also some data sources from Jilin Province Wildlife Conservation and Nature Reserve Management Office, Forestry Department Finance Department, Water Resources Department, Transportation Department, Agriculture and Animal Husbandry Bureau and Forest Seed Management Station, etc. The Group conducted field investigations and obtained a large amount of survey data and information.

Research methods. (1) Evaluation of forest ecosystem services. According to the definition of forest ecosystem service evaluation, combined with the actual situation of forest resources in Jilin Forest Industry Group, the evaluation formula for determining the physical quantity and value of forest ecosystem services is shown in Table 1.

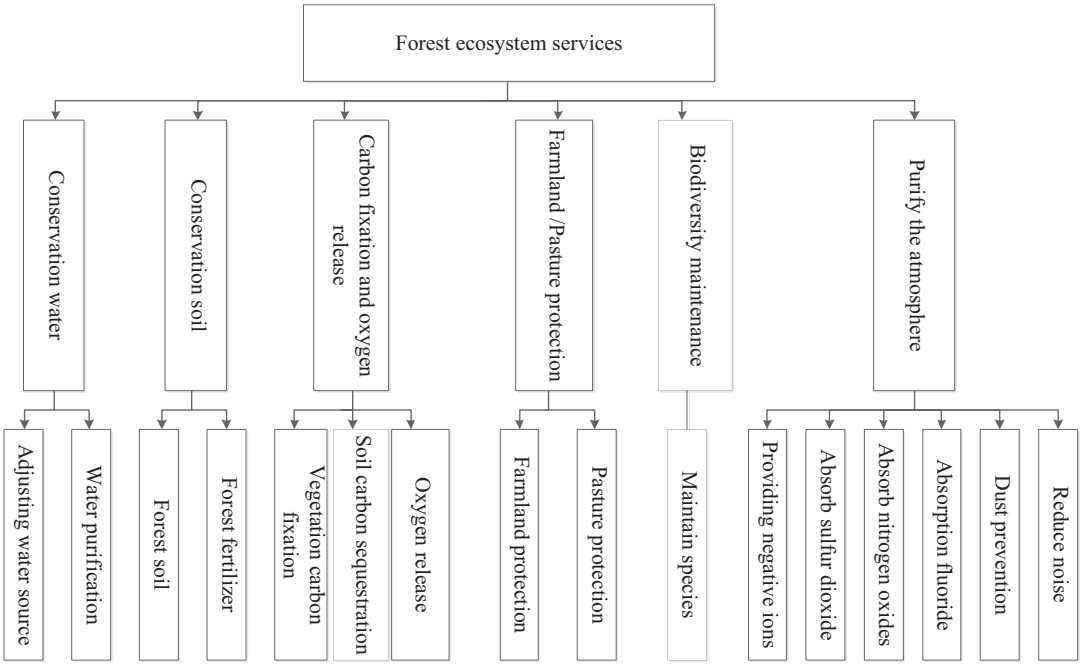

FIGURE 1
Evaluate quota system of forest ecosystem services

TABLE 1
Evaluation formula of physical quantity and value of forest ecosystem services

Service type	Index	Evaluation formula and its parameter description
Conservation water(CW)	Adjusting water source	Physical quantity: $G_R = 10A(P - E - C)$, G_R- Forest regulation water volume, m^3/a; P- Atmospheric precipitation, mm/a; E- Forest evapotranspiration, mm/a; C- Surface runoff, mm/a; A- Forest area, hm^2. Value: $U_R = G_R \times C_S$, U_R- Forest ecosystem regulates water value every year, Yuan/a; C_S- Forest water storage price, Yuan/m^3.
	Water purification	Physical quantity: Formula with the forest to regulate water volume. Value: $U_{WP} = G_R \times K$, U_P- Year of forest purification water quality, Yuan/a; K- Water purification cost（Average residential water price）, Yuan/m^3.
	Total Value	$U_{CW} = U_R + U_{WP}$, $U_{Conservation\ water}$- Forest conservation water source value, Yuan/a.
Conservation soil(CS)	Forest soil	Physical quantity：$G_{FS} = A(X_2 - X_1)$, G_{FS}- Forest year soil, t/a; X_1- Forest soil erosion modulus, $t.hm^{-2}.a^{-1}$; X_2- Soil erosion modulus without forest, $t.hm^{-2}.a^{-1}$; A- Forest area, hm^2. Value: $U_{FS} = \frac{G_{FS} \times C_C}{\rho}$, U_{FS}- Forest year solid soil value, Yuan/a; C_C- The cost of digging and transporting earth by volume, Yuan/m^3; ρ-Forest soil bulk density, t/m^3.
	Forest fertilizer	Physical quantity（Guarantee N）：$G_N = G_{FS} \times N$, G_N- Reduced nitrogen loss, t/a; N- Soil nitrogen content, %. Value（Guarantee N）：$U_N = \frac{G_N \times C_1}{R_1}$, U_N- Annual nitrogen conservation value of forest, Yuan/a; R_1- Fertilizer nitrogen content, %; C_1- Fertilizer price, Yuan/t. Physical quantity（Guarantee P）：$G_P = G_{FS} \times P$, G_P- Reduced phosphorus loss, t/a; P- Soil phosphorus content, %. Value（Guarantee P）：$U_P = \frac{G_P \times C_1}{R_2}$, U_P- Forest annual phosphorus value, Yuan/a; R_2- Fertilizer phosphorus content, %; C_1- Fertilizer price, Yuan/t. Physical quantity（Guarantee K）：$G_K = G_{FS} \times K$, G_K- Reduced potassium loss, t/a; K- Soil potassium content, %. Value（Guarantee K）：$U_K = \frac{G_K \times C_2}{R_3}$, U_K- Forest annual potassium value, Yuan/a; R_3-

Service type	Index	Evaluation formula and its parameter description
		Potassium chloride fertilizer, %; C_2- Potassium chloride fertilizer price, Yuan/t. Physical quantity（Guarantee Organic matter）: $G_M = G_{FS} \times M$, G_M- Reduced soil organic matter content, t/a； M- Soil organic matter content, %. Value（Guarantee Organic matter）: $U_M = G_M \times C_3$, U_M- Forest annual insurance organic quality value, Yuan/a; C_3-Organic price, Yuan/t. Forest soil fattening value: $U_F = U_N + U_P + U_K + U_M$, U_F- Stand year fat value, Yuan/a; U_N- Stand value of nitrogen retention, Yuan/a; U_P- Stand value of phosphorus, Yuan/a; U_K- Stand value annual potassium value, Yuan/a; U_M-Stand year warranty organic value, Yuan/a.
	Total Value	$U_{CS} = U_{FS} + U_F$, U_{CS}-Conservation soil value per year, Yuan/a; U_{FS}-Solid soil value per year, Yuan/a.
Purify the atmosphere(PA)	Providing negative ions	Physical quantity: $G_A = \frac{5.256 \times 10^{15} \times (Q_A - 600) \times A \times H}{L}$, G_A- The number of anions provided in the stand year, per unit.a^{-1}； Q_A- Negative ion concentration, pcs.cm^{-3}; H- Stand height, m; L- Negative ion lifetime, minute; A-area of forest, hm^2. Value: $U_A = G_A \times K_A$, U_A-Annual negative ion value, Yuan/a; K_A- Negative ion production cost, Yuan per unit.
	Absorb sulfur dioxide	Physical quantity: $G_{SO_2} = Q_{SO_2} \times A$, G_{SO_2} - Annual forest absorption of SO_2, kg/a ； QSO_2- The amount of SO_2 absorbed per unit area of forest, kg.hm^{-2}.a^{-1}; A- Forest area, hm^2. Value: $U_{SO_2} = G_{SO_2} \times K_{SO_2}$, U_{SO_2} - Annual forest absorption of SO_2, Yuan/a; K_{SO_2} - SO_2 Governance costs, Yuan/kg.
	Absorption fluoride	Physical quantity: $G_F = Q_F \times A$, G_F- Annual amount of fluoride absorbed by forest, kg/a; Q_F- The amount of fluoride absorbed per unit area of forest, kg.hm^{-2}.a^{-1}; A- Forest area, hm^2. Value: $U_F = G_F \times K_F$, U_F- Value of fluoride absorption in stand years, Yuan/a; K_F- Fluoride treatment costs, Yuan/kg.
	Absorb nitrogen oxides	Physical quantity: $G_{NO_x} = Q_{NO_x} \times A$, G_{NOX} - Annual amount of nitrogen oxides absorbed by forests, Yuan/kg; Q_{NOX} - Annual absorption of nitrogen oxides per unit area of forest, kg.hm^{-2}.a^{-1}; A--Forest area, hm^2. Value: $U_{NO_x} = G_{NO_x} \times K_{NO_x}$, U_{NOX} - Annual absorption of nitrogen oxides, Yuan/a; K_{NOX} -NO_x treatment costs, Yuan/kg.
	Dust prevention	Physical quantity: $G_{DP} = Q_{DP} \times A$, G_{DP}-Dust retention value per year, Yuan/kg; Q_{DP}-Annual dust amount per unit area, kg.hm^{-2}.a^{-1}; A--Forest area, hm^2. Value: $U_{DP} = G_{DP} \times K_{DP}$, U_{DP}-Dust retention value, Yuan/a; K_{DP}- Dust removal costs, Yuan/kg.
	Reduce noise	Physical quantity: $A_{RN} = \frac{1000}{D_0} \sum_{i=1}^{n} D_i \times L_i$, A_{RN}-Equivalent length of soundproof wall forest to reduce noise, m; n- Number of roads, i=1, 2， …,n; L_i- Unilateral length of the i-th highway belt, km; D_i-One-way forest belt width on the i-th road, m; D_0- The width of the forest belt equivalent to the noise barrier, m. Value: $U_{RN} = A_{FB} \times K_{RNC}$, U_{RN}-Reduce noise value per year, Yuan/a; A_{FB}- Forest belt equivalent to soundproof wall reduces noise equivalent length, m; K_{RNC}- Reduce noise costs per equivalent length per year, Yuan.m^{-1}.a^{-1}.
	Total Value	$U_{PA} = U_A + U_{SO_2} + U_F + U_{NO_x} + U_{DP} + U_{RN}$, U_{PA} - Purify the atmosphere value of forest, Yuan/a.

Service type	Index	Evaluation formula and its parameter description
Farmland /Pasture protection(FPP)	Forest agricultural protection	Physical quantity: $G_{FAP} = \sum_{i=1}^{n} G_i = R\sum_{i=1}^{n} Q_i A_i$, G_{FAP}- Annual growth of crops in the assessment per unit, kg/a; G_i- Annual increase in crops of category i, kg/a; R- Average yield increase of crops in the unit, %; Q_i- Crop yield per unit area of i-type crops, kg.hm^{-2}.a^{-1}; A_i- Sown area of i-type crops, hm^2. Value: $U_{FAP} = \sum_{i=1}^{n} G_i C_i$, U_{FAP}- Forest protection value, Yuan/a; C_i- Category i crop prices, Yuan/kg.
Biodiversity maintenance(BM)	Maintain species	Physical quantity: $H_A = \frac{1}{A}\sum_{i=1}^{n} A_i H_i = -\frac{1}{A}\sum_{i=1}^{n} A_i \sum_{j=1}^{s} P_{ij} \log_2 P_{ij}$, H_A- Regional average diversity index; A- Total forest area in a certain area, hm^2; A_i- The i-th forest type area, hm^2; H_i- Biodiversity index for the i-th forest type; n- Number of forest types; P_{ij}- Proportion of the j-th species of the i-th forest type. Value: $U_{BM} = S_{BM} \times A$, U_{BM}- Forest Year Conservation Value, Yuan/a; A--Forest area, hm^2; S_{BM}- Annual species loss opportunity cost per unit area, yuan.hm^{-2}.a^{-1}.
Carbon fixation and oxygen release(CFOR)	Soil carbon sequestration	Physical quantity（vegetation）: $G_{CFV} = 1.63 \times R_C \times A \times B_{NP}$, G_{CFV}- Annual carbon fixation of forest vegetation, t/a; R_C- carbon content of CO_2, 0.2729; B_{NP}-Net productivity of forest, t.hm^{-2}.a^{-1}; A-Forest area, hm^2. Value（vegetation）: $U_{PCS} = C_C \times G_{PCS}$, U_{PCS}- Forest plant carbon sequestration value per year, Yuan/a; C_C- Carbon price, Yuan/t.
		Physical quantity（soil）: $G_{CSS} = A \times F_S$, G_{CSS}- Annual carbon sequestration of forest soil, t/a; F_S- Per unit area of forest soil carbon sequestration, t.hm^{-2}.a^{-1}; A-Forest area, hm^2. Value（soil）: $U_{CSS} = C_C \times G_{CSS}$, U_{CSS}- Forest Soil Carbon Sequestration Value, Yuan/a; C_C- Carbon price, Yuan/t.
	Oxygen release	Physical quantity: $G_{O_2R} = 1.19 \times A \times B_{NP}$, G_{O_2R} - Oxygen release in the forest, t/a; B_{NP}- Net forest productivity, t.hm^{-2}.a^{-1}; A-Forest area, hm^2. Value: $U_{O_2} = C_{O_2} \times G_{O_2}$, U_{O_2} - Oxygen release value in forest per year, Yuan/a; C_{O_2} - O_2 value, Yuan/t.
	Total Value	$U_{CS} = U_{PCS} + U_{CSS}$, U_{CS}- Forest annual carbon sequestration value, Yuan/a; $U_{CFOR} = U_{CS} + U_{O_2}$, U_{CFOR} -the total value of Carbon fixation and oxygen release, Yuan/a.

Source：State Forestry Bureau，Forestry industry standards of the People's Republic of China LY/T1721-2008——《Specifications for Assessment of Forest Ecosystem Services in China》.

(2) Factor analysis. Factor Analysis was first proposed by Charles Spearman in 1904. The purpose was to investigate the correlation between variables and use a small number of factors to describe the interactions between multiple indicators. Relative variables were grouped into the same group, and each type of variable was changed. A factor that reflects most of the information in the original data with fewer factors. With the original data variables: x_1, x_2, x_3, ..., x_m, the relationship between variables and latent factors is expressed as:

$$\begin{cases} x_1 = b_{11}z_1 + b_{12}z_2 + b_{13}z_3 + \cdots + b_{1m}z_m + e_1 \\ x_2 = b_{21}z_1 + b_{22}z_2 + b_{23}z_3 + \cdots + b_{2m}z_m + e_2 \\ x_3 = b_{31}z_1 + b_{32}z_2 + b_{33}z_3 + \cdots + b_{3m}z_m + e_3 \\ \cdots\cdots\cdots\cdots\cdots\cdots\cdots\cdots\cdots\cdots \\ x_m = b_{m1}z_1 + b_{m2}z_2 + b_{m3}z_3 + \cdots + b_{mm}z_m + e_m \end{cases} \quad (1)$$

In formula (1), z_1-z_m is m latent factors, which are the factors included in each original variable. e_1-e_m is m individual factors that are only contained in a certain original variable and only work on this original variable, and are unique factors in each original variable. That is, the common factors and special factors are independent of each other. The purpose of the factor analysis method is to find common factors. After the results are obtained, the common factors are named according to the actual meaning. There are many methods for factor analysis. For example, the principal component analysis method can be directly used to ignore special factors. The common factor number can be determined based on the principle of maximum contribution. Assuming that the common factor is k, the initial factor model is as follows:

$$\begin{cases} x'_1 = \alpha_{11} f_1 + \alpha_{12} f_2 + \alpha_{13} f_3 + \cdots + \alpha_{1k} f_k + e_1 \\ x'_2 = \alpha_{21} f_1 + \alpha_{22} f_2 + \alpha_{23} f_3 + \cdots + \alpha_{2k} f_k + e_2 \\ x'_3 = \alpha_{31} f_1 + \alpha_{32} f_2 + \alpha_{33} f_3 + \cdots + \alpha_{3k} f_k + e_3 \\ \cdots\cdots\cdots\cdots\cdots\cdots\cdots\cdots\cdots\cdots \\ x'_m = \alpha_{m1} f_1 + \alpha_{m2} f_2 + \alpha_{m3} f_3 + \cdots + \alpha_{mk} f_k + e_m \end{cases} \quad (2)$$

In the formula (2), x'_1-x'_m is a variable normalized to the original variable whose standard deviation is 1, and the mean value is 0; f_i is the i-th factor; α_{ij} is the load of the common factor f_i, indicating that x_i depends on the weight of f_i. Since x'_1-x'_m is a variable that is normalized by the original variable x_1-x_m, the variance of each variable is 1, that is, variance(x'_i)=1. It is written as:

$$\mathrm{Va}(x') = \alpha_{i1}^2 + \alpha_{i2}^2 + \alpha_{i3}^2 + \cdots + \alpha_{im}^2 + V(e_i) = 1 \quad (3)$$

Equation (3) consists of two parts:

$$\alpha_{i1}^2 + \alpha_{i2}^2 + \alpha_{i3}^2 + \cdots + \alpha_{im}^2 \quad (4)$$

The first part, formula (4) refers to the commonality variance caused by several common factors; the second part refers to the characteristic variance $V(e)$ due to special factors. If the proportion of the common variance is greater than the total variance, the common factor will also play a greater role. The search for common variance involves factor loading and common factors.

$$V_{common} : Vc(x'_i) = \sum_{j=1}^{m} \alpha_{ij}^2 \quad (5)$$

If you take the first k factors, the common variance becomes:

$$Vc(x'_i) = \sum_{j=1}^{k} \alpha_{ij}^2 \quad (6)$$

RESULTS

Single evaluation of forest ecosystem services. The results of the single evaluation of forest ecosystem services in Jilin Forest Industry Group in 2013 are summarized in Table 2.

As can be seen from Table 2, the value of forest ecosystem services of Jilin Forest Industry Group in 2013 was 224.388 billion Yuan.

Comprehensive evaluation of forest ecosystem services. The comprehensive evaluation of forest ecosystem services mainly analyzes the factors of six single services, such as water conservation and conservation soil, to study the relationship between variables and identify potential dominant factors. The factor weights are used to give the weights of each factor, and the comprehensive weights are used to obtain the evaluation model. The service evaluation index system is constructed to include the level one and two levels. Among them, the first-level indicators refer to the service value; the third-level indicators refer to the factors that affect the service value and may have multiple collinearity with each other; and the second-level indicators refer to the few key factors extracted from the third-level indicators through factor analysis.

Construction of indicator system. (1) Establishment of a hierarchical structure model. SPSS13.0 software was used to perform factor analysis on the service values of forest ecosystems. Before extracting factors, it was checked whether most of the correlation coefficients in the correlation matrix were greater than 0.3. It was suitable for factor analysis. The correlation matrix of the original variables is shown in Table 3.

As can be seen from Table 3, most correlation coefficients in the correlation matrix table are greater than 0.3, indicating that the original data is suitable for factor analysis. Since the analysis is related to the matrix, the variance of the original factors of the service is 1, and the sum of the variance of the common factors of the 6 variables is 6. The common factor variance of the unrotated variables is shown in Table 4.

Extraction Method. Principal Component Analysis. From Table 4, it can be seen that the common factor variance of each variable is high, indicating that the extracted components can describe these variables well. According to the Kaiser-Meyer-Olkin test, the measured value is 0.730, which is close to 1; the Bartlet Test of Sphericity

TABLE 2
A single evaluation of forest ecosystem services of Jilin Forest Industry Group in 2013

Content	Value (100 million Yuan/a)	Total forest area（hm^2）	Unit area value（10 thousand Yuan/hm^2/a）
Conservation water	162.21	1241931	1.31
Conservation soil	153.09	1241931	1.23
Purify the atmosphere	1662.57	1241931	13.39
Farmland protection	91.82	1241931	0.74
Biodiversity maintenance	172.87	1241931	1.39
Carbon fixation and oxygen release	1.32	1241931	0.01
Total value	2243.88	-	-

TABLE 3
Correlation matrix of the original variables

Evaluation index		Conservation water	Conservation soil	Purify the atmosphere	Farmland protection	Biodiversity maintenance	Carbon fixation and oxygen release
correlation	Conservation water	1.000	0.665	-0.070	0.140	0.420	0.294
	Conservation soil	0.665	1.000	0.086	0.370	0.652	0.522
	Purify the atmosphere	-0.070	0.086	1.000	0.516	0.380	0.429
	Farmland protection	0.140	0.370	0.516	1.000	0.502	0.526
	Biodiversity maintenance	0.420	0.652	0.380	0.502	1.000	0.861
	Carbon fixation and oxygen release	0.294	0.522	0.429	0.526	0.861	1.000
Sig.(1-tailed)	Conservation water		0.000	0.291	0.136	0.000	0.009
	Conservation soil	0.000		0.249	0.001	0.000	0.000
	Purify the atmosphere	0.291	0.249		0.000	0.001	0.000
	Farmland protection	0.136	0.001	0.000		0.000	0.000
	Biodiversity maintenance	0.000	0.000	0.001	0.000		0.000
	Carbon fixation and oxygen release	0.009	0.000	0.000	0.000	0.000	

a Determinant =0.036.

test shows that the Bartley spherical test statistic is 199.724, and the significance level is 0.000, which is considered to exist between the correlation coefficient matrix and the unit matrix. Significant difference, the original data is suitable for factor analysis.

(2) Determination of indicator weight

The weight of the secondary indicator, that is, the key factor is determined, and the variance contribution rate of the common factor is usually used as the weight. In fact, the common factors are sorted according to the contribution rate of variance, and the eigenvalues are also sorted according to this. The common factor variance of each component is shown in Table 5.

Extraction Method. Principal Component Analysis. It can be seen from Table 5 that the eigenvalues of the first two components are greater than 1, and the cumulative contribution rate of the variance of the factors from top to bottom as a percentage of the total variance is obtained. The sum of the eigenvalues of the first two variables accounts for 76.754% of the total variance. That is, the first two variables can account for 76.754% of all original variables. The factor extraction results from Table 5, that is, the sum of the squares of the unrotated factor loads, show that the first two factor variables can summarize most of the data, and the variance that can be interpreted accounts for 76.754% of the total variance. Therefore, the result is to determine the extraction of two principal components, reducing the complexity of the original data, but will lose 23.246% of the original data. To illustrate whether the extraction factor is appropriate, do a gravel chart as shown in Fig. 2.

It can be seen from Fig. 2 that the difference of the eigenvalues between factor 1 and factor 2, factor 2 and factor 3 is large, while the difference between the factor 3, 4, 5 and 6 is small, and preliminary results are obtained. The factors can summarize most of the information, and the inflection point is at 3, so it is appropriate to extract two factors, which also confirms the results in Table 5. For the determination of the weights of the secondary indicators, the corresponding eigenvalues of the two factors are known to be 3.216 and 1.390, and the contribution rate of each factor is given by the common variance formula (6), which is 0.698 and 0.302, respectively. Therefore, the forest ecosystem service value expression is:

$$F=0.698\times F_1+0.302\times F_2 \quad (7)$$

TABLE 4
Common factor variance table for each variable not rotated

Evaluation index	Initial common factor variance	Unrotated common factor variance
Conservation water	1.000	0.895
Conservation soil	1.000	0.847
Purify the atmosphere	1.000	0.947
Farmland protection	1.000	0.781
Biodiversity maintenance	1.000	0.889
Carbon fixation and oxygen release	1.000	0.875

TABLE 5
Common factor variance table of each component

Evaluation index	Initial eigenvalue			Sum of squared extracted loads		
	Eigenval-ues	Variance contribution rate/%	Cumulative contribution rate/%	Eigen-values	Variance contribu-tion rate/%	Cumulative contribution rate/%
Conservation water	3.216	53.593	53.593	3.216	53.593	53.593
Conservation soil	1.390	23.161	76.754	1.390	23.161	76.754
Purify the atmosphere	0.559	9.314	86.068			
Farmland protection	0.446	7.439	93.506			
Biodiversity maintenance	0.269	4.482	97.989			
Carbon fixation and oxygen release	0.121	2.011	100.000			

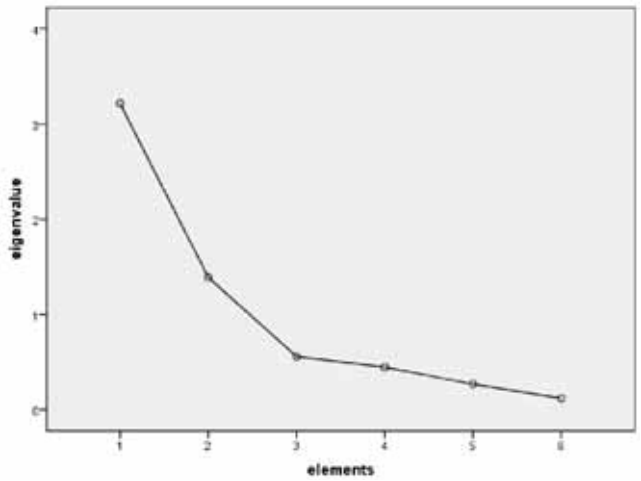

FIGURE 2
Scree plot

TABLE 6
Factor loading matrix[a]

Evaluation index	Principal Components	
	1	2
Conservation water	0.548	-0.694
Conservation soil	0.773	-0.673
Purify the atmosphere	0.499	0.705
Farmland protection	0.693	0.409
Biodiversity maintenance	0.912	-0.013
Carbon fixation and oxygen release	0.870	0.141

TABLE 7
Rotated Component Matrix(a)

Evaluation index	Principal Components	
	1	2
Purify the atmosphere	0.846	-0.170
Farmland protection	0.785	0.178
Carbon fixation and oxygen release	0.730	0.494
Biodiversity maintenance	0.654	0.336
Conservation water	-0.078	0.881
Conservation soil	0.237	0.874

Table 6 shows the factor load matrix, which shows the correlation between the original variable and each principal component, that is, which variables explain information for each factor. According to the correlation degree of each factor, the meaning of each factor can be integrated.

Extraction Method: Principal Component Analysis.a 2 components extracted. It can be seen from Table 6 that the first principal component has high correlation with conservation soil, protection of farmland/grassland, biodiversity maintenance

TABLE 10
Comprehensive evaluation index system of forest ecosystem services

Primary Index	Second Index	Third Index
Forest ecosystem services	Regulatory services（0.698）	Purify the atmosphere（0.401）
		Farmland protection（0.320）
		Carbon fixation and oxygen release（0.193）
		Biodiversity maintenance（0.087）
	Conservation soil and water services（0.302）	Conservation water（0.698）
		Conservation soil（0.302）

TABLE 11
Value of forest ecosystem services

Evaluate content	Service value /billion Yuan	The proportion of total value of each service value/%
Conservation water	34.23	6.14
Conservation soil	13.93	2.50
Purify the atmosphere	465.52	83.49
Farmland protection	20.48	3.67
Biodiversity maintenance	23.34	4.19
Carbon fixation and oxygen release	0.08	0.01
Total	557.57	-

and carbon fixation and oxygen release; the second principal component has high correlation with conservation water source, conservation of soil and purification of atmospheric environment. From the output results, it was found that the extraction result of the factor is ideal, but the correlation coefficient is close, and the factor naming is difficult. Therefore, the coefficients can be rotated to make the coefficients differentiate to 0 and 1, and the rotated factor load matrix is shown in Table 7.

Extraction Method: Principal Component Analysis. Rotation Method: Varimax with Kaiser Normalization. a Rotation converged in 3 iterations. From Table 7, it can be seen that the correlation between the first principal component and the clean air environment, farmland/grassland protection, carbon fixation and oxygen release, and biodiversity maintenance is relatively high; the correlation between the second principal component and the conservation water source and conservation soil is relatively high. The two factors are named according to the original meaning of the variable. The first factor is named as regulatory service. The second factor is named Conservation Soil and Water Service. The factor score matrix after rotation is shown in Table 8.

The covariance matrix of the estimated regression factor scores between the two principal components is shown in Table 9.

Extraction Method: Principal Component Analysis. Rotation Method: Varimax with Kaiser Normalization. Component Scores. It can be seen from Table 9 that the two principal components after rotation are completely irrelevant be-

Extraction Method. Principal Component Analysis. Rotation Method. Varimax with Kaiser Normalization. Component Scores. According to the factor score coefficient of Table 8 and the normalized value of the original variable, the score of each factor of the observable measurement can be calculated, and the observation measurement can be further analyzed. The rotated factor (main component) expression is:

FAC_1-1=-0.219×Conservation water'-0.059 × Conservation soil'+0.461×Purify the atmosphere'+0.359×Farmland protection' + 0.200 × Biodiversity maintenance'+0.267×Carbon fixation and oxygen release (8)

FAC_2-1=0.480×Conservation water'+0.412 x Conservation soil'-0.262×Purify the atmosphere'-0.066×Farmland protection'+0.201×Biodiversity maintenance'+0.112×Carbon fixation and oxygen release (9)

Using factor analysis to determine the three indicators:

F_1=0.401×Purify the atmosphere' + 0.320 × Farmland protection'+0.193×Biodiversity maintenance'+0.087×Carbon fixation and oxygen release (10)

F_2=0.698×Conservation water' + 0.302 × Conservation soil' (11)

cause orthogonal rotation factors are still orthogonal, and the rotated component load is shown in Fig. 3.

The main components of the two principal components are the horizontal and vertical coordinates. The concentration of each component is shown in Fig.3, and two secondary indicators are identified for regulating services and conservation

of soil and water services. The three indicators are the six aspects of the system. Table 10.

Forest ecosystem service value evaluation model based on the comprehensive evaluation index system of Table 10.

F=0.280×Purify the atmosphere'+0.223×Farmland protection'+0.135×Biodiversity maintenance'+0.061×Carbon fixation and oxygen release +0.211×Conservation water' + 0.091 × Conservation soil' (12)

Comprehensive evaluation of forest ecosystem services. Single service value was adjusted according to forest ecosystem service value evaluation model, results were showed in Table 11.

Table 11 shows that after adjustment, the forest ecosystem service value of the Jilin Forest Industry Group in 2013 was 55.757 billion Yuan, of which the value of the atmospheric environment service was the largest (46.552 billion Yuan, accounting for 83.49% of the total value), followed by conservation. Water resources (3.423 billion Yuan, 6.14%); biodiversity conservation (2.334 billion Yuan, 4.19%); farmland/grassland protection (2.048 billion Yuan, accounting for 3.67%); conservation soil (1.393 billion Yuan, accounting for 2.50%) Carbon sequestration and oxygen release (0.08 billion, accounting for 0.01%), in which the value of soil conservation and carbon sequestration services is low, due to lower fertilizer and carbon sequestration prices in 2013.

CONCLUSIONS AND DISCUSSION

Conclusions. First, correct the misuse of “functions” and “services”: forest ecosystem services are derived from forest ecosystem functions, “functions” are stock concepts, “services” are traffic concepts, and services can be directly or indirectly Various benefits derived from the function of forest ecosystems; re-introduction of forests after comprehensive reference to MA, "China's Sustainable Development Strategy Research Topic 2: Recognition of Forest Functions" and "China's Forest Resources and Sustainable Development" The main contents contained in the ecosystem services are defined: conservation of water resources, conservation of soil, purification of atmospheric environment, protection of farmland/grassland, conservation of biodiversity, carbon fixation and release of oxygen, and establishment and improvement of evaluation index system and methods of forest ecosystem service value.

Second, the first systematic assessment of the Jilin Forest Industry Group’s forests was conducted in conjunction with the forest management plan of the eight forestry bureaus of Jilin Forest Industry Group, China Forestry Statistical Yearbook, Jilin Statistical Yearbook, and data obtained from field research. The ecosystem service value shows that the forest ecosystem service value of Jilin Forest Industry Group in 2013 was 224.388 billion Yuan, and there was a big difference between the evaluation results and actual conditions.

Thirdly, only the value of the various service values of the forest ecosystem is evaluated separately, and the results of simply adding up the total value are questioned. The single evaluation result has a large gap with the actual ratio, and a direct sum of vectors for solving different service contents appears. With regard to issues such as repetitive accumulation and synergies, a comprehensive analysis of forest ecosystem service value accounting results using factor analysis methods was conducted. The results showed that the forest ecosystem service value of Jilin Forest Industry Group in 2013 was 55.757 billion Yuan. The result of the comprehensive evaluation process is not objective and reasonable. It not only effectively understands the status of forest resources, but also prepares natural resource balance sheets to provide the basis for the audit of environmental assets of officials and the accountability for environmental protection. It can be reversed and corrected to some extent. "GDP-only" concept of development, guidance and achievement.

Discussion. a) As the main body of terrestrial ecosystems, forests not only provide wood and forest by-products, but also provide ecosystem services such as water conservation, conservation of soil, purification of atmospheric environment, and carbon fixation and oxygen release [20-22]. These services sustain human survival. The required environmental conditions and support the global ecological balance. Asah also pointed out that forest ecosystems are closely related to climatic environment, conservation of soils, conservation of water sources, and decomposition of wastes.

Ecosystem services are of great significance [23-27]. If we continue to maintain the current forest resources status of Jilin Forest Industry Group, the newly added forest ecological service value is about 55.757 billion Yuan, of which the conservation water source value is 3.423 billion Yuan, the biodiversity conservation value is 2.334 billion Yuan, and the conservation soil value is 1.393 billion Yuan, it can be seen that the value of ecosystem services is large and sustainable.

b) The assessment method and indicator system of forest ecosystem services are not uniform. In terms of research methods and index system selection for forest ecosystem services evaluation, most domestic scholars directly use existing research results from abroad, lacking a framework for regional forest ecosystem services evaluation in a general sense, which makes the results of the research lack of comparability and evaluation results. There is also doubt.

c) There is a duplication of evaluation service content. The understanding of forest resource value accounting theory is not in place, and the differences between forest ecosystem services and resources themselves cannot be distinguished. Instead, the values of all forms of resources are considered as the value of forest resources and evaluated.

d) Research on multidisciplinary ecosystem services evaluation. Research includes not only disciplines such as ecology and forestry but also many disciplines such as sociology, economics, and management. Among them, ecology and forestry disciplines are the basis for the evaluation of ecosystem services, and economics is the main research method. Therefore, in addition to closely integrating the theoretical and methodological systems of various disciplines, the research should also be adapted to the social, economic, and cultural development stages of the time and actively provide strategic support for forest ecosystem management.

e) Previous studies have shown that the indirect use value of forest ecosystems is much higher than the direct use value. For example, Lu Chunxia et al. [28] evaluated the ecosystem services of the Qinghai-Tibet Plateau, and the results showed the economic value and ecosystem service value of the forest products. The ratio is 1:70; Xu Xinwang et al. [29-30] evaluated the value of forest ecosystem services in Anhui Province, and the results showed that ecological, economic and social benefits accounted for 74.13%, 19.67% and 6.20% of the total value of ecosystem services. However, the benefits of the forest ecosystem services of the Jilin Forest Industry Group under study have not been fully utilized. For example, the conservation water source value accounted for 6.14% of the total service value; the biodiversity conservation value accounted for 4.19%; the farmland/grassland protection value accounted for 3.67%; the value of soil conservation only accounts for 2.50%. Except for the low fertilizer and carbon sequestration prices in the region in 2013, it mainly reflects the serious degradation of forest/grassland and other ecological resources in the region, which leads to soil erosion and species reduction. And problems such as reduced quality. Therefore, we should increase natural resource protection, soil erosion control and farmland protection, continue to implement measures such as grazing bans and grazing bans, vigorously cultivate plantations, establish long-term protection mechanisms, and achieve dynamic balance between people, livestock and natural resources; Constructing facilities such as intercepting ditch in areas with serious soil erosion, actively transforming and improving sloping farmland and farmland shelterbelt in agricultural areas, establishing a system for investigating the responsibility of cultivated land protection, improving the compensation mechanism for land acquisition, and continuing to implement orderly returning farmland to land that is not suitable for cultivation. The quality of cultivated land. Without destroying the existing forest ecosystem, Jilin Forest Industry Group can rely on the advantages of forest resources to accelerate the development of the tertiary industry. For example, it can increase the development of understory farming and aquaculture and increase the development of forest by-products. We will actively build projects such as forest tourism resorts.

ACKNOWLEDGEMENT

Funding. This work was supported by the Social Science Planning Fund Project of Liaoning Province [grant number L17CGL008]; the Research Project on Economic and Social Development of Liaoning Province (grant number 2020lslktjdyb-030); and the Fund for Post-doctoral Research of Shenyang Agricultural University [grant number 770218007].

Highlights. •Concept and content of forest ecosystem service flow and forest ecosystem service function stock were confusing.

• In the Hypothesis for Different kinds of ecosystem service, evaluation of ecosystem service value exists repetitive accumulation and synergic function issues.

•Results show that different types of ecosystem services evaluation has repetitive problems.

REFERENCES

[1] Xiao-Liang, S., Ying, Z., Wei-Na, D. (2014) Empirical Analysis about Carbon Tariffs on the Influence of the Export Enterprises of China's National Economy Based on the Application of Input-output Model. Shanghai Economic Review. (10), 37-47.

[2] Zhao, J.-L., Wang, L.-X., Han, H.-R., Kang, F.-F., Zhang, Y.-L. (2013) Research Advances and Trends in Forest Ecosystem Services Value Evaluation. Chinese Journal of Ecology. 32(8), 2229-2237.

[3] Xiao-liang, S., Ke, C. (2015)Accounting Economic Value of Forest Water Conservation in Jilin Province. Bulletin of Soil and Water Conservation. 35(5), 169-172.

[4] Omer, G., Mutanga, O., Abdel-Rahman, E.M., Adam, E. (2015) Performance of Support Vector Machines and Artificial Neural Network for Mapping Endangered Tree Species Using WorldView-2 Data in Dukuduku Forest, South Africa[J]. IEEE Journal of Selected Topics in Applied Earth Observations & Remote Sensing. 8(10), 4825-4840.

[5] Xiao-Liang, S., Ying, Z. (2014) Research on Forest Ecosystem Management Applications Based on the Space-time Range of Variability [J]. China Forestry Science and Technology. 28(6), 10-14.
[6] Chen, J., Low, K.H., Yao, Y., Jaillet, P. (2015) Gaussian Process Decentralized Data Fusion and Active Sensing for Spatiotemporal Traffic Modeling and Prediction in Mobility-on-Demand Systems. IEEE Transactions on Automation Science and Engineering. 12(3), 901-921.
[7] Bright, B.C., Hudak, A.T., Kennedy, R.E., Meddens, A.J.H. (2014) Landsat Time Series and Lidar as Predictors of Live and Dead Basal Area Across Five Bark Beetle-Affected Forests[J]. IEEE Journal of Selected Topics in Applied Earth Observations & Remote Sensing. 7(8), 3440-3452.
[8] Turner, R.K., Morse-jones, S., Fisher, B. (2010) Ecosystem Valuation. Annals of the New York Academy of Sciences. 1185(1), 79-101.
[9] Bernard, F., Groot, R.S.D., José Joaquín, C. (2009) Valuation of Tropical Forest Services and Mechanisms to Finance Their Conservation and Sustainable Use: A Case Study of Tapantí National Park, Costa Rica. Forest Policy & Economics. 11(3), 174-183.
[10] Xiao-Liang, S., Ying, Z., Yong-Juan, S., Wei-Na, D. (2015) Study on Water Conservation Function of Typical Forest Vegetation in Yunnan Plateau[J]. Resources & Environment in the Yangtze Basin. 24(8), 1366-1372.
[11] Costanza, R., D'Arge, R., De Groot, R., Faberk, S., Grasso, M., Hannon, B., Limburg. Karin E., Naeem, S., O 'neill, Robert V., Paruelo, José., Raskin, Robert G., Sutton, Paul C., Belt, Marjan van den. (1997) The Value of the World's Ecosystem Services and Natural Capital[J]. World Environment. 387(6630),253-260.
[12] MA. (2003) Ecosystems and Human Well-being: A Framework for Assessment. Washington DC: American island Press. 14-21.
[13] State Forestry Bureau. (2008) Forestry Industry Standards of the People's Republic of China LY/T1721—2008: Specifications for Assessment of Forest Ecosystem Services in China-Beijing: China Standards Press.
[14] Naeem, S. (2001) How Changes in Biodiversity may Affect the Provision of Ecosystem Services//Hollowell VC, ed. Managing Human Dominated Ecosystems. St. Louis: Missouri Botanical Garden Press. 3-33.
[15] Loomes,R., O'Neill,k. (2000) Nature's Services: Societal Dependence on Natural Ecosystems. Pacific Conservation Biology. 6(2), 220-221.
[16] Tobias, D., Mendelsohn, R. (1991) Valuing Ecotourism in a Tropical Rain-forest Reserve. Ambio. 20(2), 91-93.
[17] Westman, W.E. (1977) How Much Are Nature's Services Worth? Science. 197(4307), 960-964.
[18] Wen-Jing, P., Shun-Bo, Y., Ying, F. (2014) Recreational Value Assessment by TCIA and CVM—A Case Study of Taibai Mountain National Forest Park. Economic Geography. 34(9), 186-192.
[19] Zheng, H., Li, Y.-F., Ouyang, Z.-Y., Luo, Y.-C. (2013) Progress and Perspectives of Ecosystem Services Management. Acta Ecologica Sinica. 33(3), 702-710.
[20] Xiao-Liang, S., Ke, C., Chen-Xi, L. (2015) Value Evaluation of Forest Carbon Sinks Services in China. Journal of Central South University of Forestry & Technology (Social Sciences). 9(5), 27-33.
[21] Hong-Mei, L., Xi-Jun, H., Xiao-Yan, A. (2014) Tourist's Spatial Image Cognition in the Urban Forest Park-Case Study of Hunan Forest Botanical Garden. Economic Geography. 34(10), 171-176.
[22] Xiao-Liang, S., Ying, Z. (2015) Review of Forest Water Conservation. Resource Development & Market. 31(3), 332-336.
[23] Asah, S.T., Blahna, D.J., Ryan, C.M. (2012) Involving Forest Communities in Identifying and Constructing Ecosystem Services: Millennium Assessment and Place Specificity. Journal of Forestry. 110(3), 149-156.
[24] Jin, S.I., Peng, H., Chun-Long, Z. (2011) Review of Water Conservation Value Evaluation Methods of Forest and Case Study. Journal of Natural Resources. 26(12), 2100-2109.
[25] Xiao-Liang, S. (2015) Study on Evaluation and Predictive of Forest Ecosystem Service Values for Jilin Forest Industry Group. Beijing: Beijing Forestry University.
[26] Awkerman, J.A., Marshall, M.R., Williams, A.B., Gale, G.A., Cooper, R.J., Raimondo, S. (2011) Assessment of Indirect Pesticide Effects on Worm-eating Warbler Populations in a Managed Forest Ecosystem. Environmental Toxicology & Chemistry. 30(8), 1843-1851.
[27] Xiao-liang, S., Ying, Z., Zheng-wei, H. (2014) Review of Forest Carbon Sink Measurement Methods-Based on Choice of Beijing. Forestry Economics. 36(11), 44-49.
[28] Chun-Xia, L., Gao-Di, X., Yu, X., Yun-Jiang, Y. (2004) Ecosystem Diversity and Economic Valuation of Qinghai-Tibet Plateau. Acta Ecologica Sinica. 24(12), 2749-2755.
[29] X, X.-W. (2005) Value of Forest Eco-system Services in Anhui Province. Resource Development and Market. 21(2), 96-98.

[30] Gallai, N., Salles, J.M., Settele, J., Vaissière, B.E.(2009) Economic Valuation of the Vulnerability of World Agriculture Confronted with Pollinator Decline. Ecological Economics.

Received: **27.05.2019**
Accepted: **09.11.2019**

CORRESPONDING AUTHOR

Lyu Jie
College of Economics and Management,
Shenyang Agricultural University,
Shenyang 110866 – China

e-mail: jieluesy@syau.edu.cn

© by PSP Volume 29 – No. 05/2020 pages 3505-3516 Fresenius Environmental Bulletin

FUNGAL ENDOPHYTES IN TURFGRASS AREAS IN TURKEY

Filiz Unal*

The Plant Protection Central Research Institute, Ministry Of Agriculture And Forestry, Ankara, Turkey

ABSTRACT

Fungal endophytes are epiphytic or systemic microorganisms living on plant tissues during part or all of their life cycles without causing harm to their hosts. They have been described as mutualists that enhance their host resistance against abiotic stresses, diseases, insects and mammalian herbivores by producing a broad range of fungal metabolites. Recently, these organisms have attracted extensive attention of the scientist due to their potential properties in biological control of diseases and pests. In this study, endophytic fungi were isolated from 122 turfgrass plants belonging to 7 different turfgrass species at 8 different provinces in Turkey. The ITS1-5.8S-ITS2 regions of each isolate were amplified, sequenced and performed BLAST analyzes. 419 fungal isolates were classified into 40 genera in accordance with the rDNA-ITS sequences analysis. It was determined that endophytic fungi in turfgrass areas belong to a wide variety of species and most of these species were from phylum Ascomycota.

KEYWORDS:
Fungi, endophytes, ITS sequence, turfgrass

INTRODUCTION

There are a large number of fungi species living as endophytic in grasses in nature [1]. These species can colonize grass tissues without causing apparent harm. Fungal endophytes are being recognized for their potential role as biological control agents and as metabolite sources of medical and agricultural importance [2, 3, 4]. Interest in endophyte research increased with the discovery of the clavicipitaceous (*Clavicipitaceae, Hypocreales*) endophytes of cool-season grasses, which produce toxic alkaloids associated with livestock toxicoses and increased tolerance to insect pests [5, 6, 7]. *Epichloe* spp. (formerly *Neotyphodium*) are the most popular systemic endophytes among the clavicipitaceous fungi. Dominant non-systemic endophytes of gramineae are generally familiar epiphytes, such as *Alternaria alternata*, *Cladosporium* species and *Epicoccum purpurascens*. *Alternaria alternata*, *Arthrinium* species, *Cladosporium tenuissimum*, and *Epicoccum purpurascens* are the dominant endophytes of rice (*Oryza sativa*) and maize (*Zea mays*) [8, 9]. Detrimental effects of grass endophytes on fungal pathogens have also been demonstrated. For example, isolates of *Acremonium lolii*, *A. coenophialum, Trichoderma* spp. and *Gliocladium* spp. showed antibiosis against a range of fungal plant pathogens in culture [10, 11, 12, 13, 14, 15, 16, 17]. Fungal endophyte species are took part in various classes including Dothideomycetes, Sordariomycetes, Leotiomycetes, Eurotiomycetes, and Pezizomycetes [18]. Common endophytes in grasslands are located in Pleosporales, Agaricales, Sordariales orders [19].

Endophytes may also produce secondary metabolites that directly inhibit insects or pathogens, or produce elicitors that stimulate the plant to produce secondary metabolites. For example, *Lecanicillium* spp. and *Trichoderma* spp. are both mycoparasites and insect parasites, although they also produce inhibitory metabolites [20, 21]. Some *Chatemium*, *Myrothecium, Phoma, Mortierella, Epicoccum, Sordaria* fungal species ae also used as biologic control agents in agriculture. *Chaetomium* spp. are common colonizer of soil and cellulose-containing substrates and have been reported to be a potential biocontrol agent. They are effective against seed rot and damping off caused by several seed and soil-borne plant pathogens like *Pythium ultimum*, *Alternaria raphani*, *A. brassicicola* and *Fusarium* spp. [22, 23, 24]. *C. globosum* is antagonistic to the rice blast pathogen (*Pyricularia oryzae*) [25], spot blotch of wheat caused by *Cochliobolus sativus* [26], *Ascochyta* blight of chick pea [27]. Biochemical characterization of the fungus has shown the production of xylanase and β 1,3-glucanase [28]. Besides hydrolytic enzymes, *Chaetomium* spp. are also known to produce various metabolites such as chaetomin, chaetoglobosin and BHT [29, 30] having antifungal properties against phytopathogenic fungi and nematodes [31]. It has been known that approximately 8 *Myrothecium* species, including *M. gramineum, M. roridum,* and *M. verrucarium*, have been reported worldwide. These species effectively use to control many weeds under field conditions and shows potential as an effective

bioherbicide for weed control in crop production systems [32, 33]. *Phoma* spp. has the potential as a biological control agent of weeds; for example, *Phoma herbarum* and *Phoma exigua* are effective on *Taraxacum officinale* in turfgrass [34] and *P. sorghina* is effective on poke weed [35, 36, 37]. Powder formulation of *P. herbarum* has been developed and has the potential as a biological control agent of *Eleusine indica* (goose grass) in the world. *Phoma macrostoma* is a bioherbicide being developed for selective weed control in turfgrass [38, 39]. *Sordaria* spp. have an antagonistic effect on *Armillaria mellea, Pythium aphanidermatum, Rosellinia necatrix*. *Pestalotiopsis guepinii*, *Colletotrichum capsici*, *Curvularia lunata*, *Alternaria alternata, Fusarium oxysporum* and *Lasiodiplodia theobromae* [40]. *Mortierella* spp. are saprophyte and is known to produce extracellular hydrolases such as chitinases [41]. Some *Mortierella* species demonstrated their potential as biocontrol agents of phytopathogens such as pathogenic oomycetes, *Streptomyces* spp., *Verticillium dahlia* and some insects [42, 43, 44, 45]. Some *Pestalotiopsis* species cause disease in a variety of plants, are commonly isolated as endophytes and saprophytes. Some species have both endophytic and pathogenic stages in their life cycle. At the same time, "pestaloside" compounds that some pestaliopsis species produced, cause they compete with other fungi by showing antifungal activity [46]. *Saccharomyces cerevisiae* is a yeast used as a biologic control against various pathogens in agriculture, aside from its useful features with regard to food technology.

The aim of this study was to make isolation and identification of fungal endophytes from turfgrass areas in Turkey.

MATERIALS AND METHODS

Plant collection and isolation. Survey was conducted in the largest turfgrass areas from 8 provinces (Istanbul, Antalya, Ankara, Izmir, Kayseri, Bursa, Aydın and Muğla) in Turkey in 2015. A total of 122 healthy plants (28, 22, 16, 10, 15, 13, 8 and 10 respectively) which do not show any signs of disease collected. Size of the sampling areas were determined to represent total turfgrass areas of the provinces. Healthy turfgrass sampless were collected from 0-5000 m^2, 5 000-15 000 m^2, 15 000 m^2-30 000 m^2, 30 000-60 000 m^2 and >60 000 m^2 areas from 2, 3, 5, 8 and 10 different points respectively. In the samples, 10 to 15 plant roots and green parts were taken in each sample and brought to the laboratory.

Leaf, crown and root segments (3 to 5 mm) of turfgrass were surface disinfested in 0.5% sodium hypochlorite (NaOCl) solution (1 min), rinsed three times with sterile distilled water, dried on sterile filter paper prior to plating onto Difco Potato Dextrose Agar (PDA) containing 50 mg/L of streptomycin and incubated 7-10 days.

Moleculer Identifications of Agents: Fungal DNA isolation was performed using the Qiagen DNeasy Plant Mini Kit, as specified by the manufacturer. The PCR reaction mixture and conditions were made according to [47]. DNA amplification was performed using the following optimized cycles with Techne TC-5000 thermal cycler. Primers ITS-1 (5 'TCC GTA GGT GAA CCT GCGG 3') and ITS-4 (5 'TCC TCC GCT TAT TGA TATGC 3') were used for amplification of ITS regions [48]. The polymerase chain reaction (PCR) was performed in a 50 µl reaction mixture containing 1 µl template DNA, 1 µl forward primer (10mM), 1 µl reverse primer (10mM), 5 µl reaction buffer (10x), 4 µl dNTP (each 2.5mM), 0.5 µl Taq DNA Polymerase (5 U/ µl), and 37.5 µl sterile doubledistilled water. The PCR cycling protocol consisted of initial denaturation at 94 ºC for 4 min, followed by 30 cycles of 94 ºC for 45 s, 55 ºC for 45 s, and 72 ºC for 2 min, and a final elongation step of 72 ºC for 10 min. As a negative control, the template DNA was replaced by sterile double-distilled water. The PCR products were checked using agarose gel electrophoresis and then sent for sequencing to GENOKS Gene Research and Biotechnology Company, Ankara, Turkey). The nucleotide sequences were subjected to Basic Alignment Search Tool (BLAST) analysis (http://www.ncbi.nlm.nih.gov) and compared to other sequences in GenBank.

Pathogenicity Tests: Pathogenicity tests were performed with both root and leaf inoculation grown in pots using turfgrass seeds mixture containing four cultivars (cv. *Festuca rubra*, *Lolium perenne*, *Poa pratensis* and *Festuca arundinacea*) in greenhouse conditions at 23 ± 2 ºC with a 12-h photoperiod and 50–60% RH. For root inoculations, inoculums were prepared on the moistened sterile bran in bottles The soil used in pot experiments was prepared in the form of a mixture of 2: 1: 1 garden soil: stream sand: burnt stall. Soil was sterilized three times in an autoclave at 121 ºC for 45 min on two consecutive days. Fungi-colonized bran was placed in the middle of the soil layer. Control consisted of pots without inoculum. All pots were covered with clear polyethylene and incubated for 5 days. There were six replicate pots for each treatment. After 5 days, 15 seeds of turfgrass were placed on the soil surface, covered with 10 cm^3 of steril natural topsoil, and watered with 10 ml of distilled water. After 3 weeks, the plants were washed free of soil [49].

For leaf inoculation, cultures were incubated under alternating cycles of 12 h of light and 12 h of darkness for at least 10 days. Conidia were

harvested into sterile destilled water with a sterile spatula, and suspensions were filtered through sterile cheesecloth to remove hyphal fragments. The conidia suspensions were adjusted with thoma lamella to a concentration of 1×10^5 spores per ml with 0.1% Tween 20 added for leaf inoculations. Fungi suspensions were sprayed onto the leaves of turfgrass plants that had been planted previously. The pots were covered with plastic bags for three days [50].

RESULTS AND DISCUSSION

A total of 122 healthy plants were collected from golf courses, stadiums and recreation areas in the largest turfgrass areas from 8 provinces in Turkey. As a result of isolation studies, 419 endophytic fungal isolates from 93 different species were obtained from Dothideomycetes, Sordariomycetes, Mortierellomycetes, Mucoromycetes, Eurotiomycetes, Leotiomycetes, Agaricomycetes, Saccharomycetes classes (Table 1, Figure 1). Molecular studies were conducted according to ITS 1 and ITS 4 regions of isolates. To conclude of the molecular identification studies, species showed 98-100% similarity with the isolates belonging to the same species in NCBI. According to frequency of isolates, the most common genus was *Phoma* (56 isolates) which is followed by *Trichoderma* (50 isolates) and *Epicoccum* (38 isolates) respectively. On the other hand, the most encountered species was *Phoma herbarum* with 34 isolates, which is followed by *Epicoccum nigrum* (30 isolates) and *Trichoderma harzianum* (23 isolate). In terms of plant parts, *A. gaisen, A. rosae, A. sesami, S. bicolor, A. kogelbergense* and *G. fructicola* were isolated from only leaves*, A. citri, C. bulbillosum, Trichurus terrophilus*, *D. macaronesica, D. concentrica, R. maritima, Peniophora* sp. *Sistotrema* sp.*, Lentinus* sp. were isolated from only root and the others were isolated from all two or three parts of the root, root crown and leaf (Table 1).

TABLE 1
The endophytic fungi in Turfgrass areas in Turkey

Class and Family	Species	Number of isolate	Isolation Source	*Origin	**Turfgrass Composition
	Alternaria alternata	21	Leaf, Root, root crown	Ant., Ank., İz., Ky., Bu., Mu.	Pt, Pp, C, Fa, L, Frr, Frc, ,
	A. abundans	2	Leaf, Root, root crown	Ank.	Frr, L, Pp, Frc
	A. burnsii	1	Root crown	Mu.	Fa, L, Frr, Frc, Pp,
	A. citri	1	Root	Mu.	Fa, L, Frr, Frc, Pp
	A. gaisen	1	leaf	İs.	Fa, L, Frr, Frc, Pp
	A. infectoria	3	Leaf, root	Ky., Ank.	Frr, L, Pp, Frc
Dothideomycetes Pleosporaceae	*A. rosae*	2	leaf	Ky.	Frr, L, Pp, Frc
	A. sesami	2	leaf	İs., Ant.	Fa, L, Frr, Frc, Pp, Pt, C
	Epicoccum nigrum	30	Root, root crown, leaf	İs., Ant., Ank., Ky., Bu, İz, Mu.	Fa, L, Frr, Frc, Pp, Pt, C
Dothideomycetes Didymellaceae	*E. sorghinum*	8	Root, leaf	Mu.	Fa, L, Frr, Frc, Pp
	Neoascochyta desmazieri	1	leaf	Ky.	Frr, L, Pp, Frc
	Phoma herbarum	34	Root, root crown, leaf	İs., Ant., Ank., İz., Ky., Bu., Ay., Mu.	Fa, L, Frr, Frc, Pp, Pt, C
	P. exigua	9	Root, root crown, leaf	Ank., Ky, Bu., Mu.	Fa, L, Frr, Frc, Pp, Pt
	P. glomerata	7	Root, root crown, leaf	İs., Ant., Ank., İz., Ky., Bu.	Fa, L, Frr, Frc, Pp, Pt, C
Dothideomycetes Pleosporomycetidae	*P. plurivora*	2	Root, root crown	Bu., Mu.	Fa, L, Frr, Frc, Pp
	P. cladoniicola	2	Root, root crown	Ank., Mu.	Fa, L, Frr, Frc, Pp
	P. macrostoma	2	Root, root crown	İs., Ant.	Fa, L, Frr, Frc, Pp, Pt, C
Dothideomycetes Lophiostomataceae	*Saccharicola bicolor*	5	Leaf	Bu., Ant., İz., Mu.	Frr, Frc, L, Pp, Fa, C
Dothideomycetes Cladosporiaceae	*Cladosporium perangustum*	2	Leaf	İs.	Fa, L, Fr, Pp
Sordariomycetes Sordariaceae	*Apodus oryzae*	3	Root, root crown	Ant.	Pt, C, L
	Arthrinium arundinis	3	Root, root crown	Mu., Ky.	Fa, L, Frr, Frc, Pp
Sordariomycetes Apiosporaceae	*A. kogelbergense*	1	Leaf	İs.	Fa, L, Frr, Frc, Pp
	A. sacchari	1	Root crown	Ky.	Frr, L, Pp, Frc
	Chaetomium globosum	2	Root, root crown	Ant., Bu.	Fa, L, Frr, Frc, Pp, Pt, C
Sordariomycetes Chaetomiaceae	*C. bostrychodes*	2	Root, root crown	Ant., İz.	Pt, C, Fa, L, Frr, Pp
	Pestalotiopsis clavispora	7	Root, root crown	İs., Ant., Ank. Ay., Mu.	Fa, L, Frr, Frc, Pp, Pt, C
Sordariomycetes					

Class and Family	Species	Number of isolate	Isolation Source	*Origin	**Turfgrass Composition
Sporocadaceae	*P. neglecta*	1	Root, root crown	Ant.	L, Pt, C
	P. hollandica	1	Root, root crown	İs.	L, Pp,
	P. sydowiana	1	Root, root crown	İs.	L, Pp,
Sordariomycetes Lasiosphaeriaceae	*Cladorrhinum bulbillosum*	1	Root	Ant.	L, Pt, C
Sordariomycetes Bionectriaceae	*Clonostachys rosea*	14	Root, root crown	İs., Ant, Ank., İz., Ky., Bu., Mu.	Fa, L, Frr, Frc, Pp, Pt, C
	C. rosea f. catenulata	1	Root, root crown	Bu.	Frr, L, Pp, Fa
Sordariomycetes Nectriaceae	*Corallomycetella repens*	2	Root, leaf	İs., Ky.	Fa, L, Frr, Frc, Pp
Sordariomycetes Gnomoniaceae	*Gnomoniopsis fructicola*	1	leaf	Ky.	Frr, L, Pp, Frc
Sordariomycetes Nectriaceae	*Fusarium oxysporium*	15	Root, root crown, leaf	İs., Ant., Ank., İz., Ky., Bu., Ay., Mu.	Fa, L, Frr, Frc, Pp, Pt, C
	F. solani	12	Root, root crown, leaf	İs., Ant., Ank., İz., Ky., Bu., Ay., Mu.	Fa, L, Frr, Frc, Pp, Pt, C
Sordariomycetes Stachybotryaceae	*Myrothecium verrucaria*	19	Root, root crown, leaf	İs., Ant., Ank., İz., Ky., Bu., Ay., Mu.	Fa, L, Frr, Frc, Pp, Pt, C
	M. roridum	1	Root	İs.	L, Pp,
Sordariomycetes Sarocladiaceae	*Sarocladium strictum* (=*Acremonium strictum*)	6	Root, root crown, leaf	İs., Ky., Mu., Bu.	Fa, L, Frr, Frc, Pp, C, Pt
	Sordaria fimicola,	5	Root, root crown	İz., Ky., Ay., Mu.	Fa, L, Frr, Frc, Pp, Pt, C
	S. macrospora	3	Root, root crown	İs., Bu., Ay., Mu.	Fa, L, Frr, Frc, Pp, Pt, C
	S. superba	2	Root, root crown	İs., Ant.	Fa, L, Frr, Frc, Pp, Pt, C
Sordariomycetes Stachybotryaceae	*Stachybotrys elegans*	2	Root, root crown	Mu., İz.	Fa, L, Frr, Frc, Pp, C
Sordariomycetes Hypocreaceae	*Trichoderma asperellum*	2	Root, root crown	Ant. Ank.	Pt, C, Fa, L, Frr, Frc., Pp
	T. atroviride	3	Root, root crown	İs., Ant., Ank.	Fa, L, Frr, Frc, Pp, Pt, C
	T. gamsii	5	Root, root crown	Ank., İz., Ky.	Pt, C, Fa, L, Frr, Frc, Pp
	T. hamatum,	10	Root, root crown	İs., Ant., Ank., Ky., Bu., Mu.	Fa, L, Frr, Frc, Pp, Pt, C
	T. harzianum	23	Root, root crown, leaf	İs., Ant., Ank., İz., Ky., Bu., Ay., Mu.	Fa, L, Frr, Frc, Pp, Pt, C
	T. rossicum	3	Root	İs., Ant., Ank.	Fa, L, Frr, Frc, Pp, Pt, C
	T. samuelsii	2	Root, root crown	İs., Ant.	Fa, L, Frr, Frc, Pp, Pt, C
	T. spirale	2	Root, leaf	Ant.	Fa, L, Frr, Frc, Pp, Pt, C
Sordariomycetes Microascaceae	*Trichurus terrophilus*	1	Root	Ant.	Fa, L, Frr, Pp
Sordariomycetes Hypoxylaceae	*Daldinia macaronesica*	1	Root	İs.	Fa, L, Frr, Frc, Pp
	Daldinia concentrica	1	Root	İs.	Fa, L, Frr, Frc, Pp

Class and Family	Species	Number of isolate	Isolation Source	*Origin	**Turfgrass Composition
Mortierellomycetes Mortierellaceae	*Mortierella alphina*	15	Root, root crown	İs., Ant., Ank., Bu., Ay., Mu.	Fa, L, Frr, Frc, Pp, Pt, C
	M. gamsii	5	Root, root crown	İs., Ant., Bu.	Fa, L, Frr, Frc, Pp, Pt, C
	M. minutissima	2	Root, root crown	Ant., Mu.	Fa, L, Frr, Frc, Pp, Pt, C
	M. zychae	10	Root, root crown	İs., Ant., Ank., Ky., Bu.,	Fa, L, Frr, Frc, Pp, Pt, C
	M. elongata	2	Root, root crown	Ant., Mu.	Fa, L, Frr, Frc, Pp, Pt, C
Mucoromycetes Mucoraceae	*Mucor luteus*	1	Root, root crown	İz.	L, Pp, Fa, C
	M. hiemalis	2	Root, root crown	Ank., Mu	Frr, L, Pp, Frc
	M. irregularis	1	Root, root crown	Ant.	Pt, C, Fa, L, Frr, Pp
	M. nidicola	2	Root, root crown	Ank.	Frr, L, Pp, Frc
Eurotiomycetes Aspergillaceae	*Penicillium chrysogenum*	3	Root, root crown	İs., Ant., Ank.,	Fa, L, Frr, Frc, Pp, Pt, C
	Penicillium javanicum fsp *meloforme*	1	Root	Ant.	L, Pt, C
	P. commune	5	Root, root crown	Ant., Ank. Bu., Mu.	Fa, L, Frr, Frc, Pp, Pt, C
	P. crustosum	2	Root, root crown	İs, Mu.	Fa, L, Frr, Frc, Pp
Eurotiomycetes Aspergillaceae	*Aspergillus niger*	8	Root, root crown	İs., Ant., Ank., Ay., Mu.	Fa, L, Frr, Frc, Pp, Pt, C
	A. ochraceoroseus	4	Root, root crown	Ant., Ank., İz.	Fa, L, Frr, Frc, Pp, Pt, C
	A. peyronelii	2	Root, root crown	Ank., Bu.	Fa, L, Frr, Frc, Pp, Pt, C
	A. sydowii	1	Root, root crown	İs.,	Fa, L, Frr, Frc, Pp, Pt, C
Leotiomycetes Rutstroemiaceae	*Rutstroemia maritima*	1	Root	Ank.	Frr, L, Pp, Frc
Leotiomycetes Phacidiaceae	*Phacidium lauri*	1	Root	Ank.	Frr, L, Pp, Frc
Agaricomycetes Peniophoraceae	*Peniophora* sp.	1	Root	Ant.	Pt, C, Fa, L, Frr, Pp
Agaricomycetes Hydnaceae	*Sistotrema* sp.	1	Root	Mu.	Fa, L, Frr, Frc, Pp
Agaricomycetes Polyporaceae	*Lentinus* sp.	1	Root	Ank.	Frr, L, Pp, Frc
Agaricomycetes Omphalotaceae	*Marasmiellus pumivorus*	4	Root, root crown	Ant., Mu., İz.,	Pt, C, Fa, L, Frr, Frc, Pp
Agaricomycetes Tricholomataceae	*Collybia fussipes*	2	- (Mushroom)	Ky.	Frr, L, Pp, Frc, Fa
Agaricomycetes Marasmiaceae	*Marasmius oreades*	3	Root	İs., Ky.	Fa, L, Frr, Frc, Pp, Pt, C
Agaricomycetes Psathyrellaceae	*Coprinopsis atramenteria*	2	- (Mushroom)	İz., Ank.	Pt, C, Fa, L, Frr, Pp
Agaricomycetes Strophariaceae	*Agrocybe aegerita*	2	- (Mushroom)	İz.	L, Pp, Fa, C
Agaricomycetes Agaricaceae	*Agaricus subrifescens*	1	- (Mushroom)	İz.	L, Pp, Fa, C
	Leucoagaricus naucinus	2	- (Mushroom)	İz.	Frr, L, Pp, Frc, Fa, C
	L. leucothides	2	- (Mushroom)	İz.	Frr, L, Pp, Frc, Fa, C

Class and Family	Species	Number of isolate	Isolation Source	*Origin	**Turfgrass Composition
	Rhizoctonia solani AG 7	2	Root, root crown	İz., Ant.	Fa, L, Frr, Frc, Pp, Pt, C
Agaricomycetes Ceratobasidiaceae	*Rhizoctonia* AG A	7	Root, root crown	İs., Ant., Ank., İz., Ky., Bu., Ay., Mu.	Fa, L, Frr, Frc, Pp, Pt, C
	Rhizoctonia AG B(o)	3			
	Rhizoctonia AG F	4			
	Rhizoctonia AG E	5			
	Rhizoctonia AG G	3			
	Rhizoctonia AG I	5			
	Rhizoctonia AG K	6			
Saccharomycetes Saccharomycetaceae	*Saccharomyces cerevisiae*	2	Root, root crown	İz., İs.	Fa, L, Frr, Frc, Pp, C

*İs.: İstanbul; Ant.: Antalya; Ank.: Ankara; İz.: İzmir; Ky.: Kayseri; Bu.: Bursa; Ay.: Aydın; Mu.: Muğla.
**C: *Cynodon dactylon*; Fa: *Festuca arundinacea*; Fr: *Festuca rubra*; Frr: *Festuca rubra-rubra*; Frc: *Festuca rubra-commutata*, L: *Lolium perenne*; Pp: *Poa pratensis*; Pt: *Poa trivialis.*

FIGURE 1
Some of the isolated endophytic fungi in this study on PDA, (a) *Chaetomium globosum* (b) *Epicoccum nigrum* (c) *Mucor nidicola* (d) *Sordaria fimicola*, (e) *Phoma herbarum*, (f) *Mortierella gamsii,* (g) *Myrothecium verrucaria*, (h) *Clonostachys rosea f. catenulata,* (i) *Apodus oryzae,* (j) *Rhizoctonia* AG G, (k) *Pestaliopsis clavispora,* (l) *Phacidium lauri*

In the pathogenicity assays, carried out with both the spraying and the soil inoculation methods in greenhouse conditions. None of the isolates showed any symptoms in turfgrass plants.

The second most seen *Trichoderma* genus in this study has the most commonly used species in biological control and lives in many soils and plants worldwide. The genus contains members that are plant growth promoters that act through a variety of mechanisms. *Trichoderma* species produce several lytic enzymes and antibiotics against plant pathogens, and several products made from these fungi have been commercially marketed as biopesticides, biofertilizers and soil amendments. *Trichoderma virens* is one of the well-studied species, which exhibits mycoparasitic characteristics and the ability to produce several potent epithiodiketopiperazine antibiotics that inhibit oomycetes such as *Pythium* and *Phytophthora* species. It also produces a mixture of peptaibols, which are linear peptide antibiotics that might affect certain bacteria and fungi. Some strains of *T. asperellum* and *T. harzianum* are capable of activating plant defense responses. Some strains of *Trichoderma* also have been shown to suppress a lot of important plant pathogens including

Fusarium spp, *Rhizoctonia* spp., *Pythium* spp. *Phytophthora* spp, *Colletotrichum* sp., *Rhizopus stolonifer*, *Botrytis cinerea*, *Penicillium expansum, Meloidogyne* spp., *Globodera* spp. [11, 13, 14, 15, 16, 17].

Another popular fungal genera that was isolated in our study as a potential biological control agent is *Gliocladium* species especially *G. roseum,* and they have many commercial products around the world. *Gliocladium* species have been used as biocontrol agents against various foliar, soilborne and postharvest diseases and nematodes [12, 51]. *Clonostachys rosea* f. *catenulate* (syn. *Gliocladium catenulatum*) is a mycoparasite capable of antagonizing a range of fungal plant pathogens, such as *Sclerotinia sclerotiorum*, *Rhizoctonia solani*, *Fusarium* spp., *Pythium* spp., *Botrytis* sp. [52, 53, 54, 55]. The other popular species, *Stachybotrys elegans*, effectively suppress the development of *Rhizoctonia solani* as a mycoparasite [56].

Recent researches have also revealed other promising biologic agents that could be used in the control against disease and pests in the ecosystem. For example, some studies have been performed in the world suggest that some *Myrothecium* species may serve as broad-spectrum bioherbicides [33, 57]. *Myrothecium* species, mainly *M. verrucaria* has been studied as a potential biocontrol agent for control of invasive climbing fern (*Lygodium microphyllum*), dandelion (*Taraxacum officinale*) [58], kudzu [32, 59] and amaranth weeds including *Amaranthus hybridus*, *A. spinosus* and *A. lividus* [60] on the basis of their pathogenicity to hosts. At the same time, *M. roridum* has been reported to produce toxins in culture medium. These toxins have been shown to have a potential antibiotic effect against a wide range of clinical and environmental bacteria and fungi such as: *Bacillus subtilis, Clavibacter michiganensis* pv. *Michiganesis, Botrytis cinerea, Colleotricum acutatum, Colleotricum demantium, Rosellinia necatrix, Sclerotia sclerotiorum, Diaporthe nomurai* and *Cochliobolus miyabeanus* [61, 62]. It is necessary to determine the effects of *Myrothecium s*pecies against weeds and plant pathogens in Turkey.

In this study, *Chatemium* and *Mortierella* species that their insecticidal effects were proven with studies conducted in the world were also obtained. It is necessary to determine whether they may be used in the struggle against insects which have caused economic damage to our country. Insecticidal investigations have showed that *Mortierella alpina* and *M. signyensis* caused significant mortality in waxmoth (*Galleria mellonella*) and housefly (*Musca domestica*), larvae via injection and soil inoculation, and *M. alpina* caused significant mortality in housefly larvae via baiting. An isolate of the fungus *Chaetomium globosum* produced culture broths that inhibited in vitro egg hatch and juvenile mobility of root-knot nematode (*Meloidogyne incognita*) and hatch of soybean cyst nematode (*Heterodera glycines*). Extraction and bioassay directed fractionation of the culture broth filtrate determined that flavipin, a low molecular weight compound, was the fungus metabolite responsible for most of the nematode antagonistic activity [31]. Similarly, a culture filtrate of *Aspergillus niger* strain was highly active against *Meloidogyne incognita* with marked mortality of second-stage juveniles and inhibition of egg hatching.

We isolated four *Mucor* spp. and one *Peniophora* sp. on turfgrasses. *Mucor* spp., is known as antibacterial and entomopathogen effects [63, 64]. *Peniophora* sp. inoculation reduced *Fomes annosus* in forestry but did not eliminated. *Peniophora gigantea* is used as a biological control of annosum root rot, caused by *Heterobasidion* spp., in western Europe. In the United States, *P. gigantea* was used as a biological control for annosum root rot from the 1970s to 1995. Currently, the Environmental Protection Agency is reviewing the status of *P. gigantea* as a pesticide [65, 66]. In addition to these, *Acremonium strictum* is parasitic of some pathogenic fungi and nematodes [67, 68, 69].

Since 1989, the biological product has been developed from 22 strains of *Chaetomium cupreum* and *Chaetomium globosum* in the form of pellet and powder formulation. The formulation has successfully been applied to infested field soils integrated with cultural control measures and organic amendments for the long term and they provide protection against *Phytophthora palmivora* on durian (*Durio zibethinus* L.), black pepper (*Piper nigram* L.), *Phytophthora parasitica* on tangerine (*Citrus reticulata*), *Phytophthora cactorum* on strawberry (*Fragaria* spp.), *Fusarium oxysporum* f.sp. *Iycopersici* on tomato (*Lycopersicon esculentum* L.) and basal rot of corn (*Zea mays* L.) caused by *Sclerotium rolfsii* [70].

The most isolated species was *Phoma herbarum* with 34 isolates in this study. The fungus of the genus *Phoma* has the potential to be a biological control agent of weeds, examples include *Phoma herbarum* for *Taraxacum officinale* in turfgrass and *P. sorghina* on poke weed [35, 36, 37]. Powder formulation of *P. herbarum* has been developed and has the potential as a biological control agent of *Eleusine indica* [71]. It is known that *Phoma macrospore,* one of the most important species isolated in this study, was used in the control of some weeds. *P. macrostoma* was pathogenic to many dicotyledonous plant species, but nonpathogenic to monocots. Commercial applications for weed management in turfgrass, agriculture, horticulture and forestry seem probable, while domestic management of weeds in lawns, transplanted ornamental and annual flowering

species may provide alternative markets [72]. Two bioherbicides reported to control broadleaf weeds without injuring turfgrass are *Phoma macrostoma* and thaxtomin A. Field and container experiments were conducted to evaluate pre and post efficacy of *P. macrostoma* and thaxtomin A on regionally important broadleaf weeds. In container experiments, pre applications of *P. macrostoma* provided 65 to 100% control of dandelion, marsh yellowcress, and flexuous bittercress, equivalent to that of pendimethalin [38, 39]. *P. glomerata* has mycoparozitic character [73, 74].

Saccharomyces cerevisiae, a common species existing on the surface of fruits, has been used in the food technology process for thousands of years. In recent years, *S. cerevisiae* was used as a kind of biological control agent to control *Colletotrichum acutatum* [75], *Erysiphe betae* [76], *Fusarium oxysporum* [77], *Meloidogyne incognita*, *Rotylenchulus reniformis* [78], *Penicillium digitatum* [79], *Macrophomina phaseolina*, *Fusarium solani* [80], *S. cerevisiae* showed different mechanisms of biocontrol of phytopathogenic fungi including killer phenotypes, competition for nutrients and space, hydrolytic enzymes and induction of host resistance in previous studies [75, 76, 80].

As a result, plant endophytic fungi, as a novel and important microbial resource for producing bioactive compounds originally from their hosts, have attracted many researchers' attentions, both for theoretical study and potential applications. After more than two decades of research, much progress has been achieved though there are still many issues (i.e. increasing compound yield in fermentation culture, elucidating biosynthetic pathway of the compounds in the endophytic fungi, etc.) that need to be further clarified and resolved [81]. Future studies should investigate the effects of fungi used as biological control agents, isolated from the turfgrass areas in this study against major diseases in both turfgrasses and other cultivated plants.

There is a need to further study how to control the harmful and diseases on cultivated plants that are economically important by using different endophytic fungi. After that with the studies to be done, the effects of endophytic fungi isolated from turfgrass areas in this study against major diseases in both turfgrass and other cultivated plants should be investigated.

REFERENCES

[1] Miguel, A., Sagei, L. and Paul, B. (2002) Measuring diversity of endophytic fungi in leaf fragments: Does size matter? Mycopathologia. 156, 41-45.

[2] Latch, G.C.M. (1993) Physiological interactions of endophytic fungi and their hosts. Biotic stress tolerance imparted to grasses by endophytes. Agriculture, Ecosystems and Environment. 44, 143-156.

[3] Saikkonen, K., Faeth, S.H., Helander, M. and Sullivan, T.J. (1998) Fungal endophytes: a continuum of interactions with host plants. Annual Review of Ecology and Systematics. 29, 319-344.

[4] Schardl, C.L., Leuchtmann, A., Spiering, M.J. (2004) Symbioses of grasses with seedborne fungal endophytes. Annual Review of Plant Biology. 55, 315-340.

[5] Clay, K. (1988) Fungal endophytes of grasses: a defensive mutualism between plants and fungi. Ecology 69, 10-16.

[6] Clay, K. (1990) Fungal endophytes of grasses. Annu. Rev. Ecol. Syst. 21, 275- 297.

[7] Siegel, M., Latch, G., Bush, L., Fannin, F., Rowan, D., Tapper, B., Bacon, C., Johnson, M. (1990) Fungal endophyte-infected grasses: alkaloid accumulation and aphid response. Journal of Chemical Ecology. 16, 3301-3315.

[8] Fisher, P.J., Petrini, O. (1992) Fungal saprobes and pathogens as endophytes of rice (*Oryza sativa* L.). New Phytol. 120, 137-143.

[9] Fisher, P.J., Petrini, O., Lappin Scott, H.M. (1992) The distribution of some fungal and bacterial endophytes in maize (*Zea mays* L.). New Phytologist. 122, 299–305.

[10] White, J.F., Cole, G.T. (1985) Endophyte-host associations in forage grasses: in vitro inhibition of fungi by *A. coenophialim*. Mycologia. 77, 487-489.

[11] Howell, C.R. (2003) Mechanisms Employed by *Trichoderma* Species in the Biological Control of Plant Diseases. The History and Evolution of Current Concepts. Plant Disease. 87 (1), 4-10.

[12] Iqbal, M., Dubey, M., McEwan, K.,Menzel, U., Franko, M.A., Viketoft, M., Jensen, D.F., Karlsson, M. (2018) Evaluation of *Clonostachys rosea* for control of plant-parasitic nematodes in soil and in roots of carrot and wheat. Phytopathology. 108(1), 52-59.

[13] Windham, G.L., Windham, M.T., Williams, W.P. (1989) Effects of *Trichoderma* spp. on maize growth and *Meloidogyne arenaria* reproduction. Plant Disease. 73, 493-494.

[14] Khan, T.A., Saxena, S.K. (1997) Integrated management of root knot nematode *Meloidogyne javanica* infecting tomato using organic materials and *Paecilomyces lilacinus*. Bioresour. Technol. 61, 247-250.

[15] Spiegel, Y., Chet, I. (1998) Evaluation of *Trichoderma* spp. as a biocontrol agent against soil-borne fungi and plant-parasitic nematodes in Israel. Int. Pest Manage. Rev. 3, 169-175.

[16] Saifullah, T., Thomas, B.J. (1996) Studies on the parasitism of *Globodera rostochiensis* by *Trichoderma harzianum* using low temperature scanning electron microscopy. Afro-Asian J. Nematol. 6, 117-122.

[17] Turki, A., Shammari, A.L., Bahkali, A.H., Elgorban, A.M., Maged, T., Kahky, E., Basheer A.A. (2013) The Use of *Trichoderma longibrachiatum* and *Mortierella alpina* Against Root-Knot Nematode, *Meloidogyne javanica* on Tomato Journal Of Pure And Applıed Microbiology. 7, 199-207.

[18] Rodriguez, R.J., White, Jr J.F., Arnold, E.A., Redman, R.S. (2009) Fungal endophytes: diversity and functional roles. New Phytologist. 182, 314-330.

[19] Porras-Alfaro, A., Bayman, P. (2011) Hidden Fungi, Emergent Properties: Endophytes and Microbiomes. Annu. Rev. Phytopathol. 49, 291-315.

[20] Harman, G.E., Howell, C.R., Viterbo, A., Chet, I, Lorito, M. (2004) *Trichoderma* species: opportunistic, avirulentplant symbionts. Nat. Rev. Microbiol. 2(1), 43–56.

[21] Ownley, B.H., Gwinn, K.D., Vega, F.E. (2010) Endophytic fungal entomopathogens with activity againstplant pathogens: ecology and evolution. BioControl. 55, 113-28.

[22] Harman, G.E., Eckenrode, C.J., Webb, D.R. (1978) Alteration of spermosphere ecosystems affecting oviposition by the bean seed fly and attack by soil borne fungi on germinating seeds. Annals of Applied Biology. 90, 1-6.

[23] Vannacci, G., Harman, G.F. (1987) Biocontrol of seed borne *Alternaria raphani* and *A. brassicicola*. Canadian Journal of Microbiological Research. 33, 850-856.

[24] Thiep, N.V., Soytong, K. (2015) *Chaetomium* spp. as biocontrol potential to control tea and coffee pathogens in Vietnam. International Journal of Agricultural Technology. 11(6), 1381-1392.

[25] Tyler, J.A., Richard, C., Richard, H., Belanger, R. (2001) Approaches to molecular characterization of fungal biocontrol agents: some case studies. Canadian Journal of Plant Pathology. 23, 8-12.

[26] Aggarwal, R., Tiwari, A.K., Srivastava, K.D., Singh, D.V. (2004) Role of antibiosis in the biological control of spot blotch (*Cochliobolus sativus*) of wheat by *Chaetomium globosum*. *Mycopathologia.* 15, 369-377.

[27] Rajkumar, E., Aggarwal, R., Singh, B., (2005) Fungal antagonists for the biological control of *Ascochyta* blight of chickpea. Acta Phytopathologica et Entomologica Hungarica. 40, 35-42.

[28] Ahammed, S.K., Aggarwal, R., Kapoor, H.C. (2008) Production, partial purification and characterization of extracellular xylanase from *Chaetomium globosum*. Journal of Plant Biochemistry Biotechnology. 17, 95-98.

[29] Biswas, S.K., Aggarwal, R., Srivastava, K.D., Gupta, S., Dureja, P. (2012) Characterization of antifungal metabolites of *Chaetomium globosum* Kunze and their antagonism against fungal plant pathogens. Journal of Biological Control. 26, 70-74.

[30] Di Pietro, A., Gut-Rella, M., Pachlatko, J.P., Schwinn, F.J. (1992) Role of antibiotics produced by *Chaetomium globosum* in biocontrol of *Pythium ultimum*, a causal agent of damping off. Phytopathology. 82, 131-135.

[31] Nitao, J.K., Susan, L., Meyer, F., Oliver, J.E., Schmidt, W.F., Chitwood, D.J. (2002) Isolation of flavipin, a fungus compound antagonistic to plant-parasitic nematodes. Nematology. 4(1), 55-63.

[32] Boyette, C.D., Hoagland, R.E., Abbas, H.K. (2006) Evaluation of the bioherbicide *Myrothecium verrucaria* for weed control in tomato (*Lycopersicon esculentum*). Biocontrol Science and Technology. 17, 171-178.

[33] Hoagland, R.E., Teaster, N.D., Boyette, C.D. (2013) Bioherbicidal effects of *Myrothecium verrucaria* on glyphosateresistant and-susceptible palmer amaranth biotypes. International Allelopathy Foundation. 31(2), 367-376.

[34] Brebaum, S.N., Boland, G.J (1999) First Report of *Phoma herbarum* and *Phoma exigua* as Pathogens of Dandelion in Southern Ontario. Plant Disease. 83(2), 200.

[35] Li, Y.P.; You, M. P., Khan, T.N., Finnegan, P.M., Barbettie, M.J. (2011) First Report of *Phoma herbarum* on Field Pea (*Pisum sativum*) in Australia. 95 (12), 1590.

[36] Neumann, T., Boland, G.J (2002) Influence of host and pathogen variables on the efficacy of *Phoma herbarum*, a potential biological control agent of *Taraxacum officinale*. Canadian Journal of Botany. 80, 425-429.

[37] Venkatasubbaiah, P., Van Dyke, C.G., Chilton, W.S. (1992) Phytotoxic metabolites of *Phoma sorghina*, a new foliar pathogen of pokeweed. Mycologia. 84, 715-723.

[38] Smith, J., Wherley, B., Reynolds, C., White, R., Senseman, S., Falk, S. (2015) Weed control spectrum and turfgrass tolerance to bioherbicide *Phoma macrostoma*. International Journal of Pest Management. 61(2), 91-98.

[39] Wolfe J.C., Neal J.C., Harlow C.D. (2016) Selective broadleaf weed control in turfgrass with the bioherbicides *Phoma macrostoma* and thaxtomin A. Weed Technology. 30(3), 688-700.

[40] Manoch, L., Jeamjitt, O., Dethoup, T., Kokaew, J., Eamvijarn, A., Visarathanonth, N., Chamswarng, C. (2008) Biological control of plant pathogenic fungi using *Talaromyces flavus*, *Sordaria fimicola* and some endophytic fungi. Phytopathology. 98, 97.

[41] Boer, W.D., Gerards, S., Gunnewiek, P.J.A., Modderman R. (1999) Response of the chitinolytic microbial community to chitin amendments of dune soils. Biology and Fertility of Soils. 29(2), 170-177.

[42] Wills, W., Lambe, R. (1980) *Mortierella* antagonism to oomycetes. Proceedings of American Phytopathological Society. Potomac Division, Morgantown, WV, USA.

[43] Wills, W. (1989) Integrated biological and chemical control of *Phytophthora* root rot of Azaleas and Rhododendrons. Journal American Rhododendron Society. 43(4), 205, 227-228.

[44] Tagawa, M., Tamaki, H., Manome, A., Koyama, O., Kamagata Y. (2010) Isolation and characterization of antagonistic fungi against potato scab pathogens from potato field soils. FEMS Microbiology Letters. 305(2), 136-142.

[45] Nallanchakravarthula, S. (2013) Root-Associated Microbial Communities of Different Strawberry Cultivars as Influenced by Soil Type, *Verticillium dahliae.* Kleb. and Biofumigation. Phd Thesis. Acta Universitatis Agriculturae Sueciae.

[46] Maharachchikumbura, S.S.N., Guo, L.D., Chukeatirote, E., Bahkali, A.H., Hyde, K.D. (2011) Pestalotiopsis-morphology, phylogeny, biochemistry and diversity. Fungal Diversity. 50, 167-187.

[47] Zheng, Y.K., Miao, C.P., Chen, H.H., Huang, F.F., Xia, Y.M., Chen, Y.W., Zhao, L.X. (2017) Endophytic fungi harbored in *Panax notoginseng*: diversity and potential as biological control agents against host plant pathogens of root-rot disease. Journal of Ginseng Research. 41(3), 353-360.

[48] White, T.J., Bruns, T., Lee, S., Taylor, J.W. (1990) Amplification and direct sequencing of fungal ribosomal RNA genes for phylogenetics. In: PCR Protocols: A Guide to Methods and Applications, eds. Innis, MA, Gelfand DH, Sninsky JJ, White TJ. Academic Press, Inc., New York. 315-322.

[49] Tosun, N., Turan, C. (2011) Efficacies of Application Programmes on Brown Patch Disease (*Rhizoctonia solani* Kühn.) of Turf. Anadolu, J. of AARI. 21(1), 26-35. (in Turkish).

[50] Sariasih, Y., Sutrawati, M., Hartal, L. (2015) The Potential Test of Endophytic Fungi on the Growth of Cucumber Crops and the Pathogenicity of the Pathogen *Fusarium*. International Seminar on Promoting Local Resources for Food and Health. Proceeding ISEPROLOCAL. 414-417.

[51] Zou, C.G., Tu, H.H., Liu, X.Y., Tao, N., Zhang, K.Q. (2010) PacC in the nematophagous fungus *Clonostachys rosea* controls virulence to nematodes. Environ. Microbiol. 12, 1868-1877.

[52] Sun, B.D., Liu, X.Z. (2008) Occurrence and Diversity of Insect-Associated Fungi in Natural Soils in China. Applied Soil Ecology. 39, 100-108.

[53] Rahman, M., Punja, Z.K. (2007) Biological control of damping-off on American ginseing (*Panax quinquefolius*) by *Clonostachys rosea f. catenulate* (=*Gliocladium catenulatum*). Can. J. Plant Pathol. 29, 203-207.

[54] Chatterton, S., Punja, Z.K. (2010) Factors influencing colonization of cucumber roots by *Clonostachys rosea f. catenulate*, a biological disease control agent. Biocontrol. Sci. Technol. 20, 37-55.

[55] Chatterton, S., Punja, Z.K. (2012) Colonization of geranium foliage by *Clonostachys rosea f. catenulata*, a biological control agent of *Botrytis* grey mould. Botany. 90(1), 1-10.

[56] Tweddell, R.J., Jabaji-Hare, S.H., Charest, P.M. (1994) Production of Chitinases and beta-1,3-Glucanases by *Stachybotrys elegans*, a Mycoparasite of *Rhizoctonia solani*. Appl. Environ. Microbiol. 60(2), 489-495.

[57] Walker, H.L., Tilley, A.M. (1997) Evaluation of an isolate of *Myrothecium verrucaria* from sicklepod (*Senna obtusifolia*) as a potential mycoherbicide agent. Biol. Control. 10, 104-112.

[58] Clarke, T.C., Shetty, K.G., Jayachandran, K., Norland, M.R. (2007) *Myrothecium verrucaria* a potential biological control agent for the invasive old world climbing fern (*Lygodium microphyllum*). BioControl. 52, 399-411.

[59] Boyette, C.D., Walker, H.L., Abbas, H.K. (2002) Biological control of kudzu (*Pueraria lobata*) with an isolate of *Myrothecium verrucaria*. Biocontrol Science and Technology. 12, 75-82.

[60] Yang, S.M., Brenner, D. (1997) Virulence and host range of three species of *Myrothecium* on *Amaranthus* spp. ARS USDA, TEKTRAN, USA.

[61] Turhan, G., Grossmann, F. (1994) Antagonistic Activity of Five *Myrothecium* Species Against Fungi and Bacteria. Journal of Phytopathology. 140, 97-113.

[62] Murakami, R., Shirata, A., Inoue, H. (1998) A selective medium containing the toxins of *Myrothecium roridum* for isolation from soil. J. Seric. Sci. Jpn. 67(5), 381-387.
[63] Moussa, S.A., Farouk, A.F., Opwis, K., Schollmeyer, E. (2011) Production, Characterization and Antibacterial Activity of *Mucor rouxii*. Textile Science and Engineering. 1,1.
[64] El-Ghany, T.M. (2015) Entomopathogenic Fungi And Their Role In Biological Control. Published by OMICS Group eBooks 731 Gull Ave, Foster City, CA 94404, USA.
[65] Ross, E.W., Hodges C.S, Jr. (1981) Control of *Heterobasidion annosum* colonization in mechanically sheared slash pine stumps treated with *Peniophora gigantea*. Asheville, NC: U.S. Department of Agriculture Southeast For. Expt. Stn. Res. Paper SE, 229.
[66] Tubby, K.V., Scott, D., Webber, J.F. (2008) Relationship between stump treatment coverage using the biological control product PG Suspension, and control of *Heterobasidion annosum* on Corsican pine, *Pinus nigra* ssp. laricio. For Pathol. 38, 37-46.
[67] Rivera-Varas, V.V., Freeman, T.A., Gudmestad, N.C., Secor, G.A. (2007) Mycoparasitism of *Helminthosporium solani* by *Acremonium strictum*. Phytopathology. 97(10), 1331-1337.
[68] Chalfoun, N.R., Grellet-Bournonville, C.F., Martinez-Zamora, M.G., Diaz-Perales, A., Castagnaro, A.P., Diaz-Ricci, J.C. (2013) Purification and characterization of AsES protein: a subtilisin secreted by *Acremonium strictum* is a novel plant defense elicitor. Journal of Biological Chemistry. 288, 14098-14113.
[69] Goswami, J., Kumar Pandey, R., Tewari, J.P., Goswami, B.K. (2008) Management of root knot nematode of tomato through application of fungal antagonists, *Acremonium strictum* and *Trichoderma harzianum*. Journal of Environmental Science and Health. 43, 237-240.
[70] Soytong, K., Kanokmedhakul, S., Kukongviriyapa, V., Isobe, M. (2001) Application of *Chaetomium* species (Ketomium®) as a new broad spectrum biological fungicide for plant disease control. A review article. Fungal Diversity. 7, 1-15.
[71] Rusli, M.H., Sharifah Muzzaimah, S.A., Suriza, M., Idis, A.S. (2015) Powder formulatıon of *Phoma herbarum* as biological control of goose grass (*Eleusine indica*). MPOB Information Series. 1511-7871.
[72] Bailey, K.L., Pitt, W.M., Falk, S., Derby, J. (2011) The Effects of *Phoma macrostoma* on Nontarget Plant and Target Weed Species. 58(3), 379-386.
[73] Raymond, F.S., White, F.J. (2000) *Phoma glomerata* as a Mycoparasite of Powdery Mildew. Appl. Environ. Microbiol. 66(1), 425-427.
[74] Arie, T., Kobayashi, Y., Kono, Y., Gen, O., Yamaguchi, I. (1999) Control of clubroot of crucifers by *Phoma glomerata* and its product epoxydon. 9th International Congress of Pesticide Chemistry, organised by the International Union of Pure and Applied Chemistry (IUPAC) and held in London, UK, 2-7 August 1998.
[75] Lopes, M.R., Klein, M.N., Ferraz, L.P., Silva, A.C.D. (2015) *Saccharomyces cerevisiae*: a novel and efficient biological control agent for *Colletotrichum acutatum*, during pre-harvest. Microbiol. Res. 175, 93-9.
[76] Ziedan, E.S.H.E., Farrag, E.S.H. (2011) Application of yeasts as biocontrol agents for controlling foliar diseases on sugar beet plants. J. Agr. Tech. 7(6), 1789-1799.
[77] Shalaby, E.S., El-Nad, M.F. (2008) Application of *Saccharomyces cerevisiae* as a biocontrol agent against *Fusarium* infection of sugar beet plants. Acta. Biol. Szeged. 59, 271-5.
[78] Ismail, A.E., Hasabo, S.A., El-Nagdi, W.M.A., Fadel, M.M. (2005) Efficacy of native isolates of *Saccharomyces cerevisiae*, *Trichoderma harzianum* and *T. ressei* in the biocontrol of *Meloidogyne incognita* and *Rotylenchulus reniformis* on jasmine in comparison to nematicide vydate under flood irrigation regime in Egypt. Pak. J. Nematol. 23, 317-29.
[79] Catara, A., Cirvilleri, G., Coco, V., Strano, L. (2004) Evaluation of *Saccharomyces cerevisiae* as biocontrol agent of Citrus green mold. Proc. Int. Soc. Citriculture. 2, 725-9.
[80] Attyia, S.H., Youssry, A.A. (2001) Application of *Saccharomyces cerevisiae* as a biocontrol agent against some diseases of Solanaceae caused by *Macrophomina phaseolina* and *Fusarium solani*. Egypt J. Biol. 3, 79-87.
[81] Zhao, J., Zhou, L., Wang, J., Shan, T., Zhong, L., Liu, X., Gao, X. (2010) Endophytic fungi for producing bioactive compounds originally from their host plants. Current Research, Technology and Education Topics in Applied Microbiology and Microbial Biotechnology. 567-576.

Received: **10.06.2019**
Accepted: **04.03.2020**

CORRESPONDING AUTHOR

Filiz Unal
The Plant Protection Central Research Institute,
Ministry Of Agriculture And Forestry
Ankara – Turkey

e-mail: fucar06@yahoo.com

© by PSP Volume 29 – No. 05/2020 pages 3517-3523 Fresenius Environmental Bulletin

THE TRANSFORMATION PROCESSES OF STRUVITE SLOW RELEASE FERTILLZER IN VEGETABLE BY ISOTOPIC TRACING

Rongtai Yu[1,*], Rui Deng[1], Xiaohong Zou[1], Xiang Ma[1], Zhipeng Xie[2], Changan Wang[2]

[1]School of Materials Science and Engineering, Jingdezhen Ceramic Institute, Jingdezhen, 333403, Jiangxi, P.R. China
[2]School of Materials Science and Engineering, Tsinghua University, Beijing, 100084, Beijing, P.R. China

ABSTRACT

Discharge of nitrogen and phosphorus greatly exceed the limitation in China. The precipitation of struvite, for its efficient recycling and environmentally friendly, is superior method for ammonium and phosphate removal. In this study, struvite as slow-releasing fertilizer were investigated. The results showed that the best pH for struvite release was at neutral soil, the release periods of struvite was more than two weeks, and the concentrations of ammonium and phosphate in soil were 4-6 mg/L and 2-6 mg/L at 10 day, respectively. The release rate of struvite has nothing to do with salinity, which was related to soil humidity. When struvite with N^{15} was used as slow-releasing fertilizer, it can be uptake by vegetable, especially by root, and the release period can meet vegetable growth cycle. The precipitation of struvite as slow-release fertilizer can provide opportunities for reusing ammonium and phosphate and keeping the cost of recycling and reusing of ammonium/phosphate down.

KEYWORDS:
Struvite, Isotopic tracing, Slow-release, Vegetable

INTRODUCTION

For non-renewable and irreplaceable resource, phosphorus recycling and recovery from wastewater has received widespread interesting in sewage treatment [1]. Struvite, as an effective ammonium and phosphate recycling method, has received intensively study [2-5]. Struvite crystal can be formed at room temperature with stirring in aqueous supersaturated solutions containing Mg^{2+}, NH_4^+ and PO_4^{3-} ions, the theoretical mole ratio of Mg^{2+}: NH_4^+: PO_4^{3-} is 1:1:1 [1, 5-6]. The mole ratio and pH are the key factors for struvite nucleation, which were investigated in the literatures in different wastewater and technology [7-10]. The effect of competitive ions in industrial wastewater were also studied [4,11]. Struvite precipitate technology has studied for decades, however, it is far away for application in engineering, one of the key factors is high costs of reagents.

Struvite is a slow releasing fertilizer with significant commercial value [12-13]. The content of N, P_2O_5 and Mg of pure struvite are 5.7%, 29% and 16.4% [14] As reported by Li et al [15] and Negrea et al [16], Struvite is slightly soluble in water and soil solutions, the solubility is 0.02 g/100 mL at 0ºC. A slow fertilizer with low dissolution and steady release can avoid crop burning and nutrition loss. Struvite, as a slow releasing fertilizer, have higher P_2O_5 and Mg content, and slow-release characteristics. However, to our best knowledge, the study of struvite, as a slow releasing fertilizer, is not deep and systematic. Yetilmezsoy and Sapci-Zengin [17], Ryu et al [18] used struvite as slow releasing fertilizer in cultivating plant and Chinese cabbage, respectively, the results found that the accumulation of Cu, Cd, As, Pb and Ni were decreased by using struvite as fertilizer. As far as we know, the applications of struvite as slow releasing fertilizer reported in the literatures were from the perspective of pollutant removal, not from the nature of fertilizer.

In this study, we explored struvite as slow releasing fertilizer from the point of fertilizer. The factors of solubility in soil, pH, salt concentration and soil humidity were investigated. Isotopic tracer method was used to trace the migration and transformation of nitrogen in struvite. The fertilizer efficiency of struvite were studied with different planting patterns.

EXPERIMENTAL

Materials. All the reagents were purchased from Sinopharm of China, the modified starch was purchased from Tianjin Dingfeng starch development Co. LTD., the organic fertilizer were purchased from a fertilizer Co. LTD of China, which were a product of fermentation by plant ash and animal dung; The vegetables were purchased from a farmer. All the vegetables were planting no more than 10 day after seeding.

The preparation of struvite slow-releasing fertilizer. Struvite were prepared using the modified method reported by Yu et al [19]. $NaH_2PO_4 \cdot 12H_2O$ and NH_4Cl were dissolved in deionized water (5000 mg/L, NH_4^+), and $MgCl_2$ were added. Then pH was adjusted to 9.5, the mixed solution were agitated with 200 r/min for 30 min, let it stay for 30 min, then filtered with a 0.45 μm membrane filter and washed with deionized water three times, struvite collected was dried in an oven at 40 °C for 48 h. Struvite with N^{15} were prepared using the same procedure above, the only exception was that NH_4Cl were replaced by $N^{15}H_4Cl$ (A. R).

The effect of pH on the release of nutrition by soil dissolution rate method. All the soil was collected from the top layer (0-10 cm) around the campus, and dried in an oven with 60 °C for 48 h. First, struvite was mixed with dried soil, the weight rate was 1:300, the mixture were poured into a triangular flask, and 90 mL deionized water with different pH (4-9) was sprayed to the soil in the triangular flask. Some soil was collected from the triangular flask at different time for ammonium and phosphate measured.

The effect of KCl concentration on the release of nutrition. Dried soil was mixed with struvite, the weight rate was 1:300. Then 90 mL deionized water with different KCl concentration (1-9 mg/kg) was sprayed into the mixture, some soil was collected at different time for ammonium and phosphate measured.

The effect of extracting condition on the release of nutrition. 1 gram struvite was added dialysis tubing, then imbedded into the soil, the weight rate was 1:300; and deionized water with different amount (30-200 mL) was sprayed to the mixture; some soil was collected at different time for ammonium and phosphate measured.

The effect of soil humidity on the release of nutrition. Struvite was mixed with soil, the weight rate was 1:300, then the mixture was poured into the triangular flask, an amount of deionized water (30-200 mL) was sprayed; some soil was collected at different time for ammonium and phosphate measured.

Nutrition migration in green vegetables by isotopic tracing. The basic fertilizer was different in batch experiments, struvite, urea and organic fertilizer were used as basic fertilizer, struvite with N^{15} isotope labelling was used as additional fertilizer (every factor were set 6 pot test, 1 vegetable/per pot, the vegetable were watered every two days). R0 was that vegetables were transplanted without any fertilizer, R1 was that struvite with N^{15} isotope labelling was used as basic fertilizer (1 g /each); R2 was that struvite with N^{15} isotope labelling was used as additional fertilizer after transporting day 7 (1 g /each); R3 was that struvite was used as basic fertilizer (1 g /each), and struvite with N^{15} isotope labelling was used as additional fertilizer after transporting day 7 (1 g /each); R4 was that urea was used as basic fertilizer (1 g /each), and struvite with N^{15} isotope labelling was used as additional fertilizer after transporting day 7 (1 g /each); R5 was that organic fertilizer was used as basic fertilizer (1 g /each), and struvite with N^{15} isotope labelling was used as additional fertilizer after transporting day 7 (1 g /each).

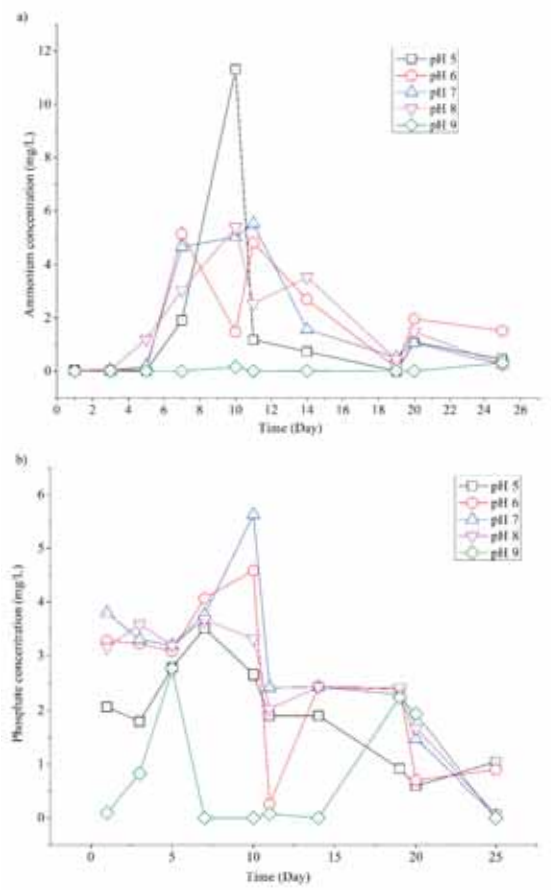

FIGURE 1
The effect of pH on the release of struvite at different days. a) The release of ammonium at different pH; b) The release of phosphate at different pH.

RESULTS AND DISCUSSION

The effect of pH on the release of nutrition by soil dissolution rate method. The value of NH_4^+ and PO_4^{3-} in parental soil was 0.24 mg/L and 0.19 mg/L, respectively. During the experiments of pH, the amount of water was 90 mL, and pH of water was adjusted to 5-9, then the mixture solution

were poured into the flask. The release rate of struvite were investigated. As showed in Figure 1, the maximum value of NH_4^+ and PO_4^{3-} in soil were about 4-6 mg/L, 2-6 mg/L at 10 day, respectively; the concentration of NH_4^+ and PO_4^{3-} in soil were decreased with the extended release time; and which were higher at neutral condition than that at acidic condition or alkaline condition.

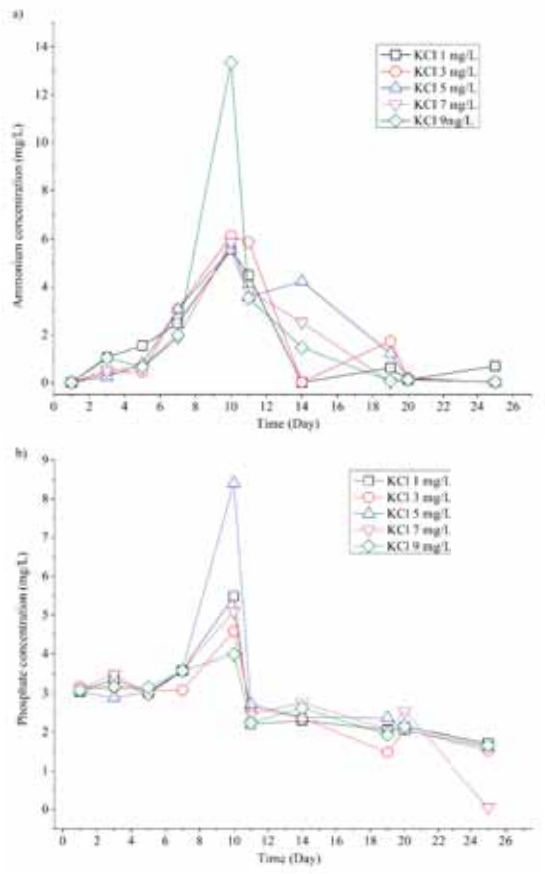

FIGURE 2
The effect of KCl on the release of struvite at different days. a) The release of ammonium at different the concentration of KCl; b) The release of phosphate at different the concentration of KCl.

Struvite would be dissolved in acidic solution, therefore, struvite mixed with soil maybe dissolve into the water when acidic solution were added, it would lead to the concentration of struvite in soil was decreased, the released amount of NH_4^+ and PO_4^{3-} reduced. When pH was too high, PO_4^{3-} would be reacted with cations in soil, and stable compounds would be formed, that was the reason why the concentration of PO_4^{3-} was decreased at higher pH. There is an equation, $NH_4^+ \cdot OH \; f \; NH_3 \cdot H_2O$, when pH is increased, the equation goes to the right, and NH_3 would be volatilized. However, there are also many kinds of microorganism in soil, and parts of struvite could be decomposed by those microorganism, nitrate, nitrate nitrogen or others would be formed, and some of NH_4^+ and PO_4^{3-} would transferred into the metabolism of microorganism. Therefore, the concentration of NH_4^+ and PO_4^{3-} in soil were decreased with the extension of release time.

The effect of KCl concentration on the release of nutrition. Salinity in different area is diversely, the release of nutrient in struvite would be restrained by salinity. The effect of salinity on the release of nutrient in struvite were investigated. As shown in Figure 2, the concentration of ammonia was dropped after the first increased, the best value was about 14 mg/L. However, the release rate of nutrient were no clear correlation with the concentration of KCl, whether ammonia or phosphate, the concentration in the soil were no clear-cut distinction when the mixed fertilize was dipped in the different concentration of KCl. The concentration of NH_4^+ and PO_4^{3-} were descended gradually during the later release period, there were about 0.2 mg/L and 2 mg/L at 25 days, respectively.

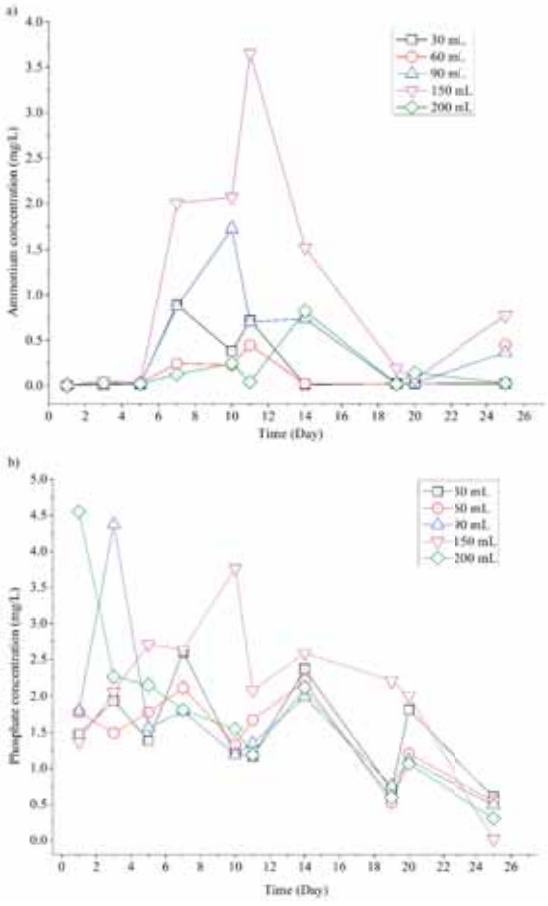

FIGURE 3
The effect of extracting condition on the release of nutrition. a) The release of ammonium at different soil humidity with dialysis tubing; b) The release of phosphate at different soil humidity with dialysis tubing.

The transformation of nitrogen and volatilization were the main reason of the decrease of ammonium at later period, and part of nitrogen would be dissolved to water. While the reaction would be the main reason of the decrease of phosphate. When there were K^+ and Ca^{2+} or other cations, it would be formed $MgKPO_4$, $Ca_3(PO_4)_2$ or $Ca_2(PO_4)OH$ with increasing PO_4^{3-} concentration. Microorganism would be degraded part of ammonium and phosphate at later period.

The effect of extracting condition on the release of nutrition. Struvite was added to dialysis tubing, the ion of NH_4^+ and PO_4^{3-} could be exuded from the dialysis tubing, while soil could not infiltrate into the dialysis tubing, the release rate of struvite were not affected by the interference factors. As showed in Figure 3 a, b, it was the curves of struvite@soil with different water. The concentration of ammonia in struvite@soil were decreased after increased with the extension of time, the best value was above 3.5 mg/L after 12 days. The concentration of phosphate was decreased with the extension of time, the best value was about 4.5 mg/L at the first week. When soil was too dry, it was not good for the release of ammonia and phosphate. If the soil was too wet, it was also not good for the release of ammonia and phosphate (Figure 3 a, b). The best humidity was 90 mL-150 mL, it was not good for the release of nutrient of struvite with too dry soil or too wet soil.

The effect of soil humidity on the release of nutrition. Soil humidity were also investigated with struvite mixed with soil directly. There were different soil humidity in agricultural planting, the analysis of simulation to planting conditions were showed in Figure 4. The concentration of ammonium and phosphate have no significant difference at the beginning, the peak value of ammonium and phosphate were occurred in the second week, and the concentration ammonium and phosphate would be declined gradually with the extension of release time. There were slight different with different humidity in the release of struvite, the concentration of ammonium in dry soil (≤ 60 mg/L) was higher than that in wet soil, while the release rule of phosphate was opposite to that of ammonium, the concentration of phosphate in wet soil was higher than that in dry soil.

Theoretically, the release rate of struvite would be increased in wet soil. However, the results of ammonium were not suitable to the rule. The dissolvability of ammonium in water was very high, when ammonium was released, ammonium would be dissolved to water, while the values in this experiment was only measured the soil. When the humidity was increased, ammonium concentration in soil would be decreased. Precipitation would be formed between phosphate and cations in soil, this is the reason that the concentration of phosphate in wet soil was a little higher than dry soil.

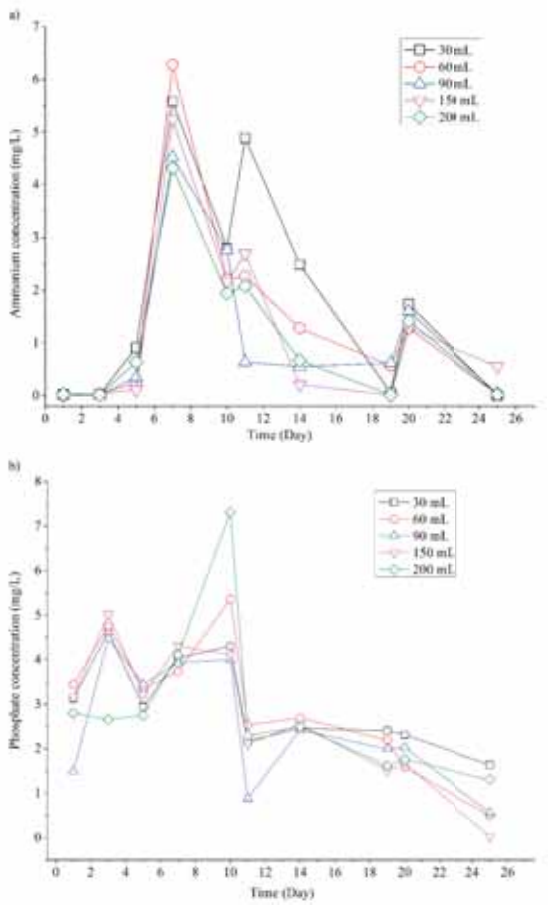

FIGURE 4
The effect of soil humidity on the release of nutrition. a) The release of ammonium at different soil humidity; b) The release of phosphate at different soil humidity.

Nutrition migration in green vegetables by isotopic tracing. The results of nitrogen and phosphorus translocation in vegetables (Figure 6) were showed in Figure 4 and Table 1. Soil and vegetables were measured respectively, vegetables were dried in an oven at 60 ºC for 24 h, and all the vegetables (leaf, root and stem) were grind and mixed (the vegetables were collected randomly), then 1 g the mixture were used for ammonium and phosphate measurement. As showed in the Figure 5, the values of ammonium and phosphate in blank sample were at low level, almost all the values in different fertilizing method were higher than that of blank sample. While the values of ammonium and phosphate in soil were different in fertilizing method. For the quick release of urea, the ammonia value in soil of R4 was a little higher than others fertilizing method in the first two weeks, and which would be decreased with the release time extension. Ammonium were not released from organic fertilizer, and vegetables maybe accelerated growth for organic fertilizer, the rate of fertilizer consumption

was also increased. Therefore, the value of ammonium in R5 was low. Struvite used as basic fertilizer or struvite as additional fertilizer (no basic fertilizer), the value of ammonium in soil were higher than others fertilizing methods.

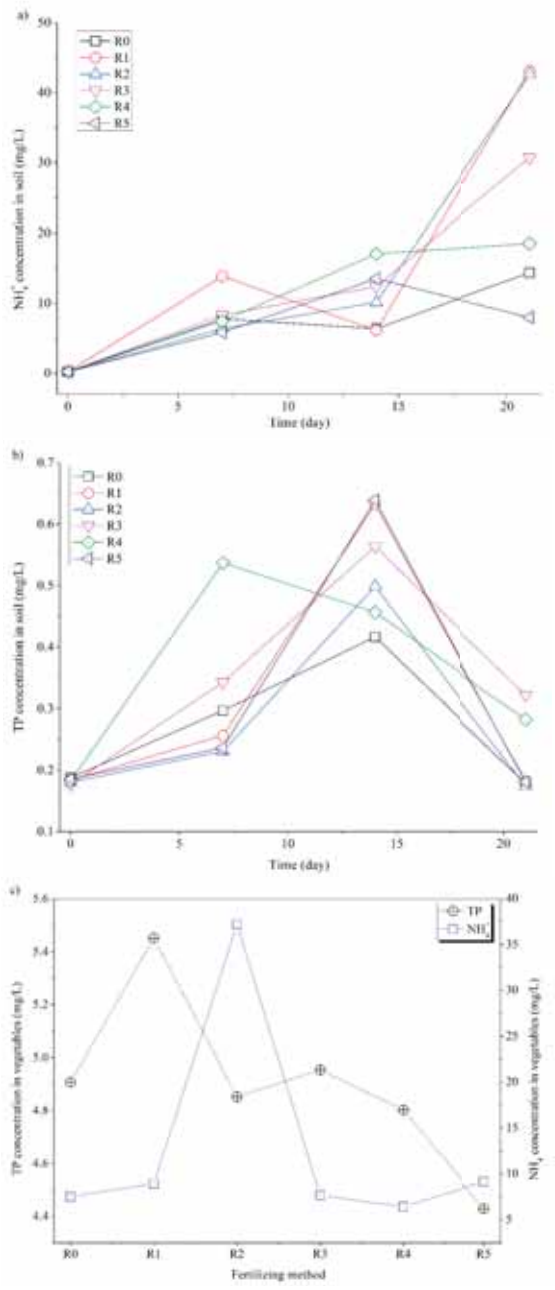

FIGURE 5
Nutrition migration in green vegetables by isotopic tracing. a) ammonium residual in soil; b) Total phosphorus residual in soil; c) the uptake of ammonium and total phosphorus by vegetables.

The release rate of phosphate was changed in different time and different fertilizing method. The release rate of phosphate would be increased at the first period when urea was used as the basic fertilizer, then decreased gradually (Figure 5 b, R4). When organic fertilizer was used as the basic fertilizer, the top value of phosphate in soil would be set back than urea as basic fertilizer (Figure 5 b, R5). The release rule of ammonium were not always identical with phosphate. When the release time was more than 20 days, the value of ammonium in R1, R2, R3 were higher than the others, while the best values of phosphate was from R3, R4. Therefore, when struvite was used as the basic fertilizer, the release of phosphate and ammonium were superior to others.

Ammonia and phosphorus in vegetables were measured. As showed in Figure 5 c, the values in vegetables have no significant difference with different fertilizing method (except ammonia of R2). That was to say, the absorption of nutrients would not be increased with different fertilizing methods. The excess of ammonium and phosphate would be enter to environment. The best case was that the release rule of the slow release fertilize was agree with the growth rhythm of vegetables.

The results of isotopic tracer were showed in Table 1. The $d^{15}N/^{14}N$ value from highest priority to lowest was R1, R3, R2, R5, R4 and R0 (without any fertilize), the best nitrogen content absorbed by plants in leaf was R1, that was to say, when struvite with N^{15} isotope labelling was used as basic fertilizer, most of nutrient were absorbed by green vegetables. While when struvite used as basic fertilizer (R2, R3), the green vegetables would be promoted growth, and green vegetables have different growth cycles for different nutrient uptake, the values of $d^{15}N/^{14}N$ in R2, R3 were different. When urea and organic fertilizer were used as basic fertilizer, the nutrient was quick release, the relative concentration of nitrogen adsorbed by vegetables from struvite with ^{15}N was lower, the values of ^{15}N in green vegetable leaf (R4, R5) were lower than other fertilization methods. In other words, when urea was used as basic fertilization, nitrogen uptake by green vegetable was prior to that of organic fertilizer, and struvite was the last one. The nutrient of ^{15}N was main uptake by green vegetable root (R1 root, stem and leaf, Table 1).

FIGURE 6
Vegetable used in the experiments

TABLE 1
The results of isotopic tracer

Sample	$^{15}N\%$	$d^{15}N/^{14}N$	Ampl28	$R^{15}N/^{14}N$
R0 leaf	5.22	2.4	2035	0.0036847
R1 leaf	4.48	60.0	1634	0.0038967
R2 leaf	4.20	27.2	1634	0.0037740
R3 leaf	7.98	36.3	2888	0.0038074
R4 leaf	7.35	6.5	2599	0.0036981
R5 leaf	6.27	18.0	2295	0.0037403
R1 root	3.30	272.5	1184	0.0046765
R1 stem	2.88	25.8	1150	0.0037689

CONCLUSIONS

Struvite was used as the slow-release fertilizer, and the factors of fertilizer efficiency were investigated by soil dissolution rate method. The release periods of struvite was more than two weeks, the peak value of NH_4^+ were about 4-6 mg/L, and PO_4^{3-} in soil was 2-6 mg/L at 10 day; the best pH for struvite slow-releasing fertilizer was at neutral condition. Salinity, like as KCl, was no clear-cut distinction with the release of struvite. Soil humidity was related to the release of nutrition, wet soil would be promote the release of phosphate, while the value of ammonium was higher in dry soil. The results of the nutrient of ^{15}N showed that the nutrient released by struvite were uptake by vegetables, and which was main uptake by root. Urea and organic fertilizer is easier for vegetables uptake, however, the release period of struvite was longer than quick effective nutrient, and when struvite used as basic fertilizer, the green vegetables were promoted growth.

ACKNOWLEDGEMENTS

This research was supported by Jiangxi Science and Technology to Support the Project (2015BBF60058) and National Natural Science Foundation of China (51668023), this research was also supported by Jiangxi provincial department of education project (GJJ170775) and Jingdezhen Science and Technology bureau project (2017GYZD016-015).

REFERENCES

[1] Barbosa, S., Barbosa, Sónia G., Peixoto, L., Meulman, B., Alves, M. M., Pereira, M. A. (2016). A design of experiments to assess phosphorous removal and crystal properties in struvite precipitation of source separated uring using different Mg sources. Chemical Engineering Journal. 298(15), 146-153.

[2] Stolzenburg, P., Capdevielle, A., Teychené, S., Biscans, B. (2015). Struvite precipitation with MgO as a precursor: application to wastewater treatment. Chemical Engineering Science. 133(8), 9-15.

[3] Lu, X., Shih, K., Li, X. Y., Liu, G., Zeng, E. Y., & Wang, F. (2016). Accuracy and application of quantitative X-ray diffraction on the precipitation of struvite product. Water Research. 90(1), 9-14.

[4] Yan, H.L., Shih, K. (2016). Effects of calcium and ferric ions on struvite precipitation: a new assessment based on quantitative X-ray diffraction analysis. Water Research. 95(15), 310-318.

[5] Munir, M. T., Li, B. , Boiarkina, I., Baroutian, S., Yu, W., Young, B. R. (2017). Phosphate recovery from hydrothermally treated sewage sludge using struvite precipitation. Bioresource Technology. 239, 171-179.

[6] Bouropoulos, N.C., Koutsoukos, P. (2000). Spontaneous precipitation of struvite from aqueous solutions. Journal of Crystal Growth. 213(3-4), 381-388.

[7] Kim, D., Min, K. J., Lee, K., Yu, M. S., Park, K. Y. (2017). Effect of pH, molar ratios and pretreatment on phosphorous recovery through struvite crystallization from effluent of anaerobically digested swine wastewater. Enviromental Engineering Research. 22, 12-18.

[8] Kwon, G., Kang, J.Y., Nam, J.H., Kim Y. O., Jahng, D. (2018). Recovery of ammonia through struvite production using anaerobic digestate of piggery wastewater and leachate of sewage sludge ash. Environmental Technology. 39, 831-842.

[9] Taddeo, R., Lepistö. (2015). Struvite precipitation in raw and co-digested swine slurries for nutrients recovery in batch reactors. Water Science & Technology. 71, 892-897.

[10] Doyle J.D., Parsons, S.A. (2002). Struvite formation, control and recovery. Water Research. 36(16), 3925-3940.

[11] Acelas, N.Y., Flórez, E., López, D. (2015). Phosphorus recovery through struvite precipitation from wastewater: effect of the competitive ions. Desalination and Water Treatment. 54(9), 2468-2479.

[12] Uysal, A., Yilmazel, Y.D., Demirer, G.N. (2010). The determination of fertilizer quality of the formed struvite from effluent of a sewage sludge anaerobic digester. Journal of Hazardous Materials. 181(1-3), 248-254.
[13] Diwani, G.E., Rafie, S.E., Ibiari, N.N.E., El-Aila, H.I. (2007). Recovery of ammonia nitrogen from industrial wastewater treatment as struvite slow releasing fertilizer. Desalination. 214(1-3), 200-214.
[14] Kumar, R., Pal, P. (2015). Assessing the feasibility of N and P recovery by struvite precipitation from nutrient-rich wastewater: a review. Environ. Sci. Pollut Res. 22, 17453-17464.
[15] Li, X.Z., Zhao, Q.L. (2002). MAP precipitation from landfill leachate and seawater bittern waste. Environ. Technol. 23, 989-1000.
[16] Negrea, A., Lupa, L., Negrea, P., et al. (2010). Simultaneous removal of ammonium and phosphate ions from wastewaters and characterization of the resulting product. Chem. Bull."Politehnica" Univ. Timisoara, Romania. 55, 136-142.
[17] Yetilmezsoy, K., Sapci-Zengin, Z. (2009). Recoery of ammonium nitrogen from the effluent of UASB treating poultry manure wastewater by MAP precipitation as a slow-releasing fertilizer. Journal of Hazardous Materials. 166, 260-269.
[18] Ryu, H.D., Lim, C.S., Kang, M.K., Lee, S.I. (2012). Evaluation of struvite obtained from semiconductor wastewater as a fertilizer in cultivating Chinese cabbage. Journal of Hazardous Materials. 221-222, 248-255.
[19] Rongtai, Y., Jinju, G., Hongqiang, R. et al. (2013). Struvite pyrolysate recycling conbined with dry pyrolysis from ammonium removal from wastewater. Bioresource Technology. 132, 154-159.

Received: **25.06.2019**
Accepted: **29.01.2020**

CORRESPONDING AUTHOR

Rongtai Yu
School of Materials Science and Engineering,
Jingdezhen Ceramic Institute,
Jingdezhen 333403 Jiangxi – P.R. China

e-mail: yurongtai@jci.edu.cn

© by PSP Volume 29 – No. 05/2020 pages 3524-3530 Fresenius Environmental Bulletin

CHANGES IN AMINO ACID COMPOSITION IN CORN SEED UNDER DIFFERENT SULFUR USAGE RATES AND APPLICATION DATES

Yakup Onur Koca*

Department of Field Crops, Faculty of Agriculture, Aydin Adnan Menderes University, Aydin, Turkey

ABSTRACT

A study was conducted to determine the impacts of two different effects of sulfur on the amino acid composition in corn seed at Aydin, Turkey, during 2013 and 2014. Sulfur doses (D1 and D2) were calculated as 400 kg ha^{-1} and 800 kg ha^{-1} with the cation exchange capacity (CEC) of the soil. SD1 and SD2 parcels (a D1 and D2 dose application on the sowing date, respectively), BD1 and BD2 parcels (a D1 and D2 dose application 60 days before the sowing date), standard fertilization without sulfur [210 $kg.ha^{-1}$ pure nitrogen (NH_4NO_3), 60 $kg.ha^{-1}$ phosphor (P_2O_5) and potassium (K_2O)] and nonfertilized parcels were established to assess the effectiveness of sulfur over time. Amino acid content (essential, conditionally essential and nonessential) of the corn seeds obtained from the different treatment parcels was measured using HPLC. According the results, significant differences among treatments and between years were found. Leucine and tyrosine increased with standard fertilization during the two years. Moreover, valine, isoleucine, lysine, cysteine and alanine increased under the SD1 treatment. Proline and cysteine increased under BD1 and isoleucine and cysteine increased under the BD2 treatment during the two years. Thus, some positive effects were noted even with only standard fertilization. Moreover, SD1 (400 kg ha^{-1} sulfur) can be recommended for practical applications because of the low application amount and ease of application with sowing. An application of 800 kg ha^{-1} sulfur (SD2) at sowing cannot be recommended, as no specific effect on amino acid composition was found.

KEYWORDS:
Amino acid, Corn, HPLC, Sulfur, Application date, Application rate

INTRODUCTION

Corn is a very significant plant for both human and animal nutrition [1]. Particularly for vegans, corn seed quality in a salad or other prepared dishes is vital with regard to food balance for essential amino acids. Moreover, it is also vital for poultry and some herbivorous animals whose major diet is only corn seed. For this reason, corn seed is among the important sources of essential amino acids required for healthy nutrition of some human and animal groups.

Because of its presence in the structure of two main amino acids (cysteine and methionine), which have a wide range of functions in the catalysis of protein blocks, sulfur is among the staminal elements for plants throughout their lives [2]. Sulfur plays a vital role in plant growth, as much as carbon or nitrogen [3, 4]. Moreover, it is essential for many primary and secondary plant metabolisms [5] and seed quality for constituents of proteins, several coenzymes and vitamins [6]. It is also associated with coenzyme A, biotin, vitamin B1, and pantothenic acid [7 - 8]. Currently, a reduction of emissions of SO_2 in the atmosphere with a preference for natural gas instead of fossil fuels has led to an increase in S deficiency in soils [9] and in plants growing in S-deficient soils [10]. Therefore, S deficiency in soils and plants has been occurring throughout the world [11].

In addition to being one of the vital elements for plants, sulfur is also a pH regulator in soil. A healthy plant only depends on the maintenance of soil alkalinity in semiarid regions of the world because there is a decrease in uptake of the main minerals (Zn, Mg, Cu, Mn, Se, S, Fe and others) at high pH levels [12]. These minerals are essential and support many vital activities in plants from protein and oil cycles to photosynthesis and energy cycles. Insufficiency of one or more of these elements negatively affects yield and quality [13, 14]. This problem is also especially important for the Mediterranean region whose soils are typically alkaline.
Sulfur can be taken up by plants after a certain period of time following application. Applied sulfur on a farm regulates the pH in the soil and then it becomes a form of sulfur that can be fully obtained by plants. The aim of this study was to determine the effects of the usage rate and application date of sulfur on amino acid composition of corn seed. Thus, we hoped to determine some information regarding the effects of some sulfur utilization rates (reducing

some stress factors by lowering the pH) and application dates (increasing the use of sulfur over time by the plant).

MATERIALS AND METHODS

This research was conducted as a factorial experiment with two factors (treatment and year) in a randomized complete-block experimental design (3 repetitions) at the trail station of Adnan Menderes University Agriculture Facility in Aydın, Western Turkey, at 37° 44' N 27° 44' E and 65 m above sea level, during 2013 and 2014. The area of the parcels used was 28 m^2 for each treatment. Aydın has a typical Mediterranean climate with hot summers and mild winters. The PR31D24 corn variety was utilized as the experiment material.

Results of the soil analysis of the experimental land showed that the soil structure was a sandy-loam soil type with the following composition: sand – 72.0%, silt – 16.7%, and clay – 11.3%. The soil was low in organic matter and had a pH of 8.4.

Treatment Combinations. The sulfur amount calculated for applications relying on the cation exchange capacity (CEC) of the soil was calculated as 400 $kg.ha^{-1}$ sulfur with elemental sulfur (S_2). The amount of sulfur for dose 1 (D1) was 400 $kg.ha^{-1}$. Twice the dose (800 $kg.ha^{-1}$) was used for dose 2 (D2). Six different treatments (considering dose, fertilization, and application date) were conducted on the experiment land changing the application time of the doses. To determine the benefits of sulfur for long time periods, the D1 and D2 doses were applied on some parcels two months (60 days) before the sowing date (BD1 and BD2) and applied on the sowing date (SD1 and SD2). Standard fertilizer [210 $kg.ha^{-1}$ pure nitrogen (NH_4NO_3) (60 $kg.ha^{-1}$ with a 15-15-15 composition was immediately applied at the beginning of cultivation and 150 $kg.ha^{-1}$ with urea (H_2NCONH_2) before the first watering), 60 $kg.ha^{-1}$ phosphor (P_2O_5) and 60 $kg.ha^{-1}$ potassium (K_2O)] parcels without sulfur and nonfertilized parcels were added. Therefore, experiments were conducted for six different treatments.

Calculation Formula of Sulfur Amount. At a 90% base saturation, 400 kg sulfur (S) ha^{-1} was applied to the soil before sowing to decrease the soil pH by 1 unit. The elemental S used in the experiment contains 99.98% S and its seed size is 80–100 mesh (0.016–0.020 μm).

Calculation of S amounts
Soil initial pH = 8.44; BD = 90

Soil goal pH = 7.44; BD = 83
Soil CEC= 15 me/100 g

Initial pH
BD.CEC = (0.90 × 15)/100 g =13.50 me/100 g
Goal pH
BD.CEC= (0.83 × 15)/100 g = 12.50 me/100 g
BD: Bulk density, **CEC**: Cation exchange capacity
Required S amount of 100 g soil = 13.50–12.50 = 1.00 me S/100 g soil
Convert to kg/ha = 25.000.000 me S/ha (1 me S = 16 mg) 25.000.000 × 16 = 400.000.000 mg S/ha = 400 kg S ha^{-1} in the soil

The sowing date was determined as April 9, 2013, and April 11, 2014. The BD1 and BD2 treatments were applied 60 days before the sowing date (February 8, 2013, and February 10, 2014). Then, the SD1 and SD2 treatments were also applied at the moment of sowing. Except for no fertilization (nothing was applied during the vegetation period) parcels, standard fertilizer was applied on all parcels as 210 $kg.ha^{-1}$ pure nitrogen (NH_4NO_3) (60 $kg.ha^{-1}$ with a 15-15-15 composition was immediately applied at the beginning of cultivation and 150 $kg.ha^{-1}$ with urea (H_2NCONH_2) before the first watering), 60 $kg.ha^{-1}$ phosphor (P_2O_5) and 60 $kg.ha^{-1}$ potassium (K_2O). When necessary, other agricultural practices used in corn farming such as irrigation, pesticide application, etc. were completed during the corn growth period.

Analysis of Corn Seed Amino Acid Composition. On the basis of dietary needs for nitrogen balance or growth, amino acids were traditionally classified as nutritionally essential or nonessential for humans and animals [15]. Essential amino acids are defined as amino acids whose carbon skeletons cannot be synthesized by the body relative to the needs [16]. Conditionally essential amino acids normally can be synthesized in adequate amounts by the organism, but must be provided from the diet to meet optimal needs under conditions in which the rates of utilization are greater than the rates of synthesis. Nonessential amino acids can be synthesized in adequate amounts by the body to meet optimal requirements [17, 18]. In our study, 17 amino acid (essential, conditionally essential and nonessential) rates were measured.

Sample Preparation. Seed samples from the experimental corn samples for each year were milled and weighed to 0.1 g. A total of 5 ml of 6 N HCl was added to the sample and then 250 µl of 2 mM phenol and 0.1 g of Na2SO3 were added. The sample was placed in an oven at 110 °C for 24 h and after that time the pH level of the sample was adjusted to 6.7–7.3 using 5 N NaOH. The supernatant was centrifuged at 4000 rpm for 5 min and then filtered through a filter and fitted to vials.

HPLC Determination. The entire amino acid content of the samples was determined using an HPLC system consisting of a Shimadzu Nexara XR

(Shimadzu Corporation, Kyoto, Japan) with a Zorbax Eclipse AAA (15 cm × 4.6 mm × 3.5 µm in size) column. Mobile phase A consisted of 40 mmol of $NaH_2PO_4.2H_2O$ adjusted to pH 7.8 with 5 N NaOH. Mobile phase B was composed of acetonitrile: methanol: water (45:45:10, vol. %). Briefly, the hydrolyzed samples and solutions of the standard amino acid mixture were automatically derived using OPA and FMOC. The column temperature was 40 °C and the injection volume was 9 µl. The amino acids were achieved by calibrating with a standard mixture of amino acids. The peak integration accuracy was enhanced by manual establishment of peak baselines using software.

Statistical Analysis. The amino acid data collected from the experiment were subjected to analysis of variance (ANOVA) using the TOTEM STAT statistical software [19]. The mean differences were compared by the least significant difference (LSD) test [20].

RESULTS AND DISCUSSION

Among more than 300 amino acids in nature, only 20 serve as building blocks of protein [21]. Because of variations in their side chains, amino acids have signally different biochemical functions [22]. Amino acids have various prominent functions in plants. In addition to their usage during protein biosynthesis, they also represent building blocks for several other biosynthetic pathways and play pivotal roles during signaling processes as well as in plant stress response [23]. The findings related to the 17 amino acid ratios measured in our study are as follows.

The least square means of amino acids were calculated through variance analysis. It was found that the treatment factor provided significantly different results for all amino acids. In addition to the year factor and the treatment × year interaction also showed significantly different results except for histidine, tyrosine and cysteine. Thus, it can be said that as an essentially natural product, the composition of the amino acids in corn seed can vary from year to year as a result of changes in the growing conditions. The years of the experiment (2013 and 2014) were separately evaluated. Amino acid values are tabulated as the essential amino acid content and the conditionally essential and nonessential amino acid content in Tables 1 and 2, respectively. Furthermore, the LSD values of the significant ones among the variation resources are presented below the tables.

The histidine, valine, methionine, threonine, isoleucine, leucine, lysine and phenylalanine values are shown as essential amino acids in Table 1. Glycine, proline, arginine, tyrosine, cysteine, aspartic acid, glutamic acid, serine and alanine values are shown as conditionally essential and nonessential amino acids in Table 2.

TABLE 1
Change of Essential Amino Acid Content with Different Sulfur Rate on Different Treatment Date Proline and Cysteine

	HIS	VAL	MET	THR	ILE	LEU	LYS	PHE
	2013							
Non-fertilization	0,25	0,32	0,17	0,24	0,22	0,69	0,21	0,35
Standard fertilization	0,25	0,32	0,19	0,24	0,22	0,74	0,21	0,35
SD1	0,24	0,36	0,19	0,20	0,25	0,84	0,23	0,35
SD2	0,20	0,27	0,17	0,24	0,21	0,73	0,15	0,32
BD1	0,24	0,32	0,18	0,24	0,23	0,74	0,18	0,35
BD2	0,22	0,33	0,14	0,18	0,25	0,80	0,21	0,36
Average (year)	0,23	0,32	0,17	0,22	0,23	0,76	0,20	0,35
	2014							
Non-fertilization	0,24	0,29	0,18	0,23	0,20	0,62	0,18	0,30
Standard fertilization	0,25	0,30	0,18	0,24	0,23	0,80	0,18	0,35
SD1	0,23	0,36	0,20	0,20	0,26	0,80	0,23	0,35
SD2	0,21	0,30	0,15	0,21	0,23	0,76	0,19	0,34
BD1	0,23	0,32	0,15	0,24	0,23	0,71	0,20	0,34
BD2	0,22	0,29	0,18	0,23	0,24	0,72	0,24	0,33
Average (year)	0,23	0,31	0,17	0,23	0,23	0,73	0,20	0,34
Average	0,23	0,32	0,17	0,23	0,23	0,75	0,20	0,34
LSD (treatment)	0,008	0,016	0,007	0,010	0,010	0,037	0,007	0,012
LSD (treatment*year)	ns	0,023	0,010	0,014	0,015	0,052	0,010	0,018

HIS: Histidine, VAL: Valine, MET: Methionine, THR: Threonine, ILE: Isoleucine, LEU: Leucine, LYS: Lysine, PHE: Phenylalanine

SD1: Sulfur application at sowing date, SD2: extra Sulfur application at sowing date, BD1: Sulfur application two months before sowing date, BD2: extra Sulfur application two months before sowing date

TABLE 2
Change of Conditionally Essential and Non-Essential Amino Acid Content with Different Sulfur Rate on Different Treatment Date

	GLY	PRO	ARG	TRY	CYS	ASP	GLU	SER	ALA
	2013								
Non-fertilization	0,33	0,66	0,44	0,27	0,37	0,54	1,25	0,45	0,51
Standard fertilization	0,31	0,63	0,39	0,28	0,27	0,50	1,24	0,38	0,50
SD1	0,31	0,63	0,37	0,29	0,36	0,46	1,27	0,31	0,52
SD2	0,24	0,60	0,30	0,27	0,25	0,42	1,18	0,37	0,47
BD1	0,29	0,70	0,38	0,29	0,41	0,50	1,30	0,42	0,52
BD2	0,30	0,53	0,33	0,27	0,34	0,42	1,24	0,33	0,51
Average (year)	0,30	0,63	0,37	0,28	0,34	0,47	1,25	0,33	0,51
	2014								
Non-fertilization	0,29	0,56	0,37	0,25	0,29	0,46	1,10	0,34	0,45
Standard fertilization	0,28	0,58	0,37	0,30	0,25	0,46	1,33	0,46	0,51
SD1	0,31	0,65	0,38	0,28	0,36	0,43	1,32	0,29	0,55
SD2	0,28	0,63	0,34	0,26	0,27	0,45	1,26	0,37	0,51
BD1	0,30	0,69	0,42	0,27	0,39	0,51	1,28	0,41	0,50
BD2	0,27	0,57	0,38	0,28	0,30	0,43	1,12	0,31	0,44
Average (year)	0,29	0,61	0,38	0,27	0,31	0,46	1,23	0,36	0,49
Average	0,29	0,62	0,37	0,28	0,32	0,47	1,24	0,34	0,50
LSD (treatment)	0,013	0,446	0,015	0,014	0,036	0,021	0,057	0,015	0,027
LSD (treatment*year)	0,018	0,631	0,021	ns	ns	0,030	0,081	0,022	0,038

GLY: Glycine, PRO: Proline, ARG: Arginine, TRY: Tyrosine, CYS: Cysteine, ASP: Aspartic acid, GLU: Glutamic acid, SER: Serine, ALA: Alanine

SD1: Sulfur application at sowing date, SD2: extra Sulfur application at sowing date, BD1: Sulfur application two months before sowing date, BD2: extra Sulfur application two months before sowing date

All essential amino acid values either increased or were unaffected with standard fertilization without sulfur compared to no fertilization during the two years. For the first year, only methionine and leucine and for the second year of the experiment only histidine, valine, threonine, isoleucine, leucine, and phenylalanine values increased with standard fertilization. In contrast to the essential amino acid rates, nearly all the conditionally essential and nonessential amino acid values either decreased or did not change with standard fertilization compared to no fertilization. Only tyrosine increased during the two years of the experiment. Thus, certain effects of standard fertilization on all essential, conditionally essential, and nonessential amino acid values cannot be noted except for leucine and tyrosine which increased during the two years. Only the leucine and tyrosine values were positively affected by the standard fertilization.

Valine, isoleucine and lysine increased with sulfur application at the sowing date (SD1) compared to standard fertilization during the two years. Moreover, cysteine and alanine values in the conditionally essential and nonessential groups also increased. The amino acids serve as precursors for the synthesis of many secondary metabolites. For example, glucosinolates develop as a defense mechanism of some plants for tissue damage caused by pests or something else [24] can be produced from alanine and some other aromatic amino acids [6]. Lysine is among the most limiting essential amino acids for plants during vegetative growth [25]. Particularly during the formation of new protein blocks, lysine in combination with methionine plays an important role. Therefore, it is thought that sulfur applied with sowing can have significant effects on plant growth to a certain degree.

Essential, conditionally essential, and nonessential amino acids did not stably react against the extra sulfur dose applied at the sowing date (SD2). Histidine, methionine and phenylalanine decreased under SD2 compared to standard fertilization during the two years. However, valine, isoleucine and lysine decreased during the first year and either increased or were stable during the second year. All conditionally essential and nonessential amino acid values decreased during the first year. Then, proline and cysteine values increased during the second year. Thus, the effect of the treatment was not exactly determined but it can be said that the extra sulfur dose induces some adverse effects during the two years. High sulfur applications may indirectly adversely affect plant growth [26]. First, the increase in the S application decreases the pH level of the soil. All the known micronutrients decrease in availability as the pH increases. This result can be perceived as positive for uptake of essential micronutrients (Zn, B, Mn, Cu, Co, Mg, Se, and Fe) [27]. However, soil-to-plant mobility of heavy metals such as mercury (Hg), cadmium (Cd), arsenic (As) and lead (Pb), which exhibit toxic properties even at very low concentrations, rapidly increases at low pH levels [12, 28]. Thus, many indirect effects may occur from slowing root growth,

inhibiting shoot growth and yield production, to decreasing chlorophyll concentration or biomass [29 - 30]. More studies on the indirect adverse effects have been completed [31, 32, 33]. The unbalanced amino acid rates and sudden decreases observed under SD2 conditions may be the result of a decrease in pH with the effect of the high sulfur application.

Effects of sulfur application two months (60 days) before the sowing date (BD1) on essential amino acid content were determined as negative with a few exceptions compared to standard fertilization. Only the isoleucine value during the first year and lysine value during the second year of the experiment increased. The effects on conditionally essential and nonessential amino acid values were determined to be irregular. Only proline and cysteine increased with the treatment during the two years. In general, the BD1 application effects were negative for essential amino acids. While there were some fluctuations, proline and cysteine values were positively affected during the two years. Many forms of stress cause an increase in the quantity of proline [34]. Thus, we believe that plants were under stress in the plots in which sulfur was applied during the early period. It can be said that some other environmental factors may have caused this stress as well as sulfur.

Isoleucine in the essential group increased with effect of the extra sulfur application two months the before sowing date (BD2) compared to standard fertilization during the two years. Valine and lysine values also increased during only one year of the experiment (the first year for valine and the second year for lysine). Similarly, cysteine in the conditionally essential and nonessential group also increased with the treatment. Other amino acid rates in the group were not stable during the two years under the BD2 treatment. Thus, it can be said that the treatment (BD2) positively affected only isoleucine and cysteine.

CONCLUSIONS

Over the past two decades, there have numerous works directed toward defining the optimal requirements of amino acids by livestock species including pigs [35], ruminants [36], birds [37], fish [38], and humans [39] under diverse developmental and environmental conditions. In addition to the literature, our results have attempted to determine the changes in amino acid compositions in corn seed under different sulfur usage rates and application dates with standard fertilization. As a result of the explication of the data obtained, the following practical results were determined.

First, the difference between the years is important. In fact, the effect of the same application during the first year was not seen at all during the second year and vice versa. Conditions that have changed over the years have led to consequences that eliminate (or alter) the effects of applications on many amino acid rates. In light of this information, the amino acid concentration can be said to strongly respond to the environmental conditions. Similar results have also been obtained in many studies on different crops [40, 41, 42]. Therefore, it can be said that the effect of environmental factors may be more dominant than application factors. In other words, whatever is applied may be reflected in the results to the extent permitted by the environment.

Second, both different sulfur doses (400 $kgha^{-1}$ and 800 $kgha^{-1}$) as well as different application times (at the sowing date and before the sowing date) and even standard fertilization were found to be effective on the amino acid composition. Standard fertilization has been shown to increase the amino acid rate of leucine and tyrosine, which are involved in many critical events, from protein synthesis to stomatal regulation in higher plants [43, 44]. Even only standard fertilization showed positive results and can be suggested in practice. The effects of SD1 on the amino acid composition were determined to be the greatest which resulted in a higher number and percentage of amino acids (valine, isoleucine, lysine, cysteine and alanine) compared to those of the other treatments. The effect of the other applications (SD2, BD1 and BD2) were less than that of SD1 for various reasons (perhaps because of the pH or heavy metals). Thus, nearly no positive effect on the amino acid rates of SD2 was observed. For this reason, SD1 can be recommended for practical applications due to the low application amount and ease of application with sowing.

REFERENCES

[1] Remison, S.U. (2005) Arable and Vegetable Crops. Benin City. Gift-Press Associates.
[2] Iqbal, P., Akmal, M., Jalal, F., Bilal, M., Said, F., Imtiaz, M., Khan, M.A., Hussain, S. and Zaheer, S. (2019) Influence of Sulfur on Nitrogen Use Efficiency, Yield and Quality of Brassica Species. Fresen. Environ. Bull. 28(8), 5779-5787.
[3] Zhou, W., He, P., Li, S. and Lin, B. (2005) Mineralization of Organic Sulfur in Paddy Soils under Flooded Conditions and Its Availability to Plants. Geoderma. 125(1-2), 85-93.
[4] Demir, I. and Basalma, D. (2018) Response of Different Levels of Nitrogen and Sulfur Doses on Oil Yield and Seed Nutrients Content of Sunflower (Helianthus annuus L.). Fresen. Environ. Bull. 27(9), 6337-6342.
[5] Ceccoti, S.P. (1996) Plant Nutrient Sulfur a Review of Nutrient Balance, Environment Impact and Fertilizers. Fert. Res. 43,117-125.

[6] Halkier, B.A. and Gershenzon, J. (2006) Biology and Biochemistry of Glucosinolates. Annual Review of Plant Biology. 57, 303-333.
[7] Tavali, I.E., Maltas, A.S., Uz, I. and Kaplan, M. (2013) The Effect of Vermicompost on Yield, Quality and Nutritional Status of Cauliflower (Brassica oleracea var. botrytis). Mediterranean Agricultural Sciences. 26, 115-120.
[8] Kucukyumuk, Z., Gultekin, M. and Erdal, I. (2014) Effects of Vermicompost and Mycorrhiza on Plant Growth and Mineral Nutrition in Pepper. Journal of Agricultural Faculty of Süleyman Demirel University. 9, 51-58.
[9] Wainwright, M. (1984) Sulfur Oxidation in Soils. Advances in Agronomy. 37, 349-396.
[10] De Kok, L.J., Bosma, W., Maas, F.M. and Kuiper, P.J.C. (1985) The Effect of Short-Term H2S Fumigation on Water-Soluble Sulphydryl And Glutathione Levels in Spinach. Plant, Cell and Environ. 8,189-194.
[11] Itanna, F. (2005) Sulfur Distribution in Five Ethiopian Rift Valley Soils under Humid and Semi-Arid Climate. Journal of Arid Environments. 62(4), 597-612.
[12] Fageria, N.K. (2002) Nutrient Management for Improving Upland Rice Productivity and Sustainability. Communications in Soil Science and Plant Analysis. 32, 603-2629.
[13] Yassen, A., Abou El-Nour, E.A.A. and Shedeed, S. (2010) Response of Wheat to Foliar Spray with Urea and Micronutrients. Journal of American Science. 6,14-22.
[14] Huang, J., Yuan, H., Liu, J., Sun, W., Xu, Y., Ma, T. and Li, M. (2018) Simultaneous Analysis of Total Phosphorus and Nitrate Nitrogen in Denitrifying Phosphorus Removal Using Near Infrared Spectroscopy. Fresen. Environ. Bull. 27(10), 6952-6959.
[15] Lupi, A., Tenni, R. and Rossi, A. (2008) Human Prolidase and Prolidase Deficiency. Amino Acids. 35, 739–752.
[16] El Idrissi, A. (2008) Taurine Increases Mitochondrial Buffering of Calcium: Role in Neuroprotection. Amino Acids. 34, 321-328.
[17] Novelli, A. and Tasker, R.A.R. (2008) Excitatory Amino Acids in Epilepsy: From the Clinics to the Laboratory. Amino Acids. 32, 295-297.
[18] Phang, J.M., Donald, S.P., Pandhare, J. and Liu, Y. (2008) The Metabolism of Proline, as a Stress Substrate, Modulates Carcinogenic Pathways. Amino Acids. 35, 681-690.
[19] Acikgoz, N., Ilker, E. and Gokcol A. (2004) Assessment of Biological Research on the Computer. Ege University Seed Technology Center, Publication No: 2 Bornova-Izmir, Turkey. ISBN: 973-483-607-8.
[20] Stell, R.G.D., Torrie, J.A. and Dickey, D.A. (1997) Principles and Procedures of Statistics. A. Biometrical Approach 3rd Edi. Mc Graw Hill Book. INC. NY.
[21] Wu, G. (2009) Amino Acids: Metabolism, Functions, and Nutrition. Amino Acids. 37, 1-17.
[22] Brosnan, J.T. (2001) Amino Acids, Then and Now—A Reflection on Sir Hans Kreb's Contribution to Nitrogen Metabolism. IUBMB Life. 52, 265-270.
[23] Suenaga, R., Tomonaga, S. and Yamane, H. (2008) Intracerebroventricular Injection of L-Arginine Induces Sedative and Hypnotic Effects Under an Acute Stress in Neonatal Chicks. Amino Acids. 35, 139-146.
[24] Mithen, R. (2001) Glucosinolates: Biochemistry, Genetics and Biological Activity. Plant Growth Regulation. 34, 91–103.
[25] Galili, G. (2002) New Insights into the Regulation and Functional Significance of Lysine Metabolism in Plants. Annual Review of Plant Biology. 53, 27-43.
[26] Cui1, Y. and Wang Q. (2006) Physiological Responses of Maize to Elemental Sulfur and Cadmium Stress. Plant Soil Environment. 52(11), 523-529.
[27] Alcântara, M.A.K. and Camargo, O.A. (2001) Retarding Factor and Dispersion-Diffusion Coefficient for Chromium (III) In Highly Weathered Soils, influenced by pH, Texture and Organic Matter (in Portuguese). Revista Brasileira de Ciência do Solo. 25, 209-216.
[28] Wang, S., Shao, Y., Zhang, N., Fu, G., He, H. and Zhu H. (2018) Effect of Cracking on Permeability of Compacted Clay Liner under Consolidation Pressure in Landfills. Fresen. Environ. Bull. 27(9), 5891-5898.
[29] Evans, L.J. (1989) Chemistry of Metal Retention by Soils. Environmental Science and Technology. 23(9), 1046-1056.
[30] Alloway, B.J. and Jackson, A.P. (1991) The Behavior of Heavy Metals M Sewage Sludge-Amended Soils. Sci. Total Environ. 100, 151-176.
[31] Tichy, R., Fajtl, J., Kuzel, S. and Kolar, L. (1997) Use of Elemental Sulfur to Enhance a Cadmium Solubilization and Its Vegetative Removal from Contaminated Soil. Nutrient Cycling in Agroecosystems. 46, 249–255.
[32] Di Toppi, S.L. and Gabrielli, R. (1999) Response to Cadmium in Higher Plants. Environmental and Experimental Botany. 41, 105-130.
[33] Elloumi, N., Ben, F., Rhouma, A., Ben, B., Mezghani, I. and Boukhris, M. (2007) Cadmium Induced Growth Inhibition and Alteration of Biochemical Parameters in Almond Seedlings Grown in Solution Culture. Acta Physiologiae Plantarum. 29, 57-62
[34] Pál, M., Horváth, E., Janda, T., Páldi E. and Szalai, G. (2006) Physiological Changes and Defense Mechanisms Induced by Cadmium-stress in Maize. Journal of Plant Nutrition and Soil Science. 169, 239-246.

[35] Wu, G., Bazer, F.W. and Davis, T.A. (2007) Important Roles for the Arginine Family of Amino Acids in Swine Nutrition and Production. Livestock Science. 112, 8-22.
[36] Firkins, J.L., Hristov, A.N. and Hall, M.B. (2006) Integration of Ruminal Metabolism in Dairy Cattle. Journal of Dairy Science. 89, 31-51.
[37] Baker, D.H. (2009) Advances in Protein-Amino Acid Nutrition of Poultry. Amino Acids. 37(1), 29-41.
[38] Li, P., Mai, K.S. Trushenski, J. and Wu, G. (2008). New Developments in Fish Amino Acid Nutrition: Towards Functional and Environmentally Oriented Aqua Feeds. Amino Acids. 37(1), 43-53.
[39] Elango, R., Ball, R.O. and Pencharz, P.B. (2009) Amino Acid Requirements in Humans: With a Special Emphasis on the Metabolic Availability of Amino Acids. Amino Acids. 37(1), 19-27.
[40] Portera, M.A. and Jonesb, A.M. (2003) Variability in Soy Flour Composition. Journal of the American Oil Chemists' Society. 80, 557-562.
[41] Garde-Cerdán, T., Lorenzo, C., Lara, J.F., Pardo, F., Ancín-Azpilicueta, C. and Salinas, M.R. (2009) Study of the Evolution of Nitrogen Compounds during Grape Ripening. Application to Differentiate Grape Varieties and Cultivated Systems. Journal of Agricultural and Food Chemistry. 57, 2410-2419.
[42] Cid, C., Palacios, J., Saiz, E., Guerrero, A. and Cerrato, Y. (2014) on Extreme Geomagnetic Storms. Journal of Space Weather and Space Climate. 4, 28.
[43] Tsune, I, Ikejima, K. and Hirose, M. (2003) Dietary Glycine Prevents Chemical-Induced Experimental Colitis in the Rat. Gastroenterology. 125, 775-85.
[44] Kim, C.J., Kovacs-Nolan, J.A. and Yang, C. (2010) l-Tryptophan Exhibits Therapeutic Function in a Porcine Model of Dextran Sodium Sulfate (DSS)-Induced Colitis. Journal of Nutritional Biochemistry. 21, 468-75.

Received: **12.07.2019**
Accepted: **04.03.2020**

CORRESPONDING AUTHOR

Yakup Onur Koca
Department of Field Crops,
Faculty of Agriculture
Aydin Adnan Menderes University
Aydin – Turkey

e-mail: yokoca@adu.edu.tr

© by PSP Volume 29 – No. 05/2020 pages 3531-3546 Fresenius Environmental Bulletin

RESEARCH ON OPTIMIZATION DESIGN OF ABNORMAL FLIP BUCKET

Lina Wang[1,*], Sai Li[1], Yingfeng Duan[1], Yagang Zhang[1], Pinran Lin[2], Chao Su[2], Wenying Li[1]

[1] Xi'an University of Science and Technology, Xi'an 710054, China
[2] DWELL Company Limited, Beijing 100085, China

ABSTRACT

This study constructs an optimization model to address ski-jump energy dissipation problems in different reservoir environments. The multi-objective genetic algorithm is applied herein as the calculation method. Due to the influence of ski-jump energy dissipation on the scouring pit in real-life engineering situations, the pressure of water flow at the point of fall influences the depth of the scouring pit, while the kinetic energy of water flow influences its shape. The optimization objective is determined at the minimum water flow pressure at the point of fall, measuring the minimum kinetic energy. The design incorporated two variables to represent the whole abnormal flip bucket, namely overflow width and height of the flip bucket. Boundary conditions were created by the solid boundary and air boundary, as well as the constant inflow rate. The optimal overflow width and height of the flip bucket were calculated through optimal computation, which can minimize the scouring force of water flow as it falls onto the ground. The results obtained provide theoretical references for practical engineering and reduce potential safety hazards. The energy in flip buckets after optimization of water flow can be fully dissipated, creating an ecosystem where water can flow unobstructed. Guiding water flow to water-deficient areas is of great significance in ensuring the long-term protection of environments and ecosystems.

KEYWORDS:
Ski-jump flow, Energy dissipation, Optimization, Ecological environment, Hydraulics

INTRODUCTION

Ski-jump energy dissipation is the common energy dissipation mode in water bodies and in hydropower engineering. With its simple structural design and economical and practical performance, ski-jump energy dissipation is often the first choice in practical engineering situations Qian [1]. There are many influencing factors during the process of ski-jump energy dissipation. This study focuses not only on full ski-jump energy dissipation but also the scouring effect as water flows onto the ground. Therefore, achieving the optimal design in ski-jump flow requires the consideration of two factors: (1) interaction of streams, such as maximum dissipation and adulteration of high-speed water flow in the air. (2) Controlling the shape and scouring force of water flow as it flows onto the ground to realize the minimum scouring force and range [2, 3].

In middle- and high-release structures, flow kinetic energy is high and it is often used in ski-jump energy dissipation. Water flows out of the flip bucket and decelerates in the air due to resistance, accompanied by a reduction in kinetic energy. Water flows onto the ground and forms scouring pits. With the increase of scouring time, fixed scouring pits are formed and kinetic energy decreases again, thus resulting in the effect of energy elimination. Given allowable environmental and topographical conditions in downstream regions, ski-jump energy dissipation is often an appropriate selection, but consideration must be given to atomized rains [4].

The shapes of the bottom and side walls in abnormal flip buckets are diverse. There are various combinations taking into consideration many practical conditions. In terrain environments, the falling point of water flow often has to be controlled at a pre-set position to protect the terrain. This can be realized by changing the shape of the flip bucket to change the water flow direction [5, 6].

In this study, the influence of overflow width and height of the flip bucket on the pressure of the water falling point, as well as the kinetic energy at the falling point were studied. When the overflow width and height of the flip bucket are fixed, optimization is then geared toward attaining minimum absolute values for pressure and kinetic energy at the falling point of water flow by using a genetic algorithm. The final optimization goal is to study the influence of the model design size of the abnormal flip bucket on ski-jump flow and provide theoretical guidance for experimental simulations and practical engineering. Results demonstrated that pressure intensity and kinetic energy were reduced compared with that in the original program, indicating reasonable optimization results were obtained.

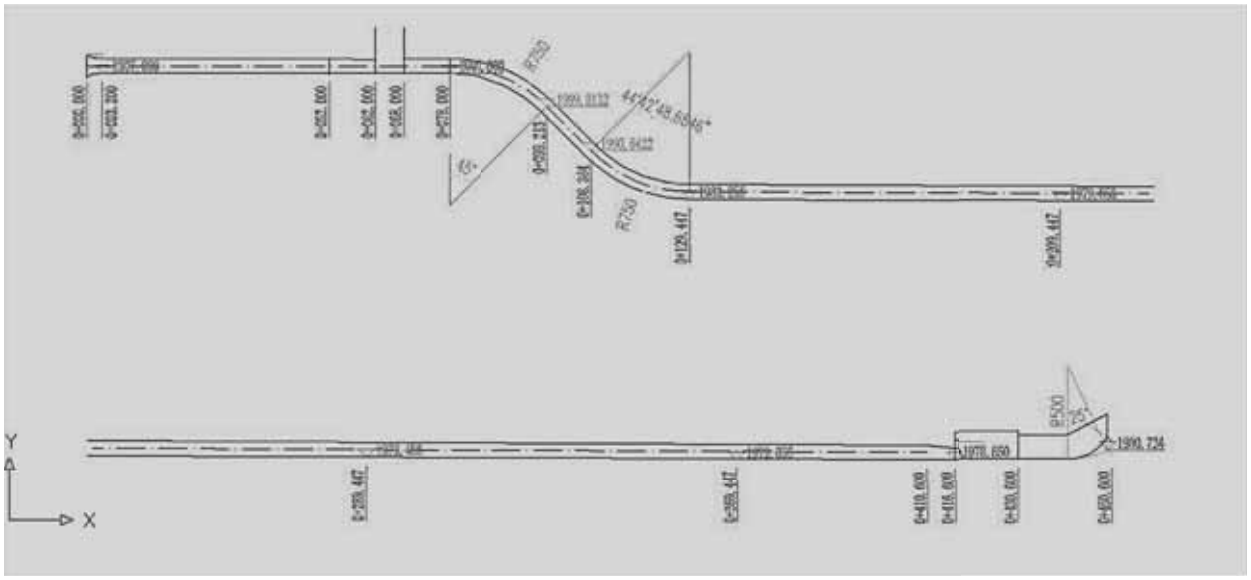

FIGURE 1
Positions of sections in the model

MATERIALS AND METHODS

Right triangular thin-walled weir flow. The right triangular thin-walled weir flow was applied by adjusting the water gate to change the flow rate. Flow rate could not be read directly, but had to be calculated by the formula $Q = C_0 H^{2.5}$ after the head on the weirs (H) was read through the U-shaped connector. In the formula, C_0 is the flow coefficient of the right triangular thin-walled weir flow, which is generally $C_0 = 1.4$.

When $H > 25cm$, the calculation formula is revised as $Q = 1.343 H^{2.47}$

where Q is the flow rate (m^3/s) and H is the head on weirs (m) [7].

Rectangular thin-walled weir flow. The flow rate of a non-submerged rectangular thin-walled weir without lateral shrinkage was calculated as $Q = mb\sqrt{2g}H_0^{1.5}$. The flow rate was adjusted continuously for multiple measurements. The stage-discharge curve was drawn based on measured results. Finally, the flow coefficient (m) was calculated [8].

Indexes for cavitations judgment - number of cavitations. The one-dimensional number of cavitations is often used as the measurement index of cavitations in actual water flow when studying cavitation problems, which is expressed as K:

$$K = \frac{p - p_v}{\frac{1}{2}\rho v^2} = \frac{(p - p_v)/\rho g}{v^2/2g}$$

where p and v are absolute pressure intensity and average flow rate at the places where water flow was not influenced by local variation of boundaries. p_v is the steam pressure and ρ is the water density.

The primary number of cavitations is determined by boundary conditions. For some boundary profiles, the number of cavitations is a fixed number and is often determined by the experiment.

The number of cavitations in actual water flow (K) and the primary number of cavitations (K_i) were compared. When $K > K_i$, no cavitation was formed. When $K \le K_i$, there was a cavitation [9].

Experimental project. The total capacity of the studied reservoir was 49.921 million m^3 and the normal pool level was 2048.50 m. The design flood level (P=2%) was 2047.90 m (major flood period) and the discharged volume of the spillway tunnel was 88.90 m^3/s. The maximum flood level (P=0.1%) was 2050.85 m and the discharged volume of the spillway tunnel was 135.00 m^3/s. The flood standard for the downstream energy dissipation and erosion control was a frequency of 30 years (P=3.33%) and the discharged volume of the spillway tunnel was 88.50 m^3/s.

The spillway tunnel was reconstructed from a diversion tunnel (Figure 1). It is on the right dam abutment and covers a length of 450.60 m (horizontal distance), including the inlet section, repairing

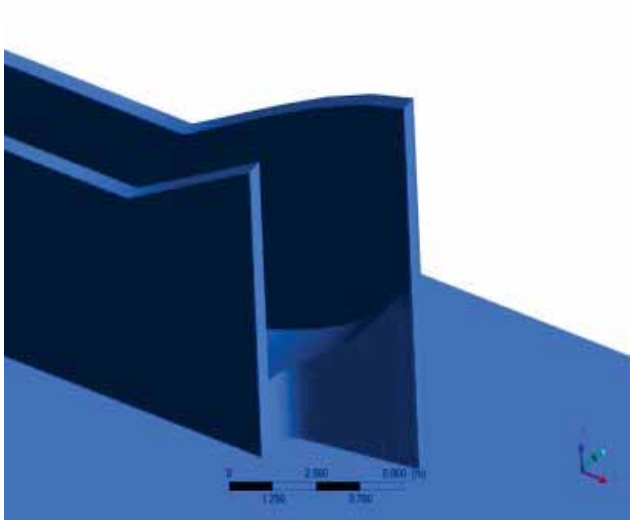

FIGURE 2
Three-dimensional diagram of the outlet section of the spillway tunnel

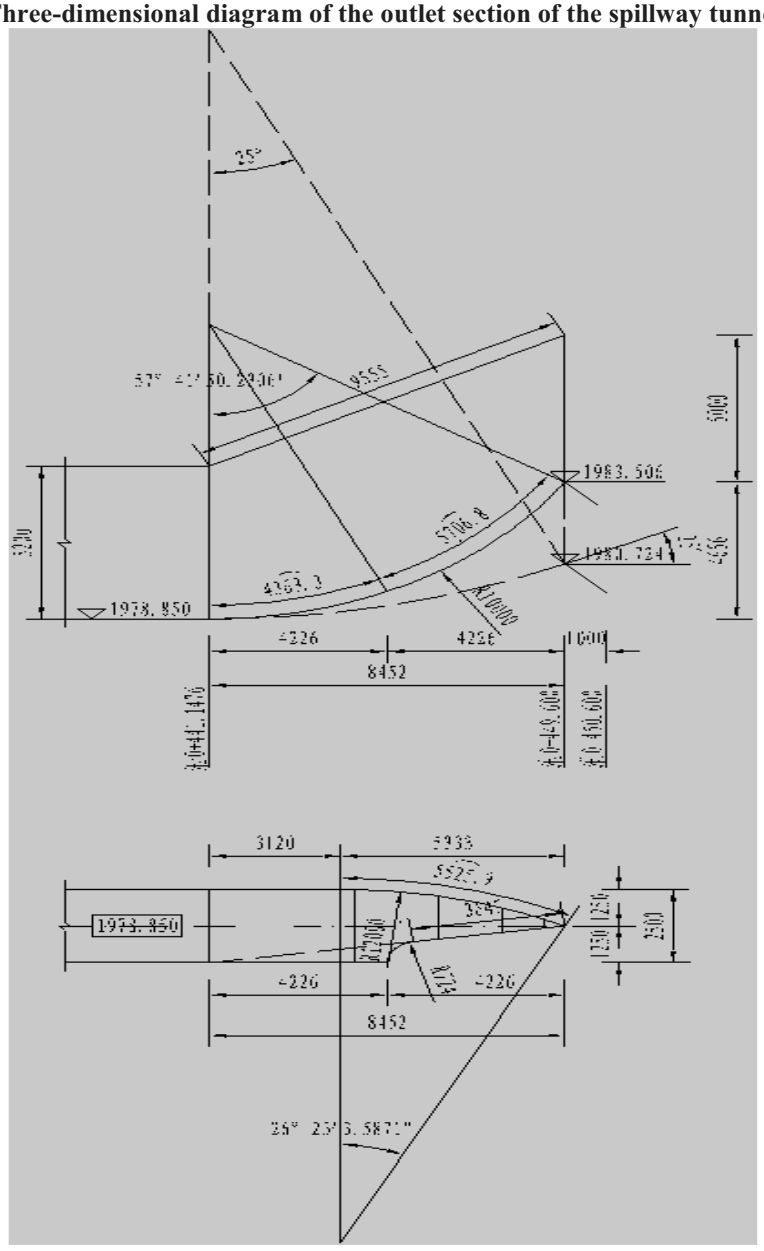

FIGURE 3
Design of the abnormal flip bucket

chamber section, Longtaitou section, pressure section, working chamber section, and outlet energy dissipation section. The floor elevation of the inlet horn section (0+000.000～0+003.200) was 2007.00 m, which connected to a 48.80-m-long round pressure section with a hole diameter of 3.20 m. The repairing chamber section was (0+062.000 ～ 0+068.000) 6.00 m long. A 10.00-m-long round-to-square pressure slope section (D3.2m→2.8×2.8 m) was set on the upstream side and another 10.00-m-long square-to-round section (3.2×3.2 m→D3.2 m) was set on the downstream. The Longtaitou section was 0+078.000～0+129.447, with a hole diameter of 3.20 m. The round pressure section was 0+129.447 ～0+410.600, where the hole diameter was 3.20 m and the longitudinal slope was 1/200. The working chamber section (0+416.000 ～ 0+430.600) was 14.00 m long and a 6.00- m-long round-to-square pressure slope section (D3.2m→2.5×2.5 m) was set up on the upstream. Subsequently, the outlet section of ski-jump energy dissipation (Figure 2) was established, which was 20.00 m long and 2.50 m wide. The elevation at the top of flip bucket was 1980.724 m, the arc radius was 20.00 m, and the ski-jump angle was 25°. An area downstream to the flip bucket was connected to a 10.00-m-long apron.

Flip bucket of spillway tunnel. The coverage and the horizontal length of the arc section of the spillway tunnel were kept constant while the arc radius decreased from 20.00 m to 10.00 m. The ski-jump angle was gradually changed from 57˚41′50.2306″ to 25˚ from the left to the right. The elevation of the nose of the weir at the left wall was 1983.506 m and the elevation on the right wall was 1979.787 m. The right wall of 0+441.148 ～ 0+449.600 was eliminated, while the left wall deflected toward the downstream from 0+444.267 at a radius of 12 m on the plane. An oblique nose of the weir was set from the ski-jump angle of 0˚ at the right wall to the axis of the 0+449.600 mileage. Meanwhile, the ski-jump flow was measured close to the nose weir to prevent a too great of an angle in the right flow. An arc connected oblique nose weir with a plane radius of 0.724 m was set in position (0+445.374) with a ski-jump angle of 25˚ on the right wall. The design of the abnormal flip bucket is shown in Figure 3.

Experiment of spillway tunnel. Experimental design. The model was designed according to gravity similarity and a normal model was applied. According to the calculations and comparisons, the final scale of the model was λL=40 and the corresponding scale parameters were:

Flow scale: λQ=λL*5/2=10119
Time scale: λT=λL/2=6.325
Flow rate scale: λV=λL/2=6.325
Roughness scale: λn=λL/6=1.849

Experimental manufacturing. The downstream terrain at the outlet of the spillway tunnel started from the arc section. It was mainly filled with scouring materials and cement dies. The pressure section and non-pressure section of the spillway tunnel were manufactured using organic glass according to the shape and size provided by the design unit (Figure 4). The roughness rate met the experimental requirements (the roughness rate of organic glass was n=0.007～0.009 and the roughness rate of concrete was n=0.014～0.017. The roughness scale of the prototype and model was 1.56～2.43.).

FIGURE 4
Experimental model of the ski-jump flow section in the spillway tunnel

Water jet shape of the spillway tunnel and downstream scouring. Taking into consideration energy dissipation and erosion control during a flood, which occurs once every 30 years (P=3.33%), the left water depth increased to 2.40 m as water flow at the outlet section was influenced by wall deflection, while on the right the depth of water did not significantly change. The cross-section of the outflow was approximately a Z-shaped section. The jet trajectory length of the left flow was 72 m and the water flow fell at 18 m on the right of the axis (downstream). The greatest height of the middle water jet was 24 m and the jet trajectory length was 96 m, while the water flow fell at 30 m to the right of the axis (downstream). The right-hand water flow was injected by different layers (the upper water flow was injected along the axis and the lower water flow was injected along the axis toward the right at 25°). The jet trajectory length was 30 m. The lower edge of the water jet was only 2.40 m away from the water surface (depth of water = 3.2 m). After continuous scouring over a period of 4 h, the left-hand flow and middle flow dropped, without a scouring pit forming. The scouring pit of the right-hand flow was 5.50 m long, 5.00 m wide and 2.40 m deep.

Taking into consideration energy dissipation and erosion control during flood conditions, the water jet from the spillway tunnel is shown in Figure 5, which is approximately “Z-shaped”. The water jet from the bottom layer is shown in Figure 6.

FIGURE 5
Left view of the ski-jump flow experiment in the spillway tunnel

FIGURE 6
Right view of the ski-jump flow experiment in the spillway tunnel

Numerical simulation contrast experimental results of the abnormal flip bucket. Standard $k-\varepsilon$ model. The standard $k-\varepsilon$ model requires solving the turbulence energy and dissipation rate equation. The transport equation of turbulence energy is deduced from an accurate equation, while the dissipation rate equation is inferred from physics and is gained from the mathematical simulation of similar round equations. The standard $k-\varepsilon$ model hypothesizes that flow has full turbulence and the influences of molecular viscosity can be neglected. Therefore, the standard $k-\varepsilon$ model is only applicable to simulations of the complete turbulence flow process. This model was proposed by Spalding and Launder in 1972 [9, 10]. The dissipation rate of turbulence (ε) is defined as:

$$\varepsilon = \frac{\mu}{\rho}\overline{\left(\frac{\partial u_i'}{\partial x_k}\right)} \tag{1}$$

The turbulence viscosity coefficient is μ, which can be expressed as the function of k and ε.

$$\mu_t = \rho C_\mu \frac{k^2}{\varepsilon} \tag{2}$$

In the standard $k-\varepsilon$ model, the transport equation of k and ε is introduced as follows.

The k equation is:

$$\frac{\partial(\rho k)}{\partial t}+\frac{\partial(\rho k u_i)}{\partial x_i}=\frac{\partial}{\partial x_j}\left[\left(\mu+\frac{\mu_i}{\sigma_k}\right)\frac{\partial k}{\partial x_j}\right]+G_k+G_b-\rho\varepsilon-Y_M+S_k \tag{3}$$

The ε equation is:

$$\frac{\partial(\rho\varepsilon)}{\partial t}+\frac{\partial(\rho\varepsilon u_i)}{\partial x_i}=\frac{\partial}{\partial x_j}\left[\left(\mu+\frac{\mu_i}{\sigma_\varepsilon}\right)\frac{\partial\varepsilon}{\partial x_j}\right]+C_{1\varepsilon}\frac{\varepsilon}{k}(G_k+C_{3\varepsilon}G_b)-C_{2\varepsilon}\rho\frac{\varepsilon^2}{k}+S_\varepsilon \tag{4}$$

where G_b is the production term caused by buoyancy. For incompressible fluid, $G_b=0$. For compressible fluid, there's:

$$G_b=\beta g_i\frac{\mu_i}{\mathrm{Pr}_i}\frac{\partial T}{\partial x_i} \tag{5}$$

where Pr_i is the turbulent Prandtl number and $\mathrm{Pr}_i=0.85$ in this model. g_i is the gravitational acceleration and β is the coefficient of thermal expansion:

$$\beta=-\frac{1}{\rho}\frac{\partial\rho}{\partial T} \tag{6}$$

G_k is the production term of the turbulence energy (k) and it is caused by the average velocity gradient:

$$G_k=\mu_i\left(\frac{\partial u_i}{\partial x_j}+\frac{\partial u_j}{\partial x_i}\right)\frac{\partial u_i}{\partial x_j} \tag{7}$$

For incompressible fluid, $Y_M=0$. For compressible fluid, there's

$$Y_M=2\rho a M_t^2 \tag{8}$$

where a is the sound velocity and $a=\sqrt{\gamma RT}$. M_t is the turbulence Mach number and $M_t=\sqrt{k/a^2}$.

In the standard $k-\varepsilon$ model, $C_\mu=0.09$, $\sigma_\varepsilon=1.3$, $C_{1\varepsilon}=1.44$, $C_{1\varepsilon}=1.44$ and $\sigma_k=1.0$.

The standard $k-\varepsilon$ model is the simplest, complete two-equation turbulence model, which has wide applicability, is economical and achieves reasonable accuracy. It is extensively applied in the industrial flow field and in heat exchange simulations [11, 12].

Comparison of calculated results. The greatest height of the water jet and the jet trajectory length were calculated as 22.88 m and 91.64 m, respectively. Simulation results are shown in Figure 7, Figure 8, Figure 9 and Table 1.

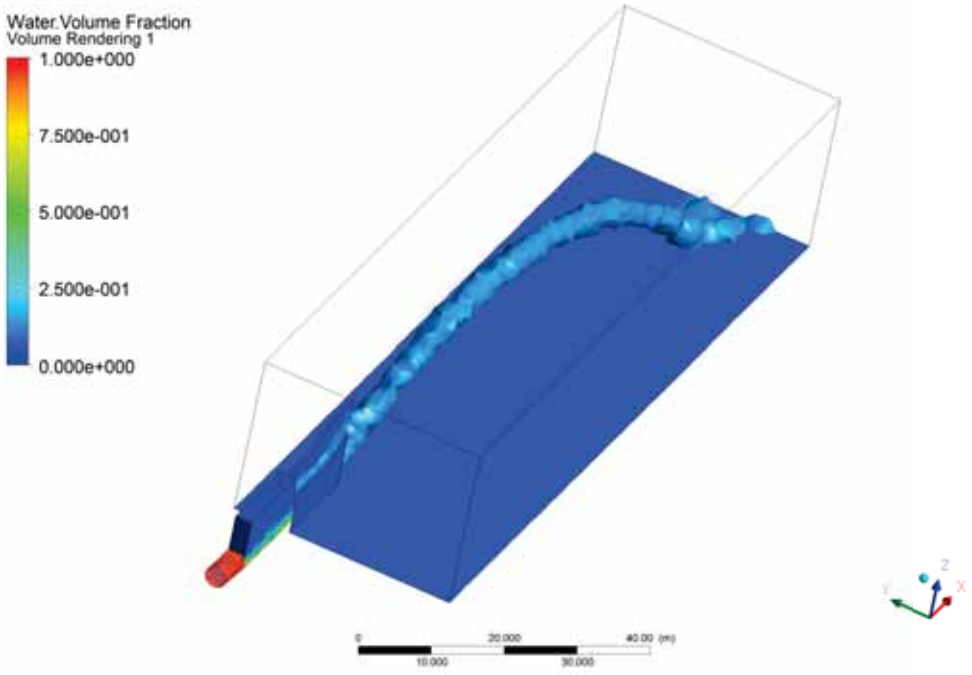

FIGURE 7
Numerical simulation of abnormal flip bucket

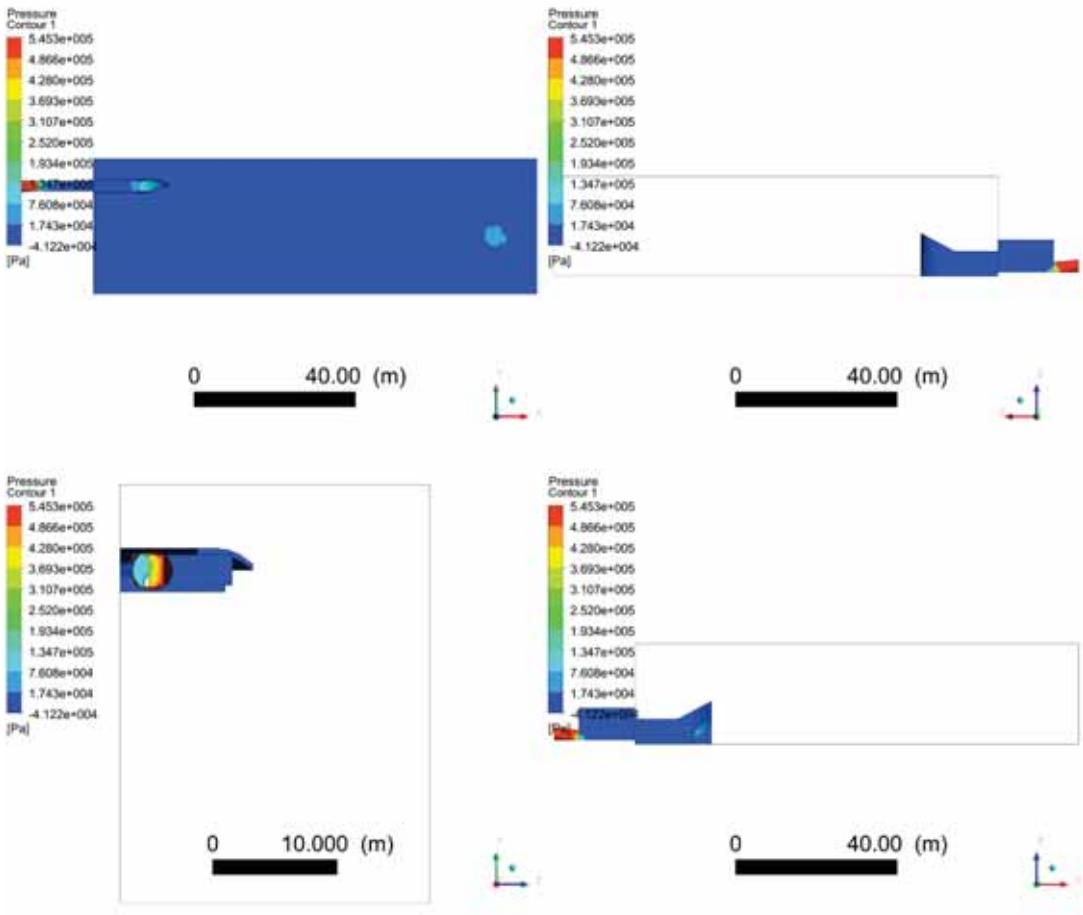

FIGURE 8
Pressure contour

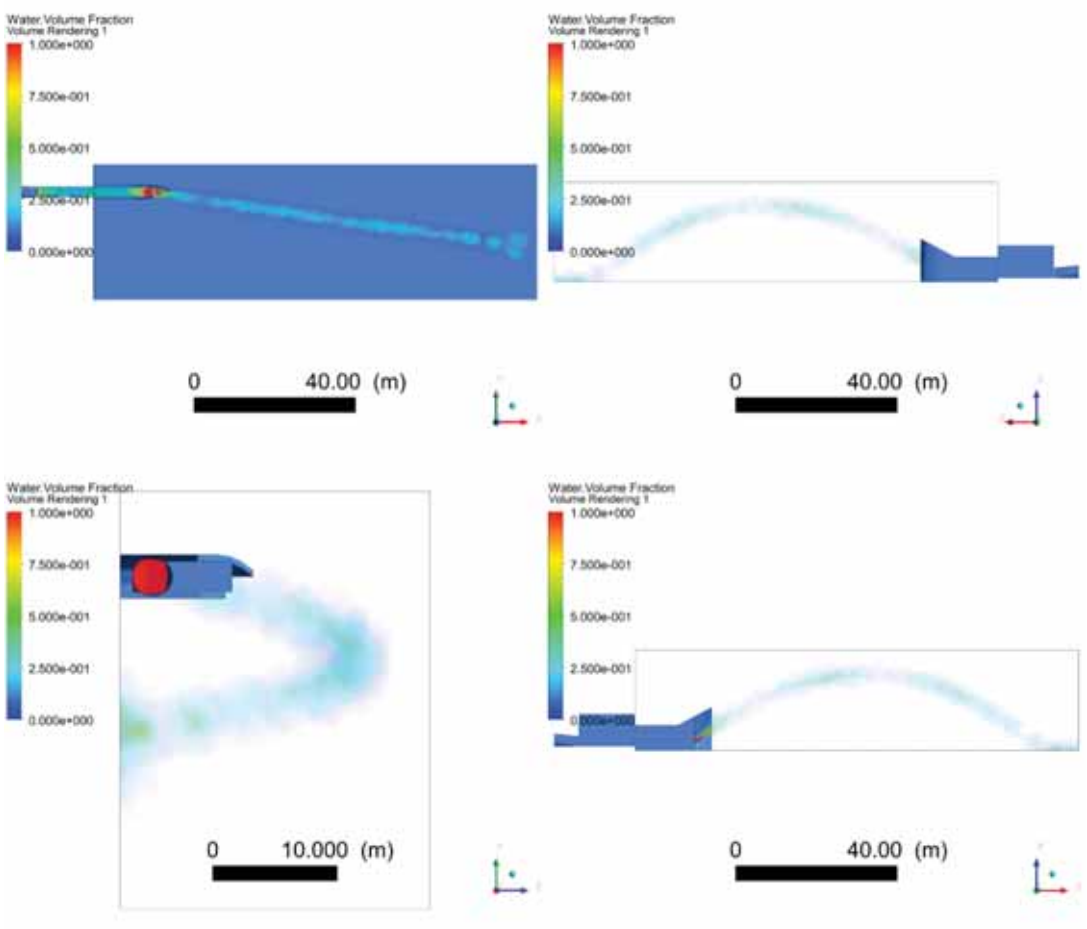

FIGURE 9
Volume rendering

TABLE 1
Hydraulic elements of spillway tunnel Q=71.96m³/s (P=3.33%)

Number of measuring points	Mileage	Measured flow rate (m/s)	Calculated flow rate (m/s)	Notes
1	0+052.000	8.95	8.95	Round-to-square
2	0+062.000	9.18	9.06	
3	0+064.500	9.18	6.77	Maintenance
4	0+064.500	9.18	6.77	Gate slot
5	0+068.000	7.03	7.81	Square-to-round
6	0+078.000	8.95	8.97	
7	0+105.000	8.95	8.92	Longtaitou
8	0+129.447	8.95	8.94	
9	0+410.200	8.95	9.01	
10	0+411.000	8.99	9.16	Pressure slope section
11	0+416.600	11.51	12.84	
12	0+420.600	31.82	32.46	After the gate
13	0+442.148	28.89	27.25	Arc section
14	0+450.600	27.77	24.79	

Analysis of calculated results. Contrast analysis between theoretical values and experimental values. Three conclusions could be gained from Table 1.

Conclusions 1. Theoretical value of speed is generally consistent with the actual value of speed.

Conclusions 2. Water flows in the pressure circular tube to keep a constant flow velocity.

Conclusions 3. The water flow rate increases suddenly after the gate and then decreases gradually. Using the calculated results, the software can effectively simulate the whole water flow process [13].

Analysis of the relationship between theoretical value and the actual environment. It can be seen from Figure 7 that ski-jump flow only has one falling point in the numerical simulation. The greatest height of the water jet and the jet trajectory length are calculated as 22.88 m and 91.64 m, respectively. These two parameters are similar to those in the experiment (24 m and 96 m, respectively). To calculate the jet trajectory length, attention shall be paid to the position with the deepest scouring pit. The actual jet trajectory length is different from the theoretical value. According to different engineering cases, the actual jet trajectory length greatly differs from the theoretical value due to variations in environmental conditions in real-world scenarios. These include thin air, low atmospheric pressure and small resistance in plateau regions with high altitude. On the contrary, there is high atmospheric pressure and strong resistance in plain regions with low altitude. In windy regions, water flow experiences aerated flow dissipation due to the influence of winds. The calculation of such aerated flow dissipation is very complicated and it is difficult to express by mathematical equations [14]. The pressure intensity distribution is shown in Figure 8 and the volume rendering of the volume fraction of water flow is shown in Figure 9.

Multi-objective optimization design of the abnormal flip bucket. The complicated optimization of ski-jump flow involves many problems. In the process of changing the ski-jump flow model, the runoff of ski-jump flow is changed (especially the abnormal flip bucket). Water flow might go from having a single falling point to multiple falling points. In the optimization of high-speed water flow, optimization goals were set to obtain maximum kinetic energy and pressure at all water falling points. Therefore, the minimums among these maximums would provide the optimal scheme [15].

Multi-objective optimization model. Objective function. The objective function is the minimum pressure caused by water flow impacting on walls and the minimum impact velocity of water fall on walls. Since the pressure is negative, its maximum is set at 0. The geometric model corresponding to the minimum pressure and minimum speed at the falling point has to be identified.

Design variables. The overflow width of the flip bucket, as well as the height of water from the flip bucket (height of the flip bucket), were defined as the design variables. They are direct influencing factors of the width and height of the water jet. The height of the flip bucket influences different arc angles in the modeling. Therefore, the angle was not used as a design variable [16, 17].

Constraint. The boundary condition of the flip bucket model was used as one constraint for optimization of ski-jump energy dissipation. The inlet flow rate was kept constant and it was used as one constraint. The movement range of the ski-jump flow in the air was defined as one constraint. A reasonable size range of the flip bucket was determined according to that in the experimental model, which was viewed as one constraint. The optimal solution could be found within this range [18].

Optimization algorithm. It is necessary to choose multiple objectives in the optimization of the flip bucket. The ski-jump flow process is very complicated. Having a single objective makes it difficult to find a relatively reasonable optimization result [19]. The multi-objective optimization algorithm can generally be divided into two types: normalized type and non-normalized type.

A normalized multi-objective optimization algorithm changes multiple objectives into a single objective for optimization, and the weight is determined subjectively by the optimizer rather than the decision maker. The normalized multi-objective optimization algorithm is very sensitive to the optimal leading shape of Pareto. It can neither process the leading valley of Pareto nor does it have high problem-solving efficiency.

The non-normalized multi-objective optimization algorithm processes multiple objectives directly by the Pareto mechanism. It does not have to transform multiple objectives into a single objective to make the leading edge of the solving set as close as possible to the leading edge of Pareto. Meanwhile, the leading edge of Pareto can be covered uniformly. The non-normalized multi-objective optimization algorithm is a multi-objective genetic algorithm. In this study, the multi-objective genetic algorithm NSGA-II was applied [20].

Optimal design scheme 1. A model was constructed and it was then meshed well. The model was input into the sculptor software, which was used for the deformation of grids of the flip bucket. Later, grids were processed by ICEM and calculated by the Ansys fluent software. Finally, the sculptor software ICEM and the Ansys fluent software of the model were integrated by Isight software (Figure 10).

Advantages. Parameterization of the calculation model was not necessary. A model was constructed and then meshed. The grid deformation was carried out directly by the sculptor software of the design model and the model size was changed. Grids were processed by ICEM, and the Ansys fluent software was applied for calculation. Finally, the optimal computation was performed after integration of the Isight software. Moreover, optimal design scheme 1 has high operation speed and saves time.

Moreover, it does not construct a model for every computation.

Disadvantages. The simulation accuracy of sculptor software in model deformation is lower than that of parameterization modeling.

Optimal design scheme 2. For parameterization of the model in the Ansys software, the mathematical relation among initial design points had to be determined. Coordinates of 10 points in the initial design were calculated by solving the equation of a circle and a proportional method corresponding to the triangle similarity:

$Angle\ is\ the\ ski-jump\ angle$

$r_1\ is\ the\ ski-jump\ arc$

$h_1\ is\ height\ of\ the\ inlet\ wall$

$h_2\ is\ height\ of\ the\ outlet\ wall$

$w\ is\ the\ inlet\ width$

$r_2\ is\ the\ radius\ of\ deflected\ arc$

$r_3\ is\ the\ radius\ of\ the\ arc,\ which\ is\ connected\ to\ the\ oblique\ flip\ bucket$

$$r_3=\frac{wr_1\sin(angle)}{4(\sqrt{(r_1\sin(angle))^2+(\frac{w}{2})^2}-\frac{w}{2}}$$

$$k_1(0,0,0)$$

$$k_2(0,h_1,0)$$

$$k_3(r_1\sin(angle),\frac{r_1}{2}+h_2-\sqrt{\frac{r_1^2}{4}-(r_1\sin(angle))^2}),0)$$

$$k_4(r_1\sin(angle),\frac{r_1}{2}-\sqrt{\frac{r_1^2}{4}-(r_1\sin(angle))^2}),0)$$

$$k_5(0,0,1)$$

$$k_6(0,0,1+w)$$

$$k_7(r_1\sin(angle)-\sqrt{r_2^2-(r_2-\frac{w}{2})^2},0,1)$$

$$k_8(\frac{r_1\sin(angle)}{2},0,1+w)$$

$$k_9(r_1\sin(angle),0,1+\frac{w}{2})$$

$$k_{10}(\frac{r_1\sin(angle)}{2}+r_3(1-\frac{w}{2\sqrt{(r_1\sin(angle))^2+(\frac{w}{2})^2}}+(\frac{w}{2})^2),0,$$

$$1+w-\frac{r_3r_1\sin(angle)}{\sqrt{(r_1\sin(angle))^2+(\frac{w}{2})^2}})$$

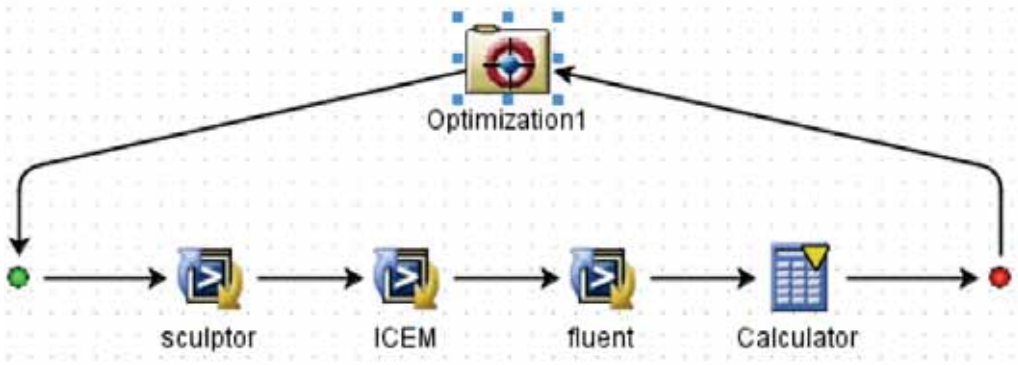

FIGURE 10
Calculation procedure for Isight software

The grid part cannot directly be realized in workbench from the construction of the model to gridding and, finally, to computation. In a word, this scheme requires recording the macro-efficiency in workbench to record the gridding program, which makes the scheme easier to use.

Advantages. This scheme can very accurately determine the relationship between model size and the optimization objective.

Disadvantages. Each computation requires constructing a new model, followed by meshing. It often requires hundreds of repeated computations, or more, to realize the optimization objective. The model construction in each computation significantly increases the workload of the computer.

Reasons for using optimal design scheme 1 as the optimization scheme. Optimal design 1 needs no modeling in each computation. Instead, it only has to draw the original design model, which changes according to the given size range. This requires a shorter computation time. Optimal design 2 requires parameterization of the model and a new model has to be constructed for each change to the computational model, thus resulting in longer computation time. Therefore, optimal design 1 was chosen for this study.

RESULTS AND DISCUSSION

Optimization results. The following optimization results were gained from repeated computation of different ski-jump flows based on the computer program:

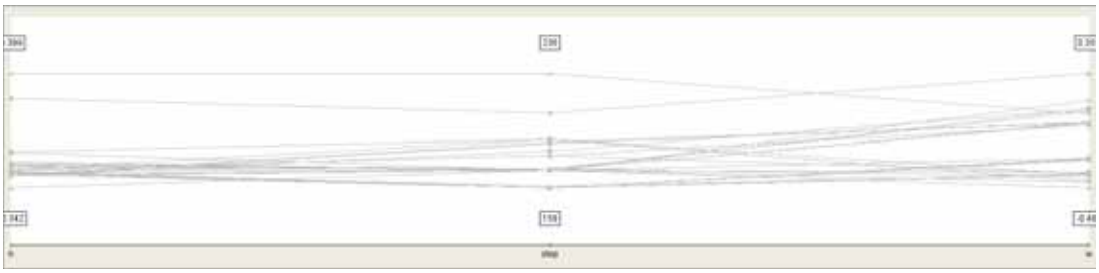

FIGURE 11
Relationship between numerical values and positions h, w and step

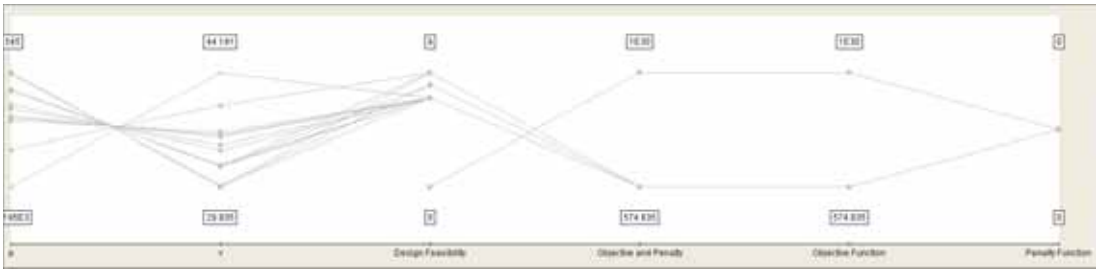

FIGURE 12
Relationship between numerical values p, w, design feasibility, objective and penalty, objective function and penalty

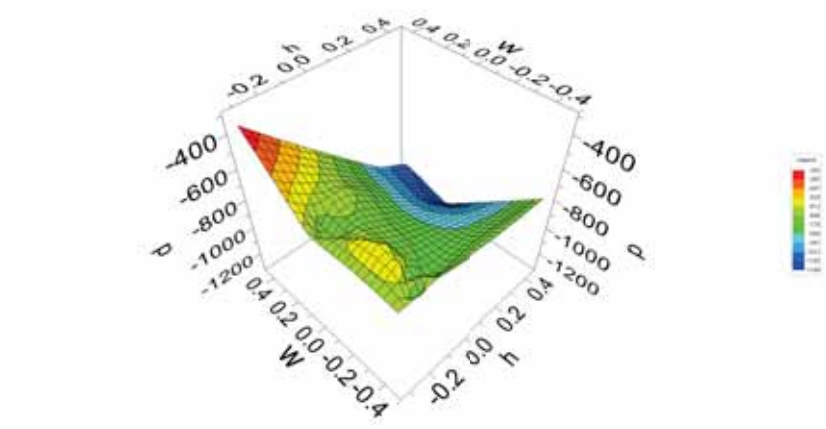

FIGURE 13
Contour map of the three-dimensional relationship of overflow width and height of flip bucket with the intensity of water pressure

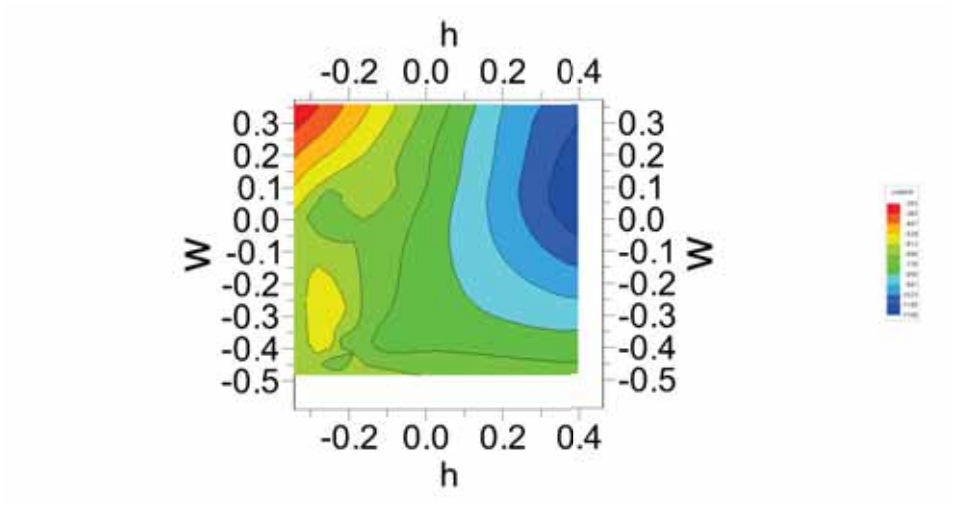

FIGURE 14
Contour map of the two-dimensional relationship of overflow width and height of flip bucket with the intensity of water pressure

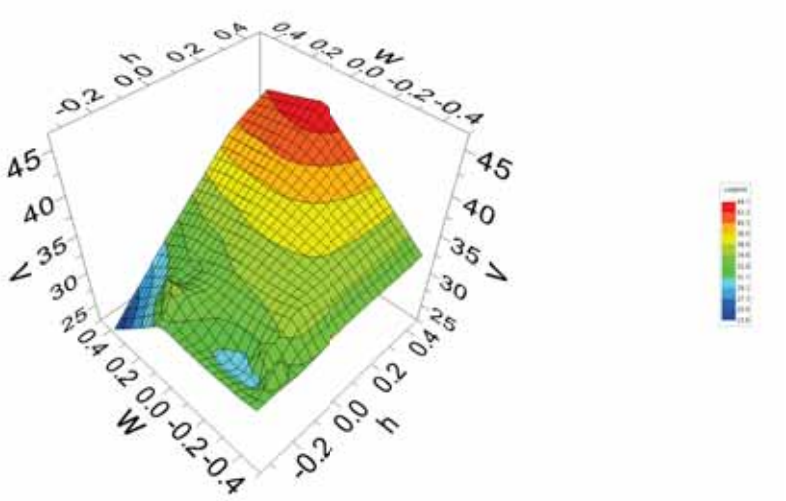

FIGURE 15
Contour map of three-dimensional relationship of overflow width and height of flip bucket with flow velocity

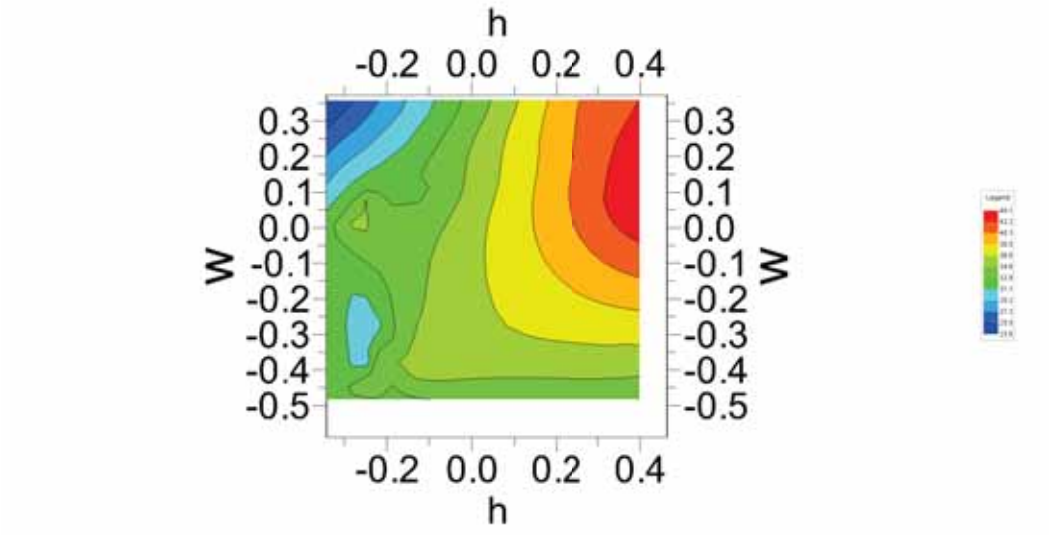

FIGURE 16
Contour map of two-dimensional relationship of overflow width and height of flip bucket with flow velocity

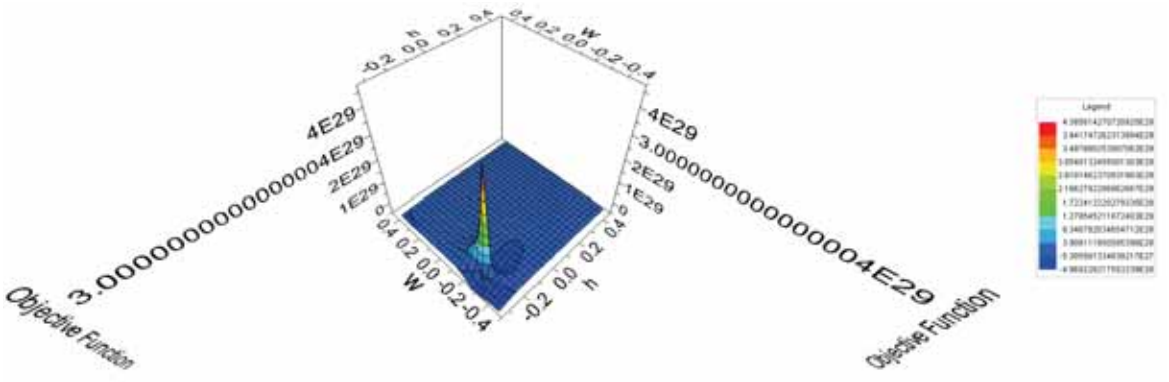

FIGURE 17
Contour map of the three-dimensional relationship of overflow width and height of flip bucket with the objective functional value

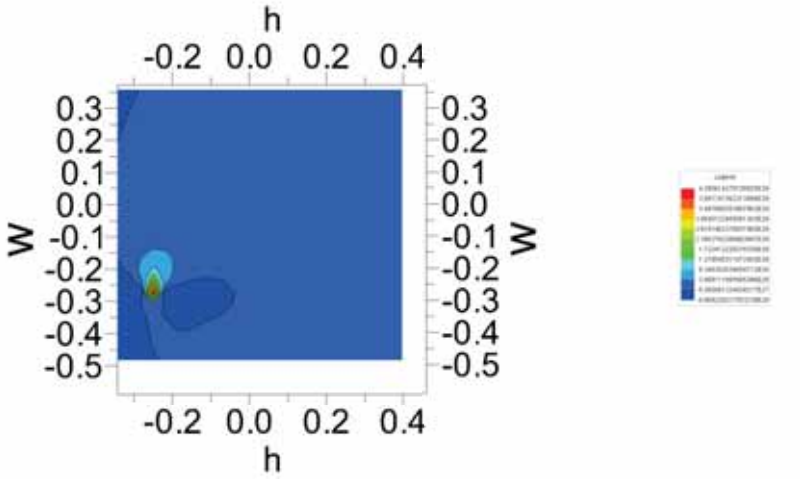

FIGURE 18
Contour map of the two-dimensional relationship of overflow width and height of flip bucket with the objective functional value

Discussion of optimization results. Analysis of computation time. Based on the above results, the water pressure against the ground over different periods varies. Therefore, the optimal body cannot consider the optimal body simply at one time point. Moreover, attention should be paid to the corresponding period of the optimal body shape. In this way, a reasonable optimal solution can be realized. In this study, this period is chosen as 1 s. Hence, the optimal body shape can only be realized during this 1-s-period and only the optimal model during this 1 s is calculated. In Table 2, the optimal solution is to decrease the overflow width by 0.26574 m and decrease the height of the flip bucket by 0.23634 m. Compared with the original scheme, this optimal solution showed an 18.29% lower pressure intensity and a 17.74% lower kinetic energy. To increase the accuracy of the research results, the computation time was increased, such as setting the time period as 10 s. This can prolong the operation time of the computer. Optimization is only performed after stabilization of water fall, because water fall from the starting point to the ground is not stable over a short period. Only stable flow can shorten the computation time for optimization.

Discussion of the relationship between the size of flip buckets and hydraulic elements. Relevant laws among hydraulic elements can be found from optimization. Optimization should not only consider the pressure of falling points and the relationship between flow velocity and the size of flip bucket [21], but also the relationship between pressure at falling points and the sizes of different flip buckets, aiming to find the size that has the greatest influence on the pressure at the falling point. Similarly, attention should be paid to the relationship between the flow velocities of falling points and the sizes of different flip buckets, finding the size that has the most influence on the kinetic energy of the falling point. In this way, the determined model size can be used in the optimization, providing an important reference for modification of the model design. Moreover, the model size can again be used as the optimal design variable for secondary optimization, again providing important references for the selection of design variables. Multiple design variables can be subjectively selected for optimization. After the optimization, the size of some flip buckets can hardly influence the objective function [22-25].

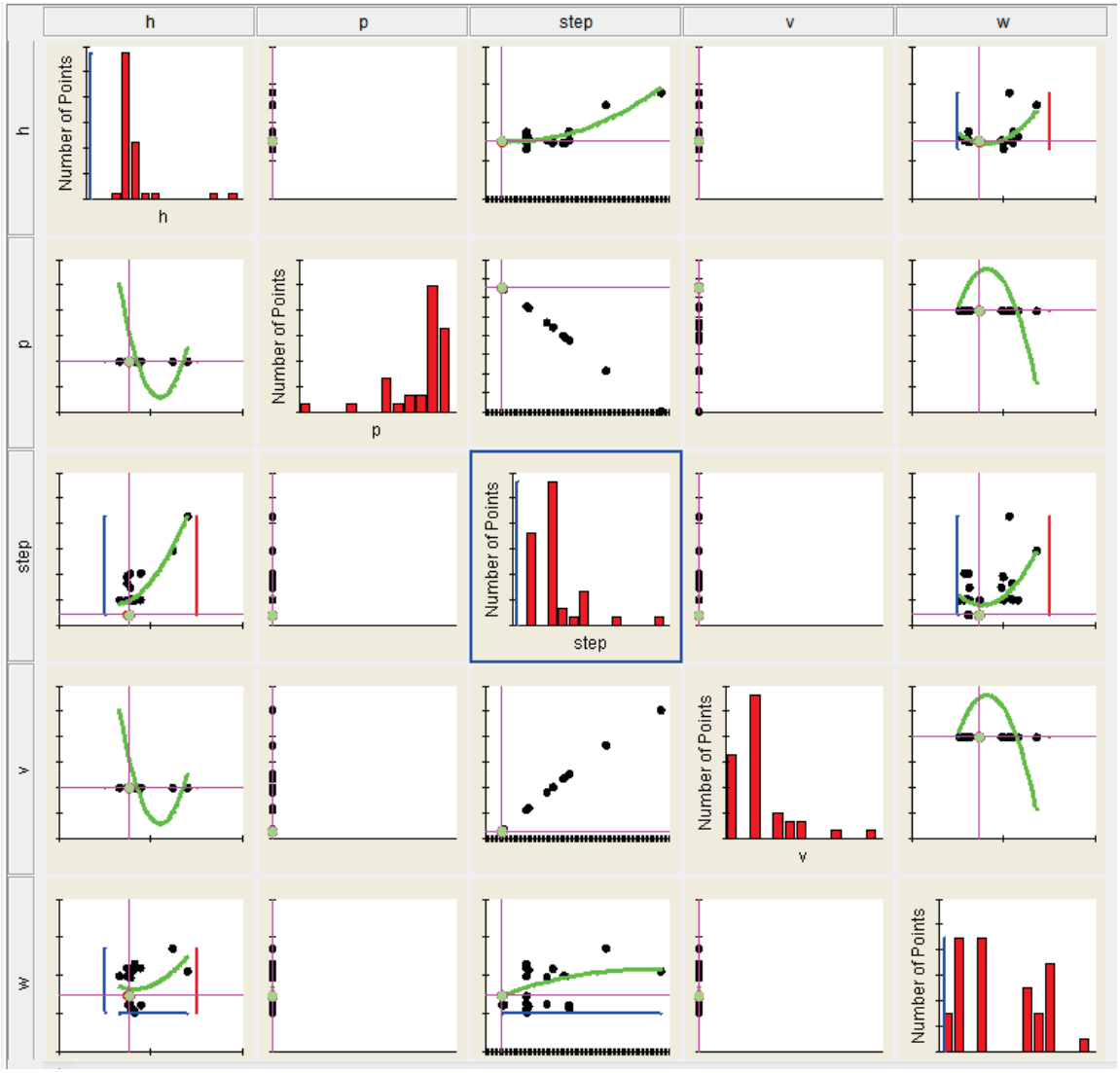

FIGURE 19
Two-dimensional numerical relationship matrix among different calculation parameters

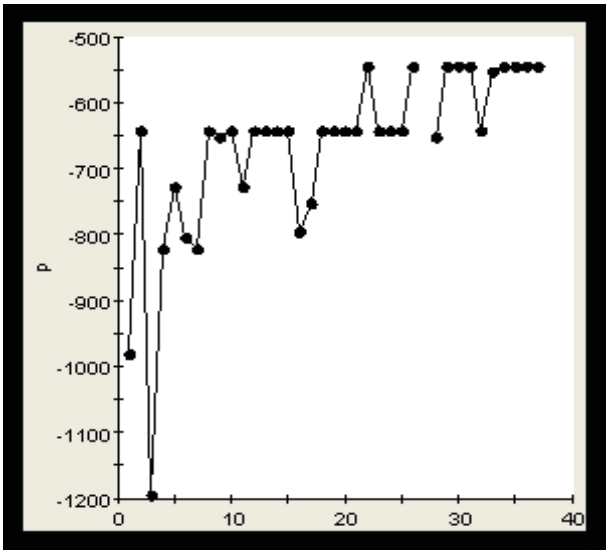

FIGURE 20
Optimization process of pressure values

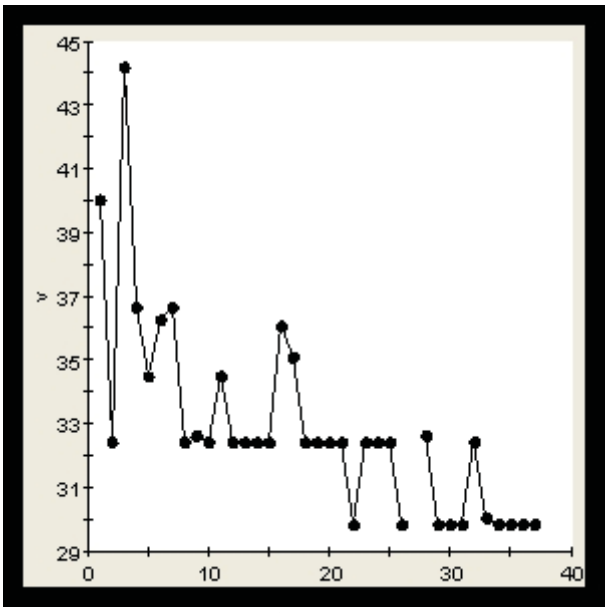

FIGURE 21
Optimization process of velocity

TABLE 2
Comparison of the optimization results and the original design scheme

Variables	Original Design Value	Optimal Value
Pressure at falling points	-667 Pa	-545 Pa
Velocity arriving at the falling points	32.89 m/s	29.83 m/s
Overflow width	3.2 m	2.93426 m
Height of flip bucket	4.6561 m	4.41366 m

Information obtained from the results diagram. The above results diagram mainly indicates the relations among all variables in the optimization. Variables include overflow width, the height of the flip bucket, computation time step, pressure at falling point, the velocity at falling point and objective functional value. The overflow width influences the scouring range of falling points of the ski-jump flow. According to model parameterization, the height of the flip bucket is closely related to the arc angle in different models. Variations of heights directly influence the size of the arc opening. The height of the flip bucket is positively related to the degree of opening and the degree of opening is positively related to the length of the flip bucket. In the above view, the degree of arc opening along the horizontal direction of the flip bucket is large. This indicates that the height of the flip bucket is related with different arc angles. Representing the height of flip bucket as different arc sizes directly in optimization can lower the workload involved in model processing. The calculation time step mainly serves to assist in optimization, its main function being to divide time periods. Time also will influence pressure and velocity at falling points. Using a single time point makes it difficult to prove that results are optimal. Hence, one time period was chosen. Pressure and velocity at falling points in one time period are variable, which can allow for better interpretation of the influences of water flow on surface scouring. The pressure at falling points mainly reflects the vertical scouring effects of flow and can also influence the depth of the scouring pit. Velocity at falling points mainly reflects kinetic energy when flow hits the ground surface and it also influences the shape of the scouring pit. The objective functional value mainly reflects the comprehensive value of two objectives. Finally, the above result diagram was analyzed. Numerical relation diagrams of different variables were drawn (Figure 11 and Figure 12). The two-dimensional and three-dimensional contour maps of relations of overflow width and height of the flip bucket with pressure and flow velocity at falling points are shown in Figure 13, Figure 14, Figure 15 and Figure 16. Based on these maps, the influence of the shape of the flip bucket on two optimization goals was analyzed. The two-dimensional and three-dimensional contour maps of relations of overflow width and height of flip bucket with objective functional value (Figure 17 and Figure 18) were used to analyze the comprehensive influence of the shape of the flip bucket on multiple objectives. The two-dimensional numerical relationship matrix among different calculation parameters (Figure 19) can identify the relations among different parameters. Finally, the optimization process of two optimization goals (Figure 20 and Figure 21) reveals multiple optimal solutions [26-31].

CONCLUSIONS

Optimization should be based on an original design scheme. The model size has to be corrected and the relationship among different model sizes must be reflected in the mathematical relation of model size in the original design scheme. In the design scheme, changing one model size might influence the size at other positions. Therefore, the chosen optimization variables should be representative and able to evaluate the whole model size. Optimization seeks to improve the original design scheme. The original design schemes mainly come from experience. Faced with varied real-life conditions, optimization only becomes meaningful by combining certain theoretical bases.

In this study, a shape modification program of the flip bucket is proposed and results are calculated by a genetic algorithm. Results demonstrated that the optimal design scheme produces a weaker scouring force from water flowing onto the ground compared with the original scheme, indicating the reasonability of the optimization results.

ACKNOWLEDGEMENTS

This study was funded by National Natural Science Foundation of China (grant number 51579089).

REFERENCES

[1] Qian, S.T. (2013) Ski-jump-step Energy Dissipators. Proceedings of the 35th IAHR World Congress. Chengdu, China.

[2] Huang, G., Xie, S., Duan, W. (2011) Optimization, Application of Energy Dissipation Works for Ski Jump Spillway at High Dams. Journal of Yangtze River Scientific Research Institute. 28, 90-93.

[3] Zhang, X., Liang, C., Fu, Q., Zhang, X. (2003) Application of Energy Approach to Estimating Scour Depth. Journal of Sichuan University. Engineering Science Edition. 35, 27-30.
[4] Liu, Z., Liu, H., Sun, S., Pan, X., Zheng, T., Li, G. (2018) Study on flood discharge atomization of ski-jump energy dissipation scheme for reconstruction project of Fengman Hydropower Station. Water Resources, Hydropower Engineering. 49, 108-113.
[5] Wu, J., Qian, S., Ma, F. (2016) A new design of ski-jump-step spillway. Journal of Hydrodynamics. 28, 914-917.
[6] Deng, J., Yang, Z., Tian, Z., Zhang, F., Wei, W., You, X., Xu, W. (2016) A new type of leak-floor flip bucket. Science China-Technological Sciences. 59, 565-572.
[7] Zhu, A., Huang, T., Zhang, Y., Lang, L. (2016) Study on ski-jump energy dissipation scheme for lower reservoir of Zhouning Pumped Storage Hydropower Station. Water Resources, Hydropower Engineering. 47, 34-39.
[8] Gou, W., Li, H., Du, Y., Yin, H., Liu, F., Lian, J. (2018) Effect of Sediment Concentration on Hydraulic Characteristics of Energy Dissipation in a Falling Turbulent Jet. Applied Sciences-Basel. 8, 1682-1683.
[9] Lara, R.D., Ota, J.J., Fabiani, A.L.T. (2018) Reduction of the erosive effects of effluent jets from spillways by contractions in the flow. RBRH. 23, 11-12.
[10] Deng, J., Wei, W., Tian, Z., Zhang, F. (2018) Design of A Streamwise-Lateral Ski-Jump Flow Discharge Spillway. Water. 10, 1585-1586.
[11] Cheng, W., Yang, Q., Chang, Z. (2018) Application of leak-floor flip bucket to spillway for Lijiayan Reservoir. Water Resources, Hydropower Engineering. 49, 63-69.
[12] Lian, J., Wang, X., Zhang, W., Ma, B., Liu, D. (2017) Multi-Source Generation Mechanisms for Low Frequency Noise Induced by Flood Discharge, Energy Dissipation from a High Dam with a Ski-Jump Type Spillway. International Journal of Environmental Research, Public Health. 14, 1482-1483.
[13] Han, C., Zhao, T., Dang, Y., Sung, F. (2009) Hydraulic control of safe operation of large-scaled hypervelocity discharge tunnel. Advances in Water Resources, Hydraulic Engineering. 1-6, 1556-1561.
[14] Wu, J., Zhang, X., Ma, F., Wu, W. (2015) Ski jump trajectory with consideration of air resistance. Journal of Hydrodynamics. 27, 465-468.
[15] Qian, S., Wu, J., Ma, F. (2016) Hydraulic Performance of Ski-Jump-Step Energy Dissipater. Journal of hydraulic engineering. 142, 5016004-5016005.
[16] Zou, P., Wang, J., Yin, H. (2007) Research on dynamic characteristics of original rock in the scour pit of energy dissipation of ski-jump. Journal of Hydroelectric Engineering. 26, 71-75.
[17] Chen, Z., Chen, Y., Huang, G. (2002) Research of configuration of narrow opening ski jump spillway, estimation of longitudinally extended width of jet. Journal of Yangtze River Scientific Research Institute. 19, 11-14.
[18] Feng, J., Wang, L., Li, R., Li, K., Pu, X., Li, Y. (2018) Operational regulation of a hydropower cascade based on the mitigation of the total dissolved gas supersaturation. Ecological Indicators. 92, 124-132.
[19] Li, Z., Bai, C., Zhang, W. (2010) Optimum Test on Bucket Dissipation of Bashan Hydropower Station's Overflow Spillway. Journal of Yunnan Agricultural University. 25, 706-711.
[20] Li, Y.W., Long, M., Zuo, L.H., Li, W., Zhao, W.C. (2019) Brittleness Evaluation of Coal Based on Statistical Damage and Energy Evolution Theory. Journal of Petroleum Science and Engineering. 172, 753-763.
[21] Wang, Y., Jiang, C., Liao, R., Yang, Y. (2015) Effect of different outlet shapes of spillway tunnel on ski-jump energy dissipation. Journal of Hydroelectric Engineering. 34, 70-76.
[22] Haghiabi, A.H. (2017) Estimation of scour downstream of a ski-jump bucket using the multivariate adaptive regression splines. Scientia Iranica. 24, 1789-1801.
[23] Buffon, F.T., Marques, M.G. (2016) Pressure determination method in dissipation basins downstream of ski jump spillways. RBRH. 21, 576-586.
[24] Wei, W., Deng, J., Liu, B. (2013) Influence of aeration, initial water thickness on axial velocity attenuation of jet flows. Journal of Zhejiang University-Science A. 14, 362-370.
[25] Lucas, J., Hager, W.H., Boes, R.M. (2013) Deflector Effect on Chute Flow. Journal of Hydraulic Engineering - ASCE. 139, 444-449.
[26] Putton, V.C., Marson, C., Fiorotto, V., Caroni, E. (2011) Supercritical Flow over a Dentated Sill. Journal of Hydraulic Engineering - ASCE. 137, 1019-1026.
[27] Leite Ribeiro, M., Boillat, J.L., Schleiss, A.J., Laugier, F. (2011) Coupled spillway devices, energy dissipation system at St-Marc Dam (France). Labyrinth, Piano Key Weirs - PKW.
[28] Yuan, Q., Wang, X., Luo, S. (2010) The Application of Two-phase Flow Numerical Simulation in Fengman Dam Overall Treatment Project. Advances in Hydraulic Physical Modeling, Field Investment, Investigation. 1, 217-221.
[29] Steiner, R., Heller, V., Hager, W.H., Asce, F., Minor, H. (2008) Deflector ski jump hydraulics. Journal of Hydraulic Engineering-ASCE. 134, 562-571.

[30] Pardo-Gomez, R. (2008) Proposed method for the hydraulic design of ski-jump energy dissipators in dam spillways, considering the occurrence of scour holes downstream of the structure. Ingenieria Hidraulica en Mexico. 23, 111-121.
[31] Schmocker, L., Pfister, M., Hager, W.H., Minor, H. (2008) Aeration characteristics of ski jump jets. Journal of Hydraulic Engineering-ASCE. 134, 90-97.

Received: **13.07.2019**
Accepted: **27.01.2020**

CORRESPONDING AUTHOR

Lina Wang
Xi′an University of Science and Technology,
Xi′an 710054 – P.R. China

e-mail: meihao7w@163.com

© by PSP Volume 29 – No. 05/2020 pages 3547-3556 Fresenius Environmental Bulletin

STUDY ON EROSION WEAR CHARACTERISTICS AND NON-SMOOTH ABRASION RESISTANCE OF ENVIRONMENT FRIENDLY JET-TYPE HYDRAULIC HAMMER JET ELEMENTS USING IN UNCONVENTIONAL OIL AND GAS RESOURCES DEVELOPMENT

Yong Huang[1,2,*], Lihong Zhu[1,2], Deyong Zou[1,2], Zepeng Chen[1,2]

[1] School of Petroleum Engineering, China University of Petroleum (East China), Qingdao 266580, P.R. China
[2] Key Laboratory of Unconventional Oil and Gas Development (China University of Petroleum (East China)), Ministry of Education, Qingdao 266580, P.R. China

ABSTRACT

High energy jet hydraulic hammer drilling technology has the characteristics of high impact power, high rock crushing efficiency and long service life. It is especially suitable for drilling in unconventional oil and gas formations (such as shale gas, natural gas hydrate and dry hot rock) with high strength, high hardness, strong abrasiveness and poor drill-ability. It is expected to solve the drilling problems in deep well and even ultra deep well hard rock formations. Meanwhile, due to the high-energy hydraulic driving mode, the technology has the advantages of recycling and environmental protection compared with the conventional drilling technology. Aiming at understanding the erosion and wear failure of jet-type hydraulic hammer jet elements, the computational fluid dynamics method was used to numerically simulate the liquid-solid two-phase flow field in the jet element. The solid particle erosion and wear characteristics of the inner wall surface of the jet element were studied and the anti-wear properties of non-smooth walls was further analyzed. The results show that there is a high-speed jet zone and vortex zone inside the jet element, which drives the solid phase particles to erode the inner wall surface and finally could cause wear. The wear zone is mainly distributed at the positions of the nozzle, cover, wedge, and side wall. Compared with the smooth wall surface, the non-smooth rough walls can increase wall shear stress and reduce wall vorticity, thus reducing the rate of solid particle erosion wear. When the wall roughness thickness is about 1mm, the wall wear is the lowest. The maximum wear rates of the nozzle, cover, plate, wedge tip, and the side walls were reduced by 76.3%, 58.2%, 52.5%, and 29.6%, respectively. This research can provide reliable theoretical support for efficient and environmental protection drilling under complex geological conditions of unconventional oil and gas resources.

KEYWORDS:
Unconventional oil and gas resources, environment friendly, jet element, liquid-solid flow, erosion wear, non-smooth surface, surface roughness

INTRODUCTION

In recent years, unconventional oil and gas resources have attracted more and more attention, but the geological situation of such resources is usually complex, such as gas hydrate formation, dry hot rock and shale oil and gas, which have the problems of deep burial, high rock hardness and poor drill-ability. Conventional drilling technology cannot effectively meet the field technical requirements. In addition, conventional drilling technology has many problems, such as low energy efficiency and obvious environmental pollution. Jet-type hydraulic hammer is a drilling auxiliary tool that uses bi-stable jet elements as the control. The jet-type hydraulic hammer uses the high-pressure jet coanda effect to switch the drilling fluid in the upper and lower cavity of the piston to drive the hydraulic hammer to work. Jet-type hydraulic hammer has several advantage characteristics such as simple structure, few moving parts, adjustable parameters, and high confining pressure resistance which has broad application prospects in deep and ultra-deep well hard rock and oil and gas drilling in complex formations [1-2]. The jet element is the core component of the jet-type hydraulic hammer. The internal drilling fluid in the jet element has a high flow rate and a large solid phase content. These solid particles could erode the jet element during the work process, wearing the inner wall of the jet element and finally losing the switching function. Field application shows that the average service life of jet elements is less than 15 hours, which severely restricts the application and promotion of hydraulic hammers [3-4]. Therefore, it is of great theoretical and engineering significance to study the erosion and wear characteristics and anti-wear measures of

jet elements for optimizing and improving the cost performance and environmental protection.

The problem of solid erosion widely exists in all major fields of modern industry and is an important cause of equipment damage or material damage [5-8]. The search for efficient anti-wear methods has been a research hotspot for scholars at home and abroad. Improving the erosion resistance of fragile equipment is the most direct and effective way, such as selecting a new type of anti-wear material [9-10] or covering the surface of the existing material with a wear-resistant layer [11-12]. However, these kind of methods could increase costs.

The collision speed and angle of the solid particles and the material surface have a significant effect on wall wear. Changing the material surface morphology could affect the near-wall flow field conditions and effectively reduce the erosion strength of the solid particles on the material [13-14]. Non-smooth surface technology is a typical material surface treatment method. By setting a number of unit cells with a certain shape on the smooth surface of the material, the characteristics of the material surface such as drag reduction, anti-adhesion and anti-wear are improved [15]. At present, this technology has been applied in many fields and achieved good results [16-17].

In this paper, with the help of computational fluid dynamics method, the liquid-solid two-phase fluid characteristics and wall wear characteristics inside the jet element are numerically simulated and the anti-wear performance of non-smooth surfaces is further analyzed. This study is trying to provide ideas and ways to solve the jet element wear failure problem.

METHODS

CFD model. In this study, the discrete model is adopted with liquid phase as the continuous phase and solid particles as the discrete phase. The governing equations are solved in the Euler and Lagrangian frameworks. In order to consider the influence of discrete phase on the continuous phase, the interphase coupling calculations are used.

(1) Continuous phase model. The continuity equation and momentum equation of liquid phase fluid are:

$$\frac{\partial \rho}{\partial t}+\frac{\partial}{\partial x_i}(\rho u_i)=0 \quad (1)$$

$$\frac{\partial(\rho u_i)}{\partial t}+\frac{\partial}{\partial x_j}\left(\rho u_i u_j\right)=-\frac{\partial p}{\partial x_i}+\frac{\partial}{\partial x_j}\left[\mu\frac{\partial u_i}{\partial x_j}-\rho\overline{u_i' u_j'}\right]+S_i \quad (2)$$

Where, ρ is the density of the liquid phase fluid, t is time, u_i and u_j are fluid velocity components, u_i' and u_j' are fluid pulsation velocity components, p is fluid pressure, μ is hydrodynamic viscosity, and S_i is a generalized source term [18].

(2) RNG K-ε turbulence model. At present, the k-ε two-equation model is the most commonly used turbulence model for engineering fluid calculation. Compared with the standard K-ε model, the RNG K-ε turbulence model has higher accuracy in complex flow simulations such as jet impingement, swirl, separated flow, and secondary flow:

$$\frac{\partial(\rho k)}{\partial t}+\frac{\partial(\rho k u_i)}{\partial x_i}=\frac{\partial}{\partial x_j}\left(\alpha_k\mu_{eff}\frac{\partial k}{\partial x_j}\right)+G_k-\rho\varepsilon \quad (3)$$

$$\frac{\partial(\rho\varepsilon)}{\partial t}+\frac{\partial(\rho\varepsilon u_i)}{\partial x_i}=\frac{\partial}{\partial x_j}\left(\alpha_\varepsilon\mu_{eff}\frac{\partial\varepsilon}{\partial x_j}\right)+C_{1\varepsilon}\frac{\varepsilon}{k}G_k-C_{2\varepsilon}\rho\frac{\varepsilon^2}{k} \quad (4)$$

Where, $\mu_{eff}=\mu+\mu_t$,

$C_{\varepsilon 1}=1.42-\frac{\eta(1-\eta/\eta_0)}{1+\beta\eta^3}$, η_0=4.377, β=0.012, $C_{2\varepsilon}$=1.68, $\eta=Sk/\varepsilon$ $S=\sqrt{2\overline{S_{ij}S_{ij}}}$ [19].

(3) Discrete Phase Model. According to Newton's second law, the orbit equation of the solid particles in the flow field can be determined by the acting force. The specific model is as follows:

$$\frac{du_p}{dt}=F_D(u-u_p)+F_B+F_x=\frac{3\mu C_D\,\mathrm{Re}(u-u_p)}{4\rho_p d_p^2}+\frac{g(\rho_p-\rho)}{\rho_p}+F_x \quad (5)$$

In the above formula: $F_D(u\text{-}u_p)$ is the drag force per unit mass of particles, F_B is the gravity of cuttings, F_x is other forces of cuttings, including Magnus force, saffman lift, Basset force, C_D is Drag coefficient, Re is Reynolds number,u is the velocity of the liquid phase fluid, u_p is the velocity of the particles, ρ_p is the density of the particles, g is the acceleration of gravity [20].

(4) Wall wear model. The wall wear rate is evaluated by the unit area and the mass lost over time, and can be expressed as:

$$R_{erosion}=\sum_{p=1}^{N_{particles}}\frac{m_p C(d_p)f(\alpha)v^{b(v)}}{A_{face}} \quad (6)$$

In the formula: R_{erosion} is the wall wear rate, $N_{\mathrm{particles}}$ is the number of collision particles, m_{p} is the particle mass flow, $C(d_{\mathrm{p}})$ is a function of the particle diameter, $f(\alpha)$ is a function of the intrusion angle, and α is the intrusion angle of the particles on the wall, v is the relative speed of the particles when they collide with the wall, $b(v)$ is a function of this relative speed, and A_{face} is the area of the wall calculation unit [21].

Division and boundary conditions. The internal flow field of the jet element can be regarded as a three-dimensional model obtained by the vertical extension of the main view plane, so the Cooper method is used for meshing. According to the ge-

ometry of the main view plane, block processing is performed. The mesh type is a quadrilateral and triangular mixed grid. Taking the main viewing plane as the source plane and scanning the source plane grid, a hexahedron + wedge-shaped mixed grid of the entire flow field is obtained. The division result is shown in Figure 1.

The jet element is responsible for the input switching of the drilling fluid inside the hydraulic hammer. Therefore, the internal jet is deflected to one side most of the time, and the wall wear is symmetrical [22]. Therefore, in order to reduce the calculation cost, this article only simulates the single-sided output of the jet. The liquid phase fluid used in the simulation is liquid water and the physical parameters of the water are: density 998.2kg/m^3, kinematic viscosity coefficient 0.001kg/ms, and initial fluid flow velocity is 25m/s.

RESULTS AND DISCUSSION

Liquid phase fluid characteristics. Figure 2 shows the characteristics of liquid phase fluid inside a jet element. It can be seen from Figure 2 that during the operation of the jet element, the drilling fluid enters from the upper nozzle position. As the cross-sectional area inside the nozzle gradually decreases, the fluid velocity continues to increase. After passing through the rectangular stable section, the drilling fluid enters the jet element working cavity in the form of submerged jet. Because the distance between the center of the jet and the two side walls is not equal, that is, there is a position difference, which causes a pressure difference between the fluids on both sides of the jet in the working chamber. With the increase of pressure difference, the jet is forced to deviate to one side, and the Coanda effect is produced. The deflected jet diffuses approximately linearly along the side wall of the working cavity, and the fluid velocity gradually decreases. Carried by the entrainment of the jet, two eddy current zones of different sizes are formed on both sides of the jet zone.

Solid phase particle motion. Figure 3 is a trajectory diagram of solid phase particles in a jet element. It can be seen from Figure 3 that during the movement of the liquid fluid, the solid particles carried by the liquid enter the internal flow field of the jet element. At first, the particles converge and accelerate at the nozzle, and then a part of the accompanying wall jet deflects to one side, and the other part turns in the vortex region [23]. During the movement of the solid particles, they constantly collide with and rub against the wall surface of the jet element, causing the wall material to detach from the matrix and eventually accumulating to form macroscopic wear.

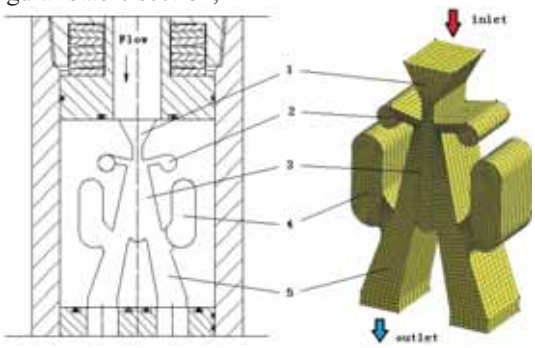

FIGURE 1
Jet element structure and grid model.
Notes: 1-nozzle; 2-signal channel; 3-working cavity; 4-empty channel; 5-output channel

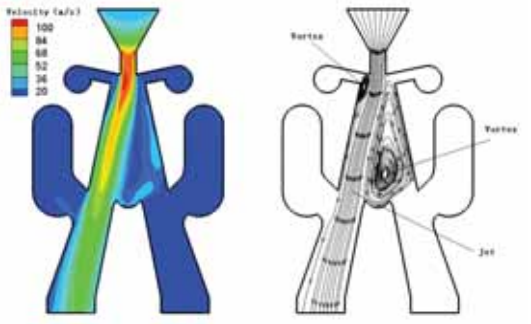

FIGURE 2
Characteristics of liquid phase fluid inside the jet element.

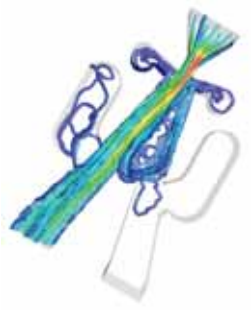

FIGURE 3
Particle trajectory in the jet element.

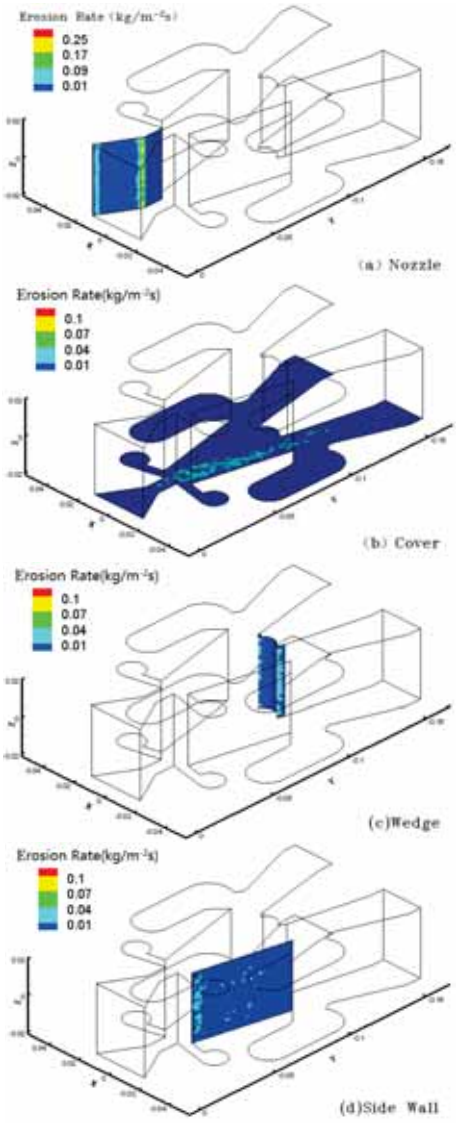

FIGURE 4
Wear distribution of jet element.

Wall wear distribution characteristics. When drilling fluid flows through the interior of the jet element, due to the different flow conditions of the liquid-solid two-phase fluid in different regions, the erosion damage caused by the drilling fluid is different. The numerical simulation results show that the wear of the jet element is mainly distributed in four areas: the nozzle, the side wall, the cover, and the wedge, which are consistent with the actual wear characteristics of the jet element in the field. As shown in Figure 4a, due to the solid phase particles converging and accelerating at the nozzle, the particle velocity and content are high, and the erosion of the wall surface is also the most serious, which is prominently shown at the interface between the acceleration section and the stable section of the nozzle. As shown in Figure 4b, the wear of the cover of the jet element is distributed in a band shape, from the nozzle stabilization section to the exhaust channel exit section, which is mainly caused by erosion of solid particles carried by the Coanda jet. The wear at the wedge is concentrated at two sharp corners. The Coanda jet and the working chamber vortex are the main causes of wear (Figure 4c). The erosion of the Coanda jet is the main cause of side wall wear which is performed in two different types: one is the wear concentration at the position of the jet wall and the other is a certain degree of erosion along the wall (Figure 4d).

Non-smooth surface erosion resistance. (1) Non-smooth surface design. The erosion and abrasion of the jet element has obvious regional characteristics, and the overall service life of the jet element can be significantly improved by improving the anti-wear ability of a specific region. The non-smooth surfaces with different roughness are set on the surface of the four erosion wear areas of the jet element to improve the wall's anti-wear performance.

TABLE 1
Roughness parameters of the wall of the jet element

Specimen	roughness thickness Ks/mm	roughness constant Cs
Smooth	0	0.5
Non-smooth 1#	0.5	0.5
Non-smooth 2#	1.0	0.5
Non-smooth 3#	2.0	0.5

In this study, the non-smooth surface characteristics of the material are equivalent to the roughness of the wall surface. The parameters for determining the wall roughness in Fluent are roughness thickness and roughness constant [24]. For non-smooth surfaces with uniformly distributed unit bodies, the height of the unit body can be taken as the roughness thickness, and the roughness constant can be regarded as a fixed value. Table 1 shows the specific parameter values. Using the above wall surface parameters, under the conditions of a fluid inlet velocity of 25 m/s, a solid phase particle diameter of 1 μm, and a solid phase content of 10%, the numerical simulations of the erosion wear effect of the jet element under different surface roughness are performed.

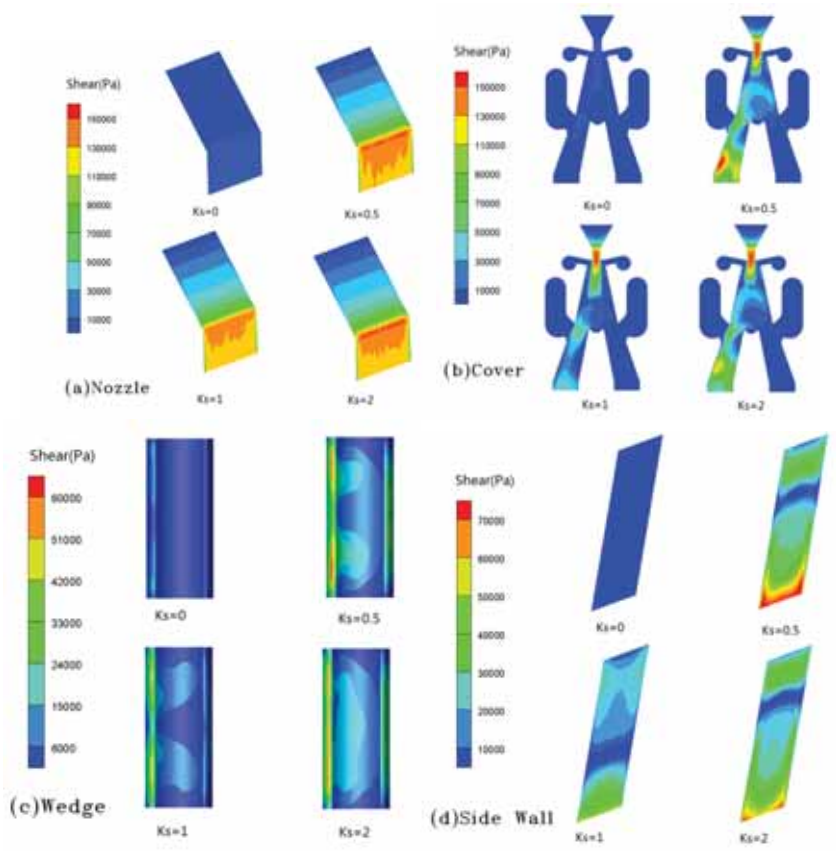

FIGURE 5
Shear stress distribution on the surface of the jet element with different surface roughness.

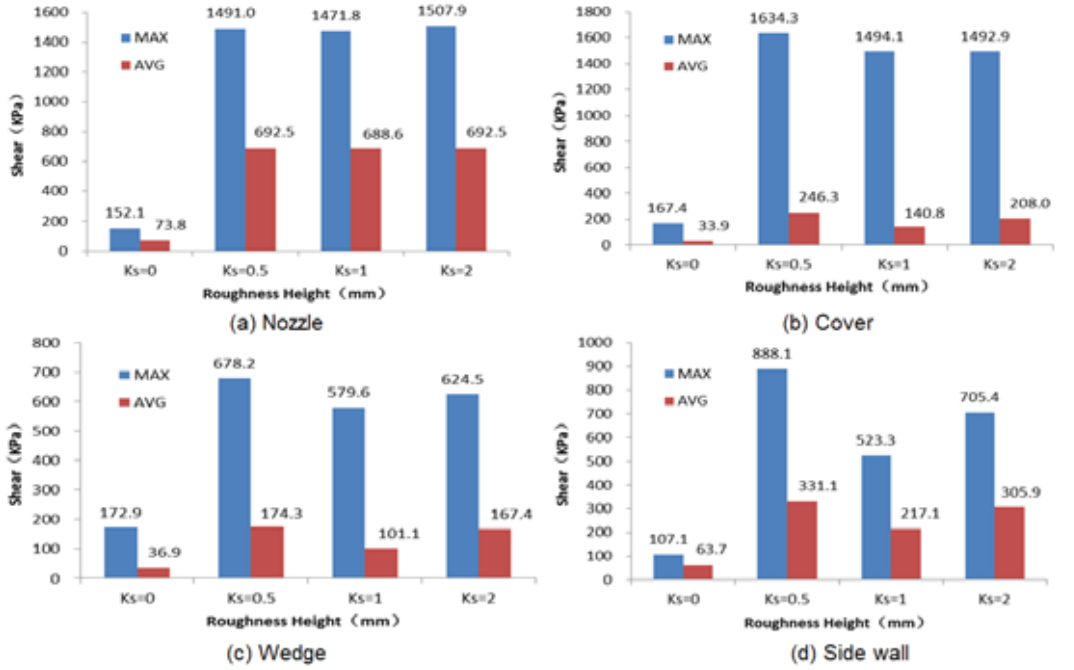

FIGURE 6
Shear stress comparison of different surface roughness walls of the jet element.

(2) Wall shear stress analysis. Figure 5 shows the shear stress distribution diagram of the wall surface of the jet element with different surface roughness. For nozzles, as the flow velocity in the nozzle increases, the nozzle shear stress gradually increases and reaches the maximum at the entrance of the stable section, and the subsequent shear stress gradually decreases with the decrease

of the flow velocity of the wall attachment fluid. For the cover, the nozzle and the output channel are the area with higher shear stress. The reason is that the velocity near the wall of these two locations is high. For the wedge, due to the effect by the vortex in the working cavity and the jet of the output channel, the shear stress at the sharp corner is the highest. While for the side wall, the shear stress at the lower part of the side wall is higher due to the deflection impact of the Coanda jet.

Figure 6 is a comparison diagram of shear stress on the wall surface of the jet element with different surface roughness. The maximum shear stress and the average shear stress of three non-smooth walls with different roughness thicknesses for the nozzle are relatively close. For cover, wedge, and side wall, when the roughness thickness is 1mm, the maximum and average values of the non-smooth wall shear stress are the smallest. While the maximum and the average shear stress of the non-smooth wall are the largest as the thickness roughness is 0.5mm. In general, the shear stress of non-smooth walls is larger than that of smooth walls, indicating that the liquid flow resistance of rough walls is large, which can effectively reduce the velocity of fluid and solid particles near the wall, thus, reducing the particle's impact on the wall.

(3) Wall vorticity analysis. Figure 7 is a wall surface vorticity distribution diagram of the jet element having different surface roughness.

For the nozzle, the area with the larger vorticity is at the entrance of the nozzle stable section. For the cover, the vorticity is affected by the nozzle jet and the vortex near the wedge, and the vorticity at the above two positions is large. The vorticity at the tip of the wedge is the highest due to the influence of the eddy current in the working cavity and the jet from the output channel and the vorticity in the middle of the side wall is high due to the deflection of the Coanda jet.

Figure 8 is a comparison diagram of wall surface vorticity with different surface roughness of the jet element. For the wall surface at different positions of the jet element, the variation law of the vorticity is not the same. For the nozzle, as the roughness thickness increases, the maximum and average values of the wall vorticity gradually decrease. For cover and wedge, the maximum and average values of vorticity on smooth walls are the highest. As the thickness is 1 mm, the maximum and average values of vorticity on non-smooth walls are the smallest. The maximum and average values of the vorticity for the side wall are the smallest when the surface roughness thickness is 0.5 mm. As the surface roughness is 1 mm, the maximum and average values of the vorticity are the largest. In general, the vorticity of the non-smooth wall of the jet element is smaller than that of the smooth wall. The surface roughness has a significant effect on the vorticity of the wall.

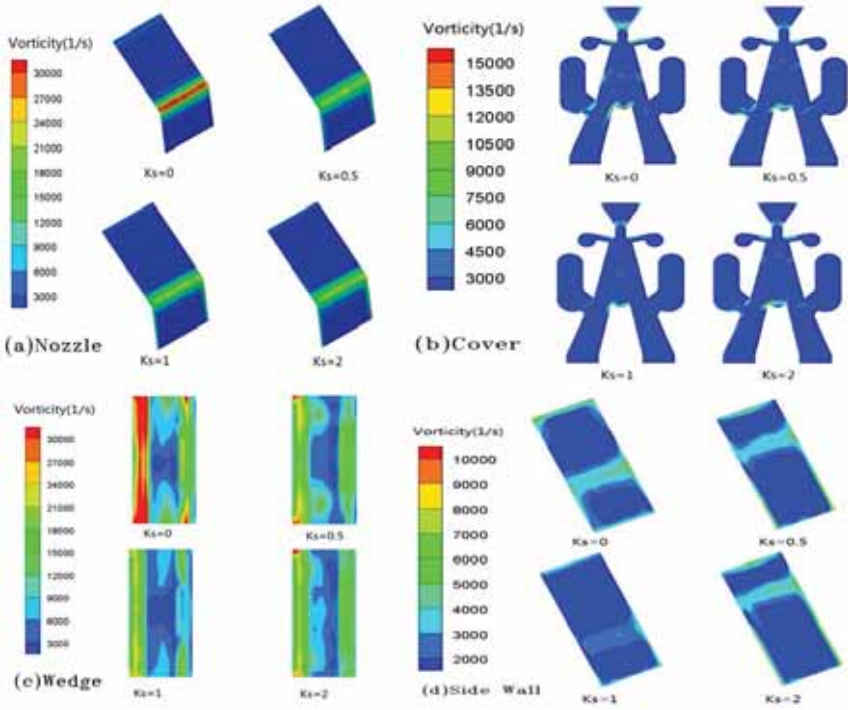

FIGURE 7
Vorticity distribution of wall surface of jet element with different surface roughness.

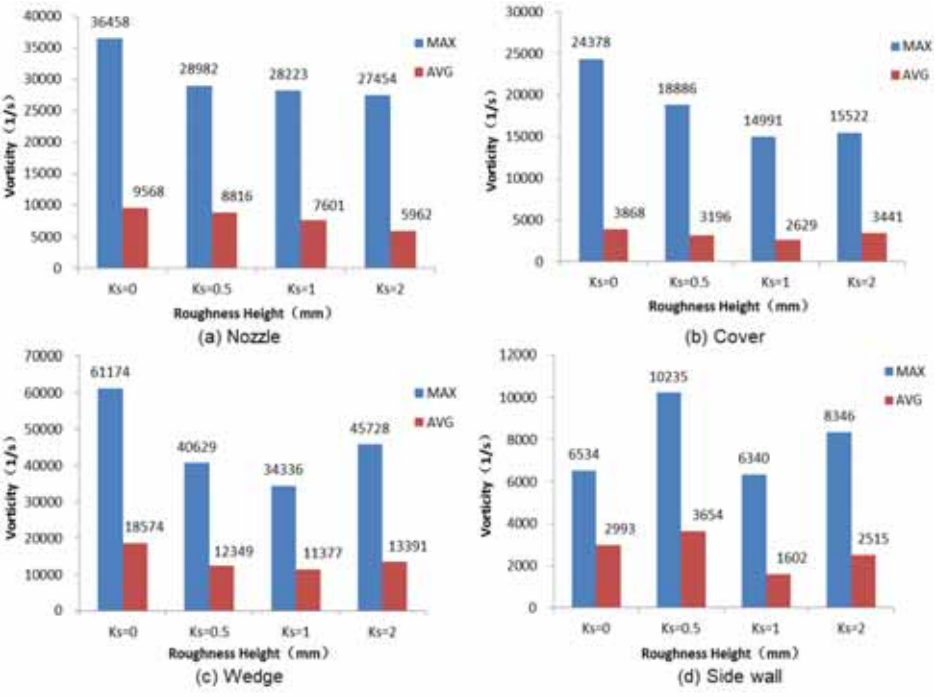

FIGURE 8
Comparison of vorticity of wall surface of jet element with different surface roughness.

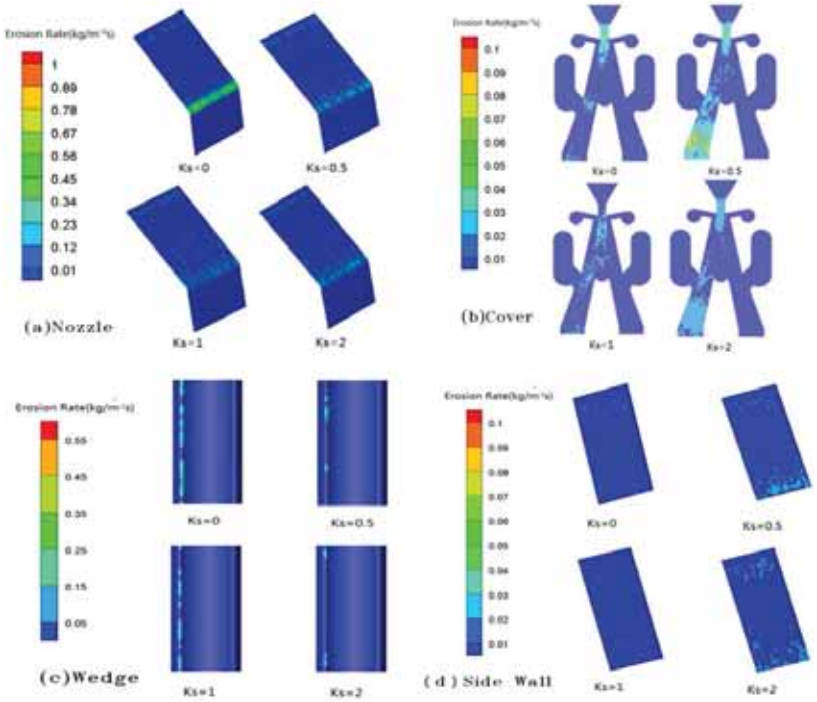

FIGURE 9
Wear distribution of wall surface of jet element with different surface roughness.

(4) Wall wear analysis. The wall wear distribution of jet elements with different surface roughness is shown in Figure 9 and Figure 10. For the nozzle, the maximum wear zone is at the entrance of the nozzle's stable section. The reason is that, on the one hand, the fluid velocity is the highest there, on the other hand, the streamline is deflected, and the particles collide with the wall. For the cover, due to the high fluid velocity at the nozzle and the output channel, the wear is concentrated in the above two places. For the wedge, the maximum wear zone appears at the sharp corner of the wedge, which is mainly affected by the output jet and the working chamber eddy current. For the side wall, the wear mainly occurs at the upper and lower ends, the upper wear area is affected by the vortex at the nozzle outlet, and the lower wear area is affected by the Coanda jet.

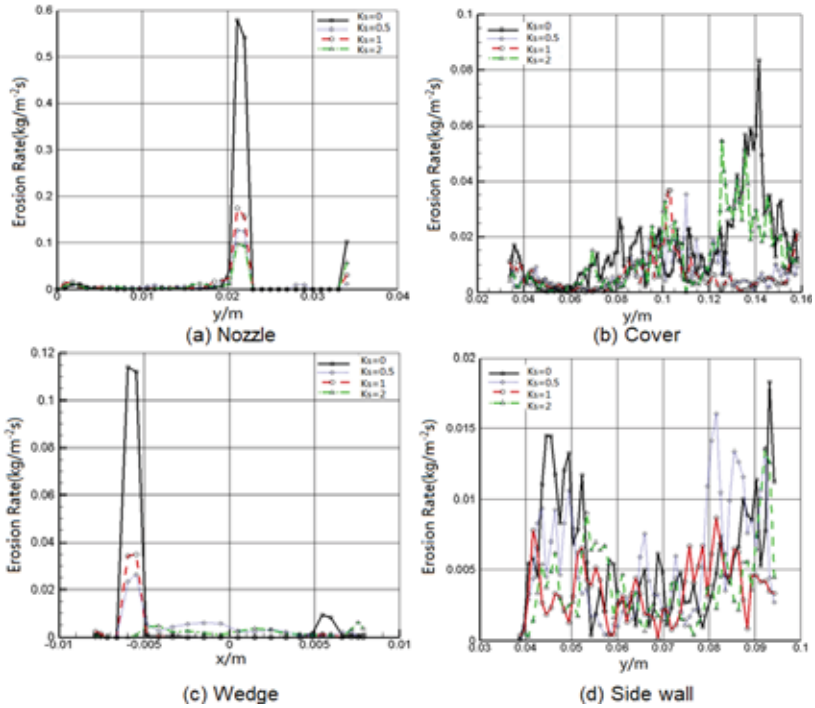

FIGURE 10
Distribution of wear rate on wall surface of jet element with different surface roughness.

Figure 11 is a comparison diagram of the wear rate of each wear region of the jet element. For the nozzle, as the roughness thickness is 1mm, the wear rate of the nozzle is the lowest, and its maximum wear rate and average wear rate are reduced by 76.2% and 71.1% compared with the smooth wall surface, respectively. For the cover, when the roughness thickness is 1mm, the wear rate of the cover is the lowest, and its maximum wear rate and average wear rate are reduced by 58.2% and 8.3%, respectively compared with the smooth wall surface. For the wedge, the wear rate decreases with increasing roughness thickness. When the roughness thickness is 2mm, the wedge wear rate is the lowest, and its maximum wear rate and average wear rate are reduced by 52.5% and 61.7% compared with the smooth wall surface, respectively. For the side wall, when the roughness thickness is 1mm, the wear rate of the side wall is the lowest, and its maximum wear rate and average wear rate are reduced by 29.6% and 2.8% respectively compared with the smooth wall surface.

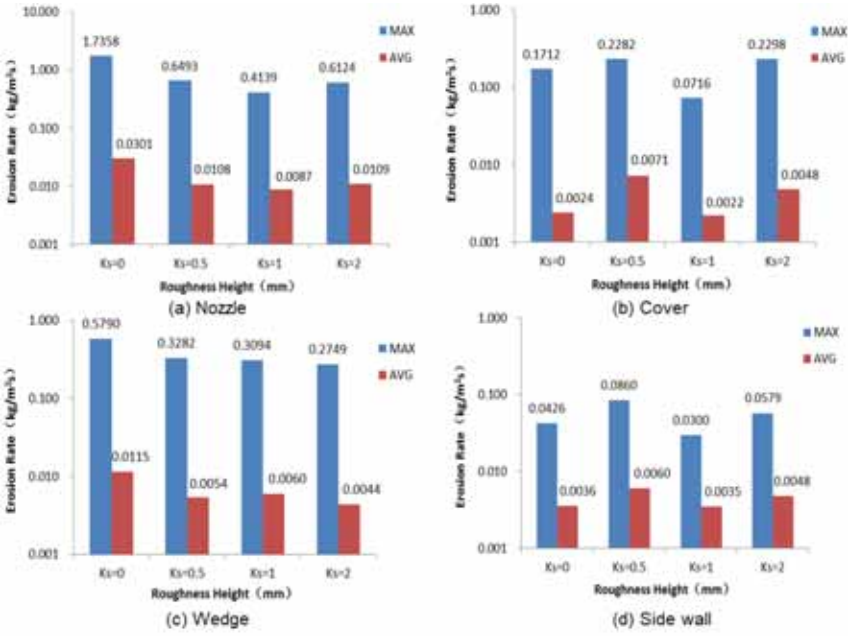

FIGURE 11
Comparison of wear rate of wall surface of jet element with different surface roughness.

CONCLUSIONS

(1) Compared with conventional drilling technology, jet hydraulic hammer drilling technology has the advantages of high impact power, high rock crushing efficiency, long service life, high energy efficiency and environmental protection, which has become one of the main options for unconventional oil and gas complex formation drilling technology. The optimization research of this technology can provide reliable theoretical support for the efficient and environmental protection development of unconventional oil and gas resources.

(2) The liquid phase fluid in the jet element exists in the form of jet and vortex, which drives the solid phase particles to erode the inner wall surface of the jet element. The wear zone mainly exists in the position of the nozzle, cover, wedge and side wall. The simulation results agree with the actual wear conditions.

(3) The shear stress of the non-smooth wall surface of the jet element is significantly increased, and the vorticity of the wall surface is significantly reduced, indicating that the liquid flow resistance of the non-smooth wall surface is relatively large, which can effectively reduce the flow velocity and vorticity of the fluid and solid particles near the wall, reducing the erosion wear of the solid particles on the wall surface. The erosion wear rate of the jet element wear area with non-smooth features is reduced to varying degrees, which has a positive effect on improving the erosion resistance of the jet element. In general, when the roughness thickness is about 1 mm, the wall has the best erosion resistance.

ACKNOWLEDGEMENTS

This work was financially supported by "The Fundamental Research Funds for the Central Universities" (No. 18CX02102A).

REFERENCES

[1] Peng, J., Wang, W., Yin, Q., Liu, H., Hu, Y., Zhao, Z. (2011) Effect of diameter of flow-dividing holes on liquid-jet hammer performance. Journal of the Beijing University of Technology. 37(4), 501-506.

[2] Suo, Z., Wang, J., Zhang, H., Li, G., Zhang, R., Jing H. (2013) Application of rotary percussion drilling on the super deep section in Tahe Field. Oil Drilling & Production Technology. 35(4), 44-46.

[3] Li, W. (2004) The experiment and research on the working life of the liquid jet amplifier of the hydraulic hammer. Changchun: Jilin University (Dissertation).

[4] Li, C., Li, F., Ren, H. (2002) Applications of hydraulic operated hammersin pilot hole drilling of kezuan-1 well. Petroleum Drilling Techniques. 30(5), 12-14.

[5] Xie, W., Deng, J., Zhou, H., He, C. (2012) Development and Prospect in Numerical Simulation of Erosion. Corrosion & Protection. 33(7), 601-604.

[6] Yu, F., Liu, M., Wang, T., Yang, X., Yan, J. (2015) Numerical research on gas-solid two-phase flow and erosion in elbows. Journal of Engineering Thermophysics. 36(4), 796-800.

[7] Zhu, X., Liu, S., Tong, H. (2010) A study on the drill pipe erosion law in gas drilling. Acta Petrolei Sinica. 31(6), 1013-1017.

[8] Wood, R., Jones, T. Ganeshalingam, J., Miles, N. (2004) Comparison of predicted and experimental erosion estimates in slurry ducts. Wear. 256, 937-947.

[9] Xie, Y., Jiang, J., Tufa, K., Yick, S. (2015) Wear resistance of materials used for slurry transport. Wear. 332-333, 1104-1110.

[10] Liu, R., Yao, J., Zhang, Q., Yao, M., Collier, R. (2015) Sliding wear and solid-particle erosion resistance of a novel high-tungsten stellite alloy. Wear. 322-323, 41-50.

[11] Santecchia, E., Hamouda, A., Musharavati, F., Zalnezhad, E., Cabibbo, M., Spigarelli, S. (2015) Wear resistance investigation of titanium nitride-based coatings. Ceramics International. 41, 10349-10379.

[12] Dallaire, S. (2013) Slurry erosion resistance of boride-based overlays containing boride crystals oriented perpendicularly to the wearing surface. Wear. 297, 1006-1015.

[13] Lin, J. Wu, F., Yu, Z. (2003) A new way to reduce wall erosion caused by solid particles. Tribology. 23(3), 231-235.

[14] Song, X., Lin, J., Zhao, J., Shen, T. (1996) Research on reducing erosion by adding ribs on the wall in particulate two-phase flows. Wear. 193, 1-7.

[15] Sun, J., Dai, Z. (2008) Bionic of non-smooth surface. Progress in Natural Science. 18(3), 241-246.

[16] Sun, N., Shan, H., Zhou, H., Chen, D., Li, X., Xia, W., Ren, L. (2012) friction and wear behaviors of compacted graphite iron with different biomimetic units fabricated by laser cladding. Applied Surface Science. 258, 7699-7706.

[17] Ren, L., Sun, S., Xu, C. (2008) Noise reduction mechanism of non-smooth leading edge of owl wing. Journal of Jilin University (Engineering and Technology Edition). 38(S), 126-131.

[18] Wang, F. (2004) Computational fluid dynamics analysis. Beijing: Tsinghua University Press. 7-13.
[19] Yakhot, V., Orzag, S. (1986) Renormalization group analysis of turbulence. I. Basic theory. Journal of Scientific Computing. 1(1), 33-51.
[20] Zhu, L., Huang, Y., Wang, R., Wang, J. (2015) A mathematical model of the motion of cutting particles in reverse circulation air drilling. Applied Mathematics and Computation. 256, 192-202.
[21] Xing, Z., Lu, Z., Zhou, Y., Liu, J. (2009) An investigation on erosion wear characteristics of sic particle reinforced steel matrix surface composite. Materials Science Forum. 620-622, 323-326.
[22] Kishore, Sampathkumaran, P., Seetharamu, S. (2005) Erosion and abrasion characteristics of high manganese chromium irons. Wear. 259(1), 70-77.
[23] Edwards, J., Mclaury, B., Shirazi, S. (2000) Evaluation of alternative pipe bend fittings in erosive service. Proceedings of ASME FEDSM '00: ASME 2000 Fluids Engineering Division Summer Meeting. Boston: ASME. 959-966.
[24] Gupta, G., Satapathy, A. (2014) Processing, characterization, and erosion wear characteristics of borosilicate glass microspheres filled epoxy composites. Polymer Composites. 36(9), 1685-1692.

Received: **18.01.2020**
Accepted: **21.02.2020**

CORRESPONDING AUTHOR

Yong Huang
School of Petroleum Engineering,
China University of Petroleum (East China),
Qingdao 266580 – P.R. China

e-mail: huangyongjlu@163.com

© by PSP Volume 29 – No. 05/2020 pages 3557-3563 Fresenius Environmental Bulletin

ASSESSMENT OF GENETIC POTENTIAL OF CITRUS GERMPLASM AGAINST CITRUS CANKER CAUSED BY *XANTHOMONAS AXONOPODIS* PV. *CITRI*

Akhtar Hameed[1,2], Muhammad Atiq[1,*], Nasir Ahmed Rajput[1], Shahbaz Talib Sahi[1], Sohaib Sarfraz[1], Hameed Ali Alsamadany[3], Abdul Mubeen Lodhi[4], Faizan Ahmed Tahir[1], Nadia Liaqat[1], Zaheer Ahmed[5]

[1]Department of Plant Pathology, University of Agriculture, Faisalabad 38000, Pakistan
[2]School of Agriculture and Environment, The University of Western Australia,WA 6009, Australia.
[3]Department of Biology, Faculty of Sciences, King Abdul Aziz University, Jeddah 21589, Saudi Arabia
[4]Department of Plant Protection, Sindh Agriculture University, Tando Jam 70060, Pakistan
[5]Department of Plant Breeding and Genetics, University of Agriculture, Faisalabad 38000, Pakistan

ABSTRACT

Thirty citrus varieties/cultivars were assessed for resistant and susceptible source against the canker disease caused by *Xanthomonas axonopodis* pv. *citri* in a field trial conducted in the research area, Department of Plant Pathology, UAF during the 2017-19 years under Randomized Complete Block Design (RCBD). Eleven varieties i.e.*Citrus japonica* (Kumquat), *Citrus pseudolimon* (GAL GAL), *Citrus sinensis* cv. *Jaffa*, *Citrus reticu*lata cv. *mungal singh*, *Citrus reticulata* cv. *tangerine*, *Citrus sinensis* cv. *pine apple*, *Citrus poncirus* (Trifoliate orange), *Citrus grandis* (Pomelo), *Citrus aurantium* (Bitter Orange), *Citrus medica* (Citron), *Citrus sinensis* cv. w*ashington navel* expressed (1.20-3.80 %) resistant response. Four genotypes namely *Citrus aurantifolia swingle* (Kagzi lime), *Citrus aurantifolia* (Key lime), *Citrus latifolia* (Persian lime), *Citrus sinensis* cv. *ruby red* exhibited (7.60-8.00 %) moderately resistant response while one variety *Citrus limonia* cv. *mayer lemon* showed (12.90 %) moderately susceptible response. Four varieties named as *Citrus reticulata* cv. *feutral's early*, *Citrus limettioides* (Sweet lime), *Citrus sinensis* cv. *succari*, *Citrus sinensis* cv. *valentia late* showed (19.00-20.70 %) susceptible response. Ten varieties namely *Citrus sinensis* cv. *red blood*, *Citrus reticulata* cv. *malta*, *Citrus limonia*, *Citrus paradisi*, *Citrus reticulata cv. kinnow*, *Citrus sinensis*, *Citrus jambhiri* (Rough lemon), *Citrus paradisi* cv. *shamber*, *Citrus paradisi* cv. *duncan*, *Citrus paradisi* cv. *foster* expressed (26.60-28.70 %) highly susceptible response against citrus canker. No citrus cultivar was found immune.

KEYWORDS:
Varieties, Cultivars, Resistant, Susceptible, Immune, RCBD

INTRODUCTION

Citrus canker caused by a notorious bacterium *Xanthomonas axonopodis* pv. *citri* (*Xac*) is one of the most economically devastating diseases affecting citrus globally [1-3]. *Xac* is a straight rod shaped, mono-flagellum, gram negative bacterium, which give yellowish colonial growth due to xanthomonadin pigment production [4]. Citrus canker produces typical necrotic lesions on stems, leaves and fruits [1,5]. The disease causes leaf fall, drying of twigs and premature fruit drop which ultimately leads towards the reduction of fruit quality and losses [6, 7]. The bacteria released on to the surface of lesions upon the presence of free water and it spreads to other plants through stomata, injuries and its vector Citrus Leaf Minor (CLM). Strong winds and rainfall also assist the pathogen dispersal to long distances and its entrance in to leaves [8]. CLM damages the leaves and further enhancing the susceptibility towards *Xac* [9]. After gaining entrance into leaves, the bacteria established and causes infection following a series of highly coordinated events; first of all the bacteria occupies the intercellular spaces, then it attaches to the mesophyll cells using type III secretion system and releases various effecter proteins and enzymes like cutinases and pectinases which causes rapid cell division and cellular enlargement. After the seven days of infection, the enlargement is at its maximum and infected portions turn into water-soaked lesions; the epidermis gets raised and began to rupture. After two weeks of initial infection the watery lesions began to dry and form multiple necrotic lesions [10]. In addition to this, overall infection is also greatly influenced by pathovar or strain type, genotype of host and corresponding environmental conditions especially during growth of new flushes of leaves [6].

Citrus canker disease is a global issue with severe disease outbreaks being reported in almost every major growing country including; USA, Brazil, Argentina, Australia and Pakistan [11]. A number of strategies are being used for the management of disease

but one of the key strategies is the use of resistant verities. Use of such disease resistant verities is of great help in disease management. It is an effective approach for long term management of disease [12, 13]. Therefore, in present study, different citrus cultivars collected from local and other major citrus growing areas of Punjab were evaluated for their resistance/susceptibility to canker by artificial inoculation of the pathogen.

MATERIALS AND METHODS

To screen out citrus varieties/cultivars against canker disease, nursery was grown for two years (2017-2019) in the research area, Department of Plant Pathology, UAF. Thirty varieties/cultivars of citrus were collected from fruit nursery, Institute of Horticulture Science, University of Agriculture Faisalabad. For maintaining the citrus nursery in healthy conditions and to avoid contamination, all the recommended horticultural practices were followed but use of any type of pesticides were avoided in order to develop disease stress. Natural inoculum of Xac was collected from nursery area, IHS, UAF for causing infection. The nursery was artificially inoculated with bacterial suspension containing 108cfu/ml determined with the help of spectrophotometer (96 micro well plate reader BioTek, model, H-QuantTM, Winooski, VT, USA). Inoculation was done on one-year old plants by spray method with the help of simple hand sprayer in the morning. Plants which were treated as control, sprayed with distilled water. Symptoms were appeared after the seven days of inoculation. The inoculated and control treatments were consisted of three replications under Randomized Complete Block Design (RCBD). Disease incidence was determined by following Croxal (1952) rating scale. According to scale, 00-00 (%) disease severity = HR, 01-05 = R, 06-10 = MR, 11-15 = MS, 16-25 = S and 26-above = HS. Following equation was used to measure disease incidence.

$$\text{Disease incidence} = \frac{\text{Total No. of Canker infected plants}}{\text{Total no. of plants}} \times 100$$

Disease ratings were taken on weekly basis from July 2017 to June 2019. LSD at 5 % probability level was used to determined disease incidence on 30 cultivars of citrus [23].

RESULTS

During 2017-18, eleven varieties i.e., *Citrus japonica* (Kumquat) (1.20), *Citrus pseudolimon* (GAL GAL) (1.40), *Citrus sinensis* cv. *Jaffa* (2.90), *Citrus reticu*lata cv. *mungal singh* (3.20), *Citrus reticulata* cv. *tangerine* (3.80), *Citrus sinensis* cv. *pine apple* (3.00), *Citrus poncirus* (Trifoliate orange) (3.00), *Citrus grandis* (Pomelo) (3.40), *Citrus aurantium* (Bitter Orange) (3.20), *Citrus medica* (Citron) (3.60), *Citrus sinensis* cv. *Washington navel* (3.40)% disease incidence expressed resistant response along with disease rating 1. Fourgenotypes namely *Citrus aurantifolia swingle* (Kagzi lime) (8.00), *Citrus aurantifolia* (Key lime) (8.00), *Citrus latifolia* (Persian lime) (8.00), *Citrus sinensis* cv. *ruby red* (7.60) exhibited moderately resistant response (rating 3) while one variety *Citrus limonia* cv. *mayer lemon* with disease incidence 12.40 showed moderately susceptible response (rating 5). Four varieties named as *Citrus reticulata* cv. *feutral's early*, *Citrus limettioides* (Sweet lime), *Citrus sinensis* cv. *succari*, *Citrus sinensis* cv. *valentia late* with disease incidence 19.40, 20.00, 20.70 and 19.00 percent respectively showed susceptible response (rating 7). Ten varieties namely *Citrus sinensis* cv. *red blood* (28.50), *Citrus reticulata* cv. *malta* (28.20), *Citrus limonia* (27.80), *Citrus paradisi* (28.70), *Citrus reticulata cv. kinnow* (28.70), *Citrus sinensis* (27.20), *Citrus jambhiri* (Rough lemon) (28.70), *Citrus paradisi* cv. *shamber* (27.90), *Citrus paradisi* cv. *duncan* (28.00), *Citrus paradisi* cv. *foster* (26.60) % disease incidence expressed highly susceptible response with (rating 9) (Table 1 and Figure 1).

From 2018-19, ten genotypes/cultivars namely *Citrus sinensis* cv. *red blood* (28.80),*Citrus reticulata* cv. *malta* (30.40), *Citrus limonia* (29.00), *Citrus paradisi* (Grape fruit) (29.40), *Citrus reticulata* (27.90), *Citrus sinensis* (27.20), *Citrus jambhiri* (Rough lemon) (28.70), *Citrus paradisi* cv. *shamber* (27.90), *Citrus paradisi* cv. *duncan* (28.00), *Citrus paradisi* cv. *foster* (26.60) % disease incidence exhibited highly susceptible response along with (rating 9) while four varieties/cultivars named as *Citrus limettioides* (Sweet lime), *Citrus reticulata* cv. *feutral's early*, *Citrus sinensis* cv. *succari*, *Citrus sinensis* cv. *valentia late* with disease incidence 20.00, 19.40, 22.70 and 19.00 respectively showed susceptible response (rating 7). One variety mayer lemon with disease incidence 12.90 percent showed moderately susceptible response with rating 5 while five varieties namely *Citrus aurantifolia* cv. *swingle* (Kagzi lime) (8.00), *Citrus aurantifolia* (Key lime) (8.00), *Citrus latifolia* (Persian lime) (8.00) and *Citrus sinensis* cv. *ruby red* (7.60) exhibited moderately resistant response along with the rating 3 while ten varieties i.e. *Citrus sinensis* cv. *Jaffa* (2.90), *Citrus reticulata* cv. *mungal singh* (3.20), *Citrus sinensis* (3.00), *Citrus reticulata* cv. *tangerine* (3.80), *Citrus poncirus* (Trifoliate orange) (3.00), *Citrus grandis* (Pomelo) (3.40), *Citrus aurantium* (Bitter Orange) (3.20), *Citrus medica* (Citron) (3.60), *Citrus sinensis* cv. *washington navel* (3.40), *Citrus pseudolimon* (GAL GAL) (1.40) and *Citrus japonica* (Kumquat) (1.20) percent disease incidence exoperissed resistant response with disease rating 1 while no one variety exhibited highly resistant response against the citrus canker (Table 2 and Figure 2).

TABLE 1
Resistance Status of Citrus Varieties against Canker Disease during 2017-18 under *in-vivo* Conditions

Sr. #	Varieties/cultivars	D.I (%)	Disease Rating	Resistance Status
1	*Citrus japonica* (Kumquat)	1.20i	1	R
2	*Citrus pseudolimon* (GAL GAL)	1.40hi	1	R
3	*Citrus poncirus* (Trifoliate orange)	3.00gh	1	R
4	*Citrus sinensis* cv. *pineapple*	3.00gh	1	R
5	*Citrus aurantium* (Bitter Orange)	3.20g	1	R
6	*Citrus reticulata* cv. *mungal singh*	3.20g	1	R
7	*Citrus sinensis* cv. *washington navel*	3.40g	1	R
8	*Citrus grandis*(Pomelo)	3.40g	1	R
9	*Citrus medica* (Citron)	3.60g	1	R
10	*Citrus reticulata* cv. *Tangerine*	3.80g	1	R
11	*Citrus sinensis* cv. *Jaffa*	2.90gh	1	R
12	*Citrus sinensis* cv. *ruby red*	7.60f	3	MR
13	*Citrus aurantifolia swingle*(Kagzi lime)	8.00f	3	MR
14	*Citrus latifolia* (Persian lime)	8.00f	3	MR
15	*Citrus aurantifolia* (Key lime)	8.00g	3	MR
16	*Citrus limonia* cv. *mayer lemon*	12.90e	5	MS
17	*Citrus sinensis* cv. *valentia late*	19.00d	7	S
18	*Citrus reticulata* cv. *feutral's early*	19.40cd	7	S
19	*Citrus limettioides* (Sweet lime)	20.00cd	7	S
20	*Citrus sinensis* cv. *Succari*	20.70c	7	S
21	*Citrus paradise* (Grapefruit)	28.70a	9	HS
22	*Citrus limonia* cv. *china lemon*	27.80ab	9	HS
23	*Citrus reticulata* cv. *Malta*	28.20ab	9	HS
24	*Citrus sinensis*	27.20ab	9	HS
25	*Citrus paradisi* cv. *Foster*	26.60b	9	HS
26	*Citrus paradisi* cv.*Duncan*	28.00ab	9	HS
27	*Citrus paradisi* cv. *Shamber*	27.90ab	9	HS
28	*Citrus sinensis* cv. *red blood*	28.50a	9	HS
29	*Citrus reticulata* cv. *Kinnow*	28.60a	9	HS
30	*Citrus jambhiri* (Rough lemon)	28.70a	9	HS

*Many values in a column sharing similar letters do not differ significantly as determined by the LSD test ($P \leq 0.05$)
R = Resistant MR = Moderately resistant MS = Moderately susceptible S = Susceptible HS = Highly susceptible

DISCUSSION

Citrus canker cause by *Xac* is a major threat among all the constraints faced by citrus crop throughout the world [1, 2, 3, 14]. Citrus canker is a major threat to the quality and exportable citrus in Pakistan. It affects cosmetic and market value. Due to this disease, 144 consignments were rejected by European Union [15]. A number of factors are involved in the development of symptoms caused by phytopathogenic bacteria. These include infection time, plant age, strain of pathogen, genetic makeup of host, infection type and environmental conditions. A lot of management strategies are available against canker disease, but the use of resistant varieties is the only long term and effective way to save the crop from the infection of *Xac*. Screening of available germplasm by using conventional breeding methods for the relative susceptibility/resistance is more accessible and robust strategy as compare to other approaches which are costly and long-term process [16] and is cost effective, short-term and best solution against the diseases all around the world [17].

TABLE 2
Resistance Status of Citrus Varieties against Canker Disease during 2018-19 under *in-vivo* Conditions

Sr. #	Varieties/cultivars	D.I (%)	Disease Rating	Resistance status
1	*Citrus japonica* (Kumquat)	1.90j	1	R
2	*Citrus pseudolimon* (GAL GAL)	2.80ij	1	R
3	*Citrus poncirus* (Trifoliate orange)	3.60hi	1	R
4	*Citrus sinensis* cv. *pineapple*	5.40g	1	R
5	*Citrus aurantium* (Bitter Orange)	4.00ghi	1	R
6	*Citrus reticulata* cv. *mungal singh*	3.20hij	1	R
7	*Citrus sinensis* cv. *washington navel*	3.80hi	1	R
8	*Citrus grandis* (Pomelo)	4.60gh	1	R
9	*Citrus medica* (Citron)	4.60gh	1	R
10	*Citrus reticulata* cv. *Tangerine*	4.00ghi	1	R
11	*Citrus limonia* cv. *mayer lemon*	13.50e	1	MS
12	*Citrus sinensis* cv. *Jaffa*	3.00ij	3	R
13	*Citrus sinensis* cv. *Ruby red*	9.80f	3	MR
14	*Citrus aurantifolia swingle* (Kagzi) lime)	9.10f	3	MR
15	*Citrus latifolia* (Persian lime)	9.00f	5	MR
16	*Citrus aurantifolia* (Key lime)	8.40f	7	MR
17	*Citrus reticulata* cv. *feutral's early*	13.80e	7	MS
18	*Citrus sinensis* cv. *valentia late*	19.20d	7	S
19	*Citrus limettioides* (Sweet lime)	20.00d	7	S
20	*Citrus sinensis* cv. *Succari*	22.00c	9	S
21	*Citrus sinensis* cv. *blood red*	28.40ab	9	HS
22	*Citrus reticulata* cv. *Malta*	27.90ab	9	HS
23	*Citrus limonia* cv. *china lemon*	27.60b	9	HS
24	*Citrus paradisi* cv. *Duncan*	27.50b	9	HS
25	*Citrus sinensis*	27.30b	9	HS
26	*Citrus paradisi* cv. *Foster*	28.80ab	9	HS
27	*Citrus paradisi* cv. *Shamber*	27.70b	9	HS
28	*Citrus jambhiri* (Rough lemon)	28.40ab	9	HS
29	*Citrus reticulata* cv. Kinnow	27.90ab	9	HS
30	*Citrus paradisi* (Grapefruit)	29.40a	9	HS

*Mean values in a column sharing similar letters do not differ significantly as determined by the LSD test ($P \leq 0.05$)
R = Resistant MR = Moderately resistant MS = Moderately susceptible S = Susceptible HS = Highly susceptible

But with the passage of time, by using these resistant and race specific varieties continuously in specific geographical area, new virulent strains of the pathogens are developed which reduce the resistance of these citrus cultivars. That is why in present study, a lot of thirty citrus varieties/cultivars were evaluated against canker and it was found that a source of resistance was available against *Xac* in some of the citrus cultivars like Kumquat.

Horizontal resistance decreases the development of disease because of the presence of multi genes and is more suitable as compared to vertical

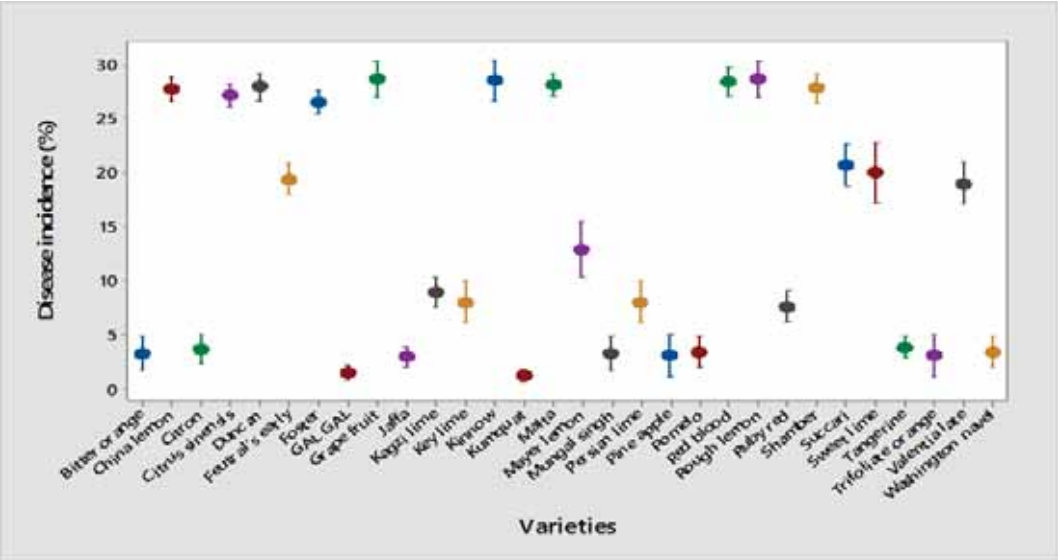

FIGURE 1
Resistance Status of Citrus Germplasm against Citrus Canker under Field Conditions during 2017-18

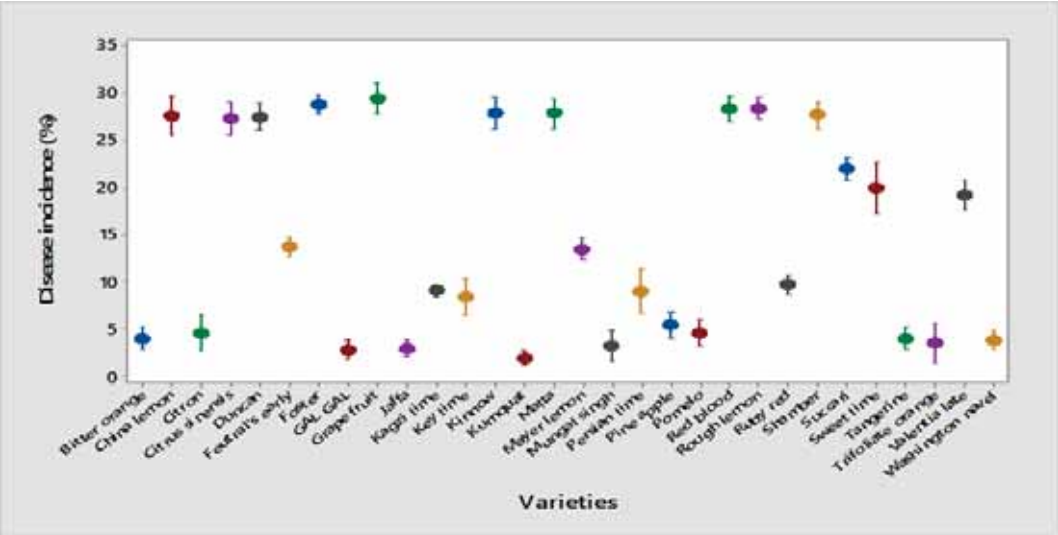

FIGURE 2
Resistance Status of Citrus Germplasm against Citrus Canker under Field Conditions during 2018-19

resistance. However, it was also noticed that susceptible varieties/cultivars provide high average yield as compared to resistant one [18]. Multiple citrus varieties were inoculated with *Xac* isolates in which most of the verities including*, C. paradisi, C.trifoliata, C. aurantifoliata, C. sinesis, Poncirus trifoliate and C. aurantrium,* turned out to be susceptible whereas *C. reticulata* showed certain degree of resistance against canker [18].Kumquat characterized as canker-resistant depending on developing fewer lesions of canker per leaf and expressing less internal bacterial populations per lesion and more importantly presence of cell death and hypersensitive response (HR) mechanism against *Xac* as compared to genotypes of susceptible cultivars [19-20]. Due to the presence of three times more production of H_2O_2 in Kumquat as compared to Grapefruit also associated with resistance against the canker disease [10]. H_2O_2 is openly associated with the resistance against pathogen attack [18] and plays an important role during PCD by constituting one of the early events of HR [9]. Accumulation of H_2O_2 induced in the plants during the interaction is likely to be induced by the impairment of endogenous H_2O_2 accumulation in bacterial pathogen. The advantage of more resistance of Kumquat against the *Xac* has been exploited for the production of intergenic hybrids through the breeding programs [19]. Kumquat can also be used as model cultivar in different research

programs for understanding the fundamental resistance mechanisms due to its highly potential genetic makeup against CC [20] with the long term goal of recognizing specific resistant genes that can be inserted into commercial citrus cultivars and avoid the more genetic variability in average yield potential as well as fruit quality. In the present study, Grapefruit was most susceptible, either lemon or some cultivars of orange are reasonably susceptible which is also documented by Amaral, [21]. McLean and Lee, [22] noticed that structural characteristics and morphology of Kumquat leaves and stomata could be a contribution factor towards CC between the grapefruit (*C. paradisi*) cultivar but [18] find out that characteristics of leaf such as cutical development, quantity of waxes which responsible for the infiltration of water, size and duration of emergence of new flushes are more important for resistance against canker disease than stomatal structure. Outcomes of the present study are also supported by [18,9] who also noticed the resistance of Kumquat and susceptibility of Grapefruit against the canker disease.

The resistant varieties/cultivars of citrus evaluated in present study can further be used, after determining their genetics in breeding programs for the production of resistant source of citrus against the canker disease. These resistant varieties having other essential horticultural characters can also be used as commercial cultivars to maximize the overall citrus yield.

ACKNOWLEDGEMENTS

This article is extracted from the doctoral dissertation of Akhtar Hameed. We are highly thankful to the Higher Education Commission of Pakistan for funding this research under the project (NRPU-HEC-6373) for this study.

REFERENCES

[1] Gottig, N., Garavaglia, B., Garofalo, C., Zimaro, T., Sgro, G., Ficarra, F., Dunger, G., Daurelio, L., Thomas, L. and Gehring, C. (2010) Mechanisms of Infection Used by *Xanthomonas axonopodis* pv. *citri* in Citrus Canker Disease. Current Research, Technology and Education Topics in Applied of Microbiology and Microbial Biotechnology. 1, 196-204.

[2] Gottwald, T. R. (2007) Citrus Canker and Citrus Huanglongbing, Two Exotic Bacterial Diseases Threatening the Citrus Industries of the Western Hemisphere. Outlooks on Pest Management. 18, 274.

[3] Tazeen, S.K., Akbar, K.F., Khan, A.M., Masood, A., Fayyaz, A., Khan, U.A. and Arooj, S. (2019) PCR Based Molecular Characterization of Citrus Bacterial Canker from Grapefruit (*Citrus Paradisi*). Fresen. Environ. Bull. 28, 3724-3728.

[4] Sharma, S.K. and Sharma, R.R. (2009). Citrus Canker Approaching Century: A Review. Tree and Forestry Science and Biotechnology. Global Science Books. 2, 54-56.

[5] Francis, M., Redondo, A., Burns, J. and Graham, J. (2009). Soil Application of Imidacloprid and Related SAR-inducing Compounds Produces Effective and Persistent Control of Citrus Canker. Eur. J. Plant Pathol. 124, 283-292.

[6] Gottwald, T.R., Sun, X., Riley, T., Graham, G.H., Ferrandino, F. and Taylor, E.L. (2002) Geo-Referenced Spatiotemporal Analysis of the Urban Citrus Canker Epidemic in Florida. Phytopathology. 92, 361-377.

[7] Graham, J.H. and Leite, R.P. (2004) Lack of Control of Citrus Canker by Induced Systemic Resistance Compounds. Plant Disease. 88, 745-750.

[8] Favaro, M.A., Roeschlin, R.A., Ribero, G.G., Maumary, R.L., Fernandez, L.N., Lutz, A., Sillon, M., Rista, L.M., Marano, M.R. and Gariglio, N.F. (2017) Relationships between Copper Content in Orange Leaves, Bacterial Biofilm Formation and Citrus Canker Disease Control after Different Copper Treatments. Crop Protection. 92, 182-189

[9] Mustafa, M., Imran, M., Rasool, A., Azeem, M., Riaz, A. and Afzal, M. (2014) Evaluation of Commercial Citrus Cultivars for Resistance to Citrus Leaf Miner and Its Management. J. Entomol. Zool. Stud. 2, 213-216.

[10] Kumar, N., Ebel, R. and Roberts, P. (2011) SOD Activity in *Xanthomonas axonopodis* pv. *citri* Infected Leaves of Kumquat. J. Hort. Sci. Biotechnol. 86, 62-68.

[11] Das, A. (2003) Citrus Canker-A Review. J. Appl. Hort. 5, 52-60.

[12] Deng, Z.N., Xu, L., Li, D.Z., Long, G.Y., Liu, L.P., Fang, F. and Shu, G.P. (2010) Screening citrus genotypes resistance to canker disease (*Xanthomonas axonopodis* pv. *citri)*. Plant Breeding. 129, 341-345.

[13] Kabas, A., Boyaci, H.F., Horuz, S., Aysan, Y. and Ilbi, H. (2018) Investigation on Identification of New Resistant Resources to Bacterial Canker and Wilt Disease. Fresen. Environ. Bull. 27, 8498-8504.

[14] Wali, S., Munir, F. and Mahmood, T. (2013) Phylogenetic Studies of Selected Citrus Species Based on Chloroplast Gene, rps14. Int. J. Agri. Biol. 15, 357-361.

[15] Maruti, T.B., Tembhurne, B.V., Chavan, R.L. and Amaresh, Y.S. (2014) Reaction of Chilli (*Capsicum annuum* L.) Genotypes and Hybrids against Fusarium wilt (*Fusarium solani*). J. Spices Aromat Crops. 23, 186-191.
[16] Jagtap, G.P., Thosar R.U. and Utpal, D. (2012) Evaluation of Plant Extracts and Bioagents for the Control of Gummosis of Mandarin Orange (Citrus Reticulate Blanko) Caused by Phytophthora Species. Afr. J. Agri. Res. 7, 4553-4558.
[17] Atiq, M., Khan, M.A. and Sahi, S. (2007) Screening of Citrus Germplasm for the Sources of Resistance against Canker Disease Caused by *Xanthomonas axonopodis* pv. *citri*. Pak. J. Phytopath. 19, 222-226.
[18] Khalaf, A., Moore, G.A., Jones, J.B. and Gmitter, F.G. (2007) New Insights into the Resistance of 'Nagami' Kumquat to Canker Disease. Physiol. Molecul. Plant Pathol. 71, 240-250.
[19] Viloria, Z., Drouillaerd, D.L., Graham, J.H. and Grosser, J.W. (2004) Screening triploid hybrids of Lakeland Limequat for Resistance to Citrus Canker. Plant Disease. 88, 1056-1060.
[20] Amaral, A.M., Carvalho, S.A., Silva, L.F.C., and Machado, M.A. (2010) Reaction of Genotypes of Citrus Species and Varieties to *Xanthomonas citri* subsp. c*itri* under Greenhouse Conditions. J. Plant Pathol. 92, 519-524.
[21] Mclean, F.T. and Lee, H.A. (1921). The Resistance to Citrus Canker of Citrus Nobilis and a Suggestion as to the Production of Resistant Varieties in Other Citrus Species. Phytopath. 11, 109-114.
[22] de Carvalho, S.A., de Carvalho Nunes, W.M., Belasque Jr., J., Machado, M.A., Croce-Filho, J., Bock, C.H. and Abdo, Z. (2015) Comparison of Resistance to Asiatic Citrus Canker among Different Genotypes of Citrus in a Long-term canker-resistance Field Screening Experiment in Brazil. Plant Disease. 99, 207-218.

Received: **23.07.2019**
Accepted: **19.02.2020**

CORRESPONDING AUTHOR

Muhammad Atiq
Department of Plant Pathology,
University of Agriculture,
Faisalabad, 38000 – Pakistan

e-mail: dratiqpp@gmail.com
dratiq1@yahoo.com

© by PSP Volume 29 – No. 05/2020 pages 3564-3570 Fresenius Environmental Bulletin

CONSTRUCTION OF ECOLOGICAL MONITORING AND EARLY WARNING SYSTEM IN COAL MINE BASED ON BIG DATA ANALYSIS

Weili Wu[1,2,*]

[1]School of Management, China University of Mining and Technology, Xuzhou 221018, China
[2]School of Mathematics and Physical Science, Xuzhou University of Technology, Xuzhou, 221018, China

ABSTRACT

In order to further improve the predictive and early warning capability of coal enterprises for heavy and serious accidents, accelerate the transformation of risk management of enterprises to prevent precautions, and to coordinate the supervision and inspection of coal mine safety at the national level, through the in-depth study of coal mine safety risk prediction and big data analysis technology, this paper builds a coal mine safety risk prediction system based on big data analysis platform. The system can dynamically display the safety production situation of coal mines, excavate and display the law of coal mine accidents, predict and display the risk of coal mine accidents, monitor and display the accident network, and display the comprehensive management of forecast data. Compared with similar systems, the prediction system based on big data analysis has certain advantages in mining accident rules, public opinion monitoring, production scheduling, command and decision-making, etc., which can effectively improve the risk prevention and control capability and decision-making efficiency of safety supervision departments and coal enterprises.

KEYWORDS:
Coal mine safety, Security Monitoring, Early Warning, Big Data Analysis

INTRODUCTION

The process of coal mine safety production is very complicated, and management personnel should implement the safety concept into all aspects of production. Information technology can realize system integration in coal mine production and dynamically present all details of production, so as to improve the supervision and control of management personnel and enlarge the management scope of management personnel and provide relevant reference data for coal mine production. Presently, in order to improve the safety of coal mine production, enterprises should strengthen the construction of internal informatization, extract some valuable information through big data analysis, establish and improve relevant control and supervision mechanisms through the summarization and sorting of potential information so as to promote the healthy development of enterprises. With the rapid development of information communication technology and the construction of information system, coal mining enterprises have collected and accumulated many data. The effective processing and analysis of these data plays an important role in coal mine safety production [1-3]. In the present researches, through unified planning and construction, data sharing of multiple professional information platforms and analysis of a large number of multi-source heterogeneous data have been realized and applied to coal mine safety management [4-8]. However, the data obtained by sampling at different time scales have not been fully mined and effectively utilized, especially the results of the regular research and archiving of historical data and the joint analysis ability of real-time monitoring data need to be further improved. To solve this problem, this paper proposes a coal mine safety monitoring and warning platform based on big data, which effectively applies big data technology to coal mine safety management. In the data processing layer, this paper proposes a tag-based big data open engine architecture of hierarchical sharing of single and multiple factors, which combines real-time data with historical data for joint analysis and mining, thus realizing the sharing of analysis models. According to the performance requirements of the platform in real application scenarios, the technical selection and architecture of coal mine safety monitoring and warning platform are designed.

MATERIALS AND METHODS

Functional requirements analysis. According to analysis of the present researches, the main causes of coal mine safety incidents include equipment failure, management error, environmental factors exceeding the standard, and operating personnel's operation errors [2, 6, 7]. Among of them, management errors and operational errors of em-

ployees are within the scope of standardized management. This paper mainly researches how to make real-time warnings on equipment failures and environmental factors exceeding the standard, thus reducing the occurrence of coal mine safety accidents. In order to realize the full mining and effective utilization of data acquired from sampling at different time scales, this paper puts forward the principles of the construction of coal mine safety monitoring and early warning platform based on big data as follows: After the analysis of lessons learned to prevent recurrence; Adopt artificial intelligence and big data technology to realize rapid intelligent early warning. Based on this, through analyzing the factors of coal mine accidents, according to China's coal mine informatization level and safety management characteristics, the functional requirements of coal mine safety monitoring and early warning platform based on big data are determined: first, the need to achieve data collection and management of coal mine safety monitoring; second, it is necessary to achieve rapid and intelligent warning of coal mine safety accidents.

Focus of big data analysis. Big data analysis focuses on data visualization analysis, data mining algorithms, predictive analysis, semantic engine, data quality and data management.

(1) Data visualization analysis mainly relies on the powerful visualization data analysis platform to correlate and analyze the massive information that is relatively scattered and the data structure is not unified, and make complete analysis charts to display the data information clearly and intuitively.

(2) Data mining algorithm is a set of trial methods to create mining model based on data, which is the theoretical core of big data analysis. The algorithm first analyzes the user's data, performs data search for specific types of patterns and trends, and uses the analysis results to define the optimal parameters for creating the mining model, and constructs different models.

(3) Predictive analysis combines a variety of advanced analytics capabilities, including special statistical analysis, data mining, machine learning, real-time scoring and so on to predict future, or other uncertain events. Use the mined data indicators to predict future events and take action accordingly.

(4) A semantic engine is the addition of semantics to existing data, which can be thought of as a semantic overlay on an existing structured or unstructured database. It enables users to get the required information faster, more accurate and more comprehensive, and improves users' Internet experience.

(5) Data quality and data management refers to the data from planning, acquisition, storage, sharing, maintenance and application, and in each stage of life cycle may be caused by all kinds of data quality problems, identification, measurement, monitoring, early warning and a series of management activities, and through the improvement and improve the management level of organization to make data quality further improved.

Big data support platform. The goal of the big data application support platform is to provide a flexible platform for analysis (Figue 1). It can satisfy business personnel to select, extract, reconstruct and combine data according to business requirements, and conduct multi-dimensional and multi-dimensional mining and analysis by using models. From the perspective of data, this platform integrates many databases with the characteristics of large data volume, heterogeneous irregular content and fast data update. From the perspective of business requirements, the platform can find the correlation of data, and realize the integration of heterogeneous big data with many types through data integration and data mining analysis of algorithm model. The platform functions include: Big data acquisition, storage, analysis and presentation.

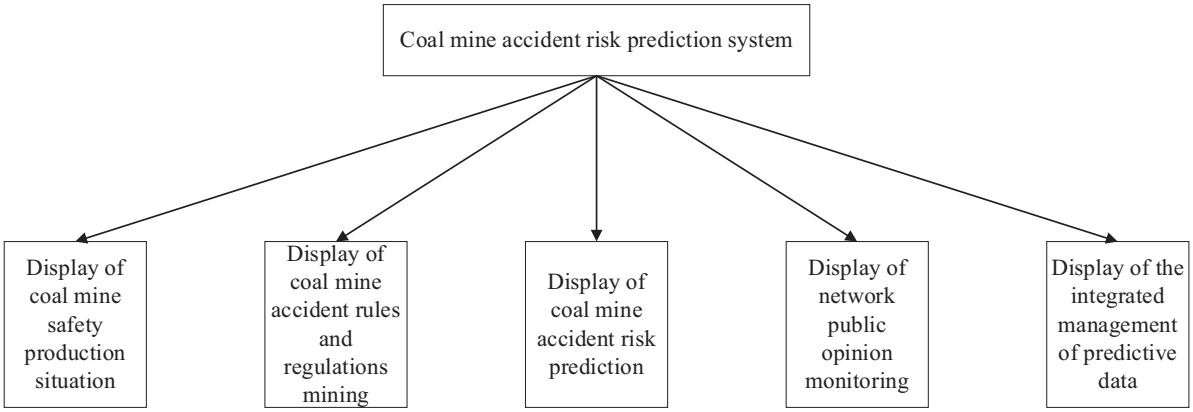

FIGURE 1
Functional structure diagram of coal mine safety risk prediction system

Platform architecture. In order to meet the functional requirements of the platform, this paper designs a coal mine safety monitoring and early warning platform based on big data by analyzing the factors of coal mine accidents. The platform architecture is shown in Figure 2, including data acquisition layer, data optimization layer, data processing layer and data application layer.

At the data acquisition layer, it is connected to the environment monitoring platform, equipment monitoring platform, security risk monitoring platform, and underground delivery platform to achieve millisecond-level data collection, so as to monitor the running status of the device in real time. The real-time data related to coal mine safety production that needs to be collected mainly include environment data and machine and equipment data. Environmental data mainly includes real-time data such as gas data, air content data, coal mine pressure data, coal mine water resources data, electromagnetic radiation data and the mining speed of working surface. Machine equipment data mainly includes real-time data of various devices, such as power data, temperature data, duration of use and so on. In order to better carry out data analysis, it is necessary to obtain basic data related to coal mine safety production, such as coal mining technology and operation specifications, regional geography and geology, personnel and equipment, and take these basic data as auxiliary reference factors.

In the data optimization layer, it mainly realizes the storage, cleaning and transformation of data. Considering the diverse types of data and the short time of data collection, the distributed file platform and NoSql database are adopted to ensure the real-time and reliability of the data storage platform.

In the process of data cleaning, measures such as filling vacant data, smoothing noise data and identifying outliers are adopted to ensure the availability of data. In the process of data conversion, the content and protocol of data exchange in coal mine are defined by setting standards for data conversion, and data from multiple data sources are merged into consistent data storage without redundancy.

In the data processing layer, statistical analysis, machine learning, data mining and other technologies and algorithms are adopted, based on real-time data and historical data of equipment and environment. Through the establishment of accident analysis model, reliability evaluation model, early warning model, the statistical analysis and mining of data are realized. In order to improve the sharing of data processing results and realize real-time warning, according to the historical data of coal mine safety incidents and related factors, labels are established on equipment and environment to facilitate quick response and discovery of security risks. The data processing layer will be described in detail in the next section.

In the data application layer, coal mine safety reliability evaluation, comprehensive analysis of coal mine safety accidents and real-time warning of coal mine safety can be realized through analyzing the correlation of coal mine safety events and data analysis model based on data processing layer, so as to realize effective utilization of real-time and non-real-time data and better ensure coal mine safety. First, coal mine safety accident comprehensive analysis; Second, coal mine safety reliability evaluation; Third, real-time warning of coal mine safety. In order to facilitate management, this paper proposes a real-time warning mechanism for coal mine safety based on hazard sources, which can be divided into spontaneous combustion warning, equipment fault warning, gas concentration warning, water hazard warning and so on.

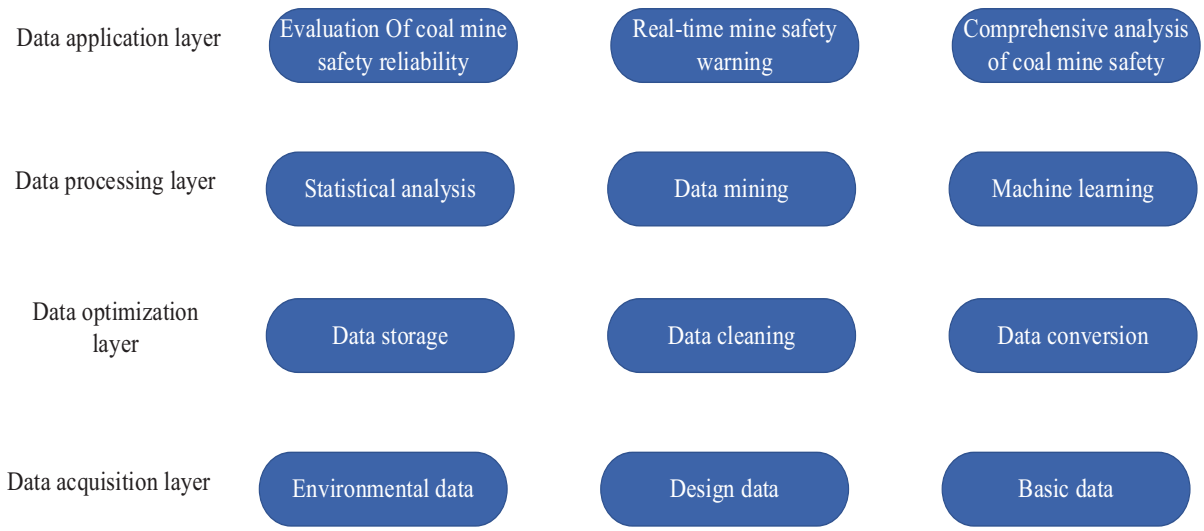

FIGURE 2
Coal mine safety monitoring and early warning platform based on big data

Key technology implementation of data processing layer

Multi-factor analysis model layer	Real-time warning model	Comprehensive analysis model	Reliability evaluation model
	Equipment failure warning, gas concentration warning, impact ground pressure warning, flood warning and so on.	Analysis of the relationship between accidents and key indicators, analysis of accident and time, analysis of the relationships between accidents and regional and so on.	Ventilation system reliability, safety monitoring reliability, equipment operation reliability, transportation roadway reliability and so on.

Correlation analysis and deep mining layers	Correlation analysis			……	Deep mining method		
	Apriori Algorithm	……	DMFIA Algorithm		SVM Algorithm	……	DBSCAN Algorithm

Single-factor label layer	Environmental single-factor label					Single-factor label for equipment				
	Water inflow		… …	Gas content		The ventilator		… …	Roadheader	
	Accident rate	Risk rating		Accident rate	Risk rating	Accident rate	Risk rating		Accident rate	Risk rating

FIGURE 3
Big data open engine architecture

RESULTS AND DISCUSSION

In order to conduct joint analysis of regular research results of historical data and real-time monitoring data, and realize rapid early warning of coal mine safety accidents, when implementing data processing layer, this paper designs a big data open engine architecture based on single-factor and multi-factor hierarchical sharing. The architecture is shown in Figure 3, including single-factor tag layer, association analysis and deep mining layer, and multi-factor analysis model layer. Firstly, is single-factor label layer: in order to improve real-time data analysis and response speed, key data sources involving security related to equipment and environment are extracted to form a single factor. Based on the single-factor data characteristics, the risk rating, accident rate and other labels are constructed. The label can quickly reflect the status of key factors of coal mine safety and achieve rapid response to coal mine safety. Secondly, is the association analysis and deep mining layer: this layer contains Apriori, fp-growth, DMFIA and other correlation algorithms, as well as logistic regression, support vector machine, clustering, decision tree and other machine learning algorithms.

These algorithms can combine big data technology with accidents such as gas outburst, coal mine water damage, coal mine fires and so on, and establish a warning model based on big data coal mine disasters. Thirdly, is the multi-factor analysis model layer: In order to realize various functions of the application layer, make full use of the existing knowledge of single-factor labels, and integrate the relationships of multiple factor labels through correlation analysis and deep mining algorithms, and generate three categories of models, including reliability evaluation model, real-time warning model and comprehensive analysis model. The following is a detailed introduction of the single-factor label and multi-factor analysis model.

Single-factor label. Generally speaking, tag is a conclusive description of the attribute state of things, a highly refined description of the attribute state, and a method to visualize abstract data, which is not only helpful for relevant personnel to understand abstract data, but also easy to realize the rapid sharing of the attribute state of things [10-12]. In

order to realize millisecond data control and fast warning of accidents, it is necessary to establish enough tag databases. Based on this, for the collected data sources, safety-related hazard sources are extracted, safety factors are sorted out and labels are established to achieve rapid response and resource sharing. For example, in terms of the environment, establish a single-factor label for hazard sources such as water pressure, water level, water inflow, gas content, gas emission, gas pressure, and oxygen concentration. In terms of equipment, single-factor labels of water pump, transformer, ventilator, shearer, roadheader and other dangerous sources are established. These labels serve as virtual representatives of the coal mine environment and equipment operating conditions, and the labels of various coal mine environments and equipment can accurately reflect their operational status. This plays a key role in real-time warning of coal mine safety. The single-factor label proposed in this paper includes the accident probability label and the risk rating label.

(1) Accident probability label. Analyze current factors and accident occurrence data, and explore the inherent relationship between the probability of accidents and current factors, so as to use the current factors to calculate the probability of occurrence of safety production accidents in coal mines. For example, transformer failure accident rate requires data sources such as rated transformer L_R, real-time operating load L_T, ambient temperature, initial load and residual time t of main transformer overload at different boundaries. The transformer failure accident rate is classified into normal, level 1 warning, level 2 warning and level 3 warning. When $L_TL_R \leq 1$, the accident rate is labeled as normal. When $L_TL_R>1$ and the remaining running time t>30min, the accident rate is labeled as level 1. When $L_TL_R>1$ and the remaining running time is 10min< t L_TL_R<30min, the accident rate is labeled as level 2. When > 1 and the remaining running time is 1min<t<10min, the accident rate is labeled as level 3.

(2) Risk rating label. Through data analysis technology, the historical data of coal mine safety production are analyzed to evaluate the risk level of coal mine safety production. Based on this, when abnormal detection of current factors is carried out, if risk rating warning occurs, timely prevention can be carried out to avoid the occurrence of safety accidents. For example, taking a transformer as an example, by analyzing data sources such as accident rate label, transformer network, and accident knowledge base, risk rating labels can be classified into normal, level 1 warning, and level 2 warning. When the accident rate is labeled abnormal and the transformer network contains backup power, the risk rating label is level 1 warning. When the accident rate label is abnormal, the transformer network does not contain backup power, and the accident knowledge base contains the accident caused by this, the risk rating label is level 2 warning.

Multi-factor analysis model. There are many research results in the early warning model, but the existing research models are relatively independent and lack of sharing [5-6, 13]. In order to realize various functions of the application layer, make full use of the existing knowledge of single-factor labels, and integrate the relationships of multiple-factor labels through correlation analysis and deep mining algorithms, and generate three categories of models, including reliability evaluation model, real-time warning model and comprehensive analysis model. For example, take the ventilation system reliability evaluation as an example, it needs to consider the ventilation system, gas monitoring system, equipment monitoring system and other factors and basic data. By sharing single-factor tags, you can quickly generate the various high-level models you need. Taking the relevant research of coal mine water disaster as an example, the basic models such as the discrimination model of water inrush source, the prediction model of water inrush level, and the evaluation model of water disaster safety can be established by analyzing the single-factor data of water pressure, water level, water inrush and so on with the correlation analysis algorithm and the deep mining algorithm. Based on these basic models, a real-time early warning model for water damage at the application level can be quickly generated for real-time warning of coal mine water hazard accidents [14, 15].

Technical implementation. In the technical implementation part, based on the analysis of existing big data platform [3, 5, 16], the technical implementation framework of coal mine safety monitoring and warning platform based on big data is proposed. This framework includes front-end acquisition layer, front-end workstation layer and back-end cluster layer. The front-end acquisition layer mainly realizes the docking with the existing acquisition system. The front-end workstation layer determines whether to issue early warning in real time by acquiring collected data and according to local rules and local cache, so as to realize the function of real-time early warning of coal mine safety. Through fast data storage, near-real-time state adjustment, model discovery and state adjustment, the back-end cluster layer realizes the functions of coal mine safety reliability evaluation and comprehensive analysis. In terms of technology selection, this paper adopts Flume, Kafka and HDFS to build acquisition architecture, and Spark, Spark Streaming and Storm to build computing architecture, so as to realize the efficient collection of coal mine safety data and improve the real-time and accuracy of platform early warning. The front-end work-

station layer and back-end cluster layer are described below.

At the front-end workstation level, the platform needs to be implemented to respond reliably to events at the millisecond level. Because the local cache can achieve sub-subtle levels of data acquisition latency. To ensure real-time performance, HBase and other in-memory databases are used to quickly acquire and update data. To overcome the memory size limit of the local cache, HBase is configured to ensure that the required data can be found in the block cache, and distributed data is distributed in the cluster nodes in a distributed memory cache. As shown in Figure 3, the front-end device generates a single-factor tag based on the collected data and compares it with the tag data in HBase to quickly determine whether to perform an alert. In the back-end cluster layer, the platform needs to process millions of pieces of data per second. This paper takes three measures to solve this problem: fast data storage, near-real-time state adjustment, non-real-time model discovery and state adjustment. The first is fast data storage: message queue platform Kafka is established between front-end devices and back-end clusters, and Kafka sends data to Flume, and Flume realizes HDFS storage of data. Secondly, near-real-time state adjustment: in order to realize real-time warning, it is usually necessary to complete the response within several seconds to several minutes after the occurrence of the event. In order to realize the near real-time state analysis, Kafka sends data to Storm/Spark Streaming, and realize the near real-time event analysis through the ability of fast calculation. Thirdly, non-real-time model discovery and state adjustment: in order to make full use of historical event data, it is necessary to complete the analysis of historical events within a few hours or days after the event is sent and dig out the hidden causes and rules. In this paper, Spark/Impala module is used for supervised and unsupervised learning of tag data. For example, using support vector machine and Bayesian network, the supervised learning of label data can distinguish risk data. K-means clustering algorithm can be used to cluster similar events, so as to determine specific categories.

CONCLUSION

In order to solve the problem that real-time data and historical data of coal mine safety are not fully analyzed and excavated, this paper analyzes the factors of coal mine accidents and designs the coal mine safety monitoring and warning platform based on big data. In order to fully analyze and mine real-time data and historical data, in the data processing layer, this paper proposes a big data open engine architecture based on label-based single-factor and multi-factor hierarchical sharing. This architecture can not only combine real-time monitoring data for real-time response, but also generate multiple models for sharing at the application layer. Through analysis, it can be known that the platform can discover, analyze and judge in advance the state that affects coal mine safety production and the data that may lead to accidents, and release the early warning information of safety production in time to minimize the probability of accidents.

ACKNOWLEDGEMENT

This research is supported by the foundation of Special Projects for Promoting Science and Technology Innovation of Xuzhou City: Construction and Empirical Study of Ecological Civilization Monitoring and Early Warning System in Coal Mining Area-Taking Xuzhou as an Example (granted by KC16SQ183).

REFERENCES

[1] Huang, Y., Cheng, W., Tang, C., Wang, C.L. (2015) Study of multi-agent-based coal mine environmental monitoring system. Ecological Indicators. 51, 79-86.

[2] Sun, S.L., Zhou, S.Q., Xue, G.Y., Ji, Z., Li, Q., Jing, D. (2009) Monitoring and early warning system for ecology and climate and its application in Hangzhou Bay. Science & Technology Review. 27, 39-47.

[3] Wu, I.C., Lu, S.R., Hsiung, B.C. (2015) A BIM-based monitoring system for urban deep excavation projects. Visualization in Engineering. 3, 2-4.

[4] Zhang, X., Fan, T.N. (2012) The Research of Distribute Temperature Monitoring System Early Warning Fire in Coal Belt Conveyor. Advanced Materials Research. 548, 890-892.

[5] Huang, M.L., Wu, B., Liu, H.K., Tan, Z.S. (2015) The Development of Shaft Monitoring and Early Warning System Based on the Technology of Fiber Bragg Grating. China Civil Engineering Journal. 48, 424-428.

[6] Lou, W.P., Zhu, X.M., Zhou, S.Q., Xue, G.Y., Cai, J.Z., Ji, Z.W. (2007) Monitoring and early warning system for agro-ecological and agriculture meteorological disaster in Shaoxing City. Transactions of the Chinese Society of Agricultural Engineering. 23, 182-186.

[7] Zhao, S.F., Chen, L.C. (2012) Hoisting Equipment of Coal Mine Condition Monitoring and Early Warning Based on BP Neural Network. Advanced Science Letters. 5, 491-496.

[8] Shan, P., Wang, C.X., Deng, H.B. (2017) Technical systems of ecological and environmental monitoring associated with large-scale coal-fired power plants: case study in Xilingol, Inner Mongolia. International Journal of Sustainable Development & World Ecology. 24, 1-6.
[9] Jiang, B.C., Gu, K.K., Ang, L., Wang, Y.Z. (2017) Dynamic Analysis on Ecological Infrastructure Quality in Coal-based Cities:A Case Study of Huainan City. Journal of Landscape Research. 2, 52-57.
[10] Schwarzenbach, R.P., Egli, T., Hofstetter, T.B., Gunten, U.V. (2010) Global Water Pollution and Human Health. Social Science Electronic Publishing. 35, 109-136.
[11] Dhillon, B.S. (2008) The safety parameters monitoring system for the coal mine based on CAN bus communication and intelligent data acquisition. Engineering Sciences. 6, 92-96.
[12] Fang, S.F., Li, D.X., Zhu, Y.Q., Ahati, J., Pei, H., Yan, J.W., Liu, Z.H. (2014) An Integrated System for Regional Environmental Monitoring and Management Based on Internet of Things. IEEE Transactions on Industrial Informatics. 10, 1596-1605.
[13] Beckie, H.J., Hall, L.M., Simard, M.J., Leeson, J., Willenborg, C.J. (2010) A framework for postrelease environmental monitoring of second-generation crops with novel traits. Crop Science. 50, 1587-1604.
[14] Jiang, J.A., Lin, T.S.,Yang, E.C., Tseng, C.L., Chen, C.P., Yen, C.W., Zheng, X.Y., Liu, C.Y., Liu, R.H., Chen, Y.F., Chang, W.Y., Chuang, C.L. (2013) Application of a web-based remote agro-ecological monitoring system for;observing spatial distribution and dynamics of Bactrocera dorsalis in;fruit orchards. Precision Agriculture. 14, 323-342.
[15] Chen, Y., Jiang, Y., Li, D. (2007) A decision support system for evaluation of the ecological benefits of rehabilitation of coal mine waste areas. New Zealand Journal of Agricultural Research. 50, 1205-1211.
[16] Dick, G.J., Eberhardt, E., Cabrejo-Liévano, A.G., Stead, D., Rose, N.D. (2015) Development of an early-warning time-of-failure analysis methodology for open-pit mine slopes utilizing ground-based slope stability radar monitoring data. Canadian Geotechnical Journal. 52, 515-529.

Received: **21.08.2019**
Accepted: **14.12.2019**

CORRESPONDING AUTHOR

Weili Wu
School of Management,
China University of Mining and Technology,
Xuzhou 221018 – China

e-mail: wuweili888@21cn.com

© by PSP Volume 29 – No. 05/2020 pages 3571-3578 Fresenius Environmental Bulletin

DETERMINATION OF HEAVY METAL CONTENTS IN ST. JOHN'S WORT (HYPERICUM SPP) IN ZONGULDAK, TURKEY

Sinem Colak[1], Kubra Yazici[2,*], Suheda Basire Akca[3]

[1]Zonguldak Bulent Ecevit University Caycuma Food and Agriculture Vocational School, Department of Chemical and Chemical Processing Technologies, 67000 Caycuma, Zonguldak
[2]Gaziosmanpasa University, Faculty of Agriculture, Department of Horticulture, Taslıciftlik Campus, 60000, Tokat, Turkey
[3]Zonguldak Bulent Ecevit University Caycuma Food and Agriculture Vocational School, Department of Park and Horticulture, 67000, Caycuma, Zonguldak

ABSTRACT

This study was carried out to determine the accumulation of heavy metals in St. John's wort (Hypericumspp.) samples grown naturally in Zonguldak province / Turkey. In the study, plant and soil samples were collected from three locations where St. John's wort plants widely grew. ICP OES was employed for determining useful heavy metal concentrations in the soil for the plant. The concentrations of Chromium (Cr), Nickel (Ni), Copper (Cu), Zinc (Zn), Cadmium (Cd), Lead (Pb), metal, and trace elements in St. John's Wort plant (flower and stem) and soil samples were analyzed using Perkin ElmerNexION 300D ICP - MS device. Pearson's Correlation analysis was used for determining the relationship between metal concentrations, and the ANOVA test was employed for determining the difference between metal concentrations arising according to the locations and samples. In addition, cluster analysis was used for identifying the similarities of metal concentrations by locations. In conclusion, according to the location evaluation, the lowest concentration of Cd and the highest concentration of Zn were found in Devrek location. In addition, the analyses indicated that heavy metals such as Cr, Cu, and Zn were found above 1 ppm in all locations. The highest heavy metal concentrations in the flower part were found in Devrek with 9.53 ppm Zn and in Çaycuma with 3.44 ppm Cu.

KEYWORDS:
Heavy metal, Environment, Soil pollution

INTRODUCTION

St. John's wort (Hypericum spp.), which belongs to Hypericaceae family, is also known as perforate St John's-wort, common Saint John's wort, and St John's wort. About 70 species of St. John's Wort (Hypericum spp.) are found wild in nature. One of a family of perennials, the plant grows all over the world except for equator and poles because it is frost resistant. It also attracts attention as a valuable plant in terms of commercial production due to especially its use in pharmaceutical production [1].

Heavy metals arise from various sources such as heavy traffic, pesticides, mining, industrial and domestic wastes, and combustion of fossil fuels [2, 3, 4]. The ions of heavy metals, which are the major environmental pollutants, are present in the air, water, and soil, and they may have serious harmful effects on humans and the ecosystem due to the toxicity of some metals [5, 6, 7]. In addition, the toxicity of heavy metal ions also shows up as an important environmental problem due to their volatility and transportability [7, 8].

Any non-biodegradable metal is considered as "heavy metal". In addition, fifty-three elements with an atomic density greater than 6 g cm-3 also fall into the heavy metal category. However, common toxic metals are chromium (Cr), manganese (Mn), copper (Cu), mercury (Hg), lead (Pb), cadmium (Cd), zinc (Zn), molybdenum (Mo), nickel (Ni), and aluminum (Al) [4, 9, 10]. Many of these elements (Fe, Zn, Mn, Cu, Ni, Mo) are essential elements for the growth and metabolism of plants, but their high concentrations are toxic to plants [10, 11,12]. These metals adversely affect the growth physiology of plants; however, they can lead to chronic and epidemic diseases when they enter the food chain [13, 14, 15]. Heavy metal stress causes biochemical, physiological, and morphological changes in plants [15, 16, 17]

Concentrations of heavy metals particularly in the edible parts of plants reduce yield, and thus food chain is adversely affected [15, 18]. As a result, soils contaminated with heavy metals are becoming a problem for human and animal health every other day [12, 19]. Minimizing heavy metal concentrations in food products is of great importance particularly for food safety [15]. In addition, essential metals such as iron, copper, nickel, and zinc are beneficial for the healthy development of the body, but their availability in high levels is not desirable. Also, metals such as mercury, lead, and cadmium show toxic effects even at very low concentrations [20,

21]. The consumption of plants that grow under environmental conditions where heavy metals are present and which contain heavy metals above acceptable levels cause heavy metal concentrations in the human body, which has adverse effects on human health. These negative effects have been studied widely [22, 23].

The plants, which have existed for centuries, are used in many fields such as food, medicine, industry, cosmetics, and decorative purposes mainly because of their medicinal values. This study aimed to determine heavy metal concentrations in flowers and stem parts of St John's wort plant (Hypericum spp.), which is used for various purposes as herbal tea, traditional treatment, and ornamental purposes, by analyzing soil samples taken from the region where they grow.

MATERIALS AND METHODS

Materials. Zonguldak province has a rugged terrain due to its location. In addition, the numerous thermal power plants in the region both restrict agricultural activities and have negative effects on the environment. Therefore, agricultural activities in the region are generally carried out in Çaycuma, Gökçebey, and Devrek districts. Various plants used in alternative medicine such as St. John's wort (Hypericumspp)grow naturally in these regions and are harvested by the local people. In this study, plant and soil samples were taken from three locations where St. John's wort plants widely grow (Table 1). Plant samples were collected between 8 and 10:00 am in dry weather from April 2018 to July 2018.

Plant residues on the soil surface were cleaned and a V-shaped hole was dug. Then a soil sample of approximately 3-4 cm in width and 30 cm in length was extracted from the smooth side of the hole by also maintaining the top part of the soil. All of the soil samples extracted from 10 different spots enough to represent the area according to the size of the land were laid on a clean cloth and mixed thoroughly. Soil samples as much as 1 kg were taken from this mixture and put into polyethylene bags.

St. John's wort plant samples taken from the pre-determined locations were dried in a 65oC oven before starting the study. The flower and stem parts of the samples taken from the oven were separated and pulverized separately. They were then put into plastic bags with ziplock, labeled, and stored in the desiccator until their chemical analyses.

Methods. 0.1 g of ground plant samples were taken and then they were burned according to wet digestion method in a Speedwave brand microwave oven in a mixture of H2O2 and 60% HNO3 acid (2: 4 ml v: v) for one hour. The burned sampleswere then filtered through blue band filter paper and made up to 10 ml with distilled water. Element concentrations were determined using the Perkin Elmer NexION 300D brand ICP-MS.

Metal analyses in the soil were determined after the wet digestion process. 0.1 mg soil sample together with 5 mL HNO3, 3 mL HCl and 1 mL HF was first burned in the microwave oven and then placed into the DAP 60 vessel system. After cooling, the samples were re-burned in the microwave oven by the addition of 3mL of boric acid. At the end of this process, completely burned samples were taken into a 15 mL falcon. 1 ml of the samples was taken and it was made up to 5 mL with ultra-distilled water. Finally, the values were obtained in the HF kit using Perkin ElmerNexION 300D brand ICP-MS device.

To determine the useful heavy metal concentrations in the soil for the plant, the analyses were conducted using Perkin Elmer Avio 200 brand ICP OES device according to 0.005 M DTPA + 0.01 M CaCl2 + 0.1 M TEA (pH 7.3) method that was reported by Lindsay and Norvell 1978 [24]. Perkin Elmer NexION 300D ICP - MS device was used for analyzing the existence of Chromium (Cr), Nickel (Ni), Copper (Cu), Zinc (Zn), Cadmium (Cd), Lead (Pb), metal, and trace elements in St John's wort plant and soil samples.

Statistical analyses were done using SPSS 22 software package and Minitab 18 software package was used for graphics. To determine the relationship between metal concentrations, Pearson's Correlation analysis was employed. The ANOVA test was used for determining the difference between metal concentrations resulting from the locations and samples. Additionally, cluster analysis was used for identifying the similarities of metal concentrations by locations.

RESULTS AND DISCUSSION

Heavy Metal Analysis in Plant Samples. In the study, the analyses of Cr, Ni, Cu, Zn, Cd, and Pb heavy metals were performed in the flower and stem parts of St. John's wort plant samples taken from 3 different locations. Figure 1 shows the metal concentrations in the flower and stem parts of St. John's Wort plant samples according to locations.

The lowest concentration of heavy metal in the flower part was Cd and its concentration varied between 0.05 and 0.02 ppm in all locations. The highest heavy metal concentrations were found to be 9.53 ppm Zn in Devrek and 3.44 ppm Cu in Çaycuma. The heavy metal concentrations in the stem were similar to those in the flower part; however, they differed by locations. The lowest heavy metal concentration was Cd and it varied between 0.13 and 0.01 ppm in all locations. The highest heavy metal concentrations were 3.92pmm Zn in Gökçebey and 3.25 ppm Cu in Devrek.

The evaluation of the locations indicated that Cr (1.77-1.1-70ppm) and Zn (3.92-3.87 ppm) concentrations were similar in the stem and flower parts in Gökçebey location. However, Pb and Cd concentrations in the stem were found to be 1.6 and 6.5 times respectively more than they were in the flower part. In the samples taken from Çaycuma region, Cr (1.67-1.95ppm) and Ni (0.24-0.38 ppm) were found in similar concentrations in the stem and flower parts. Contrary to Gökçebey location, metal concentrations were higher in the flower part in Çaycuma. Cd, Pb, Zn, and Cu concentrations in the flower part were found to be 5, 2.7, 1.9, and 2.15 times respectively higher than they were in the body part. The highest Zn concentration in Devrek location was found to be in the flower part of the St. John's wort plant and it was determined to be 2.5 times higher than it was in the stem part of the plant in Devrek region. However, Cd concentration was found to be the lowest compared to other elements. Other metal concentrations were found in similar concentrations in flower and stem parts. In a study carried out in Kütahya city on St. John's wort plant obtained from a herbalist, the concentrations of Cd, Cr, Cu, Ni, and Pb were found to be 0.12, 1.58, 7.72, 2.62 and 0.68 ppm respectively [25]. In a study carried out in Hatay, leaves and fruit were studied separately and Cd, Cr, Cu, Mn, Ni, Zn concentrations in leaves were found to be 0.1755, 0.3324, 13.73, 18.442, 4.0576, and 47.304 ppm respectively. No Cd concentration was found in the fruit and neither was Pb in leaves [26]. The findings of the current study seem to support the findings of previous studies. In another study conducted in the Sokol Mountains in West Serbia and Poland, Cd concentrations in St. John's wort plant were found to be 0.878 and 0.102 ppm, which were very high in contrast to our study [27, 28]. The 8.106 ppm Pb concentration found in the study conducted in Poland was observed to be about 66 times higher than that of St. John's wort plants in our region [28]. In summary [27, 28], according to the analyses of this study, the heavy metal concentrations of St. John's wort plant collected from 3 regions in Zonguldak province was low.

According to the overall evaluations of locations, the lowest Cd concentrations and the highest Zn concentrations were found in Devrek location. In addition, the analyses indicated that Cr, Cu, and Zn heavy metals were above 1 ppm in all locations. Table 2 shows the comparison of the mean metal concentrations in the flower and stem parts of St. John's Wort plant with standard and toxic values. Zn metal was found to be below the standard concentration value in all locations.

Metal Analysis in Soil Samples. The concentrations of heavy metals in soil samples analyzed by locations are given in Figure 2.

As is seen in Figure 2, the analysis of copper content of soil samples in accordance with the limit values reported by Linsay and Norvell indicated that all of the soil samples were in an adequate level (>0.2ppm) in terms of copper content uptake [24].

TABLE 1
Localities where St. John's wort samples were collected

Locaties of Samples	Part of the Samples	Gps Coordinates
Çaycuma	Flower-Stem	41° 25' 43.1112" North and 32° 4' 37.9416" West
Gökçebey	Flower-Stem	41° 18′ 28.5768" and 32° 8′ 29.7096"
Devrek	Flower-Stem	41° 17' 9.5424" North and 32° 0' 51.0588" West

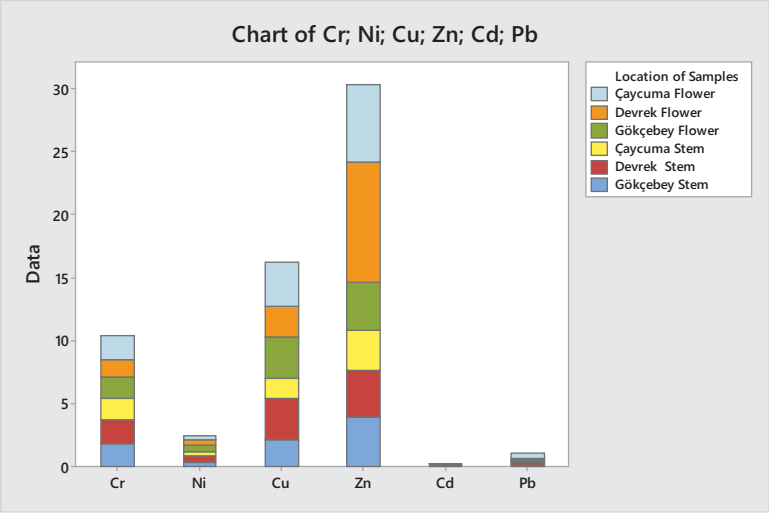

FIGURE 1
Distribution of heavy metals in the stem and flower part of the plant according to sampling locations

TABLE 2
Reference values for standard and toxic concentrations of heavy metals in plants

Element	Normal concentrations (ppm)	Toxic concentrations (ppm)	Gökçebey (ppm)	Devrek (ppm)	Çaycuma (ppm)
Cu	3-15[a]	20[b]	2,73	2,84	2,52
Ni	0.1-5[a]	30[b]	0,46	0,47	0,31
Pb	1-5[a]	20 [b]	0,12	0,13	0,28
Cr	<0.1-1[a]	2[b]	1,73	1,66	1,81
Zn	15-150[a]	200[b]	***3,89***	***6,62***	***4,65***

Reference: a, [29, 30].

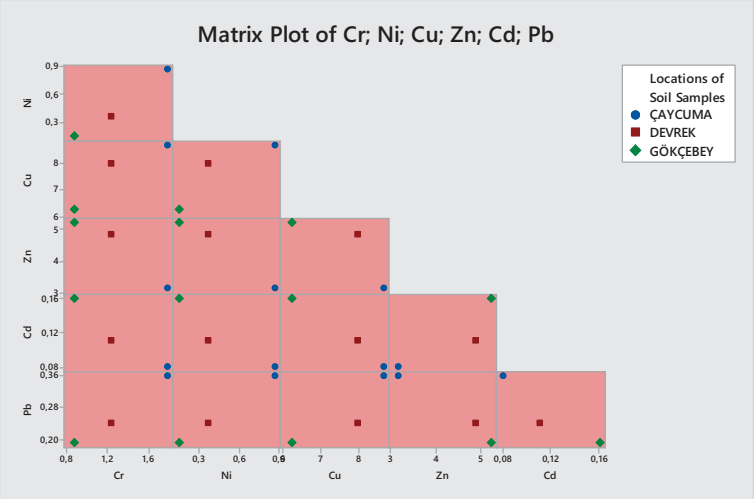

FIGURE 2
Matrix graph of Pb, Zn, Cr, Cu, Cd, Ni elements in soil samples

TABLE 3
Limit values for average heavy metal concentrations

Elementler	WHO/ FAO (ppm)	Ministry of Environment and Urbanization (ppm)	Gökçebey (ppm)	Devrek (ppm)	Çaycuma (ppm)	Adana (ppm)
Cd	3	3	0.16	0.11	0.08	0,46
Cr	100	100	0.87	1.23	1.78	59,48
Cu	100	140	6.23	7.98	8.65	35,14
Ni	50	75	0.14	0,36	0.87	94,51
Pb	100	300	0.19	0.24	0.36	51,24
Zn	300	300	5.23	4.87	3.14	60,11

Natural concentrations of heavy metals in soils depend mainly on the type and chemistry of the main materials in the soils. According to the data of World Health Organization (WHO) / World Agriculture Organization (FAO) and Ministry of Environment and Urbanization, the limit values for the average concentrations of some heavy metals found in soil are shown in Table 3. In addition, the comparison of the average heavy metal concentrations in our soil samples taken from all three regions with the average values of a study conducted in Adana region [31] indicated that the heavy metal concentrations in all three regions investigated in this study were low.

The analysis of bioavailablemetals in soil samples availability. In general, certain fractions of soil metals can be easily taken up by plants. Table 4 gives the locational comparison of heavy metal concentrations extracted with DTPA in different parts of St. John's wort plant.

As is seen in Table 4, the concentrations of Cr, Ni, and Cd for all locations and for all parts of the plant, and Pb metals found in the stem in Gökçebey location and in the flower in Çaycuma location were found to be higher than the concentrations taken up by plant from the soil (bioavailable metal concentrations). This showed that external factors such as traffic and fossil fuel use cause metal concentrations in St. John's wort plant parts.

ANOVA and Correlation Analysis. ANOVA test was employed for determining whether the element concentrations analyzed created a significant difference in soil and St. John's wort plant samples (flower and stem). Only Cu concentration

TABLE 4
Availability metal concentrations and the metal concentrations of plant samples

	Beneficial Metal Concentrations (ppm)			Plants Metal Concentrations (ppm)					
Metals	G	D	Ç	G S	D S	Ç S	G F	D F	Ç F
Cr	0,104	0,149	0,14	**1,020**	**1,193**	**0,922**	**0,980**	**0,807**	**1,078**
Ni	0,076	0,215	0,365	**0,725**	**1,176**	**0,764**	**1,275**	**0,824**	**1,236**
Cu	2,291	4,152	6,497	0,782	1,147	0,634	1,218	0,853	1,366
Zn	1,725	8,766	1,939	1,007	0,560	0,685	0,993	1,440	1,315
Cd	0,056	0,079	0,055	**1,743**	**1,631**	**0,251**	**0,257**	**0,369**	**1,749**
Pb	1,061	2,221	1,314	**1,236**	1,099	0,520	0,764	0,901	**1,480**

G: Gökçebey, D: Devrek, Ç: Çaycuma, S: Steam, F: Flower

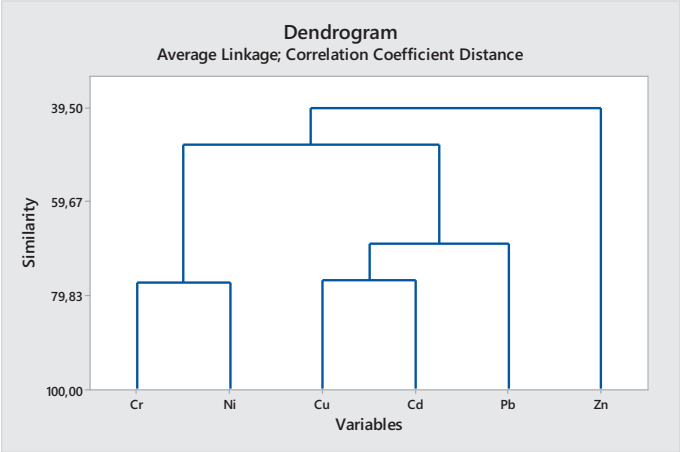

FIGURE 3
Dendrogram graph

TABLE 5
Pearson's Correlation Coefficients for total metal concentrations in soil samples

	Cr	Cu	Cd	Pb	Ni
Cr	1				
Cu	**0,93**	1			
Cd	**-0,97**	**-0,99**	1		
Pb	**0,99**	**0,88**	**-0,93**	1	
Ni	**0,99**	**0,89**	**-0,93**	**1,00***	1

*. Correlation is significant at the 0.01 level (2-tailed).

TABLE 6
Pearson Correlation table for total metal concentrations in plant samples

	Cr	Cu	Cd	Pb	Ni
Cr	1				
Cu	0,50	1			
Cd	0,34	-0,10	1		
Pb	0,52	0,38	0,14	1	
Ni	0,26	**0,82***	-0,18	-0,22	1

*. Correlation is significant at the 0.05 level (2-tailed).

(F2 = 28.571 p = 0.001) was found to yield a statistically significant difference. Pearson correlation analysis was performed for determining the relationship between total metal concentrations in soil. As seen in Table 5, a strong positive correlation was found between Cr, Cu, Pb, and Ni concentrations. Also, a strong negative correlation was found between Cd, Pb, and Ni concentrations. In addition, a statistically significant relationship was found between Pb and Ni at p <0.01 level.

Table 6 presents the results of Pearson's correlation analysis between metals found in different parts of the plant. A positive strong and significant correlation was found between Cu and Ni.

Cluster Analysis. Hierarchical clustering technique was employed for determining all heavy metal concentrations (variables) which were thought to be effective in the differentiation in soil and plant parts and which were quantitatively determined and the groups created by these concentrations. In this study, average values were used as the linkage method and the correlation coefficient was employed as a measure of distance. The dendrogram created to present the differences and similarities between the heavy metals is given in Figure 3. The evaluation of the dendrogram indicated that two main clusters belonging to the similarity ratio of 39.50 and two clusters exhibiting similar behaviors under each of the two main clusters were formed. This revealed that these clusters with similar behaviors originated from different sources. Therefore, the analysis of all of the results showed that Cr, Ni, Cd, Pb, and Cu heavy metals in the first main cluster were mostly affected by anthropogenic sources and the Zn elements found in the second main cluster were affected by lithogenic (main soil material) sources.

TABLE 7
Bioaccumulation factor values

	Gökçebey Steam	Devrek Steam	Çaycuma Steam	Gökçebey Flower	Devrek Flower	Çaycuma Flower
Cr	**1,020**	**1,193**	**0,922**	**0,980**	0,807	**1,078**
Ni	0,725	**1,176**	0,764	**1,275**	0,824	**1,236**
Cu	0,782	**1,147**	0,634	**1,218**	0,853	**1,366**
Zn	**1,007**	0,560	0,685	**0,993**	**1,440**	**1,315**
Cd	**1,743**	**1,631**	0,251	0,257	0,369	**1,749**
Pb	**1,236**	**1,099**	0,520	0,764	**0,901**	**1,480**

Bioaccumulation Factor (BAF). Heavy metals are absorbed and accumulated from the soil to different parts of the plant through their roots. In this study, the BAF factor was used for investigating heavy metal accumulation relationship in soil and plant systems. The equation of the factor is BAF = Mplant / Msoil, where Mplant refers to the element content (ppm) in the plant parts and Msoil refers the element content (ppm) in the soil where the plant grows [32]. This equation is used for estimating each element's capacity of transfer from the soil to the plant and for showing the ability of biological element transport and migration. Table 7 shows the BAF values calculated according to plant parts by locations.

In Table 7, heavy metals with BAF values equal or close to 1 indicate that St. John's wort plant is a bioaccumulator plant for that metal. Heavy metals with high BAF values in the flower part of St. John's wort plant were generally found in Gökçebey and Çaycuma and in the stem part in Devrek and Gökçebey locations. Since the data belonging to all locations and plant parts were > 0.1, the rate of transfer from soil to plant was observed to be high.

CONCLUSION

The chimney emission of thermal power plants and the heavy metals emitted within the ash in Zonguldak region combine with the nutrient cycle. Heavy metal pollution in soil, air, and water coming from thermal plants are taken up by plants through the water they absorb and therefore these pollutants are transferred to humans through food products and this leads to an adverse effect on human health. According to the regulation of the General Directorate of Food and Control, the presence of trace amounts (0.001% / 0.000001) of heavy metal in the edible parts of plants is acceptable. In Zonguldak region, heavy metal concentrations in St. John's wort plant, which is used both for treatment purposes and for its soothing properties, were found to be lower compared to other regions. However, the values were still above certain limits.

When the average concentrations of some heavy metals found in soils were examined according to the data of World Health Organization (WHO) / World Agriculture Organization (FAO) and Ministry of Environment and Urbanization, all concentrations were observed to be within the required range.

According to the BAF findings in this study, St. John's wort plant can be used as a bioaccumulator and also as a bioindicator plant for the following metals and locations for the stem part: Cr in all locations; Cd and Pb in Gökçebey and Devrek; and Ni and Cu in Devrek; and for the flower part: all heavy metals in Çaycuma; and Cr, Ni, Cu, and Zn in Gökçebey.Heavy metal input due to increased traffic, urbanization, and use of pesticides and the presence of mines and thermal power plants in Zonguldak province bring about great environmental concerns, especially for the agricultural production areas. Heavy metal pollution of St. John's wort plant which is often used as a medicinal aromatic plant in Zonguldak province is of critical importance.

REFERENCES

[1] Izmir Commodity Exchange (2016). Medicinal Aromatic Plants and Good Life, İzmir Ticaret Borsası, itb.org.tr. Turkey
[2] Dhir, B., Sharmila, P., Saradhi, P. (2008) Photosynthetic performance of Salvinianatans exposed to chromium and zinc rich wastewater. Braz. J Plant Physiol. 20, 61-70.
[3] Wei, S., Zhou, Q. (2008) Trace elements in agro-ecosystems. In: Prasad MNV (ed) Trace elements as contaminants and nutrients. Wiley, New Jersey, pp 55-80.
[4] Fahimirad S., Hatami M. (2017) Heavy Metal-Mediated Changes in Growth and Phytochemicals of Edible and Medicinal Plants. In: Ghorbanpour M., Varma A. (eds) Medicinal Plants and Environmental Challenges. Springer, Cham.
[5] Fu, F., Wang, Q. (2011) Removal of heavy metal ions from waste waters: A review. J. Environ. Manage. 92(3), 407-18.
[6] Manahan, S. (2008) Fundamentals of Environmental Chemistry. 3rd ed. CRC Press, New York.

[7] Bhavsar, K., Hurston, E., Prabhu, R., Joseph, G.P. (2017) Fibreoptic sensor todetectheavy metal pollutants in water environments. In: Proceedings of the 60th MTS/IEEE OCEANS conference (OCEANS'17): A vision for sustaining our marine futures, 19-22 June 2017, Aberdeen, UK. New York: IEEE. Article ID 8084982.

[8] Driscoll, C.T., Mason, R.P., Chan, H.M., Jacob, D.J., Pirrone, N. (2013) Mercury as a global pollutant: Sources, pathways, and effects, Environ. Sci. Technol. 47(10), 4967-4983.

[9] Herrera-Estrella, L.R., Guevara-Garcia, A.A. (2009) Heavy metal adaptation. 1-9 p. In Encyclopedia of Life Sciences (ELS). John Wiley & Sons, Ltd: Chichester. DOI: 10.1002/9780470015902.a0001318.pub2

[10] White, P.J., Pongrac, P. (2017) Plant Stress Physiology. 2nd Edition. ISBN-13:978 1 78064 729 6, Australia.

[11] Park, W., Feng, Y., Ahn, S. (2014) Alteration of leaf shape, improved metal tolerance, and productivity of seed by overexpression of CsHMA3 in Camelina sativa. Biotechnol Biofuels. 7, 96 (2014). https://doi.org/10.1186/1754-6834-7-96

[12] Chaudhary, K., Jan, S., Khan, S. (2016) Heavy metal ATPase (HMA2, HMA3 & HMA4) genes in hyperaccumulation mechanism of heavy metals. Plant metal interaction (emerging remediation techniques) 545–556.

[13] Peralta-Videa, J.R., Lopez, M., Narayan, M., Saupe, G., Gardea-Torresdey, J. (2009) The biochemistry of environmental heavy metal up take by plants: Implications for the food chain. Int. J. Biochem. Cell. Biol. 41, 1665-1677.

[14] Chakraborty, D., Rahman, M.M., Mukherjee, A., Alauddin, M., Hassan, M., Dutta R.N., Pati, S., Mukherjee SC., Roy, S., Quamruzzman, Q., Rahman, M., Morshed, S., Islam, T., Sorif, S., Selim, MD., Razaul Islam, M.D., Monower Hossain, MD. (2015) Ground water arsenic contamination in Bangladesh- 21years of research. J. Trace. Elem. Med. Biol. 31, 237-248.

[15] Kumar, S., Trivedi, P.K. (2016) Heavy Metal Stress Signaling in Plants (Chapter: 25). Plant Metal Interaction Book. Emerging Remediation Techniques, 585-603p, Elsevier Inc

[16] Gülser, F., Çığ, A., Gökkaya, T.H. (2016) Effects of Lead Contamination on Nutrient Contents of Hyacinth (Hyacinthus orientalis L. c.v. “Blue Star”). J. Int. Environmental Application and Science. 11(2), 213-215.

[17] Çığ, A., Gülser, F., Gökkaya, T., Başdoğan, G. (2017) Effect of Nickel Contamination on Nutrient contents of daffodil (Narcissuspoeticus L. c. v. Icefolies). International Journal of Secondary Metabolite (IJSM). 4(2), 99-102.

[18] Zhao, F.J., Mc Grath, S.P., Meharg, A.A. (2010) Arsenic as a food chain contaminant: mechanisms of plant up take and metabolism and mitigation strategies. Annu. Rev. Plant Biol. 61, 535-559.

[19] Rocca La, N., Andreoli, C., Giacometti, G.M., Rascio, N., Moro, I. (2009) Responses of the Antarctic microalga Koliella antartica (Trebouxiophyceae, Chlorophyta) to cadmium contamination. Photosynthetica. 47, 471-479.

[20] Al-Eed, M.A., Assubaie, F.N., El-Garawany, M.M., EL Hamshary, H., El Tayeb, Z.M. (1997) Determination of Heavy Metal levels in Common Spices. Department of Botany College of Agricultural and Food Sciences King Faisal University, P.O. Box 420, Al-Hasa 31982, Saudi Arabia.

[21] Nkansah, M.A., Opoku Amoako, C. (2010) Heavy metal content of somecommonspicesavailable in markets in theKumasimetropolis of Ghana. American Journal of Scientific and Industrial Research. ISSN: 2153-649X. 1(2), 158-163.

[22] Sarma, H., Deka, S., Deka, H., Saikia, R.R. (2011) Accumulation of Heavy Metals in Selected Medicinal Plants. Rev Environ Contam Toxicol. 214, 63–86.

[23] Okut, N. (2019) Heavy Metal Content of Some Medicinal Plants Selected from Van, Turkey. Iğdır University Journal of the Institute of Science and Technology, Research Article. ISSN: 2146-0574, eISSN: 2536-4618. 9(1), 533-544.

[24] Lindsay, W.L., Norwel, W.A. (1978) Development of a DTPA test forzinc. iron. Manganese and copper. J. Soil Sci. Am. 42, 421-428.

[25] Leblebici, S., Bahtiyar, S. D., Özyurt, M.S. (2012) Determinatıon of The Amount of Heavy Metal in Some Medicinal Plants Sold ın Herbalist in Kütahya. DPU Journal of Graduate School of Natural and Applied Sciences, 29.

[26] Ergün, N., Yolcu, H., Karanlık, S., Dikkaya, E. (2010) Heavy Metal Accumulation and Mineral Contents of Some Plants on Amanos Mountains (Hatay), Turkey. 3(2), 121-127.

[27] Đurović, D., Bulat, Z., Buha, A. Matovic, V. (2013) Cadmium, Mercury and Lead in Hypericum perforatum L. collected in Western Serbia. E3S Web of Conferences 1:15009.

[28] Fischer, A., Brodziak-Dopierała, B., Loska, K., Stojko, J. (2017) The Assessment of Toxic Metals in Plants Used in Cosmetics and Cosmetology. Int. J. Environ. Res. Public Health. 24, 14.

[29] Kloke, A., Sauerbeck, D.R., Vetter, H. (1984) The contamination of plants and soils with heavy metals and the transport of metals in terrestrial food chains. In: Nriagu, J.O. (Ed.) Changing Metal Cycles and Human Health. Dahlem Konferenzen, Springer-Verlag, Berlin, Heidelberg, New York, Tokyo. 113-141.

[30] Kastori, R., Petrović, N., Arsenijević-Maksimović, I. (1997) Heavy metals and plants. In: Kastori, R. (Ed.) Heavy Metals in the Environment. Institute of Field and Vegetable Crops, Novi. Sad, 196-257.
[31] Akyıldız, M., Karataş, B. (2018) Investigation of Heavy Metal Pollution in the Soil at Adana City Center. Çukurova University Journal of Faculty of Engineering and Architecture. 33(2), 199-214.
[32] Luoma, S.N., Bryan, G.W. (1979) Heavy metal bioavailability: Modeling chemical and biological interactions in sediment boundzinc. In: Jenne, E.A. (ed.) Chemical modeling in aqueous systems. Washington, DC: ACS Symposium Series 93. American Chemical Society, 577-604.

Received: **22.08.2019**
Accepted: **23.02.2020**

CORRESPONDING AUTHOR

Kubra Yazici
Tokat Gaziosmanpasa University
Faculty of Agriculture
Department of Horticulture
60240 Tokat – Turkey

e-mail: k-yazici-karaman@hotmail.com

© by PSP Volume 29 – No. 05/2020 pages 3579-3593 Fresenius Environmental Bulletin

DETERMINATION OF TEMPORAL CHANGE IN LAND USE BY GEOGRAPHICAL INFORMATION SYSTEMS: THE CASE OF CANDIR VILLAGE OF TURKEY

Nilufer Yazici[1,*], Bekir Inan[2]

[1]Faculty of Forestry of Isparta Applied Sciences University, Isparta, Turkey
[2]Forest District of Ministry of Forestry, Isparta, Turkey

ABSTRACT

People's pressure on nature is increasing every passing day and therefore land use patterns vary. It is important to understand the temporal changes in land use that have started in the recent past and continue at a faster pace with the anticipation that natural resources will be insufficient to meet the needs due to the increasing population and the reasons affecting this.

In this study, the land use types of Çandır village and its immediate surroundings within the boundaries of Çandır basin located in Sütçüler district of Isparta province between 1986 and 2016 were determined, changes between years of land use were calculated spatially and the reasons for the change were revealed.

In the research, stand maps and topographic maps of various measures belongs to 3 plan periods of land use, in computer environment. It was evaluated by means of GIS. Google Earth satellite imagery was also utilized. In the classification, land use forms were divided into four groups as forest, agriculture, water surface and other areas and their temporal changes were examined. Between 1986 and 2016, forest areas 875.51 ha decreased. Water surface increased by 829.12 ha and agricultural areas increased by 47.36 ha.

In 2018, land use was examined in 3 slopes and 3 elevation groups. According to this, 1051.68 hectares of study area between 0-15%, 327.09 hectare area 16-30%, 461.63 hectares area within 30% + slope groups. 1238 hectares of the Çandır village, which is the study area, is located within 200m, 437 hectares within 400m, and 233 hectares within 600m.

KEYWORDS:
Çandır village, land use, GIS, temporal change

INTRODUCTION

Today, urbanization and industrialization are experiencing the most brilliant period of human history. Human beings have caused various changes in the areas they live in since the first day of their activities on earth. The basis of these changes is to live more comfortably. The desire to live more comfortably brought humanity from nomadism to settled life, and the people who settled in certain areas aimed to make it more useful for their activities. While doing all of this, people thought of their own interests and therefore made their living spaces a little more uninhabitable every day [1-5].

As in the developing countries of the world, rapid population growth in our country have brought with it important land use problems. Problems have arisen for the new settlements and industrial areas, especially the destruction of agricultural areas, and the destruction of forests, pastures and wetlands to gain new agricultural areas. In addition, agricultural and pasture areas are used without any measures against erosion and well above their capacity. All these adversities in land use patterns lead to erosion [6-11].

Since land use/land cover change is a major factor for global change because of its interactions with climate, ecosystem processes, biogeochemical cycles, biodiversity and human activities, land use/land cover change researches have become an important aspect of global change, or global warming studies in recent decades [12-17]. Much more attention has been paid to urban land use/land cover change in the last 10 years, because ecosystems in urban areas are strongly affected by human activities and have close relations with the life of almost half of the world's population [18-21].

Due to the deterioration in land use, environmental pressures occur. Due to these pressures, the need for fast and reliable information is increasing in order to ensure the more careful use of scarce natural resources. In order to meet this need, remote sensing and geographic information systems have been developed in order to access the information on the quantity and quality of natural resources and values, and in this context, a database has been created with

fast, accurate, reliable and effective studies [22]. Remote sensing and geographic information systems provide significant advantages in monitoring of urban development and temporal changes in land use today [23]. With the invention of remote sensing and GIS techniques land use/cover mapping is a useful and detailed way to improve the selection of areas designed to agricultural, urban and/or industrial areas of a region [24]. Application of remotely sensed data made possible to study the changes in land cover in less time, at low cost and with better accuracy in association with GIS that provides suitable platform for data analysis, update and retrieval. Digital change detection techniques based on multi-temporal and multi-spectral remotely sensed data have demonstrated a great potential as a means to understanding landscape dynamics-detect, identify, map, and monitor differences in land use/cover pat-terns over time, irrespective of the causal factors [25]. Many developed countries tend to differentiate in terms of quality and quantity, both to enrich city aesthetics and doctrine, and to meet the psychological and physical needs of urban people, the open green areas that are regarded as a sign of civilization and quality of life [26]. In order to improve the stated quality and quantity, Geographic Information System (GIS) technology is currently used as a spatial technology facilitating the decision-making processes by the efficient use of spatial analysis and modeling methodologies for urban and regional planning purposes [27]. The contributions of the GIS use to urban and regional planning have been confirmed by many research studies; i.e. for the determination of the sensitive areas [28], examination of the highly urbanized cities in terms of urbanization, disaster management and etc. [29-31].

The spatial sufficiency and accessibility of the active green spaces in Avcılar District, Istanbul were evaluated using GIS technology. This study aims to draw attention to the necessity of planning systematic green spaces for the local governments preparing the development plans that shape the cities, so that high quality and healthy cities can be formed [32].

GIS for sustainable watershed management provides a flexible environment for collecting and storing data that represent watershed characteristics, building and displaying ecologically based base maps and analyzing land use changes [33-37]. GIS is also widely used in providing data for modeling works or visualization of the results obtained from modelling works [38, 39]. In the literature, it is seen that the maps created with GIS are used to provide sustainable resource management, protection of natural resources, and ecological evaluations [40, 41] In recent years, the integration of GIS and RS methods has been seen in studies examining water resources protection, shoreline changes, water body extraction, mapping of watersheds and changes in land use, etc. [42-45]. RS technology produces up-to-date, fast and precise results when examining changes to land use at different time intervals. The integrated use of GIS and RS has, however, proved to be a powerful and cost-effective approach to monitoring land use change [44, 46].

There are several studies about temporal changes in land use by using GIS [37, 47-58]. In general, remote sensing and GIS were used to determine land changes between years. The studies explore the temporal and spatial characteristics of urban expansion and land use/cover change from years. Aerial photographs and Landsat satellite images have also been used in some studies. The major factors influencing urban expansion and land use/cover change are also discussed. In general, the population, traffic conditions, industrialization, and policy are the major factors that influenced the urban expansion. In several GIS-based applications, the change in land use is analyzed and quantified via converting the raster land cover/use thematic maps to vector based maps using different resolutions with different gridding systems such as square and triangle. The used resolution is usually determined by the aim and/or scale of the applied study [59-64]. Each of these gridding systems has its own advantages when used to grid the reference land use thematic map.

This research examines the square and triangle gridding systems for the green areas classes in the third level of CORINE standards, e.g. ³arable lands´, ³green urban´ and ³open space with little or no vegetation´ classes, where the CORINE is the international standard for Coordination of Information on the Environment (CORINE) sites in Europe. The methodology followed within this research is to extract a reference land cover/use map and to generate two gridding systems, namely square and triangle grids, using 23 various cell sizes [65].

This paper deals with analyses focusing on conservation efficiency of protected areas with the objective to maintain European beech-dominated natural forests. The study area covers the territory of the Czech Republic, a typical central European country. Methods of environmental assessment of conservation effectiveness of protected areas draw on the Nature Conservation Efficiency Index (NCEI) and CORINE habitats datasets analyzed by applying Geographical Information Systems (GIS). The results of analyses of the conservation efficiency of protected areas in the conservation of beech forest habitats in the Czech Republic indicate a low level of conservation efficiency [58].

In the study, the temporal changes on the Lake Burdur shoreline are examined using GIS and RS methods in a way that will also contribute to other studies. In order to determine the temporal change of land use in Lake Burdur, Landsat satellite images of Lake Burdur from the years 1985, 2000 and 2015 were used, and a SWOT analysis of the Burdur Watershed was carried out to identify the causes of these changes [59].

In our study, the temporal changes in land use of Çandır village are tried to be revealed by using GIS and the possible reasons for this are tried to be understood and the trends on the current change are tried to be determined. In this way, it was aimed to create a base for the studies to be carried out on different subjects, especially forest planning. For this purpose, the stand maps of the Forest Management Directorate in the Çandır village for the three plan periods between 1986 and 2016 were digitized with the help of GIS and the land use types from 1986 to the present were determined, the changes in land use were calculated and the reasons for the change were put forward. The land use change that will be determined as a result of this study will be used as the basis for the determination of sustainable land use and the development works to be conducted in the coming years.

MATERIALS AND METHODS

Material. The Çandır village is located in the Sütçüler District of Isparta Province. The study area is about 20 km to Sütçüler district, 70km to Isparta and 120 km to Antalya. The study area is 1908 ha in size and its boundaries lie between 37°28´31"-37°28´16" North latitude and 30°54´19"-30°51´44" East longitude. The average height above sea level is 254 m (Figure 1). There are also Şeyhler village to the north, Kızıllı village to the south, Elsazı village to the west and Bekirağalar village to the east. The main streams and rivers that feed the area are Göksu and Aksu streams. Bowel stream, Eğregin stream and Taşçı stream form the side branches of Göksu Stream [66].

The study area located in the inner parts of the Mediterranean region is generally under the influence of Mediterranean climate and transition zone climate. The average annual rainfall in the basin is 498 mm and the average temperature is 13.5°C [67]. According to the data obtained from the 2010 Management Plans, coniferous forest areas occupy the largest share in the study area. This is followed by mixed forest areas and agricultural areas.

When the study area is evaluated in general, more than half of the general area (61.13%) consists of forested areas and 38.87% consists of deforested areas. Within the total forest area, the productive forest area is 77.05% and the degraded forest area is 22.95%. Most of the forested areas have fertile forest status. In this case, forests generally consist of “c”, “cd” and “d” stands [66].

In order to perform the study, country maps, stand maps and ArcGIS program were used. 1/25000 scale country maps used in the study area were given in Table 1. After obtaining the country maps, it was used to draw the boundaries of the Çandır dam basin to limit the study area. Çandır Dam Lake is located in the country map n25b1 (Figure 2). The boundaries of the study area were determined with the help of the numerical terrain model obtained by digitizing the equilibrium curves in the country maps on computer.

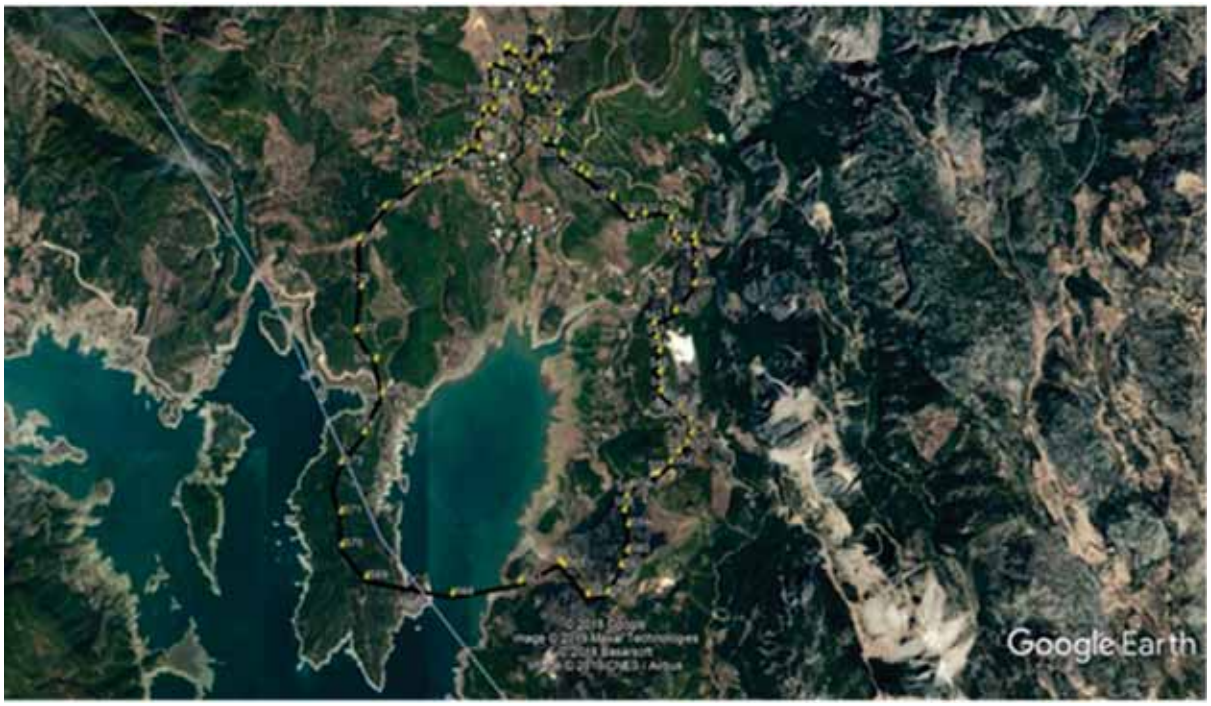

FIGURE 1
Location of the work area

FIGURE 2
Location of Çandır Dam Lake

TABLE 1
1/25000 Scale Country Map Covering the Study Area

Sheet No	Sheet Name	Print Year
1	N25b1	1960
2	N25b2	1980

One of the most important bases used in the land use assessment studies of the Çandır dam basin in 3 periods is the Forest Management Maps of Forestry Management [66]. GIS, which is also used in forestry activities due to time, money, transaction speed and wide solution area, has been utilized at different stages in the study. Some of these are digitization of equilibrium curves and stand maps and the creation of databases related to land use for different periods and conducting various analyzes and inquiries. The databases that will enable the digitization of country maps and analyzes are obtained with the ArcGIS computer program. Homeland maps were coordinated, digitized and bases were created.

Method. The thesis consists of two parts: data collection and office work. In order to reach general and theoretical information in the process of collecting data and obtaining ideas on the subject, Çandır Forest Management Chief of Sütçüler Forest Management Directorate, and Süleyman Demirel University library and electronic databases were used as base for the literature review.

In order to examine the temporal change of land use in the study area, first of all, the current management plans of the area were obtained from the Isparta Forest Regional Directorate with 1/25000 scale country maps and previous management plans remaining in the study area.

The obtained country maps were digitized with ArcGIS computer program and the boundaries of the study area were determined by obtaining a digital terrain model. With the determination of the boundaries of the study area, stand maps for each period of forest management chiefs were digitized separately by the same GIS program. The attribute databases of stand stands are arranged separately for different periods. The data created in ArcGIS environment were transferred to Microsoft Excel environment and the time changes of land use were revealed.

As there are differences in the databases obtained by digitizing the stand maps of Çandır Forest Management Directorate within the study area, these

should be collected under a single roof. Land uses in the study area were grouped under 5 groups. These groups; coniferous forests, degraded forests, water, agricultural fields and other areas. Other areas are depot, quarry, settlement, burnt and unloaded areas land use types.

RESULTS AND DISCUSSION

Based on the forest management plans, the spatial findings of the land use patterns in the study area were evaluated over the past three management plan periods.

Land use in 1986 and in 1996. The stand map prepared for the Forestry Directorate in 1986 within the study area, the land use map obtained after digitizing in ArcGIS environment and the findings obtained through the examinations and analyzes made in the databases are given below (Figure 3).

When the study area of 1908 ha is evaluated in terms of land use in 1986, the largest share in the area is composed of degraded forests (1023.88 ha) and coniferous forests (631.86 ha), agricultural areas (144.89 ha), water (71.40 ha) and other areas (35.97 ha) respectively (Figures 4 and 5).

FIGURE 3
Satellite image from 1986

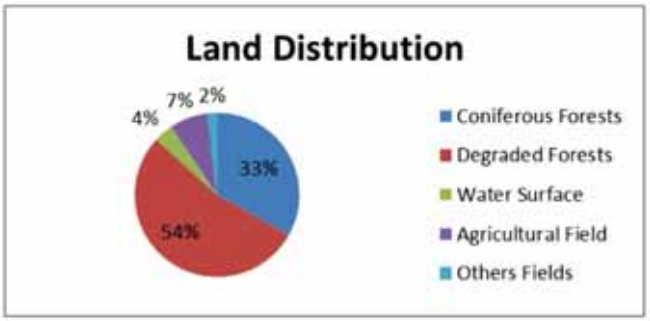

FIGURE 4
Land distribution in 1986

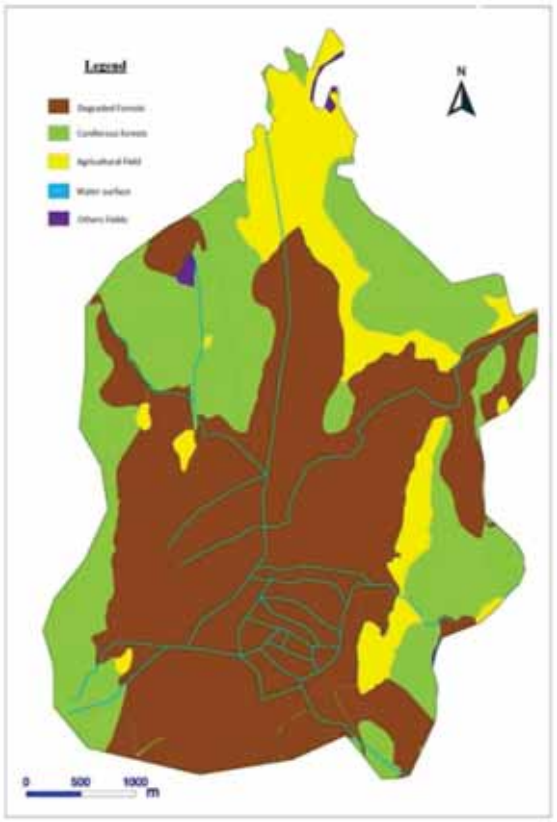

FIGURE 5
Land use in 1986

FIGURE 6
Satellite image of 1996

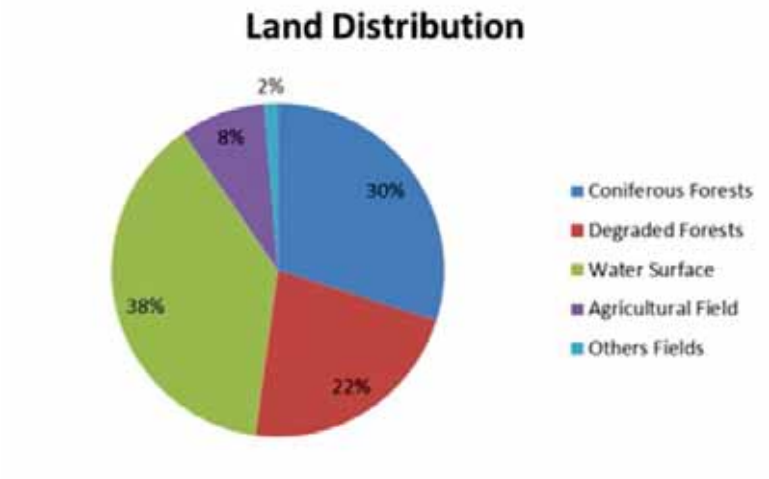

FIGURE 7
Land distribution in 1996

When the land use statuses of the databases obtained from stands in 1998 were examined, it is seen that the water area (729.53 ha) has the largest share. The water area is followed by coniferous forests (570.32 ha), degraded forests (424.98 ha), agricultural areas (158.07 ha) and other areas (25.10 ha) respectively (Figure 6, 7 and 8).

Land use in 2006 and in 2016. When the land use statuses of the databases obtained from stands in 2006 are examined, it is seen that the water area (900.52 ha) has the largest share. The water area is followed by coniferous forests (591.71 ha), degraded forests (190.65 ha), agricultural areas (189.92 ha) and other areas (35.20 ha) respectively (Figure 9, 10 and 11).

In 2016, the water area (900.52 ha) had the largest share in the study area, with coniferous forests (589.58 ha), degraded forests (190.65 ha), agricultural areas (192.05 ha) and other areas (35.50 ha) are observed (Figure 12).

In 2016 land use GIS environment stands were digitized and used as base. Blue area water in the study area, light brown coniferous forests, dark brown degraded forests, agricultural areas are shown in white and in other areas yellow (Figure 13).

As can be seen in the satellite image of 2016 (Figure 14), a large part of the study area is water area due to the start of the dam construction. The dam began to fill with water.

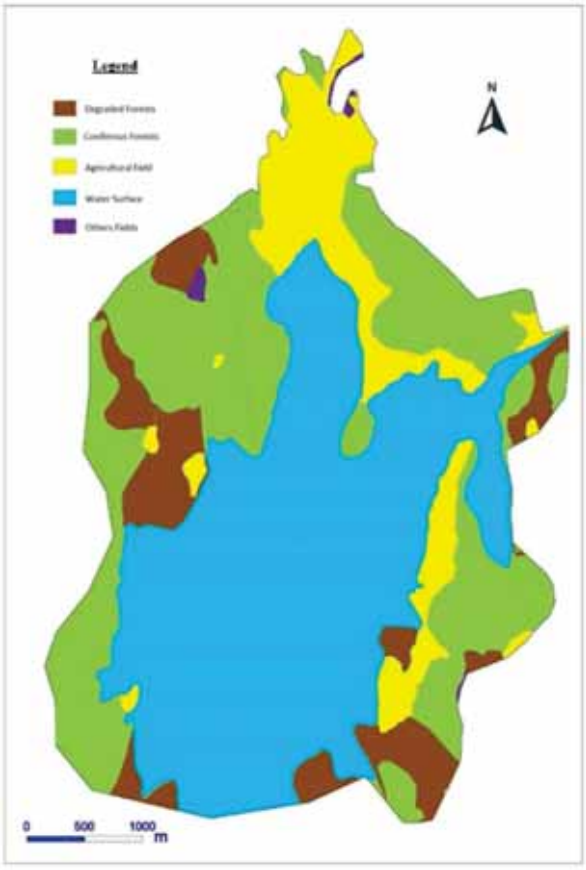

FIGURE 8
Land use in 1996

FIGURE 9
Satellite image of 2006

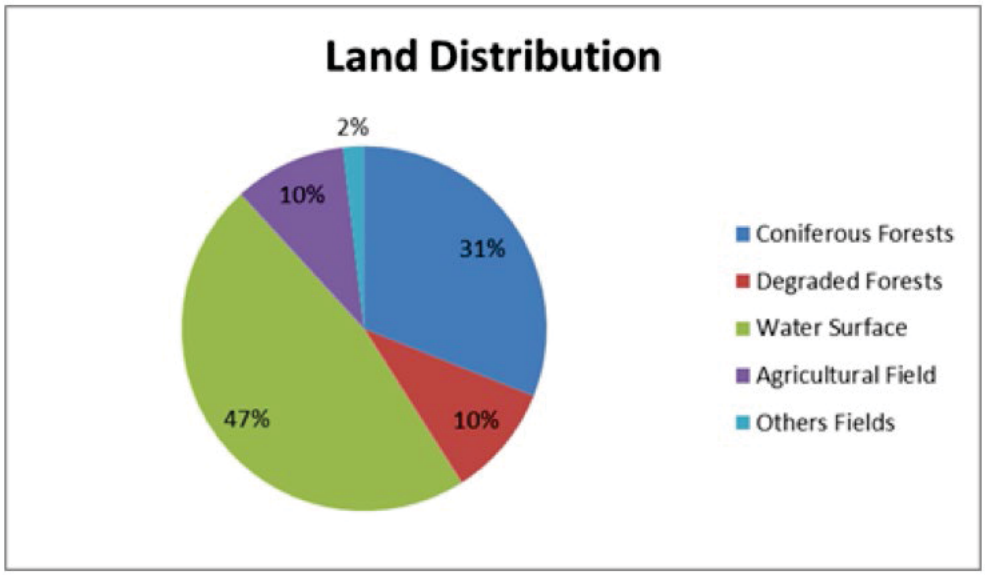

FIGURE 10
Land distribution in 2006

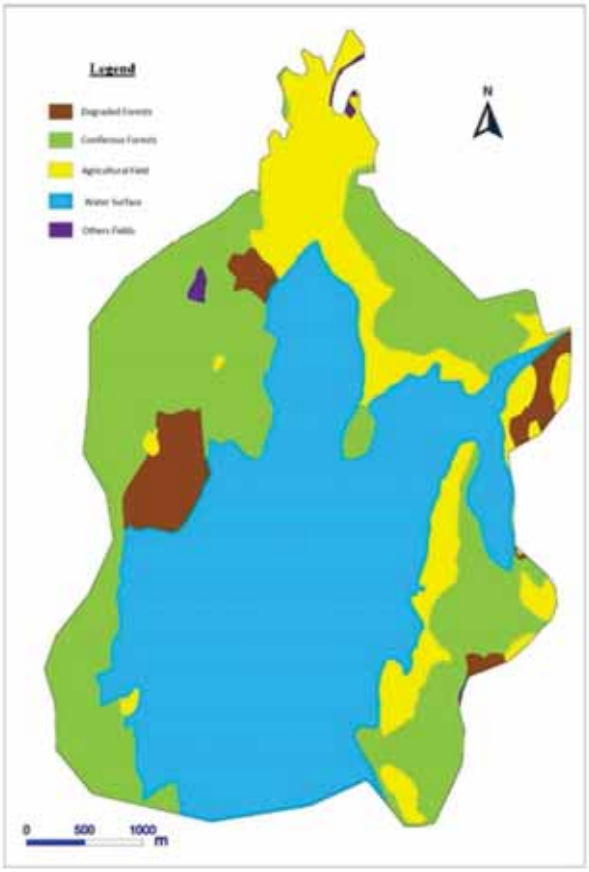

FIGURE 11
Land use in 2006

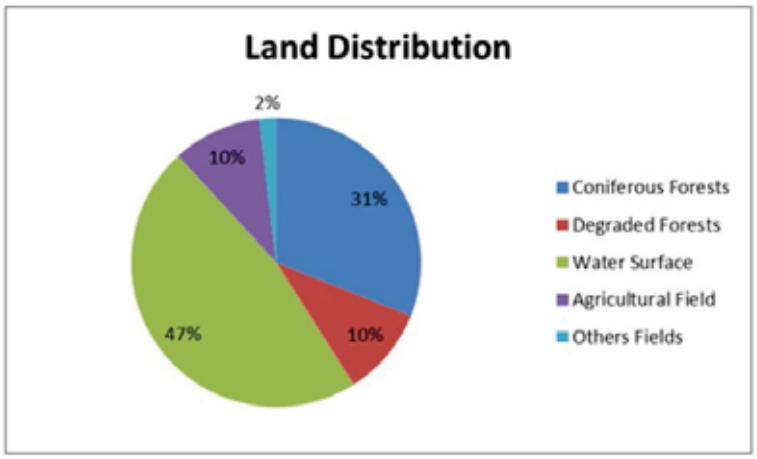

FIGURE 12
Land distribution in 2016

Using in land changes. The findings obtained by evaluating the land use changes in the study area are given below. The average slope of the basin was determined as 18% in the direction of the obtained layer (Figure 15). The blue-colored 1119.28 hectares of the study area are included in the slope groups of 0-15%, 327.09 hectares of which are shown as light brown, 16-30% and 461.63 of which are indicated with dark brown.

1238 hectares of the Çandır village, which is the study area, is located within 200m, 437 hectares within 400m, and 233 hectares within 600m (Figure 16).

In terms of periods, 1655.74 ha forest areas (coniferous and degraded forests) decreased by 660.44 ha between 1986 and 1996, and decreased by 212.94 ha to 782.36 ha in the period between 1996 and 2006. Nevertheless, there has not been a major change in forest areas between 2006 and 2016. (Table 2 and Figure 17).

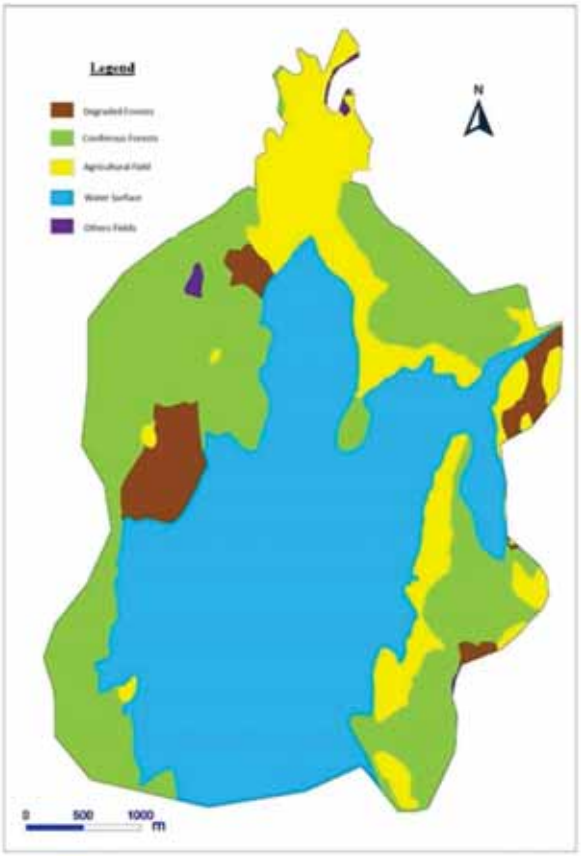

FIGURE 13
Land use in 2016

FIGURE 14
Land changes in the study area

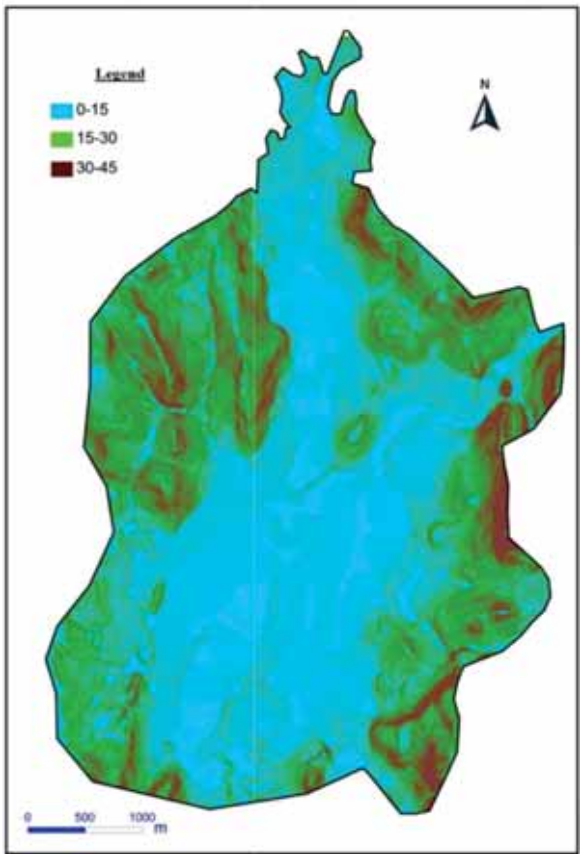

FIGURE 15
Representation of Slope Groups in GIS Environment

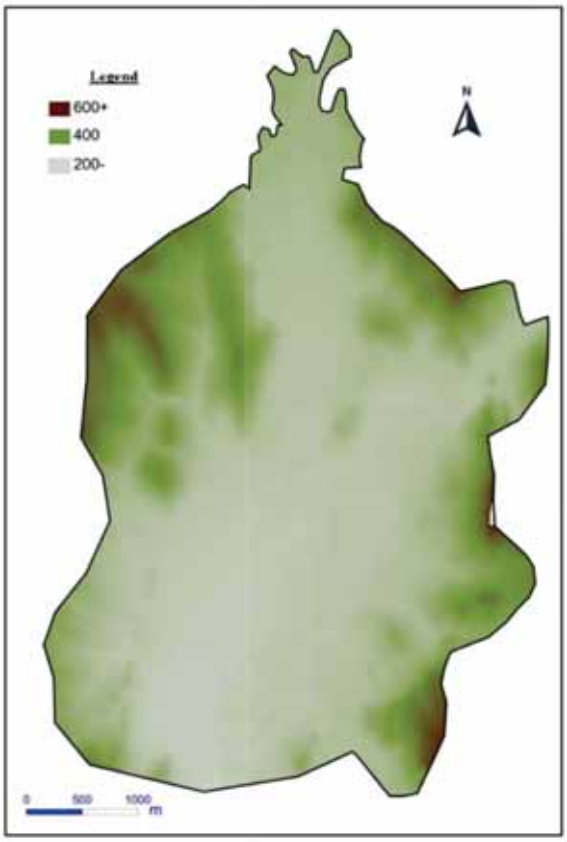

FIGURE 16
Distribution of study area in height groups

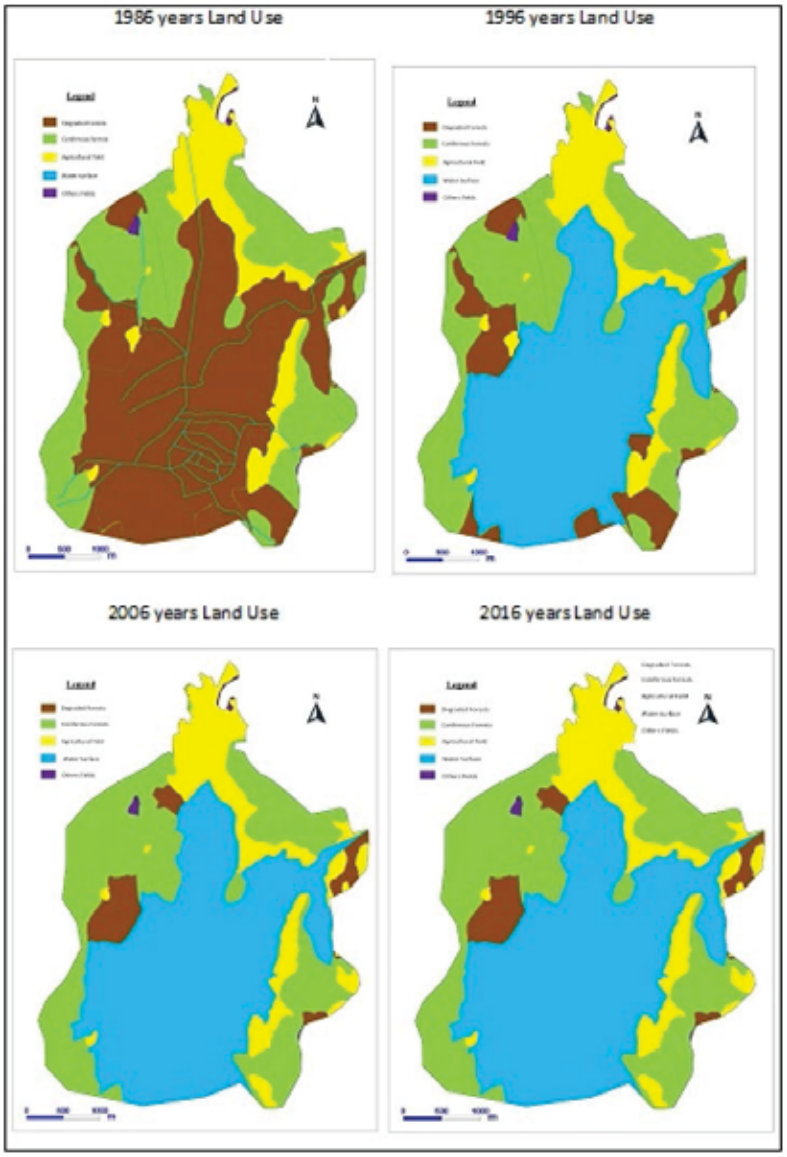

FIGURE 17
Land use changes between 1986-2016 (HA)

FIGURE 18
Karacaören Dam

TABLE 2
Land use changes between 1986-2016 (ha)

Year	Forest	Water	Agriculture	Other areas	Total
1986	1655,74	71,4	144,89	35,97	1908
1996	995,3	729,53	158,07	25,1	1908
2006	782,36	900,52	189,92	35,2	1908
2016	780,23	900,52	192,05	35,2	1908

The coniferous forests which were 631.76 ha as of 1986 decreased to 570.25 ha in 1996. It was found a decrease in coniferous and degraded forests similar to the results obtained in the land use change studies conducted in the 1987-2010 period in Düzce-Cumayeri region [68] and the results obtained in our study. In the study conducted by [69], 62817 ha forest areas (leaved, coniferous, mixed and degraded forests) increased by 1144 ha between 1986 and 1998, but decreased to 1326 ha between 1998 and 2010 and decreased to 62637 ha. It was observed. Our study is similar in terms of decrease in forest area.

In our study area, agricultural area has increased by 12.05 ha between 1986 and 1996. Between 1996 and 2016, it increased by 27.95 ha. The reason for this increase is the conversion of agricultural land into cadastral works where forest feature is destroyed. There is a similarity between our study and [68-72] in terms of increase in agricultural land.

The water area increased 659.33 ha between 1986 and 1996. The reason for this increase was the construction of the dam in 1986 and the completion of it in 1989. The Karacaören dam was constructed on the Aksu Stream on the Antalya-Isparta highway for irrigation, flood control and generation of electrical energy (Figure 18). Karacaören Dam has facilities for carp and trout production. In addition, the dam is used as urban water consumption and irrigation water. The body volume of the dam is 4.000.000 m^3. While the dam provides irrigation services on an area of 9,537 hectares, the hydroelectric power plant with a capacity of 32 MW produces 142 GWh of electricity per year [73].

There is no significant difference between the population of the village in the study area between 1986 and 1996 and 2006. In our study, although the population change experienced during the 20-year period was not very different, it was found that there was no increase in the forest areas but the forest areas decreased in this period. Many studies [74-77] stated that population growth had a negative effect on forest areas and natural resources and that these areas decreased. It was found that despite the decrease in the population between 2000 and 2010 in the villages located in the Hasanlar Dam, there was no increase in forest areas but the forest areas decreased during this period [69].

CONCLUSIONS

The increase in human needs day by day causes changes in the place where they live. Many requirements, especially shelter and food, cause people to harm the environment in an uncontrolled way. Therefore, land cover and use varies considerably over time. The importance of remote sensing technique in detecting and monitoring these changes becomes clear. Using GIS for analyzing remote sensing data facilitates environmental management planning.

Monitoring of temporal changes in land use is of great importance for future planning and conservation of natural resources. Therefore, it is extremely important to uncover the change in land use for effective and accurate management and planning of natural resources. In this context, it is necessary to analyze the accuracy of the data by using GIS and Remote Sensing methods together in the determination of land use and change by making field observations and investigations.

In this study, the temporal changes of land use patterns of Çandır village and the factors affecting these changes were tried to be determined and the reasons of the existing changes were determined.

In terms of periods, it was found that forest areas (coniferous and degraded forests) of 1652.21 ha decreased by 660.51 ha between 1986 and 1996 and decreased to 782.36 ha with a decrease of 209.34 ha between 1996 and 2016. The coniferous forests which were 631.76 ha as of 1986 decreased to 570.25 ha in 1996. The water area increased 659.33 ha between 1986 and 1996. The reason for this increase was the construction of the dam in 1989. The agricultural area increased by 12.05 ha between 1986 and 1996 and by 27.95 ha between 1996 and 2016. The reason for this increase is the conversion of agricultural land into cadastral works in areas where forest quality is destroyed. There is no significant difference between the population of the village in the study area between 1986 and 1996 and 2006. In our study, although the population change experienced during the 20-year period was not very different, it was found that there was no increase in the forest areas but the forest areas decreased in this period. This decrease was caused by the increase in demand for forest areas. It is also effective in dam construction. This indicates that factors other than the population may have an impact on the change. Therefore, it is seen that the increase in the pressure

in the forest areas is not always directly proportional to the increase in the population. It could be also concluded that:

- ✓ It should be ensured that the needs are not met by expanding the agricultural areas but by obtaining the highest yields from the existing agricultural areas,
- ✓ Monitoring the changes in land use and demographic structure in the research area over time is important for the protection and development of many natural elements, especially water yield and quality,
- ✓ The study area is located to be used in accordance with the land capability class, land-use planning with interdisciplinary units will be installed should be given direction to the work.

ACKNOWLEDGEMENTS

This study was a part of a M.Sc. thesis prepared under the supervision of Dr. Nilufer Yazici.

REFERENCES

[1] Bademci, S. (2006) Environmental Problems of Antalya City. Fırat University, Elazığ.
[2] Avtar, R., Tripathi, S., Aggarwal, K.A., Kumar, P. (2019) Population – Urbanization – Energy Nexus: A Review. MDPI Resources. 8(136), 1-21.
[3] Oğuz, H., Zengin, M. (2009) Determination of Land Cover / Land Use Changes in Erzurum City (1987-2007) by Remote Sensing and Geographical Information Systems. Dokuz Eylül University Geographic Information Symposium, 10-12 December, İzmir.
[4] Guven, A. (2016) Urban, urbanization and urban management needs. Journal of International Management, Educational and Economics Perspectives. 4(1), 21-30.
[5] Eroglu, M. (2018) Environmental Protection. Karadeniz Technical University Forestry Faculty Course Note, 80p.
[6] Bayar, R. (2003) Land use-population relations: Anamur sample. Journal of Geographical Sciences. 1(1), 97-116.
[7] Hudson, R., Rhind, D. (1980) Land Use. Methuen Pub. London.
[8] Karadağ, A. (2007) Relation between Urbanization Development and Natural Environment Process (Case of Ödemiş-İZMİR). Aegean Geographical Journal. 16, 3-16.
[9] Çamurcu, H. (2005) World Population Growth and Challenges Brought. Balikesir University, Journal of the Institute of Social Sciences. 88-105.
[10] Topal, K. (2011) As A Source of Environmental Problems Population Growth or Consumption? A Critical Approach to the Neo-Malthusian View. Turkish Journal of Administration. 470, 133-152.
[11] Yaylı, H. (2012) Development, environment and population in the context of environmental ethics. Journal of Süleyman Demirel University Institute of Social Sciences. 1(15), 151-169.
[12] Lopez, E., Bocco, G., Mendoza, M., Duhau, E. (2001) Predicting land-cover and land-use change in the urban fringe: a case in Morelia city, Mexico. Landscape and Urban. Planning. 55, 271-285.
[13] Aguilar, A.G., Ward, P.M., Smith, C.B. (2003) Globalization, regional development and mega-city expansion in Latin America: Analyzing Mexico City's peri-urban hinterland. Cities. 20(1), 3-21.
[14] Erna, L., Boccoa, G., Mendozaa, M., Duhaub, E. (2001) Predicting land –cover and land-use change in the urban fringe: a case in Morelia city, Mexico. Landscape and Urban Planning. 55, 271-285.
[15] Aguilar, A.G., Ward, P.M., Smith Sr., C.B. (2003) Globalization, regional development and mega-city expansion in Latin America: Analyzing Mexico City's peri-urban hinterland. Cities. 20, 3-21.
[16] Qiang, L., Jingshuang, L., Fengguo, D., Yanlong, S. (2017) Assessment of heavy metal pollution in agricultural soils from suburban vegetable fields under different planting time. Fresen. Environ. Bull. 26, 3542-3549.
[17] Say, N., Okten, S.O., Aysu, A., Yalcinkaya, N.M. (2017) Transformation of land use/land cover (LULC) under rapid urbanization in Adana, Turkey. Fresen. Environ. Bull. 26, 3479-3485.
[18] Stow, D.A., Chen, D.M. (2002) Sensitivity of multi-temporal NOAA AVHRR data of an urbanizing region to land-use/land cover changes and misregistration. Remote Sens. Environ. 80, 297-307.
[19] Xiao, J.Y., Shen, Y.J., Ge, J.F., Tateishi, R., Tang, C.Y., Liang, Y.Q., Huang, Z. (2006) Evaluating urban expansion and land use change in Shijiazhuang, China by using GIS and remote sensing. Landscape and Urban Planning. 75, 69-80.
[20] Carlson, T.N., Traci Arthur, S. (2000) The impact of land use – land cover changes due to urbanization on surface microclimate and hydrology: A satellite perspective. Global Planetary Change. 25, 49-65.

[21] Shen, Y., Xiao, J., Kondoh, A., Tateishi, R. (2003) Influence of land use and land cover change due to urbanization on hydrological environments: A case study. In: Proceedings of the CERES International Symposium on Remote Sensing: Monitoring of Environmental Change in Asia. Chiba University, Japan December 16-17, 25-28.

[22] İderman, E. (2006) Historical and Contemporary Land Use of Salamis Ancient City and its Surroundings by Using Remote Sensing and Geographical Information Systems. Çukurova University, Adana.

[23] Karabulut, M., Kucukonder, M., Gurbuz, M., Kaya Sandal, E. (2006) Investigation of Temporal Change of Kahramanmaraş City and Environment by Using Remote Sensing and GIS. 4th Geographical Information Systems Information Days. Istanbul.

[24] Selcuk, R., Nisanci, R., Uzun, B., Yalcin, A., Inan, H., Yomralioglu, T. (2003) Monitoring land-use changes by GIS and remote sensing techniques: case study of Trabzon. Proceedings of 2nd FIG Regional Conference Morocco. 2-5 December, 1-11.

[25] Rawat, J.S., Biswas, V., Kumar, M. (2013) Changes in land use/cover using geospatial techniques: A case study of Ramnagar town area, district Nainital, Uttarakhand, India. The Egyptian Journal of Remote Sensing and Space Sciences. 16, 111-117.

[26] Gül, A., Küçük, V. (2001) The research of Isparta and the open-green areas in urban. Turkish Journal of Forestry. 2, 27-48.

[27] Tezer, A., Onur, A.C., Albayrak, İ., Şen, Ö.L., Doğru, A.Ö., Uluğtekin, N.N. (2012) Significance of ecosystem services mapping for the integration of spatial planning and climate adaptation. AESOP 26th Annual Congress. 11-15 July 2012 METU, Ankara.

[28] Goksel, C., Mercan, D.E., Kabdasli, S., Bektas, F., Seker, D.Z. (2004) Definition of sensitive areas in a lakeshore by using remote sensing and GIS. Fresen. Environ. Bull. 13, 860-864.

[29] Kaya, S., Seker, D.Z., Tanik, A. (2012) Analysis of urbanized areas using V-I-S component model. Fresen. Environ. Bull. 21, 3243-3248.

[30] Chen, P., Meng, X., Huang, Y. (2014) The new application of GIS in urban planning: based on urban space and fire disaster. International Journal of Humanities and Management Sciences (IJHMS). 2(3), 75-77.

[31] Subasinghe, S., Estoque, R.C., Murayama, Y. (2016) Spatiotemporal analysis of urban growth using GIS and remote sensing: a case study of the Colombo metropolitan area, Sri Lanka. ISPRS Int. J. Geo-Inf. 5, 197.

[32] Kahraman, A., Dogru, A.O., Seker, D.Z., Ulugtekin, N.N., Terzi, F., Turkoglu, H., Goksel, C. (2019) Examination of the green spaces based on spatial sufficiency and accessibility through GIS. Fresen. Environ. Bull. 28, 529-534

[33] Çetin, A. (2011) Flora of Burdur Lake Area. Mehmet Akif Ersoy University, Burdur.

[34] Mert, A., Senturk, O., Guney, C.O., Akdemir, D., Ozkan, K. (2013) Mapping of some distal variables available for mapping habitat suitabilities of the species: A case study of Buldan District. GeoMed 2013 the 3rd International Geography Symposium. 10-13 June, Antalya, 489-497.

[35] Reis, S. (2008) Analyzing land use/land cover changes using remote sensing and GIS in Rize. North-East Turkey. Sensors. 8, 6188-6202.

[36] The Scıentıfic and Technologıcal Research Councıl of Turkey Marmara Research Center (TUBİTAK) (2010) Preparation of Basin Protection Action Plans - Burdur Basin. Gebze, Kocaeli.

[37] Wu, Q., Li, H.-q., Wang, R.-s., Paulussen, J., He, Y., Wang, M., Wang, B.-h., Wang, Z. (2006) Monitoring and predicting land use change in Beijing using remote sensing and GIS. Landscape and Urban Planning. 78, 322-333.

[38] Ertürk, A., Ekdal, A., Gurel, M., Yuceil, K., Tanik, A. (2004) Use of mathematical models to estimate the effect of nutrient loadings on small streams. Fresen. Environ. Bull. 13, 1350-1359.

[39] Ataol, B. (2010) Level changes in Lake Burdur. Journal of Geographical Sciences. 8(1), 77

[40] Liu, H., Wang, L., Yang, J., Nakagoshi, N., Liang C., Wang, W., Lv, Y. (2009) Predictive modeling of the potential naturel vegetation pattern in Northeast China. Ecological Research. 24, 1313-1321.

[41] Ozkan, K., Senturk, O. (2012) The Applicatıon of group discrimination techniques to predict the potential distribution of turpentine tree. In: Proceedings of International Scientific Conference People. Buildings and Environment. 7-9 October, Lednice, Czech Republic, 728-736.

[42] Şener, E., Davraz, A., İsmailov, T. (2005) Monitoring of Burdur lake level changes with multitime satellite images. Kuvarnert the Symposium Turkey ITU Eurasia Institute of Earth Sciences. 148-156.

[43] Sarp, G., Özçelik, M. (2016) Water body extraction and change detection using time series: A case study of Lake Burdur, Turkey. Journal of Taibah University of Science. 11, 381-391.

[44] Thakkar, A.K., Desai, V.R., Patel, A., Potdar, M.B. (2017) Post-classification corrections in improving the classification of Land Use/Land Cover of arid region using RS and GIS: The case of Arjuni watershed, Gujarat, India. The Egyptian Journal of Remote Sensing and Space Sciences. 20(1), 79-89.

[45] Shanwad, U.K., Patil, V.C., Honne Gowda, H., Dasog, G.S. (2008) Application of Remote Sensing technology for impact assessment of watershed management programme. J. Indian Soc. Remote. 36, 375-386.

[46] Brown, D.G., Robert Walker R., Steven Manson S., Seto K.C. (2004) Modeling land-use and land-cover change. Land Change Science. 6, 395-409.

[47] Sangavongse, S. (1995). Land use/land cover change detection in the Chiang Mai area using Landsat TM. Department of Geography and Environmental Science. Monash University, Clayton, Victoria, 3168.

[48] Pellikka, P., Clark, B., Hurskainen, P., Keskinen, A., Lanne, M.K., Masalin, P., Nyman-Ghezelbash Sirviö, T. (2004) Land use change monitoring applying geographic information systems in the Taita-Hills, SE-Kenya. In: The Proceedings of the 5th African Association of Remote Sensing of Environment Conference. Nairobi, Kenya.

[49] Kaya, S., Curran, P.J. (2005) Monitoring urban growth on the European Side of the Istanbul metropolitan area: A case study. International Journal of Applied Earth Observation and Geoinformation. 8, 18-25.

[50] Başkent, E.Z., Kadıoğulları, A.İ. (2007) Spatial and temporal dynamics of land use pattern in Turkey: A case study in İnegöl. Landscape and Urban Planning. 81, 316-327.

[51] Karakuş, C.B., Kavak, K.S., Cerit, O. (2014) Determination of Variations in Land Cover and Land Use by Remote Sensing and Geographic Information Systems Around the City of Sivas (Turkey). Fresen. Environ. Bull. 23, 667-677.

[52] Papastergiadou, E.S., Retalis, A., Apostolakis, A., Georgiadis, T.H. (2008) Environmental Monitoring of Spatio-temporal Changes Using Remote Sensing and GIS in a Mediterranean Wetland of Northern Greece. Water Resources Management. 22(5), 579-594.

[53] Grey, W.M.F., Luckman, A.J., Holland, D. (2003) Mapping urban change in the UK using satellite radar interferometry. Remote Sens. Environ. 87, 16-22.

[54] Herold, M., Goldstein, N.C., Clarke, K.C. (2003) The spatiotemporal form of urban growth: measurement, analysis and modeling. Remote Sens. Environ. 86, 286-302.

[55] Wilson, E.H., Hurd, J.D., Civco, D.L., Priloe, M.P., Arnold, C. (2003) Development of a geospatial model to quantify, describe and map urban growth. Remote Sens. Environ. 86, 275-285.

[56] Kang, H., Li, H., Zhao, S., Wang, J., Yang, K., Wang, Y., Han, Lu, Y. (2019) Land use pattern change and forecast analysis of energy and chemical industry in the Loess plateau. Fresen. Environ. Bull. 28, 2835-2841.

[57] Vrublova, K., Pohanka, G. (2019) Is environmental conservation of European beech-dominated forests efficient? Fresen. Environ. Bull. 28, 1218-1223.

[58] Temiz, F., Bozdag, A., Durduran, S.S, Gumus, M.G. (2017) monitoring coastline change using remote sensing and GIS technology: a case study of Burdur lake, Turkey. Fresen. Environ. Bull. 26, 7235-7242.

[59] Birch, C.P., Oom, S.P., Beeccham, J.A. (2007) Rectangular and hexagonal grids used for observation, experiment and simulation in ecology. Ecological Modeling. 206(3), 293-312.

[60] Frank, L.D., Schmid, T.L., Sallis, J.F. (2005) Linking objectively measured physical activity with objectively measured urban form: Findings from SMARTRAQ. American Journal of Preventive Medicine. 28, 117-125.

[61] Geurs, K., Van Wee, B. (2006) Ex-post Evaluation of Thirty Years of Compact Urban Development in the Netherlands. Urban Studies, University of Glasgow. 43(1), 139-160.

[62] Lenormand, M., Picornell, M., Cantu-Ros, O.G., Louail, T., Herranz R., Barthelemy, M., Frias-Martinez, E., San Miguel, M., Ramasco, J.J. (2015) Comparing and modeling land use organization in cities. Royal Society Open Science. 2(12) 150-449.

[63] Waddell P., Ulfarsson, G., Franklin, J. Lobb, J. (2006) Incorporating Land Use in Metropolitan Transportation Planning. Transportation Research A. 41, 382-410.

[64] Sahr, K., White, D., Kimmerling, A.J. (2003) Geodesic discrete global grid systems. Cartography and Geographic Information Science. 30, 121-134

[65] Shoman, W., Alganci, U., Demirel, H. (2019) Analyzing gridding systems for land cover/land use information: a study conducted for green areas. Fresen. Environ. Bull. 28, 694-699.

[66] Anonymous (2016) General Directorate of Forestry Information Systems Department (Date of access:08.04.2016)

[67] Anonymous (2019) Data from Turkish State Meteorological Service (Date of access: 19.01.2019).

[68] Sivrikaya, F., Çakır, G., Akay, A.E. (2011) Factors of landuse / coverchange: A case study from Turkey. Academic Journals Scientific Research and Essays. 6(17), 3684-3696.

[69] Özdemir, Y.K. (2015) Determination of Temporal Changes in Land Use in Hasanlar Dam Basin. Graduate School of Natural and Applied Sciences of Çukurova University, Düzce.
[70] Gülersoy, A.E. (2008) Relationships between Natural Environment Conditions and Land Use in Bakırçay Basin. Dokuz Eylül University Institute of Educational Sciences, İzmir.
[71] Doygun, H., Oğuz, H., Kesgin Atak, B., Nurlu, E. (2012) Investigation of the Effects of Land Use Changes on the Coastal Areas of Natural Character with Remote Sensing and GIS: Çiğli / İzmir Case. Journal of Kahramanmaraş Sütçü İmam University Faculty of Engineering. Special ıssue, 1-7.
[72] Özşahin, E., Pektezel, H., Eroğlu, İ. (2016) Temporal and Spatial Changes of Land Use in Tekirdağ City and Its Surroundings. ZFWT. 8(1), 307-326.
[73] Anonymous (2019) Data from the General Directorate of State Hydraulic Works (DSI in Turkish acronym) (Date of access: 25.06.2019).
[74] Gümüş, C. (1996) Causes of Forest Crimes in Amasya Forest Regional Directorate. Kafkas University Journal of Artvin Forestry Faculty. 1-2, 41-51.
[75] Koç, S.N. (2010) Evaluation of Restoration Works After Forest Fires in Terms of Landscape Architecture: The Case of Antalya Serik-Taşağıl Region. Kahramanmaraş Sütçü İmam University Journal of Engineering Sciences,146p.
[76] Ateşoğlu, A., Tunay, M. (2010) Spatial and Temporal Analysis of Forest Cover Changes in the Bartin Region of North Western Turkey. African Journal of Biotechnology. 9(35), 5676-5685.
[77] Özsan, M. (2011) Rural Development Surveys in Forest Villages of Beypazarı. III. Socio-Economic Problems in Forestry Congress.

Received: **22.08.2019**
Accepted: **30.12.2019**

CORRESPONDING AUTHOR

Nilufer Yazici
Faculty of Forestry of
Isparta Applied Sciences University,
TR-32260 Isparta – Turkey

e-mail: niluferyazici@isparta.edu.tr

© by PSP Volume 29 – No. 05/2020 pages 3594-3598 Fresenius Environmental Bulletin

METABOLISM TRANSFORMATION OF PHOSPHATE ACCUMULATING ORGANISMS DURING FERROUS SALT COOPERATIVE BIOLOGICAL PHOSPHORUS REMOVAL PROCESS

Hua Zhang[1,2], Yali Liu[1,2], Jian Huang[1,2,*], Jun Liu[3], Xinrui Yuan[1,2], Guijun Quan[1,2], Weiwei Sun[1,2]

[1]Key Laboratory of Anhui Province of Environmental Pollution Control and Waste Resource Utilization, Hefei, 230601, P.R. China
[2]School of Environmental and Energy Engineering, Anhui Jianzhu University, Hefei, 230601, P.R. China
[3]Anhui Zhonghuan Environmental Protection Technology Co., Ltd, Hefei, 230601, P.R. China

ABSTRACT

The present study investigated the effects of ferrous salt with different concentrations on metabolism transformation of phosphate accumulating organisms. The high-throughput sequencing technology was employed to analyze the changes of microbial community structure. Redundancy analysis was used to analyze the factors leading to changes in microbial community structure. Analysis of alpha diversity shows that low concentration ferrous salt can promote the growth of phosphate accumulating organisms, while high concentration ferrous salt can inhibit the growth of phosphate accumulating organisms. Distribution charts of microbial species show that metabolism of phosphate accumulating organisms will gradually be replaced by the metabolism of glycogen accumulating organisms when ferrous salt is excessive. Redundancy analysis showed that ferrous salt was the most important factor, and that there was a negative correlation between ferrous salt and phosphate accumulating organisms, and a positive correlation between ferrous salt and glycogen accumulating organism. The experiment is significant for further research of ferrous salt cooperative biological phosphorus removal process.

KEYWORDS:
Ferrous salt, biological phosphorus removal, microbial community structure, metabolism transformation

INTRODUCTION

Insufficient carbon is the main reason for the low efficiency of biological phosphorus removal [1, 2]. Phosphate accumulating organisms are the key microorganisms in the process of biological phosphorus removal of municipal wastewater [3, 4]. Under anaerobic conditions, phosphate accumulating organisms absorb volatile fatty acids and synthesize PHA by reducing power (NADH) produced by glycogen hydrolysis. Under aerobic conditions, phosphate accumulating organisms decompose PHA to produce energy for excessive phosphorus uptake and glycogen synthesis, and finally, phosphorus removal can be achieved by discharging excess sludge. Glycogen accumulating organisms are also the main microorganisms in biological phosphorus removal, usually coexisting with phosphorus accumulating organisms, which are similar to phosphorus accumulating organisms in metabolic processes, but have no function of phosphorus removal [5, 6]. Glycogen accumulating organisms absorb volatile fatty acids in water under anaerobic conditions and synthesize PHA by degrading glycogen in cells. Under aerobic conditions, glycogen can be recovered by oxidizing intracellular PHA [7, 8]. Ferrous salt cooperative biological phosphorus removal process is an effective way to improve the low efficiency of biological phosphorus removal, a problem caused by low carbon [9, 10]. Ferrous salt provides trace elements for microbial growth. Therefore, the removal efficiency of phosphorus has been effectively improved in wastewater treatment plants [11-14]. However, with the increasing concentration of ferrous salt, there seems to be a gradual decline in the efficiency of phosphorus removal, which indicates that the metabolic pathway and microbial community structure might be changed in biological phosphorus removal system [15]. However, there are few related studies on the change of the metabolic pathway and microbial community structure. Therefore, this study focuses on the effects of ferrous salt (0, 5, 7, 12 mg/L and 17 mg/L) on biological phosphorus removal. Sequencing technique was used to analyze the changes of microbial community structure and metabolic pathways. Redundancy analysis (RDA) was used to identify the main factors affecting the microbial community structure and metabolic changes in biological phosphorus removal. Moreover, it is also hoped that the present study can reveal the metabolic evolution of main functional microorganisms when ferrous salt is applied to biological phosphorus removal. The research may have experimental and theoretical significance for better application and

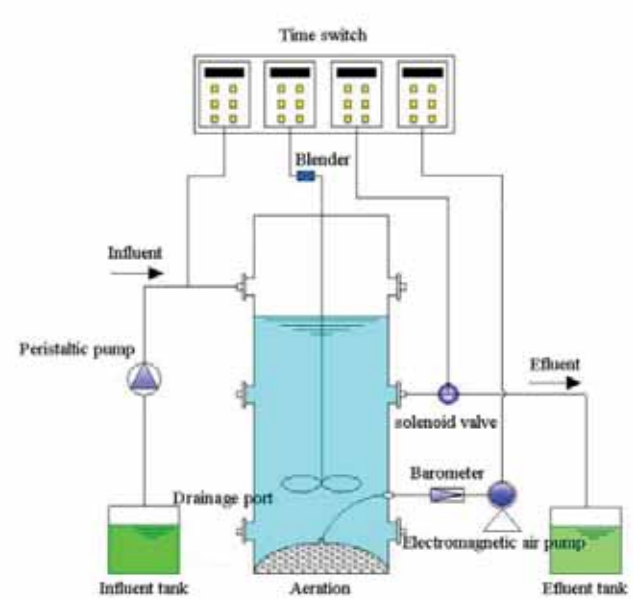

FIGURE 1
Biological phosphorus removal reactor design

TABLE 1
Experimental Water

Principal components	Unit (g/L)	Trace element	Unit (mg/L)
CH_3COONa	0.614	H_3BO_3	0.150
NH_4Cl	0.073	$CuSO_4$	0.030
KH_2PO_4	0.040	KI	0.180
$CaCl_2H_4O_2$	0.095	$MnCl_2$	0.120
$MgSO_4$	0.095	Na_2MoO_4	0.060
Peptone	0.005	$ZnSO_4$	0.120
Yeast	0.005	$CoCl_2{\cdot}6(H_2O)$	0.150
Allyl thiourea	0.004	EDTA	10.000

further research of ferrous salt synergistic biological phosphorus removal.

MATERIALS AND METHODS

Experimental device. Five sequencing batch reactor (SBR) were used in this experiment (Fig. 1). The reactor was a cylinder made of perspex with a height of 60 cm and a diameter of 20 cm. The reactor runs four cycles a day, with each cycle lasting for 360 minutes: 30 minutes for influent, 90 minutes for anaerobic, 180 minutes for aerobic, 30 minutes for precipitation, 5 minutes for drainage and 25 minutes for stabilization. The influent and effluent in each cycle are 1.0 L, the drainage ratio is 1 to 3, and the sludge concentration is 3800 mg/L.

Experimental Water. The specifications of experimental water are shown in Table 1. Ferrous sulfate solution was added to five reactors through peristaltic pump. The concentrations of ferrous salt in the five reactors were 0, 5, 7, 12 mg/L and 17 mg/L, respectively.

Experimental Method. When the reactors run steadily, 30 mL of activated sludge samples were taken from each reactor. The DNA was extracted from each sample, amplified by polymerase chain reaction, and then processed to obtain sequencing library. The original sequencing sequence is obtained from the sequencing library treated by the Illumina HiSeq 2500 platform. The optimized sequence is obtained through two-terminal split joint (sequences with more than 97% similarity is an OUT). Then we proceeded to analyze Alpha diversity, microbial community structure, and RDA.

RESULTS

Process Result and Analysis. The effect of ferrous salt on biological phosphorus removal is shown in Fig. 2. As can be seen from Fig. 2, the phosphate in effluent is 3.60 mg/L when ferrous salt

is 0 mg/L. The phosphorus in effluent was respectively 1.90, 0.28, 0.18 and 0.38 mg/L when the ferrous salt was 5, 7, 12 and 17 mg/L. The results showed that the optimal dosage of ferrous salt was 7 mg/L. Beyond that, the release capacity and intake capacity of the phosphate accumulating organisms decreased gradually with the increase of ferrous salt concentration.

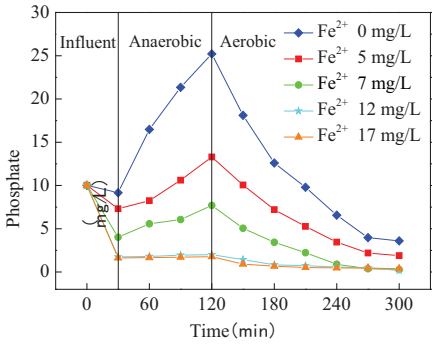

FIGURE 2
Effect of ferrous salt on orthophosphate in the typical cycle of biological phosphorus removal

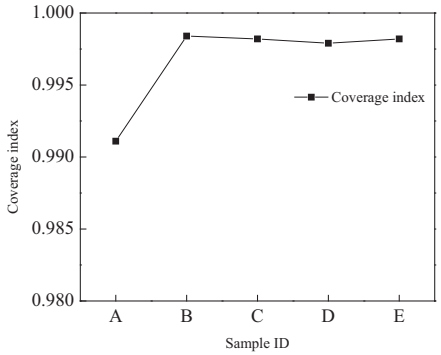

(a) Coverage index

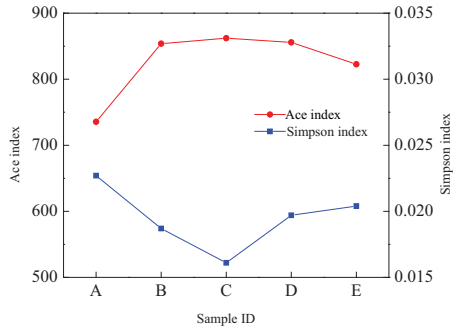

(b) Simpson index

FIGURE 3
Alpha diversity index of microorganisms in biological phosphorus removal reactor with different concentrations of ferrous salt
(A, B, C, D and E represent microbial samples with ferrous salt concentrations of 0 mg/L, 5 mg/L, 7 mg/L, 12 mg/L and 17 mg/L respectively.)

Analysis of alpha diversity index. Alpha diversity index was used to investigate the diversity of microbial species in biological phosphorus removal system at different ferrous salt concentrations. Alpha diversity index is shown in Fig. 3. Fig. 3 (a) shows that the coverage index of microbial sample is over 0.99, which shows that the results of sequence are reliable [16-17]. Fig. 3 (b) shows that Ace index first increases but then decreases, while Simpson index first decreases and then increases. These results indicate that, with the increase of ferrous salt concentration in biological phosphorus removal system, the number of microbial species first increases and then decreases. Ace index was the largest and Simpson index was the smallest when ferrous salt was 7 mg/L, which indicates that the number of microbial species was the largest at this concentration. Beyond 7 mg/L, further increase of ferrous salt concentration will lead to the gradual decrease in the number of microbial species.

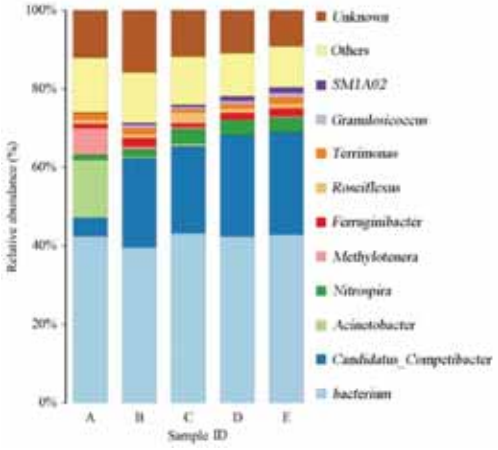

FIGURE 4
Species distribution in biological phosphorus removal reactor under different ferrous iron concentration

Analysis of metabolism and abundance of phosphate accumulating organisms and glycogen accumulating organisms. The distribution of microbial species is shown in Fig. 4. In Fig. 4, the major microorganisms are *terrimonas*, *ferruginibacter*, *acinetobacter*, *candidatus_competibacter*, *methylotenera*, *nitrospira* in the biological phosphorus removal system. *Acinetobacter* is the most important bacteria in biological phosphorus removal [18], and *candidatus competibacter* is similar to phosphorus accumulating organisms in metabolic function. Fig. 4 shows that the relative abundance of glycogen accumulating organisms increases with the increase of ferrous salt concentration, but the relative abundance of phosphate accumulating organisms decreases. The result indicates that in biological phosphorus removal system, with the increase of ferrous salt concentration, the metabolism of phosphorus accumulating organism was gradually replaced by that of

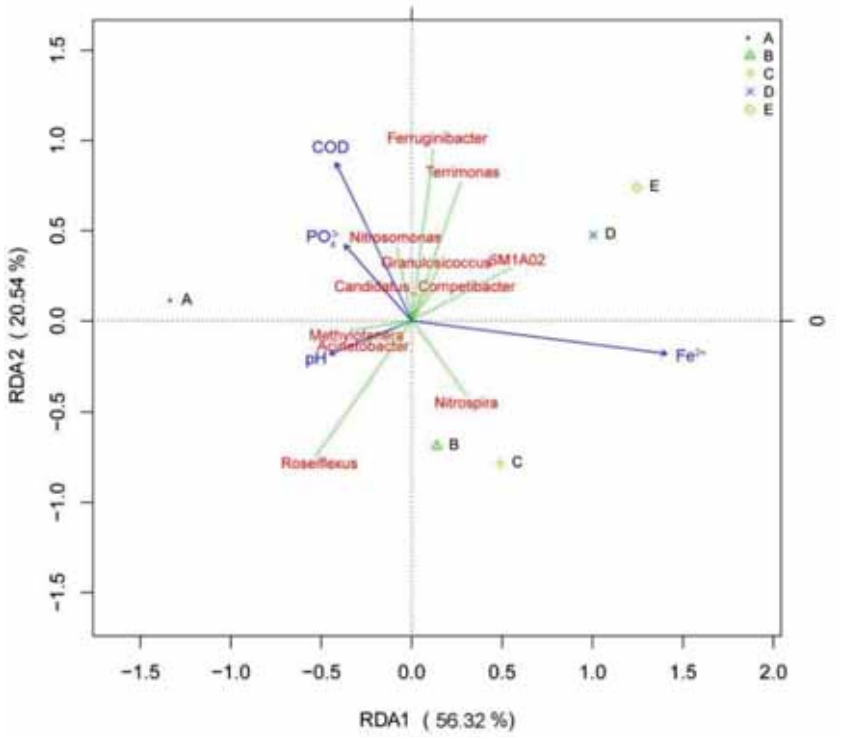

FIGURE 5
RDA Analysis of microorganism and influencing factors under different ferrous salt concentration

glycogen accumulating organism. Moreover, with the increase of the abundance of glycogen accumulating organisms, glycogen accumulating organisms gradually become the dominant bacteria and compete with phosphorus accumulating organisms for carbon, eventually inhibiting the growth and metabolism of phosphorus accumulating organisms.

Effect of ferrous salt on microorganisms. In biological phosphorus removal, the main factors influencing the microbial community structure were analyzed with redundancy analysis (RDA). The results are shown in Fig. 5: ferrous salt is the most important factor. Moreover, there was an inverse correlation between ferrous salt and *acinetobacter*. The abundance of *acinetobacter* decreased with the increase of ferrous salt concentration. However, there is a positive correlation between ferrous salt and *Candidatus_Competibacter*. The abundance of *Candidatus_Competibacter* increased with the increase of ferrous salt concentration. The results showed that the increase of ferrous salt concentration was beneficial to the growth of *Candidatus_Competibacter*.

CONCLUSIONS

Ferrous salt has influence on the biological phosphorus removal system. Low concentration of ferrous salt can promote the growth of microorganisms, while high concentration of ferrous salt can inhibit the growth of microorganisms. Moreover, with the increase of ferrous salt concentration, the relative abundance of *Acinetobacter* decreases gradually, but the relative abundance of *Candidatus_Competibacter* increases gradually. The results showed that, in biological phosphorus removal system, with the increase of ferrous salt concentration, the metabolism of phosphate accumulating organisms was gradually replaced by the metabolism of glycogen accumulating organisms. RDA analysis showed that there was a positive correlation between ferrous salt and Candida tus_Competibacter, suggesting that high concentration of ferrous salt was more conducive to the growth of glycogen accumulating organisms. It also shows that ferrous salt is the main factor affecting phosphate accumulating organisms and glycogen accumulating organisms in biological phosphorus removal system.

ACKNOWLEDGEMENTS

This research was supported by the natural Science Project for Colleges of Anhui Province (KJ2019ZD52); Anhui Province Natural Science Foundation (1808085MB34, 1908085ME142); Ph.D. start-up foundation of Anhui Jianzhu University (2018QD20); Major Research and Development Program for Key Technology of Hefei City (ZR201711290005).

REFERENCES

[1] Yuan, Y., Liu, J., Ma, B., Liu, Y., Wang, B., Peng, Y.Z. (2016) Improving municipal wastewater nitrogen and phosphorous removal by feeding sludge fermentation products to sequencing batch reactor (SBR). Bioresource Technology. 222, 326-334.

[2] Zhang, J.Y., Wang, S.Y., Hou, H.X., Zhang, H., Peng, Y.Z., Gao, Y.Q. (2011) Study on Upgrading and Reconstruction of Oxidation Ditch Process in Sewage Treatment Plant. China Water and Wastewater. 27(7), 6-9.

[3] Li, N., Wang, X.H., Kang, H., Wang X. (2013) Influence of pH on Microbial Community Structure and Metabolic Characteristics of PAOs in Biological Phosphorus Removal at Low Temperature. Environmental Science and Technology. 3, 9-11.

[4] Liu, W.T., Nakamura, K., Matsuo, T., Mino, T. (2015) Internal energy-based competition between polyphosphate- and glycogen-accumulating bacteria in biological phosphorus removal reactors-effect of P/C feeding ratio. Water Research. 31(6), 1430-1438.

[5] Fettke, J., Hejazi, M., Smirnova, J., Hcechel, E., Stage, M., Steup, M. (2009) Eukaryotic starch degradation: Integration of plastidial and cytosolic pathways. Journal of Experimental Botany. 60(10), 2907-2922.

[6] Chabre, Y.M., Roy, R. (2013) Multivalent Glycoconjugate Syntheses and Applications Using Aromatic Scaffolds. Chemical Society Reviews. 42(11), 4657-4708.

[7] Oehmen, A., Lemos, P.C., Carvalho, G., Yuan, Z.G., Keller, J., Blackall, L.L., Reis, M.A.M. (2007) Advances in enhanced biological phosphorus removal: From micro to macro scale. Water Research. 41(11), 2271-2300.

[8] Albertsen, M., Hansen, L.B.S., Saunders, A.M., Nielsen, P.H., Nielsen, K.L. (2012) A metagenome of a full-scale microbial community carrying out enhanced biological phosphorus removal. ISME Journal. 6(6), 1094-1106.

[9] Valve, M., Rantanen, P., Kallio, J. (2002) Enhancing biological phosphorus removal from municipal wastewater with partial simultaneous precipitation. Water Science and Technology. 46(4-5), 249-255.

[10] Yang, T., Zhang, J., He, S., Zhang, Y., Ma, T.Y., Yang, K. (2016) Effects of ferrous sulfate ($FeSO_4$) on dehydrogenase activity (DHA), amount of extracellular polymeric substances (EPS) and the treatment efficiency in a sequencing batch biofilm reactor(SBBR). Acta Scientiae Circumstantiae. 36(8), 2838-2843.

[11] Zhang, X.X., Wanyan, J.F., Hu, X.B., Ye, X., Ouyang, Y. (2015) Discriminant of activated sludge settling ability based on floc microscopic parameters. Acta Scientiae Circumstantiae. 35(12), 3815-3823.

[12] Rashed, E.M., El-Shafei, M.M., Heikal, M.A., Noureldin, A.M. (2014) Application of contact stabilization activated sludge for enhancing biological phosphorus removal (EBPR) in domestic wastewater. HBRC Journal. 10(1), 92-99.

[13] Banu, J.R., Do, K.U., Yeom, I.T. (2008) Effect of ferrous sulphate on nitrification during simultaneous phosphorus removal from domestic wastewater using a laboratory scale anoxic/oxic reactor. World Journal of Microbiology and Biotechnology. 24(12), 2981-2986.

[14] Ting, L.I., Dong, W., Wang, H., Lin, J.N., Zhang, Q. Ouayang, F. (2013) Effect of co-existing cations on phosphorous removal in ferrous iron oxidation of electroplating waste-water. Ciesc Journal. 64(10), 3782-3789.

[15] Fan, J., Hu, H. (2013) Effect of Chemical Addition on Biological Phosphorus Removal System. Environmental Science and Technology. 2, 41-45.

[16] Myers, A.F., Rauzy, A. (2008) Assessment of redundant systems with imperfect coverage by means of binary decision diagrams. Reliability Engineering and System Safety. 93(7), 1025-1035.

[17] Yan, B., Hong, K., Xu, Y. (2005) Metagenome Cloning-A New Approach for Novel Microbial Bioactive Compounds Discovery. Microbiology. 32(1), 113-117.

[18] Chung, K.Y., Han, S.S., Kim, H.K., Choi, G.S., Kim, I.S., Lee, S.S., Woo, S.H., Lee, K. H., kim, J.J. (2006) Inhibitory Effect of the Selected Heavy Metals on the Growth of the Phosphorus Accumulating Microorganism, Acinetobacter sp. Korean Journal of Environmental Agriculture. 25(1), 40-46.

Received: **26.08.2019**
Accepted: **19.01.2020**

CORRESPONDING AUTHOR

Jian Huang
School of Environment and Energy Engineering,
Anhui Jianzhu University,
Hefei 230601 – China

e-mail: huangjianpaper@163.com

© by PSP Volume 29 – No. 05/2020 pages 3599-3605 Fresenius Environmental Bulletin

EFFECTS OF BORIC ACID ON PROINFLAMMATION CYTOKINES, TOTAL OXIDATIVE-ANTIOXIDATIVE STATUS AND HEMATOLOGICAL PARAMETERS IN RATS APPLIED BENZO(a)PYRENE

Arzu Comba[1,*], Gokhan Oto[2], Bahat Comba[1], Hulya Ozdemir[2], Siddik Keskin[3], Gonul Arslan Akveran[4]

[1]Hitit University, Technical Sciences Vocational High School, Chemistry and Chemical Proscessing Technology Department, Corum, Turkey
[2]Yuzuncu Yıl University, Faculty of Medicine, Pharmacology Department, Van, Turkey
[3]Yuzuncü Yıl University, Faculty of Medicine, Statistic Department, Van, Turkey
[4]Hitit University, Alaca Avni Celik Vocational High School, Department of Food Processing, Corum, Turkey

ABSTRACT

The aim of this study was to evaluate effects of boric acid (BA) on tumor necrosis factor-alfa (TNF-α), interleukin 1 beta (IL-1β), interleukin-6 (IL-6), total oxidative (TOS)-total anti oxidative status (TAS) and leucocyte (WBC), erythrocyte (RBC), thrombocyte (PLT) and their other parameters in rats applied benzo(a)pyrene (B(a)P).

In this study, rats were divided into 4 groups and each group were containing 6 rats. 1st group was separated as control group. 100 mg/kg total dosage of B(a)P was applied to the 2nd group 2 times a week total in 4 equal dosage with i.p. way. Only BA 300 mg/L was applied to 3rd group in drinking water every day during 150 days. B(a)P was applied twice a week first 2 weeks, 25 mg/kg dose with i.p. way and BA were given with drinking water during 150 days to 4th group.

In the end of study was determined TNF-α and IL-1β levels in B(a)P group, increases compared with other groups. there was a statistically significant increase in levels of WBC and LY in group B(a)P+BA compared to other groups ($P \leq 0.05$). % LY level in other groups was higher; its % NEU level was lower according to control group. RBC and PLT values in BA group were higher, than the other groups. HGB was higher in group BA than group B(a)P and BA+ B(a)P; HCT was higher in group BA than group B(a)P , significantly ($P \leq 0.05$)

As a result, neutropenia and lenfositos develop in case exposure of B(a)P and BA; furthermore, combination of B(a)P and BA increases WBC. BA used alone having considerable effect on excitation of eritopoezis and thrombocytosis. BA has protective effects for organisms together with decrease in the TNF-α and IL-1β levels caused by BA cure as solution of B(a)P exposition.

KEYWORDS:
B(a)P, boric acid, inflammation, interleukin, neutropenia, TAS

INTRODUCTION

Benzo (a) pyrene (BaP), a by-product of the polycyclic aromatic hydrocarbon (PAH), occurs in incomplete combustion reactions or in burning organic substances containing carbon. BaP is one of the most discussed and studied members of PAH compounds because of its high molecular weight, its cytotoxic, mutagenic and carcinogenic properties[1]. BaP is a permanent environmental pollutant that can be absorbed by the body via oral, inhalation and skin exposure [2]. BaP arising from nutrients or contaminated aerosol circulate between the liver and the kidney and bladder. It is known that BaP easily passes through the placenta after oral, intravenous or subcutaneous administration [3]. The liver is the organ containing the most enzymes which are necessary for the bioactivation of BaP [4]. The lipophilic trait of BaP facilitates its distribution and storage in fatty tissues such as breast oil and bone marrow. It is also known that BaP in the blood is carried by chylomicrons and lipoproteins in vivo. The metabolic activation of BaP by means of cytochrome P-450 isoenzymes causes to rise various mutagenic or carcinogenic electrophiles. In particular, the benzo (a) pyrene-7,8-diol-9,10 epoxide (BPDE), a metabolite of BaP, bonds to DNA, RNA and proteins covalently [5].

Boron is a nutrient according to the World Health Organization (WHO) and it is essential for humans [6]. It is necessary for the completion of the life cycle of some advanced organisms since it plays an important role in the reproduction and development of animal cells[7]. It lessens the incidence and effect of the inflammatory diseases, too. Low boron intake affects brain function, bone health and immunity negatively [8]. In a study, histological and

histomorphometric analyses using undecalcified sections showed that at 15 days post-implantation the area of neoformed bone tissue around the boron oxide particles was significantly higher than control glass [9].

Boron forms inorganic salts called boric acid (BA) and borates by combining with oxygen and other elements. Borax, a BA salt, affects the activity of different enzymes in animal and plant systems. BA reduces the level of nitric oxide production and suppresses important inflammatory agent genes [10] and, it has antioxidant activity. The antioxidant mechanism of BA has not been fully understood but it has been reported that boron supplementation increases lipid peroxidation and thereby antioxidant activity. However, BA is a well-known component of cell membrane functions and enzymatic reactions [11]. BA is used to treat diseases such as cancer and inflammatory diseases because of anti-inflammatory and antioxidant agent trait. It reduces the toxic effects of heavy metals, prevents oxidative stress and regulates mitochondrial membrane [12].

Adipositis release tumor necrosis alpha-factor (TNF-α), interleukin-6 (IL-6) and interleukin-1 beta (IL-1β). It may trigger tumor formation in cancer cells and angiogenesis[13] by means of cytokines such as TNF-α, IL-6, ve IL-1 β -receptor agonist [13, 14]

Innate and adaptive immune cells release pro-inflammatory cytokines and these cytokines contribute cancer cell growth and tumor progression [15]. The genetic susceptibility of host and environmental factors play a role in the occurrance of clinical symptoms. The immune system responds to pathogens via production of pro-inflammatory cytokines [16]. TNF-α, a member of the cytokine family play a role in systemic inflammation, acute phase reaction and organization of immune cells. It can cause fever, apoptotic cell death, cachexia and inflammation[17, 18], gastrointestinal disorders, peptic ulcer, and gastric cancer , Alzheimer's disease, inflammatory bowel disease (IBD) [19]. IL-1β produced by immune cells, fibroblasts and epithelial cells, is initiator and enhancer of the inflammatory response and may be involved in the inflammatory response of the host and induce the expression of many other genes such as TNF-α, IL-2, IL-6, IL-12 and pro-inflammatory [20, 21].

Reactive oxygen species (ROS) are produced after metabolic and physiological events. Harmful oxidative reactions occur in the organisms in the end of enzymatic and non-enzymatic antioxidant mechanisms. When the increase in oxidants and antioxidants cannot be prevented, the oxidative / antioxidant balance shifts to the oxidative state and oxidative stress develops which cause over 100 discomfort [22-24]. There is a balance between antioxidants and oxidants in a healthy body. Health problems arise from rise of free radicals or fall of antioxidants. Total measurement of antioxidant status (TAS) and total oxidant status (TOS) is the most practical, economic and rapid way to detect oxidant [25] and antioxidant [26] amounts.

Evaluation of hemogram includes the determination of total number of red blood cell (RBC), total number of white blood cell (WBC), hematocrit (PCV), hemoglobin concentration (Hb), erythrocyte indices (MCV, MCH, MCHC), and white blood cell differential [27].

There is limited information about the effects of BA on inflammation, TAS- TOS and haematological parameters in rats which (B(a)P) is applied. Therefore, in the present study, we investigated the effect of BA on TNF-α, IL-1β, IL-6, TAS, TOS, WBC, RBC, PLT in rats (B(a)P).

MATERIALS AND METHODS

Study Groups. In this study 24 Wistar albino rats, weighing between 200 and 250 g, were used in a climate-controlled animal care facility, within a 12 h light/dark cycle. Standard rat chow and water were given to animals *ad libitum*. They were divided into 4 groups each containing 6 rats. Saline (1 mL of 0.9 % NaCl) was injected to Group 1 (Control) and 25 mg/kg B(a)P (Sigma, Code: B1760) was injected to Group 2 (B(a)P) by intraperitoneal injection way twice a week in the first two weeks of study duration. Daily dose of BA (Sigma, Code: B6768) (300 mg/L/day) was given to Group 3 (BA) within drinking water during 150 days. 25 mg/kg B(a)P by intraperitoneal injection way twice a week in the first two weeks and 300mg/L/day BA within drinking water during 150 days were given to Group 4 (B(a)P +BA). All implementations were begun simultaneously in the first day of the study. This study was approved by the local ethics committee of Yuzuncu Yil University.

Blood Collection. At the end of 150 days, blood samples were collected from all individuals and they were sacrificed by anesthetizing with i.p. injection of 70 mg/kg of ketamine HCl (Ketalar, Pfizer) and 10 mg/kg of and xylazine HCl (Rompun, Bayer).
Blood samples were taken from hearts with sterilized injector and placed into tubes with EDTA and coagulated tubes. After then bloods were separated into serum by centrifugation at 3.000 RPM during 10 min. Serum was stored (-20°C) until the analysis.

Assay. Th TNF-α, IL-1β and IL-6 levels were analysed by ELISA kits (eBioscience, Austria); TAS and TOS values were analysed using a novel automated measurement method developed by Erel et al. by colorimetric kits (Rel Assay, Türkiye) in serum. The oxidative stress index (OSI) was calculated with the ratio of TOS to TAS [25, 26].

TABLE 1
Serum TNF-α, IL-1β and IL-6 levels in all the groups (mean±SD)

Inflammation Markers	Control Group n:6	B(a)P Group n:6	BA Group n:6	B(a)P +BA Group n:6	P Value
TNF-α (pg/mL)	303,31± 22,70[b]	371,19 ± 35,49[a]	314,67 ± 30,79[b]	310,26 ± 59,46[b]	,027
IL-1β (pg/mL)	302,20 ± 87,42[b]	475,91 ± 63,46[a]	355,98 ± 81,75[b]	331,50 ±79,26[b]	,025
IL-6 (pg/mL)	163,22 ± 37,55	163,50 ±36,44	174,54 ±43,25	150,68 ±18,55	,406

a,b: in the same line values with different letters show statistically significant differences

TABLE 2
Serum TAS, TOS and OSI levels in all the groups (mean±SD)

Oxidant-Antioxidant Parameters	Control Group n:6	B(a)P Group n:6	BA Group n:6	B(a)P +BA Group n:6	P Value
TAS (mmol Trolox Equiv/L)	0,53± ,08	0,59±,07	0,51±,11	0,57±,14	,232
TOS (μmol H_2O_2 Equiv/L)	4,89±,95	4,74±1,12	3,99±1,32	5,57±1,91	,218
OSI (Arbitrary Unit)	0,92±,26	0,8±,18	0,78±,27	0,98±,11	,405

Hematology parameters, WBC, % leukocyte, RBC, HG, HCT and PLT were determined in whole blood using rat mode of veterinary blood cell counter (Abocus Junior Vet-5, Austria).

Statistical Analysis. SPSS statistical software 16.0 for Windows was used for the calculations. All data were analyzed using the Kruskal-Wallis test. Dunn test was performed to determine the different groups. Statistics Calculator was taken as significance level of 5% . The data were given as means±stantard deviation (X±SD)

RESULTS

The serum levels of TNF-α, IL-1β and IL-6 are shown in Table 1. According to the Table 1 the levels of TNF-α and IL-1β were statistically higher in group 2 than other groups (P≤0.05). The serum levels of TAS, TOS and OSI are shown in Table 2. According to the Table 2 there was no statistically difference among the groups in terms of TAS, TOS, OSI levels, (P>0.05).

The hematological parameters are shown in Table 3. According to the Table 3 the increase of WBC and LY levels in group 4 were significantly higher compared to other groups, (P≤0.05). LY% levels of group 2,3 and 4 were significantly higher (P≤0.05); hovewer, their NEU% (P≤0.01) were significantly lower than control group. The increase of RBC, HGB, HCT and PLT values were obtained in group 3; RBC and PLT were higher than other groups, HGB was higher than in group 2 and 4, HCT was higher than in group 2, significantly (P≤0.05).

DISCUSSIONS

Cytokines, multi-functional polypeptides, are synthesized by various body cells, play role in immune and inflamatuar responses, cell growth and differentiation and cicatrisation processes [28]. TNF-α, IL-6, are responsible for chronic inflammation and IL-1β, TNF-αs and IL-6 are important in processes of cell growth and differentiation [29]. IL-6 levels may rise in cancer patients and anti-apoptotic effects may be observed in tumor cells so [it plays role in pathogenesis of cancer [15, 30].

TABLE 3
The haematolojical parameters in all the groups (mean±SD)

Haematolojical Parameters	Control Group n:6	B(a)P Group n:6	BA Group n:6	B(a)P +BA Group n:6	P Value
WBC (10^9/L)	6,85±1,77[b]	6,66±1,43[b]	6,01±,80[b]	9,28±1,96[a]	,044
LY (10^9/L)	4,37±1,10[b]	5,02±1,00[b]	4,56±,78[b]	7,49±1,69[a]	,019
MO (10^9/L)	0,51±,25	0,36±,38	0,21±,26	0,48±,46	,522
NE (10^9/L)	1,99±,71	1,31±,29	1,22±,21	1,30±,17	,062
LY (%)	66,06±9,52[b]	73,86±5,25[a]	75,86±5,55[a]	78,23±6,41[a]	,031
MO (%)	7,06±3,64	4,74±4,83	3,57±4,23	5,57±5,22	,486
NE (%)	28,42±5,79[a]	19,87± 3,02 [b]	20,39±3,04[b]	16,26± 2,91[b]	,002
RBC (10^{12}/L)	7,67± ,19[b]	7,44 ±,62[b]	8,26±,60[a]	7,62 ±,39[b]	,045
HGB (g/dL)	13,96 ±,35[ab]	13,58 ±,66[b]	14,69 ±1,03[a]	13,94± ,39[ab]	,043
HCT (%)	45,81±1,23[ab]	44,20± 4,69[b]	48,71± 3,08[a]	44,94± 2,57[b]	,046
MCV (fl)	59,86±1,68	59,29±2,36	59,29±1,89	59,29±2,69	,884
MCH (pg)	18,16±,32	18,36±1,21	17,84±,47	17,92±1,47	,689
MCHC (g/dL)	30,62±,80	31,14±2,71	30,24±,27	31,04±1,55	,635
RDWc (%)	13,93±,42	14,06±,29	14,25±,37	14,47±,52	,141
PLT (10^9/L)	618,14±74,84[b]	674,14 ± 71,94[b]	774,86 ±103,93[a]	677,86 ±93,53[b]	,037
PCT (%)	,48 ±,20	,49 ±,06	,59±,19	,49 ±,07	,117
MPV (fl)	7,90 ±,69	7,27 ±,20	7,37±,30	7,19±,32	,147
PDWc (%)	34,96 ±1,15	35,44 ±,84	35,26 ±,84	34,86 ±,98	,755

a,b,c: in the same line values with different letters show statistically significant differences

Comba et al. showed that TNF-α and IL-1β levels in 3-MC group increased significantly compared to other groups. In the present study, the increase of TNF-α and IL-1β levels in group 2 was statistically higher than other groups (P≤0.05) [31].

TNF-α has toxic effect on β cells of pancreas, it ensures vein adhesion of inflamatuar cells, matures B and T lymphocytes, monocyte and macrophages [32, 33].

In addition, IL-1 increases expression of surface molecules which help the aggregation of leucocytes by affectting mononuclear and endothelium cells instead and thus triggers the chemokines synthesis which activate leucocystes [34].

Comba et al., demonstrated that LY% of every 3 groups (3 MC, BX and 3MC+BX) were significantly higher than control group however, NEU % were significantly fewer, there was no significant differences in WBC levels among groups [31].

In this study, WBC and LY levels increased significantly in group 4 according to other groups (P≤0.05). For every 3 groups while LY% levels were significantly higher (P≤0.05), NEU% levels (P≤0.01) were significantly lower than control group.

IL-1 has many inflammatoire characteristics of TNF such as affecting endothelial cells and increasing coagulation [34]. Comba et al. revealed that the number of PLT in 3-MC and 3-MC+BX groups were significantly higher than other groups (P≤0.05); HGB and HCT values in 3-MC+BX group and MCV (Mean Corpuscular Volume) values in 3-MC and 3-MC+BX groups decreased according to other groups (P≤0.05); It may change haematolojical parameters such as, PLT [31].

In this study, The RBC, Hbg, HCT and PLT values increased in BA group; RBC and PLT were higher in BA group than other groups; HG was higher in Group 3 than group 2 and 4; HCT was significantly higher in BA group than group 2 (P≤0.05).

Oxidative stress, inequality between antioxidant defense systems and free radicals, is associated with the etiology of aging and many diseases [35-37]. It is suggested that antioxidants taken from nutrition decrease oxidative stress, genotoxicity, tumor incidents and cancer risk [38].

It was shown that B compounds are effective in remaining the equality of prooxidants and anti-oxidants and they reduce tissue damage resulting from oxidative stress [39, 40]. Pawa and Ali demonstrated that B compounds limit oxidative damage by enhancing the glutathione store or inducing other free radical elimination [39].

In our study, we analyzed TOS values to assess the total oxidants effect. Likewise, we measured the

TAS level instead of evaluating antioxidant molecules separately.

Ince et al. revealed that B compounds supplementation in diet (100 mg/kg) decreases the lipid peroxidation (LPO) and malondialdehit (MDA) concentration significantly and it enhances the antioxidant defense mechanism such as GSH in blood [40]. Hovewer, in this study, there was no statistically differences among the groups for TAS, TOS, OSI levels, (P>0.05).

Comba et al. demonstrated that exposure of 3-MC and long-term usage of BX with oral way may not decrease oxidative stress [31]. This increase may be from iron deficiency in HGB and free iron increase in blood plasma. In this case free radicals and oxidative stress increase [41]. Also this stuation may be due to the difference in dose. Turkez et al. reported that B did not alter MDA concentration at low doses (5-50 mg/L) but increased it at high doses (500 mg/L) in human peripheral blood. Hovewer, in this study level of B is nontoxic [42]. B compounds are given orally to animals for a short term, the LD50 values for borax are in the range of 400-700 mg B/kg of body weight in laboratory animals [43]. Furthermore, the maximum tolerable level of B is 150 mg/kg; diet B deficiency may occur in animals when their diet contains 0.3 mg/kg B [44].

Antioxidant capacity is an important factor for all physiological standards and the performance of humans and all animals [45]. Turkez et al. observed that B compounds increased both SOD and CAT activities at low doses (15 mg/L), while they decresed (500 mg/L) them at high doses in erythrocytes [42]. Koç et al. revealed that B compounds (100 mg/kg) increased antioxidan capacity in spinal cord ıschemia/reperfusion injury [46]. Hovewer, in the present study, serum TAS levels did not change among groups. This result is consistent with the study of [40]. They showed that dietary B supplementation did not alter the plasma antioxidant capacity when compared to control group. Turkez et al. determined TAA in erythrocytes in vitro but we determined it in plasma containing many nonspecific antioxidants such as urea, uric acid, and proteins [42].

As seen, in the previous studies, it was reported that the application of different doses of BA at different period had different effects on oxidative stress and antioxidant status, but their impact on inflammation markers and the haematolojical parameters were not evaluated as distinct from our study.

As a summary in the present study, there was a statistically significant increase in the serum levels of TNF-α and IL-1β in group 2 compared to other groups(P≤0.05). There was no statistically significant difference among the groups in terms of TAS, TOS, OSI levels (P>0.05). According to the Table 3 there was a statistically significant increase in levels of WBC and LY in group 4 compared to other groups (P≤0.05).

LY% levels of each 3 groups were significantly higher than control group (P≤0.05), however NEU% levels of each 3 groups were significantly lower than control group (P≤0.01). RBC and PLT were higher than in group 3 than other groups; HGB was higher in group 3 than group 2 and 4; HCT was higher in group 3 than group 2, significantly (P≤0.05)

As a result, this experimental study has demonstrated that B(a)P may increase the level of inflammation and cancer markers like TNF-α and IL-1β and in case of exposure to B(a)P, useage of BA can decrease these levels. Only BA can be used to increase RBC, HGB, HCT, PLT levels. BA+B(a)P can increase to WBC and LY levels. B(a)P, BA or B(a)P+BA can increase LY % level and can decrease NE %. BA level and B(a)P doses in this study may not change IL-1β levels and oxidative stress factors such as TOS, TAS and OSI, and some other haematolojical parameters.

REFERENCES

[1] Juhasz, A.N., Naidu, R. (2000) Bioremediation of high molecular weight polycyclic aromatic hydrocarbons: a review of the microbial degradation of benzo [a] pyrene. International Biodeterioration and Biodegradation. 45(1,2), 57-88.

[2] Ramesh, A., Inyang, F., Hood, D.B., Archibong, A.E., Knuckles, M.E., Nyanda, A.M. (2001) Metabolism, bioavailability, and toxicokinetics of Benzo (α) pyrenein F-344 rats following oral administration. Experimental and Toxicologic Pathology. 53(4), 275-290.

[3] Verma, N., Pink, M., Petrat, F., Rettenmeier, A.W., Schmitz-Spanke, S. (2012) Exposure of primary porcine urothelial cells to benzo (a) pyrene: in vitro uptake, intracellular concentration, and biological response. Archives of Toxicology. 86(12), 1861-1871.

[4] Walle, T., Walle, U.K., Sedmera, D., Klausner, M. (2006) Benzo[A]pyrene-inducedoral carcinogenesis and chemoprevention: studies in bioengineered human tissue, Drug Metabolism and Disposition. 34(3), 346-350.

[5] Kim, J.H., Stansbury, K.H., Walker, N.J., Trush, M.A., Strickland, P.T., Sutter, T.R.(1998) Metabolism of benzo [a] pyrene and benzo [a] pyrene-7, 8-diol by human cytochrome P450 1B1, Carcinogenesis. 19(10), 1847-1853.

[6] Del Rosso, J.Q., Plattner, J.J. (2014)From the test tube to the treatment room: fundamentals of boron-containing compounds and their relevance to dermatology, The Journal of Clinical and Aesthetic Dermatology. 7(2), 13.

[7] Wei, Y., Yuan, F., Zhou, W., Wu, L., Chen, L., Wang, J., Zhang, Y. (2016) Borax-induced apoptosis in HepG2 cells involves Bcl-2, and Bax, Genet. Mol. Res. 15(2), 53.
[8] Nielsen, F.H. (2008) Is boron nutritionally relevant?, Nutrition Reviews. 66(4), 183-191.
[9] Gorustovich, A.A., López, J.M.P., Guglielmotti, M.B., Cabrini, R.L.(2006) Biological performance of boron-modified bioactive glass particles implanted in rat tibia bone marrow, Biomedical Materials. 1(3), 100.
[10] Demirci, S., Doğan, A., Aydın, S., Dülger, E.Ç., Şahin, F. (2016) Boron promotes streptozotocin -induced diabetic wound healing: roles in cell proliferation and migration, growth factor expression, and inflammation, Molecular and Cellular Biochemistry. 417(1-2), 119-133.
[11] Ince, S., Kucukkurt, I., Cigerci, I.H., Fidan, A.F., Eryavuz, A.(2010) The effects of dietary boric acid and borax supplementation on lipid peroxidation, antioxidant activity, and DNA damage in rats, Journal of Trace Elements in Medicine and Biology. 24(3), 161-164.
[12] Sogut, I., Oglakci, A., Kartkaya, K., Ol, K.K., Sogut, M.S., Kanbak, G., Inal, M.E.(2015) Effect of boric acid on oxidative stress in rats with fetal alcohol syndrome, Experimental and Therapeutic Medicine. 9(3), 1023-1027.
[13] Tilg, H., Moschen, A.R.(2006) Adipocytokines: mediators linking adipose tissue, inflammation and immunity, Nature Reviews Immunology. 6(10), 772.
[14] Kern, P.A., Di Gregorio, G.B., Lu, T., Rassouli, N, Ranganathan, G.(2003) Adiponectin expression from human adipose tissue: relation to obesity, insulin resistance, and tumor necrosis factor-α expression, Diabetes. 52(7), 1779-1785.
[15] Waldner, M.J., Foersch, S., Neurath, M.F.(2012) Interleukin-6-a key regulator of colorectal cancer development, International Journal of Biological Sciences. 8(9), 1248.
[16] Hernández, C., Serrano, C., Einisman, H., Villagrán, A., Peña, A., Duarte, I., Torres, J., Riera, F., Harris, P.R.(2014) Peptic ulcer disease in helicobacter pylori–infected children: clinical findings and mucosal immune response, Journal of Pediatric Gastroenterology and Nutrition. 59(6) 773-778.
[17] Fond, G., Hamdani, N., Kapczinski, F., Boukouaci, W., Drancourt, N., Dargel, A., Oliveira, J., Le Guen, E., Marlinge, E., Tamouza, R.(2014) Effectiveness and tolerance of anti-inflammatory drugs' add-on therapy in major mental disorders: a systematic qualitative review, Acta Psychiatrica Scandinavica. 129(3), 163-179.
[18] Güzel, M., Sönmez, M.F., Baştuğ, O., Aras, N.F., Öztürk, A.B., Küçükaydın, M., Turan, C.(2016) Effectiveness of lycopene on experimental testicular torsion, Journal of Pediatric Surgery. 51(7), 1187-1191.
[19] Rokkas, T., Sechopoulos, P., Pistiolas, D., Kothonas, F., Margantinis, G., Koukoulis, G. (2014) Population differences concerning TNF-α gene polymorphisms in gastric carcinogenesis based on meta-analysis, Annals of Gastroenterology: Quarterly Publication of the Hellenic Society of Gastroenterology. 27(2), 139.
[20] Arango Duque, G., Descoteaux, A.(2014) Frontiers in Immunology. 5, 491.
[21] Garlanda, C., Dinarello, C., Mantovani, A. (2013) The interleukin-1 family: back to the future, Immunity. 39(6), 1003-1018.
[22] Harma, M., Harma, M., Erel, O.(2005) Oxidative stress in women with preeclampsia, American Journal of Obstetrics & Gynecology. 192(2), 656-657.
[23] Yeni, E., Gulum, M., Selek, S., Erel, O., Unal, D., Verit, A., Savas, M.(2005) Comparison of oxidative/antioxidative status of penile corpus cavernosum blood and peripheral venous blood, International Journal of Impotence Research. 17(1), 19.
[24] Yanik, M., Erel, O., Kati, M.(2004) The relationship between potency of oxidative stress and severity of depression, Acta Neuropsychiatrica. 16(4), 200-203.
[25] Erel, O.(2005) A new automated colorimetric method for measuring total oxidant status, Clinical Biochemistry. 38(12), 1103-1111.
[26] Erel, O.(2004) A novel automated direct measurement method for total antioxidant capacity using a new generation, more stable ABTS radical cation, Clinical Biochemistry. 37(4), 277-285.
[27] Campbell, T.(2004) Hematology of lower vertebrates, 55 th Annual Meeting of the American College of Veterinary Pathologists (ACVP) and 39 th Annual Meeting of the American Society of Clinical Pathology (ASVCP). International Veterinary Information Service. Ithaca, NY, USA. 1104-1108.
[28] Hunt, C.D., Idso, J.P.(1999) Dietary boron as a physiological regulator of the normal inflammatory response: a review and current research progress, The Journal of Trace Elements in Experimental Medicine: The Official Publication of the International Society for Trace Element Research in Humans. 12(3), 221-233.
[29] Rodríguez-Hernández, H., Simental-Mendía, L.E., Rodríguez-Ramírez, G., Reyes-Romero, M.A. (2013) Obesity and inflammation: epidemiology, risk factors, and markers of inflammation, International Journal of Endocrinology.

[30] Greenberg, A.S., Nordan, R.P., McIntosh, J., Calvo, J.C., Scow, R.O., Jablons, D. (1992) Interleukin 6 reduces lipoprotein lipase activity in adipose tissue of mice in vivo and in 3T3-L1 adipocytes: a possible role for interleukin 6 in cancer cachexia, Cancer Research. 52(15), 4113-4116.
[31] Comba, B., Gökhan, O., Leyla, M., Özdemir, H. Comba, A.(2016) Effects of borax on inflammation, haematological parameters and total oxidant-antioxidant status in rats applied 3–methylcholanthrene, Kafkas Univ. Vet. Fak. Derg. 22(4), 539-544.
[32] Warne, J. (2003) New perspectives on endocrine signalling: tumor necrosis factor α: a key regulator of adipose tissue mass, J. Endocinol. 177, 351-355.
[33] Zarkesh-Esfahani, H., Pockley, A.G., Wu, Z., Hellewell, P.G., Weetman, A.P., Ross, R.J. (2004) Leptin indirectly activates human neutrophils via induction of TNF-α, The Journal of Immunology. 172(3), 1809-1814.
[34] Oppenheim, J.J., Ruscetti, F.W., Faltynek, C. (1987) Interleukins and interferons, Basic and Clinical Immunology. 6, 82-95.
[35] Mandelblatt, J.S., Hurria, A., McDonald, B.C., Saykin, A.J., Stern, R.A., VanMeter, J.W., McGuckin, M., Traina, T., Denduluri, N., Turner, S. (2013) Cognitive effects of cancer and its treatments at the intersection of aging: what do we know; what do we need to know?, Seminars in Oncology, Elsevier. 709-725.
[36] Padurariu, M., Ciobica, A., Lefter, R., Lacramioara Serban, I., Stefanescu, C., Chirita, R.(2013) The oxidative stress hypothesis in Alzheimer's disease, Psychiatria Danubina. 25(4), 0-409.
[37] Cojocaru, I.M., Cojocaru, M., Sapira, V., Ionescu, A.(2013) Evaluation of oxidative stress in patients with acute ischemic stroke, Romanian Journal of Internal Medicine. 51(2), 97-106.
[38] Polat, F., Turaçlar, N., Gül, E., Özdemir, Ö., Bingöl, G. (2008) Mutatıon Analysıs Of The Proto-Oncogenes Ki-Ras And C-Myc In The Soft Tissue Tumors Of The Rats That Were Formed By 3-Methylcholanthrene In Vıvo. Dumlupınar Üniversitesi Fen Bilimleri Enstitüsü Dergisi. (017) 11-18.
[39] Pawa, S., Ali, S. (2006) Boron ameliorates fulminant hepatic failure by counteracting the changes associated with the oxidative stress, Chemico-biological Interactions. 160(2), 89-98.
[40] Ince, S., Keles, H., Erdogan, M., Hazman, O., Kucukkurt, I. (2012) Protective effect of boric acid against carbon tetrachloride–induced hepatotoxicity in mice, Drug and Chemical Toxicology. 35(3), 285-292.
[41] Yilmaz, K., Kahraman, A., Bodur, S., Koçar, S., Köken, T. (2004) Reduced glutathione and antioxidant enzyme activities in erythrocytes of patients with iron-deficiency anemia, Turkiye Klinikleri, Journal of Medical Sciences 24(4), 305.
[42] Türkez, H., Geyikoğlu, F., Tatar, A., Keleş, S., Özkan, A. (2007) Effects of some boron compounds on peripheral human blood, Zeitschrift für Naturforschung. C 62(11-12), 889-896.
[43] Weir Jr, R.J., Fisher, R.S. (1972) Toxicologic studies on borax and boric acid, Toxicology and Applied Pharmacology. 23(3), 351-364.
[44] McDowell, L.R.(1992) Minerals in animal and human nutrition, Academic Press Inc.
[45] Bohloli, M., Uzun, H., Aytac, E., Toklu, A.S., Paksoy, M., Durak, H., Ipek, T. (2007) Hyperbaric oxygen (HBO) therapy after partial hepatectomy: an experimental study on oxidative stress in rats., Scandinavian Journal of Laboratory Animal Sciences. 34(2), 131-140.
[46] Koc, E.R., Gökce, E.C., Sönmez, M.A., Namuslu, M., Gökce, A., Bodur, A.S. (2015) Borax partially prevents neurologic disability and oxidative stress in experimental spinal cord ischemia/reperfusion injury, Journal of Stroke and Cerebrovascular Diseases. 24(1), 83-90.

Received: **27.08.2019**
Accepted: **25.09.2019**

CORRESPONDING AUTHOR

Arzu Comba
Hitit University
Technical Sciences Vocational High School
Chemistry and Chemical Proscessing Technology Department
19000 Çorum – Turkey

e-mail: arzucomba@hitit.edu.tr

© by PSP Volume 29 – No. 05/2020 pages 3606-3613 Fresenius Environmental Bulletin

ASSESSMENT OF WATER QUALITY; A CASE STUDY OF BUYUK MENDERES RIVER BASIN

Ebru Cokay*, Serkan Eker, Ilgi Karapinar, Hulusi Demircioglu

Dokuz Eylul University, Department of Environmental Engineering, Tinaztepe Campus, Buca Izmir

ABSTRACT

The quality of natural waters can be seriously affected by both point and not-point pollution sources such as industrial discharges, agricultural activities, water withdrawal, drought, and floods. Büyük Menderes River Basin in Turkey is subjected to these factors. It is required to evaluate its water quality for sustainable surface water management. The European Commission Water Framework Directive (WFD) was constructed to monitor water quality for rivers, lakes and transitional and coastal waters utilizing networks. Countries evaluated the Water Framework Directive and principles of WFD have been adapted to the legislation of the country over the past eighteen years. Therefore, this study was conducted in Büyük Menderes River Basin to determine its water quality classes according to the Republic of Turkey Ministry of Forestry and Water Affairs' Regulation (WAR) for Management of Surface Water. Seasonal samples were collected from 39 surveillance monitoring stations. The parameters monitored stated in the regulation were physical ones as temperature, pH, COD and BOD, nutrient parameters, etc. Annual averages of the monitored physico-chemical pollution parameters were used to determine the water quality classes of stations and the whole river basin. The results indicated that the water quality of Büyük Menderes River Basin was either class III or class IV. Besides, the water quality of Büyük Menderes River Basin was presented based on Water Framework Directive. So, two regulations (WAR and WFD) were compared with each other according to water quality classification.

KEYWORDS:
Büyük Menderes River Basin, Physico-chemical pollution, Monitoring, Water quality

INTRODUCTION

Water sources are very important to use for human activities and industrial applications. The requirement of freshwater rises in the last decade of years due to high pollution and industrial growth. Freshwater can be obtained from the river, groundwater, and lakes. However, the quality of water decreases due to industrial activities, agricultural activities, and human requirements. For that reason, the assessment of the quality of water should be managed. In Europe, Water Frame Directive was used for this aim.

EU member countries disseminated Water Framework Directive [1] which focuses on providing sustainable management of the river, lake, transition, ground and coastal waters to protect water resources. The main objective of Water Framework Directive (WFD) is to achieve "good water status". Surface, coastal and transitional waters must achieve "good ecological and chemical status" by 2027 at the latest. Implementation of the WFD and it declares a combined water protection framework in order to water management for all European countries. Countries evaluated the Water Framework Directive and principles of WFD have been adapted to the legislation of the country over the past eighteen years.

A work plan was initiated in Turkey, recently, to implement WFD in coordination with the other international/national expert groups. Water quality is evaluated based on ecological, chemical and hydromorphological status for surface waters and chemical and quantitative status for groundwater. Surveillance monitoring predominantly provides the evaluation of the overall surface water status within a river basin or sub-basin of a river basin district according to Article 7 of the WFD. Surveillance monitoring generally measures all the quality elements for the classification of ecological status including hydromorphological, chemical and physico-chemical elements.

The ecological status comprises biological quality elements such as macro invertebrate fauna, aquatic flora, phytoplankton and fish with physico-chemical quality elements (temperature, oxygenation, nutrient levels, etc.) and hydromorphological quality elements such as river continuity, flow regime, etc. [2]. Physico-chemical monitoring results and water quality assessment of some water bodies have been evaluated based on WFD [3-7]. Brack et al. [8] have reviewed fundamental, strategic and technical challenges regarding the practical implementation of the WFD. Kirmikil [9] investigates time-dependent changes in the opinions of water managers about land consolidation in rural areas. The water quality of Lake Nanhu in Wuhan, China

and the quantitative analysis of the pollutant sources in the basin were presented by Huang [10]. Akçadağ river basin in Turkey was also qualified to be used for irrigation or drinking purposes with the aid of GIS and to ensure the sustainable use of surface waters [11]. In addition, the ecological quality status of Susurluk river basin in Turkey also investigated by Albayrak [12].

The chemical status of the water is another quality parameter. The main concern for chemical status is the priority and specific pollutants. Priority pollutants, which should be monitored have been determined by directive 2008/105/EC of the European Parliament and of the Council. EU Member and candidate countries should determine pollutants, which are specific to their countries.

The Ministry of Forestry and Water Affairs in Turkey carried out different projects to determine conventional physico-chemical pollutants and the national specific pollutants. The conventional physico-chemical pollution status of the water is determined according to the Regulation of Surface Water Quality Management. The parameters monitored stated in the regulation were physical ones as temperature, pH, conductivity, color, oxygen conditions as dissolved oxygen, oxygen saturation, COD and BOD, metals, nutrient parameters like nitrogen and phosphorus. After the evaluation of these parameters, the water quality class of water bodies can be determined. There are four water classes for surface water bodies. Class I water states "Very Good" water means that the water is suitable for many uses such as drinking water, swimming, sporting activities, irrigation, and animal needs, etc. Class II water quality means "Good" water which states that the water is slightly polluted but suitable for a few uses such as drinking water, recreational purposes uses, and other fish breeding outside the Trout. Class III indicates that the water is "Middle quality ", which is polluted and can be used for some industrial purposes and agriculture after proper treatment, finally, Class IV means "Low water quality" states that water can only be used after proper treatment (surface water regulation).

In this study, a water quality class of Büyük Menderes River Basin (BMRB) was determined by the Republic of Turkey Ministry of Forestry and Water Affairs' Regulation for Management of Surface Water and Water Frame Directive. An effect of physicochemical parameters on the water quality of BMRB has been investigated. In addition, the suitable potential of water to use human and other activities will be discussed after the evaluation of analyses of physicochemical parameters based on the water quality class.

MATERIALS AND METHODS

Stations and Monitoring. The water samples from the river taken from 39 sample points which were determined by the Forestry Ministry in Turkey. Seasonal samples were collected from 14 Büyük Menderes Lake (BML) and 25 Büyük Menderes River (BMR) stations in Büyük Menderes River Basin (BMRB). Sampling stations in BMRB are given in Figure 1. Surveillance monitoring was executed for quality elements for the classification of physico-chemical parameters.

Analytical Methods. pH, temperature, dissolved oxygen, turbidity, conductivity, oxygen saturation, were recorded regularly at sampling point (station) via portable pH meter, etc. Water samples were collected into 1000 ml PFTA plastic containers and preserved at +4 ºC. Samples were filtered through 0.45 µm filter paper when required. The water quality parameters and method were as follows; COD (SM 5220 B), BOD (SM 5210 B), N-NH_4 (SM 4500-NH_3-B C D), NO3 (SM 4500-NO_3 H), P (SM 4500-P-D, SM 4500 P-B), TKN (SM 4500 Norg B, SM 4500-NH_3 C), metals; Ni, Cu, Zn, Cd, Pb (SM 3030 K, SM 3120 B). Hg analysis was conducted in ICP-AES Hydride. RES (436 nm, 525 nm, 620 nm) was determined by spectrophotometer [13]. Each analysis is done in triplicate and means the value was taken and presented in this study.

RESULTS AND DISCUSSIONS

Seasonal samples were collected from 39 surveillance monitoring stations for twelve months. Annual averages of the monitored physico-chemical pollution parameters listed in Annex V of Turkish Surface Water Quality Regulations (Table 1) were evaluated in the river basin to determine the water quality classes of stations and whole river basin.

The dissolved oxygen is important for freshwater resources because of the observation on aerobic and anaerobic conditions of water resources. Natural waters should contain the range of 5-14.5 mg O_2/L. According to EPA, the dissolved oxygen range should be ranged from 4 to 6 mg/L to ensure aquatic life in sources. To achieve a good quality of water resources, dissolved oxygen concentration should be ranged from 6 to 8 mg/L, using water quality classification for Turkish Surface Water Quality Regulations. Evaluations after sample collection from sample points showed that dissolved oxygen concentration is generally good conditions at all sampling points. Also, oxygen saturation (%) measurement showed that the water quality of BMRB is sufficient based on dissolved oxygen concentration.

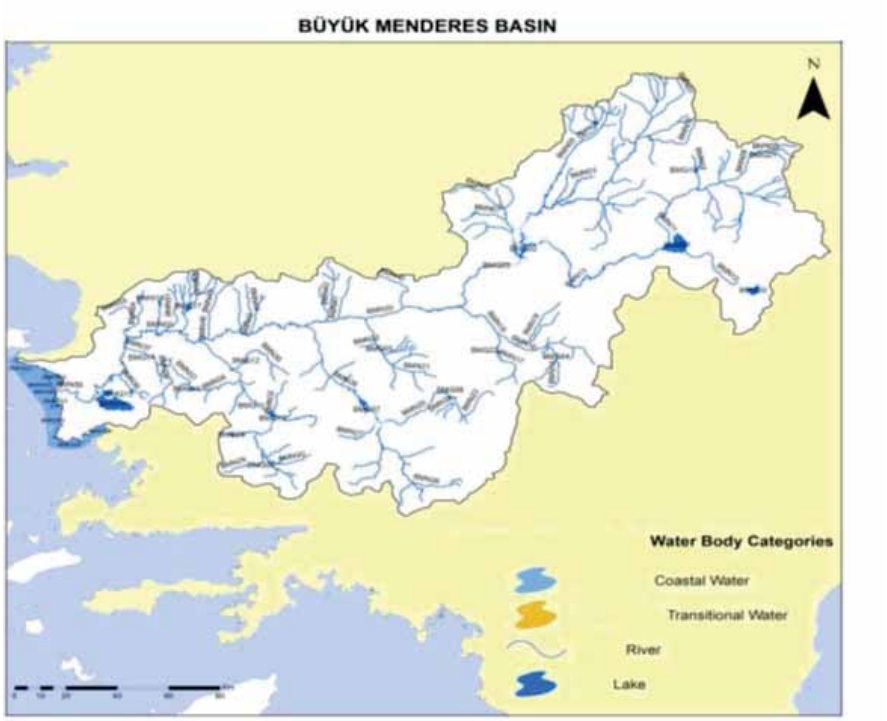

FIGURE 1
Stations in Buyuk Menderes River Basin (BMRB)

TABLE 1
Water Quality Classification Classes from
Regulation of Surface Water Quality Management (30th September 2012)

Water Quality Parameter	Class I	Class II	Class III	Class IV
COD	<25	25-50	50-70	>70
NH_4-N	<0.2	0.2-1	1-2	>2
NO_3-N (*)	<3	3-10	10-20	> 20
P (*)	<0.08	0.08-0.16	0.16-0.65	> 0.65
TKN	<0.5	1.5	5	>5
BOD	<4	4-8	8-20	>20
Ni	≤20	20-50	50-200	>200
Cu	≤20	20-50	50-200	>200
Zn	≤200	200-500	500-2000	>2000
Cd	≤2	2-5	5-7	>7
Pb	≤10	10-20	20-50	>50
Hg	<0.1	0.1-0.5	0.5-2	>2
pH	6.5-8.5	6.5-8.5	6.0-9.0	except for 6.0-9.0
Temperature	≤25	≤25	≤30	>30
Conductivity	<400	400-1000	1001-3000	>3000
Dissolved Oxygen Conc.(mg O_2/L)	> 8	6-8	3-6	<3
Oxygen Saturation (%)	>90	70-90	40-70	<40
Fecal Coliform (EMS/100 mL)	≤10	10-200	200-2000	>2000
Total Coliform (EMS/100 mL)	≤100	100-20000	20000-100000	>100000

Temperature values were sufficient based on regulations. Conductivity is also another important parameter to evaluate water quality to show solid matter concentration, alkalinity, minerals, and salinity, etc. Evaluations of samples collected from BMRB sampling points showed that conductivity values were very high at lakes and transitional sampling points.

Discharge from domestic and industrial wastewaters affects and contaminate the water

sources and water quality observed with COD or BOD concentrations. For that reason, these parameters are very important to determine organic matter concentration in surface water, to evaluate water quality and to determine water quality classification. According to Turkish Surface Water Quality Regulations, BOD and COD concentrations should be decreased from 4 mg/L and 24 mg/L, respectively to reach Class I of water quality. In addition, BOD concentrations should not exceed 6 mg/L related to the WHO water standard.

Figure 2 depicts water quality classification in the river basin via COD parameter. The class of lakes in the river basin is mostly Class I with COD<25 mg/L. Only the water quality of BML16-Bafa Lake, which is the biggest lake in the basin and receives some discharges, is in Class II with annual average COD of 28 mg/L. The COD values in the river stations were in the range of 5 to 150 mg/L. The highest COD concentrations were observed as 40 mg/L in BMR03 and 150 mg/L in BMR05 sampling points. These stations receive industrial discharges after treatment, due to organized industrial zone. Similarly, the highest BOD concentration was obtained at BMR05 sampling point with 80 mg/L annual average BOD concentration which made the station Class IV water quality (Figure 3).

Agricultural activities at BMRB affect and damage the water quality of water due to the discharge of pesticides and organic constitutes. After discharging, nitrogen concentration increases in the river. Increasing nitrogen concentration causes decreased dissolved oxygen concentration and increased algae and microorganism concentrations. For that reason, observation of N parameter at BMRB is very important. In the project, all nitrogen forms were evaluated by NO_2, NO_3, NH_4-N, Total Kjeldahl Nitrogen (TKN).

NH_4-N concentrations in the lakes of the basin are slightly higher than 0.2 mg/L which makes the lakes Class II water quality (Figure 4). Similarly, NH_4-N concentration in most of the stations in the river was between 0.2-1 mg/L that means Class II water quality. NH_4-N concentration reached to 13.6 mg/L at BMR05 and over 2 mg/L in BMR23 which makes Class IV water quality of these stations. According to Turkish Surface Water Quality Regulations, NH_4-N concentration should be decreased from 0.2 mg/L, respectively to reach Class I of water quality.

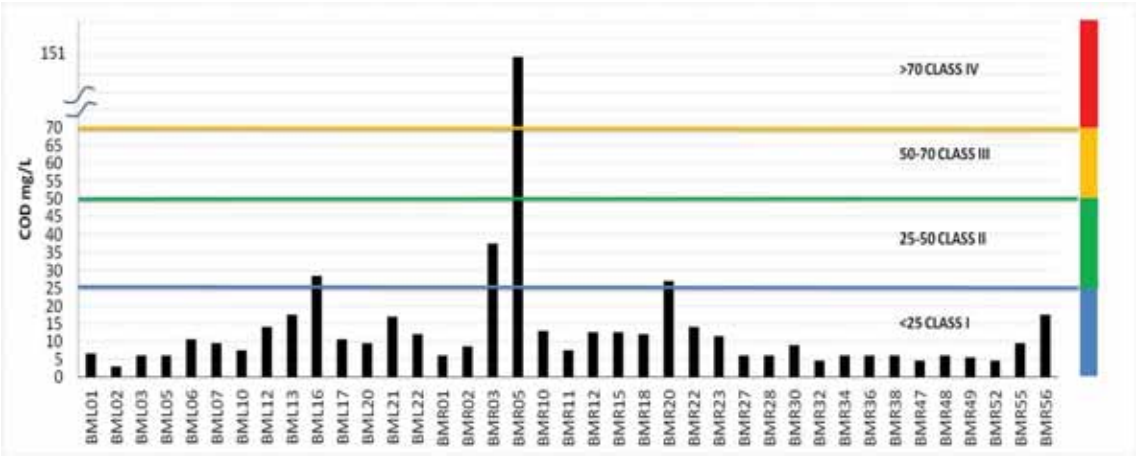

FIGURE 2
Classification of Water Quality in BMRB for COD Parameter

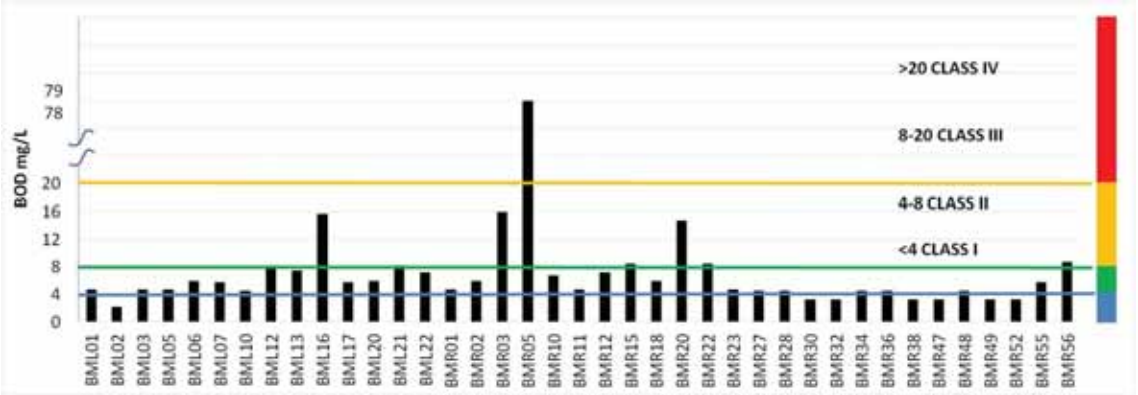

FIGURE 3
Classification of Water Quality in BMRB for BOD Parameter

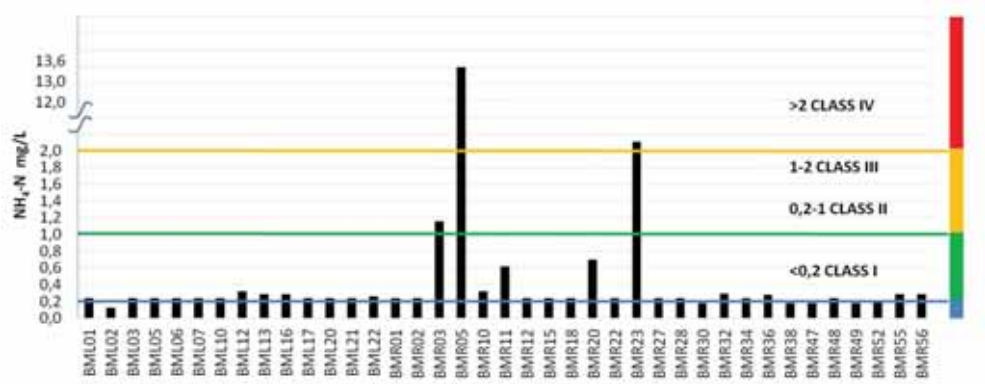

FIGURE 4
Classification of Water Quality in BMRB for NH_4-N Parameter

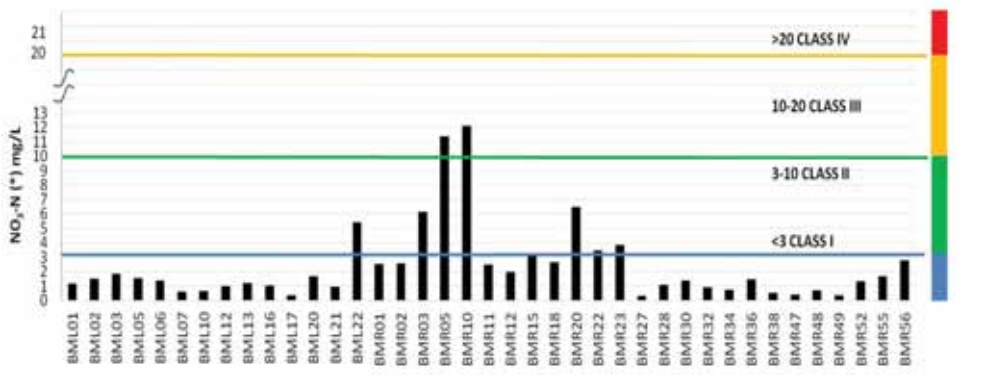

FIGURE 5
Classification of Water Quality in BMRB for NO_3-N Parameter

Annual averages of NO_3-N concentration in the lakes were mostly NO_3-N<3mg/L, which states that the water quality of lakes in the river basin are Class I (Figure 5). BMR05 and BMR10 are river stations and they are polluted especially by industrial sources. The annual average concentration of NO_3-N in these stations was over 10 mg/L indicating Class III water quality in highly polluted waters. The annual average NO_3-N concentration was not detected over 20 mg/L. In other words, none of the stations stated Class IV water quality in the river basin.

TKN concentration in most of the stations of the basin was in the range of 0.5-1.5 mg/L (Figure 6). The annual average concentrations of TKN in the stations indicated that the water quality class of the basin is mainly Class II. The highest concentrations were observed at industrial effluent discharge stations of BMR03 and BMR05 with Class IV water quality. According to Turkish Surface Water Quality Regulations, NO_3-N and TKN concentrations should be decreased from 3 mg/L and 0.5 mg/L, respectively to reach Class I of water quality.

Non-point (agricultural) or point sources (industrial or domestic wastewater) affect the water quality of surface water. These sources give nutrients to surface water. At these conditions, microorganisms and algae concentrations increase and dissolved oxygen concentration decreases and eutrophication occurs. For that reason, phosphorus concentration is an important parameter to evaluate water quality. Phosphate concentration in water is limited by EPA as 0.1 mg/L. According to Turkish Surface Water Quality Regulations, phosphate concentration should not exceed 0.08 mg/L to observe good water quality and to healthy use human activities.

Figure 7 depicts the annual average phosphorus concentration in the BMRB. Detected concentration in almost all stations was over 0.08 mg/L. The water quality of the stations was mainly Class II and Class III. Similar to other water quality parameters, phosphorus concentrations in BMR03 and BMR05 stations, which receive industrial wastewater treatment plant effluent, were above 0.8 mg/L and reaching about 2 mg/L with the water quality class of IV. The other Class IV water quality station is BMR20 which is located in Denizli area of the BMRB. There is a textile factory discharge near the sampling point. Agricultural activities and the use of pesticides are intensive. These results indicate that there is substantial phosphorus pollution in the river basin.

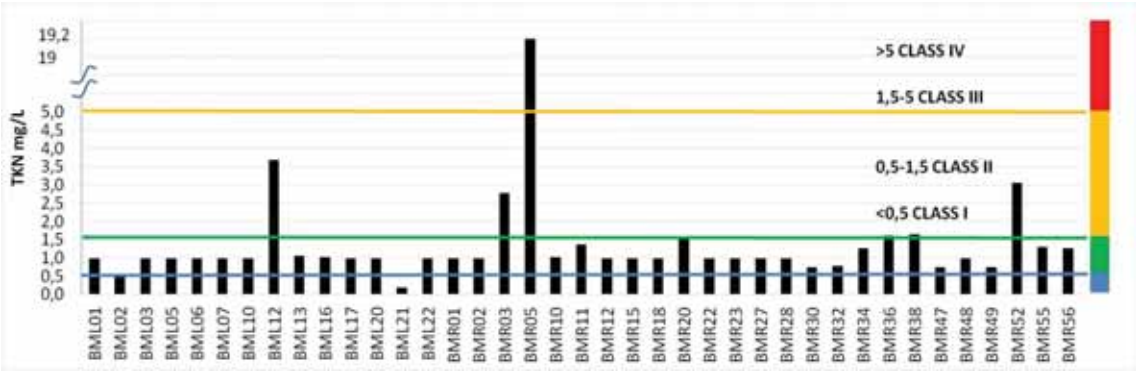

FIGURE 6
Classification of Water Quality in BMRB for TKN Parameter

Figures (4-5-6-7) show that the agricultural cultivations in this area are: sugar beets, vegetables, tree plantations, etc. The fertilization of soil by (P, N-NO_3 and N-NH_4) fertilizers created unfavorable conditions for the environment. In some cases, the NO_3 concentrations may be increased significantly in groundwater because of leaching.

Physico-chemical water classifications results were evaluated with regard to Regulation of Surface Water Quality Management accepted by the Republic of Turkey Ministry of Forestry and Water Affairs-2012 [14]. Annual averages of the monitored physico-chemical pollution parameters were used to determine the water quality class of stations and the whole river basin. The water quality class for each sample point given in Table 2.

The four groups used in the classification are expressed in different color such as Class I; Blue, Class II; Green, Class III; Orange, Class IV; Red. Twenty physico-chemical parameters were evaluated for all sampling points to determine the water quality class. The lowest quality physico-chemical parameter in the sampling point was considered in determining the class of water body. Water Quality Classification of Stations in Büyük Menderes River Basin (BMRB) was also shown in Büyük Menderes River Basin as a Table 2.The results indicated that water quality classes of the stations are Class III and Class IV. In other words, the water quality of the Büyük Menderes River Basin can be defined as Class III; middle water quality which is polluted and can be used for some industrial and agriculture purposes after proper treatment, Class IV; low water quality that can only be used after proper treatment. The reference station selection in BMRB was conducted by the Ministry. It was stated that six criteria as artificial areas, intensive agriculture, flow regulations, physico-chemical elements, industrial pressures, other pressures must be fulfilled for a site to be considered as a reference site. Reference water bodies, which are determined as “not at risk”, as a result of the risk analysis, are included in this assessment. The reference monitoring network can be extended with water bodies determined to have high status based on the data from the surveillance monitoring network and having minimum pressures among the sites that represent the water body type. Seasonal monitoring for the chemical pollutant parameters in the potential reference stations determined by the Ministry indicated that water quality class of BMR 27, BMR 32, BMR 47, BMR 48 and BMR 49 reference stations were Class III and Class IV for other reference stations as BMR 15 and BMR 36.

The regulation about Surface Water Quality Management for water quality classification based on physico-chemical parameters has been recently revised by the Republic of Turkey Ministry of Forestry and Water Affairs-2016 [15]. Some parameters were excluded, such as nitrite, and ranges of quality classes of some parameters were changed in revised regulation. Water quality classification in the basin stations does not change substantially when evaluated according to the revised regulation. The main water quality classes in the basin were Class III and Class IV.

Physico-chemical water classifications results were also evaluated with regard to the Water Frame Directive (WFD). Annual averages of the monitored physico-chemical pollution parameters were used to determine the water quality class of stations and the whole river basin. The three groups used in the classification for WFD are expressed in different colors such as High; Blue, Good; Green, Mode; Yellow. The water quality classification for sampling points relating to the Water Frame Directive (WFD) and Water Affairs’ Regulation (WAR) is given in Table 2. As can be seen in Table 2, the water quality of BMRB is good quality by means of WFD. Turkey's regulations are very strict than WFD. Because some sampling points (sixteen) observed as bad quality water named Class IV with WAR. In addition, four sampling point is found as good water quality by WFD.

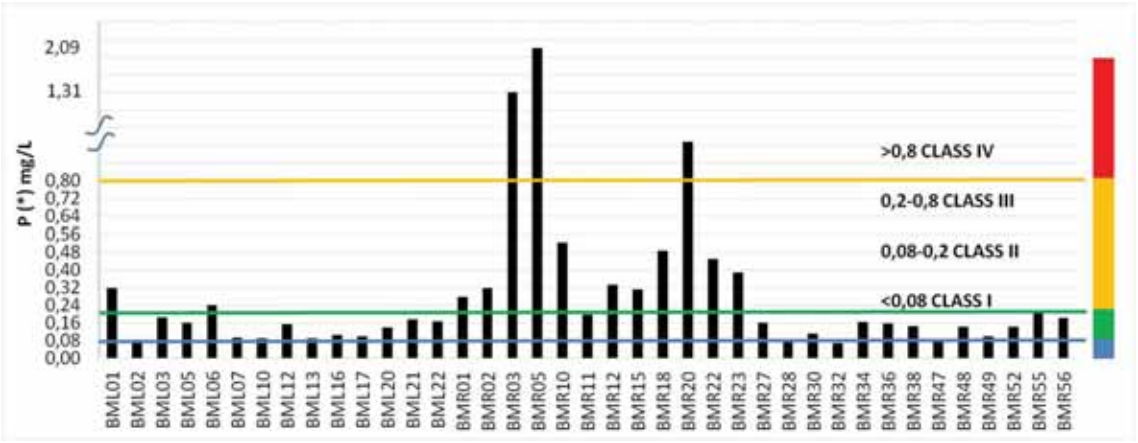

FIGURE 7
Classification of Water Quality in BMRB for P parameter

TABLE 2
The Water Quality Classification via Water Frame Directive (WFD) and Water Affairs Regulation (WAR)

Sampling Point	BMG01	BMG02	BMG03	BMG05	BMG06	BMG07	BMG10
WAR Classification	Class III	Class III	Class III	Class III	Class IV	Class III	Class III
WFD Classification	Mode	Good	Mode	Good	Good	Mode	Mode
Sampling Point	BMG12	BMG13	BMG16	BMG17	BMG20	BMG21	BMG22
WAR Classification	Class III	Class III	Class IV	Class III	Class III	Class III	Class III
WFD Classification	Mode	Mode	Mode	Mode	Mode	Mode	Good
Sampling Point	BMN01	BMN02	BMN03	BMN05	BMN10	BMN11	BMN12
WAR Classification	Class IV	Class IV	Class IV	Class IV	Class III	Class III	Class IV
WFD Classification	Mode	Mode	Mode	Mode	Mode	Mode	Mode
Sampling Point	BMN15	BMN18	BMN20	BMN22	BMN23	BMN27	BMN28
WAR Classification	Class IV	Class III	Class IV	Class IV	Class IV	Class III	Class III
WFD Classification	Mode	Mode	Mode	Mode	Mode	Mode	Mode
Sampling Point	BMN30	BMN32	BMN34	BMN36	BMN38	BMN47	BMN48
WAR Classification	Class III	Class III	Class IV	Class IV	Class III	Class III	Class III
WFD Classification	Mode	Mode	Mode	Mode	Mode	Mode	Mode
Sampling Point	BMN49	BMN52	BMN55	BMN56			
WAR Classification	Class III	Class IV	Class IV	Class IV			
WFD Classification	Mode	Mode	Mode	Mode			

CONCLUSIONS

Water quality evaluation of Büyük Menderes River Basin based on physico-chemical pollution parameters stated in WFR and Turkish National Regulations indicated that the current status of water bodies in the basin is either middle or low quality. According to WFD, the quality of the water should be improved to good status in terms of biological, hydrological and physico-chemical characteristics of basins. Therefore, management or prevention of pollution should be achieved and executed to these water bodies to reach good water status. Impact and pressure analysis will help to apply some improvement and prevention techniques such as ensuring reduction in discharge of pollutants from a point and non-point sources.

The existing treatment plants can be modified accordingly to reduce the discharge of investigated water quality parameters. Agricultural activities may be further controlled to reduce non-point sources.

ACKNOWLEDGEMENTS

This study was financially supported by TUBİTAK Main Project No: 112G12 and Subproject No: 112G083. The authors present their special thanks to Instructor Erhan Şener from Department of Geology at Suleyman Demirel University, Isparta/Turkey for his professional contribution in preparing the basin maps for the project.

REFERENCES

[1] Directive 2000/60/EC of the European Parliament and of the Council of 23 October 2000 Establishing a Framework for Community Action in the Field of Water Policy.
[2] Buijs, P. (2005) Surface Water Monitoring and Assessment under the EU Water Framework Directive. Proceedings of the 2nd International Yellow River Forum on Keeping Healthy Life of the River. 6, 236-246.
[3] Cieszynska, M., Wesolowski, M., Bartoszewicz, M., Michalska, M., Nowacki, J. (2012) Application of Physicochemical Data for Water-Quality Assessment of Watercourses in the Gdansk Municipality (South Baltic coast). Environmental Monitoring and Assessment. 184(10), 2017-2029.
[4] Fytianos, K., Siumka, A., Zachariadis, GA., Beltsios, S. (2002) Assessment of the Quality Characteristics of Pinios River, Greece. Water, Air and Soil Pollution. 136, 317-329.
[5] Traykov, I., Tosheva, A., Uzunova, E. (2010) Physicochemical Characteristics of Dam Lakes in Southwestern Bulgaria. Bulgarian Journal of Agricultural Science. 16 (3), 350-357.
[6] Ntislidou, Ch., Basdeki, A., Papacharalampou, Ch., Albanakis, K., Lazaridou, M., Voudouris, K. (2012) Ecological Water Quality and Management at a River Basin Level: A Case Study from River Basin Kosynthos in June 2011. Ecological Water Quality-Water Treatment and Reuse. 2-40.
[7] Arle, J., Mohaupt, V., Kirst, I. (2016) Monitoring of Surface Waters in Germany under the Water Framework Directive-A Review of Approaches, Methods and Results. Water. 8, 217-220.
[8] Brack, W., Dulio, V., Agerstrand, M., Allan, I., Altenburgera, R., Brinkman, M. (2017) Towards the review of the European Union Water Framework Directive: Recommendations for More Efficient Assessment and Management of Chemical Contamination in European Surface Water Resources. Science of the Total Environment. 576, 720-737.
[9] Kirmikil, M.(2019) The Evaluation of Land Consolidation Project by Water Managers in Rural Area; a Case Study in Karacabey. Fresen. Environ. Bull. 28(4A), 3097-3103.
[10] Huang, H., Won, F., Gau, Y., Zhang, Z., Annanurov, S., Zeng, X. (2019) Study on Measures to Improve Water Quality in Urban Lakes: Casing in Lake Nanhu in Wuhan. Fresen. Environ. Bull. 28, 2625-2632.
[11] Kosal, S., Sivri, N., Alver, U., Sonmez, Z., Seker, D. (2019) Quality Assessment and Chemical Composition of Surface Water in the Akcadag Basin (Malatya) in Turkey: A Case Study of Irrigation and Drinking Purposes. Fresen. Environ. Bull. 28(2), 895-901.
[12] Albayrak, S., Caglar, S., Mulayim, A., Kurt, G., Balkis, H., Cinar, N., Atabay, H., Tutak. B., Bahceci, H. (2019) A Case Study: Ecological Quality Status of Susurluk River Basin (Marmara Sea). Fresen. Environ. Bull. 28(2), 769-776.
[13] APHA, Standard Methods for the Examination of Water and Wastewater, 1998. 20th edn, American Public Health Association/American Water Works Association/Water Environment Federation, Washington DC, USA.
[14] Regulation of Surface Water Quality Management, Republic of Turkey Ministry of Forestry and Water Affairs, Official Newspaper, 30th September, 2012, Number: 28483.
[15] Regulation of Surface Water Quality Management, Republic of Turkey Ministry of Forestry and Water Affairs, Official Newspaper, 10th August, 2016, Number: 28483.

Received: **28.08.2019**
Accepted: **18.02.2020**

CORRESPONDING AUTHOR

Ebru Cokay
Dokuz Eylul University,
Department of Environmental Engineering,
Tinaztepe Campus, Buca Izmir – Turkey

e-mail: ebru.cokay@deu.edu.tr

© by PSP Volume 29 – No. 05/2020 pages 3614-3621 Fresenius Environmental Bulletin

PROBABILITY OF MAKING PROFITS IN GREENHOUSE PRODUCTION: ANTALYA - TURKEY CASE

Rahmiye Figen Ceylan*, Makbule Nisa Mencet Yelboga, Cengiz Sayin

Department of Agricultural Economics, Faculty of Agriculture, Akdeniz University, 07070, Antalya, Turkey

ABSTRACT

Greenhouse production is vital for Mediterranean countries in four season fresh fruits and vegetables supplies. However, with high investment and varying variable costs and high labour demand, greenhouse production provides fluctuating profits to producers. Accordingly, it was aimed to undermine factors affecting probability to make above average profits for 281 greenhouse operators surveyed in Antalya, Turkey in 2015. The farm level profit was detected as $10.184,63, while it was $2.639,77 per 0,1 hectares on average departing from primary data retrieved from greenhouse farmers in 2015. Accordingly, 82 greenhouse farms were making loss and 86 farms ended up with a below average profit. Following the logistic estimation of above average profit making situation, it was understood that the most important profit rising factor was ownership of the farmland. This is related with reduction of variable costs like rent or subcontractor commissions. Besides, western Antalya towns appeared as more profitable, keeping in mind the risk of lands' overuse in the long-term. However, the findings also indicated that corporatization of the sector is essential for reducing real tax payments and assuring limited responsibility of the farmers.

KEYWORDS:
Greenhouse production, profitability, logistic regression, Antalya

INTRODUCTION

Profit generation is the main objective of any sort of economic activity. Yet, profitability of an enterprise can be determined in various ways considering fixed and variable costs. Profitability of agriculture differs from other sectors with respect to time evaluation. It is well known that people involved in agriculture have to maintain their activities irrespective of their short-term profits or losses due to conditions specific to the sector.

Profitability in all terms is the ability to cover costs of productive activities and it is induced by many factors. Short term effects on agricultural profitability are more visible than other sectors as producer response to variations in consumer preferences is faster, especially for annual crops. Besides, the proximity of market structure to perfect competition is closer than other sectors especially when government intervention is minimised [1, 2, 3].

In accordance, it was intended within this study to measure factors affecting profitability of greenhouse operators in Antalya province of Turkey, where greenhouse vegetable production is a main and prominent agricultural activity [4]. Prior to proceeding, it is important to provide brief information on greenhouse production in Turkey and Antalya. The Mediterranean province of Antalya has abundant natural resources and ecological advantages to maintain four-season agricultural production. Antalya had a 1,55 % share in total agricultural lands occupied in Turkey by 2018, while its share in greenhouse production was 36,69 %. Besides, 3,57 million tonnes of vegetables were produced in plastic and glasshouses with a value of 9.5 billion TRY. This figure corresponded to 6.8% of Turkey's overall agricultural production and 64 % of national greenhouse production in 2018 [5]. When compared with 2010 data, it was understood that the share had reduced from 68 %. However, 2,82 million tonnes was the sum of the amount produced in Antalya then, signing to a 75 % rise from 2010 to 2018. These figures emphasize the dominance of the province in greenhouse production in Turkey [5, 6].

A field survey was conducted in the Centre, Kumluca and Serik towns of Antalya in 2015 in order to determine profit level of greenhouse operators. As a result of this survey, gross profit levels of 281 greenhouse operators were calculated. Gross profit for the study referred to the difference between the overall revenue retrieved for a particular farm activity and its variable costs involving seed, labour including family labour, irrigation and energy use. In opposition to fixed costs, depreciation of physical capital was included in variable costs for short term gross profit calculation [7].

After profit levels were calculated, it was intended to measure determinants of probability of an enterprise to receive above average gross profits. The factors affecting probability were considered as socio-demographic features of the farm operator and structural characteristics of the greenhouse farm. In

addition to these, the impact of taxation, which is important for government revenue generation, was considered as another effective factor [8].

Accordingly, the probability of a greenhouse operator to end up with an above average profit level was analysed with binary logistic regression. The average profit level of the focused sample was considered as a benchmark for the study. The main objective was to measure effectiveness of personal features of the operator and structural and economic characteristics of the greenhouse farm on probability to receive considerable level of profits.

MATERIALS AND METHODS

Material. The research was based on a field survey conducted in three towns (Centre, Serik and Kumluca) of Antalya that are popular for four-season plastic/glasshouse vegetable production. The sample for the survey was determined with random sampling [9]. Even though stratified sampling is preferred more in survey and scale based studies, random sample was selected for the study as all analytical processes were based on per 0,1 hectares or 0,247 acres. So, enterprise level variation was considered irrespective of the scale. Therefore, 281 operators were surveyed with 95 % confidence interval and the sample was distributed among the selected towns respecting number of greenhouse operators in these towns. Accordingly, 43 producers from the Centre, 183 producers from Kumluca and 55 producers from Serik towns of Antalya were surveyed randomly.

Methodology. The objective of the study was to measure indicators of probability to make profits for the concerned farms. The estimated probability is considered to range between 0 and 1. However, the detected probability was referred as 'making profits above average' or 'making profits below average' for the sample. Within this study, multivariate binomial logistic regression was used, which was developed to estimate dependent variables that do not have normal distribution characteristics [10]. Conversion of dependent variable referring to a choice or existence or inexistence of a situation takes place in binary choice models. The model was developed to overcome non-normality of error terms invalidating the OLS estimation assumptions [11, 12]. Therefore, the situational variable was estimated against quantitative and qualitative features involving information about greenhouse farmer, greenhouse structure and economic characteristics of the enterprise.

Within this study, the dependent variable was a dichotomous variable having values of '1 for the greenhouse farm having profit above the average profit level of the sample' and '0 for the greenhouse farm having profit below the average profit level of the sample'. Yet, the average profit level calculated for 0,1 hectares was 7.190,73 TL ($2.639,77) ($/TL exchange rate from the Central Bank of Turkey for 2015 was 1 $ = 2,7240 T.L. This rate was used hereafter.) for the sample. Therefore, the onset of the estimated equation is as following:

$$log[Pr(Y = 1 \mid x)] = ln\left[\frac{Pr(Y = 1 \mid x)}{1 - Pr(Y = 1 \mid x)}\right] = \sum \beta_i x_i + \sum \propto_i D_i + u_i$$

Here, in addition to the dependent variable (Y_i) explained above, X_i refers to the quantitative independent variables and D_i refers to the categorical variables involving information about the i^{th} greenhouse and greenhouse farmer. The proposed independent variables are as following:

TABLE 1
Description of independent variables

Abbreviation	Independent Variable	Feature
IT_{1i}	Income tax accrued to the greenhouse farm	Continuous – Quantitative – TL
PT_{2i}	Property tax accrued to the greenhouse farm	Continuous – Quantitative – TL
E_{3i}	Education level of the greenhouse farmer	Binary – (1: Secondary and above; 0: Below secondary)
A_{4i}	Age of the greenhouse farmer	Continuous – Quantitative
OS_{5i}	Ownership situation of greenhouse farm	Binary – (1: Owner; 0: Renter - subcontractor)
GG_{6i}	Structure of the greenhouse	Binary – (1: Glasshouse; 0: Greenhouse)
ID_{7i}	Classified income tax accrued to the greenhouse farm	Binary – (1 – paid tax above average of the sample; 0 – paid tax below average of the sample)
PD_{8i}	Classified property tax accrued to the greenhouse farm	Binary – (1 – paid tax above average of the sample; 0 – paid tax below average of the sample)
K_{9i}	Greenhouse takes place in Kumluca town	Binary – (1: In Kumluca; 0: In Serik or the Centre)
S_{10i}	Greenhouse takes place in Serik town	Binary – (1: In Serik; 0: In Kumluca or the Centre)
$T1_{11i}$	Declaration form of income tax – 1	Binary – (1: Enterprise; 0: Stoppage or Balance Sheet based)
$T2_{12i}$	Declaration form of income tax – 2	Binary – (1: Stoppage; 0: Enterprise or Balance Sheet based)

With continuous variables referring to income and property taxes born, binary variables respecting the average taxes paid were also included in independent variable list. It is important to note average tax levels born by these 281 greenhouse farmers. 1.067,65 TL ($391,94) was the average income tax, while average property tax was 214,68 TL ($77,71). Accordingly, dummy variables were classified due to the concerned averages.

Here, it is also essential to differentiate between the tax declaration forms of the agricultural enterprises classified under binary independent variables T1 and T2. Income taxes accrue on enterprises or producers are classified as real income tax or stoppage based income tax. Real income tax payers are also classified due to financial books they keep. While some of the producers keep their records due to agricultural enterprise accounts, some others pay taxes due to balance sheet records [13]. Taxpayers keeping agricultural enterprise books are responsible to declare their annual net income and 76 % of surveyed farms were taxed with respect to enterprise book declaration. Yet, stoppage based payers are responsible from their declarations and they are not responsible of book keeping due to their scale. 22 % of surveyed farms were taxed based on stoppages. Accordingly, large-scale farms were very limited in number that only 2 % of farms or 6 farms were taxed based on balance sheets.

In addition, checking the list of 12 independent variables, a suspect of correlation between variables can easily appear. Yet, it is also important to mention that this is a general list and exact variables inferred were determined within the analysis due to their relationships and detected correlations.

RESULTS

Profitability and Costs of Greenhouse Farms. Covered farming, covered with glass or plastic fiberglass, maintained in Antalya and relevant Mediterranean provinces, is vital both for domestic consumption and agricultural exports in Turkey. Greenhouses can control or regulate the environmental conditions for efficient plant growing [14]. 82 % of total greenhouse lands of Turkey takes place in three provinces of the Mediterranean region and Antalya ranked the first with 40 % by 2006 [15]. By 2017, the amount of land utilised for greenhouse production was 64 million hectares, of which 39 % was in Antalya [16]. Besides, Antalya is prominent in plastic/glasshouse vegetable production and the most significant products, which are important for agricultural exports as well, are different varieties of tomato and fresh pepper.

Greenhouse farming takes place in all districts of Antalya [17]. Yet, three towns were selected for the survey. The central town and the most significant producer towns of Kumluca from the west and Serik from the east of Antalya were selected. There was a multi-crop production scheme. However, 150 farms seemed to focus on tomato and 113 farms on fresh pepper production. Most of the farms (244) were composed of plastic houses with 76 %, as expected.

It is well known that greenhouse production in Antalya is maintained with a small scale capacity. Average production land was 0,45 hectares for the sample. Most of the farms constituted of pieced houses and the average number of pieces was two. Greenhouse production seemed to have its roots that average age of the plastic/glasshouses was 13,5 and most of the producers had more than 10 years of experience. Property ownership was high that 227 farmers were land owner corresponding to 85 % of the sample. Yet, for remaining renters and subcontractors, monthly rent of the whole enterprise was as $1.750. The average value calculated for owned lands was $36.197,50. These figures were used to compute the variable costs and gross income of the operators.

Considering the production and income figures, it was noted that average amount produced per year was 35 tonnes of various vegetables. The average gross income was $19.997,41, and variable cost was $9.812,78 respectively. Therefore, gross profit per farm had appeared as $10.184,63 on average. The highest farm level gross profit was recorded in Central town with $11.387,66, while the lowest was in Kumluca with $7.911,53 on.

Considering the gross profit levels, it can be noted that 113 of greenhouse farms seemed to produce a profit level above the average. The average gross profit per 0,1 hectares was $2.639,77. Accordingly, while 82 greenhouse farms were making loss, 86 farms ended with a below average profit. A significant inference is that 124 farms making either loss or below average profits were those situated in Kumluca. This can be considered as a result of traditional small scale plastic house farming and it was noted previously that glasshouse production is more profitable in terms of gross profits [18]. Besides, 31 of the farms taxed by stoppage declaration were not profitable.

When the amount of taxes born were considered, it was understood that 101 farms paid less than average income tax, while 262 farms paid below average property tax. The income tax figure referred to small scale subsistence farming once more and low property tax was related with ownership of enterprise and lands. In addition, farmers had a considerable greenhouse production experience with an average of 11 years, contributing to maintenance of the activities. To emphasize once more, significant number of farms had ended up with loss (82 farms) referring to almost 30 % of the farms. Therefore, undermining the reasons behind profitability of the greenhouse farms had been considered as important.

Characteristics of Greenhouse Farmers. Prior to estimating the relationship, farmer characteristics should be considered as they compose dummy variables explaining profitability variation of the farms. Average age of the farmers by the survey time was 42,68. This meant that greenhouse farming is mostly a business for middle aged farmers. Education level of farmers was relatively lower that 63 % of farmers had primary degrees with 8 years. There were only 14 farms operated by Bachelor's graduates. This was considered as an indicator of traditional farming practices and this quote was strengthened with the observed 'family farm' structure.

Family farms seemed to be managed by male owners, who were directly or indirectly supported by their spouses and family members. Farmers were working within the enterprise with an average of 260 days per year for productive activities. With inclusion of administrative duties, the average number of days that the producers worked in their farms with non-payment had appeared as 262. Besides, 36 producers were also holding out-of-farm jobs and they got paid 3.000 TL ($1.101,32) on average for 139 days. Spouses of the operators were working without payment in 268 out of 281 farms. Only 6 of these women were employed out of the farm as well, in

Mainly, for greenhouse farms situated in Kumluca, there appeared considerable correlation with other indicators. Income and property tax levels were correlated with their categorical reproduces as expected. In addition, tax declaration forms were correlated as well. Therefore, these variables should not be included in the regression simultaneously. Yet, the farm being glasshouse appeared as a variable that might lead multi-collinearity as it was correlated with all forms of tax declaration and property services sector with subsistence wage of the time 1.900 TL ($697,50). In addition, as well as the spouses, remaining family members were working in the greenhouse farms without payment. Therefore, the non-paid labour cost was calculated and included in variable costs of the enterprise as an alternative cost.

Factors Affecting Profitability. Afore mentioned standard equation involved all possible explanatory variables. Yet, the exact variables were determined following relationship analyses and structural tests. A priori, a significant relationship is expected between dependent and independent variables, while inexistence of the relationship is preferred between independent variables.

The correlation between dependent and independent variables were considerably low. Significance correlations with probability to receive above average profits were reached for three variables. These were the farm having situated in Kumluca town, the education level of the farmer and tax declaration forms. As most of the independent variables were dummy variables that do not have normal distribution, this is an expected situation [19]. Yet, the correlation between independent variables was checked as well and presented in Table 3.
and income tax variables. Age and level of education were in negative correlation. All signs were as expected due to the nature of the relationship. Therefore, the explanatories were selected watching these relationships.

The preliminary results for Logit estimation of profitability were indicated in Table 4.

TABLE 2
Correlation of independent variables with the dependent variable

IT_{1i}	:	-0,038 (0,53)	OS_{5i}	:	0,05 (0,40)	K_{9i}	:	-0,22 (0,00)***
PT_{2i}	:	0,04 (0,51)	GG_{6i}	:	0,03 (0,61)	S_{10i}	:	-0,08 (0,21)
E_{3i}	:	-0,109 (0,07)*	ID_{7i}	:	-0,04 (0,51)	$T1_{11i}$	:	-0,14 (0,02)**
A_{4i}	:	0,068 (0,26)	PD_{8i}	:	-0,02 (0,75)	$T2_{12i}$	:	-0,11 (0,06)*

* 90 %; ** 95 %; *** 99 % significance

TABLE 3
Correlation between Independent Variables

PT_{2i} & PD_{8i}	PD_{8i} & $T1_{11i}$	$T1_{11i}$ & $T2_{12i}$	$T2_{12i}$ & GG_{6i}	ID_{7i} & OS_{5i}
0,41 (0,00)***	-0,12 (0,05) **	-0,94 (0,00) ***	0,27 (0,00) ***	-0,11 (0,08)*
T_{2i} & K_{9i}	PD_{8i} & $T2_{12i}$	$T1_{11i}$ & GG_{6i}	$T2_{12i}$ & K_{9i}	ID_{7i} & A_{4i}
-0,14 (0,02) **	0,13 (0,03) **	-0,27 (0,00) ***	-0,38 (0,00) ***	-0,12 (0,06)*
PD_{8i} & K_{9i}	PD_{8i} & GG_{6i}	IT_{1i} & K_{9i}	GG_{6i} & K_{9i}	GG_{6i} & S_{10i}
-0,19 (0,00) ***	0,13 (0,04) **	0,43 (0,00) ***	-0,34 (0,00) ***	0,21 (0,00) ***
PD_{8i} & S_{10i}	PD_{8i} & IT_{1i}	K_{9i} & S_{10i}	E_{3i} & A_{4i}	
0,15 (0,01) **	0,18 (0,01) **	-0,67 (0,00) ***	-0,35 (0,00) ***	
IT_{1i} & ID_{7i}	IT_{1i} & OS_{5i}	E_{3i} & ID_{7i}		
0,53 (0,00) ***	-0,13 (0,03) **	0,18 (0,01) **		

* 90 %; ** 95 %; *** 99 % significance

TABLE 4
Logit estimation findings – 1

Variable	Coefficient	Z-Statistic	Probability
IT_{1i}	$-4{,}56e^{-05}$	-0,365	0,720
ID_{7i}	0,08	0,219	0,83
K_{9i}	-2,88	-5,079	0,00***
S_{10i}	-2,78	-4,726	0,00***
$T1_{11i}$	-0,68	-0,659	0,51
$T2_{12i}$	-1,19	-1,098	0,27
E_{3i}	-0,51	-1,494	0,14
GG_{6i}	-0,26	-0,746	0,46
PT_{2i}	$-1{,}40e^{-06}$	-0,012	0,99
PD_{8i}	-0,487	-0,732	0,46
A_{4i}	0,01	0,612	0,54
OS_{5i}	0,42	1,152	0,25
Constant	2,38	1,838	0,07**
McFadden R^2	0,13	**M.D.V.**	0,402
LR statistic	50,38 (0,00)***		

* 90 %; ** 95 %; *** 99 % significance

Due to the findings, other than the situation indicators and the constant estimate, the factors were insignificant. The effective factors were the greenhouses stance in either Kumluca or Serik towns. Yet, the constant appeared above the mean dependent variable and signed to negative impact of all factors. Due to McFadden pseudo R^2 statistic, which is a valid reproduction of R^2 for binary data [20], variation in the probability to make profits was explained by 13 %. The insufficient explanatory findings leaded us to reconsider the relationships among independent variables and the model was reformed accordingly.

TABLE 5
Logit estimation findings – 2

Variable	Coefficient	Z-Statistic	Probability
IT_{1i}	-0,06	-0,618	0,536
S_{10i}	-0,48	-1,471	0,14
$T1_{11i}$	-0,72	-2,488	0,01***
E_{3i}	-0,58	-2,039	0,04**
OS_{5i}	0,35	1,088	0,27
Constant	0,17	0,429	0,66
McFadden R^2.	0,14	**M.D.V.**	0,402
LR statistic	12,89 (0,02)**		
Hosmer-Lemeshow	33,65 (0,14)		
Andrews	41,77 (0,051)		

* 90 %; ** 95 %; *** 99 % significance

As a result of this estimation, individual parameter estimates did not appear fully significant and the count R^2 had appeared low as well. Yet, with reference to the binary nature of data other goodness of fit measures were checked. However, signs of the estimates fitted to the expectations and joint significance was confirmed with 12,89 at 95 % of confidence interval with Likelihood Ratio statistic. Besides, other relevant goodness of fit measures confirmed this interpretation. The probability value of Hosmer-Lemeshow test, which was above 5 %, indicated that the model had a good fit [21, 22, 23]. Andrews [24, 25] test findings were in the same line, although having a lower significance. In addition, independent variables explained 58 % of the variation, taking the constant as 0,17.

When interpretation of the parameter estimates were considered, it is first essential to compute estimated probabilities via antilog transformation as the primary results indicated log of odds, representing the logarithmic form of the probability [26].

TABLE 6
Expected Probabilities of Logit Estimates

Variable	Expected Probabilities
IT_{1i}	-0,01
S_{10i}	-0,14
$T1_{11i}$	-0,41
E_{3i}	-0,23
OS_{5i}	0,06
Constant	0,01

Accordingly, it can be briefly noted that the probability for a greenhouse farm to make profits was 1 %, when no specific factor was considered. The profit making probability rises by 6 % for farm owners. However, amount of income taxes born negatively affected the profitability. With a 1 TL ($0,37) rise in income taxes born, probability to make profits declined by 1 %.

The negative relationship between rising education level and profitability was significant. If the farmer had a secondary degree at minimum, the probability of ending with more than average profit declined by 23 %. Considering the negative correlation between age and education level of the farmer

and traditional characteristics of greenhouse farming in the region, this is an expected result. Yet, it should be kept in mind that having less profits than average does not mean making loss for all the cases.

The negative impact of tax declaration status of the farm was in conformity with the expectations. For farms, which have enterprise status and taxed based on real income, the probability of making profits declined by 41 %. This is a significant effect of taxation status on the probability. Farm having situated in Serik town of Antalya leaded to 14 % declination. This is also related with the fact that western Antalya is more prominent in greenhouse production.

The most significant probability rising factor for the selected sample was related with the ownership situation of the greenhouse. If the farmer is the owner of the facility, probability of the farm to make above average profits rose by 6 %. A question may arouse related with the property tax load of the farms. Yet, depreciation of the equipment seemed to cover property taxes and owners, in opposition to renters or subcontractors, achieved to manage their costs.

Following this computation, the probability for the i^{th} greenhouse farm of making above average profits was forecasted. Accordingly, it was detected that probability mean was 0,4. Most of the farms have a probability to receive a below average profit. 237 farms might reach 50 % of the average profit level referring to 84 % of the farms. Share of the farms having probability to receive more than average profits was 15 %, while only 3 farms assured complete profitability. Therefore, this is another indicator of traditional maintenance of the greenhouse production in the region.

RESULTS AND DISCUSSION

Greenhouse production opportunities are abundant especially in Mediterranean countries, assuring four season fresh fruits and vegetables supplies. However, after establishment of the farm, it becomes inevitable for the farmer to maintain his/her production activities irrespective of profitability of their activities in the short term. This is mostly related with high investment costs born. And also it is hard to convert greenhouse farms to open fields in the short-term. However, this does not mean continuity of activities with zero or below zero profits all the time. Accordingly, it is essential to evaluate sustainability of the sector with respect to profitability.

The intention was to determine factors affecting profit making situation among green/glasshouse farming in Antalya, Turkey based on survey data. Out of the whole sample of 281, 113 of greenhouse farms seemed to produce a profit level above the average. The average gross profit per farms was \$10.184,63, referring to \$2.639,77 gross profit per 0,1 hectares. Yet, the variation of profits depending on the situation of the farm in three different towns of Antalya, ownership situation or the taxation forms was high among the sample farms. Therefore, these situational factors and farmer characteristics were considered as factors affecting the profitability. Accordingly, the probability of an operator to receive above average profits for its activities was estimated. The gross profits calculated for 0,1 hectares was \$2.639,77. Therefore, the reasons affecting the potential to exceed this calculated average were considered as essential to project future profitability.

Due to the logistic regression estimates, it was understood that farm ownership is the most effective factor in above average profit making potential of the farm. This refers to minimisation of variable costs like rent. If farms are owned, neither rental cost nor the subcontractor commission accrues and the gross profit level of the farm, calculated with deduction of variable costs from the farm income, rises. Or else, this finding can be interpreted with regards to the high level of farmland rents in the region leading to higher variable costs.

Yet, following confirmation of the economic expectations with regards to the profitability of western Antalya, profit-reducing tax levels and taxation form of the farm had appeared as important factors. It was understood that probability to make above average profits declined for real taxpayers. It is well-known that real taxpayers both bear high taxes and they have full responsibility in terms of Turkish tax law. These book-keepers are responsible to declare their all activities and they need to cope with taxes as well as varying operational costs despite their small scale. However, considering the intensity of green/glasshouse production in the region and long-term experiences of operators in farming, this taxation effect suggests development of corporate structures. Or else, professionalization of greenhouse production is expected to produce more profits for the concerned farms.

In addition, one factor should be kept in mind. As mentioned above, western Antalya is a profitable greenhouse centre. However, we know that overuse of lands would lead loss of productivity and profitability in time. So, this confirmation on the stance of the farm should be considered as a short term finding. The dispersion of greenhouse lands with proper use of new technologies and infrastructure investments should be promoted as Mediterranean climate is widespread in Turkey, providing opportunities to new farmers.

ACKNOWLEDGEMENT

The paper is based on the data retrieved within the project entitled ‘Tagem-14/Arge/63 Taxation in Agricultural Markets and Effects of Taxation on

Price Formation: Example From Antalya Greenhouse Production' funded by General Directorate of Agricultural Research and Policies of Ministry of Agriculture and Forestry of Republic of Turkey – TAGEM.

REFERENCES

[1] Korkmaz, V. (2015) Supporting Policies for Agricultural Products: Comparison of Turkey and the EU. Unpublished MSc Thesis, University of Adnan Menderes, Turkey, retrieved on: 15.05.2019 (In Turkish)

[2] Tunc, H. (2012) Structural Features and Importance of Agriculture Sector. http://www.havvatunc.com/2012/08/13/tarim-sektorunun-yapisal-ozellikleri-ve-onemi/, retrieved on: 15.05.2019 (In Turkish)

[3] Tokatlioglu, I. (1999) Development of Competition Concept in Economic Analysis. Journal of Ekonomik Yaklasim. 10(33), 5-26. (In Turkish)

[4] Topkaya, S., Desbiez, C., Ertunc, F., (2019) Presence of Cucurbit Viruses in Ankara and Antalya Province and Molecular Characterization of Coat Protein Gene of Zucchini Yellow Mosaic Virus Turkish Isolates. Fresen. Environ. Bull. 28, 2442-2449.

[5] TUIK (2019) Turkish Statistical Institute, https://biruni.tuik.gov.tr/medas/?kn=92&locale=tr, retrieved on: 15.05.2019

[6] Kutlar, I., (2019) Analysis of the Sources of Agricultural Information Available to Greenhouse Growers in Turkey. Fresen. Environ. Bull. 28, 6825-6831.

[7] Wang, J., Wailes, E.J., Cramer, G. (1996) A Shadow-Price Frontier Measurement of Profit Efficiency in Chinese Agriculture. American Journal of Agricultural Economics. 78 (1), 146–156. https://doi.org/10.2307/1243786

[8] Aydin, F. (2007) Taxation of Agriculture in Turkey and the European Union. Asil Publications, pp. 266, Ankara. (In Turkish)

[9] Yamane, T. (2000) Elementary Sampling Methods (1st ed). Istanbul, TR: Literatur Publ. (Translated by: Esin, A., Bakır, M.A., Aydin, C. and. Gurbuzsel, E. (In Turkish)

[10] McFadden, D. (1973) Conditional Logit Analysis of Qualitative Choice Be. In: Zarembka, P., Ed., Frontiers in Econometrics (1974), Academic Press, New York, 105-142.

[11] Cox, D.R. and Snell, E.J. (1989) Analysis of Binary Data. Chalpman Hall/CRC, 2nd ed. pp: 240.

[12] Efron, B. (1988) Logistic Regression, Survival Analysis, and the Kaplan-Meier Curve. Journal of the American Statistical Association. 83(402), 414-425.

[13] GIB (2015) General Income Tax Notification, No: 290. Directorate of Revenue Administration, https://www.gib.gov.tr/290-seri-nolu-gelir-vergisi-genel-tebligi, retrieved on: 25.12.2015. (In Turkish)

[14] Korkmaz, C. and Tezcan, Y.N. (2018) A New Approach to the Determination of Heat Losses In The Greenhouse: Thermal Cameras. Fresen. Environ. Bull. 27, 7691-7690.

[15] Tuzel, Y., Oztekin, G.B., Karaman, I. (2010) Comparison of Vegetable Production in Modern and Traditional Greenhouse Enterprises in Serik Town. Journal of Ege University Faculty of Agriculture. 47(3), 223-230. (In Turkish)

[16] Sayin, C., Ceylan R.F., Mencet Yelboga M.N., Ozalp, M., Ilbasmis, E., Sav, O. (2017) Impact of Taxation on Price Formation in Agricultural Markets: Example from Antalya Greenhouse Production. Journal of Agricultural Science. 9(6), 120-130.

[17] Erdermir, T. and Erler, F. (2018) Fumigant Toxicity of Five Plant Essential Oils Against Citrus Mealybug, Planococcus Citri Rosso (Hemiptera: Pseudococcidae). Fresen. Environ. Bull. 27, 3231-3235.

[18] Ozkan, B., Hatirli S.A., Ozturk E., Aktas A.R. (2011) Profit Efficiency Analysis of Tomato Production in Antalya Province. Journal of Agricultural Sciences. 17, 34-42. (In Turkish)

[19] Jarque, C.M. and Bera A.K. (1980) Efficient Tests for Normality, Homoscedasticity and Serial Independence of Regression Residuals, Economics Letters. 6, 255–259.

[20] Gujarati, D.N. (2003) Basic Econometrics. New York: McGraw Hill Book Co.

[21] Hosmer, W. and Lemeshow S. (1989) Applied Logistic Regression. Wiley Series in Probability and Statistics, New York. pp: 375. https://doi.org/10.1002/sim.4780100718

[22] Mora, J. and Moro-Egido, A.I. (2008) On Specification Testing Ordered Discrete Choice Models. Econometrics, MDPI, 143 (1), pp.191. 10.1016/j.jeconom.2007.08.004. hal-00501801

[23] Canary, J.D. (2013) Grouped Goodness-of-Fit Tests for Binary Regression Models, Unpublished PhD thesis, University of Tasmania.

[24] Andrews, D.W.K. (1988a) Chi-square Diagnostic Tests for Econometric Models: Introduction and Applications. Journal of Econometrics. 37(1), 135-156.

[25] Andrews, D.W.K. (1988b) Chi-Square Diagnostic Tests for Econometric Models: Theory. Econometrica. 56, 1419–1453.

[26] Semple, H.M. and Brierley J.S. (2000) A Logit Analysis of Problems Affecting Domestic Food Production in Guyana. Social and Economic Studies (Sir Arthur Lewis Institute of Social and Economic Studies, University of the West Indies). 49(1), 211-224.

Received: **19.09.2019**
Accepted: **07.03.2020**

CORRESPONDING AUTHOR

Rahmiye Figen Ceylan
Department of Agricultural Economics,
Faculty of Agriculture,
Akdeniz University,
07070, Antalya – Turkey

e-mail: ceylan.figen@gmail.com

© by PSP Volume 29 – No. 05/2020 pages 3622-3632 Fresenius Environmental Bulletin

DOES GRASS-COVERED SOIL SYSTEM GUARANTEE BETTER WATER RETENTION IN SOUTHWEST CHINA DURING WINTER-TO-SPRING? THE OBSERVING EVIDENCE FROM LAB

Yingping Dong[1,2], Yongkuan Chi[2], Kangning Xiong[2,*]

[1]School of Environment, Resources, and Development, Asian Institute of Technology, 12120, Klong Luang, Pathumthani, Thailand
[2]Guizhou Normal University, School of Karst Science/ State Engineering Technology Institute for Karst Desertification Control of China, 550001, Guiyang, Guizhou, China.

ABSTRACT

Although the viewpoint of 'grass-covered land conserves water better than bare land' has been applied in ecological engineering, ecological recovery design, and policy-making as well as ecological services valuation and other academic research, etc, we challenge it could be applied equally worldwide. Based on system theory, the grass-covered pot with soil as shallow as 10cm is regarded as a minimum ecological system unit which imitates the intensive degraded Karst physical soil condition and uncovered pot severed as CK to compare with. A popular man-made grassland variety, the L. *perenne*, and a model grass variety for evapotranspiration (ET) estimations, the F. *arundinacea* were selected to test grass function in the condition of controlling water input in the lab. And the irreversible water loss, the ET, of those grass-covered soil system (GSS) and uncovered soil system (USS) are directly weighting to give precise measurement of water conservation efficiency for the whole soil system (SS) with drought stress or non-drought-stress situation under typical southwest China karst climate. The results show that grass coverage does not guarantee better water conservation for grass-covered soil systems (GSS) comparing to uncovered soil systems (USS). On the contrary, the grass community consumes more water for growth. Total water loss of GSS ranges from -6g/d/ 0.045 m^2 ~ -256g/ d/0.045 m^2 (equals to -0.13kg~-5.69kg/d/ m^2); when confronting interval drought stress at different levels, grass communities reduce the strength of photosynthesis and respiration to decrease water loss of the system. Furthermore, water transfer may happen between elder leaves to younger leaves to maintain the dynamics of the whole system. However, the total amounts of GSS are still higher than USS. Only when the extreme drought (soil moisture <5% and grass being permanently withered) occurs or within 70 hours after re-watering to this extreme drought soil, GSSs save slightly more water than USSs. Unfortunately, when soil ecosystem has the opportunity to gain water directly from the air humidity, grass coverage prevents soil system from absorbing dew supplement which is far from negligible since the maximum water gain from dew is as much as 0.133kg/m^2 somewhat higher than 1mm (0.126g/ m^2) precipitation. Altogether, GSS has never shown enough evidence on its soil water conservation competence. Additionally, 2 different grass varieties have shown different water loss amounts, drought-stressed sensitivity and response strategies depending not only varieties themselves, but also on climate variations. Relatively, L. *perenne* makes better use of water whenever it is available than F. *arundinacea* does.

KEYWORDS:
Grass-covered soil system (GSS), uncovered soil system (USS), irreversible water-loss (WL)

INTRODUCTION

As one of the biggest continuous karst worldwide and the vulnerable area (Sweeting, 1993) [1], southwest China's karst rock desertification (RD) area urgently needs ecosystem re-construction in terms of not only the rationality of land use /land cover change in macro-scale but also the creation of fine local ecological conditions in micro-scale especially sound ecology and better productivity of soil system [1]. Because RD imposed huge negative pressure on local ecology, societies, and economics surroundings to southwest China's karst region and caused extreme poverty and deconstruction of ecosystem which required integrated management [2-8].

In order to rebuilding local ecosystems and finally halt RD, great efforts have been devoted to southwest China's karst, including numerous policies i.e. Guidance on Comprehensive Recovery in southwest China karst RD area [9], Comprehensive Rehabilitation of RD Planning Framework for southwest China's RD region [10]; Ecological Construction Programs [11], China National Develop-

ment & Reform Committee and China national forest conservation program [12], and grass-based animal raising projects for poverty mitigation in the related region.

Therefore, rebuilt or newly-built grassland becomes important re-construction models for RD rehabilitation engineering [13].

The opinion of 'grassland conserves soil and water better than bare land' contributes to some central government policies or decision-making processes [14]. Due to its ecological function of soil and water conservation as well as the economic value of raising animals thus benefiting human livelihood, perennial man-made grassland turns out to be the better choice than cropland for rehabilitation or in halting further degradation in the RD region.

But 54 years' meteorological data collected from 88 sites supports a high frequent drought attack on these areas periodically from winter to spring especially March to May [15]. Unluckily, the drought situation is exacerbated by the complicated karst topography and RD conditions. Hence, 90% of all the precipitation is reported concentrating in summer [16]. Furthermore, averagely 55 days of drought annually occur in these areas with the longest drought spanning up to 35 days [17].

Drought creates much complexity for perennial grass adaption to some of these areas during the winter to spring period. It is a water shortage that affects the local ecosystem, not soil erosion caused by heavy rainfall in drought season. Hence, the grassland ecosystem services value can no longer be estimated by surface runoff reduction during this time. Instead, weather grasses buffer or compete for water with other organisms in the soil system needs to be clarified.

Soil water analysis is crucial for land cover change and also important to reflect ecological impacts of grasses, because soil water is a decisive factor for soil chemical components including SOC (soil organic carbon) and nitrogen storage which reflects potential productivity of soil ecosystem. Soil water retention is also vital for the health of soil ecology, such as tiny soil animals' living, i.e., California horn snail and soil microbes propagation as well as other forages in the soil depth of 0~120cm [18-24]

Even many methods are applied to measure soil water content including observation methods like gravimetric/ thermostat-weight technique, TDR, tension-meters method, and simulation methods as remote sensing, Gamma-ray attenuation, Ground Penetrating Radar (GPR) which applied more or less mathematic equation or models (such as Richards' equation, Compella's parametric retention model) [25-28]. These methods require labs, facilities, metadata, field verification and a rather long time for simulation but finally reach site-specific or estimated results that are difficult to use across scales or to compare with other sources of data. Because there exists some inevitable discrepancy between simulation and observatory data which might come from the collapse of macrospore in soil or the soil shrinkage due to the process [29-30]. It Additionally, soil water retention capacity or soil moisture owns so much heterogeneity in dry situations thus even proper sampling results constitute challenges to scientists and engineers [31-33].

Therefore, some simple, easy, cheap, but reliable methods at the local level and comparable results are seriously needed [34].

Considering the unique abiotic characteristic in this degrading region such as shallow and thin soil, diversified soil types, cloudy weather with high humidity, and warm winter [35], we tried to solve this problem based on 'system theory'. To regard grass-covered or uncovered pot with a certain kilogram of soil as a minimum ecological system unit, we mimic the intensive degrading karst at both soil quality and depth as shallow as 10cm with typical local thin soil. Irreversible water loss with or without drought-stress, equivalent to the ET, of GSSs or USSs are directly weighed to reflect precise water retention efficiency for the whole soil systems. Through which the results of one site can be compared with others across scales.

Our work is supposed to arouse attention on the ecological response diversity existing in introduced man-made grassland to a specific area like southwest China.

MATERIALS AND METHODS

Research Site and Materials. The Seedlings grow from Aug. 2013 to the end of Mar. 2015 in a greenhouse in Guizhou Normal University (GNU) campus, Yunyan District, Guiyang city, Guizhou province, P.R. China. Soil components were collected from the top 30cm of soil under Chinese Pine trees at the campus of Guizhou Normal University, which is typical karst calcareous soil with a high content of Ca. Experimental pot size was 15cm X 30cm X 10cm (Width X Length X Depth). 4,500~5,000g soil was added to each pot. Compound fertilizers were embedded 3cm above the bottom of each pot. Seeds of *Loliumn perenne* as typical man-made grassland variety and *Festuca arundinacea* as model grass for evapotranspiration (ET) measurement were selected and inoculated in Petri dishes to 5~6cm height, then each seedling was transferred in line of 3.0cm apart and 2.0cm width in rectangle pots.

The core experiment spans the whole winter-spring drought season from Nov. 2014 to the end of Mar. 2015 when the grass community is equally mature.

L. perenne, a most popular man-made grassland variety and F. arundinacea, a model grass

variety for evapotranspiration (ET) estimation were selected to test grass function in the condition of controlled water input in the lab. Classifying grass-covered pots into different canopy coverage ratio, two grass varieties covered systems and an uncovered bare soil system were observed in detail.

Research Method and Hypothesis. Research Hypothesis and Experimental Condition Settings. To-Test Hypothesis: Grass-covered soil system (GSS) conserves water better than uncovered soil system (USS) in drought season of SW China's karst area.

Sub-Test hypothesis: GSS losses less weight (water) than USS under various conditions.

Besides, 3 basic assumptions and a simplified premise are also essential components for testing: Assuming that all the materials grow in soil with adequate nutrients; Assuming glasses of the green house has 0 effect on grass; Assuming wind causes equal effect to all types of soil systems.

Research methods. Regarding grass and soil in the same pot as a basic ecological cell, we explored water input and output for these cells under controlled conditions.

To simplify abiotic environment that around introduced grassland ecosystem, we mimic nature in terms of geographic and meteorological conditions.

Say, geographic condition, we collect typical soil from cropland in RD area, retaining mini-stones unaffectedly, then, put them into 10cm-depth pots and setting pots in a slop angle of 15° to mimic the real typically introduced grassland situation in field.

Since historical meteorological data analysis supporting that firstly from December to March there was little amount of precipitation (around 10% annual amount); secondly, there obviously were as many rain-days, for example, as 19days for February in 2013, but little effective rainfall (10.1mm for the whole month) happened in these periods, therefore, there were very little chance for surface run-off to remove surface soil horizontally by natural precipitation. Consequently, we assume local surface run-off in our system equals to 0.

With this *ceteris paribus*, to better illustrate drought effect, we regards precipitation as the only variable parameter in our systems.

Our setting for the experiment can well represent some of the typical peak-cluster depression area for two reasons. Firstly, biotic conditions like the air temperature, humidity, depth of soil, and luminous energy et.al. retain naturally in mountainous karst area where local soil ecosystem suffers at different level of rocky desertification; secondly, chances of strong wind and heavy flood, the ignored factors, are very rare.

Three typical winter-spring droughts in terms of lasting 10-, 21-, and more than 28-days were set to compare between the grass-covered and uncovered soil systems. Grass responses and weight shifts of each system were observed and recorded in chronological order to provide detail for direct measurement or monitoring of water loss rules.

Three levels of drought stress were classified according to the measurement of soil volumetric water content as low as 15~18%; 10~15%; or <10%. First level, namely as a checkpoint for drought stress--above-vegetation appears slightly stressed; second level-- medium drought stage, there are more than 3 types of symptoms above ground including 30% of leaves withered, yellowish, and shrunk to 60~80%; Lastly, when more than 70% leaves withered, additional 10 days of drought were given to make the extreme drought stage. Because different levels of drought are natural situations in winter-spring season of SW China's Karst, thus except extreme drought stress, others are all called interval drought or normal conditions.

As CK, a group of uncovered pots are placed side-by-side with 2 groups with grass covered.

At 8:00am every morning, the maximum leaf length and width were measured and recorded. Soil volumetric water content detection was conducted every 3 days. Each pot samples 5~6 spots to get the average with least error. Around 30~60 days' later, we clipped biomass over 5cm height, and weighted leaves and stems as fresh weight, then, dry-up to get dry matter (DM) weight of the grasses.

Experiment started from full-matured of grass community (height average >20cm, coverage ratio 50~100%), with each treatment is designed to repeat 3 times.

LA104, an electronic scale with a minimum measurement unit of 1.0g, was used for fresh biomass weighting. Rulers of needle-like sharp tip are made to ensure the height measurement would not be intervened by dry grass-covered or non-even soil surface. Field Scout TDR 300+ (by Spectrum Technology, *Inc*) was used for water volumetric content detection of soil. Electro-thermal drying box (202-OAB) was set to 80°C for 48h for DM (dry matter) weighing. Finally, calculation and curve fitting were conducted with Excel-2010.

RESULTS

The Continuing Water Retaining Competence Comparison under One-off Water-input. Figure 1 shows how fast water-loss from soil system could be. The average speed of water loss under the climate of local conditions and one-time-input treatment from 2 different perspectives in terms of 1) how long it may take for 500g of water-loss; 2) how fast daily and accumulated water loss could be. Figure 1(a) shows USS required over 23

days to consume 500g water; while *L. perenne*-SS and *F. arunidinacea*-SS cost at least 6~18 and 7~20 days respectively to use-up the same amount (see Figure.1(a)).

Detailed data of 21 days sequential observation revealed that firstly, the uncovered-soil system (USS) lost 344g (76.44kg/m^2) within these day, while F. Araundinacea-SS lost 546g (121.33 kg/m^2), about 1.59 times of its uncovered partner (L. Perenne-SS lose 595g (132.22kg/ m^2), equals to 1.73 times of USS) (see Figure 1(b)). Secondly, a total of 7 days was found that GSS did not lose more water than USS. For 5 days, USS lost more water than GSS. Separately in the 1st, 2nd, 5th, 7th and 10th day, the loss amount ranged from 2 to 16g per pot (0.44~3.56 kg/ m^2) (see Figure 1(c)). For 2 days, air moisture supplements were input under the dew-point temperature to USS which caused slight net weight-gain, up to 3g to 8g (approximately were 0.67 and 1.77kg/ m^2), from air moisture. Similarly, weight-gain phenomena were also found in L. Perenne-SS and F. arundinacea-SS, less than or equal to 6g per pot (about 1.33 kg/ m^2).

Rather than isolated parameters, daily water-loss data for all type of soil system suits the moving-average analysis as Figure 1 indicates.

Systematic Water Loss Monitoring at Different Level of Drought. We tested different soil systems for 10 days in non-stressed condition, continuous drought conditions (watering every 10 days), and extreme drought conditions (20 days to 30 days), consequently, soil volumetric water content of which was less than 10% at 3.8cm and 12% at 7.6cm topsoil. Figure 2 display the results that, firstly, grasses soil system significantly consumed larger amount of water than uncovered soil system. Only if under extreme drought condition, can L. *perenne* save small amount of water which was actually only higher slightly than USS did. However, how much would that amount contribute to soil ecology was not certain.

Figure 2 displays the results that, firstly, the grass-soil system significantly consumed a larger amount of water than the uncovered soil system. Only if under extreme drought conditions, can L. perenne save a small amount of water which was only higher slightly than USS did. However, how much would that amount contribute to soil ecology was not certain.

We tested normal growth grass-soil systems treated by interval drought at two levels of canopy coverage 50% (cutting) and 100%. There were 2 to 5 times it has been observed in the repeated test that daily loss of USSs was higher than the GSSs. In repeated group 1, USSs loss slightly more water

TABLE 1
The Water Loss Observation of Different Soil System In Karst Winter

Types of System	Depth from surface (mm)	Mean ET (g/0.045m^2/d)	df	WRP in winter (d)	WL within 21 days
GSS	38	14.96±7.88	55	6~20	595
	76	15.95±8.49	55		
USS	38	11.89±6.52	55	>23	344
	76	15.95±8.49	55		

Note: GSS, grass-soil system; USS, uncovered soil system; ET, evapotranspiration; WRP, water retaining period for 500g/ 0.045m^2; WL, weight loss of the whole mini-system.

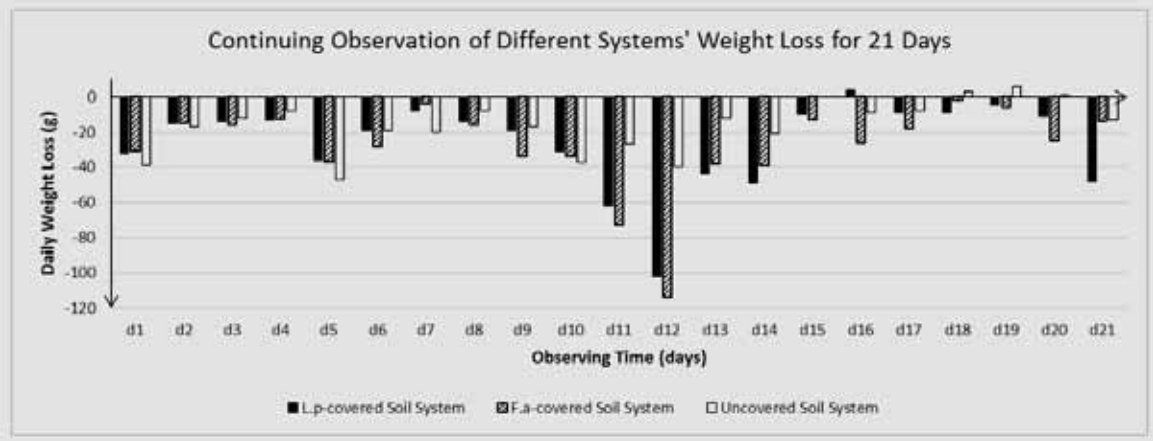

FIGURE 1
Monitoring Daily Water-Loss In Karst Winter For 21 Days (G/ 0.045m2/ Day)
Note: (a)The water loss speed in different soil system; (b) accumulated water loss for 21 days; (c) daily water loss speed and its move average.

than cutting GSSs but dramatically less than 100% coverage of the GSS. In repeated group 2, accumulated water loss of USSs remained lower than all the GSSs including cutting or full covered soil systems. This difference might be due to the different health conditions of grasses. For repeated group1 the grass as affected by a kind of small black insect before cutting.

When 70% of above-ground grass withered, the grass-soil system was exposed under extreme drought stress for an additional 10 days. In the 7 of 10 day, GSS saved more water than USS did while oppositely in non-stressed soil system. Consequently, 10-days monitoring of the extreme stressed controlled group found 97g of water loss in L .*perenne* pot (2.16kg/ m^2), 168g of loss in F. *Arundinacea* pot (3.73kg/ m^2), and 119g of loss in uncovered pot (2.64kg/m^2). Comparably, for non-stress group, L. *perenne*-SS lost 618g (13.73 kg/m^2) and F. *Arundinacea-SS* lost 463g (10.28 kg/m^2).

It is impressive that L. *Perenne* saved an average of 4.88 kg/m^2 more than uncovered under extreme drought stress conditions for the extra 10 days. But the F. *Arundinacea* spent 10.89 kg/m^2 more than USS did under regular growth conditions in a similar situation. 200ml water into GSS and USS (each treatment repeated 3 times), and observed for sequential 30days afterwards. Result details displayed in Figure 2.

Systematic Weight Loss In relation to Soil Moisture Shift. It can be told from the curves of right part of Figure 3 that USS has greater waves than both types of GSS. Because soil moisture moved within 10% during a typical cloudy winter day in USS yet only half of this amount in both GSSs. When we looked further at the left part on the hourly weight changes of systems, similar routes were found in all the 3 types of systems that the apex of water loss happened at the time of 12:00 when the highest temperature occurred in a day while the maximum water gaining of the system happened 2 hours after that. But USS ranked both the least of water loss and the maximum water gaining in the afternoon among all types of observed soil system.

In a 21 days observation time period, if soil moisture (v/v%) of 3.8cm and 7.6cm below soil surface were regarded as representatives of distribution of soil water content distribution across these two layers, both systems follow a decreased tendency close to linear correlations (GSS, R^2= 0.7602 and USS, R^2= 0.691) for the first 10 days, and stayed fuzzy situation if 21 days were analyzed overall (R^2< 0.15). These probably suggested an intensive interaction beneath the soil surface which manipulate the loss-and-gain among soil-air inter-surface. When soil moisture was abundant, the water moves mainly from the soil to the air, likewise, when top surface soil water drying, both water from the lower layer and the air moisture buffered the surface water balance.

However, USS held much higher level of soil moisture than GSS generally in both two stages and in both observed soil layers.

Systematic Water Loss Monitoring under Irrigated Condition. Soil moisture measurement may reveal soil water conditions of different soil systems more directly. Figure 3 clearly shows that the uncovered soil system (USS) loss water slower than all the GSSs if leaving out of the effect of wind. Through comparing soil volumetric water

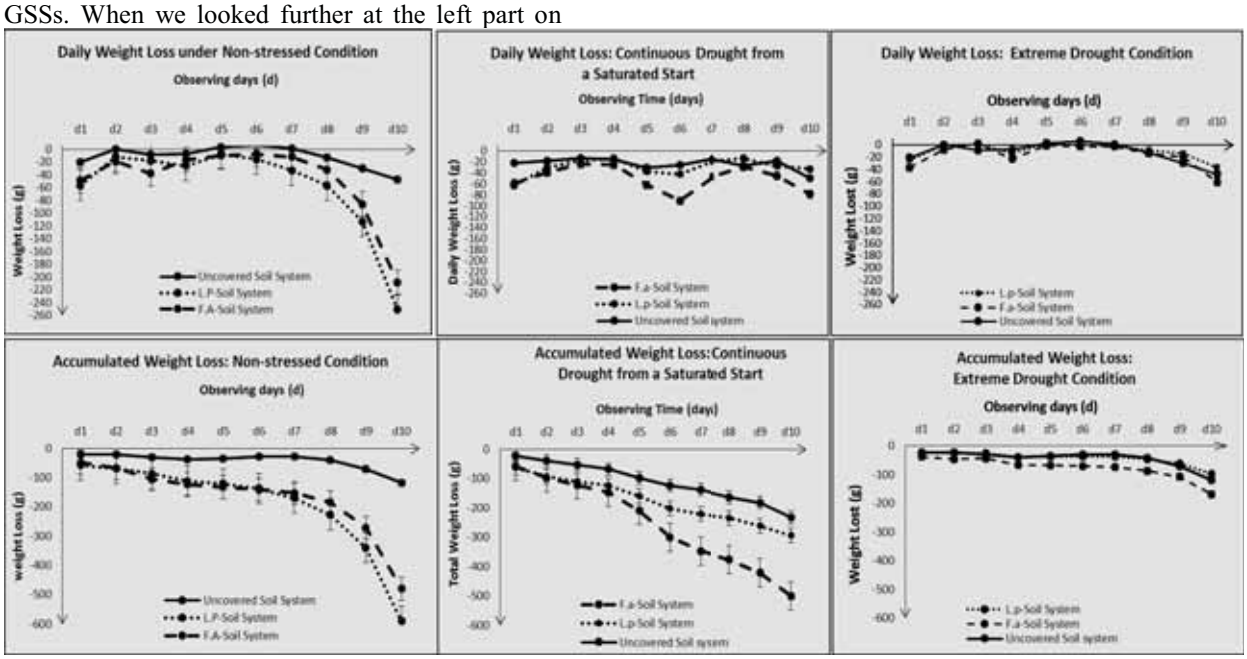

FIGURE 2

Daily Water Loss and Accumulated Change Of Grass-Soil System After 1-Week Drought Stressed (G)

Note: (a) daily water loss monitoring; (b) accumulated water loss monitoring.

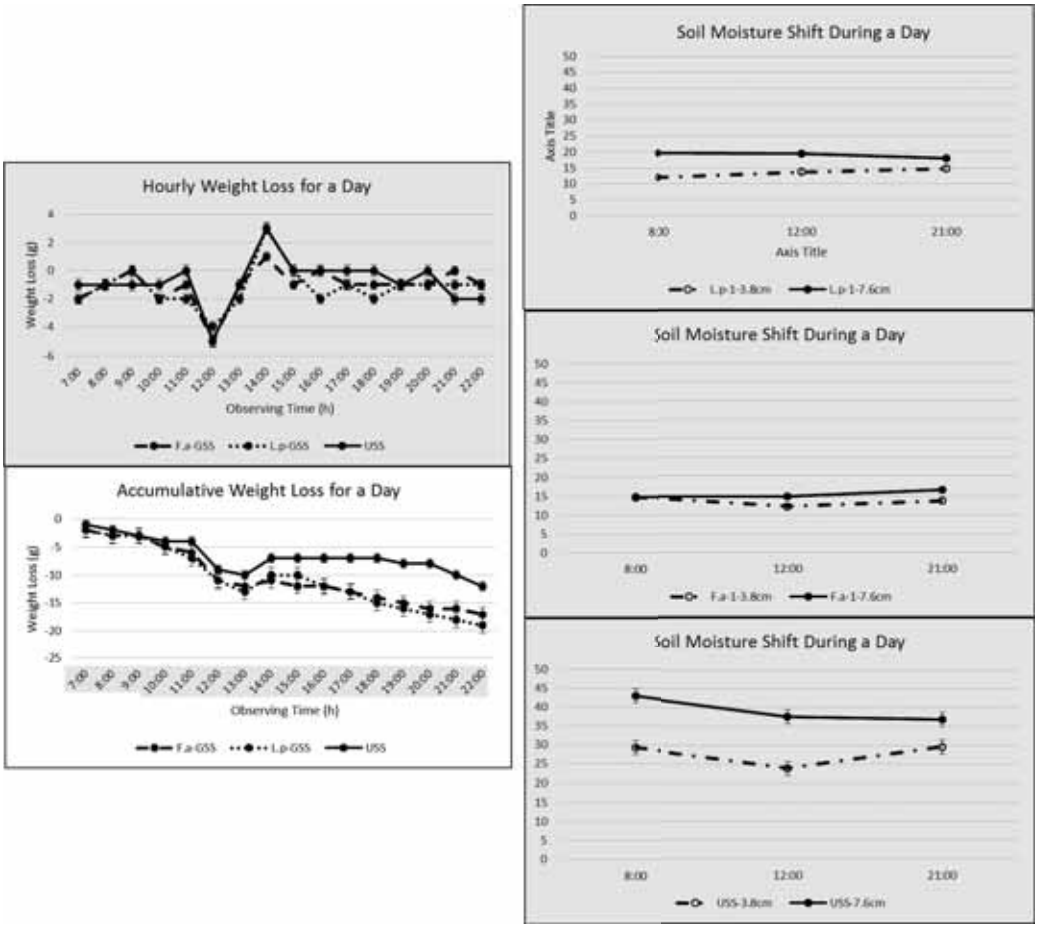

FIGURE 3
Weight and Soil Moisture (V/V%) Change of Soil System in A Typical Day

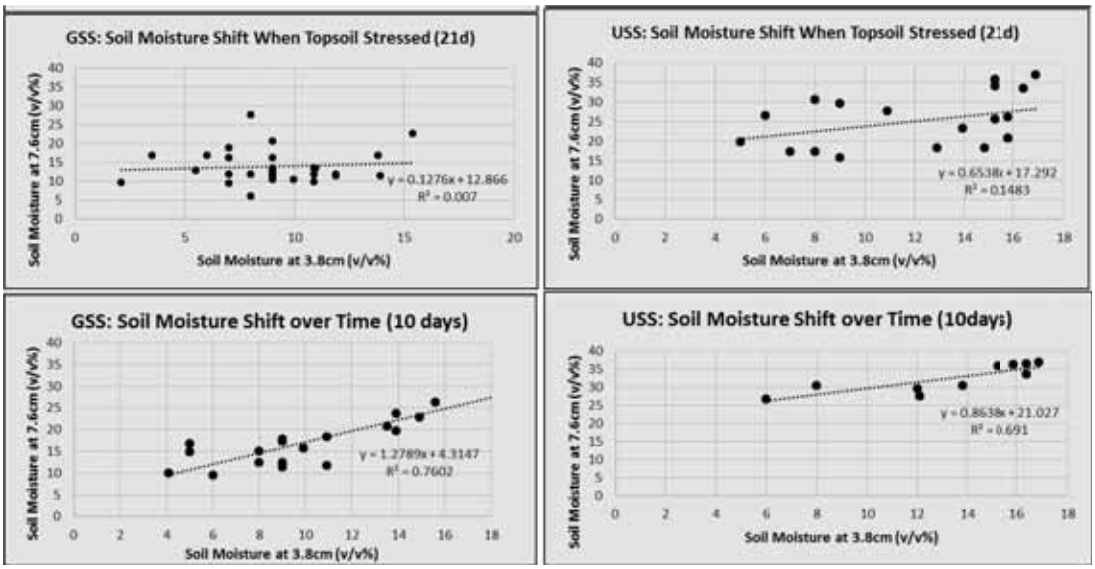

FIGURE 4
Soil Moisture Distribution Monitoring of Different Soil Systems Within 21 Days

content (VWC) at different soil layers with TDR, it can be told that soil moisture at 7.6cm layer in USS significantly was higher than in two types of GSS while mildly higher at 3.8cm below the surface soil layer. This suggested firstly, without absorbent pressure disturbance by root, water could be better retained beneath the soil surface for a longer time. Secondly, without grass covering, a high level of air humidity. Firstly, as we stated in 3.4, in winter, high air humidity can donate special water welfare to the soil system through dewdrop or drizzling. Since grass leave, no matter green or wither stop

soil from getting more water from air moisture, without grass leave, USS can harvest water from the air much easier than GSS do.

It takes 3 days for F.a drag down the surface soil moisture to 10% which is a typical dry situation, while L.p 6days and bare land 9days. In the depth of 7.6cm, it all takes more than 8days to reach soil moisture of 10%. But after 10days, non-covered soil still kept as high as 30% when F.a are suffered at 10% and L.p is approaching the threshold of dry condition.

Grass-soil systems were watered both at checkpoint status, which is the primary stage of stress in terms of surface (3.8cm) soil moisture ranging from 15% to 18% and leaf area initial shrinkage as well as at stressed status (the secondary stage-if drought extended-that grass appeared with two or more symptoms including leaf wilting, color change, increasing withering, etc.).

Figure 5 illustrates regardless of 150g or 200g water input to GSS at checkpoint or under stressed, water loss (WL) of the systems are all higher than USS which ranged from 19~113 g/0.045m^2 (42~251kg/ha/d). 0-water-input to GSS affected systems in checkpoint very little but reduced WL rapidly close to (5g/0.045m^2=11 kg/ha/d) or lower (-2~-17 g/m^2 =4.4~38kg/ha/d) than USS. The WL ratio of USS depends on the severity of drought stress. Since drought-checkpoint system with 0g input leads to much more decrease of community height in L. *perenne* (-2~-6cm) than in F. *arundinacea* (0~-2cm), after re-watering, grass-covered system used water to fill leaves, resulted in firstly a community height increasing from 5 to 8cm for *L. perenne* and 2 to 4cm for F. *arundinacea*, then width (0.2~3.5mm) and length (0~3.5cm) enlargement a single leaf.

Table 2 showed the more water input to grass-soil system under drought stress, the more water would be evaporate in the following day. If the leaves withered seriously and WL was little or negative in the previous day which suggested a endangered situation of GSS, the total loss of the whole system was largely depended on health condition of leaves. But in checkpoint, grass was still in good condition that may be easier to recover therefore grass community would extract even more water for recovering and settle for growth.

Gaining Weight from Dew. Gaining dew weight happened mostly in time period of 6:00~8:00 am or day time when the temperature was closer to dew-point and the humidity was over 80% according to our observed recorders.

The net weight gain varied from 0 to 6g per uncovered pot (5kg, 0.0045m^3 or 0.045m^2), equals to maximum 13.3kg/ha/d in the most serious degraded soil with depth of 10cm. Surprisingly this little gain helped soil system more than expected because uncovered soil was wet and soil volumetric water content at depth of 3.8cm and 7.6cm had both increased due to the dew impact. For the stressed grass at the withered checkpoint, the same amount of dew helped to recover the height of grass community dramatically at the price of greater loss of soil water.

Compared with the uncovered pot, the grass covered pot gained a maximum of 4g/0.0045m^2 (0.088kg/m^2/d, or 88kg/ha/d) which is not little when the continuous drought attacked soil-ecosystem. Conversely when canopy coverage ratio sharply decreased to 30%, the weight augment achieved 0.178 kg/m^2 /d that equals to 178kg/ ha/ d.

The way stressed grasses using dew drops. Table 2 also illustrates that regardless of 150g or 200g water input to GSS at a checkpoint or under stress, water loss (WL) of the systems all are higher than USS which ranged from 19~113 g/0.045m^2(42~251kg /ha /d). 0-water-input to GSS affected systems in checkpoint very little but reduced weight loss (WL) rapidly close to (0.5g/0.045m^2= 11 kg/ha/d) or lower (-2~-17 g/0.045m^2 = 44 ~ 38kg/ha/d) than USS. The WL ratio of USS depends on the severity of drought stress. Since drought-checkpoint system with 0g input leads to much more decrease of community height in *L. perenne* (-2~-6cm) than in *F. arundinacea* (0~-2cm) grass-soil buffer system, after re-watering, grass-covered system used water to recover grass leaves and community well-being, resulted in firstly a community height increasing from 5 to 8cm for L. perenne and 2 to 4cm for F. arundinacea, then width (0.2~3.5mm) and length (0~3.5cm) enlargement a single leaf.

DISCUSSION

According to our experimental result, uncovered-soil systems maintained water longer than grass-covered-soil system generally within soils in winter season of experimental areas in terms of both daily-loss and the accumulated loss of water. Particularly, GSSs may reach 3~4 times water consumption than their USSs partners on a single day (Figure 1). Through daily water-loss monitoring of 3 different systems matched the moving average curves as Figure 2 and Figure 5 implied, daily reduction of water was not an isolated parameter in that it affected the soil moisture of latter day and could be affected by the previous day in a coherent way.

The maximum deviation that GSSs lost more than USSs under continuous drought stress (Figure 2b) was as high as more than 70g/0.045 m^2 (~156kg/ha/d), but in extreme drought condition (Figure 5c) loss of USSs was higher than GSS which was only 14g/0.045 m^2(31kg/ha/d) maximum. This imply that even grass displayed the

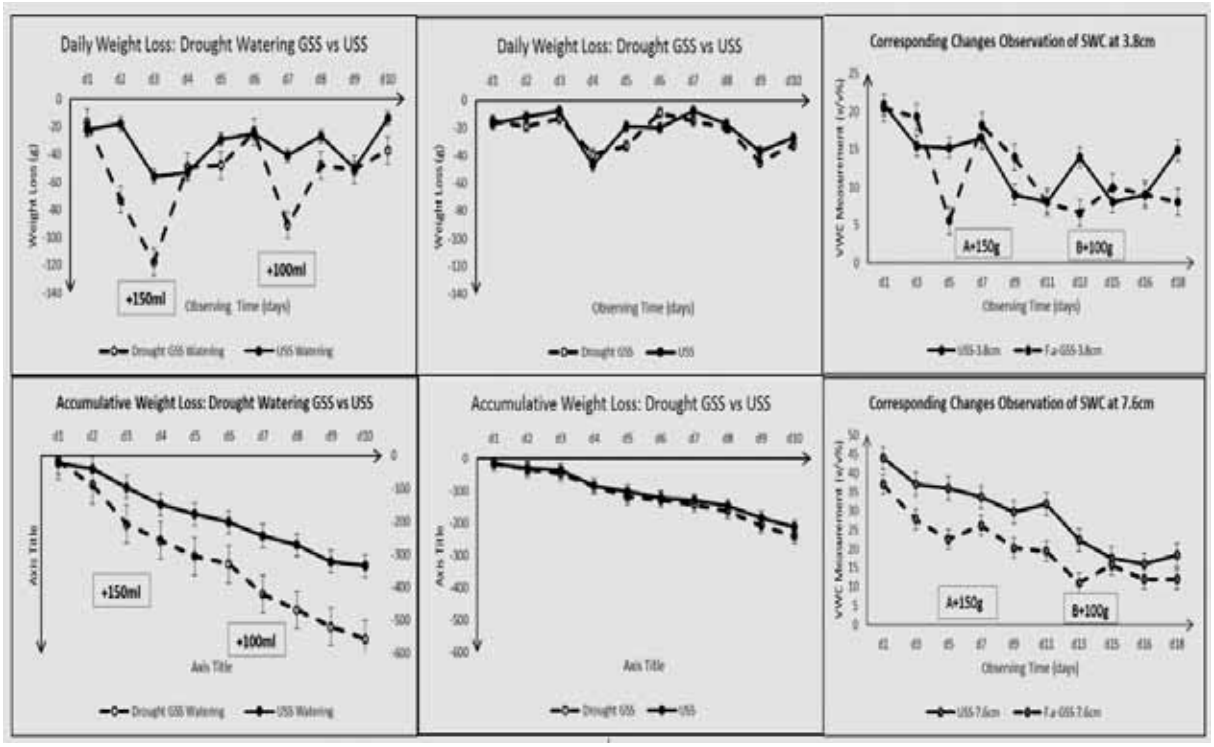

FIGURE 5
Watering Effect on Weight Loss of GSS and USS Under Drought

TABLE 2
Water Loss and Grass Morphological Appearance of The Drought Stressed Grass-Soil System

Group	Type of Soil System	Water Input	Previous Day WL	Current WL	Increment of Leave		Height
		(ml/5L)	(Current WL= X - USS) (g)		L（cm）	W（mm）	Add-ed(cm)
Group 1	F.A-SS in checkpoint	208	**133**	**119**	3.5	1	3.5
	F.A-SS under DS	207	44	85	0	1	4
	F.A-SS in checkpoint	0	68	15	0.2	-0.5	0
	F.A-SS under DS	0	5	-17	0	-0.5	0
	L.P-SS in checkpoint	201	**195**	**113**	2.1	0.2	5
	L.P-SS under DS	206	34	109	0.9	2	6
	L.P-SS in checkpoint	0	34	17	-0.9	-2	-6
	L.P-SS under DS	0	-19	-2	-17	-1	-2
	USS	**0**	**56**	**47**	-	-	-
Group 2	F.A-SS in checkpoint	149	**119**	**23**	1.9	+2.5~3.5	1
	F.A-SS under DS	152	-18	23	-0.3	2	-2
	F.A-SS in checkpoint	0	-16	32	-0.2	0~-1	-2
	F.A-SS under DS	0	15	-7	-1.7	-0.5	-1
	L.P-SS in checkpoint	149	30	28	3.5	+1~2	10
	L.P-SS under DS	152	-7	34	2.5	+0.5~2.5	8
	L.P-SS in checkpoint	0	0	8	-0.2	-1~4.0	-5
	L.P-SS under DS	0	-20	5	-2	-1~4.5	-2
	USS	**0**	**50**	**27**	-	-	-

Note: F.A-SS refers to *F.Arundinacea*-soil system; L.P-SS refers to *L.Perenne-soil* system; Uncovered-SS means soil system without vegetation covered; DS refers to Drought Stress; checkpoint means threshold of stress or not stress; W-Input is Water-Input; WL equals to Water Loss; minus USS WL= －Cureent Uncovered-soil system water loss amount; L=leave length; W=leave width. *'-' in WL means how much lower than Uncovered-SS; '-' in L, B means how much shorter than start in leave length and broad.

water-saving function under extreme drought situations when it lower the activity in evaporation but the quantity of water saving was only 1 of 5 compared to normal condition which was trivial comparing to the huge loss for leave recovering, *etc*.

Also, grass varieties showed diversified capacity in buffering soil water environment as following. When 70% of above-ground grass withered, grass-soil systems were exposed to extreme drought stress for an extended 10 days, underground organs of grasses have display their superlative water stor-

age function to prevent water loss for GSSs in Figure 2. Therefore, water loss of which is lower than USS on most days. Through comparison of water loss between GSSs and USSs, it is clear that L. perenne-SS mitigate water-loss underground more effectively than F. Arundinacea-SS because it rapidly adapted itself to the solar energy and made full use of water to hydrate and accumulate dry matter if possible. They costed less water than USSs when photosynthesis were impossible. We shared similar results with Berge on L. *perenne* environment-friendly behave in buffering soil water when drought attack[36].

Figure 5 suggests that *L. perenne*-soil system tended to be more sensible to irrigation treatment than *F. Arundinacea*-system did. The former lost much water than the latter under 2 different levels of irrigation with observable changes related to leaf area and group height etc. 150g water per pot enabled *L. Perenne* to increase community height, and enlarge length and width of leaves at multi-levels. However, it is not enough for *F. Arundinacea* to achieve similar growth unless 200g total input was given to each pot after the checkpoint of drought stress.

Re-watering soil systems causes additional water loss for GSSs, although it would improve grass well-being and increase the transferable water amount. Without water input, GSSs would lose less water than with irrigation GSS. At the same time, the grass community would allow inner water to be shifted from elder leaves to younger leaves or new buds for systematic dynamics conservation at the cost of community height and leaf area shrinkage.

12-year observation from grassland surface of SanJiang plain, northeast of China, dew is thought to be an important supplement for nature precipitation because total annual amounts of dew equate to 5.05% of precipitation of corresponding period which was about 20.68mm /a [37].

Special geologic characteristics make southwest China possible to keep high humid and temperature mostly above 0°C through the whole year which is impossible in the northeast. Together with large temperature discrepancy between day and night, naturally, more dew benefits for soil systems would be harvested in SW China's karst area. Substantially, we have observed many times that soil system gain weight in someday of winter-spring period from 2013 to 2015 instead of daily weight loss due to natural evaporation.

CONCLUSION

We have proved that the daily irreversible water loss for two types of grasses in high density growth and bare soil in a 0.0045m^3 per pot (~5kg weight) are measurable in southwest China's karst region. Therefore, both the input and output of the minimum grass-soil system can be precisely recorded.

Results show that grass coverage do not guarantee a better water conservation for GSSs comparing to USSs. Oppositely, grass community consumes more water than bare land for grass growth. When soil-system confronting interval drought stress at different levels, grass communities reduce the strength of photosynthesis and respiration to decrease water loss of the system. Furthermore, water transfer may happened from elder leaves to younger leaves to maintain the dynamics of the whole system. However, the total amounts of GSS are still higher than USS except that grassland have been exposed to extreme drought condition and first 84h after re-watering from extreme drought.

Therefore, we may safely conclude that during winter to spring climate of some southwest China's karst area, perennial grasses may not act as 'a hero of ecological conservation' [38], contrarily, they may compete soil water for growing. As a result, grass may exacerbated drought stress for local soil ecology. This result is in accord with findings that grassland owning highest annual evapotranspiration among 6 sub-regions in China since 1980s to 2005 [38]. Accordingly, average soil moisture of grassland in southwest of China is dramatically lower than cropland at 0.06~0.11m3/m3 while most of others are not worse than cropland [39].

Certainly, further evidences based on fields are welcome for local decision-making related to grassland construction, reconstruction or ecological services valuation. however, the irreplaceable lab work may provide us absolute water loss of the system which is difficult to get from fields. Therefore, considering the climate characteristics and soil limitation, our study suggests that system-theory based lab work can be a useful tool to support soil ecosystem function assessment. We also strongly recommend that perennial grassland (especially cool-season type of man-made grassland) should be avoided. Besides, hopefully our results will also enlighten measurement the method for evapotranspiration based on an ecological system as well.

System-based observation shows that dew water from air moisture is found be a good supplement to soil system in condition of precipitation shortage but perennial grass may reduce the overall gain of grass-soil system because it continues consume water to meet the need to grass alone.

In summary, instead of directly applying large-scale data for local decision-making, or policy-making, methodology innovation or re-application of useful methods that are direct, easier but reliable and system-based observation should be emphasized and applied widely in the management of rehabilitation technology.

ACKNOWLEDGEMENTS

This paper was jointly supported by "The Project of National Key Research and Development Program of China in the 13th Five-year Plan Period: Ecological Industry Model and Integrated Technology Demonstration of the Karst Plateau-Gorge Rocky Desertification Control (2016YFC05026 07)", "The Project of National Natural Science Foundation of China (No. 41561047)", "The Project for National Top Discipline Construction of Guizhou Province: Geography in Guizhou Normal University (85-01 2017 Qianjiao Keyan Fa)", and Guizhou Provincial Supporting Project (Qianjiao Keyan [2017]2925), "The Key project of Natural Science Foundation of Guizhou (Qian Ke He Foundation [2019]1431)". And many thanks to the China Scholarship Council for supporting the Ph.D. study in AIT.

REFERENCES

[1] Sweeting, M.M. (1993) Reflections on the development of Karst geomorphology in Europe and a comparison with its development in China. Z. Geomoph. 37, 127-136.

[2] Cai, Y.L. (1999) Ecological rehabilitation and development of agriculture, forestry and animal husbandry in karst mountain areas of southwest China: Status quo and trend of study. Resource Science. 21(5), 37-41. (in Chinese).

[3] Wang, S.J. (2003) Karst Rocky Desertification - the most serious ecological and geological environment problem in southwest China. Bulletin of Mineralogy, Petrology and Geochemistry. 22(2). (in Chinese).

[4] Wang, S.J., Li, Y.B., Li, R.L. (2003) The background, succession and rehabilitation of Karst Rocky Desertification. Quaternary Sciences. 23(6), 657-666 (in Chinese).

[5] Li, Y.B., Luo, G.J., Bai, X.Y., Wang, Y.Y., Wang, S.J., Xie, J., Yang, G.B. (2014) The correlations among arable land, settlement and karst rocky desertification-cases study based on typical peak-cluster depression. Acta Ecologica Sinica. 34(9), 2195-2207.

[6] Huang, Q.H., Cai, Y.L., Wang, X.C. (2007) The research frontier of southwest of China karst rocky desertification area. J. of Natural Disaster. 02, 106-111. (in Chinese).

[7] Cao, X.Y. (2004) The economic impact of rocky desertification to Guizhou national minority ethnic and its counterplan. J. of Guizhou Minority. 24, 116-118.

[8] Cai, Y.L. (1999) Ecology reconstruction and Agriculture, Forestry, Husbandry development of southwest of China karst mountain area: The Status Quo and Trends. Resource Sciences. 05, 39-43. (in Chinese).

[9] Zuo, X.J., Zuo, T.A., Xu, S.J. (2010). Benefit evaluation on the control mode for typical karst rocky desertification in guizhou province, China. Asian Agricultural Research. 2(7), 60-64.

[10] Tang, Y., Jia, H.F., Jiang, Q.G., Wang, J. (2011). Comprehensive rehabilitation planning of deserted pits and the case study in plain area of Beijing, China. Landscape & Urban Planning. 99(2), 123-132.

[11] Lü, Y.H., Fu, B.J., Feng X.M. (2012) A policy-driven large scale ecological resto-ration: quantifying ecosystem services changes in the Loess Plateau of China. PLoS ONE. 7(2), e31782.

[12] Liu, J., Li, S., Ouyang Z. (2008) Ecological and socioeconomic effects of China's policies for ecosystem services. Proceedings of the National Academy of Sciences. 105(28), 9477-9482.

[13] Su, X.L. (2005) KRD and Ecological Environment Management. Earth and Environment. 33(4), 20-28.

[14] Huo, L.N. (2010) Analysis of different vegetation communities function of soil conservation and water retention in Yunan mountainous area. Dissertation. Henan Agriculture University.

[15] Yuan, S.J., Miao, Q.L., Gu, X.P. (2007) Analysis on the Spring Drought in the Karst Region of Yunnan and Guizhou Plateau in China. Scientia Geographica Sinica. 27(6), 796-800. (in Chinese).

[16] Zhao, Z.Q., Hou, L.S., Cai, Y.L. (2006) The process and mechanism of soil degradation in karst area in Southwest China. Earth Science Frontiers. 3. (in Chinese).

[17] Xu, D.D., Gu, X.P., Wu, J.M. (2006) Some researches on spatiotemporal distribution regularities of drought in the karst region over Yunnan and Guizhou. J. of Guizhou Metheorology. 30(2), 9-11. (in Chinese).

[18] Nacinovic, M.G.G., Mahler, C.F., Souza, A.A. (2014) Soil erosion as a function of different agricultural land use in Rio de Janeiro. Soil and Tillage Research. 144, 164-173.

[19] Wiesmeier, M., Spörlein, P., Geuß, U. (2012) Soil organic carbon stocks in southeast Germany (Bavaria) as affected by land use, soil type and sampling depth. Global Change Biology. 18(7), 2233-2245.

[20] Fierer, N., Schimel, J.P., Holden, P.A. (2003) Variations in microbial community composition through two soil depth profiles. Soil Biology and Biochemistry. 35(1), 167-176.

[21] Schütz, K. (2009) Flooding forested groundwater recharge areas modifies microbial communities from top soil to groundwater table. FEMS Microbiology Ecology. 67(1), 171-182.

[22] Eilers, K. (2012) Digging deeper to find unique microbial communities: the strong effect of depth on the structure of bacterial and archaeal communities in soil. Soil Biology and Biochemistry. 50, 58-65.
[23] Lorda, J., Lafferty, K.D. (2012) Shading decreases the abundance of the herbivorous California horn snail, *Cerithidea californica*. Journal of Experimental Marine Biology and Ecology. 432, 148-155.
[24] Kulmatiski, A., Beard, K.H. (2013) Root niche partitioning among grasses, saplings, and trees measured using a tracer technique. Oecologia. 171(1), 25-37.
[25] Dobriyal, P., Qureshi, A., Badola, R. (2012) A review of the methods available for estimating soil moisture and its implications for water resource management. Journal of Hydrology. 458, 110-117.
[26] Worsching, H., Becker, R., Schlaeger, S., Bieberstein, A. and Kudella, P. (2006) Spatial-TDR moisture measurement in a large scale Levee model made of Loamy soil material. Proceedings of the TDR 2006: Third International Symposium and Workshop on Time Domain Reflectometry for Innovative Soils Applications, Purdue University, IN, USA, September.
[27] Weihermüller L., Siemens J., Deurer M. (2007) In situ soil water extraction: A review. Journal of Environmental Quality. 36(6), 1735-1748.
[28] Lunt, I.A., Hubbard, S.S., Rubin, Y. (2005) Soil moisture content estimation using ground-penetrating radar reflection data. Journal of Hydrology. 307(1), 254-269.
[29] Brocca, L., Melone, F., Moramarco, T. (2010) ASCAT soil wetness index validation through in situ and modeled soil moisture data in central Italy. Remote Sensing of Environment. 114(11), 2745-2755.
[30] Farley, K.A., Kelly, E.F., Hofstede, R.G.M. (2004) Soil organic carbon and water retention after conversion of grasslands to pine plantations in the Ecuadorian Andes. Ecosystems. 7(7), 729-739.
[31] Harden, C.P., Hartsig, J., Farley, K.A. (2013) Effects of land-use change on water in Andean páramo grassland soils. Annals of the Association of American Geographers. 103(2), 375-384.
[32] Wang, J., Fu, B.J., Qiu, Y. (2000) Spatiotemporal Variability of Soil Moisture in Small Catchment on Loess Plateau—Semivariograms. Acta Geographica Sinca. 55(4) 428-438. (in Chinese).
[33] Zhang, J.G., Chen, H.S., Su, Y.R. (2006) Spatial Variability of Soil Moisture Content and Reasonable Sampling Number in Cluster-Peak Depression Areas of Karst Region. J. of Soil and Water Conservation. 20(2). (in Chinese).
[34] Boardman, J. (2006) Soil erosion science: Reflections on the limitations of current approaches. Catena. 68(2), 73-86.
[35] Xiong, K.N., Li, J., Long, M.Z. (2012) Typical soil and water loss characters and crucial problem identification of RD rehabilitation zone in Karst area. Acta Geographica Sinca. 67(7) (in Chinese).
[36] Li, F., Wang, S.J., Liu, Y.S. (2005) Changes of soil quality in the process of karst rocky desertification and evaluation of impact on ecological environment. Acta Ecologica Sinica. 25(3). (in Chinese).
[37] Chi, Y.K., Xiong, K.N., Xiao, H., Chen, H., Huang, D.H., Wen, Y.Q., Shen, X.Y. (2018) A comparative study on meat quality between Guizhou semi-fine wool sheep and a series of semi-fine wool sheep in southwest China. Fresen. Environ. Bull. 27(6), 4239-4238.
[38] Franzluebbers, A.J., Hubbs, M.D., Norfleet M.L. (2012) Evaluating soil organic carbon sequestration potential in the Cotton Belt with the soil conditioning index. Journal of Soil and Water Conservation. 67, 378-389.
[39] Bing, L.F., Su, H.B., Shao, Q.Q., Liu, J.Y. (2012) Characteristics Analysis on China Terrestrial Surface Evapotranspiration and Soil Moisture Variation in late 30 years. J. of Geo-information Science. 14(1),1-13. (in Chinese)

Received: **20.09.2019**
Accepted: **28.11.2019**

CORRESPONDING AUTHOR

Kangning Xiong
Guizhou Normal University，
School of Karst Science/
State Engineering Technology Institute for Karst Desertification Control of China,
550001, Guiyang, Guizhou – China

e-mail: xiongkn@163.com

© by PSP Volume 29 – No. 05/2020 pages 3633-3640 Fresenius Environmental Bulletin

RESEARCH ON THE RELATIONSHIP BETWEEN URBANIZATION SPACE AND SUSTAINABLE DEVELOPMENT

Dan Huang*

School of Tourism and Geography Science, Yunnan Normal University, Yunnan 650500, China.

ABSTRACT

The development of new-style urbanization and the level of eco-environmental benefits in Yunnan Province are quite different in space. The development is not a synchronous relationship, but also indirectly reflects the prominence of ecological environment problems in the development of new-style urbanization. How to coordinate the development relationship among them has become a key issue under the current concept of sustainable development.

Through the study of new-style urbanization and sustainable development, this paper analyzes its space-time coupling relationship and aims to provide a scientific reference for the coordinated development of urban and rural areas in Yunnan Province.

The coupling level and coordination evaluation model used to analyze the space-time coupling relationship between new-style urbanization and sustainable development in Yunnan Province, this paper estimates the new-style urbanization level and sustainable development benefit of Yunnan Province, and develops from spatial difference analysis.

Among the spatial distribution of new-style urbanization levels, only Kunming City is at a high level, only Yuxi City and Qujing City are at the upper limit, and the remained 13 cities (states) are below the lower limit. Among the spatial distribution of sustainable development benefits, only Diqing is at a high level, with Nujiang and Lijiang at the upper limit, and the remained 13 cities (states) are below the lower limit.

The level of new-style urbanization development and sustainable development benefit in Yunnan Province is quite different in space. From the perspective of spatial distribution, its new-style urbanization level is characterized by from the central growth to the periphery growth. Based on the concept of sustainable development, this paper formulates relevant policies according to the actual situation of regional development, which strengthens cooperation and exchange among cities (states). It is a key link to narrow regional differences and promote new-style urbanization level. The rapid development of new-style urbanization has high requirements for sustainable development. The new-style urbanization and sustainable development of Yunnan Province have not yet reached a state of cooperation, but the level of coordination is constantly improving. To reduce the irrational distribution of resources, the irrational use of resources in the new-style urbanization development is the key to improve the development of new-style urbanization in Yunnan.

KEYWORDS:
Yunnan Province, new-style urbanization, sustainable development, relationship

INTRODUCTION

The elements of the ecological environment are based on important factors in the ecological environment. It refers to the elements of nature (material and energy) or effects that are closely related to human beings, which affect the human production and life activities (the second nature formed by manual intervention). It includes natural matter elements such as animals, plants, microorganisms, land, minerals, oceans, rivers, sunlight, atmosphere, and water, as well as artificial materials on the ground and underground with the related facilities. In the past 40 years of reform and opening up, China's urbanization has made great progress. The level of urbanization has increased from 17.9% in 1978 to 58.5% in 2017. The resident population of urban areas has also increased from 170 million in 1978 to 810 million in 2017. Billion has created the achievements of the world [1, 2]. With the deepening of reforms, China's economic development has entered a new normal. This new normal is based on the sustainable development, which does not undermine sustainable development. China's urbanization development is relative to that of developed countries in Europe and America for hundreds of years. There are still large gaps in the development process, and there are many problems in development, such as urban household registration, rural hollowing out, and land reclamation. These problems have become an important obstacle

to the development of urbanization in China in the new era [3- 5]. With deepening the green development, new-style urbanization with urban and rural planning, industrial interaction, ecological livability, and harmonious development has become an important direction of urbanization development in China in the new era. However, for a long time, people misunderstand the concept of urbanization and believe that non-agriculturalization is the direction of urbanization development, resulting in ecological problems such as over-exploitation of agricultural land use, low land efficiency, low utilization rate, and severely restricting China [6]. From the perspective of resource utilization, the limited resource resources of urbanization in the new-style urbanization and the waste of resources caused by the loss of rural population have become the key issues to solve urgently. Therefore, the coordinated development of new-style urbanization and sustainable development is studied. From the perspective of the evolution of space-time, it is important to analyze the development level of new-style urbanization, which is based on the development of urban and rural integration, industrial interaction, and ecological livability [7, 8].

Xu Li [9] analyzed the development level and spatial characteristics of new-style urbanization in Changzhou City, Jiangsu Province. The results show that the development level of new-style urbanization in Changzhou is from good to good, and the development level and optimization trend of new-style urbanization in different districts and counties are quite different. Wang Chongling et al. [10] used the coordination level and coupling level evaluation model to analyze the space-time coupling relationship between the new-style urbanization and human settlements development in Ningxia, they analyzed the temporal and spatial evolution characteristics of the coupling level of five prefecture-level cities. The results show that the new-style urbanization and human settlements coordination index and coupling index of Ningxia have shown a good upward trend, and the coordination relationship between new-style urbanization and human settlements is mostly in a highly coordinated stage. In terms of space, the coupling coordination level is not much different, and based on the research results, optimization strategies such as optimizing urban spatial pattern are proposed. Wang Shujia et al. [11] studied the coordinated development of sustainable development-economic-new-style urbanization in the Beijing-Tianjin-Hebei region with a coupled and coordinated development model. The results show that the coordinated development level of Beijing-Tianjin-Hebei has significant spatial and temporal differentiation, and its advantages and constraints are different. The backwardness of Hebei economy and new-style urbanization has become the bottleneck for the overall coordinated development of the region. Summarizing previous studies, it is found that the new-style urbanization theory and empirical research are rich, but lack of research on new-style urbanization and sustainable development, and there is bias in the research area. There are few studies on the development of urbanization in underdeveloped areas. Based on the study of new-style urbanization and sustainable development in Yunnan Province, this paper analyzes the space-time coupling relationship, which provides a scientific reference for the coordinated development of urban and rural areas in Yunnan Province.

RESEARCH AREA OVERVIEW AND DATA SOURCES

Overview of the study area. Yunnan Province is located in the southwestern border of China. Its southwestern part is adjacent to Myanmar, Laos, and Vietnam. The borderline is 4 060 km2 and there are more than 20 mirrored roads. In 2017, the resident population of Yunnan Province was 48 million, of which the urban population was 22.41 million, and the rural population was 25.59 million. The province's urbanization rate reached at 46.7%, up 9.2% from 2010, but still it is lower than the national level 58.5%. Therefore, Yunnan Province actively seized the state's support policies for the development of the western region, and proposed the urban agglomeration in central Guizhou, the secondary urban agglomerations in western Yunnan, the secondary urban agglomerations in southeastern Yunnan, the secondary urban agglomerations in northwestern Yunnan, and the southwestern Guizhou. The construction of six urban agglomeration in the urban agglomerations and the secondary urban agglomerations in northeast Yunnan will improve the development level of new-style urbanization in Yunnan Province [12,13]. Yunnan Province has 8 provincial cities including Kunming, Qujing and Yuxi, and 8 ethnic autonomous prefectures such as Dali, Honghe and Diqing. It is a large province with multi-ethnic culture. There are many mountainous areas in Yunnan Province, such as basins, valleys and hills, and the types of landforms are complex. Complex geomorphological features hinder the development of new-style urbanization in Yunnan Province. Among them, the urbanization level in the central and eastern areas of Gansu is relatively high, but the mountainous areas and canyons in western Yunnan have relatively lagging the level of urbanization development [14]. Yunnan has abundant light energy resources, the dry and wet seasons are distinct, and the temperature difference among the four seasons is small. Yunnan Province is rich in natural resources, and its per capita water resources are four times the national average. However, complex geomorphological conditions increase the difficulty of using water resources. Based

on the location conditions and urbanization development status of Yunnan Province, combined with the development connotation of new-style urbanization, this paper studies the coordinated development relationship between new-style urbanization and sustainable development in Yunnan Province from the perspective of Tempo-spatial expanded dimension, which analyzes the coordinated development level of both. We will provide suggestions for the coordinated development of new-style urbanization and sustainable development under the guidance of the sustainable development, which promote the coordinated development of urban and rural areas in the context of the new-style urbanization development of Yunnan Province in the new era.

Data source. The research data of this paper originated from the following tips. (1) Yunnan Statistical Yearbook (2009~ 2016). (2) Statistical Yearbook of various provincial cities and autonomous prefectures in Yunnan Province (2009~ 2016). (3) Statistics of National Economic and Social Development of Yunnan Province Bulletin (2009~ 2016).

RESEARCH METHOD

Constructing the indicator of coupling system. With the continuous advancement of new-style urbanization and sustainable development, the synergistic development effect of both has gradually become an important research content under the concept of sustainable development. The main goal of the new-style urbanization is how to solve the resource and environmental problems in the traditional urbanization development, and the sustainable development construction plays an important role in promoting the ecological habitability, industrial interaction, and urban-rural integration of the new-style urbanization [15]. The starting point of this paper is based on this foundation. Therefore, based on the principles of operability, comprehensiveness, and scientificity, the evaluation indicators of new-style urbanization and sustainable development in Yunnan Province are selected. By referring to previous studies and the connotation of new-style urbanization development, the new-style urbanization evaluation system consists of population, economy, society, urban-rural integration, and space, and comprehensively covers the new concept of sustainable development. The sustainable development level, sustainable development pressure, and sustainable development protection in the indicators selection of sustainable development benefit system constitute the stress-state-response model of its benefit measurement. It comprehensively reflects the level of human settlements in urban and rural areas, the pressure of urbanization development on sustainable development and the protection of sustainable development.

Estimation of new-style urbanization Level and Sustainable Development Benefits in Yunnan Province. Efficacy function. The variable $U_i(i=1,2,3,\ldots,m)$ is set as the order parameter of the new-style urbanization and sustainable development coupling system in Yunnan Province. U_{ij} represents the index j of the order parameter i, and X_{ij} (j=1, 2, 3, …, n) is the index j value of the order parameter i. If α_{ij}, β_{ij} are the upper limit and lower limit of the order parameters of the new-style urbanization and sustainable development coupling system, the original data is standardized by the extreme difference standardization. The orderly efficacy coefficient U_{ij} of the new-style urbanization and sustainable development of the coupled system in Yunnan Province can be expressed as follows.

$$U_{ij}=\begin{cases}(X_{ij}-\beta_{ij})/(\alpha_{ij}-\beta_{ij}) & Uij \text{ is positiveEfficacy function}\\ (\alpha_{ij}-X_{ij})/(\alpha_{ij}-\beta_{ij}) & Uij \text{ is negativeEfficacy function}\end{cases} \quad (1)$$

Entropy method to calculate index weights. In this paper, the entropy method is used to calculate the weights of various indicators of the new-style urbanization and sustainable development system. To a certain extent, it can avoid the subjective influence of human factors. The specific calculation steps are as follows.

(1) Make a weight change for each indicator S_{ij} :

$$S_{ij}=U_{ij}/\sum_{i=1}^{n}U_{ij} \quad (2)$$

(2) Calculate the entropy value hi of the indicator j.

$$h_i=-\frac{1}{\ln n}\sum_{i=1}^{n}S_{ij}\ln S_{ij} \quad (3)$$

(3) Calculate the difference αj of the indicator j.

$$\alpha_j=1-h_j \quad (4)$$

(4) Calculate the weight λj of the indicator j.

$$\lambda_j=\alpha_j/\sum_{i=1}^{n}\alpha_j \quad (5)$$

New-style urbanization level and sustainable development benefit calculation. The product of the weight of the evaluation index j of the new-style urbanization and sustainable development subsystem and the standardized value of the indicator is used as the evaluation score W_{ij} of the indicator in this year. The sum of all the indicators in the system is the total score of the new-style urbanization or land use ecological benefits of the year.

$$W_{ij} = U_{ij} \times \lambda_j \quad (6)$$

$$F_i = \sum_{j=1}^{m} W_{ij} \times 100 \quad (7)$$

Where, W_{ij} represents the score of the evaluation index j for the year i of Yunnan Province. λ_j is the weight of the indicator j, and W_{ij} is the normalized value of the indicator j of the year i of Yunnan Province. F_i represents the total score of new-style urbanization level or land use ecological benefit in Yunnan Province in the year i. Since the calculated indices are all between 0 and 1, the calculation results are weighted by the percentage system, which describe the spatial distribution characteristics of the new-style urbanization and sustainable

TABLE 1
Index system of the new urbanization and ecological environment coupling system

System layer	Criterion layer	Selection basis	Indicator layer	Attributes	Weights
New urbanization	Economic urbanization	The level of economic development	The proportion of secondary and tertiary industries in GDP (%)	positive	0.125
			GDP per capita (yuan / person)	positive	0.052
			Per capita disposable income of urban residents (yuan)	positive	0.091
			Proportion of retail sales of urban residents (%)	positive	0.051
	Social urbanization	Habitat Environmental Quality	Health technical personnel per 1,000 people (person)	positive	0.063
			Proportion of cultural industry expenditure (%)	positive	0.036
			Number of buses per 10,000 people (vehicles)	positive	0.084
			Number of beds in health centers and hospitals per 1,000 people (zhang)	positive	0.046
	Population urbanization	Demographic and social pressure	Proportion of urban population (%)	positive	0.057
			Proportion of non-agricultural population (%)	positive	0.039
			Urban employment rate (%)	positive	0.079
	Spatial urbanization	Responding to Urbanized Land Use	Urban population density (%)	positive	0.102
			Proportion of built-up area (%)	positive	0.021
			Per capita highway open mileage (km2)	positive	0.032
	Urban-rural integration	Coordination of urban and rural development	Per capita income of urban and rural residents (%)	Moderate	0.034
			Per capita social consumption of urban and rural residents (%)	Moderate	0.021
			Urban and rural employment ratio (%)	Moderate	0.057
Ecosystem	Ecological environment level	Green development concept	Forest cover rate(%)	positive	0.043
			Water resources per capita (m3 / person)	positive	0.060
			Park green area per capita (m2)	positive	0.095
			Green coverage of built-up area (%)	positive	0.042
			Proportion of wetland area (%)	positive	0.036
	Ecological environmental pressure	Ecological environment status	Water consumption per 10,000 yuan of GDP (m3)	negative	0.104
			Urban sewage discharge per unit area (m3 / km2)	negative	0.067
			Industrial exhaust emissions (m3 / 10,000 yuan)	negative	0.085
			Industrial wastewater discharge (t / 10,000 yuan)	negative	0.078
			Production of industrial solid waste (t / 10,000 yuan)	negative	0.062
	Conservation of ecosystem	Ecological environment governance	Industrial pollution treatment investment (10,000 yuan)	positive	0.102
			Urban sewage treatment rate (%)	positive	0.094
			Industrial solid waste utilization rate (%)	positive	0.075
			Afforestation area (km2)	positive	0.056

TABLE 2
Benefits Distribution of new-style urbanization and Sustainable Development in Yunnan Province

Equal division	＜30	30＜X≤40	40＜X≤50	50＜X≤60	> 60
New-style urbanization	Low level	Little level	Mild level	Little High level	High level
sustainable development	Low efficiency	Little efficiency	Mild efficiency	Little High efficiency	High efficiency

development level in Yunnan Province more objectively and clearly. The classification of new-style urbanization level and sustainable development benefit scores is shown in Table 2.

New-style urbanization and sustainable development coupling level evaluation model. Coupling level model. Coupling is a phenomenon in which two systems interact to coordinate development. Therefore, referring to the capacity coupling coefficient model in physics [18], the calculation formula of the coupling level of the new-style urbanization and sustainable development subsystems is as follows:

$$C = \left[(U_1 * U_2) / (U_1 + U_2)^2 \right]^{1/2} \quad (8)$$

The value C in the formula (8) is $0 \le C \le 1$. When C is equal to 1, the coupling level of both systems is the largest, indicating that both systems are in a benign resonant coupling state, and the coupled system will tend to a new ordered structure. When C is equal to 0, the coupling level of both systems is the smallest, and the systems are in an independent disorder state. According to the division basis of the physics coupling stage, the new-style urbanization and sustainable development coupling state is divided into four stages. The results are shown in Table 3.

Coupling coordination level model. Because of the lack of coupling, the overall effect of responding to new-style urbanization and sustainable development. Therefore, it is impossible to reflect the level of coordination between new-style urbanization and sustainable development. It is necessary to construct a new model of coupling level of urbanization and sustainable development. The formula is as follows:

$$D = (C * F)^{1/2}, F = \alpha U_1 + \beta U_2 \quad (9)$$

In equation (9), D is the coupling coordination level, C is the coupling level, and F is the comprehensive coupling evaluation index of the new-style urbanization and sustainable development, which reflects the overall synergistic effect of both systems. α and β are undetermined coefficients, and the final coupling coordination level is calculated. Referring to the research of Wu Han et al [18], the coupling coordination level is divided into five levels, and the results are shown in Table 4.

RESULTS AND DISCUSSION

Analysis of the relationship between new-style urbanization and sustainable development. Coupling level is a measure of the orderly synergy between the new-style urbanization and sustainable development. The level of coordination is the cooperation among the various elements in both systems, and the new-style urbanization and sustainable development have a dynamic coupling

TABLE 3
Coupling phase division

Coupling level	C=0	(0.1, 0.3]	(0.3, 0.5]	(0.5, 0.8]	(0.8, 1)	C=1
Coupling phase	Disorder	Low levelcoupling	Antagonism	Run-in phase	High level coupling	Order

TABLE 4
Classification of new-style urbanization and sustainable development coupling coordination level

Hierarchical sequence	I	II	III	IV	V
Coordination level	(0.1, 0.2]	(0.2, 0.4]	(0.4, 0.6]	(0.6, 0.8]	(0.8, 1.0]
Coordination level	Seriously uncoordinated	Mild uncoordinated	Primary coordination	Good coordination	High Quality coordination

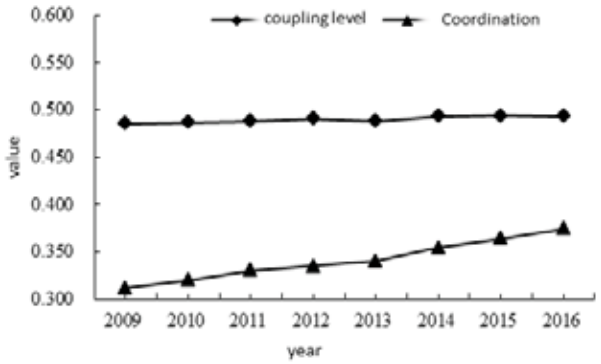

FIGURE 1
Coordination degree of new urbanization and ecological environment in Yunnan Province

TABLE 5
Coupling degree of new urbanization and ecological environment in each city (state) of Yunnan Province

Year	2009	2010	2011	2012	2013	2014	2015	2016	Level of coupling
Kunming City	0.447	0.450	0.451	0.455	0.433	0.462	0.465	0.450	Antagonists
Yuxi	0.487	0.496	0.490	0.490	0.489	0.482	0.490	0.490	Antagonists
Qujing City	0.489	0.480	0.482	0.490	0.492	0.494	0.495	0.495	Antagonists
Zhaotong	0.490	0.492	0.499	0.500	0.500	0.500	0.500	0.500	Break in
Baoshan	0.498	0.495	0.499	0.500	0.500	0.502	0.500	0.503	Break in
Lijiang City	0.494	0.495	0.499	0.500	0.496	0.499	0.500	0.500	Break in
Pu'er City	0.504	0.500	0.499	0.499	0.499	0.500	0.499	0.502	Break in
Lincang	0.499	0.499	0.501	0.500	0.500	0.503	0.499	0.500	Break in
Dehong	0.496	0.450	0.498	0.500	0.499	0.500	0.499	0.500	Break in
Nu River	0.431	0.469	0.469	0.459	0.450	0.499	0.500	0.500	Break in
Diqing	0.459	0.450	0.469	0.469	0.469	0.459	0.460	0.460	Antagonists
Dali	0.489	0.499	0.499	0.500	0.500	0.499	0.500	0.500	Break in
Chuxiong	0.499	0.501	0.499	0.500	0.500	0.499	0.500	0.500	Break in
Red river	0.492	0.480	0.89	0.489	0.490	0.489	0.490	0.490	Antagonists
Wenshan	0.499	0.499	0.499	0.498	0.499	0.500	0.500	0.500	Break in
Xishuang-banna	0.498	0.499	0.499	0.500	0.498	0.500	0.502	0.500	Break in

TABLE 6
Coordination levels of new urbanization and ecological environment in each city (state) of Yunnan Province

Year	2009	2010	2011	2012	2013	2014	2015	2016	Degree of coordination
Kunming City	0.41	0.42	0.42	0.43	0.41	0.44	0.44	0.45	Primary disorders
Yuxi	0.37	0.37	0.38	0.37	0.38	0.36	0.36	0.37	Mild disorder
Qujing City	0.34	0.32	0.35	0.35	0.34	0.35	0.36	0.37	Mild disorder
Zhaotong	0.30	0.32	0.31	0.32	0.32	0.32	0.33	0.33	Mild disorder
Baoshan	0.31	0.33	0.32	0.32	0.33	0.32	0.33	0.34	Mild disorder
Lijiang City	0.30	0.31	0.31	0.32	0.33	0.33	0.34	0.36	Mild disorder
Pu'er City	0.28	0.29	0.31	0.32	0.32	0.33	0.34	0.36	Mild disorder
Lincang	0.27	0.29	0.30	0.31	0.32	0.33	0.33	0.34	Mild disorder
Dehong	0.29	0.29	0.30	0.31	0.32	0.32	0.34	0.35	Mild disorder
Nu River	0.30	0.31	0.32	0.33	0.33	0.35	0.36	0.37	Mild disorder
Diqing	0.30	0.32	0.33	0.34	0.37	0.38	0.39	0.41	Primary coordination
Dali	0.32	0.33	0.35	0.34	0.36	0.35	0.36	0.37	Mild disorder
Chuxiong	0.29	0.30	0.32	0.32	0.33	0.32	0.34	0.35	Mild disorder
Red river	0.30	0.31	0.32	0.32	0.33	0.33	0.34	0.36	Mild disorder
Wenshan	0.26	0.27	0.28	0.30	0.30	0.31	0.32	0.34	Mild disorder
Xishuang-banna	0.34	0.34	0.36	0.36	0.35	0.37	0.38	0.39	Mild disorder

relationship. According to formula (8) and formula (9), the coupling level and coordination level of new-style urbanization and sustainable development in Yunnan Province and each city (state) are calculated. The results are shown in Figure 1, Table 5 and Table 6.

It can be seen from Figure 1. The coupling level of new-style urbanization and sustainable development in Yunnan Province was stable during the period from 2009 to 2016, and the fluctuation range was small. The average coupling level was 0.490, which was in the enthalpy stage. By checked and balanced with each other, they are close to the running-in stage of (0.5, 0.8], which indicates that the rapid development of new-style urbanization has higher requirements for sustainable development and has a certain coercive effect, so it has a mutual competition. The level of coordinated development has continued to rise from 2009 to 2016. However, it is still at a level of slight imbalance. It shows that the new-style urbanization and sustainable development of Yunnan Province has not yet reached the cooperation, but its coordination level is constantly improving. Coordinated development of cities and states are shown in Yunnan Province from Table 5 and Table 6. In terms of situation, Kunming, Qujing, Diqing and Honghe are in the embarrassing stage, while the rest of the cities

(states) barely reach the running-in stage, including Baoshan City in the southwest of Guizhou. The coupling between urbanization and sustainable development is the highest, but Kunming, which has a relatively high economic output, has the lowest coupling level. At the same time, only Kunming and Diqing reach at the primary coordination level, and the rest of the cities State is in a mildly disordered state.

From the time-space evolution of the coupling and coordinated development of new-style urbanization and sustainable development in Yunnan Province from 2009 to 2016, the coupling level of Kunming City declined in 2016, while other cities (states) showed an upward trend of varying levels of fluctuation. However, in terms of the level of coordination, Kunming reached 0.45 in 2016, which is at the highest level among cities (states). However, the coordination level of other cities (states) is in a steady rising stage, among which the growth rates of *Diqing* Prefecture has fastest increase from 0.30 in 2009 to 0.41 in 2016, the growth is obvious. Based on the spatial differentiation of new-style urbanization levels and ecological benefits, the development of coordination level has affected by regional economic level, ecological basis, population pressure, and sustainable development governance. Therefore, based on the status quo of new-style urbanization development in Yunnan Province, the key should be to strengthen exchanges and cooperation among regions, which reduce the irrational resource allocation and the irrational use of resources in the development of new-style urbanization.

CONCLUSION

Through the calculation of the new-style urbanization level and sustainable development benefit of Yunnan Province, and based on the coupling coordination level model, the coupling and coordination relationship is studied. The conclusions are as follows. First, the level of new-style urbanization development and sustainable development benefits in Yunnan Province is quite different in space. From the perspective of spatial distribution, its new-style urbanization level is characterized by decreasing from the central to the periphery. Based on the concept of sustainable development, relevant policies are formulated by the regional development. The reinforcement of cooperation and exchanges among cities (states) is to narrow regional differences, which promotes new-style urbanization levels. Second, the new-style urbanization has high requirements for sustainable development. The new-style urbanization and sustainable development of Yunnan Province have not yet reached at the state of cooperation, but the coordination level is constantly improving. Third, the irrational distribution reduction of resources and the irrational used in the new-style urbanization, it is the key to improve the development of new-style urbanization in Yunnan.

REFERENCES

[1] Zhang, Z.B. (2013) Strategic Significance and Reform Challenges of New Urbanization. Journal of National School of Administration. (1), 48-54.

[2] Yao, S.M., Zhang, P.Y., Yu, C. (2014) The Theory and Practice of New Urbanization in China. Geographical Science. 34(6), 641-647.

[3] Wang, H.Z. (2016) Research on the Inner Relationship between New Urbanization and Ecological Environment in China. Journal of Shijiazhuang University of Economics. 39(4), 43-48.

[4] Zhan, J.R., Wang, Z.Y. (2016) Research on Chongqing New Urbanization Construction under Low Carbon Economy. China Agricultural Resources and Regional Planning. 37(12), 57-61.

[5] Pei, W., Deng, L. (2017) Mechanism and Realization Path of Synergistic Promotion of New Urbanization and Ecological Civilization Construction. Journal of Northwest University for Nationalities (Philosophy and Social Sciences Edition). (1), 106-113.

[6] Wang, G.H., Zhao, X.Y., Huang, Y.S. (2018) Research On the Relationship Between New Urbanization and Coordinated Development of Ecological Environment. Economic Issues. (3), 112-117.

[7] Li, X.Q., Jiang, B., Chu, N.C. (2017) Coupling and Coordination Analysis of Urban Intensive Land Use and New Urbanization-Taking Three Urban Clusters in China as an Example. Resources And Environment In The Yangtze Basin. (7), 31-39.

[8] Tian, S.Z., Fang M.Y., Li G.L. (2017) Population-Land-Economy-Social Urbanization Level Measurement and Coupling Coordination Analysis - Based on Panel Data of 31 Provinces. Journal of Shijiazhuang University of Economics. 40(4), 49-57.

[9] Chenery, H.B. (1957) In: Patterns of Development:1950-1970. Oxford University Press, Oxford.

[10] Lucas, R.E. (1988). On the Mechanics of Economicis Development. Journal of Monetary Economicis. (1), 3-42.

[11] Moomaw, R.L., Shatter, A.M. (1996) Urbanization and Economic Development:A Bias toward Large Cities. Journal of Urban Economics. (1), 21-32.

[12] Xu, L. (2018) Evaluation of New Urbanization Development Level and Analysis of Its Spatial Characteristics-Taking Changzhou City, Jiangsu Province as an Example. Chinese Journal of Agricultural Resources and Regional Planning. 38(6), 61-66.
[13] Wang, C.L., Han L., Zhu Z.L. (2018) Analysis of the Temporal and Spatial Coupling Relationship between New Urbanization and Human Settlement Environment Development in Ningxia. Chinese Agricultural Science Bulletin. (26), 83-89.
[14] Wang, S.J., Ren, L., Kong, W. (2018) Research on the Coordinated Development of Eco-environment-Economy-New Urbanization in Beijing-Tianjin-Hebei Region. East China Economic Management. (10), 61-69.
[15] Shen, L.Y., Ochoa, J.J., Shah, M.N., Zhang, X.L. (2011) The Application of Urban Sustainability Indicators-Acoparison between Various Practices. Habitat International. 35(1), 17-29.
[16] Wu, J.Q., Luo H.S., Chen C.Y. (2014) Research on the Coordinated Development of Urbanization and Industrial Ecology in Yunnan——A Coordination Evaluation Model Based on Improved Entropy Method. Resources Development and Market. 30(2), 138-140.
[17] Peng, B.W., Wu, Y.D., Cao, H.H. (2016) Analysis of Coordinated Development of Tourism and New Urbanization Based on System Coupling——Taking Yunnan Province as an Example. World Geography Research. 25(2), 103-114.
[18] Zheng, J.C. (2015) Research on the Relationship between New Urbanization Promotion and Regional Economic Development——An Empirical Analysis Based on Data from Yunnan Province. Economic Problems Research. (9), 65-71.
[19] UN-Habitat. (2002) In: Sustainable Urbanization Achieving Agenda21.UN-Habitat, Nairobi.
[20] Bettencourt, L.M., Lobo, J., Helbing, D., Kuhnnert, C., West, G. B. (2007) Growth,innovation,scaling,and the pace of life in cities. Proceedings of the National Academy of Sciences. 104(17), 7301-7306.
[21] Hezri, A.A. (2004) Sustainability Indicator System and Policy Processes in Malaysia: A Framework for Utilization and Learning. Journal of Environmental Management. (73), 357-371.
[22] Rong, H.Q. (2013) On China's New Urbanization Construction and Ecological Environment Protection. Modern Economic Research. (8), 5-9.
[23] Zhang, X.F. (2017) Analysis and Evaluation of Land Use Efficiency and New Urbanization Coordination-Based on Empirical Analysis of the Middle Reaches of the Yangtze River. Chinese Journal of Agricultural Resources and Regional Planning. 38(4), 62-68.
[24] Han, W. (2017) Analysis of the Coupling Coordination Relationship between New Urbanization and Ecological Environment in Zhejiang Province. Journal of Ningbo University (Humanities Science Edition). 30(4), 118-123.
[25] Zhang, C.Y. (2014) Coupling Evaluation Model of Tourism Industry and New Urbanization. Statistics and Decision. (14), 28-31.
[26] Liu, C.Y., Liu, Y.Y., Ding, R.G. (2018) Coupling Analysis of New Urbanization and Ecological Environment in Fujian Province. Chinese Journal of Applied Ecology. 29(9), 3043-3050.

Received: **25.09.2019**
Accepted: **19.02.2020**

CORRESPONDING AUTHOR

Dan Huang
School of Tourism and Geography Science,
Yunnan Normal University,
Yunnan 650500 – China.

e-mail: huangdan_ynnu@163.com

© by PSP Volume 29 – No. 05/2020 pages 3641-3649 Fresenius Environmental Bulletin

CEPHALARIA SYRIACA (L.): INVESTIGATION OF ANTIMICROBIAL, ANTIBIOFILM, ANTIOXIDANT POTENTIAL AND SEED MORPHOLOGY

Esra Atalan[1], Ali Savas Bulbul[2,*],Yusuf Ceylan[3]

[1]Bartin University,Graduate School of Natural andApplied Sciences, Department of Biology, Bartin, Turkey
[2]Kahramanmaras Sutcu Imam University, Faculty of Arts and Sciences, Department of Biology, Kahramanmaras, Turkey
[3]Bartin University, Faculty of Science, Department of Molecular Biology and Genetics, Bartın, Turkey

ABSTRACT

Plants that have been used in the treatment of many diseases for centuries are now used for industrial and medical purposes. *Cephalaria* genera in the Dipsacaceae family have properties such as mitigating and relaxing. *Cephalaria syriaca* L., commonly found in Anatolia, is generally used in industry due to the fatty acids it contains. It is also used as the additive to wheat flour.

This study aimed to investigate the antibacterial activity of DMSO extracts of oil derived from the seed of *Cephalaria syriaca* (L.) grown in Turkey against twenty bacterial strains. For this purpose, disk diffusion, minimum inhibitory concentration (MIC) and minimum bactericidal/bacteriostatic concentration (MBC) methods were used. Antifungal activity of DMSO extracts against a fungus strain was examined by disc diffusion method.

Antioxidant activities of seed oil extracts were investigated using DPPH (2,2-diphenyl-1-picrylhydrazyl) radical scavenging assay. In addition, seed morphology was examined using a stereomicroscope and scanning electron microscope (SEM). In conclusion, the extracts had the highest antibacterial activity against *Staphylococcus epidermidis* and *Enterobacter aerogenes* extracts, and the highest antibiofilm activity against *Proteus vulgaris*, with 39.94 ± 9.25%.

KEYWORDS:
Antibiofilm activity, antimicrobialactivity, antioxidantactivity, *Cephalaria syriaca*, morphology

INTRODUCTION

Utilization of the plants in the prevention and treatment of human diseases dates back to ancient times. Medically important plants in Turkey and in other countries are used by people from the past to present [1, 2]. It is also being benefitted from essential oils as feed supplements. In addition, they exert antimicrobial activities against a wide range of microorganisms including bacteria, protozoa, and fungi [3]. Besides their antimicrobial activities, they also have antiseptic, antioxidant, digestive stimulant and enzymatic properties [4].

Herbal antimicrobial agents have been used for centuries to preserve and keep food. It is known that herbs have been used as a medicine from BC 2700 until today. In recent years, foodborne diseases have commonly been seen throughout the world. Preventive methods are used in the food industry in order to prevent the spread of these diseases, which pose a serious problem for both human health and food industry. Natural or synthetic substances, which are used as the preservative due to their antimicrobial activity, are the most important of these methods. With the recent emergence of the adverse effects of foods containing chemical substances, the increasing trend has been towards natural antimicrobial substances all over the world. For this purpose, research on natural antimicrobial products that could be used in the food industry is also increasing [5].

Phytochemical studies on the genus *Cephalaria* belonging to the Dipsacaceae family indicate that various compounds such as iridoids, flavonoids, triterpenes, alkaloids, and lignans have been used in conventional medicine for centuries. Most of these compounds exhibit antimicrobial, antifungal, antioxidant and cytotoxic activities [6]. It is known that there are about 12 species of *Cephalaria* genus in Turkey. However, the species *Cephalaria syriaca* L. is exclusively widespread throughout Anatolia [7]. *C. syriaca* is an annual, very hardy plant that grows as weeds in wheat fields [7, 8].

MATERIALS AND METHODS

Plant materials. *Cephalaria syriaca* (L.) seeds used here were supplied from the Central Research Institute for Field Crops.

Plant extraction. *C. syriaca* seed was kept overnight at the laboratory environment for drying and then pulverized. Oil was extracted from pulverized *C. syriaca* seed with petroleum ether in

soxhlet apparatus. Rotary evaporator was used to remove the solvent. The obtained pure *C. syriaca* oil was dissolved with DMSO and prepared at different concentrations (70 µl/ml, 50 µl/ml, 30 µl/ml and 10 µl/ml).

Antimicrobial activity. Microorganisms and media. Twenty bacterial strains (*Klebsiella pneumoniae, Staphylococcus aureus, Proteus vulgaris, Escherichia coli CFAI, Serratia marrescer, Staphylococcus epidermidis, Alfa Streptococcus haemolyticus, Enterococcus faecium, Pseudomonas aeruginosa, Listeria monocytogenes, Enterococcus durans, Salmonella kentucky, Enterobacter aerogenes, Salmonella infantis, Pseudomonas fluorescens, Enterococcus faecalis, Listeria innocua, Salmonella enteritidis, Salmonella typhimurium* and *Bacillus subtilis*) were used to test antibacterial activity of seed extracts, while *Candida albicans* strain was used to determine antifungal activity of seed extracts. LB broth (Luria Bertoni) was used in bacterial subculture and MIC analysis, while Mueller-Hinton agar (MHA) was used MBC and disk diffusion. In addition, Potato Dextrose Agar (PDA) was also used for the development of fungi.

Disc diffusion assay. Disc diffusion method described previously by Andrews [9] was used to investigate the antimicrobial activity. Sterile discs were impregnated with four different concentrations of culture media and positive and negative controls. The discs were placed onto the bacteria cultured in MHA medium and incubated at 37°C for 16-18 hours. Similarly, the discs were placed onto the fungus cultured in PDA medium and incubated at 25°C for 24-48 hours. AZM (Azithromycin) antibiotics for bacteria and Oceral for fungi were used as positive controls.

Minimum inhibition concentration (MIC). The minimum inhibition concentration values (MIC) of the extract were determined according to the method applied by Basile et al. [10]. An equal volume of 70 µl / ml was added to the LB broth added on the 96-well microplates, then serial dilution was performed. After serial dilution, bacterial culture was added and incubated at 37°C for 16-18 hours. Then it was measured using spectrophotometer at 600 nm. The evaluation was performed depending on the positive and negative controls.

Minimum bactericidal/bacteriostatic concentration (MBC). Samples were taken from the wells where MIC values are calculated, and cultured on MHA (Mueller Hinton Agar) solid medium. It was then incubated at 37°C for 18-24 hours.

Antibiofilm activity. Antibiofilm properties of the prepared concentrations were determined using the method described by Merritt et al. [11]. Bacteria were incubated within a 96-well microplate at 37 °C for 48 hours. Following incubation, the solutions present in the wells were completely discharged, washed and allowed to dry. After drying, it was fixed using 95% methanol and allowed to dry again. 0.1% crystalline violet solution was added to each of the dried wells and allowed for staining. The microplates were then washed and allowed to dry. Just after drying, 33% glacial acetic acid solution was added to the wells containing gram-positive bacteria and 95% ethanol solution was added to the wells containing gram-negative bacteria. 15 minutes later, the microplates were read at 600 nm on a spectrophotometer. The same treatments were also applied to the wells containing the positive controls. The % inhibition value of the biofilm formation was calculated from the measurement results using the following formula.

% Inhibition formula: % Inhibition = (Acontrol- ASample / Acontrol) x100

AControl: Absorbance valuesfor the control group at 600 nm

ASample: Absorbance valuesfor the sample group at 600 nm

Antioxidant activity. The antioxidant property of the oil was determined using the method developed by Blois [12]. 1 mL of extracts prepared at different concentrations (4.375 µl / ml -70 µl / ml) and 1 mL of Ascorbic acid (4.375 µl / ml -70 µl / ml) used as the standard were placed into glass tubes. 4 mL of 0.1 mM solution of DPPH (dissolved in ethanol) was added onto it. It was kept in the dark at room conditions for 30 minutes, subsequently, absorbance values at 517 nm were measured. DPPH radical scavenging activity was calculated the measurement results using the following formula.

$$\%\ \text{DPPH radical scavenging activity} = \frac{\text{Control Absorbance - Sample Absorbance}}{\text{Control Absorbance}} = x\ 100$$

Seed Morphology. The morphology and systematic importance of *C. syriaca* seed were determined using stereomicroscope according to the method developed by Fırat and Başer [13]. Olympus SZ2-LGB digital photography system and scanning electron microscope (SEM) were used for morphological examination. The seed width and length were measured, then their photographs were taken. Tescan MAIA3XMU model electron microscope in Bartın University Central Research Laboratory was used for detailed surface shapes of seed samples. Microphotographs at different magnifications were gained for each seed examined.

RESULTS AND DISCUSSION

Disc diffusion results. Disc diffusion results of the concentrations are shown in Table 1. All the plant extracts exhibited antimicrobial activity at different concentrations. The highest inhibition value was observed at concentrations of 10 µl/ml and 30 µl/ml among the extracts. A concentration of 10 µl/ml created a 10.66 mm diameter inhibition zone on *Staphylococcus epidermidis*, whereas a concentration of 30 µl / ml formed a 10.33 mm diameter inhibition zone on *Enterobacter aerogenes*. Pure oil from *C. syriaca* and 70 µl/ml concentration of *C. syriaca* showed antifungal effect against *C. albicans*. Other concentrations produced no antifungal effect.

MIC and MBC Results. MIC method was used to determine the lowest amount of the active ingredient necessary for preventing the growth of microorganisms. MIC results of microplates after 16-18 hours of incubation are shown in Table 2. MIC results were supported by MBC test results, which are shown in Figure 1. MICs were detected at 35 µl/ml concentrations against *Klebsiella pneumoniae, Salmonella infantis, Pseudomonas fluorescens, Enterococcus faecalis* and *Listeria innocua*. MICs were obtained at 17.5 µl/ml concentration against other bacteria. MBC analysis performed according to the detected MIC concentrations showed that these concentrations have bacteriostatic effects on bacteria. Taken all together, MIC, MBC, and disk diffusion results support each other.

TABLE 1
Inhibition zones (mm) of *C. syriaca* seed oil extracts

	Inhibition zone (mm)*						
Microorganisms	*C. syriaca* pure oil	*C. syriaca* 70 µl/ml	*C. syriaca* 50 µl/ml	*C. syriaca* 30 µl/ml	*C. syriaca* 10 µl/ml	%100 DMSO	+ Control
Klebsiella pneumoniae	5,66	7,5	7	7,66	7,5	7	15
Staphylococcus aureus	6,33	4,5	8,16	7,66	9,16	8,66	20
Proteus vulgaris	6,83	6,83	4,66	9	8,33	7,16	21
Escherichia coli	8,5	8	8	8,5	8,66	7,16	9
Serratia marcescens	8,16	7,33	8,16	8,33	6,83	8	23
Staphylococcus epidermidis	7,16	8,33	9,8	10	10,66	8,16	22
Alfa Streptococcus haemolyticus	8,33	7,66	6,66	7,5	7,5	4,33	18
Enterococcus faecium	7	7,66	8,33	9,66	6,83	4,5	20
Pseudomonas aeruginosa	7,66	7,16	8,66	9,66	6,66	6,66	22
Listeria monocytogenes	7,16	7,16	7,33	9	7,5	4,66	20
Enterococcus durans	6,66	7	7	8,16	7,16	7,66	22
Salmonella kentucky	7	8	7,66	8,16	8,33	6,66	21
Enterobacter aerogenes	7,33	8,66	9,33	10,33	7,66	7,33	19
Salmonella infantis	6,83	7,16	8,16	8,16	6,33	8	22
Pseudomonas fluorescens	7,83	7,83	7,33	8	6,83	7	24
Enterococcus faecalis	7,66	7,33	7,66	6,83	6,5	6,83	18
Listeria innocua	7,16	6,66	7,5	8,5	6,83	7	20
Salmonella enteritidis	7,83	6,83	7,16	7	6,83	6,66	24
Salmonella typhimurium	2,6	7,5	7,16	8,16	5,33	4,83	25
Bacillus subtilis	7	7,33	8,16	7,16	6,5	7,16	19
Candida albicans	6,83	2,16	0	0	0	0	35

TABLE 2
MIC values of *Cephalaria syriaca* seed oil extracts

	Minimum Inhibition Concentration (MIC)
Microorganisms	***Cephalaria syriaca***
Klebsiella pneumoniae	35 µl/ml
Staphylococcus aureus	17,5 µl/ml
Proteus vulgaris	17,5 µl/ml
Escherichia coli	17,5 µl/ml
Serratia marcescens	17,5 µl/ml
Staphylococcus epidermidis	17,5 µl/ml
Alfa Streptococcus haemolyticus	17,5 µl/ml
Enterococcus faecium	17,5 µl/ml
Pseudomonas aeruginosa	17,5 µl/ml
Listeria monocytogenes	17,5 µl/ml
Enterococcus durans	17,5 µl/ml
Salmonella Kentucky	17,5 µl/ml
Enterobacter aerogenes	17,5 µl/ml
Salmonella infantis	35 µl/ml
Pseudomonas fluorescens	35 µl/ml
Enterococcus faecalis	35 µl/ml
Listeria innocua	35 µl/ml
Salmonella enteritidis	17,5 µl/ml
Salmonella typhimurium	17,5 µl/ml
Bacillus subtilis	17,5 µl/ml

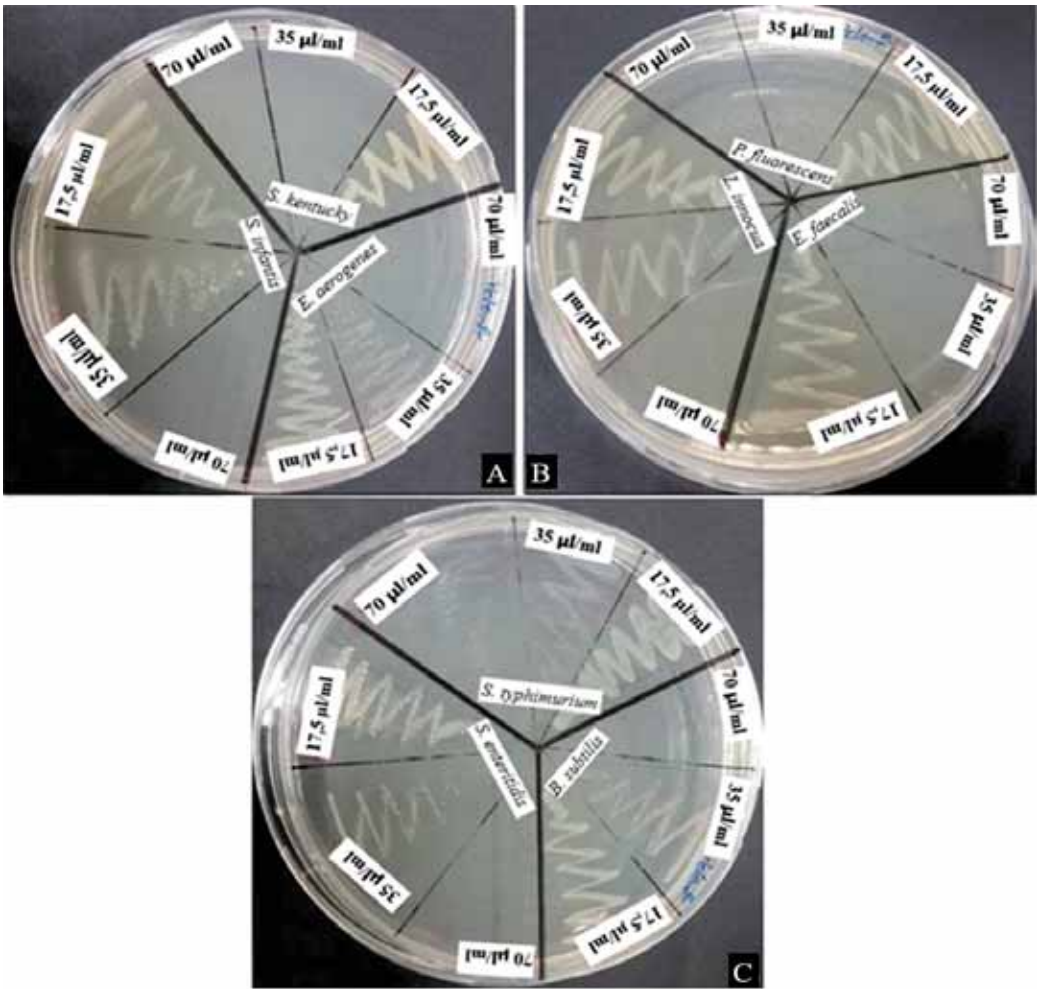

FIGURE 1

MBC results of 70 µl / ml, 35 µl / ml, 17.5 µl / ml concentrations of *Cephalaria syriaca* seed oil [*S. infantis* (A), *S. kentucky* (A), *E. aerogenes* (A) *P. fluorescens* (B), *E. faecalis* (B), *L. innocua* (B), *S. enteritidis* (C), *S. typhimurium* (C) and *B. subtilis* (C)].

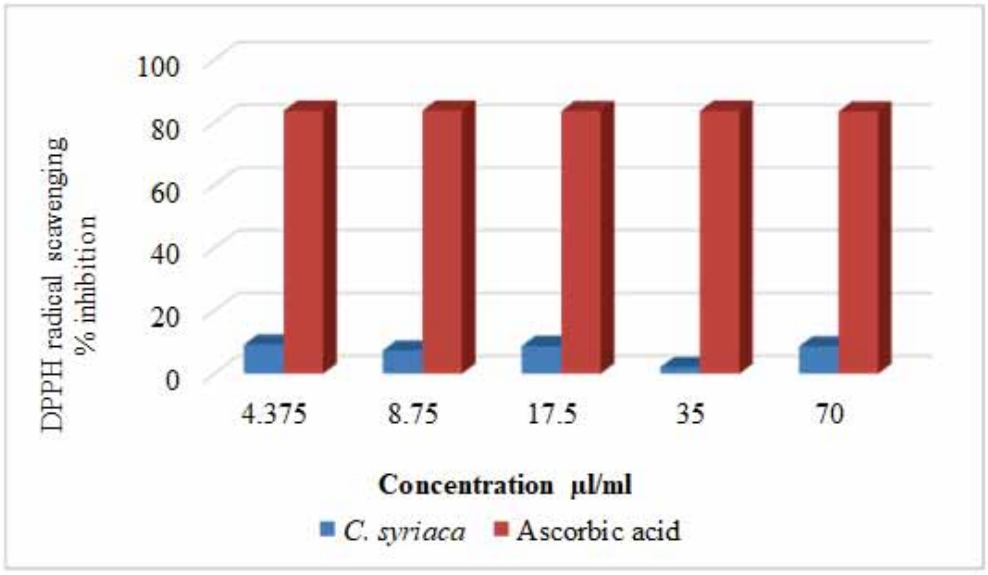

FIGURE 2

DPPH radical scavenging activity (% inhibition values) of *Cephalaria syriaca* seed oil extract sandstandard antioxidant agents

Results of Antioxidant Activity (DPPH). Antioxidant activity of concentrations (70 µl/ml, 35 µl/ml, 17.5 µl/ml, 8,75 µl/ml, 4,375 µl/ml) were established by DPPH radical scavenging activity. The results are shown in Table 3 and Figure 2. Ascorbic acid was used as a standard substance. As shown in Figure 2, when compared the studied concentrations with the standard substance, plant extracts did not have high activity. The highest value was obtained at 4.375 4,3l µl/ml, while the lowest value was observed at 35 µl/ml.

Antibiofilm results. The present results showed that seed oil extracts from *C. syriaca* exhibited the highest antibiofilm activity against *P. vulgaris* and 35 µl/ml concentration inhibited biofilm formed by *P. vulgaris* by 39.94 ± 9.25%. However, the studied concentrations did not have antibiofilm activity against *L. monocytogenes* and *E. durans*. The percent of biofilm inhibitory concentration is shown in Table 4.

General Seed Morphology. Data on seed morphology obtained by stereo microscopy and scanning electron microscopy are shown in Table 5. Surface ornamentation was determined as reticulate and verrucate. Electron micrograph of seed is shown in Figure 3 and its surface ornamentation in Figure 4.

TABLE 3
Percent agein hibition values (according to concent rations) of DPPH radical scavenging activity of *Cephalaria syriaca* seed oil extracts and standard antioxidant agents.

Concentration	*Cephalaria syriaca* extract	Ascorbic acid
70 µl/ml	9,27 ± 8,16	83,75 ± 0,46
35 µl/ml	7,4 ± 3,79	83,85 ± 0,63
17,5 µl/ml	8,79 ± 0,58	83,66 ± 1,02
8,75 µl/ml	2,06 ± 1,57	83,76 ± 0,69
4,375 µl/ml	8,7 ± 4,98	83,55 ± 0,19

TABLE 4
Percentages inhibition of biofilm formation of plant extracts used in research.

	Antibiofilm Activity				
Microorganisms	*C. syriaca* 70 µl/ml	*C. syriaca* 35 µl/ml	*C. syriaca* 17,5 µl/ml	*C. syriaca* 8,75 µl/ml	*C. syriaca* 4,375 µl/ml
K. pneumoniae	0	0	9,83 ± 8,99	0	0
S. aureus	0	13,61 ± 13,49	20,83 ± 9,57	1,04 ± 0,89	0
P. vulgaris	30 ± 2,73	39,94 ± 9,25	16,4 ± 11,58	17,06 ± 7,47	0
E. coli	17,68 ± 8,29	34,64 ± 14,49	31,85 ± 12,47	24,85 ± 6,89	20,72 ± 5,84
S. marcescens	28 ± 16,72	32,49 ± 6,53	29,35 ± 7,85	14,58 ± 12,68	0
S. epidermidis	0	26,77 ± 2,80	27,16 ± 1,63	21,8 ± 3,07	12,82 ± 4,81
Alfa S. haemolyticus	0	0	22,78 ± 6,15	15,39 ± 5,61	11,09 ± 3,22
E. faecium	13,69 ± 8,45	17,21 ± 15	18,51 ± 3,53	16,31 ± 14,26	7,68 ± 7,5
P. aeruginosa	27,93 ± 3,20	35,94 ± 5,28	38,5 ± 7,37	30,21 ± 13,97	17,65 ± 14,8
L. monocytogenes	0	0	0	0	0
E. durans	0	0	0	0	0
S. kentucky	28,94 ± 9,26	39,26 ± 7,76	38,12 ± 3,89	25,64 ± 8,84	11,08 ± 10,49
E. aerogenes	28,63 ± 12,78	24,74 ± 11,01	11,64 ± 8,51	0	0
S. infantis	27,35 ± 5,59	25,44 ± 5,57	20,27 ± 13,49	12,6 ± 11,78	0
P. fluorescens	23,79 ± 3,06	28.38 ± 6,84	24,59 ± 11,17	12,82 ± 12,29	8,22 ± 7,14
E. faecalis	0	0	9,64 ± 3,22	5,67 ± 3,12	0
L. innocua	0	9,48 ± 4,29	10,23 ± 6,64	9,12 ± 8,30	7,34 ± 6,52
S. enteritidis	20,06 ± 10,99	20,11 ± 12,06	0	0	0
S. typhimurium	4,15 ± 2,30	-	-	-	-
B. subtilis	2,36 ± 2,17	-	-	-	-

TABLE 5
Seed dimensions (values in mm) and seed morphological findings.

Taxon	Seed length	Seed width	Seed length / Width ratio	Seed color	Seed shape	Hilum length	Hilum width	Surface ornamentation
C. syriaca	5,97±0,43	2,27±0,24	2,63	Yellowish brown	Elipsoid	0,33±0,08	0,49±0,14	Reticulate and verrucate

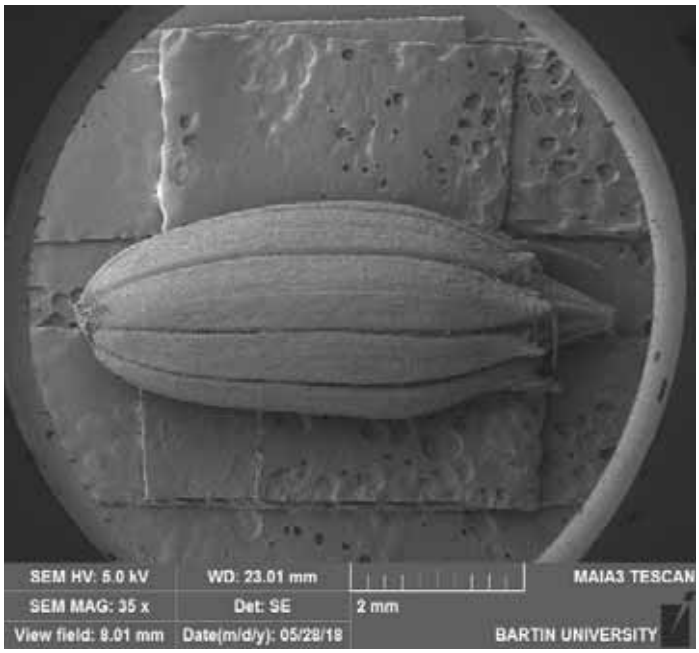

FIGURE 3
SEM images of *Cephalaria syriaca* seed.

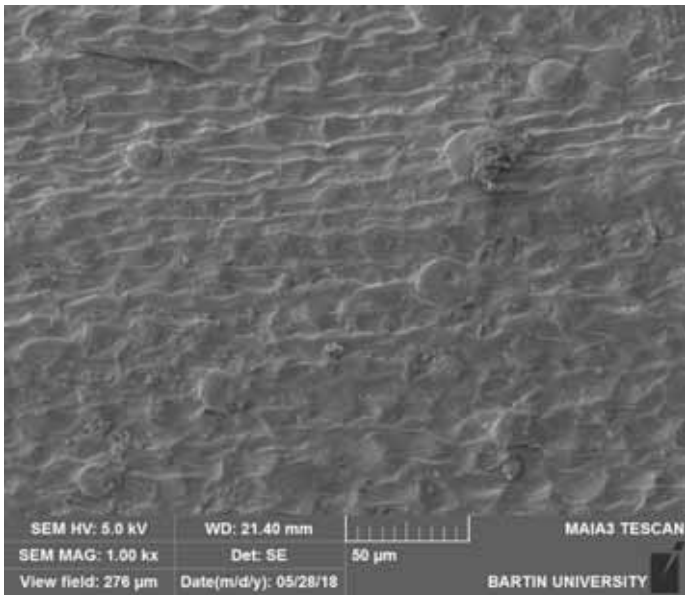

FIGURE 4
SEM image of surface ornamentation.

DISCUSSION AND CONCLUSION

Perdetzoglou et al. [14] investigated the fatty acid and sterol compositions of eight taxa belonging the genus *Lomelosin* (Dipsacaceae) and the antibacterial activities of extracts obtained from *Lomelosia minoana* subsp. *asterusica*, *Lomelosia sphaciotica* var. *sphaciotica* and *Lomelosia sphaciotica* var. *decalvans* against *E. coli*, *P. aeruginosae, S. aureus, S. epidermidis, K. pneumoniae* and *E. cloacae*. They reported that plant extracts showed no antimicrobial activity against *P. aeruginosae* and *K. pneumoniae*. In their study, however, the extract derived from *L. sphaciotica* var. *sphaciotica* showed the highest activity against E. cloacae and the lowest activity against *S. aureus*. *Lomelosin* genus in that study and *C. syriaca* in the present study belong to the same family (Dipsacaceae). Contrary to their results, we observed that *C. syriaca* exhibited antimicrobial effects on *E. coli, P. aeruginosae, S. aureus, S. epidermidis* and *K. pneumoniae*.

Ertürk et al. [15] investigated the antimicrobial activities of commercially purchased thyme and mint essential oils (against 12 gram-positive bacteria, 8 gram-negative bacteria, 1 mycobacterium and 7 yeast strains). They found that the antimicrobial effect of thyme essential oil was higher than that of

mint essential oil. When compared inhibition zone diameters of thyme and mint essential oils, thyme values (24.27 ± 3.99 mm) were greater than mint values (16.55 ± 6.17 mm). Mint essential oil showed the highest activity against *C. albicans* (27 ± 1 mm), while it had no effect on *E. faecalis, E. coli, P. aeruginosa* and *S. typhimurium*. Thyme essential oil produced the highest antimicrobial effect against *L. welshimeri* (30 mm) and *S. aureus* (29 ± 1 mm) whereas it showed no action against *P. aeruginosa*. In our study, essential oil of *C. syriaca* had an antimicrobial effect on *P. aeruginosa, S. aureus, E. faecalis, E. coli, P. aeruginosa, S. typhimurium* and *C. albicans* within the range of 10.66-5.5 mm.

Şirin et al. [16] examined the antimicrobial activities of *Ramalina farinacea* (L.) Ach and *Usnea intermedia* (A.Massal) Jatta lichens (against *Bacillus cereus* ATCC 7064, *Bacillus licheniformis* ATCC 14580, *Citrobacter freundii* ATCC 8090, *E. faecalis* ATCC 29212, *E. coli* ATCC 25992, *Klebsiella oxytoca* ATCC 8724, *L. innocua* ATCC 33090, *P. vulgaris* ATCC 8427, *P. aeruginosa* ATCC 27853, *S. enteridis* ATCC 13076, *S. typhimurium* CCM 5445, *Shigella flexneri* ATCC 12022, *S. aureus* ATCC 6538P, *S. epidermidis* ATCC 3699, *Streptococcus pyogenes* ATCC 19615, *Yersinia pestis* ATCC 19428, *C. albicans* ATCC 90028, *Candida glabrata* ATCC 90030, *Candida lipolytica* ATCC 8660, *Candida parapsilosis* ATCC 22019, *Candida tropicalis* ATCC 4563, *Cryptococcus neo-formans* ATCC 32045, *Debaryomyces hansenii* DSM 70238 and *Saccharomyces cerevisiae* ATCC 9796). They reported that both *R. farinacea* (L.) Ach. and *U. intermedia* (A. Massal) Jatta lichens had the highest antimicrobial activity against *C. albicans*; the first showed the highest antimicrobial activity against *S. enteritidis*, and the latter against *S. pyogenes*. In our study, essential oil of *C. syriaca* showed an antimicrobial effect against *S. enteritidis* and *C. albicans*, with the highest against *S. epidermidis*.

Kara et al. [17] investigated the antimicrobial effects of extracts from *Malva sylvestris* L., *Taraxacum officinale* Weber, *Rumex crispus* L., *Althaea officinalis* L. and *Alkanna tinctoria* (on *H. pylori* ATCC 49503, *S. aureus* ATCC 33862, *B. subtilis* ATCC 6633, *E. cloacae* ATCC 13047, *E. coli* ATCC 25922, Proteus mirabilis ATCC 7002, P. aeruginosa ATCC 10145, *K. pneumoniae* (Kİ), *C. albicans* ATCC 60193 and *Saccharomyces cerevisiae* NRRLY 12632). They observed that extracts from *M. sylvestris* L. and *T. officinale* Weber showed the highest activity against *K. pneumoniae* (15 mm); however, the extracts were not effective against *P. aeruginosa* and *C. albicans*. The extracts of *M. sylvestris*, *A. officinalis* and *A. tinctoria* had the lowest antimicrobial activity against *B. subtilis*, *P. mirabilis* and *S. cerevisiae*, and *S. aureus* and *S. cerevisiae*, and *S. cerevisiae*, respectively. In our study, the essential oil of *C. syriaca* had an antimicrobial effect on *S. aureus*, *B. subtilis*, *E. coli*, *P. aeruginosa*, *K. pneumoniae* and *C. albicans*.

Bülbül et al. [18] studied the antimicrobial activity of extracts from *Acanthophyllum acerosum* and *Acanthophyllum microsepherium* (against *E. aerogenes* ATCC 13048, *K. pneumoniae*, *S. enteritidis* ATCC 13075, *S. typhimurium* SL1344, *S. aureus* ATCC 25923, *S. epidermidis* DSMZ 20044, *B. subtilis* DSMZ 1971, *E. coli* CFAI, *E. coli* ATSS 2592, *S. infantis*, *S. kentucky*, *P. aeruginosa* DSMZ 50071, *E. faecium*, *E. durans*, *L. innocua*, *E. faecalis* ATCC 29212, *P. fluorescens* P1, *L. monocytogenes* ATCC 7644 and *C. albicans* ATCC 10231). They noticed that extract of *A. acerosum* had no antimicrobial activity *E. faecium*, *E. durans*, *L. innocua*, *E. faecalis*, *P. fluorescens*, *L. monocytogenes* and *C. albicans* while showing the activity against other microorganisms within the range of 1,83 and 6,67 mm. *A. acerosum* had MIC values at 10 mg/ml against *K. pneumoniae, S. epidermidis, E. coli* CFAI, *S. kentucky*, *P. fluorescens, E. faecalis* and *S. aureus*. They also found that although the extract of *A. microsepherium* had the effect (diameter in 6-7 mm) on *K. pneumoniae, S. enteritidis, S. typhimurium, S. epidermidis*, *S. kentucky* and *E. faecium*, it did not have MIC value against any microorganism. When compared with their findings, we observed the higher antimicrobial effect of *C. syriaca* essential oil.

Witkowska-Banaszczak et al. [19] investigated the antimicrobial and antioxidant activities of the essential oils derived from leaves and flowers of *Succisa pratensis* Moench and of their extracts dissolved in different solvents (against (*S. aureus* NCTC 4163, *P. aeruginosa* NCTC 6749, *C. albicans* ATCC 10231 and *T. mentagrophytes* ATCC 9533). They found that the essential oil from the flowers showed more antimicrobial effect than that from the leaves. They also found that these essential oils had the highest antimicrobial activity against *P. aeruginosa, S. aureus, T. mentagrophytes* and *C. albicans*, but methanol and water extracts showed the moderate or weak effect on these microorganisms. In addition, the methanol extract derived from the leaf had the most potent antioxidant activity. In the present study, the essential oil of *C. syriaca* had the antimicrobial effect on *P. aeruginosa* (MIC = 17.5 µl / ml), *S. aureus* (MIC = 17.5 µl / ml) and *C. albicans*.

Hung et al. [20] isolated six caffeoylquinic acid derivatives from *Dipsacus asper* Wall (Dipsacaceae) and examined its antioxidant activity. They determined that isolated compounds are potent DPPH scavengers and also inhibit LDL oxidation mediated through Cu^{2+} ions. They also demonstrated that *D. asper* and its active phenolic compounds may be useful in preventing the development and progression of atherosclerotic disease. We revealed

that the essential oil of *C. syriaca* exhibits low antioxidant DPPH radical scavenging activity.

Karaca et al. [21] investigated the antibacterial and antibiofilm activities of methanol and ethanol extracts of three medicinally important macrofungi [(*Lentinus edodes* (Berk.) Sing. (Shiitake), *Lactarius deliciosus* Fr. and *Ganoderma lucidum* (Curtis) P. Karst.)]. For this purpose, they studied their effects on *P. aeruginosa* and *S. typhimurium*. They found that methanolic extracts of all three macrofungi exhibit antimicrobial activity at high concentrations (100 mg/ml). Ethanolic extracts did not show antimicrobial activity, whereas all the extracts demonstrated antibiofilm activity. *G. lucidum* extract had the highest antibiofilm activity. We observed that in addition to antimicrobial activity, *C. syriaca* extracts had the highest antimicrobial activity against *P. vulgaris* and low antibiofilm activity against *S. typhimurium*.

Al-Dhabi et al. [22] dissected the antimicrobial and antibiofilm activities of chloroform extracts obtained from fresh fruits of *Couroupita guianensis* (against *B. subtilis* MTCC 441, *Micrococcus luteus* MTCC 106, *E. aerogenes* MTCC 111, *S. aureus* MTCC 96, *Shigella flexneri* MTCC 1457, *Salmonella paratyphi*-B, *K. pneumoniae* MTCC 109, *P. aeruginosa* MTCC 741, *P. vulgaris* MTCC 1771, *S. typhimurium* MTCC 1251, *C. albicans* MTCC 227 and *Malassesia pachydermatis*). They found that chloroform extracts showed good antimicrobial and antibiofilm activities and that inhibition zone diameter with regard to antibacterial activity ranged from 0 to 26 mm. They also showed that the extracts have 52% of antibiofilm activity (2 mg/ml) against *Pseudomonas aeruginosa*. In the present study, the antibiofilm activity of *C. syriaca* extracts ranged from 17 to 35%, while their antimicrobial activity was from 5.5 to 10.66 mm.

Boj˘nanský and Fargašová [23] found that the seed color of the *Knautia drymeia* Heuff from the Dipsacaceae family is yellowish-brown and the seed length ranges from 5.4 to 2-2.4 mm. This species is indigenous to Central and Southern Europe, and grows on wet, humous, stony and loamy grounds among light forests and shrubberies. When these results are compared with our findings, the seed morphology of *C. syriaca* and *K. drymeia* resembles each other.

Cephalaria syriaca is used in bread making by adding to wheat flour, which allows us to investigate the antimicrobial and antioxidant effects. Disc diffusion, MIC and MBC results of *C. syriaca* suggest that it has an antimicrobial effect. It is understood from our results that it has a low antioxidant effect and has an antibiofilm activity at different concentrations. Its seed morphology is similar to what is reported by previous studies.

C. syriaca, which is a common plant and grows in all environments, is thought to be able to contribute to industrial areas and economy. Without bringing costs, it is foreseen that it may be used by adding to biofilm acting materials. Considering the areas of usage of *C. syriaca* in the industry, its growing conditions and its addition to bread flour, this study would contribute to the literature and shed light on future studies.

REFERENCES

[1] Ilçım, A., Dıgrak, M. and Bağcı E. (1998) TheInvestigation of AntimicrobialEffect of SomePlantExtract. Turkish Journal of Biology. 22, 119-125.

[2] Kırbağ, S. and Zengin, F. (2006) Antimicrobial Activies of Some Medical Plants in Elazığ Region.Yuzuncu Yıl University Journal of Agricultural Sciences. 16(2), 77-80.

[3] Turan, F., Gürağaç, R. and Sayın, S. (2012) TheUse of Essential Oils in Aquaculture. 5(1), 35-40.

[4] Şengezer, E. and Güngör, T. (2008) Essentialoilsandtheireffects on animals. Lalahan Journal of Farming Research Institute. 48(2), 101-110.

[5] Yücel Şengün, İ. and Öztürk, B. (2018) Some Natural Antimicrobials Of Plant Origin. Anadolu University Journal of Science and Technology C- Life Sciences and Biotechnology. 7(2), 256 - 276.

[6] Sultana, N., Tek, A.L. and Serçe, S. (2017) Karyotype analysis of *Cephalaria syriaca* cv. Karahan, a new cultivar developed from a wild population. International Symposium on Medicinal Aromatic and Dye plants, Malatya, 403-410.

[7] Katar, D., Arslan, Y., Subaşı, İ. and Kodaş, R. (2012) The effect of different sowing dates on yield and yield components of *Cephalaria* (*Cephalaria syriaca*) under. Biological Diversity and Conservation. 5/3,48-53.

[8] Altunbaş, O. (2015) Pyrolysis Plant Of Pelemir. Selçuk University, Graduate School Of Natural And Applied Sciences, Konya.

[9] Andrews, J.M. (2003) BSAC standardized disk susceptibility testing method (version 6). J. Antimicrob. Chemother. 60, 20-41.

[10] Basile, A., Vuotto, M.L., Ielpo, TL., Moscatiello, V., Ricciardi, L., Giordano, S. and Cobianchi, R.C. (1998) Antibacterial activity in *Rhynchostegium riparoides* (Hedw.) Card. Extract (Bryophyta). Phytotherapy Research. 12, 146-148.

[11] Merritt, J.H., Kadouri, D.E. and O'Toole, G.A. (2015) Growing and Analyzing Static Biofilms. Chapper 1. Curr Protoc Microbiol, USA, Unit 1B. 1.

[12] Blois, M.S. (1958) Antioxidant determinations by the use of stable free radical. Nature. 1199-1200.

[13] Fırat, M and Başer, B. (2015) Pollen and seed morphology of species *Physocardamum davisii* and *Bornmuellera cappadocica*. Biological Diversity and Conservation. 8(3),168-172.
[14] Perdetzoglou, D., Kofınas, C., Chınou, I., Loukıs, A. and Gally, A. (1996) A comparative study of eight taxa of *Lomelosia* RAF. (Dipsacaceae) from Greece, according to their fatty acid and sterol composition and antibacterial activity. Feddes Repertorium. 1-2, 37-42.
[15] Ertürk, R., Çelik, C., Kaygusuz, R. and Aydın, H. (2010) Antimicrobial activities of commercial essential oils of thyme and mint. Cumhuriyet Medical Journal. 32, 281-286.
[16] Şirin, N. and Dülger, B. (2015) The Studies on Antimicrobial Activities of the Lichens *Ramalina farinacea*(L.) Ach. And *Usnea intermedia* (A. Massal.) Jatta. Düzce University Journal of Science and Technology. 3, 340-349.
[17] Kara, A.A., Algur Ö.F. and Köseoğlu M.Ş. (2016) Antimicrobial Activities of Some Herbs on *Helicobacter pylori*. Cumhuriyet University Faculty of Science, Science Journal. 37(2), 129-140.
[18] Bülbül, A., Ceylan, Y. and Armağan, M. (2018) Investigation of Antibacterial and Antifungal Properties of *Acanthophyllum acerosum* and *Acanthophyllum microcephalum*. Research Journal of Biological Sciences. (2), 14-17.
[19] Witkowska-Banaszczak, E. and Długaszewska, J. (2017) Essential oils and hydrophilic extracts from the leaves and flowers of *Succisa pratensis* Moench. and their biological activity. Journal of Pharmacy and Pharmacology, 69(11), 1531-1539.
[20] Hung, T.M., Na, M., Thuong, P.T., Duy Su, N., Sok, D., Song, K.S., Seong, Y.H. and Bae, K. (2006) Antioxidant activity of caffeoyl quinic acid derivatives from the roots of *Dipsacus asper* Wall. Journal of Ethnopharmacology. 188–192.
[21] Karaca, B., Akata, I. and Çöleri Cihan, A. (2017) Antimicrobial and antibiofilm activities of *Lentinus edodes*, *Lactarious delicious*, and *Ganoderma lucidum*. Kastamonu University Journal of Forestry Faculty. 17 (4), 660-668.
[22] Al-Dhabi, N.A., Balachandran, C., Raj, M.K., Duraipandiyan, V., Muthukumar, C., Ignacimuthu, S., Khan, I.A and Rajput, V.S. (2012) Antimicrobial, antimycobacterial and antibiofilm properties of *Couroupita guianensis* Aubl. fruit extract. BMC Complementary and Alternative Medicine. 12, 242.
[23] Bojnanský, V. and Fargašová, A. (2007) Taxonomy and morphology of seeds. In Atlas Of Seeds And Fruıts Of Central And East-European Flora Springer Netherlands. 1-954.

Received: **01.10.2019**
Accepted: **18.02.2020**

CORRESPONDING AUTHOR

Ali Savas Bulbul
Kahramanmaraş Sütçü İmam University,
Avşar Campus, Faculty of Arts and Sciences,
Department of Biology,
46100 Kahramanmaraş – Türkiye

e-mail: asavasbulbul@gmail.com

© by PSP Volume 29 – No. 05/2020 pages 3650-3655 Fresenius Environmental Bulletin

THE EFFECTS OF DIFFERENT HANGING RATIOS ON CATCHING EFFICIENCY OF GILLNETS IN NORTHEASTERN TURKISH AEGEAN COASTS

Ugur Altinagac[1,*], Alkan Oztekin[1], Ugur Ozekinci[1], Adnan Ayaz[1], Cenkmen Ramazan Begburs[2]

[1]Canakkale Onsekiz Mart University, Faculty of Marine Science and Technology, Canakkale, Turkey
[2]Akdeniz University Faculty of Fisheries, Antalya, Turkey

ABSTRACT

In this study, it was aimed to determine the effect of hanging ratio on the catch per unit effort in gillnets. The study was carried out at 0-30-meter depth in the Northeastern Aegean coast of Turkey between October 15, 2015 - October 15, 2017. In this study, 9 different gillnets for fishing red mullets (*Mullus barbatus*) and striped mullets (*Mullus surmuletus*) with 18-20-22 mm mesh size and 0.35-0.50-0.65 hanging ratio were used. At the end of the study, a total of 6961 and 365.97 kg of fish were caught with gillnets, 51 species belonging to 26 families. There was no statistically significant difference between catch per unit effort (CPUE) of nets with different hanging ratios in number and weight based on both each rigged piece of net and in total catch ($P > 0.05$).

When the catch efficiency of the trial nets with different hanging ratios was examined per each rigged piece of net, it was determined that the nets with E=0.65 hanging ratio caught the highest number and weight amount of fish in total catch.

KEYWORDS:
Catch per Unit of Effort, Northern Aegean, Hanging Ratio, Gillnet, Catch Efficiency, Çanakkale, Gökçeada

INTRODUCTION

Gillnets are fishing tools that stand upright thanks to floats and leads and consist of one or more walls and help fish or other water species be entangled from their gills or other body parts into the nets. They are used both in sea and inland waters, on the surface or medium waters or bottom [1, 2]. Passive gears are relatively simple in their design, construction and use [3]. Gillnets are mainly used in a passive way but also used in an active way [1, 4, 5, 6].

Although there are many factors affecting selectivity in trammel nets, it has been reported by many researchers that the main factor is the mesh size [6, 7, 8, 9, 10]. In addition to the mesh size, the factors reported to be effective include the elasticity, firmness, thickness and visibility of the net thread, the method of net use, the body shape and behaviour of the fish, and the way that the fish were caught in the mesh of the net other than the pectoral field [11, 12, 13, 10]. One of the factors considered to affect selectivity is the hanging ratio. The hanging ratio is a measure of how tense the net is along the float line and lead line in the construction of the net. In a rigged net, hanging ratio is a measure obtained by dividing the line length by the original (unrigged) net length [14]. In other words, it is the net length rigged in a unit line [15, 10, 16].

The shape of the mesh size of the net within water is associated with the hanging ratio, and it has been indicated by many researchers that it may affect species selectivity [11, 12, 10, 16]. The hanging ratio is significant in fish catching by getting entangled into the net, observation or getting attached to the net from different body extensions. As the hanging ratio of the rigged nets decreases, the probability of the big fish belonging to the same species getting entangled into the net increases [16]. With the increase of hanging ratio, the fish catching is more likely to happen by observing the net via gillnets. In marine fishing in European coasts, it was reported that the hanging ratio of the commercial extension nets used in flatfish catching ranged between 0.25 and 0.65, and the hanging ratio of nets used in fusiform fish catching ranged between 0.4 and 0.6 [17].

Today, due to their economic value many fish species are under the problem of overfishing worldwide [18]. Red mullets are commercially valuable species among Turkey demersal fish species [19, 20, 21]. Some studies have been conducted on the biology of this species [22, 23, 24, 25, 26, 27], catching, catching efficiency and selectivity [20, 28, 29, 30, 31] However, there is no research on the effect of hanging ratio on catch efficiency in gillnets used in the fishing of this species. In this study, it was aimed to determine the effects of hanging ratio on catching efficiency in target species and to identify the most suitable hanging ratio in simple gillnets intensely used in the red mullets.

FIGURE 1
Sampling fields in Çanakkale and Gökçeada coasts

MATERIALS AND METHODS

The study was carried out between October 2015 and October 2017 in the areas where commercial fishing activities are carried out in the North Aegean between 0-30 m depths. A total of 37 fishing operations were carried out on the coasts of Çanakkale and Gökçeada (Figure 1).

In the study, 9 different net types were formed by rigging the nets with 36-40- and 44mm stretched mesh sizes and with E= 0.35-0.50 and 0.65 hanging ratios. The thread thickness of the nets is multifilament 210 denier/3 no and the mesh height is 40. A package net has between 4545 and 5555 mesh number in length. A plan illustrating the technical characteristics of the nets is given below (Figure 2).

The nets used in the study are designed via 1 package (200 m length, 40 vertical mesh height) net, when done with different hanging ratios, the net with the E=0.35 hanging ratio gave 70 m length, the net with the E=0,50 hanging ratio gave 100 m length and the net with E=0.65 hanging ratio gave 130 m length. All nets were tied to one another and thrown into the sea and were used with the semi-circular method in a passive way.

Catch per Unit Effort (CPUE) Calculations. Total catch efficiency calculations for the 37 operations carried out in the study were obtained through dividing the total amount of catches by the number of operations in fish number and weight. The rigged net lengths obtained from a package of net vary according to the hanging ratio. Hence, catch efficiencies obtained at the end of the study were calculated in number and weight in total catch and as per each rigged piece of net, in a way to include the target species and the most caught species.

While calculating the catch per unit effort (CPUE), it was calculated by using the CPUE= ΣC/(Fn x 3 rigged pieces of net) formula since 3 of the nets in each hanging ratio were used. In the formula, ΣC represents the total catches (in terms of number and weight), Fn represents the number of operations.

Statistical comparisons were made in terms of number and weight, both total catch and per each rigged piece of net. In addition, the total catch values were compared by combining the fish caught by the nets with the same hanging ratio and with 3 different mesh sizes. Tukey test was used for pairwise comparisons and variance analysis was used for weight comparison.

RESULTS

As a result of 37 catch operations carried out throughout the study, 51 species belonging to 26 families were caught, a total of 6961 and 365.977 kg of fish were caught in total. In trials, mainly black scorpionfish (*Scorpaena porcus*) with 71.9 kg and striped mullets (*Mullus surmuletus*) with 62.5 kg took the first two places. These fish were followed by the picarel (*Spicara maena*) 52.2 kg, bogue (*Boops boops*) 41.8 kg and annular seabream (*Diplodus annularis*) 18.4 kg. Another target in these nets, the red mullets (*Mullus barbatus*), was the seventh with 14.9 kg of fish, and a total of 86.2 kg catches were carried out for the remaining 44 species, which are called other species (Table 1).

As a result of the calculations about the catch per unit effort of the trial nets rigged with the different hanging ratios used in the study (Table 2), it was indicated that the target species striped mullet (*Mullus surmuletus*) and red mullet (*Mullus barbatus*) were caught slightly higher both in number and quantity through the nets with E = 0.65 hanging ratio.

In the study, Tukey test was used for pairwise comparisons, and variance analysis was performed for weight comparisons, due to the high variance between the amount of fish caught no statistically significant difference was found in total catch between the average of number and weight efficiencies of the fish caught by the nets with different hanging ratios both based on each rigged piece of net and total catch data (P> 0, 05).

In the comparisons carried out for nets of different hanging ratios with the same mesh size, no statistically significant difference was found in catch efficiencies per each rigged piece of net and total catch efficiencies for both target mullet species (*Mullus* sp.) and the black scorpionfish, blotched picarel and annular seabream, which are entangled into the nets intensely (P> 0.05).

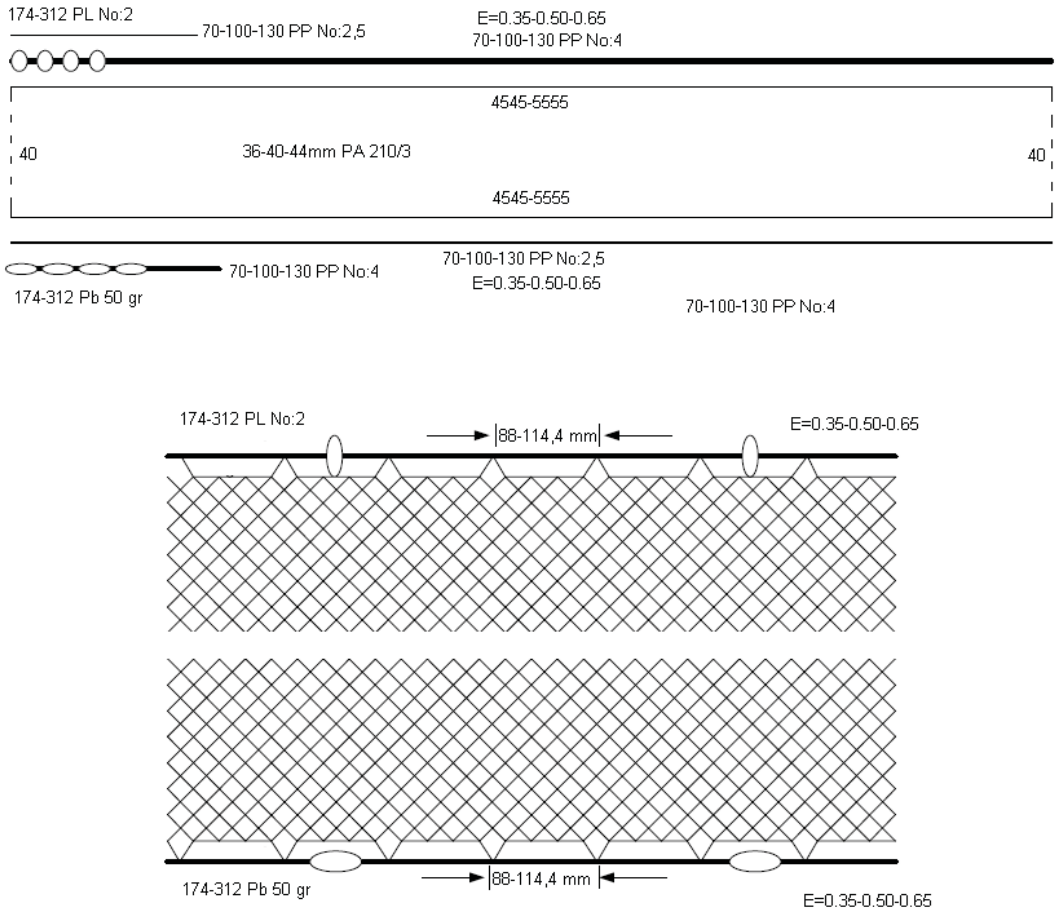

FIGURE 2
Technical plan of experimental nets

TABLE 1
The quantities of species caught in the study in number and weight (g) according to trial nets rigged with hanging ratio factors

Species	Total catch							
	E=0,35	E=0,50	E=0,65	ΣN	E=0,35	E=0,50	E=0,65	ΣW
	N	N	N		W	W	W	
Black scorpionfish *(Scorpaena porcus*)	407	287	415	1109	27419	19140	25316	71875
Striped mullet (*Mullus surmuletus*)	252	280	476	1008	18115	18736	25677	62528
Blotched picarel (*Spicara maena*)	548	282	396	1226	22521	11720	18036	52277
Bogue (*Boops boops*)	166	183	369	718	8688	11633	21506	41827
Annular seabream (*Diplodus annularis*)	204	246	262	712	5226	6538	6655	18419
Painted comber (*Serranus scriba*)	75	118	137	330	4299	5793	7853	17945
Red mullet (*Mullus barbatus*)	92	96	114	302	4290	5159	5457	14906
Others	462	569	525	1556	29240	28679	28281	86200
Total	2206	2061	2694	6961	119798	107398	138781	365977

(N: number, W: grams, E: hanging ratio).

Although there is no statistically significant difference between the hanging ratios, when looking at the by-catch black scorpionfish in weight and blotched picarel caught by E = 0.35 is more. On the other hand, it is seen that the target species, striped mullet and red mullet are caught more in E = 0.65 hanging ratio.

One of the interesting results of this study is that the gillnets with E=0.50 hanging ratio caught at least fish in the total catch. The gillnets with E=0.35 hanging ratio may have caught fishes by entanglement and tension of the gillnets with E= 0.65 hanging ratio may have caught more fish because of reduced underwater visibility.

TABLE 2
Catch per unit effort (CPUE) per each rigged piece of net for the species caught in the trial nets

Species	Catch per Unit Effort (CPUE) ΣC_N / (Fn x 3 nets)			Catch per Unit Effort (CPUE) ΣC_W / (Fn x 3 nets)		
	E=0,35	E=0,50	E=0,65	E=0,35	E=0,50	E=0,65
	N	N	N	W	W	W
Black scorpionfish *(Scorpaena porcus*)	3,667	2,586	3,739	247,00	172,40	228,10
Striped mullet (*Mullus surmuletus*)	**2,270**	**2,523**	**4,288**	**163,20**	**168,80**	**231,30**
Blotched picarel (*Spicara maena*)	4,937	2,541	3,568	202,90	105,60	162,50
Bogue (*Boops boops*)	1,495	1,649	3,324	78,27	104,80	193,70
Annular seabream (*Diplodus annularis*)	1,838	2,216	2,360	47,08	58,90	59,95
Painted comber (*Serranus scriba*)	0,676	1,063	1,234	38,73	52,19	70,75
Red mullet (*Mullus barbatus*)	**0,829**	**0,865**	**1,027**	**38,65**	**46,48**	**49,16**
Others	4,162	5,126	4,730	263,40	258,40	254,80

(N: number, W: gram, ΣC_N: total number of catches, ΣC_W: total weight of catches, Fn: number of operations.)

DISCUSSION AND CONCLUSION

When the average catch efficiencies per each rigged piece of net according to the hanging ratios of the nets are examined, a similar result can be seen that the net with E = 0.65 hanging ratio catch other species except for picarel in both the target species, striped mullet and red mullets, and non-target species. As a result of the statistical analysis performed at the end of 37 operations on the number and unit of total catches obtained as the catch yield per each rigged piece of net only before considering the lengths of the nets, it was determined that the catch efficiency did not show statistically significant variations according to different hanging ratios per each rigged piece of net (P> 0,05). Orsay and Duman [32] conducted experiments by dyeing monofilament nets of 55 mm mesh size in 4 different colours in Keban Dam Lake. As a result of the experiments, it was found that nets with E = 0.50 hanging ratio yielded more catches compared to nets with E = 0.67 hanging ratio. In a similar study carried out by Orsay and Dartay [33] between 2004-2006 in the Keban Dam Lake, they performed experiments on monofilament nets with 40 mm mesh size which they dyed in four different colours in E= 0.50 and E=0.67 hanging ratios. In the study, although they obtained more catches with the black coloured nets based on hanging ratios of the nets, they only found a statistically significant difference in the blue coloured net with E = 0.50 hanging ratio. Since these two studies were carried out in inland waters and because visibility of the nets was reduced since a coloured monofilament net was used in fish catching, the entanglement properties of the relevant nets increase as the hanging ratio decreases, which might have affected the results [17, 16].

Balık and Çubuk [32] performed experiments in zander (*Stizostedion lucioperca*) fishing in Eğirdir Lake with monofilament gillnets rigged with four different hanging ratios. While catch efficiency per each rigged piece of net was large as the hanging ratio grew, it was determined that when catch efficiency was set to 100 meter net and 1.5 m standard in height, more zander (*Stizostedion lucioperca*) fish were caught in gillnets rigged with low hanging ratio. In a similar study, Aydın and Yüksel [35] carried out experiments with nets having five different hanging ratios (0.30-0.40-0.50-0.60 and 0.70) in 60 m in length in *Luciobarbus mystaceus* (Palas, 1814) fishing in Keban Dam Lake. As a result of the experiments, they found that the nets rigged with 0.40 hanging ratio are more efficient than other nets. In the present study, nets were used in different lengths according to the hanging ratio. Normally, although there is no statistical catch difference between the nets with hanging ratio of E= 0.65, they seemed to have a higher number of catches (Table 1). In a study conducted in Çanakkale coasts using the same nets in length, catch amounts showed variations in different hanging ratios according to mesh size [9]. Parsa et al. [36] experimented with two different floating nets used in catching large pelagic fish on the coasts of Bushehr. As a result of the study, it was found that the hanging factor does not affect the catch efficiency. Similar results were obtained in a study conducted in Australia [37].

The catch efficiency of the striped mullet (*Mullus surmuletus*), the species most commonly entangled in the nets, black scorpionfish (*Scorpaena porcus*), blotched picarel *(Spicara maena*) and annular seabream (*Diplodus annularis*) at the end of 37 operations were compared statistically both in number and weight, both per each rigged piece of net and total catch. Studies carried out on species in the seas have not been able to clearly reveal the effect of hanging ratio on catch efficiency [9, 36, 37]. This situation strengthens the possibility that it might be related to the body structure of the fish. In this study, considering this situation, the absence of a protrusion in the body structure of striped mullet, red mullet, picarel and annular seabream, etc. which will increase the entanglement probability of the fish into the net may have resulted in such a finding. The fact that the black scorpionfish was not caught in other

operations may be insufficient for statistical comparison. As a matter of fact, when the catch efficiency (CPUE) is examined, the nets with E = 0.35 hanging ratio caught blotched picarel and black scorpionfish in weight higher than the nets from other hanging ratios.

In the studies conducted on hanging ratio in inland waters, it was seen that the hanging ratio effected the catch efficiency, while studies conducted on seas did not present findings that it affected catch efficiency. This situation raises doubts that the hanging ratio is not a factor that directly affects the catch efficiency. The visibility factor of the net and the speed at which the fish hit the net along with the hanging ratio raise the probability of increasing the catch yield [7, 8, 9].

As a result, considering the target and non-target species of the gillnets to be used in striped mullet and red mullet catching in the North Aegean Sea, it is recommended to use nets with hanging ratios E = 0.65 for target species.

ACKNOWLEDGEMENTS

This study has been supported by TÜBİTAK project No. 115O897. We would like to express our gratitude to Osman Odabaşı, Erman Uğur, Ogün Şirin, Ergün Tanay and Hayati Yağlı, who have been very helpful.

REFERENCES

[1] Kara, A. (1992) Trammel nets in the Aegean Region and research on the development of trammel nets fishing. PhD Thesis. Ege University Graduate School of Natural and Applied Science. (in Turkish.)

[2] Sasi H. (2019) Assessment of water quality and fisheries activities in upper Akcay River in Denizli-Muğla Province. Fresen. Environ. Bull. 28, 2707-2718

[3] Atessahin, T., Duman, E. (2018) Fish catching trials with two different types of fish pots in Keban Dam Lake (Turkey-Elazığ) Fresen. Environ. Bull. 27, 1472-1479

[4] Sainsbury, C.J. (1995) Commercial fishing methods. 3rd Eds. Fishing News Books Ltd. Farnham, 359p.

[5] Ünsal, S., Kara, A. (1996) Classification of catching methods. Ege Journal of Fisheries and Aquatic Sciences, İzmir. 13, 461-469.

[6] Brandt, A.V. (1984) Fish catching methods of the world. Fishing News Books Ltd., Farnham, Surrey, England, 418p.

[7] Ayaz A., İşmen İ., Özekinci U., Altınağaç U., Özen Ö., Yığın C.Ç., Cengiz Ö., Ayyıldız H., Öztekin, A. (2010) Studies on determining bycatch ratio and bottom gill net selectivity in north Aegean Sea. Project Report. TUBITAK Project No: 106Y021, 177p.

[8] Kumova, C.A. (2013) Effect of hanging ratio to catch efficiency and selectivity in gillnets. M.Sc. Thesis. Canakkale Onsekiz Mart University Graduate School of Natural and Applied Sciences Chair for Fisheries. 63p.

[9] Kumova, C.A., Altınağaç, U., Öztekin, A., Ayaz, A., Aslan, A. (2015) Effect of Hanging Ratio on Selectivity of Gillnets for Bogue (*Boops boops*, L. 1758). Turkish Journal of Fisheries and Aquatic Sciences. 15, 561-567.

[10] Yüksel, F., Aydın, F. (2012) Gillnet selectivity and factors affecting selectivity. e-Journal of New World Sciences Academy. 7(2), 5A0070.

[11] Clark, J.R. (1960) Report on selectivity of fishing gear in fishing effort, and effect of fishing on resources and the selectivity of fishing gear. ICNAF Spec. Publ. 2, 27-56.

[12] Hamley, J.M. (1975) Review of Gillnet Selectivity. Journal of the Fisheries Research Board of Canada. 32, 1943-1969.

[13] Özdemir S., Erdem, Y., Sümer, Ç. (2005) Catch efficiency and catch composition of the gillnets having different structure and material. Fırat University Journal of Science and Engineering. 17 (4), 621-627.

[14] Hubert, W.A., Pope, K.L., Dettmers, J.M. (2012) Passive capture techniques. In: Zale, A.V., Parrish, D.L., and Sutton, T.M. (eds.) Fisheries Techniques. 3rd edition. American Fisheries Society, Bethesda, Maryland. 223-265.

[15] Hoşsucu, H. (2002) Fisheries I. Fishing Gear and Technology. (in Turkish), s. 247, İzmir, Ege. University Fisheries Faculty pub.No:55, Bornova-İzmir.

[16] Karlsen, L., Bjarnason, B.A. (1987) Small-scale fishing with driftnets. FAO Fish. Tech. Pap. 284.

[17] Hovgard, H., Lassen, H. (2000) Manual on estimation of selectivity for gillnet and longline gears in abundance surveys. FAO Fisheries Technical Paper No: 397, Rome 84p.

[18] Sangun, L., Basusta, N., Guney, O.I. (2018) Determination of catch composition in the bottom trawling using multivariate statistical methods in eastern Mediterranean. Fresen. Environ. Bull. 27, 6317-6323.

[19] Kalaycı, F., Yeşilçiçek, T. (2012) Investigation of the selectivity of trammel nets used in red mullet (*Mullus barbatus*) fishery in the Eastern Black Sea, Turkey. Turkish Journal of Fisheries and Aquatic Sciences. 12, 937-945.

[20] Dinçer, A.C., Bahar, M. (2008) Multifilament gillnet selectivity for the red mullet (*Mullus barbatus*) in the eastern Black Sea coast of Turkey, Trabzon. Turkish Journal of Fisheries and Aquatic Sciences. 8, 355-359.
[21] Bolat, Y., Tan, D. (2017) Selectivity of multifilament trammel nets of different mesh sizes on the red mullet (*Mullus barbatus* L., 1758) in Western Mediterranean, Turkey. Iranian Journal of Fisheries Sciences. 16(1), 127-137
[22] Akyüz, E.F. (1957) Observations on the Iskenderun Red Mullet (*Mullus barbatus*) and its environment. Proc. Gen. Counc. Medit. 38, 305-331.
[23] Kara, F., Gurbet, R. (1990) Distribution of the demersal fish of economical value and their stock assesment in the Northern Aegean Sea. Ege University, AFS project No: 1988/003, İzmir, 43 pp. (in Turkish).
[24] Toğulga, M., Mater, S. (1992) A comparison of data on the population dynamics of *Mullus barbatus* L. from the Izmir Bay in 1973 and 1990. Ege University, Journal of Faculty of Science. Series B. 14(2),11-28
[25] Çelik, Ö., Torcu, H. (2000) Investigations on the biology of red mullet (*Mullus barbatus* Linnaeus, 1758) in Edremit Bay, Aegean Sea, Turkey. Turk. J. Vet. Anim. Sci. 24, 287-295.
[26] Atar, H.H., Mete, T. (2009) Investigating of Some Biological Features of Red Mullet (Mullus Sp. Linnaeus, 1758) Distributing in Mersin Bay. Biyoloji Bilimleri Araştırma Dergisi. 2(2), 29-34.
[27] Genç, Y. (2014) Red Mullet Fisheries in the Black Sea, Turkish Fisheries in the Black Sea. Düzgüneş, E., Öztürk, B., Zengin, M. (Eds.) Published by Turkish Marine Research Foundation (TUDAV), Publication number: 40, Istanbul, Turkey, 340-360.
[28] Özekinci U. (1997) Determination of gillnets selectivitiy using with the indirect methods to gillnetting catches Red Mullet (*Mullus barbatus*) and Annular Breams (*Diplodus annularis*). International Mediterranean Fisheries Congress, Izmir, Turkey, 9-11 April 1997. 1(1), 653-659
[29] Aydın, İ., Gökçe, G., Metin, C. (2007) The effects of monoflament and multiflament PA netting twine on catch composition of the red mullet gillnets. Ege Journal of Fisheries and Aquatic Sciences, 23 (3-4), 285-289.
[30] Dinçer, A.C., Bahar, M. (2008) Multifilament Gillnet Selectivity for the Red Mullet (*Mullus barbatus*) in the Eastern Black Sea Coast of Turkey, Trabzon. Turkish Journal of Fisheries and Aquatic Sciences. 8, 355-359.
[31] Aydın, İ., Metin, C. (2008) Effects of mesh numbers of red mullet gillnets through the depth of the net on catch composition. Journal of Fisheries Sciences.com. 2(3), 210-215.
[32] Orsay, B., Duman, E. (2010) Catching efficiency of various hanging ratio and colour monofilament gill nets. Journal of Fisheries Sciences.com. 4(4), 362-375.
[33] Orsay, B., Dartay, M. (2011) Catch Efficiency of Monofilament Gill Nets Configured at Various Colors and Hanging Ratios. Journal of Animal and Veterinary Advances. 10(9), 1219-1226.
[34] Balık, İ., Çubuk, H. (2001) Effect of hanging ratio on efficiency and selectivity of gillnets on capture of pikeperch (*Stizostedion lucioperca* (L.)) and tench (*Tinca tinca* L.). Ege Journal of Fisheries and Aquatic Sciences. 18(1-2), 149-154.
[35] Aydın, F., Yüksel, F. (2014) Investigation of Selectivity of Gillnets Equipped with Different Hanging Ratios Using in the Catching of Luciobarbus mystaceus (Pallas, 1814). Tunceli Universitesi Bilim ve Gençlik Dergisi. 2(1), 1-14
[36] Parsa, M., Paighambari, S.Y., Ghorbani, R., Shabani, M.J. (2014) Effects of Hanging Ratio on the Catch Rate and Catch per Unit Effort (CPUE) of Tuna Drifting Gillnets in Bushehr Coastal Waters, Persian Gulf (Iran). World Journal of Fish and Marine Sciences. 6(3), 214-218.
[37] Gray, C.A., Broadhurst, M. K., Johnson, D.D., Young, D.J. (2005) Influences of hanging ratio, fishing height, twine diameter and material of bottom-set gillnets on catches of dusky flathead *Platycephalus fuscus* and non-target species in New South Wales, Australia. Fisheries Science. 71, 1217-1228

Received: **08.10.2019**
Accepted: **11.02.2020**

CORRESPONDING AUTHOR

Ugur Altinagac
Canakkale Onsekiz Mart University,
Faculty of Marine Science and Technology,
Canakkale – Turkey

e-mail: altinagac@comu.edu.tr
ualtinagac@yahoo.com

© by PSP Volume 29 – No. 05/2020 pages 3656-3662 Fresenius Environmental Bulletin

THE EFFECT OF IRON ION ON CLOGGING AND MICROBIAL COMMUNITY STRUCTURE OF GROUNDWATER HEAT PUMP RECHARGE

Han Kang*, Dan Li, Chunyue Zang, Rongyao Gao, Mouwei Wang, Jun Pan

School of Municipal and Environmental Engineering, Shenyang Jianzhu University; No.25, Hunnan Middle Road, Hunnan New District, Shenyang City, Liaoning, P.R.China

ABSTRACT

In order to imitate the clogging process of groundwater recharge, the sand columns were used to simulate the recharge clogging experiment. Four gradient experiments of 9, 6, 3 and 0 mg/L iron ion concentrations were designed to measure items, such as the water flux and the porosity to study the development law of groundwater recharge clogging under different iron ion concentrations. The results showed that as the iron ion concentrations became higher, the decay of water flux was more obvious, the clogging was more serious. And the clogging tended to be stable as the recharge developed. When the ratio of iron and manganese ions in recharge water was 2:1, the most serious clogging occurred. Moreover, by monitoring aquifer microorganisms and using high throughput sequencing technique (HTS), the changes of microbial community structure and its relationship with clogging were studied. It was verified that there were three dominant microorganisms in the system: *Pseudomonas* sp., *Flavobacterium* sp. and *Pseudarthrobacter* sp., and among them a competitive relationship existed. It was also found that the iron ion concentrations greatly influenced the microbial community structure in solution. High iron ions restrained the competition of the three dominant microorganisms in the system and had adverse effects on other microorganisms.

KEYWORDS:
Artificial recharge, Clogging, Iron and manganese ions, HTS, Microorganisms

INTRODUCTION

The recharge clogging is a main factor to the inefficiency of groundwater recharge, which greatly affects the evaluation of the groundwater source heat pump system [1-3]. The inefficiency of recharge often leads to the failing of EER (energy efficiency ratio) in groundwater source heat pump system [4]. There are many factors that can affect the evolution process of artificial recharge clogging, hence the artificial recharge clogging is a complex process of physical-chemical-biological interaction [5-9] .

According to the research of Ye et al., the solution ionic strength and the flow velocity have effects on colloid clogging in saturated porous media during artificial recharge [10]. Huang et al. [11] simulated the physical clogging during groundwater artificial recharge and deduced the empirical formula of percolation. It's concluded that the recharge process leads to the formation of the silt layer, as a result, the outflow rate decreases rapidly [12]. The factors that influence chemical clogging are complex. According to the current research, iron usually reacts with oxygen in recharge water and produces precipitation. According to Du et al., the chemical clogging is mostly associated with iron oxyhydroxide precipitation [13,14]. Biological clogging is also common in recharge water. The biomass accumulation could lead to biological clogging [15-17]. In irrigation experiments, Lu et al. also mentioned that biological fouling had influence on water treatment [18]. The microbial community structure of groundwater often changes with time during artificial recharge [19-21]. During groundwater recharge process, the living environment of microorganisms changes, which alters the microbial population structure in the system.

The recent studies about recharge clogging mostly focused on the macroscopic aspect, however the microscope research especially at microbial aspect was weak. In this study, the relationship between iron ions and recharge clogging was studied through laboratory simulated recharge clogging experiment. Also by using HTS, the succession of microbial population structure in recharge water was further explored. Based on the test results, the microbial species and community structure were analyzed, and the relationship with the clogging was discussed.

MATERIALS AND METHODS

Experimental Instruments. The experimental instruments were made from clear plexiglass (93 cm high, 10 cm internal diameter and 1.0 cm thick). The four instruments A1, A2, A3 and A4 were vertically mounted. The experiment of simulated groundwater recharge process was operated in plexiglass instruments. To sampling water, manual valves were set 1, 5, 9, 12, 15 cm away from the outlet on one side of each instrument. The sand was placed inside the four instruments, and the particle size of the sand was 0.25-0.85 mm.

Artificial Recharge Water. The artificial water pumped into the four instruments A1, A2, A3 and A4, was solutions of $(NH_4)_2Fe(SO_4)_2 \cdot 6H_2O$ with four different concentrations: 63 mg/L, 42mg/L, 21mg/L and 0 mg/L, thus the iron ion concentrations were 9, 6, 3 and 0 mg/L respectively, and pH was 7.0. Other main components were as follows: KNO_3 3.5 mg/L, $MnCl_2 \cdot 4H_2O$ 1.5 mg/L, Na_2SO_4 120 mg/L and $NaNO_2$ 0.06 mg/L.

Experimental Method. Sand Filing. To eliminate the Boundary Effect, the petrolatum was used to be smeared around the inside wall before the experiment. Then stones of large grains were placed at the bottom of the instruments. Afterwards the screened sand was filled and tamped to 70 cm height. In order to saturate the sand column, distilled water was slowly poured from the top opening until the water film appeared on the surface of porous media. At this time, the lower outlet valve was opened to empty the distilled water, after completely emptied it was closed.

Experiment Performance. The use of artificial water also ensured a fairly consistent composition of inflow for the experiments. Pre-configured iron ion solution was added into four instruments, and the iron ion concentrations in A1, A2, A3 and A4 were 9, 6, 3 and 0 mg/L. The liquid level was maintained at 20 cm above the sand column, and the instruments corresponded to a residence time of 8 h. In order to reduce the influence of hydrodynamics on the permeability of porous media, the supplying liquid was injected at a constant flow rate during the experiment. Four parallel experiments were conducted for 70 days and meanwhile the water flux and porosity were monitored daily.

Testing Items and Methods. (a) Water Flux

According to the change of water flux in soil column section, the degree of clogging can be expressed as

$$Q = \frac{V}{t} \quad (1)$$

Where:

Q is the water flux through the cross section of soil column (ml/s);

V is the volume of water flowing out of emptied soil column (ml);

t is the time required for emptying soil column(s).

(b) Porosity. The given total volume of soil column was V, tap water was injected from the top into the sand column. Until the liquid level was even to the sand column, open the outlet valve at the bottom, recording effluent volume V1, the porosity can be expressed as

$$n = \frac{V_1}{V} \quad (2)$$

Where:

n is the porosity;

V_1 is the total volume of drainage;

V is the total volume of soil column.

(c) Testing of Microbial Community Structure. The detailed operations were as follows: the sand in the instruments was washed just after finishing the experiment. Then the washing water was retained and separated from sand by centrifuge. Afterwards the supernatant was filtered through a filter machine, until the microorganisms in it were completely adsorbed on the 0.22-micron filter membrane. The microbial DNA was extracted and sent to biological company (Shanghai Major-bio Bio-Pharm Technology Co., Ltd) for HST testing, then the results were analyzed.

RESULTS

Experimental Results of Recharge Clogging. Variation of Water Flux. As shown in Fig.1, the water flux was demonstrating a downward trend, and Fig.2 showed the percentage of the decay was demonstrating an upward trend. At the beginning of the experiment, during 1 d to 10 d: the most obvious water flux decay occurred in A1, with Q reducing from 2.97 ml/s to 1.60 ml/s, rapidly decreasing by 46.1%; whereas A2 decayed weakly with Q decreasing by 29.3%,in comparison to 39.9% in A3 and 34.3% in A4. During 11 d to 30 d, the water flux in A1 reduced from 1.62 ml/s to 1.18 ml/s, only decreasing by 27.2%, yet in A2 it reduced from 2.01 ml/s to 1.02 ml/s, rapidly decreasing by 49.3%. While in A3 and A4 the reduction was 44.6% and 43.6%. During 31 d to 50 d, the water flux in A1 and A2 reduced by 21.6% and 16.7% respectively, while in A3 and A4 the reduction was 7.95% and 8.79%. During 51 d to 70 d, the water flux in four instruments kept decreasing slowly, and the decay was not significant, respectively decreasing by 20.4%, 19.6%, 18.8% and 17.9%.

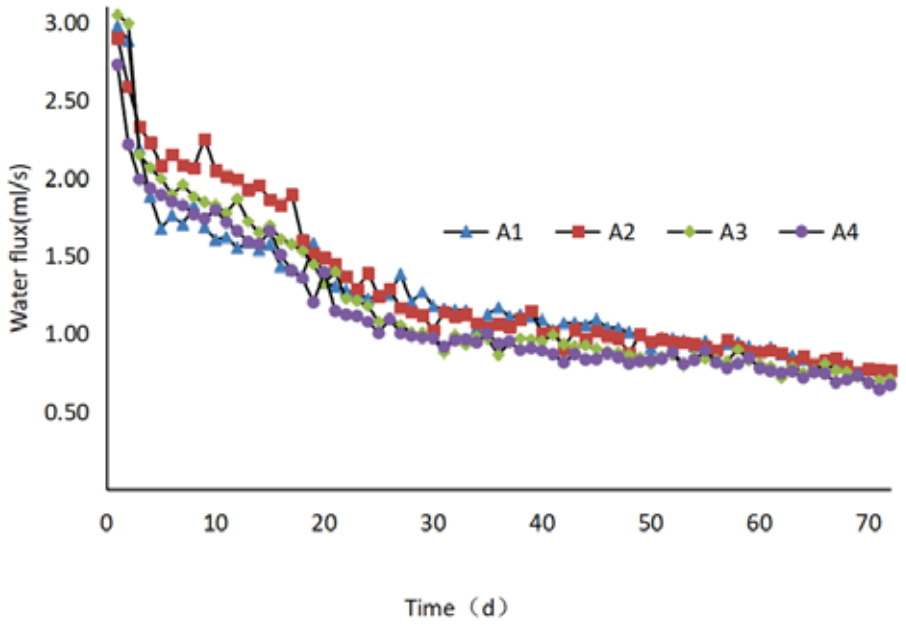

FIGURE 1
The water flux at different iron ion concentrations

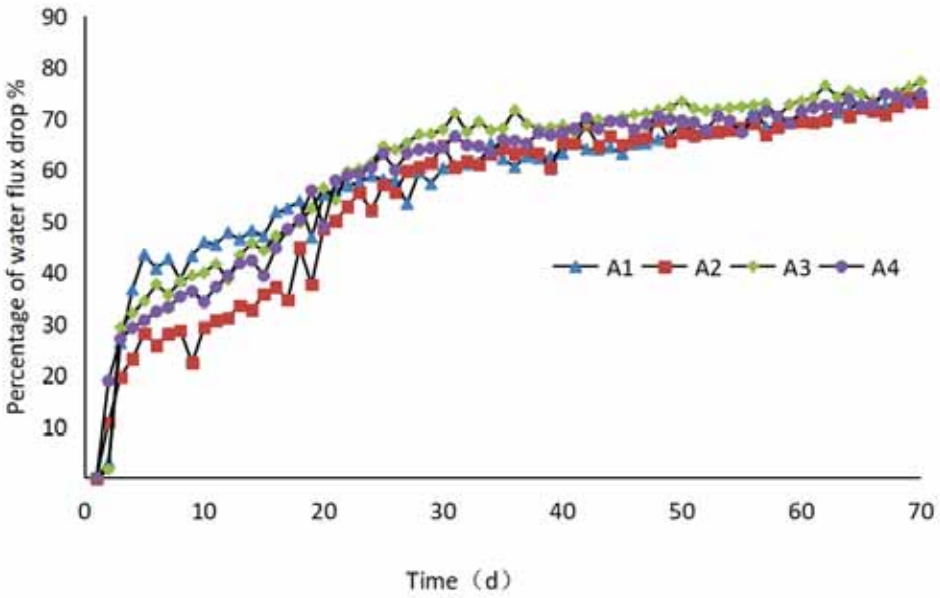

FIGURE 2
The percentage of water flux decay at different iron ion concentrations

Porosity variation law. As shown in Fig.3, at 1d the porosity in A1, A2, A3 and A4 were 0.2396, 0.266, 0.2802 and 0.2627, and at 10d decreased by 1.42%, 2.71%, 16.9% and 22.6% respectively. During 11 d to 60 d, the decay of porosity remained slow, among them the most obvious decay occurred in A1, reducing from 0.2362 to 0.1703, decreasing by 27.9%. During 60 d to 70 d, the porosity in four instruments decreased obviously, while in A1 and A2 the reduction of porosity was gentle, decreasing by 14.5% and 8.83%. The porosity in A3 reduced from 0.1703 to 0.1318, decreasing by 22.6%. By contrast, in A4 there was the most rapid decay rate in porosity, decreasing by 27.1%.

HTS Results. As shown in Fig.4, there were three microorganisms: *Pseudomonas* sp., *Flavobacterium* sp. and *Pseudarthrobacter* sp., in A1 they accounted for about 29% in the total microorganisms. Yet in A2, A3 and A4, the total proportions of the three dominant microorganisms all reached more than 60%. The proportion of *Pseudomonas* sp. was the largest, *Flavobacterium* sp. ranked second, *Pseudarthrobacter* sp. was the last. The proportions of these three dominant microorganisms were influenced by each other at different iron ion concentrations. When the concentration of iron ion was 0 mg/L, *Pseudomonas* sp. was optimum,

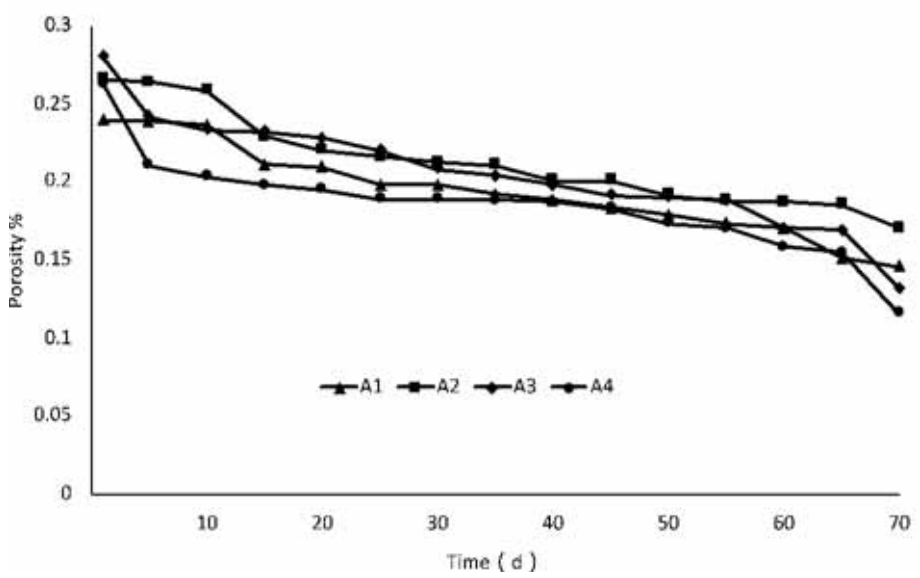

FIGURE 3
The sand column porosity at different iron ion concentration

with the proportion up to 57%, compared to 8% for *Flavobacterium* sp. and 11% for *Pseudarthrobacter* sp.. When it came to 3mg/L, the proportion of *Pseudomonas* sp. went down to 27%, while *Flavobacterium* sp. and *Pseudarthrobacter* sp. had superiority, with their proportions going up to 20% and 16%. The rest microorganisms also showed different evolutionary changes at different iron ion concentrations. *Polaromonas* sp. was only after the three dominant microorganisms in the system, with the proportion up to 13% in A1, then in A2, A3 and A4 the proportion were 2.5%, 2% and 1.2%. *Arcicella* sp. had the proportion of 15% in A1, but only 0.5% in A2. Meanwhile it was not found in A3 and A4. *Massilia* sp. had the proportion of 1%, 0.9% and 2.3% in A1, A2 and A3, but in A4 its proportion rose to 5.3%.

Effect of Iron Concentrations on Water Flux. According to the results, in the medium period 27 d-46 d, the decay percentages on water flux in A1, A2, A3 and A4 were 11.56%, 6.17%, 5.46% and 4.67%. It was obvious that the iron ion concentration of A1 was the highest, yet A4 it was the lowest. It showed the decay was slowly down with the decreasing of iron ion concentrations. This might be due to the chelate of iron ions, anhydrous ferric oxide (HFO), which was insoluble in water, causing the clogging of porous media. By the end of the experiment, after 65 d, because of the blockages accumulating on the surface of porous media, there was not a continuous decline on water flux. Thus the condition of recharge clogging tended to be stable. Therefore, with the increasing of iron ion concentrations, the amount of chelates increased, the clogging was more serious, the water flux decreased. During the process, the decreasing of water flux tended to be slow and the clogging condition tended to be stable.

Effect of Iron Ion Concentrations on Porosity. In the medium period of the experiment, the porosity of the four groups decreased slowly. But among them, in A1 it declined fastest, by contrast, respectively 15.62%, 18.93% and 26.01% faster than A2, A3 and A4. The ratio of Iron and Manganese ion in A1, A2, A3 and A4 were 6:1, 4:1, 2:1 and 0:1. It could be obtained that in A2 the ratio was 2:1, the porosity declined fastest and most obvious. It might be due to the complex produced in Ferric and Manganese ionic reaction, which was hard to electrolyze [22,23]. As a result, it led to the clogging. Therefore, when the ratio of Iron and Manganese ion was 2:1, the most complete reaction led to the most blockages, the clogging was the most obvious.

Effect of Ferric Ion Concentration on Microbial Population Structures. By analyzing the HTS results, it could be obtained that there were three dominant microorganisms: *Pseudomonas* sp., *Flavobacterium* sp. and *Pseudarthrobacter* sp.. The total proportion of them in the system remained around 60% during the experiment, while there was a competitive relationship among them. When *Flavobacterium* sp. and *Pseudarthrobacter* sp. increased, *Pseudomonas* sp. decreased. When the concentration of iron ion was 0, *Pseudomonas* sp. became optimum. As the concentration went up, its competition declined, which showed that the increasing of iron ion concentrations would be harmful to *Pseudomonas* sp.. When the concentration of iron ion was 0, *Polaromonas* sp. was measured very rare in the experiment, yet *Arcicella* sp. was not found, but the proportion of *Massilia* sp. went up.

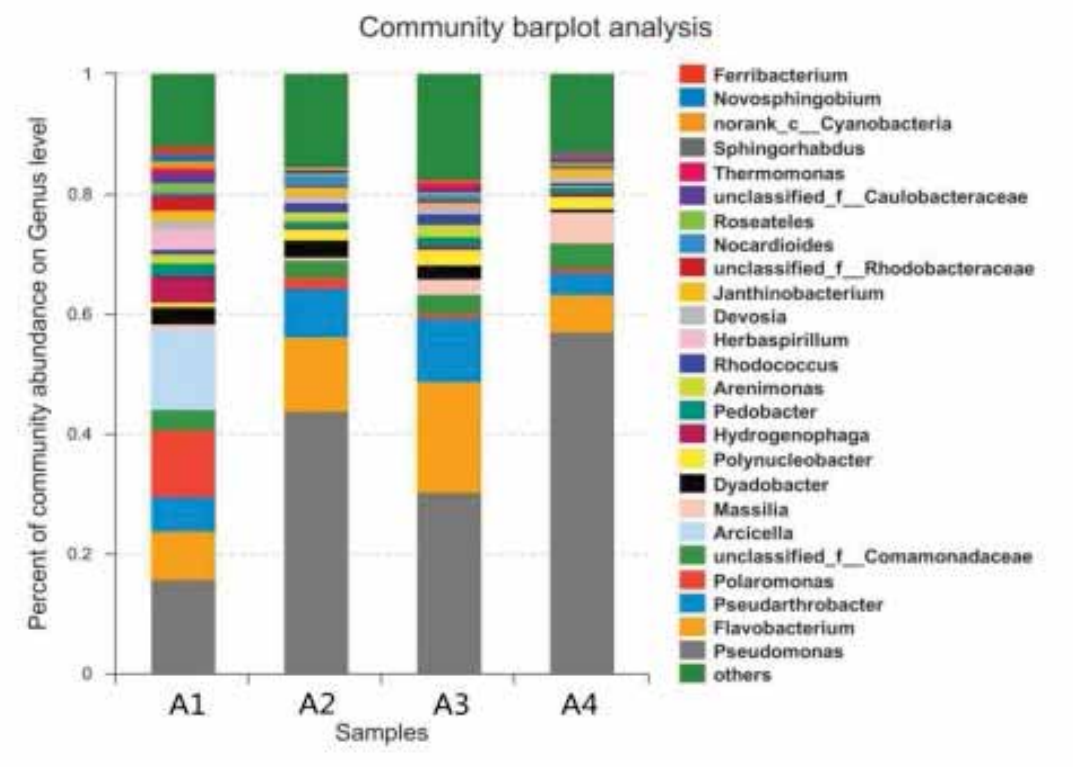

FIGURE 4
Percent of community abundance on genus level in solutions of different iron ion concentrations

The proportion of *Polaromonas* sp. and *Arcicella* sp. rose up at a higher iron ion concentration, but *Massilia* sp. declined. Meanwhile the total abundance of the three dominant microorganisms reduced from 64% to 29%, indicating that high iron concentrations promoted *Polaromonas* sp. and *Arrcicella* sp. but restrained *Massilia* sp., *Pseudomonas* sp., *Flavobacterium* sp. and *Pseudarthrobacter* sp.. It was also obtained that the three dominant microorganisms had tolerance range for iron ion concentrations. High iron concentrations restrained them in the whole system. Therefore, the Iron ion concentrations had a significant effect on microbial community structure. High iron concentrations had positive effects on *Polaromonas* sp. and *Arcicella* sp., but harmful to *Massilia* sp.. Within the tolerance range, the higher iron ion concentration, the larger the proportion of *Pseudomonas* sp., *Flavobacterium* sp. and *Pthrobacter* sp., as well as more competitive. But beyond the tolerance range the competition would be restrained.

CONCLUSION

(1) The iron ion concentrations in recharge water affected the decay degree of water flux. The chelates produced could block the interior of porous media. When the concentrations went up, more chelates were produced, the water flux decayed more obviously, the clogging became more serious. During the process, the decay of water flux tended to be gentle and the condition of recharge clogging tended to be stable.

(2) The iron ion concentrations in recharge water affected the porosity. When the concentrations went up, the porosity declined, the clogging became more serious. When the ratio of Iron and Manganese ion was 2:1, more blockages were produced, leading to the clogging in porous media. And the present porosity was the smallest, indicating the clogging was the most serious.

(3) The Iron ion concentrations had a significant effect on microbial community structure. High iron ion concentrations promoted *Polaromonas* sp. and *Arcicella* sp., but restrained *Massilia* sp.. Within the tolerance range, when the iron ion concentrations became higher, the proportion of the dominant microorganisms was higher, and they became more competitive. But beyond the tolerance range their competition would be restrained.

ACKNOWLEDGEMENTS

This work was supported by the Department of Science & Technology of Liaoning province (Grant No. 20170520224) and SJZU Postdoctoral Innovation Fund Project (Grant No. SJZUBSH201718).

REFERENCES

[1] Parimalarenganayaki, S., Elango, L. (2018) Quantification of groundwater recharge and river bed clogging by daily water level measurements in a check dam. Arabian Journal of Geosciences. 11, 174-181

[2] Shu, L. C., Zhang, Y. J., Xu, Y., Wu, P. P., Abunu, A., Esther, C. M. (2017) Experimental Study on Gas Phase Blockage Characteristics of Groundwater Artificial Recharge. Advances in Water Science. 28, 756-762.

[3] Kandra, H., McCarthy, D., Deletic, A. (2015) Assessment of the impact of stormwater characteristics on clogging in stormwater filters. Water Resources Management. 29, 786-791.

[4] Lin, Y.C., Liu, L. C. (2014) Application effect evaluation of groundwater ground-source heat pump systems in Beijing. Journal of HV & AC. 44, 63-66.

[5] Cannavo, P., Coulon, A., Charpentier, S., Béchet, B., Beaudet, L. V. (2018) Water balance prediction in stormwater infiltration basins using 2-D modeling: An application to evaluate the clogging process. International Journal of Sediment Research. 33, 371-384.

[6] Ma, Z. Y., Xu, Y., Zhai, M. J., Wu, M. (2017) Clogging mechanism in the process of reinjection of used geothermal water: A simulation research on Xianyang No.2 reinjection well in a super-deep and porous geothermal reservoir. Journal of Groundwater Science and Engineering. 5, 311-325.

[7] Daniele, P., Marco, B. P., Diogo, B., Daniel, F. G., Xavier, S. V., Daniel, M. T. (2012) Probabilistic analysis of maintenance and operation of artificial recharge ponds. Advances in Water Resources. 36, 23-35.

[8] Kang, H., Wang, M. W., Zang, C. Y., Pan, J. (2017) Research status and prospect of recharge clogging of groundwater heat pump. Journal of Earth Environment. 8, 320-326.

[9] Nan, T., Shao, J. L., Cui, Y. L. (2016) Column test-based features analysis of clogging in artificial recharge of groundwater in Beijing. Journal of Groundwater Science and Engineering. 4, 88-95.

[10] Ye, X. Y., Du. X. Q., Zhang, H. X., Cui, R. J. (2017) Effects of solution ionic strength and flow velocity on colloid clogging in saturated porous media during artificial recharge. Journal of Chemical Industry and Engineering. 68, 4793-4801.

[11] Huang, X. D., Shu, L. C., Cui, J. L., Tong, K., Zhou, Q. P. (2014) Test on the Characteristic of Physical Clogging During Groundwater Artificial Recharge and Derivation of Percolation Empirical Formula. Journal of Jilin University (Earth Science Edition). 44, 1966-1972.

[12] Zyed, M., Mariem, K., Philippe, S. (2016) Coupling Effects of Flow Velocity and Ionic Strength on the Clogging of a Saturated Porous Medium. Transport in Porous Media. 112, 265-282.

[13] Du, X. Q., Zhang, H. X., Ye, X. Y., Lu, Y. (2018) Flow Velocity Effects on Fe (III) Clogging during Managed Aquifer Recharge Using Urban Storm Water. Water. 10, 358-369.

[14] Siriwardene, N. R., Deletic, A., Fletcher, T. D. (2006) Clogging of stormwater gravel infiltration systems and filters: Insights from a laboratory study. Water Research. 41, 1433-1440.

[15] Hao, Y. L., Chang, Q. L., Qu, A. Y. (2019) Preparation and adsorption phosphate property of Fe-Mn oxide/diatomite composite. Acta Petrologica Et Mineralogica. 38, 273-278.

[16] Qiu, W., Li, W. Y., He, J. G., Zhao, H. Y., Liu, X. M., Yuan, Y. X. (2018) Variations regularity of microorganisms and corrosion of cast iron in water distribution system. Journal of Environmental Sciences. 74, 177-185.

[17] Xing, X. C., Wang, H. B., Hu, C., Liu, L. Z. (2018) Characterization of bacterial community and iron corrosion in drinking water distribution systems with O_3-biological activated carbon treatment. Journal of Environmental Sciences. 69, 192-204.

[18] Lu, Y., Du, X. Q., Fan, W., Chi, B. M., Yang, Y. S. (2012): Prediction of Microbial Clogging in Groundwater Artificial Recharge. - Journal of Hunan University (Natural Science) 39(01): 77-80.

[19] Parimalarenganayaki, S., Brindha, K., Sankaran, K., Elango, L. (2015) Effect of recharge from a check dam and river bank filtration on geochemical and microbial composition of groundwater. Arabian Journal of Geosciences. 8, 8069-8076.

[20] Su, X. S., Meng, X. F., Zhang, W. J., Shi, X. F., He, H. Y. (2015) Change of the Groundwater Microbial Community During Artificial Recharge Process. Journal of Jilin University (Earth Science Edition). 45, 573-583.

[21] Zhang, X. Y., Ye, X. Y., Du, X. Q., Wen, Y. J., Han, J. C. (2014) Study on the Effect of Microbial Clogging on Medium Permeability during Artificial Recharge of Groundwater. Journal of Safety and Environment. 14, 146-150.

[22] Lao, T. Y., He, J. T., Huang, S. Y., He, B.N., Lian, Y.Q. (2019) Simulated Assessment of Gas Production and Microbial Proliferation and Metabolism on Porous Media Clogging in Groundwater Nitrate Remediation by Nano Emulsified Vegetable Oil. Acta Scientiae Circumstantiae. 42, 1-11.

[23] Zhu, J., Lou, Z. M., Wang, Z. X., Xu, X. H. (2014) Preparation of Iron and Manganese Oxides/Carbon Composite Materials for Arsenic Removal from Aqueous Solution. Progress In Chemistry. 26, 1551-1561.

Received: **05.10.2019**
Accepted: **31.01.2020**

CORRESPONDING AUTHOR

Han Kang
School of Municipal and Environmental Engineering, Shenyang Jianzhu University; No.25, Hunnan Middle Road, Hunnan New District, Shenyang City, Liaoning, P.R.China

e-mail:3.7-kh@163.com

© by PSP Volume 29 – No. 05/2020 pages 3663-3670 Fresenius Environmental Bulletin

RELATIONSHIP BETWEEN DIAGENESIS, MATURITY AND PHYSICAL PROPERTIES OF TIGHT SANDSTONE RESERVOIRS IN SULIGE GAS FIELD

Gaorun Zhong, Xiaoli Zhang*, Xi Zhao, Xiaolin Wang, Junhui Lu, Yajun Li

State key laboratory for Continental Dynamics, Department of Geology, Northwest University, Xi'an, 710069, China

ABSTRACT

Diagenesis and maturity are critical elements influencing the physical properties of tight sandstone reservoirs. The relationships between diagenesis, maturity and physical properties of He8 members in the Southeast Sulige Gas Field, Ordos Basin, China, were systematically investigated by core observation, scanning electron microscopy, X-ray diffraction analysis, physical properties analysis, particle size analysis and cathode luminescence data. The results show the following: (1) The diagenesis of the reservoir in the study area as it reaches the middle diagenesis stage B. (2) The porosity reduction and loss rate of different rock types are obviously different under different diageneses. During compaction of quartz sandstone, the porosity reduction caused by compaction was 6.43–10.35% and the porosity reduction rate was 18.62–29.71%. For compaction of lithic quartz sandstone, the porosity reduction caused by compaction was 6.65–10.66%, and the porosity reduction rate was 19.54%~31.77%. Then, during compaction of lithic sandstone, the porosity reduction caused by compaction was 5.66%~11.57% and the pore reduction rate was 17.50–36.06%. During cementation, the average porosity loss rates of quartz sandstone, lithic sandstone and lithic sandstone caused by cementation were 31.32%, 33.85% and 36.13%, respectively. (3) Rock types and maturity directly determine the physical properties of tight reservoirs. Reservoir porosity and face ratio have a good positive correlation with the relative content of quartz, and the reservoir porosity is negatively correlated with the content of debris. The sandstone with high compositional maturity and structural maturity still has a large number of original pores after compaction. The porosity and permeability of the sandstone reservoir are positively correlated with the average grain size of rock particles.

KEYWORDS:
Ordos Basin, He8 member, Diagenesis, Physical properties, Sulige Gas Field

INTRODUCTION

The Sulige Gas Field is located in the Northern Ordos Basin, China. It entered the exploration and development stage in June 2000, and its annual production exceeded 137.0×10^8 m^3 in 2011, with proven geological reserves of 3.0×10^{12} m^3 [1-3]. Permian He 8 and Shan 1 are the main gas-bearing strata, the He8 section gas reservoir buried depth is commonly 3200–3500m [4], the average reservoir permeability is $0.73\times10^{-3}\mu m^2$, the formation pressure is 24.6–29.1 MPa, the coefficient of average pressure is 0.9, and most of the gas saturation is less than 70.0%. Low permeability, low pressure and low gas saturation are the typical characteristics of this gas reservoir, and sand body and reservoir physical properties are the main controlling factors of natural gas distribution. Numerous studies have shown that the tight reservoirs are closely related to the sedimentary evolution process, diagenesis and tectonics [5]. Previous research has shown that the composition and structural characteristics of sandstone are the internal factors controlling the formation of effective reservoirs and diagenetic fluid, while the effective reservoir is closely related to a diagenetic environment and burial process [6]. Mineral composition and structural characteristics in sandstone jointly affect diagenesis and pore evolution process, and reservoir physical properties are closely related to sandstone maturity and diagenesis. However, the pore types of reservoirs in different regions are different, and such corresponding relationship does not have universal regularity [7,8]. During diagenetic evolution, mechanical compaction and cementation are the main reasons for reservoir densification, which are destructive diagenesis. Dissolution can promote the formation of secondary pores and effectively improve reservoir properties, which is constructive diagenesis, and authigenic clay minerals play a dual role in the formation of effective reservoirs. Different diagenesis types cause different loss rates of reservoir original porosity. Andrew et al. [9] proposed a model for calculating porosity loss caused by compaction and quartz cementation. Mohammad et al. [10] calculated the loss rate of porosity of carbonate reservoir by taking Biot coefficient as the rock

strength index for carbonate sedimentary reservoir. Salman et al. [11] and Yang Renchao et al. [12] improved relevant parameters according to different areas and calculated the porosity reduction amount and porosity reduction rate of clastic rock reservoirs. In actual production, the diagenetic facies of tight sandstone reservoirs are usually divided according to the characteristics of clastic composition, diagenetic mineral assemblage, interstitial composition, diagenetic type and pore evolution [13].

The Southeast Sulige Gas Field is located in the Northern Shaanxi Slope of the Ordos Basin in the regional structure adjacent to the Hengshan mountain in the south, extending to Yulin in the east and Wushenqi in the north, with an area of 2800 km^2 (Figure 1). The sedimentary face of Permian He8 members is dominated by the braided river delta plain system. The upper Paleozoic strata in Southeast Sulige are Carboniferous Benxi, Permian Shanxi, Xiashihezi, Shangshihezi and Shiqianfeng formation, and the total thickness of the formation is usually 700–800 m. The main gas formation in the Southeast Sulige Gas Field is the He8 members, and the cumulative gas thickness is generally 0.6–19.4 m, with an average of 6.6 m. The gas saturation of most reservoirs is less than 70.0%, the drilling rate of gas formation is 77.0%, and the open flow rate of the gas test is 0.4–38.2 $\times 10^4$ m^3/d, 5.9$\times 10^4$ m^3/d on average [14].

MATERIALS AND METHODS

Southeast Sulige Gas Field is a hot block that has been developed in recent years, so it is very important to study the relationship between sandstone maturity, diagenesis and reservoir physical properties for the predicting natural gas sweet span. This paper presents completed core observations of 59 wells, scanning electron microscopy (SEM) images of 86 samples, X-ray diffraction analysis of 20 samples, routine physical properties of 400 samples, particle size analysis of 73 samples, and cathode luminescence of 20 samples.

RESULTS

Lithologic characteristics of reservoirs. According to the core observation, thin section identification and SEM data, the main reservoir rocks in the He8 members are lithic quartz sandstone and lithic sandstone, with a small amount of quartz sandstone. The rock clastic compositions are mainly quartz and debris, with a small amount of feldspar. Among them, the content of quartz in the He8 members ranges from 52.7% to 94.1%, with an average of 74.4%, and the content of rock debris ranges from 7.5% to 38.8%, with an average of 24.9%. The content of feldspar is less than 8.0%. The interstitial fillings mainly consist of siliceous, calcite and tuff; and clay minerals mainly consist of illite, kaolinite and chlorite. In the He8 members, siliceous, calcite and tuff account for 23%, 12% and 7% of the total interstitial fillings, respectively; while Illite, kaolinite and chlorite account for 36%, 18% and 4% of the total interstitial fillings, respectively. The grain size of sandstone is generally medium and fine sandstone, and the grain size range is greater than 0.3 mm. The sorting property.

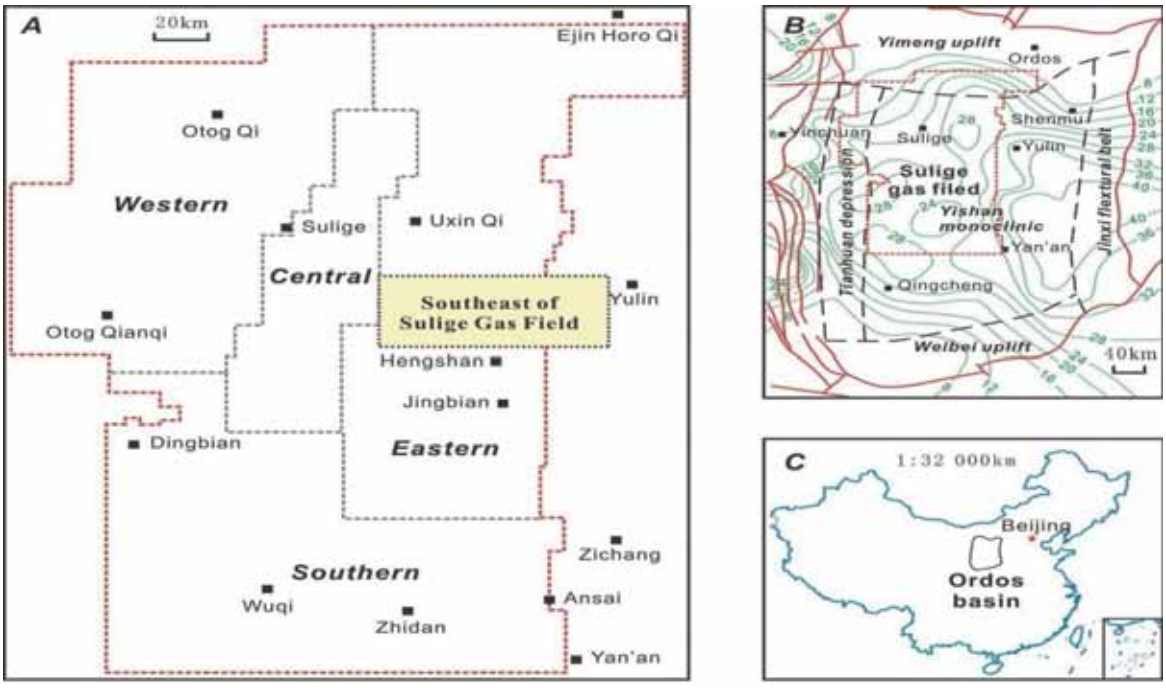

FIGURE 1
The location of the Southeast Sulige Gas Field in the Ordos Basin, China

of particles is from medium to good, mainly with a sub-angular structure. It is believed that the particles have high structural maturity and composition maturity. The high maturity of compositional and structural indicate that the characteristics are far from provenance. The sedimentary characteristics of the sediments are consistent with those of a braided river delta plain

Diagenesis and authigenic minerals. The sandstone in He8 members of the study area has strong compaction, with most of the particles in linear contact and smaller particles in concave and convex contact (Figure 2a). Quartz grain fracture and mica or clastic deformation can be observed because of strong compaction. In SEM, mica and debris fill the pores (Figure 2b), while quartz overgrowth is also widely distributed (Figure 2c), occupying the pore space. Strong compaction reduces the original porosity and narrows the throat. Cementation is one of the important factors for the deterioration of the properties of tight sandstone [15], and there are three cementation types in the Southeast Sulige Gas Field: (1) Siliceous cementation is characterised by secondary enlargement of quartz (Figure 2c). (2) Authigenic clay mineral cementation mainly includes illite, kaolinite and chlorite. Illite is usually distributed in pores in the form of filamentous (Figure 2d). Kaolinite is usually distributed in pores in the form of book-like or vermicular shapes. Chlorite is distributed on the surface of particles in a thin film (Figure 2e). (3) The carbonate cementation of the tight sandstone in the study area is dominated by calcite and ferric calcite with poikilitic structure. In the quartz cathode luminescence spectrum, calcite is usually bright yellow or orange-yellow, while kaolinite is blue (Figure 2f). Under certain diagenetic conditions, the debris, matrix and cement in sandstone may be dissolved [16]. Dissolution mainly includes debris, feldspar, and quartz particles (Figure 2g, h and i)..

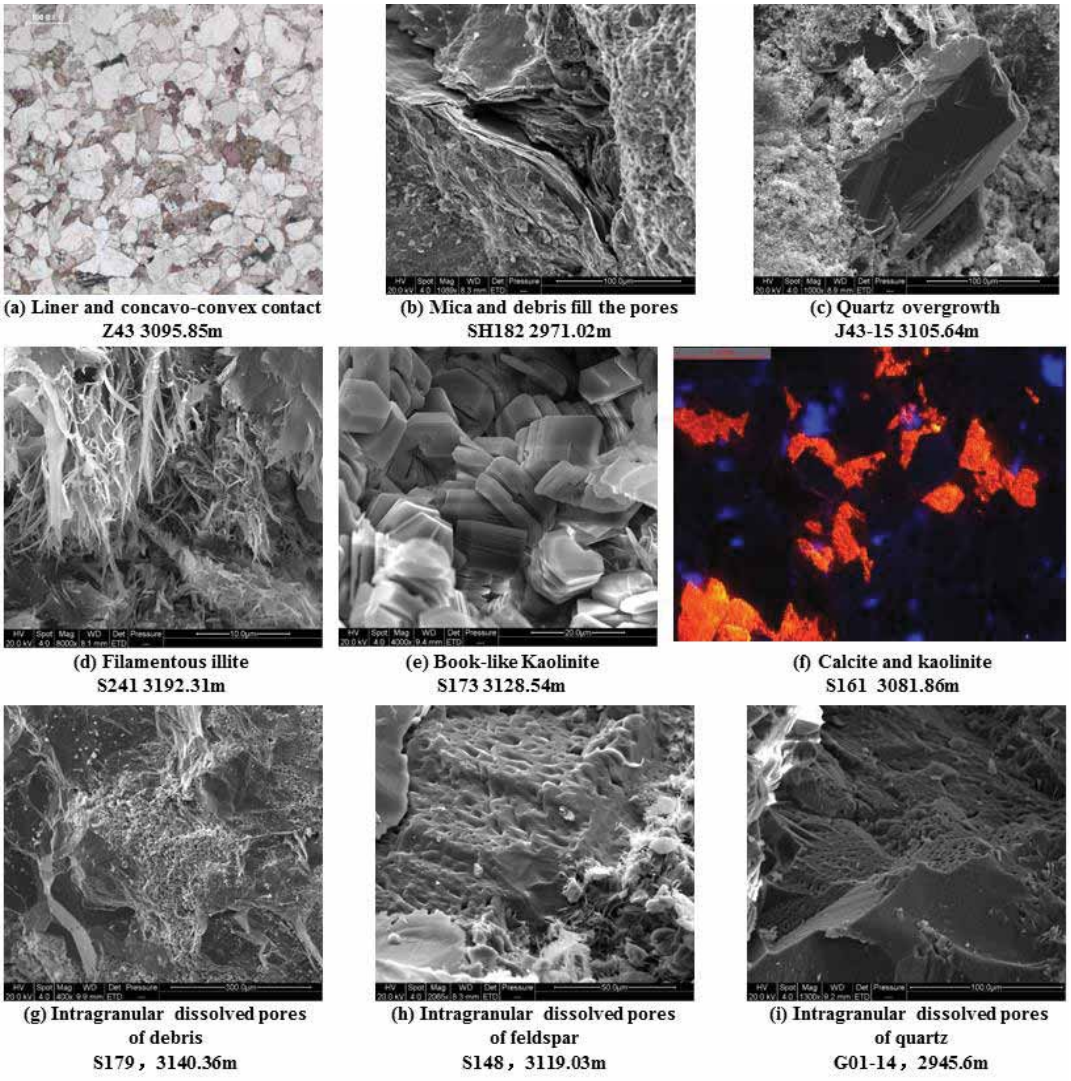

FIGURE 2
Types and characteristics of diagenesis in the Southeast Sulige Gas Field

The intragranular dissolves pores, interparticle dissolved pores and moldic pores of debris, feldspar, quartz particles and cements were formed in sandstones by dissolution in the acid medium during the middle diagenetic stage in the study area. At the same time, microfractures can be developed by dissolution. The width of microfractures formed during dissolution is generally 5 to 50μm, accounting for 1.0% to 2.0% of the total porosity. This width greatly increases the permeability of tight sandstone reservoir and provides a channel for gas charging in the later stage

Determination of diagenetic stages. According to the organic maturities, diagenetic minerals and homogenisation temperature of fluid inclusions of sandstone reservoirs in the Southeast Sulige Gas Field, the diagenetic stages of sandstone reservoirs are classified according to the national standard of the oil and gas industry (SY/ t5477-2003). The main parameters are as follows: (1) The buried depth of the He8 section is from 3200 to 3500 m. Ro values mainly range from 0.75% to 2.1%, indicating the organic matter in He8 sandstone reservoir has reached a high maturity stage. (2) The quantitative composition analysis of illite (44.10%), Kaolinite (13%), chlorite (5%) is followed by the illite/montmorillonite, kaolinite and chlorite at 20.01%, 17.95% and 17.86%, respectively, and the ratio of illite/montmorillonite is less than 20. (3) The test data of diagenetic fluid inclusions of sandstone show that the temperature distribution of diagenetic fluid inclusions of sandstone is uniform, ranging from 95℃ to 165℃, and the peak value ranges from 105℃ to 155℃. The uniform temperature distribution mainly corresponds to the middle diagenetic stage B.

According to the diagenetic minerals, diagenetic phenomena and uniform temperature of fluid inclusions, the diagenetic sequence of sandstone reservoirs in the He8 members in the Southeast Sulige Gas Field was determined (Figure 3).

Diagenesis controls on reservoir properties. Diagenesis is an important cause of reservoir densification and an important content of tight reservoir research. According to the SEM results, X-ray diffraction analysis, cast thin section and conventional thin section observations under the microscope, the results show that the reservoir pore types in the He8 members in the Southeast Sulige Gas field are mainly dissolution holes and intergranular holes, followed by residual intergranular holes and micropores, and microfractures are very rare. Diagenetic types include compaction, cementation and dissolution. Compaction and cementation are important factors leading to the rapid decrease of porosity and permeability of sandstone reservoirs. Dissolution promotes the development of secondary pores and effectively improves the porosity and permeability of reservoirs, which are key to making tight reservoirs become effective reservoirs. In addition, kaolinite and siliceous cementation reduce the physical properties of the reservoir but improve the mechanical strength and compaction resistance of the rock, which is conducive to preserving reservoir pores.

Compaction causes a rapid decrease in porosity. Compaction results in a rapid decrease in the original porosity of the reservoir. The mechanical compaction in the early stage changed the point contact between rock particles into line contact, and the particles rotated, shifted and aligned. At the same time, the plastic particles were squeezed out and filled between the pores, resulting in the loss of a large number of original intergranular pores in the reservoir. Because the mineral composition, grain size and grain maturity of different types of rocks are different, diagenesis can transform reservoirs of different types of rocks to different degrees. Therefore, while quantitatively calculating the degree of reservoir physical transformation by compaction, the influence of different rock types on reservoir physical properties can be compared and analysed.

The original porosity of the sandstone reservoir is calculated by using the sorting coefficient. The calculation formula is (Beard D C and Weyl P K, 1973; Scherer M, 1987) [17, 18]:

$$\Phi_P=20.91+22.90/S_o \quad (1)$$

Here, Φ_P represents the original porosity, and S_o represents the sorting coefficient.

The amount of porosity reduction of compaction (Φ_C) and the ratio of porosity reduction of compaction (Φ_{DC}) are calculated by the following formulas:

$$\Phi_C=\Phi_P- V_F - V_M -\Phi_N +\Phi_S \quad (2)$$

$$\Phi_{DC}=\Phi_C/\Phi_P\times 100\% \quad (3)$$

Here, V_F represents the cement content percentage, V_M represents the matrix percentage, Φ_N represents the current porosity percentage, Φ_S represents the dissolution porosity percentage, and Φ_P represents the original porosity percentage.

According to the calculation of Equations (1)-(3), the calculation results showed that for the quartz sandstone, the original porosity was 34.00–37.10%, with an average of 35.61%; the porosity reduction caused by compaction was 6.43–10.35%, with an average of 9.19%; and the porosity reduction rate was 18.62–29.71%, with an average of 25.80%. For lithic quartz sandstone, the original porosity was 31.36–36.04%, with an average of 33.19%; The porosity reduction caused by compaction was 6.65–10.66%, with an average of 8.62%; and the porosity reduction rate was 19.54–31.77%, with an average of 25.22%. For the lithic sandstone, the original porosity was 30.53–36.96%, with an average of 31.86%; the porosity reduction caused by compaction was 5.66%~11.57%, with an

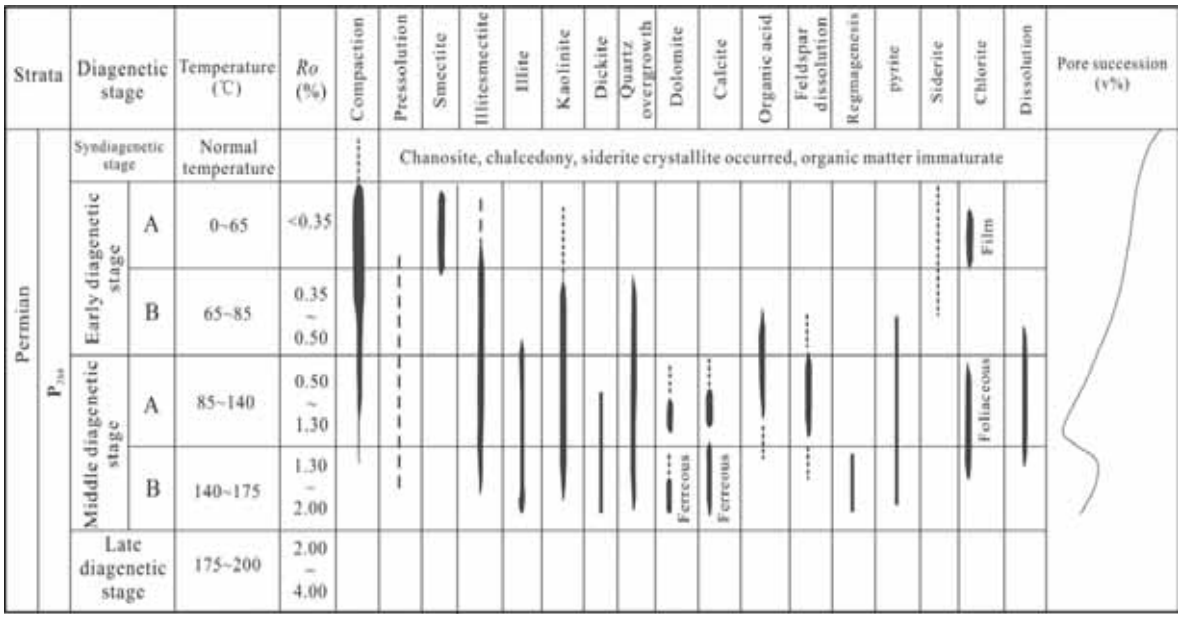

FIGURE 3
Reservoir diagenesis stages of He8 members in the Southeast Sulige Gas Field

average of 7.95%; and the hole reduction rate was 17.50–36.06%, with an average of 24.10%.

Cementation further blocks the pores. Because of the changes of the diagenetic environment such as burial depth, temperature, pressure and pore water chemical properties of reservoirs, the diagenetic precipitation and cementation of authigenic minerals further reduce the porosity and permeability [19,20]. The cementing materials in the reservoir of the He8 members in the study area are mainly kaolinite, illite and chlorite, siliceous cementing and carbonate cementing, and among them, the autogenous kaolinite is filled in the pores in the form of book or vermicular, blocking a lot of primary intergranular porosity, significantly making the physical properties of the reservoir worse and reducing the permeability of the reservoir. However, authigenic kaolinite reflects that sandstone is an open system with good permeability. The aggregation of kaolinite crystals is usually concentrated in relatively large pore sizes, indicating that the presence of a large number of kaolinite crystals also increases the reservoir compression resistance to some degree. Filling pores may play a certain role in protecting the primary pores. In subsequent diagenetic evolution, a large number of intercrystalline micropores of kaolinite can be formed, also contributing to reservoir physical properties. The presence of siliceous cementation reduces the porosity of the reservoir and increases the compression resistance of the reservoir and inhibits the development of compaction, helping preserve the original intergranular pores of the reservoir. Chlorite is usually distributed on the surface of rock particles in the form of a thin film or lining and prevents the secondary increase of quartz and other self-upper minerals and has an obvious protective effect on the primary pores. Illite cementation is usually filamentous and distributed in the pore and plays an important role in reducing the porosity and permeability of sandstone reservoirs. Carbonate minerals are usually evenly dispersed in the pores, making the reservoir densified. However, with the change of diagenetic environment, some carbonate cementitious materials are dissolved, forming secondary pores.

Employing the following formula, we can calculate the original porosity and the ratio of porosity reduction caused by cementation (Φ_{FD}):

$$\Phi_{FD}= (V_F-\Phi_N\times V_M) /\Phi_P\times 100\% \quad (4)$$

Here, V_F represents the interstitial percentage, V_M represents the intergranular percentage, Φ_N represents the current porosity percentage, and Φ_P represents the original porosity percentage.

According to Equation (4), the average porosity loss rates of quartz sandstone, lithic sandstone and lithic sandstone caused by cementation are 31.32%, 33.85% and 36.13%, respectively.

Dissolution promotes the development of secondary pores. The sandstone reservoir of He8 members in the study area reaches period B of the middle diagenetic stage. Before the middle diagenetic stage, the organic matter transforms into hydrocarbons and carbon dioxide in the process, and the pore fluid is strongly acid. In the acidic diagenetic environment, the dissolution of debris, feldspar and tuff minerals forms a large number of secondary pores, and the dissolution of some cementitious materials in the residual intergranular pores forms intergranular dissolution pores, improving the porosity of sandstone. After reaching

the middle diagenetic stage, the organic acid in the pore fluid gradually decreases, and the diagenetic environment gradually changes from acidic to alkaline. At this time, some quartz particles undergo dissolution, forming a small number of dissolution pores in quartz grains. Through SEM and thin section observations, the statistical results show that the dissolution hole accounts for 53% of the reservoir in the study area.

DISCUSSION

The calculation results show that the original porosity form quartz sandstone, lithic quartz sandstone to lithic sandstone gradually decreases, but the compaction of quartz sandstone porosity loss rate is highest, followed by lithic quartz sandstone and lithic sandstone. The main reason for this formation is because the average contents of chlorite thin film in lithic quartz sandstone and lithic sandstone (1.50%) were significantly higher than those of quartz sandstone (0.35%), and the existence of chlorite film plays an important role to protect the original intergranular pores.

Rock types and maturity directly determine the physical properties of tight reservoirs. According to the thin section observation statistics, reservoir porosity has a good positive correlation with the relative content of quartz, reservoir porosity has a negative correlation with the content of debris (Figure 4a), and the reservoir face ratio has a positive correlation with the quartz content (Figure 4b). According to the relation diagram of porosity and permeability of different types of rocks (Figure 5), quartz sandstone has the best physical properties (the average porosity is 9.7% and the average permeability is 2.8×10^{-3} μm^2), followed by lithic quartz sandstone (The average porosity is 7.9% and the average permeability is 0.56×10^{-3} μm^2), and the worst physical properties of lithic sandstone (the average porosity is 6.1%, and the average permeability is 0.10×10^{-3} μm^2).

The sandstone with high compositional maturity and structural maturity still has a large number of original pores after compaction. The porosity and permeability of the sandstone reservoir are positively correlated with the average grain size of rock particles (Figure 6), and the correlation coefficients are 0.93 and 0.95, respectively.

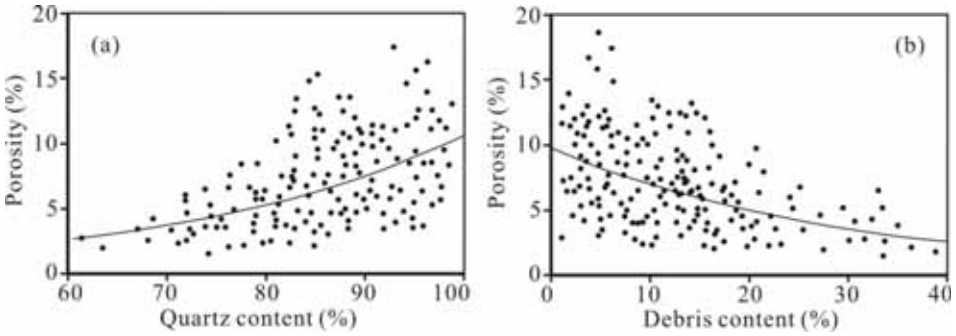

FIGURE 4
Relationship between quartz content, debris content and porosity

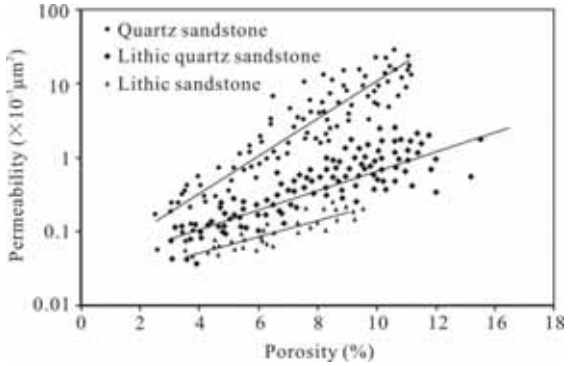

FIGURE 5
The relationship between porosity and permeability of different rock types

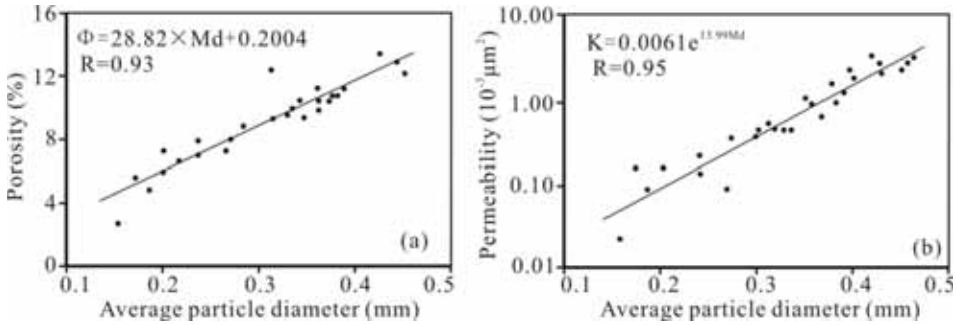

FIGURE 6
The relationship between porosity, permeability and average particle diameter

CONCLUSION

According to the diagenetic minerals, diagenetic phenomena and diagenetic temperature uniformity in the Southeast Sulige Gas Field, diagenesis has reached the middle diagenetic stage B.

Because the mineral compositions, grain sizes and grain maturities of different types of rocks are different, the diagenesis can transform reservoirs of different types of rocks to different degrees. During compaction, for the quartz sandstone, the porosity reduction caused by compaction was 6.43–10.35%, and the porosity reduction rate was 18.62–29.71%. For the lithic quartz sandstone, the porosity reduction caused by compaction was 6.65–10.66%, and the porosity reduction rate was 19.54–31.77%. For the lithic sandstone, the porosity reduction caused by compaction was 5.66–11.57%, and the hole reduction rate was 17.50–36.06%. During cementation, the average loss rate of porosity of quartz sandstone, lithic quartz sandstone and lithic sandstone caused by cementation were 31.32%, 33.85% and 36.13%, respectively.

Dissolution makes the biggest contribution to the improvement of reservoir physical properties. Dissolution pores account for 53% of the total pores in the reservoir. In middle diagenetic stage A, the reservoir was in an acidic diagenetic environment and the lithic, feldspar and tuff minerals dissolved, forming a large amount of secondary porosity. In middle diagenetic stage B, the diagenetic environment gradually changed from an acidic environment to alkaline environment, and quartz particles underwent dissolution and formed a few dissolution pores.

Rock types and maturity directly determine the physical properties of tight reservoirs. Reservoir porosity and face ratio have a good positive correlation with the relative content of quartz, while the reservoir has a porosity negative correlation with the content of debris. The physical properties of different rock types are obviously different, and quartz sandstone has the best physical properties, followed by lithic quartz sandstone and lithic sandstone. The sandstone with high compositional maturity and structural maturity still has a large number of original pores after compaction. The porosity and permeability of the sandstone reservoir are positively correlated with the average grain size of rock particles.

ACKNOWLEDGEMENTS

We acknowledge the State Key Laboratory of Continental Dynamics for assisting with the completion of this project.

REFERENCES

[1] Zou, C.N., Tao, S.Z., Zhang, X.X., He, D.B., Zhou, C.M., Guo, X.H. (2009) Geologic characteristics, controlling factors and hydrocarbon mechanisms of China's Large Gas Provinces of low porosity and permeability. Sci. China Ser D-Earth Sci. 52(8), 1068-1090.

[2] Zou, C., Zhu, R., Wu, S., Yang, Z., T, S., Yuan, X., Hou, L., Yang, H., Xu, C., Li, D., Bai, B., Wang, L. (2012) Types, characteristics, genesis and prospects of conventional and un conventional hydrocarbon accumulations: taking tight oil and tight gas in China as an instance. Acta Petrolei Sinica. 33(2), 173-187.

[3] Li, J., Guo, B., Zheng, M., Yang, T. (2012) Main types, geological features and resource potential of tight sandstone gas in China, Natural Gas Geoscience. 23(4),607-615.

[4] He, D.-B., Jia, A.-L., Tian, C.-B., Guo, J.-L. (2004) Diagensis and genesis of effective sandstone reservoirs in the Sulige Gas Field. Petroleum Exploration and Development. 31(3), 69-71.

[5] Pan, X., Wang, H., Wang, Z., Liu, Y., Gao, X., Wang, L., Xiao, S. (2019) Differential Diagenesis of Delta Plain Sandstone and Its Control on Reservoir Classification: A case study on Yan'an Formation in Yinjiacheng area, southwestern Ordos Basin. Acta Sedimentologica Sinica. 37(5), 1031-1043.

[6] Wang, X., Mou, C. (2013) Diagenesis and diagenetic facies of reservoir in He8 section of Shihezi Formation in east II part of Sulige Gas Field. Natural Gas Geoscience. 24(4), 678-689.
[7] Taylor, T.R., Giles, M.R., Hathon. L., Diggs, T.N., Braunsdorf, N.R., Birbiglia, G.V., Kittridge, M.G., Macaulay, C.I., Espejo, I.S. (2010) Sandstones diagenesis and reservoir quality prediction: Model, myths and reality. AAPG Bulletin. 94(8), 1093-1132.
[8] Ajdukiewicz, J.M., Landed, R.H. (2010) Sandstones reservoir quality prediction: The state of the art. AAPG Bulletin. 94(8), 1083-1091.
[9] Andrew, R., Jon, G. (1992) Model calculations of loss of porosity in sandstones as a result of compaction and quartz cementation. Marine and Petroleum Geology. 9(3),319-323.
[10] Mohammad, M.A., Mai, K.B., Ida, L.F., Kathrine, H., Birte, R., Zakir, H., Anette, S.K. (2010) Biot's coefficient as an indicator of strength and porosity reduction: Calcareous sediments from Kerguelen Plateau. Journal of Petroleum Science and Engineering. 70(3-4), 282-297.
[11] Salman, B., Robert, H.L., Linda, B. (2002) Anomalously high porosity and permeability in deeply buried sandstone reservoirs: origin and predictability. AAPG Bull. 86(2), 301-328.
[12] Yang, R.-C., Wang, X.-P., Fan, A.-P., Han, Z.-Z., Zhao, J., Wang, Y.-L. (2012) Diagenesis of Sandstone and Genesis of Compact Reservoirs in the East II part of Sulige Gas Field, Ordos Basin. Acta Sedimentologica Sinica, 30(1), 111-119.
[13] Zou, C.-N., Tao, S.-Z., Zhou, H., Zhang, X.-X., He, D.-B., Zhou, C.-M., Wang, L., Wang, X.-S., Li, F.-H., Zhu, R.-K., Luo, P., Yuan, X.-J., Xu, C.-C., Yang, H. (2005) Genesis, classification and evaluation method of diagenetic facies. Petroleum Exploration and Development. 35(5), 526-540.
[14] He, Z.X., Fu, J.H., Xi, S.I., Fu, S.T., Bao, H.P. (2003) Geological features of reservoir formation of Sulige gas field. J Oil. 23(2),6-12.
[15] Wang, F., Tian, J.C., Li, F.J., Zhao, J.X., Li, M.R. (2009) Diagenesis of reservoirs in the upper Paleeozoic member 8 formation in the Sulige area. J Lanzhou Univ, 45(4).18-29.
[16] Wang, J., Zhao, Y.C., Liu, W., Wang, J.H. (2006) The main factors of Reserves quality and "are plus alkaline" Superimposed instant effect in Tabamiao, Ordos basin. Earth Sci. 31(2), 221-227.
[17] Beard, D.C., Weyl, P.K. (1973) Influence of texture on porosity and permeability of unconsolidated sand. AAPG Bulletin. 57(2),349-369.
[18] Scherer, M. (1987) Parameters influencing porosity in sandstones: A model for sandstone porosity prediction. AAPG Bulletin. 71(5), 485-491.
[19] Ehrenberg, S.N. (1989) Assessing the relative importance of compaction processes and cementation to the reduction of porosity in sandstones: discussion. AAPG Bulletin. 73(10), 1274-1276.
[20] Salman, B., Robert, H.L., Linda, B. (2002) Anomalously high porosity and permeability in deeply buried sandstone reservoirs: origin and predictability. AAPG Bull. 86(2), 301-328.

Received: **12.10.2019**
Accepted: **20.02.2020**

CORRESPONDING AUTHOR

Xiaoli Zhang
State key laboratory for Continental Dynamics
Department of Geology, Northwest University
Xi'an, Shaanxi Province 710069-China

e-mail: xiaoli_nwu@163.com

© by PSP Volume 29 – No. 05/2020 pages 3671-3678 Fresenius Environmental Bulletin

COUPLING AND COORDINATION ANALYSIS BETWEEN TOURISM DEVELOPMENT AND ECOLOGICAL ENVIRONMENT IN JIANGSU PROVINCE

Tao Sun[1], Qiaoqiao Shen[1,2,*]

[1]College of Economics and Management, Nanjing University of Aeronautics and Astronautics, Nanjing 210016, Jiangsu, China
[2]Jiangsu Vocational Institute of Commerce, Nanjing 211168, Jiangsu, China

ABSTRACT

The paper takes 2006-2018 as the investigation period, constructs the tourism industry and ecological environment evaluation index system, and the entropy weight method determines the index weight, evaluates the comprehensive level of tourism industry and ecological environment in Jiangsu area and each city; introduces the coupling coordination degree model The quantitative development of the coordinated development degree in Jiangsu Province was carried out, and the evolution trajectory of its coordination relationship was analyzed based on the calculation results. The results show that the coupling coordination degree has an upward trend in the long run, and the coupling level is in the antagonistic stage for a long time. The coupling coordination degree is highly coordinated from low to intermediate. However, the speed and development trajectory of the two are not consistent, indicating that the two have not yet reached a high degree of coordination. Based on the local coordinated development trend and the environmental economic basis, the countermeasures and suggestions for coordinating the coordinated development of Jiangsu tourism industry and ecological environment are put forward.

KEYWORDS:
Tourism industry, ecological environment, coupling, coordination, green economy

INTRODUCTION

In the past 40 years of reform and opening up, with the rise of mass tourism, the relationship between tourism and economic development has attracted wide attention. The environmental problems brought about by tourism activities and economic growth has also received much attention. The tourism industry has always been recognized as "smoke-free". The status of the industry has been questioned. At the same time, the ecological and environmental problems caused by the extensive economic development have caused national anxiety. Unreasonable tourism planning and development have threatened the originally fragile ecological environment. Therefore, it is reasonable to deal with regional tourism activities, economic development and environmental protection. The system relationship has become a top priority. The party's "Nineteenth National Congress" report clearly stated that "accelerating the reform of the ecological civilization system and building a beautiful China" emphasizes that man and nature are the communities of life, and that human beings must respect nature, conform to nature, and protect nature. The development of tourism resources must profoundly practice the development concept of "Green Water Qingshan is Jinshan Yinshan". The green ecological environment is the foundation of tourism resource development and the guarantee of tourism development. On the other hand, the protection of ecological environment is the development of tourism resources. The ecological environmental protection is the premise of the development of reasonable tourism resources. Therefore, under the background of ecological civilization construction, the coupling degree and coupling coordination degree of tourism resource development and ecological environment need to be evaluated. The spatial and temporal differences between the coupling degree and coupling coordination degree need to be considered, how to promote the development of tourism resources and the coordinated development of ecological environment. Need to be discussed. However, due to the vast territory of China and the obvious differences between regions, the study of specific regions has important practical significance for the government to formulate differentiated proposals.

The main contributions of this paper are as follows: (1) The evaluation index system of tourism industry development and ecological environment coupling and coordination is constructed, and the weight of evaluation index is determined by entropy weight method combined with expert advice, and the science of index system construction is guaranteed from both subjective and objective perspectives. (2) Using the coupling degree model to measure the coupling degree and coupling coordination degree of tourism industry and ecological environment, determine the coupling relationship between the two, and analyze the empirical results to provide a theoretical reference for the coordinated development of

Jiangsu tourism industry and ecological environment.

LITERATURE REVIEW

In recent years, scholars who have a sustainable and synergistic view of tourism development have been increasing, and the academic community has begun to realize that the relationship between tourism economy and ecological environment is symbiotic interaction, coupled and coordinated development. Wall and Wright (1977) pioneered the concept and research methods of tourism impact on the environment, and analyzed the relationship between tourism activities and environmental factors and their impact mechanisms [1]. Meethan (1997) pointed out that for urban tourism; the quality of urban environment is highly concerned by tourists [2]. Cole (1994) argues that tourism development can improve the environmental quality of tourism destinations [3]. Stephen (1992) analyzed the impact of tourism development on the environment and believed that tourism development has both positive and negative effects on the ecological environment [4]. Milne (2008) draws a similar conclusion to Stephen through a study of Pacific island countries [5]. Zhang Jinhe and Zhang Jie (2004) used the tourism ecological footprint model to analyze the tourism ecological footprint of Huangshan City, and believed that tourism development has the characteristics of global ecological impact [6]. Zhong Xia and Liu Yihua (2012) used the principal component analysis method and the coupled coordination degree function modeling method to quantitatively analyze the coupling coordination degree of tourism-economy-ecological environment in 21 cities of Guangdong Province [7]. Dong Yajuan et al. (2013) used the coupling coordination function and its quantitative model to analyze the coupling and coordination relationship between urban inbound tourism flow and tourism environment in Xi'an City [8]. Song Jinxi et al. (2002) explored the impact of tourism economic development on the environment of Xi'an [9]. Wan Xucai et al. (2003) based on the perspective of tourists, through comprehensive research on the quality of urban tourism environment in Nanjing and Suzhou [10]. Wang Hui et al. (2006) used coordinated development theory to study the coordinated development between Shanghai and Dalian's tourism economic system and ecological environment system [11]. Cui Feng (2008) believes that the construction of Shanghai's ecological environment is moderately ahead of the development of tourism economy [12]. Pang Wen et al. (2011) pointed out that the coupling coordination degree can effectively judge the coupling relationship between urban tourism economy and ecological environment and the state of coordinated development [13]. Wang Xiaohong (2012) systematically discussed the necessity and feasibility of synergy theory in tourism development, and put forward the matters that should be paid attention to in the development of tourism synergy [14]. Wu Yaoyu et al. (2012) believe that the key to achieving coordinated development between tourism economy and ecological environment is the development of ecotourism resources [15]. Wang Zhaofeng et al. (2012) also conducted related research on the coupling relationship between tourism industry and urbanization, and found that tourism industry and urbanization development has the characteristics of mutual influence and coupling development [16]. Gao Nan et al. (2013) analyzed the coupling degree of tourism system and eco-environment system in 31 provincial-level regions of China from 2001 to 2011, and obtained the overall situation of moderate coupling and coordination [17]. Yang Dongquan and Zhang Zhiming (2014) scholars also conducted an empirical study on the coupling relationship between tourism industry and ecological environment, and found that the coupling degree of the two shows an increasing trend [18]. Jia Fengmei and others took Heilongjiang Province as an example. The study found that rural urbanization and the ecological environment system are in a highly coordinated state [19]. Luo Nengsheng et al. (2014) also found that the coupling degree of urbanization and ecological environment system showed an upward trend [20].

In summary, the research on the relationship between tourism and the environment at home and abroad has gradually evolved from qualitative research to quantitative research. Foreign studies started earlier, mainly focusing on tourism capacity, tourism carrying capacity and sustainable tourism development, while domestic research started late. But the starting point is higher, a large number of quantitative models are introduced, and the relationship between tourism and the environment is analyzed from multiple angles and aspects. In the related research of coupling coordination degree, the research content mainly focuses on the coupling and coordinated development of tourism economy and environment. Most of the research scope focuses on the national region, and there is no small-scale comparative analysis of specific regional scope. Most of the research perspectives use time series vertical comparison, lack of region. The internal space Jiangsu tourism industry development and ecological environment evaluation index system, the coupling degree model and the coupling coordination degree model are introduced to calculate the coupling degree and coupling coordination degree of Jiangsu tourism development and ecological environment from 2006 to 2018, and with the help of statistical analysis tools SPSS 20.0 and The GIS software ArcGIS 10.2 analyzes its temporal evolution and horizontal spatial pattern characteristics. On this basis, it proposes measures to promote the development of Jiangsu tourism industry and the coordinated development of ecological environment, with a view

to promoting the sustainable development of tourism and ecological environment in Jiangsu.

MATERIALS AND METHODS

Coupling is originally a terminology derived from logistics. It originally refers to the phenomenon in which two or more circuit elements interact, affect each other and finally achieve synergy. Coupling degree is an index to evaluate the trust relationship between systems. The closer the system is, the stronger the coupling is, and the worse the independence is. Later, in the fields of agronomy, biology, geography and other related fields, especially in the study of eco-economic systems, this concept was widely adopted. This paper defines the interaction between tourism development and ecological environment through the interaction and mutual influence of their respective system elements as the tourism development-ecological environment coupling. The change in the degree of coupling determines the tendency of the system to move from disorder to order when it reaches the critical region. The coupling process between tourism development and ecological environment can be divided into two processes: forward coupling and negative coupling, showing two results. Positive coupling means that the ecological environment is good and the tourism efficiency is rising. The two show a positive state of mutual promotion and symbiosis. The negative coupling refers to the deterioration of the ecological environment, the low efficiency of tourism development, and the mutual vicious circle situation weakening.

Evaluation index system construction and weight determination. From the above analysis, it can be concluded that there is a coupling relationship between the tourism economy and the ecological environment, and the two exhibit the characteristics of mutual influence, mutual restraint and common development. Therefore, the construction of a suitable evaluation index system is the basis for evaluating the coordination of tourism economic development and ecological environment. However, relevant indicators on economic development and resource and environmental assessment have not yet been uniformly measured in the academic world, and the tourism economy and ecological environment system are extensive and have many indicators, which cannot be accurately calculated one by one. Therefore, this paper evaluates the construction of the indicator system is based on the research results of the predecessors. According to the statistical data collected by the author as much as possible, the overall correspondence, the appropriate proportion, the key points, the combination of the total indicators and the mean indicators, data availability and comparability are followed. Based on the principle, the evaluation index system and the weights for evaluating the coordination degree of tourism industry and regional environment in Jiangsu Province are selected as shown in Table 1.

Standardized processing of data. The tourism resource development and ecological environment subsystem contains several indicator layers. The dimension between the indicators and the direction of the force are different. Therefore, the data needs to be standardized on the indicators to eliminate the measurement unit differences and forces between the data. Inconsistent problem, the formula is as follows:

$$x_i^{'} = \begin{cases} \frac{x_i - \min(x_i)}{max(x_i) - min(x_i)} & (with\ positive\ effect) \\ \frac{max(x_i) - x_i}{max(x_i) - min(x_i)} & (with\ negative\ effect) \end{cases} \quad (1)$$

Weight determination method. The analytic hierarchy process is used to calculate the weight value Rj of each index in the index system, and the consistency matrix is tested to ensure the rationality of the weight. When the random consistency CR<0.1 is set, the matrix consistency is satisfactory, and the weight vector of the index layer to the target layer is calculated, and the obtained weight Rj is reasonable.

$$R_j = \frac{g_j}{\sum_{j=1}^{n} g_j},\ j = 1,2,3,\ \cdots n,\ R_j \in (0,1) \quad (2)$$

$$g_j = 1 - h_j \quad (3)$$

$$h_j = -k \sum_{i=1}^{m} \left(P_{ij} lnlnP_{ij}\right) \quad (4)$$

$$k = \frac{1}{lnlnm} \quad (5)$$

$$P_{ij} = \frac{x_{ij}^{'}}{\sum_{i=1}^{m} x_{ij}^{'}} \quad (6)$$

Where: Rj is the weight of the jth indicator; g_j is the difference coefficient of the jth indicator; h_j is the entropy of the j indicator. According to the above steps, the evaluation index and index weight of tourism development and ecological environment coupling degree can be obtained.

Coupling coordination model. According to the capacity coupling system model in physics, the coupling degree model of Jiangsu tourism and ecological environment can be popularized, namely:

$$C = \left[\frac{u_1 u_2}{\left(\frac{u_1 + u_2}{2}\right)^2}\right]^{1/2} \quad (7)$$

In Formula (7), C represents the degree of coupling, ranging from 0 to 1; when C=0, it indicates that tourism economic development has no correlation with ecological environment; when C=1, it indicates that tourism economy and ecological environment have the best coupling degree.

$$T = \alpha u_1 + \beta u_2 \quad (8)$$

In Formula (8), T represents the comprehensive evaluation index of tourism economic system and ecological environment system, and α and β are undetermined coefficients, because tourism economic

TABLE 1
Indicator system and weights of tourism industry and ecological environment system evaluation

System	Subsystem	Evaluation index	Nature	Weights
Tourism industry system	Economic benefit	Number of tourists (10,000 people)	+	0.0012
		Tourism foreign exchange income (100 million US dollars)	+	0.0123
		Tourism income accounts for the proportion of tourism revenue in the province (%)	+	0.0233
	Infrastructure	Number of tourism practitioners (person)	+	0.0988
		Number of tourist attractions	+	0.0322
		Tourism infrastructure investment (US$10,000)	+	0.0432
Ecological environment system	Economic	GDP per capita (yuan/person)	+	0.0224
		Total import and export (US$10,000)	+	0.0553
		Per capita disposable income (yuan/person)	+	0.0221
		Financial revenue (100 million yuan)	+	0.0987
		Tertiary industry as a percentage of GDP (%)	+	0.0332
	Ecology	Per capita park green area (m2/person)	+	0.0189
		Pollution-free treatment rate of domestic garbage (%)	+	0.0223
		Forest cover rate (%)	+	0.0661
		Industrial wastewater discharge (10,000 tons)	-	0.0221
		Industrial carbon dioxide emissions (10,000 tons)	-	0.0881
		Industrial soot emissions (10,000 tons)	-	0.0543
	Service	Railway density (km/million km2)	+	0.0321
		Internet penetration rate (%)	+	0.0663
		Intelligent device penetration rate (Ministry / 100 people)	+	0.0339
	Society	Population urbanization rate (%)	+	0.0332
		Average number of students per 10,000 students (person)	+	0.0872
		Number of employees in the cultural industry (person)	+	0.0328

TABLE 2
Coupling degree and coupling coordination degree classification

C-value interval	Coupling type	D-value interval	Coupling coordination type
$0<C\leq0.3$	Low level coupling	$0<D\leq0.4$	Low coupling coordination
$0.3<C\leq0.5$	Antagonistic stage	$0.4<D\leq0.6$	Moderate coupling coordination
$0.5<C\leq0.8$	Run-in stage	$0.6<D\leq0.8$	Highly coupled coordination
$0.8<C<1$	High level coupling	$0.8<D<1$	Extreme coupling coordination

system and ecological environment system have the same status and role for urban development, therefore, α and the value of β is taken as 0.5.

$$D = \sqrt{C \times T} \quad (9)$$

In Formula (9), D represents the degree of coupling coordination, ranging from 0 to 1; the closer the value of D is to 1, the better the degree of coupling between the tourism economic system and the ecological environment system. In order to more intuitively express the relationship between the coordination degree of tourism economic system and ecological environment system, this paper classifies the coupling coordination degree; the specific classification is as follows Table 2.

RESULTS

Data source. Based on the objectivity, convenience and authenticity of data collection, the original data used in this paper mainly comes from the "Jiangsu Statistical Yearbook" and "China Tourism Statistics Yearbook". If the data in the yearbook and the statistical bulletin are inconsistent, the data in the Jiangsu Statistical Yearbook shall prevail, and the missing data shall be supplemented by the data on tourism and ecological civilization in the official website of the tourism bureaus of Jiangsu Province.

Coupling degree time evolution analysis. Based on the statistical data of Jiangsu Province in 2006-2018, the data was processed first, and then the tourism industry and regional economic evaluation index were calculated according to the coupling degree and coupling coordination model. Based on this, the coupling degree and coupling coordination degree of the two industries are calculated as shown in Table 3. From the calculation results in Table 3, we can find:

(1) Time series analysis of systematic evaluation index. From the overall development status, the evaluation index of tourism industry and ecological environment in Jiangsu Province in 2006-2018 showed the opposite time series characteristics: the

TABLE 3
The results of Coupling coordination degree value and level

Year	Tourism Industry Composite Index U1	Ecological environment comprehensive index U2	Comprehensive coordination index T	Coupling C	Coupling coordination D	Coupling level	Coordination level	Coupling coordination feature
2006	0.0421	0.5844	0.2021	0.2966	0.3122	Low level coupling	Low coupling coordination	Tourism industry relatively lagging
2007	0.0444	0.5723	0.2035	0.2989	0.3144	Low level coupling	Low coupling coordination	Tourism industry relatively lagging
2008	0.0551	0.5564	0.2098	0.3243	0.4045	Antagonistic stage	Moderate coupling coordination	Tourism industry relatively lagging
2009	0.1567	0.5532	0.4156	0.3676	0.4311	Antagonistic stage	Moderate coupling coordination	Tourism industry relatively lagging
2010	0.2766	0.5133	0.3955	0.3844	0.4342	Antagonistic stage	Moderate coupling coordination	Tourism industry relatively lagging
2011	0.3312	0.4676	0.3987	0.4235	0.4543	Antagonistic stage	Moderate coupling coordination	Tourism industry relatively lagging
2012	0.3655	0.4521	0.4123	0.4378	0.5023	Antagonistic stage	Moderate coupling coordination	Tourism industry relatively lagging
2013	0.4441	0.4311	0.4377	0.4765	0.5124	Antagonistic stage	Moderate coupling coordination	Ecological environment relatively lagging
2014	0.4933	0.4088	0.4876	0.4744	0.6034	Antagonistic stage	Highly coupled coordination	Ecological environment relatively lagging
2015	0.5123	0.3756	0.5024	0.4823	0.6054	Antagonistic stage	Highly coupled coordination	Ecological environment relatively lagging
2016	0.5678	0.3511	0.5551	0.4899	0.6063	Antagonistic stage	Highly coupled coordination	Ecological environment relatively lagging
2017	0.6671	0.3789	0.6033	0.4904	0.6074	Antagonistic stage	Highly coupled coordination	Ecological environment relatively lagging
2018	0.7523	0.4233	0.6228	0.4977	0.6087	Antagonistic stage	Highly coupled coordination	Ecological environment relatively lagging
Mean	0.3622	0.4668	0.4190	0.4188	0.4920	Antagonistic stage	Moderate coupling coordination	Tourism industry relatively lagging

former showed a large upward trend, which reflected the good development trend of tourism in Jiangsu Province, although the rapid rise of the tourism economic evaluation index after 2009, it can be seen that the tourism development has great flexibility. After the financial crisis, government tourism stimulated the development of tourism, which made the tourism industry grow rapidly; the ecological environment evaluation index showed a fluctuating decline. The trend, from 0.5844 in 2006 to 0.3511 in 2016, then tends to pick up, indicating that the ecological environment in Jiangsu Province is deteriorating, but since the 13th Five-Year Plan, the government has listed ecological civilization as a national development strategy, ecological environment. The improvement has become the focus of Jiangsu's development, and the ecological environment has rebounded.

In stages, from 2006 to 2012, although Jiangsu's tourism economic development lags behind the protection and construction of the ecological environment, it has a rapid growth rate and contains great potential for development; 2012-2018, Jiangsu Province's ecological environment protection and construction lags behind the development of the tourism industry, indicating that the tourism economy has continued to maintain a stable and substantial growth since 2012. However, with the continuous expansion and development of the tourism industry, the quality of the ecological environment is also declining, but it has begun to appear in 2016. The slight increase indicates the awareness of environmental protection in Jiangsu Province.

(2) Analysis of the evolution characteristics of the coupling degree and coupling coordination degree of ecotourism and tourism environment in Jiangsu Province. The coupling degree between Jiangsu tourism industry and ecological environment is between 0.3 and 0.5. According to the above classification of coupling degree, the coupling degree between Jiangsu tourism industry and ecological environment is in the antagonistic stage, and the early 2006 and 2007 are at low level coupling. The stage

indicates that the degree of coupling is gradually increasing, but the coupling level is generally low during 2006-2010, which is lower than the average level of 0.4188. After 2010, the coupling degree of both is higher than the average level. In 2018, the coupling degree of the two is the highest point is reached at 0.4977, which is very small compared to the coupling type run-in phase. From the calculation results of coupling degree, it can be seen that the coupling degree has been in the antagonistic stage during 2008-2018 and has not yet reached the running-in period, indicating that the coupling degree between Jiangsu tourism industry and ecological environment is not optimistic, and it is in a state of mutual competition for a long time. Further policy needs to be adopted to promote the coordinated development of the two.

It can be seen from Table 3 that the coordination degree of ecotourism and tourism environment in Jiangsu Province between 2006 and 2018 is between 0.3 and 0.61, and the average value does not exceed 0.5. The characteristics of ecotourism development and tourism environment are relatively obvious. Not coupled in an ideal state. From the numerical point of view, the coordination degree of ecotourism and tourism environment in Jiangsu Province has been on an upward trend from 2006 to 2018, and the coordination level has also been coordinated from low to medium coordination, and finally highly coordinated. From the trend point of view, with the increase of time, 2006 and 2007 are low coordination, 2008-2013 is moderate coordination, 2014-2018 is highly coordinated, and the coupling coordination degree in 2018 is 0.6087, due to recent years. The emergence of a series of new forms of tourism such as eco-tourism, recreation and tourism, and health tourism has tied tourism and the ecological environment firmly together, and the people's ecological concept has been continuously enhanced. Taking ecological environmental protection as an opportunity to promote tourism. The reform and upgrading have accelerated the integration and development of the two, and the coupling and coordination between the two have achieved remarkable results. Despite this, there is still much room for improvement in the development of ecotourism in Jiangsu Province, and it takes longer to work with the tourism environment. Mainly because the development of tourism in Jiangsu Province is still in an extensive development model, the integration with the tourism environment needs to be strengthened, and some major events will also affect the coordinated development of eco-tourism and tourism environment in Jiangsu Province.

CONCLUSION

The ecotourism industry has a close relationship with the regional integrated environment, which is interdependent and mutually influential. The regional environment is a necessary condition for the rapid development of the tourism industry, and the development of the tourism industry has also promoted the improvement of the regional environment. Taking Jiangsu Province as an example, this paper analyzes the comprehensive evaluation index and coupling and coordination development of the two systems by constructing the evaluation index system of tourism industry system and regional environmental system, and using the coupling coordination degree model. The main conclusions are as follows aspect:

The degree of coupling between the tourism industry system and the regional environmental system in Jiangsu Province remained stable. The significant correlation between the comprehensive index and the stability of the coupling degree between the two systems fully demonstrates that there is a dynamic coupling relationship between the tourism industry and the regional environment, and the two influence each other. Therefore, the benign interaction and integration of the two systems through coupling is an important way to promote the development of the tourism industry and improve the comprehensive environment of the region.

From the perspective of the overall time series evolution of Jiangsu tourism industry development and ecological environment coupling, 2006 and 2007 are in a low level coupling stage. From 2008 to 2018, the coupling between Jiangsu tourism industry development and ecological environment is mainly in the antagonistic stage, and the coupling degree is not high. The annual order has not changed much. After 2016, the coupling degree has improved significantly, reaching its peak in 2018. The coupling degree is generally on the rise. After 2009, the rate of increase is fast and tends to be stable. However, the coupling degree between Jiangsu tourism industry and ecological environment is not optimistic. The average value of 2006-2018 is only 0.4188, which is still at a low level. It has been in a state of mutual competition for a long time, and the interaction between the two is less, which restricts the coordinated development of the two.

From the overall time series evolution of Jiangsu tourism industry development and ecological environment coupling coordination degree, 2006 and 2007 are in a low degree of coupling and coordination stage. From 2008 to 2013, Jiangsu tourism industry development and ecological environment coupling coordination degree are mainly in moderate coupling coordination. In the stage, from 2014 to 2018, it was in the stage of high coupling and coordination, and the degree of coupling coordination has been greatly improved. The tightness of the two is deepened and the interaction response is enhanced. The coupling coordination degree also shows a trend of rapid increase and then slows, and the coupling and coordination benefits grow steadily. The annual order fluctuation of the coupling coordination degree is slightly larger than the coupling degree. Although

the coupling and development degree of the tourism industry system and the regional environmental system is continuously enhanced, the average value from 2006- 2018 is only 0.4920, and the coupling coordination level is generally low. In the future, Jiangsu Province should make full use of good regional environmental conditions, increase support for the development of the tourism industry, enhance the level of coupling and coordinated development of the two systems, and tap into the development potential of the tourism industry.

In summary, in areas where the tourism industry is lagging behind, we should actively cultivate the growth of regional tourism industry, and create special tourism products such as beautiful villages, forest towns, customs towns, cultural districts, etc., and actively develop global tourism demonstration zones and improve tourism. Infrastructure conditions, carefully constructing tourism industry clusters, forming a new format for the development of regional tourism industry; in the region where the ecological civilization construction is lagging, we must take the implementation of the concept of ecological civilization as the core, and build green tourism products as the main line, without sacrificing The eco-environment develops the old road of tourism industry at the cost, seeks the convergence point of the coordinated development of tourism industry development and ecological civilization construction, promotes the innovation of "tourism+" format, reduces the impact of tourism activities on the ecological environment, and realizes the green development of regional tourism industry.

DISCUSSION

(1) Promote green production and consumption, and promote the development of low-carbon tourism. In the context of a low-carbon economy, Jiangsu Province has strengthened its awareness of ecological responsibility and promoted low-carbon emission reduction of tourism enterprises. Tourist attractions should vigorously promote light-weight and energy-saving public transport, and encourage tourists to choose low-carbon or zero-carbon travel methods such as hiking and bicycles. Tourist hotels should promote energy-saving technologies in related architectural design, refrigeration, heating, lighting, water supply, etc., implement tourism contract energy management, and promote the green development of tourism enterprises. At the same time, it is necessary to improve the low-carbon environmental awareness of tourists, guide and encourage simple and civilized tourism behaviors, and use low-carbon consumption throughout the tourism process: ready-to-eat, live, travel, travel, purchase, and entertainment [21].

(2) Strengthen the coordination and cooperation of tourist attractions, and play the role of radiation in popular scenic spots. One of the important reasons for the decline in the quality of the ecological environment in tourist attractions is that the number of tourists exceeds the carrying capacity of the ecological environment in the scenic spot. Therefore, there is a need to plan and effectively divert traffic from hot spots. On the one hand, it is beneficial to alleviate the negative impact on the scenic spot due to the excessive number of tourists. On the other hand, it can also exert the diversity advantages of tourism resources in the region and create a new tourism brand. Jiangsu tourists are more concentrated in central city tourist attractions, and relatively more remote areas are less attractive to tourists. It is necessary to divert tourists through scenic spots and through trains to meet the needs of tourists in the scenic spots and enhance the experience of tourists in scenic spots [22].

(3) Increase investment in environmental protection and enhance the environmental awareness of tourism participants. Local governments and tourism management departments at all levels should regard the protection of the ecological environment as the lifeline for the development of the tourism industry, and always tighten the string of ecological and environmental protection, and take practical and effective measures to promote the ecological development of tourism industry. First, we must increase financial support, spend great efforts to control air pollution, water pollution, waste pollution, etc., and lay the foundation for the reshaping of the tourism environment. Second, we must actively promote relevant legislation, using the power of the system and the law as the ecological environment. The third is to guide the tourism behavior of the majority of tourist participants, strengthen the environmental awareness of tourism operators and ordinary tourists, and actively guide the tourists to consciously abide by environmental protection conventions through environmental protection publicity, environmental knowledge and other forms, and consciously maintain Tourism ecological environment.

(4) Strengthen macroeconomic regulation and control, fully embody the important role of the government. The government's macroeconomic regulation and control of the economy is an important way to achieve coordinated and sustainable development of the two. Establish a truly comprehensive decision-making body, establish a tourism economic and ecological environment coordination policy committee, make scientific decisions on tourism economic development and ecological environment issues in Jiangsu Province, and realize the integration between the environmental department and the tourism economic development department.

Make decisions to improve the coordination between the two.

REFERENCES

[1] Wall, G., Wright, C. (1977) The environmental impact of outdoor recreation. Ontario: University of Waterloo.

[2] Meethan, K. (1997) York: Managing the tourist city. Cities, 14(6), 333-342.

[3] Cole, D.N. (1994) Backcountry impact management: Lessons from research. Trends. 31(3), 10-14.

[4] Stephen,L.J.Smith. (1992) Recreational Geography: Theory and Methodology. Higher Education Press.

[5] Milne, S. (1990) The impact of tourism development in small Pacific Island States: an overview. New Zealand Journal of Geography. 89(1), 16-21.

[6] Zhang, J., Zhang, J. (2004) Tourism Ecological Footprint Model and Empirical Analysis of Huangshan City. Journal of Geographical Sciences. 59(5), 763-771.

[7] Zhong, X., Liu, Y. (2012) Analysis of the coordinated development of tourism -- Economic-ecological environment in Guangdong Province. Tropical Geography. 32(5), 568-574.

[8] Dong, Y., Ma, Y., Li, Z. (2013) Research on the coupling and coordination relationship between Xi'an inbound tourism flow and urban tourism environment. Regional Research and Development. 23(1), 98-101.

[9] Song, J., Wang, B., Li, H. (2002) Environmental effects and environmental remediation of tourism development in Xi'an. Journal of Northwest University (Natural Science Edition). 32(6), 683-686.

[10] Wan, X., Zhang, A., Li, G. (2003) Comprehensive Evaluation of Urban Tourism Environment Quality Based on Tourists-Analysis of Cases of Nanjing and Suzhou. Economic Geography. 23(1), 113-116.

[11] Wang, H., Lin, J., Jiang, B. (2006) Analysis of the coordinated development of tourism and environment in Dalian. Marine Environmental Science. 25(1), 84-87.

[12] Cui, F. (2008) Research on the coordinated development of tourism economy and ecological environment in Shanghai. China Population Resources and Environment. 18(5), 64-69.

[13] Pang, W., Ma, Y., Tang, Z. (2011) Study on the Coupling Relationship between Tourism Economy and Ecological Environment and Coordinated Development-Taking Shanghai and Xi'an as Examples. Statistical Information Forum. 26(12), 44-48.

[14] Wang, X. (2012) Research on Tourism Development Based on Synergetics Theory. Journal of Jilin Province Economic Management Cadre College. 26(1), 37-39.

[15] Wu, Y., Cui, F. (2012) Measurement and analysis of the relationship between tourism economy and ecological environment in Nanjing. Tourism Forum. 5(2), 79-83.

[16] Wang, Z., Yu, H. (2012) Research on the coupling development of tourism industry development and small town construction in Zhangjiajie. Economic Geography. 7, 165-171.

[17] Gao, N., Ma, Y., Li, T. (2013) Research on Coordinated Development of Tourism Industry and Urbanization Based on Coupling Model—Taking Xi'an as an Example. Tourism Journal. 28(1), 62-68.

[18] Yang, Z., Zhang, Z. (2014) Research on Coordinated Development of Tourism Economy and Ecological Environment Based on Coupling Model-Taking Guilin City as an Example. Journal of Northwest Forestry University. 29(3), 262-268.

[19] Jia, F., Zhou, L., Liu, H. (2013) Study on the Coupling Relationship between Urbanization and Ecological Environment in Heilongjiang Province. Hunan Agricultural Sciences. 12, 145-148.

[20] Luo, N., Li, J., Luo, F. (2014) Study on the Coupling Relationship between Urbanization and Ecological Environment—Taking Changzhutan Urban Agglomeration as an Example. Huxiang Forum. 1, 47-52.

[21] Liu, D.-H., Yang, Y.-C. (2011) Research on Coordination Degree of Regional Economy-Tourism-Ecological Environment-Taking Anhui Province as an Example. Resources and Environment in The Yangtze Basin. 20(7), 892-896.

[22] Luo, P. (2002) Problems and Countermeasures of Tourism Ecological Environment in Fujian Forest Park. Subtropical Resources and Environment. 17(4), 47-49.

Received: **22.10.2019**
Accepted: **12.02.2020**

CORRESPONDING AUTHOR

Qiaoqiao Shen
College of Economics and Management,
Nanjing University of
Aeronautics and Astronautics,
Nanjing 210016, Jiangsu – China

e-mail: suntao@nuaa.edu.cn

© by PSP Volume 29 – No. 05/2020 pages 3679-3689 Fresenius Environmental Bulletin

WIND TUNNEL SIMULATION OF RETAINING WALL EFFECTS ON WIND-SAND ENVIRONMENT

Min Yan, Hejun Zuo*, Gangtie Li

Inner Mongolia Key Laboratory of Aeolian Physics and Desertification Engineering,
College of Desert Control Science and Engineering, Inner Mongolia Agricultural University, Hohhot,
Inner Mongolia Autonomous Region, China

ABSTRACT

It is necessary to find rules of wind–sand migration around impenetrable structures, select effective wind–sand regional protection systems, set appropriate parameters and determine appropriate similarity ratios for wind-tunnel simulation models. The paper uses three models of different height in simulating the wind flow field and obtaining the sand transport law in a wind tunnel. Results show that when airflow acts on the windproof sand-retaining wall vertically, there is a sharp change in wind speed at a distance of 5H windward of the wall that does not change with the indicated wind speed. Affected by the windproof sand-retaining wall, the windward side conforms to the structural characteristics of wind–sand flow at different indicated wind speeds. Sand accumulation is mainly concentrated in the 0–10 cm layer near the surface; this layer accounts for 91.22% of the total sand transport volume on average. The leeward side no longer follows the rule of wind–sand flow, and the sand transport capacities of 10, 20 and 30 cm walls mainly concentrate in the height ranges of 20–60, 40–80 and 50–90 cm, respectively; these ranges respectively account for 91.46%, 94.66% and 63.33% of the total sand transport capacity. Simulation experiments are carried out in a wind tunnel with a test-section of 1.2 m × 1.2 m. A model height of about 20 cm is recommended. The ratio of the model height to the section length is 1:6, and the model be paved with the section width as far as possible.

KEYWORDS:
Wind and sand barrier, Airflow field, Configuration of drifting sand flux, Wind tunnel simulation

INTRODUCTION

Construction and operation activities of linear sand-control projects in sand damage areas of China are increasing year by year in alignment with the country's "One Belt and One Road" and "Western Development" strategies. The characteristics of sparse vegetation, strong wind, long-lasting winds, greater quantities of sand-carrying materials in the air and uneven spatial and temporal distributions have seriously affected traffic, buildings and human production as well as people's daily lives [1]. To protect the environment and reduce the harm of quicksand, different measures of wind prevention, sand fixing and sand blocking are widely applied in arid and semi-arid areas; e.g., the application of shelter forests [2], sand-retaining walls [3, 4], high vertical sand barriers [5], tiled sand barriers [6, 7] and comprehensive protection systems [8-10].

High vertical wind-and-sand-resistance measures are especially important as indispensable engineering sand-control measures in windy and sandy areas facing serious wind and sand disasters. Many studies have investigated the characteristics of the airflow velocity field, wind–sand flow structure, erosion and deposition transport rules and protection benefits through field observation, wind tunnel experiments and numerical simulation [11-13]. It has been found that a functional high-density polyethylene mesh with upper and lower densities has a good sand prevention effect and that an inclined plate insert has an obvious energy dissipation effect. It has been determined that the sand blocking effect is best when the porosity is 40% to 45% and that the wind-and-sand blocking effect is best when the row spacing is 5H [14] (H means the height of the sand net). Perera [15] found that the recirculation bubble that forms behind fences disappeared when the porosity e was >30%. Ventilation measures, mainly involving the wind load, aerodynamics and induced morphological dynamics, have been widely studied since the beginning of the 20th century. Simply put, porosity and its distribution are generally considered to be the most important factors determining the performances of sand control measures that drive the design and control for a given height and incoming wind.

In contrast, to the best of our knowledge, there has been surprisingly little scientific research on the aerodynamics and morphological dynamics of the wind-blown-sand solid barrier; i.e., the research of the absence with porosity. Only Baines [16], Good [17] and Letchford [18] conducted wind tunnel tests to simulate the aerodynamic characteristics of a solid vertical wall under two-dimensional conditions. Furthermore, the wind–sand migration law of this wind–

sand blocking measure is obviously different from that of the wind ventilation measure and there have been few studies on the airflow characteristics and wind–sand flow structure on the leeward side [13, 19]. In addition, the best similarity ratio of the model is not given in a wind tunnel experiment. According to geometric similarity, motion similarity, dynamic similarity, thermodynamic similarity and mass similarity of the models, most of the models use their own characteristic parameters to determine a reasonable range [20-22], and it is thus necessary to screen the similarity ratio of the model.

Vertical baffle is a wind-blown-sand solid barrier with the porosity by "0", and is very useful structures used in agriculture and other applications for the last several years. Besides crop protection, vertical baffles are frequently used for the protection against wind loads of other low-rise buildings and objects or linear engineering sand damage [23]. Along with their wind loading reducing ability vertical windbreak baffles have also been found to be efficient in successfully affecting sand damage by railway and highway in arid region [24, 25]. Since the wind flow and configuration of drifting sand flux are a very complicated phenomenon that is largely affected by many factors, however, a complete quantitative analysis on the effects of vertical baffles have not been performed. Therefore, it is necessary to conduct in-depth analysis on the vertical baffle. Due to its impermeability and large size, field observation is confronted with unprecedented difficulties, and the wind tunnel experiment has become an ideal environment to solve this problem.

Owing to the limitations of the field observation and the uncertainty of numerical simulation under the environmental conditions of a windy and sandy area, it is not easy to obtain the rules of wind-sand movement for tall protective measures of windproof, and it is not easy to monitor the benefits of wind and sand blocking at different heights. In addition, under specific wind–sand environment conditions, the outermost part of a wind–sand protection system of a railway in linear engineering needs to be blocked by tall measures with no air permeability, so as to avoid the direct harm of wind–sand flow on rail lines and locomotives. Conducting a wind tunnel experiment is therefore an effective way to simulate the law of wind and sand migration. The paper places models in the airflow field of a wind tunnel in simulation experiments, analyzes the motion law of the models near the airflow resistance and under the action of sediment and sediment characteristics, reveals the wind-sand special comprehensive environment against the windshield sand wall under the action of the sand transport rule, and considers comprehensive prevention and control measures for linear project experimental model choosing and its application in the construction of the system to provide a theoretical basis and data for future work.

MATERIALS AND METHODS

(1) Wind test. Wind tunnel experiments were carried out in the Shapotou soil and wind tunnel laboratory of the Cold and Arid Regions Environmental and Engineering Research Institute, Chinese Academy of Sciences. The dc held blowing low-speed wind tunnel was 37.08 m, the length was 21 m and the cross-section was 1.2 m by 1.2 m. The whole lifting of the section of the bottom can make 1°. The wind energy ratio was 0.55, the average turbulence intensity was 0.6%, the turbulence scale was $\varepsilon < 1‰$, and the axial static pressure gradient was $\Delta p/\Delta x = 0$ in the experiments. The free-stream wind velocity in the wind tunnel ranged from 1.2 to 30.8 m/s. The working principle of the wind tunnel is shown in Figure 1. According to the similarity characteristics of airflow motion, a wind tunnel can generally reach an aerodynamic self-modeling state if the Reynolds number is controlled around $Re = 10^6$. The Reynolds number is calculated as [26]

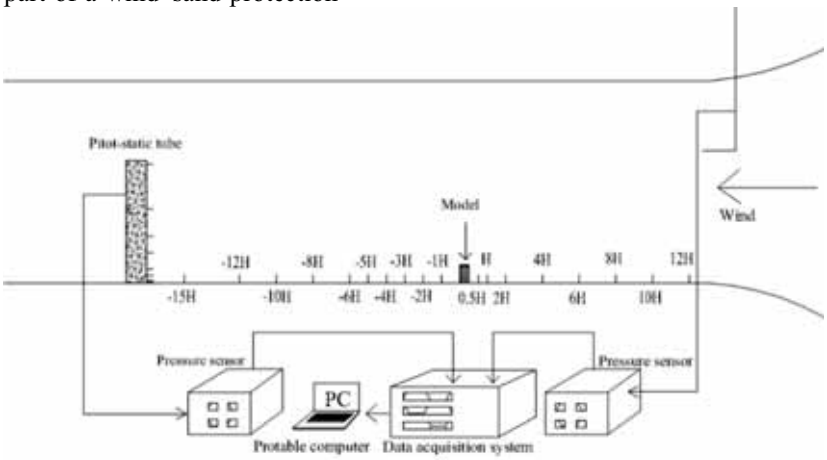

FIGURE 1
Schematic of the Wind Speed Measurement System and Experimental Setup

$$Re = \rho v L / \mu \quad (1)$$

where ρ is the flow density, v is the wind speed in the tunnel, L is the model dimension and μ is the viscosity coefficient.

(2) Experimental Materials. Each model was made of wood and had a height of 10, 20 or 30 cm. The design of the wind tunnel experiments did not consider the responses of sand particles of different size to each model, and the source of sand samples did not affect the smooth implementation of the experimental scheme or the analysis, summary and refinement of experimental test accuracy and general rules. Eolian sand samples were therefore obtained at the edge of the Tengger Desert, where the laboratory is located. The particle size distribution is given in Table 1. The experimental scene is shown in Figure 2.

TABLE 1
Characteristics of Sand Particle Size Distribution

Grain size (μm)	< 100	100 ~ 200	200 ~ 300	300 ~ 400
Percentage (%)	4.31	76.20	19.14	0.35

FIGURE 2
Experimental Scene
(a) model in the wind tunnel and (b) sand morphology due to the presence of the model

Measurement of the Flow Velocity Field around Each Model. A wind tunnel experiment was conducted to determine the characteristics of the airflow velocity field for models of different height in the case of clean air. The models had heights of 10, 20 and 30 cm and the indicated wind speed was set at 6, 8, 10 and 12 m/s. The wind speed was measured using a pitot-tube differential pressure measurement system at heights of 0.3, 0.6, 1.5, 3, 12, 20, 35 and 60 cm and horizontal distances of before the model of 1H, 2H, 3H, 4H, 5H, 6H, 8H, 10H, 12H and 15H and after it with 0.5H, 1H, 2H, 4H, 6H, 8H, 10H and 12H (Figure 1).

Measurement of Drifting Sand Flux around Each Model. A wind tunnel experiment was conducted to determine wind and sand flow under the conditions of sand-carrying wind in the case of a void (without a model) and before and after each model. The models had heights of 10, 20 and 30 cm and the indicated wind speed was set at 6, 8, 10 and 12 m/s. A continuous-equal-height-step sand-deposition instrument was used to measure the wind and sand flow. The wind–sand flow on the windward side of the model was measured at a distance of 3H and the height of the sand deposition instrument was 20 cm (10 layers). The wind–sand flow on the leeward side of the model was measured at 3H and the height of the sand deposition instrument was 100 cm (50 layers).

Measurement of Sand Morphology around Each Model. A wind tunnel experiment was conducted to determine the wind tunnel (without a model: CK) and sand flow before and after models having heights of 10, 20, and 30 cm. The indicated wind speed was set at 6, 8, 10 and 12 m/s for 10, 10, 5, and 3 min respectively. The three-dimensional coordinates of sand accumulation were obtained using a ruler and Vernier calipers. The center line intersection of the wind tunnel floor on windward and leeward sides of the model was taken as the origin of coordinates, and points were selected to measure the three-dimensional coordinates of the sand accumulation. A three-dimensional morphological map was drawn using the geostatistics software Surfer 11.0.

(3) Data Analysis. The wind speed in the tunnel was calculated as [20]:

$$v = 4.05\sqrt{\frac{P}{p} \times \frac{T}{293} \times \Delta h} \quad (2)$$

where v is the wind speed, P is the standard atmospheric pressure (mmHg), p is the atmospheric pressure (mmHg), T is the temperature (K) and △h is the pitot-tube differential pressure (mmH_2O).

The sediment flux was calculated as [27]:

$$Q = \frac{q}{A.t} \quad (3)$$

where Q is the sediment flux, q is the sediment runoff, A is the unit area of the sand inlet of the sand collector and t is the transportation time.

The area and volume of the accumulated sand bottom were calculated using the geostatistics software Surfer 11.0.

RESULTS

Effect of Model on the Airflow Velocity Field. (1) Airflow Velocity Field for Models of Different Height. Figure 3 show the change rules of the airflow velocity field for indicated wind speeds of 6, 8, 10 and 12 m/s in the wind tunnel without a model (CK) and with models having heights of 10, 20 and

30 cm. It is seen that all streamlines have a parallel arrangement at different indicated wind speeds. The airflow changes appreciably when the model is blocked. Under the effect of vertical wind, the wind velocity began to fluctuate at 5H. Lower airflow interference by model flow encryption, wind strengthened, before –3H to model is an air uplift area, and to form an area of strong wind above the model and the leeward side of the lower air to form an area of weak or no wind, the upper airflow diffusion changed, wind speed gradually recovered from 9H to 10H. As the model height increased, the distance of effective protection afforded by the model in the leeward weak-wind or calm area did not change appreciably and was within the range of 0 to 9H after the model. However, the protection range in the vertical gradient increased with the height of the model. With an increase in the indicated wind speed, changes in the secondary airflow on the windward side and leeward side of the model tended to be the same, and it is thus considered that a change in the indicated wind speed had no appreciable effect on the change law of the airflow velocity field.

(2) Change Law of the Vertical Flow Velocity Profile for Models of Different Height. The gradient of the vertical air velocity profile changed for different indicated wind speeds of 6, 8, 10 and 12 m/s and different heights of windward and leeward model positions as shown in Figure 4. It is seen that the wind speed at 3H on the windward side increased by different degrees with an increase in height for different indicated wind speeds. The airflow below 3 cm in the near stratum was appreciably affected by the models, with the average air speed dropping to 2.11, 3.07, 3.95 and 4.83 m/s or 35.13%, 38.34%, 39.51% and 40.25% of the indicated wind speed respectively. The airflow uplift gradually strengthened with an increase in height. The average airflow velocity increased with the wind speed gradient, by 47.37%, 43.68%, 40.73% and 38.75% respectively compared with the airflow velocity in the near stratum. Above a vertical height of 2H, the airflow speed was basically unaffected by the models and returned to the indicated wind speed. There was no obvious change law with an increase in model height on the windward side.

Figure 4c and 4d shows wind speed curves on the leeward side at 3H. Affected by the model, 10- and 20-cm model leeward with 3–20 cm height wind speed reduction process was most obvious, and 30-cm model with 3–35 cm wind speed reduction process was most obvious, four groups of average air velocity were instructs the wind speed was reduced by 95.07%, 94.91%, 95.81% and 93.24% respectively, the leeward side 0 to 2H range, wind speed and even zero. With an increase in the vertical height, the airflow velocity above 35 cm was

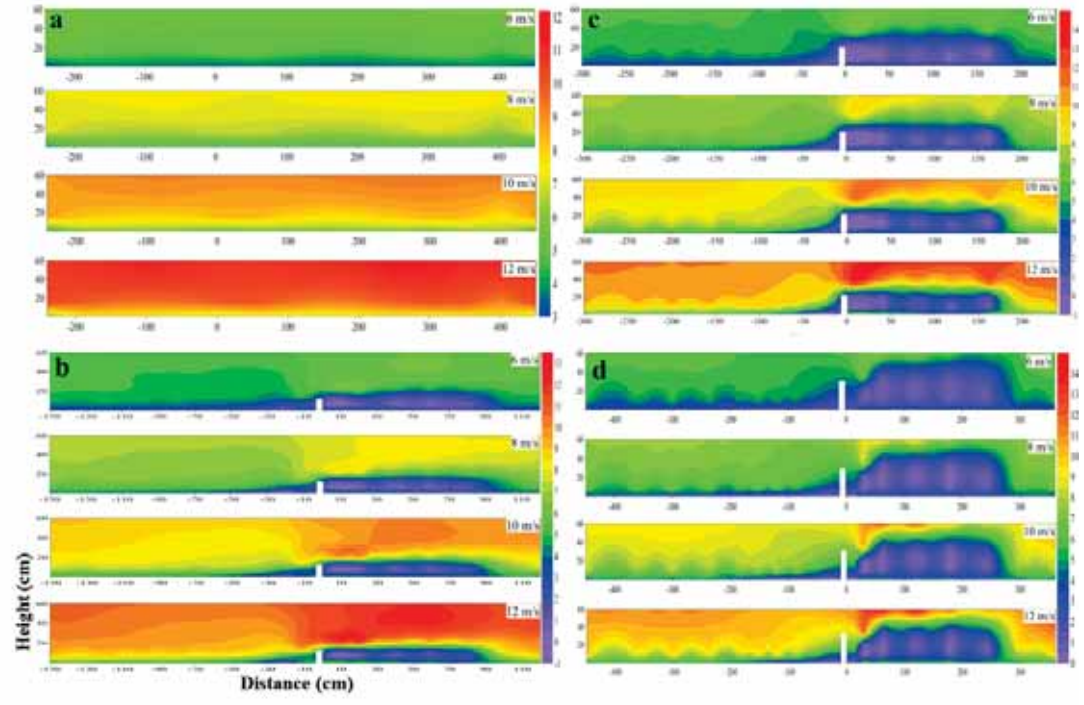

FIGURE 3
Characteristics of The Wind-Tunnel Airflow Velocity with Different Models
(a) Characteristics of the wind tunnel (without model: CK): airflow velocity for different wind speed gradients. (b) Characteristics of the wind-tunnel airflow velocity for different wind speed gradients and the 10-cm model. (c) Characteristics of the wind-tunnel airflow velocity for different wind speed gradients and the 20-cm model. (d) Characteristics of the wind-tunnel airflow velocity for different wind speed gradients and the 30-cm model.

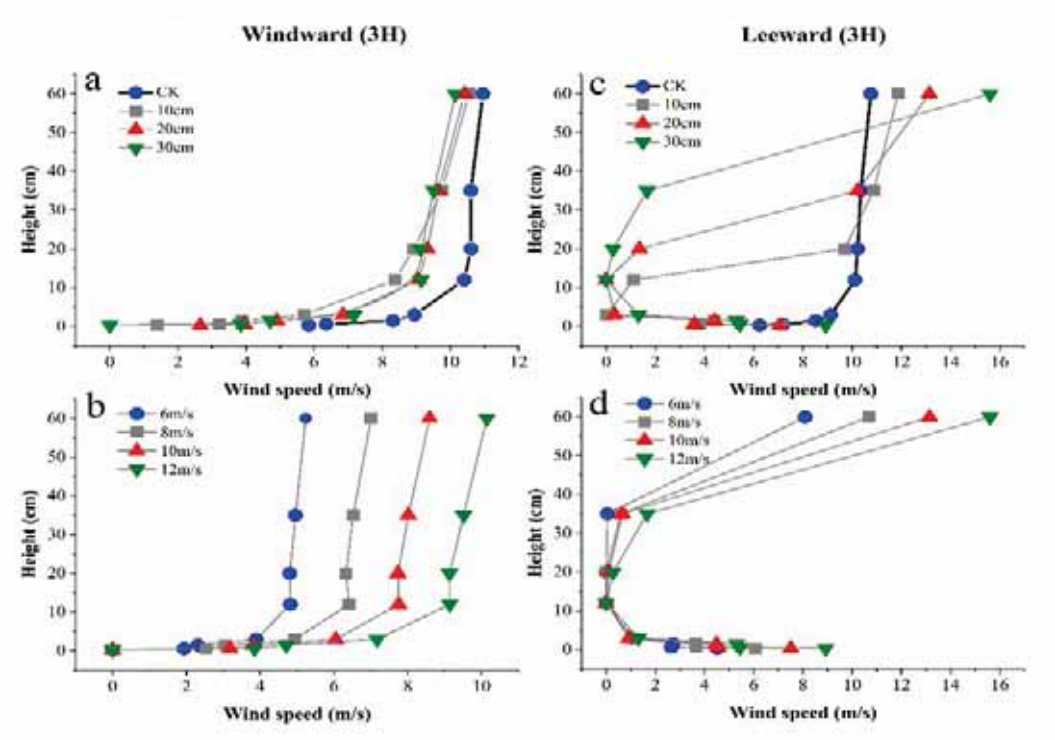

FIGURE 4
Vertical Flow Velocity Profile Characteristics of Baffles of Different Height
(a) 3H windward for an empty tunnel and different models with a wind speed of 12 m/s, (b) 3H windward of the 30-cm model for different indicated wind speeds, (c) 3H leeward of different models for an indicated wind speed of 12 m/s and (d) 3H leeward of the 30-cm model for different indicated wind speeds.

basically unaffected by the model and returned to the indicated wind speed. Moreover, the indicated wind speed had no appreciable effect on the wind profiles on the windward and leeward sides of the models.

Effect of Models on the Vertical Distribution of Wind–Sand Flow and the Sand-Blocking Characteristics. (1) Structural Characteristics of Wind-Sand Flow for Models of Different Height. Figure 5 shows curves of the wind–sand flow structure change at different positions on the windward and leeward sides of models of different height when the indicated wind speed was 6, 8, 10 and 12 m/s. It is seen that when there was no model in the wind tunnel, the change rules of sand transport at 3H on the windward side and at 3H on the leeward side were similar. When a model was present, the near-surface sediment transport volume before and after the model followed different rules with a change in height, for different indicated wind speeds. The overall sediment transport volume decreased with an increase in height. Windward sediment transport was mainly concentrated at heights of 0–10 cm; the height range of 0–10 cm accounted for 90.87%, 92.70% and 90.15% of the total windward sediment transport for the models having heights of 10, 20 and 30 cm respectively. Affected by the impermeable model, the leeward side no longer followed the structural law of wind–sand flow. Sand transportation for the models having heights of 10, 20 and 30 cm was mainly in the range of 20–60, 40–80 and 50–90 cm, accounting for 91.46%, 94.66% and 63.33% of the total leeward sand transport volume respectively (Table 2). The sediment transport volume was a maximum at the positions of 40, 60 and 80 cm respectively. This variation rule was unaffected by the indicated wind speed. However, with an increase in the indicated wind speed, the average sediment transport volume of each layer appreciably increased. The leeward side was basically without sand at indicated wind speeds of 6 and 8 m/s and was higher at 12 m/s than at 10 m/s by a factor of 2.92 on average.

(2) Characteristics of The Model Sand Resistance for Models Of Different Height. Figure 6 shows the sand accumulation patterns before and after the three models (having heights of 10, 20 and 30 cm) for different indicated wind speeds (6, 8, 10 and 12 m/s). It is seen that the surface area and amount of sand accumulation around a model increased as the height of the model increased. At the same indicated wind speed, the surface area and amount of sand accumulation around the model with a height of 30 cm were respectively 2.18 and 3.23 times those of sand accumulation around the model with a height of 10 cm (Table 2). When the

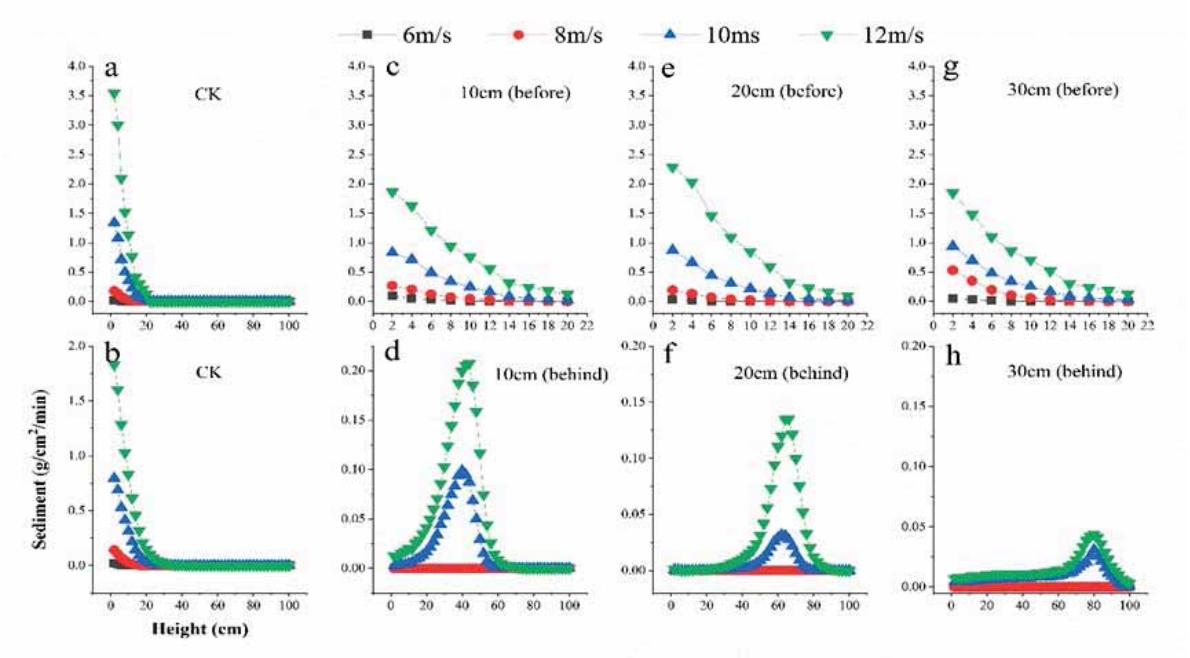

FIGURE 5
Reattachment Distance of Airflow for Different Wind Directions

(a) wind–sand flow structure at 3H on the windward side without a model (CK), (b) wind–sand flow structure at 3H on the leeward side without a model (CK), (c), (e), and (g) wind-sand flow structures at 3H on the windward side for 10-, 20-, and 30-cm models, respectively, and (d), (f), and (h) wind–sand flow structures at 3H on the leeward side for 10-, 20-, and 30-cm models, respectively.

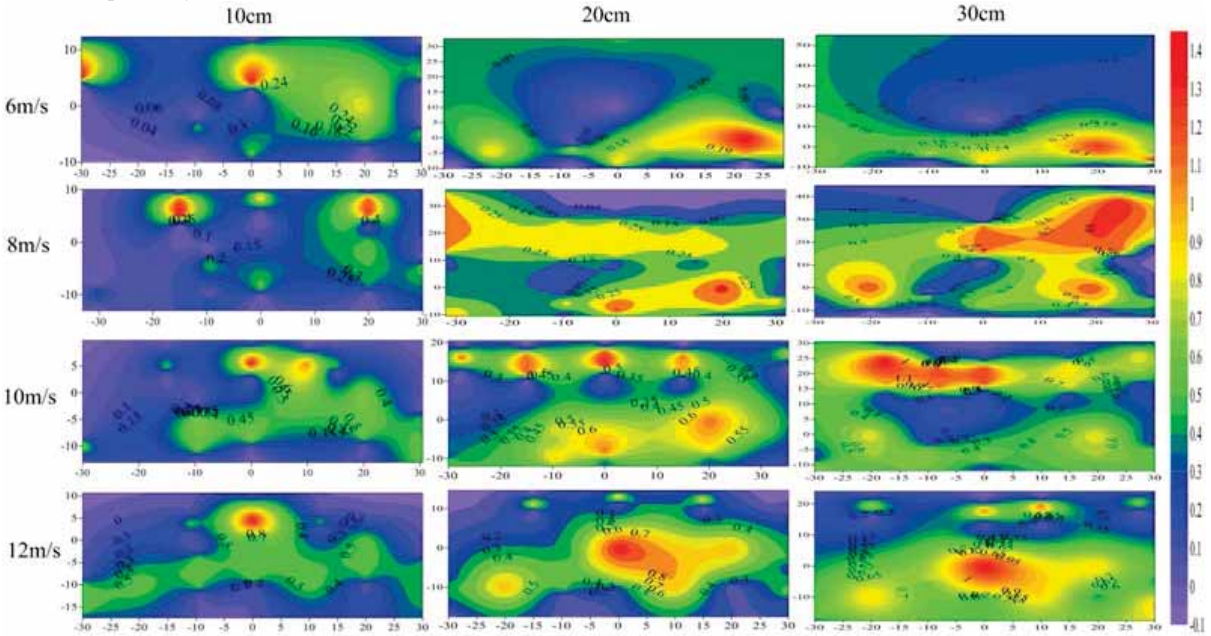

FIGURE 6
Characteristics of Sand Morphology for Models of Different Height

indicated wind speed was 6, 8 10 and 12 m/s, the average surface area of the model of the same height was respectively 1850.88, 1977.81, 2466.05 and 2647.32 cm^2. Sediment accumulation was 317.23, 615.47, 811.36 and 892.59 cm^3, respectively.

Determination of the Model Similarity Ratio in the Wind Tunnel. Figure 7 shows the effects of the three models on wind speed at heights of 3 cm (Figure 7a) and 60 cm (Figure 7b) for different observation points near the surface at different indicated wind speeds (6, 8, 10 and 12 m /s). It is seen that the wind speed at each observation point in the range of 0 to 8H before the model and 0 to 10H after the model was disturbed by the model, resulting in the wind speed fluctuating. For different indicated wind speeds, the effect of the same model on the wind speed was similar, while the

TABLE 2
Sediment Transport Characteristics of Baffle Models at Different Indicated Wind Speed

Model	Indicate wind speed （m/s）	Q_1 (g/cm^2/min)	Q_2 (g/cm^2/min)	Q_{0-10}/Q_1	Q_{20-60}/Q_2	Q_{40-80}/Q_2	Q_{50-90}/Q_2	S （cm^2）	V （cm^3）
CK	6	0.042	0.035	88.00	0.00%	0.00%	0.0%	0.00	0.00
	8	0.504	0.418	92.60	0.30%	0.00%	0.0%	0.00	0.00
	10	4.456	3.336	89.10	1.80%	0.00%	0.0%	0.00	0.00
	12	13.103	8.676	86.20	3.90%	0.20%	0.7%	0.00	0.00
10 cm	6	0.193	0.000	98.68	0.00%	0.00%	0.00%	1316.16	177.40
	8	0.757	0.000	94.14	0.00%	0.00%	0.00%	1321.90	291.53
	10	2.959	1.026	88.24	92.72	34.87	2.74%	1452.34	374.84
	12	7.813	2.472	81.94	90.20	42.69	7.35%	1467.28	501.74
20cm	6	0.062	0.000	99.07	0.00%	0.00%	0.00%	1883.88	242.30
	8	0.457	0.000	97.41	0.00%	0.00%	0.00%	2121.05	485.69
	10	2.781	0.289	89.86	48.37	95.08	86.31	2481.01	719.99
	12	9.121	1.360	84.64	38.81	94.24	88.13	2569.57	829.71
30 cm	6	0.105	0.000	95.49	0.00%	0.00%	0.00%	2352.61	532.00
	8	1.289	0.000	96.22	0.00%	0.00%	0.00%	2490.48	1069.18
	10	3.100	0.464	87.49	31.96	54.61	63.87	3464.80	1339.26
	12	7.350	0.768	81.41	29.27	50.95	62.78	3905.11	1346.33

between models having different similarity ratios was large. The wind speed at a height of 3 cm fluctuated greatly. The degree of influence before the model decreased in the order of 30 cm > 10 cm > 20 cm while the degree of influence after the model decreased in the order of 30 cm > 10 cm > 20 cm. The degree of influence of the similarity ratio of the models on wind speed at a height of 60 cm decreased in the order of 30 cm > 10 cm > 20 cm before the model and decreased in the order 30 cm > 10 cm > 20 cm after the model. It is seen that the effect of the 30-cm model on wind speed was greater than that of the 10-cm model and that of the 20-cm model. Combined with the effect of the wind speed at two extreme heights, the disturbance of the wind speed at different heights by the 20-cm model was the least.

DISCUSSIONS

The existence of the sand-retaining wall that "once" flow on the surface of the Earth as a special form of "secondary" flow, lead to the wall of airflow in both flow speed and flow direction on all great changes have taken place, especially the air of momentum and energy transfer mode becomes more complex, the change and effect the sand-retaining wall deposition and migration regularity of sand flow [28, 29]. As a matter of fact, a sand-retaining wall is an artificial obstacle rising above a surface, and the dynamic process of its sand prevention is controlled by the complex interaction among the wall, terrain, wind direction, air flow and sand accumulation [30]. The results of the present paper show that the airflow around obstacles in the runtime, on the windward side due to the blocking effect of obstacles on airflow prone to separation, forming part of the uplift and accelerated air, after over obstacles, leeward side was affected by the pressure differential, control air flow are the major factors weight attached form air flow, air flow and obstacle, obstacles, etc. When the airflow acts on the sand-retaining wall, the windward airflow divides into lower decelerating airflow, middle uplifting accelerating airflow and upper turbulence, forming an area of weak wind. When the airflow crosses the sand-retaining wall, the boundary layer separates, and part of the airflow continues to lift and accelerate, forming a zone of strong wind at the top of the windproof sand-retaining wall. The remaining airflow decelerates or becomes opposing airflow on the leeward side, forming a zone of weak or no wind. This result is consistent with wind-tunnel test results for an impermeable arch and wind barriers of different type [31].

The results of the wind tunnel experiments reported in the literature show that the sand resistance rate is one of the most intuitive parameters with which to characterize the sand resistance effect of the sand-retaining wall due to multiple factors. Additionally, many sand observations have revealed obvious differences in the shape and position of sand accumulating before and after a sand-retaining wall. After different wall on both sides of the wall shows that the sand flow, air flow disturbance situation, there are differences at different positions in local,

deceleration zone, the sand material after the sand-retaining wall, in the position away from the wall must be the biggest probability in sand, then under the action of a force to the movement, the deposited sand has different forms [32-34]. The simulation results of the present paper show that the sand-retaining wall windward conforms to the structural characteristics of sand flow, affected by the wall, on the leeward side no longer follow the rules of wind sand flow, and with an increase in wall height, the main sediment discharge layer increased gradually in the vertical direction; i.e., over short distances, the suspended load sand flow does not easily fall form many sand deposition. The forms of sand accumulation on the leeward side of the wall are different from each other because of the law of sand migration. Compared with the measures of wind permeability and sand obstruction, there are appreciable differences in the structure of wind–sand flow on the lee side. Air flow through pores results in wind erosion on the near surface behind the barrier, forming a wind–sand flow structure similar to that in front of the barrier. However, there is much less sand transport behind the barrier than in front of the barrier. Sand-resisting measures of structure differences, leading to an appreciable difference, were found on the leeward side of the protective range. Wind tunnel experiments and field observations show that the nylon net porosity is 40% to 45%, under different instructions wind barrier after 10H to 12H wind speed back to indicate wind [35]. According to the calculated shelter index, wind barriers with porosity of 0.3-0.4 could provide the longest effective shelter distance, and a 2-row-a-belt scheme with inter-row spacing of 5-7 H (H as the height of wind barriers) is the most effective. The optimal inter belt spacing is suggested as 12-15 H depending on local wind velocity [36]. It has to do with this paper, wind-tunnel simulation results to determine different height of the retaining wall barrier 8 H to 12 H results are consistent.

The sand barrier belt is an important part of a wind–sand protection system in linear engineering, and different sand barrier measures are widely used in highway and railway protection systems. However, there is no unified conclusion on the reasonable heights of different measures, especially the determination of the model height in wind tunnel simulations [37, 38]. Scholars have made field observations of the protective effects of 1.5-, 2.0-, and 2.5-m sand barriers to investigate the effect of the wall height. Results show that when the wall structure was the same, on the leeward side of a retaining wall, sediment decreasing trend changes with an

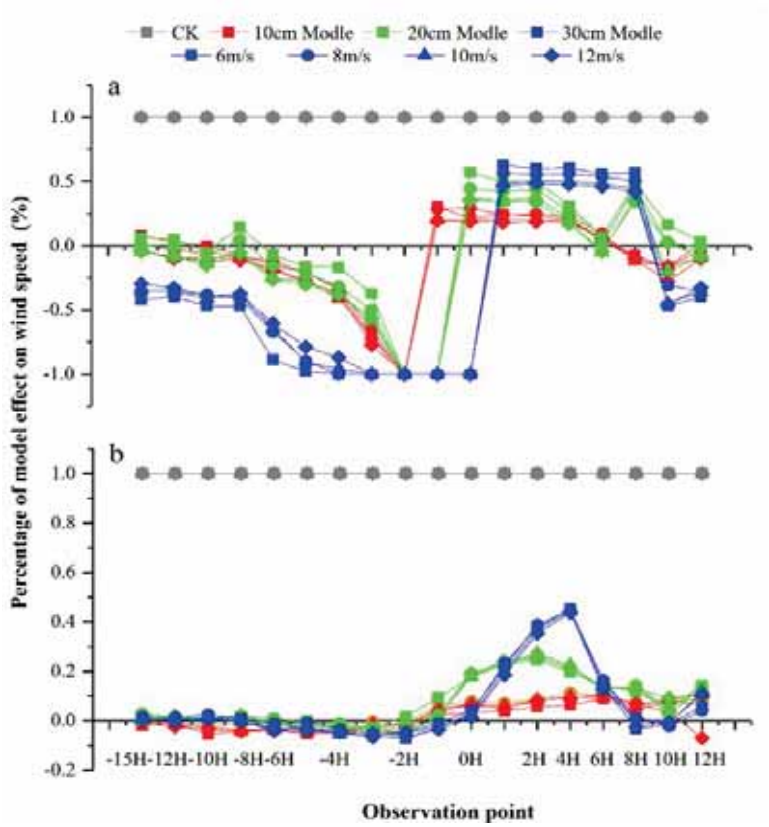

FIGURE 7
Effects of the Model Height on Wind Speed
(a) effect of the model height on the wind speed near the surface (at a height of 3 cm) for different wind speed gradients and (b) effect of the model height on the wind speed near the surface (at a height of 60 cm) for different wind speed gradients.

increase in height, the higher the height, the wind with the smaller sediment. It can be shown that when the vertical height exceeds the set height of the sand-retaining wall, the movement of the upper layer carrying sand flow is gradually reduced by the disturbance of the sand-retaining wall, and the gap between the amount of sand collected by the wind behind the sand-retaining wall gradually reduces. It is considered that the wind–sand protection effect of a 2.0-m sand-retaining wall is better than that of a 2.5-m wall and that of a 1.5-m wall; i.e., with an increase in wall height, the added protective effect gradually flattens out from a rapid increase initially and, with a further increase in height, the protective effect only slightly increases or even declines [39].

The simulation results of the present paper show that the sand blocking benefits of 2.0- and 3.0-m sand-retaining walls are better than those of 1.0-m walls. For the same indicated wind speed gradient, the sediment accumulation and sediment resistance are about 2 to 3 times those for the 1.0-m sand-retaining wall. However, the increase in the protective benefit is more gradual for the 3.0-m sand-retaining wall than for the 2.0-m sand-retaining wall. It can be shown that a wall should be no higher than 3.0 m in practical engineering applications. The present paper further analyzed the disturbance of the wind speed by models of appropriate height having different similarity ratios. Results show that the degree of influence before the model on wind speed decreased in the order of 30 cm > 10 cm > 20 cm while that after model decreased in the order of 30 cm > 10 cm > 20 cm. The effect of the 30-cm model on wind speed was obviously greater than that of the 10-cm model and that of the 20-cm model; i.e., the 20-cm model least disturbed the wind speed at different heights. In conclusion, it is advisable to set the height of the model at about 20 cm in future wind tunnel experiments. The model similarity ratio was about 1:6 considering that the section size of the wind tunnel used in the present study was 1.2 m × 1.2 m.

CONCLUSIONS

When airflow acts on a sand-retaining wall vertically, there is an inflection point of a sharp change in wind speed at a distance of 5H from the windward side of the wall that does not change with the indicated wind speed. The position of the zone of strong wind gradually moves to the windward side with an increase in height. The change rule of the wind flow on the leeward side is basically the same for different heights of the wall.

Affected by the sand-retaining wall, the windward side of the model conforms to the structural characteristics of wind–sand flow at different indicated wind speeds. Sand accumulation mainly concentrates in the 0–10-cm layer near the surface; this layer accounts for 91.22% of the total sand transport volume on average. The leeward load does not follow the rules of sand flow, and the sand transport capacities of the walls with heights of 10, 20 and 30 cm are mainly concentrated in the ranges of 20–60, 40–80 and 50–90 cm respectively; these ranges respectively account for 91.46%, 94.66% and 63.33% of the total sand transport capacity.

The simulation experiments of the present study were carried out in a wind tunnel with test-section dimensions of 1.2 m × 1.2 m, and the ratio of the model height to section length was about 1:6. The sand-retaining wall should thus be 2 to 3 m tall in application.

ACKNOWLEDGEMENTS

This work was supported by the National Key Research and Development Program of China (No. 2016YFC0501009). We thank Glenn Pennycook from Liwen Bianji, Edanz Group China (www.liwenbianji.cn./ac), for editing the English text of this manuscript.

REFERENCES

[1] Xie, S.B., Qu, J.J., Pang, Y.J. (2017) Dynamic wind differences in the formation of sand hazards at high and low altitude railway sections. Journal of Wind Engineering and Industrial Aerodynamics. 169, 39-46.

[2] Zhao, W.Z., Hu, G.L., Zhang, Z.H., He, Z.B. (2008) Shielding effect of oasis-protection systems composed of various forms of wind break on sand fixation in an arid region: A case study in the Hexi Corridor, Northwest China. Ecol. Eng. 33, 119-125.

[3] Xu, X.L., Zhang, K.L., Kong, Y.P., Chen J.D., Yu, B.F. (2006) Effectiveness of erosion control measures along the Qinghai-Tibet Highway, Tibet plateau, China. Transp. Res. Part D. 11, 302-309.

[4] Dong, Z., Li, H.L., Wang, J., Ding, G.D., Sun, B.P. (2007) Wind tunnel test on effect of controlling wind and deposited sand of geogrid sand-barrier. Sci. Soil Water Conserv. 5, 35-39.

[5] Xiao, J.H., Yao, Z.Y., Qu, J.J. (2015) Influence of Golmud-Lhasa section of Qinghai-Tibet railway on blown sand transport. Chinese Geographical Science. 25, 39-50.

[6] Zhang, C.L., Zou, X.Y., Cheng, H., Yang, S., Pan, X.H., Liu, Y.Z., Dong, G.R. (2007) Engineering measures to control windblown sand in Shiquanhe town, Tibet. J. WindEng. Ind. Aerodynamics. 95, 53-70.

[7] Zhang, S., Ding, G.D., Yu, M.H., Gao, G.L., Zhao, Y.Y., Wu, G.L., Wang, L. (2018) Effect of straw checkerboards on wind proofing, sand fixation, and ecological restoration in shifting sandy land. Environmental Research and Public Health. 15(10), 2184.
[8] Zhang, K.C., Qu, J.J, Liao, K.T., Niu, Q.H., Ha, Q. (2010). Damage by wind-blown sand and its control along Qinghai-Tibet railway in China. Aeolian Research. 1, 143-146.
[9] Cheng, J.J., Xue, C.X. (2014) The sand-damage–prevention engineering system for the railway in the desert region of the Qinghai-Tibet plateau. J. Wind. Eng. Ind. Aerodyn. 25, 30-37.
[10] Wang, T., Qu, JJ., Ling, Y.Q., Liu, B.L., Xiao, J.H. (2018) Shelter effect efficacy of sand fences: A Comparison of Systems in a Wind Tunnel. Aeolian Research. 30, 32-40.
[11] Zhang, C.L., Zou, X.Y., Pan, X.H., Yang, S., Wang, H.T. (2007) Near-surface airflow field and aerodynamic characteristics of the railway-protection system in the Shapotou region and their significance. Journal of Arid Environ. 71, 169-187.
[12] Li, B., Sherman, D.J. (2015) Aerodynamics and morphodynamics of sand fences: a review. Aeolian Research. 17, 33-48.
[13] Luca, B., Davide, F., Andrea, L.G. (2018) Solid barriers for windblown sand mitigation: Aerodynamic behavior and conceptual design guidelines. Journal of Wind Engineering and Industrial Aerodynamics. 173, 79-90.
[14] Lee, S.J., Park, K.C., Park, C.W. (2002) Wind tunnel observations about the shelter effect of porous fences on the sand particle movements. Atmospheric Environment. 36(9), 1453-1463.
[15] Perera, M.D.A.E.S. (1981) Shelter Behind Two-dimensional Solid and Porous Fences. Journal of Wind Engineering and Industrial Aerodynamics. 8, 93-104.
[16] Baines, W. (1963) Effects of velocity distribution on wind loads and flow patterns on buildings, In: Proceedings of Conference "Wind Effects on Buildings and Structures". National Physical Laboratory, 198-225.
[17] Good, M.C., Joubert, P.N. (1968) The form drag of two-dimensional bluff-plates immersed in turbulent boundary layers. J. Fluid Mech. 31(3), 547-582.
[18] Letchford, C.W., Holmes, J.D. (1994) Wind loads on free-standing walls in turbulent boundary layers. J. Wind Eng. Ind. Aerodynamics. 51, 1-27.
[19] Walker, I.J., Nickling, W.G. (2002) Dynamics of secondary airflow and sediment transport over and in the lee of transverse dunes. Progress in Physical Geography. 26, 47-75.
[20] Bagnold, R.A. (1941) The Physics of Blown Sand and Desert Dunes. Methuen, New York.
[21] Wu, R.L., Wang, Z.Y. (1985) Principles of wind tunnel design. Beijing Institute of Aeronautics Press, Beijing, 9-20.
[22] Butterfield, G.R. (1999) Near-bed mass flux profiles in Aeolian sand transport: High-resolution measurements in a wind tunnel. Earth Surface Processes and Landforms. 24(5), 393-412.
[23] Giannoulis, A., Stathopoulos, T., Briassoulis, D., Mistriotis, A. (2012) Wind loading on vertical panels with different permeabilities. J. Wind Eng. Ind. Aerodynamics. 107–108, 1-16.
[24] Chang, W.R. (2006) Effect of porous hedge on cross ventilation of a residential building. Building and Environment. 41, 549-556.
[25] Luca, B., Marko, H., Lorenzo, R. (2018) Wind-blown sand along railway infrastructures: A review of challenges and mitigation measures. Journal of Wind Engineering and Industrial Aerodynamics. 177, 340-365.
[26] Wu, W.Y. (1982) Hydromechanics (the second volume). Peking University Press, Beijing, 228-241.
[27] Nicholas, P.W., Jeffrey, E.H., Justin, W.Z., Ericha, M.C., Christopher, H.H., Ted, M.Z., Gregory, S.O., Thomas, E.B., Benjamin, J.B., Robert, B., Scott, D.C., Brad, F.C., Michael, C.D., Justin, D.D., Fred, A.F., Kris, M.H., Philip, H., Valerie, L., Noel, A.L., Loretta, J.M., Mark, A.N., Norfleet, M.L., Frederick, B.P., Matt, A.S., Brenton, S.S., Jean, L.S., John, T., Negussie, H.T., David, T., Robert, S.U., Larry, W. (2016) The nation wind erosion research network: building a standardized long-term data resource for Aeolian research, modeling and land management. Aeolian Research. 22, 23-36.
[28] McEwan, I.K., Willetts, B.B. (1993) Adaptation of the near-surface wind to the development of sand transport. Journal of Fluid Mechanics. 252, 99-101.
[29] Liu, X.P., Dong, Z.B. (2004) Experimental investigation of concentration profile of a blowing sand cloud. Geomorphology. 60, 371-381.
[30] Dong, Z.B., Wang, H.T., Zhang, X.H., Michael, A. (2004) Height profile of particle concentration in an aeolian saltating cloud: A wind tunnel investigation by PIV MSD. Geophysical Research Letters. 30, 1-4.
[31] Yan, M., Zuo, H.J., Wang, H.B., Li, G.T. (2019) Wind tunnel simulation of an opencut tunnel airflow field along the Linhe-Ceke Railway, China. Aeolian Research. 39, 66-76.
[32] Zou, X.Y., Wang, Z.L., Hao, Q.Z. (2001) The distribution of velocity and energy of saltating sand grains in a wind tunnel. Geomorphology. 36, 155-165.
[33] Dong, Z.B., Luo, W., Qian, G. (2007) A wind tunnel simulation of the mean velocity fields behind upright porous fence. Agric. For. Meteorol. 146, 82-93.

[34] Zhang, N., Kang, J.H., Lee, S.J. (2010) Wind tunnel observation on the effect of a porous wind fence on shelter of saltating sand particles. Geomorphology. 120, 224-232.
[35] Yuan, X.X., Wang, H.F., Lei, J.Q., Li, S.Y., Kang, X.G., Ma, X.X. (2016) Wind tunnel simulation of windbreak effect of double-row Nylon net fence with different interval. Journal of Desert Research. 36(5), 1238-1246.
[36] Fang, H., Wu, X.X., Zou, X.Y., Yang, X.F. (2018) An integrated simulation-assessment study for optimizing wind barrier design. Agricultural and Forest Meteorology. 263, 198-206.
[37] Wang, X.M., Dong, Z.B., Chen, G.T. (2000) On efficiency of sand-controlling system along the Tarim Desert High-way in Taklamakan Desert. Journal of Chinese Geography. 10(2), 141-150.
[38] Zhang, Y.P., Wang, T., Zhao, S.P., Wang, S.H. (2019) Influence of wind-break wall on aerodynamic characteristics of positive feeder of overhead contact line of Lanzhou-Xinjiang high-speed railway. Journal of Railway Science and Engineering. 16(7), 1628-1636.
[39] Zhang, S.B. (2016) Experimental study on design parameters of retaining wall for sandstorm section of Lanzhou -Urumqi high-speed railway. Railway Standard Design. 60(6), 4-8.

Received: **24.10.2019**
Accepted: **04.03.2020**

CORRESPONDING AUTHOR

Hejun Zuo
College of Desert Control Science and Engineering,
Inner Mongolia Agricultural University,
Hohhot ,Inner Mongolia Autonomous Region 010018 – P.R. China

e-mail: zuohj@126.com

© by PSP Volume 29 – No. 05/2020 pages 3690-3697 Fresenius Environmental Bulletin

TRANSPORT OF Pd/Fe NANOBIMETAL MODIFIED BY CARBOXYMETHYL CELLULOSE IN POROUS MEDIA

Jinkui Zhong*, Xiaoxiao Sun, Zhengxin Wang, Liguo Wang, Li Ding, Qiaozhen Yang, Liu Li, Jianyu Zhang

School of Environmental and Municipal Engineering, Lanzhou Jiaotong University, Lanzhou 730070, China

ABSTRACT

Nano zero valent iron (nZVI), nano palladium-iron bimetallic (Pd/Fe), nZVI stabilized with carboxymethyl cellulose (CMC) (CMC-Fe), and Pd/Fe modified with CMC (CMC-Pd/Fe) were prepared by liquid phase reduction method, and characterized by scanning electron microscopy (SEM). The sedimentation and transport experiments of the four kind of nano particles in porous media were conducted to investigate the dispersion of the materials. The effects of different nano-iron, nano-iron concentration, amount of CMC modification, grain size, and flow rate of injection on nano irons transport were investigated by column experiment. The results show that the particle size of nano particles modified by CMC gets smaller, and the degree of dispersion is improved. The catalyst Pd has little effect on the sedimentation of nano-iron. Under the same conditions, the transport of nZVI and Pd/Fe modified with CMC in the porous medium is obviously better than that of nZVI and Pd/Fe, while the difference of transport between CMC-Fe and CMC-Pd/Fe is not significant. With increase of the nano-iron concentration, the amount of CMC modification, the particle size of the medium and the flow rate, the transport of the modified nano-iron in the medium increases.

KEYWORDS:
Carboxymethyl cellulose, nano bimetallic, dispersion, transport

INTRODUCTION

Nano zero valent iron (nZVI) has ideal properties, such as smaller particle size, larger specific surface area, stronger reducibility and higher surface activity [1, 2]. It can degrade chlorinated organic compounds [3, 4, 5], organic dyes [6, 7, 8], pesticides [9, 10, 11], heavy metals [12, 13], and other pollutants in water. Thus, nZVI is considered as a potential remediation material for contaminated groundwater [14, 15, 16]. Many remediation projects for contaminated groundwater have been carried out via using nZVI around the world, of which more than 60% were in the United States [17]. However, the pure nano-particles are easily agglomerated into large particles, and deposited on the surface of porous media, or intercepted in the pores of porous media due to the magnetic force and van der Waals force between nZVI particles, so transport capability of nZVI is inhibited [18, 19]. Under typical groundwater conditions, the distance of transport of pure nZVI in porous media is only a few centimeters [20]. In addition, the size of nZVI particles increases after agglomeration, which results in the reduction of specific surface area, the reactivity and the efficiency of removing pollutants. Furthermore, nZVI is easily oxidized in the air, which results in the inactivation of nZVI particles. The above shortcomings limit the application of nZVI in remediation field for contaminated groundwater [21].

Studies have shown that surface coating of nZVI can increase the electrostatic repulsion and steric hindrance of the surface of nZVI particles, overcomes the magnetic force and van der Waals force between the particles, and reduces aggregation in porous media [22]. It could also improve transport ability of nZVI in porous media and prevent nZVI from being oxidized [23]. At present, some researchers used CMC-Fe in remediation of contaminated groundwater, the results showed that dispersion and transport capability of nZVI have been greatly improved [24, 25, 26]. Adding noble metal catalyst such as Pd, Pt, Ag, Cu and Ni could greatly improve the property of remediation [17]. It could be proved that Pd was the best catalyst in the reaction of dehalogenation. However, there has restricted knowledge concerning Pd/Fe nanobimetal transport in porous media, most especially in the existence of the modifier-CMC. Therefore, a basic understanding of the influence of hydrology on modified Pd/Fe is demanded to assess the transport based on the site conditions, thus helping to control the transport of nZVI. Until now, no study on effects of hydrology on CMC-coated Pd/Fe particles transport has been conducted.

The aim of this study was to explore stabilization and transport of CMC-Pd/Fe in porous media by sedimentation and column experiments. Particularly, the influence of nano-iron concentration, CMC modification amount, medium particles size and flow rate on the mobility of particles was investigated. This study is good for a better insight of stabilization,

mechanism and parameters controlling CMC-Pd/Fe particles and retention in porous media.

MATERIALS AND METHODS

Materials. Ferrous sulfate hydrate ($FeSO_4 \cdot 7H_2O$) and carboxymethyl cellulose (CMC, 98%) were purchased from Kaixin Chemical Industry Co., Ltd (China). Sodium borohydride ($NaBH_4$) was obtained from National Pharmaceutical Group Co., Ltd (China). Potassium hexachloropalladate (K_2PdCl_6, Pd≥26.3%) was supplied from Aladdin reagent Co., Ltd (China). Ethanol (C_2H_5OH) was purchased from Damao Chemical Reagent Factory sodiumn (China). The chemicals above mentioned are all analytical purity. All solutions were prepared with deionized water. The quartz sand was immersed in concentrated hydrochloric acid for 12 hours. Then the quartz sand was washed with deionized water and dried in an oven. Finally, the quartz sand was sieved with a standard sieve with 20, 30, and 40 mesh.

Methods. Preparation of nano-particles. (1) Preparation of nZVI. Preparation of nZVI was operated by transferring $NaBH_4$ aqueous solution dropwise into a three-necked flask with electric stirring involving 100 mL $FeSO_4$ aqueous solution and stirring at speed of 500 r/min at room temperature. This operation was performed in high-purity nitrogen. The reaction equation is stated as reaction 1.

$$Fe^{2+} + 2BH_4^- + 6H_2O \rightarrow Fe + 2B(OH)_3 + 7H_2 \quad (1)$$

(2) Preparation of Pd/Fe. After nZVI was prepared, 6 mL of 100 mg/L K_2PdCl_6 solution (K_2PdCl_6 particles were dissolved with a certain amount of HCl, and then diluted with deionized water to the desired concentration) was added. Pd/Fe can be prepared by stirring continuously until the solution color changes from orange to gray. This process is given below in reaction 2.

$$PdCl_6^{2-} + Fe \rightarrow Pd(s) + Fe^{2+} + 6Cl^- \quad (2)$$

(3) Preparation of CMC-Fe. The fresh $FeSO_4$ aqueous solution was added to the CMC solution, and stirred for 15 min under nitrogen atmosphere. Then, the $NaBH_4$ aqueous solution was added dropwise till the production of a large number of black particles.

(4) Preparation of CMC-Pd/Fe. After CMC-Fe was prepared, it was stood for 10 min. Then the K_2PdCl_6 solution was added drop-wise at a uniform rate, and the mixture was stirred continually for 15 min under nitrogen atmosphere.

Sedimentation experiment of particles. Amount of 10 ml prepared nanoparticles suspension was transferred into a colorimetric tube with plug, then sealed, allowed to stand to observe the difference in sedimentation performance of different systems. Different suspensions of nanoparticle were placed in a 10 mm glass cuvette, and the absorbance was measured by an ultraviolet spectrophotometer at a wavelength of 508 nm. A value was recorded every minute for the first 35 min. For the next 55 min, it is recorded every 5 min. The relative absorbance (A/A_0) is plotted as a function of time.

Transport experiments. The plexiglass column used in the experiment was Φ2.5cm×25cm. The treated quartz sand was uniformly filled into the column. The gauze was placed at both ends of the column. And the both ends of the column was filled with glass beads with a height of 0.5 cm (particle diameter of 0.3 cm) to facilitate the flow distribution. Then, 10 pore volumes (PVs) deionized water and 5 PV background electrolyte solution ($NaHCO_3$) was pumped into the column through a peristaltic pump to wash the experimental column for removing the turbidity of background and obtaining stable flow regime, evenly distribution of the surface charge in media.

The nZVI suspension of 10 PV was pumped into the simulated sand column under different conditions through a peristaltic pump. The concentration of iron ions was determined after digesting with nitric acid at specified time intervals (0, 0.5, 1.0, 1.5, ...10 PV). After the end of the experiment, the media in the simulated column was taken out every 2 cm. Then the iron ion concentration was determined after digesting with nitric acid. Finally, the spatial distribution of nZVI in the simulated sand column was examined.

Analytical method. The iron content is measured by flame atomic absorption method. The absorption wavelength is 248.3 nm, the high voltage is 620.2 V, the working lamp current is 6.0 mA, the acetylene flow rate is 0.9 L/min, the air flow rate is 6.0 L/min, the flame height is 7.5 mm, and the number of measurements is 3 times.

RESULTS AND DISCUSSION

SEM. The SEM images of four kinds of nZVI was shown in Figure 1. As shown in Figure 1(a), the bare nZVI was composed of spherical particles, and the particles are agglomerated with each other at a particle diameter of about 50 to 100 nm, which results in limited mobility and poor dispersion. As shown in Figure 1(b), nano Pd/Fe bimetallic particles are clustered together or adhered to other particles in a dendritic or layered structure. The dispersibility is not significantly improved compared to the bare nZVI indicates that Pd can not influence the dispersibility of nZVI obviously. The CMC-Fe particles are

dispersed in the CMC, and the average particle diameter is about 10-50 nm (Figure 1(c)). The particles of CMC-Fe are spherical and have high overall dispersion. Figure 1(d) shows that CMC-Pd/Fe particles are highly dispersed with a particle size of about 30-50 nm. It shows that CMC, as an anionic polymer modifier, can overcome the magnetic force and surface tension between nano-iron particles, reduce the agglomeration of particles, and improve the dispersion of particles.

Sedimentation of four kind of nZVI. Figure 2 shows the sedimentation curves of different nano-iron particles dispersed in water. The sedimentation velocity of nZVI and Pd/Fe is fast, which occurs at the beginning. The A/A_0 drops from 1 to 0.5 in the first 5 min, then continues to decrease in 10 min. During the period of 10 min to 20 min, the rate of sedimentation slows down and gradually stabilizes after about 60 min, so it can be speculated that the two nano-irons settled completely after 60 min. The sedimentation of 50% CMC-Pd/Fe starts from the 4th min, and the A/A_0 reaches the minimum at the 18th min. Then, the A/A_0 is maintained at about 0.05 during the period of 18 min to 40 min. Finally, the A/A_0 increases to about 0.09 after 40 min. The A/A_0 of 100% CMC-Fe, 100% CMC-Pd/Fe, and 300% CMC-Pd/Fe do not vary within 90 min. It can be inferred that the three nano particles does not settle or have a little extent of sedimentation within 90 min.

The dispersibility of nZVI, Pd/Fe, 50% CMC-Pd/Fe, 100% CMC-Fe, 100% CMC-Pd/Fe and 300% CMC-Pd/Fe increased in turn, indicating CMC can enhance the dispersion of nano-iron and reduce its sedimentation, while the excess amount of CMC does not further reduce its sedimentation dramatically. Pd has little effect on the sedimentation of nano-iron. Therefore, the 100% modification amount is economical and effective.

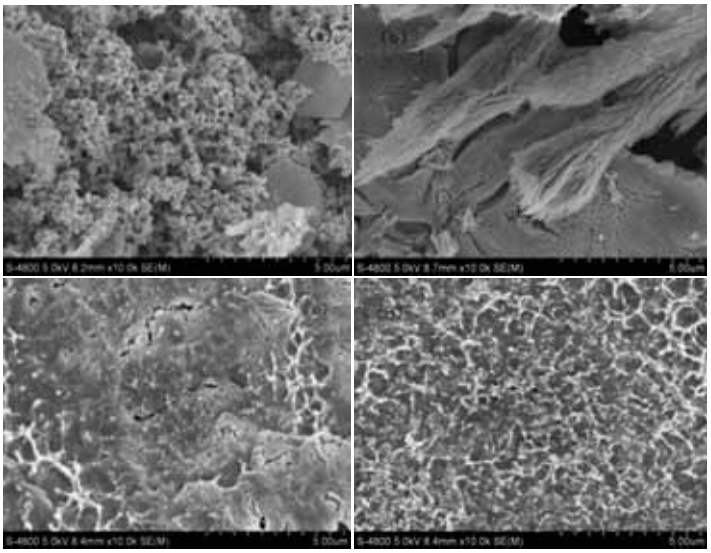

FIGURE 1
SEM images of Nano iron: (a) nZVI, (b) Pd/Fe, (c) CMC-Fe, (d) CMC-Pd/Fe

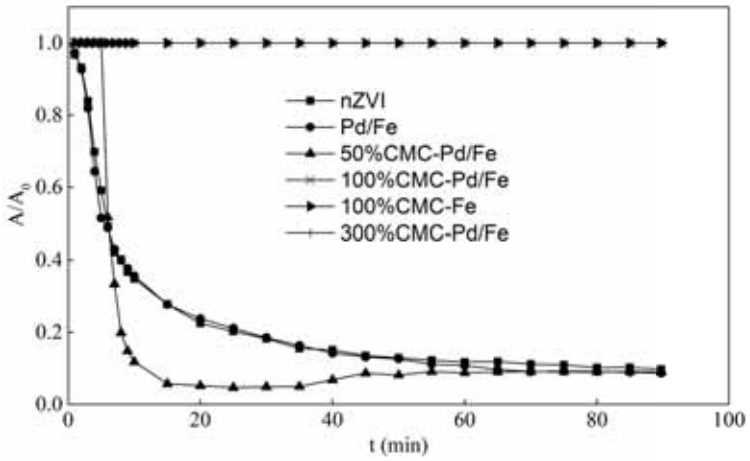

FIGURE 2
Sedimentation curves of nano-iron

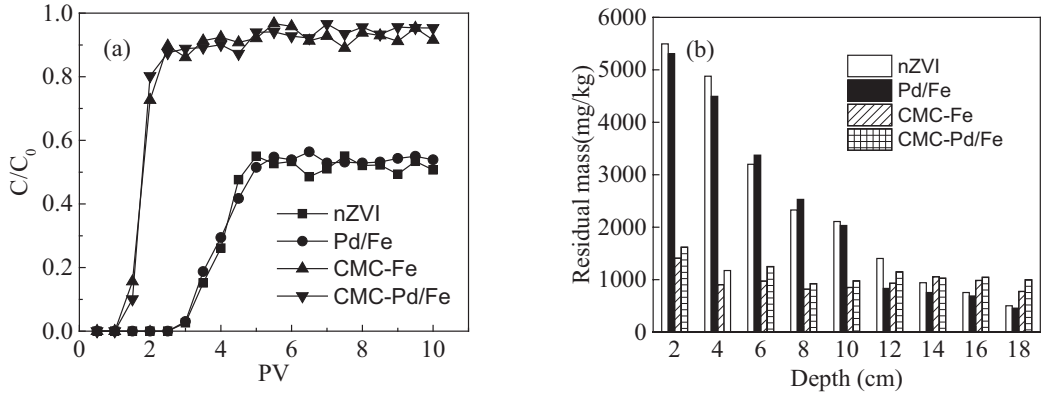

FIGURE 3
Different nano-iron penetration curve (a) and the residual in quartz sand (b)

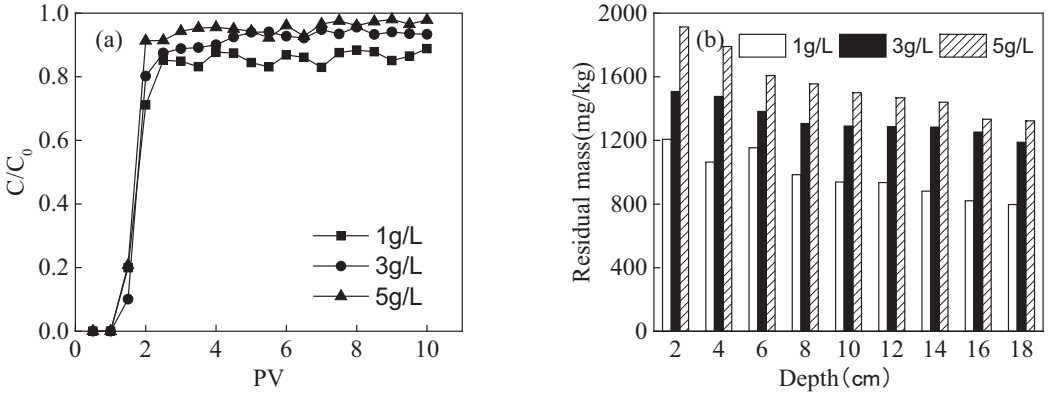

FIGURE 4
Different nano-iron concentration penetration curve (a) and the residual in quartz sand (b)

Transport of nZVI in porous media under different conditions. Effect of types of nZVI on transportation. Figure 3 shows the breakthrough curves and iron content of different types of nano particles in simulated sand column at different depths. The experimental conditions are pH 6.46, the size of quartz sand 20 mesh, the flow rate 6 mL/min, the CMC modification amount 100% and the concentration of iron 3 g/L. Figure 3(a) show that the relative concentration (C/C_0) increases dramatically as the injection volume increases, and gradually becomes equilibrium. CMC-Fe, CMC-Pd/Fe and nZVI tend to balance in 2, 2, and 4 PV, respectively. The C/C_0 of CMC-Fe and CMC-Pd/Fe does not have obvious difference, and the C/C_0 of nZVI and Pd/Fe is not high. It indicates that the transport of modified nano-iron with CMC is better than the ones without CMC, and Pd has no effect on the transport of nano-iron.

Figure 3(b) shows that the residual amount of nano particles in the sand column gradually decreases from the bottom to the top of the column. The residual amount at the bottom is more than 5000 mg/kg, while the one at the top is only about 800 mg/kg. The distribution of CMC-Fe and CMC-Pd/Fe is uniform in each section of porous medium, and the residual amount is always between 1000 and 1500 mg/kg. Results show that modified nZVI with CMC can overcome the magnetic force and van der Waals force between particles, and can produce repulsion with negatively charged quartz sand, and enhance dispersion stability and delivery [17]. Unmodified nano-irons accumulate at the bottom of the column will block the pores of the porous medium, hinder the transport of the nano-iron particles, which results in less nano-iron at the top [17]. The transport of modified nano-iron is significantly better than that of the unmodified nano-iron. The subsequent experiments are carried out using CMC-Pd/Fe.

Effect of nano-iron concentration on transport of CMC-Pd/Fe. Figure 4 shows the breakthrough curves of different concentrations of CMC-Pd/Fe and the residual amount in the sand column. As can be seen from Figure 4(a), the C/C_0 is zero before the injection volume of CMC-Pd/Fe reached 1 PV. After that, with increasing injection volume, C/C_0 increases rapidly and stabilizes at 2 PV. The equilibrium C/C_0 increases as the injection concentration increases. When the concentration of nano-iron is 1, 3 and 5 g/L, the equilibrium C/C_0 is

about 0.8, 0.9 and 0.9 respectively. These results indicated that increasing the concentration of CMC-Pd/Fe is beneficial to its transport because there is a corresponding exponential relationship between C/C_0 and the depth direction of the porous bed [27]. The equilibrium adsorption capacity of CMC-Pd/Fe is fixed in porous media. High concentration of CMC-Pd/Fe makes the porous medium easier reach adsorption saturation compared to low concentration of CMC-Pd/Fe, which results in higher C/C_0 and better mobility. Figure 4(b) shows that high concentration of CMC-Pd/Fe cause more residual than the low concentration of CMC-Pd/Fe in each section of the porous medium. The residual amount of CMC-Pd/Fe in the sand column from the bottom to the top for 1, 3, and 5 g/L is about 1200 to 800 mg/kg, 1500 to 1300 mg/kg, and 1900 to 1400 mg/kg, respectively. These show that more nano-iron will deposit on the surface of the porous medium or be filled in the pores of the porous medium as enhancing the concentration of CMC-Pd/Fe [27]. The subsequent experiments were carried out using 3 g/L.

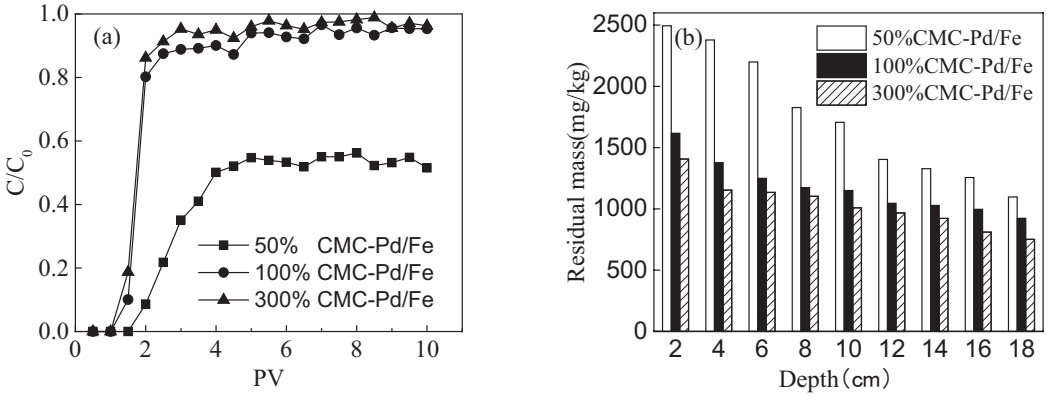

FIGURE 5
Different CMC concentration penetration curve (a) and the residual in quartz sand (b)

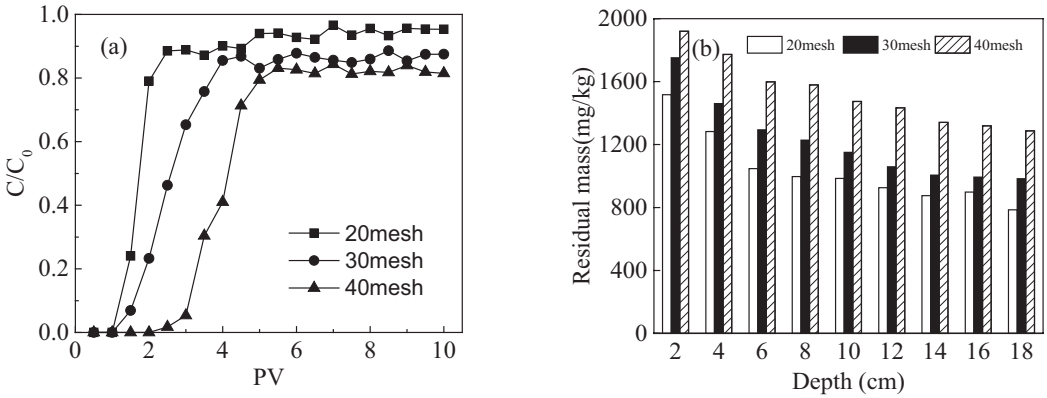

FIGURE 6
Different quartz sand particle size penetration curve (a) and the residual in quartz sand (b)

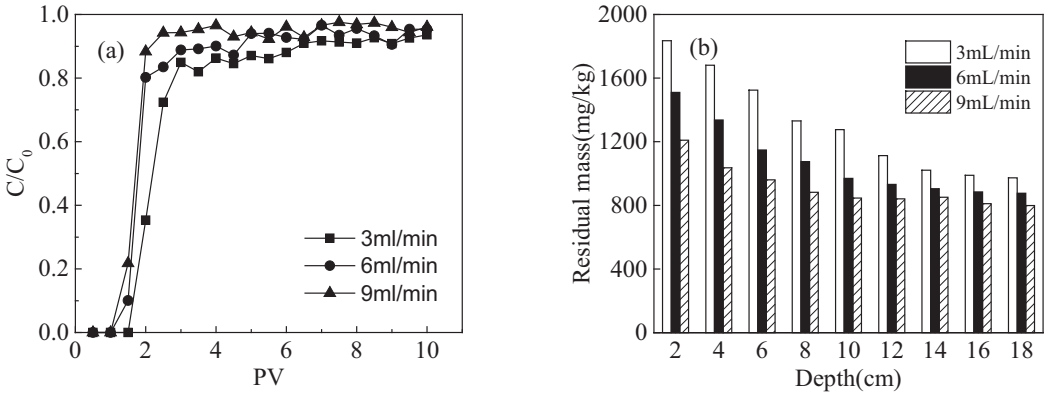

FIGURE 7
Different flow rate penetration curve (a) and the residual in quartz sand (b)

Effect of amount of CMC modification on the migration of CMC-Pd/Fe. Figure 5 shows the effect of amount of CMC modification on the transport of CMC-Pd/Fe. The C/C_0 is zero for 100% CMC-Pd/Fe and 300% CMC-Pd/Fe before the injection volume less than 1 PV, and then increased rapidly, until the C/C_0 became equilibrium after 2 PV. Although the equilibrium C/C_0 for 300% CMC-Pd/Fe was slightly higher than that for 100% CMC-Pd/Fe, the difference was not significant. The C/C_0 of 50% CMC-Pd/Fe equals zero before 2PV of injection, then increases rapidly, finally tends to balance after 4 PV. The C/C_0 at equilibrium is about 0.5, which is less than that of 100% CMC-Pd/Fe and 300% CMC-Pd/Fe. These results show that increasing CMC results in the reduction of residual amount of CMC-Pd/Fe in each section of sand column. It is indicated that an appropriate increase of the amount of modifier can enhance the transport of CMC-Pd/Fe. When the CMC modification amount is 50%, the electrostatic repulsion provided by CMC cannot completely overcome the magnetic force and van der Waals force between particles. Some of the nano-irons agglomerated and deposited on the surface of the porous medium results in weak transport. It was observed that the dispersion and the transport of the nano-iron are improved when the CMC modification amount was increased up 100%. The nano-iron has a good dispersibility when the modification amount is 100% and 300%, which reduces the residual amount [28]. The dispersibility and the transport of nano-iron could not be further improved even though the amount of CMC reached 300% compared to 100%.

Effect of grain size on CMC-Pd/Fe transport. Figure 6 shows the breakthrough curves of CMC-Pd/Fe and the residual amount in different particle size porous media. The C/C_0 of CMC-Pd/Fe rises up as the particle size of the medium increases. In 20 and 30 mesh porous media, the C/C_0 of CMC-Pd/Fe is zero before the injection volume is 1 PV, then increases rapidly, finally tends to be balanced after 2 PV and 4 PV, respectively. The equilibrium C/C_0 is 0.9 and 0.8 for 20 and 30 mesh porous media, respectively. In the 40 mesh porous medium, the C/C_0 of CMC-Pd/Fe is zero before 3 PV, then rapidly increases, finally the C/C_0 is stable at about 0.7 after 5 PV. Figure 6(b) shows that decreasing the grain size can lead to increasing of residual amount of CMC-Pd/Fe. It is mainly because the declining of particle size of the medium can result in decreasing of porosity and increasing adsorption capacity of CMC-Pd/Fe on surface of media. CMC-Pd/Fe deposits on the surface of the porous medium in a large amount, and the migrated CMC-Pd/Fe decreases, so the C/C_0 becomes smaller and the residual amount increases.

Effect of flow rate of injection on transport of CMC-Pd/Fe. Figure 7(a) shows that the C/C_0 of CMC-Pd/Fe increases as the flow rate increases. When the flow rate is 6 and 9 ml/min, the C/C_0 of CMC-Pd/Fe is zero before the injection volume is 1 PV, then increases rapidly, finally the C/C_0 is stable at about 0.9 after 2 PV. When the flow rate is 3 ml/min, the C/C_0 is almost zero before the injection volume is 2 PV, then increases rapidly, finally the C/C_0 reaches equilibrium after 3 PV. Figure 7(b) shows that the residual amount of CMC-Pd/Fe in each section of the porous medium decreases as the flow rate increases, and the overall distribution from the bottom to the top is relatively uniform. These results indicated that the flow rate affects the time that CMC-Pd/Fe reaches equilibrium, and has little effect on the equilibrium C/C_0. This is mainly because the shear force of the water flow increases as the flow rate increases, and the adsorption of the nano-iron particles by the medium can be overcome. Results show that the flow rate of 3 mL/min has achieved good results, further increasing the flow rate does not significantly improve the transport.

CONCLUSIONS

This study mainly investigated the sedimentation properties and transport of modified nano-iron characteristics in porous media under different conditions. The main conclusions are as follows:

(1) The dispersibility of the nano-iron modified by CMC is greatly improved, and the particles size of nZVI modified with CMC gets smaller through the image of SEM. Results of sedimentation experiment have revealed that CMC can be a potential material for nZVI application because of its capability to improve the stability of nZVI particles. The inorganic catalyst Pd has little effect on the nano-iron sedimentation.

(2) Under the same conditions, the transport of nZVI modified with CMC in porous media is significantly better than that of pure nZVI and Pd/Fe. However, Pd has no effect on the transport of nano-iron.

(3) With the increase of nano-iron concentration, CMC modification amount, medium particle size and flow rate, the transport of modified nano-iron in the medium is enhanced significantly.

ACKNOWLEDGEMENTS

This work was supported by the National Natural Science Foundation of China (21467013, 21167007), the National Natural Science Foundation of Gansu (1508RJZA095), Innovation and Entrepreneurship Program of Lanzhou Jiaotong University (2019CXCYKC18).

REFERENCES

[1] He, F., Zhao, D., Paul, C. (2009) Field assessment of carboxymethyl cellulose stabilized iron nanoparticles for in situ destruction of chlorinated solvents in source zones. Water Research. 44(7), 2360-2370.

[2] Fu, F., Ma, J., Xie, L., Tang, B., Han, W., Lin, S. (2013) Chromium removal using resin supported nanoscale zero-valent iron. Journal of Environmental Management. 128, 822-827.

[3] Vilardi, G., Rodríguez-Rodríguez, J., Ochando-Pulido, J.M., Verdano, N., Martinez-Ferez, A., Di Palma, L. (2018) Large Laboratory-Plant application for the treatment of a Tannery wastewater by Fenton oxidation: Fe(II) and nZVI catalysts comparison and kinetic modelling. Process Safety and Environmental Protection. 117, 629-638.

[4] Zhang, Z., Shen, Q., Cissoko, N., Wo, J., Xu, X. (2010). Catalytic dechlorination of 2,4-dichlorophenol by Pd/Fe bimetallic nanoparticles in the presence of humic acid. Journal of Hazardous Materials, 182(1), 252-258.

[5] Xi, Y., Megharaj, M., Naidu, R. (2011) Dispersion of zerovalent iron nanoparticles onto bentonites and use of these catalysts for orange II decolourisation. Applied Clay Science. 53(4), 716-722.

[6] Shu, H.Y., Chang, M.C., Chen, C.C., Chen, P.E. (2010) Using resin supported nano zero-valent iron particles for decoloration of Acid Blue 113 azo dye solution. Journal of Hazardous Materials. 184(1-3), 499-505.

[7] Satapanajaru, T., Chompuchan, C., Suntornchot, P., Pengthamkeerati, P. (2011) Enhancing decolorization of Reactive Black 5 and Reactive Red 198 during nano zerovalent iron treatment. Desalination. 266(1-3), 218-230.

[8] Xi, Y., Megharaj, M., Naidu, R. (2011) Dispersion of zerovalent iron nanoparticles onto bentonites and use of these catalysts for orange II decolourisation. Applied Clay Science. 53(4), 716-722.

[9] El-Temsah, Y.S., Oughton, D.H., Joner, E.J. (2013) Effects of nano-sized zero-valent iron on DDT degradation and residual toxicity in soil: a column experiment. Plant and Soil. 368(1-2), 189-200.

[10] Dror, I., Jacov, O. M., Cortis, A., Berkowitz, B. (2012) Catalytic Transformation of Persistent Contaminants Using a New Composite Material Based on Nanosized Zero-Valent Iron. ACS Applied Materials and Interfaces. 4(7), 3416-3423.

[11] Thompson, J.M., Chisholm, B.J., Bezbaruah, A.N. (2010) Reductive dechlorination of chloroacetanilide herbicide (alachlor) using zero-valent iron nanoparticles. Environmental Engineering Science. 27(3), 227-232.

[12] Tang, L., Feng, H., Tang, J., Zeng, G., Deng, Y., Wang, J., Liu, Y., Zhou, Y. (2017) Treatment of arsenic in acid wastewater and river sediment by $Fe@Fe_2O_3$, nanobunches: The effect of environmental conditions and reaction mechanism. Water Research. 117, 175-186.

[13] Jiang, D., Zeng, G., Huang, D., Chen, M., Zhang, C., Huang, C., Wan, J. (2018) Remediation of contaminated soils by enhanced nanoscale zero valent iron. Environmental Research. 163, 217-227.

[14] Lin, K.S., Mdlovu, N.V., Chen, C.Y., Chiang, C. L., Dehvari, K. (2018) Degradation of TCE, PCE, and 1,2–DCE DNAPLs in contaminated groundwater using polyethylenimine-modified zero-valent iron nanoparticles. Journal of Cleaner Production. 175, 456-466.

[15] Dong, L., Lin, L., Li, Q., Huang, Z., Tang, X., Wu, M., Li, C., Cao, X., Scholz, M. (2018) Enhanced nitrate-nitrogen removal by modified attapulgite-supported nanoscale zero-valent iron treating simulated groundwater. Journal of Environmental Management. 213, 151-158.

[16] Kang, Y., Yoon, H., Lee, W., Kim, E., Chang, Y. (2018) Comparative study of peroxide oxidants activated by nZVI: Removal of 1,4-Dioxane and arsenic(III) in contaminated waters. Chemical Engineering Journal. 334, 2511-2519.

[17] Crane, R.A., Scott, T.B. (2012) Nanoscale zero-valent iron: Future prospects for an emerging water treatment technology. Journal of Hazardous Materials. 211-212, 112-125.

[18] Su, Y., Zhang, W.-J., Liang, X.-C., Qin, C.-Y., Li, L.-L., Zhao, Y.-S. (2015) Enhanced delivery of nanoscale zero valent iron by foam in porous media. China Environmental Science. 35(06), 1700-1708.

[19] Schrick, B., Hydutsky, B.W., Blough, J.L., Mallouk, T.E. (2004) Delivery Vehicles for Zerovalent Metal Nanoparticles in Soil and Groundwater. Chemistry of Materials. 16(11), 2187-2193.

[20] Jiemvarangkul, P., Zhang, W.X., Lien, H.L. (2011) Enhanced transport of polyelectrolyte stabilized nanoscale zero-valent iron (nZVI) in porous media. Chemical Engineering Journal. 170(2), 482-491.

[21] Yang, J., Wang, X., Zhu, M., Liu, H., Ma, J. (2014) Investigation of PAA/PVDF–NZVI hybrids for metronidazole removal: Synthesis, characterization, and reactivity characteristics. Journal of Hazardous Materials. 264, 269-277.

[22] Tesh, S.J., Scott, T.B. (2015) Nano-composites for water remediation: A Review. Advanced Materials. 26(35), 6056-6068.

[23] Dong, H., Guan, X., Lo, I.M. (2012) Fate of As(V)-treated nano zero-valent iron: determination of arsenic desorption potential under varying environmental conditions by phosphate extraction. Water Research. 46(13), 4071-4080.

[24] Naja, G., Halasz, A., Thiboutot, S., Ampleman, G., Hawari, J. (2008) Degradation of Hexahydro-1,3,5-trinitro-1,3,5-triazine (RDX) Using Zerovalent Iron Nanoparticles. Environmental Science and Technology. 42(12), 4364-4370.
[25] Qiu, X., Fang, Z., Yan, X., Gu, F., Jiang, F. (2012) Emergency remediation of simulated chromium (VI)-polluted river by nanoscale zero-valent iron: Laboratory study and numerical simulation. Chemical Engineering Journal. 193-194, 358-365.
[26] He, F., Zhao, D., Liu, J., Roberts, C. (2007) Stabilization of Fe−Pd Nanoparticles with Sodium Carboxymethyl Cellulose for Enhanced Transport and Dechlorination of Trichloroethylene in Soil and Groundwater. Industrial and Engineering Chemistry Research. 46(46), 29-34.
[27] Ofenvironment, D. (2013) Stockholm Convention on Persistent Organic Pollutants (POPs). Air Quality and Climate Change. 47(1), 187-196.
[28] Yu, X.B., Wei, C.H., Ke, L., Wu, H.Z., Chai, X. S., Hu, Y. (2012) Preparation of trimethylchlorosilane-modified acid vermiculites for removing diethyl phthalate from water. Journal of Colloid and Interface Science. 369(1), 344-351.
[29] Xian H. (2014) A Study on Remediation of Cr(VI) and TCE in Water by CMC Stabilized Nano Zero-Valent Iron. Beijing: China University of Geosciences.
[30] Li, K.-X., Zhang, Y.-X., Lan, S.-S., Liu, X.-R., Chang, S., Zhang, F. (2017) Transport of CMS-Na modified zero-valent iron particles in saturated porous media. Applied Chemical Industry. 46(5), 820-824.

Received: **24.10.2019**
Accepted: **19.02.2020**

CORRESPONDING AUTHOR

Jinkui Zhong
School of Environmental and
Municipal Engineering,
Lanzhou Jiaotong University,
Lanzhou 730070 – China

e-mail: zhongjk@ mail.lzjtu.cn

© by PSP Volume 29 – No. 05/2020 pages 3698-3702 Fresenius Environmental Bulletin

THE TREATMENT OF Cr^{6+} CONTAINING WASTEWATER BY Fe/C MICRO-ELECTROLYSIS SYSTEM

Pingping Yang, Yanyan Liu, Hongying Wang, Junfeng Chen*, Meizhen Tang, Renjun Wang, Yushan Wei, Yuewei Yang

Department of Environmental Science, School of Life Sciences, Qufu Normal University, Qufu 273165, P.R. China

ABSTRACT

Chromium plating waste water contains a large number of heavy metal ions, some organic and inorganic substances and other harmful substances. After comprehensive comparison and measurement, Iron-carbon micro-electrolysis was adopted to treat it. The influence of various variables including iron/carbon ratio, pH and reaction time, on the treatment effect of chrome-containing wastewater was studied. As for results, the removal rate of Cr^{6+} reached 65.98%, 73.24%, 95.37% respectively when the iron/carbon was 1:1, pH was 3, reaction time is 20mins. At last, the experiment was done under these three optimal conditions. Under the optimal conditions, the removal rate of Cr^{6+} attained 97.38% according to the outcome.

KEYWORDS:
Chromium plating waste water, iron-carbon micro-electrolysis, optimal condition

INTRODUCTION

There are two main forms of chromium in wastewater containing chromium, which are Cr^{6+} and Cr^{3+} [1]. With much stronger toxicity compared with Cr^{3+}, Cr^{6+} can cause serious damage to people's internal organs, even lead to death when the circumstance is serious [2]. Chromium-containing wastewater will threaten and even endanger organisms in the water, affect the development of related industries; when it enters the soil, it will destroy the fertility of the soil, do harm to plants and crops, and thus reduce agricultural production [1]. At present, there are physical, chemical, biological and physicochemical methods for treating chrome-containing wastewater [3]. Generally, they can be divided into the following several categories. (1) Reductive precipitation: This method is to use some reagents that can oxidize Cr^{6+}into Cr^{3+}, and then add alkaline materials like NaOH to precipitate $Cr^{3+}$and remove the chromium at last [4]. Though, to achieve this, the requirements for facility and investment are lower, it is possible for the product to pollute the environment again. (2) Biochar adsorption: At present, porous carbon materials have got large development space for repairing chromium ion pollution. Among them, biochar, as a green adsorbent, has a very broad research and application prospect. However, the limited sorption as well as low-efficient reduction reactions between surface functional groups lead to lower removal rate of Cr^{6+} [5]. (3) Electrolytic reduction: it means that heavy metals can be removed by electrolysis. However, this method is just suitable for recycling heavy metals now [6]. (4) Ion-exchange resin method. This method has advantages including recycling water and needing lower expense. However, it is used less now because it has high requirements for technology as well as investments and can't remove chromium completely [7]. (5) In addition to the above methods, there still are a series of other treatment methods such as evaporation concentration method, electroosmosis method, neutralization method, liquid membrane method and photocatalytic degradation [8].

Fe/C micro-electrolysis technology was taken advantage of to carry out our experiment. This technology is also known as internal electrolysis and zero-valent iron method, whose reaction principle is to achieve the purpose of removing Cr^{6+} through the electrode reaction of iron and carbon in a certain electrolyte solution [9]. In terms of micro battery, iron is usually used as the cathode and carbon as the anode [7]. The main factors affecting Fe/C micro-electrolysis technology include Fe/C ratio, influent PH, reaction time, etc. [10]. However, the desired effect can be achieved only under the most suitable conditions including the optimal iron-carbon ratio, influent PH, reaction time.

Due to the advantages of low cost, high efficiency and low energy consumption, iron-carbon micro-electrolysis technology has been widely used in many fields [11]. By studying the three main factors, the best treatment effect of Fe/C micro-electrolysis technology on Cr^{6+} wastewater can be found.

MATERIALS AND METHODS

Laboratory reagents. 100 mg/L chrome standard reserve solution, 50 mg/L chrome-containing wastewater, reductive iron powder, activated carbon, 10% NaOH solution, 5% hydrochloric acid,

0.1 mol/L NaOH solution, 0.1 mol/L hydrochloric acid, diphenyl-dihydrazine, acetone, 1+1 phosphoric acid, 1+1 sulfuric acid.

Treatment of iron and carbon materials. Preparation of treatment reagent. (1) 10% NaOH: The water with 10 g of sodium hydroxide was stirred until dissolution. Since when sodium hydroxide dissolves in water, the temperature will rise. The solution should be cooled before being transferred to a 1-L volumetric flask and shaken well. (2) 5% hydrochloric acid: 105.6ml of 37% concentrated hydrochloric acid was added to 864.9ml water.

Reductive iron powder. 10% sodium hydroxide and hydrochloric acid were soaked for 10 minutes and 20 minutes respectively. The former is washed with tap water, while the latter is washed with distilled water.

Activated carbon. It was first washed with tap water and then soaked in Cr^{6+} wastewater of 50 mg/L for three hours, being absorbed and saturated gradually, so as to eliminate the interference of external factors. Finally, it was put into a drying box and sealed or reserved.

Experimental instruments and equipment. Electric mixer, UV-visible spectrophotometer, electric constant temperature drying box, pH meter, electronic balance, beaker, pipette, rubber head dropper, volumetric bottle, glass rod, measuring cylinder, colorimetric dish, glass bottle, conical bottle.

The experimental method. 200 mL Cr^{6+} wastewater was put into a beaker and treated with reduced iron powder and activated carbon. Under the stirring function of electric mixer with a rotating speed of 245 r/ min, wastewater was treated by micro-electrodes formed between iron and carbon. After the reaction, the concentration of chromium ion was detected by spectrophotometer, and determined in comparison with the standard curve obtained by Diphenyl carbonyl dihydrazine method and then the removal rates could be calculated. The optimal reaction conditions were determined by comparing different removal rates.

RESULTS AND DISCUSSION

Effect of iron - carbon ratio on treatment effect of Cr^{6+} wastewater. 200 mL of simulated wastewater was put into a beaker, and the pH of water inlet was adjusted to be 2, and the total amount of reductive iron powder and activated carbon was 25 g. The ratios of iron and carbon were set as 1:2, 1:1, 2:1 and 3:1, respectively. The rotation speed was set as 245 r/min, and the stirring time was set as 30 mins. Let it stand still for ten minutes after mixing. Their absorbance was measured by diphenyl carbonyl dihydrazine method and compared with the standard curve.

It can be seen from Figure 1 that the removal rate of Cr^{6+} is proportional to the iron-carbon ratio within a certain range. When the iron-carbon ratio is 1:1, the treatment effect of chrome-containing wastewater is the best. Compared with the original wastewater, 65.98% Cr^{6+} is removed, which is far higher than the removal effects of the other three kinds of Cr^{6+} wastewater with three different iron-carbon ratios, indicating that under this ratio, the most primary batteries are formed between iron and carbon and other iron - carbon ratios above or below this ratio are not ideal. When the weight of iron powder is higher than that of activated carbon, due to its reducibility, iron powder plays a reductive role after reacting for a long time, resulting in a low removal rate [12]. When the amount of iron powder is lower than the amount of activated carbon, the number of batteries will decrease. And because excess activated carbon has already achieved saturated, it will not absorb the pollution of the wastewater, leading the removal rate down [13, 14].

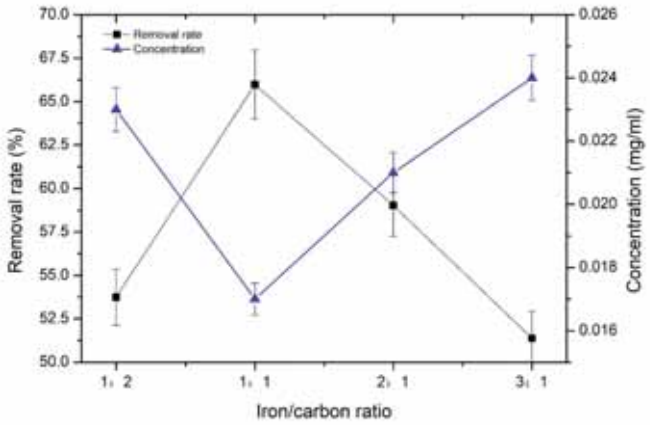

FIGURE 1
The removal rate and concentration changes by different iron/carbon ratios

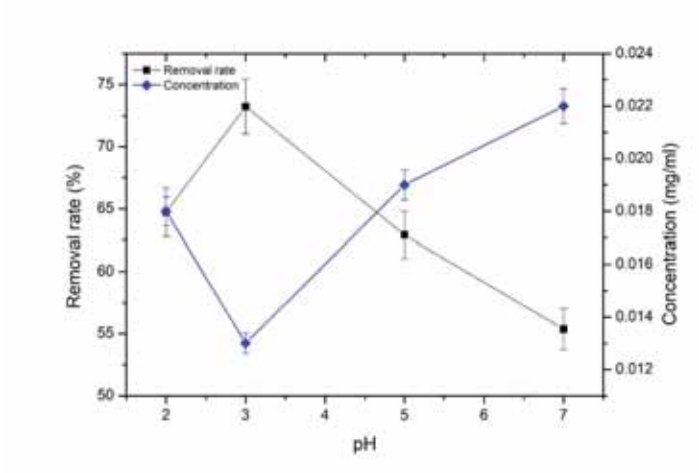

FIGURE 2
The removal rate and concentration changes by different pH settings

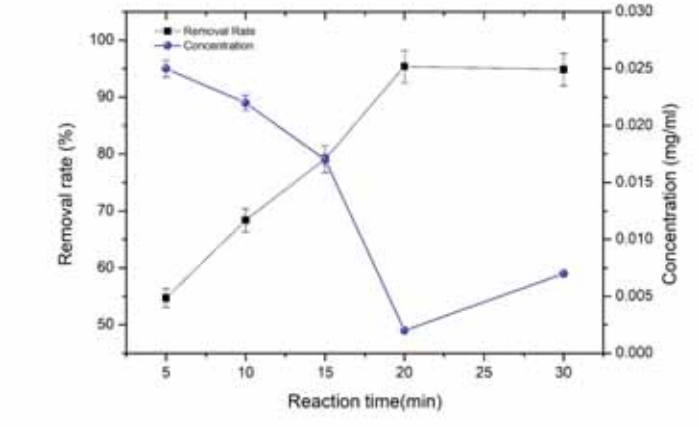

FIGURE 3
The removal rate and concentration changes by different reaction time settings

Effect of influent pH on treatment effect of Cr^{6+} wastewater. 200 mL of simulated wastewater was put into a beaker, and the amount of iron and carbon was set as 25 g. According to the above experiments, the iron and carbon ratio should be set as 1:1. Then, the pH of water inlet was set as 2, 3, 5 and 7, respectively. After stirring, let it stand still for 10 minutes. Then some solution was checked in the colorimetric tube, and compared with the standard curve.

The removal rate of Cr^{6+} also presents a proportional relationship with the inlet pH within a certain range from Figure 2. When pH is 3, the removal rate of Cr^{6+} was 73.24%, and the wastewater concentration reduces to 13 mg/L correspondingly. Therefore, a PH of 3 is regarded as the optimal condition. At a pH of 3, the acidity is higher and the iron is more easily corroded, so the galvanic cell runs faster. At a pH of 2, the solution becomes too acidic to operate the galvanic cell well. At a pH of 5 and 7, they are not as acidic as the solution with a pH of 3. Besides, the oxygen that enters the beaker during agitation speeds up the operation of galvanic cell [15, 16].

Effect of reaction time on treatment effect of Cr6+ wastewater. 200 mL Cr^{6+} wastewater was put into a beaker and stirred with same speed. The iron-carbon ratio was set as 1:1 and PH as 3 according to the two above experiments. The reaction time were set as 10 mins, 15 mins, 20 mins, 30 mins, respectively. Their absorbance is measured by diphenyl carbonyl dihydrazine method and compared with the standard curve.

It can be seen that the relationship between the removal rate of $Cr^{6+}$and reaction time roughly demonstrates s-shaped from Figure 3. After stirring, the best removal effect is achieved under the condition of 20 mins' reaction time, with removal rate being 97.38%. The concentration of wastewater is reduced to 2 mg/L, which is much higher than the removal effect under the condition of other three kinds of reaction times. Therefore, the best reaction time is 20 mins. The reason why the treatment effect increases with time is that the longer the time, the easier iron powder is to reduce to Fe^{3+} [17]. Only when the reaction time is sufficient, high removal rate can be achieved.

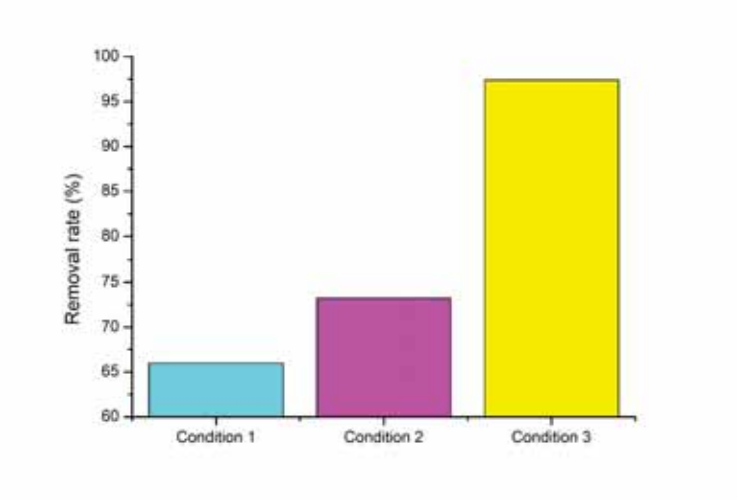

FIGURE 4
The removal rates under three different conditions
Condition 1: the ratio of iron to carbon is 1:1, the inlet pH is 2, and the reaction time is30 mins;
Condition 2: the ratio of iron to carbon is 1:1, the inlet pH is 3, and the reaction time is 30 mins;
Condition 3: the ratio of iron to carbon is 1:1, the inlet pH is 3, and the reaction time is 20 mins.

Treatment effect of Cr^{6+} wastewater under optimal conditions. It can be found from Figure 4 that when iron carbon ratio is 1:1, inlet pH is 3, reaction time is 20 mins, the best treatment result can be achieved with removal efficiency reaching 97.38%, much better than other removal rates under other conditions. Therefore, this is the best reaction condition.

The reaction mechanism is as follows:

(1) The electrode reaction：

Anodic reaction：$Fe-2e^{-}\rightarrow Fe^{2+}$

Cathode reaction: $O_2+4H^{+}+4e^{-}\rightarrow 2O^{2-}+4[H]\rightarrow 2H_2O$

Under aerobic conditions, C can accept electrons and transfer them to Cr^{6+} or oxygen, thus accelerating the reduction reaction [18].

(2) Redox reaction:

From the electrode reaction equation above, it can be seen that Fe^{2+} and [H] will be generated at the electrodes of the galvanic cell respectively. Both of these two substances can increase or decrease the valence of heavy metal ions in the wastewater, so as to achieve the purpose of removing pollutants [19]. In this experiment, Cr^{6+} can both oxidized into Cr^{3+} by these two substances, and thus the toxicity of waste water is decreased [20].

CONCLUSIONS

The application of Fe/C micro-electrolysis technology can remove Cr^{6+} from industrial wastewater effectively. The effects of iron and carbon ratio, inlet pH and reaction time on the removal of Cr^{6+} were discussed. When the Fe/C ratio was 1:1, the removal rate of Cr^{6+} was the highest, 65.98%. When the pH of water was adjusted to 3, the removal rate of Cr^{6+} was the highest, reaching 73.24%. When the reaction time was set as 20 mins, the removal rate of Cr^{6+} was the highest, reaching 95.37%. As can be seen from Figure 4, when the three optimal conditions were selected as the operating conditions, the removal rate of Cr^{6+} in the wastewater is as high as 97.38%, achieving an ideal treatment effect. In a word, this study would provide an example for the treatment of chromium-containing wastewater using Fe/C micro-electrolysis.

ACKNOWLEDGEMENTS

The authors gratefully thank the financial support provided by Shandong Provincial Natural Science Foundation (ZR2019BB040), the National Natural Science Fund of China (NO. 31901188, NO. 31700433, and NO. 31672314) and Shandong Provincial Agricultural Fine Species Project (2019LZGC020).

REFERENCES

[1] Lu, X., Li, B., Guo, L., Zhang, G., Wang, P. (2019). Reduction and Stabilization Remediation of Hexavalent Chromium (Cr6+)-contaminated Soil. Ekoloji Dergisi. 28(107), 973-980.
[2] Kozlowski, H., Kolkowska, P., Watly, J., Krzywoszynska, K., Potocki, S. (2014). General aspects of metal toxicity. Current Medicinal Chemistry. 21(33), 3721-3740.
[3] Rajput, S., Pittman Jr, C.U., Mohan, D. (2016). Magnetic magnetite (Fe3O4) nanoparticle synthesis and applications for lead (Pb2+) and chromium (Cr6+) removal from water. Journal of Colloid and Interface Science, 468, 334-346.

[4] Jobby, R., Jha, P., Yadav, A.K., Desai, N. (2018). Biosorption and biotransformation of hexavalent chromium [Cr (VI)]: a comprehensive review. Chemosphere, 207, 255-266.
[5] Shen, Y.S., Wang, S.L., Tzou, Y.M., Yan, Y.Y., Kuan, W.H. (2012). Removal of hexavalent Cr by coconut coir and derived chars–the effect of surface functionality. Bioresource Technology. 104, 165-172.
[6] Jin, W., Du, H., Zheng, S., Zhang, Y. (2016). Electrochemical processes for the environmental remediation of toxic Cr (VI): A review. Electrochimica Acta. 191, 1044-1055.
[7] Zhang, W., Li, X., Yang, Q., Wang, D., Wu, Y., Zhu, X., Wei, J., Liu, Y., Hou, L., Chen, C. (2019). Pretreatment of landfill leachate in near-neutral pH condition by persulfate activated Fe-C micro-electrolysis system. Chemosphere, 216, 749-756.
[8] Li, D., Han, J. (2019). Homogeneous Photocatalytic Iron Slag Reduction Cr6+ from Chromium Wastewater Containing High-Salt in Constructed Wetland. Polish Journal of Environmental Studies. 28(5), 3745-3752.
[9] M a, Z., Yang, Y., Jiang, Y., Xi, B., Yang, T., Peng, X., Lian, X., Yan, K., Liu, H. (2017). Enhanced degradation of 2, 4-dinitrotoluene in groundwater by persulfate activated using iron–carbon micro-electrolysis. Chemical Engineering Journal, 311, 183-190.
[10] Zhang, C., Zhou, M., Ren, G., Yu, X., Ma, L., Yang, J., Yu, F. (2015). Heterogeneous electro-Fenton using modified iron–carbon as catalyst for 2, 4-dichlorophenol degradation: influence factors, mechanism and degradation pathway.Water Research. 70, 414-424.
[11] Huang, C., Peng, F., Guo, H. J., Wang, C., Luo, M. T., Zhao, C., X, L., Chen, X., Chen, X. D. (2018). Efficient COD degradation of turpentine processing wastewater by combination of Fe-C micro-electrolysis and Fenton treatment: long-term study and scale up. Chemical Engineering Journal. 351, 697-707.
[12] Mueller, F., Gutsche, A., Nirschl, H., Geiger, D., Kaiser, U., Bresser, D., Passerini, S. (2017). Iron-doped ZnO for lithium-ion anodes: impact of the dopant ratio and carbon coating content. Journal of The Electrochemical Society. 164(1), A6123-A6130.
[13] Li, X., Zhou, M., Pan, Y. (2018). Enhanced degradation of 2, 4-dichlorophenoxyacetic acid by pre-magnetization Fe-C activated persulfate: Influential factors, mechanism and degradation pathway. Journal of Hazardous Materials. 353, 454-465.
[14] Yang, K., Jin, Y., Yue, Q., Zhao, P., Gao, Y., Wu, S., Gao, B. (2017). Comparison of two modified coal ash ferric-carbon micro-electrolysis ceramic media for pretreatment of tetracycline wastewater. Environmental Science and Pollution Research. 24(13), 12462-12473.
[15] Zhu, X., Chen, X., Yang, Z., Liu, Y., Zhou, Z., Ren, Z. (2018). Investigating the influences of electrode material property on degradation behavior of organic wastewaters by iron-carbon micro-electrolysis. Chemical Engineering Journal. 338, 46-54.
[16] Zhang, L., Yue, Q., Yang, K., Zhao, P., Gao, B. (2018). Enhanced phosphorus and ciprofloxacin removal in a modified BAF system by configuring Fe-C micro electrolysis: investigation on pollutants removal and degradation mechanisms. Journal of Hazardous Materials. 342, 705-714.
[17] Yang, B., Gao, Y., Yan, D., Xu, H., Wang, J. (2018). Degradation characteristics of color index direct blue 15 dye using iron-carbon micro-electrolysis coupled with H2O2. International Journal of Environmental Research and Public Health. 15(7), 1523.
[18] Yang, Z., Ma, Y., Liu, Y., Li, Q., Zhou, Z., Ren, Z. (2017). Degradation of organic pollutants in near-neutral pH solution by Fe-C micro-electrolysis system. Chemical Engineering Journal. 315, 403-414.
[19] Li, P., Liu, Z., Wang, X., Guo, Y., Wang, L. (2017). Enhanced decolorization of methyl orange in aqueous solution using iron–carbon micro-electrolysis activation of sodium persulfate. Chemosphere. 180, 100-107.
[20] Han, Y., Li, H., Liu, M., Sang, Y., Liang, C., Chen, J. (2016). Purification treatment of dyes wastewater with a novel micro-electrolysis reactor. Separation and Purification Technology. 170, 241-247.

Received: **25.10.2019**
Accepted: **11.02.2020**

CORRESPONDING AUTHOR

Junfeng Chen
Department of Environmental Science,
School of Life Sciences,
Qufu Normal University,
Qufu 273165 – P.R. China

e-mail: chenjunfeng@qfnu.edu.cn or
chenjunfeng2011@163.com

© by PSP Volume 29 – No. 05/2020 pages 3703-3713 Fresenius Environmental Bulletin

SPATIAL DISTRIBUTION AND COMPOSITION OF MICROPLASTICS ALONG NINGBO COAST IN SUMMER

Shengnan Zhao[1,3], Yifeng Zhu[1,3,*], Shuoqian Mao[2], Meiling He[3]

[1]School of Marine Science, Ningbo University, Ningbo, 315211
[2]Ningbo Institute of Oceanography, Ningbo, 315832
[3]Key Laboratory of Applied Marine Biotechnology, the Ministry of Education, Ningbo University, Ningbo, 315211

ABSTRACT

Microplastics in the seawater of Ningbo quantitatively and qualitatively were characterized. Water samples were collected with 77 μm mesh net by vertical towing in summer 2016. The results indicated that microplastics were ubiquitous in the seawater of Ningbo, 2361 microplastics were found in 19 stations, and the concentration of microplastics ranged from 4.0-165.0 piece/m^3, in average of 38.0 piece/m^3; the majority of plastics ranged from 1000 μm to 5000 μm in size, which constituted 43.8% of the total samples, in average of 1116.0 μm. The most frequent geometries were fibers, taking 90.5% of the total, followed by particles for 7.2%. The most frequent color were colored ones, followed by transparent, and black, accounted for 36.8%, 35.4%, and 21.9% of the total samples, respectively. The most frequent chemical composition of microplastics were polyethylene terephthalate and polyethylene, accounted for 53.6% and 25% of the total, respectively. The microplastics pieces were mostly originated from plastic litter from terrestrial sources. This study provided important reference for better understanding microplastic levels in seas.

KEYWORDS:
Microplastic, Ningbo coast, characteristics, spatial distribution

INTRODUCTION

Marine plastic pollution is a serious environmental problem. In 2010, the total amount of plastic waste entering the sea from land was about 4.8 million to 12.7 million tons [1]. It is estimated that by 2050, global plastic waste will reach 12 billion tons [2]. These plastics are mainly derived from waste generated by human activities such as sewage and garbage discharged from land, fisheries and navigation, of which land sources account for about 80% [3]. Under the influence of physics, chemistry and biology, large plastic waste will gradually decompose into micro-plastics with a particle size of no more than 5 mm [4]. These micro-plastics are either suspended in seawater or deposited on the seabed [5], which has great harm to the ecological environment, micro-plastic has become one of the main pollutants in the ocean [6, 7]. At present, research on marine microplastic pollution has aroused great concern from the whole society, and the research scope involves the source of microplastics [8] and distribution [9, 10], biofeeding [11-13], ecological risk [14], research methods, etc. [15, 16].

In China, monitoring marine plastic pollution has gradually aroused the concern. According to the "2018 China Marine Ecological Environment Bulletin" [17], plastic is still the main type of marine debris, the average density of the micro-plastics in the surface water layer is 0.42 piece/m^3 of the Bohai Sea, Yellow Sea and South China Sea monitoring area. In recent years, Chinese researchers have investigated the contamination of micro-plastics in some estuaries and sea areas, such as the Yangtze River estuary [18], Jiaojiang River [19], Oujiang River and Minjiang Estuary [20], and South China Sea [21], Bohai Sea [22], Donghai Sea[23] and Hong Kong Sea. Results obtained are quite different due to the different survey environments and sampling methods [24], and most of the research is directed to micro-plastics in surface seawater, rarely involving in the entire water column. Many studies have shown that microplastics are accumulated in the deep sea [25, 26], and deep coastal water is considered as another under-recognized microplastic "reservoir" [27]. To this end, this study conducted a vertical trawl analysis of micro-plastics in Ningbo's coastal waters, and explored the spatial distribution and composition characteristics of micro-plastics in the sea.

MATERIALS AND METHODS

Survey Station. From June 15th to 17th, 2016, the "Runjiang 1" scientific survey vessel (loaded 659.2 tons, Zhoushan Runhe Marine Technology Development Service Co., Ltd.) was used for vertical trawl sampling. In order to explore the possible differences in microplastics between nearshore and offshore stations, a total of 19 survey

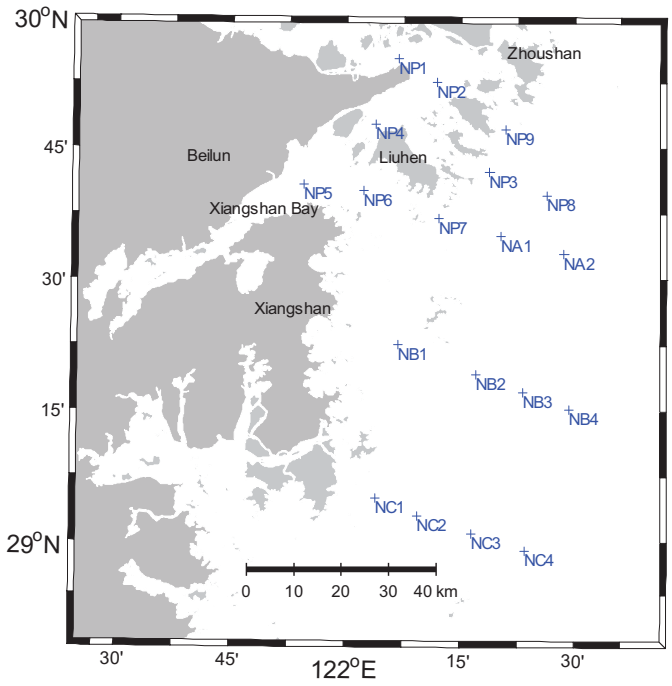

FIGURE 1
Map of Sampling stations

sites were set up (Figure 1), and stations near the coastline were classified into nearshore waters (NP1, NP2, NP3, NP4, NP5). , NP6, NP7, NP9, NB1, NC1), the rest are offshore waters.

Sample Collection. For each station, a plankton III filter is used to vertically tow from the sea floor to the surface (water depth 19-100 m), sieve aperture is 77 μm, trawl speed is 0.5-0.8 m/s, the mesh diameter of filter screen is 0.37 m, the net length is 1.4 m, and the network port is equipped with a digital flow meter (Hydro-Bios, Germany). After the sampling was completed, the flowmeter data was recorded and the filter volume was converted. The filter was rinsed with distilled water for three times at least, the sample was transfer from the filter to a vial with volume of 1 L, and it was fixed with 5% formalin, it was immediately stored in sealed form.

Sample digestion and measurement analysis. Due to the high content of organic matter in the collected sample, it needs to be digested. The sample was poured into a tall beaker of 1 L, 20 ml of 30% hydrogen peroxide and 65% nitric acid mixture was added (Volume ratio is 1:3), and it was sealed with aluminum foil. The induction cooker was heated up and the temperature was maintained at 75-90°C, during which 20 ml of the mixture was added until the organic matter is completely digested (about 2 h in total) [28, 29], and filtered was carried out via the glass fiber filter paper (GF/A, Whatman, UK) with a pore size of 1.6 μm and diameter of 47 mm after cooling, and the residue of the inner wall was repeatedly washed with distilled water, all of the samples were collected on a nitrocellulose membrane.

The filtered filter was placed in a petri dish, and the microplastic was selected under a microscope using a dissecting needle and forceps. The principle of confirmation of microplastics is: cell-free or organic structure; the fiber thickness is the same and the ends are not tapered; the fibers are not separated or twisted; the color of the particles is uniform and the particles are not flickering [30, 31]. At the same time, the characteristics of each microplastic, such as the shape and color, were recorded. The camera (Leica DFC7000 T, Leica, Germany) was used to take photos, and the micro-plastic size information was measured using the software (Leica Application suite V4). Microplastics are classified into five fractions according to the range of microplastics, <100 μm, 100-500 μm, 500-1000 μm and 1000-5000 μm, respectively.

56 micro-plastics with typical shapes and colors were selected. The XploRA ONE high-sensitivity Raman spectrometer manufactured by HORIBA Scientific was used to detect the chemical composition of micro-plastics. At the same time, suspicious samples were detected, the recognition accuracy was improved, and the micro-plastics were placed with tweezers. On the quartz plate, it was focused on a sample platform under a 50-fold objective lens, and the excitation wavelength was 785 nm, and a Raman spectrum in the range of 0-3500 cm^{-1} was collected.

Since micro-plastics are widely used in the environment [32], in order to prevent pollution, the

operator wears experimental clothes and nitrile gloves during the operation; All experimental containers and tools are washed with distilled water for 2 to 3 times. And the samples to be analyzed were all covered with aluminum poise; three blank control groups were set.

Data processing. All raw data preprocessing and statistical analysis were programmed in the R 3.2.5 language. In the data analysis, the difference between the parameters of the offshore and offshore waters was determined by independent sample t test. The number of micro-plastics, the abundance, the length, the number of colors, the number of shapes and the number of particles are numerically distributed using Matlab 7.8 software. The spatial interpolation is based on the triangular-cube method. It is assumed that each interpolation must be interpolated within the range of three actual observations to avoid extrapolation of the results of the interpolation process [33].

RESULTS AND DISCUSSION

Quantitative characteristics and spatial distribution of micro-plastics in survey stations. According to the survey, the total number of micro-plastics obtained by 19 stations was 2,361 (Table 1), and no pollution was found in the blank group, so no blank correction was needed. The distribution abundance of microplastics is between 4.0 and 165.0 piece/m^3, and the average abundance is 38.0 piece/m^3. The length of the micro-plastics in the surveyed sea area was between 20.4 and 4937.0 μm, the average length was 1116.0 μm, and the average width of the micro-plastics was 24.4 μm. In the sea area, four kinds of micro-plastics were detected, and four colors were used, covering the four granular groups.

Abundance in the vicinity of the sea area of of Xiangshan Port (NP5) is the highest rom the spatial distribution of micro-plastic abundance in the surveyed sea area (Figure 2A), reaching 165.0 piece/m^3, and it is high in the coastal waters of Xiangshan County (NP6, NB1 and NC1), with abundance of 75.5 piece/m^3, 44.0 piece/m^3, 70.0 piece/m^3, and the farther from the shore is, the lower the abundance is. The percentage of the number is the highest in the NP2 station near Zhoushan Island, and the port area in Xiangshan Port is also higher, and the other sea areas are lower (Figure 2B). According to the length distribution map (Figure 2C), the average length of microplastics in Zhoushan Island and Xiangshan Port port area is shorter, and the longer microplastic distribution area is on the south side of the surveyed sea area.

Microplastic composition. Figure 3 is a photomicrograph of a typical microplastic. The four microplastics in this investigation are fibers, particles, fragments, and films (Table 2), based on [34]: fibrous fingers are longer than width. , filamentous plastic; granular refers to smooth spherical plastic; fragmented refers to irregular and hard plastic; film refers to flat, flat and smooth plastic. Among them, the number of fibers accounted for the vast majority, the number of percentages reached 90.5%, and the abundance reached 35.8 piece/m^3. The number of particles and fragments is 2nd and 3rd, respectively, and the total number of the two is only 9.3%, and the number of films is less.

TABLE 1
Quantitative characteristics of microplastics in each station

Station	Water sample collection / m^3	Total number/piece	Percentage /%	Abundance/(piece/m^3)	Average length (range) /μm	Average width /μm	Number of forms / species	Number of colors / species	Number of particles/ piece
NP1	17.6	186	7.9	10.6	960.7 (60.9-4808.9)	29.2	3	4	4
NP2	9.6	332	14.1	34.6	1072.1 (61.9-4701.8)	20.6	3	4	4
NP3	2.9	162	6.9	55.9	824.7 (63.3-4080.4)	22.9	3	4	4
NP4	5.9	143	6.1	24.2	993.8 (35.3-4515.4)	25.6	3	4	4
NP5	1.4	231	9.8	165.0	1117.9 (97.7-4830.6)	16.2	3	4	4
NP6	2.0	151	6.4	75.5	913.7 (20.4-4782.4)	24.0	4	4	4
NP7	2.0	106	4.5	53.0	1078.9 (58.4-4255.7)	21.1	4	4	4
NP8	4.7	58	2.4	12.3	1066.5 (50.3-3400.0)	45.3	3	3	4
NP9	2.5	60	2.5	24.0	835.7 (37.1-4919.8)	38.1	2	3	4
NA1	6.4	98	4.2	15.3	1058.2 (135.7-3140.2)	22.5	3	4	4
NA2	4.3	177	7.5	41.2	1159.9 (110.6-4937.0)	26.6	3	4	4
NB1	2.5	110	4.7	44.0	1262.4 (243.1-4752.5)	36.4	2	4	4
NB2	1.7	64	2.7	37.6	1254.6(436.2-3427.9)	23.3	2	4	4
NB3	7.2	67	2.8	9.5	1369.7 (244.6-4217.3)	19.3	2	3	4
NB4	9.5	38	1.6	4.0	1459.2 (144.5-4264.2)	25.6	3	4	3
NC1	1.7	119	5.0	70.0	1664.6 (80.1-4256.5)	21.0	3	4	4
NC2	3.4	82	3.5	24.1	1327.7 (102.1-4690.1)	22.5	3	3	3
NC3	5.4	43	1.8	8.0	1157.2 (162.3-3530.9)	17.0	1	3	3
NC4	9.7	134	5.7	13.8	1269.1 (103.0-4844.5)	23.9	3	3	3
Mean ± standard deviation	5.3±4.0	124.3±71.2	5.3±3.0	38.0±36.4	1116.0±867.3 (20.4-4937.0)	24.4±67.2	2.8±0.7	3.7±0.5	3.8±0.4

Note: The number of particles is the number of micro-plastic lengths covering the number of granular groups.

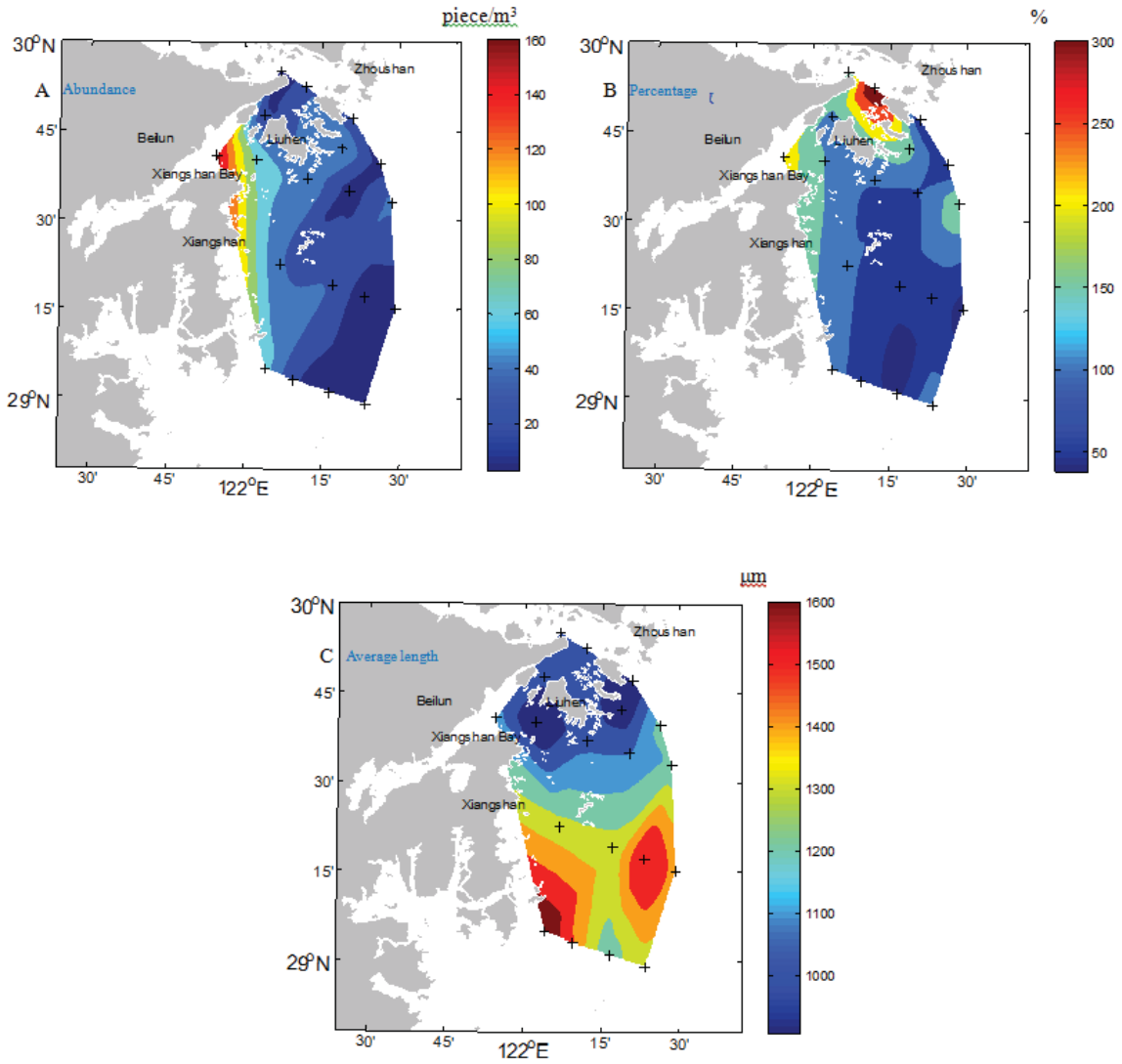

FIGURE 2
Spatial distribution of microplastics abundance, individual percentage and length

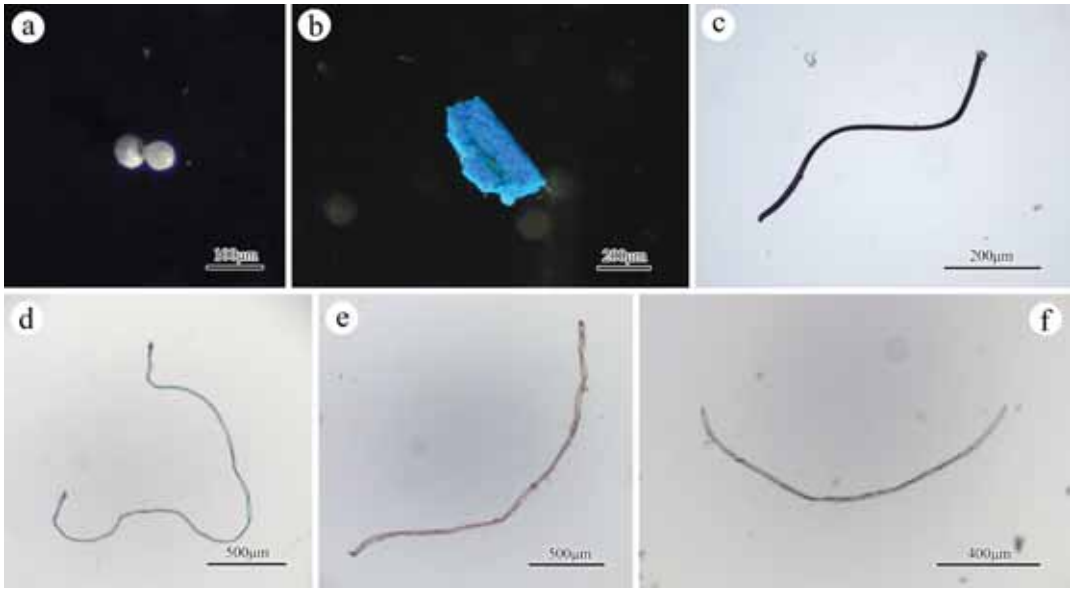

FIGURE 3
Images of different microplastics; a is white particles, b is blue fragments, c, d, e, and f are black, green, red, and transparent fiber

TABLE 2
Characteristics of different-shaped microplastic in the sea area

Morphology	Total number/piece	Percentage /%	Abundance/(piece/m$^{3)}$	Length /μm	Width /μm
Fiber	2137	90.5	35.8±36.7	1206.4±856.1	18.1±9.8
Particle	170	7.2	1.4±1.9	159.0±31.8	137.1±21.3
Fragment	50	2.1	0.7±0.6	666.7±716.9	335.6±440.1
Film	4	0.2	0.1±0.2	1266.4±673.3	453.3±179.7

TABLE 3
Characteristics of different-sized microplastic in the sea area

Size	Total number/piece	Percentage /%	Abundance/(piece/m$^{3)}$	Length /μm	Width /μm
Less than 100 μm	28	1.2	0.5±0.8	70.9±11.9	37.2±17.0
100-500 μm	548	23.2	8.3±10.4	324.3±61.7	27.5±15.2
500-1000 μm	752	31.8	12.4±11.9	742.8±19.5	24.3±8.4
1000-5000 μm	1033	43.8	16.8±17.1	1848.3±125	27.0±15.1

TABLE 4
Characteristics of different-colored microplastic in the sea area

Color	Total number/piece	Percentage /%	Abundance/(piece/m$^{3)}$	Length /μm	Width /μm
Colored	869	36.8	15.0±14.9	1079.3±830.9	26.2±86.2
Transparent	835	35.4	13.5±12.9	1353.6.±896.8	23.1±59.4
Black	517	21.9	8.3±11.2	1013.9±798.9	18.4±16.7
White	140	5.9	1.2±1.3	303.5±448.4	123.8±127.8

TABLE 5
Spatial difference in quantitative characteristics of microplastics

Group	Total number/piece	Percentage /%	Abundance /(piece/m$^{3)}$	Length /μm	Width /μm	Number of forms / species	Number of colors / species	Number of particles/ piece
Nearshore waters	160.0±72.6*	6.8±3.1*	55.7±41.4*	1067.4±876.7*	25.5±61.8	3.0±0.6	3.9±0.3*	4.0*
Offshore waters	84.6±42.8	3.6±1.8	18.4±12.4	1235.8±129.1	25.1±7.6	2.6±0.7	3.4±0.5	3.6±0.5

Note: * represents a significant difference between the seas(P<0.05).

According to the divided particle size group (Table 3), the length of the microplastics is mainly distributed in 3 grain sizes of 100 μm to 5000 μm, and the total number, the percentage of the number and the abundance of the 1000-5000 μm particle size group are the highest, the average length of the fraction is 1848.3 μm; and <100 μm microplastics are rare.

Microplastic samples were divided into four categories according to color, transparent, white, black and colored (Table 4). The proportion of the four colors of microplastics was 36.8% in color, 35.4% in transparency, 21.9% in black, and 5.9% in white.

Comparison of sea area differences in micro-plastic quantity characteristics. After the different stations were divided into nearshore and offshore waters (Table 5), except for the significant difference between the width and shape of the microplastics (P>0.05), the total number, the percentage of the number, the abundance, There were significant differences in length, number of colors and number of grains between the two sea areas (P<0.05). Moreover, except for the significantly lower length of microplastics in the coastal waters, other parameters are higher than offshore waters.

In the four microplastic forms (Figure 4A), the fibrous abundance of the two sea areas was significantly higher than the other forms. Moreover, the fibrous abundance in the coastal waters was significantly higher than that in the offshore waters (P<0.05), and no significant differences were found between the other seas in different sea areas (P>0.05). According to different grain size analysis (Figure 4B), the abundance of each grain level is higher in offshore waters than in offshore waters, and the <100 μm, 100-500 μm, 500-1000 μm grain size groups are significantly higher than offshore waters. (P<0.05). Among the four colors (Figure 4C), the color and transparency abundance is the highest, and the abundance of all color microplastics is generally higher in offshore waters than in offshore waters. Colored and white are significantly different in different sea areas (P<0.05).

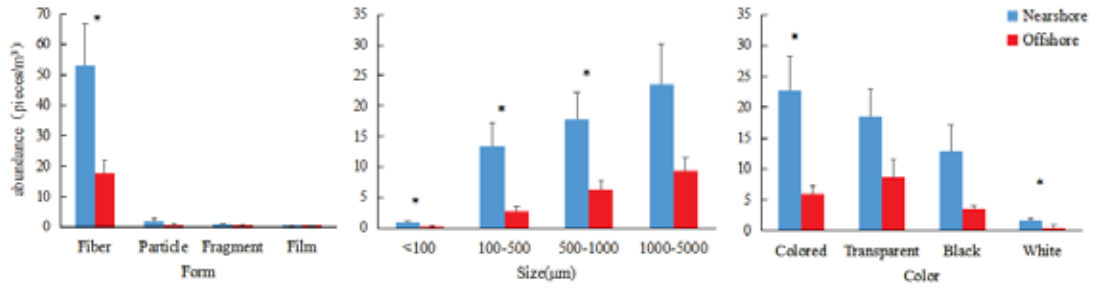

FIGURE 4
Comparison of abundance differences of microplastics between different sea areas; * represents that there is a significant difference between the sea areas (P<0.05); the error bars represent standard errors.

Microplastic chemical composition. The Raman spectrum was analyzed by Raman spectroscopy to obtain a Raman spectrum (Figure 5), in which polyethylene terephthalate accounted for 53.6%, polyethylene (Polyethylene) accounted for 25%, and polypropylene (polypropylene). accounted for 16.1%, and polyvinyl chloride accounted for 5.4%. The main vibration peaks of polyethylene terephthalate are 1602 and 1716 cm^{-1} [35], which are caused by the stretching vibration of carbon and oxygen atoms in the carboxyl group and the asymmetric stretching vibration between carbon atoms in the benzene ring. The main vibration peaks of polyethylene are 1059, 1125, 1289 and 1429 cm^{-1} [36]; the main vibration peaks of polypropylene are 809, 841, 971, 1149, 1166 and 1451 cm^{-1} [37]; the characteristic peaks of polyvinyl chloride are 625 and 684 cm-1, which are caused by the stretching vibration between carbon and chlorine atoms [38].

Composition characteristics of microplastics along the coast of Ningbo. Most marine microplastic pollution studies are limited to surface waters [39, 40]. In fact, there is also a large amount of microplastics in the water column [41]. Many

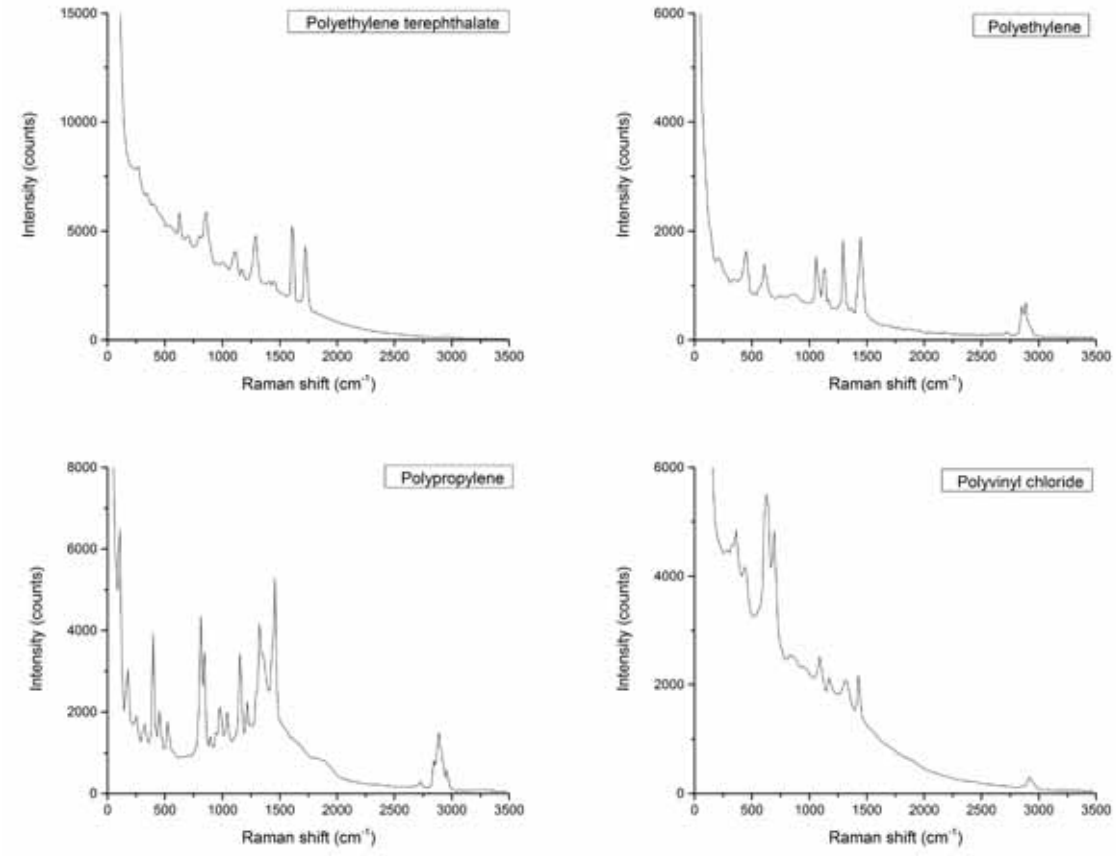

FIGURE 5
Raman spectra of samples

TABLE 6
Comparison between this study and other literatures

	Filter aperture /μm	Abundance (piece/m$^{3)}$	Main morphology	Main ingredient
This study	77	38.0	Fiber	PET、PE、PP、PVC
Baltic Sea [48]	174	310	Fiber	—
Baltic Sea [45]	174	32.2	Fiber	PET、PA、PE、PP、PS、PVC、PMMA
Arctic Ocean [46]	250	46	Fiber	PET、PA、PVC、PP
Lions Bay, France [47]	200	0.23	Fiber	PET、PA、PE、PAN、PVC、PP

factors will affect the vertical distribution of micro-plastics in seawater. Lighter-weight plastics such as polyethylene and polypropylene will float on the surface of the sea, and plastics such as polyethylene oxide and polyethylene terephthalate with higher density will sink; wind-driven turbulence can migrate micro-plastics from the surface of seawater to the sub-layer of seawater [42]; biofilms formed by algae and protozoa on the surface of micro-plastics will increase it. Density causes sedimentation [43]; marine animals swallow microplastics and expel them together with feces, causing microplastics to flow in deep waters [44]. A study in Monterey Bay, Calif., found that micro-plastics at an altitude of 200 to 600 m from the sea are extremely high, reaching 15 piece/m^3. The deep sea, as the largest ecosystem on Earth, stores large amounts of micro-plastics for the ocean. Creatures have potential hazards. At present, the understanding of micro-plastics in water columns is still scarce, and more data is needed to understand the vertical distribution of micro-plastics and the impact on marine life.

In this study, a vertical trawl sampling of the coastal waters of Ningbo was carried out using a 77 m filter. The results show that the micro-plastics exist in a large amount in the entire water column, with an average abundance of 38.0 piece/m^3, which is significantly higher than that of the adjacent East China Sea surface micro-plastic 1.02 piece/m^3 (screen pore size 60 m). Table 6 shows the sampling methods and results of other literatures. The sampling points of these studies are also located along the coast and are greatly affected by human activities. After comparison, the results of 38.0 piece/m^3 in this study and the microbial abundance of the Baltic Sea [45] and the Arctic Ocean [46] were similar, 32.2 piece/m^3 and 46 piece/m^3 respectively, but the filter aperture of both is larger than 77 m in this study. The large aperture means that it is possible to miss some of the smaller micro-plastics, which may cause an underestimation of abundance. In addition, the results of this study are higher than the 0.23 piece/m^3 of Lefebvre et al. [47], which is lower than the 285.7 piece/m^3 of the Baltic Sea [48] in 2017, which may be related to the sampled water depth.

The micro-plastics with a length of 1000 μm to 5000 μm in this sea area are the main components (43.6%), and the colors are mainly colored (37.1%) and transparent (35.3%). There are 4 types of micro-plastics detected, and most of the fibers (90.5%) are similar to those of other full-water sampling. The Baltic fiber type accounts for 75%, and the fibers in the Arctic Ocean water column account for 94%, the micro-plastic fiber type in the Sea of Lions Bay in France is as high as 99.1%; most surface seawater research has similar reports, and the micro-plastic fiber type in the Gulf of Mexico accounts for 72.5% of the total, the fiber type in the Northeast Pacific Ocean accounts for about 75%. Many studies have shown that a large number of fibrous microplastics in the ocean are associated with human discharge of sewage and garbage. According to Browne et al. [49], the sewage discharged from the washed synthetic fabric contains a large amount of micro-plastic fibers (mainly polyester fiber and acrylic fiber) with an abundance of 1 piece/L, and an average of 1900 pieces per wool fabric. Micro-plastic fibers; Napper et al. [50] found that the washing machine washed 6 kg of synthetic fabric, discharging 4.96×10^5 polyester fibers and 7.28×10^5 acrylic fibers. Bai Mengyu et al. [51] studied the occurrence characteristics of micro-plastics in the inflow and outflow of wastewater from China's coastal cities, and the micro-plastic emissions. It was found that the abundance of micro-plastics in the influent water was as high as 117 piece/L, and the abundance after treatment was 52 piece/L, the shape is mainly fibrous, and the treated sewage will eventually be released into rivers and oceans. Fishing activities in the coastal areas are very frequent. The commonly used fishing nets, fishing nets, fishing lines and other fishing gears are all made of plastic. If the damaged fishing gear is not properly disposed, it will become plastic waste and enter the ocean. Cracked into a large number of tiny micro-plastic fibers.

Raman spectroscopy detected that the composition of micro-plastics was mainly PET (53.6%) and PE (25%). Most of the fibers were PET, and most of the fragments were PE. Similar to the results of the Lions Bay and the Baltic Sea, but the study of surface seawater is dominated by PE and PP [52]. The lower ratio of PE to PP in this study may be due to the small amount of water collected by the vertical trawl on the surface of the sea. Polymers are distributed in water columns of different depths due to density. Low-density polymers such

as PE and PP usually float on the surface of the sea and are easily collected by surface trawls, as opposed to PET and PVC. The polymer has a higher density and has a low capture rate in the surface seawater but is abundant in the water column.

The distribution of micro-plastics in Ningbo sea area has obvious land-source characteristics. The results show that the distribution of micro-plastics in the coastal waters of Ningbo is very uneven, and the abundance of micro-plastics in each station ranges from 4.0 to 165.0 piece/m^3. After analyzing the offshore and offshore waters, it was found that the micro-plastic abundance (56.1 piece/m^3) in the coastal waters was significantly higher than that in the offshore waters (18.8 piece/m^3), and the distribution of color number and number of particles. There are also significantly more offshore waters than offshore waters. The reason for this difference is mainly due to the fact that most of the microplastics in the ocean originate from land, which is terrestrial.

Ningbo is located on the coast, with developed economy and dense population. Human activities produce a large amount of plastic garbage such as food packaging bags, fast food boxes, plastic bottles, etc. Under the influence of the environment, it will be broken into micro-plastics, which can enter the sea directly through the coast or river; Cleaners, skin care products and textiles all contain large amounts of microplastics that are difficult to treat by the wastewater treatment plant and eventually discharged into the sea. The initial source of micro-plastics can also be judged by identifying the type of polymer. Polyethylene (PE), polyethylene terephthalate (PET), polypropylene (PP) and polyvinyl chloride (polyethylene chloride) were detected in the samples. PVC). These plastic components are all components of human production and common objects in life, reflecting obvious land-source characteristics. PE is commonly used in the production of packaging products, straws, fishing nets, cables, etc.; PET has the advantages of water resistance, oil resistance and high temperature resistance, and is mostly used for packaging materials such as disposable beverage bottles, bathroom products, cosmetic boxes, etc. PP can be used for making weaving Bags, various household appliances, outdoor furniture; PVC is used to make water pipes, children's toys, etc. These plastic products have a short service life and are easy to enter the environment after being discarded, becoming a source of marine microplastics.

Micro-plastics do not stay in the coastal waters from the land to the ocean. They will gradually diffuse, dilute and redistribute to the distant shore under the influence of water flow and wind [53], and some will be lame. Marine organisms such as shrimps, fish, and fish feed on different water layers. These ocean currents and biological processes cause the micro-plastic abundance of offshore waters to be lower than that of nearshore waters. Many studies have also reported that micro-plastics in the sea are closely related to human activities. On densely populated coasts, the abundance of micro-plastics is significantly higher than that of offshore waters. The micro-plastics abundance in central Stockholm, Sweden is 10 times higher than offshore waters; in Plymouth, UK, micro-plastic abundance decreases from 1.5 piece/m^{-3} as offshore distance increases At 0.5 piece/m^{-3}; in the northeastern Pacific, the micro-plastic abundance in the offshore waters is 279 piece/m^{-3}, while the ashore abundance is as high as 1710-7630 piece/m^{-3}; the microplastic abundance of surface floating in the Yangtze River estuary to the East China Sea is (4137.3±2461.5) piece/m^{-3} and (0.167±0.138) piece/m^{-3}, which also shows that the micro-plastic abundance shows a significant decline from land to ocean, showing land-source characteristics.

CONCLUSION

(1) Vertical trawls (mesh 77 μm) of summer micro-plastics in the coastal waters of Ningbo showed a maximum of 165.0 pieces/m^{-3}, an average abundance of micro-plastics of 38.0 pieces/m^{-3}, and an average length of micro-plastics of 1116.0 m. The length varies from 20.4 to 4937.0 m, and the length is mainly between 1000 and 5000 m (43.6%). A total of 4 micro-plastics were detected, with fiber type accounting for the majority (90.5%), color mostly colored (36.8%), transparent (35.4%) and black (21.9%); chemical composition with polyterephthalic acid Ethylene glycol (53.6%) and polyethylene (25%) dominated.

(2) The micro-plastics are unevenly distributed in space, and the abundance in the coastal waters that are greatly affected by human activities is large. The farther away from the coast, the lower the abundance. Comparing the nearshore and offshore waters, it is found that the abundance, color number and size of microplastics are significantly higher than offshore waters except for the slightly lower length of microplastics in the coastal waters. The results show that most of these microplastics come from the land and migrate to oceans through ocean currents and winds.

ACKNOWLEDGEMENT

This research was supported by the Program of “Xinmiao” (Potential) Talents in Zhejiang Province (2017R405057).

REFERENCES

[1] Jambeck, J.R., Andrady, A., Geyer, R., Narayan, R., Perryman, M., Siegler, T., Wilcox, C., Law, K.L. (2015) Plastic waste inputs from land into the ocean. Science. 347, 768-771.

[2] Henry, B., Laitala, K., Klepp, I.G. (2019) Microfibres from apparel and home textiles: Prospects for including microplastics in environmental sustainability assessment. Science of The Total Environment. 652, 483-494.

[3] Anderson, Z.T., Cundy, A.B., Croudace, I.W., Warwick, P.E., Celis-Hernandez, O., Stead, J.L. (2018) A rapid method for assessing the accumulation of microplastics in the sea surface microlayer (SML) of estuarine systems. Scientific Reports. 8, 942-943.

[4] Cesa, F.S., Turra, A., Baruque-Ramos, J. (2017) Synthetic fibers as microplastics in the marine environment: a review from textile perspective with a focus on domestic washings. Science of The Total Environment. 598, 1116-1129.

[5] Coppock, R.L., Cole, M., Lindeque, P.K., Queirós, A.M., Galloway, T.S. (2017) A small-scale, portable method for extracting microplastics from marine sediments. Environmental Pollution. 230, 829-837.

[6] Cole, M., Lindeque, P., Halsband, C., Galloway, T.S. (2011) Microplastics as contaminants in the marine environment: a review. Marine Pollution Bulletin. 62, 2588-2597.

[7] Kramm, J., Völker, C. (2018) Understanding the Risks of Microplastics: A Social-Ecological Risk Perspective. Freshwater Microplastics. 58, 223-237.

[8] Sillanp, M., Sainio, P. (2017) Release of polyester and cotton fibers from textiles in machine washings. Environmental Science & Pollution Research International. 24, 19313-19321.

[9] Frere, L., Paul-Pont, I., Rinnert, E., Petton, S., Jaffré, J., Bihannic, I., Soudant, P., Lambert, C., Huvet, A. (2017) Influence of environmental and anthropogenic factors on the composition, concentration and spatial distribution of microplastics: a case study of the Bay of Brest (Brittany, France). Environmental Pollution. 225, 211-222.

[10] Klein, S., Dimzon, I.K., Eubeler, J., Knepper, T.P. (2018) Analysis, occurrence, and degradation of microplastics in the aqueous environment. Freshwater Microplastics. 58, 51-67.

[11] Steer, M., Cole, M., Thompson, R.C., Lindeque, P.K. (2017) Microplastic ingestion in fish larvae in the western English Channel. Environmental Pollution. 226, 250-259.

[12] Kolandhasamy, P., Su, L., Li, J., Qu, X., Jabeen, K., Shi, H. (2018) Adherence of microplastics to soft tissue of mussels: a novel way to uptake microplastics beyond ingestion. Science of the Total Environment. 610, 635-640.

[13] Sun, X., Li, Q., Zhu, M., Liang, J., Zheng, S., Zhao, Y. (2017) Ingestion of microplastics by natural zooplankton groups in the northern South China Sea. Marine Pollution Bulletin. 115, 217-224.

[14] Mattsson, K., Hansson, L.A., Cedervall, T. (2015) Nano-plastics in the aquatic environment. Environmental Science: Processes & Impacts. 17, 1712-1721.

[15] Hidalgo-Ruz, V., Gutow, L., Thompson, R.C., Thiel, M. (2012) Microplastics in the marine environment: a review of the methods used for identification and quantification. Environmental Science & Technology. 46, 3060-3075.

[16] Qiu, Q.X., Tan, Z., Wang, J.D., Peng, J.P., Li, M.M., Zhang, Z.M. (2016) Extraction, enumeration and identification methods for monitoring microplastics in the environment. Estuarine, Coastal and Shelf Science. 176, 102-109.

[17] Ministry of Ecology and Environment (MEE) of the People's Republic of China, 2018. 2018 Bulletin on China's Marine Ecological Environment. Beijing: Ministry of Ecology and Environment (MEE) of the People's Republic of China, 1-61.

[18] Zhao, S.Y., Zhu, L.X., Wang, T., Li, D.J. (2014) Suspended microplastics in the surface water of the Yangtze Estuary System, China: First observations on occurrence, distribution. Marine Pollution Bulletin. 86, 562-568.

[19] Zhu, X.T., Yi, J., Qiang, L.Y., Cheng, J.P. (2018) Distribution and Settlement of Microplastics in the Surface Sediment of Yangtze Estuary. Environmental Science. 39, 2067-2074.

[20] Zhao, S.Y., Zhu, L.X., Li, D.J. (2015) Microplastic in three urban estuaries, China. Environmental Pollution. 206, 597-604.

[21] Cheung, P.K., Cheung, L.T.O., Fok, L. (2016) Seasonal variation in the abundance of marine plastic debris in the estuary of a subtropical macro-scale drainage basin in South China. Science of The Total Environment. 562, 658-665.

[22] Zhang, W.W., Zhang, S.F., Wang, J.Y., Wang, Y., Mu, J.L., Wang, P., Lin, X.Z., Ma, D.Y. (2017) Microplastic pollution in the surface waters of the Bohai Sea, China. Environmental Pollution. 231, 541-548.

[23] Liu, T., Sun, X.X., Zhu, M.L., Liang, J.H., Zhao, Y.F. (2018) Distribution and composition of microplastics in the surface water of the east china sea. Oceanologia et Limnologia Sinica. 49, 62-69.

[24] Di Mauro, R., Kupchik, M.J., Benfield, M.C. (2017) Abundant plankton-sized microplastic particles in shelf waters of the northern Gulf of Mexico. Environmental Pollution. 230, 798-809.
[25] Chiba, S., Saito, H., Fletcher, R., Yogi, T., Kayo, M., Miyagi, S., Ogido, M., Fujikura, K. (2018) Human footprint in the abyss: 30 year records of deep-sea plastic debris. Marine Policy. 96, 204-212.
[26] Jamieson, A.J., Brooks, L.S.R., Reid, W.D.K., Pierntey, S.B., Narayanaswamy, B.E., Linley, T.D. (2019) Microplastics and synthetic particles ingested by deep-sea amphipods in six of the deepest marine ecosystems on Earth. Royal Society Open Science. 6, 180667-180668.
[27] Choy, C.A., Robison, B.H., Gagne, T.O., Erwin, B., Firl, E., Halden, R.U., Hamilton, J.A., Katija, K., Lisin, S.E., Rolsky, C., Van Houtan, K.S. (2019) The vertical distribution and biological transport of marine microplastics across the epipelagic and mesopelagic water column. Scientific Reports. 9, 7843-7844.
[28] Yonkos, L.T., Friedel, E.A., Perez-Reyes, A.C., Ghosal, S., Arthur, C.D. (2014) Microplastics in four estuarine rivers in the Chesapeake Bay, U. S. A. Environmental Science & Technology. 48, 14195-14202.
[29] Zhou, Q. (2016) Characteristics and ecological risks of micro-plastics in typical coastal tidal flats and offshore environments. Beijing: University of Chinese Academy of Sciences.
[30] Mohamed, N.H., Obbard, J.P. (2014) Microplastics in Singapore's coastal mangrove ecosystems. Marine Pollution Bulletin. 79, 278–283.
[31] Gorokhova, E. (2015) Screening for microplastic particles in plankton samples: how to integrate marine litter assessment into existing monitoring programs. Marine Pollution Bulletin. 99, 271-275.
[32] Liu, K., Zhang, F., Song, Z., Zong, C., Wei, N., Li, D. (2019) A novel method enabling the accurate quantification of microplastics in the water column of deep ocean. Marine Pollution Bulletin. 146, 462-465.
[33] Watson, D. (1992) Contouring: A Guide to the Analysis and Display of Spatial Data. Oxford: Pergamon Press.
[34] Kershaw, P.J., Turra, A., Galgani, F. (2019) Guidelines for the monitoring and assessment of plastic litter and microplastics in the ocean. GESAMP Reports & Studies Series 99.
[35] Purvis, J., Bower, D.I., Ward, I.M. (1973) Molecular orientation in PET studied by polarized Raman scattering. Polymer. 14, 398-400.
[36] Allen, V., Kalivas, J.H., Rodriguez, R.G. (1999) Post-consumer plastic identification using Raman spectroscopy. Applied Spectroscopy. 53, 672-681.
[37] Nielsen, A.S., Batchelder, D.N., Pyrz, R. (2002) Estimation of crystallinity of isotactic polypropylene using Raman spectroscopy. Polymer. 43, 2671-267.
[38] Ritter, U., Scharff, P., Pinchuk, T.M., Dmytrenko, O.P., Bulavin, L.A., Kulish, M.P., Prylutskyy, Y. I., Zabolotnyy, M.A., Grabovsky, Y. E., Bilyy, M.M., Rugal, A.G., Shut, A.M., Shlapatska, V.V. (2010) Radiation modification of polyvinyl chloride nanocomposites with multi-walled carbon nanotubes. Materialwissenschaft und Werkstofftechnik. 41, 675-681.
[39] Desforges, J.P.W., Galbraith, M., Dangerfield, N., Ross, P.S. (2014) Widespread distribution of microplastics in subsurface seawater in the NE Pacific Ocean. Marine Pollution Bulletin. 79, 94-99.
[40] Gewert, B., Ogonowski, M., Barth, A., MacLeod, M. (2017) Abundance and composition of near surface microplastics and plastic debris in the Stockholm Archipelago, Baltic Sea. Marine Pollution Bulletin. 120, 292-302.
[41] Li, Y.W., Long, M., Zuo, L.H., Li, W., Zhao, W.C. (2019) Brittleness Evaluation of Coal Based on Statistical Damage and Energy Evolution Theory. Journal of Petroleum Science and Engineering. 172, 753-763.
[42] Reisser, J., Slat, B., Noble, K., Plessis, K.D., Epp, M., Proietti, M.C., De Sonneville, J., Becker, T., Pattiaratchi, C. (2015) The vertical distribution of buoyant plastics at sea: an observational study in the North Atlantic Gyre. Biogeosciences. 12, 1249-1256.
[43] Kooi, M., van Nes, E.H., Scheffer, M., Koelmans, A.A. (2017) Ups and downs in the ocean: Effects of biofouling on vertical transport of microplastics. Environmental Science & Technology. 51, 7963-7971.
[44] Cole, M., Lindeque, P., Fileman, E., Clark, J., Lewis, C., Halsband, C., Galloway, T.S. (2016) Microplastics alter the properties and sinking rates of zooplankton faecal pellets. Environmental Science & Technology. 50, 3239-3246.
[45] Zobkov, M.B., Esiukova, E.E., Zyubin, A.Y., Samusev, I.G. (2019) Microplastic content variation in water column: The observations employing a novel sampling tool in stratified Baltic Sea. Marine Pollution Bulletin. 138, 193-205.
[46] Kanhai, L.D.K., Gårdfeldt, K., Lyashevska, O., Hassellöv, M., Thompson, R.C., O'Connor, I. (2018) Microplastics in sub-surface waters of the Arctic Central Basin. Marine Pollution Bulletin. 130, 8-18.

[47] Lefebvre, C., Saraux, C., Heitz, O., Nowaczyk, A., Bonnet, D. (2019) Microplastics FTIR characterisation and distribution in the water column and digestive tracts of small pelagic fish in the Gulf of Lions. Marine Pollution Bulletin. 142, 510-519.
[48] Bagaev, A., Mizyuk, A., Khatmullina, L., Isachenko, I., Chubarenko, I. (2017) Anthropogenic fibres in the Baltic Sea water column: Field data, laboratory and numerical testing of their motion. Science of the Total Environment. 599, 560-571.
[49] Browne, M.A., Crump, P., Niven, S.J., Teuten, E., Tonkin, A., Galloway, T., Thompson, R. (2011) Accumulation of microplastic on shorelines woldwide: sources and sinks. Environmental Science & Technology. 45, 9175-9179.
[50] Napper, I.E., Thompson, R.C. (2016) Release of synthetic microplastic plastic fibres from domestic washing machines: effects of fabric type and washing conditions. Marine Pollution Bulletin. 112, 39-45.
[51] Bai M.-Y., Zhao S.-Y., Peng G.-Y., Gao L., Li D.-J. (2018) Occurrence, characteristics of microplastic during urban sewage treatment process. China Environmental Science. 38(5): 1734-1743.
[52] Kanhai, L.D.K., Officer, R., Lyashevska, O., Thompson, R.C., O'Connor, I. (2016) Microplastic abundance, distribution and composition along a latitudinal gradient in the Atlantic Ocean. Marine Pollution Bulletin. 115, 307-314.
[53] Goldstein, M.C., Rosenberg, M., Cheng, L. (2012) Increased oceanic microplasticdebris enhances oviposition in an endemic pelagic insect. Biology Letters. 8, 817-820.

Received: **28.10.2019**
Accepted: **25.01.2020**

CORRESPONDING AUTHOR

Yifeng Zhu
School of Marine Science,
Ningbo University, Ningbo, 315211

e-mail: zhuyifeng8888@21cn.com

© by PSP Volume 29 – No. 05/2020 pages 3714-3723 Fresenius Environmental Bulletin

REGIONAL ADAPTATION AND BREAKTHROUGH OF THE LIVELIHOOD WAY OF THE MOUNTAIN ETHNIC GROUPS IN THE SOUTHEAST FRINGE OF HIMALAYA FROM THE PERSPECTIVE OF SPACE PRODUCTION

Peishen Li[1,2], Zhisheng Zhou[1,*]

[1]College of Tourism and Geography, Yunnan Normal University, Yunnan, China
[2]School of Business and Tourism Management, Yunnan University, Yunnan, China

ABSTRACT

The southeastern fringe of Himalayas is the extension of Himalayas to the southeast. In geography, Himalayas transformed from east to west, and now it transformed from northwest to southeast. Geopolitically, it includes vast areas in northwestern Yunnan, southern Tibet, northern Myanmar, and northeastern India. The steep altitude difference and the vertical climate distribution together create a regional natural space with diversity. From the perspective of space production, the mountain ethnic groups living in this area create a set of livelihoods respectively, which are compatible with the complex and diverse natural spaces in the process of interacting with the natural space. The exchange behavior among ethnic groups is the beginning of the way in which the mountain peoples of different livelihood types breakthrough their own livelihoods. The emergence of trade activities will link the mountainous ethnic groups of different livelihood types across the Himalayas into a whole with a common cultural identity. The process by which its livelihoods achieve breakthroughs in the process of space production is also a process of different cultural blending.

KEYWORDS:
Space production, southeastern fringe of Himalaya, mountain ethnic group, livelihood way, breakthrough

INTRODUCTION

Henri Lefebvre (1974), who supposes that space is a product of society, a result of purposeful social practice, and a product of social relations, proposed space production. Space is never cavernous. It often contains certain definitions. Different social forms have different production methods. Each production method has a corresponding and unique space for production. Any nation has its own survival space [1]. In order to survive in this particular space, humans must adjust their behavior to adapt to the environment to meet the needs of food, water, and shelter. This method and means necessary for food, clothing, and housing is a livelihood. The means of livelihood refers to the whole set of living-making means adopted by the human community, which adapt to different environments. The survival and development of any nation depends not only on the natural space made up of the natural environment, but also on the complex social and spiritual spaces formed on the basis of natural space [2]. Under the interaction of specific natural space, social space and spiritual space, the nation and its culture can have slowly formed and developed. As a means of utilizing and coordinating the natural and social environment of the nation, it has also been formed and continuously improved. The mountainous group refers to the minority group living in the jungle where the terrain is relatively high, and the non-host country, which the agriculture is based on mountain agriculture.

In the 1960s, scholars engaged in mountain research in northern Thailand began to use the *"Hilltribes"* and *"Highlanders/ Uplanders"*, which addresses to mountain groups. In 2005, the term *"Zomia"* in Mizo-Kuki-Chin refers to the vast area from the highlands of central Vietnam to the northeastern part of India, its geographical scope includes Vietnam, Thailand, Cambodia, Laos and Myanmar as well as China's Yunnan, Guizhou, Sichuan and Guangxi provinces. In 2009, *Scott* once again interpreted the geographical concept "*Zomia*", who believed that several ethnic groups living here interacted with each other through material exchange and trade between the highlands and the lowlands, thus escaping civilized rule. The southeastern fringe of the Himalayas in this paper is also within the scope of "*Zomia*". Its regional scope mainly includes the northwestern part of Yunnan, the southeast of Tibet, the northeastern India and the northern Myanmar. Due to the similar development of productive forces and similar geographical environment, the mountainous ethnic groups in this region have similar economic life and cultural characteristics. Thereby forming a similar way of livelihood, and thus forming their own unique form of

space production. From the dimension of "reproduction" of space, we can see that with the development of society, the mountain ethnic groups continue to breakthrough their closed livelihood types. A close relationship among different types of livelihoods is created, linking the Himalayan region into a whole space with common cultural characteristics.

LIVELIHOOD TYPES OF THE MOUNTAIN ETHNIC GROUP IN THE SOUTHEASTERN FRINGE OF THE HIMALAYAS

The geographical space of the alpine valleys on the southeastern fringe of the Himalayas promotes the spatial pattern of the three-dimensional distribution of the mountain ethnic groups. This usually leads to different livelihood types of the same people because of different survival spaces. For example, Tibetans are also living in plateau grasslands for nomadic living, some are living in mountain valleys for farming, and some other Tibetans are living in the transitional zone of agriculture and farming with animal husbandry.

Plateau animal husbandry type. Tibetans, Sherpas and other ethnic groups living above 4,500 meters above sea altitude are typical representatives of the highland animal husbandry economy. They rely on herding and raising Tibetan sheep, Tibetan goats, yaks, horses, and other livestock to live a nomadic life. Because the climate characteristics vary from place to place, the time of rotation varies. The herdsmen of northern Tibet whispered: "Spring is released in the summer and the mountain is released; in the autumn, the hillside is placed on the beach." The Tibetan monks in southern Tibet said: " In the spring, the water is grazing, and in the summer, it is grazing in the mountains; in the autumn, it grazes on the hillside and in winter, it grazes along the riverbank." In the humid and semi-humid areas in the southeastern part of the Qinghai-Tibet Plateau, the pastures are divided into summer-autumn, winter-spring, and spring-autumn. In this way, the people who choose the livestock livelihood method in the plateau often form a situation in which the whole family grazes. Generally choose to live in a place with water plants, and arrange the production of agricultural and sideline industries centered on the pasture. The fixed houses are not used for storing food and valuable households. People generally live in pastures in pastures, usually in the same room as humans and animals.

Types of farming livelihood. Rotation system of shifting cultivation. This method of livelihood is to choose a piece of land in the forest every year. After cutting down the trees, the roots and weed leaves of the dead wood are cleaned, dried, and then burned with fire. The burned land uses charcoal as fertilizer and then turns the ground. Under the corn, buckwheat, potato and other crops, no need to fertilize, and the land fall after the harvest is completed. The cycle of fallow is determined according to the situation of vegetation restoration. Generally, it takes seven or eight years if it takes less than three or five years. In the next year, new mountain farming will be burned, and then fallow. This kind of fallow land is called a rest in our country, and it is called *Jhoom* in northeastern India. The mountainous people using traditional farming methods are distributed in the northwestern part of Yunnan, in the south and in the south of Tibet, including the Tibetan, *Derung*, *Nu people, Lisu people, Jingpo nationality, De'ang people, Wa people, Lahu people, Yi people, Hani people, Jinuo people*, *Zemia Nagas, Gallo people, Mizo people* in northeastern India, and *Kachin* in the highlands of northern Myanmar. The *Kachin* people called this land a monsoon rainland. A clear set of methods has summed up for how to plant this kind of forestland. In addition, the *Nagas, Chin, and Garos* of the northern Burma are all users of the rotation system. In India, the *Dimasa Kachari* was chosen by the village head "*Gumpola*" to select "*Jhoom.*" The *Mikirs* decided by the village elder "*Hawar*".

Rice farming type. The mountainous people adopting this type of farming mainly include *Bai, Yi, Hani, Achang, Keno, Pumi* and most of *Menba, Tujia, Jingpo, Naxi, Lahu*, and so on. *Tibetans and Luoba* ethnic group also have a small part of this type of livelihood. Among them, white, alfalfa, Hani and other ethnic groups have a long history of growing rice. The Hani people are also famous for their good terraces. They have terraced terraces that stretch from the valley to the top of the mountain, and use the natural conditions of how high the mountains are and how high the water is. Terraced irrigation is introduced through the *Laoshan Shuigou. Kayin* and the northern part of Shan State, which are in the upper reaches of Myanmar's Qin-Dunjiang and Irrawaddy rivers, and the Kaya and Naga in the mountains of Myanmar. China, Myanmar, and India are typical representatives of mountainous irrigation terraces. They are good at planting rice, oued, corn in the mountains. In addition, it barley supplemented by fishing, hunting and raising pigs, and raising cattle. The Yi residents living in the lowlands have made a living by planting rice. While living in the west of the *Hugong* Valley, they are more likely to belong to *Kachin* (*Jingpo*). The western frontiers of the Assam region of India are usually also rice-growing areas. The *Nujiang* River and the *Derung* River Basin in the northwestern part of Yunnan belong to the alpine valley and the climate is relatively cold. Most of the geographical areas are suitable for land rice cultivation. Tradi-

tional cultivated crops mainly include alfalfa, millet, alfalfa, sorghum, barley, and oats.

Farming, animal husbandry, hunting, collecting mixed type. This is the livelihood of Tibetans living at 4,500 meters below sea altitude and some Yi people living in Wumeng Mountain and Liangshan Mountain area, some Qiang Nationality, Lisu nationality, and Nu people living in *Gaoligong* Mountain. The habitats of these ethnic groups are cold and high in climate. In addition to cultivating crops with short growth cycle, cold tolerance, and drought resistance, such as barley, wheat, buckwheat, rapeseed, and peas, they also graze sheep, Tibetan goats, yaks, oxen, goats, and horses. Grazing is a regional vertical grazing based on seasonal changes. This grazing method is conducive to balancing the consumption of diverse forage resources, so that livestock can breed throughout the year. Its form of expression is: people living in the warm and humid climate of the valley to cultivate crops, in the summer moved to the mountain pastures above 3,500 meters above sea altitude to find rich resources such as Cordyceps, Coptis, Matsutake and other nature gifts. This type of livelihood in the "summer in mountain, winter into the deep valley" combines the traditional farming, animal husbandry, and collection industries, showing a distinct vertical distribution of livelihood types. In this way, people can get all the natural resources from the lowland valley to the Plateau Mountains. Similarly, as a sideline of ploughing, due to the implementation of multi-species mixed planting, there are also many plant species, which increases the coverage of the surface and is conducive to controlling soil erosion. Tibetans refer to this way of livelihood as "Semedro" or "Sam Mabrog" [3]. In addition, fishing and hunting has greatly expanded the variety of living materials of mountain people, enabling people living in the mountains to survive in the harsh natural environment. Through archaeological excavations of the ruins of the Cangwu and Haimenkou sites, we believe that at the latest in the Neolithic Age, there were already Bai people's ancestors living in the Cangshan and Bohai Sea areas. They were engaged in simple farming, animal husbandry, fishing and hunting production, insects on the mountain forests, rivers, and lakes. The fish and shrimp are all visible. The Yi and Nu people have fishing nets in almost every family, and households have bows. The fishing and hunting life not only enriched the food types of mountain residents, but also prompted people to invent a variety of fishing and hunting tools such as forks, nets, bows, slingshots, javelins, and meteors.

REGIONAL ADAPTATION OF LIVELIHOOD TYPES - PRODUCTION PROCESSES IN SPACE

Henri Lefebvre divides space into three categories: natural space, spiritual space, and social space. He believes that natural space can have measured and depicted accurately within a certain range, which derived from the natural material space. Spiritual space is a kind of constructed space such as human consciousness, signs, and symbols, and so on. It is a concept and imagination of space. Social space refers to the space created by people in real life or in social life, including various things and relationships, which promote the flow of material objects and information [4]. Since human beings always move within a certain space, such human activities will inevitably reflect the natural ecology of a particular natural space, and the ideology and production relations that are compatible with the natural space cannot transcend the influence of the natural ecological environment.

Natural space formed by livelihood types. Himalayas are located on the fringe of the southern foot in Qinghai-Tibet Plateau, it is from northwest to southeast across the China and South Asian subcontinent, which is from the Nanga-Palbat peak in Kashmir (8125 meters above sea altitude) to the Nanga Bawa peak at the turn of the *Yarlung Zangbo* River. It is 2,850 kilometers above sea altitude, with a total length of 2,450 kilometers and a width of 200 to 350 kilometers. More than 110 peaks are over 7350 meters above sea altitude, with an average elevation of over 4,000 meters and more than 6,000 meters covered with snow. As the terrain gradually rises from the southeast to the northwest, the hot and humid summer southeast monsoon traces back to the plateau along the valley, and its influence has gradually weakened from the southeast to the northwest. The climate type adapts to it also gradually transitions from warm-wet to dry-cold. This forms a natural space composed of mountain forests, alpine meadows, alpine grasslands, and alpine desert landscapes.

There are mountain ranges such as Gaoligong Mountain, Nu Mountain and Yunling in the regional space. The rivers such as Derung River, Nujiang River, Minjiang River and Jinsha River are gathered. Many mountain valleys make the natural space of this area and the vast Himalayan snow-capped mountains. The natural spaces are extremely similar and together with the Himalayan region constitute a complete and vast geographical unit [5]. The natural factors of high temperature, lack of oxygen, and the vertical change of the biological climate and the horizontal changes directly lead to the large difference in the vegetation types of the grassland in this region. In line with the natural landscape in the area, Tibetans generally live in a

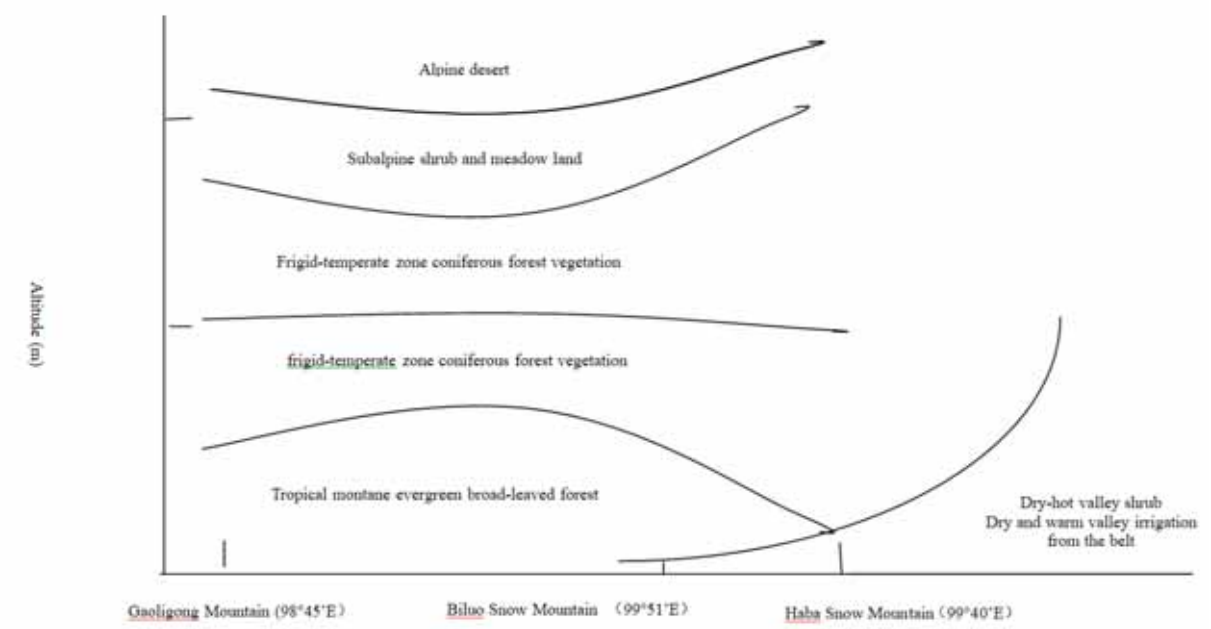

FIGURE 1
27" 30' vertical natural zone change along north latitude
Source: Yang Qinye and Shen Kangda, vertical natural belts in the Hengduan Mountains area, northwestern Yunnan. Acta Geologica Sinica, 1984 (02), pp. 141-147.

valley from an altitude of 1,800 meters to a mountain area of 3,500 meters above sea altitude. The corresponding livelihoods cover the three-dimensional vertical livelihood from the valley to the mountain. The yak, which is widely bred by Tibetans and has strong adaptability to the ecological environment, can adapt to the thin and cold highlands of the air, and adapt to the arid and hot valleys. It can live freely and progenize in the harsh natural environment. Even more Tibetans provide dairy products such as ghee and milk residue. Tibetans living in the temperate valleys have long formed a combination of farming, animal husbandry and harvesting methods of "In summer, they are active in the mountains, and in winter they are active in the deep valley.", showing obvious characteristics of vertical distribution of livelihoods. Mountain-canyon ecological environment survival choice.

The Sherpas people live mainly on the mountain plains of the southern Tibetan Plateau and northern Nepal. They are located in subtropical and warm temperate zones with an average elevation of about 2000 meters. The climate is warm and humid, and the original forests are densely covered. The mild climate provides good conditions for the Sherpas to develop animal husbandry. However, due to the lack of improved livestock breeds and pastures, and the habit of Grass pruning, the Sherpa can only change the pastures with the change of climate, forming winter and spring festivals under the mountains, and moving to the higher mountains during the summer rainy season. After the fall, the nomadic livelihood method is very similar to that of the Tibetans. This type of livelihood, in which individuals or families move with the seasons, is widespread among nomads in the southeastern Himalayas [6].

Spiritual space formed by livelihood types. Different social forms have different production methods, and each production method has its own corresponding and unique space production.

This is because the society is in an established and exclusive mode of production. Its special nature has created space. The practice of space not only defines space, but also gives space society practicality. In such an inheritance, there must be a trace of history, and the characteristics of society are superimposed in space [7]. From this perspective, it is not difficult to understand that the Himalayas are both a concept of a geographical space and a concept of a cultural space. In the formation and development of different livelihood types in the natural space of the southeastern fringe of the Himalayas, the spiritual space that is compatible with it has also formed and developed.

In the southeastern fringe of the Himalayas, there is Tibetan Buddhism that is mainly popular in the northern mountains of the Himalayas. It prevails in Hinduism in the southern Himalayas of the Indian plains and in Islam, which is prevalent between the plains of Assam in India and the southeastern Himalayas. Among these different religious beliefs, Tibetan Buddhism has the largest number of believers in the region and the widest space for communication. Tibetan Buddhism believes that the world is a place that can provide support for sentient beings, but at the same time, it is a material system, which changes constantly. In this way, it is

not difficult for us to understand that Tibetan Buddhism believes that human activities change the natural environment, and the deterioration of the natural environment affects human survival. Therefore, the nomadic people represented by the Tibetan people in the southeastern fringe of the Himalayas have developed a mixed farming and animal husbandry basis based on the cattle, horses, sheep, and other animals provided by the local people in the natural environment of the mountain-gorge. At the same time, these animals are often deified, so we can usually see the clues in the numerous animal figures in Tibetan Buddhist monasteries. This is also the embodiment of the spiritual space that is constructed because of the production of natural space.

It is noteworthy that the southeastern fringe of the Himalayas also has "primitive religions" that are common in different nationalities and cultures. They are divided into natural worship, totem worship, reproductive worship, hero or ancestor worship. Even though each nation has its own different religious beliefs, it is more or less able to find the existence of primitive religion. Taking nature worship as an example, nature worships all things and spirits. They firmly believe that nature, earth, day, month, star, landscape, trees, and other natural things are full of vitality, that is, people and everything are interdependent and symbiotic. The reason is as follows. On the one hand, the natural conditions of the southeastern fringe of the Himalayas are harsh, natural disasters such as avalanches and mudslides occur, and there is serious alpine hypoxia. The local people have placed their hopes on life above the supernatural forces. Under the control of the pan-spiritual beliefs, most of the ancestors living in the Himalayas prayed for the gods to bless the race, the abundance of crops and their own safety. On the other hand, they are grateful for the gifts, food, shelter, and other resources that nature has given, and express their gratitude in a pious manner to repay the grace of nature. In addition, this spiritual space is constructed in the natural space production process.

Social space formed by livelihood types. The social space contains the production relationship and the reproduction relationship. The production relationship is the social relationship formed in the process of material data production. It is the social form of production mode, that is, the division of labor and the organization according to the hierarchical social function. The social relationship of reproduction is the gender. The social relationship of reproduction is the relationship between the physiological relationship of two sexes and the age group within the family organization [8]. In these relationships, marriage is a social behavior and a social phenomenon. It is determined by the economic foundation of a certain society. It changes with the development of social productivity, which promotes social and social productivity.

In the various ethnic groups on the southeastern fringe of the Himalayas, there have been marriage systems such as group marriage, polyandry, polygamy, and monogamy. In general, the southeastern fringe of the Himalayas is a relatively concentrated area of polygamy marriage system, which is still meeting the production and reproduction needs of mountain residents. Among the 430 Tibetan families on the Sino-Indian border, the proportion of brothers and wives is 65.6%. The polyandry system has several forms of brothers and wives, friends and wives, and very few fathers and sons. The most common is that several brothers share a wife in a family. The main reason for forming a polyandry system is to maintain the concept that a big family does not separate. The southeastern fringe of the Himalayas is vast, sparsely populated, with a bad climate, lack of resources, frequent natural disasters, traffic jams, and it is difficult for small families with few people to survive in such natural spaces. In order to maintain a livelihood and promote further family prosperity, the use of polygamous marriage methods is more labor-intensive, raising fewer children, and the family, land, cattle and sheep will not be dispersed. Therefore, families with polyandry are often richer than monogamous families. Monogamous families are adopted. Once the males in the family are separated, they will split the property of the family and weaken the power of the extended family. Furthermore, the spiritual space of the southeastern fringe of the Himalayas - Tibetan Buddhism believes that contraceptive measures and abortion are equivalent to killing, which is not allowed for the teachings of Dharma. However, the scarcity of resources and the harsh living environment in Tibet have made many families aware of controlling population growth. In this way, whether it is polygamy or polyandry, the essence of both forms of marriage is to maintain the scale of the family economy and the concentrations of property, which prevent the outflow of family property. It is also possible to concentrate the family's means of production and the marriage form of the workforce and thus become the best form of marriage that best suits the region. This is the product of the production of mountainous groups in the natural space of the southeastern Himalayas, and the direct reaction of the social relations of various ethnic groups across the Himalayas in social space.

BREAKTHROUGHS IN LIVELIHOOD TYPES - SPACE REPRODUCTION PROCESS

Lefebvre believes that with the development of the historical stage, production in space begins to shift to the production of space. "The production of space" refers to the production of space itself rather

than the production inside space. It is a process of creating a space product, which meets the needs of reality through the reconstruction or resetting of material data in physical space. The production of space is human [9]. The process of creating space products that meet the needs of their own survival and development, that is, through the flow of energy, raw materials, and labor, the traditional economic and cultural types break the original isolation and existence, and represent the spatial integrity.

Business contacts - the interconnection of different types of livelihoods. In the southeastern fringe of the Himalayas, the mountain ethnic groups show the natural selection and adaptation in the interaction between human and natural space through the livelihood methods of plateau animal husbandry economy, farming economy and mixed farming economy, which is the process of space production. However, the emergence of trade and communication has further promoted the further exchange and interaction between the mountainous people and the natural space. It has also become a common strategy for the Himalayas to adapt to nature and develop in the natural space, and to reproduce the space.

The emergence of the original exchange. The different subsistence types of the mountain population in the southeastern Himalayas have become the basis for the exchange of products between ethnic groups or clans in different regions. The exchange of clan products before the social division of labor is only an accidental exchange behavior, which is mainly manifested in the gifting and rebates of different groups of different livelihood types. For example, the *Derung* and Yi people living in the *Hengduan* Mountains in the southeastern fringe of the Himalayas will bring their own special local products to visit relatives and friends after the harvest, and the master will give back their own special local products. This friendly and enthusiastic exchange takes place several times. However, this primitive exchange, which is limited in both the number of times and the number of exchanges, is a gift. It promotes the germination of product exchange and creates a powerful force that drives human society to the era of commodity economy today. It is also this kind of original exchange, which opens the prelude to the interconnection between different types of livelihoods. It enables the mountain people living in the Himalayas to engage in different types of livelihoods through trade practices, and gradually develop into an interconnected whole.

Development of inter-ethnic transactions. Among the various mountain groups in the southeastern fringe of the Himalayas, the form of trade exchange between the various ethnic groups and the surrounding areas is mainly realized through material exchange and non-governmental trade between different types of livelihoods in the mountain and dam areas [10]. The ethnic groups living in mountainous areas, semi-mountainous areas and dam areas depend on each other for interdependence. Ethnic groups in high-altitude areas require tea and salt at low altitudes, while groups in low-altitude areas require medicinal materials, wood, fur, and mountain goods at high altitudes [11]. At the same time, inter-ethnic trade between Lhasa and Bhutan took place through Mughal and Kashmiri through India's Patna and Nepal. The Bai merchants continued to transport Yunnan's tea, salt, homespun and other daily necessities to the Kangzang area. A special wool blanket deal connects Nepal with North India. This inter-ethnic trade activity is carried out through trade routes formed by rivers and canyons in the Himalayas, which are closely linked to different livelihood types. In the inter-ethnic exchange, each ethnic group also broke through its original type of livelihood and formed the reproduction of the living space of its respective ethnic group.

Formation of regional trade networks. The development of inter-ethnic transactions promoted the development of the inter-ethnic trading circle, and the inter-ethnic trading circle promoted the formation of the Himalayan regional trade network. As the inter-ethnic trading space continues to expand, channels between different regions and countries within the Himalayas have gradually opened up, and even remote trade activities across the Himalayas have emerged. These trade routes connect regional ancient roads between ethnic groups in various regions and form a wider trade network. A large number of documents document the close links between the different subsistence types of the Himalayas through the trade routes such as the "Southern Silk Road", "Five-foot Road", "The Sichuan Poisonous Road" and "Tea-horse Ancient Road". For example, Tibetan monks, toasts, wealthy businessmen, and civilians, either to support their families or to make profits, have rushed to Lijiang, Zhongdian, and the arrow furnace to set up business names, run caravans, and travel hard to the ancient road of business on the snowy plateau. Items such as shackles, ironware, lacquerware and bamboo sticks appear in Southeast Asia, South Asia and even in West Asia, while jewelry, spices, glazes, wool products and other artifacts in South and Central Asian countries can also be found in the Mainland. From the Shizhai Mountain in Jinning, Yunnan, more than 2,000 years ago, the ancient tombs of the ancient monks were excavated in India. It is inferred that the ancient Shu Kingdom, which was in the interior of China, was associated with West Asia, South Asia and Southeast Asia and the Indian Ocean more than 2,000 years ago. The

ethnic groups along the fringe have close trade relations, and the Beihai currency closely links the ethnic groups in the Himalayas to form a broad trade circle. This situation further confirms that the Himalayan region may be a complete regional market for a considerable period. With the establishment of the capitalist world system, India and Myanmar have become the UK's trade markets, and the countries and regions of the Himalayas have also become part of the world market system and have been included in the global trade network.

In the context of economic globalization in recent years, the growth environment of similar cordyceps, pine mushrooms and other globally integrated Cordyceps markets has enabled farmers and herders in the Himalayas to form a common dependence on the Cordyceps market and form a similar "New collection economy" type. The transition of production methods is accompanied by the creation of new spaces, which reflects the process of creating space products that meet the needs of their own survival and development, as well as the holistic nature of the Himalayan region.

Consistency of spiritual space. With the development of trade activities, the livelihood types of the mountainous ethnic groups in the Himalayas are also evolving, showing the trend of transition and development towards settled farming. The reasons for the change are in addition to the influence of commercial activities, but also in the Himalayan region. The reduction in the spatial extent of livestock and ploughing reduces in the number of organisms. This transformation has objectively promoted the links between the various ethnic groups with the settlement of farming culture. The interconnection between different types of livelihoods will be integrated into the completely Himalayan region, and different ethnic groups will conduct business activities on many trade channels. At the same time, the culture of diverse forms is also colliding, so that the spiritual space formed on this basis tends to be consistent in this process.

We have noticed that all kinds of religions popular in the Himalayas have shown special attention to space and all things that the original religion advocates show the worship of natural space. Bon religion and shamanism divide the universe into three layers of heaven conception, earth, and underground. The three generations of Buddhism, the four major ministries, and the Nirvana realm all emphasize the sense of space. Obviously, the open natural space of the Himalayas has long-term effects on the formation of spiritual spaces for people, who have lived and produced here for a long time. As a common survival space of many local ethnic groups, people's strong and firm belief in the Himalayas has enabled the ethnic groups to understand, connect and identify in culture, and promote the consistency of spiritual space.

At the same time, along with the development of commercial activities, Tibetan Buddhism spread to other ethnic minority settlements in Lijiang, Dali and Nujiang. The main temple of the Bai nationality and the three temples of the *Naxi* people have recognized by the Tibetans. More typical is the Maquan River, the source of the Yarlung Zangbo River, the Peacock River from the source of the Ganges River, the Xiangquan River, and the Shiquan River, the source of the Indus River, near the Gang Rinpoche in Ali, Tibet. At the source of the great rivers, people in the Himalayas rely on these rivers to supply water, and through these natural passages to conduct business activities, merchants as the carrier of communication to connect these relatively independent cultural systems. As a result, Gang Rinpoche has also become a mountain of common belief in Hinduism, Jain religion, Bon religion, and Buddhism. The beliefs of these four religions to the gods of Mount Rinpoche are from the mountains of the local primitive nature worship to spiritual beliefs. Through the natural passages carrying business activities near the Gangriboche Mountain, different ethnic groups and believers converge, infiltrate and integrate with each other, which ultimately forms a strong cultural root of the religious beliefs in the area, and also contributes to the consistency of spiritual space.

The integrity of social space. The trade between the mountainous ethnic groups of different livelihood types has brought frequent contacts of various ethnic groups. The commodities used for inter-ethnic exchange have condensed people's emotions and concepts, which subtly exported certain national values and customs. The lifestyles of various ethnic groups, the continuous absorption, and blending of values have gradually formed a more consistent social space for the mountainous groups on the southeastern fringe of the Himalayas.

At present, most of the ethnic groups in the southeastern fringe of the Himalayas have a monogamous marriage system. Among them, the *Hani, Yi, Achang, Jingpo, Naxi and Yi* people include the *Kachin people* in northern Myanmar, the common characteristics of the *Naga, Mizo, and Mikir* in northeast India. Young men and women have full freedom of love before marriage. Most ethnic groups in the Himalayas adopt “public housing” to facilitate the social activities of young men and women. Young people sing and talk about love in public houses or in the mountains. In addition, some of the concepts and customs left over from the typical marriages of the aunts who were very popular among the mountainous peoples on the southeastern fringe of the Himalayas have become the mate selection criteria for the mountainous groups in the southeastern fringe of the Himalayas today. For example, *Jingpo, Yi* and other ethnic

groups follow the symbolic ritual of "*you nver xian wen jiu*".

The more obvious feature is the link between different ethnic groups and ethnic groups through trade activities, the mutual integration of ethnic groups and ethnic groups is increasing, and the marriage system within the ethnic group is gradually disintegrated. It is located in *Bingzhongluo* Town, *Gongshan* County in the upper and middle reaches of the Nujiang River, with more than 10 kinds. In the case of ethnic groups living together in a village, inter-ethnic marriage is more common. There is even a family member with Tibetans, Nu, Bai, Han, Derung, Naxi and other ethnic groups. However, family members respect each other. Do not interfere with each other; the family is harmonious and happy. Tibet's Chawalong, near the Gaoligongshan area in northwestern Yunnan, was once an important town in Tea-horse Ancient Road. The old people in Chawalong's old age will speak many words, such as Suli, Naxi, and Nu (Morang) national languages. Most ethnic minorities living in the Nujiang River Basin have many Tibetan customs in their daily lives. The common marriage system and customs have linked the Himalayan region into a whole. The ethnic groups of different livelihood types have realized the reproduction of social space in the development of trade in the southeastern fringe of the Himalayas.

RESULTS AND DISCUSSION

The diverse natural spaces of snowberg mountains, canyons, meadows, rivers and lakes on the southeastern fringe of the Himalayas are the basis for the livelihoods of mountain ethnic groups living in this region, and the different types of livelihoods are not only adapted to nature in the southeastern Himalayas. The survival strategy developed in the natural survival activities is also the interaction result of mountain residents in the natural space, which is the space production compatible with the harsh natural space of the Himalayan region.

As social productivity continues to advance, trade activities among ethnic groups begin to emerge, linking mountain ethnic groups of different livelihood types. The formation and development of trade routes such as "five feet road", "The Sichuan poisonous Road", "Tea-horse Ancient Road" and "the Southern Silk Road" are the products of objective social history development along the route or in the production process of a certain space. It is also the product of the common needs of all ethnic groups living in the Himalayas. Objectively, the ethnic groups of different livelihood types have continuously blended and interacted, so that the growing trade network connects the traditional types of livelihoods that were originally isolated and existed, and the southeastern fringe of the Himalayas is connected to the vast areas across the overall area of Himalayas.. At the same time, the process of the convergence and integration of different ethnic cultures on these trade routes is also the process of spatial reproduction of the various ethnic groups.

Since modern times, the economic and social development of various ethnic groups and regions in the Himalayas and the common needs of business activities have been the basis for the formation of trade channels and their long-standing support. The existence of these trade channels further promotes the inter-communication among the various ethnic groups and brings the Himalayan region closer together. However, with the changes in the modern international order, the world pattern has also undergone major changes. The Himalayan region also presents complexities in terms of ethnic relations and borders.

Spiritual space and social space are not only the carrier of culture, but also "produce" new spiritual and social spaces carrying different cultures in the interaction and communication of culture and space, so space is also a place of "reproduction". . The current "The Belt and Road" strategy proposed by China is a systematic and ambitious concept. It is a reflection of the geography, ethnicity, and culture across the Himalayas from the dimensions of the new era. It is the concrete manifestation of production in space. The stages are required across the development of the Himalaya countries and regions. Throughout the vast area across the Himalayas, it has been a "space" of ethnicity and its economic and cultural diversity since ancient times. The spread and interaction of different nationalities and their cultures constitute the main theme of the history of the Himalayans. Diversity is the development of the Himalayan culture in the mainstream of history. The objective geomorphology and the long-term development of history have led to various exchanges or connections between the various countries and regions across the Himalayas at the ethnic, economic, political, and cultural levels. It reflects the development and evolution of social history in Asia and the world, and it has extremely rich and profound connotations. So far, the spiritual space and social space formed based on natural space have also become more consistent, making the southeastern Himalayas a "space" for the nation and its economic and cultural diversity. This is not only the result of the interaction between the nation and the "space", but also the result of the "space" shaping the national culture.

ACKNOWLEDGEMENTS

This paper is funded by the project: National Social Science Fund Major Project "Study on the History of Exchange and Interaction Development

in the Tri-Border of China, Myanmar and India" (NO.: 0130060402001).

The research content of this paper is funded by the project: the national social science general project "Study on the coordinated integration of the Lisu culture identity and Chinese cultural identity" (project number: 18BMZ034).

REFERENCES

[1] Henri, L. (1991). The Production of Space. Wiley-Blackwell. 154-155.
[2] Sun, Q.Y. (2004) Cultural Anthropology Course. Beijing: National Publishing House. 163-164.
[3] Shen, H.M. (2016) The Himalayan Ecology-Social and Cultural Integrity - Also on the Path and Method of Regional Research in Yunnan Meili Tibetan Area. Journal of Southwest University for Nationalities (Humanities and Social Sciences Edition) .7,1-7.
[4] Christoph von, F. (1979) [English] - Haimendorff. The economic life of Sherbba in Nepal. Translation by Wu Zelin. Beijing: Mimeographed. 3-5.
[5] Bao, Y.M. (2005) Space Culture and Urban Research Wenhui Daily. 11, 6
[6] Gong, B.Z.X. and Q, C. (2011) On the Ecological Thoughts and Social Influence of Tibetan Buddhism. Journal of Sichuan University for Nationalities (bimonthly Founded in 1986) .1-4.
[7] Zhang, Q.G. (2010) The Main Reasons for the Harmonious Coexistence of Multi-ethnic Religions in Yunnan.Religion Studies of the World. (3), 19-25.
[8] Lu, H.L. Cultural Interaction across the Himalayas: Prehistoric Archaeological Studies in Western Tibet. Science Press, Beijing. 176-177
[9] Jiang, L.X. (2005) Economic and Cultural Types: The Material Basis of Ethnic Relations in Southwest China. Journal of Southwest University for Nationalities (Humanities and Social Sciences Edition). 26 (5), 26-29.
[10] Gu, H., Tan, Q.L. Multi-Historical History and Identity of Cross-border Ethnic Groups in Yunnan. Journal of Yunnan Nationalities University (Philosophy and Social Sciences Edition). 26(1), 60-64.
[11] Ma, G.J. (2009) Economic Development and Ecological Adaptation - Taking the Changes of Traditional Livelihoods of the Three Ethnic Groups in Yunnan - Guizhou Plateau as an Example. Guizhou Ethnic Research. 3,127-132.
[12] Qiu, R.F. (2010) The Traditional Model of the Symbiotic Development of Diversity Culture in Minority Areas. Frontiers. 1, 76-79.
[13] He, Y.H., He, D.Y. (2007) The Historical Origins of the Indian Himalayas in India and the Tibetan and Burmese Ethnic Groups in Southwest China. Journal of Southwest University for Nationalities (Humanities and Social Sciences Edition). 5, 18-22.
[14] Gao, E.H. (2018) The field research on the field of space production theory. "Bohai University Master Thesis".6, 5-6.
[15] Ci, R.Z.M. (2013) A survey report on monogamy and polygamy marriage in Qiangbai Village, Nianxi Township, Jiangda County, Changdu District. Tibet Development Forum. 4, 68-72.
[16] Wang, X.Y. (2014) From ethnic marriage to transnational marriage: the change of ethnic minority marriage circle on China - Myanmar border. Thought Front. 6, 54-57.
[17] Duan, J.S., Li, H.K. (2016) Geography, Ethnic Groups, Culture - A Historical and Realistic Reflection on the "Belt and Road" Strategy and the Relationship between the Southwest Frontiers. Journal of Northern Nationalities University (Philosophy and Social Sciences Edition). 3, 43-47.
[18] Gong,B.J.D. (2018) Study on the Commercial Activities and Cultural Exchanges between the Ancient Tea Horses and the Ancients. Journal of Sichuan Nationalities University. 2,1-7.
[19] Lv, H. L. (2015) Research on Early Tombs in Western Himalayas. Acta Archaeologica Sinica. 1, 1-34.
[20] Zhang, M.L., Zou, N.Q. (2018) Study on the Migration Flow and Inter-ethnic Relationship of the Tai-Yu People in the Interpretation and Interpretation Areas of Yunnan, Tibet, and India. Journal of Ethnology. 4, 39-48
[21] Xia, M. (2002) The Religious and Cultural Function of the Songs - An Introduction to the Himalayan Mountain Songs. China Tibetology. 1, 92-98.
[22] He, Y.M., Zhao, S.L. (2014) Analysis of the Variety of Marriage and Family Forms in Tibet during the Qing Dynasty and the Republic of China. Journal of Guizhou Nationalities. 8, 189-193.

Received: **30.10.2019**
Accepted: **10.02.2020**

CORRESPONDING AUTHOR

Zhisheng Zhou
College of Tourism and Geography,
Yunnan Normal University,
Yunnan – China.

e-mail: zhouzhisheng_ynu@163.com

© by PSP Volume 29 – No. 05/2020 pages 3724-3731 Fresenius Environmental Bulletin

DETERMINING THE FORAGE YIELD AND CERTAIN CHARACTERISTICS OF SOYBEAN (*GLYCINE MAX*.L.) VARIETIES WITH DIFFERENT SOWING DATES

Melih Okcu[1,*], Halil Yolcu[2]

[1]Atatürk University, Faculty of Agriculture, Department of Field Crops, Erzurum, Turkey
[2]Department of Plant and Animal Production, Kelkit Aydın Dogan Vocational School, Gumushane University, Gumushane, Turkey

ABSTRACT

This research was conducted at Gumushane University, in the field of application of Gumushane University Vocational School of Higher Education during 2014-2015. The research was carried out in 3 replications according to the exact blocks trial pattern of chance during the season of breeding between 2014 and 2015. İn the research Nova, Arısoy, A-3127, Sa-88, Ataem-7, Bravo, Yeşilsoy and Yemsoy varieties were used, and different three sowing dates (1 April,15 April, 30 April).

According to the results, the highest values in terms of green grass and ADF values were given by Yeşilsoy cultivar. Yeşilsoy cultivar took the first place with 12123.3 kg / ha^{-1} in terms of green grass yield. In terms of hay yield, Arısoy cultivar gave the highest value with 5003 kg / ha^{-1}. The highest values in ADF, NDF and Crude protein content were Bravo 37.51%, Ataem-7 37.48%, Bravo 46.72%, Yeşilsoy 46.48%, Bravo 13.96%, Ataem-7 13%, 95 respectively gave the highest values. In terms of sowing time, sowing time of 1 April gave the highest results among the parameters examined. Therefore, while sowing time on April 1 was determined as the most suitable planting, Nova, Arısoy, Ataem-7, Yeşilsoy and Yemsoy varieties were the prominent varieties in terms of green, dry grass and crude protein.

KEYWORDS:
Soyabean, *Glycine max*.L., sowng date, forage yield

INTRODUCTION

As a member of the legume family, soybean is an annual summer crop and the seeds of soybean contains, on average, 18-24% fat, 36-40% protein, 26% carbohydrates and 8% mineral content. It is a widely utilized crop in various fields on account of its high grade protein that closely resembles animal based protein in quality, containing highly valued amino acids that acts both as nourishment for the stages of growth and development and as a booster for the said processes [1-2]. Soybean, which has the leading position in protein output per unit area of land cultivation, because its pulp offers high protein content after the extraction of vegetable oil from, is utilized in poultry rations in abundance as a high grade animal feed and also as a green fertilizer [3].

The most important attribute of soybean, comparative to other animal and plant based protein sources, is that it offers the highest and the cheapest protein output. For the lower production costs and high nutritional value it provides, soybean protein is preferred over milk, egg and meat protein in food production [4]

There are many limiting factors to soybean production. Included in this list of factors are inappropriate sowing dates, climate change, low germination rate, sub-par seed quality and humidity stress. Amongst these elements, sowing dates and plant densities are the highest impacting factors on the growth and development process, the bean yield [5] and the seed quality [6]. Discovering different soybean varieties and determining the agronomic mistakes made might be helpful in minding this gap.

Sowing date is a variable which has a substantial impact on the yield [7-8] and is one of the most significant cultural applications in soybean production [9]. Considering the economical aspect and the increase in yield, sowing date, is an excellent approach to soybean. [10-11].

Sowing at various sowing dates, impacts the developmental stages of soybean as a a result of different factors. These factors are, the variations in photoperiod [12-13], the air temperature [14], the distribution and the quantity of precipitation [15]. Sowing date has a substantial effect on the yield and the development of soybean. Early sowing in season may cause sub-par germination rates and limited growth. When the product is subjected to higher temperatures, in a day that is shorter than the critical length, it moves towards early maturing. If this occurrence takes place before plant reaches the sufficient height, the yield of soybean diminishes and the plant stays compact [16]. However, late sowing may shorten the vegetative stage and as a result, this diminishes overall dry matter accumulation, weakens reproductive organ

properties and potentially causes reduced yields [17].

This study is done to determine some of the properties and the yield of forage from soybean at various sowing dates.

MATERIALS AND METHODS

Plant Material. The research was conducted at Gumushane University, in the field of application of Gumushane University Vocational School of Higher Education during 2014-2015. The research was carried out in 3 replications according to the exact blocks trial pattern of chance during the season of breeding between 2014 and 2015. İn the research Nova, Arısoy, A-3127, Sa-88, Ataem-7, Bravo, Yeşilsoy and Yemsoy varieties were used, and different three sowing dates (1 April,15 April, 30 April) the parcel length was 6 m and width was 2.8 m and each parcel was formed 4 ordinary. 3 kg N, 6 kg P_2O_5 and 8 kg K_2O [18] were used as fertilizer at the time of sowing and also soybean bacteria culture (*Rhizobium Japonicum*).

In the experiment, there was no disease and harmful struggle or chemical struggle. When the plants were 8-10 cm long, weeds were taken by hand or with anchor and weeds were made between the rows. Half of each parcel was harvested after completion of physiological maturity for seed yield during the full flowering period for green grass yield, except for the beginning and edge rows of 0.50 cm in harvest.

According to the research conducted in 2014.2015 and the average for many years, the temperature did not fall below zero in 2014, while the temperature did not fall below zero in 2015 in February-November months. The highest temperature in July (20.20 C^0), the lowest temperature (-1.70 C^0) in January. According to the average of many years, the maximum rainfall in May (65.8 mm), the lowest rainfall in August (12,1 mm) was observed (Table 1.). Research land is poor in terms of PH: 7.6-7.8 and organic matter 2.21% in mild alkaline reaction with clay-tinned structure. The experimental area contains salt 0,04%, lime 0,99%, phosphorus 1,52 kg/da, potassium 32 kg/da (Table 2.).

Statistical Analysis. Results the results were analyzed with the help of SPSS 20.0 package program (SPSS Inc., 2010) according to the randomized blocks trial pattern. Differences between the mean were determined by Duncan multiple comparison test

TABLE 1
Parameters for Research years (2014-2015) and long years average (1960-2015)

MONTHS	2014 Monthly Total Rainfall (mm)	2014 Monthly Average Temperature (C^0)	2014 Monthly Average Relative Humidity (%)	2015 Monthly Total Rainfall (mm)	2015 Monthly Average Temperature (C^0)	2015 Monthly Average Relative Humidity (%)	Avarage Temperature For Many Years (C^0)	Sunbathing Period For Many Years	Humidity For Many Years	Average total precipitation for many years
JANUARY	28.5	0.8	59.1	55.5	-0.6	58.3	-1.7	1.20	68.5	35.2
FEBRUARY	22.1	2.5	45.6	34.4	2.2	55.8	-0.5	3.46	65.7	32.2
MARCH	45.3	6.5	46.8	67.4	5.5	50.4	3.7	5.02	63.5	41.8
APRİL	38.1	11.3	46.4	46.8	7.5	49.4	9.4	6.06	61.5	60.3
MAY	66.7	14.7	52.4	45.3	13.8	49.9	13.7	7.30	62.3	65.8
JUNE	31.0	17.8	44.1	40.6	17.9	52.3	17.2	9.12	61.1	44.3
JULY	19.3	21.7	36.7	2.8	20.9	38.7	20.2	10.04	60.2	12.7
AĞUST	12.4	23.0	34.9	5.7	22.8	42.2	20.1	9.46	60.5	12.1
SEPTEMBER	51.5	17.6	43.1	9.6	20.7	36.8	16.6	8.59	60.5	19.7
OCTOBER	61.4	11.5	54.1	50.1	12.5	55.8	11.4	5.33	64.7	42.0
NOVEMBER	51.6	4.9	55.0	79.4	6.0	52.4	5.1	2.12	68.3	41.1
DECEMBER	14.2	4.9	58.6	31.7	-1.9	64.9	0.4	0.51	69.7	39.9

TABLE 2
Soil parameters of the experiment area

Saturation (%)	pH	EC (ds/m)	Salt (%)	Lime (%)	Organic Matter (%)	Phosphorus (kg/da)	Potassium (kg/da)
44.0	7.44	1.48	0.04	0.99	2.21	1.52	32

RESULTS AND DISCUSSION

Fresh Grass Yield. The highest yield, in terms of forage and dry hay, has been acquired with 12123 kg/ha^{-1} from the Yeşilsoy variety and is followed by 12048 kg/ha^{-1} from the Yemsoy variety. The results of forage yields shows resemblance to; [19-20-21-22]. In terms of forage yield the highest value has been acquired with 10694,46 kg/ha from the sowing date of April 1st while the lowest value is acquired with 8822,51 kg/ha from the sowing date of April 15 (Table.3). [22] reported to acquire the highest forage yield from Erensoy variety and the lowest forage yields from Blaze, Adasoy, Nova, Cinsoy and May-5312 varieties. In terms of dry hay yield, while Arısoy variety takes the lead with 5003 kg/ha, it is followed by SA-88 variety with 4670 kg/ha. In terms of dry hay yield, the highest yield has been acquired with 4365 kg/ha from the sowing date of April 30 while the lowest yield has been acquired with 3893 kg/ha from the sowing date of April 15 (Table.3). On the subject of dry hay yield [22] has reported to achieve the highest dry hay yield from the Turksoy variety while acquiring the lowest yield from the Adasoy variety. In this study the highest yield has been achieved with Arısoy variety. Meanwhile, in a study done in Punjab, [17] achieved the highest biological efficiency amongst 3 different sowing dates with 5637 kg/ha from the sowing date of June 5, regarding the biological efficiency of varieties the highest value has been achieved with 5551 kg/ha from SL-744 variety. [23], in the study regarding 5 different sowing dates, reported to achieve the highest biological efficiency with 4430,5 kg/ha from the sowing date of January 28, in regards to varieties, the highest biological efficiency have been achieved with 4221,3 kg/ha from the Faisal variety. [24], in the study regarding 3 different sowing dates, reported to achieve the highest biological efficiency with 3095,58 kg/ha^{-1} from the sowing date of D_1 (25th MW). [24], in the study done in Bangladesh regarding the yield of soybean and the seed quality, reported to achieve the highest biological efficiency with 3995 kg/ha^{-1} from the sowing date of November 25.

TABLE 3
The effects of different sowing time and different soybean varities on some grass quality of soybean 2014

Varieties	Planting time	Fresh grass yield (kg/ha^{-1})	Hay yield (kg/ha^{-1})	ADF (%)	NDF (%)	Crude protein content (%)
NOVA	1 April	6540	3440	33.82	44.90	16.11
	15 April	10610	4100	32.26	43.22	14.10
	30 April	5200	3790	34.01	41.01	14.60
	Mean	**7450 d**	**3778 d**	**33.36 e**	**43.04 c**	**14.94 b**
SA-88	1 April	8430	4840	34.76	42.70	14.02
	15 April	13460	4820	35.23	42.84	11.42
	30 April	409**0**	2770	34.48	42.63	13.26
	Mean	**8660 c**	**4143**	**34.82 d**	**42.72 d**	**12.90 d**
ATAEM-7	1 April	16300	5780	38.54	45.10	14.20
	15 April	5950	2550	38.46	44.17	14.26
	30 April	5600	3410	37.27	45.78	14.66
	Mean	**9283,3 b**	**3913**	**38,09 a**	**45,02 b**	**14,37 c**
BRAVO	1 April	11090	3690	36,15	45,21	13,16
	15 April	2840	2110	37,84	46,04	14,86
	30 April	3980	2740	38,22	45,14	15,05
	Mean	**5970 e**	**2847**	**37,40 b**	**45,46 ab**	**14,36 c**
A-3127	1 April	7630	3850	35,18	45,74	14,58
	15 April	4160	2920	38,16	46,04	14,05
	30 April	5920	3940	34,14	44,10	14,26
	Mean	**5903,3 e**	**3570**	**35,83 c**	**45,29 ab**	**14,30 c**
ARISOY	1 April	8050	3960	33,13	45,20	16,10
	15 April	5970	3960	32,16	46,14	15,20
	30 April	11590	5430	31,20	46,03	14,90
	Mean	**8540 c**	**4450**	**33,25 e**	**45,79 a**	**15,40 a**
YEŞİLSOY	1 April	7500	3130	32,10	44,40	12,15
	15 April	10700	4100	33,01	48,20	11,13
	30 April	15000	4700	32,14	45,23	13,05
	Mean	**11070 a**	**3977**	**32,42 f**	**45,94 a**	**12,11 e**
YEMSOY	1 April	11000	3800	35,10	44,70	9,65
	15 April	9500	3300	32,01	40,01	8,86
	30 April	12500	4500	34,15	36,10	9,30
	Mean	**11000 a**	**3867**	**33,75 e**	**40,27 e**	**9,27 f**
Sowing Time Avarages	1 April	**9567,50**	**40613**	**34,85**	**44,74**	**13,75**
	15 April	**7899**	**3482,5**	**34,89**	**44,58**	**12,99**
	30 April	**7985**	**3910**	**34,45**	**43,25**	**13,64**
P	V	**	**	**	**	**
	S	**	**	**	**	**
	VxS	**	**	**	**	**

2015

Varieties	Planting time	Fresh grass yield (kg/ ha^{-1})	Hay yield (kg/ ha^{-1})	ADF (%)	NDF (%)	Crude protein content (%)
NOVA	1 April	8180	4300	32.56	43.56	15.47
	15 April	13320	5130	34.04	45.53	12.64
	30 April	6500	4730	35.89	40.82	14.66
	Mean	**9333.33 d**	**4720 d**	**34.16 b**	**43.23 c**	**14.26 a**
SA-88	1 April	10540.20	6050	34.44	41.69	13.05
	15 April	16950.20	6060	37.33	41.80	10.33
	30 April	5120	3460	36.74	42.55	12.64
	Mean	**10870.13 b**	**5190 b**	**36.17 ab**	**42.01 d**	**12.00 c**
ATAEM-7	1 April	20360.20	7170	38.81	45.41	13.40
	15 April	7430	3190	39.46	46.58	13.35
	30 April	7000	4270	32.35	45.69	13.63
	Mean	**11596.73 b**	**4876.60 c**	**36.87 ab**	**45.89 b**	**13.53 b**
BRAVO	1 April	13870.20	4620	34.89	46.01	13.96
	15 April	3550	2640	37.59	46.06	12.36
	30 April	4970	3420	40.38	51.88	14.36
	Mean	**7463.40 e**	**3560 f**	**37.62 a**	**47.98 a**	**13.56 b**
A-3127	1 April	9530.60	4810	34.78	46.69	13.62
	15 April	5200	3650	40.83	48.63	13.00
	30 April	7400	4920	32.83	43.68	13.23
	Mean	**7376.87 f**	**4460 e**	**37.58 a**	**46.33 a**	**13.28 b**
ARISOY	1 April	10060.20	4928	32.28	49.26	15.19
	15 April	7470	4960	34.57	46.02	14.30
	30 April	14490	6780	33.25	45.69	13.85
	Mean	**10673.40 c**	**5556 a**	**33.37 c**	**46.99 a**	**14.45 a**
YEŞİLSOY	1 April	8930	3720	32.95	45.40	11.07
	15 April	12740	4880	33.55	49.35	10.14
	30 April	17860	5590	32.74	46.29	12.02
	Mean	**13176.60 a**	**4730 d**	**33.08 c**	**47.01 a**	**11.07 d**
YEMSOY	1 April	13100	4520	34.40	44.89	8.65
	15 April	11310	3920	31.68	40.48	7.79
	30 April	14880	5350	36.23	36.18	8.20
	Mean	**13096.6 a**	**4590 e**	**34.10 b**	**40.52 e**	**8.21 e**
Sowing Time Avarages	1 Nisan	**11821.4**	**4540**	**34.39**	**44.99**	**13.05**
	15 Nisan	**9746.28**	**4300**	**36.13**	**45.56**	**11.74**
	30 Nisan	**9777.5**	**4820**	**35.05**	**44.10**	**12.83**
P	V	**	**	**	**	**
	S	**	**	**	**	**
	VxS	**	**	**	**	**
	VxSxY	**	**	**	**	**
Average of Varities	NOVA	**8391.67**	**4250**	**33.76**	**43.14**	**14.60**
	SA-88	**9765.07**	**4670**	**35.50**	**42.37**	**12.45**
	ATAEM-7	**10440.02**	**4395**	**37.48**	**45.46**	**13.95**
	BRAVO	**6716.70**	**3205**	**37.51**	**46.72**	**13.96**
	A-3127	**6640.09**	**4015**	**36.71**	**45.81**	**13.79**
	ARISOY	**9606.70**	**5003**	**33.31**	**46.39**	**14.93**
	YEŞİLSOY	**12123.3**	**4350**	**32.75**	**46.48**	**11.59**
	YEMSOY	**12048.5**	**4230**	**33.93**	**40.40**	**8.74**
Average of Year	2014	**8484.6**	**3818**	**34.87**	**44.19**	**13.45**
	2015	**10448.4**	**4710**	**35.37**	**45.00**	**12.55**
	Mean	**9466.5**	**4264**	**35.12**	**44.60**	**13.00**
Average of Sowing Time	1 April	**10694.46**	**4301**	**34.62**	**44.87**	**13.40**
	15 April	**8822.51**	**3893**	**35.51**	**45.07**	**12.37**
	30 April	**8881.25**	**4365**	**34.75**	**43.68**	**13.24**
	V	**	**	**	**	**
	S	**	**	**	**	**
	VxS	**	**	**	**	**
	VxSxY	**	**	**	**	**

V: Varieties; S:Sowing time. Y:Year. VxS: Varieties x Sowing time between interaction. VxSx Y: Varieties x Sowing timex Year between interaction NS: No Significiant; *p<0.05, **p<0,01 a,b,c,d,e,f : Differences between media carrying different letters in the same column are important.

Hay Yield. The results on the yield of dry hay is concluded to be lower than the [20-17-26-22]. This difference may caused by the differences in the spots chosen for growing. In comparison to other leguminous forage crops, the dry hay yield of soybean is lower than Trifolium [27] and Onobrychis, forage yield has been also lower, however it is similar to Vicia and Lathyrus [28-29]. While it has been compared to other leguminous plants in regards of its advantages and drawbacks,

because soybean has been sowed as a primary or secondary feed crop, it can easily be included in a regular sowing regimen. In respect of forage and dry hay yield, interactions between; soybean varieties, differences between sowing dates, variety x sowing date; variety x sowing date x yearly applications have been found to be significant at 1% (Table.3).

ADF and NDF. ADF and NDF values have been found to be between, 33,08% with 38,09% and 40,27% with 47,98% respectively. Highest NDF value has been acquired with 46,48% from the Yeşilsoy variety while the lowest NDF value has been acquired with 40,40% from the Yemsoy variety. While the highest ADF value has been acquired with 37,51% from the Bravo variety, the lowest ADF has been acquired from the Yeşilsoy variety with 32,75% (Table.3). [22] reported to acquire the highest ADF value with 44,1% from the Yeşilsoy variety and the highest NDF value with 54,9% from the Erensoy variety. In this study, the highest NDF value has been acquired with the Yeşilsoy variety. By sowing dates, the highest ADF and NDF values have been acquired as 35,51% from the sowing date of April 15 and the lowest values have been acquired as 34,62% from the sowing date of April 1, respectively. In regards of ADF and NDF values, interactions between; soybean varieties, differences between sowing dates, variety x sowing date; variety x sowing date x yearly applications have been found to be significant at 5% (Table.3). The ADF and NDF values have been similar to [30], [17-20-22-26]. However the NDF values are lower than [31-32-33-34]. Typically the fiber content, rather than high fat components, have been in between the ratio reported for feed crops as Trifoluim [35-36]. In regards of ADF and NDF values, while it was similar to Trifolium and Onobrychis, it was lower than Vicia and Lathyrus [28-37-38-39].

Crude Protein. Crude protein content have found to be between 8.21% and 15.40%. The highest crude protein content have been acquired from the Arısoy and the Nova varieties (Table.3). The lowest value has been acquired from the Yemsoy variety. [22] reported to acquire, the highest crude protein value with 13,2% from the Ataem-7 variety, the lowest values with 10,8% from the Nazlıcan and the Erensoy varieties and with 12,3% from the Yemsoy variety. In this study the highest NDF value have been acquired from the Yeşilsoy variety. The results of crude protein content has been similar to the values [19-40] reported. However it has been found to be lower than [17-20-26] and higher than the values proposed by [22]. This may be caused by soil properties and climate change. Soybean, when harvested as a feed crop whilst the seeds are in the development phase [41] , on account of a well established variety has the potential of producing 12% to 20% protein, it is comparable to Trifolium on both quality and quantity of its protein content [42]. The interactions between genotypes gets determined by the harvesting maturity of the plants and the environmental factors [43-44]. Thus it has been concluded that the interactions between soybean varieties are significant. As reported by [45], soybean feed contains, on average, 20,2% crude protein. Crude protein ratios of soybean, whilst showing resemblance to Vicia and Onobrychis, is lower than Trifolium and Lathyrus [47-28-37-46].

CONCLUSION

The most significant element that impacts yield, is the sowing date. As being a widely applied cultural practice and as it has a direct effect on the yield, sowing date is one of the more important applications. Sowing date, by impacting upon the developmental stages of soybean, directly influences the yield. While particularly, the late sowing dates and the detrimental environmental conditions has a negative impact, the temperature and the photoperiod have an impact as well. Soybean that has been sowed later in the vegetative period will have a shorter time frame to complete its vegetative development.

In this study, the forage yield and some of its qualities from soybean with various sowing dates have been determined. Amongst these parameters studied between soybean varieties, the highest forage yield and the ADF values have been acquired with the Yeşilsoy variety. In regards to the forage yield with 12123,3 kg/ha^{-1} the Yeşilsoy variety has deemed to have the first place. In regards to dry hay yield, the Arısoy variety with 5003 kg/ha^{-1}, has provided the highest value. Considering the ADF, the NDF and the crude protein content, highest values have been acquired as 37,51% from Bravo, 37,48% from ATAEM-7, 46,72% from Bravo, 46,48% from Yeşilsoy, 13,96% from Bravo and 13,95% from ATAEM-7 respectively. Amongst the studied parameters, the interactions between; variety, sowing date, year, variety x sowing date, variety x sowing date x year found to be very significant (Table.3). In regards of sowing dates, the sowing date of April 1 has provided the highest values amongst the studied parameters. Therefore, while the sowing date of April 1 has concluded to be the most appropriate sowing date, the varieties of Nova, Arısoy, ATAEM-7, Yeşilsoy and Yemsoy, in regards to their crude protein content, forage yield and dry hay yield, has been concluded to be advisable to farmers.

ACKNOWLEDGEMENT

This research was supported by funds of Department of Scientific Research Project Management of Gumushane University with the project number 15.B0123.02.01.

REFERENCES

[1] Bellaloui, N., Hu, Y., Mengistun, A., Kassem, M.A., Abel, C.A. 2013. Effects of foliar boron application on seed composition, cell Wall boron and seed δ ^{15}N and δ ^{13}C isotopes in water-stressed soybean plants. Frontiers in Plant Science. 4, 1-12.

[2] Bohn, T., Cuhra, M., Travail, T., Sanden, M., Fagan, J. and Primicerio, R. 2014. Compositional differences in soybeans on the market: glyphosate accumulates in Roundup Ready GM soybeans. Food Chemistry. 153, 207-215.

[3] Okcu, M., Tozlu, E., Pehluvan, M., Kaya, C., Kumlay, M., Dizikısa, T. 2007. A study on the adaptation of soybean (Glycine Max. L) cultivars under Erzurum-Pasinler ecological conditions. 1st National Oil Seed Crops and Biodiesel Symposium. 28-31 May 2007, 219-224. Samsun

[4] Ali, N. (2010) .Soybean Processing and Utilization, The Soybean Botany, Production and Uses, Editor", Singh, G.

[5] Zhang Q.-Y., Qing-lu G., Herbert S.J, Yansheng L. and Hashemi, A.M. (2010). Influence of sowing date on phenological stages, seed growth and marketable yield of four vegetable soybean cultivars in North-eastern USA. African J. Agri. Res. 5(18), 2556-2562.

[6] Rahman, M.M., Hampton, J.G. and Hill, M.J. (2005). Soybean seed yield as affected by time of sowing in a cool temperature environment. Seed Sci. Technol. 7, 1-15.

[7] Calvino, P,A., Sadras, V.O., Andrade, F.H. (2003a). Quantification of environmental and management effects on the yield of late-sown soybean. Field Crops Res. 83, 67-77.

[8] Calvino, P.A., Sadras, V.O., Andrade, F.H. (2003b). Development, growth and yield of late-sown soybean in the southern Pampas. Europ. J. Agro. 19, 265-275.

[9] Robinson, A.P., Conley, S.P., Volenec, J.J., Santini, J.B. (2009). Analaysis of high yielding, early-planted soybean in India. Agron. J. 101, 131-139.

[10] Hoeft, R.G., Nafziger, E.D., Johnson, R.R., Aldrich, S.R. (2000). Modern corn and soybean production. MCSP Publications, Champaign, L.J.

[11] Naeve, S.L., Potter, B.D., Quiring, S.R., O'Neil, T.A., Kurle, J.E. (2004). Influence of soybean plant and population and row spacing on development and yield across planting dates in Minnesota. Available at www.soybeans.umn.edu/pdfs/2004asaposter_1_spacingplanting_screen .pdf. University of Minnesota, Minneapolis.

[12] Han, T.F., Wu, C.X., Tong, Z., Mentreddy, R.S., Tan, K.H. and Gai, J.Y. (2006). Post flowering photoperiod regulates vegetative growth and reproductive development of soybean. Environmental and Experimental Bot., 55, 120-129.

[13] Kumudini, S.V., Pallikonda, P.K. and Steele, C. (2007). Photoperiod and e-genes influence the duration of the reproductive phase in soybean. Crop Sci. 47, 1510-1517.

[14] Chen, G.H., Wiatrak, P. (2010). Soybean development and yield are influenced by planting date and environmental conditions in southeastern coastal plan, United States. Agron. J. 102, 1731-1737.

[15]]Hu, M. and Wiatrak, P. (2012). Effect of planting date on soybean growth, yield and grain quality: Review. Agron. J. 104, 785-790.

[16] Boquet, D.J and Clawson, E.L. (2007). Planting dates for soybean varieties in North Louisiana. Ouisiana Agriculture Magazine, LSUA, Center.com.

[17] Ram, H., Singh, G., Aggarwal, N. (2010). Effect of Time of Sowing on The Performance of Soybean [Glycine Max (L.) Merrill] In Punjab. J. Res. Punjab Agric. Univ. 47 (3 and 4), 127-31, Sep. and Dec. 2010.

[18] İlisulu, K. (1973) . Oil Crops and Breeding. Ankara University, Faculty of Agriculture. Chair of Industrial Crops. Caglayan Bookstore. p. 195-199. Ankara.

[19] Martin, R.C., Astatkie, T., Cooper, J.M. (1997). The effect of soybean variety on corn-soybean intercrop biomass and protein yields. Canadian Journal of Plant Sci. 289-294.

[20] Undersander, D. (1999). Soybeans for hay or silage.http//:www.uwex.edu./ces/forage/pubs/SOYBNFOR.html

[21] Brown,C.2003.Soybeanasaforag crop. http://www.omafra.gov.on.ca/english/crops/facts/soybean_forage.html

[22] Kokten, K., Seydosoglu, S., Kaplan, M., Boydak, E. 2014. Forage Nutritive Value of Soybean Varieties. Legume Research. 37 (2), 201-206.

[23] Rehman, M., Khaliq, T., Ahmad, A., Wajid, S.A., Rasul, F., Hussain, J., Hussain, S. (2014). Effect of Planting Time and Cultivar on Soybean Performance in Semi-Arid Punjab, Pakistan. Global Journal of Science Frontier Research: D. Agriculture and Veterinary. 14(3), 41-45.

[24] Jaybhaye, R.P., Shinde, B.P., Asewar, V.B. (2015). Response of soybean to sowing dates and spacing under rainfed condition. International Journal of Tropical Agriculture. 33(2), 474-750.

[25] Kundu, K.P., Roy, S.T., Khan, H.S., Parvin, K., Mazed, M.E.H. (2016).Effect of sowing date on yield and seed quality of soybean. Journal of Agriculture and Ecology Research International. 9(4), 1-7.

[26] Blount, A.R.S., Wright, D.L., Sprenkel, R.K., Hewitt, T.D, Myer R.O. (2009). Forage soybeans for grazing hay and silage. University of Florida, IFAS Extension. SS-AGR-180.

[27] Saruhan ,V., Kusvuran, A. (2011). Deteremination of yield performances of some lucerne cultivars and genotypes under the Southeastern Anatolia Region conditions.Aegean Univ. Agricultural Faculty Journal. 48(2), 133-140.

[28] Kaplan, M. (2013). Effects of harvest time on the yield and quality of common vetch (Vicia sativa L.)genotypes. Erciyes Universtiy, Journal of Science, not published, in print media.

[29] Karadag, Y., Ozkan, M., Albay, S., Kir, H. (2012). Determination of Yield and Yield Components of Some Grasspea (*Lathyrus sativus* L.)lines in Tokat-Kazova ecological conditions. Research Journal of Agricultural Science. 5, 11-13

[30] Smith, N.E., Collar L.S., Bath D.L., Dunkley W.L. and Franke A.A., (1981). Digestibility and Effects of Whole Cottonseed Fed to Lactating Cows. J. Dairy Sci. 64, 2209-2215.

[31] Albro, J.D., Weber, D.W., Delcurto, T. (1993). Comparison of whole, raw soybeans extruded soybeans, or soybean meal and barley on digestive characteristics and performance of weaned beef steers consuming mature grass hay. Journal of Animal Science. 71,26-32.

[32] Mertens, D.R. (1997). Creating a system for meeting the fiber requirements of dairy cows. J. Dairy Sci. 80(7), 1463-1481.

[33] Bodine, T.N., Purvis, H.T., Ackerman C.J., Goad, C.L. (2000). Effects of supplementing prairie hay with corn and soybean meal on intake, diestion and ruminal measurements by beef steers. Journal of Animal Science. 78(12), 3144-3154.

[34] Sheaffer, C.C., Orf, J.H., Devine , T.E., Jewett, J.G. (2001). Yield and quality of forage soybean. Agronomy Journal. 93, 99-106.

[35] Julier, R., Lila, M., Furstoss, V., Travers, V., Huyghe, C. (1999). Measurement of cell-wall digestibility in lucerne using the filter bag technique. Animal Feed Science and Technology. 79, 239-245.

[36] Robinson, P.H., Mathews, M.C., Faadel, J.G. (1999). Influence of storage time and temperature on in vitro digestion of neutral detergent fiber at 48 h. and composition to 48 h in sacco neutral detergent fiber digestion. Anim. Feed Sci. Technol. 80, 257-266

[37] Basaran, U., Mut, H., Onal-Asci, O., Acar, Z., Ayan I. (2011). Variability in forage quality of Turkish grass pea (Lathyrus sativus L.) landrace. Turk J. Field Crops. 16, 9-14.

[38] Kaplan, M. (2011). Determination of potenrial nutritive value of sainfoin (Onobrychis sativa) hays harvested at flowering stage. Journal of Animal and Veterinary Advances. 10 (15), 2028-2031.

[39] Canpolat, O., Kalkan, H., Filya, I. (2013). The use of honey locust pods as a silage addiditve for alfalfa forage. Kafkas Univ. Vet. Fac. Journal. 19 (2), 291-297.

[40] Wanapat, M., Promkot, C., Khampa, S. (2007). Supplement of cassava hay as a protein replacement for soybean meal in concentrate supplement for dairy cows. Pakistan Journal of Nutrition. 6(1), 68-71.

[41] Fehr, W., Caviness, C. (1980) .Stages of soybean development. Iowa Cooperation Service, Special Report, 80.

[42] Hintz, R.W. and Albrecht, K.A. (1994). Dry matter partitioning and forage nutritive value of soybean plant components. Agron. J. 86, 59-62

[43] Cummins, D.C. (1981).Yield and quality changes with maturity of silage type sorghum fodder. Agronomy J. 73(6), 988-990.

[44] Filya, I. (2004).Nutritive value and aerobic stability of whole crop maize silage harvestedat four stages of maturity. Animal Feed Science and Technology. 116,141-150.

[45] Tobia, C., Villalobos, E., Rojas, A., Soto, H., Moore, K.J. (2008). Nutritional value of soybean (Glycine max L. Merr.) silage fermented with molasses and inoculated with Lactobacillus brevis 3. Livestock Research for Rural Development. 20 (7), 1-9.

[46] Kanani, J., Lukefahr, S.D., Stanko, R.L. (2006) .Evaluation of tropical forage legumes (Medicago sativa, Dolichos lablab, Leucaena leucocephala and Desmanthus bicornutus) for growing goats. Small Ruminant Research. 65, 1-7.

[47] Rahmati, T., Azarfar, A., Mahdavi, A., Khademi, K., Fatahnia, F., Shaikhahmadi, B. and Darabighane, B. (2012). Chemical composition and forage yield of three Vicia varieties (Vicia spp.) at full blooming stage. Italian Journal of Animal Science. 11(57), 309-311.

Received: **31.10.2019**
Accepted: **08.02.2020**

CORRESPONDING AUTHOR

Melih Okcu
Atatürk University,
Faculty of Agriculture,
Department of Field Crops,
Erzurum- Turkey

e-mail: melihokcu@hotmail.com

© by PSP Volume 29 – No. 05/2020 pages 3732-3737 Fresenius Environmental Bulletin

STUDY ON MAIZE HETEROTIC GROUPS AND HETEROTIC MODELS IN NORTHERN CHINA IN DIFFERENT ECOTYPES

Jia-Bin Ci, Wei Yang, Xue-Jiao Ren, Liang-Yu Jiang, Yi-Fan Wei, Wei-Guang Yang*

Faculty of Agronomy, Jilin Agricultural University, Changchun 130118, China

ABSTRACT

Aimed to present a 3 heterotic models hypothesis based on maize germplasms divided into Reid group, non-Reid group and DOM group in north China, inbred lines bred from between either 2 groups. Crosses (5×6) were formed according to the North Carolina design II (NC II) scheme, and popular cultivar "Xianyu 335" served as control. The experiment was carried out in 3 ecological zones during 2-year with densities of 50000, 60000, and 80000 plants per ha, respectively. Excellent hybrid crosses with high, stable yield and density tolerance were screened out. 1 cross of model I, 4 crosses of model II, 2 crosses of model III showed strong heterosis. Results demonstrate clearly that the "3 heterotic groups and 3 heterotic models" hypothesis for maize heterosis application is effective and simple, and Models II and III are suitable for north China.

KEYWORDS:
Maize, Heterosis, Heterotic groups, Heterotic models, Ecotypes

INTRODUCTION

Usually, maize heterotic groups were divided into multi-groups and heterotic models in China [1-8], which brought huge work to test the combining ability of inbred lines. On the other hand, major germplasms Tangsipingtou and Lvda red cob were still indispensable for north China spring maize region [9-12]. Importance of these two gremplasms shall be underestimated if they were divided into Non-Reid groups according to the Reid×Non-Reid heterotic model. Summering up researches, based on the principle of simple, practical, and effective, a principle of 3 heterotic groups (Reid group, Non-Reid group and DOM groups) and 3 heterotic germplasms were proposed. The heterotic groups were independent. With tested materials selected from one group, lines from the other two groups could be test materials. For example, inbred line A (Reid germplasm, Reid) as the tested line, lines B (Non-Reid germplasm, Non-Reid) and C (DOM germplasm, DOM) could be test lines, with heterosis present in A×B and A×C. With tested materials selected from between 2 groups, lines from the 3rd group could be test materials. For example, with the second cycle line D (Reid×DOM) as the tested line, line C (Non-Reid) could be test line, with heterosis exhibited in D×C. For further research and proving of it, this study was conducted hope to provide a theory base for maize heterosis usages in northern China.

MATERIALS AND METHODS

Materials. The heterotic models were Non-Reid × DOM (model I), Reid × DOM (model II), and Reid × Non-Reid (model III). PH6WC (Reid), PH4CV (Non-Reid), PH5AD (Non-Reid), 93287 (DOM) and M5972 (DOM) were selected as the skeleton inbred lines for improving.

For each heterotic model, 4 improved lines and 1 skeleton inbred line were the tested lines. 6 inbred lines from the 3rd group served as test lines. Liao3180 and M54 were added to Model III as tested lines according to their pedigree. (Table 1).

Crosses (5×6) were formed according to the NC II design in 2015, and the cultivar "Xianyu 335" served as the control.

Methods. Experiments were carried out in 3 densities during 2 years. Baicheng in western Jilin Province (semiarid ecotype), Changchun in middle of Jilin Province (sub-humid ecotype) and Huadian in eastern Jilin Province (humid ecotype) were selected as tests sites. Randomized design consisting of 3 replications were hired, with densities at 50,000, 60,000, and 80,000 plants per ha respectively. 2 rows in the middle were harvested to measure plot yield (kg×6.5 m^2) after maturity. Field managements were consistent with regular field plots.

Statistical analysis. Heterosis was analyzed in accordance with the middle parent heterosis (MPH) and over standard heterosis (OSH) methods [13]. The data were analyzed using DPS (Data Processing System) software 9.50 [14].

$$MPH(\%) = \frac{F1 - MP}{MP} \times 100\%; \quad MP = \frac{P1 + P2}{2};$$

$$OSH(\%) = \frac{F1 - CK}{CK} \times 100\%;$$

RESULTS AND DISCUSSION

Heterosis performance according to 3 heterotic models. Table 2 and Table 3 show the average MPH and variation range of 30 hybrid crosses in ecotypes and densities according to heterotic models in 2016 and 2017, respectively. Results demonstrated that mean MPH values of 30 crosses were greater than 100% with only one exception. Further analysis indicated that the lowest MPH was 46.4%, while the highest reached 221.6%. Therefor the 3 heterotic models were suitable and could be a guidance for heterotic breeding.

Results in 2016 showed that heterosis performance varied in ecotypes. Regarding the densities in Changchun, the average MPH values of Models II and III were significantly higher than Model I, with 145.4% 130.8%, and 115.1%, respectively. Similar results obtained in Huadian, whose average MPH values of Models II, III and I were 163.2%, 149.4% and 120.1%, respectively. In Baicheng, the average MPH of Model III reached 135.4%, significantly higher than Models I and II, which were 115. 0% and 104.5%, respectively.

In 2017, similar results were observed. The average MPH values of Models II and III in Changchun were significantly higher than Model I, at 142.0%, 139.5%, and 112.6%, respectively; in Huadian, these values were 144.2%, 153.5%, and 120.9%, respectively. In Baicheng, the average MPH of Model III (144.6%) was significantly higher than Model I (111.3%) and Model II (77.9%) (Table 3).

The average MPH values over two years were listed in Table 4. Results show that Model III reached the highest at 142.2%, followed by Model II (129.5%) and Model I (115.8%). Model III and Model II are more useful in spring maize region.

TABLE 1
Materials and design for three heterosis models of maize

Heterotic model	Tested lines	Germplasms	Test lines	Test lines germplasms
Model I: Non-Reid × DOM	JD7-1 JD7-2	PH4CV×93287	PH6WC PHGJ4 J1595 J1590 Zheng58 J1259	Reid
	JV2-1 JV2-2	PH4CV×M5972		
	PH4CV			
Model II: Reid × DOM	JC7-1 JC7-2	PH6WC×93287	J9D207 J1577 J1881 PH4CV PHB1M PH5AD	Non-Reid
	JC2-1 JC2-2	PH6WC×M5972		
	PH6WC			
Model III: Reid × Non-Reid	JCV-1 JCV-2	PH6WC×PH4CV	93287 J1828 J2239 M5972 T106 S122	DOM
	JCD-1	PH6WC×PH5AD		
	Liao3180	From PN3180		
	M54	From American cultivar×Tie7922 (Reid)		

TABLE 2
MPH (%) of 30 crosses for heterosis models in ecotypes and densities in 2016

Locations	Model	Parameters	Densities (10 000/ha)			Mean value
			5	6	8	
Changchun	Model I	MPH	113.1	127.2	104.9	115.1
		Variation range	66.1–154.4	66.8–194.8	70.8–133.1	
	Model II	MPH	163.1	136.8	136.1	145.4
		Variation range	129.4–221.6	95.1–178.8	84.2–182.2	
	Model III	MPH	150.5	138.0	103.9	130.8
		Variation range	118.3–176.9	107.2-169.8	74.9–123.7	
Huadian	Model I	MPH	132.9	119.7	107.7	120.1
		Variation range	95.4–218.9	76.7–144.4	71.9–127.7	
	Model II	MPH	197.6	150.5	141.6	163.2
		Variation range	142.9–261.6	111.7–187.0	109.6–199.3	
	Model III	MPH	168.02	152.5	127.8	149.4
		Variation range	134.8–200.0	120.7–178.6	97.7–153.6	
Baicheng	Model I	MPH	128.6	104.7	111.5	115.0
		Variation range	65.2–214.6	68.7–49.6	84.2–144.4	
	Model II	MPH	114.4	100.9	98.4	104.5
		Variation range	86.8–157.3	70.6–121.6	65.5–124.5	
	Model III	MPH	160.7	126.4	119.2	135.4
		Variation range	135.2–198.1	99.5–156.0	87.5–152.9	

TABLE 3
MPH (%) of 30 crosses for three heterosis models in different ecological zones and densities in 2017

Locations	Model	Parameters	Densities (10000/ha)			Mean Value
			5	6	8	
Changchun	Model I	MPH	112.2	121.4	104.3	112.6
		Variation range	68.0–146.2	70.8–147.0	72.1–125.5	
	Model II	MPH	158.6	135.9	131.6	142.0
		Variation range	132.3–195.8	98.2–172.2	97.1–176.1	
	Model III	MPH	150.1	138.7	129.7	139.5
		Variation range	120.7–173.4	114.5–170.8	95.5–158.0	
Huadian	Model I	MPH	118.35	123.15	121.26	120.9
		Variation range	75.7–178.2	84.0–141.2	91.7–137.8	
	Model II	MPH	160.9	134.5	137.1	144.2
		Variation range	139.5–181.7	109.3–154.7	102.9–176.8	
	Model III	MPH	156.3	159.1	145.0	153.5
		Variation range	131.8–179.0	131.3–184.2	108.1–180.9	
Baicheng	Model I	MPH	125.5	101.5	106.9	111.3
		Variation range	95.8–186.0	80.8–117.2	83.1–122.5	
	Model II	MPH	91.4	65.5	76.9	77.9
		Variation range	67.6–119.0	46.4–80.0	58.0–91.6	
	Model III	MPH	162.4	146.1	125.3	144.6
		Variation range	137.3–196.7	110.3–187.9	92.2–158.3	

TABLE 4
MPH (%) in ecotypes and densities over 2 years

Models	Year		Mean value over 2 years
	2016	2017	
Model I	114.9	116.7	115.8
Model II	121.3	137.6	129.5
Model III	145.9	138.5	142.2

TABLE 5
Screening of heterotic crosses under different densities for heterotic Model I in 2016–2017

50,000/ha			60,000/ha			80,000/ha		
Heterotic crosses	Plot yield (kg/6.5 m^2)	Yield increase (%)	Heterotic crosses	Plot yield (kg/6.5m^2)	Yield increase (%)	Heterotic crosses	Plot yield (kg/6.5m^2)	Yield increase (%)
JV2-1×J1590	8.33	8.26	JV2-2×J1590	8.90	15.58	JV2-2×J1590	7.79	12.32
PH4CV×J1590	8.31	7.97	JV2-1×J1590	8.71	13.12	JV2-1×J1590	7.78	12.22
JV2-1×J1595	8.23	6.89	JV2-1×PH6WC	8.47	10.02	JD7-2×J1590	7.69	10.88
JV2-2×J1595	8.23	6.87	JV2-2×J1595	8.46	9.90	JD7-1×J1590	7.61	9.74
JV2-2×PH6WC	8.21	6.62	PH4CV×J1590	8.43	9.40	JV2-1×J1595	7.54	8.72
JV2-2×J1590	8.18	6.31	JV2-1×J1595	8.37	8.62	JV2-2×J1595	7.51	8.27
JD7-2×J1590	8.04	4.50	JD7-2×J1590	8.36	8.53	JV2-1×PHGJ4	7.46	7.57
			JV2-2×PH6WC	8.33	8.18	JV2-2×PHGJ4	7.44	7.34
			JD7-1×J1590	8.24	6.94	JD7-2×PH6WC	7.40	6.71
			JV2-2×PHGJ4	8.23	6.82	JV2-1×PH6WC	7.39	6.58
			PH4CV×J1595	8.12	5.41	JD7-2×J1595	7.37	6.27
						JV2-2×PH6WC	7.36	6.08
						PH4CV×J1590	7.34	5.88
						JD7-1×J1595	7.28	5.05
						JD7-1×PH6WC	7.24	4.42
						JD7-1×PHGJ4	7.24	4.36
						JD7-2×PHGJ4	7.22	4.11
CK (Xianyu 335)	7.70			7.09	0.00		6.93	
Heterotic crosses Num.	7			11			17	
Strong heterotic crosses Num.	1			8			6	

Screening of heterosis hybrid crosses in 3 heterotic models. Strong heterotic crosses were selected according to the standard that the yield should significantly increase by more than 8% compared with control "Xianyu 335". Results were shown in the Table 5, Table 6 and Table 7.

According to model I, with 50000 plants per ha, 7 hybrid crosses were superiors with yield significantly overtook control. Among them, 1 hybrid cross

showed strong heterosis. With 60000 plants per ha, there were 17 crosses were superiors and 1 with strong heterosis. Strong heterosis crosses were identified under high density, the low density-tolerance of "Xianyu 335" may be a reason for these phenomena.

According to Model II, with 50,000 plants per ha, 10 superior and 4 strong heterosis crosses emerged. With 60,000 plants per ha, 10 superior and 6 strong heterosis crosses emerged. With 80000 plants per ha, there were 7 superior and 6 strong heterosis crosses emerged.

According to Model III, with 50,000 plants per ha, 7 superior and 3 strong heterosis emerged. With 60,000 plants per ha, 7 superior and 3 strong heterosis crosses emerged. With 80,000 plants per ha, 13 superior and 5 strong heterosis superior crosses emerged.

TABLE 6
Screening of heterotic crosses under different densities for heterotic Model II in 2016–2017

50,000/ha			60,000/ha			80,000/ha		
Heterotic crosses	Plot yield (kg/6.5 m^2)	Yield increase (%)	Heterotic crosses	Plot yield (kg/6.5 m^2)	Yield increase (%)	Heterotic crosses	Plot yield (kg/6.5 m^2)	Yield increase (%)
JC2-2×J1577	8.75	11.99	JC2-2×J1577	8.66	11.52	JC2-2×J1577	8.25	16.06
PH6WC×J1577	8.63	10.51	JC7-2×J1577	8.63	11.13	JC7-2×J1577	8.14	14.46
JC7-2×J1577	8.55	9.42	JC2-2×J1881	8.55	10.04	JC2-1×J1577	7.98	12.28
JC2-2×J1881	8.48	8.51	PH6WC×J1577	8.47	9.02	JC7-1×J1577	7.95	11.78
JC7-2×J1881	8.44	7.97	PH6WC×J1881	8.40	8.19	PH6WC×J1577	7.91	11.30
JC2-2×PH4CV	8.28	5.98	JC2-2×J9D207	8.40	8.09	JC2-2×J1881	7.88	10.81
JC2-2×PH5AD	8.24	5.50	JC7-2×J1881	8.33	7.23	JC2-2×J9D207	7.56	6.33
PH6WC×J1881	8.12	3.93	JC7-1×J1577	8.31	7.05			
JC7-1×J1577	8.11	3.81	PH6WC×J9D207	8.31	7.04			
JC7-2×J9D207	8.10	3.61	JC2-2×PH4CV	8.23	5.91			
CK (Xianyu 335)	7.81			7.77			7.11	
Heterotic crosses Num.	10			10			7	
Strong heterotic crosses Num.	4			6			6	

TABLE 7
Screening of heterotic crosses under different densities for heterotic Model III in 2016–2017

50,000/ha			60,000/ha			80,000/ha		
Heterotic crosses	Plot yield (kg/6.5 m^2)	Yield increase (%)	Heterotic crosses	Plot yield (kg/6.5 m^2)	Yield increase (%)	Heterotic crosses	Plot yield (kg/6.5 m^2)	Yield increase (%)
JCV-2×J1828	8.33	8.73	Liao3180×T106	8.56	8.82	Liao3180×T106	7.58	10.54
JCV-2×J2239	8.30	8.35	JCV-1×J1828	8.54	8.55	JCV-2×J1828	7.53	9.81
Liao3180×T106	8.28	8.05	JCV-2×J1828	8.54	8.52	JCV-2×J2239	7.53	9.79
JCD-1×J1828	8.27	7.93	JCV-2×J2239	8.45	7.37	JCV-1×J1828	7.46	8.67
JCD-1×J2239	8.23	7.42	JCV-1×J2239	8.45	7.32	JCV-1×J2239	7.45	8.55
JCV-1×J1828	8.13	6.06	JCD-1×J2239	8.43	7.07	JCD-1×J1828	7.36	7.31
JCV-1×J2239	7.99	4.29	JCD-1×J1828	8.40	6.73	M54×S122	7.32	6.64
						JCD-1×J2239	7.25	5.66
						JCV-2×93287	7.19	4.83
						M54×J2239	7.12	3.76
						Liao3180×J1828	7.10	3.52
						M54×J1828	7.07	3.01
						JCD-1×T106	7.07	2.99
CK (Xianyu 335)	7.66			7.87			6.86	
Heterotic crosses Num.	7			7			13	
Strong heterotic crosses Num.	3			3			5	

TABLE 8
Major popular cultivars, parents and heterosis models in the spring maize zone of northern China

Cultivar	Parent	Heterosis model	Suitable area
Xianyu 335	PH6WC×PH4CV	Reid×Non-Reid (Model III)	North spring maize region
Xianyu 696	PH6WC×PHB1M	Reid×Non-Reid (Model III)	North spring maize region
Xianyu 508	PH6WC×PHB1M	Reid×Non-Reid (Model III)	Middle subhumid maize region
Denghai 9	65232×8723	Reid×Non-Reid (Model III)	Middle subhumid maize region
Zhengdan 958	Zheng58×Change7-2	Reid×DOM (Model II)	North spring maize region
Jingke 968	Jing724×Jing92	Reid×DOM (Model II)	West semiarid maize region
Jingke 665	Jing725×Jing92	Reid×DOM (Model II)	West semiarid maize region
Jidan 27	Si-144×93287	Reid×DOM (Model II)	Eastern humid maize region
New Tiedan 10	C8605-2×Dan340	Reid×DOM (Model II)	Middle subhumid maize region
Dan 2109	C8605-2×Dan598	Reid×DOM (Model II)	Middle subhumid maize region
Nongda 108	P178×HuangC	Reid×DOM (Model II)	Middle subhumid maize region
Huangmo	Huangzao4×Mo17	Non-Reid ×DOM (Model I)	West semiarid maize region
Zhongdan 2	Mo17×Zi330	Non-Reid ×DOM (Model I)	West semiarid maize region
Danyu 13	Mo17×E28	Non-Reid ×DOM (Model I)	North spring maize region
Jidan 180	Mo17×Ji853	Non-Reid×DOM (Model I)	West semiarid maize region
Jidan 342	Ji1037×Ji853	Non-Reid×DOM (Model I)	West semiarid maize region
Sidan 19	Si-444×Mo17	Non-Reid×DOM (Model I)	West semiarid maize region
Zedan 33	918×Ze461	Non-Reid×DOM (Model I)	West semiarid maize region

Screening results of heterotic crosses in 3 densities during 2 years demonstrated that the yield of JV2-1×J1590 was significantly increased by 8.26% compared with "Xianyu 335" in model I. JC2-2×J1577, PH6WC×J1577, JC7-2×1577, JC2-2×J1881, in model II, JCV-2×J1828 and Liao3180 ×T106 in model III were excellent crosses with strong heterosis, high yield, stable yield and density tolerance.

Liao3180×T106 (also known as Tiannong 9) was a popular cultivar, with better yield and disease resistance than "Xianyu 335". In this study, the emerging of it as a strong heterotic cross indirectly verified that the models were suitable for maize production.

The 3 heterotic groups and 3 heterotic models are convenient and practical for maize breeding in northern China

Multiple heterotic groups and heterotic models principle brought considerable work and cost. It is efficient to improve breeding by building simple and practical heterotic models.

Traditionally the American model of heterosis was 2 groups (Reid, Lancaster) with heterotic model Reid × Lancaster, which developed into (Reid, Non-Reid), with heterotic model Reid × Non-Reid (Wu, 2014). In accordance with this model, Tangsipingtou and Lvda Red cob germplasms should be divided to Non-Reid group, which did not fit the breeding practice in northern China. The "3 heterotic groups and 3 heterotic models" principle were proposed according to the former studies. Under the guidance of it, genetic improvements and breeding of inbred lines have been carried out [15-17], and clear results had been achieved.

The principle that lines selected from one group tested by other 2 groups lines was proved to be practical, and reasonable. Main popular cultivars in northern China were bred in accordance with it, such as Xianyu335, Zhengdan958, and Jingke968.

This experiment was followed the principle that "lines selected from between 2 groups tested by the 3rd group lines", hope to research and prove it furtherly.

Results showed that there was strong heterosis for the crosses followed the 3 heterotic groups in ecotypes and densities, with high yield, stable yield and density tolerance crosses emerged. Meaning the "3 heterotic groups and 3 heterotic models" principle was practical, effective and suitable for northern China.

Test location of maize is representative. Representative ecotypes were considered as testing locations. Placed in Songnen Plain, Jilin Province is a major spring maize production area in northern China. According to geography, the province can be roughly divided into 3 ecotypes: a western semiarid region, a central semi-humid region and an eastern humid region. Western semiarid region lacks rain with saline and infertile soil, drought is the main cause of yield reduction. As abundant rainfall and fertile soil, central semi-humid region is the major maize production area. However, lodging caused by high wind speed during the growth period as well as disease cause yield reductions. Eastern humid region, chilling damage affects high yields. In consideration of these characteristics, the test locations of the 3 different ecotypes were representative.

Densities gradient system consisting of 50,000 plants per ha, 60,000 plants per ha, and 80,000 plants per ha were set according to the actual and trending of maize production in Jilin Province.

CONCLUSION

The experiment was carried out in 3 ecological zones during 2-year with densities of 50000, 60000,

and 80000 plants per ha, respectively. Excellent hybrid crosses with high, stable yield and density tolerance were screened out. 1 cross of model I, 4 crosses of model II, 2 crosses of model III showed strong heterosis. Results demonstrate clearly that the "3 heterotic groups and 3 heterotic models" hypothesis for maize heterosis application is effective and simple, and Models II and III are suitable for north China.

ACKNOWLEDGEMENTS

This work was funded by The National Key Research and Development Program of China (Grant number 2016YFD0101202); and Sciences and Technology Development Program of Jilin Province (Grant number 20170307009NY).

REFERENCES

[1] Khan, Z.H., Khalil, S.K., Ikramullah, Ali, M., Iqbal, A., Islam, B., Ali, K., Ali, W., Ahmad, M., Afridi, S.G, Shah, F. (2019) Physical characteristics of cobs and kernels in sweet corn under varying planting environments. Fresen. Environ. Bull. 28, 6568-6573.

[2] Li, M., Yang, D., Yang, Z., Wen, S.X., Zhu, G.X., Gou, W.L., Li, C. (2019) Effects of sludge addition amount on soil physico chemical properties and growth of maize seedlings in rocky desertification areas of Guizhou Province. Fresen. Environ. Bull. 28, 6816-6824.

[3] Yue, H.W., Bu, J.Z., Wei, J.W., Zhang, Y.L., Chen, S.P., Peng, H.C., Xie, J.L., Jiang, X.W. (2019) Evaluation of the adaptability and stability of maize cultivars through gge biplot analysis. Fresen. Environ. Bull. 28, 6719-6732.

[4] Yagiz, A., Konuskan, O. (2019) Changes of some germination characteristics with different phenological stages in maize. Fresen. Environ. Bull. 28, 9886-9891.

[5] Abd El-Aty, M.S., El-Sayed, A.A., Amer, E.A., Rizk, M.S. (2018) Evaluation and classification of sixteen new yellow maize inbred lines using linextester analysis in different locations under Egyptian environment. Fresen. Environ. Bull. 27, 4986-4994.

[6] Liu, W.G., Zhang, Z.J., Zhao, W.Q., Yang, W.G., Lu, M. (2016) Genetic analysis of Jidan maize varieties using fluoescent SSR markers. Journal of Northwest A & F University (Nat. Sci. Ed.). 10, 25-36.

[7] Wang, M., Zhang, H.W., Yue, Y.H., Jin, M.H., Zhang, Z.J., Liu, W.G. (2012) Analysis of Germplasm Basis and Heterosis Model of Maize of Jilin Province in the Past Twenty Years. Journal of Jilin Agricultural Sciences. 1, 27-31.

[8] Zeng, S.X. (1990) The maize germplasm base of hybrids in China. Scientia Agricultura Sinica. 23, 1-9.

[9] Li, S.S. (1997) Breeding and utilization of maize cultivar "Huangzao 4". Beijing Agricultural Sciences. 1, 19-21.

[10] Jiang, L.Z., Gao, Y., Zhang, J.H. (2007) Review on breeding and application of maize Lv Germplasm. Liaoning Agricultural Sciences. 2, 47-49.

[11] Wu, Y. (2014) The research of heterotic group and heterosis model of the northern maize of China. Changchun: Jilin Agricultural University.

[12] Zhao, W.Y., Liu, R.Z., Liu, X. (2009) The Utilization Expect of the Danyu Inbred Lines of Lv Series in the Corn Production of China. Journal of Maize Sciences. 6, 24-26.

[13] Li, Y.W., Long, M., Zuo, L.H., Li, W., Zhao, W.C. (2019) Brittleness Evaluation of Coal Based on Statistical Damage and Energy Evolution Theory. Journal of Petroleum Science and Engineering. 172, 753-763.

[14] Tang, Q.Y. (2002) Practical statistic analysis and DPS data processing system. Beijing: Science Press.

[15] Dong, Y., Yang, W., Ren, X.J., Li, R., Wang, L.P., Xv, X., Yang, W.G. (2017) Research on Heterosis and Combining Ability of Yield per Plant in Reid Improved Lines of Maize under Different Densities. Journal of Jilin Agricultural University. 2, 1-7.

[16] Sun, G.X., Ren, X.J., Yang, W., Ci, J.B., Zhang, Y., Yang, W.G. (2015) Study on Density-Tolerance of Improved Lines of Chang 7-2 and its hybrids. Journal of Jilin Agricultural University. 2, 141-147.

[17] Wang, Y.F., Luan, Y., Li, Y.H., Zhou, T., Xu, D.Y., Gao, Y., Yang, W.G. (2016) Research of Yield Potential and Stability on Improved Lines from Maize Basic Populations. Journal of Maize Sciences. 5, 8-14.

Received: **03.11.2019**
Accepted: **08.02.2020**

CORRESPONDING AUTHOR

Wei-Guang Yang
Faculty of Agronomy,
Jilin Agricultural University,
Changchun 130118 – China

e-mail: shaoshao889q@163.com

© by PSP Volume 29 – No. 05/2020 pages 3738-3755 Fresenius Environmental Bulletin

AUTUMN SEASONAL COLOR OPTIMIZATION METHOD FOR THE SCENIC FOREST OF PURPLE MOUNTAIN FOREST PARK

Zi Wang[1,2], Mingyang Li[1,2,*], Chunhua Qian[1,2,3]

[1]College of Forestry, Nanjing Forestry University, Nanjing, China
[2]Co-Innovation Center for Sustainable Forestry in Southern China, Nanjing, China
[3]Department of Intelligent Agriculture, Suzhou Agricultural Vocational and Technical College, Suzhou, China

ABSTRACT

At present, the seasonal color landscape of scenic forests receives substantial attention, but there is no scientific or reasonable solution for the lack of color in the landscape. The purpose of this study is to explore an optimization method that is suitable for the autumn forest color landscape in order to provide a reference for the construction of color landscape in forest parks. The autumn seasonal color optimization method for scenic forests that is proposed in this paper is the dominant color substitution method. This method takes the urban forest park as the orientation basis, takes the forest subcompartment as the unit, determines the subcompartments that need to be optimized with a sensitivity analysis and color aesthetics evaluation, and takes the overmature forest subcompartments as the ultimate object of optimization; then, the corresponding submethod (dominant color substitution in subcompartments submethod or dominant color substitution outside the subcompartments submethod) is selected according to their characteristics to optimize the subcompartments . The results show that, after optimization, the proportion of stands with a high-quality color aesthetic increased from 56.91% to 58.61%, and the proportion of stands with more than one color type in autumn increased by 1.67%. In the ecological function, the biomass of subcompartments increased by 185.83 $t \cdot hm^{-2}$ in total, the Shannon-Wiener Index and the Pielou Index of tree species of all subcompartments also increased after optimization. In conclusion, an ecology-aesthetic color landscape optimization method for autumn scenic forests is proposed in temperate, warm temperate and subtropical regions of China.

KEYWORDS:
Autumn seasonal color, Ecology, Dominant color substitution method, Purple Mountain

INTRODUCTION

Different aspects of the colors of biological species have been widely studied [1-3]. In studies on sea animals, Sheppard [4] focused on the property of shells, and Donner et al. [5] analyzed the changing data on coral bleaching, which was related to the health level of coral. Birds have attracted the attention of many researchers; for example, Ridgway [6] wrote an ornithology book using more than one thousand types of color to describe the birds. Because the colors of bird eggs [7] are diverse, they have been the objects of research as well.

Schifferstein et al. [8] utilized different vegetables, such as tomatoes, carrots and cucumbers, as study resources to explore the relationship and the effect between foreground color and background color. They found that the foreground color related to the background color and that it also depended on the background color. This meant that the color of foreground would change simultaneously with the diversification of the background color [9].

Concerning tree species color, studies have mainly concentrated on the colors of leaves of woody species [10-12]. For example, Grose [13] compared the leaf color of native species with that of exotic species growing in Australia. The results showed that the leaves of exotics were colorful and dark, while there were fewer and lighter leaf colors of endemic trees. Additionally, the effect of genetic isolation on the leaf color of local vegetation was critical. Finally, homogenization, which was observed with urban expansion, could be reflected by the leaf color.

Color photographs are often treated as fundamental research data, and the process of taking photographs varies, such as images from satellites, drones [14] and cameras [15-19]. Because the near-surface presence can be seen in more detail in images taken by camera [20], studies assessing forest scenic aesthetics always utilize camera images as the primary data for gaining near-surface information, such as the foliage and color of trees. In agriculture and grass seasonal landscapes, Schüpbach et al. [21] selected 244 colored photo-

graphs for respondents to assess. They put the season color as a factor and evaluated the values of recreation and aesthetics in the study area. In addition, color photographs are almost always an indispensable data source in studying the scenic beauty of other landscapes, such as corridor and mountain landscapes.

In a color description, Welland [22] included a range from pure white to yellow to describe the color of diamonds. In fact, more color descriptions can be found for woody plants. Fridell Anter [23] noted that woody landscapes were always dominated by the color of green in some urban and rural regions. Grose [24] used the colors termed mid-green, dark green and glossy green to define leafage color information, while Merzlyak and Gitelson [25] selected foliage with colors of uniform green, green-yellow, yellow-green and yellow without anthocyanin pigment as a source to study autumn leaves. In the study of color, color can be defined quantitatively according to a color system. Itten's hue circle [26] is a color system that with a hue ring divided into 12 parts with different colors. With the development of the color system, new color systems, such as the Pantone series and the Natural Color System of Sweden, have been used in many research fields, such as in studies of buildings or plants. In addition, the Munsell soil color chart is often used to analyze and compare the color of soils.

Autumn seasonal color. Seasonal autumn color is typical and representative, thus attracting many researchers to its study. Woody vegetation with yellow leaves related to autumn phenology dominates northern Europe [27], just as species with red leaves dominate in other parts of the world. In temperate regions, the percentage of the tree species is approximately 15%, and the leaf color will change from green to yellow or to red in fall. Furthermore, the proportion can reach 70% in certain regions, such as New England [28, 29]. Grose [30] pointed out that a species that characteristically has orange leaves in some areas might differ in its characteristic leaf color in other areas.

Actually, the changing leaf color of woody plants is affected by the unmasking of carotenoids, as well as the breakdown of chlorophyll [31], which is considerably related to the leaves' intense yellow coloration. In terms of red coloration, anthocyanins are often treated as a functional indicator because they are beneficial for branches and the trunk in enhancing the recovery rate of foliar nitrogen and other resources through the protection of photooxidation and photoinhibition [32-37]. However, many researchers [38] have found that red autumnal leaf coloration is not produced by anthocyanins but by mid-senescence leaves synthesizing de novo. Tropical young leaves with a red color are as the result of physiological causes, such as scavenging reactive oxygen species and defense from photoinhibition [39].

As temperature and precipitation are thought to control leaf color changes and leaf-fall [40-42], climate changes may also affect the phenology of autumn colors (Archetti et al. 2013) with ecological implications [43]. In New England, Archetti et al. [44] used a substantial amount of long-term data to study the variability in the timing and cumulative amount of the autumn color of eight species and predicted changes in the phenology of autumn colors until the year 2099 by using a process-oriented model. The result showed that climate change will lead to an overall increase in the amount of autumn colors for most species.

In vertical phenological variation, trees of different heights provide a small-scale ecological distinction within the forest. Although differences in the leaf coloration and leaf-fall dates for trees at diverse forest heights or life stages are not reported [45, 46], vertical variation affects leaves' autumnal phenology. Gressler et al. [47] observed that the differences in the relative humidity and light availability are related to autumn phenological variations. In addition, air temperature and light were analyzed as microenvironmental drivers, which have an impact on the extent of differences in leaf senescence in the overstory, mesostory and understory, which are the three vertical canopy positions. Richardson and O'Keefe [48] found that overstory individuals of two study species presented earlier leaf coloration and leaf-fall than did conspecific understory trees, whereas the other three species showed the opposite changes.

Seasonal variations in leaf color in different seasons are frequently compared, especially those of spring and autumn. Lev-Yaduna et al. [49] found that some tree species with red leaves in the fall would have more or less red coloring in their spring leaves. Additionally, approximately 50% of species with red spring leaves had yellow autumn leaves. Klosterman and Richardson [14] calculated the color indices from drone imagery of oak-dominated temperate deciduous forest and found that the plant area index correlated with the canopy greenness index in the spring green-up. Furthermore, it correlated with the canopy redness index in autumn senescence. Concerning leaf herbivore faunas, spring and autumn faunas are unidentical, which is related to selection of leaf coloration in spring or autumn [50, 51].

The study of autumn vegetation seasonal color landscape is mainly divided into two aspects. On the one hand, the quantitative study of landscape color can be found in many theses. Zheng took common garden plants in autumn as a research object, while Zhuang quantified the landscape color of a natural secondary forest plant community and an artificial community of Wutong in Shenzhen. Different types of landscape aesthetic evaluations, such

as mountain and river landscapes, are based on the scenic beauty evaluation method (SBE method). Because this method can objectively reflect the aesthetic value of the actual landscape, it is also adopted in the study of the aesthetic evaluation of autumn color landscape. Zheng et al. [52] used a community survey to carry out an aesthetic evaluation of scenic forests by the SBE method. Based on different elevation levels, the autumn landscape color was quantified, and the color distribution and aesthetic quality of different plant communities were obtained. Chen et al. [53] studied the forest landscape in spring, summer and autumn in the mountainous area of Western Beijing, evaluated the landscape aesthetically by using the SBE method, established a multiple regression model for predicting the quality of scenic aesthetics based on various landscape factors, including the types of seasonal color, and proposed the corresponding operational technical principles of autumn seasonal color landscape.

Reasons for choosing autumn color landscape as the research object in Purple Mountain Forest Park. The color landscape of Purple Mountain Forest Park in spring is mainly concentrated on Meihua Mountain, which is a mature garden landscape with a good quality color landscape and is highly popular among the public. In summer, the color landscape is dominated by artificially planted herbs and woody flowers, and the forest fulfills more service functions, such as providing shade and cool; however, the ornamental value of the landscape is not high. In winter, due to the low temperature, rain, wetness, and sometimes fog and haze, there are fewer outdoor activities, so the value of a colorful landscape in winter is low.

Compared with the forest landscape of Purple Mountain forest park during these three seasons, the autumn color landscape has its own uniqueness and must be optimized. First, autumn is the main viewing season for the scenic forest color landscape, and the forest landscape is the main part of the landscape. Second, the autumn leaf tree species are widely distributed throughout Purple Mountain forest park, with a large service radius. Third, the autumn color landscape offers visitors multiangle viewing, such as viewing the forest from within the forest and overlooking the forest from high altitudes, with prominent multilevel viewing service functions. Finally, tourists' preference for the seasonal color landscape is very high, and there are many tourists in autumn. At present, there are also major problems that are urgently in need of being solved; that is, there is no targeted optimization method for the color landscape in some areas with poor-quality color landscapes. Therefore, poor landscapes cannot be improved, which results in an inadequate ornamental service function of the autumn color landscape in the scenic forest.

The purpose of this paper is to explore targeted autumn color landscape optimization methods in order to improving the quality of the autumn color landscape as well as providing a reference for the optimization of autumn landscapes in other areas.

MATERIALS AND METHODS

Study area. This study focused on the Purple Mountain National Forest Park, which lies in the city of Nanjing, Jiangsu, China (Fig. 1). The forest park is located at 32°16′15″N, 118°48′00″W and has a total area of 3008.8 km. It belongs to the transition zone between the north subtropical zone and the warm temperate zone, with abundant sunshine resources and distinct seasons. The park is a mixed growth area of deciduous broad-leaved forest and evergreen broad-leaved forest with abundant plant species and an obvious transitional vegetation composition. It is a substantial city forest green space with a forest coverage rate reaching 70.2% and accounting for 15.6% of the total forest area in Nanjing.

Purple Mountain National Forest Park is well-known, attracting a large number of visitors. In recent years, the average annual passenger flow has fluctuated approximately 8 million times, and the number of climbers has fluctuated approximately 9 million times. The tourist volume of Purple Mountain Forest Park is bimodal, i.e., occurring in spring (March-May) and in autumn (October). An analysis of the proportion of local tourists in each month shows that the main reason for the seasonal weakening of the forest park is the participation of local tourists. This seasonal weakening is the unique advantage of urban forest parks. The study of statistical data shows that, among the three major scenic spots of Sun Yat-sen Mausoleum, Ming Xiaoling Mausoleum and Linggu Temple, the proportion of visitors to Sun Yat-sen Mausoleum is the lowest (14%), while the proportions of Linggu Temple (30.2%) and Ming Xiaoling Mausoleum (26.8%) are higher. Purple Mountain has been recognized as one of the forty best tourist attractions in China since 1991, and it was assessed as a national civilized scenic spot in 1999. The urban forest park was designated an "AAAA level tourist area" and was certified by the ISO14000 environmental management system in 2000.

Data collection. Direct data. Data resources include the forest resources survey data of Purple Mountain in 2017; World View 3 satellite image of Purple Mountain on October 29, 2017 (panchromatic band + multispectral band + shortwave infrared band + CAVIS band). The spatial resolution of the panchromatic band is 0.31×0.31 m, the multispectral band is 1.24×1.24 m, the shortwave infrared band is 3.70×3.70 m, and

the CAVIS band is 30.00×30.00 m.); the NDVI (Normalized Difference Vegetation Index) in autumn data and the DEM (Digital Elevation Model) data.

Data on autumn season color preferences of visitors. Visitors' preferences data are obtained mainly through questionnaires, and 140 participants participated in the survey. There were three main portions of the survey: tourist background information (TB), favorite autumn landscape color (PC) and favorite seasonal color types (CT). Questionnaire survey sites were scattered in every scenic spot of Purple Mountain Forest Park. Before the questionnaire was used as a survey, teachers of relevant specialties at Nanjing Forestry University reviewed the questionnaire (Table 1).

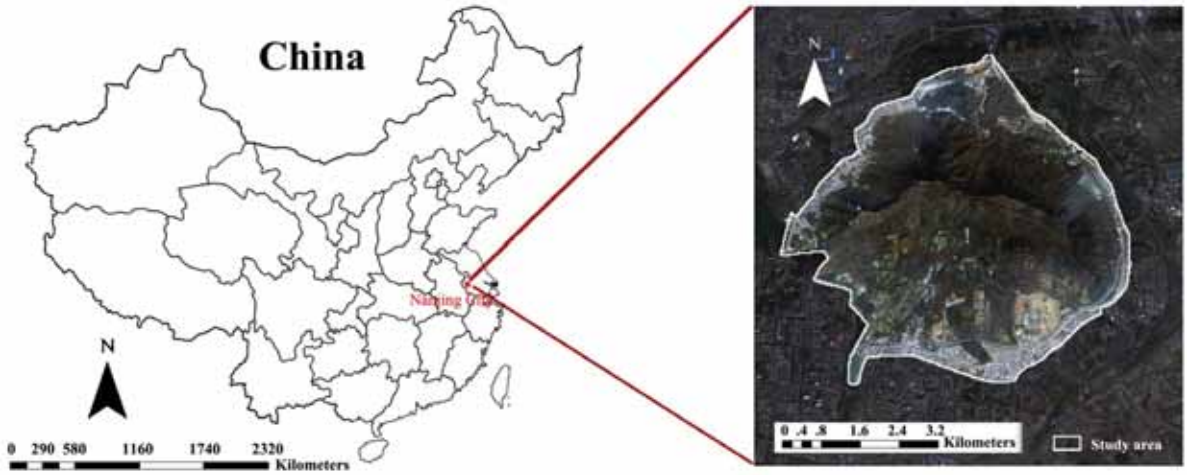

FIGURE 1
Location of Purple Mountain, Nanjing, Jiangsu

TABLE 1
Questionnaire designed in 3 categories: visitors' background (TB), visitors' one preferred color of forest landscape in fall (PC), visitors' preferred autumn-color types. The aim and options of the survey are shown as well.

Questionnaire	Acronym	Options	Explanations
Visitors' background	TB	Age: a) <18 b) 18-29 c) 30-50 d) >50 Occupation: a) Student b) Worker c) Manager d) Others	The basic background information of the visitors is determined, and the visitors participated in the next color-aesthetic evaluation are selected according to the proportion of the background.
Visitors' one preferred color of forest landscape in fall	PC	a) Red b) Red-orange c) Orange d) Orange-yellow e) Yellow f) Yellow-green g) Green	To determine the visitors' favorite autumn landscape color, and determine the preference ranking of each color, as the basis for optimizing the color landscape.
Visitors' preferred autumn-color types	CT	a) None (Green) b) One (e.g., red-orange) c) Two (e.g., red and yellow) d) Three or above (e.g., red, orange and yellow-green)	To determine the preference ranking of visitors for autumn color types, as a basis for optimizing color landscape.

In the process of investigation, we mainly adopted a one-to-one approach. First, investigators introduced themselves and asked tourists if they were willing to participate in the survey. If the answer was no, investigators chose other tourists. If visitors were willing to participate in the questionnaire, the questionnaire was sent on paper to participants for them to answer [54-57]. After that, the investigators asked whether the participants were willing to participate in the following aesthetic evaluation of landscape color. If the answer was yes, investigators recorded the contact mode of the participants to facilitate the follow-up contact.

Data on color aesthetic evaluation. Landscape aesthetics are related to the physical attributes of landscape, including color and structure. Because scenic color photographs can objectively reflect the real landscape, they are often used as data sources for landscape aesthetic evaluation [58, 59]. Therefore, the database of the aesthetic evaluation of color landscape is also based on the collection of on-site color pictures, but autumn seasonal color is the main content of the photographs.

Diverse light intensity environments in forests [60] decline with the vertical gradient and have a critical impact on the autumn phenology of trees [61, 62]. The initial and final periods of the autumn phenology, leaf coloring and leaf-fall are different for different strata (overstory, mesostory and understory); however, the overstory trees peaked at a similar time as the mesostory trees. Therefore, more visible autumnal color is simultaneously distributed in the highest and second-highest canopy levels, which were selected as the main body of each photograph.

Color landscape photographs were collected in October and November 2017. A total of 1324 photographs were collected; i.e., 2 pictures were taken in each subcompartment. The two photographs (in each subcompartment) were randomly sampled, and one of the two photographs was selected. In addition, 662 photographs were selected as the research data.

To truly reflect the color-aesthetic characteristics of the forest seasonal landscape and to make the landscape more comparable, the photography should be carried out according to the following criteria: (1) choose sunny and high visibility weather conditions to photograph; (2) photograph under direct sunlight conditions, if possible; (3) give priority to upward landscapes; (4) select forest seasonal color landscapes in the forest subcompartment as the photograph object; (5) use the central coordinates of the forest subcompartments as the coordinates of the photography site; (6) choose the time that best reflects the autumn landscape characteristics; and (7) use an iPhone 7 Plus mobile phone as the photographing tool to shoot areas without buildings, transmission lines, wildlife, equipment or other nonlandscape elements.

Different types of landscape aesthetic evaluations [63] and forest seasonal color landscape aesthetic evaluations make photographs that can be made into slides. Thus, this study randomly presents all photographs in the form of slides.

Because the details may bias the judges, only a brief explanation is given to the judges before the judgement begins. The explanation does not involve details about the research, such as the photographing place, tree species, sanitary felling and the condition. Daniel and Boster [64] were the first to provide "standardized instructions" before judging, which have been widely used since. We also used this method to explain the background, significance and requirements. The age and occupational background information of the judges should be consistent with that of the participants in the questionnaire survey, and no color-blind judges should be included. Each judge scores the slides in the same order by using the same evaluation form. There are seven points on the evaluation form, and each one represents a class of color-aesthetic landscape quality grade: 1 point (very poor), 2 points (poor), 3 points (medium-poor), 4 points (medium), 5 points (medium-good), 6 points (good), and 7 points (very good). According to the principle of psychophysical evaluation, each slide is projected for 10 seconds. The judges record the response value of each landscape on the evaluation response table according to the sequence of slides.

To eliminate the differences in color-aesthetic standards due to gender and individual subjective differences between different judges, the evaluation values are standardized as follows:

$$Z_{ij} = \left(R_{ij} - \overline{R}_j\right) \Big/ S_j \quad (1)$$

$$\overline{R}_j = \frac{1}{n} \sum\nolimits_{i=1}^{n} R_{ij} \quad (2)$$

$$S_j = \sqrt{\frac{1}{n-1} \sum\nolimits_{i=1}^{n} \left(R_{ij} - \overline{R}_j\right)^2} \quad (3)$$

where Z_{ij} is the standardization value of the j^{th} judge for the i^{th} scene; R_{ij} is the color-scenic assessment score of the j^{th} judge for the i^{th} scene; R_j is the mean value of the color-scenic assessment score of the j^{th} judge for the same vertical-structure landscapes; and S_j is the color-scenic assessment score and standard deviation of the j^{th} judge for the same vertical-structure landscapes.

Quantification of seasonal color type. As a result of autumn seasonal color, the forest landscape is mainly illuminated by light, and the color appearance is presented by the leaves. According to the scenic photographs of the investigation subcompartments, the tree stand

landscape (canopy) is taken as the main color extraction object. Based on Itton's 12-color hue ring theory, the HSB color model is used to refine the color ring to 24 color hue values. Furthermore, the color types are defined by the interval of the color hue value. The number of colors in each subcompartment landscape is extracted by using ColorImpact software.

Technical process: Using the software, the number of color components of each photograph is adjusted to the maximum value (64), and then the color hue values of each component are quantified. According to the color hue value intervals of the color ring, the category of each color is defined, to determine the number of autumn seasonal color categories of each landscape.

Optimal region determination. The determination of the optimal region is mainly based on the location of the urban national forest park. The urban national forest park has the following five basic characteristics:

1. The forest park is located in the urban planning area, which is directly affected by urban life and urban expansion.

2. The park has a long history of cultural and cultural landscapes, which are the essence of urban landscape or historical and cultural cities.

3. The main body of the forest park is mostly an urban natural landscape environment, and it is the largest and most concentrated ecological green space in the urban area. At the same time, it also functions as an urban public green space.

4. The organic integration of the natural landscape and human landscape is conducive to the development and utilization of tourism resources.

5. Tourism development is recent, the infrastructure conditions are good, tourism development is fairly basic, and the number of tourists is substantial. The forest park can play a variety of functions by coordinating the contradictions among the needs of scenic tourism, ecological protection and public leisure [65].

Therefore, as a national forest park, Purple Mountain has been endowed with many functions, such as natural protection, landscape tourism and leisure for citizens. Basically, it can be summarized as having two major service functions: ecology and aesthetics [66].

Optimal region determination based on ecological sensitivity. Eco-sensitivity refers to the degree of response of the ecosystem to human disturbance and natural environment change, thus indicating the degree of difficulty and the possibility of regional ecological environment problems occurring [67]. The sensitive areas are more likely to have ecological environmental problems when they are affected by unreasonable human activities. The essence of the ecological sensitivity assessment is the process of identifying potential ecological problems in the context of the current natural environment and implementing them into specific spatial regions [68]. Through the evaluation of ecological sensitivity, highly sensitive areas that are not easy to recover after a disturbance can be screened out to provide target orientation for the determination of an ecological space that is based on the perspective of improving the internal stability of the ecosystem. It can also provide a scientific basis for the decision-making of prevention and treatment efforts to solve regional ecological environment problems [69]. Because the ecological sensitivity of Purple Mountain is closely related to vegetation and topography, it is vulnerable to human disturbance [70]. Therefore, the vegetation index (NDVI), slope (generation of DEM data), distance from the road, and distance from residential areas are extracted as ecological sensitivity evaluation indicators.

In spatial principal component analysis (SPCA), several spatial variables are analyzed and transformed in two-dimensional space, and a few irrelevant comprehensive indicators are extracted to achieve the best synthesis and simplification of high-dimensional variables. In this study, SPCA was introduced to analyze and screen the four evaluation indicators. Taking the cumulative contribution rate of more than 95% as the basis and criterion, the first principal component was selected as the final result of the ecological sensitivity analysis [71]. The mean value was taken as the threshold break-point, and the study area was divided into two parts: the high-sensitivity and low-sensitivity ecological areas. The high-sensitivity area is the protected area, and the low-sensitivity area is the main area of color optimization.

Technological process: Based on the ArcGIS software platform, three grid layers, namely, slope, distance from road and distance from residential area, were generated by two modules, namely, surface analysis and cost-weighted distance, in the spatial analysis tool. Then, the three raster layers and NDVI raster layers were divided into the same number of levels after being unified by unit through the "Reclassify" module. The principal components module was used to analyze the principal components of the four layers. For the raster layer after principal component analysis, the mean value of the raster is the threshold breakpoint, which can be divided into two categories: the nonoptimum area and the optimum area (Fig. 2).

Optimal region determination based on color aesthetics. The result of the SBE method is determined by the characteristics of the landscape itself and the aesthetic scale of the evaluators; it is the most widely used and recognized psychophysical method in landscape evaluation [72, 73]. Research on the seasonal color of forest landscape is also based on this method to evaluate seasonal

landscape aesthetics. Therefore, this study also adopts this method to evaluate the color aesthetics of the autumn landscape.

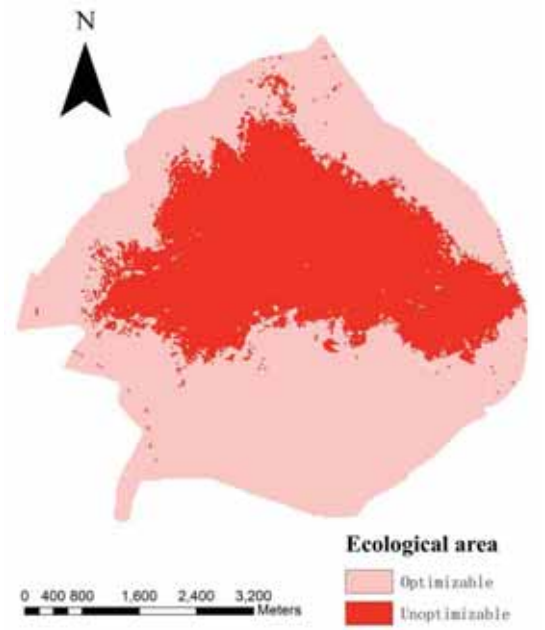

FIGURE 2
Ecological optimized area

The Kriging method is a linear unbiased optimal estimation of unknown sample points based on the data of some known sample points in the finite forest area of unknown sample points, which takes into account the shape, size and spatial orientation of sample points, the spatial position relationship between sample points and the unknown sample points, and the structural information provided by the variogram. Thus, this method is applied in this study. Because ordinary Kriging is the most common interpolation method, this study chooses the ordinary Kriging interpolation method from the many Kriging methods. In addition, it is a linear estimation of regionalized variables; it requires that data be changed into a normal distribution, and the expected value of the artificial regionalized variable Z is an unknown constant. Based on the analysis of the interpolation accuracy of different semivariance theoretical models of forest survey factors in Purple Mountain [74], the Kriging interpolation model was selected for this study as the best index model with both fitting accuracy and prediction accuracy.

Technical process: Using ArcGIS as the software platform, the center points of 662 subcompartments vector files in the research area were extracted by a "Feature to point" module. The point vector files with the same coordinates of the values of color beauty attributes are input, and the "Ordinary" Kriging method is selected through the "Kriging" module in the "Spatial Analysis" tool. The "Exponential" semivariance theory model was used to generate the Kriging interpolation trend surface of the seasonal color aesthetics landscape. For the generated raster layers, the average value of the raster was used as the threshold breakpoint, which can be divided into two categories: the non-optimization area (better color landscape quality) and the optimization area (worse color landscape quality) (Fig. 3).

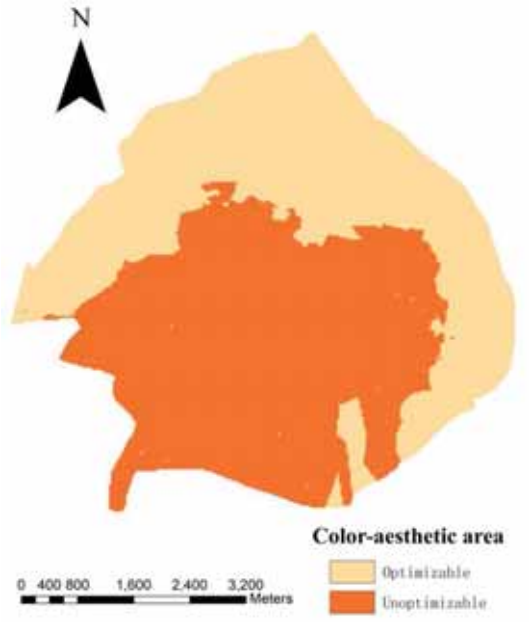

FIGURE 3
Color-aesthetic optimized area

According to the above two approaches, the forest subcompartment was treated as the unit, and these subcompartments were located in the overlapping areas of ecology and color aesthetics and can be selected as the object of optimization (the pink areas) (Fig. 4).

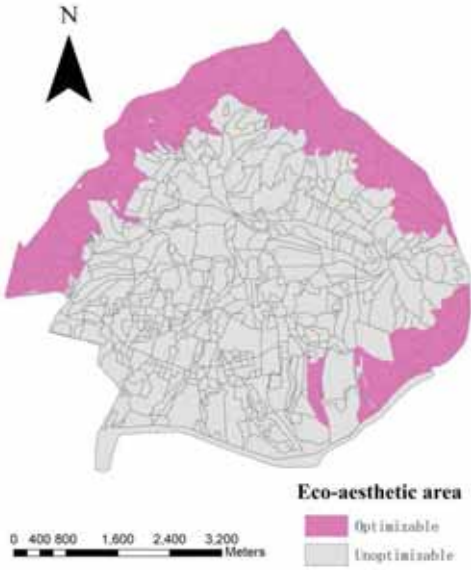

FIGURE 4
Eco-aesthetic optimized subcompartments

Optimum objects determination based on the particularity of scenic forest management. As the scenic forest is a special kind of forest, it is generally allowed to cut only old and rotten trees

with pruning and sanitary felling (GB 26902-2011-T Technical Regulations for the Construction of Tropical and Subtropical Eco-scenic Forest - National Standards and National Standards). Overmature forests are extremely vulnerable to wind fall and death due to infection with diseases and insect pests because of their old age, as well as to aging with fewer ecological benefits. It is necessary to renew the forest to maintain the stability of the forest ecosystem. Therefore, in this study, forest subcompartments with overmature forests in the age group stage were utilized as the ultimate optimization objects (Fig. 5).

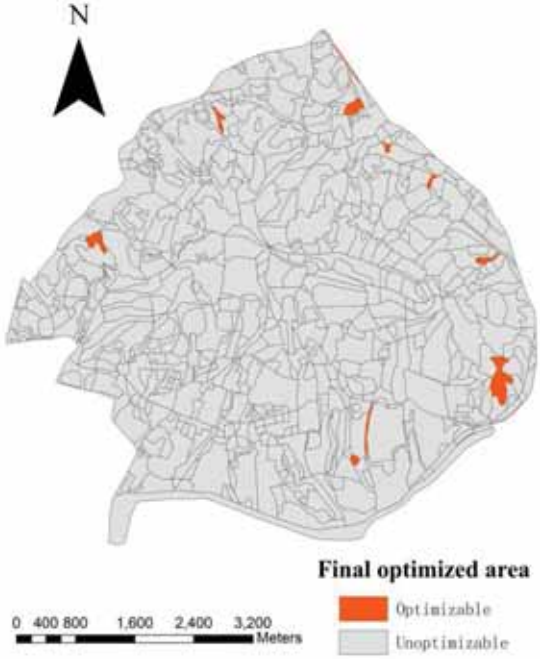

FIGURE 5
Final optimized subcompartments

Forest subcompartment optimization method. Because the viewing horizon of autumn landscape color in scenic forest is relatively limited, the viewing area of high-quality color landscape can be broadened by increasing the number of dominant colors, and the quality of seasonal color landscape inside and outside of the forest can be effectively improved to achieve the goal of optimization. At the same time, dominant color-leaf tree species can form relatively stable plant communities, thereby stabilizing the optimization of the color landscape.

The method of color optimization that was proposed in this study is called the dominant color substitution method. It means that an autumn landscape with poor color quality can achieve the purpose of landscape color substitution only by replacing dominant tree species in the landscape to improve the color quality of the seasonal landscape. This concept is based on the premise that the proportion of the original main tree species in the subcompartments remains unchanged. For example, if the original stand of a subcompartment is mixed forest, then the stand property of the attribute of the subcompartment is still mixed forest after optimization. Additionally, the proportion of each tree species in the initial stand of this subcompartment remains unchanged, and only the dominant tree species (the largest tree species) in the stand are replaced by the target tree species, to achieve the result of color optimization.

In this method, the autumn landscape color aesthetic evaluation score is used as the basis for judging the quality of the color landscape. According to the ranking results of "CT", the number of autumn seasonal color types is optimized from the beginning to the end. The ranking of "PC" is used as the basis for the optimization of the color composition of the seasonal landscape. The optimal tree species selection is mainly based on the dominant color-leaved tree species in the study area. Specifically, it can be divided into two methods: dominant color substitution in forest subcompartments and dominant color substitution outside forest subcompartments.

Dominant color substitution in forest subcompartments. This method was applied to the color landscape with replaceable colors in the subcompartments. According to the information on the tree species in the subcompartments, autumn color-leaf tree species are selected as the target of color replacement so that the purpose of color replacement in autumn can be achieved through color-leaf tree species replacement, and then the quality of the color landscape can be improved.

When there is only one color-leaved tree species in the subcompartments, the tree species is regarded as the target tree species of color replacement to replace the dominant color of the dominant tree species, and then to optimize the color landscape.

When there is more than one species of color-leaved trees in the subcompartment, all color-leaved trees will be selected. According to the actual color landscape of each tree species in the subcompartments, and the ranking results of "CT" and "PC", tree species will be screened from front to back in order to optimize. When the landscape presents autumn color, but there is no significant difference in the color hue, all of the replaceable dominant color tree species are selected as the best color-leaved tree species, as these represent the original proportion of tree species in the subcompartment for which to distribute tree species in the new forest subcompartment. When there is no autumn phase color in the landscape, the optimal color-leaf tree species are selected according to the qualitative description of the autumn color-leaf tree species as part of the theory of color change, as a means to replace the dominant tree species. At the same time, after optimization, forest management measures, such as thinning and sanitary felling, are needed to improve the autumn color landscape quality.

Dominant color substitution outside forest subcompartments. The method is applied to the color landscape of nonreplaceable colors (autumn-colorless leaf species) in subcompartments. The selection area of the target dominant color should be concentrated in the area to be optimized with low ecological sensitivity. The selected target color-leaved tree species should have the same lifestyle as one of the main tree species in the optimized subcompartment. Based on the premise of satisfying the above conditions, according to the ranking results of "CT" and "PC", the tree species were screened, in order, from front to back, and the specific process is consistent with the above mentioned "Dominant color substitution in forest subcompartments".

Ecological function index. In the ecological systems, biomass, interaction and information are three fundamental notions [75]. They can operate at different hierarchical levels, with the characteristics of increasing complexity. Biodiversity is at the basis of this complexity, which means that with more diversity, there is more information and interaction [76]. Furthermore, the hierarchical organization of all organisms and the functional characteristics of each level can define biodiversity as well. Urban forest plays a critical role in storing carbon through above-ground biomass. In addition, the woods provide numerous ecosystem services that support the wellbeing of urban dwellers [77]. Thus, biomass and biodiversity (wood) were chosen as the ecological indicators by which to judge the optimization method in this paper.

Biomass of tree species. Fang et al. [78] proposed the widely used method [79, 80] of the continuous function of conversion factor to estimate the forest biomass and introduced the model of biomass and accumulation with the calculation parameters of the dominant tree species, which overcame the shortcomings of the static conversion parameters of the biomass conversion factor method. This method is also used in this study to predict the biomass. The equation is as follows:

$$B = a * V + b \quad (4)$$

In the formula, B is the stand biomass per hectare (m^3/hm^2), V is the stand volume per hectare (t/hm^2), and a and b are the parameters. The biomass is calculated in subcompartments.

Tree species diversity index. For tree species diversity, we calculate Shannon's diversity (H) and Shannon's evenness (J).

$$H = -\sum_{i=1}^{S} p_i \ln p_i \quad (5)$$

$$J = H / \ln S \quad (6)$$

In the formula, p_i is the proportion of the number of i species in the total number of tree species, and S is the total number of tree species. The tree species diversity index is calculated in the subcompartments as well.

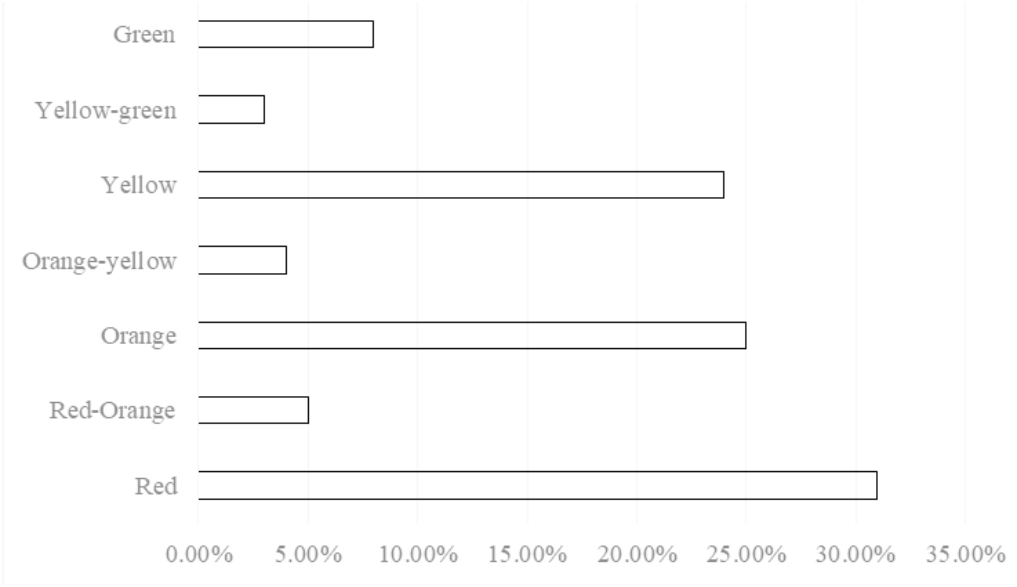

FIGURE 6
Visitors' one preferred color of forest landscape in fall(PC)

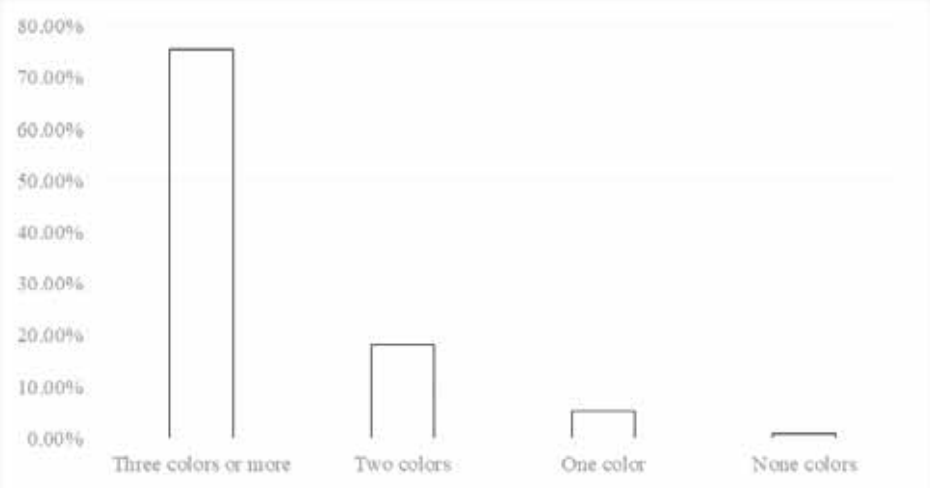

FIGURE 7
Visitors' preferred autumn-color types(CT)

TABLE 2
Eigenvalues and contribution rates of the spatial principal components

PC	Eigenvalue	Contribution rates	Accumulated contribution rates
1	3672.8027	99.73%	99.73%
2	5.2953	0.15%	99.88%
3	2.7464	0.07%	99.95%
4	1.723	0.05%	100.00%

RESULTS AND DISCUSSION

"PC" and "CT" According to the survey data, the ranking results of "PC" from high to low are red, orange, yellow, green, red-orange, orange-yellow, and yellow-green (Fig. 6). Among them, red (31%), orange (25%) and yellow (24%) are the three most attractive colors to tourists, which are the most representative seasonal colors in autumn. Red-orange, orange-yellow and yellow-green are preferred by fewer people. The results of "CT" show that with the decrease in the number of autumn color types in the landscape, the tourists' preference gradually decreases (Fig. 7). Among them, the landscape with three or more seasonal color features is the most popular among the visitors, with a percentage as high as 75%. However, the preference of no colors (green) is the lowest, with only 1% concentration of the population.

After extracting the autumn phase color types from each forest sample photograph, the correlation coefficient between the number of autumn phase color types and the aesthetic evaluation value of the color landscape is 0.307 according to Spearman's correlation analysis, which showed a very significant positive correlation ($P < 0.01$). This shows that the more seasonal color types there are, the higher the aesthetic quality of the seasonal landscape, and the greater the degree of attraction to tourists. Thus, the number of seasonal color types can be used as the basis for color landscape optimization. In the process of optimizing color selection, we should use the "rich seasonal colors" and "red, orange and yellow are the main landscape color components" as the reference.

"SPCA". In the SPCA of the regional ecological sensitivity, the cumulative contribution rate of the first principal component reached 99.73% (Table 2), which shows that it can positively reflect the current situation of ecological sensitivity in the study area. Therefore, the first principal component is selected for analysis.

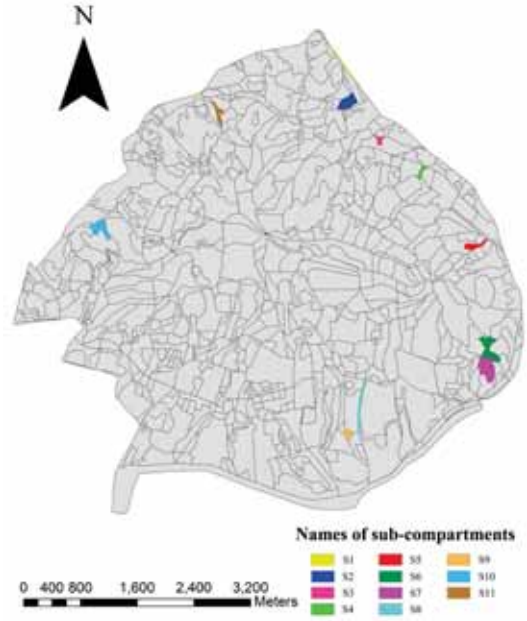

FIGURE 8
Names of subcompartments

Forest subcompartments optimization. In the optimization region, based on the management characteristics and principles of scenic forest, the number of forest subcompartments that can be optimized is 11 (Fig. 8). Different colors represent different subcompartments. And the labels and the distribution of all the subcompartments are displayed in the figure. Based on the attributes of each subcompartment, it is optimized separately by one of the two optimized submethods (Table 3). Among them, five forest subcompartments are optimized by using the method of dominant color substitution in the forest subcompartments. Based on the autumn color-leafed tree species in the subcompartments, with mainly Maple (Liquidambar formosana), Sawtooth oak (Quercus acutissima) and Oriental oak (Quercus variabilis) selected as the optimum dominant tree species. The best autumn facial color can be qualitatively described as red, red-orange, orange, orange-yellow and yellow.

Because there are no autumn color-leafed tree species in the subcompartments, the remaining six forest subcompartments use the method of dominant color substitution outside the forest subcompartments. After optimization, Maple, Sawtooth oak and Oriental oak were also selected as the dominant tree species, and the best autumn facies color was also described qualitatively as red, red-orange, orange, orange-yellow and yellow. After optimization, the main tree species composition was allocated according to the proportion of the original tree species composition in forest subcompartments.

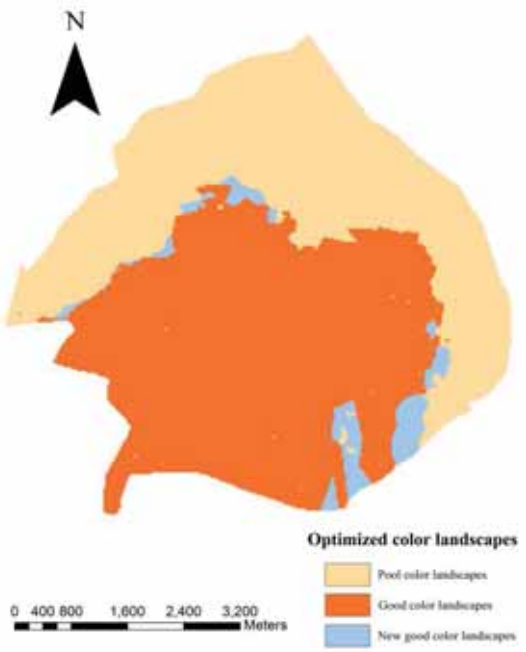

FIGURE 9
Optimized colored landscapes distribution

The function of color aesthetics optimization. In the study area, all subcompartments with optimized target tree species as dominant species are extracted, i.e., subcompartments with Maple, Sawtooth oak and Oriental oak as dominant species. According to different target tree species, the color aesthetic assessment value is divided into three parts, and the color aesthetic evaluation mean of each target tree species is calculated and used as the color aesthetic evaluation value of subcompartments after

TABLE 3
Forest subcompartment optimization

The number of optimized subcompartments	Optimization method	Name	Qualitative description of seasonal colors with new high preference after optimization	Major tree species composition after optimization
11	Dominant color substitution outside forest subcompartments	S1	Orange, orange-yellow, yellow	Oriental oak (100%)
		S2, S9	Red, red-orange, orange, orange-yellow, yellow	Maple (60%), Wingceltis (*Pteroceltis tatarinowii)* (40%)
		S3, S7	Orange, orange-yellow, yellow	Sawtooth oak (100%)
		S6	Orange, orange-yellow, yellow	Oriental oak (80%), Locust(*Robinia pseudoacacia)* (10%), Masson Pine (*Pinus massoniana)* (10%)
	Dominant color substitution in forest subcompartments	S4	Red, red-orange, orange, orange-yellow, yellow	Maple (100%)
		S5	Orange, orange-yellow, yellow	Sawtooth oak (100%)
		S8, S10	Orange, orange-yellow, yellow	Oriental oak (100%)
		S11	Red, red-orange, orange, orange-yellow, yellow	Sawtooth oak (60%), Fir (*Cunninghamia lanceolata)* (40%)

optimization. Then, the new color aesthetic evaluation value is added to the 11 optimized subcompartments, vector files with new attribute values are input and the Kriging space interpolation method is used (the specific process is identical with "Optimal region determination of color aesthetics") to obtain the trend map of the color aesthetics evaluation of the autumn landscape after optimization (Fig. 9). After optimization, the aesthetic quality of the autumn color landscape has been improved to a certain extent. Generally, based on the current situation, the high quality of color landscape areas in the central and south-central regions have the trend of expanding to surrounding areas. Although the quality of color landscape in the northern region has not been significantly improved, it has been significantly improved in the southern and southeastern areas, which covers the main scenic spots of Purple Mountain.

Specifically, the percentage of stands with a higher color aesthetic quality grade, that is, their evaluation score was higher than the mean value (mean=-0.082156), increased from 56.91% to 58.61%, while the stands with a lower quality grade decreased by 1.7% after optimization (Fig. 10). The number of autumn color types also increased, and the proportion of forest stands with more than one color type increased by 1.67% (Fig. 11). Therefore, both the quality evaluation of color aesthetics and the number of seasonal color categories have been improved to a certain extent after optimization.

The function of ecological optimization. Comparison of the tree species biomass before and after optimization. Based on the sample plot storage data of 11 forest subcompartments and the conversion model of forest storage and biomass, the volume of each hectare in the subcompartments before and after optimization was calculated (Table 4). The results show that in all subcompartments, the biomasses of the six subcompartments, S1, S3, S4, S5, S7 and S10, increased after optimization, while those of the other five subcompartments decreased after optimization. From the total biomass of subcompartments using the same suboptimization method, the biomass of the dominant color substitution outside forest subcompartments method increased by 161.89 $t \cdot hm^{-2}$, and the biomass of dominant color substitution in forest subcompartments method increased by 23.94 $t \cdot hm^{-2}$. Overall, the biomass of all subcompartments increased by 185.83 $t \cdot hm^{-2}$ after optimization, which indicates that the ecological function of 11 subcompartments improved after optimization.

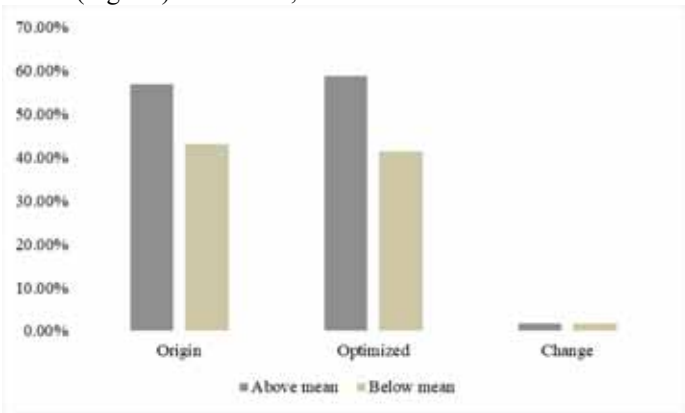

FIGURE 10
Autumn color-aesthetic assessment value comparison analysis

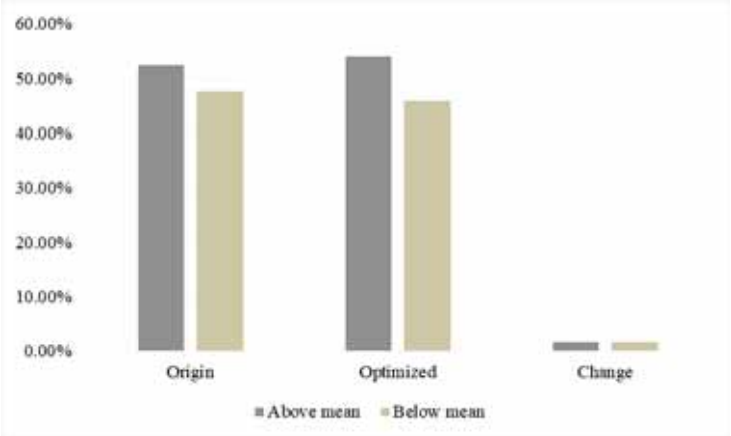

FIGURE 11
Autumn color types comparison analysis

TABLE 4
Biomass comparison analysis

Optimization method	Name	Biomass before optimization ($t \cdot hm^{-2}$)	Biomass after optimization ($t \cdot hm^{-2}$)	Biomass change ($t \cdot hm^{-2}$)	Biomass change with two suboptimization method ($t \cdot hm^{-2}$)	Biomass change in total ($t \cdot hm^{-2}$)
Dominant color substitution outside forest subcompartments	S1	255.39	344.23	88.85	161.89	185.83
	S2	181.45	127.29	-54.16		
	S3	86.24	164.65	78.41		
	S6	153.97	133.84	-20.13		
	S7	94.54	176.33	81.80		
	S9	74.06	61.18	-12.88		
Dominant color substitution in forest subcompartments	S4	114.59	125.63	11.04	23.94	
	S5	122.12	157.44	35.31		
	S8	154.57	138.20	-16.37		
	S10	101.01	106.20	5.19		
	S11	87.24	76.01	-11.23		

Comparison of the tree species diversity index before and after optimization. After optimization, the diversity of the tree species in the study area improved to a certain extent. The Shannon-Wiener Index increased from H=0.2475142 before optimization to H'=0.2475978 after optimization (Fig. 12); the Pielou Index also increased from J=0.0696174 to J'=0.0696409 (Fig. 13). From the numerical point of view, the change was a slight growth. However, from the overall color optimization point of view, not only the autumn color landscape quality was improved, but the species diversity was also optimized, thus reflecting the ecological and color aesthetic characteristics of the whole color optimization method.

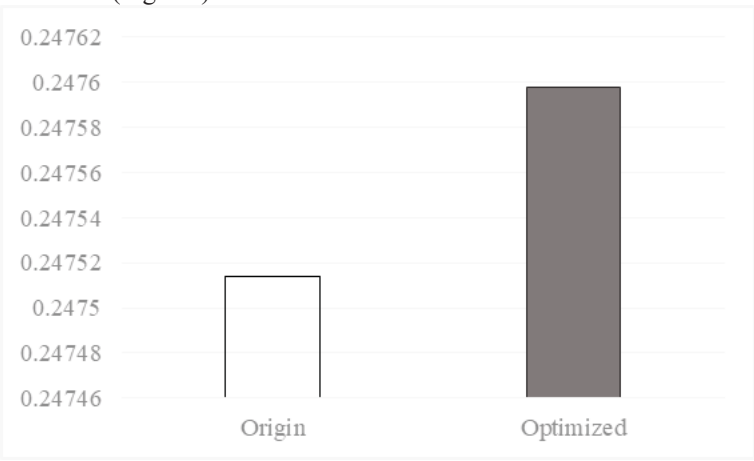

FIGURE 12
Shannon-Wiener(H) Index comparison analysis

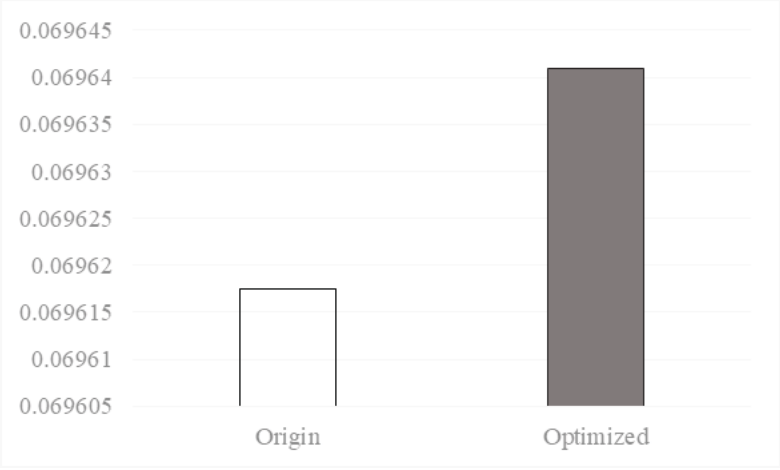

FIGURE 13
Pielou(J) Index comparison analysis

Through the optimization of this research method, the area of the quality of color landscape improvement was small because the color optimization method in this study was based on the ecological and aesthetic functions of scenic forest, and then the forest subcompartments with poor color landscape quality in autumn were optimized. The number of optimized forest subcompartments was limited by the characteristics and management requirements of the scenic forest itself. With increasing forest age, many new forest subcompartments will be suitable for optimization. Therefore, the seasonal landscape color optimization of scenic forests is a long-term and sustainable project. Although obvious and immediate results of optimization cannot be achieved, it is a more scientific and reasonable optimization method, and it is also suitable for the study area of the autumn landscape color optimization method.

In each step of the whole color optimization method, the data should be updated at the same time to ensure real-time data and to improve the accuracy of color optimization. For the questionnaire survey, we can use the questionnaire for several years and then determine the public preference of seasonal color in each survey period. With the evidence of color optimization, the seasonal color preferences of the public are determined by the average value of the public preference across successive annual questionnaires. In the process of sample photograph collection, the consistency of the location coordinates of each survey data is ensured, and the continuity of data is guaranteed. In this study, the optimized seasonal color aesthetic trend distribution was based mainly on the aesthetic evaluation of landscape color and the average value of each color type of the optimized tree species because the suboptimization method has not yet been implemented, so it is not clear what the actual scenic forest color landscape after optimization will be. Of course, if this method is applied in practice, the feasibility of this optimization method can be better verified by evaluating the color types and color aesthetics of the real landscape after optimization, and the optimization method can be improved and perfected based on all aspects of reality. In the future research, we can add evaluation factors, such as economic benefit evaluation, judge the tourism economic value of color landscape, and improve the evaluation method.

Because the optimization object of this method is a seasonal forest landscape, whether the optimized forest community has seasonal characteristics becomes the main basis for whether this method can be popularized and applied. Among the different climate types, the zonal forest type is composed of deciduous broad-leaved forests in temperate and warm temperate zones. The appearance of this forest community shows an obvious seasonal change and is almost completely distributed in the northern hemisphere. For example, forest communities in Northeast China and North China are mainly composed of deciduous broad-leaved forests. The dominant species are deciduous trees of Fagaceae and Betulaceae. The subtropical region has a distinct climate throughout the year. The typical forest community type is evergreen broad-leaved forest. The distribution of the tree layer is mainly made of Fagaceae and Lauraceae evergreen broad-leaved species. Thus, the autumn color landscape of scenic forests in China is mainly distributed in temperate, warm temperate and subtropical regions. Because the study area, Purple Mountain Forest Park, is located in the transition zone between the north subtropical zone and the warm temperate zone, it is a mixed-growth area of deciduous broad-leaved forest and evergreen broad-leaved forest with abundant plant species and an obvious transitional vegetation composition. The target tree species that are selected by the autumn color optimization method belong to temperate zone, warm temperate zone and subtropical suitable tree species, and this color optimization method is suitable for forest autumn landscape color optimization in temperate, warm temperate and subtropical regions of China. However, due to the climatic characteristics of the cold temperate zone, the summer is short and the winter is long. The zonal vegetation is mainly composed of the northern coniferous forest. The typical forest type in the tropical zone is the tropical rain forest, with small annual temperature differences, high temperature and rain throughout the year, with no obvious seasonal alternation. Therefore, from the point of view of a suitable tree species, this method is not suitable for cold temperate and tropical zones.

The evaluation of color aesthetics, the preference for color types and the selection of color-leaf tree species are all based on local data in the study area. Thus, when this method is applied to other areas, it is necessary to make changes according to the local conditions, including the local geographical environment, ecological environment, cultural environment, and social environment, under the unchanged planning framework. Then, the method can be developed into a practical, feasible, and scientific method.

Many provinces and municipalities in China are focusing on the construction of a "color forest"; this study can provide a reference, especially for autumn color landscape optimization methods. Although this study does not propose a color method for the other three seasons in addition to autumn, it is based on the characteristics of the study area and the economic and ecological benefits, and the optimization value is not considered significant. However, for other regions in China, because the forest species and forest communities are different, the landscapes in the four seasons are also not the same. In addition, the public's preference for each

season's landscape varies from place to place. Therefore, the application of the landscape forest seasonal color landscape optimization method for the other three seasons is worthy of further study. Finally, on the basis of the four seasons and the one-season color landscape optimization method for scenic forests, a comprehensive, four-season landscape color planning approach is formed, which can provide services for the construction of forest color landscape in different regions.

CONCLUSIONS

In this study, a color optimization method for autumn landscapes is proposed, which optimize the color scenic aesthetic function and ecological function of scenic forests in forest park. Additionally, the method is suitable for the optimization of autumn forest color landscapes in temperate, warm and subtropical regions of China.

ACKNOWLEDGEMENTS

This research was funded by the Top-notch Academic Programs Project of Jiangsu Higher Education Institutions, China (TAPP, [PPZY2015A062]).

REFERENCES

[1] Zencirkiran, M., Ender, E., Cetiner, S., Gorur, A., Eraslan, E., Tanriverdi, O.D., Celik, B.H. (2018) A research on Kocaeli geophytes and their ornamental purposes for sustainable landscape design. Fresen. Environ. Bull. 27, 6042-6052.

[2] Tarakci Eren, E., Duzenli, T. (2017) Determination of the visual preference levels and perceptual differences in the appearance of certain taxa in different seasons. Fresen. Environ. Bull. 26, 689-700.

[3] Polat, Z., Kilicaslan, C., Kara, B., Deniz, B. (2015) Visual quality assessment of trees and shrubs in the south campus of Adnan Menderes University in spring. Fresen. Environ. Bull. 24, 4303-4315.

[4] Sheppard, R. (1823) Descriptions of seven new British land and fresh-water shells, with observations upon many other species, including a list of such as have been found in the county of Suffolk. Trans. Linn. Soc. Lond. 14, 148-170.

[5] Donner, S.D., Skirving, W.J., Little, C.M. (2005) Global assessment of coral bleaching and required rates of adaptation under climate change. Glob. Chang. Biol. 11, 2251-2265.

[6] Ridgway, R. (1912) Color Standards and Color Nomenclature, with Fifty-three Colored Plates and Eleven Hundred and Fifteen Named Colors. Washington, D.C.

[7] Martínez-Padilla, J., Dixon, H., Vergara, P., Pérez-Rodriguez, L., Fargallo, J.A. (2010) Does egg colouration reflect male condition in birds? Naturwissenschaften. 97, 469-477.

[8] Schifferstein, H.N.J., Howell, B.F., Pont, S.C. (2017) Colored backgrounds affect the attractiveness of fresh produce, but not it's perceived color. Food Qual. Prefer. 56, 173-180.

[9] Stockman, A., Brainard, D.H. (2009) Color vision mechanisms. In Bass, M., DeCusatis, C., Enoch, J., Lakshminarayanan, V., Li, G., Macdonald, C., Maharajan, V., van Stryland, E. (Eds.), The Optical Society of America Handbook of Optics. New York: McGraw-Hill.

[10] Juniper, B.E. (1994) Flamboyant flushes: a reinterpretation of non-green flush colors in leaves. Int. Dendrol. Soc. Yearbook. 1993, 49-57.

[11] Lev-Yadun, S., Holopainen, J.K. (2009) Why red-dominated American autumn leaves and yellow-dominated autumn leaves in Northern Europe? New Phytol. 183, 506-512.

[12] Richards, P.W. (1996) The Tropical Rain Forest. In 2nd (Ed.), *An Ecological Study*. Cambridge: Cambridge University Press.

[13] Grose, M.J. (2016) Green leaf colors in a suburban Australian hotspot: Color differences exist between exotic trees from far afield compared with local species. Land. Urban Plan. 146, 20-28.

[14] Klosterman S., Richardson, A.D. (2017) Observing Spring and Fall Phenology in a Deciduous Forest with Aerial Drone Imagery. Sensors. 17, 2852-2869.

[15] Brown, T.C., Daniel, T.C. (1986) Predicting scenic beauty of timber stands. Forest Sci. 32, 471-487.

[16] Daniel, T.C., Wheeler, L., Boster, R.S., Best Jr., P.R. (1972) An application of signal detection analysis to forest management alternatives. Man-environment Systems. 3, 330-344.

[17] Matín, B., Ortega, E., Otero, I., Arce, R.M. (2016) Landscape character assessment with GIS using map-based indicators and photographs in the relationship between landscape and roads. J. Environ. Manage. 180, 324-334.

[18] Meitner, M.J. (2003) Scenic beauty of river views in the Grand Canyon: relating perceptual judgments to locations. Land. Urban Plan. 68, 3-13.

[19] Schirpke, U., Tasser, E., Tappeiner, U. (2013) Predicting scenic beauty of mountain regions. Land. Urban Plan. 111, 1-12.

[20] Kosmala, M., Crall, A., Cheng, R., Hufkens, K., Henderson, S., Richardson, A.D. (2016) Season Spotter: Using Citizen Science to Validate and Scale Plant Phenology from Near-Surface Remote Sensing. Remote Sens. 8, 726-748.
[21] Schüpbach, B., Junge, X., Lindemann-Matthies, P., Walter, T. (2016) Seasonality, diversity and aesthetic valuation of landscape plots: An integrative approach to assess landscape quality on different scales. Land Use Policy. 53, 27-35.
[22] Welland, M. (2009) Sand: A Journey through Science and the Imagination. Oxford: Oxford University Press.
[23] Fridell Anter, K. (1996) Inherent colors of vegetation stones and ground. Stockholm: Scandinavian Color Institute AB.
[24] Grose, M.J. (2007) 'Green above, paler below': Descriptions in the literature of the biodiversity of the colors of trees from southwest Australia. Journal of the Royal Society of Western Australia. 90, 179–194.
[25] Merzlyak, M.N., Gitelson, A. (1995) Why and What for the Leaves Are Yellow in Autumn? On the Interpretation of Optical Spectra of Senescing Leaves(*Acer platanoides L.)*. J. Plant Physiol. 145, 315-320.
[26] Itten, J. (1973) The Art of Color: the subjective experience and objective rationale of color. New York: Van Nostrand Reinhold.
[27] Holopainen, J.K., Peltonen, P. (2002) Bright autumn colors of deciduous trees attract aphids: nutrient retranslocation hypothesis. Oikos. 99, 184-188.
[28] Archetti, M. (2009) Phylogenetic analysis reveals a scattered distribution of autumn colors. Ann. Bot. 103, 703-713.
[29] Archetti, M., Döring, T.F., Hagen, S.B., Hughes, N.M. (2009) Leather S.R. Unravelling the evolution of autumn colors: an interdisciplinary approach. Trends Ecol. Evol. 24, 166-173.
[30] Grose, M.J. (2012) Plant colour as a visual aspect of biological conservation. Biol. Conserv. 153, 159-163.
[31] Chichester, C.O., Nakayama, T.O.M. (1965) Pigment changes in senescent and stored tissues. In: Goodwin, T.W. (Ed.), Chemistry and Biochemistry of Plant Pigments. New York: Academic Press.
[32] Close, D.C., Beadle, C.L. (2003) The ecophysiology of foliar anthocyanin. Bot. Rev. 69, 149-161.
[33] Feild, T.S., Lee, D.W., Holbrook, N.M. (2001) Why leaves turn red in autumn. The role of anthocyanins in senescing leaves of red-osier dogwood. Plant Physiol. 127, 566-574.
[34] Hoch, W.A., Zeldin, E.L., McCown, B.H. (2001) Physiological significance of anthocyanins during autumnal leaf senescence. Tree Physiol. 21, 1-8.
[35] Liu, X., Yu, W., Wang, G., Cao, F., Cai, J. (2016). Comparative Proteomic and Physiological Analysis Reveals the Variation Mechanisms of Leaf Coloration and Carbon Fixation in a Xantha Mutant of Ginkgo biloba L. Int. J. Mol. Sci. 17, 1794-1799.
[36] Matile, P. (2000) Biochemistry of Indian summer: physiology of autumnal leaf coloration. Exp. Gerontol. 35, 145-158.
[37] Ougham, H.J., Morris, P., Thomas, H. (2005) The colors of autumn leaves as symptoms of cellular recycling and defenses against environmental stresses. Curr. Top. Dev. Biol. 66, 135-160.
[38] Lee, D.W., O'Keefe, J., Holbrook, N.M., Feild, T.S. (2003) Pigment dynamics and autumn leaf senescence in a New England deciduous forest, eastern USA. Ecol. Res. 18, 677-694.
[39] Lee, D.W., Brammeler, S., Smith, A.P. (1987) The selective advantages of anthocyanins in developing leaves of mango and cacao. Biotropica. 19, 40-49.
[40] Estrella, N., Menzel, A. (2006) Responses of leaf coloring in four deciduous tree species to climate and weather in Germany. Clim. Res. 32, 253-267.
[41] Kozlowski, T.T., Pallardy, S.G. (1997) Physiology of Woody Plants. New York: Academic Press.
[42] Richardson, A.D., Bailey, A.S., Denny, E.G., Martin, C.W., O'Keefe, J. (2006) Phenology of a northern hardwood forest canopy. Glob. Chang. Biol. 12, 1174-1178.
[43] Richardson, A.D., Black, T.A., Ciais, P., Delbart, N., Friedl, M.A. (2010) Influence of spring and autumn phenological transitions on forest ecosystem productivity. Philos. T. Roy. Soc. 365, 3227-3246.
[44] Archetti, M., Richardson, A.D., O'Keefe, J., Delpierre, N. (2013) Predicting climate change impacts on the amount and duration of autumn colors in a New England Forest. PLoS One. 8, e57373.
[45] Augspurger, C.K. and Bartlett, E.A. (2003) Differences in leaf phenology between juvenile and adult trees in a temperate deciduous forest. Tree Physiol. 23, 517-525.
[46] Seiwa, K. (1999) Changes in leaf phenology are dependent on tree height in Acermono, a deciduous broad-leaved tree. Ann. Bot. 83, 355-361.
[47] Gressler, E., Jochner, S., Capdevielle-Vargas, R.M., Morellato, L.P.C., Menzel, A. (2015) Vertical variation in autumn leaf phenology of *Fagus sylvatica L.* in southern Germany. Agric. For. Meteorol. 201, 176-186.

[48] Richardson, A.D., O'Keefe, J. (2009) Phenological differences between understory and overstory: a case study using the long-term Harvard Forest Records. In Noormets, A. (Ed.), Phenology of Ecosystem Processes: Applications in Global Change Research. New York: Springer.
[49] Lev-Yaduna, S., Yamazakib, K., Holopainenc, J.K., Sinkkonend, A. (2012) Spring versus autumn leaf colors: Evidence for different selective agents and evolution in various species and floras. Flora. 207, 80-85.
[50] Dixon, A.F.G., Hopkins, G.W. (2010) Temperature seasonal development and distribution of insects with particular reference to aphids. In Kindlmann, P., Dixon, A.F.G., Michaud, J.P. (Eds.), Aphid Biodiversity under Environmental Change. Dordrecht: Springer.
[51] Feeny, O. (1970) Seasonal changes in oak leaf tannins and nutrients as a cause of spring feeding by winter moth caterpillars. Ecology. 51, 565-581.
[52] Zheng, Y., Zhang, W.Q., Wu, Q.N., Chen, Z.R., Wang, Y.C., Ding, G.C., Chen, S.P., Fu, W.C., Zhu, Z.P., Huang, S.P., Wu, J.J., Dong, J.W. (2016) The Color Quantization of the Fall Scenic Forest in Jinsi Canyon National Forest Park in Shanxi Province. Journal of Northwest Forestry University. 31, 275-280.
[53] Chen, X., Jia, L., Wang, Y., Zhou, R., Li, X. (2008) Landscape estimation and management technique principles of different seasonal scenic and recreational forests in West Mountain, Beijing. Journal of Beijing Forestry University. 30, 39-45.
[54] Goffe, P.L. (1995) The benefits of improvements in coastal water quality: a contingent approach. J. Environ. Manage. 45, 305-317.
[55] Lee, C.K. (1997) Valuation of nature-based tourism resources using dichotomous choice contingent valuation method. Tourism Manage. 18, 587-591.
[56] Majumdara, S., Deng, J., Zhang, Y., Pierskalla, C. (2011) Using contingent valuation to estimate the willingness of tourists to pay for urban forests: A study in Savannah, Georgia. Urban For. Urban Gree. 10, 275-280.
[57] Togridou, A., Hovardas, T., Pantis, J.D. (2006) Determinants of visitors' willingness to pay for the National Marine Park of Zakynthos, Greece. Ecol. Econ. 60, 308-319.
[58] Arthu, L.M. (1977) Predicting scenic beauty of forest environments: Some empirical test. Forest Sci. 23, 151-160.
[59] Buhyoff, G.J., Wellman, J.D., Daniel, T.C. (1982) Predicting scenic quality for mountain pine beetle and western spruce budworm damaged forest vistas. Forest Sci. 28, 827-838.
[60] Chazdon, R.L., Pearcy, R.W. (1991) The importance of sunflecks for forest understory plants: photosynthetic machinery appears adapted to brief, unpredictable periods of radiation. BioScience. 41, 760-766.
[61] Lewis, J.D., Mckane, R.B., Tingey, D.T., Beedlow, P.A. (2000) Vertical gradients in photosynthetic light response within an old-growth Douglas-fir and western hemlock canopy. Tree Physiol. 20, 447-456.
[62] Yoshimura, K. (2010) Irradiance heterogeneity within crown affects photosynthetic capacity and nitrogen distribution of leaves in Cedrela sinensis. Plant Cell Environ. 33, 750-758.
[63] Vries, S., De Groot, M., Boers, J. (2012) Eyesores in sight: Quantifying the impact of man-made elements on the scenic beauty of Dutch Landscapes. Land. Urban Plan. 105, 118-127.
[64] Daniel, T.C., Boster, R.S. (1976) Measuring landscape aesthetics: The scenic beauty estimation method. Colorado: Department of Agriculture, Forest Service, Rocky Mountain Forest and Range Experiment Station.
[65] Yang, H. (2002) Systematic Analysis and Pattern Reorganization and Improvement of Sun Yat-sen Mausoleum Scenic Area. Modern Urban Research. 2002, 9-13.
[66] Li, M., Wang, B., Liu, L. (2007) Research on the Management Division Method of Urban National Forest Park Based on Both the Ecological and Aesthetical Functions. Forest Resources Management. 1, 75-79.
[67] Ouyang, Z. (2011) China's eco-environmental sensitivity and its spatial heterogeneity. Acta Ecol. Sin. 20, 9-12.
[68] Pan, F., Tian, C., Shao, F. (2011) Evaluation of ecological sensitivity in Karamay, Xinjiang, Northwest China. Acta Geographica Sinica. 66, 1497-1507.
[69] Chen, X., Peng, J., Liu, Y., Yang, Y., Li, G. (2017) Constructing ecological security patterns in Yunfu city based on the framework of importance-sensitivity-connectivity. Geographical Research. 36, 471-484.
[70] Li, M., Zhou, Q., Huang, W., Liu, F. (2012) Geomatics-Based Analysis of Landscape Security Pattern for Wild Animals in Eastern Suburb of Nanjing City- A Case Study of Hydropotes inermis. Journal of Southwest Forestry University. 32, 70-75.
[71] Wang, Q., Fu, M., Wei, L., Han, Y., Shi, N., Li, J., Quan, Z. (2016) Urban ecological security pattern based on source-sink landscape theory and MCR model: A case study of Ningguo City, Anhui Province. Acta Scien. Circum. 36, 4546-4554.

[72] Chen X. (2000) Research on evaluation of forest landscapes and construction of scenic and recreation forest in west Beijing mountain area: With reference to the development of forest recreation in Taihang Mountain area. Beijing: Beijing Forestry University.
[73] Wang, Y., Chen, X. (1999) Application of psychophysical method in evaluation of foreign forest landscapes. Scientia Silvae Sinicae. 35, 110-117.
[74] Li, M., Liu, M., Liu, M. (2010) GIS-based geostatistical analysis of forest inventory factors. Journal of Nanjing Forestry University (Natural Science Edition). 34, 66-70.
[75] Jørgensen, S. (2012) Introduction to Systems Ecology. Boca Raton: CRC Press.
[76] La, N.A., Dalia, D., Hanna, M., Luisa, P.M., Camino, L., Benis, E., Davide, G., Neville, D.C. (2017) Ecosystem services classification: A systems ecology perspective of the cascade framework. Ecol. Indic. 74, 392-402.
[77] Carrus, G., Scopelliti, M., Lafortezza, R., Colangelo, G., Ferrini, F., Salbitano, F. (2015) Go greener, feel better? The positive effects of biodiversity on the well-being of individuals visiting urban and peri-urban green areas. Land. Urban Plan. 134, 221-228.
[78] Fang, J., Liu, G., Xu, S. (1996) Biomass and net production of forest vegetation in China. Acta Ecol. Sin. 16, 497-508.
[79] Cao, L., Ruan, H., She, G. (2016) Estimation of forest biomass dynamics in subtropical forests using multi-temporal airborne LiDAR data. Remote Sens. Environ. 178, 158-171.
[80] Shen, W., Li, M. (2016) Quantifying Live Aboveground Biomass and Forest Disturbance of Mountainous Natural and Plantation Forests in Northern Guangdong, China, Based on Multi-Temporal Landsat, PALSAR and Field Plot Data. Remote Sens. 8, 595-596.

Received: **03.11.2019**
Accepted **16.02.2020**

CORRESPONDING AUTHOR

Mingyang Li
College of Forestry,
Nanjing Forestry University,
Nanjing, China

e-mail: lmy196727@126.com

© by PSP Volume 29 – No. 05/2020 pages 3756-3763 Fresenius Environmental Bulletin

MORPHOLOGICAL AND MOLECULAR CHARACTERIZATION OF LOCAL FABA BEAN (*VICIA FABA* L.) ACCESSIONS USING INTER-SIMPLE SEQUENCE REPEAT (ISSR) MARKERS

Nihat Yilmaz*

Kayseri University, Safiye Cikrikcioglu Vocational College, Kayseri, Turkey

ABSTRACT

Faba bean (*Vicia faba* L.) is an agronomically important crop and has value for both food and feed. In the present study, 38 faba bean accessions were collected from 94 different provinces of Northern Cyprus. Plant materials examined to determine genetic diversity using by morphological features. The morphological characterization was performed according to UPOV (The International Union for the Protection of New Varieties of Plants) and IPGR (Institute of Plant Genetic Resources) criteria. This study revealed that the 38 faba beans were classified into 15 morphologically different groups. One genotype was chosen to represent each of the 15 different groups, a totally representative 15 genotypes and a control variety were used for molecular characterization. ISSR markers were used to detect genetic diversity among the groups. Based on molecular data, a total of 108 DNA bands were obtained with 10 ISSR primers and 103 of them were polymorphic. The average polymorphism rate was determined to be 88.32%.

KEYWORDS:
Germplasm, Genetic diversity, Local accessions, DNA

INTRODUCTION

Faba bean (*Vicia faba* L.) belongs to the family of Leguminosae and is an excellent alternative plant for the nutrition of people and in improving soil fertility, as are all legumes. It is a valuable vegetable protein source, which can be consumed both fresh and dried because it contains high protein content. The dry broad bean content contains in different varieties varies from 26% to 41% in terms of both human and animal nutrition [1,2,3,4].

The importance of plant genetic resources is increasing day by day. In agreement with the development of this awareness, many countries are expanding their efforts to collect and protect their local materials, and these efforts are being carried out jointly with the support of international organizations. Ancient and valuable local varieties and populations are valuable and their acquired resistance to diseases, pests, and abiotic factors. By using this kind of material, new varieties can be obtained which are resistant and/or tolerant to diseases, pests, salinity, and drought under the different environmental conditions. These also form a valuable source for current unknown needs, which will emerge in the future [5].

Cyprus Island, the cradle of many migration and trade routes, the third biggest island after Sardinia and Sicily in the middle of the Mediterranean Sea, is very rich in plant gene sources. Although having so many specifications, no study has been conducted about the collection, characterization, preservation, and evaluation of vegetable gene sources in Northern Cyprus. In the past, studies were generally about wild plants. However, there is no study about the collection and preserving of plant forms called "farmer variety" or "local variety." Yet, it is an inevitable truth that these accessions encountered the danger of extinction or, more certainly, genetic erosion because of not being able to compete with modern varieties. These seeds, which are our missing values or in a broad sense plant genetic material, will be an onlooker to the improvement of agriculture in the country, together with our future and most importantly to the extinction of heritage, which can be left to the next generations [5].

In this study, it was aimed to collect and morphologically characterize of faba bean accessions grown in Northern Cyprus. ISSR markers were also used to understand genetic diversity among the groups formed as a result of the morphological characterization. These significant genetic resources of faba bean could be used in breeding programs and the protection of local genetic resources.

MATERIALS AND METHODS

Plant Material. This research was conducted in three stages: collection, morphological characterization, and molecular characterization. In the first stage of the study, the local faba bean accessions

were collected from different region of Northern Cyprus. In the second stage, morphological characterization studies on the collected genetic material of the faba bean were performed according to UPOV and IPGR criteria used total of 44 traits. In the third stage, molecular characterization studies using ISSR markers were conducted on the results of the morphological characterization of the selected accessions.

DNA Extraction. A total of 15 faba bean accessions were used for the molecular characterization and one reference variety named Sevilla. Genomic DNA was isolated from young leaves of 10–days seedlings using CTAB method according to Doyle and Doyle (1990) [6]. DNA concentrations were determined by means of a semi-automatic microplate reader (Power Wave HT, BIO-TEK Instruments, Inc., Winoos, VT, USA) and DNA concentrations were prepared at 10 ng/µl for PCR studies. In this study, the DNA isolation was screened with the ISSR markers given in Table 2 to determine genetic similarities and differences. 20 ISSR primers were tested and 10 ISSR primers, which were polymorphic and easy to score, were selected for this study.

The ISSR DNA amplification (PCR) was conducted in a reaction volume of 15 µl containing 2µl genomic DNA, 6µl of 2xPCRmix (Fermentas), 1.5µl $MgCl_2$ (Fermentas), 1.5µl Taq Polymerase (Fermentas), and 1.45µl ddH_2O, 2µl primer (20 ng) (Operon).

PCR amplification was performed with pre-denaturalization at 94°C for 3 min, followed by 35 cycles at 94°C 1 min, 53°C 50 min, 72°C 2 min and the final extension at 72°C for 7 min before cooling at 4°C A total of 15µl of PCR product was loaded onto the loading wells of 1.5% agarose gel (added to 0.5 mg / ml ethidium bromide in gel) by adding 3 110 l of 6x loading solution on the products obtained from PCR, and run under 110 Volts for 3 hours in electrophoresis tanks and photographed under UV computer-aid. The polymorphism rates of ISSR markers were calculated according to the following formula: Polymorphism (%) = The number of polymorphic bands / Total number of bands x 100.

Data Scoring and Analysis. The gel images obtained as a result of the molecular analysis were evaluated and the band sizes in the base pair units obtained as a result of the scoring were recorded in a table containing the bands of all the primers. In the case of the presence of the DNA band (1), in the case of absence (0) values were given and the binary matrix dendrogram table data file was prepared. The only clearly reproducible band was scored and differences in band intensity were not considered. Data analysis was conducted using only polymorphic bands The NTSYS (Numerical Taxonomy Multivariate Analysis System) 2.1 computer package program was used for the analysis of the data obtained by using both molecular and morphological features and the level of genetic relationship was determined by UPGMA (Unweighted Pair Group Method Arithmetic Average) grouping of similarity matrix according to the Rohlf (1993) [7] method. Similarly, indexes were calculated according to Dice (1945) method [8]. All data were also analyzed by Principle Coordinate (PCoA) using PAST program [17]. First, a similarity matrix was generated using Dice coefficients. This matrix was then used for PCoA. Polymorphism information content (PIC) values were calculated according to Smith et al. (1997) [16], using the algorithm for all primer combinations as follows: $PIC = 1 - \Sigma fi^2$, where fi^2 is the frequency of the it^h allele.

RESULTS AND DISCUSSION

The Findings of Collections of Faba Bean Accessions. A total of 94 points were visited on the route of the sampling lines, including 5 major regions (Nicosia, Morphou, Kyrenia, Famagusta, and Iskele). 94 places were assessed during the trips and 38 samples were collected from these areas and their best agro-morphological features were taken into consideration. The visited points and names of the accessions in the research are given in Table 1.

The Findings of Morphological Characterization among Accessions. The findings obtained from the study were evaluated generally, and it was seen that at the end of morphological characterization, based on the morphological specifications, the accessions of the faba beans, could be separated from each other. These findings were examined separately, based on species and in detail. By the end of the morphological characterization studies done on 38 different/separate faba bean accessions, the accessions were generally separated into 15 different groups. Ammar et al. [2] reported that forty faba bean accessions of field performance results showed a significant amount of variation for their agro-morphological studied parameters. Similar results were obtained as in our study. It was determined that there were important differences from the point of growing shape. Accessions were primarily divided into two different groups as determined (limited growing) and indeterminate. Having the determinate growing shape specification, Bak-02, Bak-06, Bak-20, Bak-29 and Bak-30 code numbered accessions was separated from the other 33 accessions with their specifications. Because of these morphological characterization studies done in this determinate group, the Bak-02,

TABLE 1
Collected Faba Bean Accessions Used in the Study and their Location of the Collection.

No	Accessions Number	Location of Collection	No	Accessions Number	Location of Collection
1	Bak-01	Yeşilırmak	20	Bak-20	Bostancı
2	Bak-02	Yedidalga	21	Bak-21	Doğancı
3	Bak-03	Yedidalga	22	Bak-22	Beyarmudu
4	Bak-04	Yedidalga	23	Bak-23	Vadili
5	Bak-05	Aydınköy	24	Bak-24	Akdoğan
6	Bak-06	Güzelyurt	25	Bak-25	Vadili
7	Bak-07	Bağlıköy	26	Bak-26	Vadili
8	Bak-08	Bostancı	27	Bak-27	Ergazi
9	Bak-09	Bostancı	28	Bak-28	Beyarmudu
10	Bak-10	Güzelyurt	29	Bak-29	Lapta
11	Bak-11	Yedidalga	30	Bak-30	Alsancak
12	Bak-12	Doğancı	31	Bak-31	Alsancak
13	Bak-13	Doğancı	32	Bak-32	İnönü
14	Bak-14	Aydınköy	33	Bak-33	Tatlısu
15	Bak-15	Doğancı	34	Bak-34	Yeni Boğaziçi
16	Bak-16	Alsancak	35	Bak-35	Tatlısu
17	Bak-17	Zümrütköy	36	Bak-36	Büyükkonuk
18	Bak-18	Lapta	37	Bak-37	Çınarlı
19	Bak-19	Bostancı	38	Bak-38	Çınarlı

Bak-06, Bak-20, Bak-29, and Bak-30 accessions showed similarities with each other. From the point of flowering specification, the Bak-02, Bak-06, Bak-20, Bak-29, and Bak-30 numbered accessions went into the late group and from the point of pod shape together with being short structured, they had a broad pod structure. This group's other similar structure was containing 2 or 3 seeds in their pods, from the point of seed number they contain, and their seed weight showed high similarity. The Bak-02, Bak-06, and Bak-20 accessions formed the first group because of their faba bean distribution being at the top and they were called Group 1. The Bak-29 and Bak-30 numbered accessions showed differences in their faba bean distribution found at the bottom and in the middle and formed Group 2.

All the remaining 33 accessions were found to have an indeterminate growing shape. Being in this indeterminate group, these accessions' plant characteristics, leaf and flower forms were determined as similar to each other together with no big differences being found.

The quantitative characteristic determining differences among these accessions appeared as pod and seed characteristics. According to this, it was determined that they were separated into four main elements from the point of pod characteristics and seed number;

- Very tall; seven or nine seeds
- Tall; four or six seeds
- Medium height; three or five seeds
- Short; two or three seeds

In the results of the characterization studies done among these three groups, similarities and differences were put forth. The faba accessions having the tallest pod form and seven-nine seed number Bak-25, Bak-26, Bak-37, Bak-38 and the control plants were called Group 3. It was determined that this group's accessions, from the point of general plant characteristics, leaf, time of flowering, flower forms, pod, and seed characteristics had similarities. These accessions' other common characteristic was their pod forms' not being flat and straight and showing a strong faba bean curvature.

Although showing similarities with all the characteristics mentioned for Group 3, The Bak-05 accession was put in Group 4 because of its very low seed weight. It was determined that the Bak-01, Bak-03, Bak-10, Bak-11, Bak-12, Bak-13, Bak-15, Bak-16, Bak-19, Bak-21, and Bak-31 numbered examples were closely similar to each other from the points of short pod and number of seeds they contained (2-3 seeds), their time early flowering, pod form's being flat-even, their curvature's being absent or very weak, and, their plant, leaf, and flower characteristics. They were called Group 5.

Although showing big similarities to the accessions in Group 5, the Bak-24 and Bak-32 numbered accessions showed as a different group and were named Group 6, as they were late, from the point of time of flowering and they had higher seed weight.

The Bak-17 numbered accession should have been added to Group 6 as it had 2 or 3 seeds in its pods, and they were late from the point of time of flowering, plant, leaf, and flower. However, with the

pod length being shorter and the pod width's being narrower, it was separated from the other accessions and named Group 7.

The Bak-04, Bak-08, Bak-09, and Bak-33 numbered accessions were found very similar to each other, as they were early from the point of plant, leaf, flower forms, time of flowering, and they had 3 or 5 seeds in their pods. However, some differences among these accessions were observed. For example, compared to Bak-08 and Bak-09, Bak-04 was found to have a shorter pod length and for this reason, it was called Group 8. The Bak-33 numbered accession was also found similar as it contained 3 or 4 seeds in its pod form, but, as it was found short from the point of pod length, had a different dry seed shape in cross-section, and was found to have low seed weight, it was called Group 9. The Bak-08 and Bak-09 numbered accessions were found similar to each other from the point of all specifications and were named Group 10.

With 3 or 4 seed content, broad and short formed pod, being medium late as the time of flowering, and being in the heavy seed weight group, Bak-18 showed differences and was evaluated as a separate group and named Group 11.

The Bak-14, Bak-22, Bak-23, Bak-27, Bak-28, Bak-34, Bak-35, and Bak-36 numbered accessions were found similar to each other as they were medium late with their plant and leaf characteristics and their seed number in the pod was between 4 and 6. Although they had many common characteristics, it was identified that there were minor morphological differences among them. In this situation, the Bak-14, Bak-22, and Bak-35 numbered accessions showed differences as their stem distribution of faba bean was at the top and the others were in the middle and bottom, so were separated into Group 12. It was determined that Bak-27, Bak-28, Bak-34, and Bak-36 showed very close similarities to each other from the point of all characterizations and they were evaluated as Group 13. The Bak-23 showed differences from the point of pod length as it was taller, and it was separated and named Group 14.

Despite having a 4 or 5 seeds pod form, the Bak-07 was separated from all other accessions and called Group 15. This genotype's pod weight was found lighter (lower) than all other genotype's pod weights and it was also found different from the points of dry seed shape in median longitudinal and cross-section.

There were important duplications in the examples collected according to the evaluations done, considering all these results and it would be appropriate to choose and maintain one accession from each one of these 15 groups. According to this:

The first group: Bak-02/ The second group: Bak-29/ The third group: Bak-38/ The fourth group: Bak-05/ The fifth group: Bak-13/ The sixth group: Bak-24/ The seventh group: Bak-17/ The eighth group: Bak-04/ The ninth group: Bak-33/ The tenth group: Bak-08/ The eleventh group: Bak-18/ The twelfth group: Bak-22/ The thirteenth group: Bak-28/ The fourteenth group: Bak-23/ The fifteenth group: the Bak-07 was chosen and protected for the gene bank.

A dendrogram was obtained by using 44 morphological traits in 38 faba bean accessions and the similarity between accessions varied between 0.84-1.00. The faba bean accessions were divided into 2 main groups and the first main group included 15 faba bean accessions while the other accessions were in the second group. In Group 1, the Bak-25, Bak-26, and Bak-38 accessions were found to be similar and differed from other populations by having the tallest pod form and seven-nine seed number, whereas in Group 2, the Bak-01, Bak-03, Bak-13, and Bak-16 accessions were similar to each other from the points of short pod and number of seeds they contained (2-3 seeds), their time early flowering, pod form's being flat-even, their curvature's being absent or very weak, and, their plant, leaf, and flower characteristics, The accessions Bak-11, Bak-12, Bak-15, Bak-21, and Bak-31 were similar. Likewise, the Bak-08 and Bak-09 accessions were found to be similar to each other from the point of all specifications in Figure 1.

The Findings of Molecular Characterization among Accessions: In the molecular characterization study using 15 faba bean accessions, 10 ISSR primers were used to produce 108 bands and 103 of them were polymorphic The size of amplified DNA fragments ranged from 150 to 1300 bp. Percentage of polymorphic bands ranged from 100% to a minimum of 57.14% with an average of 88.32% in Table 2. In our study; we used 19 ISSR primers and all ISSR primers proved to be informative. PIC values obtained from ISSR primers were ranged from 0.42-0.82.

The dendrogram obtained by the characterization of the faba bean genotype using 10 ISSR primers is presented in Figure 2. PCoA plot was also generated based on the ISSR data (Figure 3). According to the dendrogram based on ISSR data, genetic similarity among faba bean accessions was determined between 0.65-0.86 and similar accessions were found Bak-33 and Sevilla variety used as a control plant. These results are also being relatively close with those obtained by Salazar-Laureles et al. [3], who found that genetic distances showed an average range from 0.38 to 0.83. The findings show that genetic variation was quite high among the local faba bean accessions using the ISSR marker system.

There are thousands of completed researches in the world about plant genetic resources and many researchers are still being conducted. Faba beans have been reported to contain important local

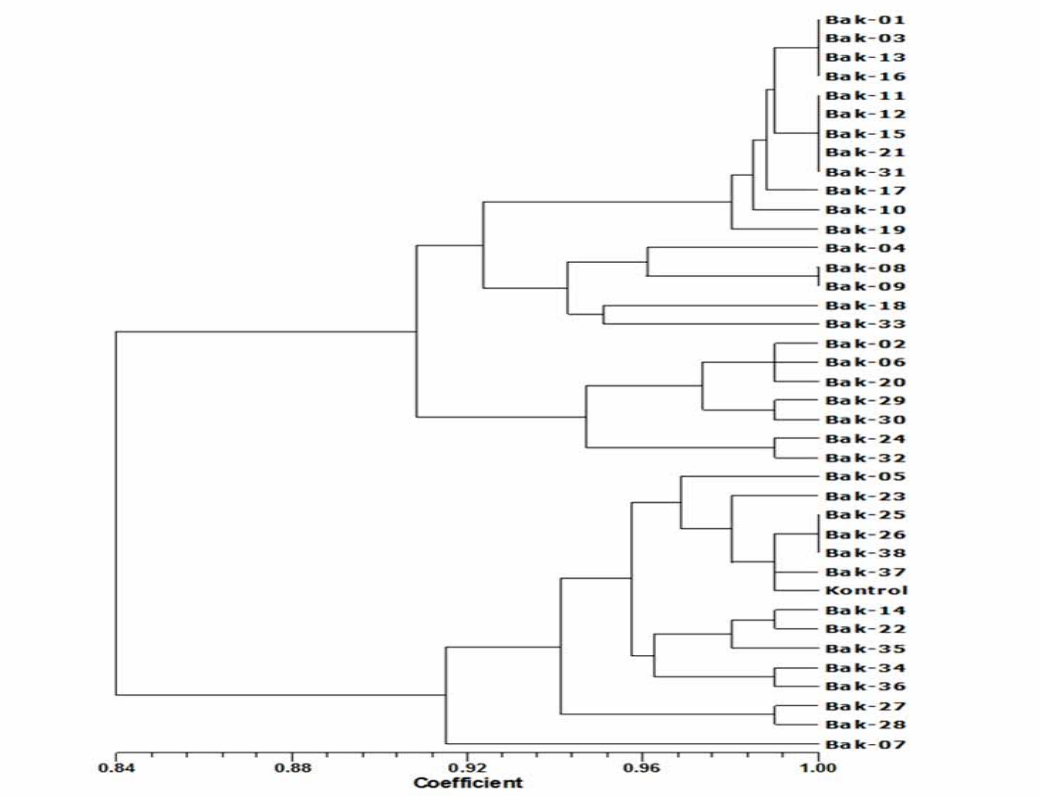

FIGURE 1
Dendrogram Obtained by Using 44 Morphological Features in 38 Faba Bean Accessions and a Control Variety.

TABLE 2
Size Ranges (Bp), the Total Number (N) and Number of Polymorphic Bands (Np), Percentage Of Polymorphism (% P) Of ISSR Primers among the Faba Bean Accessions

Primer	Size range (bp)	Total No. of bands	No. of polymorphic bands	Percentage of polymorphic bands (%)	PIC
CA6AC	380-1000	12	12	100.00	0.48
HVHTCC7	250-1300	11	11	100.00	0.42
BDBCA7C	150-500	7	4	57.14	0.54
TCC5RY	250-1100	7	7	100.00	0.69
GACA4	350-1000	11	11	100.00	0.82
GA8YG	390-1100	11	10	90.91	0.71
AGC6G	350-1100	9	9	100.00	0.60
AG7YC	300-1100	10	7	70.00	0.45
GAA6	400-1000	9	9	100.00	0.66
CAC3GC	350-1000	13	12	92.31	0.76
Average		10	9	88.32	0.61
Total		130	117	1148.12	

nutrients based on the vegetables. Yılmaz et al. [9] also reported that Cyprus has a rich flora where important components of Mediterranean flora are found in Cyprus cuisine. In this study, which supports this report, it was determined that accessions were collected into 15 different groups as a result of the morphological characterization studies performed on 38 different faba bean accessions.

The use of faba bean accessions collected from the island of Northern Cyprus, from a certain geographical area, is the prediction that the genetic distance between these accessions may be close to each other. The findings show that the genetic variation between the faba bean accessions was quite wide using the ISSR marker system. In the morphological and molecular characterization study done on faba

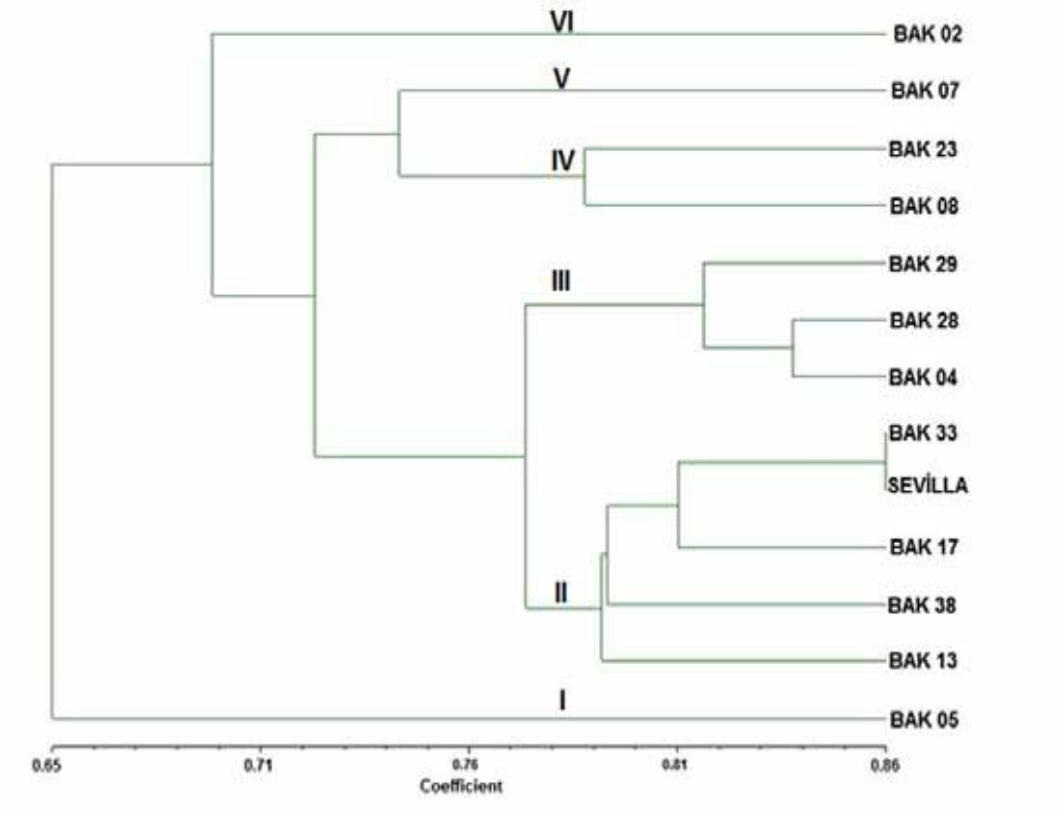

FIGURE 2
Dendrogram from the UPGMA Grouping Analysis of 15 Faba Bean Accessions Based on ISSR Molecular Markers

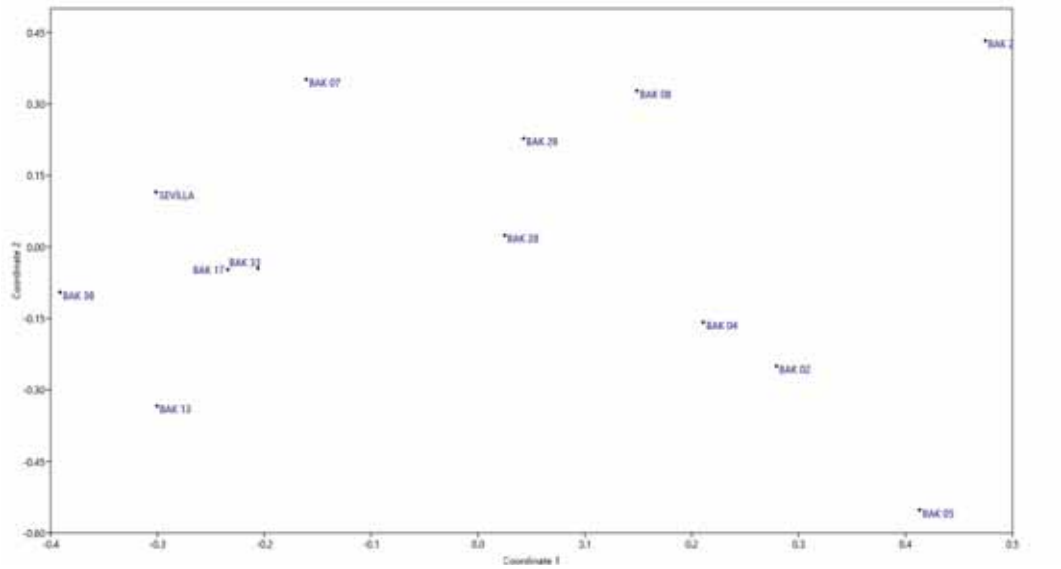

FIGURE 3
Principle Coordinate Analysis of 15 Faba Bean Accessions Based on ISSR Molecular Markers

beans, the molecular genetic differences among accessions were reported in the obtained data.

In the same study, it was found that there was a high genetic diversity among accessions [10]. Madakbaş [11] also reported that the seeds of 51 bean accessions obtained from the İzmir Aegean Agricultural Research Institute, showed morphological, pod features, and differences from the ecological conditions of Samsun province and were found to have a high variation in bean accessions.

Terzopoulos and Bebeli [12], and Wang et al. [13] reported that genetic diversity in faba bean is closely associated with the habitat in which it grows geographic origin and ecologic distribution.

While all these results were generally evaluated, the morphological characterization studies performed in the material obtained were considered insufficient because some of the observations and measurements were sensory (subjective) and they are also affected by environmental conditions. For this reason, different molecular markers are sufficient and not influenced by environmental factors [2]. Molecular markers are provided more reliable information for evaluating and assessing the genetic diversity of germplasm among faba beans [14, 2]. On the other hand, the results indicated that ISSR is more advantageous in showing faba bean accessions differences rather than differences based on morphological appearance [15]. Therefore, the fact that there was no previous morphological characterization study in Northern Cyprus has increased the importance of this study and it was considered that morphological characterization studies alone are insufficient. In such studies, it was concluded that it would be beneficial to carry out molecular characterization studies to provide more reliable results.

ACKNOWLEDGEMENTS

This study is financially supported by The Scientific and Technological Research Council of Turkey (TUBITAK), Project number: 110-O-117. The authors thank to TUBITAK for the financial support.

REFERENCES

[1] Pekşen, E., Gülümser A. (2007) Comparison of Faba Bean (*Vicia faba* L.) Genotypes Sown in Autumn and Spring for Some Plant Characters and Seed Yield. J. of Fac. of Agric., OMU. 22(1), 79-85.

[2] Ammar, H.M., Alghamdi, S.S., Migdadi, M.H, Khan, A.M., El-Harty, H.E., Al-Faifi, A.S. (2015) Assessment of Genetic Diversity among Faba Bean Genotypes Using Agro-Morphological and Molecular Markers. Saudi Journal of Biological Science. 22, 340-350

[3] Salazar-Laureles, E.M., Pérez-López, D.J., González-Huerta, A., Azquez-García, M.L., Valadez-Moctezuma, E. (2015) Genetic Variability Analysis of Faba Bean Accessions Using Inter-Simple Sequence Repeat (ISSR) Markers. Chilean Journal of Agricultural Research. 75(1) January-March.

[4] Ateş, A.Ç., Fidan, H., Yılmaz, N., Konuksal, A. (2017) Botrytis Fabae and Bean Common Mosaic Virus (BCMV) Are the Most Common Diseases of Faba Bean (*Vicia faba* L.) in TRNC. Akademik Ziraat Dergisi. 6 (2), 115-122.

[5] Yılmaz N., Alas T., Abak K. (2012) Collection of Local Vegetables Genotypes with Their Wild Relatives in North Cyprus. Acta Hort. (ISHS). 960, 135-138.

[6] Doyle, J., Doyle, J.L. (1990) Isolation of Plant DNA from Fresh Tissue. Focus. 12,13-15.

[7] Rohlf, F.J. (1993) Numerical Taxonomy and Multivariate Analysis System. Exeter Software, Dept. of Ecology and Evolution, State University of New York.

[8] Dice, L.R. (1945) Measures of the Amount of Ecologic Association between Species. Ecology. 26, 297-302.

[9] Yılmaz, N., Baktır, İ., Tozlu, İ. (2007) Three Important Vegetables of Northern Cyprus Cuisine: Wild Asparagus (*Asparagus stipularis* Forssk), Molehiya (*Corchorus olitorius* L.), Kolakas (*Colocasia esculenta* L. Schott). V. Ulusal Bahçe Bitkileri Kongresi, Erzurum, 4-7 Eylül 2007.

[10] Erdinç, E. (2012) Some Genetic Variation between Genotypes and Anthracnose Disease in Turkey (Colletotrichum Lindemuthian I (Sacc. and Magn.) Lambs. Scribe.) Determining the Stability of the Phenotypic and Molecular Methods. Ph.D Thesis, Graduate School of Natural and Applied Sciences, Van-Turkey.

[11] Madakbaş, S.Y., Ergin, M. (2011) Morphological and Phenological Characterization of Turkish Bean (Phaseolus Vulgaris L.) Genotypes and their Present Variation States. African Journal of Agricultural Research. 6 (28), 6155-6166.

[12] Terzopoulos, P.J., Bebeli, P.J. (2008) Genetic Diversity Analysis of Mediterranean Faba Bean (*(Vicia faba* L.) with ISSR Markers. Field Crops Research. 108(1), 39-44.

[13] Wang, HF., Zong, X.X., Guan, J.P., Yang, T., Sun, X.L., Ma, Y., Redden, R. (2012) Genetic Diversity and Relationship of Global Faba Bean (*Vicia faba* L.) Germplasm Revealed by ISSR Markers. Theor. Appl. Genet. 124, 789-797.

[14] Alghamdi, S.S., Migdadi, H.M, Ammar, M.H., Paull, J.G. Siddique, K.H.M. (2012) Faba Bean Genomics: Current Status and Future Prospects. Euphytica. 186, 609-624.

[15] Arslan, E., Tamkoç, A. (2009) The Application of ISSR-PCR to Determine the Genetic Relationship and Genetic Diversity between Narrow Leaved Bluegrass (*Poa angustifolia*) and Rough Bluegrass (*Poa trivialis*) Accessions. Turk J. Biol. 35, 415-423.

[16] Smith, J., Chin, E., Shu, H., Smith, O., Wall, S., Senior, M., Mitchell, S., Kresovich, S., Ziegle, J. (1997). An evaluation of the Utility of SSR Loci as Molecular Markers in Maize (*Zea mays* L.): Comparisons with Data from RFLPs and Pedigree. Theoretical and Applied Genetics. 95, 163-173.

[17] Hammer, Ø., Harper, D.A., Ryan, P.D. (2001) PAST: Paleontological Statistics Software Package for Education and Data Analysis. Palaeontologia Electronica 4(1), 9.

Received: **04.11.2019**
Accepted: **21.02.2020**

CORRESPONDING AUTHOR

Nihat Yilmaz
Kayseri University,
Safiye Cikrikcioglu Vocational College,
Melikgazi, Kayseri – Turkey

e-mail: nhyl01@gmail.com
nihatyilmaz@kayseri.edu.tr

© by PSP Volume 29 – No. 05/2020 pages 3764-3777 Fresenius Environmental Bulletin

CRITERIA FOR DETERMINING WATER BASIN BOUNDARY AND THE IMPORTANCE PLANNING DECISIONS IN SUSTAINING WATER RESOURCES

Leyla Suri*

Istanbul Commerce University, Faculty of Architecture and Design, Department of Architecture, Istanbul, Turkey

ABSTRACT

Together with earth and air, water is one of the most vital sources. The need for drinking, potable and irrigation water is increasing day by day, with the increase in population and expansion of the settlement areas. Only 0.03 of the total water resources on earth is fresh water and 0.75 of the fresh water resources are in the glaciers and in the form of permanent snow. Turkey is not in the region receiving direct precipitation due to its geographical location and it is among the countries which will possibly have water shortage in the future. Therefore, it is vital to store and protect the precipitation that forms the fresh water source. Expanding settlement areas and increasing human activities reduce water yield in water basins, from which water is provided. Water basin preservation plans are prepared to protect supplies from pollution. The preservation zones are defined by standard distances in the prepared plans. However, water is collected in the same reservoir with surface or underground movements in the water basin. Elements that may pollute the water supply, defined by the plan and legislation, may also be present in these areas. Defining polluting sources depending on the distance in a water basin is not considered scientific. The nature, density and continuity of the polluting sources are among the criteria for determining water yield. In current practices, a drainage divide generally constitutes the water basin preservation zone. Determining the side boundaries of the water basin solely by drainage divide is not sufficient to understand the actual feeding zone of the reservoir. Slope, age and presence of faults and cracks in the underground beds have an essential impact in determining the side boundaries of the water basin. The purpose of the study is to emphasize the importance of fresh water resources, to draw attention to the pollution sources in the water basins, and to reveal the importance of geological structures in the water basin. The subject is discussed based on the analysis of a natural water basin system and an inductive method. The findings reveal that plans and laws are effective tools for preserving water basins. Current legislation and the planned decisions of Istanbul Elmalı water basin are examined, in order to clarify the issue. It is observed that the criteria for preservation and sustainability of water basins need to be shown in detail for legislation. The geological structure analysis in water basins is expected to be a guide for future plans.

KEYWORDS:
Water basin, Elmalı water basin, water basin boundaries, geological structures in the water basin

INTRODUCTION

The survival of the earth population depends on the sustainable use of air, water and earth resources. Factors, such as settlement area demands, due to increasing population, industrial activities, uncontrolled and excessive use of natural resources have a negative impact on the ecosystem. Environmental issues, arising from human activities, are main issues, which need to be resolved with the help of scientific approaches. In addition, water is vital for agricultural production and any industrial activity [1].

The sustainability of natural resources and ensuring optimum benefit by maintaining resources, require multi-disciplinary studies in the fields of natural and social sciences. Natural systems have a delicate balance interacting mutually. At the same time, the relationship between industry and natural resources should be taken into consideration and the carrying capacity should be measured, in order to maintain the required socio-economic development and to achieve the optimum balance [2]. Changes in any of the system elements affect each other and also the entire system. “Water” is among the main sources of life for the creation and survival of all creatures. The water resources on earth are 97% composed of salt water. Three-fourths of the fresh water supplies that constitute 3% of the total water resources, are on the other hand, in the form of permanent snow at the ice bergs, and are not usable [3]. The distribution of the usable fresh water (0.0075 of the available water resources) is as follows [4]:

- Underground waters 95 %
- Lakes and rivers 3.5 %
- Soil moisture 1.5 %

Turkey is not in the region receiving direct precipitation due to its geographical location and it is among the countries that will likely have water shortage in the future. Therefore, it is vital to store and protect the rainfall that forms the fresh water source. Pollution arising from expanding settlement areas and increasing human activities reduces water yield in water basins, from which water is provided. Whereas planning of water resources in 1970s was mainly aimed at preventing floods and regulating river regime, increasing environmental pollution in the following years increased the need for a planned development of the water basins, where drinking and potable water has been obtained. Water basin preservation plans are prepared in order to protect water supplies from pollution. The plans should be prepared with scientific analyzes which ensure the sustainability of natural resources and the applicability of the plan decisions. The preservation zones are defined by standard distances in the prepared plans. However, water product in the short, medium and long distance is collected in the same reservoir with surface or underground movements in the water basin. Elements that may pollute the water supply should be defined by the plan and legislation may also be present in these areas. Defining polluting sources depending on the distance in a water basin is not considered scientific (SAME sentences was already used above). The quality, density and continuity of the pollutant sources are among the criteria for determining the effects on water yield. In current practices, drainage divide, which is determined by combining the highest ridges of the topography, generally constitutes the boundaries of the water basin preservation zone. Determining the side boundaries of the water basin solely by drainage divide is not sufficient to understand the actual feeding zone of the reservoir. The slope, age and presence of faults and cracks in the underground beds have an important impact in determining the side boundaries of the water basin. The purpose of the study is to emphasize the importance of fresh water resources, to draw attention to the pollution sources in the water basins, and to reveal the importance of geological structures in the water basin. The plan decisions of Elmalı water basin in the Anatolian Side of Istanbul Province are examined in line with this purpose as a sample.

MATERIALS AND METHODS

Water basins contain system elements of natural, terrestrial and aquatic nature. They can also be described as subsystems of the ecosystem, which can provide and maintain their natural cycle without any human intervention. However, legal and administrative practices incompatible with urban systems and water basin ecosystem create disruptive (anthropogenic) effects. Anthropogenic effects have been discussed with cause and effect relationship (induction), and the structure and function of the water basin ecosystem have been examined. Along with the elements of natural system, laws, plans and administrative practices within the scope of urban systems were used as input materials of the study. The mutual relationships of natural water basin system and urban systems have been analyzed with systematic approach. Accordingly, the effects on the existing section, parameters of the system and the interaction between the parameters have been analyzed and alternative approaches for a sustainable water basin management have been proposed.

System and ecosystem. Churchman defines system as "the whole formed by the dependent parts (elements) interacting with each other". Understanding the system is possible with a holistic approach to the system, its surrounding, resources, components, function, purpose, performance criteria and management [5]. In other words, according to the definition by Arslan, system is "the name of a whole comprising of units having stable and meaningful relationships" [6]. The general structure of the system can be summarized as follows:

- System is the functional whole in which the units covered are in a mutual relationship,
- It can be a sub-system or unit of the surrounding systems,
- All or parts of the system may intersect with other systems,
- Systems are usually open systems, and
- There is a functional, continuous, stable relationship between units and systems.

Ecosystem is used to describe the whole or a part of the biosphere (Rocks and soil on the surface of earth (lithosphere), water surfaces (hydrosphere), lower levels of the atmosphere and all living creatures constitute biosphere altogether). Natural cycles run numerous system networks in the Biosphere regularly and stably. Accordingly, the system created by biotic (living) and abiotic (non-living) beings in nature with the mutual connections among them is called Ecological System or Ecosystem [7]. The definition of ecosystem can be described as [8] "a unit of spot comprising of biotic and abiotic creatures that are in mutual relations and feeding and renewing itself through the circulation of substance and energy between these creatures" [9]. In balanced ecosystems, the substance cycle is continuous, energy inputs and outputs are equal, and there is a balance defined as golden balance (Figure 1) between producers, consumers and decomposers.

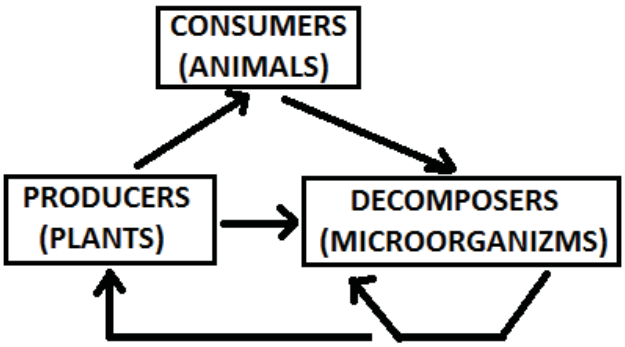

FIGURE 1
The Golden Triangle of the Balanced Ecosystem

The preservation and sustainability of the balance depends on the return of the materials consumed by the food chain to the system for reproduction. The existence of raw material in the ecosystem is definite, and should return to the system after use. If the used raw materials do not return to the system, if there is an excessive increase or decrease in system elements, if the interconnections break [10], and if there are external effects on the system, the golden balance may collapse. Interventions by the human beings to the vegetation in the water basins and the wastes mixed into the soil and water will break the connection between the elements, will affect the substance cycle, energy input-output, and ecosystem elements, and will disrupt the balance of the water basin ecosystem [8].

Water basin and water basin ecosystem. The water basins discussed within the scope of the study can be categorized into four groups. Water Basin Classifications by Region can be done as follows;

a. Catchments/Watersheds (i.e. Small-Scale Water Basins)	A<100ha
b. Medium-Scale Water Basins	100ha<A<1000ha
c. Drainage Basins (i.e. Large-Scale Water Basins)	1000ha<A<10000ha
d. Very Large-Scale Water Basins	A<10000ha

The small-scale water basins are called "catchments" or "watersheds" and large-scale water basins are called "drainage basins". With its 83.4 km2 area [11], Elmalı Water Basin, the plan decisions, which are examined within the scope of this study, is classified within small-scale water basins.

Some of the water basin definitions in the literature are given below:

"It is the water catchment area surrounded by ridges called water lines (drainage divide) where rainfalls or spring water flow into the same course or lake" [12]. "It is a piece of land with a concave topographic structure that is bounded by the drainage divide passing from the ridges and where the surface water collected on it as a result of precipitation can reach a single outlet" [13].

The natural system formed together by the forest, water, river, vegetation, lake, microorganisms, fauna, soil and other factors, such as climate and geomorphology in the water basin zone, can be defined as "Water basin ecosystem". The water basin ecosystem has, both terrestrial and aquatic features. Therefore, the water basin ecosystem is extremely complex in terms of elements, functions and interactions. The boundaries of the water basin ecosystem should be known in order to determine the system elements and to be able to analyze, plan and implement accordingly.

Water movement in water basin ecosystem. The source of water is precipitation, and water is one of the renewable natural resources. It is stored in the atmosphere, oceans, on the surface of and underneath the ground, and is constantly circulating between these resources. Water vaporizing from the earth and oceans reaches the atmosphere and the water vapor in the atmosphere condenses and reaches back to the earth in the form of snow or rain. Some of the water reaching the earth falls to the open water surfaces, such as seas, lakes and rivers and some falls on the soil, vegetation and forest surfaces. Water falling to the soil reaches to the groundwater tables partly by surface flow and partly by flowing towards the underground, and feeds the moving and standing water resources.

The water yield in the streams feeding the reservoir in the water basins is connected to the surface and underground flows. The part of the rainfall that cannot be infiltrated by soil, flows towards the streams with the surface flow. Surface flows may cause the stream beds and reservoirs to fill and become polluted with the materials they carry from the surface. Problems of sudden deluge and water flood may occur as well as a transfer of more pollutants to the resource, especially in the zones turned into open areas and firm ground by human activities.

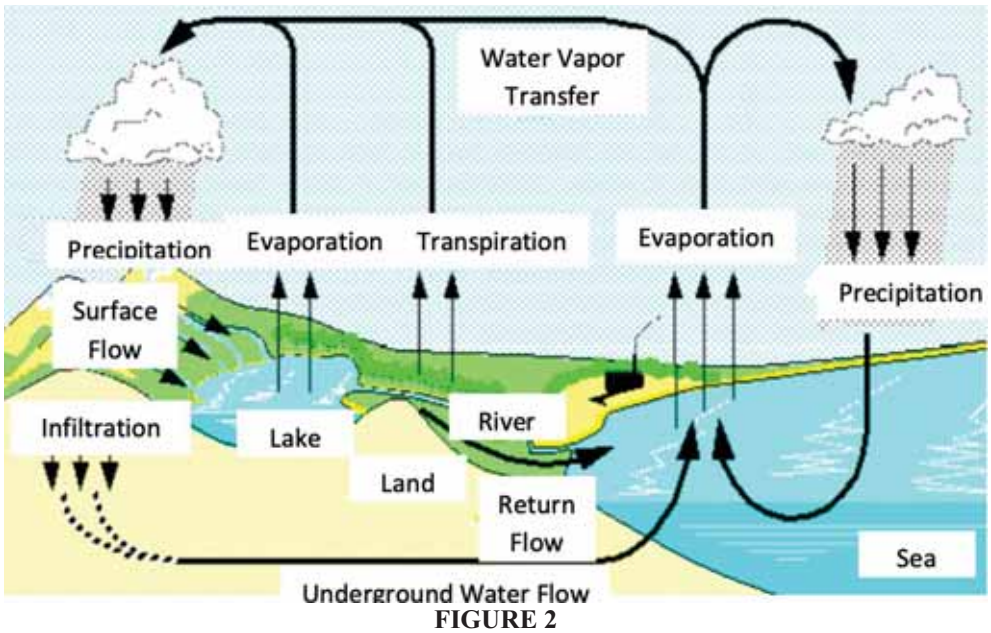

FIGURE 2
Hydrologic cycle [14]

Water leaking underneath the surface is filtrated and cleaned through soil layers and reaches the underground water reserves after a longer period, but still regularly. In case of the event of the water amount penetrating into the soil, becomes higher than the amount of water the soil can retain, some of the excess water infiltrating towards the deeper levels of soil, may reach the surface of the soil again as spring water, whilst some of the water may mix with streams and lakes, and also some of it may mix with underground water. The order of the stream flows depends on the water reaching the stream by infiltrating through the soil or by surface flow. Human factor is effective on vegetation and soil. Decreasing vegetation affects the hydrological status of the water basin and increases erosion and sedimentation. It is preferred that water feeding the reservoir comes from the underground in the water basin system, to obtain water regularly in all seasons and to control its quality and quantity.

Obtaining the quality of plentiful water regularly in all seasons and optimizing the water yield is directly proportional to the collection of rainfalls in underground water reservoirs (maximum vegetation, minimum firm ground). Protection of the soil and preventing loss of soil layers by erosion, are the primary factors for the retaining of and transmission to the underground of the precipitation. Vegetation cover, especially forest surface covered with litter has an important function in the protection of the soil. Providing there has no intervention to the water resource, other than the natural system and the water is not used in a way that will have a negative effect on the water yield. Its sustainability can be ensured by the hydrological cycle.

Uncontrolled development of human activities, draining wetlands and swamps, erosion, uncontrolled discharge of contaminated liquids and solid materials, reduction of forestlands due to unconscious use and similar negative inputs, disrupt the balance of the ecosystem. With the abovementioned anthropogenic effect, the ecological balance of the terrestrial and aquatic systems, which are the subsystems of the ecosystem, is affected from each other and enters into the process of disruption. The problems in the hydrological cycle lead to disruption of the regime, pollution and decrease in the amount of the surface and underground water.

Water basin boundaries. As it can be seen from the definitions of water basin and water basin ecosystem, the water basin boundary is defined as the boundary of the area (water basin) that collects surface water and transmits it to the reservoir, the boundary passing through the highest ridges of the surface topography (drainage divide, ridgeline). However, a part of the rainwater coming from the surface reaches the reservoir from the underground with a vertical movement. Accordingly, the geological structure underneath the ground is one of the most important factors needing to be analyzed in detail, due to its effect on the correct determination of the water basin feeding zone and on the quality of the water product. The underground water moving to the lower layers of the soil, with vertical movement, fills the cavities and cracks. It can reach all the way to the streams, through the cracks and faults or extract to the surface as spring water at a certain point. When the water reaches the impermeable bed, it collects there and reaches to streams and lakes in the form of underground flow. The underground water surface is generally similar to the surface of the topography and high at the hills and low at the rivers [15]. It is probable for the precipitation coming to the water basin to go out of the water basin by underground flow in the lands

with karstic nature. This situation which is related to the geomorphologic structure of the land, affects the amount of the water in the water basin. The phases of water, from atmosphere to the reservoir in the water basin ecosystem, are given in Figure 3.

It can be said that the "drainage divide" forms the side boundaries of the water basin in the natural water basin ecosystem. The definition can be considered to be sufficient when analyzed only in respect to the surface flow. However, the same may not true for underground water. The existence of faulted and cracked structures is possible at old formations, belonging to the Paleozoic Era. Particularly, the karstic nature of the region may increase the likelihood of emerging differences in the reservoir feeding zones, between the surface water and underground water. Although there are no pollutants in the zones, where the water basin boundary is determined by the surface topography, there may be elements outside the drainage divide polluting the reservoir through underground water [16]. Since the underground water surface is generally similar to the topography [15], it can be presumed that the side boundaries of the water basin are the same in terms of surface water and underground water. On the other hand, when the slopes of surface and underground beds are not the same, the water basin feeding zone may include sections outside the drainage divide. Therefore, geological and geomorphologic studies are important for determining the side boundaries of water basins. During the basin plan analytical study stage, knowing the actual basin feeding zone shall be accurate for calculating the water balance sheet, providing optimal benefit from water [17] and determining water basin plan decisions. Side boundaries of the water basin, proposed to be determined according to the slope of the impermeable bed, are schematized in Figure 4. On the left, the drainage divide formed by surface topography determines the boundary outside the slope of the impermeable bed, and on the right the slope of the impermeable bed underneath the ground determines the boundary outside the drainage divide.

Slopes of the underground beds are, on the other hand, another issue to be considered in determining the side boundaries of the water basin (Figure 5).

In Figure 5, it can be seen on the left that the underground beds direct water to the reservoir outside the drainage divide and it is suggested that the boundaries of the water basin should be passed out of the drainage divide, considering the slope of the bed and the slope of the impermeable bed in this section. On the right side, however, the slope of the bed and the slope of the impermeable bed coincided with the boundary of the drainage divide.

To sum up, determination of the side boundaries of the water basin requires a broad analysis of several factors, such as the surface topography, the geomorphology of the impermeable bed, the slope direction of the underground beds, the age and permeability of the geological formations and, whether they are faulted and cracked.

The part of the atmosphere up to 11-12 km can be considered as the upper boundary of the water basin ecosystem [9] and the surface of the impermeable bed can be regarded as the lower boundary [18].

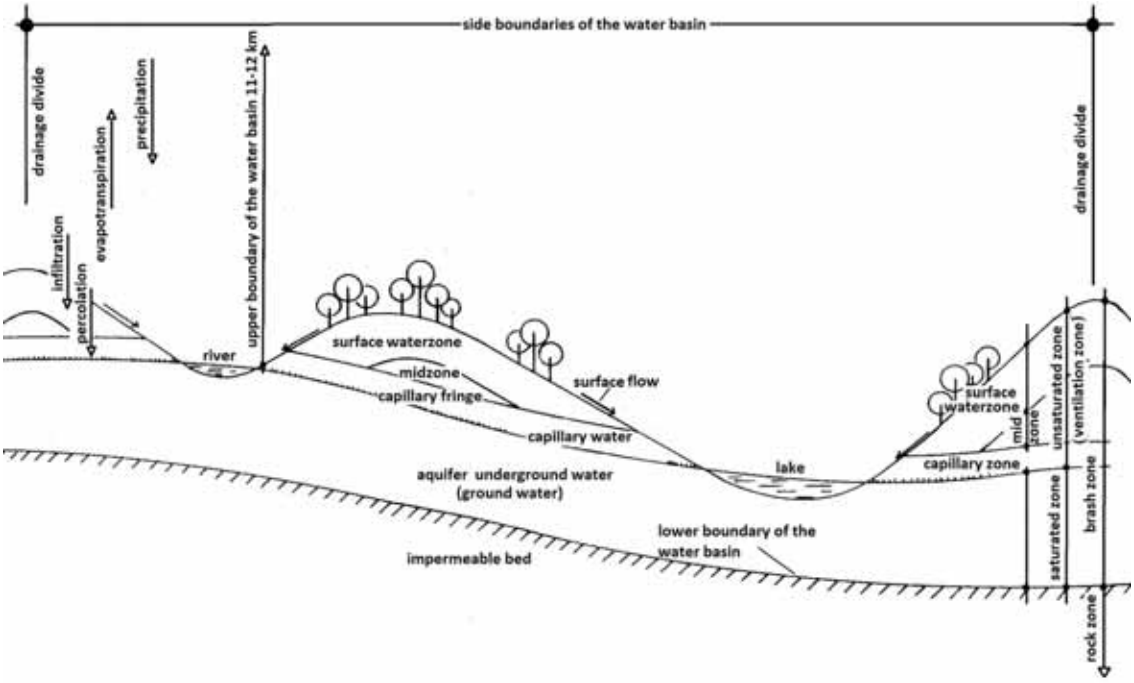

FIGURE 3
Water movement in water basin ecosystem [8]

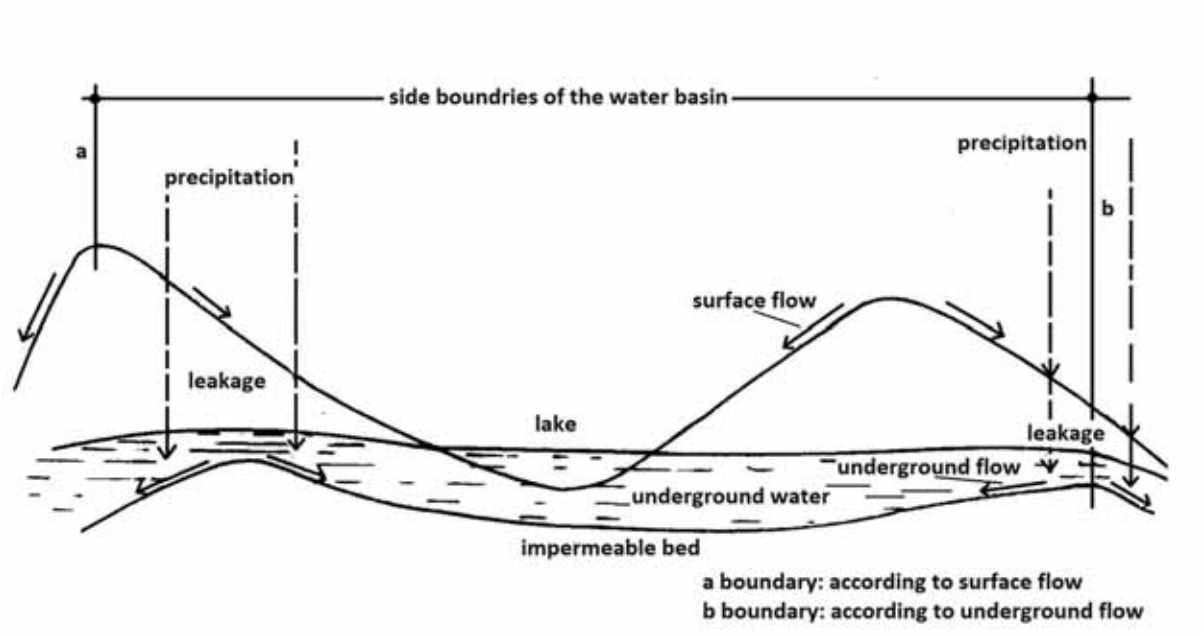

FIGURE 4
Side boundaries according to the slope of the impermeable bed (Adapted from [8])

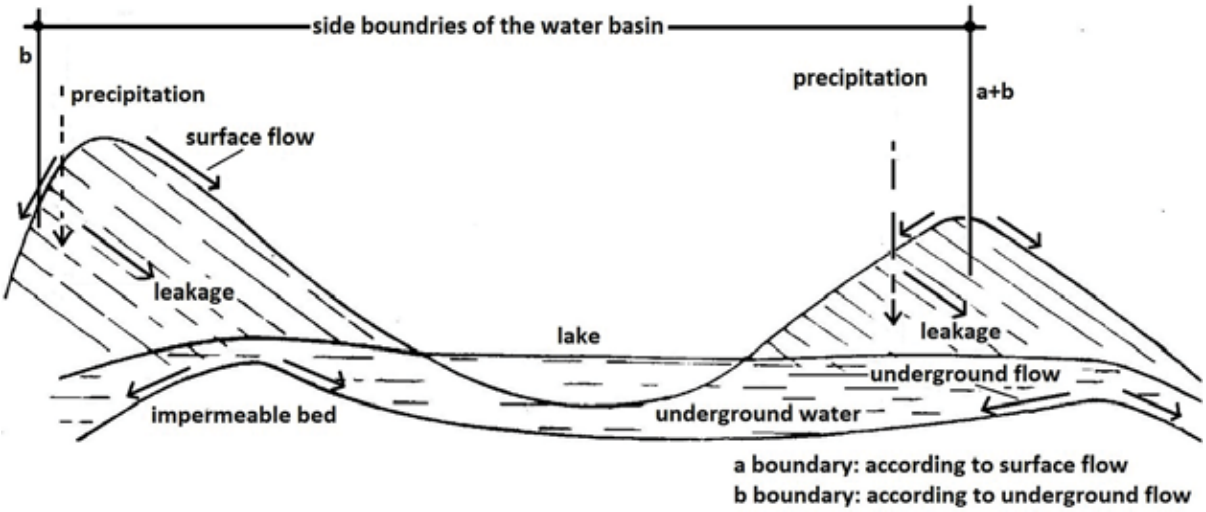

FIGURE 5
Side boundaries according to the slope of the bed (Adapted from [8])

Laws, regulations and plans on water basins are issued with the aim of preserving and sustaining the resources. Determining the elements, targeted to be preserved and sustained in the natural characteristics of the water basin ecosystem and increasing the water yield, are directly proportional to the knowledge of the actual feeding zone of the water basin outside the drainage divide, in other words, the boundaries of the water basin. Except from its role in determining the boundaries of the water basin, the underground geological and geomorphologic structure in the water basin has also the features of directing the underground water, cleaning it by filtration, and changing its minerals and quality consistent with the tectonic movements and permeability of the rocks.

Sources polluting water basin ecosystem. While the reservoir is fed by the surface and underground movements of water, the materials and pollutants carried with the water also reach the reservoir. Elements which do not exceed the carrying capacity of the renewable natural systems and are native in the natural system, can be cleaned within the natural cycles of the system. However, pollutants arising from human activities, which the natural system is not familiar with, are out of the cleaning capability of the natural system, and have a high volume and continuity, collect in air-water-soil resources and are transmitted to the reservoir. Departing from the aforementioned golden triangle rules creates irreversible situations in the water basin ecosystem or causes costly measures to be

taken. Accordingly, the amount of water in the basin decreases, quality of the water disrupts and the opportunity to access the water regularly in all seasons (The amount, quality and regime of the basin water can be briefly referred to as "water yield") is restricted. Plans should be handled with a holistic approach [19]. The factors reducing the yield of water in the basin can be summarized as: Decrease in the forest surface and vegetation other than forest, loss of soil by erosion in open areas, unconscious agricultural activities, expansion of settlement and industrial zones (firm ground), presence of unhealthy areas such as garbage patches and wrong site selection for them, discharge of wastes directly to the water resource, soil or air, mine exploration works, large infrastructure projects, such as highways, and so on.

The impact of the pollution of vital water resources, caused directly by human activities, increases due to climate change. Laws, regulations and plan studies should seek ecological and economical solutions that will eliminate the anthropogenic effects in water resources.

The Elmalı Dam Catchment Basin Protection Plan has been examined with the stated purpose.

RESULTS

Elmalı Dam is located 15 km away from Istanbul city center, on the eastern side of the Bosporus and on the west side of Ömerli Dam, in the Anatolian Side of Istanbul and the Kocaeli Peninsula. It is within the borders of Beykoz, Çekmeköy, Sancaktepe, and Maltepe Districts and is one of the smallest dams in Istanbul, with an area of approximately 83 km2 and 15 million m3 water retaining volume.

Two dams constructed over Elmalı Stream (Elmalı 1, 1926-1948) and Çavuşbaşı Stream (Elmalı 2, 1955) operate in an integrated way.

Elmalı Dam is fed by several streams (Figure 7) (Sakıran Stream, Arnavut Stream, Çiftlik Stream, Armutyatağı Stream, Çekmeköy Stream, Değirmen Stream, Karaağaç Stream, Köprü Stream (Kemer Stream)) [21].

The population and settlement areas in the Elmalı Basin began to increase rapidly, especially in 1980s as in the entire metropolis of Istanbul. The construction of the second bridge at the Bosporus (Fatih Sultan Mehmet Bridge) and linking roads (TEM) in 1984, also establishing organized industrial zones, such as Dudullu and IMES in the basin and its hinterland, brought the demand for accommodation areas forward. On the other hand, Zoning Amnesty, the Law on Supporting the Development of Forest Villagers and similar laws, regulations permitting the uses that might cause settlement and pollution in the water basins, presence of the county municipalities, having the authority to make and implement independent plans beyond the responsibility of the Istanbul Metropolitan Municipality, during the specified period, upper scale plan decisions which did not include adequate solutions for subscale plans and implementations towards the sustainability of the natural ecosystem features of the water basins and similar reasons, led to a decrease in the water yield in the basin with high population and settlement pressure [8].

As it can be seen in Table 1, areas that retain and transmit the water to the soil and prevent erosion, such as forest lands and bushes, decreased by 57% between the specified years, but the settlement areas forming firm grounds on the basin increased by 40% (Table 1, Figure 8). Settlement areas cause pollution by industrial activities and domestic waste. At the same time, firm ground increases the surface flow and transmits the pollutants on the surface to the water resources on one hand, and prevents regular water flow towards the underground beds and negatively affects the amount and regime of the water on the other hand.

FIGURE 6
Location of Elmalı drinking water basin [20]

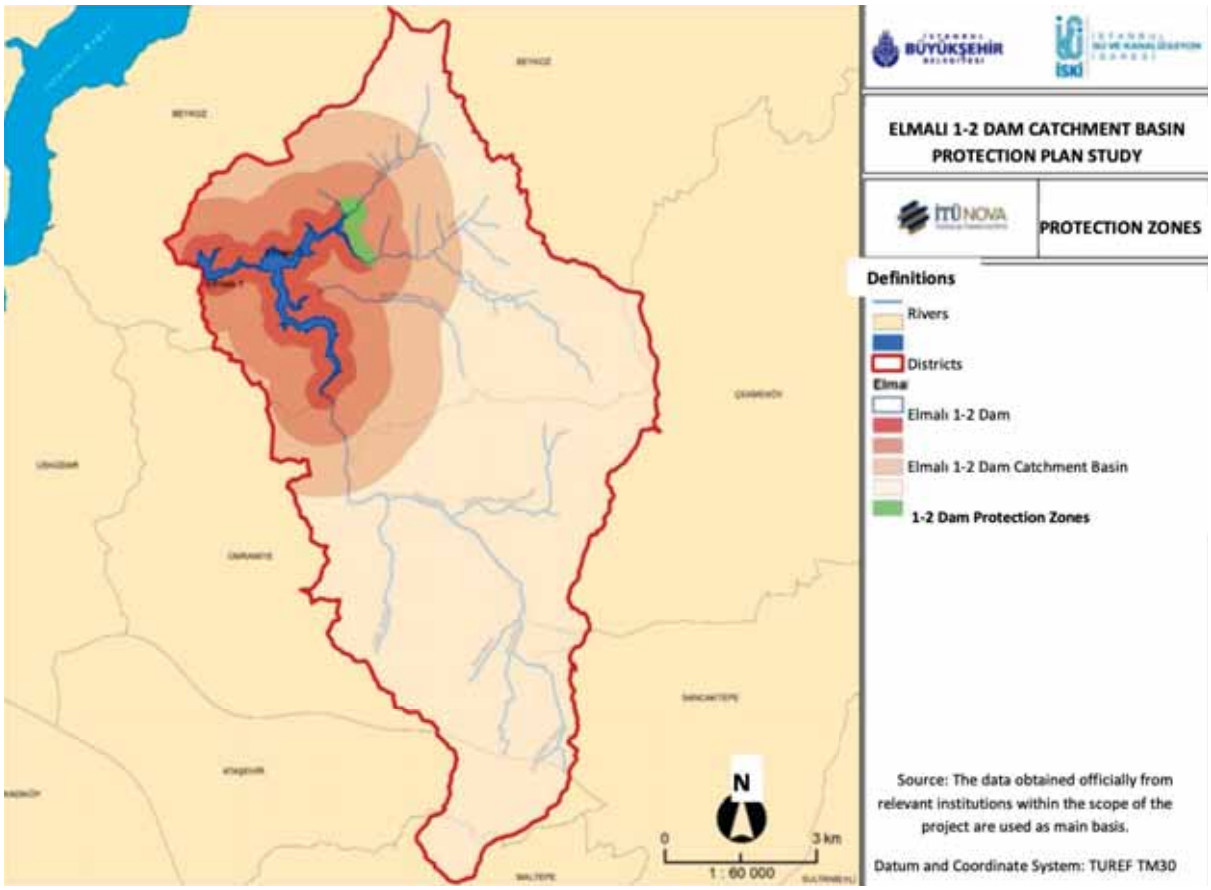

FIGURE 7
Streams and preservation zones in Elmalı drinking water basin [23]

TABLE 1
Changing in the Land Use in Elmalı Drinking Water Basin [20]

Category/ Year	1995		2005		2013	
	Ha	%	Ha	%	Ha	%
Arid Land	92	1	61	1	59	1
Agriculture	423	5	117	1	84	1
Forest	4135	50	3778	45	3757	45
Settlement	2444	29	3233	39	3378	40
Water	97	1	72	1	72	1
Bushes	1150	14	1080	13	991	12
Total	8341	100	8341	100	8341	100

The settlement areas are centered in the southern part of the water basin and are surrounding the Baklacık, Budak, Çekmeköy, Kemer, Karaağaç, Değirmen… streams, feeding the basin. Over the years, the settlement areas have also increased in the north of the water basin.

The amount, quality and regime of water is directly proportional to the presence of vegetation in the water basin. Studies show that in the forest lands which consume less water and are covered with litter, the amount of precipitation is 15%-50% higher compared to the surrounding areas [24]. More water is retained in the soil, nearly half of the precipitation becomes usable water product (this ratio is 14% in open areas) [13], rain splash and wind erosion is not seen, and the amount of water transmitted to the lower layers increases as the hollow structure of the soil increases [7].

If the population sizes are listed in proportion with basin areas, Elmalı, Alibey, Sazlıdere and Ömerli Water Basins come first [21]. The increasing water demand, and the decreasing and polluted water supply, create an economic burden by promoting the construction of new water transport pipes and treatment plants, at high costs. As the available resources fail to meet the water demand in Istanbul, water is provided from longer distances (Melen, Yeşilçay, Istıranca, Sakarya) (Figure 9).

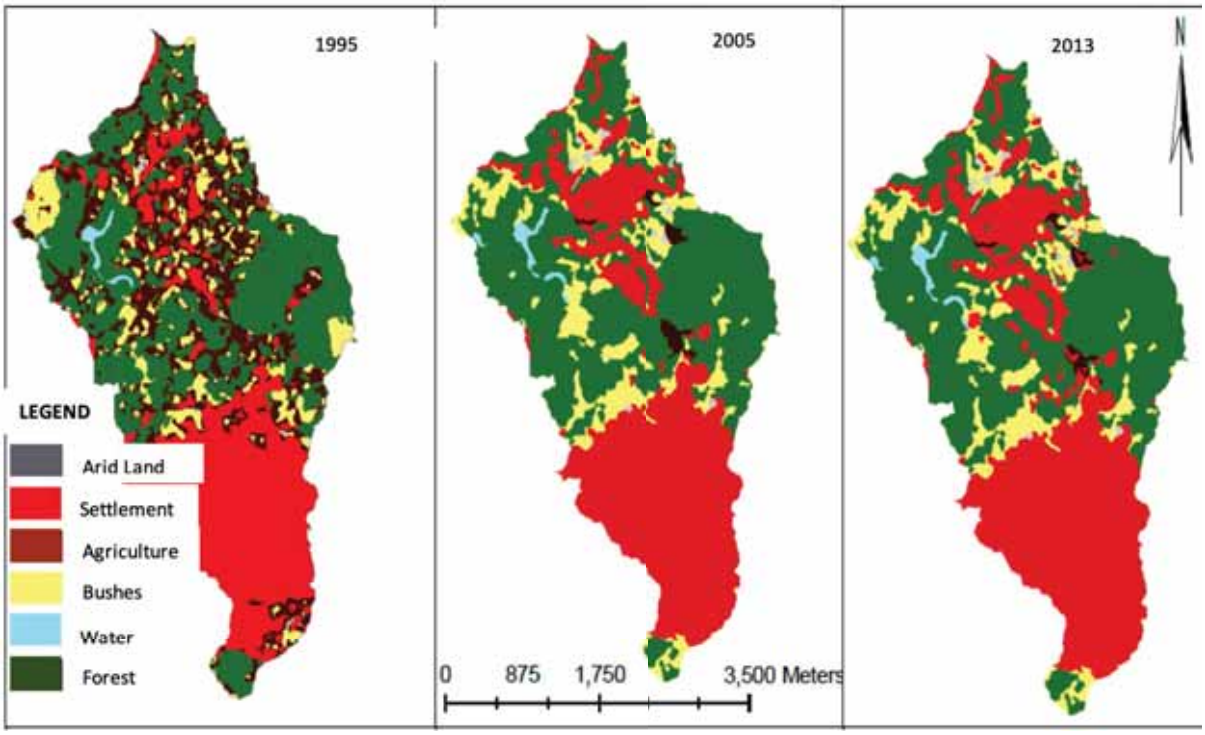

FIGURE 8
Changing land use in Elmalı drinking water basin by years [20]

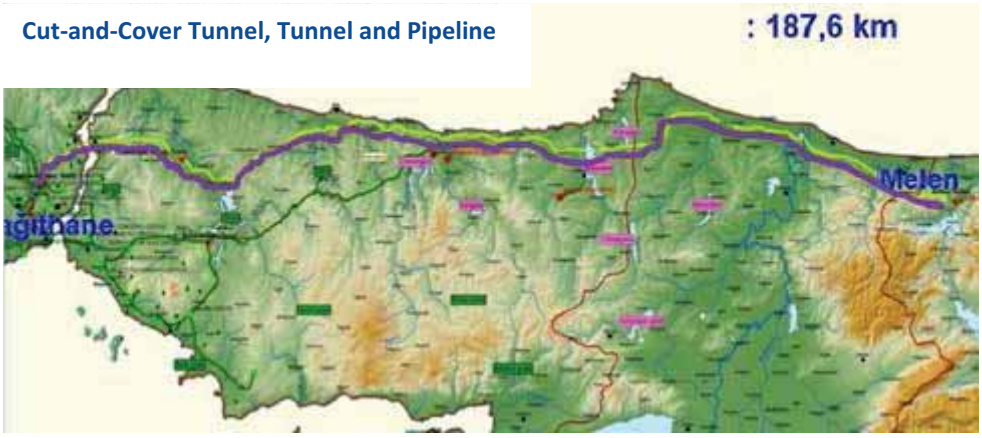

FIGURE 9
Water Supply System from Melen River to Istanbul [25]

Fresh water basin ecosystems formed according to the river resources, provide sustainability in the nearby hinterland, in proportion to the capacity, as long as there is no pressure from other systems. However, directing the resource according to the relatively higher water demands at longer distances, negatively affects the features of the ecosystem in the immediate surroundings of the resource.

Elmalı 1-2 Dam Catchment Basin Protection Plan. The given information on the water basin ecosystem and Elmalı Basin in a summary, has been tried to be examined within the scope of Elmalı Dam Catchment Basin Protection Plan. The impact of the plan on the basin, and the headings considered important, are mentioned in the paragraph below.

It was stated that Elmalı 1-2 Dam Catchment Basin Protection Plan has been approved by the consent of the Ministry of Agriculture and Forestry, dated 20.03.2019 and entered into force [23], was prepared for the purpose of establishing all legal and technical principles, regarding the preservation and sustainability of the water yield of the dam for providing drinking water, and regulating of all kinds of activities within the dam catchment basin.

Determination of the water basin boundaries, as a result of geological studies, including the details explained in the previous sections, and knowing the actual feeding zone of the water basin, gains importance in the realization of the purposes of the plan. There is no small-scale geological map which shows the current situation of the region. Detailed

geological studies need to be conducted in the basins [26].

The strict short-, medium-, long-distance preservation zones in the regulations and plans are defined under the title of 'water basin preservation zones' in Elmalı water basin plan as: reservoir green diversion zone ((dam reservoir boundary) areas between 0-300 m), reservoir preservation zone (300-700 m), short distance preservation zone (700-1000 m) and long distance preservation zone (1000-basin border). Apart from these, "Controlled Use Zone" which covers "the region which was established before the preparation of the Preservation Plan, is compulsory for settlement and urban development, and where human activities are intense and necessary measures are taken to minimize the negative effects of these activities on the dam catchment basin ecosystem" are identified (Figure 10).

The mentioned area is the settlement area with dwellings and facilities adjacent to the northeastern border of the reservoir. In the settlement next to the reservoir, and which is stated to be densely populated, but preserved in the plan, minimizing the pollution caused by human activities will result in high costs. Settlements cause problems, resulting from the formation of firm ground. The number of organisms carrying diseases easily increases in the areas where domestic waste is collected, the pollution reaches to the water resources with the water infiltrating through the surface and this carries high risks of illnesses [27] . A detailed analysis of the geological structure of the region is required and the region has to be converted into soft ground with vegetation, instead of firm ground, by clearing the region of the settlement, which may be aimed in time.

The concept of "preservation zones", implemented with standard values, was brought to the agenda in accordance with the protocol signed between the General Directorate of State Hydraulic Works and the Ministry in 1976, and was used with the purpose of providing preservation around the drinking water resources, until zoning plans were made. It was written in the relevant protocol that: "...Regulations shall be prepared for the protocol areas following the detailed local researches in the regions priorities of which to be determined. The strict, short and medium distance preservation zones may be expanded in the regulations to be prepared for these regions considering the boundaries determined by the protocol to be minimum..." The preservation zone distances have been used as standard values in the plans, and regulations approved later, instead of performing the basin-specific studies, proposed in the protocol. The same applies to the Elmalı Water Basin Plan. As it can be understood from the definition of water basin, water feeding the dam reservoir from the surface and underground reaches the lake by covering the entire basin.

The plan [23] states that the number of building stocks in the controlled use zone, adjacent to the dam reservoir, has to be reduced in time. The solution of the property problem and the term 'in time' may not be covered in practice. While the gross density is 30 people/ha in this region, maxTAKS (TAKS: Base density rate):30 value is regarded as firm ground in urban scale. The statement under the same heading that 'the existing industrial plants and commercial enterprises that do not generate waste water can continue their activities without generating industrial waste water' does not comply with the water basin ecosystem.

The values of density depending on the distances are increased in the same plan. The table adapted from the plan by the author is below. (Table 2).

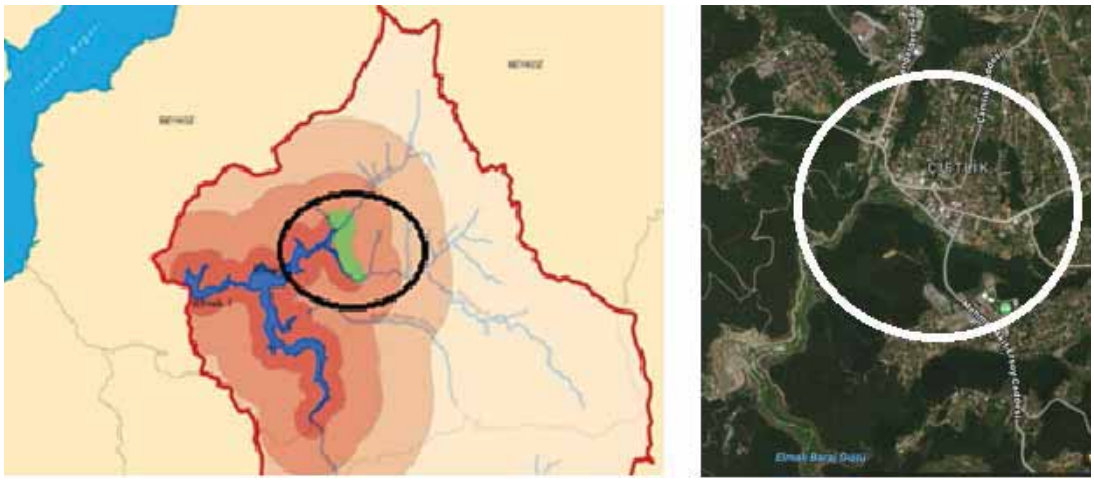

FIGURE 10
Elmalı Water Basin Plan Controlled Use Zone
(Prepared by referring to [23] and Google Map source)

TABLE 2
Elmalı 1-2 Dam Catchment Basin Protection Plan [23]

Elmalı 1-2 Dam Catchment Basin Protection Plan	Gross Density person/hectare		BCR	Function
CONTROLLED USE ZONE	30		30	Dwellings, commercial buildings, new highways, railways can be constructed.
RESERVOIR PRESERVATION ZONE	50		30 (dwelling) 50 (social infrastructure)	Dwellings, universities, student dormitories, guesthouses, boarding primary schools, boarding secondary schools, boarding high schools, accommodation facilities, tourism facilities except for those qualified as boardinghouses, congress and conference centers, socio-cultural facilities, primary care clinics, new highways and railways can be constructed. The existing industrial plants and commercial facilities can continue to operate, existing cemetery can be used.
SHORT DISTANCE PRESERVATION ZONE	Beykoz Ümraniye Çekmeköy Sancaktepe Ataşehir Maltepe	60 80 60 40 60 20	-	In addition to the above, the existing Organized Industrial Zone is preserved. The existing fuel stations are allowed to continue their fuel and LPG/CNG supply activities under the condition that they meet TSI standards and perform preliminary treatment on their waste water and connect to the collector line. New tourism facilities are not allowed, except for environmentally friendly ecotourism facilities, the existing cemetery can be used, mining activities are conditionally allowed, solid waste transfer stations are conditionally allowed, new highways and railways can be constructed. Pet shops, shelters and training camps for pets, salesrooms, accommodation facilities, such as guesthouses, boardinghouses, and hotels or training areas can be constructed.
LONG DISTANCE PRESERVATION ZONE	Beykoz Ümraniye Çekmeköy Sancaktepe Ataşehir Maltepe	75 140 100 120 140 25	-	In addition to the above, recreation facilities, fuel stations and similar other facilities and roads can be constructed. The existing organized industrial zone is protected, regular storage mine tailings disposal plants are allowed in the Long-Distance Preservation Zone after 3 (three) km horizontally from the border of Short-Distance Preservation Zone. The existing fuel stations, gas filling stations and chemical substance depots are allowed to carry out filling activities, fuel and LPG supply activities, under the condition that they meet TSİ standards, except for service activities in the stations, solid waste transfer stations are conditionally allowed. The mining activities and tailings generated as a result of these activities are conditionally allowed. Pet shops, shelters and training camps for pets, salesrooms, accommodation facilities, such as guesthouses, boarding houses, and hotels or training areas can be constructed.

DISCUSSION AND CONCLUSIONS

As it can be seen in Table 2, Elmalı Dam Catchment Basin Preservation Plan could allow the construction of all uses within the water basin, including unhealthy facilities that may be located in urban fabric, such as dwellings, industrial plants, fueling facilities, social-cultural facilities, cemeteries and an organized industrial zone. CO2 emissions from the energy consumption in the settlements and fossil fuels, used by cars [28] also directly reach the air, water and soil resources in the basin. Provisions for the conditional allowance of some facilities involve several difficulties, as it can be seen in similar implementations today. SCHEDULE 2 annexed to the plan under the heading 'Working program for the implementation of the measures' includes the program for the management of domestic, industrial, hazardous and special wastes, medical wastes and mineral tailings. Taking land use decisions which the natural system is not familiar with and is not able to clean, and which will cause a development beyond its carrying capacity, cannot be regarded as one of the scientific methods. Pollution of the water basin, with the plan decision, regulations and implementations supporting the plan decisions, cause the irreversible depletion of the polluted resources, and Figure 8 reflects how this happens in practice. Treatment of the polluted resource and transportation of water from other regions are implementations with high costs.

Pollution within the water basin boundaries shall be carried to the dam reservoir by the water (Figure 11).

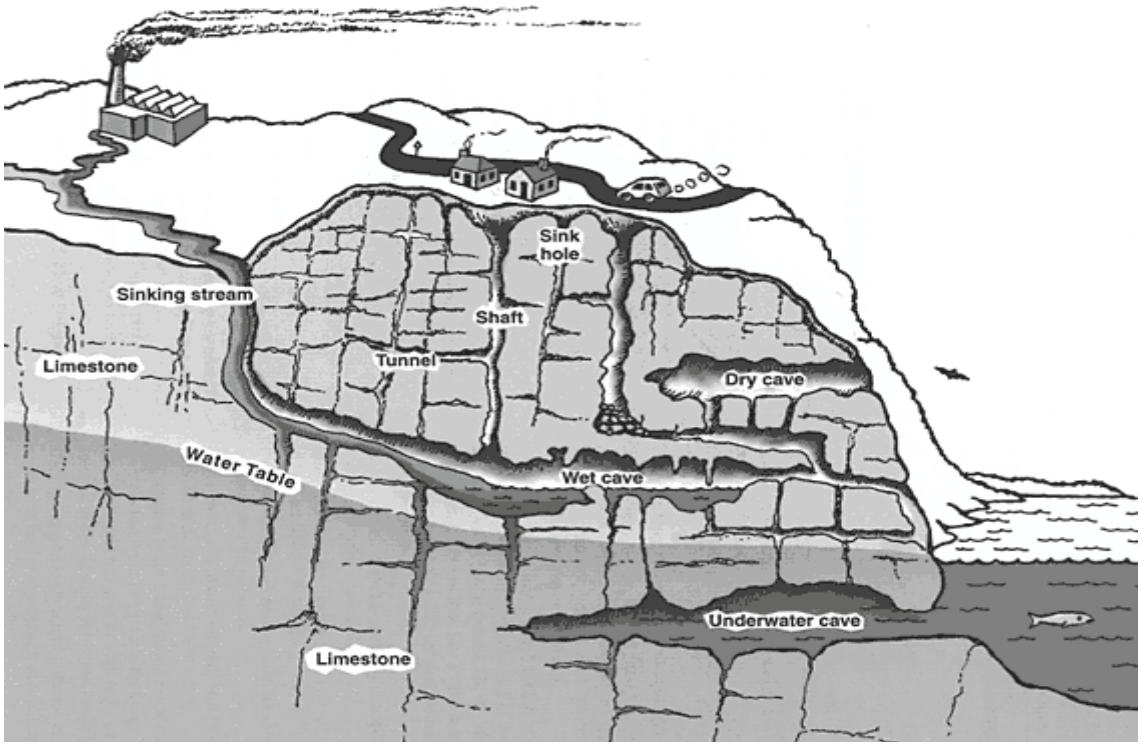

FIGURE 11
Water in the basin reaching to the dam reservoir regardless of distance [4]

The preservation mentality, depending solely on the surroundings of the dam reservoir, without analyzing the water basin ecosystem elements, definition of standard distance, and increasing settlement conditions in proportion to the distance of the preservation zones to the reservoir, do not comply with scientific data and are far from a planning mentality. It is considered beneficial to prepare water basin plans and boundaries in the context of detailed geological maps. It may be suggested, that water permeability of the formations, the chemical reaction of the rocks, according to the content of the water coming, the capacity and capability to filtrate-store different organisms within the water, contribution of the rocks to the quality of the water, the hollow-faulted-cracked structure or impermeability of the formation and similar analysis of the geological maps, should be handled with vertical sections in sensitive areas if necessary, with the participation of relevant disciplines.

Solutions sought as emergency action plans, in order to meet the current needs cannot produce solutions to the water shortage fundamentally and in the long run. It should be aimed to sustain water resources by benefiting from their natural features. Accordingly:

- Calculation of the population of the plan, in line with the carrying capacity [29] of the resource,
- Determination of the land use decisions in the plans, in reference to the calculated population and the natural structural features of the water basin,
- Including measurements to prevent regional accumulations in the plan decisions,
- Including provisions which support the planned decisions in the laws can be counted among the principles of sustainable fundamental solutions.

Urban systems which put pressure on the water basin ecosystem, should be planned in an integrated way in the upper stage, within the sociocultural structure of the societies, and should have content that provides a sustainable solution, applicable to the plans at lower stages.

ACKNOWLEDGEMENTS

This manuscript presented at the International Conferences on Science and Technology ICONST 2019.

REFERENCES

[1] Zheng, Y., Zhang, L., Zhang, G., Yang, B., Liu, T., Liu, S. (2019) Study on Water Environment Planning in an Ecological City as Sustainable Development Perspective. Fresen. Environ. Bull. 28, 7964-7970.

[2] Atabay, S. (1998) Sustainable development and environmental management - South East Anatolia project example. 38th Congress of the European Regional Science Association: "Europe Quo Vadis? - Regional Questions at the Turn of the Century". 28 August - 1 September 1998, Vienna, Austria.
[3] Eruz, E. (1991) Conservation and Importance of Forest Water Relationship. Bulletin of Istanbul University, Institute of Marine Sciences and Geography, 7, Istanbul. (In Turkish)
[4] Yolcubal, İ. (2015) Hydrogeology Lecture Notes. Kocaeli University Department of Geological Engineering, Kocaeli. (In Turkish)
[5] Churchman, C.W. (1968) The Systems Approach. Dell Publishing Co. 29-30.
[6] Arslan, R. (1993) Evaluation Techniques in Urban Planning. Yildiz Technical University Faculty of Architecture Department of Urban and Regional Planning Publications, 270, Istanbul, 32. (In Turkish)
[7] Çepel, N. (1995) Forest Ecology. Istanbul University Faculty of Forestry Publications, 433, Istanbul. (In Turkish)
[8] Suri, L. (2000) Planning and Management in Potable Water Basins, Case of Ömerli Potable Water Basin. Doctoral Thesis. Yildiz Technical University Institute of Science, Istanbul. (In Turkish)
[9] Erinç, S. (1984) The Ambient Ecology and Changes in Degradational Ecosystem. Istanbul University Institute of Naval Sciences and Geography Publications, Istanbul. (In Turkish)
[10] Işık, K. (1997) Urban Ecosystem Model and Environmental Problems. Symposium on Cities and Ecology in Preserving Nature. 19.12.1997. The Society of Nature Conservation in Turkey, Istanbul University Faculty of Forestry, Istanbul University Environmental Problems Research and Application Center and Istanbul Technical University Faculty of Architecture, Istanbul. (In Turkish)
[11] İSKİ (1999) Istanbul Water Supply, Sewerage and Drainage, Waste Water Treatment and Removal Master Plan Study. Istanbul Metropolitan Municipality, the Directorate General of Istanbul Water and Sewerage Administration. (In Turkish)
[12] Uzunsoy, O. and Görcelioğlu, E. (1985) Basic Principles and Practices in Water Basin Rehabilitation Works. Istanbul University Faculty of Forestry Publications, 371, Istanbul. (In Turkish)
[13] Balcı, N. (1976) The Role of Vegetation - Especially Forests- in Hidrology, Land Use and Soil Stability. 1st Seminar on Forest Cadaster 15 January-22 February 1974, Istanbul University Faculty of Forestry, Directorate General of Forestry Publications, Item No: 607, Serial No: 13, Ankara. (In Turkish)
[14] Koç, G. (2018) Basin Processes. https://docplayer.biz.tr/68637086-Hidrolojik-dongu-su-dongusu.html. (In Turkish)
[15] Erguvanlı, K. and Yüzer, E. (1984) Geology of Underground Waters (Hydrogeology). Istanbul Technical University Faculty of Mines, Istanbul. (In Turkish)
[16] Oktay, F., Eren, R., Çinal, H., Aktaş, M., Akmeşe, I., Üner, K. (1997) The Importance of Geological Factors in Determining the Boundaries of the Water Basin Protection Area - Examination of Büyükçekmece Water Basin Case", Symposium on Preservation and Management of Water Resources, 2-3 June 1997, İSKİ, Istanbul Technical University and Turkish Water Foundation, Istanbul. (In Turkish)
[17] Öztaş, T. (1997) Problems Originating from Ecology in Modern Cities. Symposium on Cities and Ecology in Preserving Nature. 19.12.1997. The Society of Nature Conservation in Turkey, Istanbul University Faculty of Forestry, Istanbul University Environmental Problems Research and Application Center and Istanbul Technical University Faculty of Architecture, Istanbul. (In Turkish)
[18] Seyhan, E. (1977) Fundamentals of Hydrology, Geographical Institute of the University of Utrecht University center "De Uithof" Transitorium II Heidelberglaan 2, the Netherlands. (Fundamentals of Hydrology, Geografisch Instituut der Rijksuniversiteit te Utrecht Universiteitscentrum "De Uithof" Transitorium II Heidelberglaan 2, Nederland).
[19] Aksu, G.A. (2014) Holistic Landscape Planning Approach. Istanbul Commerce University, Journal of Science. 13-26. (In Turkish)
[20] Geymen, A. (2016) Monitoring Natural Resources in Water Basins using Geographical Information Systems: Case of Elmalı Water Basin. Kahramanmaraş Sütçü İmam University Journal of Natural Sciences. 19(2), 174-180. (In Turkish)
[21] ISKI (2018) Drinking Water Basins Regulation, 01.10.2018-00873813 (In Turkish)
[22] T.C., Ç.Ş.B. (2018) Istanbul Provincial Environmental Status Report for 2017. Istanbul Provincial Directorate of Environment and Urbanization, Section of Environmental Impact Assessment, Istanbul. (In Turkish)
[23] İSKİ (2019) Elmalı 1-2 Dam Catchment Basin Protection Plan. Approved by the consent of the Ministry of Agriculture and Forestry no. 921501 dated 20.03.2019, Press Advertising Association Advertisement No: ILN00969336, Yeni Söz Newspaper. 23.03.2019, Istanbul. (In Turkish)
[24] Çepel, N. (1994) Landscaping Ecology, Istanbul University Faculty of Forestry Publications, 429, Istanbul. (In Turkish)

[25] İlhan, A., Yıldız, D., Tokaç, F.Z., Kurnaz, M.L., Türkeş, M. (2014) Water Crisis in Istanbul and Collective Solution. ISBN no: 978-605-62639-4-1, Martı Offset, Istanbul. (In Turkish)
[26] Var, D. (2008) Examination of Southern Part of Elmalı Water Basin in terms of Surface and Underground Water Pollution. Master Thesis. Istanbul Technical University Institute of Science Department of Geological Engineering, Istanbul. (In Turkish)
[27] Şanlısoy, A. (2002) Problems in Water Catchment Basins in Istanbul, Causes and Solution Proposals. Master Thesis. Istanbul Technical University Institute of Science. (In Turkish)
[28] Civelekoğlu, G., Bıyık, Y. (2018) Investigation of Carbon Footprint Change from Transportation Sector. Bilge International Journal of Science and Technology Research. 2(2), 158. (In Turkish)
[29] Luo, M., Huang, E., Ding, R., Lu, X. (2019) Research on Water Resources Carrying Capacity Based on Maximum Supportable Population. Fresen. Environ. Bull. 28, 100-110.

Received: **05.11.2019**
Accepted: **28.01.2020**

CORRESPONDING AUTHOR

Leyla Suri
Istanbul Commerce University,
Faculty of Architecture and Design
Department of Architecture,
Istanbul – Turkey

e-mail: lsuri@ticaret.edu.tr,
leylasuri14@gmail.com

© by PSP Volume 29 – No. 05/2020 pages 3778-3789 Fresenius Environmental Bulletin

EFFECT OF POTASSIUM APPLICATION ON THE GROWTH AND Fe/Zn USE EFFICIENCY OF SALT-TOLERANT AND SENSITIVE MAIZE GENOTYPES IN RESPONSE TO SALINITY

Munaza Batool[1,*], Muhammad Amjad Bashir[2], Muhammad Abdul Qayyoum[1], Arif Hussain[1], Syeda Amber Hameed[3], Suilman Mohammad Alghanem[4], Muhammad Saqib[5]

[1]Department of Soil and Environmental Sciences, Faculty of Agricultural Sciences, Ghazi University Dera Ghazi Khan Punjab, Pakistan
[2]Department of Plant Protection, Faculty of Agricultural Sciences, Ghazi University Dera Ghazi Khan Punjab, Pakistan
[3]Department of Zoology, Faculty of Sciences, Ghazi University Dera Ghazi Khan Punjab, Pakistan
[4]Department of Botany, Faculty of Sciences, University of Tabuk Kingdom of Saudia Arabia
[5]Department of Soil and Environmental Sciences, Faculty of Agricultural Sciences, University of Agricultural Faisalabad Punjab, Pakistan

ABSTRACT

Status of mineral nutrient in plant body play an important role in improving its response to any environmental hazard like water stress, salt stress and heavy metal stress etc. Along with other mineral nutrients, potassium has an important task regarding plants endurance under salt stress condition. It is very important for maintaining turgor and membrane potential, balancing osmotic potential, controlling stomatal movement and activating enzymes. Addition of potassium in growing medium improved salinity tolerance in rice, wheat and corn. Results of previous research depicted that high concentration of potassium in plant body greatly reduced the production of reactive oxygen species. With the objective to combat salinity stress in maize a pot study to investigate the effect of K application on the growth and Fe/Zn use efficiency of salt-tolerant and sensitive maize genotypes. In this experiment two maize (*Zea mays* L.) genotypes, one salinity sensitive and one salinity tolerant (on the basis of study I) were used. Seeds of each cultivar were sterilized in $HgCl_2$ solution (0.1%) for 10 min and after rinsing these seeds with distilled water they were sown in plastic pots containing well washed gravels. The seedlings were allowed to grow for 15 days. Uniform sized seedlings were transferred to a hydroponic system comprising of plastic tubs filled with Hoagland's nutrient solution (half strength). The treatments in this experiment include different levels of NaCl and potassium. The concentrations of potassium were 1 and 1.5 mM of the Hoagland nutrient solution with 0 or 100 mM NaCl. The salinity treatment was developed by adding sodium chloride (NaCl) to the nutrient solution after four days of transplantation to the hydroponic system. There were four replications of each treatment. The plants were allowed to grow in the treatment solutions for 28 days and at harvest the data regarding root/ shoot lengths, root/shoot fresh and dry weights were recorded. The oven dried shoot samples were analyzed for ion contents including Zn, Fe, Na^+ and K^+. It was concluded that in saline soil maize yield may improve by the application of K and increase of the concentration in maize grains can improve human nourishment.

KEYWORDS:
Maize, Salinity, Salt, saline, Potassium, Zinc

INTRODUCTION

Potassium plays a vital role in enhancing the yield and quality of maize grain. Many physiological processes of plants, affecting plant growth and yield such as photosynthesis, activation of enzymes, plant water relation and assimilation are affected by potassium application. Potassium is an important nutrient as nitrogen and phosphorus for grain crops [1]. Potassium (K) is an essential plant macronutrient and plays an important role in many physiological processes vital to plant nutrient and water uptake, nutrient transport, and growth, especially under adverse conditions. K fertilizer is the primary K source in most modern agricultural systems. The application rates of nitrogen (N) and phosphorus (P) fertilizers have increased annually, whereas the application rate of fertilizer K is still insufficient. Potassium plays a vital role in enhancing the yield and quality of maize grain. Many physiological processes of plants, affecting plant growth and yield such as photosynthesis, activation of enzymes, plant water relation photosynthesis, activation of enzymes, plant water relation. Potassium is an important nutrient as nitrogen and phosphorus for grain crops. The deficiency symptoms of potassium apparently have been not shown on maize crop but the yield decreases drastically, if there is severe deficiency then symptoms also can be observed [2]. Soils in Pakistan are generally considered rich in potassium but increase in cropping intensity, extensive removal of straw from the field, excessive use of tube well water and

soil applied K get field, excessive use of tube well water and soil applied K get fixed with clay minerals have resulted in considerable fixed with clay minerals have resulted in considerable exhaust of soil potassium [3]. Moreover, the price of fertilizers is getting higher and become expensive to the farmers. The deficiency symptoms of potassium apparently have been not shown on maize crop but the yield decreases drastically, if there is severe deficiency then symptoms also can be observed [2].

It is very important for maintaining turgor and membrane potential, balancing osmotic potential, controlling stomatal movement and activating enzymes. An appropriate K^+/Na^+ is imperative for maintaining turgor, and cell osmoregulation, stomata opening and closing, synthesis of Status of mineral nutrient in plant body play an important role in improving its response to any environmental hazard like water stress, salt stress and heavy metal stress etc. Along with other mineral nutrients, potassium has an important task regarding plants endurance under salt stress condition. High production of reactive oxygen species due to salt stress lead to membrane damage and result in potassium leak from cell due to K^+ efflux channel. Addition of potassium in growing medium improved salinity tolerance in rice, wheat and corn. The present study has been conducted to study the effect of K application on the growth and Fe/Zn use efficiency of salt-tolerant and sensitive maize genotypes in response to salinity.

MATERIALS AND METHODS

Study Site. The research work reported in this experiment has been conducted at the Institute of Soil and Environmental Sciences, University of Agriculture, Faisalabad, Pakistan. This work has been conducted to evaluate the performance of different maize genotypes against salinity.

Experiment detail and analysis. In this experiment two maize (*Zea mays* L.) genotypes, one salinity sensitive and one salinity tolerant (on the basis of study I) were used. Seeds of each cultivar were sterilized in $HgCl_2$ solution (0.1%) for 10 min and after rinsing these seeds with distilled water they were sown in plastic pots containing well washed gravels. The seedlings were allowed to grow for 15 days. Uniform sized seedlings were transferred to a hydroponic system comprising of plastic tubs filled with Hoagland's nutrient solution (half strength). This solution was covered with thermo-pore white sheet having holes. The plants were supported in the holes of thermo-pore sheets. Each tub was supplied with 100 liter Hoagland's nutrient solution. The treatments in this experiment include different levels of NaCl and potassium. The concentrations of potassium were 1 and 1.5 mM of the Hoagland nutrient solution with 0 or 100 mM NaCl. The salinity treatment was developed by adding sodium chloride (NaCl) to the nutrient solution after four days of transplantation to the hydroponic system. The pH of the treatment solution was maintained between 5.5 and 6.5 by using dilute NaOH or HCl solutions. The treatment solutions in all the tubs were aerated by bubbling air in the nutrient solutions. There were four replications of each treatment. The plants were allowed to grow in the treatment solutions for 28 days and at harvest the data regarding root/ shoot lengths, root/shoot fresh and dry weights were recorded. The oven dried shoot samples were analysed for ion contents including Zn, Fe, Na^+ and K^+.

Plant Analyses. Sodium, potassium, iron and zinc determination. The shoot samples were oven dried at 75°C for 48 hours. The dry root and shoot weights were recorded. The dried and ground shoot samples were digested in a di-acid (HNO_3:$HClO_4$ ratio of 2:1) mixture (Jones and Case, 1990). For this purpose, the dried ground material was placed in digestion tubes, 10 mL of di-acid mixture was added and incubated over night at room temperature. Tubes were placed in a digestion block and heated up to 350 °C until fumes were produced and continued to heat for another 30 minutes. Digestion tubes were removed from the block and allowed to cool. The tubes were placed again into the digestion block until fumes were produced for 20 minutes. Again digestion tubes were removed. Above step was repeated until the cool material became colorless. After digestion volume was made 50 ml with distilled water and used for ionic analysis. The ionic concentration for Na^+ and K^+ in plant samples was determined by Sherwood- 410 Flame Photometer with the help of self-prepared standard solutions using reagent grade salt of NaCl and KCl respectively. The Zn concentration in the digest was estimated by an atomic absorption spectrophotometer (PerkinElmer, 100 Analyst, Waltham, USA).

RESULTS

Shoot and root growth. The salinity (100 mM NaCl) resulted in a significant decline in shoot fresh and dry weights of both the maize genotype (Figure 1, Figure 2). The difference among genotypes, treatments and their interaction was significant for both these parameters. In control treatment, (no salt, no potassium) genotypes did not differ significantly however in the saline treatments they differed significantly from each other and this difference widened with more salt concentration in the growing medium. Like shoot growth salinity resulted in the corresponding decline in the root growth as well (Figure 3, Figure 4). The main effects as well as their interaction were significant for both root fresh and dry weights. Reduction in fresh and dry weights of root

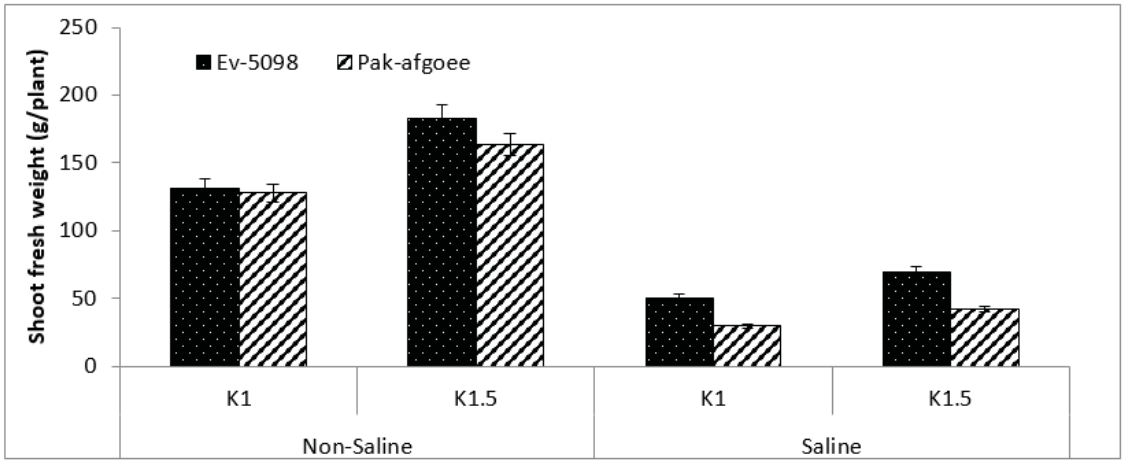

FIGURE 1
Effect of K application on shoot fresh weight of maize genotypes under non-saline and saline conditions

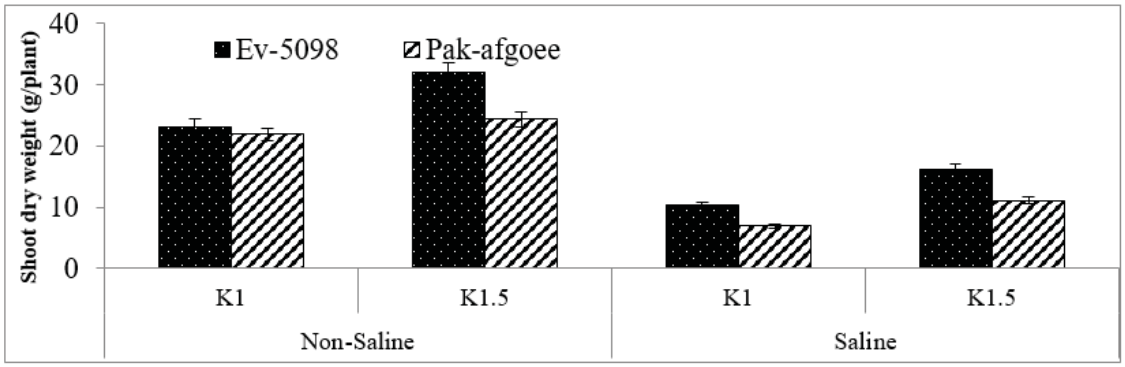

FIGURE 2
Effect of K application on shoot dry weight of maize genotypes under non-saline and saline conditions

was more in the case of salt sensitive than salt tolerant genotype. The length of both shoot and root was also decreased due to salinity stress (Figure 5, Figure 6). The genotypes did not differ significantly from each other under control condition. *Ev-5098* produced more root and shoot weight and length at 100 mM NaCl level with potassium application K@ 1.5x as compared to Pak-afgoee and it was also statistically significant from each other.

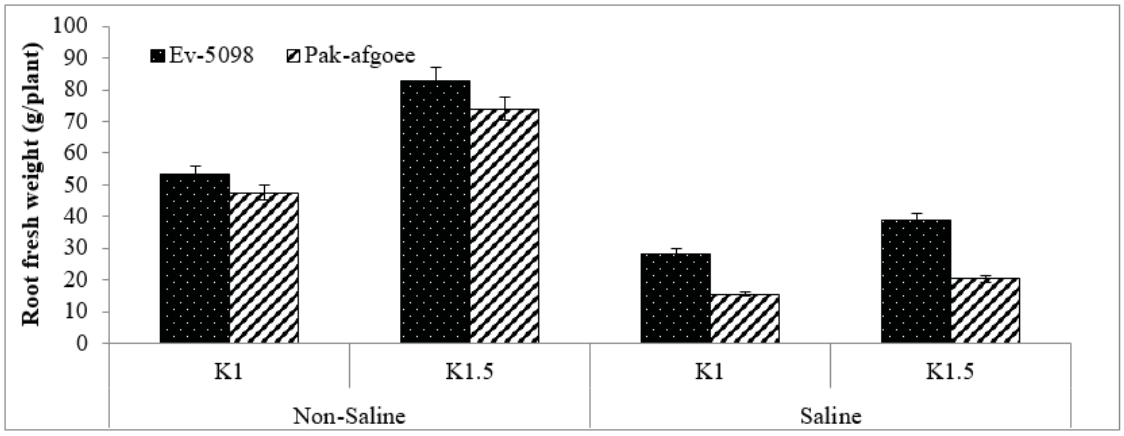

FIGURE 3
Effect of K application on root fresh weight of Maize genotypes under non-saline and saline conditions

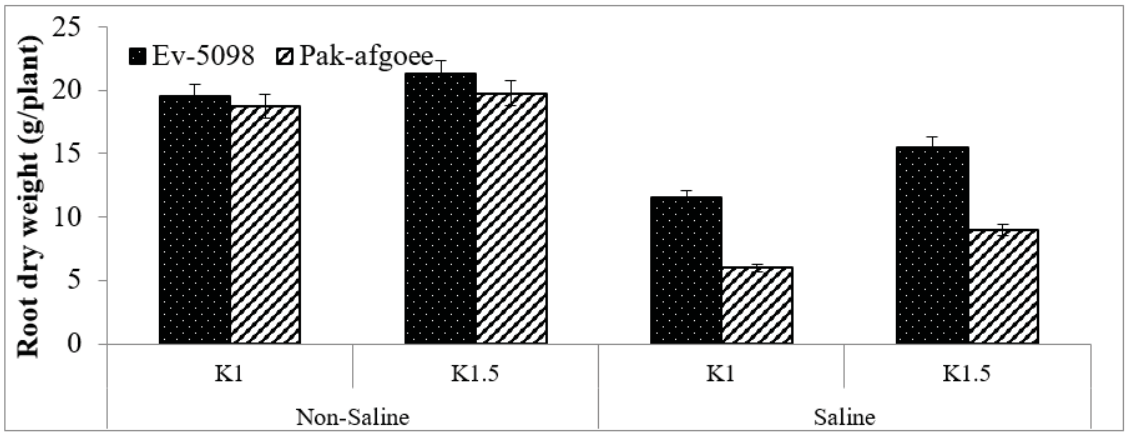

FIGURE 4
Effect of K application on root dry weight of Maize genotypes under non-saline and saline conditions

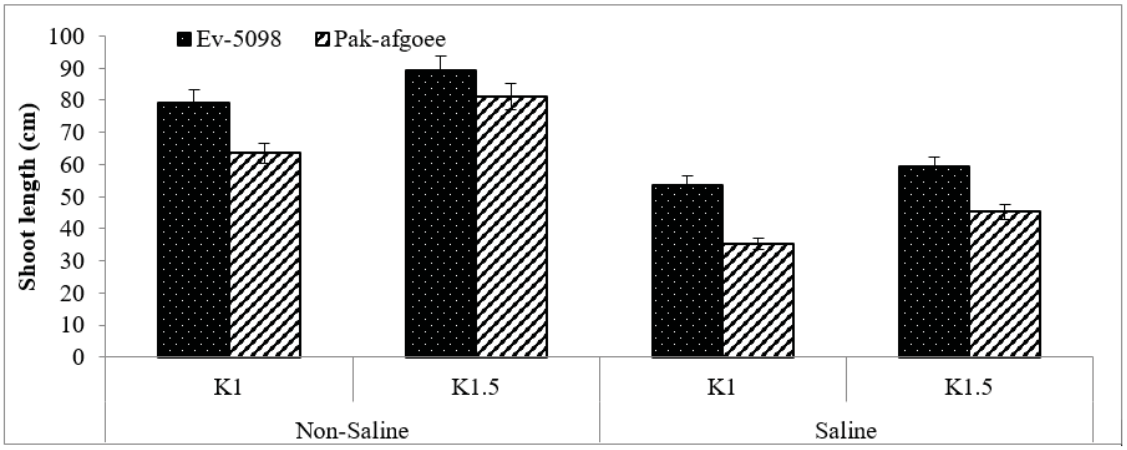

FIGURE 5
Effect of K application on shoot length of Maize genotypes under non-saline and saline conditions

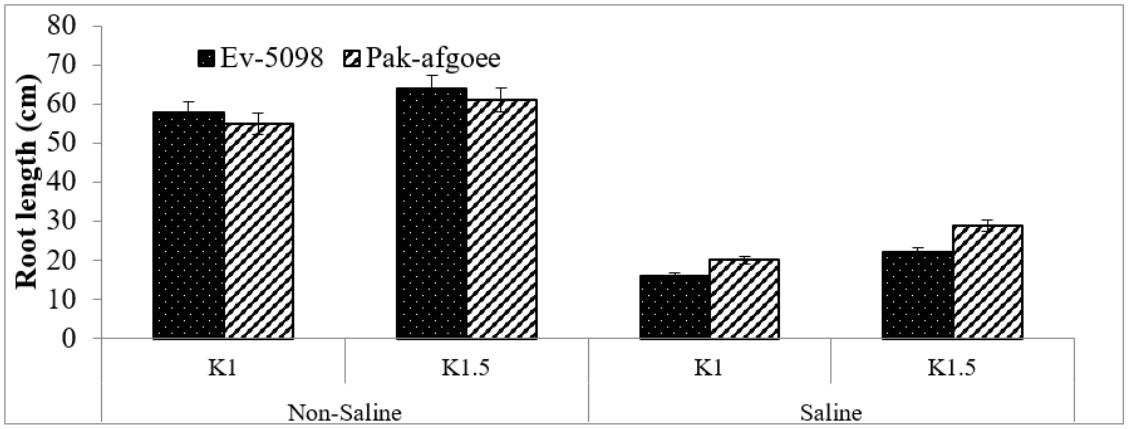

FIGURE 6
Effect of K application on root length of Maize genotypes under non-saline and saline conditions

Leaf ionic composition. Salinity significantly (P<0.05) increased the leaf Na^+ concentration in both genotypes (Figure 7). The individual as well as interactive effects of salinity, potassium and genotype were found significant. The comparison of genotypes under both treatments of potassium showed that with 100 mM NaCl application, Ev-5098 had lower concentration of Na^+ as compared to Pak-afgoee which is salt sensitive genotype. The difference between genotypes was the maximum at 100 mM NaCl with K1.5x. In this treatment, the maximum Na^+ concentration was found in the leaf of Pak-afgoee. The concentration of K^+ as against of Na^+ decreased significantly at 100 mM NaCl level of salinization (Figure 8). The highest K concentration in leaf was observed under non-saline condition with K application @ 1.5. The comparison of genotypes at salinity level (100 mM NaCl) and with potassium application K1.5 showed that *Ev-5098* accumulated more K^+ in leaf as compared to Pak-afgoee. It is showed from Figures 10 and 11 that the Zn concentration and Zn use efficiency improved under salinity (100 mM NaCl) with the application of potassium. The highest leaf Zn concentration was observed in leaf of Ev-5098 under saline environment with K1.5x application as compared to Pak-afgooe. Similarly, the highest Zn use efficiency was recorded in this genotype under saline condition while it was less as compared to non-saline condition. Similar trend was observed in Fe leaf concentration (Figure 11) and Fe use efficiency (Figure 12). The genotype Ev-5098 contains higher Fe in leaf with K application @ 1.5x and 100 mM NaCl than Pak-afgoee. In case of Fe use efficiency, Ev-5098 showed more Fe use efficiency under saline condition as compared to Pak-afgooe.

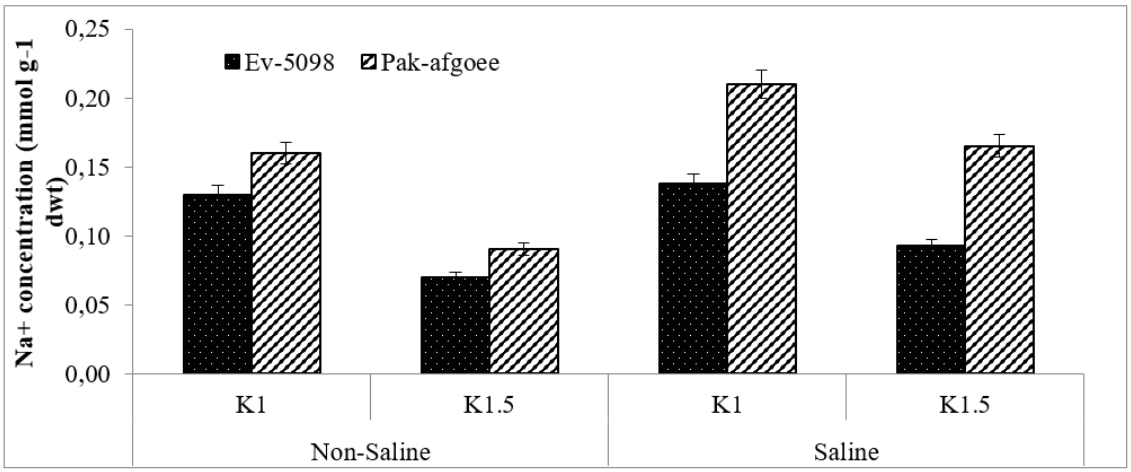

FIGURE 7
Effect of K application on sodium concentration of Maize genotypes under non-saline and saline conditions

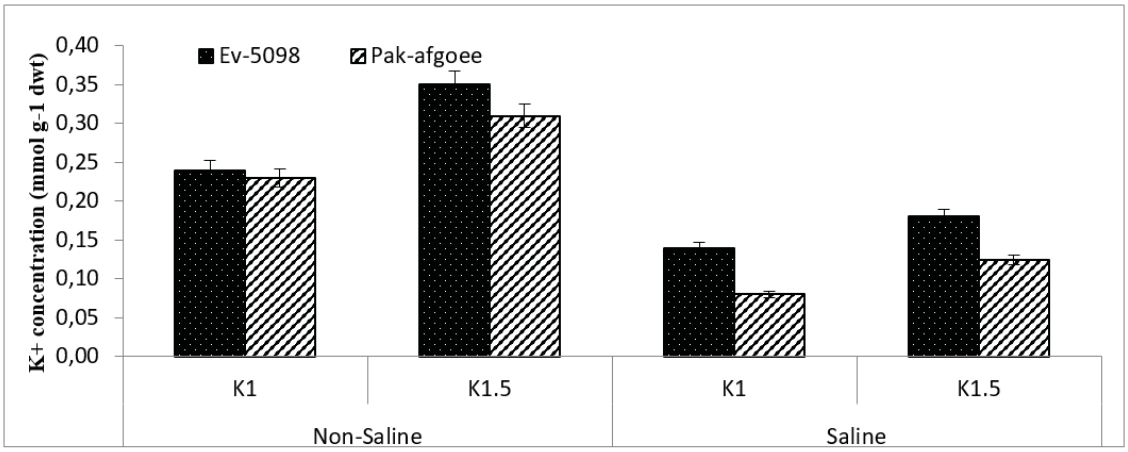

FIGURE 8
Effect of K application on potassium concentration of Maize genotypes under non-saline and saline conditions

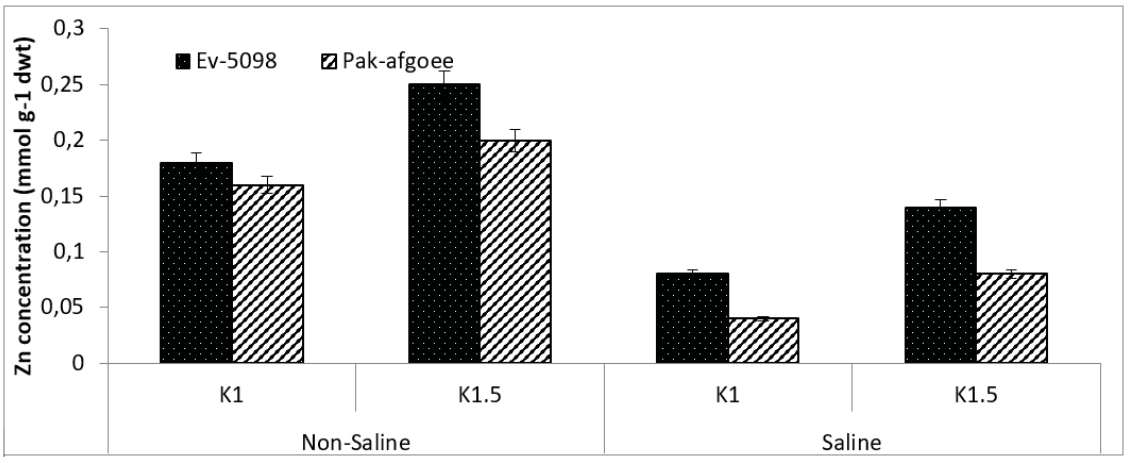

FIGURE 9
Effect of K application on zinc concentration of Maize genotypes under non-saline and saline conditions

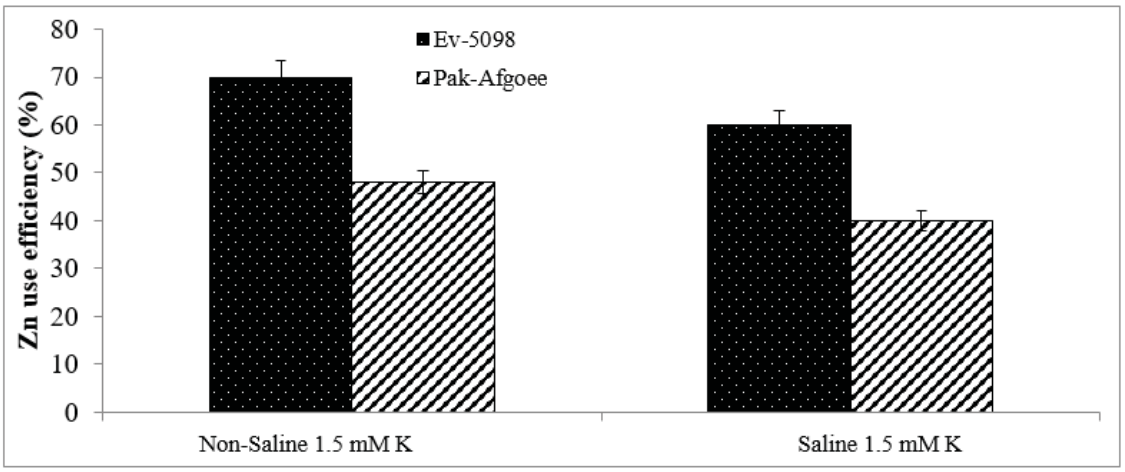

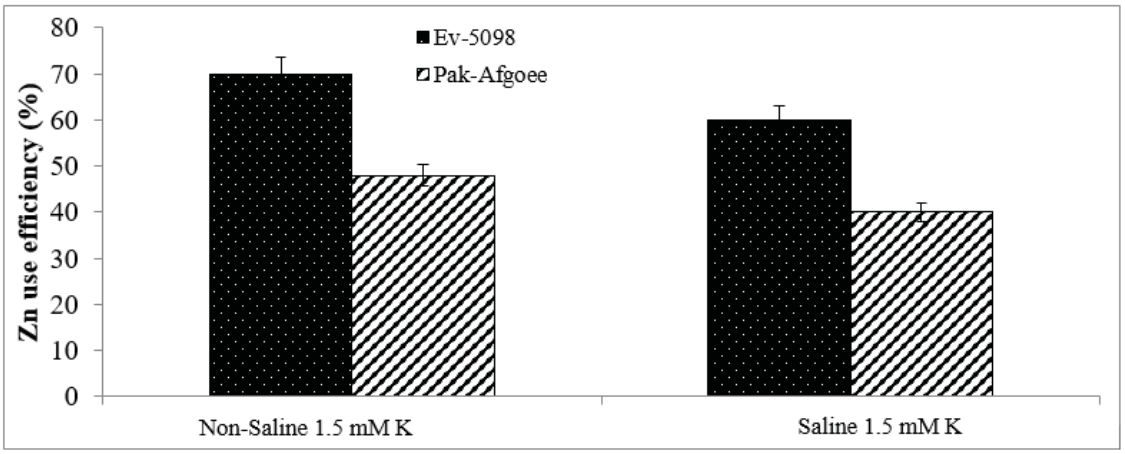

FIGURE 10
Effect of K application on zinc use efficiency of Maize genotypes under non-saline and saline conditions

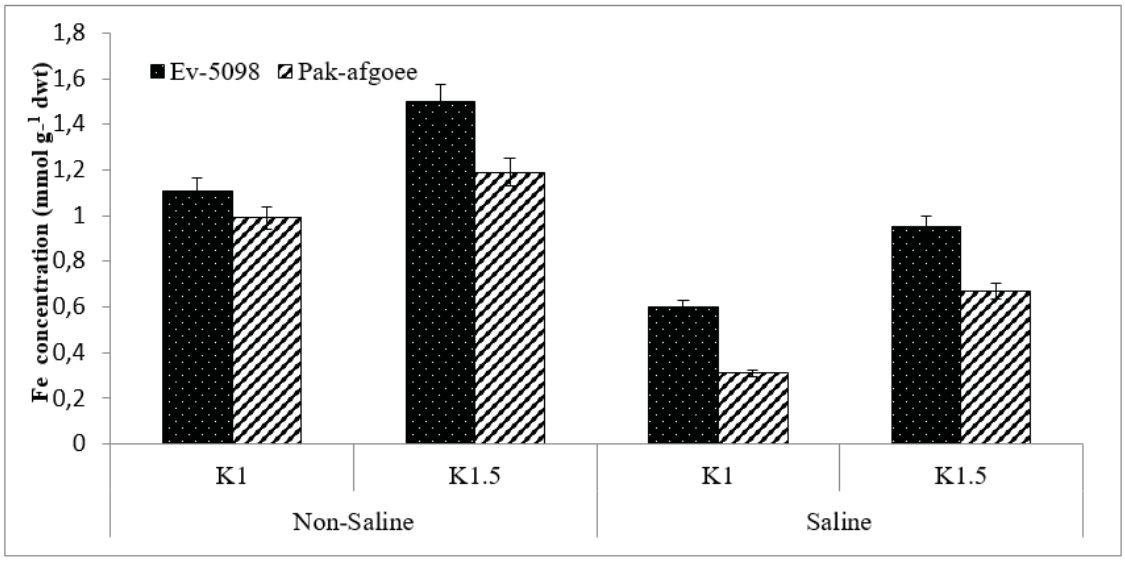

FIGURE 11
Effect of K application on iron concentration of Maize genotypes under non-saline and saline conditions

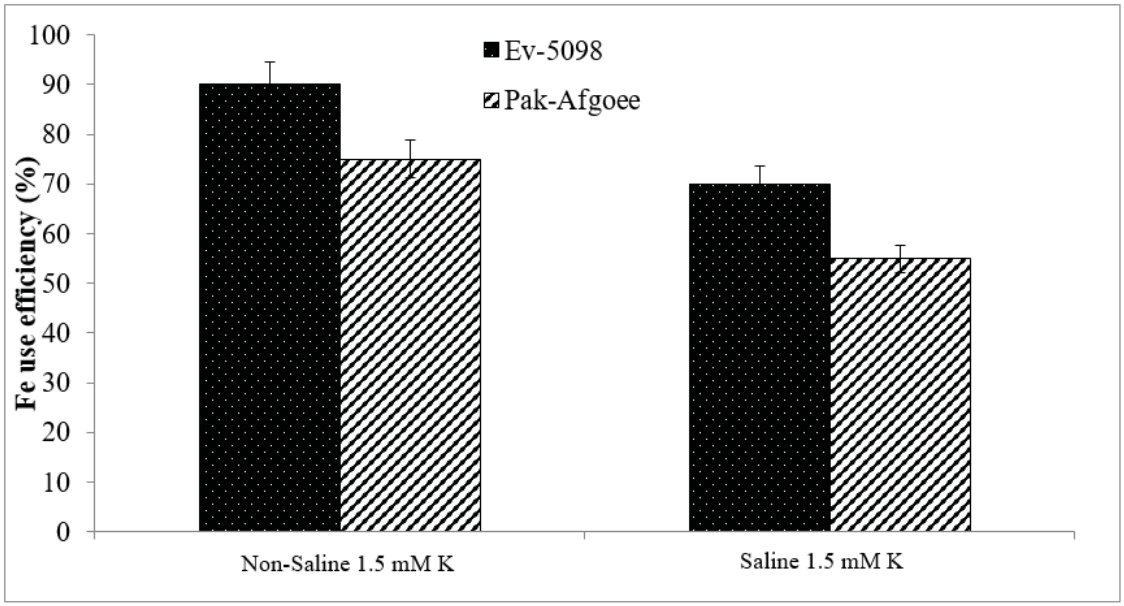

FIGURE 12
Effect of K application on iron use efficiency of Maize genotypes under non-saline and saline conditions

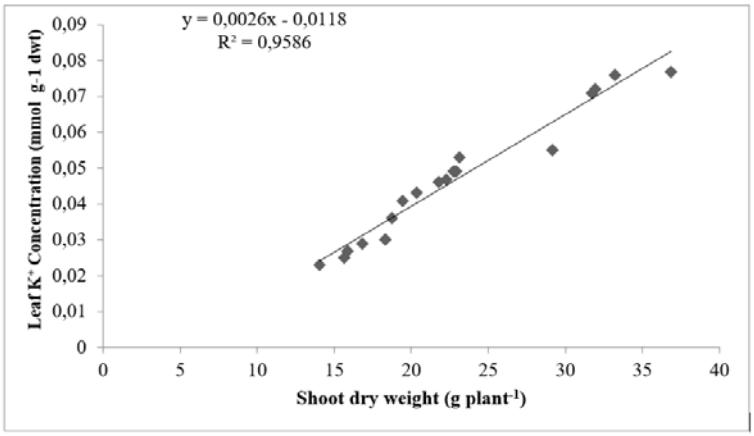

FIGURE 13
Relationship between leaf K^+ and shoot dry weight (g $plant^{-1}$) of different maize genotypes

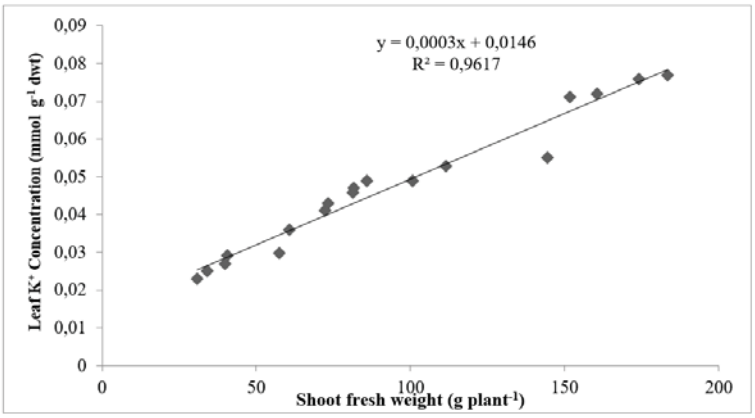

FIGURE 14
Relationship between leaf K^+ and shoot fresh weight (g $plant^{-1}$) of different maize genotypes

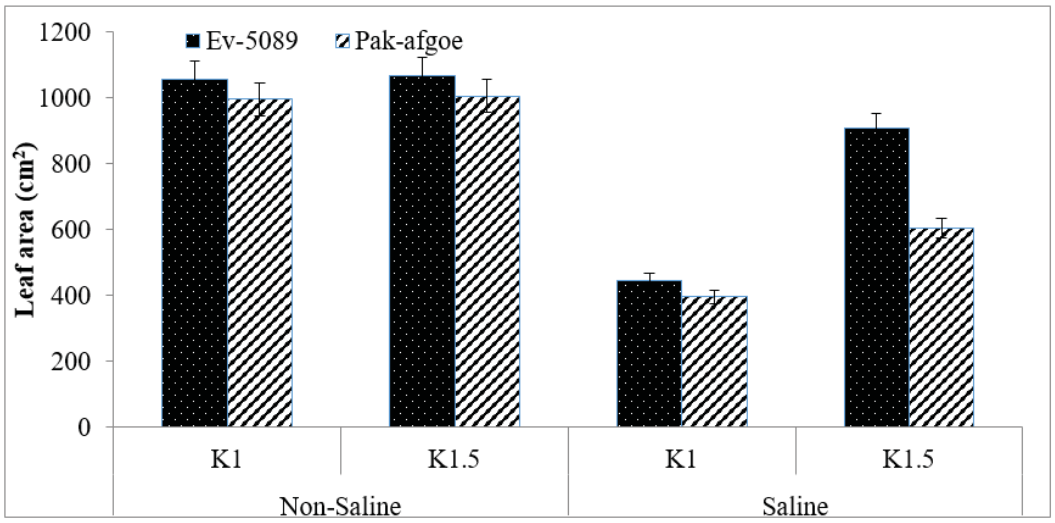

FIGURE 15
Effect of K application on Leaf area of Maize genotypes under non-saline and saline conditions

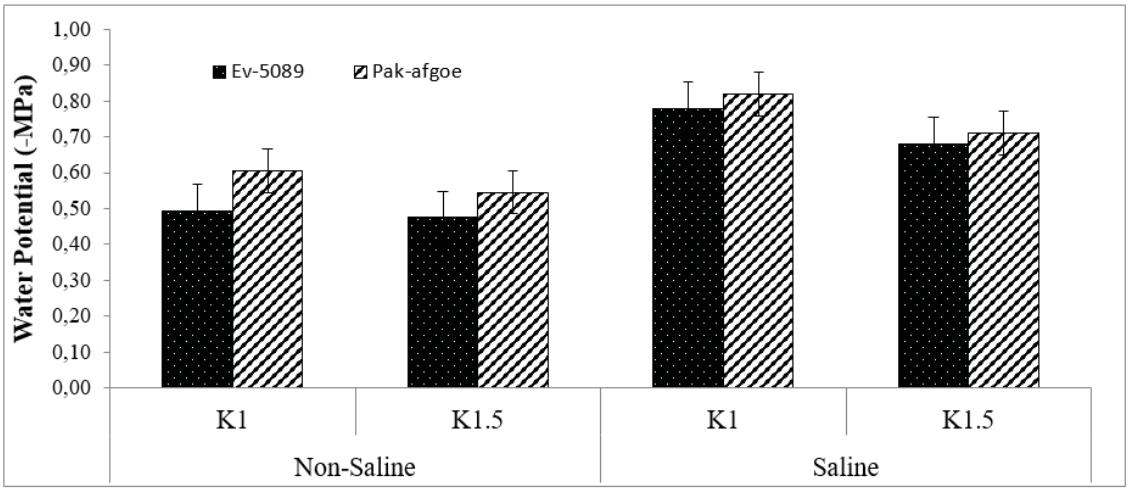

FIGURE 16
Effect of K application on Water potential of Maize genotypes under non-saline and saline conditions

Leaf area. The data regarding leaf area shows that the mean leaf area of the maize genotypes has been decreased significantly under saline conditions while application of potassium reduces the negative effect of salinity (Figure 15). The individual as well as interactive effects of salinity, potassium and genotypes were found significant. The comparison of genotypes showed that with 100 mM NaCl application, Ev-5098 had higher leaf area as compared to Pak-afgoee which is salt sensitive genotype. Under 100 mM NaCl level of salinity, the minimum leaf area was found in Pak-afgoee with low K application in nutrient solution.

Water potential (-MPa). The data regarding water potential show that the mean water potential of the maize genotypes has been decreased significantly under saline conditions while application of potassium minimizes the negative effect of salinity (Figure 16). The individual as well as interactive effects of salinity, potassium and genotypes were found significant. The comparison of genotypes showed that with 100 mM NaCl application, Ev-5098 had higher water potential as compared to Pak-afgoee which is salt sensitive genotype. Under 100 mM NaCl level of salinity, the minimum water potential was found in Pak-afgoee with low K application in nutrient solution.

Photosynthesis Rate (µmol CO_2 m^{-2} s^{-1}). The data regarding photosynthesis rate shows that the photosynthesis rate of the maize genotypes has been decreased significantly under saline conditions while application of potassium decreases the negative effect of salinity (Figure 17). The individual as well as interactive effects of salinity, potassium and genotypes were found significant. The comparison of genotypes under K application of 1.5x showed that with 100 mM NaCl application, Ev-5098 had higher photosynthesis rate as compared to Pak-afgoee which is salt sensitive genotype. Under 100 mM NaCl level of salinity, the minimum photosynthesis rate was found in Pak-afgoee with 1xK application in nutrient solution.

Transpiration Rate (mmol H_2O m^{-2} s^{-1}). The data regarding transpiration rate show that the mean transpiration rate of the maize genotypes has been decreased significantly under saline conditions while application of potassium decreases the negative effect of salinity (Figure 18). The individual as well as interactive effects of salinity, potassium and genotypes were found significant. The comparison of genotypes showed that with 100 mM NaCl application, Ev-5098 had higher transpiration rate as compared to Pak-afgoee. Similar genotypic trend was observed 1x K and 100 mM NaCl application in nutrient solution.

Stomatal conductance (mmol m^{-2} s^{-1}). The data regarding stomatal conductance shows that the mean stomatal conductance of the maize genotypes has been decreased significantly under saline conditions while application of potassium improves their growth under saline conditions (Figure 19). The individual as well as interactive effects of salinity, potassium and genotypes were found significant. The comparison of genotypes showed that under 100 mM NaCl application, Ev-5098 had higher stomatal conductance as compared to Pak-afgoee which is salt sensitive genotype. Similar genotypic trend was observed for stomatal conductance with 1x K and 100 mM NaCl application.

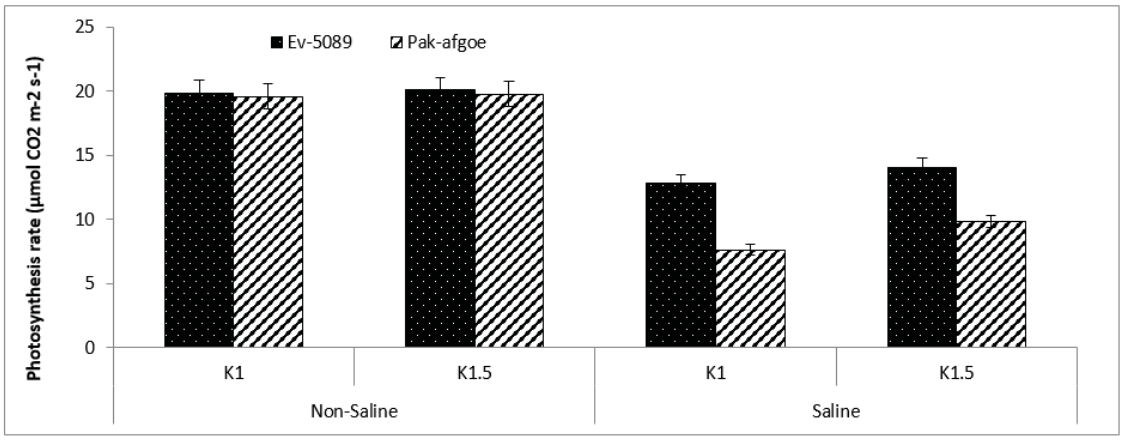

FIGURE 17
Effect of K application on Photosynthesis Rate of Maize genotypes under non-saline and saline conditions

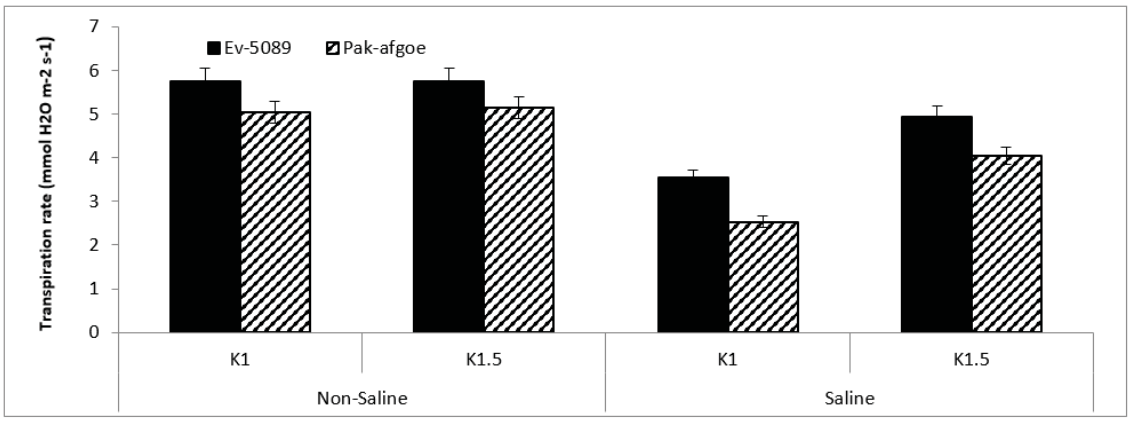

FIGURE 18
Effect of K application on Transpiration Rate of Maize genotypes under non-saline and saline conditions

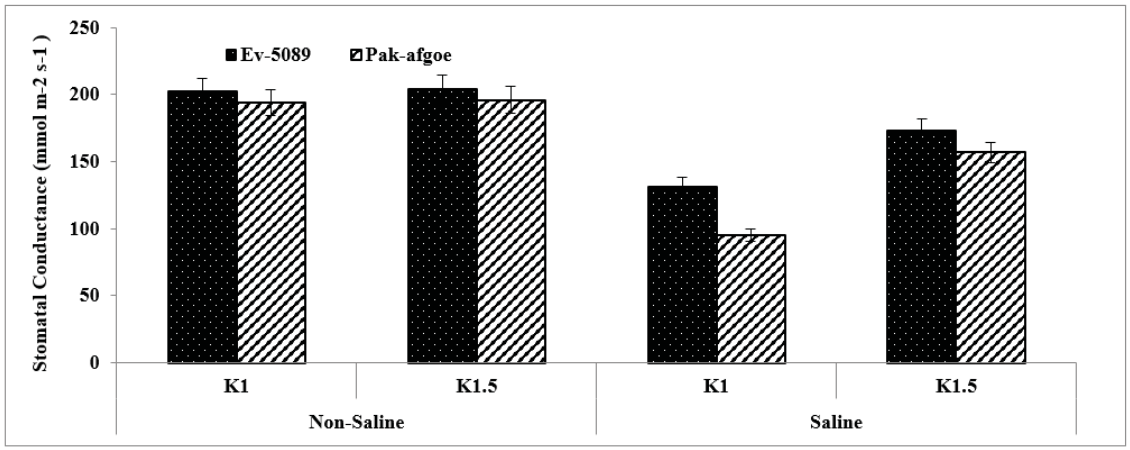

FIGURE 19
Effect of K application on Stomatal conductance of Maize genotypes under non-saline and saline conditions

DISCUSSION

The present study showed that potassium had a significant (P<0.05) role in amelioration of the effect of salinity on maize crop. Salinity reduced the shoot fresh and dry weight, root and shoot length but this reduction was less with the application of potassium fertilizer. Reduction in shoot fresh and dry weight of maize genotypes in the presence of NaCl was attributed to ion toxicity as excess Na^+ resulted in nutritional and metabolic imbalances. [5] reported that higher accumulation of Na^+ damaged plant metabolism and reduced plant growth. The two maize genotypes under study responded to salt stress depending upon their capabilities to selectively uptake K^+ over Na^+. Better growth of salt-tolerant genotype under salt stress was related to its higher accumulation of K+ than salt-sensitive genotype, which is also evident from earlier studies in barley [6, 7]. In another study, [8] confirmed that genotype with lowest Na^+ concentration produced greatest biomass. Application of K significantly reduced the toxic effects of NaCl and improved plant growth in maize hybrids. This was due to antagonistic effect of K^+ with Na^+ [9]. Similarly, enhancement in growth and dry matter yield was reported in rice by the addition of K in saline soil [10]. High Na^+ accumulation in maize genotype Pak-afgoee could be one of the reasons of its sensitivity to NaCl stress while Ev-5098 might be salt tolerant due to low accumulation of Na^+ and high accumulation of K^+ in leaf. The lower uptake of Na^+ in salt tolerant genotype may be related to its selectivity of K^+ over Na^+. Similar, finding was observed by [11] who reported that due to selective absorption and preferential loading of K^+ in xylem, salt tolerant plant accumulated low sodium and high potassium. However, salt tolerant maize genotype showed low affinity for Na^+ over K^+ by maintaining low Na^+/K^+ ratio as compared to salt sensitive.

Zinc is crucial element for optimal flowering, size of fruit and crop production. It is also necessary for all photosynthetic tissues and for chlorophyll biosynthesis [12]. Zinc has countless effect on necessary plant life processes, such as (i) nitrogen metabolism, uptake of nitrogen and protein quality; (ii) photosynthesis-chlorophyll synthesis, carbon anhydrase activity; (iii) resistance to biotic and abiotic stresses by protection against oxidative stress [13]. Crop yields and the quality of crop products are normally damaged when the supply of available zinc for plants is insufficient. In plants, zinc plays an important role as a structural constituent or regulatory cofactor of different enzymes and proteins [14].

In this study the salt sensitive genotype Pak-afgoee showed more negative value of water potential than salt tolerant genotype EV-5098. Salinity lowers the water potential and disturbs the ion distribution [15] and plants adjust their water potential to more negative levels [16]. Similar results were observed by [17] that salt stress lowered the water potential in maize leaves. However, salt tolerant plants have ability to adjust their tissue water potential to a level that is lower than that of water potential of saline medium in which they are growing [18]. Under salinity lower osmotic potential is most depressing effect in plants for nutrient and water uptake. Chlorophyll content in plants has a strong negative correlation with salt stress. The leaf chlorophyll contents, net photosynthetic rate, stomatal conductance and transpiration rate have a strong negative correlation with leaf Na^+ concentration and a strong positive correlation with leaf K^+ concentration. Salinity decreases chlorophyll content and affects the photosynthetic electron transport thus inhibiting the PS-II activity as a result of salt toxicity in chloroplasts [19].

REFERENCES

[1] Ahmed, G.A., Hassanein, M.S. and Gazzar, M.M.E. (2006) Growth and yield response of two wheat cultivars to complete foliar fertilizer compound "Dogoplus". Egypt. J. Appl. Sci. Res. 2, 20-26.

[2] Pettigrew, W.T. (2008) Potassium influences on yield and quality production for maize, wheat, soybean and cotton. Physiol. Plant. 133, 670-681.

[3] Ahmad, A.H.M., Bukhsh, A., Ahmad, R., Iqbal, J., Mudassar, Maqbool, M., Ali, A., Ishaque, M. and Hussain, S. (2012) Nutritional and physiological significance of potassium application in maize hybrid crop production. Pak. J. Nutr. 11, 187-202.

[4] Malik, D.M., Chaudhry, R.A. and Hussan, G. (1989) Crop response to potash application in the Punjab. In: Role of Potassium in improving fertilizer use efficiency. Proceedings of the Workshop on the Role of Potassium in improving fertilizer use efficiency. March 21-22, 1989. National Fertilizer Development Center, Planning and Development Division, Islamabad, Pakistan. 187-190.

[5] Abid, A., Hussain, M., Habib, H.S., Kiani, T.T., Anees, M.A. and Rahman, M.A. (2016) Foliar spray surpasses soil application of potassium for maize production under rainfed conditions. Turk. J. Field Crops. 21, 36-43

[6] Chen, X.Q. and Yu, B.J. (2007) Ionic effects of Na^+ and Cl on photosynthesis in *Glycine max* seedlings under isoosmotic salt stress. J. Plant Physiol. Mol. Biol. 33(4), 294-300.

[7] Lynch, J. and Läuchli, A. 1(984) Salt stress disturbs the calcium nutrition of barley (*Hordeum vulgare* L.). New Phytol. 99, 345-354.

[8] Lee, D.H., Kim, Y.S. and Lee, C.B. (2001) The inductive responses of the antioxidant enzymes by salt stress in the rice (*Oryza sativa* L.). J. Plant Physiol. 158, 737-745.

[9] Liang, Y.C., Sun, W., Zhu, Y.G. and Christie, P. (2007) Mechanism of silicon mediated-mediated alleviation of abiotic stresses in higher plants. A Review. Environ. Pollution. 14(2), 422-428.
[10] Carden, D.E., Walker, D.J., Flowers, T.J. and Miller, A.J. (2003) Single-cell measurements of the contributions of cytosolic Na+ and K+ to salt tolerance. Plant Physiol. 131, 676-683.
[11] Ali, S., Riaz, K.A., Mairaj, G., Arif, M., Fida, M. and Bibi, S. (2008) Assessment of different crop nutrient management practices for yield improvement. Aust. J. Crop Sci. 2(3), 150-157.
[12] Bayuelo-Jimenez, J.S., Craig R. and Lynch J.P. (2002) Salinity tolerance of *Phaseolus* species during germination and early seedling growth. Crop Sci. 42, 1584-1594.
[13] Crosbie, T.M. and Pearce RB (1982) Effects of recurrent phenotypic selection for high and low photosynthesis on agronomic traits in two maize populations. Crop Sci. 22, 809-813.
[14] Flowers, TJ (2004) Recent advances in genetics of salt tolerance in tomato. Plant Cell, Tissue Organ Cult.76, 101-119.
[15] Alloway, B.J. (2008) Zinc in soils and plant nutrition. Brussels, Belgium and Paris, France: IZA and IFA. 139-143.
[16] Rontein, G.B. and Hanson, A.D. (2002) Metabolic engineering of osmoprotectant accumulation in plants. Metab. Eng. 4, 49-56.
[17] Koyro, H.W. (2006) Effect of salinity on growth, photosynthesis, water relations and solute composition of the potential cash crop halophyte *Plantago coronopus* (L.) Env. Exp. Bot. 56, 136-146.
[18] Munns, R. (2005) Genes and salt tolerance: bringing them together. New Phytol. 167, 645-663.
[19] Sudhir, P. and Murthy, S.D.S. (2004) Effects of salt stress on basic processes of photosynthesis. Photosyn. 42, 481-486.

Received: **06.11.2019**
Accepted: **28.01.2020**

CORRESPONDING AUTHOR

Munaza Batool
Soil Science Laboratory
Ghazi University
Dera Ghazi Khan Punjab – Pakistan

e-mail: mbatool@gudgk.edu.pk

© by PSP Volume 29 – No. 05/2020 pages 3790-3797 Fresenius Environmental Bulletin

EXPERIMENTAL STUDY ON ADVANCED PURIFICATION TECHNOLOGY OF POLYMER-CONTAINING WASTEWATER FROM OILFIELD

Chenglong Shu[1,3,*], Longfei Guo[2], Dong Hao[1], Yongzong Li[2], Yuru Jiang[4]

[1]No.7 Oil Production Plant, Changqing Oilfield Company, PetroChina, Xi'an, Shaanxi 710200, P.R. China
[2]No.8 Oil Production Plant, Changqing Oilfield Company, PetroChina, Xi'an, Shaanxi 710021, P.R. China
[3]Department of Geology, Northwest University, Xi'an, Shaanxi 710069, P.R. China
[4]No.11 Oil Production Plant, Changqing Oilfield Company, PetroChina, Xi'an, Shaanxi 710200, P.R. China

ABSTRACT

The reuse and high viscosity loss rate of polymer-containing wastewater are the key issues to be solved urgently during the development of oil and gas fields. In this study, polysilicon aluminum flocculant (PSiAF) was synthesized in laboratory to investigated the advanced purification of polymer-containing wastewater, and its purification performance and viscosity stability were tested. The main factors affecting polymer solution viscosity, such as pH, ion concentration, salt and suspended solids, were analyzed. In addition, the scaling trend of purified water under stratigraphic conditions was simulated by Oil Scalechem prediction software. The results indicated that the effect of Fe^{2+}, Ca^{2+}, Mg^{2+}, S^{2-} and suspended solids content in solution on the viscosity of the polymer solution was greater than that of the others, and it must be controlled in preparing polymer solution. The optimal dosing formula of the flocculant with the performance of removal of turbidity and calcium was as follows, 50 mg/L polymerized ferrous sulfate (PFS) + 200 mg/L PSiAF + 8 mg/L setting agent. The content of Ca^{2+}, Mg^{2+} and residual polymer of the purified water, obtained by deepened processing with the flocculant, decreased sharply, and the oil content and suspended solid content was lower, moreover, the purified water hardly contained Fe^{2+}. The average particle size of suspended particles（SS）in purified water was less than 100 nm, which was smaller than the pore diameter or the cores, so formation could not be blocked by SS. As a result, the purified water could be reused for preparing the polymer flooding solution.

KEYWORDS:
Polymer flooding, polysilicon aluminum flocculant, stratigraphic conditions, polymerized ferrous sulfate, suspended particles, setting agent

INTRODUCTION

Polymer-containing wastewater is a new type of oily, suspended solids wastewater system with complex composition and stable water quality[1]. It mainly has the following characteristics: high salinity, large suspended solids, oil content, high polymer concentration, high viscosity, no significant changes in long-term placement[2,3]. The application of polymer oil recovery technology can significantly improve oil recovery. The relevant test results showed that the polymer flooding technology can increase the crude oil production by 11 times and reduce the water content of the crude oil. Moreover, the technology is suitable for many different oil fields at home and abroad, such as Daqing Oilfield and Shengli Oilfield in China, 183 polymer flooding fields in America, Alran oilfield in the former Soviet Union and Horsefly Lake oilfield in Canada, etc [4-7].

However, the widespread use of polymer flooding technology also brings several serious problems[8-11]. If the polymer sewage is not recycled, the water consumption is very large, at the same time, the discharged polymer sewage will cause some serious environmental pollution. Polymer-containing wastewater has the characteristics of polymer content, oil content and suspended matter content exceeding the standard, serious emulsification, small oil drop and stable emulsion. At the same time, a large amount of water is needed to prepare polymer solution. How to use polymer flooding produced water to prepare polymer solution has become a key technical problem to be solved in tertiary oil recovery[12,13]. On the one hand, the fresh water resources used to prepare polymer solution are becoming increasingly scarce, and the problem of "man well competing for water" is more prominent. On the other hand, with the implementation of the new environmental protection law, the pressure of the third production sewage discharged to the standard is increasing, and the treatment of a large number of polymer flooding produced water has become an urgent problem to be solved in the oilfield. If polymer solution can be

prepared from polymer flooding produced water, water resources can be saved, environmental pollution can be reduced and economic benefits can be improved. However, due to the complex oil-water system formed in the polymer flooding process, and a large number of minerals exist in the sewage in different forms, the viscosity of polymer solution prepared by sewage is often much lower than that prepared by clean water[14].

In order to solve these problems, it is necessary to find out the main control factors that affect the viscosity of polymer solution in sewage, and then carry out research on reduction measures for various influencing factors, so as to finally form a relatively economic and effective polymer flooding development matching sewage preparation flooding polymer solution technology. In this study, an innovative treatment agent, polysilicon aluminum flocculant, was synthesized in laboratory to investigated the advanced purification of polymer-containing wastewater, and its purification performance and viscosity stability were evaluated. The main factors affecting polymer solution viscosity were analyzed. Aeration pretreatment and road agent system screening experiments were carried out combined with polymer flooding wastewater treatment process. In addition, viscosity retention agent is added to the treated water to improve the viscosity retention rate of polymer solution prepared for wastewater.

MATERIALS AND METHODS

Materials. Hydrolyzed polyacrylamide (HPAM) with DH of 24%, provided by Beijing Hengju oilfield chemical agent company. Ferric chloride, ferrous chloride, sodium sulfide, calcium chloride, potassium sulfate, magnesium chloride, thiosulfuric acid Sodium, hydrochloric acid, sodium hydroxide, sulfuric acid, $Na_2SiO_3 \cdot 9H_2O$ and $Al_2(SO_4)_3 \cdot 18H_2O$ were all purchased from Shanghai Aladdin Biochemical Technology Co., Ltd. The viscosity retention agent PA was composed of sodium thiosulfate, sodium polyaspartic acid and sodium fumarate in a certain proportion, which has the functions of deoxidization and complexation of calcium and magnesium. PFS and setting agent were supplied by Gongyi Huakang water treatment materials Co., Ltd. The water sample was oil recovery wastewater from polymer flooding.

Apparatus. The rheometer Rs-600 was purchased from HaakeTechnik GmbH Co., Ltd., Germany. ScaleChem scale prediction software was supplied by USA OIL Co., Ltd., USA. The dynamic laser particle sizer Nano ZS was produced by Malvern instruments Co., Ltd., UK. High performance liquid chromatography waters 2695 was supplied by Watson Technology Co., Ltd., USA. Plasma emission spectrometer OPTIMA 5300DV (ICP) was purchased from PerkinElmer instruments Co., Ltd., USA.

Experiment procedure. Prior to the experiment, take some water and add into a certain amount of $Na_2SiO_3 \cdot 9H_2O$, and the appropriate reaction temperature needs to control in this period[15,16]. Adjust the pH value with sulfuric acid, and prepare the polysilicate solution after aging. Then add in a certain amount of $Al_2(SO_4)_3 \cdot 18H_2O$ and concentrated sulfuric acid to obtain the low viscosity polysilicate solution. Drop the prepared polysilicate into the prepared polysilicate three times in the aluminum solution, the pH value is adjusted to about 2.0 with concentrated sulfuric acid after each drop. The reaction is heated and stirred for a period of time. After standing, the polysilicate is added continuously. After all drops are added, the product is aged for a period of time. The white flocculant PSiAF is obtained after drying. The water purification performance of the synthesized product has no obvious change after 3 months, which can meet the requirements of industrial production.

Take some polymer-containing wastewater from the settling tank, and add into a certain amount of $FeCl_2$ solution to adjust the pH value to 7. Then aerate a certain time at the gas flow rate of 2 L/min. The flocculant, coagulant aid and sedimentation aid of the set concentration were successively add into the aerated wastewater, stir and stand, take the supernatant to measure the turbidity, so as to evaluate the treated water quality[17].

The apparent viscosity of the system was measured by rheometer Rs-600 at 34 °C and 10 S^{-1} shear rate[18]. The polymer content in wastewater was measured by HPLC and detected by UV detector. The silicon content in the system was measured by ICP with standard curve method.

RESULTS AND DISCUSSION

Analysis of sewage quality before treatment. The polymer-containing wastewater was sampled from the demulsification system of polymer flooding produced liquid. The water type is weak alkaline water of sodium bicarbonate type, and Table 1 lists the results of water quality analysis. The content of inorganic matter in the effluent from polymer flooding is relatively stable, containing a certain amount of divalent iron and no sulfide. The polymer content in the incoming liquid varies with the recovery degree. In the peak period of increasing oil, the content is between 400 to 500 mg/L. it can be seen by naked eyes that there are relatively stable colloidal particles in the water.

TABLE 1
The analysis results of wastewater containing polymer quality

Parameter	Value	Parameter	Value
Si/(mg·L^{-1})	1.22	oil/(mg·L^{-1})	358.5
Ca^{2+}、Mg^{2+}/(mg·L^{-1})	104.73	Suspended solids/(mg·L^{-1})	224.5
Fe^{2+}/(mg·L^{-1})	0.1	polymer/(mg·L^{-1})	500.0
Fe/(mg·L^{-1})	0.1	Zeta potential/mV	-32.5
Dissolved oxygen/(mg·L^{-1})	0.01	Median particle size/μm	5.97
S^{2-}/(mg·L^{-1})	7.17	PH	7.51
Volatile Phenol/(mg·L^{-1})	0.29	Water type	$NaHCO_3$

PH, inorganic cation and anion. The initial viscosity of polymer solution (polymer concentration 1500 mg/L, temperature 25 °C) with different pH and inorganic cations and anions is shown in Figure 1. It can be seen that the viscosity of polymer solution is the highest when the pH value is 9, and the reasonable pH value should be controlled between 7 and 9, while the pH value of the water from the treatment station is just within this range, so it is unnecessary to adjust the pH value of the water. No matter what kind of inorganic ions, they can reduce the viscosity of polymer solution. The content of Ca^{2+} and Mg^{2+} has a great influence on the viscosity of polymer solution. The content of Ca^{2+} and Mg^{2+} should be strictly controlled below 100 mg / L when sewage is used to prepare polymer solution. The existence of a small amount of Fe^{2+} will cause a significant decrease in the viscosity of polymer solution[19]. When the content of Fe^{2+} is greater than 4 mg/L, the loss rate of solution viscosity is 83%. Therefore, it is better not to contain Fe^{2+} in the waste water for preparing polymer solution[20]. In addition, in order to prevent other reducing ions in the water from reducing Fe^{3+} to Fe^{2+}, Fe^{3+} in the waste water needs to be strictly controlled below 3 mg/L. The effect of S^{2-} on the viscosity of polymer is similar to a straight line with a negative slope. When the mass concentration of S^{2-} is 25 mg/L, the viscosity loss of polymer solution is 33%. S^{2-} is removed by aeration or air flotation.

Dissolved oxygen. Take simulated water from sewage treatment station, apply nitrogen for 10 min, and prepare deaeration water. The polymer solution with mass fraction of 0.1% was prepared with deaerated and non deaerated simulated water respectively. The solution prepared with deaerated water was added with nitrogen for another 10 minutes to drive away a small amount of oxygen brought in during the dissolution process. The effect of dissolved oxygen content on the viscosity of polymer

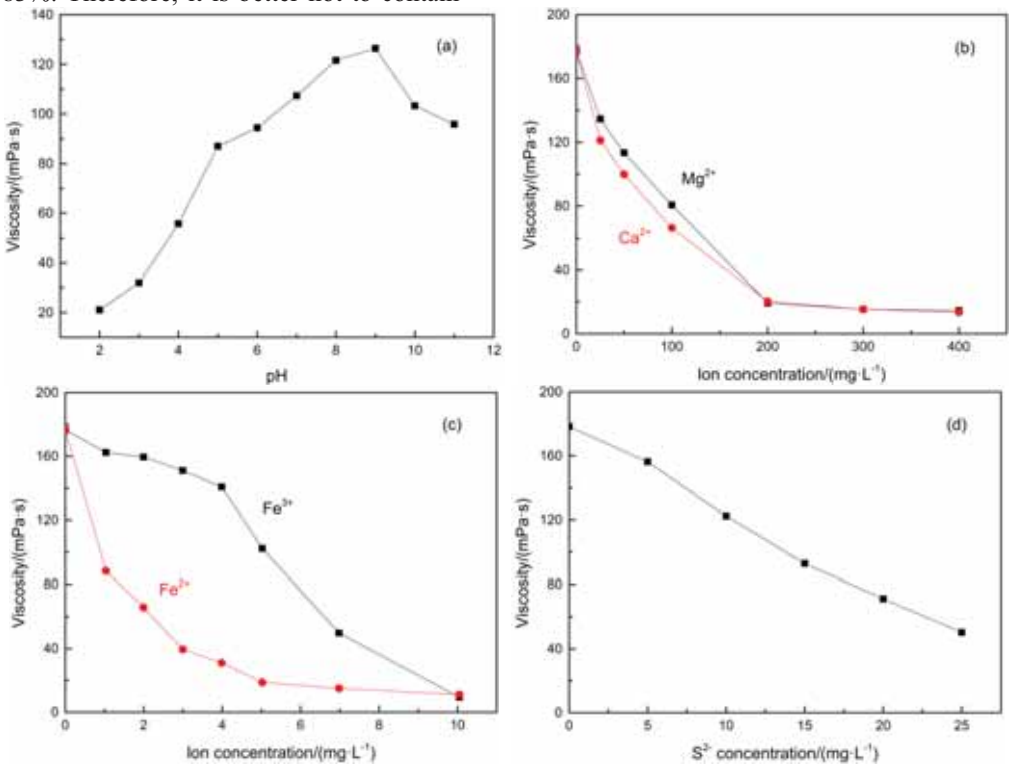

FIGURE 1
Effect of pH, inorganic cation and anion concentration on viscosity of polymer solution

TABLE 2
Effect of dissolved oxygen on viscosity of polymer solution

Placement time/d		7	30	60	90
Solution viscosity /(mPa·s)	Prepared with deaerated water	16.25	15.73	15.04	14.87
	Prepared with non-deaerated water	15.62	15.06	14.12	13.28

solution is shown in Table 2. It can be seen that the initial viscosity of the polymer solution prepared with deaerated water is 4.0% higher than that of the solution without deaeration (dissolved oxygen content 0.1 mg/L), and the viscosity of both solutions decreases with time. This may be related to the introduction of oxygen or other unknown factors in the solution[21,22]. However, after 90 days,the viscosity of the solution prepared with deaerated water is 12.0% higher than that of the solution prepared without deaerated water, which indicates that dissolved oxygen participates in the degradation of polymer. Considering that dissolved oxygen can promote the free radical reaction of Fe^{2+}, S^{2-}, the content of dissolved oxygen in water must be strictly controlled when polymer solution is prepared with sewage[23].

Suspended matter content. Polymer-containing wastewater contains residual polymer, which is wrapped with other suspended solids to form stable colloidal particles. Dilute the effluent from the settling tank of polymer flooding sewage station with simulated water to obtain the polymer containing sewage with different turbidity, filter it with coarse filter paper to remove mechanical impurities, prepare 0.1% polymer solution, and investigate the effect of polymer containing suspension on the viscosity of polymer solution. It can be seen from Table 3 that for polymer flooding produced water with different turbidity, the higher suspended matter content (turbidity greater than 20ntu) has a negative impact on the viscosity of polymer solution, resulting in a significant reduction in viscosity. When the content of suspended solids is high, due to the adsorption loss on the solid surface, polymer molecules flocculate and settle, resulting in the decrease of solution viscosity. On the other hand, under the condition of water invasion, the hydroxyl group is connected with the carboxyl group of HPAM by hydrogen bond or the amide group of HPAM by hydrogen bond, which leads to the adsorption of HPAM molecules on the surface of clay minerals and the loss of viscosity of polymer solution[24]. Therefore, when polymer solution is prepared with polymer flooding wastewater, the suspended solids must be removed.

Advanced purification of wastewater - containing polymer. In order to eliminate the disadvantageous factors to the viscosity of polymer solution in sewage effectively, polysilicate aluminum flocculant with strong turbidity reduction ability was synthesized according to the water quality characteristics of polymer flooding sewage, and the process parameters of deepening treatment were further optimized.

Aeration pretreatment. Aeration can eliminate reducing ions in water and degrade residual polymer molecules. Take the water from polymer flooding sewage treatment station, add 0.2% Fe^{2+}, adjust the pH value to 7 with hydrochloric acid, initiate oxidation-reduction reaction, accelerate the degradation of residual polymer in sewage, and form iron-containing flocculant under the action of oxygen, which plays the role of preliminary flocculation and turbidity reduction. At room temperature, the gas flow rate was controlled to 2 L/min and 3 L/min respectively. The effect of aeration time on flocculation was investigated. The flocculant formula is: 300 mg/L PSiAF + 2 mg/L settling aid, and the experimental results are shown in Table 4. We can that under the set gas flow rate, it is appropriate to control the aeration time at 4 numbers and 6 minutes. The aeration time is too short, the reaction is not complete, and it is not easy to flocculate into larger particles; the aeration time is too long, and the dissolved gas in the solution is too much, which adsorbs on the external surface of the flocs, affecting the flocs sinking. The gas flow rate has little

TABLE 3
Effect of suspended solids content in wastewater on viscosity of polymer solution

Dilution factor	0	1	2	3	4
Turbidity /NTU	123.5	50.1	30.5	20.3	10.2
Polymer concentration (/ mg·L^{-1})	465.7	230.4	143.4	109.5	80.7
Viscosity (/mPa·s)	10.62	12.10	13.98	14.33	16.62

TABLE 4
Effect of aeration time on water purification

Aeration time /min		2	4	6	8
Turbidity /NTU	Flow rate 2L/min	8.2	3.5	3.2	5.0
	Flow rate 3L/min	7.8	3.1	3.6	4.8

effect on the flocculation effect. It may be that the gas provided at low flow rate is enough for polymer oxidation reaction, so the gas flow rate was set as 2 L/min.

Drug formula screening. The aerated water samples were divided into four groups, each group was 200 mL, the stirring speed was 250 r/min, 50 mg/L coagulant aid PFS was added, then different doses of flocculant psias-1 were added, the interval was 1 min, then 8 mg/L precipitant aid was added, the interval was 30 s. After that, stir for 1 min at the speed of 60 r/min, and leave for 10 min. observe the effect of different flocculants on the water purification effect, and determine the turbidity of the supernatant. It can be seen from Table 5 that when the dosing concentration of the flocculant psias-1 is 200 mg/L, the turbidity decreases from 15.6 NTU to 2.8 NTU, and the supernatant is clear. When the dosage of the flocculant continues to increase, the decrease of turbidity is not obvious, so the best dosage of the flocculant PSiAF is determined as 200 mg/L.

Dosage of coagulant aid. The water samples were divided into five groups. According to the above methods and the optimized conditions of screening, the addition amount of fixed flocculant PSiAF was 200 mg/L, and a certain amount of coagulant aid PFS was added to observe the effect of different concentrations of coagulant aid on water purification, and the turbidity of supernatant was measured. The experimental results are shown in Table 6, and It can be seen that within the range of 0 number of 150 mg/L, the effect of coagulant aids on turbidity is not great, but when no coagulant aids are added, due to the acidity of polysilicate aluminum flocculant, the flocs will float up; once the coagulant aids are added, even if the content is only 50 mg/L, the flocs will also float up to sink. In order to effectively control the settlement of floc and facilitate sludge discharge, the best dosage of coagulant aid is 50mg/L.

Through optimizing the purification process, the best flocculant formula was selected as follows: 50 mg/L PFS + 200 mg/L PSiAF + 8 mg/L sedimentation aid.

Water quality after further treatment. The water quality of Polymer-containing wastewater after further treatment has changed a lot compared with that before treatment, see Table 7 for details. It can be seen from that after the deepening treatment, the content of Ca^{2+}, Mg^{2+} and residual polymer in the water is greatly reduced, free of reductive ferrous ion and sulfide, and the oil content and suspended matter content are low. The zeta potential of treated water increased and the median particle size decreased, indicating that the colloid has been destabilized and the water type has not changed. However, in order to improve the viscosity retention of polymer, it is necessary to add deoxidizer to reduce the dissolved oxygen content in water.

Prediction of scale formation and particle size of aggregates in sewage treatment. Use the scaling simulation software to simulate the purified polymer flooding sewage under the formation conditions (temperature 25 °C number 40 °C, pressure 10 number 12 MPa), and the results can be see in Figure 2. The particle size distribution of the aggregate in the purified water (added with 20 mg/L PA) was measured on the laser particle size analyzer, and the results are shown in Figure 3 (three parallel measurements). According to the scaling simulation, there is a certain scaling trend of calcium carbonate in the injected water under the formation conditions, but the absolute amount of calcium carbonate is not large. Under the pressure of 12 MPa, the precipitation of 11 water is less than 6 mg, which is similar to the scaling trend of heavy oil sewage with good water quality. After adding polysilicon flocculant, there is a certain amount of SiO_2 in the water body, but its scale amount and scale tendency are far from saturated state, so it will not precipitate out of the water. In addition, because the scaling software can only simulate the conventional ions in water, it can be confirmed by measuring the particle size of particles by laser particle sizer when adding special agent system. It can be seen that the average particle size of calcium carbonate produced in the water body is less than 100 nm after the polymer flooding purified water is added with viscosity retention agent, which is a solid particle of nanometer scale, and its diameter is far smaller than the average pore roar radius of the reservoir, which is not enough to cause formation plugging.

TABLE 5
Effect of flocculant addition on water purification

PsiAF dose(/mg·L^{-1})	Floc size	Settling velocity	Suspension floc content	Supernatan	Supernatant turbidity/NTU
100	smaller, loose	slower	more	gray	15.6
150	large, dense	fast	less	clear	3.4
200	large, more dense	faster	less	clear	2.8
250	large, more dense	faster	less	clear	3.8

TABLE 6
Effect of coagulant addition on water purification

PsiAF dose(/mg·L^{-1})	Floc situation	Settling velocity	Suspension floc content	Supernatan	Supernatant turbidity/NTU
0	floating	slow floating	less	clear	10.3
25	sinking	slow	less	clear	5.0
50	sinking	fast	less	clear	2.8
100	sinking	fast	less	clear	5.4
150	sinking	fast	less	clear	8.5

TABLE 7
The analysis results of wastewater after advanced purification

Parameter	Value	Parameter	Value
Si/(mg·L^{-1})	14.68	oil/(mg·L^{-1})	3.2
Ca^{2+}、Mg^{2+}/(mg·L^{-1})	35.32	Suspended solids/(mg·L^{-1})	2.5
Fe^{2+}/(mg·L^{-1})	0	polymer/(mg·L^{-1})	3.6
Fe/(mg·L^{-1})	0	Zeta potential/mV	-15.4
Dissolved oxygen/(mg·L^{-1})	0.1	Median particle size/μm	1.34
S^{2-}/(mg·L^{-1})	0	PH	8.21
Volatile Phenol/(mg·L^{-1})	0	Water type	$NaHCO_3$

TABLE 8
The viscosity variation of the polymer solution prepared by advanced purification of wastewater with placement time

Dosing water	Viscosity after placement at different times (/mPa·s)			Relative viscosity/%
	Initial value	30 d	60 d	
Polymer flooding simulated sewage	15.62	15.06	12.21	21.8
Polymer flooding purification of sewage	17.16	16.04	13.30	14.8

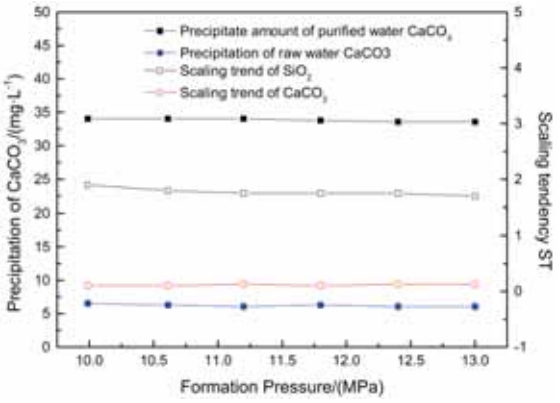

FIGURE 2
Simulation of scaling trend of polymer flooding purified water

Viscosity change of polymer solution prepared by polymer flooding purified sewage. Table 8 gives the initial viscosity and viscosity stability of HPAM solution (containing 20 mg/L viscosity maintaining agent PA) with mass fraction of 0.1% prepared by polymer flooding simulated sewage and polymer flooding purified sewage respectively. Relative viscosity loss is defined as the ratio (%) of the difference between viscosity and initial viscosity of polymer solution after 90 days. It can be seen from Table 8 that the initial viscosity of polymer solution prepared by polymer flooding simulated sewage is 15.62 MPa·s, while the viscosity of polymer solution prepared by deep purified water (including viscosity retention agent) reaches 17.16 MPa·s, which is increased by more than 9%. Through deep purification, reducing ions and residual polymers in solution are removed, turbidity of water for solution preparation is reduced, and long-term viscosity stability is obtained to improve, when 20 mg/L of viscosity retention agent is added to the solution, the dissolved oxygen in the solution is effectively reduced, and the relative viscosity loss of the solution after 90 days is less than 15%, which meets the requirements of sewage preparation of polymer solution.

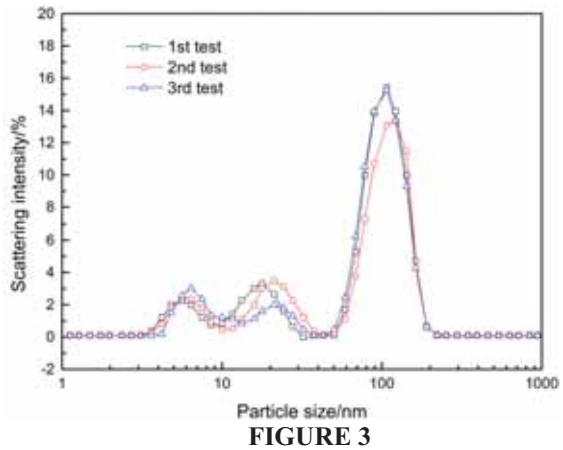

FIGURE 3
Particle size of polymer flooding purified water

CONCLUSIONS

In this study, the advanced purification technology of polymer-containing wastewater was investigated by experiment and numerical simulation. The main factors affecting polymer solution viscosity, as PH, inorganic cation and anion, dissolved oxygen and suspended matter content, were all analyzed and discussed. Moreover, the optimal dosing formula of the flocculant with the performance of removal of turbidity and calcium was obtained. The main conclusions are as follows: (1) Fe^{2+}, Ca^{2+}, Mg^{2+}, reducing substances and dissolved oxygen in polymer-containing wastewater have great viscosity loss to the solution, and the initial viscosity of the solution will be greatly reduced when the salinity exceeds 4000 mg/L. (2) The synthesized PSiAF is suitable for the advanced treatment of wastewater containing polymer with low dosage and good effect of turbidity removal and calcium reduction. After the treatment with 50 mg/L PFS + 200 mg/L PSiAF + 8 mg/L precipitant aid, the tendency of carbonate scale scaling is small, and the particle size of solid particles is far smaller than the formation pore roar radius, which can meet the requirements of polymer flooding sewage depth purification. (3) The initial viscosity of the polymer solution prepared by the advanced purification of polymer-containing wastewater is higher, and the viscosity loss in three months is less than 15%, which meets the requirements of the preparation of polymer solution by sewage.

ACKNOWLEDGEMENTS

This work was not funded by any funds.

REFERENCES

[1] Li, J., Xiong, Y., Wang, X.J. (2019) Synthesis and flocculation of a novel flocculant for treating wastewater produced from polymer flooding. Environmental Technology. 3, 1-29.

[2] Wang, B.H., Chen, Y., Liu, S.Zi. (2006) Photo catalytical visbreaking of wastewater produced from polymer flooding in oilfields. Colloids and Surfaces A, Physicochemical and Engineering Aspects. 287(1-3), 170-174.

[3] Yuan, S.L., Xu, G.Y., Cai, Z.T., Jiang, Y.S. (2003) Molecular simulation studies on the interaction between different polymers in aqueous solution. Colloid and Polymer Science. 281(1), 1-6.

[4] Fu, F.L., Xie, L.P., Tang, B. (2012) Application of a novel strategy-advanced fenton-chemical precipitation to the treatment of strong stability chelated heavy metal containing wastewater. Chemical Engineering Journal. 189-190, 283-287.

[5] Xie, L.P., Fu, F.L., Tang, B. (2012) Removal of chromium from CrEDTA synthetic wastewater using advanced fenton-hydroxide precipitation process. Advanced Materials Research. 550-553, 2005-2008.

[6] Mahran, D., Eliyahu, S., Abraham, J.D. (2019) Enhanced flocculation activity of polyacrylamide-based flocculant for purification of industrial wastewater. Polymers for Advanced Technologies. 22(16), 88-96.

[7] Meeussen, J.C.L., Keizer, M.G., Riemsdijk, W.H.V. (1992) Dissolution behavior of iron cyanide (Prussian Blue) in contaminated soils. Environmental Science and Technology. 26(9), 1832-1838.

[8] Dalton, C.C., Iqbal, K., Turner, D.A. (2002) Iron phosphate precipitation in Murashige and Skoog media. Physiologia Plantarum. 57(4), 472-476.

[9] Klas, S.Y., Dubowski, O. (2011) LahavChemical stability and extent of isomorphous substitution in ferrites precipitated under ambient temperatures. J. Hazard. Mater. 193, 59-63.

[10] Alexandra, W., Ana, M., Ferraria, A.M.B., Do, R. (2019) Purification of monoclonal antibodies in a stirred cell with polyethyleneimine odified polyethersulfone ultrafiltration membrane. Journal of Chemical Technology and Biotechnology. 8(32), 12-16.

[11] Misra, R.K., Jain, S.K., Khatri, P.K. (2011) Iminodiacetic acid functionalized cation exchange resin for adsorptive removal of Cr(VI), Cd(II), Ni(II) and Pb(II) from their aqueous solutions. J. Hazard. Mater. 185, 1508-1512.

[12] Barakat, M.A., Schmidt, E. (2010) Polymer-enhanced ultrafiltration process for heavy metals removal from industrial wastewater. Desalination. 256, 90-93.

[13] Nowack, B. (2002) Environmental chemistry of aminopoly carboxylate chelating agents. Environ. Sci. Technol. 36, 4009-4016.

[14] Englehardt, J.D., Meeroff, D.E., Echegoyen, L., Deng, Y., Raymo, F.M., Shibata, T. (2007) Oxidation of aqueous EDTA and associated organics and coprecipitation of inorganics by ambient iron-mediated aeration. Environ. Sci. Technol. 41, 270-276.

[15] Fu, F.L., Wang, Q., Tang, B. (2010) Effective degradation of C.I. Acid Red 73 by advanced Fenton process. J. Hazard. Mater., 174, 17-22.

[16] Sthiannopkao, S., Sreesai, S. (2009) Utilization of pulp and paper industrial wastes to remove heavy metals from metal finishing wastewater. J. Environ. Manage. 90, 3283-3289.
[17] Kurenkov, V.F., Hartan, H.G., Lobanov, F.I. (2002) Degradation of Polyacrylamide and Its Derivatives in Aqueous Solutions. Russian Journal of Applied Chemistry. 75(7), 66-72.
[18] Rachid, E.M., Frigon, J.C., Hawari, J., Marroni, D., Serge, R.G. (2002) Combining photolysis and bioprocesses for mineralization of high molecular weight polyacrylamides. Biodegradation. 13(4), 102-108.
[19] Zhao, Z., Liu, Z., Wang, H. (2018) Sequential application of Fenton and ozone-based oxidation process for the abatement of Ni-EDTA containing nickel plating effluents. Chemosphere. 2002, 238-245.
[20] Shokrollahzadeh, S., Azizmohseni, F., Golmohammad, F. (2008) Biodegradation potential and bacterial diversity of a petrochemical wastewater treatment plant in Iran. Bioresource Technology. 99(14), 6127-6133.
[21] Wang, T., Wang, Q., Soklun, H. (2019) A green strategy for simultaneous Cu(II)-EDTA decomplexation and Cu precipitation from water by bicarbonate-activated hydrogen peroxide/chemical precipitation. Chemical Engineering Journal. 370, 1298-1309.
[22] Rao, N., Rao, H., Granville, M., Christine, I. B. (2016) Determining how polymer-bubble interactions impact algal separation using the novel posi-dissolved air flotation process. Separation and Purification Technology. 201, 1011-1026.
[23] Zhu, F., Shi, C.M., Cheng, C. (2013) Flocculation performance of trimethoxysilane modified polymer flocculant for wastewater from effluent A/O bioreactor. Advanced Materials Research. 634-638, 330-333.
[24] Gao, B., Jia, Y., Zhang, Y. (2011) Performance of dithiocarbamate-type flocculant in treating simulated polymer flooding produced water. Journal of Environmental Sciences. 23(1), 37-43.

Received: **11.11.2019**
Accepted: **14.01.2020**

CORRESPONDING AUTHOR

Chenglong Shu
Department of Geology,
Northwest University,
Shaanxi 710069 – China

e-mail: haojie93@126.com

© by PSP Volume 29 – No. 05/2020 pages 3798-3803 Fresenius Environmental Bulletin

PREPARING AND OPTIMIZING A NEWLY AFFINITY GEL FOR PURIFICATION OF CARBONIC ANHYDRASE ISOENZYMES

Serap Beyaztas Uzunoglu[1,*], Yildiz Yalcin[1], Tayfun Uzunoglu[2], Seref Karadeniz[3], Habibe Kurt[1]

[1]Department of Molecular Biology and Genetics, Science and Art Faculty, Balikesir University, Balikesir, Turkey
[2]Department of Physics, Science and Art Faculty, Balikesir University, Balikesir, Turkey
[3]Scientific and Technological Application and Research Center, Duzce University, Duzce, Turkey

ABSTRACT

Human carbonic anhydrase isozymes have been purified from the hemolysate, directly by using the original affinity gel in chemical structure of Sepharose 4B-L-tyrosine- sulfathiazole. Different solution buffers were used for obtaining the purified CA isozymes from the affinity column. Most suitable elution buffers were determined for CA I and CA II isoenzymes pH 6.3, 25 mM Na_2HPO_4/1.0 M NaCl and pH 5.6, 0.1 M $NaCH_3COO$ / 0.5 M $NaClO_4$ respectively. The purification values for CA I and CA II have been obtained as 635.71 and 666.71 folds with 28.41% and 46.19% yield respectively. The ionic strength and optimum pH values of the original affinity gel have been determined for each isozyme of CA. Maximum binding was achieved 0.3 ionic strength and pH 8.7 for both CA I and CA II. The single bands was indicated for each isoenzymes by SDS-polyacrylamide gel electrophoresis.

KEYWORDS:
Carbonic anhydrase, isozymes, affinity gel, affinity chromatography, purification.

INTRODUCTION

The carbonic anhydrase (CA, EC 4.2.1.1) contains a zinc ion which is important for catalysis. CAs catalyse the conversion of CO_2 to the bicarbonate ion and protons. The CA reaction is included in many physiological and pathological processes, including respiration, pH and CO_2 homeostasis, electrolyte secretion, gluconeogenesis, lipogenesis and ureagenesis; bone resorption; calcification; and tumorigenicity [1- 3]. Sixteen isozymes have been characterized up to now in mammals [1,2]. Carbonic anhydrase isoenzymes are sensitive to sulphonamides with different IC_{50} and Ki values. For example, CA II is more sensitive to sulphonamides than CA I [4]. Mammalian blood is cheapest and most speedily available from number of sources for CA isoenzymes [4-8]. Several purification methods known in the literature for CA isoenzymes [9-14].

Affinity chromatography is potent and practicable means of purifying proteins. [15] Affinity chromatography is a widely used method for CA isoenzymes with high yield and purification fold of the enzyme from various sources [9-14]. It is provided suitable ligands with a highly specific interaction for target protein [16-17]. The purification method is advantage of many proteins for specific and suitable ligands with particularity, high stability, and high volume [14]. Sulfonamides are used as ligands specific and strong inhibitors of CA in these methods [3, 4, 6, 8, 18, 19, 20]. In the literature have been described using a variety of matrices, spacer arms and ligands for affinity gels [9-14].

The present study had been synthesized an original affinity gel with Sepharose 4B used as a matrix, l-tyrosine used as a spacer arm was covalently attached to the matrix. Sulfathiazole is the ligand for affinity gel for carbonic anhydrase purification. The present study characterizes the accomplished purification of carbonic anhydrase from erythrocytes using an original affinity gel and to achieve high purification a selective elution step.

MATERIALS AND METHODS

Materials. Sepharose 4B, L-tyrosine, sulfathiazole, protein assay reagents, enzyme purification chemicals for buffers, enzyme assay chemicals for buffers and chemicals for electrophoresis were obtained from Sigma Aldrich Co. (Milan, Italy) and Merck Chem Co. (Milan, Italy). All other chemicals were of analytical grade.

Preparation of affinity gel. The affinity gel was prepared with 4 g cyanogens bromide (BrCN) in 1:1 dilution of Sepharose 4B and water. The mixture was adjusted to pH 11 with 4M NaOH in an ice bath and maintained at that pH for 10-15min. Mixture was transported to a Buchner funnel and washed with cold 0.1 M $NaHCO_3$ buffer pH 10 and was transported to a beaker in the same buffer. L-tyrosine solution in cold 0.1 M $NaHCO_3$ (pH 10)

buffer was coupled to BrCN activated Sepharose-4B-Ltyrosine. The suspension was completed by stirring with a magnet for 90 min [10]. The suspension was washed with 1L cold distilled water.[14, 20] The affinity gel was obtained by diazotisation of sulfathiazole and coupling of this compound to the Sepharose-4B-L-tyrosine. The reaction was stabilized at pH 9.5 in suspension which was mixed for 3h at room temperature. After incubation, the suspension was washed with 1L cold distilled water and 0.05 M Tris-SO_4 (pH: 7.5) buffer solution and was stored in a buffer solution containing 0.05 M Tris-SO_4 (pH: 7.5).

Purification of carbonic anhydrase from human erythrocytes. Human blood samples were obtained from the Balikesir University Faculty of Medicine, using tubes containing anticoagulant. The blood samples were centrifuged at 5000 rpm for 20 min and the plasma and buffy coat were removed. Erythrocytes were washed two times with NaCl (0.9%) and the erythrocytes were hemolyzed with cold water [14]. The tissue samples were centrifuged at 15000 rpm for 40 min at 4°C and the ghosts, intact cells and precipitate were removed. The pH of the hemolysate was adjusted to 8.5 with solid Tris. The hemolysate was applied to the Sepharose 4B-L-tyrosine-sulfathiazole affinity column equilibrated with 25 mM Tris /0.1 M Na_2SO_4 (pH: 8.5) buffer. The affinity gel was washed with 25 mM Tris/22 mM Na_2SO_4 (pH 8.5) buffer, and CA isozymes were eluted under different elution conditions.

Protein determination. The protein in the column eluates was determined with UV-VIS spectrophotometer by the absorbance at 280 nm. Protein quantitative determination was obtained by absorbance measurements at 595nm according to the Bradford method, using bovine serum albumin as the standard [21].

Enzyme assay. Carbonic anhydrase activity was assayed by the hydration of CO_2 according to the method of Maren method [22] which is based on the determination of the time required for the pH of solution decreasing from 10.0 to 7.4 due to the hydration of CO_2.

SDS polyacrylamide gel electrophoresis. SDS polyacrylamide gel electrophoresis was applied after purification of the enzymes. It was performed in 10 and 3% acrylamide concentrations, containing 0.1% SDS according to the Laemmli procedure [23] for the running and stacking gel, respectively.

RESULTS AND DISCUSSION

Enzyme purification is laborious and time consuming process. For this reason, the purification method can be rapid and efficient. In this process, the enzymatic activity must not be reduced and the three-dimensional structure must not be denatured.

CA isoenzymes have been purified with different yields and purification folds from different sources [9-14]. Different purification methods have been used for CA isoenzymes [10,12,14] CA isoenzymes were purified first by Arslan et al. trough affinity chromatography, in their study, Sepharose-4B-Ltyrosine- p-aminobenzenesulfonamide gel and the enzyme was purified 416.8 times [10]. It was reported that EUPERGIT C250L- Ethylenediamine-4-isothiocyanato benzenesulfonamide gel were purified 184 times as a result of total hCA I and h CA II isoenzymes [12]. In another study, Sepharose 4B-Ethylenediamine-4-isothiocyanato benzenesulfonamide gel was used; the isoenzymes were purified approximately 672 and 580 times [14].

TABLE 1
Purification scheme of CA-I and CA-II from human erythrocytes by Sepharose-4B-L-tyrosine-sulfathiazole affinity chromatography

Purification Step	Volume (mL)	Total Activity (U)	Activity (U/mL)	Protein Amount (mg/mL)	Total Protein (mg)	Specific Activity (U/mg)	Overall Yield (%)	Overall Purification (fold)
Hemolysate	25 ml	53	2.12	32.21	805.25	0.0658	100	-
Affinity Chromatography	3 mL	15.06	5.02	0.12	0.36	41.83	28.41	635.71

TABLE 2
CAII

Purification Step	Volume (mL)	Total Activity (U)	Activity (U/mL)	Protein Amount (mg/mL)	Total Protein (mg)	Specific Activity (U/mg)	Overall Yield (%)	Overall Purification (fold)
Hemolysate	25 ml	53	2.12	32.21	805.25	0.0658	100	-
Affinity Chromatography	3 mL	24.48	8.16	0.186	0.558	43.87	46.19	666.71

SCHEME 1
The new affinity gel for purification of CA isoenzymes.

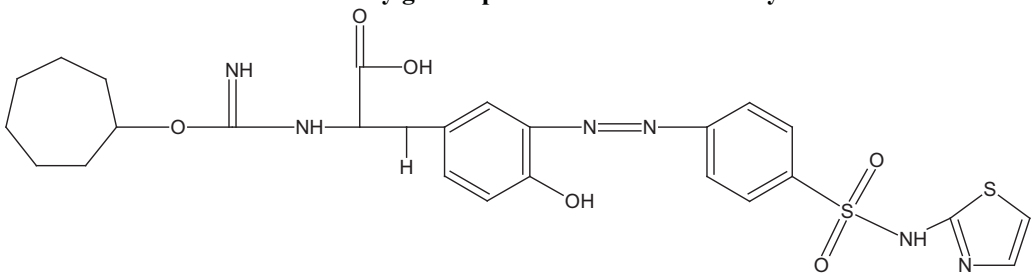

Sepharose 4B L-tyrosine Sulfathiazole

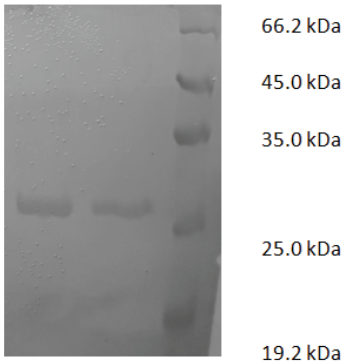

In study of Bozdag et al. (2015), hCA I enzyme was purified 672 times with 62 % yield and hCA II enzyme was purified 580 times with 43 % yield. In this study, hCA I enzyme was purified 635.71 times with 28.41 % yield and hCA II enzyme was purified 666.71 times with 46.19 % yield. It seems that the method of Bozdag et al. is better because approximately same purification fold with more yields for hCA I but in our study is better than the others with purification folds and yield for hCA II.

The present study, we design an original affinity gel for purifying the CA isoenzymes from human erythrocytes by using affinity chromatographic method. The novel affinity gel was prepared to purify the carbonic anhydrase isoenzymes. For this aim, the functional group $–NH_2$ of L-tyrosine was covalently attached to the matrix sepharose 4B by means of an amide bond. After that, L-tyrosine was attached to the activated gel as a spacer arm, and finally diazotised sulfathiazole was clenched to the meta position of L-tyrosine molecule as ligand. In this way, Sepharose-4B-L-tyrosine-Sulfathiazole affinity gel was obtained (Scheme 1). Sulfathiazole was chosen as a ligand, since it is a specific inhibitor of CA [24].

We synthesized Sepharose 4B- L-tyrosine-sulfathiazole affinity gel by change of washing and elution conditions for purifying the CA isoenzymes. The hemolysate was applied to the affinity column equilibrated with 25 mM Tris /0.1 M Na_2SO_4 (pH 8.5) buffer. The affinity gel was washed with 25 mM Tris/22 mM Na_2SO_4 (pH 8.5) buffer, and CA isoenzymes were purified under different elution status. The eluates were described by protein determination at 280 nm and assaying CO_2 hydratase activity for CA I and CA II. The isoenzymes CA I and CA II were purified up to 635.71 and 666.71 fold with a recovery ratio of 28.41% and 46.19% respectively in Table I. These values are better than some of the reported affinity gels, and equivalent to others [9-14]. Purified enzymes were acquired exhibiting a single band on SDS-PAGE, corresponding to a molecular weight of approximately 29 kDa (Figure 1).

We used only one chromatographic technique, Sepharose 4B-L-tyrosine-sulfathiazole affinity chromatography by change of elution conditions and binding capacities. CA I and CA II were eluted using the affinity gel with different elution buffers (Figure 2). The most suitable elution buffers were 1 M NaCl /50 mM Na_2HPO_4 (pH 6.3) for CA I and 0.1 M CH_3COONa/0.5 M $NaClO_4$ (pH 5.6) for CA II. The binding capacities of the affinity gel for the CA I and CA II isozymes were determined at different ionic strengths (Figure 3) and pH buffers (Figure 4). For this purpose, elution buffers were used with different compounds at different concentrations. We used for elution CA I and CA II pH 6.3 and 5.6 buffers respectively. The binding capacities of the affinity gel for the CA I and CA II isoenzymes were found at different pH buffers in the range from 6.5-9.0. For specification of optimum ionic strength, enzyme activity was found using

different concentrations of $NaSO_4$, pH 6.3 and pH 5.6, in the range from 0.1 to 0.52. The enzyme was seen to exhibit the maximum binding was achieved ionic strengths around 0.3. So that we prepared the optimum pH for CA I and CA II, 50 mM Na_2HPO_4/1.0 M NaCl and 0.1 M $NaCH_3COO$/0.5 M $NaClO_4$ buffers respectively. Buffers were prepared in the pH range of 6.5-9.0 (Figure 4), maximum binding was determined for CA I and CA II pH 8.7. These results displayed differences with other studies in the literature [9-14].

Sulfathiazole exhibited quite effective inhibition to CA I and CA II with 77.01 nM IC_{50} value [24]. In another study was seen with sulfanilamide for CA I and CA II isoenzymes as IC_{50} values of 24.53 nM and 100.73 nM, respectively [24]. IC_{50} values for sulfathiazole was effective inhibitor than sulfanilamide for CA II [24]. In this study, we used sulfathiazole for a ligand to synthesized affinity gel. The purification fold and yield Sepharose 4B-L tyrosine-sulfanilamide gel for CA I was better than CA II [10]. But, gel synthesized by us, purification fold and yield for CA II was better than CA I. In

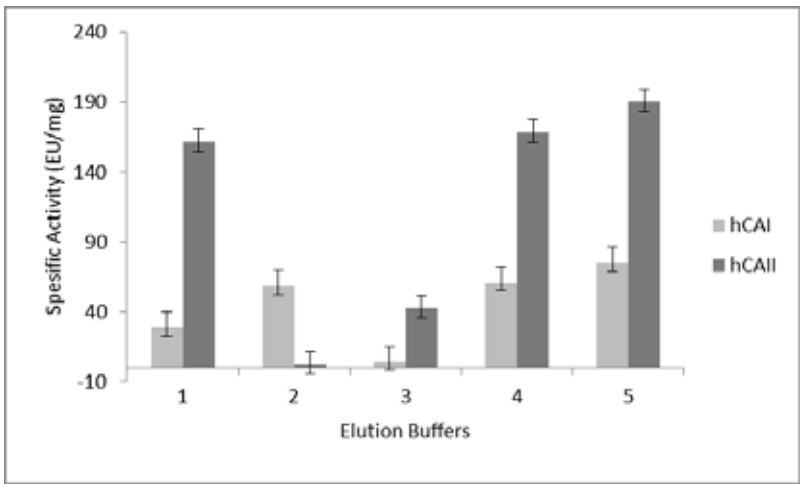

FIGURE 1
SDS-PAGE pattern (Lane 1 : hCA II, Lane 2: hCA I, Lane 3: Marker)

1. 50 mM Na_2HPO_4/1 M NaCl (pH:6.3)- 50 mM Na_2HPO_4/0.2 M KSCN (pH:6.3);
2. 0.1 M KI/ 0.1 M Tris-SO_4 (pH:7.0) -0.1 M $NaCH_3COO$/ 0.5 M $NaClO_4$ (pH:5.6);
3. 0.1 M KI/ 0.1 M Tris-SO_4(pH:7.0) - 50mM Na_2HPO_4 / 0.2 M KSCN(pH:6.3);
4. 50 mM Na_2HPO_4/1 M NaCl (pH:6.3)-0.1 M $NaCH_3COO$ / 0.5 M $NaClO_4$ (pH:5.6)
5. 1 M NaCl / 22 mM Na_2HPO_4 (pH:6.3), 0.1 M $NaCH_3COO$ / 0.5 M $NaClO_4$ (pH: 5.6)

FIGURE 2
Effect of different buffers for elution hCA I and hCA II

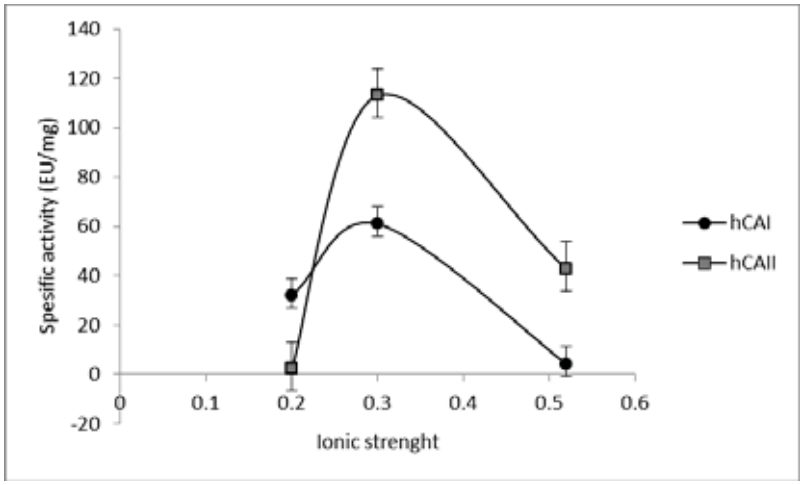

FIGURE 3
Effect of ionic strength

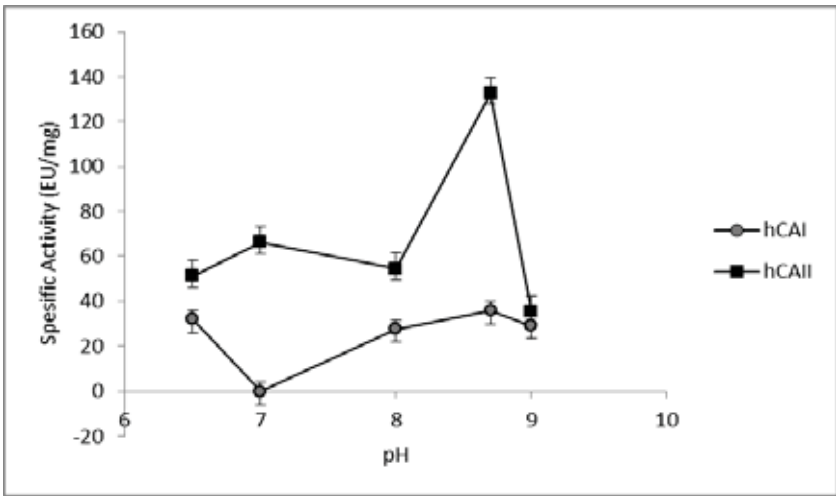

FIGURE 4
Effect of pH

addition, the binding capacities of the affinity gel for the CA I and CA I were best values another studies [9-14]. Thus, Sepharose 4B-L tyrosine - sulfathiazole affinity gel is displayed to be favourable for the purification of CA I and CA II in active form. These results show that the procedure used in the purification is good enough to be used in further studies. It is interesting, when we changed the compounds of the buffer, pH and ionic strengths, purification fold of CA II was better than CA I. By changing the elution conditions is advantage of purification of CA isoenzymes.

We focussed in this study to develop an original and easy chromatographic method for the purification of CA isoenzymes. Affinity chromatography is a suitable technique which is easily applicable for the rapid purification. For this purpose, in our study describes an original affinity gel synthesis was prepared using Sepharose 4B with sulfathiazole, an inhibitor of carbonic anhydrase, which is also commercially purchasing as well. In this reaction, L-tyrosine was used as a spacer arm for controlling the steric effects between the matrix and ligand. Hydroxyl groups that Sepharose contains, provide the binding of the ligand to the matrix in mild conditions. The purification of an each isozyme has been controlled by SDS-polyacrylamide gel electrophoresis.

ACKNOWLEDGEMENT

This work has been supported by TUBITAK with 2209-A - University Student Research Project Support Program.

Conflicts of Interest. All authors declared that they have no conflicts of interest.

REFERENCES

[1] Supuran, C.T. (2016) Structure and function of carbonic anhydrases, Biochem. J. 473(14), 2023-2032.
[2] Supuran, C.T., Scozzafava, A. (2007) Carbonic anhydrases as targets for medicinal chemistry, Bioorg. Med. Chem. 15(13), 4336-4350.
[3] Supuran, C.T. (2008) Carbonic anhydrases: novel therapeutic applications for inhibitors and activators, Nat. Rev. Drug. Discov. 7(2), 168-181.
[4] Supuran, C.T. (2008) Carbonic anhydrases, an overview, Curr. Pharm. Des. 14(7), 603-614.
[5] Vullo, D., Franchi, M., Gallori, E., Pastorek, J., Scozzafava, A., Pastorekova, S., Supuran, C.T. (2003) Carbonic anhydrase inhibitors. inhibition of the tumor-associated isozyme IX with aromatic and heterocyclic sulfonamides, Bioorg. Med. Chem. Lett. 13(6), 1005-1009.
[6] Vullo, D., Voipio, J., Innocenti, A., Rivera, C., Ranki, H., Scozzafava, A., Kaila, K., Supuran, C.T. (2005) Carbonic anhydrase inhibitors. inhibition of the human cytosolic isozyme VII with aromatic and heterocyclic sulfonamides, Bioorg. Med. Chem. Lett. 15(4), 971-976.
[7] Vull,o D., Innocenti, A., Nishimori, I., Pastorek, J., Scozzafava, A., Supuran, C.T. (2005) Carbonic anhydrase inhibitors. inhibition of the transmembrane isozyme XII with sulfonamides - a new target for the design of antitumor and antiglaucoma drugs?, Bioorg. Med. Chem. Lett. 15(4), 963-969.
[8] Nishimori, I. (2004) In carbonic anhydrase -its inhibitors and activators CRC Press: Boca Raton.
[9] Armstrong, J.M., Myers, D.V., Verpoorte, J.A., Edsall, J.T. (1966) Purification and properties of human erythrocyte carbonic anhydrases, J. Biol. Chem. 241, 5137-5149.

[10] Arslan, O., Nalbantoglu, B., Demir, N., Ozdemir, H., Küfrevioglu, O.I. (1996) A new method for the purification of carbonic anhydrase isozymes by affinity chromatography, Turk J. Med. Sci. 26,163-166.
[11] Zhu, X.L., Sly, W.S. (1990). Carbonic anhydrase IV from human lung. purification, characterization, and comparison with membrane carbonic anhydrase from human kidney, J. Biol. Chem. 265(15), 8795-8801.
[12] Sahin, A., Isik, S., Arslan, O., Supuran, C.T., Guler, O.O. (2015) A new affinity gel for the purification α-carbonic anhdrases, J. Enzyme Inhib. Med. Chem. 30(2), 224-228.
[13] Sharma, A., Bhattacharya, A., Singh, S. (2009) Purification and characterization of an extra cellular carbonic anhydrase from Pseudomonas fragi, Process Biochem. 44(11), 1293-1297.
[14] Bozdag, M., Isik, S., Beyaztas, S., Arslan, O. Supuran C. (2015) Synthesis of a novel affinity gel for the purification of carbonic anhydrases, J. Enzyme Inhib. Med. Chem. 30(2), 240-244.
[15] Berg, J.M., Tymoczko, J.L., Stryer, L. (2002) Biochemistry, W.H. Freeman and Company.
[16] Hage, D.S., Anguizola, J.A., Bi, C., Li, R., Matsuda, R., Papastavros, E., Pfaunmiller, E., Vargas, J., Zheng, X. (2012) Pharmaceutical and biomedical applications of affinity chromatography: recent trends and developments, J. Pharm. Biomed. Anal. 69, 93-105.
[17] Ozensoy, O., Puccetti, L., Fasolis, G., Arslan, O., Scozzafava, A., Supuran, C.T. (2005) Carbonic anhydrase inhibitors. inhibition of the tumor associated isozymes IX and XII with a library of aromatic and heteroaromatic sulphonamides, Bioorg. Med. Chem. Lett. 15(21), 4862- 4866.
[18] Supuran, C.T. (2010) Carbonic anhydrase inhibitors, Bioorg. Med. Chem. Lett. 20(12), 3467-3474.
[19] Supuran, C.T., Scozzafava, A., Casini, A. (2003) Carbonic anhydrase inhibitors, Med. Res. Rev. 23(2), 146-189.
[20] Arslan, O. (2001) Inhibition of bovine carbonic anhydrase by new sulfonamide compounds, Biochem. (Mosc). 66, 982-983.
[21] Bradford, M.M. (1976) A rapid and sensitive method for the quantitation of microgram quantities of protein utilizing the principle of protein-dye binding, Anal. Biochem. 72, 248-251.
[22] Maren, T.H. (1960) A simplified micromethod for the determination of carbonic anhydrase and its inhibitors, J. Pharmacol. Experiment. Ther. 130, 26-29.
[23] Laemmli, D.K. (1970) Cleavage of structural proteins during assembly of the head of Bacteriophage T4, Nature. 227, 680-683.
[24] Gokcen, T., Gulcin, I., Ozturk, T., Goren, A.C. (2016) A class of sulfonamides as carbonic anhydrase I and II inhibitors, J. Enzyme Inhib. Med. Chem. 31(2), 180-188.

Received: **13.11.2019**
Accepted: **19.01.2020**

CORRESPONDING AUTHOR

Serap Beyaztas Uzunoglu
Department of Molecular Biology and Genetics, Science and Art Faculty,
Balikesir University,
Balikesir – Turkey

e-mail: beyaztas@balikesir.edu.tr

© by PSP Volume 29 – No. 05/2020 pages 3804-3811 Fresenius Environmental Bulletin

STUDY ON THE INFLUENCE OF ECOLOGICAL GARDEN LANDSCAPE DESIGN ON WATER ENVIRONMENT

Haifeng Wang[1,2], Li Fei[1,2,*], Wang Chong[3]

[1]School of Water Conservancy and Hydroelectric Power,Hebei University of Engineering, Handan 056000, China
[2]Dept.Landscape Archtecture and Urban Design, Woosuk University, Korea 55338
[3]Power China Beijing Engineering Corporation Limited Beijing 100024, China

ABSTRACT

The objective of this study was to focus on influence of ecological garden landscape design on water environment. The effects of hydraulic loading rate (HLR), pH, initial total phosphorus concentration and pollutant loading rate (PLR) on pollutants removal were investigated. This study finds that although the influent loading rates were highly variable, the subsurface wastewater infiltration (SWI) system performed well in treating the sewage effectively. Hydraulic and pollutant loading rates had negative influence on the pollutants removal. Pollutant removal efficiencies decreased with loading rates increasing. The performance of the underground infiltration system is very stable, and various pollution indicators also have certain removal efficiency. After the underground infiltration rate system treatment of raw water, TP and so on have all declined, and the quality of landscape water has been significantly improved.

KEYWORDS:
Ecological landscape, Design, Water environment, SWI

INTRODUCTION

In recent years, the original form of the earth's surface has been changed drastically by land development and urban expansion. A large number of human behaviors, such as deforestation, river diversion and underlying surface hardening, lead to the loss or occupation of a tremendous amount of habitat, which is closely related to the lives of animals and plants and results in the deterioration of the atmosphere and the water environment. In the process of urbanization, the natural landscape's patch fragmentation and poor patch connectivity have become a more serious issue, and the ecological environment is faced with the problem of species extinction and serious pollution [1].

Landscape has important practical significance for protecting species diversity, preventing soil erosion, filtering pollutants, resource management and global change [2]. It improves the ability of bio-circulation and exchange, and improves the stability of ecosystem. With increasing emphasis on urban ecological environment, more and more attention has been paid to urban ecological landscape.

Subsurface wastewater infiltration (SWI) system has proved to be a good alternative for wastewater advanced treatment with the consideration of efficiency and cost [3-6]. In China, more attention to the SWI system has been obtained since the late 1990s when non-point source pollution control was introduced [7]. Since then, large scale SWI systems have been applied in many areas around the world to treat municipal wastewater. Some demonstration treatment systems were also established in American, Australia, Russia, Japan, China and other countries, gained popularity as a cost effective wastewater management option in both developed and developing countries [8-12]. Nowadays, the major research focus about the SWI system is the design, performance and mechanisms of pollutant removal [13-18]. In SWI treatment, wastewater is firstly treated by conventional physico-chemical or biological treatment and then allowed to infiltrate through aerated unsaturated zone wherein it gets purified through processes such as filtration, adsorption, chemical reaction and biodegradation. SWI system has demonstrated a consistent capacity to decompose organic matte [19].

Therefore, the objective of this study was to focus on influence of ecological garden landscape design on water environment. The effects of hydraulic loading rate (HLR), pH, initial total phosphorus concentration and pollutant loading rate (PLR) on pollutants removal were investigated.

MATERIALS AND METHODS

Ecological garden landscape design. It should follow the principles of regional natural conditions, follow the principles of environmental protection, follow the principles of plant ecology, and follow applicable and economic principles.

System description. The SWI systems were 1.6 m long and 1.3 m wide with a depth of 1.1 m. The matrix was 7% activated sludge, 62% brown

soil and 31% coal slag mixed evenly in volume ratio. The beds were planted with common grass, which was mainly for landscape planting.

RESULTS AND DISCUSSION

Effects of HLR on TP removal. During the operation period, PLR 20.00 g BOD/m^2 d and HLR 0.040, 0.060, 0.080 and 0.100 m^3/m^2 d were presented to test the effect of HLR on the TP removal. As seen from Figures 1-4, HLR had obvious influence on the TP removal in the SWI system. In the current study, TP removal efficiency decreased with the HLR increasing. The average removal efficiency of decreased from 82.10% under HLR 0.040 m^3/m^2 d to 68.42% under 0.100 m^3/m^2 d.

In a SWI system, organic matters will be absorbed by the soil, then broken down by the microbiota through fermentation and/or respiration, and mineralized as a source of energy or assimilated into biomass. With respect to the TP removal, short-term or long-term storage is the main removal mechanisms in the SWI system. Previous studies have shown that at phosphorus loading rates of less than 5 g P/m^2 year, the SWI system can absorb more than 90% of the total incoming phosphorus. According to the results, to achieve high effluent quality and hydraulic efficiency in a SWI system, HLR of 0.080 m^3/m^2 d was optimal.

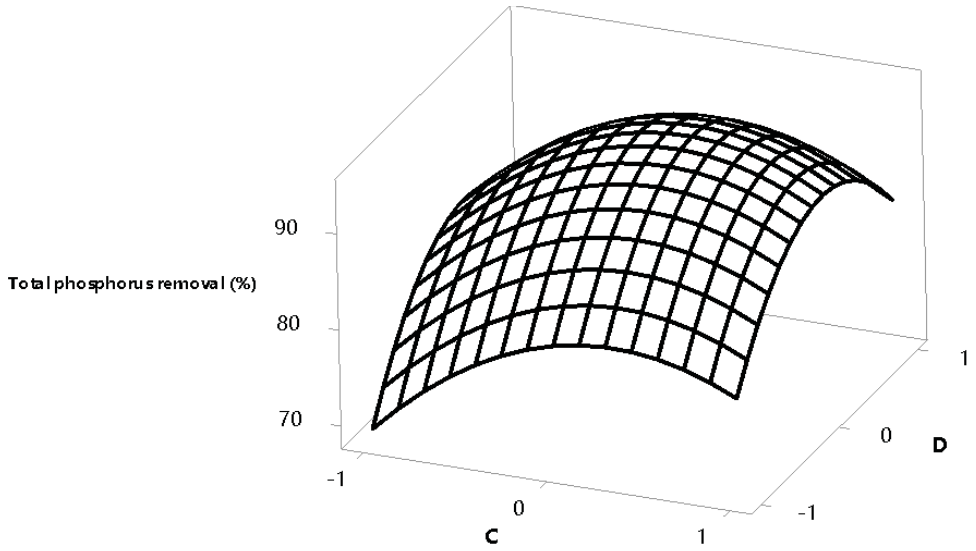

FIGURE 1
Surface Plot of Total phosphorus removal (%) vs D, C

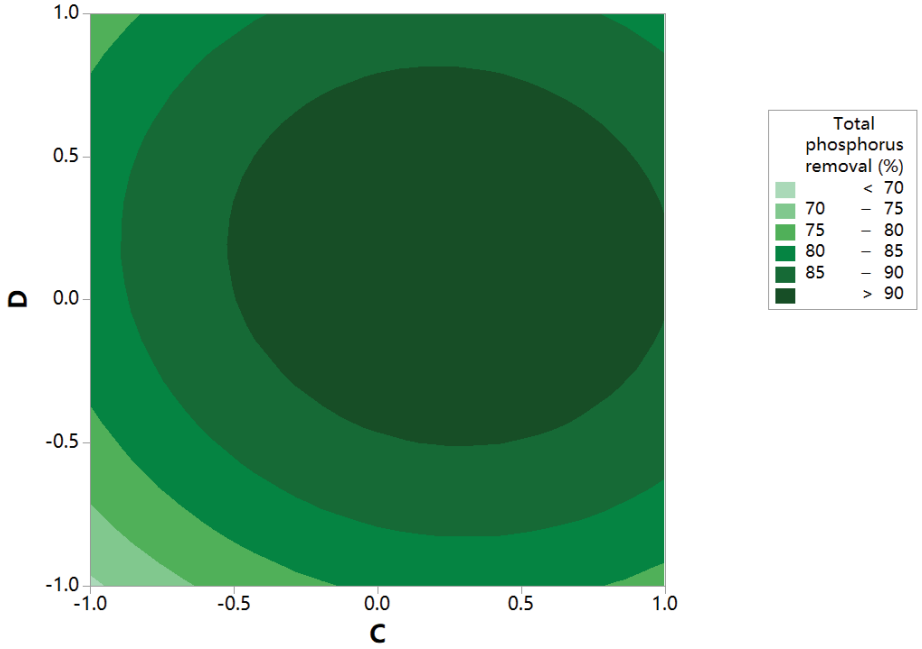

FIGURE 2
Contour Plot of Total phosphorus removal (%) vs D, C

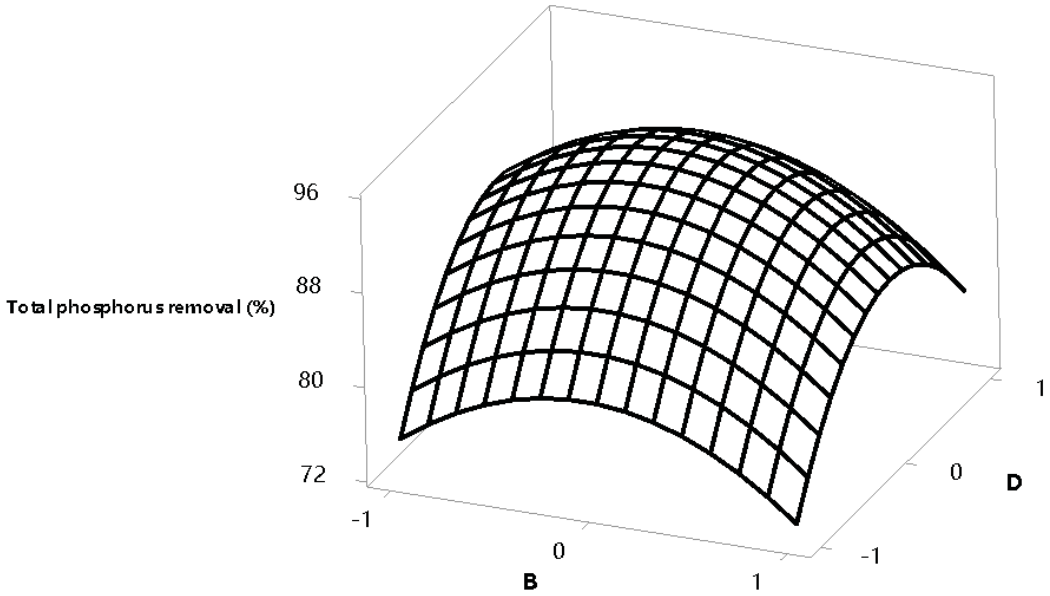

FIGURE 3
Surface Plot of Total phosphorus removal (%) vs D, B

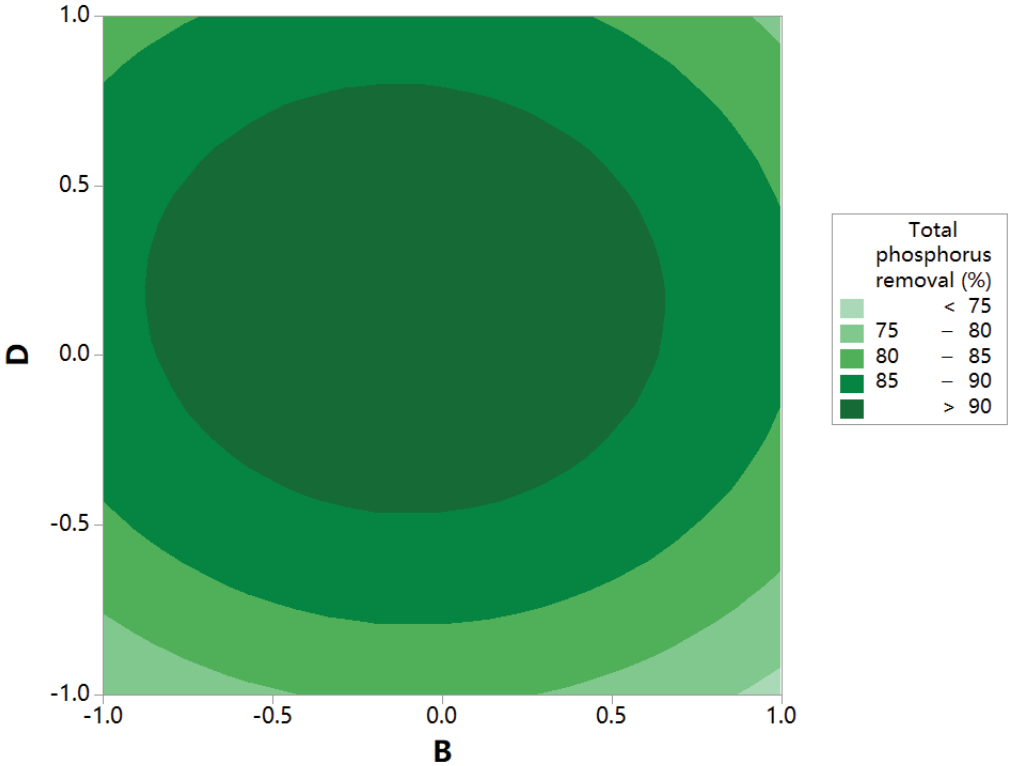

FIGURE 4
Contour Plot of Total phosphorus removal (%) vs D, B

Effects of PLR on TP removal. During the operation period, HLR 0.080 m^3/m^2 d and PLR 8.00, 12.00, 16.00 and 20.00 g BOD/m^2 d were presented. The effects of PLR on TP removal were presented in Figures 5-8. Overall, TP removal decreased with the PLR increasing, especially when PLR increased from 16.00 g BOD/m^2 d to 20.00 g BOD/m^2 d, removal efficiencies dropped from 92.87% to 87.25 % for TP. The results were a consequence of competition between heterotrophic bacteria and autotrophic bacteria. The increase of PLR which resulted in a higher organic loading shifted a favor of heterotrophic bacteria against autotrophic bacteria contribution. The results revealed that high pollutant removal is brought under low PLR.

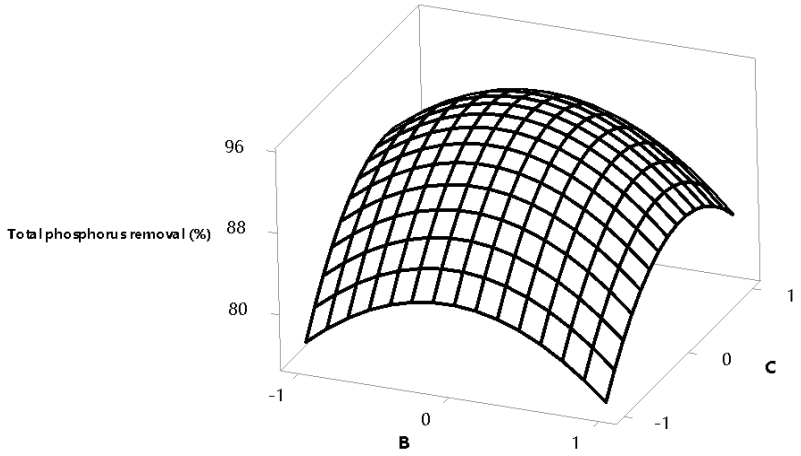

FIGURE 5
Surface Plot of Total phosphorus removal (%) vs C, B

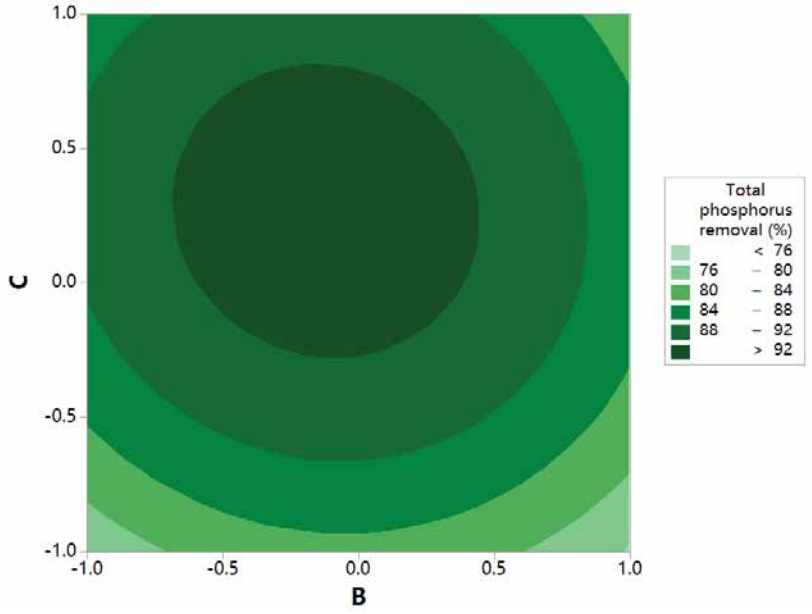

FIGURE 6
Contour Plot of Total phosphorus removal (%) vs C, B

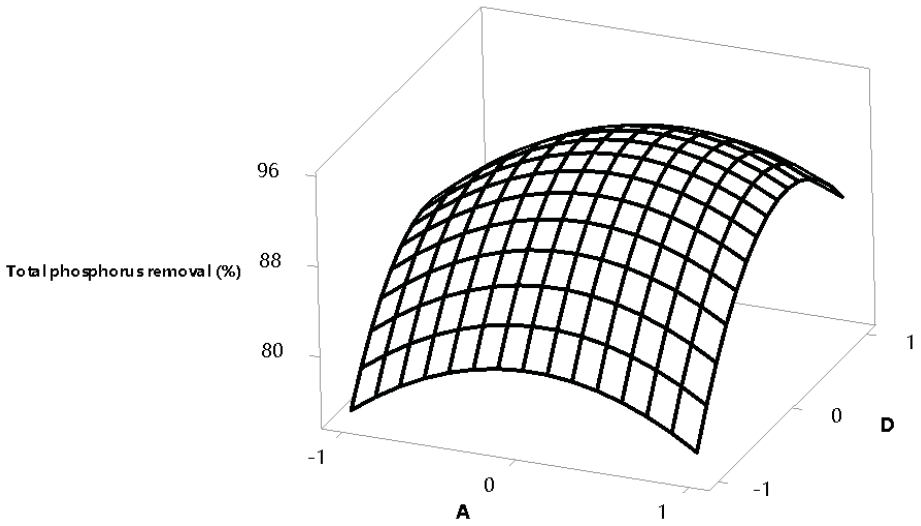

FIGURE 7
Surface Plot of Total phosphorus removal (%) vs D, A

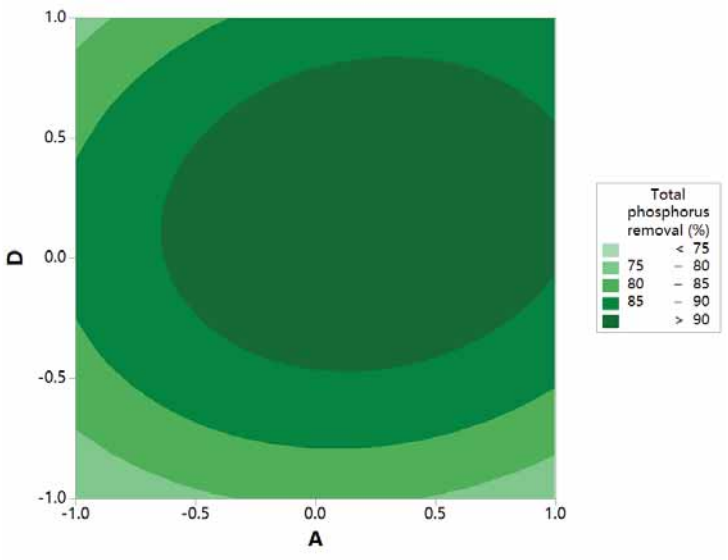

FIGURE 8
Contour Plot of Total phosphorus removal (%) vs D, A

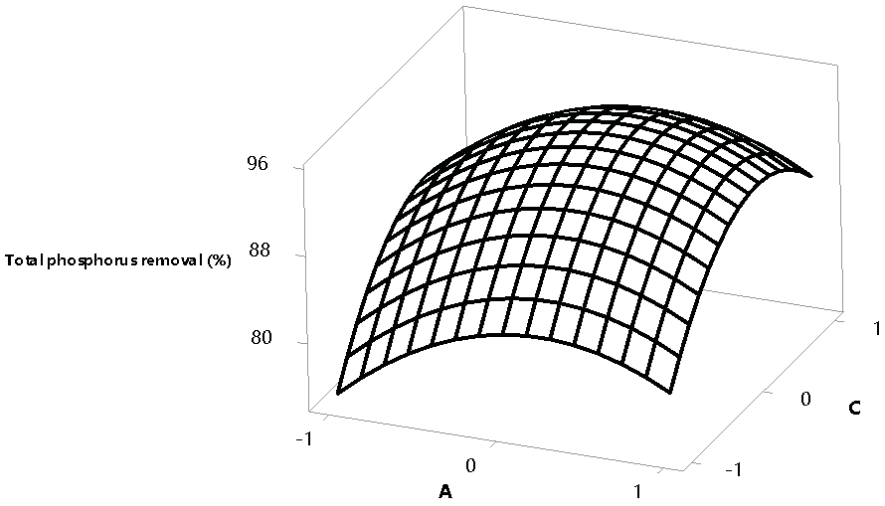

FIGURE 9
Surface Plot of Total phosphorus removal (%) vs C, A

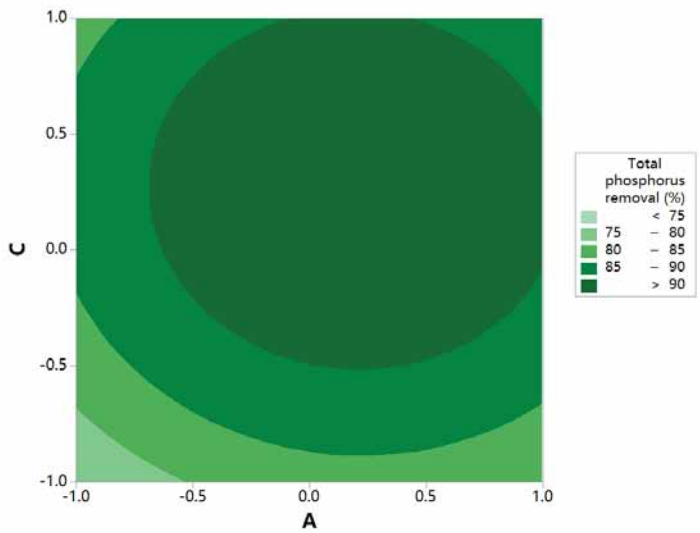

FIGURE 10
Contour Plot of Total phosphorus removal (%) vs C, A

Effects of pH on TP removal. After 3 weeks' start-up phase, the average removal is 91.8 ± 0.7% for TP under HLR of 0.080 m^3/m^2 d and PLR of 16.00 g BOD/m^2 d. TP removal change little when pH changes (Figures 9 and 10). The effluent concentrations for TP is 0.3 mg/L. According to the Water Quality Standard for Urban Miscellaneous Water Consumption in China, the effluent of the SWI system can be used for cleaning, flushing toilets and irrigating the landscape.

Effects of initial total phosphorus concentration on TP removal. Effects of initial total phosphorus concentration on TP removal is shown in Figures 11 and 12. After the water body is fully digested in the anaerobic state in the underground percolation tank, the composition of the water body changes. In the daytime operation of the underground infiltration system, the changes in various pollution indicators in the water body are not too large, indicating that the performance of the underground infiltration system is stable and has certain removal efficiency. TP removal increased when initial total phosphorus concentration increased at first but decreased subsequently. After the underground infiltration rate system treatment of raw water, TP and so on have all declined, and the quality of landscape water has been significantly improved.

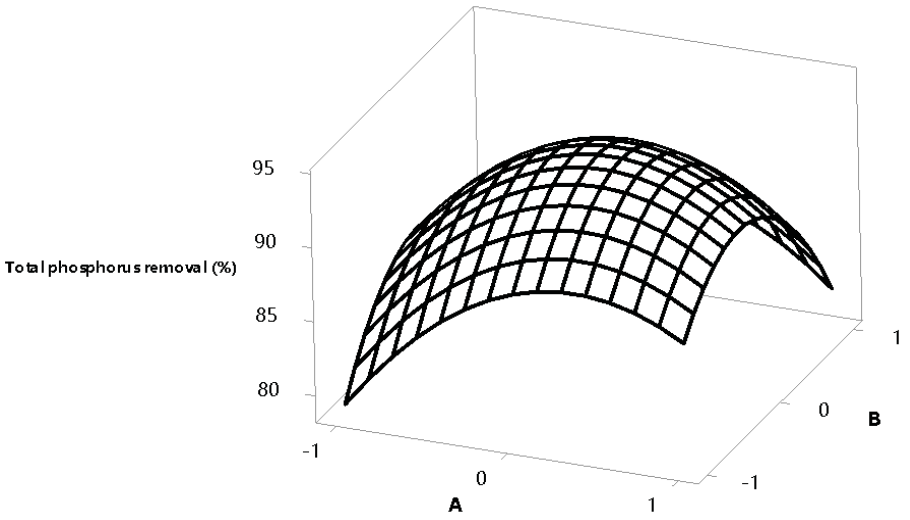

FIGURE 11
Surface Plot of Total phosphorus removal (%) vs B, A

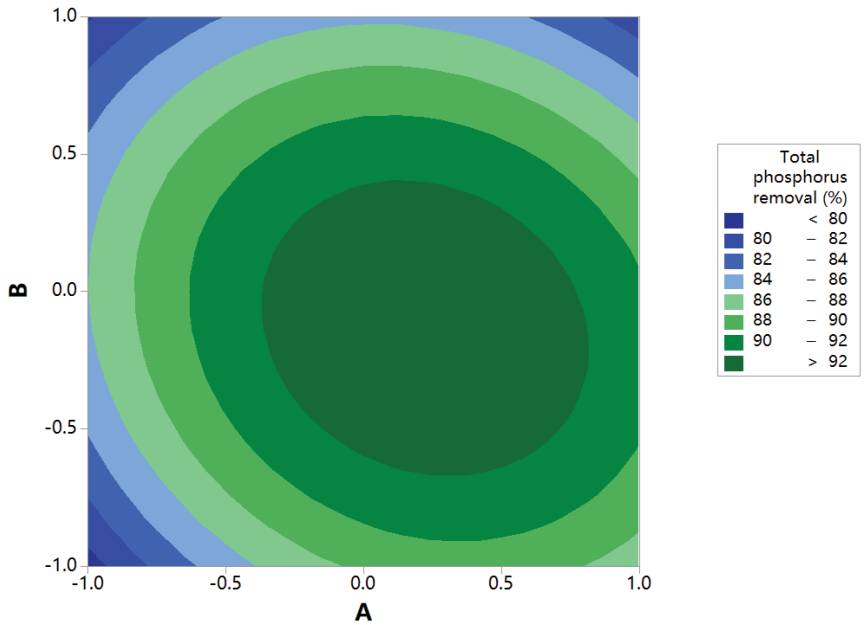

FIGURE 12
Contour Plot of Total phosphorus removal (%) vs B, A

CONCLUSIONS

Influence of ecological garden landscape design on water environment is studied. This study finds that although the influent loading rates were highly variable, the SWI system performed well in treating the sewage effectively. Hydraulic and pollutant loading rates had negative influence on the pollutants removal. Pollutant removal efficiencies decreased with loading rates increasing. The performance of the underground infiltration system is very stable, and various pollution indicators also have certain removal efficiency. After the underground infiltration rate system treatment of raw water, TP and so on have all declined, and the quality of landscape water has been significantly improved.

REFERENCES

[1] Liang, C., Li, Y., Chai, B., Wu, H. (2019) Evaluating the effects of intermittent aeration and biochar addition on enhancing removal performance of subsurface wastewater infiltration systems with loess soil. Bioresource Technology Reports. 5, 12-19.

[2] Yan, X. (2011) Study on Urban Ecological Corridor of Shanghai Pudong New Area. Anhui Agricultural University, Hefei.

[3] Qin, W., Dou, J.F., Ding, A.Z., Xie, E., Zheng, L. (2014) A study of subsurface wastewater infiltration systems for distributed rural sewage treatment. Environ. Technol. 35, 2115-2121.

[4] Wang, X., Sun, T., Haibo, L., Yinghua, L., Pan, J. (2010) Nitrogen removal enhanced by shunt distributing wastewater in a subsurface wastewater infiltration system. Ecological Engineering. 36(10), 1433-1438.

[5] Liang, C., Li, Y., Chai, B., Wu, H. (2019) Evaluating the effects of intermittent aeration and biochar addition on enhancing removal performance of subsurface wastewater infiltration systems with loess soil. Bioresour. Technol. Rep. 5, 12-19.

[6] Pan, J., Fei, H., Song, S., Yuan, F., Yu, L. (2015) Effects of intermittent aeration on pollutants removal in subsurface wastewater infiltration system. Bioresource Technology. 191, 327-331.

[7] Duan, R., Fedler, C.B. (2010) Performance of a combined natural wastewater treatment system in West Texas. J. Irrig. Drain. Eng. 136, 204-209.

[8] Zhang, J., Huang, X., Wei, J., Hu, H.Y., Shi, H.C. (2002) Nitrogen and phosphorus removal mechanism in subsurface wastewater infiltration system, China. Environ. Sci. 22, 438-441.

[9] Degen, M.B., Reneau Jr. R.B., Hagedom, C., Martens, D.C. (1991) Denitrification in onsite wastewater treatment and disposal systems. Virginia Water Resour. Res. Center Bull. 171, 1-113.

[10] Li, Y.H., Li, H.B., Sun, T.H., Wang, X. (2011) Study on nitrogen removal enhanced by shunt distributing wastewater in a constructed subsurface infiltration system under intermittent operation mode. J. Hazard. Mater. 189, 336-341.

[11] Sun, Y., Qi, S., Zheng, F., Huang, L., Pan, J., Jiang, Y., Hou, W., Xiao, L. (2018) Organics removal, nitrogen removal and N_2O emission in subsurface wastewater infiltration systems amended with/without biochar and sludge. Bioresour. Technol. 249 , 57-61.

[12] Vymazal, J. (2011) Plants used in constructed wetlands with horizontal subsurface flow: a review. Hydrobiologia. 674, 133-156.

[13] Ji, B., Yang, K., Zhu, L., Jiang, Y., Wang, H., Zhou, J., Zhang, H. (2015) Aerobic denitrification: a review of important advances of the last 30 years. Biotechnol. Bioprocess Eng. 20, 643-651.

[14] Li, Y.W., Long, M., Zuo, L.H., Li, W., Zhao, W.C. (2019) Brittleness Evaluation of Coal Based on Statistical Damage and Energy Evolution Theory. Journal of Petroleum Science and Engineering. 172, 753-763.

[15] Li Y.-H., Li, H.-B., Sun, T.-H., Wang, X. (2011) Effects of hydraulic loading rate on pollutants removal by a deep subsurface wastewater infiltration system. Ecological Engineering. 37, 1425-1429.

[16] Kong, Z., Feng, C., Chen, N., Tong, S., Zhang, B., Hao, C., Chen, K. (2014) A soil infiltration system incorporated with sulfur-utilizing autotrophic denitrification (SISSAD) for domestic wastewater treatment. Bioresour. Technol. 159, 272-279.

[17] Li, H.B., Li, Y.H., Sun, T.H., Wang, X. (2012) The use of a subsurface infiltration system in treating campus sewage under variable loading rates. Ecol. Eng. 38, 105-109.

[18] Zou, S., Yao, S., Ni, J. (2014) High-efficient nitrogen removal by coupling enriched autotrophic-nitrification and aerobic-denitrification consortiums at cold temperature. Bioresour. Technol. 161, 288-296.

[19] Zheng, M.Z., Hu, L., Dong, R.J., Wu, D.M., Cheng, S.P., Cui, J.Y. (2011) Environmental effect of turf-soil system disposing nitrogen in biogas fertilizers. Trans. CSAE. 27 , 294-299.

Received: **15.11.2019**
Accepted: **13.02.2020**

CORRESPONDING AUTHOR

Li Fei
Hebei University of Engineering School of Water Conservancy and Hydroelectric Power,
Handan 056000, China

e-mail: 364066428@qq.com

© by PSP Volume 29 – No. 05/2020 pages 3812-3817 Fresenius Environmental Bulletin

EFFECTS OF DIFFERENT ASPECTS AND HARVEST TIMES ON ESSENTIAL OIL RATIO AND COMPONENTS OF WILD THYME (*THYMBRA SPICATA* L. VAR. *SPICATA*)

Emine Aslan, Dogan Arslan*

Siirt University, Faculty of Agriculture, Field Crops Department, 56000 Siirt, Turkey

ABSTRACT

The study was carried out to determine the quality characteristics of *Thymbra spicata* L. var. *spicata* which has a natural distribution in the flora of Siirt province, Turkey. The dried leaves and flowers of *Thymbra spicata* L. var. *spicata*, which is used in folk medicine in Anatolia, are consumed as spices and tea, and young shoots are used as salads. The essential oil content of the plant varies between 0.5 and 3.4%. A significant portion of essential oil in *Thymbra spicata* L. var. *spicata* is composed of carvacrol. In this study, essential oil ratio and essential oil components of *Thymbra spicata* L. var. *spicata* collected from different aspects (north, south, east, west) and at different harvest times (pre-flowering, full flowering and post-flowering) were determined. The samplings were carried out according to the split plots into randomized blocks experimental design with 4 replications. The results showed that essential oil ratio varied between 2.13 and 3.15%. The highest essential oil ratio (3.15%) was obtained from the west aspect during the full flowering period, while the lowest essential oil ratio (2.13%) was obtained from the east aspect at post-flowering period. A total of 38 components were identified in the essential oil as 19 main components and 19 others in very small quantities (total of 2%). The main component of the essential oil was carvacrol (39.29-65.97%).

KEYWORDS:
Harvest time, Time Aspect, Carvacrol, Terpinene, Timol, Myrcene, p-Cymene

INTRODUCTION

Thyme species, which have a wide natural expansion range in the world and Turkey, are quite commonly used plants for medicinal and aromatic purposes. Thyme species are the members of Lamiaceae family which grows in a wide area from the North Pole to the Himalayas, from South East Asia to Hawaii and Australia, to America and Africa, however, the thyme has a very intensive distribution particularly in the Mediterranean Region. The Lamiaceae family is a cosmopolitan family represented by 236 genera and about 7133 species in the world. The Lamiaceae family, the third richest plant family of Turkey, is represented with 48 genus, 565 species and total of 782 taxa (603 species, subspecies and 179 varieties). Three hundred and forty-six of these taxa (271 species, 75 subspecies and varieties) are endemic to Turkey. [1, 2, 3].

Thymbra. spicata L. var. *spicata* belongs to the genus *Thymbra* and is a perennial shrub. *Thymbra* species of naturally grown in dry sunny slopes and high dry meadows has two varieties and four taxa in Turkey, which are *T. spicata* L. (var. *spicata*, var. *intricata* P.H. Davis) and *T. sintenisii* Bornm. & Aznav. (var. *sintenisii*, var. *isaurica* P.H. Davis) [4, 5, 6, 7]. This variety is known as "Zahter" in Southeastern Anatolia Region of Turkey. The dried leaves and flowers are consumed as spices and tea while the young shoots are as salad. The essential oil content of the plant varies between 0.5 and 3.4% and carvacrol constitutes a significant portion of the essential oil. Carvacrol is dissolved in water; thus, herbal teas prepared with *Thymbra spicata* L. *var. spicata* are recommended for colds, coughs and stomach aches. The plant is also used as a painkiller in the treatment of skin diseases such as parasites and eczema. Thyme has a strong antibiotic effect on bacteria and fungi due to the phenol content. Therefore, the plant is widely used in the production of perfume, soap, shampoo, liquor, toothpastes, canned tomato paste, sauces and sausages in addition to the use as aromatizer (fragrance and flavor) in food products, especially meat products [8, 9, 10, 11, 12]. In addition, the essential oil obtained from *Tymbra spicata* L. var. *spicata* is effective on some plant pathogenic bacteria and weed control in agriculture [13, 14]. In this study, the effects of different aspects and harvest periods on the essential oil content and essential oil components of *Tymbra spicata* L. var. *spicata* were investigated.

MATERIALS AND METHODS

Material. The study was carried out to determine the quality characteristics of *Thymbra spicata*

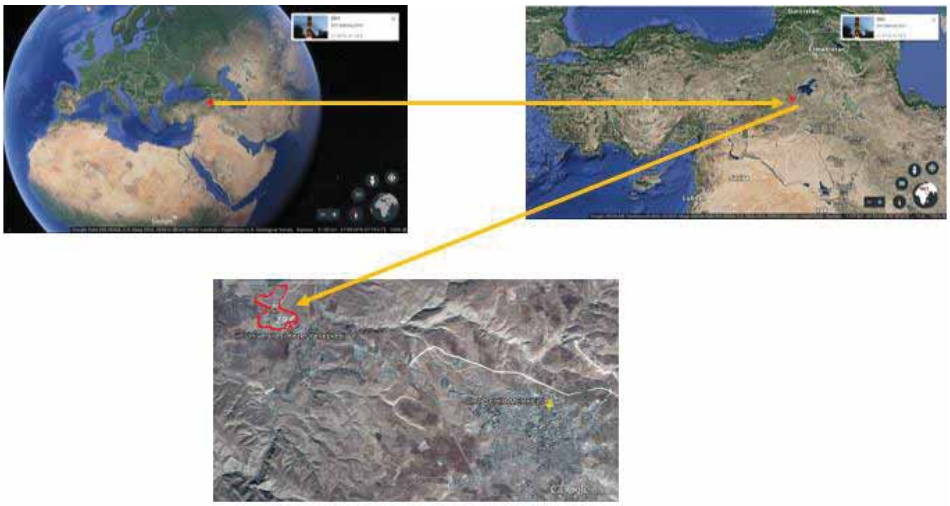

FIGURE 1
Satellite image of the study area

TABLE 1
Some climatic data during the experiment (2016) and for the long-term (1938-2015)

YEARS	2016					LONG TERM				
MONTHS	Mean Temperature (°C)			Mean Humidity (%)	Tot. Precipitation (mm)	Mean Temperature (°C)			Mean. Humidity (%)	Tot. Precipitation (mm)
	Mean	Max.	Min.			Mean	Max.	Min.		
April	16.6	26.5	4.2	47.5	104.2	14.4	19.1	8.9	57.9	96.0
May	19.9	30.6	8.0	48.9	63.1	20.0	25.2	13.5	48.5	44.6
June	26.5	38.4	14.8	32.7	8.6	27.0	32.1	18.9	32.3	9.3
July	31.4	41.6	20.6	24.5	1.6	31.2	36.9	23.4	26.9	1.2
August	32.3	41.8	22.4	20.5	0.9	30.1	36.8	23.1	21.6	0.9
September	25.0	36.3	12.4	29.8	0.0	25.1	32.2	18.7	12.9	4.9
Mean	25.28	35.87	13.73	33.99	29.73	24.63	30.38	17.76	33.36	26.15

Source: Siirt Meteorological Stations Records, Provincial Meteorological Directorate.

var. *spicata* which has a natural distribution in the flora of Siirt province, Turkey. The study area has an altitude of 580 m and is located between 37º 96´ north latitude and 410º 85´ east longitude. The satellite image of the study area was shown in Figure 1. The data on average temperature (ºC), average relative humidity (mm) and total precipitation (mm) for 2016 and long-term (1938-2015) averages of Siirt province were given in Table 1.

The average monthly temperature in 2016 differs from the long-term averages, and the average minimum and the maximum temperatures in 2016 were higher than the long-term averages (Table 3.1). Monthly average relative humidity and total rainfall did not differ significantly compared to the long-term averages; however, total monthly precipitations were higher than the long-term averages. The average maximum temperature (41.8 °C) in 2016 was recorded in August and the average lowest temperature (4.2 °C) was recorded in April.

Method. Plant samplings were carried out according to the split plots into randomized blocks experimental design with 4 replications. The different aspects (north, south, east, west) were the main plots and harvest periods (pre-flowering, full flowering and post-flowering) were the sub-plots. determined as fallows; Ten g of air-dried plant sample was placed into a 500 ml flask and 100 ml of deionized water was added to determine the essential oil ratio. The components of essential oil obtained by distillation in Clevenger apparatus for 4 hours were determined by using a gas chromatography-mass spectrometry the essential oil ratio and essential oil components of the *Thymbra spicata* L. var. *spicata* were (Thermo Scientific Trace 1310 and ISQ Single Quadrupole). The MS model (Thermo TG-WAX-MS 0.25 mm inner diameter x 60 m length, 0.25 µm film thickness) column was used in the gas chromatography-mass spectrometry. The mass range was adjusted to m/z 50-550 amu. Scan Mode was used for data collection. The MS transfer line temperature

was 250°C, the MS ionization temperature was 250°C and the column temperature was initially 60°C, kept for 6 minutes and increased to 230 °C with a 4 °C min^{-1} heat increase rate.
The analysis was completed by incubating the samples at 230 °C for 15 minutes. The structure of each compound was defined by Xcalibur software using mass spectra (Wiley 9, Nist demo and mainlib).

Statistical analysis of the data (variance analysis) was carried out by using JMP Statistical Software according to Split Plot into Randomized Block experimental design with four replications. Least Significant Difference (LSD) test at 95 and 99% probability levels was used as post-hoc where variance analysis indicated significant differences.

TABLE 2
Sample collecting dates for different growth periods of plants in the study area

	Pre-flowering	Full Flowering	Post-flowering
Thymbra spicata* L. var. *spicata	10.04.2016	02.05.2016	30.06.2016

TABLE 3
Effects of different aspects and harvest times on essential oil ratio (%) and essential oil composition of *Thymbra spicata* L. var. *spicata*

TIME **	ASPECT**				MEAN **
	North	East	South	West	
Pre-flowering	2.23f	2.28ef	2.55c	2.23f	2.32*c*
Full Flowering	2.23f	2.86b	2.44d	3.15a	2.67*a*
Post-flowering	2.33e	2.13g	2.44d	2.60c	2.38*b*
Mean	2.26c	2.42b	2.48b	2.66a	2.46
CV	2.51				
LSD (% 1)	0.08 (Aspect), 0.04 (Harvest Time), 0.09 (Aspect x Harvest Time)				
**	significant at 1%				

RESULTS AND DISCUSSION

Essential Oil Ratio (%). Mean essential oil ratios of *Thymbra spicata* L. var. *spicata* and the groups were given Table 3.

The effects of aspects and harvest times and the interaction of aspect x harvest time on essential oil ratio were statistically significant (Table 3). The highest essential oil ratio was obtained at the full flowering period. Mean essential oil ratio at pre-flowering period was 2.32%, at full flowering was 2.67%, and post-flowering was 2.38% (Table 3). The essential oil ratio of plants collected from different aspects ranged from 2.26 to 2.66%. The highest value was obtained from the plants collected in west aspect (2.66%) and the lowest value was obtained from the plants collected in north aspect (2.26%) (Table 3). Aspect x harvest time interaction indicated that the highest essential oil ratio (3.15%) was obtained from the plants in the west aspect at the full flowering period, while the lowest essential oil ratio (2.13%) was obtained from the plants in the east aspect post-flowering period.

The highest essential oil ratio was obtained in full flowering period and in the west aspect. Therefore, the results concluded the importance of choosing western aspects if thyme is to be collected or grown for essential oil. The essential oil ratios obtained in this study were higher than those reported by 10, 12, 15 and 16 while similar to those recorded by 17 and 18. The differences in essential oil ratios reported can be attributed to the differences in climate, ecological conditions and flora.

Essential Oil Compositions (%). The values of the essential oil composition were given in Table 4. Carvacrol (39.29-65.97%) was the highest essential oil component followed by γ-terpinene (12.5-26.54%), p-cymene (0.05-20.99) and Cymene (12.92-20.74%) (Table 4). In addition to the 19 main components given in the table, α-Terpineol, Linalool, Sabinene, trans-Sabinene hydrate, 2,3-Dimethyl-2-Butanol, 2-methyl-2-Pentanol, Ocimene, 1-Pentanol, Acetone, Aromadendrene, GermacreneD, Benomyl, 3-octanol, Tetraethyl pyrophosphate, 2,4-Dichlorophenethylamine, Trans-dihydrocarvone, Cyclohexanone and 4-Hxylresorcinol, Dihydrocarvone were also found in the essential oil, which were constituted 2% of the total and called as “others” in the table.

The mean carvacrol ratio in the pre-flowering period was 65.97% in the north, 65.06% in the south, 59.31% in the west and 57.15% in the east aspect. The mean carvacrol ratio in full flowering period was 61.29% in the south, 57.6% in the east, 52.77% in the north and 47.96% in the west aspect. The mean carvacrol ratio of essential oil in post-flowering period was 58.26% in the east, 45% in the north, 41.17% in the south and 39.29% in the west aspect. The results showed that the north aspect and the full flowering period should be preferred if the plant is to be harvested or produced to obtain carvacrol.

The γ-Terpinene among the other components of the essential oil had the highest ratio (26.54%) at post flowering period in west aspect; the highest (4.14%) ratio of α-terpinene was obtained at post-flowering period in the west aspect and the highest ratio of thymol (0.95%) was found in the north aspect at post-flowering period (Table 4). The highest ratio (0.94%) of β-Pinene was recorded in north aspect at post-flowering period and the highest ratio (27.58%) of β-Myrcene was obtained in the north aspect at pre-flowering period.

β-phellandrene was at the highest ratio (1.87%) in the west aspect at pre-flowering and β-caryophyllene was at the highest ratio (2.41%) in the east aspect at the post-flowering period. The highest ratio of Camphene (0.28%) was recorded in the east aspect at full flowering and the highest Spathulenol (0.33%) was in the west aspect at the post-flowering period. Limonene was at the highest ratio (0.50%) in the south aspect at post-flowering period, while P-cymene was at the highest ratio (20.99%) in the east aspect at the pre-flowering period. The highest ratio of Caryophyllene oxide (0.92%) was obtained in the west aspect at post-flowering period.

Myrcene was at the highest ratio (23.8%) in the South aspect at post-flowering, while 1-octen-3-ol (0.45%) was at the highest ratio in the north aspect at post-flowering period. The highest Borneol ratio (0.59%) was obtained in the north aspect at post-flowering period, while the highest α-Caryophyllene ratio (3.81%) was obtained in the west aspect at full flowering period. The Cymene was at the highest ratio (20.74%) in the south aspect at pre-flowering period and Terpinolene was at the highest ratio (0.58%) in the south aspect at full flowering period. The results revealed that the Carvacrol had the highest ratio (54.24%) compared to the other components of the thyme essential oil.

Essential oil components and essential oil ratios obtained in this study are similar to the findings of different researchers [15, 19, 20, 21].

CONCLUSIONS

The results showed that essential oil ratio of *Thymbra spicata* L. var. *spicata* ranges 2.13 and 3.15%. The effects of different aspects and harvest times on essential oil ratio was statistically significant. The composition of the essential oil was also affected by different aspect and harvest times. Carvacrol was the main component of the essential oil in all harvest times and aspects. The highest essential oil ratio was obtained in the west aspect at full flowering period while the highest carvacrol ratio was obtained in the north aspect at full flowering period. The results concluded that both the aspect and harvest times should be taken into consideration for collecting from nature and cultivation of *Thymbra spicata* L. var. *spicata*.

ACKNOWLEDGEMENT

The authors thank to Siirt University Scientific Research Projects **(2016-SİÜFEB-23)** Department for their financial support. At the same time, this article is produced from a master's thesis.

TABLE 4
Essential oil compositions and ratios (%) of *Thymbra spicata* L. var. *Spicata* collected from different aspects and at different harvest times

ESSENTIAL OIL COMPONENTS		Carvacrol	γ-terpinene	α-terpinene	Timol	β-Pinene	β-Myrcene	β-phellandrene	β-caryophyllene	Camphene	Spathulenol	Limonene	p-cymene	Caryophyllene oxide	Myrcene	1-octen-3-ol	Borneol	α-Caryophyllene	Cymene	Terpinolene	Others
Harvest Time	Aspect																				
Pre-flowering	North	65,97	-	-	-	0,94	27,58	0,3	0,51	-	-	-	-	-	-	-	-	-	-	-	4,7
	East	57,15	15,1	1,8	0,18	-	-	-	2,08	0,23	-	0,25	20,99	0,42	-	0,29	-	-	-	-	1,51
	South	65,06	12,5	1,33	-	-	-	-	1,45	-	-	0,18	17,91	-	0,67	0,33	0,16	-	-	-	0,41
	West	59,31	14,22	-	-	0,08	0,94	0,05	0,87	-	-	0,21	0,05	0,41	-	0,34	-	1,52	20,74	-	1,26
Full Flowering	North	52,77	23,71	3,54	-	0,19	2,19	-	2,11	0,18	-	0,35	-	-	-	0,27	0,26	-	13,95	0,13	0,35
	East	57,6	19,58	3,18	0,21	0,25	-	0,28	2,02	0,28	0,21	0,35	-	0,54	2,36	-	0,23	-	12,92	-	-
	South	61,29	17,09	2,83	0,32	0,19	-	0,24	1,76	-	0,13	0,29	10,85	0,4	1,83	0,18	0,23	-	-	0,12	2,25
	West	47,96	23,6	-	0,68	0,34	2,8	0,38	2,32	-	0,16	0,43	15,81	0,52	-	0,34	0,34	3,81	-	-	0,51
Post Flowering	North	45,00	23,01	-	0,95	0,28	2,38	0,35	2,41	-	0,32	0,43	-	0,87	-	0,45	0,59	3,32	19,12	0,17	0,35
	East	58,26	17,71	2,8	0,7	0,25	-	0,28	2,15	-	0,19	0,34	13,72	0,61	2,09	0,28	0,38	-	-	0,15	0,9
	South	41,17	25,11	3,61	-	0,35	-	-	-	-	0,28	0,66	-	0,85	23,8	0,43	-	-	-	0,58	3,16
	West	39,29	26,54	4,14	0,87	0,4	-	-	-	-	0,33	0,5	19,48	0,92	-	0,45	0,51	-	-	-	6,57
Mean		54,24	19,83	2,90	0,56	0,33	6,33	0,53	1,83	0,23	0,23	0,36	14,12	0,62	7,17	0,34	0,34	2,39	16,69	0,23	2,00

REFERENCES

[1] Harley, R.M., Atkins, S., Budantsev, A.L., Cantino P.D., Conn, B.J., Grayer, R., Harley, M.M., De Kok, R.P.J., Krestovskaja, T., Morales, R., Paton, A.J., Ryding, O. and Upson, T., (2004) Labiatae. Kubıtzkı K., (Ed), The Families and Genera of Vascular Plants, Springer-Verlag, Berlin, Heidelberg, New York. 6, 167

[2] Celep, F., Dirmenci, T. (2017) Systematic and Biogeographic Overview of Lamiaceae in Turkey. Naturel Volatiles and Essential Oils. 4 (4), 14-27.

[3] Kahraman, A., Celep, F., Doğan, M. (2009) Morphology, Anatomy and Palynology of *Salvia indica* L. (Labiatae), World Applied Sciences Journal. 6(2), 289-296.

[4] Arani, A. M., Naderi M., Goldansaz S. M. (2015) Effect of Harvesting Time on Essential Oil Content and Composition of *Thymbra spicata.* Journal of Medicinal Plants and By-products. 1, 51-55

[5] Daneshvar-Royandezagh, S., Khawar, K.M., Ozcan, S. (2009) In Vitro micropropagation of garden thyme (*Thymbra spicata* L. var. *spicata* L.) collected from Southeastern Turkey using Cotyledon Node. Biotechnology and Biotechnological Equipment. 23(3), 1319-1321.

[6] Kizil, S. (2010) Determination of essential oil variations of *Thymbra spicata* var. *spicata* L. naturally growing in the wild flora of east Mediterranean and Southeast Anatolia Regions of Turkey. Industrial Crops and Products. 32(3), 593-600.

[7] Davis, P.H. (1982) Labiatae, Flora of Turkey and the East Aegean Islands, University Press Edinburg. 73, 383-384

[8] Baytop, T., (1999) Treatment with plants in Turkey, Past and Present. Second Edition, Nobel Bookstores. (in Turkish).194, 245-255.

[9] Tuzun, H. (1986) Possibility and Benefits of Medicinal Plants Cultivation in Turkey. VI. Herbal Medicine Raw Materials Meeting. May 16-19, 1986. Ankara (in Turkish).

[10] Kıvanç, M., and A. Akgül. (1988) The inhibitory effect of different black thyme (*Thymbra spicata L.*) doses on growth of Escherichia coli at different temperatures. Doğa, Turkish Journal of Agriculture and Forestry. 12(3), 248-252. (in Turkish)

[11] Tansı, S. (1991) Investigation of drog yield and ecological, ontogenetic and morphogenetic variability in Karabas thyme (*Thymbra spicata L.*). Cukurova Uni. Institute of Science and Technology Field Crops Department. PhD Thesis. 153 (in Turkish).

[12] Başaran, S., Güler, K.H., Güler, S. (2010) Fresh/Dry Weight Ratio of Some Important Non-wood Forest Products Naturally Distributed in the Western Mediterranean Region. General Directorate of Forestry, Western Mediterranean Forestry Research Institute. 60, 19-21 (in Turkish)

[13] Basim, H., Yegen, O., Zeller, W. (2000) Antibacterial Effect of Essential Oil of *Tymbra spicata* L. var. *spicata* on Some Plant Pathogenic Bacteria. Journal of Plant Diseases and Protection, 279 (3), 279-284.

[14] Önen, H. (2003) Bioherbicidal Effects of Some Plant Essential Oils. Turkey Herbology Journal. 6(1), 39-47. (in Turkish).

[15] Ravid, U., Putievsky, E. (1985) Composition of essential oils of *Thymbra spicata* and *Satureja thymbra*. - Chemotypes, Planta Med. 4, 337-338.

[16] Zeybek, U., Haksel, M. (2011) Important medicinal plants and their uses in Turkey and the World. ALFA Printing and Distribution Ltd. 112-115. İzmir. (in Turkish).

[17] Tonçer, Ö., Kızıl, S. (2005) Determination of Yield and Components in Wild Thyme (Thymbra spicata L. var. spicata) as Influenced by Development Stages. Horticultural Science (HORTSCI). 32(3), 100-103

[18] Özderin, S., Fakir, H. Dönmez, İ.E. (2014) Determination of Essential Oil Ratio and Components of Some Thyme Species Naturally Distributed in Muğla-Ula Region, II. National Mediterranean Forest and Environment Symposium, Isparta. (in Turkish) 96-103.

[19] Toncer, O., Karaman, S., Diraz E., Sogut T., Kizil, S. (2016) Diurnal Variation Effects in Essential Oils of Wild Thyme (*Thymbra spicata* var. *spicata* L.) Under Cultivation Conditions. 19 (8), 2037-2048

[20] Tümen, G., Ermin, N., Özek, T., Kürkçüoglu, M., Baser, K. H. C. (1994) Composition of Essential Oils from Two Varieties of *Thymbra spicata* L. Journal of Essential Oil Research. 6(5), 463-468.

[21] Kızıl, S., Toncer, O., Dıraz, E., Karaman, S. (2015) Variation of Agronomical Characteristics and Essential Oil Components of Zahter (*Thymbra spicata* L. var. *spicata*) Populations in Semi-Arid Climatic Conditions. Turk Journal Field Crops. 20(2), 242-251

Received: **15.11.2019**
Accepted: **27.02.2020**

CORRESPONDING AUTHOR

Dogan Arslan
Department of Field Crops,
Faculty of Agricultural,
Siirt University
56000 Siirt – Turkey

e-mail: darslan23@gmail.com
doganarslan@siirt.edu.tr

© by PSP Volume 29 – No. 05/2020 pages 3818-3826 Fresenius Environmental Bulletin

RESEARCH ON A NOVEL EVALUATION CRITERION OF RURAL PUBLIC SPACE ENVIRONMENTAL CAPACITY BASED ON AHP FUZZY METHOD

Bo Han*, Jia Yu

College of Architecture and Civil Engineering, Qiqihar University, Qiqihar Heilongjiang 161006, China

ABSTRACT

The environmental capacity of public space is an important part of rural construction, which directly affects the construction of rural construction and social stability. Therefore, the AHP (Analytic Hierarchy Process) fuzzy method based on the evaluation method of the rural public space capacity in the cold region was studied. When the AHP analysis method was used to determine the weights of indicators at all levels, the importance of the pair-based evaluation indexes was evaluated with the Delphi method and expert opinions, and the judgment matrix of the evaluation index of the rural public space environmental capacity was constructed. The fuzzy comprehensive evaluation method is adopted to obtain relevant factors on the basis of layer upon layer extrapolation, and to obtain the influence degree of social and economic aspects of the environmental capacity of the public space in the cold countryside. In other words, the weight of the evaluation index of the environmental capacity of the public space in the cold countryside is calculated and the consistency test is carried out. According to the index weight, this paper constructs the evaluation index system of the public space environmental capacity of the villages in the cold region, which is mainly composed of four evaluation systems of society-nature-economy-resource, and adopts this system to evaluate the environmental capacity of the public space of the villages in the cold region. The experimental results show that the proposed method can effectively evaluate the environmental capacity of rural public space in cold regions, and the stochastic consistency ratio and calculation time of the judgment matrix are the shortest, and the index weight value has the best reliability.

KEYWORDS:
AHP fuzzy method, cold country, public space, index weight, environmental capacity

INTRODUCTION

The village refers to a rural settlement with a certain population and land use size [1] and specific economic, social and natural landscape characteristics. The cold region of northern China has its own unique climatic characteristics. The climatic characteristics are mainly characterized by low temperature, more snowfall, less sunshine, and shorter nights [2]. In China, the proportion of cold cities in the northeast and north China is relatively high. The most typical cities in China are Harbin, Qiqihar, Changchun and Shenyang. The villages on the outskirts of these typical cold cities are cold villages.

Due to the cold climate, backward economic development and the lag of rural planning and construction, China's coldland villages are becoming more and more aging. As early as 1990, the World Health Organization proposed a development strategy of "healthy aging" [3]. The purpose is to delay the development of middle-aged aging, and promote the mental health and physical health of the elderly. The opening of the public space in the cold countryside not only provides the elderly with a place for outdoor sports, but also enables the elderly to relax and relieve stress in the public space environment. It also strengthens the communication between the elderly and the open contact of the elderly through the public space. The elderly open to the public through the open space of the public space, improve physical fitness, strengthen daily communication, and actively participate in old age activities, which can not only help to promote the mental health and physical health of the elderly, but also promote social health. [4].

The cold climate has certain influence on the rural public space. The impact has advantages and disadvantages. In the cold environment, the residents create the spatial vocabulary of the cold country in the process of resisting the cold climate. Besides, coldland villages can strengthen the ice and snow culture, create ice and snow landscapes, promote ice and snow activities according to their climatic characteristics to attract foreign tourists to visit, result in changing the appearance of cold rural areas, and promoting local economic development. The disadvantages is that due to the large tempera-

ture drop in winter and the frequent occurrence of rain and snow, in this cold environment [5], the travel rate of rural residents is reduced, and recreational activities are also significantly reduced, so the use rate of facilities in public spaces is reduced. At the same time, the maintenance of public space facilities is more difficult. The greening plants in the public space of the cold rural areas are dying with the temperature drop, and the soil is also frozen, and the overall vitality of the cold rural areas is declining. The species is relatively simple. After the invasion of cold air, plants appear to be broken, dead, frostbitten, etc. [6]. The rural landscape has become monotonous. And with the opening of the public space in the cold countryside, the pollution of the environment is intensified. Based on the premise of human development and natural ecological balance, the public space of the cold rural area can accommodate the maximum load value of pollutants, which is the public space environment capacity of the cold rural areas. The capacity of pollutants in public spaces in rural areas is limited. The size of the space, the characteristics of each environmental element, and the physical and chemical properties of the pollutant itself directly affect the size of the environmental capacity [7]. The larger the public space, the larger the environmental capacity. At the same time, the more unstable the physical or chemical properties of the pollutant, the greater the capacity of the environment.

The evaluation process of environmental capacity is complex. In order to effectively evaluate the environmental capacity of rural public space in cold regions, this paper proposes a method for estimating the capacity of rural public space environment based on AHP fuzzy method. This method can not only effectively evaluate the public space of cold rural areas. Compared with other evaluation methods, it has the advantages of small calculation time, low calculation repetition rate, and small random consistency ratio, and the evaluation quality is high.

MATERIALS AND METHODS

Using AHP analysis to determine the weight of indicators at all levels. Analytic Hierarchy Process, also known as AHP is the method of dividing decision-related elements into multiple levels, such as goals, plans, and criteria, and performing qualitative and quantitative analysis on multiple levels [8]. The analysis method can not only analyze complex decision problems, but also mathematically process the thinking process of decision making, and use a small amount of quantitative information during the period based on the intrinsic properties and internal relations of the problem. Therefore, the analytic hierarchy process is applicable to the environment in which decision results cannot be accurately measured.

(1) Constructing a judgment matrix for hierarchical ordering and consistency checking. 1) Construct a judgment matrix. In the field of analytic analysis, researchers usually obtain the element value of the judgment matrix by their own experience [9]. Then they can understand the evaluator's judgment on the importance of each level of indicators according to the value of the judgment matrix element, and the integer value within 10 and the reciprocal scale value. The method combines the Delphi method, and on the basis of consulting experts, the importance evaluation of the two-two evaluation indicators is completed, and the judgment matrix structure of the rural space public space environmental capacity evaluation index is realized. 2) The operation judges the matrix feature vector value and the maximum eigenvalue. Suppose that the judgment matrix has an element i [10] on any row, and the product of the multiplication (Pi) of the elements (i) is expressed as:

$$P_i = \prod_{j=1}^{n} a_{ij} \tag{1}$$

The n root of the root P_i can be expressed as:

$$\overline{Q}_i = \sqrt[n]{P_i} \tag{2}$$

$\overline{Q}_i$ is a vector, and can be expressed as $\overline{Q}_i = \left(\overline{Q}_1, \overline{Q}_2, ..., \overline{Q}_n\right)$, after the vector is normalized, the formula is obtained:

$$Q_i = \frac{\overline{Q}_i}{\sum_{i=1}^{n} \overline{Q}_i} \tag{3}$$

$Q = \left\{Q_1, Q_1, ..., Q_n\right\}$ is called characteristic vector value.

Adopted $\delta_{\max}$ as the largest eigenvalue of the judgment matrix, and the maximum eigenvalue can be expressed as:

$$\delta_{\max} = \sum_{i=1}^{n} \frac{\left(AQ\right)_i}{nQ_i} \tag{4}$$

The element $\left(AQ\right)_i$ in equation (4) can be seen as the i th element in AQ.

(2) Fuzzy comprehensive evaluation. Fuzzy comprehensive evaluation method is the method of fuzzy mathematics which is used for the things that affect many factors and reflects the influence of various factors affecting the upper event factors. The method obtains the influence degree of relevant factors on the social and economic aspects of the overall target on the basis of layer-by-layer push [11], and quantifies relevant factors to promote the

realization of fuzzy comprehensive evaluation of rural public space environmental capacity.

1) Establish an evaluation target indicator set and an evaluation target set. Construct a set of evaluation indicators for public space environmental capacity in rural areas, which can be expressed as $M=\{m_1,m_2,...,m_n\}$. Construct a target set of environmental capacity assessment for rural public space in cold regions, which can be expressed as $H=\{h_1,h_2,...,h_n\}$.

Through the target set, the state of the public space environment capacity of the cold rural areas can be determined, and the three levels of excellent, good and bad are respectively represented by I, II and III, and the scores of the three levels are 90, 60, 30 respectively. The cold space rural public space environmental capacity assessment target set can be expressed as: $H=\{h_1,h_2,...,h_n\}=\{excellent,good,bad\}$. 2) Single factor fuzzy evaluation analysis. Analysis of a single indicator m_i and judge the evaluation object's program to evaluate the membership of each element of the target set, this process is called single factor fuzzy evaluation analysis. Choosing the appropriate membership degree can promote the realization of fuzzy comprehensive evaluation [12]. By analyzing the characteristics of rural public space environmental capacity index, the rural spatial public space capacity index is divided into qualitative evaluation index and quantitative evaluation index. The evaluation index is based on the membership function of the evaluation index [13]. Suppose a membership function is $\alpha_{ij}(y_i)$, and the membership function represents the degree to which the evaluation index x_i belongs to the standard value y_j and satisfies $\alpha_{ij}\in[0,1]$. When the standard function of the membership value increases with the increase of the index, the membership function curve of the rising trapezoidal distribution is most suitable. When the standard function of the membership value increases with the decrease of the index, the membership function curve of the descending trapezoidal distribution is most suitable [14]. So the expression of the membership function is:

$$\alpha_{ij}(y_i)=\begin{cases}(y_{j-1}-x_i)/(y_{j-1}-y_i), x\in[y_i,y_{i-1}]\\(x_i-y_{j+1})/(y_j-y_{i+1}), x\in[y_i,y_{i+1}]\\0\end{cases} \quad (5)$$

3) The total evaluation matrix calculation. After determining the value of each evaluation index, the membership degree of the relevant indicator belongs to different levels according to each evaluation index value, and the membership degree can also be regarded as a total evaluation matrix which can be expressed as:

$$D=\begin{pmatrix}\alpha_{11},\ldots,\alpha_{1m}\\ \ldots\ ,\ \ ...,\ \ \ ...\\ \alpha_{z1},\ldots,\alpha_{zm}\end{pmatrix} \quad (6)$$

In equation (6), the membership function α_{ij} represents the degree to which the evaluation index x_i belongs to the standard value y_i; m and z represent the number of levels and the number of evaluation indicators, respectively.

4) Fuzzy comprehensive evaluation. First set a vector C, then the solution formula of the vector C can be expressed as:

$$C=Q\times D=(Q_1,Q_2,...,Q_n)\begin{pmatrix}\alpha_{11},\ldots,\alpha_{1n}\\ \ldots\ \ ,...,\ \ \ ...\\ \alpha_{z1},\ldots,\alpha_{zn}\end{pmatrix}=(c_1,c_2,...,c_n) \quad (7)$$

In equation (7), Q and D represent the weight coefficient vector and the total evaluation matrix, respectively, and satisfy $\max(c_1,c_2,...,c_n)=c_j$. j represents the state level of the public space environment capacity of the cold country.

In the vector formula C, c_j is the degree of membership of the public space environment capacity state in the cold country.

The process of change c_j is the process of changing the state of the public space environment in the cold rural areas. Finally, the index weights need to be obtained [15], and the index weights are solved in the process of membership degree of each level in the evaluation results. Since each level of the cold rural public space environmental capacity evaluation index has its own state level score, the average weighting of the scores for each level is required, and the formula can be expressed as:

$$\beta_j=\frac{c_j^k}{\sum_{j=1}^{n}c_j^k},\ j=1,2,...,n \quad (8)$$

In the formula of the weighted average solution, it will be regarded $\beta_1,\beta_2,...,\beta_n$ as a set of weights $\beta_j\in(\beta_1,\beta_2,...,\beta_n)$, and each level of the weight of the group will be given the same level parameter [16-18], and the level parameter can be set as u_j and the final result of weight q can be calculated by the following formula:

$$q = \sum_{j=1}^{n} \beta_j u_j \quad (9)$$

Construction of evaluation index system. Based on the results of the index weights obtained above, combined with the actual situation of the rural public space and the traditional social-natural-economic-resource system evaluation system, the cold space rural public space environmental capacity evaluation index system is constructed (Figure 1).

In Figure 1, the first-level indicators are social environmental capacity, natural environmental capacity, economic environmental capacity, resource-environmental capacity, and the secondary indicators are evaluation indicators such as population density, suitability of livelihood methods, ethnic fitness, and water use conditions. The population density of the cold rural areas, the adaptability of livelihood methods, the national fitness and the water use conditions constitute the social environmental capacity [19], and the social environmental capacity also reflects the social inclusiveness of the rural public space in the cold regions. The climate suitability, planting suitability, water environment quality and ecological environment of the coldland villages constitute the natural environment capacity, reflecting the suitability of the natural environment of the cold rural public space. Per capita GDP, per capita grain production, per capita net income, income structure constitute economic environment capacity, measure the development of related industries in rural public space while per capita arable land, per capita construction land, and per capita water resources constitute resource environmental capacity [20]. These parameters measure the extent to which land resources and water resources limit agricultural development.

After determining the set of reviews for the comprehensive evaluation results, the grading criteria for the evaluation can be established, as shown in Table 1.

TABLE 1
Judgement level quantization table

Level	Capacity	Score
I	Excellent	90
II	Good	60
III	Bad	30

When scoring the relevant indicators in the constructed cold space rural public space environmental capacity evaluation index system, the quantitative indicators are classified into I, II, and III according to the above criteria, and the relevant scores are 90, 60, and 30 respectively.

RESULTS AND ANALYSIS

Taking Suibin County in Heilongjiang Province as the research area, the landscape of Suibin County has its own characteristics, and its whole is inclined to the northwest, with an average elevation of 1473.5 meters. The southeastern part of Suibin County is an earth-rock forest area, the west is a loess hilly area, and the riverside is a river valley area. Its annual average temperature, average

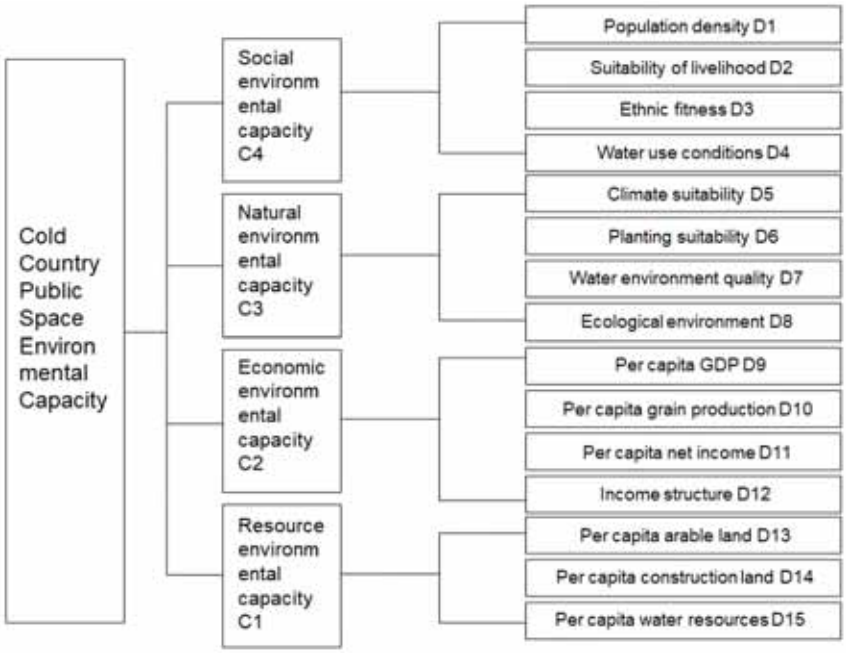

FIGURE 1
Evaluation index system of public space environmental capacity in cold rural areas.

rainfall, and annual sunshine hours are 9°C, 688.4mm, and 2401.37h, respectively. It is a temperate continental climate and belongs to the cold country of China.

Comprehensive evaluation of environmental capacity of rural public space in cold regions. The four weight values for the social environmental capacity, natural environmental capacity, economic environmental capacity, and resource environmental capacity of Suibin County at this time are 0.12, 0.22, 0.32, and 0.34, respectively. The AHP fuzzy method is used to determine the weight of the index layer of the four weight values, and based on this, the evaluation matrix is constructed. The matrix feature vector is obtained by the evaluation matrix. Table 2 to Table 5 are the index weight calculation results.

The consistency check of the social environmental capacity index weight, the natural environment capacity index weight, the economic environment capacity index weight, and the resource environmental capacity index weight of the above Suibin County is completed. Since the matrix is established as a consistent matrix, the test process usually uses the judgment matrix. The random consistency ratio is used as a test indicator.

The random consistency ratio of the judgment matrix L_F is:

$$L_F = \frac{\omega - q}{q(t-1)} \quad (10)$$

ω is the number of iterations in the calculation, t is expressed as a parameter for calculating the usage time. The larger the value L_F, the more serious the inconsistency of the matrix. Therefore, when $L_F < 0.098$ is satisfied, it can be considered that the consistency test result is satisfactory. If it is not met, the consistency test result is not satisfactory, and the weight coefficient of the relevant indicator needs to be changed again.

It can be seen from the calculation that the values of C1 to C4 are 0.022, 0.057, 0.001, and 0.010, respectively. These values fit $L_F < 0.098$, thus, it is considered that the weight values of C1 to C4 are highly reliable.

A comprehensive evaluation of the public space environmental capacity of Suibin County was carried out, and the results are shown in Table 6. Table 6 Comprehensive evaluation results of public space environmental capacity in Suibin County.

TABLE 2
Social environmental capacity indicator weights

C1	D1	D2	D3	D4	Weight
D1	0.98	2.98	1.98	2.48	0.410231
D2	0.31	0.98	0.23	0.48	0.078218
D3	0.48	3.98	0.98	1.23	0.255613
D4	0.38	1.98	0.78	0.98	0.171032

TABLE 3
Natural environment capacity index weights

C2	D5	D6	D7	D8	Weight
D5	0.98	0.38	1.48	1.18	0.196766
D6	2.48	0.98	1.98	1.48	0.369845
D7	0.65	0.48	0.98	1.98	0.195186
D8	0.81	0.65	0.48	0.98	0.152759

TABLE 4
Economic environment capacity index weights

C3	D9	D10	D11	D12	Weight
D9	0.98	0.78	0.88	1.18	0.214742
D10	1.23	0.98	1.18	1.98	0.300809
D11	1.09	0.81	0.98	1.48	0.243505
D12	0.81	0.48	0.65	0.98	0.156528

TABLE 5
Resource environment capacity indicator weights

C4	D13	D14	D15	Weight
D13	0.98	1.65	1.18	0.383665
D14	0.58	0.98	0.48	0.193872
D15	0.81	1.98	0.98	0.360130

TABLE 6
Comprehensive evaluation results of environmental capacity of public space in Suibin County

Standard floor	Indicator layer	Membership	Score	Evaluation value
C1	D1	excellent	90	75
	D2	good	60	
	D3	excellent	90	
	D4	good	60	
C2	D5	excellent	90	75
	D6	good	60	
	D7	good	60	
	D8	excellent	90	
C3	D9	poor	30	37.5
	D10	good	60	
	D11	poor	30	
	D12	poor	30	
C4	D13	excellent	90	80
	D14	good	60	
	D15	excellent	90	

TABLE 7
Comparison of performance of various methods

Methods		C1	C2	C3	C4	Average
SWOT	Calculating time /ms	12	10	11	13	11.5
	Calculation repetition rate /%	67.8%	54.2%	59.0%	61.3%	60.60%
	Random consistency ratio	0.12	0.10	0.13	0.12	0.12
BCG	Calculating time /ms	10	12	9	10	10.25
	Calculation repetition rate /%	20.1%	22.8%	19.3%	16.4%	19.7%
	Random consistency ratio	0.096	0.10	0.093	0.11	0.10
The method in this study	Calculating time /ms	6	4	7	5	5.5
	Calculation repetition rate /%	1.20%	3.10%	0.20%	0.90%	1.35%
	Random consistency ratio	0.022	0.057	0.001	0.010	0.0225

It can be seen from Table 6 that the analysis of the comprehensive capacity of public space environment in Suibin County, the weight of social environmental capacity index, the weight of natural environment capacity index, and the weight of economic environment capacity index are all above 60, which is in line with the requirements.

(1) Social environment: Since the setting and expansion of public space are carried out in Suibin County, there will be no religious conflicts and cultural background changes due to geographical differences. The setting and expansion of public space in Suibin County will adapt to the social environment. The social environment is inclusive for immigrants;

(2) Natural environment: basically, no change, good suitability;

(3) Economic environment: Table 6 shows that the economic environmental capacity index of Suibin County is 37.5. The low score is because the overall situation of economic development is not ideal due to its own topography. The planned per capita GDP and per capita net income are quite different from the national average. The income structure is not diversified in large cities, and its income source is single. Moreover, the industrial structure of Suibin County is not much different from the extensive economy dominated by traditional agriculture. The regional economy still needs continuous reform;

(4) Resource and environment aspects: Due to heavy snowfall in winter, fertile land, abundant water resources, and vigorous development in agriculture, the resources and environment fully meet the requirements of the public space environment capacity of Suibin County.

Method reliability verification. In the above test on the comprehensive evaluation of the public space environmental capacity of Suibin County, it is mentioned that the values L_F of C1~C4 are 0.022, 0.057, 0.001, and 0.010, respectively, which are all satisfied $L_F < 0.098$. It can be considered that the weight values of C1~C4 are highly reliable. In order to verify the performance advantages of the proposed method, the SWOT analysis method, the BCG matrix method and the method of this paper are used to calculate the random consistency ratio of C1~C4. The calculation results are shown in Table 7.

In order to express the content of Table 7 more intuitively, the calculation time, calculation repetition rate, and random consistency ratio of different methods are plotted, as shown in Figure 2 to Figure 4.

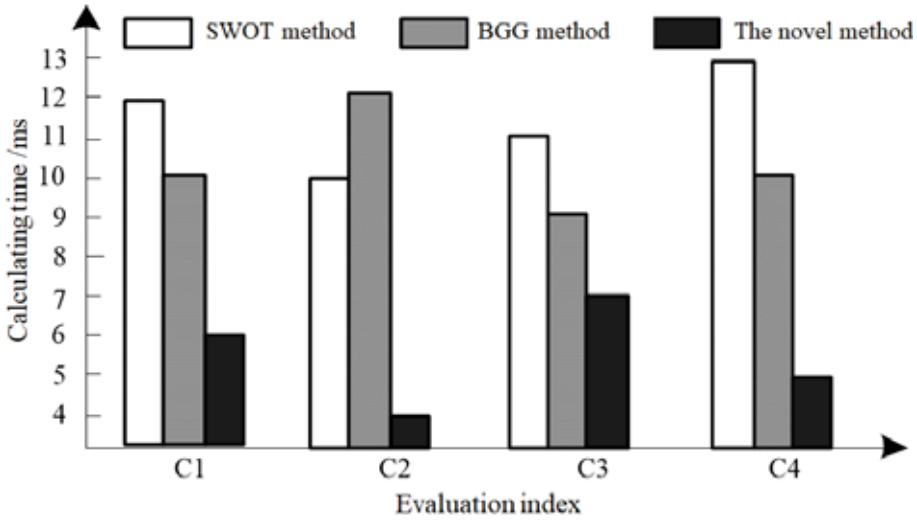

FIGURE 2
Calculation time using different methods.

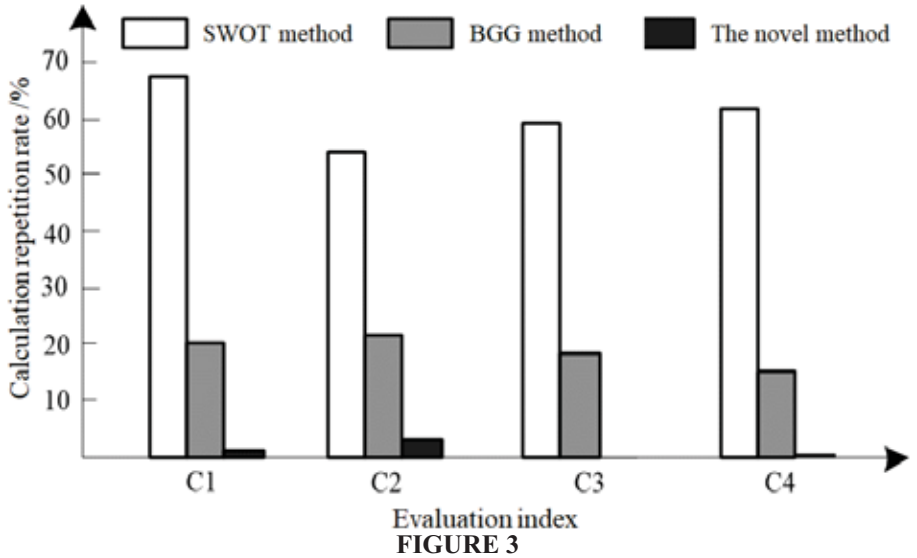

FIGURE 3
Calculated repetition rate using different methods.

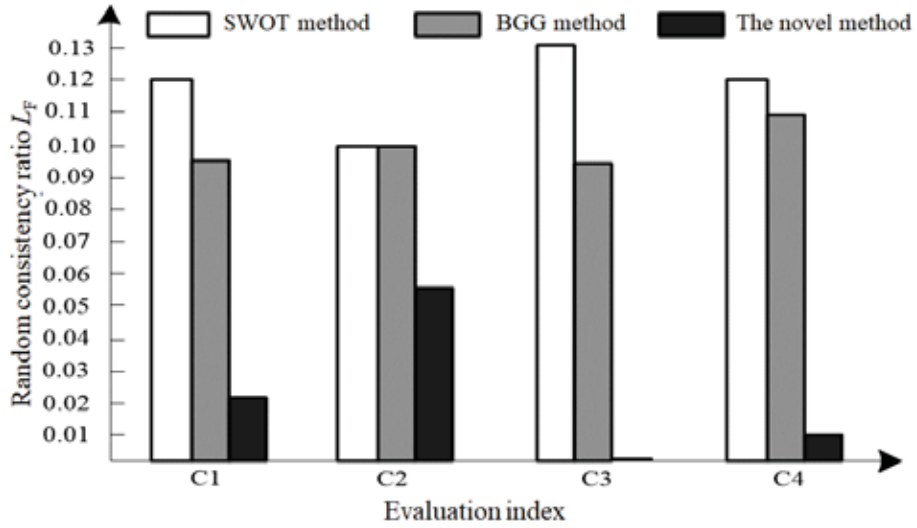

FIGURE 4
Random consistency ratio using different methods

The results show that the method of calculating the random consistency ratio L_F has the shortest time and the minimum random consistency ratio is kept below 0.05, which is completely satisfied $L_F < 0.098$, and the weight coefficient of the relevant index does not need to be changed again. Therefore, the calculation repetition rate is also minimal and can be basically ignored. It can be seen that the method can not only shorten the calculation time, but also avoid the waste of resources due to repeated calculations, and the reliability of the evaluation index weight value is strong, which can realize the high-quality evaluation of the rural public space environment capacity.

CONCLUSIONS

The construction and expansion of rural public space in the cold region is conducive to the daily communication and physical health of the elderly. Therefore, the evaluation of the environmental capacity of the rural public space in the cold region is particularly important. However, due to the complex dynamic system of the public space environment capacity of the cold country, the dynamic system is characterized by multi-factor, multi-level and multi-objective. The single analysis method often cannot satisfy its systemic, comprehensive and accurate. Therefore, this paper combines the fuzzy comprehensive evaluation method and the analytic hierarchy process to use the AHP fuzzy method to calculate the social environment capacity, economic environment capacity, natural environment capacity and resource environment capacity as a whole, and dynamically calculate the weight of the rural public space environmental capacity evaluation index. The calculation is also a kind of quantitative calculation, and based on the calculation results, the evaluation index system of rural public space environment capacity is constructed, which effectively evaluates the environmental capacity of rural public space in the cold area. The evaluation process not only shortens the calculation time, but also the index weight. The value is highly reliable and the evaluation quality is high.

ACKNOWLEDGEMENTS

The authors would like to express their sincere thanks to all the persons who have contributed to this work.

REFERENCES

[1] Luo, J., Zhou, J. (2015) Evaluation of Major Mining Economic Zones of China and Their Future Development Strategy. China Soft Science. 33(6), 175-183.
[2] Zhang, L., Qi, Y., Li, H., Xu, X., Wang, X. (2015) Water quality and water environmental capacity for the small subsidence lakes in the Huainan and Huaibei coal mine areas, Anhui Province. Chinese Journal of Ecology. 34(4), 1121-1128.
[3] Zhang, G., Li, L., Wang, Y., Xue, C., Wang, J. (2016) The Eco-tourism Environmental Capacity of the Shahu Lake Scenic Area in Ningxia, China. Journal of Desert Research. 36(4), 1153-1161.
[4] Ke, L., Wang, Q., Xu, L., Jiang, X., Yang, S. (2015) The coastwise surplus water environment capacity computing model based on GIS. Marine Sciences. 39(7), 112-117.
[5] Du, P. (2015) Analysis and Study of the PEIA for Intercity Railway Network. Journal of Railway Engineering Society. 32(2), 93-96.
[6] Wang, S., Qi, S., Yu, D., Zhang, Y., Wan, L. (2015) Forecast and evaluation of water environment quality based on WASP model: a case study on Harbin section of Songhua River. Journal of Natural Disasters. 72(1), 89-92.
[7] Bai, H. (2016) Study on water environmental carrying capacity evaluation and gross control based on environmental capacity. Environmental Pollution and Control. 38(4), 103-106.
[8] Wang, Y., Gao, J., Liu, Z., Zhang, Z. (2016) Pollution Load and Environment Capacity in Tonghu Lake Basin. Wetland Science. 14(3), 354-360.
[9] Zhang, Y., Cao, W., Chen, J., Li, Y., Wang, Z., Huang, W. (2015) Study on Water Environmental Capacity of Reservoired River in Jiulong River Basin. Journal of Fujian Normal University (Natural Science Edition). 12(6), 85-89.
[10] Liu, H., Cai, B. (2018) Advance in Research and Application on Aquaculture Carrying Capacity. Progress In Fishery Sciences. 39(3), 44-56.
[11] Chen, L., Zeng, W., Wu, H. (2015) Research on the Seasonal Water Environmental Capacity for Weihe River. Yellow River. 37(2), 72-74.
[12] Zheng, W. (2019) The coordination degree of economic environment and water ecological civilization of urban scale expansion: a case study of Guangdong Province. Jiangsu Agricultural Sciences. 47(10), 330-335.

[13] Lu, Y., Sun, W. (2017) Estimation of NO2 remainder atmospheric environmental capacity and layout optimization of emission sources based on CALPUFF model: A case study in Hefei. Environmental Pollution and Control. 39(12), 1358-1362.
[14] Wen, J., Yang, C., Fu, Y. (2017) Study on allocation of water environmental capacity of Huntaihe River Watershed. Water Resources and Hydropower Engineering. 48(11), 150-155.
[15] Nadi, S., Samiei, M., Salari, H. (2017) A New Multi-Criteria Evaluation Model Based on the Combination of Non-Additive Fuzzy Ahp, Choquet Integral and Sugeno λ-MEASURE. 44(15), 423-428.
[16] Zhao, X., Ji, Y., Li, X. (2018) Evaluation of Post-grouting Bearing Capacity of Cast-in-situ Bored Pile Based on Self-balance Method. IOP Conference Series Earth and Environmental Science. 189(11), 22-28.
[17] Samuel, O., Asogbon, G., Sangaiah, A. (2017) An Integrated Decision Support System Based on ANN and Fuzzy_AHP for Heart Failure Risk Prediction. 68(17), 163-172.
[18] Peng, H., Liu, Y., Gao, X. (2017) Calculation of intercepted runoff depth based on stormwater quality and environmental capacity of receiving waters for initial stormwater pollution management. 24(31), 1-9.
[19] Li, S., Yang, T., Zhu, S. (2017) A method for screening copper-tolerant rice (Oryza sativa L.) cultivars based on hydroponic experiments and cluster analysis. International Journal of Phytoremediation. 19(12), 1093-1099.
[20] Zhu, J., Wang, E., Sun, W. (2019) Application of Monte Carlo AHP in ranking coastal tourism environmental carrying capacity factors. Asia Pacific Journal of Tourism Research. 24(7), 644-657.

Received: **21.11.2019**
Accepted: **20.02.2020**

CORRESPONDING AUTHOR

Bo Han
College of Architecture and Civil Engineering,
Qiqihar University,
Qiqihar Heilongjiang 161006 – China

e-mail: 3613546205@qq.com

© by PSP Volume 29 – No. 05/2020 pages 3827-3832 Fresenius Environmental Bulletin

MONITORING DEFORESTATION BY MULTITEMPORAL DATA USING REMOTE SENSING TECHNOLOGIES: A CASE STUDY OF SINOP-TURKEY

Asli Sabuncu*

Kandilli Observatory and Earthquake Research Institute, Geodesy Department, Bogazici University, Istanbul, Turkey

ABSTRACT

This paper intends to map and monitor Land Use Land Cover (LULC) changes and forest degradation derived from Landsat satellite images using remote sensing technologies. For this aim, Sinop province of Turkey was selected as the case study area. LULC changes and forest degradation have been studied using Landsat data sets between the years 1987-2019. 3 Landsat 5 TM imageries were dated 27 July 1987, 06 July 1997 and 16 June 2007 and 2 Landsat 8 OLI/TIRS imageries were dated 13 July 2017 and 10 July 2019 were used in order to analyze the data. In this context, Support Vector Machine algorithm which is the most trusted supervised classification method and Normalized Difference Vegetation Index (NDVI) were applied to all Landsat data to demonstrate forest and built-up changes in every decade. Seven land use classes were determined. These classes were; Waterbody, agriculture, sand, built-up areas, vegetation, forest and bare soil/rock. Noteworthy changes were observed in the classes of built-up areas and forest from the year of 1987 to 2019. Besides, accuracy assessments were carried out and the kappa statistics for Landsat 5 and Landsat 8 data were calculated 0.94, 0.99, 0.89, 0.98 and 0.99 respectively. Unfortunately, in the case study area, forest degradation will be continued due to the installation of nuclear power plant station in the following years.

KEYWORDS:
LULC, Change Detection, Deforestation, Sinop-Turkey, Support Vector Machine Classification, Landsat, Forest degradation

INTRODUCTION

Forests play significant role in affecting the Earth's climate due to the importance of carbon deposition in terms of globally. Plants and soils in the forest manage and regulate the global carbon balance by holding carbon dioxide (CO_2) through photosynthesis and releasing it through the respiratory tract. In general, loss of biodiversity, disruption water cycle, soil erosion and global warming are extremely severe ecological problems which are results of deforestation and forest degradation. Forests are playing significant role not only animals but also for humans and their following generation in terms of ecological issues. Since 1960s' over the half of the tropical forests have been destroyed and deforestation rate has been increased rapidly. In the last decade, 13 million of ha/year of forests have been deforested in the world and the rate of the forest degradation is extremely high [1]. In Turkey, the total amount of forest and forest areas are 27 million ha and only 1.6% of this figure is under protection. Turkey is among the richest countries in the world in terms of different plant species. An estimated more than 10,000 vascular plants live in the territory of Turkey and about 34% of them were classified as endemic species [2-3-4].

The most important algorithm to detect Land Use Land Cover changes over time is remote sensing nowadays. In the literature, remote sensing approaches have been used in order to detect land use land cover changes in time and scale in many significant scientific papers. Besides using remote sensing approaches in LULC changes over time gives opportunity to get results with low costs, less time consumption and better accuracy. This technique also allows scientists to update results when the new data is available [5-6-7].

MATERIALS AND METHODS

Study Area and Materials. Sinop province is located among Turkey's most northern tip Inceburun which is surrounded by Kastamonu in the west, Çorum in the south, Samsun in the east and Black Sea in the north. The city is situated between 34°13'59.73" - 35°27'17.83" Eastern Meridians and 41°42'32.61" - 41°20'19.68" Northern Parallels with an altitude of 25m. above sea level. Besides, the province area covers about 5860 km^2 of the total land of Turkey. (Figure 1) Sinop province is dominated densely forested areas and vegetation as it receives highly rainfall during most part of the season. Sinop province has warm and humid weather in summer

with an average daytime 26 celsius and cool and wet weather in winter with an average 5 celsius at the daytime.

Besides, three important nature parks and areas are situated in the border of Sinop province. These are Bozburun Wildlife Development Area; Hamsilos Nature Park, and Sarıkum Nature Reserve [8]. Hamsilos Nature Park or Hamsilos Bay is the only fjord of Turkey which is located near Inceburun. Sarıkum Nature Reserve is one of the most important wetland and lagoon of the Black Sea region which has been declared as Nature Reserve Area. Sinop Province is slated to be the Sinop Nuclear Power Plant which has been started to construct in 2017 and will be completed in 2028. Sinop Nuclear Power Plant will be the Turkey's second nuclear power plant after Akkuyu nuclear power plant established on the Mediterranean coast the province of Mersin. The Nuclear Power plant includes 4 different reactors. The first unit of the construction will be completed by 2023 and the final phase will be finished and activated by 2028. Thus, this construction will be caused important environmental changes and severe ecological disturbance in the study area [9].

During the remote sensing analysis, multi-temporal data were used to detect the extent of forest degradation in the region in the long term. In the analyses, 3 Landsat 5 TM which were dated at 27 July 1987, 06 July 1997 and 16 June 2007 and 2 Landsat 8 OLI/TIRS data which were dated at 13 July 2017 and 10 July 2019 acquired from USGS Archive [10]. These data were used to map and evaluate the decadal land cover changes due to the forest degradation. All optical satellite data belonging to nearly or almost to the same season in order to avoid the seasonal changes as much as possible. Besides all data cloud coverage was lower than 10 %. The specifications of the used satellite images acquired for forest degradation and LULC change detection are given in the Table 1.

Methods. In the literature, there are numerous classification approaches that have been developed and widely used in order to monitoring a great range of ecological problems. In this study, the most trusted and reliable pixel based image analysis classification method which is Support Vector Machine (SVM) algorithm was used. SVM is a machine learning image analysis classification method that is used in many different areas. SVM pixel based classification and spectral vegetation index (NDVI) were the two different steps to evaluate the results of the case study forest degradation quantitatively and qualitatively. All analyses were performed in this study for SVM classification and its accuracy assessment via ENVI version 4.8 (Exelis Vis. Inf.Sol.) and NDVI calculation using ArcGIS v.10.0 (ESRI) software packages.

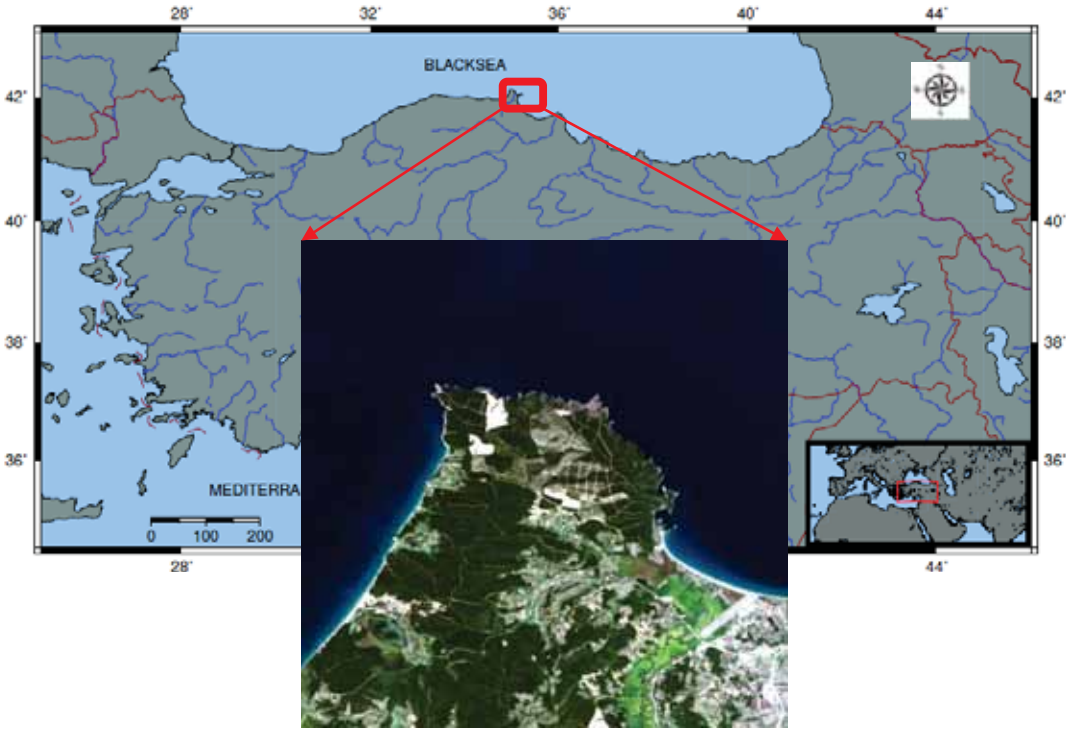

FIGURE 1
The Geographical Location of the Study Area

TABLE 1
The Characteristics of Landsat 5 and Landsat 8 Datasets Used in this Study

	Landsat 5 TM		Landsat 8 OLI/TIRS	
Bands	Spectral Resolution (μm)	Spatial Resolution (m)	Spectral Resolution (μm)	Spatial Resolution (m)
B1	0.45 - 0.52	30	0.435-0.451	30
B2	0.52 - 0.60	30	0.452-0.512	30
B3	0.63 – 0.69	30	0.533-0.590	30
B4	0.76 – 0.90	30	0.636-0.673	30
B5	1.55 – 1.75	30	0.851-0.879	30
B6	10.40 – 12.50	120* (30)	1.566-1.651	30
B7	2.08 – 2.35	30	2.107-2.294	30
B8	-	-	0.503-0.676	15 (Pan.)
B9	-	-	1.363 -1.384	30
B10	-	-	10.60 -11.19	100*
B11	-	-	11.50 -12.51	100*

*TM Band 6 was acquired at 120-meter resolution, but products are resampled to 30-meter pixels.
*TIR bands are acquired at 100 m. resolution, and resampled to 30 min delivered data product.

Image Classification – Support Vector Machine Algorithm. The fundemantal of SVM algorithm is to find an optimal boundary which is represented by a hyperplane in the feature space between two classes due to minimize the classification error [11]. SVM is one of the most known non-parametric classification algorithm that has been performed widely in terms of classification process in remote sensing [12,13,14].

The main LULC classes identified in Sinop Peninsula through the image analysis are Vegetation, Forest, Built-up, Agriculture land, Bare soil and Rocky, Waterbody, Sand. Vegetation cover represents lands with herbaceous types of cover while forest cover represents lands dominated by woody vegetation such as deciduous and evergreen forests. Built-up class is defined as land covered by structures and other man – made structures such as buildings, dams, roads, asphalts. Agriculture land cover represents areas where the dominated fields are related to agriculture. Bare soil and rocky surface represent the lands with exposed soil, rocks etc. which are observed near the sea side in general. Waterbody class is the biggest class that covers the sea, small and big, natural or artificial fresh and salt water bodies in the study area whereas sand class is the smallest one covers the lands with exposed to sands and dune. For the years of 1987-2019, the spatiotemporal changes in the aforementioned features for the case study area are displayed in Figure 2. Moreover, Support Vector Machine supervised classification algorithm was used for quantitative analysis of Landsat 5 TM and Landsat 8 OLI/TIRS datasets. A significant phase for the evaluation of the results of SVM classification process is the accuracy assessment. The classification of accuracy was carried out through the confusion matrix and the overall accuracies and Kappa coefficients of the all datasets are shown in Table 2.

Normalized Difference Vegetation Index (NDVI) Calculation. Green vegetation performs photosynthesis using chlorophyll in its leaves. During photosynthesis, the portion of the

TABLE 2
SVM Classification Accuracy Assessment

Date	Overall Accuracy (%)	Kappa Coefficient
1987	96.5962	0.9493
1997	99.9103	0.9913
2007	98.5691	0.8923
2017	99.5356	0.9632
2019	99.2969	0.9559

electromagnetic energy from the sun in the wavelength range of 0.63 μm to 0.69 μm corresponding to red light is used. Therefore, a satellite image that measures the reflection of red light will have low numerical values in areas with dense vegetation [15]. Normalized Difference Vegetation Index (NDVI) is the most commonly used index for detecting green vegetation in remote sensing applications and monitoring positive and negative results over time. NDVI is the mathematical expression of near infrared and red band images [16] (Formula 1). NDVI is expressed in the range of [-1 to +1]. In vegetation-intensive regions, NDVI approaches to +1, while vegetation is sparse and in bare soil, the NDVI value moves away from + 1 and approaches zero. NDVI index values of different objects such as cloud, water and snow are close to -1 [17].

$$NDVI = (NIR- Red)/ (NIR + Red) \quad (1)$$

NDVI maps for the case study area of the years 1987, 1997, 2007, 2017 and 2019 were produced. NDVI technique was applied to all data to track vegetation coverage and changes in the case study area for the time period. When the NDVI indexed maps were examined, there was a significant forest degradation between 1997-2019 in the region. The forest degradation has started at

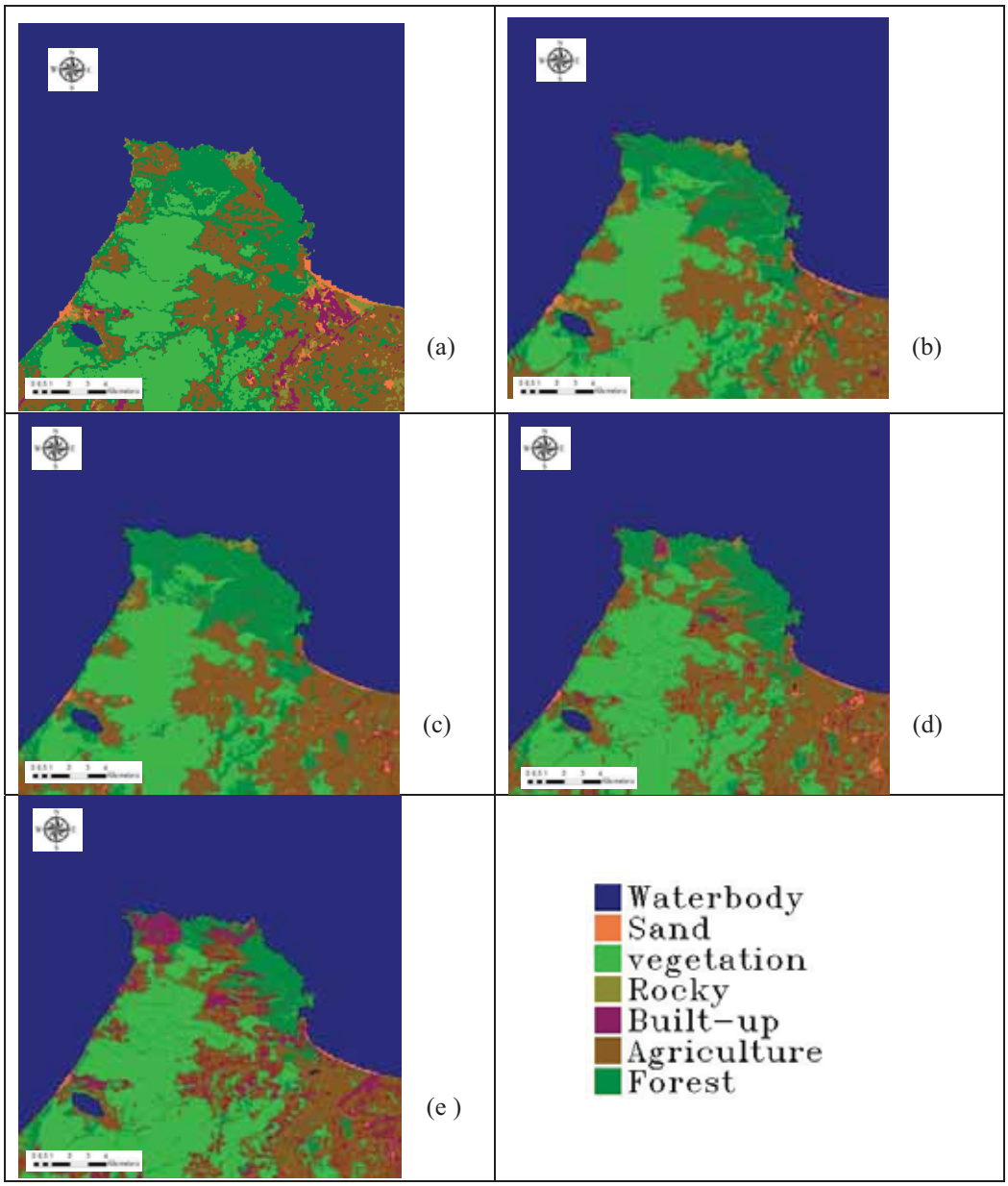

FIGURE 2
LULC Maps of Landsat Datasets (© USGS) Datasets. (a) 1987. (b) 1997. (c) 2007. (d) 2017. (e) 2019. (f) Definition of the Classes

1997 and it has reached at its highest value at 2019 (Figure 3).

RESULTS

This paper used 10-year interval (1987, 1997, 2007, 2017 and 2019) of Landsat data and ancillary NDVI data in order to display the changes in the long run for the case study area. According to LULC change detection analysis and mapping to forest degradation performed for the period of 1987 – 2019, the main change was observed in two classes; forest and built-up. As shown, the findings of this study clearly prove that the negative effects on the forest areas was mainly observed by using satellite images (Table 3). There was a rapid increase in the built-up land cover especially from 2017 to 2019. Analyzing the table 3, it is clearly seen that, forest land cover has been decreased continuously from 1997 to 2019. It was observed that rapid forest degradation occurred in the case study area with a decrease 51 % in forest class and increase 28 % in built-up class from the year 1987 to 2019.

DISCUSSION AND CONCLUSIONS

Forest degradation and deforestation are the most dangerous threat for the forests of the whole world. It is important to monitor, map and assess for-

est loss especially to mitigate degradation in the forest area to take environmentally sensitive decisions. In recent years, remote sensing products such as optical and radar images are useful for accurately mapping land use land cover analysis. Thanks to both types of sensors (optical and radar) have a synoptic view and to produce fast, accurate and periodic data, data analysis can be performed quickly and accurately. Spectral Vegetation index such as NDVI is the most known index among remote sensing approach. NDVI is the best vegetation index in order to detect the healthy vegetation and forest with satellite images. Support Vector Machine is the best algorithm to detect and evaluate the changes over time in specific location in the long run. As shown in this study, the multi-temporal Landsat 5 TM and Landsat 8 OLI/TIRS satellite images cover the Sinop peninsula and its vicinity have been classified in order to detect and evaluate the land use land cover changes and forest degradation which has been occurred in the decadal period from 1987 to 2019. Noteworthy changes were observed in the classes of built-up areas and forest from the year of 1987 to 2019.

Unfortunately, it is highly expected that, deforestation in the case study area will continue and cause urbanization due to the Sinop nuclear power plant installation. When all phases of the power plant construction will finish, it will change the land cover land use in Sinop Peninsula and may lead to inevitable environmental problem.

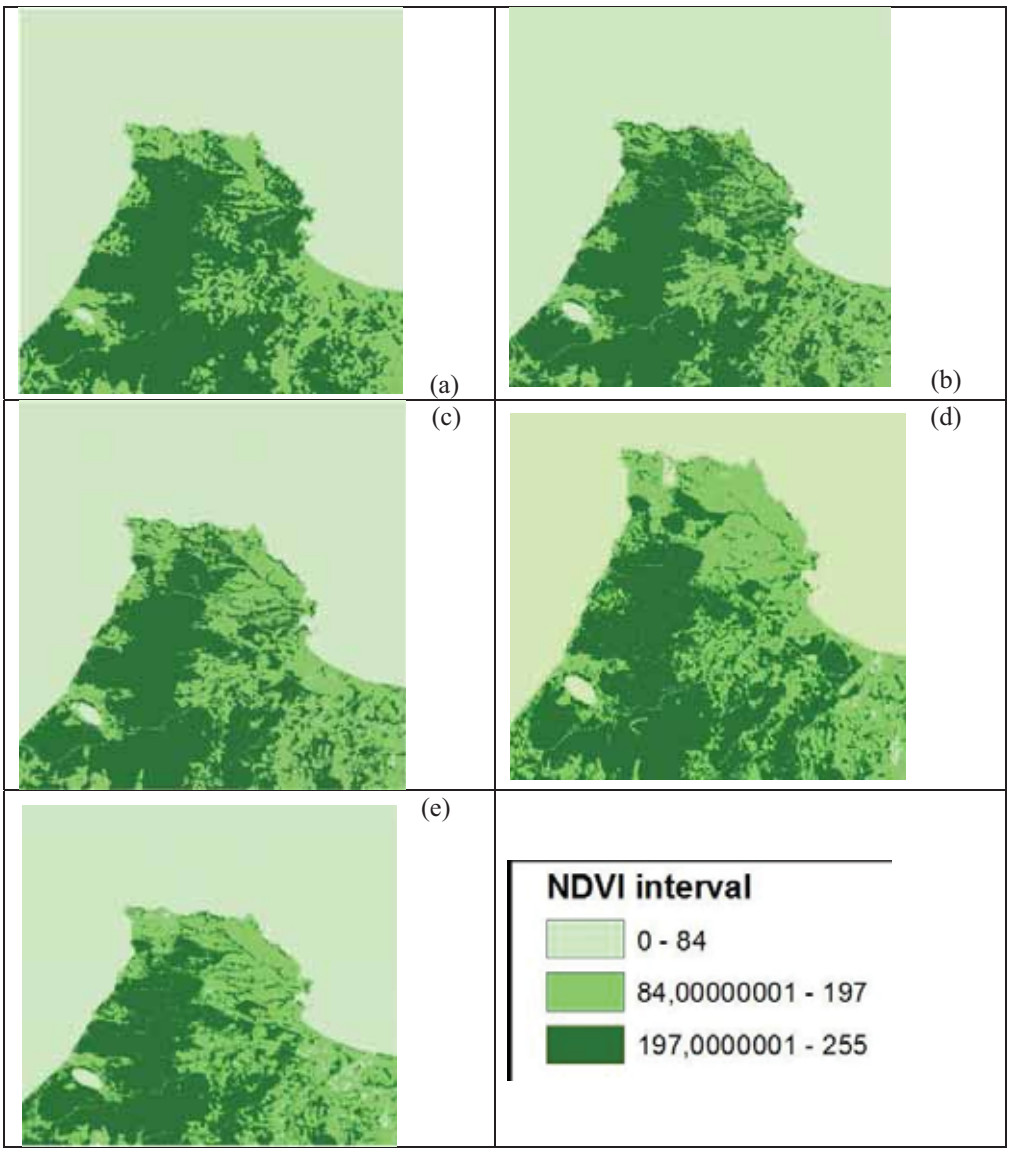

FIGURE 3
The Classification of NDVI (a) 1987. (b) 1997. (c) 2007. (d) 2017. (e) 2019.

TABLE 3
The Total Area Covered (Km^2) by Forest and Built-Up Classes in Sinop Peninsula between the Years 1987 and 2019

Land Cover	1987 (Km^2)	1997 (Km^2)	2007 (Km^2)	2017 (Km^2)	2019 (Km^2)
Forest	41.1876	33.1578	35.9289	21.0438	20.9952
Built-Up	5.0832	2.9646	2.0151	5.4243	18.1953

ACKNOWLEDGEMENTS

The author would like to thank to the United States Geological Survey (USGS) – https://earthexplorer.usgs.gov/ for providing us Landsat 5 TM, Landsat 8 OLI/TIRS and also full archive of Landsat satellite images.

REFERENCES

[1] Moutinho, P. (2012) Deforestation Around the World. Dr. Paulo Moutinho (Ed.), ISBN: 978-953-51-0417-9, InTech.1-372.
[2] Özhatay, N., Kültür, Ş. (2006) Check-list of Additional Taxa to the Supplement Flora of Turkey III. Turkish Journal of Botany. 30, 281-316.
[3] Özhatay, N., Kültür, Ş., Aslan, S. (2009) Check-list of Additional Taxa to the Supplement Flora of Turkey IV. Turkish Journal of Botany. 33, 191-226.
[4] Özhatay, F.N., Kültür, Ş., Gürdal, M.B. (2011) Check-list of Additional Taxa to the Supplement Flora of Turkey V. Turkish Journal of Botany. 35, 589-624.
[5] Jovanovic, D., Govedarica, M., Sabo, F., Bugarinovic, Z., Novovic, O., Beker, T., Lauter, M. (2015) Land Cover Change Detection by Using Remote Sensing: A case Study of Zlatibor (Serbia). Geographica Pannonica. 19(4), 162.
[6] Lambin, E.F., Geist, H.J., Lepers, E. (2003) Dynamics of Land Use and Land Cover in Topical Regions. Annual Review of Environment and Resources. 28(1), 205.
[7] Mukhiddin, J., Alim, P., Sven, F., Johannes, H. (2019) Analysis of Land Use Land Cover Change Detection of Bostanlik District, Uzbekistan Pol. J. Environ. Stud. 28(5), 3235-3242.
[8] T.C. Sinop Valiligi. (2019). http://www.sinop.gov.tr/cografya. Access date: 06/10/2019.
[9] Çolak, E., Chandra, M., Sunar, F. (2019) The Use of Multi-Temporal Sentinel Satellites in the Analysis of Land Cover Land Use Changes Caused by the Nuclear Power Plant Construction. The International Archives of the Photogrammetry, Remote Sensing and Spatial Information Sciences. XLII-3/W8.
[10] USGS (2019) Earth Explorer Web page. https://earthexplorer.usgs.gov. Access date: 22/09/2019.
[11] Vapnik, V.N. (1995) The Nature of Statistical Learning Theory. 2. Springer-Verlag. New York. 1-314.
[12] Mountrakis, G., Im, J., Ogole, C. (2011) Support Vector Machines in Remote Sensing: A Review. ISPRS Journal of Photogrammetry and Remote Sensing, 66 (3), 247-259.
[13] Pal, M., Maxwell, A.E., Warner, T.A. (2013) Kernel-based Extreme Learning Machine for Remote-sensing Image Classification. Remote Sensing Letters. 4 (9), 853-862.
[14] Maxwell, A.E., Warner, T.A., Strager, M.P., Pal, M. (2014) Combining Rapid Eye Satellite Imagery and Lidar for Mapping of Mining and Mine Reclamation. Photogrammetric Engineering and Remote Sensing. 80 (2), 179-189.
[15] Tucker, C. (1979) Red and Photographic Infrared Linear Combination For Monitoring Vegetation. Remote Sensing of Environment. 8, 127-150.
[16] Kandemir E., Research on determining the relationships between NDVI values in remote sensing and species distribution in natural vegetation, Master Science Thesis, Ege University, İzmir, 2010 [in Turkish].
[17] Hatfield, J.L., Kanemasu, E.T., Asrar, G., Jackson, R.D., Pinter, P.J. Jr., Reginato, R.J., Id, S.B. (1985) Leaf Area Estimates from Spectral Measurements Over Various Planting Dates of Wheat. Int. J. Remote Sensing. 6 (1), 67-75.

Received: **23.11.2019**
Accepted: **07.03.2020**

CORRESPONDING AUTHOR

Asli Sabuncu
Kandilli Observatory and Earthquake
Research Institute Geodesy Department
Bogazici University
Istanbul – Turkey

e-mail: asliboun@gmail.com

© by PSP Volume 29 – No. 05/2020 pages 3833-3839 Fresenius Environmental Bulletin

ENVIRONMENTAL QUALITY ASSESSMENT OF GEOPARK BASED ON FUZZY COMPREHENSIVE EVALUATION TAKING BIJIE JIMING SANSHENG GUIZHOU GEOPARK AS AN EXAMPLE

Taian Zuo[1,2,*]

[1]School of Tourism Management and Services, Chongqing University of Education, Chongqing 400067, China
[2]College of Ecological Engineering, Guizhou University of engineering science, Bijie, Guizhou 551700, China

ABSTRACT

Environmental quality is the basis for the survival and development of tourism. The evaluation of environmental quality of geological parks can be carried out from space, time and elements. In terms of spatial regional environmental assessment, most of them focus on the evaluation of geopark attractions or scientific research values. Tourism environmental assessment research has not received widespread attention. Based on the fuzzy comprehensive evaluation system, this paper takes Bijie Jiming Sansheng• Guizhou geopark as an example, and it constructs a geological park environmental quality evaluation index system and discusses the multi-element comprehensive evaluation method of geological park environmental under the extensive investigation and expert group scoring. At the same time, the quantitative quality evaluation of the environment of Jiming Sansheng geopark was carried out.

KEYWORDS:
Geological parks, environmental evaluation index system, fuzzy comprehensive evaluation, Bijie Jiming Sansheng-Guizhou geopark

INTRODUCTION

The geopark environment is a complex environmental system consisting of natural environment, humanistic social environment and tourism business environment with the tourist as the main space unit [1-3]. Whether it can develop healthily, there are the same internal factors and external influences like other things, and the external environment is the basis for the existence of geoparks. Because visitors are increasingly demanding the environment outside the geological resources, especially the urban environment, the social environment, ecological environment and resource environment play an important role in ensuring the development of the geological park [4-7]. The advantages and disadvantages of the external environment have become an important yardstick for directly weighing the competitiveness of geoparks. The scientific evaluation of the geopark environment is the basis for the rational development of geological resources and the sustainable development of address resources, and also the importance of geological resources for sustainable development.

Bijie Jiming Sansheng• Guizhou geopark is located in Linkou Town, Dayin Town, Yanzikou Town and Tuanjie Township, Qixingguan District, Guizhou Province. The total planned area is 116.91 square kilometers (Figure 1). The park consists of Yueliangshan scenic area (39.91 square kilometers), Mianyuhe scenic area (36 square kilometers), and Jiming scenic area [8-9]. Many geological heritage resources such as karst gorges, caves, natural bridge, Tiankeng, peak cluster, karst doom, stone forest and pictographic mountains, and waterscape, geological section, paleontology, environmental geological relics and geological structure relics are as complementary.

Guizhou's landform belongs to the plateau mountains in southwestern China. The terrain is high in the west but low in the east. It is inclined from the central to the north, east and south, with an average elevation of about 1, 100 meters. There are many mountainous areas in Guizhou Plateau. The landforms can be broadly divided into four basic types: plateau, mountain, hill and basin, of which 92.5% are mountainous and hilly. There are many mountains in the territory, and the mountains are stacked on top of each other.

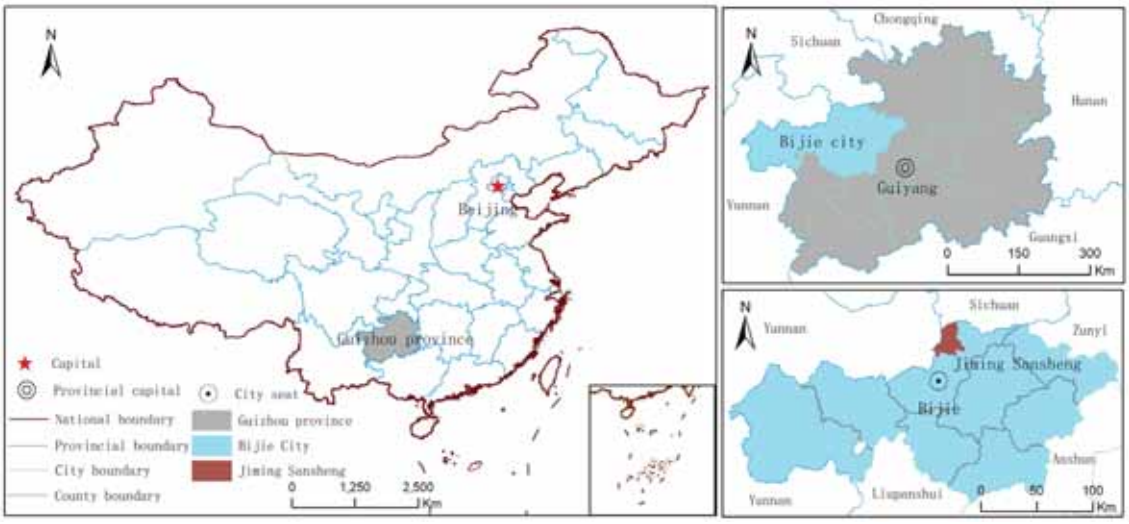

FIGURE 1

Geographical distribution map of the research object

MATERIALS AND METHODS

The fuzzy comprehensive evaluation method can be divided into two levels: single-level fuzzy evaluation and multi-level fuzzy evaluation, and the multi-level fuzzy evaluation method is based on the single-level fuzzy evaluation [10-12].

Single-Level Fuzzy Comprehensive Evaluation Model. The specific implementation steps for the single-level fuzzy comprehensive evaluation model are as follows (Eq.1):

(1) Given two finite universes.

$$U = \{u_1 \quad u_2 \quad \cdots \quad u_m\} \qquad V = \{v_1 \quad v_2 \quad \cdots \quad v_n\} \tag{1}$$

Let U, V be 2 finite universes. Where U is a collection of all evaluation factors, called the evaluation factor set, with m elements; V is a collection of all the reviews, called a comment set, with n evaluations.

(2) Determine the weight. In the comprehensive evaluation, the size of the assessment level factors must be considered, and a fuzzy subset W={w1, w2,..., wm} on the set of factors U, the number of weight set elements and the evaluation index must be formed. The number is equal, which is m. Where wi is the weight of ui to um, that is, the measure of the magnitude of the effect ui on the evaluation level. Generally, the value is given by expert scoring and combined with matrix operation.

(3) Determine the evaluation matrix. Because the evaluators are different, even if the evaluation of the same indicator also produces different results, the evaluation result is expressed by the degree to which the ui evaluation index makes the vi evaluation scale. This possible degree is called membership degree. Recorded as rij. Then, the corresponding membership degree vector of the single factor evaluation of the index ui is Ri, Ri=(ri1, ri2...rij, . . . , rin), i=1, 2, . . . , m.

The evaluation matrix of m evaluation factors is: Where R is a fuzzy relation matrix on U to V. At this time, weigh (U, V, R) as the evaluation space (Eq.2),

$$\mathrm{R} = \begin{bmatrix} R_1 \\ R_2 \\ \vdots \\ R_m \end{bmatrix} = \begin{bmatrix} r_{11} & r_{12} & \cdots & r_{1n} \\ r_{21} & r_{22} & \cdots & r_{2n} \\ \vdots & \vdots & \vdots & \vdots \\ r_{m1} & r_{m2} & \cdots & r_{mn} \end{bmatrix} \tag{2}$$

Where $r_{ij} = d_{ij} / d$ $(0 \le r_{ij} \le 1,\ i = 1, 2, ..., m;\ j = 1, 2, ..., n)$, The middle d represents the number of experts participating in the evaluation, and the d_{ij} represents the number of experts who have made the evaluation scale v_j in the evaluation of the index u_i. It can be seen that the larger the r_{ij} value, the greater the possibility of making a v_j evaluation for u_i.

(4) Calculate the evaluation results. It is known that W and R, using the synthetic operation of the fuzzy transform, obtain a fuzzy subset on the domain V, that is, the comprehensive evaluation result, which is generally written as $B=W\times R$.

Multi-Level Fuzzy Comprehensive Evaluation Model. The multi-level fuzzy evaluation method is based on the single-level fuzzy evaluation. The specific steps are as follows [13-15]:

(1) For the evaluation factor set U, according to a certain attribute, it is divided into i subsets to obtain a second level evaluation factor set;

(2) For each evaluation factor in the subset, according to the weight Wi and the evaluation ma-

trix R_i, the evaluation is performed according to the single-level fuzzy comprehensive evaluation method, and the comprehensive evaluation result of the i subset is obtained $B_i=W_i \times R_i=[b_{i1}, b_{i2}, ..., b_{in}]$;

(3) Then evaluate the upper-level factors, and the evaluation decision matrix is (Eq.3):

$$R = \begin{bmatrix} B_1 \\ B_2 \\ \vdots \\ B_m \end{bmatrix} = \begin{bmatrix} b_{11} & b_{12} & \cdots & b_{1n} \\ b_{21} & b_{22} & \cdots & b_{2n} \\ \vdots & \vdots & \vdots & \vdots \\ b_{m1} & b_{m2} & \cdots & b_{mn} \end{bmatrix} \quad (3)$$

(4) According to the weight distribution of each subset, $W(\wedge)$ is obtained, and the comprehensive evaluation result $B(\wedge)=W(\wedge)\times R$ is obtained. If necessary, we can continue to divide and obtain a fuzzy comprehensive evaluation model of three levels or more. The calculation method is calculated in such a way that it is calculated step by step. Therefore, the evaluation result $B(\wedge)$ is not only the comprehensive evaluation result of each subset in U, but also the comprehensive evaluation result of all evaluation factors in U.

RESULTS AND DISCUSSION

Establishment of Indicator System. The selection principle of environmental quality evaluation index system of Jiming Sansheng geopark should not only follow the general principles of objectivity, science and integrity, but also consider the following two aspects: (1) The evaluation index system should fully consider the geological Features of Jiming Sansheng geopark, and select the typical indicators [16]; (2) Indicators should be recognized and used by the evaluators, and easy to grasp the rating level. According to the above principles, the environmental quality assessment of Jiming Sansheng geopark is divided into two levels (Table 1): Primary factors, including tourism resource environment, tourism service environment, natural ecological environment, and social and cultural environment. Secondary factors, including resource rareness, resource abundance, aesthetic value, sustainable development, resources protection, traffic and hotel, tourist facilities, information construction, tourism service quality, atmosphere and water, sanitary conditions, green rate, tourism demand ability, tourism investment ability, tourism policy, local residents quality, tourism awareness, tourism awareness, a total of 17.

Determination of Indicator Weight. Determining the weight of each indicator plays an important role in the evaluation of tourism environmental quality. Whether the weight is reasonable or not is directly related to the scientific nature of the evaluation system. We have adopted the Analytic Hierarchy Process (AHP) [6, 17-19] when determining the weights of the indicators in the established evaluation system. First, construct the judgment matrix, compare and analyze the importance of indicators; second, the index weight coefficient is calculated; again, the consistency check is performed on the judgment matrix; finally, the weight is calculated. Through the above steps, we obtained the weights of the indicators at all levels of the evaluation system (Table 1)

(2) Calculation of index weight coefficient. By constructing five judgment matrices, hierarchical ordering and consistency check steps, the weight values of each individual factor are obtained (Table 1).

(3) Evaluation model operation. Let the evaluation factor set $U=\{Y_1, Y_2, Y_3, Y_4\}$, in which each element subset $Yi=\{E_{i1}, E_{i2}, ..., E_{ij}\}$ is set accordingly (Table 1). The rating level is divided into 6 levels, that is, very good (I level), good (II level), better (level III), poor (level IV), very poor (V level), quite poor (level VI), Then the comment set $V=\{v_1, v_2, v_3, v_4, v_5, v_6\}=\{very\ good, good, better, poor, very\ poor, quite\ poor\}$.

After the statistical calculation of the results of the evaluation of the evaluation experts, the evaluation decision matrix of the second-level factors is analyzed and compiled as:

In the same way, the value of results is calculated. From the secondary factor weight Wi (see Table 1) and the evaluation decision matrix R_i in each subset, according to the synthetic algorithm, the matrix calculation is used to obtain the i subset of the tourism environment of Guizhou Province (i=1, 2, 3, 4). The results of the comprehensive evaluation are B_1, B_2, B_3 and B_4.

$$B_1 = W_1 \times R_1 = (0.145 \quad 0.240 \quad 0.408 \quad 0.073 \quad 0.085 \quad 0.060)$$
$$B_2 = W_{21} \times R_2 = (0.000 \quad 0.000 \quad 0.223 \quad 0.408 \quad 0.240 \quad 0.130)$$
$$B_3 = W_3 \times R_3 = (0.000 \quad 0.198 \quad 0.628 \quad 0.110 \quad 0.075 \quad 0.000)$$
$$B_4 = W_4 \times R_4 = (0.000 \quad 0.020 \quad 0.298 \quad 0.378 \quad 0.235 \quad 0.070)$$

Based on the single-factor fuzzy comprehensive evaluation result B, the comprehensive evaluation decision matrix of each subset in U can be obtained (Eq.4).

$$R = \begin{bmatrix} B_1 \\ \vdots \\ B_n \end{bmatrix} = \begin{bmatrix} b_{11} & \cdots & b_{1m} \\ \vdots & \vdots & \vdots \\ b_{n1} & \cdots & b_{nm} \end{bmatrix} = \begin{bmatrix} 0.145 & 0.240 & 0.408 & 0.073 & 0.085 & 0.060 \\ 0.000 & 0.000 & 0.223 & 0.408 & 0.240 & 0.130 \\ 0.000 & 0.198 & 0.628 & 0.110 & 0.075 & 0.000 \\ 0.000 & 0.020 & 0.298 & 0.378 & 0.235 & 0.070 \end{bmatrix} \quad (4)$$

Finally, according to the first-order factor weight W in Table 2, the value of the decision matrix R is also comprehensively evaluated to carry

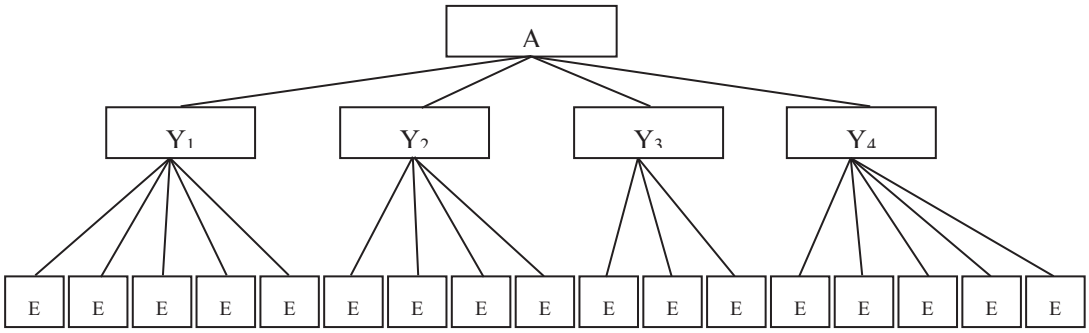

FIGURE2
AHP hierarchy diagram of tourism environment assessment

TABLE 1
Geological Park Environmental Quality Evaluation Index ystem

	First-order influence factor			Secondary influence factor		
	Samples	Factor	Calculation	Number	Factor	Calculation
Geological park environmental quality comprehensive evaluation index A	Y_1	Tourism resource environment	0.41	E_{11}	Resource rareness	0.29
				E_{12}	Resource abundance	0.29
				E_{13}	Aesthetic value	0.19
				E_{14}	Sustainable development	0.19
				E_{15}	Resources protection	0.05
	Y_2	Tourism service environment	0.36	E_{21}	Traffic and hotel	0.12
				E_{22}	Tourist facilities	0.36
				E_{23}	Information construction	0.11
				E_{24}	Tourism service quality	0.41
	Y_3	Natural ecological environment	0.11	E_{31}	Atmosphere and water	0.07
				E_{32}	Sanitary conditions	0.15
				E_{33}	Green rate	0.79
	Y_4	Social and cultural environment	0.12	E_{41}	Tourism demand ability	0.39
				E_{42}	Tourism investment ability	0.25
				E_{43}	Tourism policy	0.08
				E_{44}	Local residents quality	0.08
				E_{45}	Tourism awareness	0.20

The calculation steps are as follows:
(1) Establish an AHP hierarchy diagram. In this paper, the evaluation of tourism environment in Guizhou Province is taken as the overall goal (A). Compared with the overall goal, four first-level factors (Y) are the criterion layer and 17 second-level factors (E) are the target layer (Figure 2).

out the fuzzy transformation synthesis operation, and the comprehensive evaluation results of the tourism environment quality in Jiming Sansheng geopark are obtained:

$$B = W \times R = (0.0595 \quad 0.1225 \quad 0.3519 \quad 0.2338 \quad 0.1577 \quad 0.0798)$$

Overall Result Analysis. According to the above judgment results, and the principle of maximum membership degree, the maximum degree of membership is 0.3519, the corresponding comment is "better", but the "very good" and "good" are 0.0595 and 0.1225, respectively. The first 3 levels overall. The level accounts for 0.5339, just over half, indicating that the environmental quality of Jiming Sansheng geopark is not optimistic, many areas still need to be improved.

Subsystem Result Analysis. For the vertical comparison of R values, the scores of the three levels of "very good", "good" and "better" are Y_1 (0.793), Y_2 (0.223), Y_3 (0.825), and Y_4 (0.318). According to the order from large to small, $Y_3 > Y_1 > Y_4 > Y_2$, where the value of Y_3 and Y_1 is around 0.8, indicating that the natural ecological environment and tourism resources environment of Jiming Sansheng geopark are relatively superior, while tourism service environment and social culture environment are relatively poor.

TABLE 2

***p*, *q* values of Ei in the second-level factor and datasheet of standard sum**

Evaluation factor E_i	E_{11}	E_{12}	E_{13}	E_{14}	E_{15}	E_{21}	E_{22}	E_{23}	E_{24}
p	1.0	0.75	0.75	0.0	0.0	0.25	0.25	0.0	0.25
q	0.0	0.25	0.25	1.0	1.0	0.75	0.75	1.0	0.75
P	0.4	0.3	0.3	0.0	0.0	0.33	0.33	0.0	0.33
Q	0.0	0.1	0.1	0.4	0.4	0.23	0.23	0.3	0.23
Evaluation factor E_i	E_{31}	E_{32}	E_{33}	E_{41}	E_{42}	E_{43}	E_{44}	E_{45}	/
p	0.5	0.0	1.0	0.5	0.25	0.5	0.25	0.0	/
q	0.5	1.0	0.0	0.5	0.75	0.5	0.75	1.0	/
P	0.33	0.0	0.67	0.33	0.17	0.33	0.17	0.0	/
Q	0.33	0.67	0.0	0.14	0.21	0.14	0.21	0.29	/

Comparative analysis of the results of various factors. Ignore the internal differences in the comment level [17-19], and divide the comments into 2 levels from a vague point of view, that is, the reviews are “good” (including very good, good and better) and the reviews are “poor” (including poor, very poor and quite poor) Two levels, and the factors in the first-level factor Yi are correspondingly added to the first three items and the last three items of the membership degree, and the sum is standardized (Table 2).

The specific formula is (Eq.5, Eq.6):

$$p_i = \sum_{j=1}^{3} r_{ij} \quad q_i = \sum_{j=4}^{6} r_{ij} \tag{5}$$

$$P_i = p_i \Big/ \sum_{i=1}^{n} p_i \quad Q_i = q_i \Big/ \sum_{i=1}^{n} q_i \tag{6}$$

The value of *p, q* is calculated from the r_{ij} in the corresponding matrix of the previous, which are the first 3 and the last 3 of the membership degree of the second factor E_i. The sum of the terms *P, Q* is the summed data of the sum of *p* and *q* [20-23].

As can be seen from the data in Table 2, in the sub-environment system: E_{11} (resource rareness), E_{12} (resource abundance), E_{13} (aesthetic value), E_{21} (traffic and hotel), E_{22} (tourist facilities), E_{24} (tourism service quality), E_{33} (green rate), E_{41} (tourism demand ability), E_{43} (tourism policy), the nine environmental factors have higher P_i values. That is, the evaluation value is “good”, and the *P* value of E_{33} (0.67) is the highest, indicating green rate is best among all the better factors. And E_{14} (sustainable development), E_{15} (resources protection), E_{23} information construction), E_{32} (sanitary conditions), E_{42} (tourism investment ability), E_{44} (local residents quality), E_{45} (tourism awareness), the seven environmental factors have higher Q_i values. That is, the evaluation value is "poor", and the *Q* value of E_{32} (0.67) is the highest, indicating that the sanitary conditions is poor among all the poor factors.

CONCLUSIONS

(1) In this paper, a systematic analysis method and a method of consulting expert groups are used to establish an environmental assessment index system for the Jiming Sansheng geopark, including 4 first-level indicators and 17 secondary indicators of tourism resources environment, tourism service environment, natural ecological environment and social and cultural environment.

(2) The indicators better reflect the various elements of the tourism environment at the provincial level, and they are systematic, scientific and objective. The construction of this indicator system is conducive to better quantitative evaluation and analysis of the tourism environment at the provincial level. However, since the data acquisition of this evaluation index system is based on the method of expert scoring, there will be certain deviations in the specific operation and data processing, which is an important factor affecting the evaluation results.

(3) According to the evaluation results, the Environmental Quality Review of Jiming Sansheng geopark accounted for 53.39% of the total level, while “very good” and “good” accounted for only 18.2%, indicating that the overall environmental quality is not optimistic. As far as the primary indicators are concerned, the tourism resource environment has a score of 0.793, and the natural ecological environment has a target of 0.825. Especially the tourism resource environment and the natural ecological environment are relatively close to each other, indicating that these two aspects are relatively superior. The scores of Tourism service

environment and social and cultural environment are all around 0.3, which is relatively low, indicating that the environmental quality of these two aspects is relatively poor. The reasons are: on the one hand, it is related to the special geographical environment of Guizhou; on the other hand, the geopark has just been established.

ACKNOWLEDGEMENTS

This work was financially supported by the Guizhou Scientific and Technological Cooperation Program Evaluation on Ecological Carrying Capacity of Karst Dualistic Water Resources in Caohai National Nature Reserve, China (No. LH20157594).

REFERENCES

[1] Zheng, D., Wang, H. (2014) Condition assessment of regenerative heater based on fuzzy comprehensive evaluation. Applied Mechanics and Materials. 687-691, 206-211.

[2] Chu, H., Xu, G., Yasufuku, N., Yu, Z., Liu, P., Wang, J. (2017) Risk assessment of water inrush in karst tunnels based on two-class fuzzy comprehensive evaluation method. Arabian Journal of Geosciences. 10(7), 179-196.

[3] Wei, D., Xuan, Y., Zhe, U. (2006) Study on spatial fuzzy comprehensive assessment of ecological and environmental quality in west Jilin province. Arid Zone Research. 23(1), 155-160.

[4] Xiao, I., Xin, U. (2012) Fuzzy comprehensive evaluation of atmospheric environmental quality in Xi'an city based on entropy of weight of evaluating indicators. Environmental Science Technology. 35(4), 195-199.

[5] Mu, Z., Tao, U., Yan, I. (2011) Assessment of groundwater specific vulnerability in Guangzhou based on fuzzy comprehensive evaluation. Geoscience. 1(4), 148-152.

[6] Xin, L., Zhi, I., Liang, G., Ke, S., Bao, H. (2017) Durability assessment of foamed mixture lightweight soil based on analytic hierarchy process and fuzzy comprehensive evaluation (AHP-FCE). Journal of Hohai University. 45(4), 332-339.

[7] Xu, Y., Du, P., Wang, J. (2017) Research and application of a hybrid model based on dynamic fuzzy synthetic evaluation for establishing air quality forecasting and early warning system: A case study in China. Environmental Pollution. 223, 435-448.

[8] Singh, M., Soni, K. (2017) A comprehensive review of fuzzy-based clustering techniques in wireless sensor networks. Sensor Review. 37(3), 168-180.

[9] Zhang, X., Li, J., Liu, J., Peng, W., Zhang, Z. (2018) Stability evaluation of soft rock supporting system of inclined shaft based on fuzzy comprehensive evaluation method. Journal of Liaoning Technical University (Natural Science Edition). 37(3), 476-481.

[10] Wu, Y., Li, Y., Zhang, L., Guo, L., Li, H., Xi, B., Wang, L., Li, C. (2017) Assessment of lakes ecosystem health based on objective and subjective weighting combined with fuzzy comprehensive evaluation. Journal of Lake Sciences. 23(3), 356-375.

[11] Hong, O., Fen, L. (2018) Linguistic dynamic analysis based on interval type II fuzzy comprehensive evaluation. Pattern Recognition and Artificial Intelligence. 11(1), 102-119.

[12] Wang, M., Zhang, J., Zhang, W. (2017) The application of fuzzy comprehensive evaluation method in the software project risk assessment. the 2017 International Conference. ACM. 9(2), 56-69.

[13] Zheng, D., Wang, H. (2014) Condition assessment of regenerative heater based on fuzzy comprehensive evaluation. Applied Mechanics and Materials. 687-691, 206-211.

[14] Kennish, J. (1980) Environmental quality. Dictionary Geotechnical Engineering/worterbuch Geotechnik. 20(11), 200-227.

[15] Zhang, G., Spickett, J., Rumchev, K., Lee, H., Stick, S. (2006) Indoor environmental quality in a 'low allergen' school and three standard primary schools in western Australia. Indoor Air. 16(1), 74-80.

[16] Zagreus, L., Huizenga, C., Arens, E., Lehrer, D. (2004) Listening to the occupants: a web-based indoor environmental quality survey. Indoor Air. 14(s8), 65-74.

[17] Miao, Z., Jing, I., Ming, J., Jun, L., Ling, B. (2006) Evaluation on environmental quality of Pb, Zn and Cu contents in vegetable plantation soils and vegetables in Hangzhou suburb. Environmental Science. 27(4), 742-747.

[18] Feio, J., Almeida, P., Craveiro, C., Calado, J. (2007) Diatoms and macroinvertebrates provide consistent and complementary information on environmental quality. Fundamental and Applied Limnology / Archiv für Hydrobiologie. 169(3), 247-258.

[19] Rehdanz, K., Maddison, D. (2008) Local environmental quality and life-satisfaction in Germany. Ecological Economics. 64(4), 787-797.

[20] Kalf, F., Crommentuijn, T., Plassche, D. (1997) Environmental quality objectives for 10 polycyclic aromatic hydrocarbons Ecotoxicology. Environmental Safety. 36(1), 89-97.
[21] Kyle, C. (1997) Editorial: urban environmental quality: an emerging educational challenge. Journal of Research in Science Teaching. 34(1), 1-21.
[22] Hanley, N., Mcgregor, G., Swales, K., Turner, K. (2009) Do increases in energy efficiency improve environmental quality and sustainability?. Ecological Economics. 68(3), 692-709.
[23] Dabert, P., Barrington, S., Burton, C. (2009) Livestock waste treatment systems for environmental quality, food safety, and sustainability. Bioresource Technology. 100(22), 5527-5536.

Received: **26.11.2019**
Accepted: **21.02.2020**

CORRESPONDING AUTHOR

Taian Zuo
School of Tourism Management and Services, Chongqing University of Education,
Chongqing 400067, China

e-mail: dilikexue2012@sina.com

© by PSP Volume 29 – No. 05/2020 pages 3840-3852 Fresenius Environmental Bulletin

STUDY ON PERFORMANCES ON GREEN AND ECOLOGICAL CONCRETE OF NEAR SURFACE MOUNTED (NSM) WITH MPC ADHESIVE BASED ON ECOLOGICAL THEORY

Liwen Zhang[1,*], Zhouqiang Liu[1], Tao Geng[1], Wenhua Zhang[2], Qinghu Shang[1], Yanggui Deng[1]

[1]Department of Civil Engineering, Guangzhou University, Guangzhou, 510006, China
[2]Department of Civil Engineering, Nanjing Forestry University, Nanjing, 210037, China

ABSTRACT

NSM fiber reinforced polymer (FRP) is a reliable and environmentally friendly rehabilitation and strengthening method for deficient concrete structures. However, it was not applied widely in practice due to some drawbacks of its typical adhesive material-epoxy: longer curing time, higher curing temperature, and instability in light. MPC, an inorganic cementitious blend, appears a fast-setting, higher early strength development, lower setting temperature, good fire and corrosion resistance. As a result, it may improve the applications of NSM using MPC as a new adhesive material. This paper concentrated on a preliminary exploration for the MPC bond performance. A mixture proportion optimization was carried out firstly for extending the MPC's setting time for casting specimens and improving its lowered bond strength caused by extending the setting time. Then, a total of 12 NSM specimens in 6 sets experienced direct pull-out tests to investigate the feasibility of the MPC NSM system and its different performances with the epoxy NSM system under various curing ages. The results showed that the MPC is proper for NSM system in practice although its bond strength and ductility is weaker than general epoxy. Additionally, the bond strength of the MPC is increasing approximately linearly with the curing age increasing at least before 28 days.

KEYWORDS:
Green, Ecological, Near Surface Mounted, FRP, Epoxy

INTRODUCTION

Near surface mounted (NSM) fiber reinforced polymer (FRP) has been adopted for years in strengthening works of concrete structures as a reliable rehabilitation and strengthening method [1-3]. In NSM system, adhesive layer used to connect FRP and concrete substrate undoubtedly plays a key role determining performances of the whole system [4-7]. Thus, an adhesive material with better properties is essential for ensuring the effectiveness of NSM system. Epoxy resin generally is accepted as the adhesive material due to its good mechanical and thermal behaviors, better chemical and corrosion resistance, and excellent bond performances than common cement grout [8]. However, there are some deficiencies in this epoxy adhesive material, e.g., curing time is longer, curing temperature is higher, and secondary pollution is prone to produce [9-12]. These deficiencies obviously restrict applications of NSM system in the strengthening works. Magnesium phosphate cement (MPC) is an inorganic cementitious blend of magnesium oxide (MgO) and ammonium dihydrogen phosphate ($NH_4H_2PO_4$) or alkali phosphate salt. This blend used in rapid repairs of pavement has high bond strength and low shrinkage rates. Specially, it appears a fast-setting (several minutes), higher early strength development (about 20 MPa within 1 hour), lower setting temperature, good fire and corrosion resistance [13-15]. As a result, it may improve the applications of NSM using MPC instead of epoxy resins as the adhesive material in NSM system.

For strengthened concrete structures with NSM FRP, it often fails due to debonding between FRP and concrete substrate [16-20]. That means it is essential to understand the bond characteristics of NSM FRP for predicting the capacity of NSM FRP and effectively applying this strengthening method. Extensive studies for the bond characteristics have been conducted by bond tests and numerical simulations in the last decades. These existing studies covered a wide range of parameters including FRP material types [21], FRP cross-sectional shapes [8,22], FRP surface configurations [22], groove dimension [6,18,23,24], adhesive types [25,26], and bond length [3,20,27,28]. However, the studies were completed based on NSM system with epoxy or cement grout adhesive. The results of these studies could not properly describe the bond characteristics of NSM system with MPC adhesive because of distinct properties between MPC and the

two aforementioned adhesive materials. For that reason, a study concentrating on the bond characteristics of NSM FRP with MPC was conducted through a direct pull-out test. This paper isa part of the study, which has an objective of exploring whether it is feasible to employ MPC instead of epoxy as the adhesive material in NSM system and investigating the distinction of the bond behavior between MPC NSM system and epoxy NSM system under different curing ages. A total of 12 specimens in 6 sets with a concrete block having a section size of 300 × 150 × 150 mm underwent direct pull-out tests, in which 6 specimens (3 sets) adopted MPC adhesive and the others still employed epoxy adhesive. In addition, an experiment aiming to optimize mix proportion of MPC was carried out ahead of the pull-out test for improving the lower property of MPC caused by introducing borax to prolong setting time of MPC for casting specimens.

MATERIALS AND METHODS

Basic mix proportion of MPC. MPC, also known as magnesium phosphate ceramics, are clinker-free cements that have strong chemical bonding and high mechanical strength through acid-base reactions between magnesia and phosphate acid (H_3PO_4) or soluble acid phosphates, such as ammonium dihydrogen phosphate ($NH_4H_2PO_4$), sodium dihydrogen phosphate (NaH_2PO_4), or potassium dihydrogen phosphate (KH_2PO_4). It is a so fast-setting cement binder, which completes initial setting only in a few minutes, that leads to inadequate time for casting specimens before MPC complete setting. On that ground, some addition agents such as borax are needed to be added in the MPC to increase its setting time [29-31]. A work focusing on the mix proportion of MPC was carried out before the pull-out tests for obtaining an optimizing MPC both considering performance and setting time.

The water-cement ratio of 0.15 (where cement means the compound of MgO and $NH_4H_2PO_4$)was adopted as a basic mix proportion. Three factors, molar ratio of MgO to $NH_4H_2PO_4$, fly ash proportion, and borax proportion, were investigated in this optimizing work, which varied from 4 to 6, 0% to 45%, and 8% to 14%, respectively. The mix proportion investigation was divided to three groups which are displayed in Table 1. Prismatic specimens including the parameters in the table were employed in the 2-day and 28-day

TABLE 1
Mix proportion investigation details and results

Groups	Molar ratio	Borax proportion (%)	Fly ash proportion (%)	Setting time (min)	Compressive strength (MPa) 2days	28 days
1	3	10	\	11	23.5	42.6
	4			9	25.1	47.5
	5			7	31.3	59.3
	6			4	33.0	63.1
2	5	8	\	4	33.3	62.8
		10		7	31.3	59.3
		12		10	27.8	52.7
		14		14	24.1	49.5
3	5	10	0	7	31.3	59.3
			15	6	36.3	65.5
			30	5	32.5	62.6
			45	9	27.1	53.4

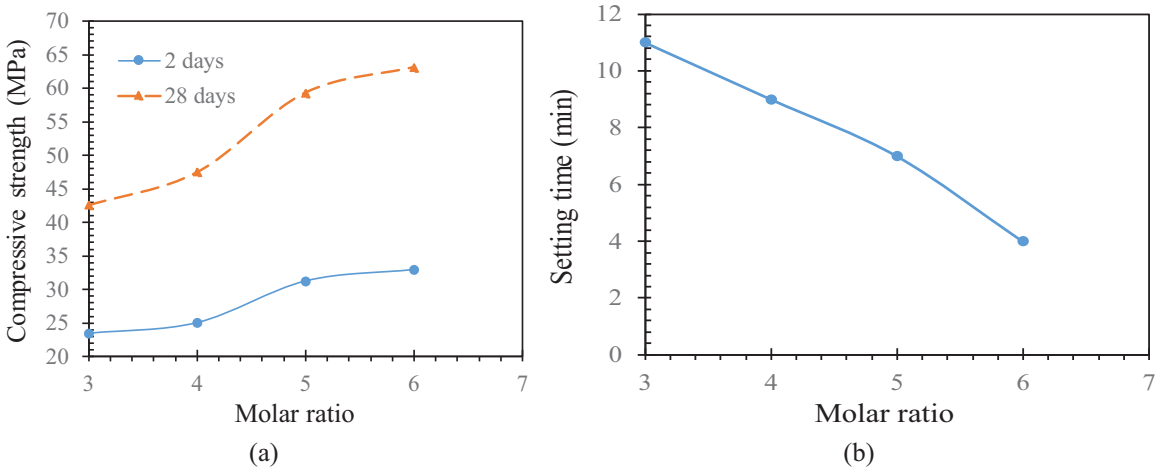

FIGURE 1
Effect of molar ratio. (a) Compressive strength; (b) Setting time

compression tests according to GB/T 17671-1999, with size of 40 mm × 40mm × 160mm for evaluating the influences of the factors on MPC performances. For each specimen, setting time was determined by the modified Vicat needle method according to ASTM standard C807-05 [32].

RESULTS AND DISCUSSION

Figures 1 (a) and (b) offer the influence of the molar ratio on the MPC setting time and compressive strength, respectively. The figures appear that the setting time is decrease with the increase of the molar ratio. However, the 2 days and 28 days compressive strength of the MPC displays an increase tendency, which increases to 33.0 MPa from 23.5 MPa and 63.1 MPa from 42.6 MPa, respectively. The borax affects the MPC in the opposite direction. The setting time, as shown in Figure 2 (a), keeps growth with the borax increasing, but the compressive is decreasing as described in Figure 2 (b).As for the fly ash shown in Figures 3 (a) and (b), it appears similar influence of the molar ratio on the MPC with its proportion increasing; but when its proportion exceeds a certain limit, e.g., about 20%--30% in Figures 3 (a) and (b), the influence reverses.

The appearances of Figure 1-Figure 3 indicate that the setting time varies with the factors on the contrary to the properties of the MPC, that is, the setting time is increasing while the properties is declining. As a result, median values of the factors are adopted as the basic mix proportion in order to both obtain adequate setting time and favorable performances of MPC. Table 2 lists the basic mix proportion of the MPC used to be as adhesive material of NSM FRP system investigated in the following pull out test.

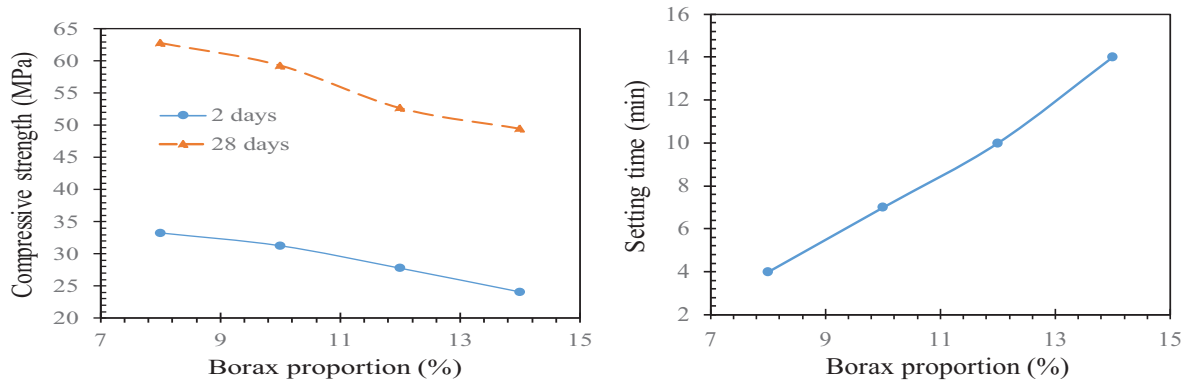

FIGURE 2
Effect of borax proportion. (a) Compressive strength; (b) Setting time

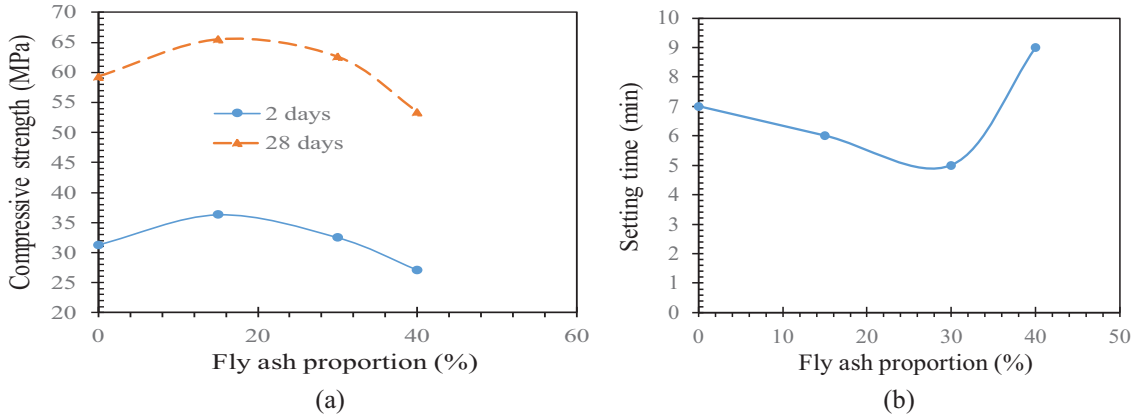

FIGURE 3
Effect of molar ratio. (a) Compressive strength; (b) Setting time

TABLE 2
Basic mix proportion

Water-cement ratio	Molar ratio	Borax proportion (%)	Fly ash proportion (%)	Setting time (min)	Compressive strength (MPa)
0.15	5	10	15	6	36.3

TABLE 3
Test parameters

Specimen designation	Curing age (Day)	Adhesive material
G-E-T2-1 G-E-T2-2	2	Epoxy
G-E-T7-1 G-E-T7-2	7	
G-E-T14-1 G-E-T14-2	14	
G-M-T2-1 G-M-T2-2	2	MPC
G-M-T7-1 G-M-T7-2	7	
G-M-T14-1 G-M-T14-2	14	

Note:G =GFRProd; E = epoxy;M = MPC; T2,T7, and T14 = the curing age of 2 days, 7days, and 14 days, respectively;the last Arabic numeral - 1= the first specimen in one set; and the last Arabic numeral - 2= the second specimen in the set.

(a) (b)

FIGURE 4
GFRP rods and tensile test. (a) GFRP rods; (b) Tensile test

TABLE 4
Properties of GFRP rods

Provided by	Tensile strength (MPa)	Elastic modulus (GPa)	Tensile strain (%)
Manufacturer	910	45	2.03
Lab test	1050	48	2.21

TABLE 5
Properties of Sikadur-32LP

Epoxy	Shear strength (MPa)	Flexural tensile strength (MPa)	Compressive strength (MPa)	Tensile strength (MPa)	Bonding strength (MPa)
Sikadur-32LP	3.3	35	70	20	3

Pullout testof NSM. General. A direct pull-out test was carried out for investigating the bond performances of the NSM with MPC. The investigation concentrates on the bond performances under various curing ages of the MPC. A total of 12 concrete blocks in 6 sets were casted in which each set consisted of 2 identical specimens. The 3 sets of the specimens used MPC as adhesive material, and other 3 sets still adopted epoxy as the contrast of the MPC specimens. The curing ages of 2 days, 7 days, and 14 days are involved in the test considering the properties of the epoxy. Table 3 offers the test scheme and the specimen numbers.

Materials. The average 28-day compressive strength of the concrete blocks was 21.5 MPa through the standard cylinder compression test of ASTM C39/39M [33]. GFRP round ribbed rods were employed with a diameter of 10 mm, as shown in Figure 4 (a). The mechanical properties of the rods were examined in laboratory again (Figure 4 (b)) according to ACI 440.3R-0434besides the data provided by its manufacturer, just as summarized in Table 4. Sikadur-32LPwas selected as the adhesive material of the specimens with epoxy. Table 5 lists the epoxy's properties provided in its introduction. The MPC optimized in section 2 was used as the adhesive material of the specimens with MPC. Its properties and mix proportion can be obtained from Table 2.

Test setup and specimens. The shape of a prism was selected as the specimens' configuration with a dimension of 150 mm ×150mm× 300 mm according to the typical dimensions used in most literatures [35-38]. All the specimens were given a bonded length of 250 mm, which was about 25 times the rods' diameter on average [22,23,38-40], in order to ensure a sufficient bond for developing the full bond strength in materials. A through groove was carved on one surface of each specimen with a square section of 20 mm ×20 mm. Additionally, the internal surfaces of the grooves were roughened for increasing the bonded strength between the concrete and FRP rods. The two adhesive materials, the MPC and the epoxy, were filled in the grooves when the FRP rods have been deployed. Figure 5 offers the configuration details of the specimens.

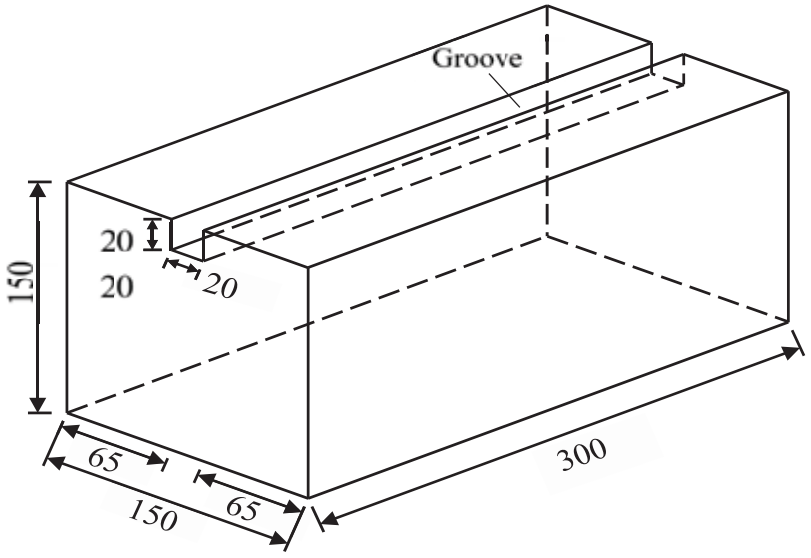

FIGURE 5
Configuration of specimens (mm)

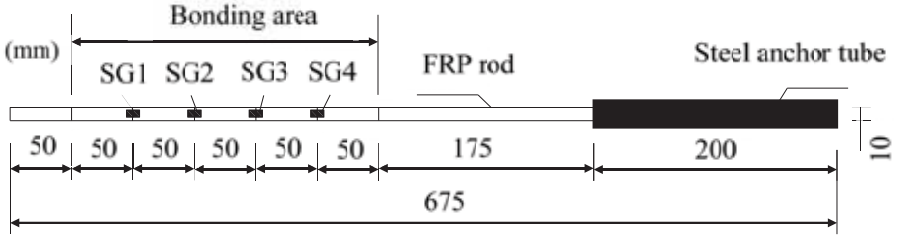

(a)

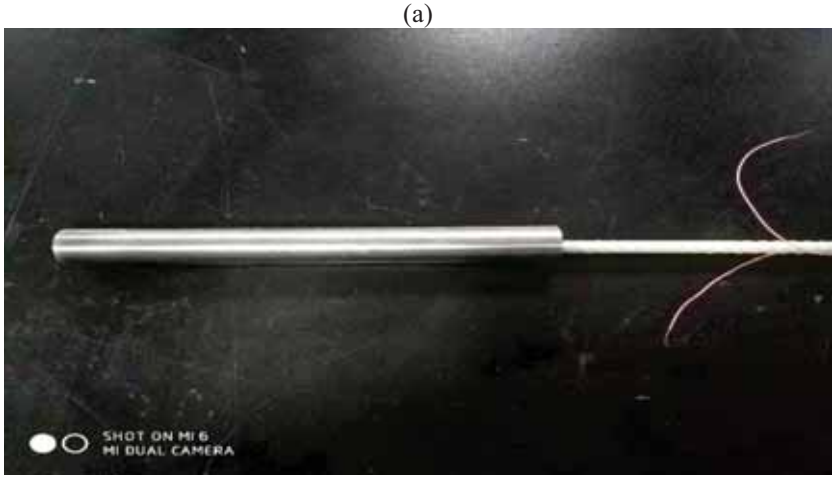

(b)

FIGURE 6
Strain gauge layout and anchorage. (a) Strain gauge layout; (b) Anchorage in loading end

FIGURE 7
Pull-out test setup

The FRP rods were washed off with alcohol before the test. Four strain gauges (SG) were set on each FRP rod along the rod's axis according to Figure 6(a) after the washed rods underwent air-drying process. A 200 meters long steel tube with the diameter of 30 mm was used to cover the FRP rod in its loading end, Figure 6 (b), in order to prevent the FRP rod from being broken by a loading clam [36,37,41]. Epoxy was filled in the steel tube for ensuring adequate bond between the steel tube and the FRP rod.

Once the filled adhesive materials were cured for designed ages, specimens would be used for the direct pull-out test displayed in Figure 7. Auniversal testing machine was employed to carry out the test. Two steel plates were placed on the top and bottom of the specimens, respectively, and were fixed on the testing machine with four threaded rods in order to avoid any possible movement of the specimens. The loading was implemented relying on the displacement of the load clamp with a rate of 1 mm / s. Two linear variable displacement transformers (LVDTs) were installed at the loading end and the free end, respectively, to measure the corresponding displacements.

General observation. Most tests were continuing until the specimens were broken except for two set specimens of G-E-T2 and G-E-T7.The tests for these two set specimens were terminated when their loaded displacement approximated to the measure range of the LVDTs at the loading end. Although the two set specimens remained intact in appearance, their downward load-displacement curves indicated that capacity of the specimens was weakened due to internal damage of the specimens.

Due to the limited loaded displacement, slight changes were observed from G-E-T2 and G-E-T7 during the whole pull-out processing. But for specimens of G-E-T14, those started to crack diagonally from the loading end to the edge of the specimens in the later stage of loading. Then, the specimens appeared an obvious splitting crack at the bonding area and failed for an instant with a loud noise. The sets for specimens with MPC, however, looked like nothing happened before abrupt damage of these specimens.

Failure modes. As the limited loaded displacement problem precedingly mentioned, the specimens of G-E-T2 and G-E-T7 was basically intact in appearance, as shown in Figure 8 (a) and (b). Figure 8(c), appeared visible concrete and epoxy cover breakages along the bond length of FRP rods, although few fractures were observed in internal epoxy adhesive layer and the interface of epoxy-GFRP. Large spalling of concrete cover occurred at the sets of specimens with the MPC, as described in Figure 9 (a), (b), and (c) that indicates a better bonding performance of MPC with concrete than epoxy. Severe MPC breakages were also observed in the specimens. However, most portions of the FRP rods was contacted with the MPC pieces. It means that MPC has an enough bonding strength with FRP rods even though itself strength was weaker than epoxy. Additionally, similar concrete failure modes of the specimens with MPC at each curing age shows that MPC has adequate bond strength to prevent the FRP rods slippage after two days curing.

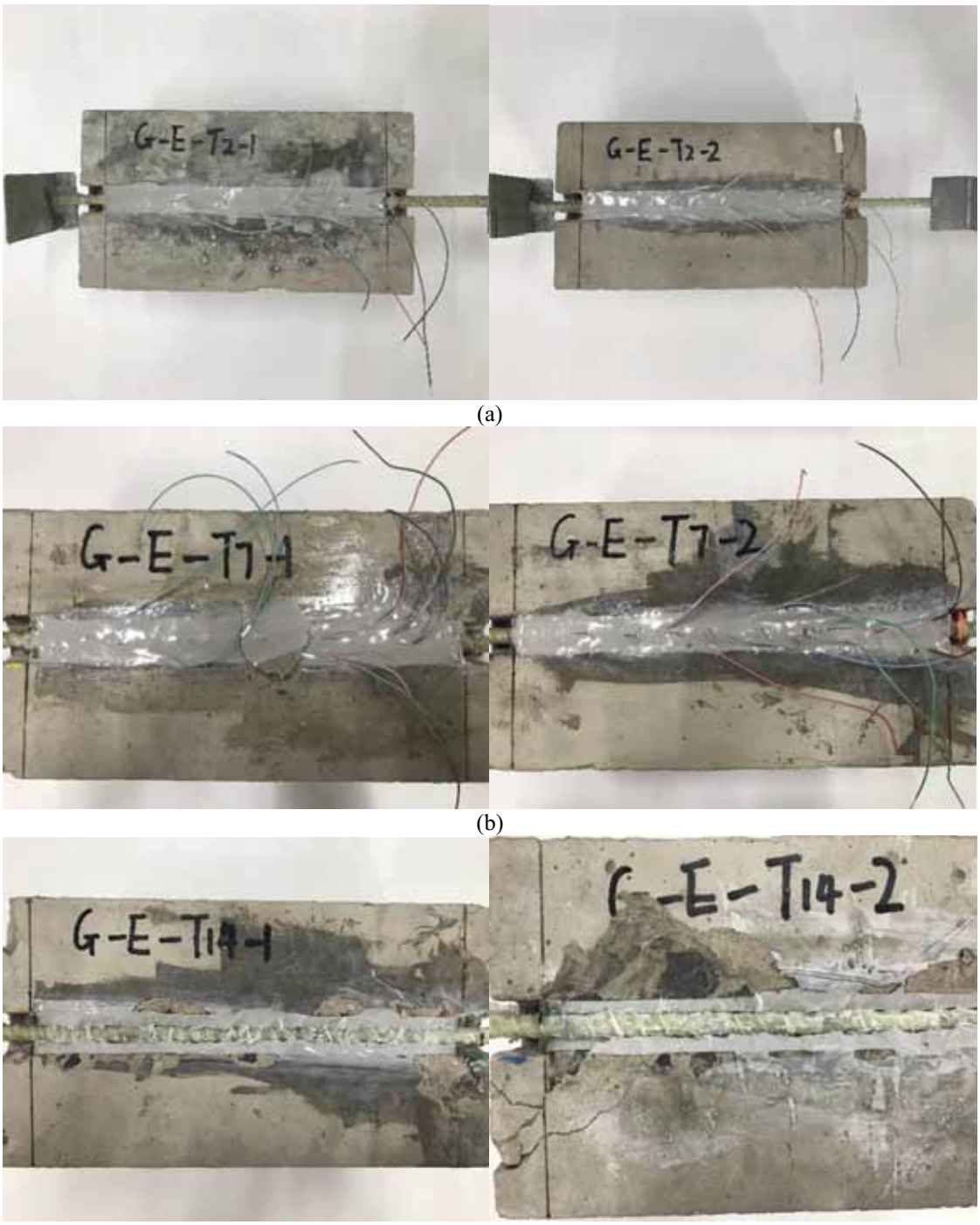

FIGURE 8
Failure modes of specimens with epoxy. (a) G-E-T2; (b) G-E-T7; (c) G-E-T14

Load-displacement response. Typical convex parabolas are observed from the load-displacement curves of specimens with epoxy, i.e., sets of G-E-T2, G-E-T7, and G-E-T14 shown in Figure 10 except for G-E-T14-2 of which the curve is cut off at about its peak value due to abruptly damage of the specimen. The expected increase of pull out forces with curing age increasing is presented in Figure 10, on the contrary, peak displacements corresponding to the pull-out forces appear decline with the curing age increasing. For example, the peak displacement decreases from about 5.4 mm(remarked by a red dash line with round caps) to 4.2 mm(remarked by a green dash line with round caps) when the curing age increases from 2 days (G-E-T2-1) to 7 days (G-E-T7-1). This unexpected phenomenon means that the ductility of epoxy specimens is lower with the curing age increasing.

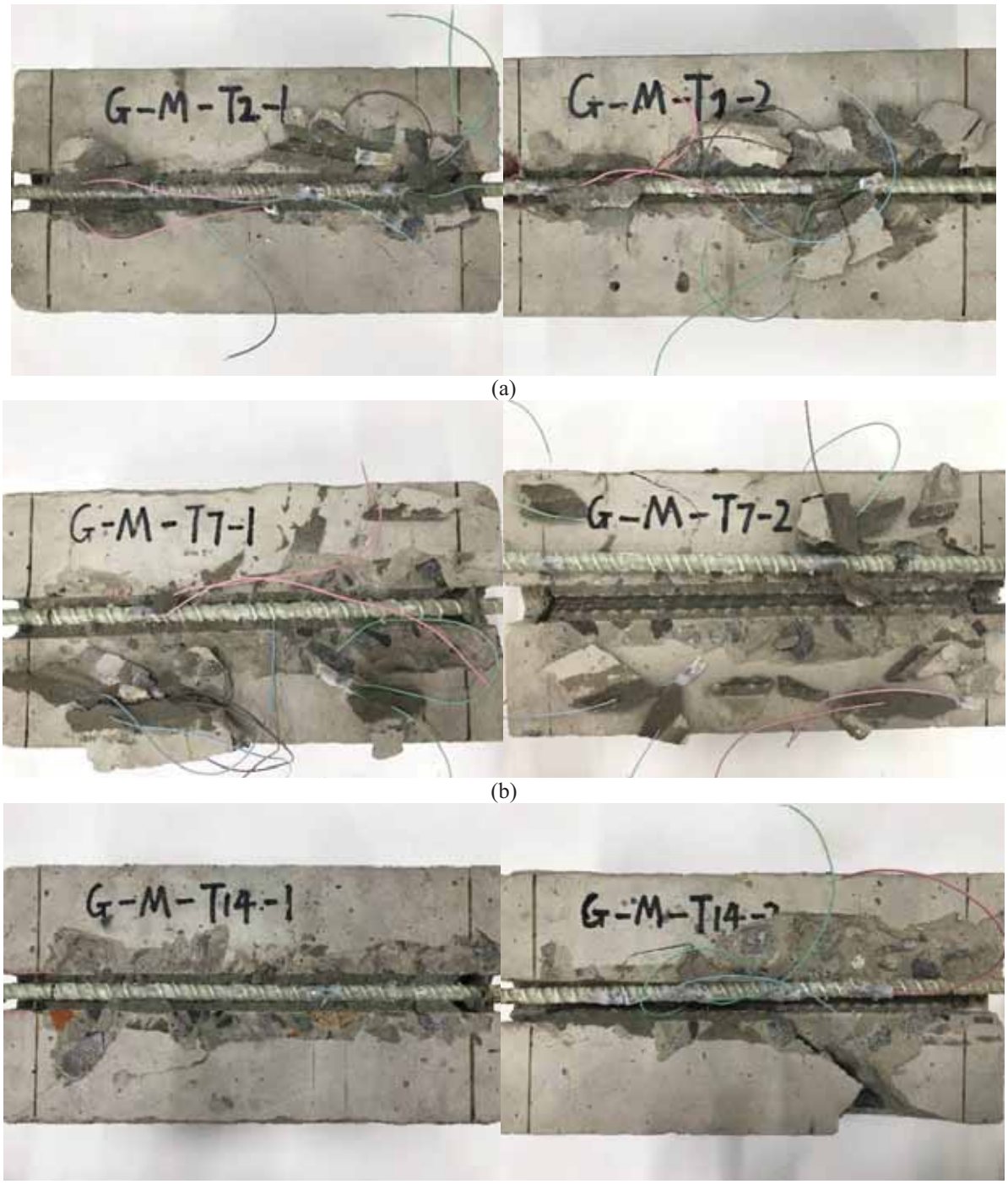

FIGURE 9
Failure modes of specimens with MPC. (a) G-M-T2; (b) G-M-T7; (c) G-M-T14

MPC specimens present similar convex parabolic load-displacement curves with the epoxy specimens apart from very short decline branches shown in Figure 11. It is also observed that the MPC specimens have much smaller peak displacement than the epoxy specimens. Additionally, the MPC specimens do not display a significant increment of the peak displacements with curing age increasing like the epoxy specimens. The peak displacement only decreases from about 2.5 mm(remarked by a purple dash line with round caps) to about 2.3 mm (remarked by a black dash line with round caps) when the curing age increases from 2 days (G-M-T2-1) to 14 (G-M-T14-1) days. These imply that MPC specimens have less ductility than epoxy specimens and their ductility vary slightly after 2 days curing.

Curves of average pull-out force with curing ages are collected in Figure 12 for specimens with the two adhesive materials in order to investigate the different effects of the curing age on the pull-out force of the specimens, more clearly. From

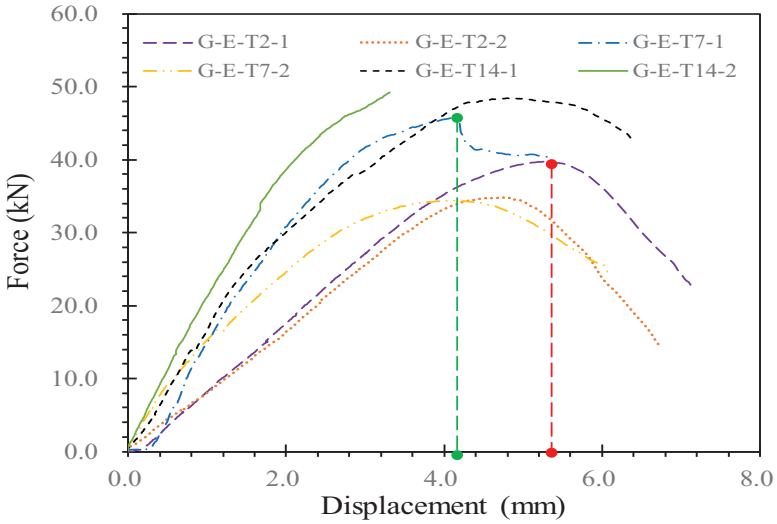

FIGURE 10
Load-displacement curves of specimens with epoxy

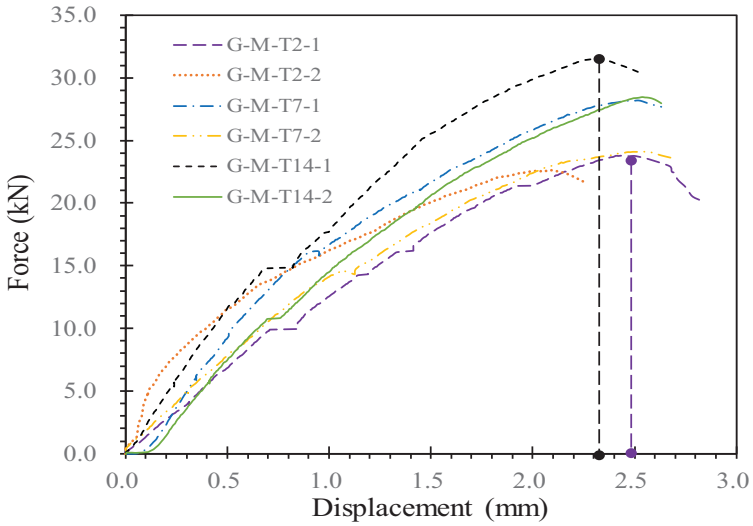

FIGURE 11
Load-displacement curves of specimens with MPC

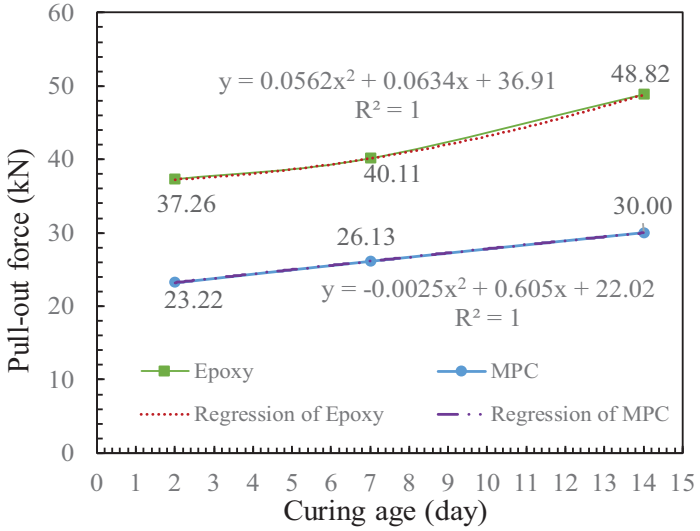

FIGURE 12
Pull out force-curing age curve

Figure 12, Specimens with the epoxy appear larger pullout force than specimens with MPC. The pull-out forces of all specimens increase as the curing age increases. For the specimens with the epoxy, their pull-out force increases according to aquadratic parabola; but for the specimens with the MPC, their pull-out force displays a more linear growth curve. Although pull-out tests after 14 days curing age have not been conducted, it could still be predicted that the bond strength of the MPC is increasing until at least 28 days from the improving properties of the MPC before 28 days. Two curves of the pull-out forces are regressed to two equations with the correlation coefficient of 1 shown in Figure 12, respectively, for evaluating the pull-out force during various curing days. Note that, these two equations are mostly proper to specimens having curing age from 2 days to 14days.

Bond stress-slip curves. Figure 13 offers bond stress-slip curves of specimens with the epoxy. Abbreviated letters of SG1, SG2, SG3, and SG4 represent strain gauges 1, 2, 3, and 4, respectively. Obviously, the bond strength is increasing with curing age increasing. In the case of 2 days curing age, e.g., G-E-T2-1, it presents the maximum bond strength of about 11 MPa; when the curing age increases to 14 days, the bond strength (G-E-T14-1) grows to about 30 MPa. However, the peak slip corresponding to the bond strength presents a decreased trend with the curing age increasing Bond stress-slip curves of specimens with the MPC displayed in Figure 14 appear similar configurations with the bond stress-slip curves of the specimens with the epoxy except for less bond strength. The bond strength of the specimens with the MPC still increases with their curing age increasing but slightly than the bond strength of the specimens with the epoxy. Most bond strengths only increase from about 5 MPa to 7 MPa when the curing age extends from 2 days to 7 days. As expected, the specimens with the MPC also shows much less slip value than the specimens with the epoxy. The slips presented in Figure 14 are a fraction of a millimeter for all specimens with the MPC, however, these values raise to several millimeters for the specimens with the epoxy, as described in Figure 13.

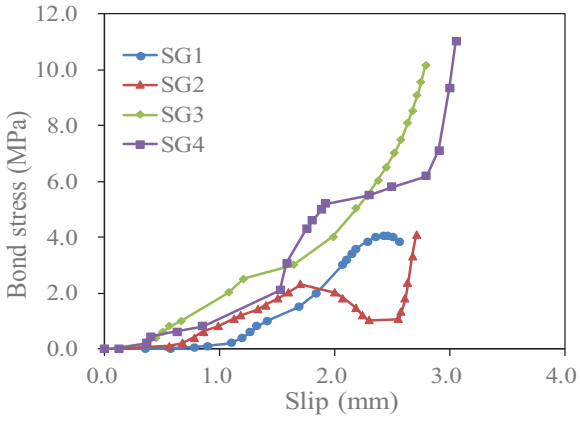

(a) G-E-T2-1

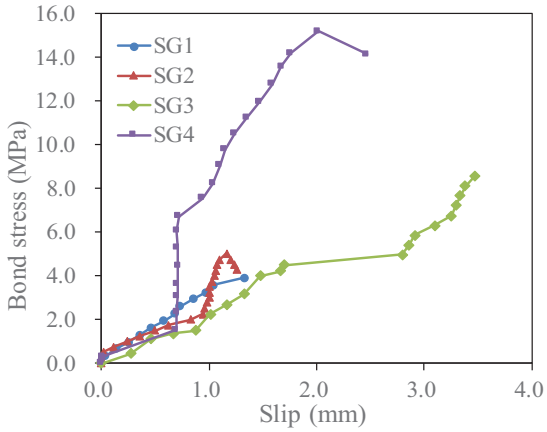

(b) G-E-T-7-1

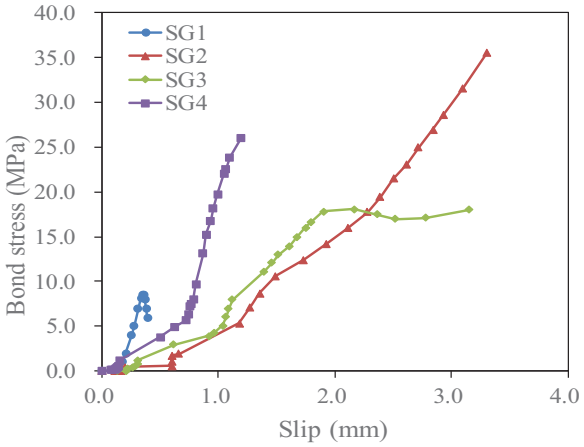

(c) G-E-T14-1

FIGURE 13
Bond stress-slip curves of specimens with epoxy

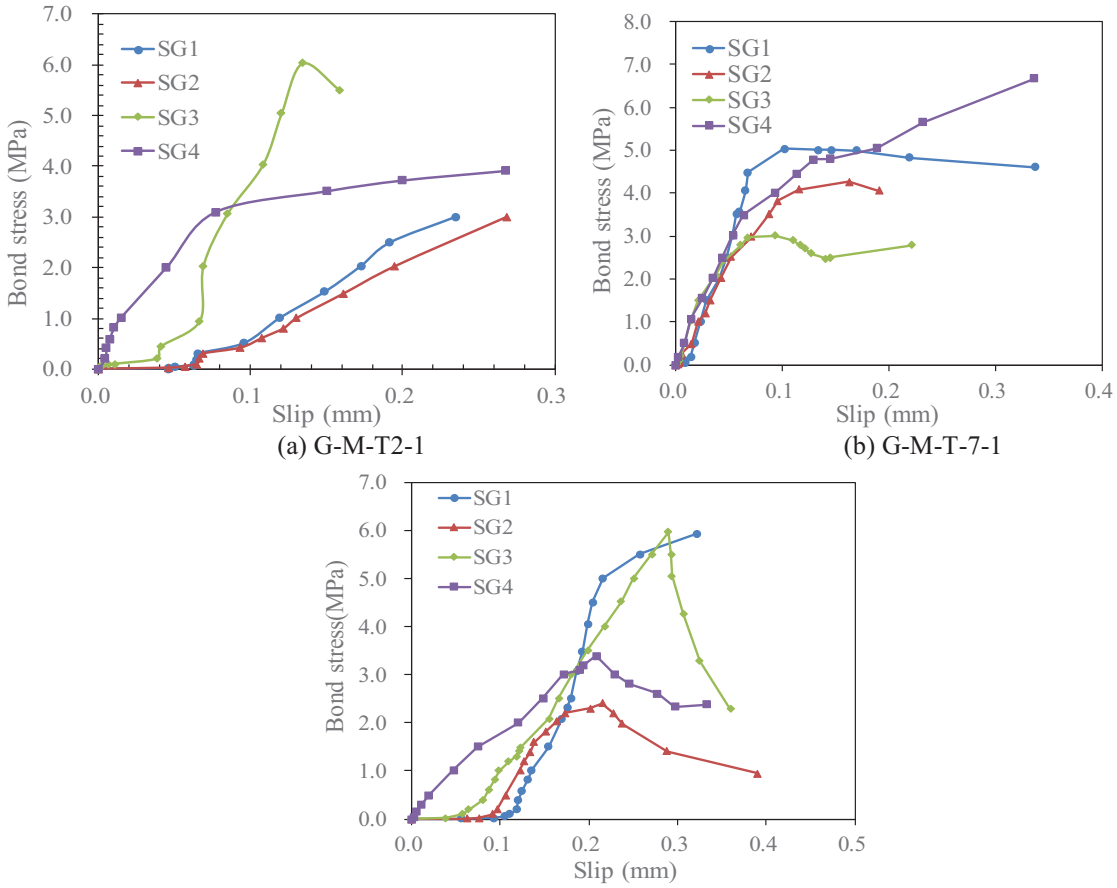

(a) G-M-T2-1 (b) G-M-T-7-1

(c) G-M-T14-1

FIGURE 14
Bond stress-slip curves of specimens with MPC

CONCLUSIONS

MPC is adopted to instead of epoxy as an adhesive material in NSM FRP systems for improving drawbacks of longer curing time, higher curing temperature, and light instability in typical NSM FRP systems with the epoxy. In order to preliminarily investigate the bond performances of this new adhesive material, mix proportion optimization of MPC and pull-out tests of 12 specimens were carried out in this study. Some conclusions are summarized as follows:

(1) Neat MPC is too fast-setting to apply to the NSM system in practice. Some additional agents are needed for slowing the setting time, but it may lower its properties. As a result, a mix proportion optimizing is necessary before being used in the NSM system.

(2) Borax could delay the setting time of MPC, however, it reduced the performance of the MPC. Although a handful of fly ash could improve the performance of the MPC, it speeds up the setting process of MPC. Additionally, the effect of the fly ash proportion on the MPC would reverse when the fly ash proportion exceeded a certain limit.

(3) Failure modes of concrete cover breakage for specimens with the MPC indicate that the MPC has adequate bond strength proper for structure strengthen using NSM technique after no more than two curing day even though weaker than general epoxy. And, the bond strength of the MPC is increasing linearly basically with curing time increasing until to 14 curing days.

(4) A study around effect of other agents and fibers on the MPC bond performance will be soon carried out in purpose of improving the bond strength and ductility of MPC.

ACKNOWLEDGEMENT

The authors acknowledge the financial support received from the National Natural Science Foundation of China (Project No. 51608137).

REFERENCES

[1] De Lorenzis, L., Nanni, A., La Tegola, A. (2000) Flexural and shear strengthening of reinforced concrete structures with near surface mounted FRP rods. International Meeting on Composite Materials, Milan, Italy.

[2] De Lorenzis, L., Nanni, A. (2002) Bond between near-surface mounted fiber-reinforced polymer rods and concrete in structural strengthening. Aci. Struct. J. 99, 123-132.
[3] Hassan, T., Rizkalla, S. (2003) Investigation of bond in concrete structures strengthened with near surface mounted carbon fiber reinforced polymer strips. J. Compos. Constr. 7, 248-257.
[4] Yan, X., Miller, B., Nanni, A., Bakis, C.E. (1999) Characterization of CFRP rods used as near surface mounted reinforcement. In: The 8th International Conference on Structural Faults and Repair, Edinburgh, Scotland.
[5] Merdas, A., Fiorio, B., Chikh, N. (2002) Bond Behavior of Carbon Laminate Strips into Concrete by Pullout-bending Tests. Bond in Concrete 2002, Budapest.
[6] De Lorenzis, L., Rizzo, A., La Tegola, A. (2002) A modified pull-out test for bond of near-surface mounted FRP rods in concrete. Composites Part B: Engineering. 33, 589-603.
[7] De Lorenzis, L. (2002) Strengthening of RC structures with near surface mounted FRP rods, University of Leece, Italy.
[8] De Lorenzis, L., Lundgren, K., Rizzo, A. (2004) Anchorage length of near-surface mounted fiber-reinforced polymer bars for concrete strengthening - Experimental investigation and numerical modeling. Aci. Struct. J. 101, 269-278.
[9] Ma, J., Mo, M. S., Du, X. S., Dai, S. R., Luck, L. (2008) Study of Epoxy Toughened by in Situ Formed Rubber Nanoparticles. Applied Polymer. 110, 304-312.
[10] Xie, R., Theophanous, T., Aguirre, F., Verghese, N., Valette, L., Pham, H. (2011) Advanced Epoxy Resins with Enhanced Toughness for Demanding Applications. International Conference on Thermosets, Stuttgart.
[11] Wang, Z., Yang, X., Wang, Q., Hahn, H.T., Lee, S.G. (2011) Epoxy resin nanocomposites reinforced with ionized liquid stabilized carbon nanotubes. International Journal of Smart and Nano Materials. 2, 176-193.
[12] Gao, J., Li, J., Benicewicz, B.C., Zhao, S., Hillborg, H., Schadler, L.S. (2012) The Mechanical Properties of Epoxy Composites Filled with Rubbery Copolymer Grafted SiO_2. Polymers-Basel. 4, 187-210.
[13] Yang, Q., Zhu, B., Wu, X. (2000) Characteristics and durability test of magnesium phosphate cement-based material for rapid repair of concrete. Materials and Structures. 33, 229-234.
[14] Seehra, S.S., Gupta, S., Kumar, S. (1993) Rapid setting magnesium phosphate cement for quick repair of concrete pavements. Cement Concrete Res. 23, 254-266.
[15] Abdelrazig, B.E.I., Sharp, J.H., EI-Jazairi, B. (1998) The chemical composition of mortars made from magnesia-phosphate cement. Cement Concrete Res. 1, 415-425.
[16] Teng, J.G., De Lorenzis, L., Wang, B., Li, R., Wong, T.N., Lam, L. (2006) Debonding failures of RC beams strengthened with near surface mounted CFRP strips. J. Compos. Constr. 10, 92-105.
[17] Seracino, R., Jones, N.M., Ali, M. S., Page, M. W., Oehlers, D J. (2007) Bond Strength of Near-Surface Mounted FRP Strip-to-Concrete Joints. J. Compos. Constr. 11 (4), 401-409.
[18] Novidis, D., Pantazopoulou, S. J., Tentolouris, E. (2007) Experimental study of bond of NSM-FRP reinforcement. Constr. Build. Mater. 21 (8), 1760-1770.
[19] De Lorenzis, L., Teng, J.G. (2007) Near-surface mounted FRP reinforcement: An emerging technique for strengthening structures. Composites Part B: Engineering. 38 (2), 119-143.
[20] Oehlers, D.J., Haskett, M., Wu, C., Seracino, R. (2008) Embedding NSM FRP Plates for Improved IC Debonding Resistance. 12(6), 635-642.
[21] Zhang, H., He, L., Li, G. (2015) Bond failure performances between near-surface mounted FRP bars and concrete for flexural strengthening concrete structures. Eng. Fail Anal. 56, 39-50.
[22] Lee, D., Cheng, L., Hui, J.Y. (2013)Bond Characteristics of Various NSM FRP Reinforcements in Concrete. J. Compos. Constr. 17(1), 117-129.
[23] Lee, D., Cheng, L. (2013) Bond of NSM systems in concrete strengthening - examining design issues of strength, groove detailing and bond-dependent coefficient. Constr. Build. Mater. 47, 1512-1522.
[24] Peng, H., Hao, H., Zhang, J., Liu, Y., Cai, C.S. (2015) Experimental investigation of the bond behavior of the interface between near-surface-mounted CFRP strips and concrete. Constr. Build. Mater. 96, 11-19.
[25] Al-Mahmoud, F., Castel, A., François, R., Tourneur, C. (2011) Anchorage and tension-stiffening effect between near-surface-mounted CFRP rods and concrete. Cement and Concrete Composites. 33 (2), 346-352.
[26] Sharaky, I.A., Torres, L., Baena, M., Mias, C. (2013) An experimental study of different factors affecting the bond of NSM FRP bars in concrete. Compos. Struct. 99, 350-365.
[27] Mohamed Ali, M. S., Oehlers, D. J., Griffith, M. C., Seracino, R. (2008) Interfacial stress transfer of near surface-mounted FRP-to-concrete joints. Eng. Struct. 30 (7), 1861-1868.

[28] Hassan, T., Rizkalla, S. (2002) Bond mechanisms of near surface mounted FRP bars and strips for flexural strengthening of concrete structures. In: Proceedings of the First International Conference on Structural Health Monitoring of Innovative Civil Engineering Structures, Winnipeg, Canada.
[29] Ding, Z., Li, Z. (2005) High-Early-Strength Magnesium Phosphate Cement with Fly Ash. Aci. Mater. J. 102 (6), 375.
[30] Qiao, F., Chau, C. K., Li, Z. (2010) Property evaluation of magnesium phosphate cement mortar as patch repair material. Constr. Build. Mater. 24 (5), 695-700.
[31] Xu, B., Lothenbach, B., Leemann, A., Winnefeld, F. (2018) Reaction mechanism of magnesium potassium phosphate cement with high magnesium-to-phosphate ratio. Cement Concrete Res. 108, 140-151.
[32] ASTM standard C807:2008. Standard Test Method for Time of Setting of Hydraulic Cement Mortar by Modified Vicat Needle.
[33] ASTM C39/39M:2009. Standard Test Method for Compressive Strength of Cylindrical Concrete Specimens.
[34] ACI 440.2R-08:2008. Guide for the design and construction of externally bonded FRP systems for strengthening concrete structures.
[35] Khshain, N.T., Al-Mahaidi, R., Abdouka, K. (2015) Bond behaviour between NSM CFRP strips and concrete substrate using single-lap shear testing with epoxy adhesive. Compos. Struct. 132, 205-214.
[36] Coelho, M.R.F., Sena-Cruz, J.M., Neves, L.A. C.A (2015) review on the bond behavior of FRP NSM systems in concrete. Constr. Build. Mater. 93, 1157-1169.
[37] Gopinath, S., Murthy, A.R., Patrawala, H. (2016) Near surface mounted strengthening of RC beams using basalt fiber reinforced polymer bars. Constr. Build. Mater. 111, 1-8.
[38] Al-Abdwais, A., Al-Mahaidi, R. (2016) Modified cement-based adhesive for near-surface mounted CFRP strengthening system. Constr. Build. Mater. 124, 794-800.
[39] Chen, C., Cheng, L. (2016) Fatigue Bond Characteristics and Degradation of Near-Surface Mounted CFRP Rods and Strips in Concrete. J. Compos. Constr. 20 (3), 1-14.
[40] Lee, H., Lee, W., Jung, W.T., Chung, W. (2017) Bond characteristics of near-surface-mounted anchorage for prestressing. Constr. Build. Mater. 148,748-756.
[41] Bilotta, A., Ceroni, F., Barros, J.A., Costa, I. (2016) Bond of NSM FRP-Strengthened Concrete: Round Robin Test Initiative. J. Compos. Constr. 20(1), 1-16.

Received: **01.12.2019**
Accepted: **26.01.2020**

CORRESPONDING AUTHOR

Liwen Zhang
Department of Civil Engineering,
Guangzhou University,
Guangzhou 510006 – China

e-mail: zhangliwen9988@aliyun.com

© by PSP Volume 29 – No. 05/2020 pages 3853-3859 Fresenius Environmental Bulletin

DEVELOPMENT CHARACTERISTICS AND DISTRIBUTION CONTROL FACTORS OF OIL RESERVOIRS IN SOUTHERNWESTERN QAIDAM BASIN, CHINA

Bing Hao[1,*], Pengfei Li[2], Xuan Huo[2], Jianhua Zhong[1], Chunqi Xue[1]

[1]School of Geoscience, China University of Petroleum (East China), Qingdao 266580, China
[2]PetroChina Coalbed Methane Company Limited, Baode Xinzhou 036600, China

ABSTRACT

China's Qaidam Basin has the highest elevation in the world. Its complex geological conditions have always been a huge challenge for oil and gas exploration. A systematic summary of the types and distribution patterns of developed reservoirs in the Qaidam Basin is essential to guide oil and gas exploration in this area. In this paper, taking the Yuejin No. 2 East High Point oilfield in the southwestern area of the Qaidam Basin as an example, the petrological characteristics of the Paleogene and Neogene reservoirs and the controlling factors of oil and gas distribution in this area were systematically studied. The results show that the rock type of the target layer is mainly lithic feldspar sandstone, followed by feldspar sandstone. The ratio (Q / (F + R)) of quartz (Q) to feldspar (F) and rock debris (R) is generally between 0.4 and 1.3, with an average of 0.7, indicating that the composition maturity of the sediment is low. The ratio of the framework particle content (G) to the mixed base content (M) (G / M) is between 4.6 and 26.7, with an average of 8.8, indicating that sandstones generally have low mixed base content, low sedimentation medium density, fast sedimentation speed, and low structural maturity. The cements are mainly carbonate cements, and some zeolite cements, gypsum cements, and argillaceous cements are also developed. The oil-bearing well section of the target layer is long, and the continuous oil-bearing well section is 1 300-1 500 m. The oil-bearing area on the plane is widely distributed, and the oil layer is developed thicker in the high structural parts. The oil and gas distribution of the reservoirs in the whole area is mainly controlled by multiple structures, lithology and sedimentary facies. The type of reservoir in this area is structural-lithologic reservoir.

KEYWORDS:
Qaidam Basin, Paleogene, Neogene, oil reservoir, development characteristics, controlling factors

INTRODUCTION

The Qaidam Basin, located in the northern part of the Tibetan Plateau, has the highest elevation in the world. Its average elevation is 2 900 m. Since 1954, there have been 32 proven oil and gas fields in the Qaidam Basin, with proven oil and gas geological reserves of 11.7×10^8 t crude oil equivalent. However, since the beginning of basin exploration in the 1950s, its complex geological conditions have been a huge challenge for oil exploration [1-2]. Subject to the lagging of the guiding ideology of sedimentation, hydrocarbon generation, and accumulation theory, oil and gas exploration in the basin was not discovered on a large scale in the 30 years after the 1970s. Therefore, systematically summarizing the types and distribution rules of developed reservoirs in the Qaidam Basin is important to guide oil and gas exploration in this area [3-8].

Reservoir petrological characteristics, diagenesis and heterogeneity are important research contents for complex oil and gas reservoir evaluation [9-12]. These research contents are also important evaluation factors that determine the formation, type and distribution of the reservoir [13-14]. The key factor for tight reservoir development is the permeability of the reservoir, and the main factor affecting the permeability is the microscopic pore structure of the rock [15-17]. The microscopic pore structure inside the rock is mainly affected by the petrological characteristics, diagenesis and heterogeneity of the reservoir [18-20]. In this paper, taking the Yuejin No. 2 East High Point oilfield in the southwestern region of the Qaidam Basin as an example, the petrological characteristics and controlling factors of oil and gas distribution of the main reservoirs in this area are systematically studied. This research has important reference value for accelerating the exploration and development of tight reservoirs in the area.

MATERIALS AND METHODS

The study area is located in the Yuejin No. 2 East High Point Oilfield in the southwestern Qaidam Basin. The stratigraphic unit division in this area is

TABLE 1
Stratigraphic summary of the study area.

Layer				Code	Evolutionary stage		Structural cycle
System	Series	Formation	Segment				
Quaternary	Pleistocene	Qigequan	/	Q_{1+2}	Fold rise period	Delta frontal subfacies and river facies.	Late Himalayan cycle
Neogene	Pliocene	Shizigou	/	N_2^3			
		Shangyoushashan	/	N_2^2		Lake sediment deposition, delta front subfacies deposition.	
		Xiayoushashan	/	N_2^1	Large depression period		
	Miocene	Shangganchaigou	/	N_1			
Paleogene	Oligocene	Xiaganchaigou	Upper	E_3^2			Early Himalayan cycle
			Lower	E_3^1	Fault depression transitional stage	The river floods the plain facies and the delta plain subfacies.	
	Ancient Eocene	Lulehe	/	E_{1+2}			

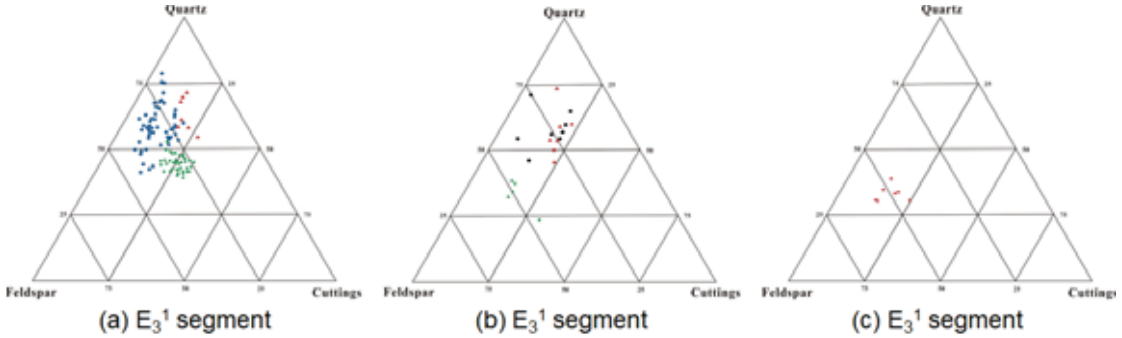

FIGURE 1
Triangular diagram of sandstone classification in each layer of the study area.

shown in Table 1. The main oil-bearing sections of the study area from bottom to top are: the lower segment of the Xiaganchaigou Formation (E_3^1), the upper segment of the Xiaganchaigou Formation (E_3^2), the Shangganchaigou Formation (N_1), and the Shangganchaigou Formation (N_2^1). The buried depth of the reservoir is 770 – 2 280 m. In the longitudinal direction, the length of the oil-bearing well section is generally around 1 400 m, and the average single-layer thickness is 3.1 m.

Because the oil and gas content of different reservoir groups is very different, in order to reveal the development status and distribution characteristics of the reservoir, this paper uses drilling and logging data to comprehensively interpret the oil reservoir and sand [21-24]. The experimental testing items of reservoir petrology analysis include thin slice analysis, mineral component identification and petrophysical property testing. The size of the samples for thin section analysis and identification of mineral components was 2 cm × 2 cm, and the testing instrument was an OLYMPUS microscope. Petrophysical property testing items include porosity and permeability. The testing instruments are KXD-II porometer and permeameter (QT-2).

Rock type. Based on the statistical analysis of core slice analysis data of 5 wells in Yuejin No.2 oilfield, the petrological characteristics were studied. The rock types of Yuejin No. 2 are classified according to the SY / T5579-2000 standard, and are mainly lithic feldspar sandstone, followed by feldspar sandstone (Figure 1). Sandstone generally contains carbonates; a small amount of sandstone is gypsum-bearing or gypsum debris feldspar sandstone. Part of the oil-rich medium and fine sandstone is loose sand. The granular composition of the rocks is relatively fine, mainly composed of fine sandstone, ultrafine sandstone, medium-fine sandstone, and fine-grained sandstone, followed by medium sandstone, coarse sandstone, and conglomerate sandstone.

Rock debris component. The content of feldspar and rock debris are relatively high, between 20-30% and 15-20%, respectively. The quartz content generally varies between 30-43%. Feldspar is dominated by plagioclase and orthoclase, and a small amount is plagioclase. The rock debris are mainly igneous and metamorphic rock debris, and there are fewer sedimentary rock debris. A small amount of crystalline limestone rock debris with small particle size and good roundness can be seen.

Rock structure. The shape of sandstone particles in the reservoir is angular and subangular with poor roundness. From the analysis of the particle size of the coring data, it can be seen that the reservoir is mainly fine medium sandstone and fine sandstone, and the degree of separation is poor [25-26]. As the particle sortability decreases, the main particles that make up the rock transition from one to two or three. The smaller the particles, the more muddy the rock is. The cementation forms of rocks are mainly pore-

type and contact-type, and the interstitial materials are mainly distributed between the grains and the grain surface (Figure 2). When anhydrite is the main cementation, the rocks are mainly matrix cementation.

Rock maturity. The ratio (Q / (F + R)) of quartz (Q) to feldspar (F) and rock debris (R) is generally between 0.4 and 1.3, with an average of 0.7, indicating that the composition maturity of the sediment is low. The ratio of the framework particle content (G) to the mixed base content (M) (G / M) is between 4.6 and 26.7, with an average of 8.8, indicating that sandstones generally have low mixed base content, low sedimentation medium density, fast sedimentation speed, and low structural maturity. Detrital particles are mainly sub-angular-sub-circular, and the sorting waits until the difference is poor, which also shows that the rocks are of medium to low maturity. Overall, the sandstone in this area has near-source, unreformed sediments and low-mature petrological characteristics.

Cementitious characteristics. The data of rock thin sections and cast thin sections were used to study the characteristics of mineral cementation.

(1) Carbonate cement. Carbonate cement is the main interstitial material in this area, and it is common in all sand layers from shallow to deep [27-28]. 80-90% of its mineral composition is calcite, and the rest is dolomite and a small amount of iron calcite and iron dolomite. Calcite is mostly mud-like or powder-like, and a few are plaque-shaped and fill the intergranular pores. Calcite secondary enlarged edges were seen on some calcite particles, indicating that the formation of calcite cements has multiple phases. Some mud crystal calcite cements recrystallize into bright crystal calcites. The analysis of thin sections shows that the content of calcite cements in sandstone varies greatly, ranging from 2-26%, and generally accounts for 50-70% of the total cement. The content of dolomite in sandstone is not high, and it usually changes between 2-10%. In some horizons, such as the middle sandstone of the N_1 horizon in Well Yue12, the dolomite content can be as high as 25%, forming a dolomitic cementation layer. The content of iron calcite and iron dolomite is <5%. The generation sequence of the above carbonate minerals is roughly:

Calcite→Dolomite and iron calcite→Iron dolomite

Most of the calcite crystals analyzed by scanning electron microscopy were filled with erosive particles and filled the intergranular pores; the dolomite rhombic crystals were slightly eroded and the edges were smooth.

(2) Zeolite cement. The zeolite cements appearing in this area are sodium zeolite-alumite. It only appears intermittently in the lower layer of N_1 and the upper layer of E_3^1. The intergranular pores filled with calcite are filled in continuous crystals or agglomerates, and the content is generally less than 5%. The formation of zeolite is later than that of calcite. Although its content and distribution are far inferior to those of calcite and anhydrite, the damage to the pores is quite obvious [29]. Wells such as Yue 12 are in the N_1 and E_3^1 formations, and the sandstones appearing in zeolite have poor oil-bearing properties, and have changed from oil-saturated-oil-containing grades to oil-stain-oil-immersed grades.

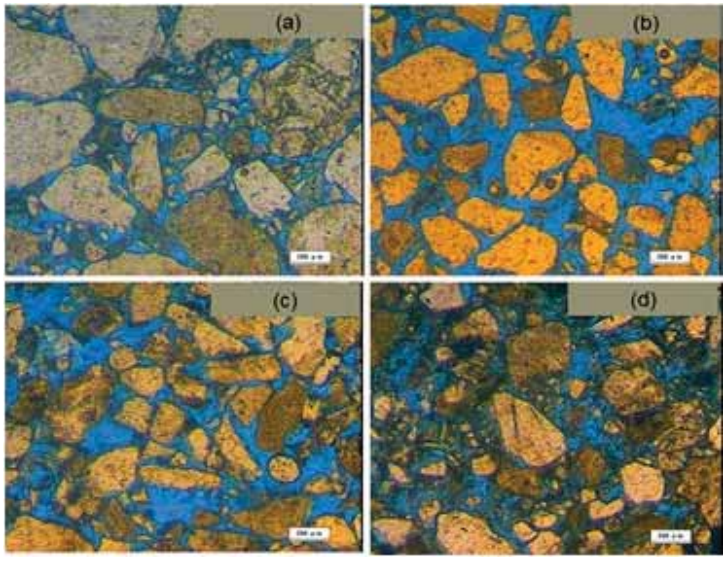

FIGURE 2
Microscopic characteristics of target rock samples.
Notes: (a) Cast thin section image of Well Jian 1 (pore cementation); (b) Cast thin section image of Well Jian 1 (contact cementation); (c) Cast thin section image of Well Jian 2 (contact cementation); (d) Cast thin section image of Well Jian 2 (pore cementation).

TABLE 2
Statistical results of reservoir petrophysical parameters in each interval of the study area.

Horizon	Average porosity (%)	Average permeability ($10^{-3}\mu m^2$)	Pore throat radius (μm)	Average pore throat radius (μm)	Throat sorting coefficient	Throat variation coefficient
N_2^1	20.46	250.07	2.12 − 15.59	6.58	6.45	0.47
N_1	22.03	253.2	3.82 − 57.15	9.81	4.26	0.38
E_3^1	15.6	208.9	1.90 − 19.21	5.87	4.71	0.403

(3) Gypsum cement. It is an important interstitial material in the deep (lower E_3^1) reservoirs in this area. It is mainly anhydrite, gypsum is rare, and other layers rarely occur. The depth at which anhydrite begins to appear is often the depth at which analite disappears. The content of anhydrite varies widely, from 2-25%, with extremely uneven distribution. Its content and crystallization habit are obviously related to the particle size of sandstone. The anhydrite that appears in fine sandstone is mostly scattered or scattered in the pores, and the content is not high, usually less than 10%. When it coexists with marl cement in the intergranular pores of sandstone, it is a good reservoir. However, in medium-coarse-grained or coarse-grained sandstone, anhydrite often forms a continuous crystal to form a base cement paste or paste-containing sandstone. The content of anhydrite usually reaches 20-25%, which becomes the main component of the cement and is a poor reservoir.

Scanning electron microscope showed plate-like anhydrite crystals filled in the intergranular pores. Regarding the generation sequence of anhydrite and calcite, it is common to see that calcite is island-shaped in anhydrite cementite cement in the rock thin sections [30]. We can often see anhydrite growing around calcite (the boundary morphology is the same as calcite), but no calcite is wrapped in anhydrite, indicating that anhydrite cemented later than calcite. Therefore, the formation of anhydrite and anhydrite in the sandstone cement in this area are later than the early calcite cement. The cementation sequence of them is calcite → analcite → anhydrite. The former was explained by the latter in turn, and the cementation of anhydrite occurred at the latest.

(4) Argillaceous cement. It is another major interstitial material in this area. It is often mixed with mud crystal carbonate to form marl cement and fills the pores. The argillaceous cements are mainly montmorillonite, illite / smectite mixed layer, illite, chlorite and kaolinite. Among them, the mineral content of montmorillonite or the illite / smectite mixed layer varies between 2 and 42%. It appears in the N_2^1-N_1 horizon and disappears in the E_3^1 interval. Illite is the main component in argillaceous interstitials, and its content varies from 50-80%. From shallow to deep, the content also increases significantly with depth. Chlorite and kaolinite are both low in content and not much changed at 20-40%. From shallow to deep, the composition of clay minerals changes regularly:

Montmorillonite or illite / smectite mixed layer (disorderly)-- Illite -- Chlorite + Kaolinite

↓

Illite / smectite mixed layer (orderly)-- Illite -- Chlorite + Kaolinite

↓

Illite -- Chlorite + Kaolinite

With the increase of the burial depth, the argillaceous interstitial material has undergone the transformation of clay minerals from montmorillonite → illite / smectite mixed layer → illite. This shows that they are no longer terrestrial heterogeneous bases controlled by denuded areas, but have been modified by the diagenetic environment during the burial-diagenesis process, forming a new clay mineral facies. It has evolved from heterogeneous interstitials to cements that participate in various diagenesis [31]. The content of argillaceous interstitial components in sandstone varies greatly, accounting for 15-60% of the total cement, and generally between 30-50%.

Reservoir properties. In the longitudinal direction of Yuejin No.2, the petrophysical properties of the N_1 reservoir are the best, with an average porosity of 22.03% and an average permeability of 253.2×10^{-3} μm²; followed by the petrophysical properties of the N_2^1 reservoir, with an average porosity of 20.46% and an average permeability of 250.07×10^{-3} μm²; E_3^1 reservoirs have relatively poor petrophysical properties, with an average porosity of 15.6% and an average permeability of 208.9×10^{-3} μm². The target layers as a whole belong to mesoporous and medium-permeability reservoirs (Table 2).

RESULTS

Reservoir distribution characteristics. The distribution area of each oil layer in the target layer is wide, and there are many layers and large thicknesses. The area is dominated by tectonic lithologic reservoirs, and the reservoirs are mainly concentrated in the high structural parts. For the upper fault system, the N_2^1 and N_1 reservoirs are thicker, with a maximum thickness of 30-50 m, and the N_2^1, N_1, and E_3^2 reservoirs develop unconformities, so the reservoirs are thin and the maximum thickness is between

10-20 m. The maximum oil layer thickness of other oil layer groups is between 20-30 m. For the lower fault system, the E_3^1 reservoir is affected by lithology and the reservoir is thicker, with a maximum thickness of 27.3 m and a maximum thickness of E_3^1 of about 10 m.

On the whole, the characteristics of oil and gas distribution are mainly as follows: Except for the two thin oil layers E_3^1 and E_3^1, the other oil layers are relatively well developed. And the oil-bearing well section is long, and the continuous oil-bearing well section is 1 300-1 500 m. The oil-bearing area is widely distributed on the plane, and the oil layer develops thicker in the high part of the structure.

Controlling factors of reservoir distribution. The oil and gas distribution of the reservoirs in the whole area is mainly controlled by multiple structures, lithology and sedimentary facies. The type of reservoir in this area is structural-lithologic reservoir, so the difference of oil-gas-water interface between different fault blocks in different horizons is large, and there is no unified oil-water interface.

Oil and gas are enriched in high parts near the No. 1 inversion fault. The structure of Yuejin No. 2 East High Point Oilfield is a lithological structure trapped reservoir that is complicated by faults and is dominated by structural control and affected by lithology. The basic structure is a fault anticline structure complicated by faults. The sedimentary thickness of the top layer of the oilfield structure is slightly thinner than that of the wing, and the sedimentary particles are relatively coarse, which is the same sedimentary structure. According to the small-layer sedimentary facies belt and the corresponding oil layer configuration, it is found that the distribution of the oil layer is closely related to the facies zone. The oil layer is mainly distributed in the subdivision channel belt.

The type of reservoir in this area is lithologic structural trap reservoir. The specific characteristics are as follows: The plane distribution of the reservoir is controlled by the structure, and the distribution of the reservoir is mainly concentrated in the high structure. The thickness distribution of the reservoir in the oil-bearing range is relatively stable. Oil and gas are formed around fault traps in the surrounding area, and the thickness of the oil layer on the plane does not change much. As shown in Figure 3, lithology and faults form a shield together. Due to the influence of lithology and petrophysical properties on the plane, the thickness of the reservoir changes greatly.

CONCLUSIONS

(1) The rock type of the target layer in the Yuejin No. 2 East High Point oilfield is mainly lithic feldspar sandstone, followed by feldspar sandstone. The content of feldspar and rock debris are relatively high, between 20-30% and 15-20%, respectively. The quartz content generally varies between 30-43%. Feldspar is dominated by plagioclase and orthoclase, and a small amount is plagioclase.

(2) The ratio (Q / (F + R)) of quartz (Q) to feldspar (F) and rock debris (R) is generally between 0.4 and 1.3, with an average of 0.7, indicating that the composition maturity of the sediment is low. The ratio of the framework particle content (G) to the mixed base content (M) (G / M) is between 4.6 and 26.7, with an average of 8.8, indicating that sandstones generally have low mixed base content, low sedimentation medium density, fast sedimentation speed, and low structural maturity. The cements are mainly carbonate cements, and some zeolite cements, gypsum cements, and argillaceous cements are also developed.

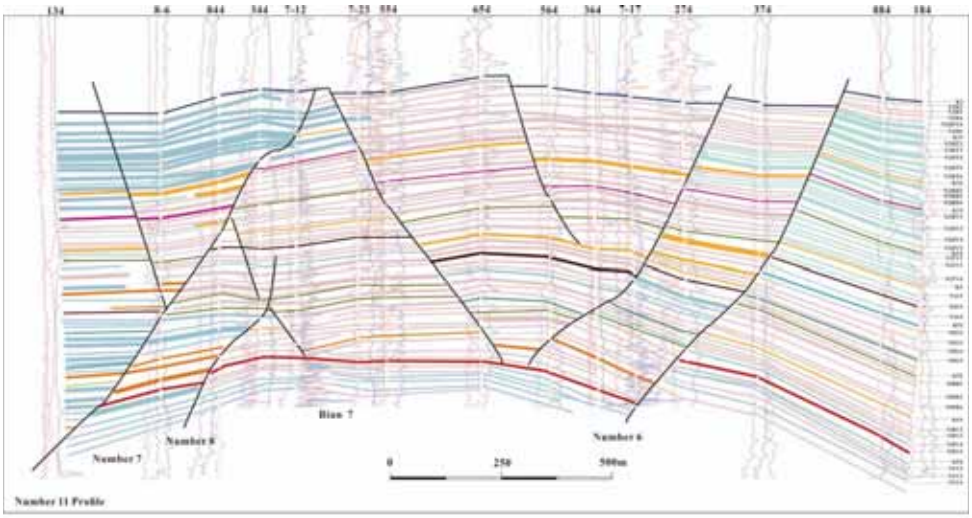

FIGURE 3
Reservoir profile of the N_2^1-N_1 formation in Wells 134-184 in the study area.

(3) The oil-bearing well section of the target layer is long, and the continuous oil-bearing well section is 1 300-1 500 m. The oil-bearing area on the plane is widely distributed, and the oil layer is developed thicker in the high structural parts. The oil and gas distribution of the reservoirs in the whole area is mainly controlled by multiple structures, lithology and sedimentary facies. The type of reservoir in this area is structural-lithologic reservoir.

ACKNOWLEDGEMENTS

The authors would like to show their sincere thanks to those persons who have helped this work and all the authors of the references.

REFERENCES

[1] Zhang, X.C., Sun, Z.D., Zhao, J.S., Pan, Y.Y., Wu, M.Z. (2014) Study on the influence of strike-slip fault displacement on reservoir in Northern slope, Tazhong area. Geoscience. 28(5), 1017-1022.

[2] Peters, K. (1986) Guidelines for evaluating petroleum pyrolysis. AAPG Bulletin. 70, 318-329.

[3] Hakimi, M., Abdullah, W., Shalaby, M. (2010) Source rock characterization and oil generating potential of the Jurassic Madbi formation, onshore East Shabowah oilfields, Republic of Yemen. Organic Geochemistry. 41, 513-521.

[4] Klemme, H., Ulmishek, G. (1991) Effective petroleum source rocks of the world: Stratigraphic distribution and controlling depositional factors. AAPG Bulletin. 75(12), 1809-1851.

[5] Lasaga, A., Luttge, A. (2001) Variation of crystal dissolution rate based on a dissolution step wave model. Science. 291(5512), 2400-2404.

[6] Lasaga, A., Lüttge, A. (2004) Mineralogical approaches to fundamental crystal dissolution kinetics. American Mineralogist. 89(4), 527-540.

[7] Davisson, M., Criss, R. (1996) Na - Ca - Cl relations in Basinal fluids. Geochimica et Cosmochimica Acta. 60(15), 2743-2752.

[8] Cao, Y., Liu, L., Chen, D., Wang, C., Yang, W., Kang, L., Zhu, X. (2017) Partial melting during exhumation of Paleozoic retrograde eclogite in north Qaidam, Western China. Journal of Asian Earth Sciences. 148, 223-240.

[9] Guo, P., Liu, C., Yu, M., Ma, D., Wang, P., Wang, K., Mao, G., Zhang, Q. (2017) Paleosalinity evolution of the Paleogene perennial Qaidam Lake on the Tibetan Plateau: Climatic vs. tectonic control. International Journal of Earth Sciences. 107(5), 1641-1656.

[10] Chen, X., Xu, R., Schertl, H., Zheng, Y. (2018) Eclogite-facies metamorphism in impure marble from north Qaidam orogenic belt: Geodynamic implications for early Paleozoic continental-arc collision. Lithos. 310-311, 201-224.

[11] Fisher, J., Boles, J. (1990) Water-rock interaction in Tertiary sandstones, San Joaquin Basin, California, USA: Diagenetic controls on water composition. Chemical Geology. 82, 83-101.

[12] Peters, K., Walters, C., Moldowan, J. (2005) The biomarker guide (Volume 2): Biomarkers and isotopes in petroleum exploration and earth history. Cambridge: Cambridge University Press.

[13] Horita, J., Zimmermann, H., Holland, H. (2002) Chemical evolution of seawater during the Phanerozoic: Implication from the record of marine evaporites. Geochimica et Cosmochimica Acta. 66(21), 3733-3756.

[14] Qin, Y., Feng, Q., Chen, G., Chen, Y., Zou, K., Liu, Q., Jiao, Q., Zhou, D., Pan, L., Gao, J. (2018) Devonian post-orogenic extension-related volcano-sedimentary rocks in the northern margin of the Tibetan plateau, NW China: Implications for the Paleozoic tectonic transition in the north Qaidam orogen. Journal of Asian Earth Sciences. 156, 145-166.

[15] Liu, Y., Qiu, Z., Zhong, H., Nie, Z., Li, J., Huang, W., Zhao, X. (2019) Bitumen Recovery from Crude Bitumen Samples from Halfaya Oilfield by Single and Composite Solvents-Process, Parameters, and Mechanism. Materials. 12(17), 2656.

[16] Yang, J., He, Y., Luo, Y. (2019) Application of Improved Newberry Model in Geostress Prediction of Coal Measure Tight Sandstone Formation. Fresen. Environ. Bull. 28, 6965-6971.

[17] Lv, D., Wang, D., Li, Z., Liu, H., Li, Y. (2016) Depositional environment, sequence stratigraphy and sedimentary mineralization mechanism in the coal bed- and oil shale-bearing succession: A case from the Paleogene Huangxian Basin of China. Journal of Petroleum Science and Engineering. 148, 32-51.

[18] Lv, D., Zhang, M., Wang, H., Song, G., Zhou, Z., Meng, Y., Yong, P., Yang, Q. (2016) Petroleum accumulation conditions of the Paleogene Shahejie formation in Qingdong Sag of Bohai Bay Basin, Eastern China. Arabian Journal of Geosciences. 9(3), 228.

[19] Lv, D., Chen, J., Li, Z., Zheng, G., Song, C., Liu, H., Meng, Y., Wang, D. (2014) Controlling factors, accumulation model and target zone prediction of the coal-bed methane in the Huanghebei Coalfield, north China. Resource Geology. 64(4), 332-345.

[20] Moon, V. (1993) Microstructural controls on geomechanical behavior of ignimbrite. Engineering Geology. 35(4), 19-31.

[21] Zhu, R., Lou, Z., Yun, L. (2008) Occurrence and distribution of formation water in the Ordovician reservoirs of the Tahe Oilfield. Chinese Journal of Geology. 43(2), 228-237.
[22] Yin, S., Lv, D., Ding, W. (2018) New method for assessing microfracture stress sensitivity in tight sandstone reservoirs based on acoustic experiments. International Journal of Geomechanics. 18(4), 1-16.
[23] Kharaka, Y., Law, L., Carothers, W. (1986) Role of organic species disvolved in formation water from sedimentary basins in mineral diagenesis. In: Gautier, D.L. (ed.) Role of Organic Matter in Sediment Diagenesis. Soc. Econ. Paleontol. Mineral. Spec. Publ. 38, 111-122.
[24] Kukal, G. (1984) A systematic approach for the effective log analysis of tight gas sands. In: Proceedings of the SPE Unconventional Gas Recovery Symposium. Society of Petroleum Engineering of AIME, Pennsylvania, New York.
[25] Connolly, C., Walter, L., Baadsgaard, H., Longstaffe, F. (1990) Origin and evolution of formation waters, Alberta Basin, Western Canada Sedimentary Basin. Applied Geochemistry. 5, 375-413.
[26] Yin, S., Han, C., Wu, Z., Li, Q. (2019) Developmental characteristics, influencing factors and prediction of fractures for a tight gas sandstone in a gentle structural area of the Ordos Basin, China. Journal of Natural Gas Science and Engineering. 72, 1-14.
[27] Yin, S., Zhao, J., Wu, Z., Ding, W. (2018) Strain energy density distribution of a tight gas sandstone reservoir in a low-amplitude tectonic zone and its effect on gas well productivity: A 3D FEM study. Journal of Petroleum Science and Engineering. 170(6), 1-16.
[28] Yin, S., Han, C., Wu, Z., Li, Q. (2019) Developmental characteristics, influencing factors and prediction of fractures for a tight gas sandstone in a gentle structural area of the Ordos Basin, China. Journal of Natural Gas Science and Engineering. 72, 1-14.
[29] Ursula, I.V., Jorge, O.P. (2014) Artificial neural networks applied to estimate permeability, porosity and intrinsic attenuation using seismic attributes and well-log data. Journal of Applied Geophysics. 107, 45-54.
[30] Knauth, L., Beeunas, M. (1986) Isotope geochemistry of fluid inclusions in Permian halite with implications for the isotopic history of ocean water and origin of saline formation waters. Geochimica et Cosmochimica Acta. 50, 419-433.
[31] Peters, K., Moldowan, J. (1993) Guide for the application of biological markets. New Jersey: Prentice-Hall.

Received: **03.12.2019**
Accepted: **16.02.2020**

CORRESPONDING AUTHOR

Bing Hao
School of Geoscience,
China University of Petroleum (East China),
Qingdao 266580 – China

e-mail: 312034461@qq.com

© by PSP Volume 29 – No. 05/2020 pages 3860-3869 Fresenius Environmental Bulletin

EFFECTS OF DIFFERENT STORAGE TEMPERATURES AND DURATIONS ON ESSENTIAL OF COMPONENTS OF *MENTHA PIPERITA*

Meryem Yesil*

Department of Crop and Animal Production, Vocational School of Technical Sciences, Ordu University, Ordu, 52200, Turkey

ABSTRACT

This study was conducted to identify the storage temperature and duration providing the least quality losses in essential oil of *Mentha piperita* of Lamiaceae family with a great economic significance throughout the storage. The *Mentha piperita* leaves harvested at the beginning of flowering were dried in a drying cabin at 35 °C. Essential oils were extracted with the aid of Clevenger device, placed into glass vials. The control group was analyzed for essential oil components and ratios right after the distillation and the experimental groups were analyzed after storage of essential oil samples in a fridge at 2 °C, 4 °C, 6 °C, -18 °C, -20 °C and -22 °C temperatures for 1, 3 and 6 months with the aid of a GC-MS device. Present findings revealed that storage conditions had significant effects on essential oil components. As compared to essential oil components of the control group, 3 months of storage at storage temperatures of below 0 °C could be recommended for α-pinene, β-pinene, 1,8-cineole, pulegone, piperitone and caryophyllene components, 6 months of storage at 2°C for menthone, 6 months of storage at -20°C for menthol and 6 months of storage at -18 °C for caryophyllene component.

KEYWORDS:
Essential oil components, *Mentha piperita*, storage duration, storage temperature

INTRODUCTION

Essential oils are obtained from plants or herbal drugs through water or water vapor distillation. They are liquid at room temperature, but frozen sometimes, volatile, redolence and greasy mixtures. They are called with different names such as “volatile oils” since they can volatilize at room temperature whey they were exposed to open air, “etheric oils” since they volatilize like ether, “essential oils” since they have nice smell and are used in perfumes [1]. Plant essential oils have been used for years for various scientific and commercial purposes. They are mostly used in cosmetics, drugs, food industry, aromatherapy and phytotherapy [2]. Essential oils have various analgesic (pain relieving), antiseptic (preventing propagation of microbes), antifungal (against fungi), antiviral (preventing virulence), bactericide (against bacteria), sedative (tranquillizer), stimulant, antioxidant (preventing negative impacts of free radicals) effects. These attributes may vary with the type of essential oil, but they all have common antibiotic, disinfectant and immune system boosting effects [3, 4, 5, 6].

With such significant attributes, essential oils have a high economic value, thus aromatic and medicinal plants with a high essential oil content have been farmed in several countries [7]. However, essential oils with quite a high economic value are significantly influenced by the plants from they originated, ecological conditions under which they were grown, various agronomic practices, drying methods and storage durations [8, 9]. Previous researchers reported changes in essential oils of *Salvia sclarea* L. Rhyu, *Satureja hortensis* L., Bauer et. al., *Caryophyllus aromaticus* L. and Gopalakrishnan *Elettaria cardamomum* L. throughout the storage [10, 11, 12]. Misharina, stored *Coriandrum sativum* L. essential oil under room temperature at dark and light environment for 1, 2, 4, 6, 9 and 12 months and indicated that chemical changes took place in essential oils at light environment might result in negative outcomes in human health [13]. Therefore, each material has a certain expiration date. The essential oils of aromatic and medicinal plants which are used as industry raw material are easily influenced by storage temperatures and durations and such factors may shorten the shelf life of essential oils. Together with increased awareness on health, industrial sector has started to place emphasis on food security. Especially in food industry and the other industries directly related to human health, a special emphasis should be placed on post-harvest processes of essential oils just to prevent any negative impacts of essential oils on human health and also to prevent economic losses. Erroneous storage and packaging may readily alter chemical composition of essential oils, then reduce industrial value of essential oils and consumer satisfaction.

TABLE 1
Descriptive statistics and multiple range test results for α-pinene (%)

°C	1-Month			3-Month			6-Month		
	Average	Std. Error	Std. Deviation	Average	Std. Error	Std. Deviation	Average	Std. Error	Std. Deviation
Control	*1.600*^{A}	*0.006*	*0.010*						
2	1.297Aa^{B}	0.050	0.087	1.383Aa^{A}	0.033	0.057	1.103Aa^{B}	0.015	0.025
4	1.383Aab^{A}	0.024	0.042	1.543Aa^{A}	0.061	0.105	1.120Ab^{B}	0.012	0.020
6	1.097Ab^{B}	0.063	0.110	1.593Aa^{A}	0.097	0.167	1.067Ab^{B}	0.019	0.032
-18	1.347Aab^{A}	0.064	0.110	1.520Aa^{A}	0.091	0.157	1.040Ab^{B}	0.006	0.010
-20	1.220Ab^{B}	0.118	0.205	1.653Aa^{A}	0.012	0.021	1.197Ab^{B}	0.127	0.220
-22	1.237Ab^{B}	0.003	0.006	1.613Aa^{A}	0.048	0.083	1.087Ab^{B}	0.012	0.021
P-Value	Storage Duration: 0.000 Storage Temperature: 0.232 Storage Duration x Storage Temperature: 0.044*								

*, significant ($p<0.05$)
The means indicated with the different capital letters in the same storage duration are significantly different ($p<0.05$)
The means indicated with the different small letters in the same storage temperature are significantly different ($p<0.05$)
^{B}, Significantly different from the control sample according to Dunnett's test ($p<0.05$)

In this study, effects of different storage temperatures and durations on essential oil composition of *Mentha piperita* plants were investigated.

MATERIALS AND METHODS

Material. The *Mentha piperita* species used in present experiments were supplied from The Medicinal Plant Collection Garden of Ordu University Agricultural Faculty.

Method. Material propagation, fertilization and harvest. About 5-7 cm root-scions of *Mentha piperita* were rooted in turf-filled viols and transplanted into the field on 15 May 2018 at 40 cm row spacing and 30 cm on-row plant spacing. Each plot had 16 rows with 30 plants on each. Plot total area was 54 m^2. DAP (18%) and TSP (42%) fertilizers were applied at planting as to have 5 kg/da of each.

M. piperita shoots were harvested at the beginning of flowering and leaves were separated from the shoots and dried in a drying oven at 35 °C.

Extraction and storage of essential oils. Essential oils were extracted with a Clevenger apparatus in 3 replicates. Essential oil extracts were placed into glass vials and stored in fridges set at 2 °C, 4 °C, 6 °C, -18 °C, -20 °C, -22 °C for 1, 3 and 6 months.

Essential oil components. Essential oil components were determined with the aid of GC-MS (GC/MS-QP2010 Shimadzu brand) device. Helium was used as the carried gas. GC-MS parameters were as follows:
Column: TRB-5MS (30 m x0.25 mm x0.25 µm)
Injection Temperature: 250 °C
Injection Mode: Split
Flow Control Mode: Pressure
Pressure: 80 kPa
Split Ratio: 25
Column Temperature program: 40 °C 2 min
4 °C/min 240 °C 3 min
Ion source Temperature: 200°C
Interface Temperature: 250°C
Start Time: 0 min End Time: 55 min
Acquisition Mode: Scan
Start m/z: 40 End m/z: 4000

Data assessment. Data normality was checked by Kolmogorov-Smirnov test, variance homogeneity was checked by Levene's test. Two-way ANOVA procedure was applied to experimental data in accordance with completely randomized block design with 3 replications. Significant means were compared with the aid of Tukey's multiple comparison test. Dunnett's test was used to compare the control group with the experimental groups. In present calculations and assessments, significance level (α) was considered as 5%. Statistical calculations were performed with the aid of SPSS v25 (IBM Inc., Chicago, IL, USA) software.

RESULTS AND DISCUSSION

The major essential oil components of *Mentha piperita* were presented in this study. Two-way variance analyses revealed that storage duration x storage temperature interactions had significant effects on α-pinene, 1,8-cineole and pulegone components ($p<0.05$) and on β-pinene, menthone, menthol, piperitone, caryophyllene and germacrene-D components ($p<0.001$).

α-pinene ratio (%). Storage durations alone (1, 3 and 6 months) did not have significant effects on α-pinene contents (Table 1). Considering the storage durations, it was observed that 3 months of storage significantly increased α-pinene ratios as compared to the other storage durations ($p<0.05$).

TABLE 2
Descriptive statistics and multiple range test results for β–pinene (%)

°C	1-Month			3-Month			6-Month		
	Average	Std. Error	Std. Deviation	Average	Std. Error	Std. Deviation	Average	Std. Error	Std. Deviation
Control	*3.003*^{A}	*0.009*	*0.015*						
2	2.433ABa^{B}	0.015	0.025	2.550Ba^{B}	0.049	0.085	1.447Ab^{B}	0.012	0.021
4	2.487Aa^{B}	0.023	0.040	2.680ABa^{B}	0.029	0.050	1.443Ab^{B}	0.023	0.040
6	2.207Bb^{B}	0.034	0.059	2.757ABa^{B}	0.074	0.129	1.370Ac^{B}	0.012	0.020
-18	2.440ABb^{B}	0.090	0.156	2.760ABa^{B}	0.066	0.114	1.327Ac^{B}	0.009	0.015
-20	2.337ABb^{B}	0.139	0.240	2.933Aa^{A}	0.028	0.049	1.423Ac^{B}	0.015	0.025
-22	2.287ABb^{B}	0.012	0.021	2.947Aa^{A}	0.013	0.023	1.477Ac^{B}	0.038	0.065
P-Value	Storage Duration: 0.000 Storage Temperature: 0.027 Storage Duration x Storage Temperature: 0.000***								

***, significant ($p<0.001$)
The means indicated with the different capital letters in the same storage duration are significantly different ($p<0.05$)
The means indicated with the different small letters in the same storage temperature are significantly different ($p<0.05$)
^{B}, Significantly different from the control sample according to Dunnett's test ($p<0.05$)

The α-pinene ratio of control samples (1.600%) decreased at 6 °C (1.097%), -20 °C (1.220%), -22 °C (1.237%) storage temperatures of 1-month storage duration and at all storage temperatures of 6-month storage duration ($p<0.05$), but storage temperatures did not result in significant changes in α-pinene ratios of 3-month storage duration ($p>0.05$). In 3-month storage, α-pinene ratios increased at -20 °C (1.653%) and -22 °C (1.613%) storage temperatures. The greatest decrease in α-pinene ratio (1.600%) was observed at -18 °C (1.040%) of 6-month storage and it was followed by 6 °C (1.067%) of 6-month storage (Table 1). These findings comply with the findings of the earlier studies indicating that essential oils were significantly influenced by plant origins, ecological conditions, agricultural practices, drying method, storage durations and conditions [8, 9, 14]. Bahmanzadegan et al., investigated the effects of different storage temperatures and durations on essential oils of *Myrtus communis* L. and stored essential oils at 4 ^{0}C, -20 ^{0}C and room temperature for 3 months [15]. Researchers reported that α-pinene, limonene, 1,8-cineole and α-terpinene ratios decreased at room temperature and α-terpineol and geranyl acetate ratios increased at the end of 3-month storage. Increases were also observed in α-terpineol and geranyl acetate ratios, increasing essential oil quality, at the end of the storage at room temperature. It was concluded that minimum change and original quality was achieved at -20 ^{0}C storage temperature. Najafian, conducted a study with the essential oils of *Melissa officinalis* species and reported α-pinene ratio as 0.9% right after distillation, 1.2% at the end of 1-month storage at 4 °C, 0.8% at the end of 2-month storage, 0.8% at the end of 3-month storage and 0.5% at the end of 5-month storage. In present study, α-pinene ratios also increased numerically at the end of 3-month storage at -20 °C and -22 °C storage temperatures [16].

β-pinene ratio (%). Considering the storage durations alone, it was observed that β-pinene ratio at the end of 1-month storage at 4 °C (2.487%) was significantly greater than the β-pinene ratio at 6 °C (2.207%) ($p<0.05$). The other temperatures did not result in significant changes in β-pinene ratios of 1-month storage. The β-pinene ratio at 2 °C of 3-month storage (2.550%) mathematically increased at the other temperatures, but such increases were found to be significant only at -20 °C (2.933%) and -22 °C (2.947%) storage temperatures ($p<0.05$). The β-pinene ratios decreased at the end of 6-month storage as compared to the other storage durations (Table 2).

Considering the increase in storage durations, it was observed that 6-month storage at 2 ^{0}C decreased β–pinene ratio (1.447%) as compared to 1-month (2.433%) and 3-month (2.550%) storage. A similar case was also observed for 4 ^{0}C storage temperature (6-month: 1.443%, 1-month: 2.487%, 3-month: 2.680%). However, fluctuations were observed in β–pinene ratios at 6 °C, -18 °C, -20 °C and -22 °C storage temperatures, β–pinene ratios increased at the end of 3-month storage and significantly decreased at the end of 6-month storage ($p<0.05$) (Table 2).

Dunnett's test results revealed that β-pinene ratio of control oil (3.003%) decreased at all storage durations and temperatures. However, such decreases were found to be significant at all temperatures of 1 and 6-month storage durations and 2, 4, 6 and -18 °C temperatures of 3-month storage ($p<0.05$), but were not found to be significant only at -20 °C and -22 °C temperatures of 3-month storage ($p>0.05$) (Table 2). Choi and Sawamura, stored *Citrus tamurana* essential oils at -21, 5, 20 and 30 °C temperatures for 1, 3, 6 and 9 months and reported undesired chemical changes with the prolonged storage durations [17]. Misharina et al., extracted essential oils of *Majarona hortensis* species and stored essential oils in dark-color bottles for 3, 6, 9 and 12 months at room temperature, dark and light environments [18]. Researchers indicated insignificant changes in essential oil components when they were stored under dark conditions. In dark environments, there were not almost any changes in α-thujene, α- and β-pinene, β-myrcene and α-phellandrene ratios and α-terpinene and limonene ratios decreased at the

end of 1-year storage. However, in light environments, there were significant changes in α-phellendrene and α-terpinene ratios throughout the storage and quality losses were reported for storage durations greater than 3 months under light conditions. In present study, a significant decrease was recorded in β-pinene ratios in all treatments except for 3-month storage at -20 °C and -22 °C. Crutchet et al., obtained essential oils of *Mentha piperita* leaves right after distillation and 21-day storage at 0 °C and analyzed the essential oil components [19]. Researchers reported the β–pinene ratio as 0.12% right after distillation and as 0.19% after 21-day storage at 0 °C. Present findings were not complying with the results of that study, since β–pinene ratios decreased at all storage conditions.

1,8 - cineole ratio (%). Considering the storage durations alone, it was observed that 1,8-cineole did not influenced by storage temperatures (2, 4, 6, -18, -20, -22 °C) of 1, 3 and 6-month storage durations ($p>0.05$), but increasing storage durations influenced 1,8-cineole ratios at 6 ^{0}C and -22 °C storage temperatures ($p<0.05$) (Table 3). The 1,8-cineole ratio at 6 °C of 1-month (9.980%) and 6-month (9.533%) storages were significantly lower than the 1,8-cineole ratio of 3-month storage (11.253%) ($p<0.05$). A similar case was also observed at -22 °C, the greatest ratio (11.637%) was observed at the end of 3-month storage.

The 1,8-cineole ratio of the control sample (11.357%) increased only at -22 °C of 3-month storage (11.637%), but such an increase was not found to be significant ($p>0.05$). Similarly, the other temperatures of 3-month storage did not yielded significant changes in 1,8-cinole ratios (Table 3). Significant decreases were observed in 1,8-cineole ratios at all storage temperatures, except for 2 °C of 1-month storage (10.583%) and -20 °C of 6-month storage (10.553%) ($p<0.05$), the greatest decrease was observed at 6 °C of 6-month storage (9.533%) and it was followed by 6 °C of 1-mpnth storage (9.980%). Previous researchers also indicated that essential oil ratios and components of medicinal and aromatic plants were influenced by drying methods, storage conditions and durations [20, 21]. Kazaz et al., stored rose petals at 0 and 3 °C for 7, 14, 21 and 28 days [22]. Researchers reported the greatest essential oil component ratios for the distillations right after the harvest, decreasing citronellol ratios with increasing storage durations and insignificant effects of storage temperatures on essential oil components. In present study, 1,8-cineole ratios decreased with increasing storage durations and 1,8-cineole ratios were significantly influenced by storage temperatures. Sharma and Kumar, investigated the storage-induced changes in essential oil composition of damask rose (*Rosa damascene* Mill.) and analyzed essential oil components right after the harvest (control samples) and after 10, 20 and 30 days of storage at 4±0.5 °C and -20 °C [23]. Researchers indicated that the most appropriate essential oil composition was achieved from the distillation of fresh petals, however in cases where instant distillation of petals were not possible in large harvest sites, it was indicated that 20 days storage at -20 °C did not have any negative effects on rose oil quality and international standards were achieved for essential oil components. Najafian, was not able to identify 1,8-cineole in essential oils of *Melissa officinalis* right after distillation, but reported periodically increasing 1,8-cineole ratios at the end of 1-month storage at 4 °C (2.5%), 2-month of storage (4.4%), 3-month storage (6.8%) and 4-month storage (8.2%). Such a finding was not complying with the present results, since the 1,8-cineole ratio was high right after the harvest and decreased at all storage conditions, except for 3-month storage at -22 °C [16].

Menthone ratio (%). Menthone ratios were not influenced significantly by all storage temperatures of 1-month storage ($p>0.05$) (Table 4). However, significant decreases were observed at 2 °C (30.537%), 4 °C (30.460%) and -18 °C (31.043%) of 3-month storage and 2 °C (29.907%), 6 °C (30.323%), -18 °C (28.400%), -20 °C (29.203%) and -22 °C (30.513%) of 6-month storage ($p<0.05$).

TABLE 3
Descriptive statistics and multiple range test results for 1,8 cineole (%)

°C	1-Month			3-Month			6-Month		
	Average	Std. Error	Std. Deviation	Average	Std. Error	Std. Deviation	Average	Std. Error	Std. Deviation
Control	*11.357*^{A}	*0.179*	*0.311*						
2	10.583Aa^{A}	0.097	0.168	10.643Aa^{A}	0.185	0.320	10.360Aa^{B}	0.203	0.351
4	10.393Aa^{B}	0.113	0.196	11.197Aa^{A}	0.157	0.272	10.280Aa^{B}	0.101	0.176
6	9.980Ab^{B}	0.381	0.660	11.253Aa^{A}	0.081	0.140	9.533Ab^{B}	0.482	0.834
-18	10.427Aa^{B}	0.263	0.456	11.163Aa^{A}	0.197	0.342	10.187Aa^{B}	0.044	0.076
-20	10.310Aa^{B}	0.461	0.798	11.267Aa^{A}	0.130	0.225	10.553Aa^{A}	0.052	0.091
-22	10.290Ab^{B}	0.147	0.255	11.637Aa^{A}	0.079	0.137	10.000Ab^{B}	0.097	0.168
P-Value	Storage Duration: 0.000 Storage Temperature: 0.123 Storage Duration x Storage Temperature: 0.032*								

The means indicated with the different capital letters in the same storage duration are significantly different ($p<0.05$)
The means indicated with the different small letters in the same storage temperature are significantly different ($p<0.05$)
^{B}, Significantly different from the control sample according to Dunnett's test ($p<0.05$)

TABLE 4
Descriptive statistics and multiple range test results for menthone (%)

°C	1-Month			3-Month			6-Month		
	Average	Std. Error	Std. Deviation	Average	Std. Error	Std. Deviation	Average	Std. Error	Std. Deviation
Control	*33.117*^{A}	*1.421*	*2.461*						
2	36.400Aa^{B}	1.511	2.616	30.537Bb^{A}	0.436	0.755	29.907Bb^{B}	0.186	0.321
4	33.753Aa^{A}	0.667	1.155	30.460Bb^{A}	0.383	0.664	33.860Aa^{A}	0.485	0.840
6	35.430Aa^{A}	1.006	1.742	34.587Aa^{A}	0.468	0.810	30.323Bb^{A}	0.778	1.348
-18	35.250Aa^{A}	0.220	0.381	31.043Bb^{A}	0.298	0.516	28.400Bb^{B}	0.058	0.100
-20	35.513Aa^{A}	1.019	1.765	35.393Aa^{A}	0.223	0.386	29.203Bb^{B}	0.075	0.131
-22	33.650Aab^{A}	0.126	0.218	35.230Aa^{A}	0.139	0.241	30.513Bb^{A}	0.216	0.374
P-Value	Storage Duration: 0.000 Storage Temperature: 0.004 Storage Duration x Storage Temperature: 0.000***								

***, significant ($p<0.001$)
The means indicated with the different capital letters in the same storage duration are significantly different ($p<0.05$)
The means indicated with the different small letters in the same storage temperature are significantly different ($p<0.05$)
^{B}, Significantly different from the control sample according to Dunnett's test ($p<0.05$)

At the same storage temperatures, decreasing menthone ratios were observed with increasing storage durations (1, 3, 6 months) at 2 °C, 6 °C, -18 °C and -20 °C storage temperatures, but the same decrease was not observed at 4 °C and -22 °C. The menthone ratio of 33.753% at 4 °C decreased to 30.460% at the end of 3-month storage, but increased back to 33.860% at the end of 6-month storage. The menthone ratio of 33.650% at -22 °C of 1 -month storage increased to 35.230% at the end of 3-month storage, but decreased back to 30.513% at the end of 6-month storage (Table 4).

The menthone ratio of control sample was 33.117%, the value increased with 1-month storage at 2^{0}C (36.400%), but significantly decreased with 6-month storage at 2 °C (29.907%), -18 °C (28.400%) and -20°C (29.203%) ($p<0.05$) (Table 4). A significant increase or decrease was not observed at different storage temperatures of the other storage durations ($p>0.05$). Menthone is a predecessor component of menthol and high levels are not desired for this component. Menthone ratios mathematically increased at all temperatures of 1-month storage (2 °C =36.400%, 4 °C =33.753%, 6 °C =35.430%, -18 °C =35.250%, -20 °C =35.513%, -22 °C =33.650%); at 6 °C (34.5875), -20°C (35.393%) and -22 °C (35.230%) storage temperatures of 3-month storage and at 4 °C (33.860%) of 6-month storage, but decreased at the other storage temperatures and durations. Curutchet et. al., investigated the effects of storage on essential oil components of *M. piperita* species and reported menthone ratio as 46.8% for samples subjected to distillation right after the harvest, as 448.7% for the samples stored at 0 °C for 21 days [19]. In present study, increased menthone ratios were observed at all temperatures of 1-month storage. Such changes in menthone ratios were attributed to ongoing chemical transformations.

Menthol ratio (%). The menthol ratios at 6 °C (25.573%) and -22 °C (24.607%) temperatures of 1-month storage were significantly different from the menthol ratio at -18 °C (20.713%), but the changes in menthol ratios at the other storage temperatures were not found to be significant ($p>0.05$). In case of 3-month storage, significant changes were observed in menthol ratios with storage temperatures. The greatest menthol ratio was observed at 2 °C (19.600%), it was followed by -18 °C (18.100%), 4 °C (17.937%), 6 °C (16.257%) and the lowest menthol ratios were observed at -20 °C (14.800%) and -22 °C (14.373%). In 6-month storage, generally high menthol ratios were observed at 2 °C, 4 °C, 6 °C, -18 °C, -20 °C and -22 °C storage temperatures and the greatest value was observed at -20 °C (27.100%).

Dunnett's test revealed that samples stored at -18 °C for 1 month (20.713%), at 2 °C (19.600%), 4 °C (17.937%), 6 °C (16.257%), -18 (18.100%) for 3 months and at 4 °C for 6 months (20.077%) had similar menthol ratios with the control samples (18.010%) ($p>0.05$), but the menthol ratios at different storage temperatures and durations were significantly different ($p<0.05$) (Table 5). As compared to the menthol ratio of the control sample, the lowest menthol ratio was observed at -22 °C of 3-month storage (14.373%) and the greatest menthol ratio was observed at -20 °C of 6-month storage (27.100%). Kumar et al., investigated storage-induced changes in essential oil composition of Isparta rose (*Rosa damascena* Mill.) petals [24]. Researchers performed distillation of control samples right after the harvest and stored the other samples at 4 °C, 18±1 °C and 25±1 °C temperatures and 90±5% relative humidity for 4, 8, 12, 16, 20 and 24 hours and extracted essential oils of samples after storage. Increasing citronellol+nerol components were reported with increasing storage durations. Crutchet et al., reported the menthol ratio of *M. piperita* essential oil as 21.6% right after the distillation and as 23.5% after 21-day storage at 0 °C. In present study, menthol ratios increased at all temperatures of 1 and 6-month storage [19].

Pulegone ratio (%). Descriptive statistics for pulegone ratios are provided in Table 6. Considering the storage durations alone, it was observed that all storage temperatures of 1, 3 and 6-month storage durations, except for -18 °C of 6-month storage, did not result in significant changes in pulegone ratios ($p>0.05$). However, pulegone ratio at -18°C of 6-month storage (3.250%) was significantly different from the pulegone ratios of the other samples ($p<0.05$). Again, the pulegone ratio at -18 °C of 6-month storage (3.250%) was significantly lower than the ratios of the other samples (1-month: 5.203%, 3-month: 4.930%) ($p<0.05$). Increasing storage durations influenced the pulegone ratios at the other temperatures, but such influences were not found to be significant ($p<0.05$) (Table 6).

The pulegone ratio of the control samples (3.340%) increased in all of the other samples, except for -18 °C of 6-month (3.250%) and such an increase was found to be significant at 2 °C (4.677%), 4°C (4.707%), -18 °C (5.203%) of 1-month storage, 2 °C (4.627%), 4 °C (4.903%), -18 °C (4.930%), -20 °C (4.640%) of 3-month storage and 2°C (4.607%), 4 °C (4.880%), 6°C (4.743%) of 6-month storage ($p<0.05$), but not found to be significant in the other samples ($p>0.05$). Kumar et al., reported lower hexadecane, nonadecane and methyl eugenol ratios of Isparta rose (*Rosa damascena* Mill.) for the samples subjected to GC-MS analyses right after the harvest than for the stored samples. In present study, pulegone ratio of the control samples (3.340%) also increased with the storage [24].

Piperitone ratio (%). Statistical analyses for piperitone ratios are provided in Table 7. Considering the storage durations alone, it was observed that only the samples stored at 2 °C (1.113%) and -22 °C (0.987%) for 1-month had significantly different piperitone ratios ($p<0.05$), similar piperitone ratios were observed at the other storage temperatures. In 3 and 6-month storages, the changes in piperitone ratios were not found to be significant ($p>0.05$).

TABLE 5
Descriptive statistics and multiple range test results for menthol (%)

°C	1-Month			3-Month			6-Month		
	Average	Std. Error	Std. Deviation	Average	Std. Error	Std. Deviation	Average	Std. Error	Std. Deviation
Control	*18.010*^{A}	*0.826*	*1.430*						
2	22.173ABab^{B}	0.962	1.665	19.600Ab^{A}	0.300	0.520	25.100Aa^{B}	0.692	1.198
4	23.183ABa^{B}	1.174	2.034	17.937ABCb^{A}	0.220	0.381	20.077Bab^{A}	0.527	0.914
6	25.573Aa^{B}	0.266	0.461	16.257ABCb^{A}	1.151	1.993	24.283Aa^{B}	0.233	0.404
-18	20.713Bb^{A}	0.263	0.456	18.100ABb^{A}	0.336	0.581	26.630Aa^{B}	0.111	0.192
-20	23.783ABa^{B}	1.607	2.783	14.800BCb^{B}	0.425	0.737	27.100Aa^{B}	0.610	1.056
-22	24.607Aa^{B}	0.058	0.101	14.373Cb^{B}	0.461	0.798	23.940Aa^{B}	0.784	1.357
P-Value	Storage Duration: 0.000 Storage Temperature: 0.011 Storage Duration x Storage Temperature:.:0.000***								

***, significant ($p<0.001$)
The means indicated with the different capital letters in the same storage duration are significantly different ($p<0.05$)
The means indicated with the different small letters in the same storage temperature are significantly different ($p<0.05$)
^{B}, Significantly different from the control sample according to Dunnett's test ($p<0.05$)

TABLE 6
Descriptive statistics and multiple range test results for pulogene (%)

°C	1-Month			3-Month			6-Month		
	Average	Std. Error	Std. Deviation	Average	Std. Error	Std. Deviation	Average	Std. Error	Std. Deviation
Control	*3.340*^{A}	*0.322*	*0.557*						
2	4.677Aa^{B}	0.237	0.411	4.627Aa^{B}	0.084	0.145	4.607ABa^{B}	0.041	0.070
4	4.707Aa^{B}	0.326	0.564	4.903Aa^{B}	0.119	0.206	4.880Aa^{B}	0.056	0.096
6	4.113Aa^{A}	0.314	0.544	4.537Aa^{A}	0.117	0.203	4.743ABa^{B}	0.092	0.159
-18	5.203Aa^{B}	0.167	0.289	4.930Aa^{B}	0.090	0.156	3.250Bb^{A}	1.000	1.732
-20	4.313Aa^{A}	0.321	0.556	4.640Aa^{B}	0.155	0.269	4.303ABa^{A}	0.037	0.064
-22	4.600Aa^{A}	0.000	0.000	4.413Aa^{A}	0.074	0.127	3.897ABa^{A}	0.262	0.454
P-Value	Storage Duration: 0.054 Storage Temperature: 0.308 Storage Duration x Storage Temperature: 0.014*								

*, significant ($p<0.05$)
The means indicated with the different capital letters in the same storage duration are significantly different ($p<0.05$)
The means indicated with the different small letters in the same storage temperature are significantly different ($p<0.05$)
^{B}, Significantly different from the control sample according to Dunnett's test ($p<0.05$)

TABLE 7
Descriptive statistics and multiple range test results for piperitone (%)

°C	1-Month			3-Month			6-Month		
	Average	Std. Error	Std. Deviation	Average	Std. Error	Std. Deviation	Average	Std. Error	Std. Deviation
Control	*1.253*^{A}	*0.009*	*0.015*						
2	1.113Aa^{B}	0.032	0.055	1.120Aa^{B}	0.010	0.017	1.027Aa^{B}	0.037	0.064
4	1.037ABa^{B}	0.003	0.006	1.107Aa^{B}	0.009	0.015	1.050Aa^{B}	0.010	0.017
6	1.050ABab^{B}	0.012	0.020	1.120Aa^{B}	0.031	0.053	0.930Ab^{B}	0.015	0.026
-18	1.060ABab^{B}	0.026	0.046	1.123Aa^{B}	0.028	0.049	0.960Ab^{B}	0.006	0.010
-20	1.037ABb^{B}	0.018	0.031	1.180Aa^{A}	0.026	0.046	0.953Ab^{B}	0.022	0.038
-22	0.987Bb^{B}	0.003	0.006	1.03Aa^{A}	0.012	0.021	1.043Aa^{B}	0.042	0.072
P-Value	Storage Duration: 0.000 Storage Temperature: 0.074 Storage Duration x Storage Temperature: 0.000***								

***, significant ($p<0.001$)
The means indicated with the different capital letters in the same storage duration are significantly different ($p<0.05$)
The means indicated with the different small letters in the same storage temperature are significantly different ($p<0.05$)
^{B}, Significantly different from the control sample according to Dunnett's test ($p<0.05$)

TABLE 8
Descriptive statistics and multiple range test results for caryophyllene (%)

°C	1-Month			3-Month			6-Month		
	Average	Std. Error	Std. Deviation	Average	Std. Error	Std. Deviation	Average	Std. Error	Std. Deviation
Control	*3.710*^{A}	*0.006*	*0.010*						
2	3.083Cc^{B}	0.080	0.139	3.970Aa^{A}	0.031	0.053	3.533Bb^{A}	0.048	0.084
4	3.687Ab^{A}	0.074	0.127	4.150Aa^{B}	0.061	0.106	3.690ABb^{A}	0.050	0.087
6	2.940Cb^{B}	0.165	0.286	3.833Aa^{A}	0.026	0.045	3.663ABa^{A}	0.072	0.124
-18	3.537ABb^{A}	0.023	0.040	4.137Aa^{B}	0.019	0.032	3.853ABab^{A}	0.178	0.309
-20	2.930Cb^{B}	0.070	0.121	3.970Aa^{A}	0.046	0.080	3.810ABa^{A}	0.066	0.114
-22	3.217BCb^{B}	0.009	0.015	4.043Aa^{B}	0.082	0.142	4.047Aa^{B}	0.043	0.075
P-Value	Storage Duration: 0.000 Storage Temperature: 0.000 Storage Duration x Storage Temperature: 0.000***								

***, significant ($p<0.001$)
The means indicated with the different capital letters in the same storage duration are significantly different ($p<0.05$)
The means indicated with the different small letters in the same storage temperature are significantly different ($p<0.05$)
^{B}, Significantly different from the control sample according to Dunnett's test ($p<0.05$)

The 1, 3 and 6-month storages at 2 °C and 4 °C did not result in significant changes in piperitone ratios ($p>0.05$). However, 6 °C (1-month: 1.050%, 3-month: 1.120%, 6-month: 0.930%), -18 °C (1-month: 1.060%, 3-month: 1.123%, 6-month: 0.960%), -20 °C (1-month: 1.037%, 3-month: 1.180%, 6-month: 0.953%) temperatures resulted in insignificant changes in 1 and 3-month storages ($p>0.05$), but resulted in significant decreases in 6-month storage ($p<0.05$). At -22 °C storage temperature, piperitone ratio was measured as 0.987%, but the ratios increased at the end of 3-month (1.203%) and 6-month (1.043%) storages ($p<0.05$).

As compared to the piperitone ratio of the control samples (1.253%), the ratios decreased in all of the stored samples and such a decrease was found to be significant at all temperatures of 1-month storage, at 2, 4, 6 and -18 °C temperatures of 3-month storage and again all temperatures of 6-month storage ($p<0.05$) (Table 7).

Caryophyllene ratio. Considering the storage durations alone, in 1-month storage, the greatest caryophyllene ratio was observed at 4 °C (3.687%) and the lowest caryophyllene ratio was observed at -20 °C (2.930%). In 3-month storage, the greatest ratio was observed at -18 °C (4.137%) and the lowest ratio was observed at 6 °C (3.833%). In 6-month storage, the ratio at -22 °C (4.047%) was greater than the values of the other samples, it was followed by -18 °C (3.853%) and the lowest ratio was observed at 2°C (3.533%). Considering the increasing storage durations, the greatest caryophyllene ratios were observed at 2 °C, 4 °C, 6 °C, -18 °C and -20 °C of 3-month storage, but the caryophyllene ratios decreased at the end of 6-month storage. Only the caryophyllene ratio at -22 °C of 3-month storage (4.043%) mathematically increased in 6-month storage (4.047%) (Table 8).

As compared to the caryophyllene ratio of the control samples (3.710%), the caryophyllene ratios significantly decreased at 2 °C (3.083%), 6 ^{0}C (2.940%), -20 °C (2.9305) and -22 °C (3.217%) of

1-month storage ($p<0.05$), but significantly increased at 4°C (4.150%), -18 °C (4.137%), -22 °C (4.043%) of 3-month storage and at -22 °C (4.047%) of 6-month storage ($p<0.05$). In general, the lowest ratio was observed at -20 °C (2.930%) of 1-month storage and the greatest ratio was observed at 4°C (4.150%) of 3-month storage. Rowshan et al., investigated the effects of storage conditions on essential oil composition of *Thymus daenensis* and analyzed essential oil components after storage at 4 °C, -20 °C and room temperature for 1, 2 and 3 months [25]. The researchers recommended -20 °C for the preservation of main components and indicated that essential oil quality was preserved at low temperatures. In present study, caryophyllene ratios increased at -18 °C, -20 °C and -22 °C of 3-month storage as compared to the control samples.

Germacrene-D ratio (%). In 1-month storage, the greatest germacrene-D ratio was observed at 4 °C (3.903%) and the lowest germacrene-D ratio was observed at 6 °C (3.227%). The case was different in 3-month storage with the greatest ratio at -18°C (4.050%) and the lowest ratio at 6 °C (3.460%). In 6-month storage, the germacrene-D ratio at -18 °C was measured as 4.077%, it was followed by -22 °C (4.013%) and the lowest ratio was observed at 2 °C (3.003%).

At 2 °C storage temperature, the greatest germacrene-D ratio was observed in 3-month storage (3.737%) and it was followed by 1-month (3.260%) and 6-month (3.003%) storages. At 4 °C storage temperature, germacrene-D ratios decreased with increasing storage durations, the germacrene-D ratio was 3.903% at the end of 1-month storage, 3.853% at the end of 3-month storage and 3.217% at the end of 6-month storage. At 6 °C storage temperature, germacrene-D ratios were ordered as 3-month (3.460%), 1-month (3.227%) and 6-month (3.140%) storages. At -18 °C and -20 °C storage temperatures, germacrene-D ratios increased with increasing storage durations. However, a similar case was not observed at -22 °C, the germacrene-D ratio of 1-month storage (3.205%) increased at the end of 3-month storage (3.897%), but decreased back to 3.870% at the end of 6-month storage.

The germacrene-D ratio of the control samples (4.023%) increased mathematically at -18 °C of 3-month storage (4.050%) and 6-month storage (4.077%), but such increases were not found to be significant ($p>0.05$). The germacrene-D ratios decreased at the other storage temperatures (Table 9).

CONCLUSION

Present findings revealed that essential oil components of control samples influenced by storage temperatures and durations. The results of Dunnett's test can be summarized as follows:

- The α-pinene ratios were not significantly influenced by 4 °C and -18 °C of 1-month storage and all temperatures of 6-month storage, but mathematically increased at -20 °C and -22 °C of 3-month storage. The greatest decrease was observed at the end of 6-month storage.
- The β-pinene generally decreased under present storage conditions. Such a decrease was found to be significant at all temperatures of 1 and 6-month storages and at 2 °C, 4 °C, 6 °C and -18 °C of 3-month storage, but -20 °C and -22 °C did not result in significant changes in β-pinene ratios.
- The 1,8-cineole ratios were not significantly influenced by all temperatures of 1-month storage, 2 °C of 3-month storage and -20 °C of 6-month storage, the ratio mathematically increased at -22 °C of 3-month storage, but the other storage temperatures and durations decreased 1,8-cineole ratios.
- The menthone ratios significantly increased at 2 °C of 1-month storage and significantly decreased at 2 °C, -18 °C and -20 °C of 6-month storage. Menthone ratios either increased or decreased at the other storage temperatures, but such changes were not found to be significant.

TABLE 9
Descriptive statistics and multiple range test results for germacrene-D (%)

°C	1-Month			3-Month			6-Month		
	Average	Std. Error	Std. Deviation	Average	Std. Error	Std. Deviation	Average	Std. Error	Std. Deviation
Control	*4.023*^{A}	*0.102*	*0.176*						
2	3.260BCb^{B}	0.087	0.151	3.737BCa^{B}	0.009	0.015	3.003Bb^{B}	0.009	0.015
4	3.903Aa^{A}	0.015	0.025	3.853ABa^{A}	0.069	0.120	3.217Bb^{B}	0.023	0.040
6	3.227Cab^{B}	0.137	0.238	3.460Ca^{B}	0.038	0.066	3.140Bb^{B}	0.012	0.020
-18	3.823Aa^{A}	0.053	0.092	4.050Aa^{A}	0.020	0.035	4.077Aa^{A}	0.043	0.075
-20	3.250BCb^{B}	0.012	0.020	3.897ABa^{A}	0.032	0.055	3.870Aa^{A}	0.046	0.079
-22	3.517Bb^{B}	0.017	0.029	3.930ABa^{A}	0.090	0.156	4.013Aa^{A}	0.015	0.025
P-Value	Storage Duration: 0.000 Storage Temperature: 0.000 Storage Duration x Storage Temperature: 0.000***								

***, significant ($p<0.001$)
The means indicated with the different capital letters in the same storage duration are significantly different ($p<0.05$)
The means indicated with the different small letters in the same storage temperature are significantly different ($p<0.05$)
^{B}, Significantly different from the control sample according to Dunnett's test ($p<0.05$)

- The menthol ratios significantly increased at 2 °C, 4 °C, 6 °C, -20 °C and -22 °C of 1-month storage and at 2 °C, 6 °C, -18 °C and -22 °C of 6-month storage, but significantly decreased at -20 °C and -22 °C of 3-month storage. The other storage temperatures and durations did not result in significant changes in menthol ratios.

- The pulegone ratios generally increased at all temperatures of all storage durations. Such increases were found to be significant at 2 °C, 4 °C and -18 °C of 1-month storage, 2 °C, 4 °C, -18 °C and -20 °C of 3-month storage and 2 °C, 4 °C and 6 °C of 6-month storage, but the changes in the other storage temperatures were not found to be significant.

- The -piperitone ratios significant decreased with the storage. Such decreases were not found to be significant at -20 °C and -22 °C of 3-month storage, but significant at all temperatures of the other storage durations.

- The caryophyllene ratios significantly decreased at 2 °C, 6 °C, -20 °C and -22 °C of 1-month storage and significantly increased at 4 °C, -18 °C and -22 °C of 3-month and -22 °C of 6-month storage.

- The germacrene-D ratios decreased at 2 °C, 6 °C, -20 °C and -22 °C of 1-month, 2 °C and 6 °C of 3-month and 2 °C, 4 °C and 6 °C of 6-month storage. The greatest increase was observed at 18 °C of 6-month storage, but this increase and the increases at the other storage conditions were not found to be significant.

Present findings revealed that storage conditions had significant effects on essential oil components. It was concluded based on present findings that in case of storage of *Mentha piperita* essential oil, 3 months of storage at storage temperatures of below 0 °C could be recommended for α-pinene, β-pinene, 1,8-cineole, pulegone, piperitone and caryophyllene components, 6 months of storage at 2 °C for menthone, 6 months of storage at -20 °C for menthol and 6 months of storage at -18 °C for caryophyllene component.

ACKNOWLEDGEMENTS

This study was supported by Scientific Research Projects Department of Ordu University (with the project number of BY-1722).

REFERENCES

[1] Çalıkoğlu, E., Kıralan, M., Bayrak, A. (2006) What is essential oil, how to produce and an overview of the situation in Turkey. Turkey 9. Food Congress: May 24-26, Bolu, 569-570.

[2] Hammer K.A., Carson C.F., and Riley T.V. (1999) Antimicrobial activity of essential oils and other plant extracts. Journal of Applied Microbiology. 86(6), 985-990.

[3] Cellat, K. (2011) Essential oil extraction and investigation of components of some endemic plants. Çukurova University Institute of Natural and Applied Sciences Department of Chemistry. Adana.

[4] Czerniewicz, P., Chrzanowski, G., Sytykiewicz, H., Sprawka, I., Leszczynski, B. (2016) Aphidicidal and Deterrent Activity of Phenolic Acid Extracts from Some Herbal Plants Towards *Myzus Persicae* Sulz. and *Rhopalosiphum Padi* L. Fresen. Environ. Bull. 25, 5714-5721.

[5] Erdemir, T., Erler, F. (2018) Fumigant Toxicity of Five Plant Essential Oils Against *Citrus Mealybug*, *Planococcus Citri* Risso (Hemiptera: Pseudococcidae). Fresen. Environ. Bull. 27, 3231-3235.

[6] Anjum, S., Khadim, R., Shah, S.Z.A., Hamid, A., Jan, S.A., Shinwari, Z.K., Ghafoor, A. (2019) Biochemical Characterization of Geographically Diverse *Mentha* Species from Azad Jammu and Kashmir. Fresen. Environ. Bull. 28, 1347-1355.

[7] Özgüven, M., Kırıcı S. (1999) Research on Yield, Essential Oil, Contents and Components of Mint (*Mentha*) Species in Different Ecologies. Tr. J. of Agriculture and Forestry. 23(5), 465-472.

[8] Arabhosseini, A., Huisman, A., van Boxtel, W., Muller, J. (2007) Long-term effects of drying conditions on the essential oil and color of tarragon leaves during storage. Journal of Food Engineering. 79(2), 561-566.

[9] Yeşil, M. (2012) Effects of Nitrogen and Phosphor Dosages on the Quality and Agricultural Characteristics of *Mentha spicata* L. and *Mentha villoso-nervata* L. Genotypes. Ataturk University Graduate School of Natural and Applied Sciences, Erzurum.

[10] Rhyu, H.Y. (1979) Gas chromatographic characterization of sages of various geographic origins. J. Food Sci. 44, 758-762.

[11] Bauer, K., Garbe, D., Surbur, Y. (1992) Common Fragrance and Flavour Materials. Weinheim: VCH Verlagsgesellschaft.

[12] Gopalakrishnan, N. (1994) Studies on the storage quality of carbon dioxide-extracted cardamom and clove bud oils. Agric. Food Chem. 42, 796-798.

[13] Misharina, T.A. (2001) Influence of the Duration and Conditions of Storage on the Composition of the Essential Oil from Coriander Seeds. Applied Biochemistry and Microbiology. 37(6), 622-628.

[14] Singh, A.K., Singh, K., Naqvi, A.A., Thakur, R.S. (1990) Effect of storage of herb on the quality and yield of oil in mint species. Research and Industry. 35(3), 46–48.
[15] Bahmanzadegan, A., Rowshan, V., Saharkhiz, M.J. (2015) Essential Oil Composition of *Myrtus communis* L. Under Different Storage Conditions. TEOP. 18(6), 1467-1475.
[16] Najafian, S. (2014) Storage Conditions Affect the Essential Oil Composition of Cultivated Balm Mint Herb (Lamiaceae) in Iran. Industrial Crops and Products. 52(2014), 575-581.
[17] Choi, H.S., Sawamura, M. (2002) Effects of Storage Conditions on the Composition of *Citrus tamurana* Hort ex Tanaka (*Hyuganatsu*) Essential Oil. Biosci. Biotechnol. Biochem. 66(2), 439-443.
[18] Misharina, T.A., Polshkov, A.N., Ruchkina, E.L., Medvedeva, I.B. (2003) Changes in the composition of the essential oil of marjoram during storage. Appl. Biochem. Microb. 39(3), 353–358.
[19] Curutchet, A., Dellacassa, E., Ringuelet, J.E., Chaves, A.R., Vina, S.Z. (2014) Nutritional and sensory quality during refrigerated storage of fresh-cut mints (*Mentha piperita* and *M. spicata*). Food Chemistry. 143, 231-238.
[20] Baydar, H., Kazaz, S., Erbaş, S., Örücü, Ö.K. (2008) The Effects of Cold Storage and Drying on Essential Oil Content and Composition in Oil-Bearing Rose (*Rosa damascena* Mill.) Flowers. Süleyman Demirel University Agriculture Faculty Journal. 3(1), 42-48.
[21] Polatçı, H., Tarhan, S. (2009) Effect of Different Drying Methods on Drying Time and Quality of Reyhan (*Ocimum basilicum*) Plant. Gazi Osman Pasa University, Agriculture Faculty Journal. 26(1), 61-70.
[22] Kazaz, S., Erbaş, S., Baydar, H. (2009) The Effects of Storage Temperature and Duration on Essential Oil Content and Composition Oil Rose (*Rosa damascena* Mill.). Turkish J. of Field Crops. 14(2), 89-96.
[23] Sharma, S., Kumar, R. (2016) Effect of temperature and storage duration of flowers on essential oil content and composition of damask rose (*Rosa* × *damascena* Mill.) under western Himalayas. Journal of Applied Research on Medicanal and Aromatic Plants. 3(1), 10-17.
[24] Kumar, R., Sharma, S., Sood, S., Agnihotri, V. K., Singh, B. (2013) Effect of diurnal variability and storage conditions on essential oil content and quality of damask rose (*Rosa damascena* Mill.) flowers in north western Himalayas. Scientia Horticulturae. 154 (2013), 102-108.
[25] Rowshan, V., Bahmanzadegan, A., Saharkhiz, M.J. (2013) Influence of storage conditions on the essential oil composition of *Thymus daenensis* Celak. Industrial Crops and Products. 49(2013), 97-101.

Received: **06.12.2019**
Accepted: **28.01.2020**

CORRESPONDING AUTHOR

Meryem Yesil
Department of Crop and Animal Production,
Vocational School of Technical Sciences
Ordu University
Ordu – Turkey

e-mail: meryemyesil@hotmail.com

© by PSP Volume 29 – No. 05/2020 pages 3870-3878 Fresenius Environmental Bulletin

NUMERICAL SIMULATION ON THE EFFECT OF YIELD ON HYDRATE DECOMPOSITION IN THE PRODUCTION STAGE OF DEEPWATER WELLS

Zhi Zhang*, Zhe Zhang

State Key Laboratory of Oil and Gas Reservoir Geology and Exploration, Southwest Petroleum University, Chengdu 610500, China

ABSTRACT

During the production of deep well involving hydrate stratum, the hydrate will dissociate when the heat of shaft transfers to the hydrate stratum, and the generated excess pore pressure may cause risk to the shaft integrity. In this paper, the calculation model for hydrate dissociation distance and gas production is established based on the seepage mechanics and heat and mass transfer theories, in which the dissociation distance and gas production of hydrate under different shaft-stratum temperature conditions are calculated and the impact of hydrate saturation and porosity of hydrate stratum on the dissociation distance and gas production is analyzed, as a result, the increases of the saturation of natural gas hydrate and the porosity of hydrate stratum will result in the increases of dissociation distance and gas production of hydrate, and the impact degree decreases gradually as the frontal surface reduces; meanwhile, the impact of saturation of natural gas hydrate on the hydrate dissociation distance and related gas production is more obvious than the impact of porosity of hydrate stratum, moreover, the control of shaft temperature via controlling the production can effectively reduce the dissociation distance and gas production of the hydrate stratum.

KEYWORDS:
Natural gas hydrate, hydrate decomposition, dissociation distance, gas production, modeling research, deep water

INTRODUCTION

During the production of deep well involving hydrate sediment, the high-temperature stratum fluid enters the shaft via the formation and moves to the wellhead, so the temperature distribution in the shaft changes accordingly and a temperature difference appears between the hydrate and the hydrate sediment, resulting in the heat exchange. This heat transfer process will break the stability of the hydrate and let them dissociate around the well as shown in Figure 1. The hydrate dissociation will cause the decrease in mechanism strength of the hydrate stratum, resulting in a sharp increase to the stratum pore pressure [1-2], large-scale deformation and even destruction of stratum containing hydrate e.g. submarine landslide [3-5], sediment collapse [6], submarine pockmark [7-9], etc., and further significant risk to drilling and exploitation [10-12]. If the pore pressure of stratum after the hydrate dissociation is higher than the collapse resistance of cement sheath, there will be some risks, for example, the cement sheath may be damaged [13-15], the casing may be destroyed by collapse [16], and the shaft barrier may become incomplete. If the pore pressure of formation after the hydrate dissociation is higher than the collapse resistance of cement sheath [17], there will be some risks, for example, the cement sheath may be damaged, the casing may be destroyed by collapse, and the shaft barrier may become incomplete [18-21].

Zhang et al. [15] proposed an analyzing model to describe the hydrate dissociation with thermal stimulation of porous media. This model regards the hydrate dissociation as a process to generate gas and water at the movable dissociation boundary. The boundary separates the dissociation belt including gas and water from the dissociation belt including hydrate. As a result, a similarity solution of conservation equation is obtained in the form of diagram. Sayuri et al. [21] proposed a numerical model relating to the natural gas hydrate dissociation in the stratum with seabed hydrate deposits, and further studied the relationship between the increase in stratum pore pressure and stratum strain in consideration of the phase change of hydrate from solid state to fluid state, namely, the water and gas generate in the stratum. Tsypkin et al. [22] applies the correction mathematical model to research the formation and dissociation kinetics of hydrate. In the calculation experiment, the impact of the heating strength, gas well production, and gas-bearing bed permeability on the formation and dissociation kinetics of natural gas hydrate is studied, and the calculation results indicated that no matter how long the distance between the wells, the hydrate saturation growth rate and its absolute value are greatly related with the permeability and production.

In 2012, Su et al. [23], by making use of different stratum conditions, only decreased the pressure inside the shaft to induce the hydrate dissociation,

and through the research and comparison, they proved that the high stratum permeability and impermeable boundary will obviously affect the dissociation and gas production of hydrate. In 2014, Wang et al. [24], in consideration of the enthalpy change function of natural gas hydrate, established the shaft temperature field equation during the deep gas well testing process, and combined this equation and the phase balance condition of hydrate formation and the calculation method of the pressure filed, as a result, they worked out a method for predicting the natural gas hydrate forming area during the commissioning process of the deep gas well. In 2017, Gong et al. [25] established the dynamic heat transferring model of drilling fluid circulating process as per the measured data of the hydrate stratum and proved that the excess pore pressure will be directly affected by the hydrate saturation degree, therefore the change of saturation needs to be monitored in real time to reduce the risk of geological disaster caused by the hydrate stratum in the shallow stratum in deep water area. Tsypkin et al. [26] proposed a model showing the process that natural gas hydrate dissociates from the methane hydrate reservoir while the pressure and temperature decreases inside the gas well. The equation constitutes the mass conservation equation, momentum balance equation, and energy conservation equation, and the model calculation results show that the dissociation rate increases while the pressure reduction and the initial saturation of natural gas hydrate increase, and degrades sharply while the distance from the bounder gets larger and larger. Currently, the research on the hydrate dissociation process is concentrated on the drilling natural gas hydrate or the exploration of hydrate, but there are few discussions concerning on the impact of the hydrate dissociation of deep well exploration on the shaft integrity. In this paper, the heating dissociation process of hydrate stratum is studied, the model is constructed for the dissociation of hydrate stratum during the heat transferring process from the shaft to the hydrate stratum, and the radial dissociation distance and gas production of the hydrate stratum is calculated quantitatively, thereby providing evidence for the excess pore pressure produced from hydrate dissociation as well as offering the engineering significance to evaluate whether the increase in external shaft load caused by the excess pore pressure will cause risk to the shaft integrity during the production process [27-28].

MATERIALS AND METHODS

The dissociation of natural gas hydrate is a complicated phase-change heat and mass transfer process, and the dissociation and seepage process will be affected by the physicochemical property of natural gas hydrate, the property of porous media in formation skeleton, as well as the geological condition of the natural gas hydrate stratum. For the radially symmetric natural gas hydrate stratum in two dimensions as shown in Figure 1, assuming the non-permeable overlying strata available for heat exchange exist in the upper and lower part, the dissociation of natural gas hydrate is mainly affected by the seepage of gas and liquid phases as well as the hydrate dissociation dynamics caused by the transferring process of the heat inside the shaft to the natural gas hydrate stratum.

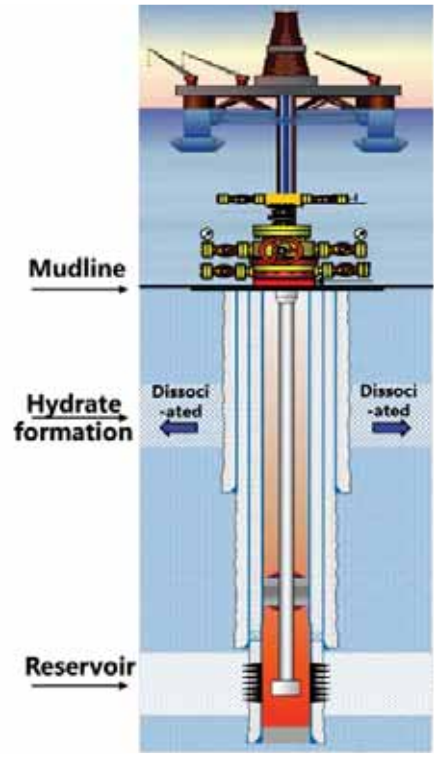

FIGURE 1
Hydrate Dissociation Diagram of Deep Well Involving Hydrate Stratum

The kinetic equation for the hydrate dissociation is established based on the hydrate during the dissociation process, the methane gas generated by the hydrate dissociation, as well as the mass conservation equation and energy conservation equation of water.

Mass conservation equation of methane gas:

$$-\frac{1}{r}\frac{\partial\left(r\rho_g v_{gr}\right)}{\partial r}-\frac{\partial\left(\rho_g v_{gz}\right)}{\partial z}+m_g=\frac{\partial\left(\phi\rho_g S_g\right)}{\partial t} \tag{1}$$

Mass conservation equation of water:

$$-\frac{1}{r}\frac{\partial\left(r\rho_w v_{wr}\right)}{\partial r}-\frac{\partial\left(\rho_w v_{wz}\right)}{\partial z}+m_w=\frac{\partial\left(\phi\rho_w S_w\right)}{\partial t} \tag{2}$$

Mass conservation equation of natural gas hydrate dissociation:

$$m_h=\frac{\partial\left(\phi\rho_h S_h\right)}{\partial t} \tag{3}$$

Where: t—time, s; r—radial distance, m; z—axial distance, m; ρ_g—density of methane gas, kg/m^3; ρ_w—density of water, kg/m^3; ρ_h—density of natural gas hydrate, kg/m^3; m_g—production rate of methane gas, kg/m^3·s; m_w—production rate of water, kg/m^3·s; m_h—production rate of natural gas hydrate, kg/m^3·s; v_{gr}—seepage velocity of methane gas along radial direction, m/s; v_{gz}—seepage velocity of methane gas along axial direction, m/s; v_{wr}—seepage velocity of water along radial direction, m/s; v_{wz}—seepage velocity of water along axial direction, m/s.

Since the porous media is filled by natural gas hydrate in solid state, only the methane gas and water are seeping in the porous media during the dissociation process, and according to the Darcy law. Seepage velocity of methane gas along r direction:

$$v_{gr} = -\frac{Kk_{rg}}{\mu_g}\frac{\partial P_g}{\partial r} \tag{4}$$

Seepage velocity of methane gas along z direction:

$$v_{gz} = -\frac{Kk_{rg}}{\mu_g}\frac{\partial\left(P_g - \gamma_{gz}\right)}{\partial z} \tag{5}$$

Seepage velocity of water along r direction:

$$v_{wr} = -\frac{Kk_{rw}}{\mu_w}\frac{\partial P_w}{\partial r} \tag{6}$$

Seepage velocity of water along z direction:

$$v_{wz} = -\frac{Kk_{rw}}{\mu_w}\frac{\partial\left(P_w - \gamma_{wz}\right)}{\partial z} \tag{7}$$

Saturation degree and capillary pressure:

$$k_{rw} = \left(S_w^*\right)^{n_w};\quad k_{rg} = \left(S_g^*\right)^{n_g} \tag{8}$$

$$S_w^* = \frac{S_w - S_{wr}}{1 - S_{wr}};\quad S_g^* = \frac{S_g - S_{gr}}{1 - S_{gr}} \tag{9}$$

Natural gas hydrate, free methane gas, and free water fill up to the clearance of porous media:

$$S_h + S_g + S_w = 1 \tag{10}$$

Capillary pressure:

$$p_c = p_{ce}\left(\frac{\frac{S_w}{S_g + S_w} - S_{wr}}{1 - S_{wr}}\right)^{-n_c} \tag{11}$$

Where: p_{ce}—nominal capillary pressure, Pa; S_{wr}—bound water saturation, dimensionless; n_c—empirical index, dimensionless.

Equation of gas dynamic viscosity:

$$\mu_g = 2.45\times10^{-6} + 2.88\times10^{-8}T + 3.28\times10^{-12}T^2 - 3.78\times10^{-15}T^3 + 2.09\times10^{-8}\rho_g + 2.51\times10^{-10}\rho_g^2 - 5.82\times10^{-13}\rho_g^3 + 1.84\times10^{-16}\rho_g^4 \tag{12}$$

Providing the hydrate is evenly distributed on the rock particle surface of hydrate deposit stratum, without any displacement during the dissociation process, the Masuda model [23] with decreased permeability is referred to, then the relation between the absolute permeability of hydrate deposit stratum and hydrate saturation degree is:

$$K = K_0\left(1 - S_h\right)^N \tag{13}$$

Where: K_0—absolute permeability of deposit stratum when the hydrate stratum is 0, dimensionless; N—permeability reduction index, dimensionless.

K_{rg} and K_{rw} are worked out:

$$K_{rw} = \left(\frac{\frac{S_w}{S_g + S_w} - S_{wr}}{1 - S_{wr} - S_{gr}}\right)^{n_w} \tag{14}$$

$$K_{rg} = \left(\frac{\frac{S_g}{S_g + S_w} - S_{gr}}{1 - S_{wr} - S_{gr}}\right)^{n_g} \tag{15}$$

Where: S_{wr}—residual saturation of water, dimensionless; S_{gr}—residual saturation of methane, dimensionless; n_w—empirical coefficient, dimensionless; n_g—empirical coefficient, dimensionless.

Energy conservation equation of heat transfer:

$$\rho C\frac{\partial T}{\partial t} + \rho Cv\frac{\partial T}{\partial x} - \frac{\partial}{\partial x}\left(\lambda\frac{\partial T}{\partial x}\right) = m_h\Delta H \tag{16}$$

Where: λ—heat conduction coefficient, W/(m·k); C—specific heat, J/(kg·K); ΔH—latent heat of phase change during hydrate dissociation, J/kg.

Where:

$$\rho C = \phi\left(S_g\rho_g C_g + S_h\rho_h C_h + S_w\rho_w C_w\right) + \left(1+\phi\right)\rho_s C_s \tag{17}$$

$$\rho Cv = \rho_g v_g C_g + \rho_w v_w C_w \tag{18}$$

$$\lambda = \phi\left(S_w\lambda_w + S_g\lambda_g + S_h\lambda_h\right) + \left(1-\phi\right)\lambda_s \tag{19}$$

$$\Delta H = H_0 + C_0 T \tag{20}$$

Where: ρ_s—density of rock particles, kg/m^3; C_g, C_w, C_h, C_s—specific of gas, water, hydrate and rock particles, J/(kg·K); ϕ—porosity, dimensionless; H_0, C_0—known constant, to be determined by experimental data; λ_g, λ_w, λ_h, λ_s—heat transfer coefficient of gas, water, hydrate and rock particles, W/(m·K).

According to the chemical equation $CH_4{\cdot}N_HH_2O \rightarrow CH_4 + N_HH_2O$:

$$m_{\mathrm{h}} = -m_{\mathrm{g}} \frac{M_{\mathrm{h}}}{M_{\mathrm{g}}} \tag{21}$$

$$m_{\mathrm{w}} = -m_{\mathrm{g}} \frac{N_{\mathrm{H}} M_{\mathrm{w}}}{M_{\mathrm{g}}} \tag{22}$$

Where: N_H—number of hydrates, dimensionless; M_w, M_h—molar mass of water and hydrate, kg/mol.

Where:

$$m_{\mathrm{h}} = k_{\mathrm{d}} M_{\mathrm{h}} A_{\mathrm{s}} \left(p_{\mathrm{eq}} - p_{\mathrm{g}} \right) \tag{23}$$

Where: p_{eq}—phase equilibrium pressure of hydrate, Pa; A_s—reaction specific surface area of hydrate dissociation in deposits, m^{-1}; k_d—dissociation constant of hydrate, mol/(s·Pa·m^2). p_{eq}, k_d and A_s respectively refer to:

$$p_{\mathrm{eq}} = p_0 e^{4.93 - \frac{T_{\mathrm{a}}}{T}} \tag{24}$$

$$k_{\mathrm{d}} = k_0 e^{-\frac{\Delta E}{RT}} \tag{25}$$

$$A_{\mathrm{s}} = \sqrt{\frac{\left(\phi_{\mathrm{wg}}\right)^3}{2K}} \tag{26}$$

Where: p_0—known constant, Pa; T_a—known constant, K; K_0—fixed rate constant of hydrate dissociation, mol/(s·Pa·m^2); ϕ_{wg}—effective porosity, $\phi_{wg} = \phi(1\text{-}S_h)$; ΔE—activation energy of hydrate dissociation, J/mol.

The energy conservation equation showing the process that shafts transfer heat to the hydrate stratum,

$$\begin{aligned} &-\frac{1}{r}\frac{\partial}{\partial r}\left(r\lambda_m \frac{\partial T}{\partial r}\right) + \frac{\partial}{\partial z}\left(\lambda_m \frac{\partial T}{\partial z}\right) - \frac{1}{r}\frac{\partial}{\partial r}\left(r\rho_g v_{gr} h_g + r\rho_w v_{wr} h_w\right) \\ &-\frac{\partial}{\partial z}\left(\rho_g v_{gz} h_g + \rho_w v_{wz} h_w\right) + q_{out} + q_{ab} \\ &= \frac{\partial}{\partial t}\left[(1-\phi)\rho_s h_s + \phi S_h \rho_h h_h + \phi S_g \rho_g h_g + \phi S_w \rho_w h_w\right] \end{aligned} \tag{27}$$

Where: λ_m—thermal conductivity of the whole reservoir stratum, W/m·K; λ_m can represent the function of porous medium and branch thermal conductivities,

$$\lambda_m = \phi_f \left(\lambda_w S_w + \lambda_g S_g\right) + \left(1 - \phi_v\right)\lambda_s + \left(\phi_v - \phi_f\right)\lambda_h \tag{28}$$

Where: ϕ_f—porosity of fluid, dimensionless; ϕ_v—porosity of porous medium, dimensionless; λ_s—thermal conductivity of porous medium material, W/m·K; λ_w—thermal conductivity of water, W/m·K; λ_g—thermal conductivity of methane gas, W/m·K; λ_h—thermal conductivity of hydrate, W/m·K; q_{out}—roof and bottom boards heat transfer, J/m^3·s; q_{ab}—heat absorbed by the dissociation of hydrate, J/m^3·s; ρ_s—density of porous medium material, kg/m^3; ρ_w—density of water, kg/m^3; ρ_g—density of methane gas, kg/m^3; ρ_h—density of hydrate, kg/m^3.

RESULTS

Assuming the temperature difference between the temperatures of wellbore in the deep well and the hydrate sediment stratum around the well is 65°C, the temperature of the stratum is gradually rising due to the temperature difference in the process of production, the equilibrium state of hydrates is broken, and hydrates are ceaselessly resolved and generate gas. Based on what mentioned above, hydrate heating dissociation seepage and thermal transmission model is built as per the energy conservation law equation, the law of conservation of mass equation and the kinetics of hydrate dissociation equation. Combine with parameters related to hydrate stratum around the deep well, discuss the influences of the saturation of different natural gas hydrates and porosity of different strata in natural gas hydrate sediment stratum around the deep well on the radial dissociation distance of hydrates in a shaft and on the gas production of hydrate dissociation. Basic parameters of the hydrate sediment stratum around the deep well is shown in Table 1.

TABLE 1
Model parameters of Geology of Typical Hydrate Sediment Stratum around the Deep Well

Parameter	Value	Parameter	Value
Water depth	1000m	Temperature of mud line	4°C
Position of hydrate	BML500-600m	Area of hydrate sediment	1000m^2
Formation pressure	19-20.8MPa	Formation temperature	16.5-19°C
Porosity	0.40	Permeability	0.2D
Density of hydrate	905kg/m^3	Density of water	1035 kg/m^3
Saturation of hydrate	0.35	Saturation of water	0.65
Gas density (formation conditions)	120kg/m^3	Density of rock	2600kg/m^3
Density of water	1000kg/m^3	Thermal conductivity of hydrate	0.5787J/(m×s×°C)
Thermal conductivity of rock	3.5J/(m×s×°C)	Thermal conductivity of water	0.6134J/(m×s×°C)
Gas thermal conductivity	0.07J/(m×s×°C)	Thermal conductivity of the roof	3.588J/(m×s×°C)
Heat capacity of the roof	900J/(kg×°C)	Heat capacity of gas	2.265×103J/(kg×°C)
Hydrate dissociation enthalpy	6.283×104J/mol	Heat capacity of rock	900J/(kg×°C)
Heat capacity of hydrate	1.8×10-3J/(kg×°C)	Heat capacity of water	4.5×103J/(kg×°C)
Compressibility factor of water	4×10-4MPa^{-1}	Compressibility factor of hydrate	3×10-4MPa^{-1}
Compressibility factor of rock	1.12×10-3MPa^{-1}	Compressibility factor of gas	0.1MPa^{-1}

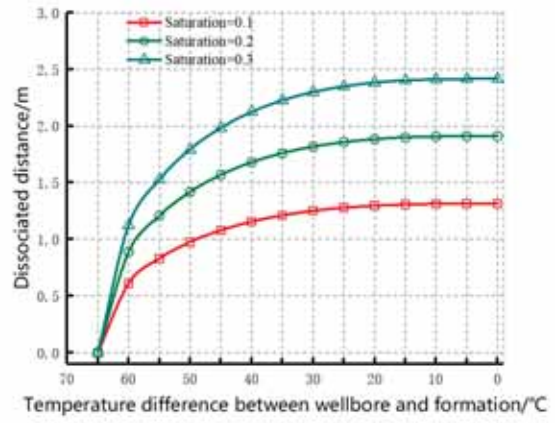

FIGURE 2
Relation between Temperature Difference and Dissociation Distance on the Basis of the Saturation of Different Natural Gas Hydrates

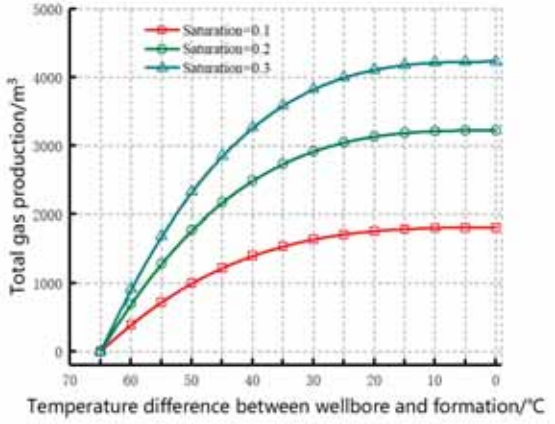

FIGURE 3
Distribution Curve of Accumulated Gas Production of Saturation of Different Natural Gas Hydrates

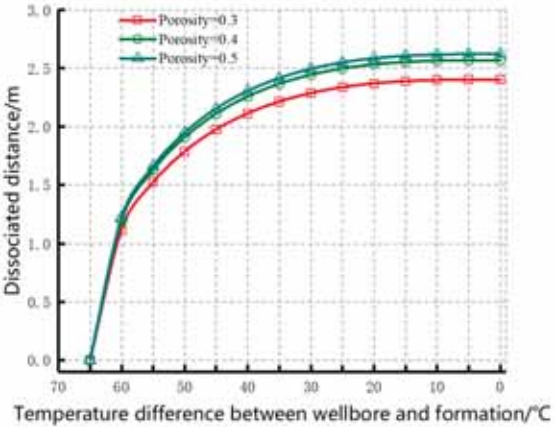

FIGURE 4
Relation between Temperature Difference and Dissociation Distance of Porosity of Different Hydrate Strata

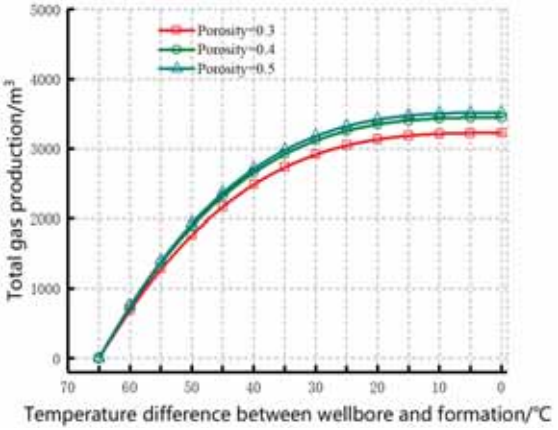

FIGURE 5
Distribution of Accumulated Gas Production of Porosity of Different Hydrate Strata

On the premise of keeping the remaining parameters constant and changing the saturation of hydrate only, discuss the dissociation distance and gas production of hydrates as the saturation of natural gas hydrate is respectively 10%, 20% and 30%. The relation curve between temperature difference and distance on the basis of the saturation of different gas hydrates is shown in Figure 2.

With the increase of saturation of natural gas hydrate, temperatures of shafts will have an obviously great influence on the distance of nearby strata. In addition, at the same condition of saturation of natural gas hydrates, as the temperature difference decreases, the dissociation distance will gradually increase and the growth rate of dissociation distance will gradually reduce; When the temperature difference between temperatures of shafts and the stratum is 65°C, as the increase of saturation of natural gas hydrate, dissociation distance will dramatically increase; while the temperature difference is 0°C, the temperature will achieve a balance; while hydrate stops dissociation, the maximum dissociation distance will be respectively 1.31m, 1.91 m and 2.42 m as the saturation of hydrate in natural gas hydrate sediment stratum is 10%, 20% and 30%; meanwhile, the dissociation distance at 20% saturation of natural gas hydrate is 1.46 times that at 10% saturation of natural gas hydrate. While the dissociation distance at 30% saturation of natural gas hydrate is 1.27 times that at 20% saturation of natural gas hydrate. As the increase of saturation of natural gas hydrate, the increasing trend of dissociation distance decreases and the influence decreases with the saturation increasing.

As shown in Figure 3, discuss the respective influence of saturation 10%, 20% and 30% of natural gas hydrate on the gas production of hydrate sediment stratum around dissociation. The figure shows that, in the process of temperature difference between shafts and the stratum varying from 65°C to 0°C, with the increase of saturation of natural gas hydrate, while the temperature difference is 0°C, the

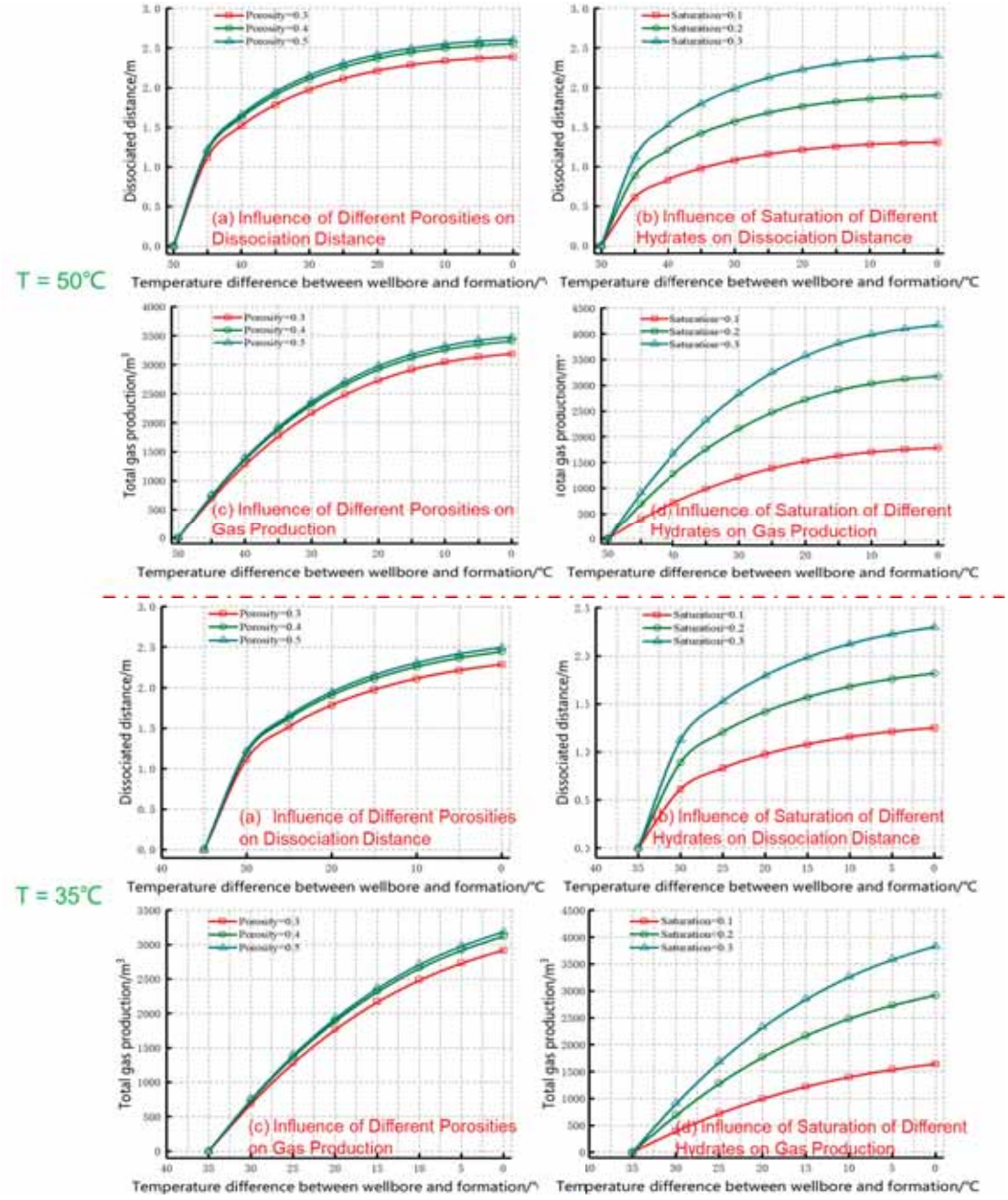

FIGURE 6
The influences of the saturation or porosity of different natural gas hydrates on dissociation distance and gas production

temperature will achieve a balance; while the saturation of hydrate in natural gas hydrate sediment stratum is 10%, 20% and 30%, the maximum gas production will respectively be 1813.3m^3, 3223.8m^3 and 4231.0m^3. Meanwhile, the gas production at the 20% saturation of natural gas hydrate is 1.78 times that at the 10% saturation of natural gas hydrate. While the dissociation distance at 30% saturation of natural gas hydrate is 1.31 times that at 20% saturation of natural gas hydrate. This indicates that the saturation of natural gas hydrate has a great influence on the gas production of hydrate dissociation.

This is shown in Figure 4. As the increase of porosity of hydrate sediment stratum, the dissociation distance of hydrate will increase. While the temperature difference between the temperatures of nearby shafts and the stratum is 65°C, with the increase of porosity of hydrate stratum, the dissociation distance will slightly increase and the maximum dissociation distance will be 9.9%; while the temperature difference between the temperatures of the place of shaft heat transfer and the stratum is 0°C, the farthest dissociation distance that porosity influences is still short, namely 2.40m, 2.56m and 2.62m

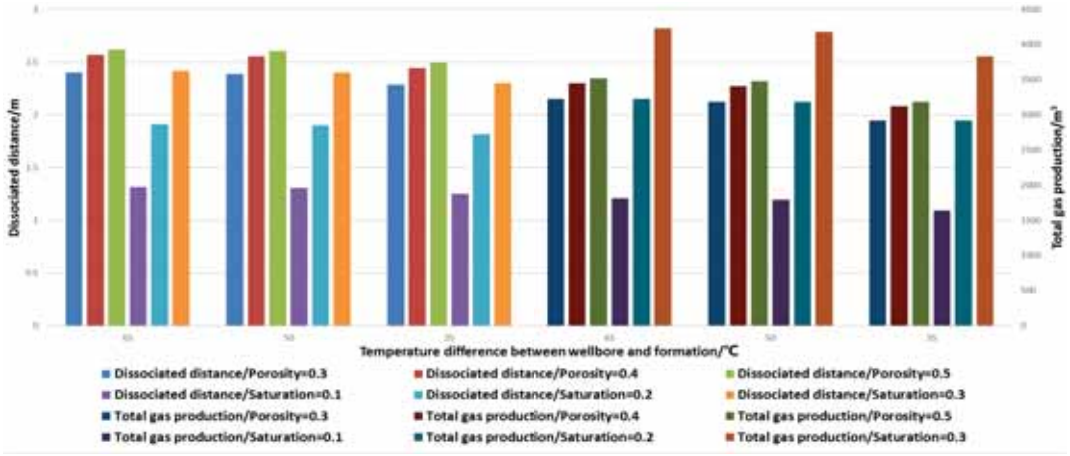

FIGURE 7
Comparison of Dissociation Distance and Gas Production Based on Different Temperature Differences

TABLE 2
Dissociation Distance of and Gas Production of Hydrate Stratum Based on Different Shafts and Temperature Differences of Strata

Temperature difference between wellbore and formation	Formation condition	Dissociated distance/m	Total gas production/m^3
65°C	Porosity=0.3	2.40	3223.78
	Porosity=0.4	2.57	3446.32
	Porosity=0.5	2.62	3517.41
	Saturation=0.1	1.31	1813.32
	Saturation=0.2	1.91	3223.78
	Saturation=0.3	2.42	4231.04
50°C	Porosity=0.3	2.39	3186.98
	Porosity=0.4	2.55	3406.99
	Porosity=0.5	2.61	3477.26
	Saturation=0.1	1.31	1792.61
	Saturation=0.2	1.90	3186.99
	Saturation=0.3	2.40	4182.75
35°C	Porosity=0.3	2.29	2981.86
	Porosity=0.4	2.44	3120.35
	Porosity=0.5	2.49	3184.71
	Saturation=0.1	1.25	1641.79
	Saturation=0.2	1.82	2918.86
	Saturation=0.3	2.30	3830.80

respectively. Among which, there is 6.9% difference between the farthest dissociation distance at 40% porosity and at 30% porosity, 2.2% difference between the farthest dissociation distance at 50% porosity and 40% porosity, and 9.2% difference between the farthest dissociation distance at 50% porosity and 30% porosity. The increase is not significant. Meanwhile, on the basis of the same porosity of hydrate stratum, as the gradual decrease of temperature difference, the distance that porosity influences will gradually increase, but the growth rate of dissociation distance will gradually reduce.

As shown in Figure 5, with the increase of porosity of hydrate stratum, the gas production of hydrate dissociation will slightly increase. In addition, on the basis of the same porosity of hydrate stratum, as the gradual decrease of temperature difference, the growth rate of accumulated gas production will gradually reduce; while the temperature difference between the temperatures of nearby shafts and the stratum is 65°C, with the increase of porosity of hydrate stratum, gas production will slightly increase and the maximum difference of corresponding gas production is 9.5%; while the temperature difference between the temperatures of the place of shaft heat transfer and the stratum is 0°C, the difference between the final gas production at 40% porosity of hydrate stratum and that at 30% porosity of hydrate stratum is 7.2%, and the difference between the final gas production at 50% porosity of hydrate stratum and that at 40% porosity of hydrate stratum is 2.3%. The influence of temperature difference. The influence of the final gas production is still little. The maximum difference is still 9.5%.

Assuming the temperature differences between the temperatures of shafts in the deep well and the hydrate sediment stratum around the well are 50°C and 35°C, the influences of the saturation or porosity of different natural gas hydrates on dissociation distance and gas production are shown in Figure 6.

It shows from Figure 6 to Figure 7 and Table 2 that, as the temperature difference between the temperatures of shafts and the stratum decreases from

65°C to 35°C, the dissociation distance and gas production of hydrate stratum decrease based on different porosities or saturations. While the temperature difference is 50°C and the porosity is 0.5, the dissociation distance is 2.61m and the gas production is 3477.26m^3, respectively accounting for 99.2% of the dissociation distance and 98.9% of the gas production in the same case while the temperature difference is 65°C; while the saturation is 0.3, the dissociation distance is 2.40m and the gas production is 4182.75m^3, respectively accounting for 99.2% of the dissociation distance and 98.9% of the gas production in the same case while the temperature difference is 65°C. While the temperature difference is 35°C and the porosity is 0.5, the dissociation distance is 2.49m and the gas production is 3184.71m^3, respectively accounting for 95.0% of the dissociation distance and 90.5%of the gas production in the same case while the temperature difference is 65°C; while the saturation is 0.3, the dissociation distance is 2.30m and the gas production is 3830.80m^3, respectively accounting for 95.0% of the dissociation distance and 90.5%of the gas production in the same case while the temperature difference is 65°C.

CONCLUSIONS

(1) Increases of the saturation of natural gas hydrate and the porosity of hydrate stratum will result in the increases of dissociation distance and gas production of hydrate;

(2) As the heat transfer is carrying out, the temperature difference between phase transition and frontal surface gradually decreases and the influences of saturation of hydrate and stratum porosity on dissociation distance and gas production decrease.

(3) Change of saturation of natural gas hydrate will distinctly influence the dissociation distance of hydrate and corresponding gas production. While the change of porosity of hydrate stratum will slightly influence the dissociation distance and gas production of hydrates.

(4) Reducing the temperature difference between shafts and the hydrate stratum can decrease the radial distance of dissociation of hydrate sediment stratum and the gas production of hydrate dissociation, control the increase of shaft external load caused by the excess pore pressure, and reduce the integrity risk of shafts in the deep well.

ACKNOWLEDGEMENTS

The authors are grateful for the support of the Program for National Science and Technology Major Project of the Ministry of Science and Technology of China (2016ZX05026-002, 2016ZX05028-001, 2016ZX05024-005), the Sichuan Science and Technology Program, China (2016JQ0010), and the PetroChina Innovation Foundation (2017D-5007-0315).

REFERENCES

[1] Zhang, B., Guan, Z., Zhang, Q. (2015) Prediction and analysis on annular pressure of deepwater well in the production stage. Acta Petrolei Sinica. 36(8), 1012-1017.

[2] Holtzman, R., Juanes, R. (2011) Thermodynamic and hydrodynamic constraints on overpressure caused by hydrate dissociation: A porescale model. Geophysical Research Letters. 38(38), L14308.

[3] Paull, C., Buelow, W., Ussler, W. (1996) Increased continental-margin slumping frequency during sea-level lowstands above gas hydrate–bearing sediments. Geology. 24(2), 143.

[4] Rothwell, R., Reeder, M., Anastasakis, G., Stow, D., Thomson, J., Kihler, G. (2000) Low sea-level stand emplacement of megaturbidites in the western and eastern Mediterranean Sea. Sedimentary Geology. 135(1), 75-88.

[5] Mienert, J., Vanneste, M., Stefan, B., Karin, A., Haflidi, H., Hans, P. (2005) Ocean warming and gas hydrate stability on the mid-Norwegian margin at the Storegga Slide. Marine and Petroleum Geology. 22(1-2), 233-244.

[6] Arzbacher, S., Rahmatian, N., Ostermann, A., Massani, B., Loerting, T., Jörg, P. (2019) Macroscopic defects upon decomposition of CO_2 clathrate hydrate crystals. Physical Chemistry Chemical Physics. 21, 9694-9708.

[7] Vogt, P., Gardner, J., Crane, K. (1999) The Norwegian–Barents–Svalbard (NBS) continental margin: Introducing a natural laboratory of mass wasting, hydrates, and ascent of sediment, pore water, and methane. Geo-Marine Letters. 19(1-2), 2-21.

[8] Rensbergen, P., Batist, M., Klerkx, J., Hus, R., Poort, J., Vanneste, M., Granin, N., Khlystov, O. (2011) Sublacustrine mud volcanoes and methane seeps caused by dissociation of gas hydrates in Lake Baikal. Geology. 30(7), 631-634.

[9] Zühlsdorff, L., Spie, V. (2004) Three-dimensional seismic characterization of a venting site reveals compelling indications of natural hydraulic fracturing. Geology. 32(2), 101.

[10] Maslin, M., Mikkelsen, N., Vilela, C., Haq, B. (1998) Sea-level –and gas-hydrate–controlled catastrophic sediment failures of the Amazon Fan. Geology. 26(12), 1107.

[11] Chen, F., Yapa, P. (2001) Estimating hydrate formation and decomposition of gases released in a deepwater ocean plume. Journal of Marine Systems. 30(1-2), 21-32.

[12] Phrampus, B., Hornbach, M. (2012) Recent changes to the Gulf Stream causing widespread gas hydrate destabilization. Nature. 490(7421), 527-530.
[13] Zhang, Z., Zhang, L. (2015) Study on thermal stress of free casing in high temperature and high yield gas well. Journal of Safety and Environment. 15(4), 98-102.
[14] Zhang, Z., Xu, B., Shi, T. (2007) Application of reliability theory in strength design of casing string. West-China Exploration Engineering. (8), 49-51.
[15] Zhang, Z., Wang, B., Li, Z. (2016) Study on mechanics of multi-packer completion string in high pressure gas well. Journal of Southwest Petroleum University (Science and Technology Edition). 38(6), 172-178.
[16] Zhang, Z., Li, Y., Zhang, C. (2013) Wellbore integrity design of high temperature gas wells containing CO2. Natural Gas Industry. 33(9), 79-86.
[17] Xu, H., Zhang, Z., Xiong, J. (2014) Effect of free casing on stress and integrity of cement ring in high temperature and high pressure gas well. Drilling & Production Technology. 37(2), 75-78.
[18] Zhang, Z., Zhou, Y., Fu, J. (2010) Wellbore integrity design method for sulphur-bearing gas Wells. Natural Gas Industry. 30(3), 67-69.
[19] Zhang, Z., He, Y., Wang, Y. (2017) Research on risk evaluation of well integrity for sour gas wells. Journal of Safety Science and Technology. 13(4), 101-107.
[20] Wang, Y., Feng, J., Li, X., Zhang, Y. (2018) Influence of well pattern on gas recovery from methane hydrate reservoir by large scale experimental investigation. Energy. 152, 34-45.
[21] Sayuri, K., Fusao, O., Tomohiko, F. (2010) A chemo-thermo-mechanically coupled analysis of ground deformation induced by gas hydrate dissociation. International Journal of Mechanical Sciences. 52(02), 365-376.
[22] Tsypkin, G. (2005) Effect of decomposition of a gas hydrate on the gas recovery from a reservoir containing hydrate and gas in the free state. Fluid Dynamics. 40(1), 117-125.
[23] Su, Z., He, Y., Wu, N., Zhang, K., Moridis, G. (2012) Evaluation on gas production potential from laminar hydrate deposits in Shenhu Area of south China Sea through depressurization using vertical wells. Journal of Petroleum Science and Engineering. 86-87, 87-98.
[24] Wang, Z., Sun, B., Wang, X., Zhang, Z. (2014) Prediction of natural gas hydrate formation region in wellbore during deep-water gas well testing. Journal of Hydrodynamics. 26(4), 568-576.
[25] Gong, Z., Ren, S., Zhang, L., Cui, G., Liu, Y., Wang, Y. (2017) Shallow Gas and Shallow Water Flow Induced by Natural Gas Hydrate Dissociation in Deep Water Sediments. OTC-27624-MS.
[26] Tsypkin, G. (2001) Mathematical model for dissociation of gas hydrates coexisting with gas in strata. Doklady Physics. 46(11), 806-809.
[27] Nimblett, J.N., Shipp, R.C., Strijbos, F. (2005) Gas Hydrate As A Drilling Hazard: Examples From Global Deepwater Settings. Offshore Technology Conference. 2-5 May, Houston, Texas.
[28] Liang, H., Song, Y., Chen, Y. (2010) Numerical simulation for laboratory-scale methane hydrate dissociation by depressurization. Energy Conversion and Management. 51(10), 1883-1890.

Received: **09.12.2019**
Accepted: **01.02.2020**

CORRESPONDING AUTHOR

Zhi Zhang
State Key Laboratory of Oil and
Gas Reservoir Geology and Exploration,
Southwest Petroleum University,
Chengdu 610500 – China

e-mail: 2115543711@qq.com

© by PSP Volume 29 – No. 05/2020 pages 3879-3884 Fresenius Environmental Bulletin

EFFECTIVE PLANT REGENERATION METHOD FROM CALLUS CULTURES, OBTAINED FROM DIFFERENT EMBRYO SOURCES, IN WINTER WHEAT (*TRITICUM AESTIVUM* L.) WITH THIDIAZURON (TDZ)

Berk Benlioglu*, Nilufer Kocak Sahin

Department of Field Crops, Faculty of Agriculture, Ankara University, 06110 Diskapi, Ankara,Turkey

ABSTRACT

The different embryonic resources of certain winter wheat cultivars (*Triticum aestivum* L.) are explained in vitro in order to improve an effective plant regeneration system through callus inititiation, using different thidiazuron (TDZ) doses. In the case of each genotype or embryo source, thidiazuron has been seen to benefit plant regeneration by increasing the number of plants regenerated and transferred into the soil at a rate of between 1.18 and 3.7 times the controls. Within the embryo sources, immature embryos and within the cultivars, Bezostaja-1 responded to TDZ based common winter wheat regeneration treatments by producing the highest number of regenerants. Nevertheless, the 1 mg l^{-1} dose of TDZ caused significant reductions within the studied parameters. The method applied in this research can be used in winter wheat, gene transfer studies and transgenic plant production.

KEYWORDS:
Embryo resources, winter wheat, Thidiazuran (TDZ), plant regeneration

INTRODUCTION

Although common wheat (*Triticum aestivum* L.) is one of the most important cereals for human nutrition, it still requires improvement through biotechnological intervention in combination with conventional breeding. However, for biotechnological applications, improved plant tissue culture systems are required. So far, in tissue culture studies, various explants of common wheat such as immature embryos [1-5], mature embryos [5-9], immature leaves [10, 11], immature inflorescences [5, 12-15] and meristamatic shoot segments [16] were used and the regeneration of fertile plants was reported with varying degrees of success. In addition to conventional plant growth regulators, chemicals that were synthesized for different purposes have been continously tested because of their effects on improving tissue culture response among plants. One such chemical, Thidiazuran (TDZ: N-phenyl-N'-(1,2,3-thidiazol-yl)urea) was registered as a cotton defoliant by Schering AG (Berlin, Germany) in 1976 [17]. Beginning in the 1980's TDZ has become a point of research in tissue culture studies due to its effects on morphogenesis among various plant species. Although the majority of studies involving TDZ are on dicotyledonous species [18, 19], very little information is available for monocotyledonous species, and especially for cereals [4, 7, 16, 20]. The aim of this study is to investigate the effects of TDZ on plant regeneration using callus cultures obtained through three embryo explant sources (immature, mature, and endosperm- supported-mature) in five different cultivated varieties of common winter wheat in Turkey.

MATERIALS AND METHODS

Plant Material. Five genotypes of winter wheat cv. Basak-95, Bezostaja-1, Gerek-79, Tosun-21 and line T- 111 were used as sources of immature, mature and endosperm-supported mature embryos. The plants were grown in the field during the winter of 2017-2018 and harvested in the following May.

Explant Preparation And Culture Manipulation. Immature seeds were harvested from main spikes 15-18 days after anthesis, surface-sterilized in 70% (v/v) ethanol for 1 min and in commercial bleach (5% sodium hypochlorite) for 30 min, and then washed several times in sterile distilled water. Immature embryos were aseptically excised from caryopsis and placed with the scutellum upwards on solid agar medium in sterile Petri dishes for 14 days at 26±1°C in darkness. The basal medium used in this study consisted of MS macro- and micro-elements [21] supplemented with 20 mg l^{-1} sucrose, 2 mg l^{-1} 2,4-D, and 7 mg l^{-1} agar. The media were adjusted to pH 5.8 and autoclaved for 20 min at 121°C and 1.1 kg/cm^2 pressure. For shoot initiation, calli were transferred to TDZ (0.25, 0.50, 0.75, 1 mg l^{-1}) - containing MS medium supplemented with 20 mg l^{-1} sucrose and 7 mg l^{-1} agar for 5 weeks at 26±1°C in a 16 h light (2000 lux) 8 h dark photoperiod. Each

treatment consisted of 15 embryos or seeds per Petri dish with three replicates.

Mature seeds were surface-sterilized in 70% (v/v) ethanol for 5 min, rinsed twice with sterile distilled water, incubated further in commercial bleach for 30 min and rinsed several times in sterile distilled water [22, 23]. The surface-sterilized seeds were incubated at 33°C for 2 h in sterile distilled water for imbibition. The mature embryos were easily separated from the endosperm in imbibed seeds and placed, scutellum up on MS medium supplemented with 20 mg l^{-1} sucrose, 2 mg l^{-1} 2,4-D and 7 mg l^{-1} agar and incubated at 26±1°C for 14 days in darkness [24]. After this incubation, the calli were transferred to TDZ (0.25,0.50, 0.75, 1 mg l^{-1}) - containing MS medium supplemented with 20 mg l^{-1} sucrose and 7 mg l^{-1} agar for shoot initiation and growth for 5 weeks at 26±1°C in a 16 h light 8 h dark photoperiod.

Endosperm-supported mature embryo culture was carried out according to Ozgen et al. [3], with minor modifications. Mature seeds were surface-sterilized in 70% (v/v) ethanol for 5 min, washed twice with sterile distilled water, incubated further in commercial bleach for 25 min and rinsed several times in sterile distilled water. The seeds were then imbibed in sterile distilled water for 2 h at 33°C. For callus induction, mature embryos were aseptically moved slightly with a scalpel from the imbibed seeds. The seeds with moved embryos were placed furrow downwards in sterile 10 cm Petri dishes containing 7 ml of 2,4-D solution (8 mg l^{-1}). The dishes were kept at 26±1°C in total darkness for 14 days. The developed calli were removed from the seeds and transferred on to a hormone-free MS mineral salts, supplemented with 2 mg l^{-1} glycine, 20 mg l^{-1} sucrose and 7 mg l^{-1} agar in Petri dishes. The transferred callus cultures were kept at 26±1°C in darkness for 3 weeks, and then for shoot initiation, calli were transferred to TDZ (0.25, 0.50, 0.75, 1 mg l^{-1}) - containing MS medium supplemented with 20 mg l^{-1} sucrose and 7 mg l^{-1} agar for 5 weeks at 26±1°C in a 16 h light (2000 lux) 8 h dark photoperiod.

When shoots and roots were established, plantlets, 1-2cm in height, were transferred to baby-jars containing hormone-free MS medium supplemented with 20 mg l^{-1} sucrose and 7 mg l^{-1} agar for 1 month. When the roots of these plantlets reached to 10-12 cm in length, they were transferred to soil in pots. Each pot was covered with a plastic bag for 1 week to maintain high humidity under a 16 h light 8 h dark photoperiod at 26±1°C. After 3 weeks, the plants were vemalised for 2 weeks at 4°C and subsequently transferred to soil and grown in the greenhouse to maturity to ensure fertility and seed set.

Data Collection And Analysis Callus fresh weights were measured under sterile conditions for every 15 embryos with three replicates before the calli were transferred to the shoot initiation medium in ali TDZ doses.

The effect of TDZ on culture responses was determined by analysis of variance and least significant difference tests. The data recorded in percentages were transformed to arcsine before analysis. Correlation coefficients between the different characters were calculated for each procedure [25].

RESULTS AND DISCUSSION

Callus Induction. For immature embryos, callus induction became evident on the first day of culture whereas for endosperm-supported embryos and mature embryos, callus proliferation occurred within 2 or 3 days of culture.

Although TDZ was not present at this stage, immature embryos responded consistently within the individual genotype sets. The callus inductions ranged from 93.3% to 100 % (Table 1). All five genotypes produce callus at an average of 97.7%.

For mature embryos, Line 111, Bezostaja-1 and Tosun-21 displayed consistent callus inductions within individual genotype sets ranging from 88.9% to 100%. In this group, Başak-95 (73.3% vs. 86.7%) and Gerek-79 (77.7% vs. 86.6%) displayed significant differences in callus induction. All five genotypes produce callus on an average of 89.4%.

For endosperm-supported embryos, Line 111, Bezostaja-1 and Gerek-79, were the genotypes displaying consistent callus inductions ranging from 93.3% to 100%. However, Basak-95 (79.9% vs. 95.5%) and Tosun-21 (88.8% vs. 93.3%) showed significant differences in callus inductions. Nevertheless, all five genotypes produced callus at an average of 94.2%.

The callus induction data we have obtained is in accordance with data obtained elsewhere [5, 13, 14, 26] reconfirming the superior potential of immature embryos, which were followed in this study by endosperm-supported mature embryos and finally by mature embryos in the callus induction process.

For the callus weight as a measured parameter, varietal differences between genotypes were apparent for all embryo sources. For the immature embryos, the average callus weights ranged significantly, from 0.68 g (Başak-95) to 1.12 g (Line 111). However, the highest average callus weights were obtained from endosperm-supported embryos ranging from 0.86 g (Bezostaja-1) to 2.81 g (Line 111). Also a low but significant ($p<0.05$) positive correlation ($r=0.230$) between callus induction and callus weight has been observed for this group (Table 2). The lowest average callus weights were obtained from mature embryos ranging from 0.47 g (Gerek-79) to 1.02 g (Line 111) with a moderate but significant ($p<0.01$) positive correlation ($r=0.380$) between the callus induction percentage and the callus weight (Table 2).

The order of embryo sources in relation to callus weight parameters is clearly in accordance with

the results we have obtained previously [13]. During callus formation, endosperm- supported embryos have the advantage of mobilizing more nutrients from the endosperm, in addition to the nutrients present in the MS medium, which might contribute to the highest average callus weights we have obtained. The immature embryos lacking this support, produced the second highest average callus weights, most likely due to the juvenile cells they posses when compared to least average callus weight-yielding mature embryos.

Plant Regeneration. In order to observe the effects of TDZ on plant regeneration, all genotypes for each embıyo source have been subjected to TDZ treatments ranging from 0 (control) to 1 mg l^{-1}. The genotypes responded differently to TDZ doses by varying their regeneration capacities.

For immature embryos, the callus cultures of Line 111, whereas Başak-95 responded to 0.5 mg l^{-1} of TDZ by displaying positive but non-significant plant regeneration capacity differences compared to the controls. The regeneration capacity of Bezostaja-1 (0.75 mg l^{-1}) and Gerek-79 (0.50 mg l^{-1}) are affected in a significant positive manner when compared to the Controls. Tosun-21 is found to be the only genotype displaying a negative but non-significant regeneration capacity difference than the control at a 0.75 mg l^{-1} TDZ application. All genotypes, except Bezostaja-1, are affected negatively compared to a 1 mg l^{-1} TDZ application by displaying significant differences of regeneration capacity when compared to the controls (Table 1).

Mature embryos responded to TDZ treatments by displaying either negative but non-significant plant regeneration capacity differences compared to the controls: Bezostaja-1 (0.25 mg l^{-1}), Gerek-79 (0.25 mg l^{-1}) and Tosun-21 (0.75 mg l^{-1}) or negative, but with a significant difference when compared with the control: Line 111 (0.5 mg l^{-1}). Başak-95 was found to be the only genotype which responded to 0.25 mg l^{-1} TDZ treatment positively, although the difference is a non-significant one. All genotypes are affected negatively by 1 mg l^{-1} TDZ application displaying significant differences of regeneration capacity when compared to the controls.

For endosperm-supported embryos, non-significant plant regeneration capacity differences were observed between TDZ treatments and controls. These differences were either positive: Line 111 (0.5 mg l^{-1}), Başak-95 (0.75 mg l^{-1}) and Gerek-79 (0.5 mg l^{-1}) or negative (Bezostaja-1 and Tosun-21 at 0.75 mg l^{-1}). All genotypes were affected negatively by a 1 mg l^{-1}TDZ application displaying significant differences in regeneration capacity when compared with controls.

In contrast to the inconsistent plant regeneration capacity results, there are clear significant positive effects of TDZ on the number of regenerated plants.

For immature embryos, all genotypes, except Gerek-79 at 0.5 mg l^{-1} responded to 0.75 mg l^{-1} of TDZ treatment increasing the number of regenerated plants from 1.38-folds (Gerek-79) to 3.25-folds (Başak-95) when compared to controls.

Mature embryo-based callus cultures also responded to TDZ treatments by increasing the number of regenerated plants when compared to controls. This increase was 1.18-folds for Line 111 (0.5 mg l^{-1}), 1.33-folds for Başak-95 (0.75 mg l^{-1}), 1.94-folds for Bezostaja-1 (0.75 mg l^{-1}), 1.5-folds for Gerek-79 (0.25 mg l^{-1}) and 1.6-folds for Tosun-21 (0.75 mg l^{-1}).

The same positive trend was also observed when endosperm-supported mature embryo-based callus cultures were subjected to TDZ treatments. The increase was 2.48-folds for Line 111 (0.25 mg l^{-1}), 1.65-folds for Başak-95 (0.75 mg l^{-1}), 3.7-folds for Bezostaja-1 (0.5 mg l^{-1}), 2.65-folds for Gerek-79 and finally 2.48-folds for Tosun-21 (0.25 mg l^{-1}).

For all three embryo sources a moderate amount of significant correlation soil is also evident between the regeneration capacity of the callus, as well as for a number of plants growing in (Table 2).

For all genotypes, the application of 1 mg l^{-1} of TDZ reduced the number of plants growing in the soil significantly when compared to the controls. Three exceptions from the immature embryo group contradicted this observation, namely: Line 111 (non-significant), Başak-95 (significant) and Bezostaja-1 (significant)). One exception can be observed from the endosperm-supported mature embryo group (Bezostaja-1 (significant)). These genotypes at the aforementioned embryo source groups increase the number of plants obtained through TDZ applications at 1 mg l^{-1}.

The highest numbers of plants are regenerated when immature embryos were used [3, 5, 13, 14, 26] which is followed more or less equally by mature and endosperm-supported mature embryos in this study. In this respect, this is the first report comparing the efficiency of endosperm-supported mature embryos with immature and mature embryos towards common winter wheat regeneration under the influence of TDZ.

CONCLUSIONS

In conclusion, we found that TDZ at a concentration of up to 0.75 mg l^{-1} with immature embryos as the embryo source was optimal for common winter wheat regeneration. However, above this concentration, TDZ seems to possess growth inhibitory effects on the regeneration process of most genotypes of winter wheat. Although the precise mechanism of TDZ action is not known, a variety of plausible mechanisms have been previously proposed [19]. More recently, the role of TDZ in plant regeneration

TABLE 1
Culture responses from 3 embryo sources of five common winter wheat genotypes

Embryo sources and Genotypes	Callus induction (%)					Callus weigt (g)				
	Dosages (mg/l)					Dosages (mg/l)				
Immature	0	0.25	0.50	0.75	1	0	0.25	0.50	0.75	1
Line 111	100.0a	97.8a	100.0a	100.0a	100.0a	0.90a-e	0.85bc	1.12a	1.02a-c	1.10a
Basak-95	97.8a	95.5a	97.7a	100.0a	97.8a	0.80cd	0.68e	0.84b-e	0.68e	0.71e
Bezostaja-1	95.5a	97.7a	100.0a	97.8a	97.7a	0.79de	0.70e	0.81c-e	0.85b-e	0.75e
Gerek-79	100.0a	97.7a	93.3a	93.3a	100.0a	0.73e	1.06ab	0.91a-e	1.08a	1.01a-d
Tosun-21	100.0a	97.8a	95.5a	95.5a	93.3a	0.75e	0.76e	0.82c-e	0.79de	0.78de
Mean	98.7±0.9	97.2±0.5	97.3±1.3	97.3±1.3	97.8±1.2	0.79±0.03	0.81±0.07	0.90±0.6	0.88±0.07	0.87±0.08
Mature										
Line 111	93.3a-c	100.a	97.7ab	97.7ab	97.7ab	0.87a-c	1.02a	0.91ab	0.85a-d	0.79a-f
Basak-95	86.7a-e	82.2c-f	73.3f	75.5ef	75.5ef	0.72b-h	0.76b-g	0.57e-h	0.81a-e	0.66b-h
Bezostaja-1	93.3a-c	95.5ab	93.3a-c	97.8ab	88.9a-d	0.61c-h	0.66b-h	0.72b-h	0.68b-h	0.64c-h
Gerek-79	82.2c-f	84.4b-f	86.6a-e	77.7d-f	82.2c-f	0.47h	0.55e-h	0.49h	0.51gh	0.52gh
Tosun-21	95.5ab	97.8ab	100.0a	91.1a-c	88.9a-d	0.53f-h	0.60d-h	0.73b-h	0.59d-h	0.48h
Mean	90.2±2.5	92.0±3.6	90.2±4.8	88.0±4.8	86.6±3.7	0.64±0.07	0.72±0.08	0.69±0.07	0.69±0.06	0.62±0.05
Endosperm sup. mature										
Line 111	95.5ab	93.3ab	97.8ab	95.5ab	95.5ab	2.78a	2.81a	2.19b	2.15bc	2.01b-d
Basak-95	88.9b	79.9c	93.3ab	88.8b	95.5ab	1.19h-k	1.32f-k	1.60d-h	1.31f-k	1.46e-j
Bezostaja-1	93.3ab	100.0a	100.0a	93.3ab	100.0a	1.01jk	0.86k	1.72b-g	1.54d-ı	1.90b-e
Gerek-79	100.0a	95.5ab	97.8ab	97.8ab	93.3ab	1.77b-f	1.65d-h	1.68c-h	1.61d-h	1.31f-k
Tosun-21	93.3ab	91.1ab	93.3ab	88.8b	93.3ab	1.39f-j	1.18h-k	0.98jk	1.24g-k	1.06ı-k
Mean	94.2±1.8	92.0±3.4	96.4±1.3	92.8±1.8	95.5±1.8	1.63±0.3	1.06±0.3	1.63±0.2	1.57±0.2	1.55±0.2
Embryo sources and Genotypes	Regeneration Capacity[a] (%)					Number of Regenerated Plant				
	Dosages (mg/l)					Dosages (mg/l)				
Immature	0	0.25	0.50	0.75	1	0	0.25	0.50	0.75	1
Line 111	91.1a-c	80.0c-d	93.1ab	88.8a-d	75.5e	7.0h-j	6.0ı-k	7.6gh	12.3ab	7.3g-ı
Basak-95	86.2a-e	83.4b-e	88.6a-d	84.4a-e	77.2de	3.6m	7.0h-j	8.3e-h	11.7bc	5.3kl
Bezostaja-1	81.4b-e	79.3c-e	84.4a-e	95.5a	88.7a-d	8.3e-h	5.7jk	8.0f-h	13.7a	9.3de
Gerek-79	82.1b-e	88.9a-d	90.4a-c	61.9f	55.5f	6.0ı-k	8.6e-g	9.6de	8.3e-h	5.3kl
Tosun-21	86.6a-e	63.5f	76.7e	81.9b-e	40.5g	6.0ı-k	8.3e-g	7.3g-ı	10.6cd	4.0lm
Mean	85.5±1.75	79.0±4.2	86.6±2.2	82.5±2.2	67.5±8.6	6.2±0.8	7.1±0.6	8.2±0.4	11.3±0.9	6.2±0.3
Mature										
Line 111	88.1a-c	75.5c-f	66.0e-h	66.0e-h	45.5j-l	5.3b-e	6.0a-c	6.3ab	5.3b-d	2.7g-k
Basak-95	74.3d-f	76.4b-f	73.1d-g	68.7d-h	56.1h-j	3.0g-j	2.0jk	3.7e-h	4.0d-g	1.3k
Bezostaja-1	90.5a	79.2a-e	66.6e-h	74.7d-f	64.7f-ı	3.6e-h	5.0b-e	6.3ab	7.0a	2.3h-k
Gerek-79	89.3ab	81.6a-d	66.7e-f	59.7g-ı	36.1l	4.0d-g	6.0a-c	5.3b-d	4.0d-g	1.6jk
Tosun-21	72.0d-g	52.2ı-k	59.9g-ı	68.2d-h	40.0kl	3.3f-ı	4.0d-g	4.6c-f	5.3b-d	1.6jk
Mean	82.8±4.0	73.0±5.3	66.5±2.1	67.5±2.4	48.5±5.3	3.8±0.4	4.6±0.7	5.2±0.5	5.1±0.6	1.9±0.3
Endosperm sup. Mature										
Line 111	83.6cd	88.0b-d	86.4b-d	67.5e	32.7f	2.7g-ı	6.7a	6.0ab	4.0d-g	1.66ıj
Basak-95	92.8a-d	94.8a-c	90.4a-d	97.4ab	88.3b-d	4.0d-g	4.7b-e	6.0ab	6.6a	3.0f-ı
Bezostaja-1	100.0a	97.8ab	97.8ab	92.9a-d	62.1e	1.7ıj	4.7b-e	6.3a	4.0d-g	2.7g-ı
Gerek-79	84.1cd	86.2cd	84.3cd	81.7d	61.5e	2.0ıj	4.3c-f	5.3a-d	3.7e-h	1.0j
Tosun-21	100.0a	87.8b-d	83.3d	92.3a-d	66.8e	2.3h-j	5.7a-c	4.3c-f	4.0d-g	1.7ıj
Mean	92.1±3.6	90.3±2.3	88.4±2.6	86.4±2.2	62.3±8.9	2.5±0.4	5.2±0.4	5.6±0.4	4.5±0.5	2.0±0.4

[a] : Number of regenerable calli (Nodular calli with green spots) / number of calli induced x 100
Means followed by the same letter are not significantly different at the 0.05 probability level

in relation to a metabolic cascade that includes signal perception is discussed elsewhere, as well as the accumulation and transport of endogenous plant signals such as auxins and melatonin, a system of secondary messengers, and a concurrent stress response [27].

Regardless of what the action mechanism is, the use of TDZ in cereal tissue culture, in particular the common winter wheat, clearly improved the regeneration process from 1.18 to 3.7-folds up to a concentration of 0.75 mg l^{-1} in this study. This procedure of a TDZ-based regeneration of common winter wheat plants we have developed can be used in transgenic as well as molecular wheat breeding studies in the future.

TABLE 2
Correlations between different characters in callus cultures from different embryos of five common winter wheat genotypes (*upper line*, immature embryos; *middle line*, mature embryos; *lower line*, endosperm – supported mature embryos)

Characters	Correlation coefficients between characters			
	1	2	3	4
(1) Callus induction (%)	-	0.188	0.114	0.033
	-	0.380**	-0.034	0.422**
	-	0.230*	-0.232*	-0.154
(2) Weight of callus (g)		-	-0.038	0.059
		-	0.127	0.328**
		-	-0.233*	0.136
(3) Regeneratiyon capacity of callus (%)			-	0.434**
			-	0.450**
			-	0.474
(4) Number of plants growing in soil				-
				-
				-

*,** : Significantly different from zero at 0.05 and 0.01 probability, respectively.

REFERENCES

[1] Sears, R.G. and Deckard, E.L. (1982) Tissue culture variability in wheat: callus induction and plant regeneration. Crop Science. 22(3), 546-550.

[2] Felfoldi, K. and Purnhauser, L. (1992) Induction of regenerating callus cultures from immature embryos of 44 wheat and 3 triticale cultivars. Cereal Research Communications. 273-277.

[3] Ozgen, M., Turet, M., Altinok, S. and Sancak, C. (1998) Efficient callus induction and plant regeneration from mature embryo culture of winter wheat (*Triticum aestivum* L.) Genotypes. Plant Cell Reports. 18, 331-335.

[4] Shan, X., Li, D. and Qu, R. (2000) Thidiazuron promotes in vitro regeneration of wheat and barley. In Vitro Cellular and Developmental Biology-Plant. 36(3), 207-210.

[5] Chauhan, H., Desai., S.A. and Khurana, P. (2007) Comparative analysis of the differential regeneration response of various genotypes of *Triticum aestivum*, Triticum durum and Triticum dicoccum. Plant Cell, Tissue and Organ Culture. 91(3), 191-199.

[6] Ozias-Akins, P. and Vasil, I.K. (1983) Improved efficiency and normalization of somatic embryogenesis in *Triticum aestivum* (wheat). Protoplasma. 117(1), 40-44.

[7] Ganeshan, S., Chodaparambil, S.V., Båga, M., Fowler, D.B., Hucl, P., Rossnagel, B.G. and Chibbar, R.N. (2006) In vitro regeneration of cereals based on multiple shoot induction from mature embryos in response to thidiazuron. Plant Cell, Tissue and Organ Culture. 85(1), 63-73.

[8] Kato, K., Chowdhury, S.H. and Harada, S. (1991) Effect of culture condition on plant regeneration capacity of mature embryo derived callus in wheat (*Triticum aestivum* L.). Wheat Inf. Serv. 72, 95–97.

[9] Beyaz, R. and Yıldız, M. (2017) The Effects Of Co-Cultıvatıon In Wheat (Triticum sp.) and Flax (Linum usitatissimum L.) On Shoot Regeneratıon Capacity Of Explants. Fresen. Environ. Bull. 26(12A), 8239-8245.

[10] Ahuja, P.S., Pental, D. and Cocking, E.C. (1982) Plant regeneration from leaf base callus and cell suspensios of *Triticum aestivum*. Z Pflanzenzüchtg 89: 139-144.

[11] Zamora, A.B. and Scott, K.J. (1983) Callus formation and plant regeneration from wheat leaves. Plant Science Letters. 29(2-3), 183-189.

[12] Ozias-Akins, P. and Vasil, I.K. (1982) Plant regeneration from cultured immature embryos and inflorescences of *Triticum aestivum* L. (wheat): evidence for somatic embryogenesis. Protoplasma. 110(2), 95-105.

[13] Maddock, S.E., Lancaster, V.A., Risiott, R. and Franklin, J. (1983) Plant regeneration from cultured immature embryos and inflorescences of 25 cultivars of wheat (*Triticum aestivum*). Journal of Experimental Botany. 34(7), 915-926.

[14] Redway, F.A., Vasil, V., Lu, D. and Vasil, I. K. (1990) Identification of callus types for long-term maintenance and regeneration from commercial cultivars of wheat (*Triticum aestivum* L.). TAG Theoretical and Applied Genetics. 79(5), 609-617.

[15] Barro, F., Martin, A., Lazzeri, P.A. and Barcelo, P. (1999) Medium optimization for efficient somatic embryogenesis and plant regeneration from immature inflorescences and immature scutella of elite cultivars of wheat, barley and Tritordeum. Euphytica. 1.8, 161-167.
[16] Sharma, V.K., Hänsch, R., Mendel, R.R., and Schulze, J. (2005) Influence of picloram and thidiazuron on high frequency plant regeneration in elite cultivars of wheat with long-term retention of morphogenecity using meristematic shoot segments. Plant Breeding. 124(3), 242-246.
[17] Arndt, F., Rusch, R., Stilfried, H.V., Hanisch, B. and Martin, W.C. (1976) SN49537, A new defoliant. Plant Physiology. 57, 99.
[18] Lu, C.Y. (1993) The use of thidiazuron in tissue culture. In Vitro Cellular and Developmental Biology-Plant. 29(2), 92-96.
[19] Murthy, B.N.S., Murch, S.J. and Saxena, P.K. (1998) Thidiazuron: A potent regulator of in vitro plant morphogenesis. In Vitro Cellular and Developmental Biology-Plant. 34(4), 267.
[20] Hong, Y X. and Zhen, Z. (1999) Improvement in plant regeneration from callus in wheat. Acta Phytophysologia Sinica. 25, 388-394.
[21] Murashige, T. and Skoog, F. (1962) A revised medium for rapid growth and bio assays with tobacco tissue cultures. Physiologia Plantarum. 15(3), 473-497.
[22] Olcer, H. and Mecit, B. (2012) Polyphenol Oxidase Activities In Embryo and Endosperm Of Wheat Seeds During Germination Under Boron Stress. Fresen. Environ. Bull. 21(10), 2936-2941.
[23] Yıldız, M. and Beyaz, R. (2019) The Effect of Gamma Radiation on Agrobacterium tumefaciens ± Mediated Gene Transfer In Durum Wheat (Triticum durum Desf.). Fresen. Environ. Bull. 28(1), 488-494.
[24] Beyaz, R. (2019) The Effect of Seed Size on In Vitro Seed Germınatıon, Seedling Growth and Tissue Culture Response Of Callus From Mature Embryos Of Wheat (Triticum sp.). Fresen. Environ. Bull. 28(1), 502-508.
[25] Steel, R.G. and Torrie, J.H. (1960) Principles and procedures of statistics. Principles and Procedures of Statistics.
[26] Tuberosa, R., Ravaglia, S. and Lucchese, C. (1988) Callus induction and plant regeneration in Italian cultivars of bread wheat. Agric. Med. 118, 361-365.
[27] Jones, M.P., Cao, J., O'Brien, R., Murch, S.J. and Saxena, P.K. (2007) The mode of action of thidiazuron: auxins, indoleamines, and ion channels in the regeneration of Echinacea Purpurea L. Plant Cell Reports. 26(9), 1481-1490.

Received: **09.12.2019**
Accepted: **27.02.2020**

CORRESPONDING AUTHOR

Berk Benlioglu
Department of Field Crops,
Faculty of Agriculture,
Ankara University,
06110 Diskapi, Ankara – Turkey

e-mail: benliogluberk@hotmail.com

© by PSP Volume 29 – No. 05/2020 pages 3885-3893 Fresenius Environmental Bulletin

RESEARCH ON CH_4 AND N_2O REGIONAL SIMULATION OF DIFFERENT WATER AND FERTILIZER AND BIO-CARBON REGULATION MODES IN RICE FIELD IN COLD REGION BASED ON DNDC MODEL

Yanyu Lin[1,2], Shujuan Yi[2,3,*], Zhongxue Zhang[4], Dan Xu[4],Tangzhe Nie[5]

[1]College of Civil Engineering and Water Conservancy, Heilongjiang Bayi Agricultural University, Heilongjiang Daqing 163319, China
[2]Quality Supervision and Testing Center for Agricultural Processed Products of Ministry of Agriculture (Daqing), Heilongjiang Daqing 163319, China
[3]College of Engineering, Heilongjiang Bayi Agricultural University, Heilongjiang Daqing 163319, China
[4]School of water conservancy and civil engineering, Northeast Agricultural University, Harbin, Heilongjiang 150030, China
[5]School of Water Conservancy and Electric Power Heilongjiang University, Harbin, Heilongjiang 150080, China

ABSTRACT

Rice field is an important source of greenhouse gas emissions. In order to explore the characteristics of CH4 and N2O emissions from rice field in the Northeast cold region, this paper takes rice field in *Qing'an* County of Heilongjiang Province as the research object, and three factors as water, nitrogen fertilizer and biocarbon are selects. In this paper, the DNDC model is used to simulate and estimate the CH4 and N2O emissions under traditional management and optimization modes. The results show that the CH4 emissions in the optimized mode reduced by 54.64% compared with the traditional model, which is from rice fields in the county during the growing season. Under the optimized model, the N2O emissions during the growing season of rice fields in the county were reduced by 20.45% compared with the traditional model. The results of sensitivity factor analysis show that the effect of water depth on CH4 emissions from rice field is positively correlated, while the effect on N2O emissions is reversed. The total amount of nitrogen fertilization in the test range showed a certain inhibitory effect on rice field CH4 emissions, and it significantly promoted N2O emissions. The growth of biocarbon would inhibit rice field CH4 and N2O emissions. The results provide a scientific basis, which scientifically estimates greenhouse gas emissions from rice fields in China and formulates strategies to reduce greenhouse gas emissions from cold temperate rice fields.

KEYWORDS:
Northeast cold rice field, CH_4 and N_2O, Water and fertilizer and biocarbon, Emission reduction

INTRODUCTION

In recent decades, global warming caused by the growth of greenhouse gas concentrations in the atmosphere has gradually become the focus of global environmental problems. Carbon dioxide (CO2), methane (CH4) and nitrous oxide (N2O) are considered the three most important greenhouse gases [1]. Recently, the concentration of CH4 in the global atmosphere is increasing at an annual rate of 0.8%, and the concentration has reached 1.75 ppmv. The concentration of N2O in the atmosphere has reached 0.7 ppbv, and the average annual growth rate is about 0.26% ~ 0.3% [2-3]. There is no intervention in the previous agricultural policy. By 2030, CH4 emissions from agricultural sources are expected to increase by 60% and N2O by 35% to 60% from 2005. Therefore, controlling greenhouse gas emissions from agricultural sources will reduce global warming to vital role.

Different from other dry farming systems, the unique "soil-water-crop-climate" interactive environment of rice fields becomes a more special agricultural ecosystem [4]. According to research data in 2009, global methane emissions from rice field are 50 million tons per year [5]. In order to meet the needs of global population growth, the global rice field will double in the next decade [6], which means that methane emissions will increase by 50%. For a long time, most researches on N2O have focused on dryland soils, while N2O emissions from rice field are considered to be very low and can even be ignored [7]. However, in recent years, scientists have found that N2O emission is also an important source of rice field [8].

The DNDC model estimates the emissions of trace gases such as CO2, CH4, and N2O in the soil by coupling the denitrification and decomposition processes driven by the soil environment. It is the most successful ecological process to simulate terrestrial biogeochemical cycles in the world [9]. Many scholars at home and abroad have used this

model to simulate and predict greenhouse gases, and the results are quite satisfactory [10-12]. In this study, the simulation results of DNDC are scaled from a micro-ecosystem to the regional level. By determining high-emission areas and high-emission management measures, we explore the impact of different water and fertilizer and biocarbon application amounts on greenhouse gas emissions. Its accurate estimation method can effectively complement the current traditional research methods, so that the best mitigation measures can be determined according to local conditions.

INTRODUCTION TO THE DNDC MODEL

DNDC model construction. Denitrification-decomposition (DNDC) is a biogeochemical model based on the four concepts of element abundance, coupling, circulation, and dynamics. It can be used to simulate regional greenhouse gas emissions scenarios. The principle of the DNDC model applied to the area is similar to other GIS databased models. The entire simulation area needs to divide into several small "units". The soil properties and climatic parameters in the Unit are the same by default. The soil properties and climatic parameters of different "units" depend on the GIS database, which has defined. Different types of farmland systems can be customized as independent farmland management measures. However, farmland management measures are unique for each unit [13-14].

Model sensitivity factor analysis. The sensitivity analysis of the model is to find out from many uncertain factors the sensitivity factors, which have an important effect on the greenhouse gas emission of rice fields. At the same time, the influence and sensitivity level of the factor analyzed and calculated on the target results. In order to compare these simulation results, the sensitivity index introduced can be used to judge the influence level of these factors on the output of the model [15]. The formula is as follows.

$$S = \left(\frac{O_2 - O_1}{O_{avg}}\right) / \left(\frac{I_2 - I_1}{I_{avg}}\right) \quad (1)$$

In the formula, S is the relative sensitivity index. I_1 and I_2 are the minimum and maximum values of the input parameters, respectively. I_{avg} is the average of I_1 and I_2. O_1 and O_2 are the output values relative to the I_1 and I_2 models, respectively. O_{avg} is the average of O_1 and O_2. When the absolute value S is higher, it indicates that the input factor has a greater influence on the simulation result, and a negative value indicates that there is a "reciprocal relation" between the input parameter and the simulation result.

RESULTS AND ANALYSIS

DNDC model construction. In order to apply the model to the estimation of CH4 and N2O emissions from black soil rice field in the cold region of *Qing'an* County, the climate includes daily maximum, minimum temperature, and daily precipitation, soil includes bulk density, Texture, clay content, organic matter and pH, and agricultural practices includes land utilization type, crop area, crop planting and harvesting periods, inorganic and organic fertilizer use. Meteorological information was provided by the Qing'an County Meteorological Station of the China Meteorological Administration. Soil information was taken from "Soil of Qing'an County" and provided by the Soil Census Office of Qing'an County, Heilongjiang Province. The farming information comes from field surveys of 14 townships in Qing'an County. The DNDC model was used to calculate the CH4 and N2O emissions from the rice field in each township, as shown in Table 1.

TABLE 1
Simulation results of total emissions of CH4 and N2O in the growing season in 2018

Location	Rice area（hm^2）	Total CH4 emissions（10^4kgC）	Total N2O emissions（10^2kgN）
Qing'an town	2350	8.48	7.46
Huansheng Township	3551	12.82	11.28
Minle Town	687	2.48	2.18
Jubaoshan Xiang	1426	5.15	4.53
Daluo town	3633	13.12	11.54
Jianmin Xiang	4865	17.57	15.45
Xinsheng Township	9422	34.02	29.33
Fengshou Township *	14933	43.03	49.64
Ping'an Town *	7917	22.81	26.31
Hardworking town	8211	29.65	26.08
Development Township	11667	42.12	37.06
Tongle Township	5426	19.59	17.23
Get rich	9579	27.60	31.84
Jiusheng Town	11535	33.24	38.34
total	95202	311.69	308.91

Note: * indicates the demonstration town of water-saving irrigation in Qing'an County

Simulation analysis of CH4 and N2O emissions from rice field under different water and fertilizer and biocarbon regulation modes in the study area. Overview of the study area. The research area is located at Heilongjiang Rice Irrigation Test Center Station (125 ° 44'E, 45 ° 63'N) in Qing'an County, Suihua City, Heilongjiang Province. It is a typical cold black soil region. The average annual temperature is at 2.5 ° C, the average annual precipitation is 550 mm, and the average annual water surface evaporation is 750 mm. The crop's hydrothermal growth period is 156 to 171 days, and the frost-free period of the year is 128 days. The climate is characterized by a continental monsoon climate in the cold temperate zone. The soil type is albic type rice soil with a bulk density of 1.01 g/cm3 and a porosity of 61.8%. Basic physical and chemical properties of soil have the following relationship. The organic matter mass ratio is 41.4 g/kg, pH value is 6.40, total nitrogen mass ratio is 15.06g / kg, total phosphorus mass ratio is 15.23g/kg, total potassium mass ratio is 20.11g / kg, alkaline hydrolyzed nitrogen mass ratio is 154.36mg/kg, effective phosphorus mass ratio is 25.33mg / kg and quick-acting potassium mass ratio is 157.25 mg/kg.

Test design. The experiment adopted the optimal design of saturated D311 [16] to study the effects of irrigation, nitrogen fertilizer, and biochar on the CH4 emissions during the rice growing season under controlled irrigation conditions. The water and fertilizer refer to the local farmers' standards, and the irrigation amount is 5000~ 10000 m3 / hm2, nitrogen fertilizer (pure nitrogen) 50 ~ 150kg / hm2, biocarbon 0~ 40t / hm2. The specific design scheme is shown in Table 2.

Simulation analysis of DNDC model. In this study, in 2019, traditional water and fertilizer and biocarbon management mode, that is, optimized seeding modes for rice were selected to simulate the total CH4 and N2O emissions from rice field in *Qing'an* County during the growing season. The normal management mode is the normal water and fertilizer and biocarbon application level, which is the treatment of this test11. The optimized management model adopts the optimized water and fertilizer management scheme obtained through the optimal design test, that is, the irrigation amount is 4591~ 5420 m3 / hm2, the nitrogen application amount is 100.11~ 112.54kg / hm2, and the biocarbon amount is 21.29~ 22.14t / hm2 [17]. The simulation results are shown in Table 3. It can be seen in Figure 1 and Figure 2 for a comparison of specific township emissions.

TABLE 2
Optimal design processing table for saturated D-311

Processing number	Coded value			Actual value		
	X_1	X_2	X_3	W（m^3/hm^2)	N(kg/hm^2)	BC(t/hm^2)
1	0	0	2	5000	100	40
2	0	0	-2	5000	100	0
3	-1.414	-1.414	1	3200	65	30
4	1.414	-1.414	1	6800	65	30
5	-1.414	1.414	1	3200	135	30
6	1.414	1.414	1	6800	135	30
7	2	0	-1	7500	100	10
8	-2	0	-1	2500	100	10
9	0	2	-1	5000	150	10
10	0	-2	-1	5000	50	10
11	0	0	0	5000	100	20

TABLE 3
Simulation of total CH4 and N2O emissions from rice field during different growing seasons in Qing'an County

Rice field area（hm^2）	Management model	CH4 total emissions（10^6kgC）	N2O total emissions（10^4kgN）	total GWP（$kgCO_2/hm^2$）
95202	Traditional model	5.71	3.96	1322.83
	Optimization mode	2.59	3.15	1003.33

Note: Total GWP（$kgCO_2/hm^2$）=25f(CH4)+298f(N2O)

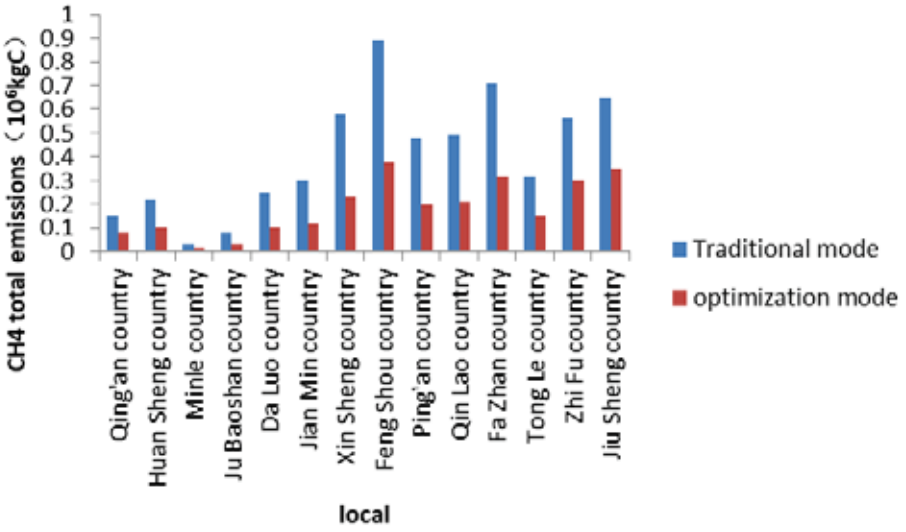

FIGURE 1
Effects of CH4 reduction in various townships under different control modes

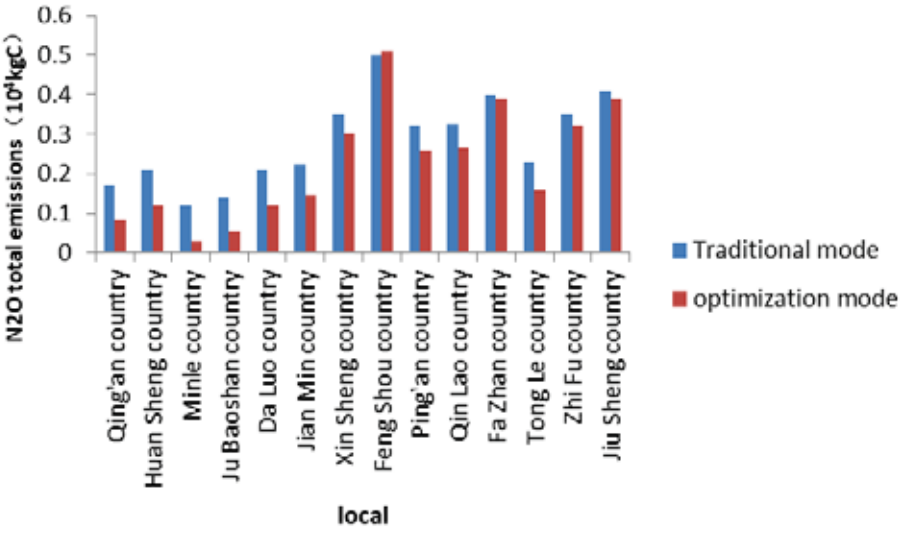

FIGURE 2
N2O emission reduction effect of various townships under different control modes

TABLE 4
Simulation of total CH4 and N2O emissions from rice field during different growing seasons in Qing'an County

Parameter	Background value	test value	Sensitivity index
Soil texture	Clay loam	Sandy loam, loam, sandy clay loam, clay	-1.3097
Soil SOC content (%)	2.53	1.518,2.024,3.036,3.542	0.6308
Soil pH	5.94	5,7,8	0.2325
Annual average temperature (℃)	1.69	reduce 2℃and 4℃,add 2℃ and 4℃	0.1243
Annual rainfall (mm)	57.7	reduce 10% and 20%,add 10% and 20%	-0.0407
Water layer depth (cm)	10	0,2,5,10	0.3256
Total nitrogen fertilizer application (kg / hm2)	100	50,65,135,150	-0.1429
Amount of biochar applied	20	0,10,30,40	-1.2044

TABLE 5
Parameter settings for sensitivity analysis and sensitivity index (S) for the effect on N2O flux

Parameter	Background value	test value	Sensitivity index
Soil texture	Clay loam	Sandy loam, loam, sandy clay loam, clay	-0.2667
Soil SOC content (%)	2.53	1.518,2.024,3.036,3.542	0.7075
Soil pH	5.94	5,7,8	-1.4444
Annual average temperature (℃)	1.69	reduce 2℃and 4℃,add 2℃and 4℃	0.4483
Annual rainfall (mm)	57.7	reduce 10%and 20%,add 10%and 20%	-0.0943
Water layer depth (cm)	10	0,2,5,10	-0.2727
Total nitrogen fertilizer application (kg / hm2)	100	50,65,135,150	1.4571
Amount of biochar applied	20	0,10,30,40	-0.0008

Sensitive factor analysis. In this study, eight variables were selected from three aspects of soil properties, climatic factors, and farmland management methods as the parameters to test for the sensitivity analysis of CH4 and N2O in rice fields, which are soil texture, soil SOC content, soil pH, annual average temperature, and annual temperature, rainfall, water depth, total nitrogen fertilizer application and biochar application. The basic scenario (background value) in this article is based on the actual climate, soil environment, and agricultural management measures at the test site, and the alternative scenario (test value) is based on changing one of the parameters to be tested without changing other parameters in the basic scenario. The parameter values are established, it can be seen in Table 4 and Table 5.

The analysis results in Table 4 show that soil properties are the main influencing factors of CH4 emission fluxes in black soil rice field in cold regions, and soil texture factors are the most sensitive, with a sensitivity index of -1.3097. This shows that the CH4 emission from clay soil is significantly lower than that of loamy and sandy soil, and the content of clay particles in cold black soil is higher. The release of CH4 increased with the growth of soil organic carbon (SOC) content and pH, but the sensitivity of soil pH was relatively small. The reason can be explained that the soil texture determines the permeability of soil and the decomposition rate of soil organic matter, so it can affect the soil redox potential and the supply of substrates that produce CH4 microorganisms, which in turn affects CH4 emissions from rice fields. Higher SOC content can increase the concentration of soluble organic carbon (DOC) by increasing the decomposition rate of the soil. The increased DOC also increases the methyl group production of CH4 in the wetland soil [18]. *Oremland et al.* [19] pointed out that most of the methanogens in soil have a pH adaptation range of 6- 8, and the optimal pH is about 7. In the meteorological factors, temperature is more sensitive to the impact of CH4 emissions in rice fields than rainfall. Higher temperatures driving soil temperature can increase the activity of soil microorganisms, which promote the growth of rice, thereby promoting the production and emission of CH4 in rice fields. The influence level of rainfall on black soil rice field on CH4 emissions is insignificant compared with the irrigation model. From the sensitivity analysis of farmland management methods, it can be seen that the depth of the water layer is the most sensitive factor, and the CH4 emissions from rice fields increase with the depth growth of the water layer. The results on the suppression of CH4 emissions are the same, when the layer thickness is close to 0 water level, which further reflects that rice field water management may become an economically feasible CH4 emission reduction measure. The growth of the total nitrogen fertilizer application has a certain inhibitory effect on rice field methane and will promote rice yield, but long-term application has a greater impact on soil and ecological environment. The sensitivity index of the biocarbon application amount was -1.2044, which showed that it had an inhibitory effect on CH4 emissions from rice fields.

The analysis data in Table 5 show that the sensitivity index of soil texture to rice field N2O is -0.2667. As the soil clay content increases, rice field N2O emissions gradually decrease, and CH4 emitted from clay soil is lower than that of loam and sandy soil. The clay content of ground black soil is relatively high, which is the reason why the observed N2O emission flux is lower than that observed in southern rice field. The sensitivity index of soil SOC content to rice field N2O is 0.7075, which indicates that the growth of soil SOC content has a promoting effect on rice field N2O emissions. In general, the concentration (content) of soil matrix is greater such as organic carbon, NO3-, and NO2-, the soil N2O emission flux is larger [21]. The sensitivity index of soil pH to rice field N2O emissions shows that the growth in soil pH is inversely related to N2O emissions. When the soil is in an acidic condition, the inhibitory effect of acidic conditions on N2O reduction is stronger than that on NO3-, resulting in a larger proportion of N2O to

N2 in the reactants. As the soil pH is worth increasing, the reduction of N2O to N2 is accelerated, which is leading to decrease in the ratio of N2O to N2 in the reactants, which is a reduction in N2O emissions [22]. Among the meteorological factors, the sensitivity index of temperature to rice field N2O emissions is 0.4483, that is, the growth in temperature will promote rice field N2O emissions. Rainfall can change the soil water state. Dissolved oxygen in the rainwater can increase the redox potential of the soil and change the supply of oxygen, which affects N2O emissions. However, the rice field is not affected by rainfall [23]. The sensitivity index of rainfall to N2O emissions from paddy fields in this paper is also significantly smaller. From the analysis of farmland management methods, the sensitivity index of water layer depth to rice field N2O emissions is -0.2727, indicating that rice field N2O emissions decrease as the water layer depth increases. Soil water content determines the aeration status of the soil and affects the activity of nitrifying bacteria and denitrifying bacteria. This has an impact on N2O emissions. Total nitrogen fertilizer application is the most sensitive factor in farmland management. The increase of total nitrogen fertilizer application has a significant promotion effect on N2O emission from paddy fields. Therefore, in the greenhouse gas emission reduction, the application amount of nitrogen fertilizer should be considered. The sensitivity index of the applied amount of biochar to rice field N2O emissions is -0.0008, which indicates that the applied amount of biochar has no significant effect on rice field N2O emissions. However, the amount of biochar applied has a suppressive effect on N2O emissions from rice fields.

DISCUSSION

The DNDC model has a good point simulation of CH4 and N2O in the black soil rice field, which simulated the CH4 and N2O emission peaks and seasonal emission rules of the rice field in the study area. However, there are some unsatisfactory places. The model lags behind the actual observed peak value of the CH4 simulation, and the simulated value of the main peak is too high. The simulation of the N2O peak is earlier than the actual observed peak, and the simulated value of the emission peak is higher. The reason is that the data input of biocarbon is not accurate enough, and it can only be entered after it is converted into straw amount. Therefore, the simulation of greenhouse gas emissions from rice fields based on biocarbon as the input parameter is the place where the model needs to improve.

At present, it is difficult to make comprehensive observations of greenhouse gases in larger areas in consideration of factors such as observation conditions, labor, equipment, and funds. DNDC model is used to simulate the CH4 and N2O emissions of rice fields under different natural conditions and different field management methods, which can become a powerful tool for quantitative estimation of greenhouse gas emissions in black rice soil. Due to the limitation of test time and labor in this study, the sampling points did not cover the entire research area, and only the rice field of Heilongjiang Province Rice Irrigation Test Center (Ping'an Town) was selected for the test. In order to make the model better applied, as many ground observations as possible should be carried out, which is necessary for further verification of the model reliability, timely adjustment of model parameters and improvement of the simulation accuracy of the model. The influencing factors that cause large changes in CH4 and N2O emissions from rice field include three aspects, which are soil attribute factors, climatic factors, and farming management methods. However, soil properties change little from time scale, and climate factors cannot be controlled artificially. Therefore, from the perspective of operability, greenhouse gas emission reduction can only be achieved by changing farmland management methods. In this study, no matter what kind of water and fertilizer and biocarbon mode, CH4 is the main greenhouse gas, we should focus on controlling CH4 emissions while reducing N2O emissions, to reduce the comprehensive greenhouse effect of CH4 and N2O in rice fields and reduce environmental pollution. Existing literature has different views on the effect of applying biocarbon on CH4 emissions from rice fields. Singh BP, Sonoki T, Yang Min et al [24-26] believe that biocarbon applied to rice fields can affect soil pH, organic matter content, and redox potential. Physicochemical properties such as temperature, nitrogen form, air permeability, and soil moisture can reduce the activity and abundance of methanogenic bacteria in rice fields, which increase the activity and abundance of methane oxidizing bacteria, thereby inhibiting CH4 emissions.

In addition, the large specific surface area and loose porosity of biocarbon help soils absorb a large amount of CH4, provide a carbon source for methane oxidizing bacteria, promote soil CH4 oxidation, and reduce the transport of CH4 to the atmosphere. However, *Knoblauch C, Singla A, Chen S, et al. [27-29]* believe that the application of biocarbon containing more unstable components in rice fields will increase soil activated carbon pools, promote rice growth and increase root exudates, which are methanogens. Adequate carbon sources provided. At the same time, the application of biocarbon in rice fields may promote CH4 emissions by adjusting soil physical and chemical properties such as soil temperature, pH, and water retention capacity. It may also be that the biochemical-inhibiting chemicals inhibit the activity of methane oxidizing

bacteria, thereby promoting CH4 emissions. In addition, the application of biocarbon in rice fields may directly promote CH4 emissions by promoting electron transfer. However, the impact on rice field N2O emissions is certain. Studies show that the application of biocarbon in rice fields reduces N2O emissions. The reason is that biocarbon reduces the denitrifying bacteria in rice fields by affecting physicochemical properties such as soil porosity, pH, texture, and permeability and its enzyme activity, thereby inhibiting N2O emissions from rice fields [30- 31]. The simulation results of the DNDC model show that the amount of biocarbon application has an inhibitory effect on the CH4 and N2O emissions from rice fields. In field management, it is necessary to increase the application or choose a reasonable water and fertilizer and biocarbon management method.

CONCLUSION

(1) The DNDC model is used to estimate the CH4 and N2O emissions during the growing season of rice fields in Qing'an County are 5.71 × 106 kg C and 3.96 × 104 kg N, respectively. The model further simulated the CH4 and N2O growth season emissions of rice fields in Qing'an County under the traditional mode and the optimization mode. The CH4 emissions during the growing season of rice fields in the county under the optimization mode were 2.59 × 106 kg C, which was 54.64 lower than that in the traditional mode. %. In the optimization mode, the county's rice field N2O growing season emissions were 3.15 × 104 kg N, which was 20.45% less than the traditional model's rice field N2O growing season emissions.

(2) The sensitivity analysis of CH4 and N2O in this paper show that CH4 and N2O emissions in soil properties decrease with the growth of soil clay content. It increases with the growth of soil organic carbon content. CH4 emissions increase with the pH growth (within the test range). N2O emissions decrease with the pH growth. Temperature of the meteorological factors is more sensitive to the effects of CH4 and N2O emissions in rice fields. Higher temperatures will promote the production and emission of CH4 and N2O from rice fields. The increase in rainfall has a reciprocal relation to both CH4 and N2O emissions, but the sensitivity coefficients are small, indicating that the impact of rainfall on greenhouse gases in cold rice field is not insignificant. In the farmland management method, the depth effect of the water layer on the CH4 emission from the rice field is positively correlated, and the effect on the N2O emission is opposite. The total amount of nitrogen fertilization in the test range showed a certain inhibitory effect on CH4 emissions in rice fields, and it significantly promoted N2O emissions. The increase for application on CH4 and N2O emissions in rice fields showed little effect, but appears as an inhibitory effect.

(3) Based on the simulation results of this study and the sensitivity factors analysis of rice fields CH4 and N2O, the following greenhouse gas emission reduction currently considered operationally feasible are proposed. The rice field implements water-saving irrigation, focuses on controlling CH4 emissions, and performs reasonable fertilization. Taking into account N2O emissions with biocarbon, the comprehensive greenhouse effect produced by rice fields CH4 and N2O is reduced, and environmental pollution is reduced. The amount of biocarbon application has an inhibitory effect on the CH4 and N2O emissions from rice fields. In field management, it should be applied as much as possible or a reasonable method of water and fertilizer and biocarbon management should have selected.

ACKNOWLEDGEMENTS

This work is funded by Heilongjiang Provincial Postdoctoral General Funding Program(LBH-Z18255), Heilongjiang Bayi Agricultural University Support Program for San Heng San Zong (TDJH201907), Heilongjiang Bayi Agricultural University Talents Plan Program (XYB201801), Key Laboratory of Efficient Use of Agricultural Water Resources, Ministry of Agriculture, PRChina (2017004). The Ministry of Agriculture's Agricultural Products Quality Supervision, Inspection and Testing Center (Daqing) postdoctoral workstation also supports this research.

REFERENCES

[1] IPCC. Agriculture. In Climate Change (2007): Mitigation of Climate Change. Contribution of Working Group III to the Fourth Assessment Report of the Intergovernmental Panel on Climate Change.Metz B, Davidson O R, Bosch P R et al. Eds. Cambridge University Press, Cambridge, U K, IPCC, 2007.

[2] IPCC. In Climate Change (2001): The Scientific Basis. Contribution of Working Group I to the Third Assessment Report of the Intergovernmental Panel on Climate Change [Houghton,J. T., Ding,Y., Griggs,D.J., Noguer, M., van der Linden, P. J., Dai,X., Maskell,K., Johnson (eds),C.A.]. Cambridge University Press, Cambridge, United Kingdom and New York, NY, USA, 2001.

[3] WMO. Scientific Assessment of Ozone Depletion:(2002).Global Ozone research and monitoring project report No. 47. World Meteorological Organization, Geneva, 2003, 498 pp.

[4] Johnson Beebout, S.E., Angeles, O.R., Alberto, M.C.R., Buresh R.J. (2009) Simultaneous minimization of nitrous oxide and methane emission from rice rice field is improb able due to redox potential changes with depth in a greenhouse experiment without plants. Geoderma. 149, 45-53.

[5] Qiu, J. (2009a) China cuts methane emissions from rice fields. Nat. News. https://doi.org/10.1038/news.2009.833.

[6] Seshadri, S. (2007) Methane emission, rice production and food security. Current Science. 93, 1346-1347.

[7] Khalil, M.A.K., Rasmussen R.A., Wang M.X., et al. (1990) Emission of trace gases from Chinese rice fields and biogas generators:CH4, N2O, CO, CO2, chlorocarbons and hydrocarbons. Chemosphere. 20, 239-244.

[8] Stehfest, E, Bouwman, L. (2006) N2O and NO emission from agricultural fields and soils under natural vegetation: summarizing available measurement data and modeling of global annual emissions. Nutrient Cycling in Agroecosystems.16, 208-228.

[9] United States EPA. Inventory of U S. Greenhouse Gas Emissions and Sinks 1990-1994.EPA-230-R-96-006,1995.

[10] Li, C.S., Frolking, S.E., Harriss, R.C.,Terry, R.E. (1994) Modeling nitrous oxide emissions from agriculture:A Florida casestudy. Chemosphere. 28,1401-1415.

[11] Grant, B., Smith, W.N., Desjardins, R. et al. (2004) Estimated N2O and CO2 emissions as influenced by agricultural practices in Canada. Climatic Change. 65, 315-332.

[12] Li, C.S., Mosier, A., Wassmann, R., Cai, Z.C.,Zheng, X.H., Huang, Y., Tsuruta, H., Boonjawat, J., Lantin, R. (2004) Modeling greenhouse gas emissions from rice-based production systems:Sensitivity and upscaling. Global Biogeochemical Cycles. 18,10.1029 /2003GB002045.

[13] Liu, F., Wu, M., Yang, M. (2020) Research progress of DNDC model and its application prospects in alpine ecosystems. Journal of Glaciology and Geocryology. 42 (2/5).

[14] Li, C.S., Frolking, S., Frolking, T.A. (1992A) model of nitrousoxide evolution from soil driven by rainfall events. Journal of GeophysicalResearch-Atmospheres. 97, 9759-9776.

[15] Walker, S.E., Mitchell, J.K., Hirschi, M.C., Johnsen, K.E. (2000) Sensitivity analysis of the root zone water quality model. Transactions of the ASAE. 43, 841-846.

[16] Xu, Z. (1997) Regression analysis and experimental design. Beijing: China Agricultural Press. 102-143.

[17] Lin, Y., Yi, S., Zhang, Z., Wang, M., Nie, T. (2019) Effects of Water and Fertilizer and Biocarbon Regulating Models on the Comprehensive Warming Potential of Greenhouse Gas in Rice field in Northeast China. Fresen. Environ. Bull. 5, 3602-3606

[18] Li, C. (2007) Quantifying greenhouse gas emissions from soils:Scientific basis and modeling approach. Soil Science and Plant Nutrition. 53, 344-352.

[19] Oremland, R.S., Marsh, L., Des Marais, D.J. (1982) Methanogenesis in Big Soda Lake, Nevada: an alkaline, moderately hypersaline desert lake. Applied and Environmental Microbiology. 43(2), 462-468.

[20] Ren, L., Wang, G., Zhang, R. (2002) Experimental study on methane emissions from rice field in the Chengdu Plain. Chinese Journal of Atmospheric Sciences. 26 (6), 731-743.

[21] Gao, Z., Chen, X., Zhang, F. (2004) Research progress on N2O emissions from farmland. Ecology and Environment. 13 (4), 661-665.

[22] Qi, Y., Dong, Y. (1999) Production and emission of soil nitrous oxide and its influencing factors. Acta Geographica Sinica. 54 (6).

[23] Zheng, X., Wang, X., Wang, Y. (1996) Effects of soil moisture on N2O production and emission in a rice-wheat rotation ecosystem. Journal of Applied Ecology. 7 (3), 273-279.

[24] Singh, B.P., Cowie, A.L. (2014) Long- term influence of biocarbon on native organic carbon mineralisation in a low- carbon clayey soil. Scientific Reports. 4(3),1-9.

[25] Sonoki, T., Furukawa, T., Jindo, K., Suto, K., Masakazu, A., Sanchez-Monedero, M.A. (2013) Influence of biocarbon addition on methane metabolism during thermophilic phase of composting. Journal of Basic Microbiology. 53(7), 617-621.

[26] Yang, M., Liu, Y., Sun, X., Dong, D., Wu, W. (2013) Biomass charcoal increases methane oxidation activity in rice fields. Journal of Agricultural Engineering. 29(17), 145-151.

[27] Knoblauch, C., Maarifat, A.A., Pfeiffer, E.M., Haefele,S.M. (2011) Degradability of black carbon and its impact on trace gas fluxes and carbon turnover in rice field. Soil Biology & Biochemistry.43(9),1768-1778.

[28] Singla, A., Inubushi, K. (2014) Effect of biocarbon on CH4 and N2O emission from soils vegetated with rice. Rice & Water Environment. 12(1),239-243.

[29] Chen, S., Rotaru, A.E., Shrestha, P.M., Malvankar, N.S., Liu, F., Fan, W., Nevin, K.P., Lovley, D.R. (2014) Promoting interspecies electron transfer with biocarbon. Scientific Reports. 4(20), 163-168.

[30] Yagi, K., Tsuruta, H., Minami, K., Kanda K. (1994) Methane emission from Japanese and Thai rice field[C]//Minami K,Mosier A R,Sass R L. CH4 and N2O:Global emission and controls from rice fields and other agricultural and Industrial sources. NIAES Series2, Tokyo:Yokendo Publishers,:41-53.
[31] Zou, J., Huang, Y. (2003) Zong Lianggang, et al. CO2, CH4 and N2O emissions from rice field and their influencing factors. Journal of Environmental Sciences. 23(6), 758-764.

Received: **10.12.2019**
Accepted: **16.02.2020**

CORRESPONDING AUTHOR

Shujuan Yi
College of Engineering,
Heilongjiang Bayi Agricultural University,
Heilongjiang Daqing 163319 – China.

e-mail: yishujuan_2005@yeah.net

© by PSP Volume 29 – No. 05/2020 pages 3894-3904 Fresenius Environmental Bulletin

APPRAISAL OF CHROMIUM CONTENTS IN WHEAT GRAINS IRRIGATED WITH WASTEWATER

Asma Zafar[1], Zafar Iqbal Khan[1], Kafeel Ahmad[1], Muhammad Nadeem[2], Humayun Bashir[1,*]

[1]Department of Botany, University of Sargodha, Sargodha, Pakistan
[2]Institute of Food Science and Nutrition, University of Sargodha, Sargodha, Pakistan

ABSTRACT

Present study was carried out in different areas of Punjab, Pakistan in order to explore the effect of diverse sources of water (ground, sewage, industrial) on the chromium contents of soil and various varieties (Punjab-2011,Seher-2006,Faisalabad-2008, Watan) of wheat plant in two cropping years. The great health hazard has been associated with the exposure of food crop to the toxic heavy metals. It was noticed that the main reason of elevated level of heavy metals in the soil and wheat plant is due to the increased irrigation with wastewater. The concentration of chromium in all types of water, soil and wheat plant (root, shoot, grains) samples was varied from (2.80-3.40 mg/l), (1.78-3.24 mg/kg), (1.42-2.28, 1.14-2.86, 0.78-1.48 mg/kg), respectively. The chromium concentration in all types of water samples was found higher than the maximum permissible level (0.1 mg/l). However, the chromium contents in soil (65 mg/kg) and wheat grains (2.3 mg/kg) samples were found within the maximum permissible levels. All the samples showed the bio-concentration factor, pollution load index, daily intake of metal and health risk index for chromium less <1 while the bioaccumulation factor, translocation factor and enrichment factor of chromium were found >1 for some samples. Regular monitoring of wheat crop is recommended in light of these results to lessen the health risks in humans.

KEYWORDS:
Chromium, Permissible level, Bio-concentration factor, Health hazard

INTRODUCTION

In the world of developing countries for the irrigation of agriculture soil wastewater is used without any proper treatment which is most industrially and domestically polluted, which pose many adverse effects on proper growth of plants and also on the fertility of land. The continual use of untreated sewage water not only results in the high concentration of heavy metals in soil and plants, but also show adverse effects on human through their access to food chain [1]

The term heavy metal refers to any metallic chemical element that has relatively high density and is toxic and poisonous at low concentrations. Heavy metals are metallic, naturally occurring compounds that have a very high density greater than 5 g/cm^3; compared to other metals at least five times the density of water. They are one of the most persistent pollutants in soil and water [2]

It has been verified that chromium does not have any biological importance and is declared as a non-essential metal for mammals. Cr (III) has the property of being bounded by organic materials so, it is unable to move in water and soil. The maximum permissible level for chromium in plants and water is 1.30 mg/kg and 0.1 mg/l, respectively, as suggested by Khan et al [3]

Chromium is ubiquitous in nature and ranges in different concentration in environment. Cr (III) is usually present in environment and Cr (VI) is totally produced by human activities. General exposure to Cr (VI) is through emissions from industries. Cr (VI) is used as anticorrosive agent in various cooling system, combustion eg- Cigarette smoke and ash from power plants [4]

The most common exposures routes for chromium are as under- ingestion, dermal contact and inhalation. Human health is adversely affected due to the exposure of chromium and these health effects are categorized in two types, carcinogenic and non-carcinogenic and have three types of exposure duration[5] Acute (14 days or less), intermediate (75-364 days) and chronic (365 days or more). But Unites States Environmental Protection Agency had reported that chromium is carcinogenic only if taken through the route of inhalation.

Crop consumption is the main source by which toxic heavy metals are transferred in the human body. This transfer of toxic heavy metals can cause life-threatening diseases like cancer, which mostly occurs in the human digestive system [6]

The usage of wastewater in a regular way can protect plants and soil from its adverse effect, but still, it can pose a threat to them. The consumption of the foods which are cultivated with wastewater ir-

rigation poses a health risk to human as implementing by many scientific studies. However, domestic sewage sludge is a reservoir of important nutrients but special care is required in order to prevent the excessive entrance of those compounds which have adverse effects [7]. Current will be helpful to control the metal toxicity and updating permissible levels regarding to wheat irrigated with different water sources. The main aim of the current study is to explore the chromium level in staple food crop wheat irrigated with various types of water and their possible effects on the health of animals and human.

MATERIALS AND METHODS

Study Area. The research was carried out in 7 cities (Faisalabad, Gujranwala, Sargodha, Bhakkar, Kasur, Gujrat, and Chiniot) of Punjab, Pakistan (Figure 1). The various wheat fields of five varieties irrigated with ground, sewage and industrial water were selected for the sample collection of water, soil and wheat plant (root, shoot, grain). All composite samples of seven cities were pooled into one replicate, and then divided into four samples. These four samples of each variety for each type of water source were collected to form one composite sample. All sampling was done in two cropping years (2017-2018).

Sampling Design. Sampling was done using the Randomized Complete Block Design (RCBD).

Water, Soil and Wheat Plant Sampling. All types of water (100 ml each), soil, and wheat plant samples (root, shoot, grains) were collected by following the standard methods [8] [9] [10].

Water, Soil and Wheat Plant Digestion. All the water, soil and wheat plant samples were digested by following the standard procedures [11] [12].

Analytical Procedure to Determine Metal. Atomic Absorption Spectrophotometer Perkin-Elmer, AAS-5000) was used to assess the level of chromium.

FIGURE 1
Map of Study Sites

Bioaccumulation Factor. The metal bioaccumulation factor (BAF) is calculated as the ratio of the heavy metal concentration of crop to soil and was calculated as follows [13]

$$BAF = \frac{[Metal]_{Shoot}}{[Metal]_{Soil}}$$

Translocation Factor. The ability of the plant to relocate the stored metals from one portion to the other the ratio of the heavy metal concentration from one part to the other is calculated by using translocation factor (TF). In the current study, the wheat root-shoot TF was calculated as follows [13]

$$TF = \frac{[Metal]_{Shoot}}{[Metal]_{Root}}$$

Bioconcentration Factor. Bioconcentration factor was assessed by using ensuing formula [14]
BCF= Chromium in wheat grain (mg/kg)/ Chromium in soil (mg/kg)

Enrichment Factor. Enrichment factor was analysed by using the following formula Buat-Menard and Chesselet[15]

$$EF = \frac{[(M)Grain/(M)soil]_{Samples}}{[(M)Grain/(M)soil]_{Standard}}$$

Standard value of Chromium in wheat grains= 2.3
Standard value of Chromium in soil= 9.07

Daily Intake of Metals. The daily intake of heavy metals (DIM) assessed by both the daily intake of wheat and the chromium concentration in crops [16]

$$DIM = C_{metal} \times D_{food\ intake} / B_{average\ weight}$$

DIM= Daily intake of chromium
C_{metal} is the chromium contents in wheat grains (mg/kg)
D_{food} intake represents the daily consumption of wheat grain (mg/kg)
$B_{average\ weight}$ is the normal weight of the body (kg).
The daily intake by the ingestion of wheat grains is 0.242 (kg/person),[17] and 55.9 kg is used as the average weight of the body[17]

Health Risk Index. If the value of HRI is <1, people will be not affected by the ingestion of these wheat grains. The following formula was used to evaluate the HRI [18]

$$HRI = DIM/R_fD$$

Where R_fD= Oral reference dose for chromium

Pollution Load Index. The pollution load index (PLI) was used to assess the total amount of contamination in the soil. This index is handy to determine the quality of soil after the accumulation of heavy metals PLI > or equal to 1 shows the high level of contamination and lousy quality. The pollution load index was examined [19]
PLI= Concentration of chromium in investigated soil/ Reference value of chromium in soil

Statistical Analysis. The results from all the samples were subjected to analysis of variance (ANOVA) as applicable and best fitted to field analysis like to completely randomised block design. Data obtained from each attribute were subjected to statistical analysis using Minitab 16 software. Three-way ANOVA (3-factor factorial design) was applied to find out significant differences among mean values. Tuckey test was applied in conjunction with ANOVA. The set of all pairwise comparison is treated through Tuckey test altogether. And lettering denotes difference among means [20].

RESULTS

Water. Data from analysis of variance revealed that water source, year and water source×year significantly (p<0.05) affected the concentration of Cr in the irrigation water from various sources (Table 2).

The chromium concentration in all types of water samples varied from 3.40 to 2.80 mg/l (Figure 2). Mean results for the chromium concentration in different types of irrigation water revealed that the highest contents of chromium was noticed in industrial water in cropping year 2 and the lowest was observed in ground water in cropping year 1.

Soil. The results from analysis of variance for chromium showed that variety, water source, year, variety×water source and variety×water source×year had significant (p<0.05) effect on concentration of Cd in soil irrigated with different sources of water. Analysis of variance revealed that variety×year and water source×year had non-significant (p>0.05) effect on Cd concentration in soil, irrigated by different water sources (Table 3).

Chromium concentration in various soil samples ranged from 1.78 to 3.24 mg/kg (Figure 3). Data showed that the chromium concentration in soils of various varieties of wheat irrigated with ground water in two cropping years was found highest 2.96 mg/kg in soil of variety Faislabad-2008 in year 1, and the lowest concentration 2.26 mg/kg was found in soil of variety Watan in year 1. Maximum concentration 3.24 mg/kg of chromium in soil of different varieties of wheat irrigated with sewage water in year 1 and year 2 was observed in soil of variety Galaxy-2013 in cropping year 2, and the lowest concentration 2.23 mg/kg was noticed in soil of variety Watan in year 1. Results indicated that the lowest chromium concentration 1.78 mg/kg in various samples of soil, irrigated with industrial water was found in soil of variety Watan in year 2 and the highest 2.75 mg/kg was found in soil of variety Faislabad-2008 in year 2.

Root. Chromium concentration was significantly (p<0.05) affected by all sources except for variety×year and variety×water source×year, which

had non-significant (p>0.05) effect on concentration of chromium in roots of wheat plants (Table. 3).

Chromium contents in various types of wheat root samples varied from 1.42 to 2.28 mg/kg (Figure 4). Generally, chromium was present in all types of wheat root samples but the highest amount of chromium was observed in the variety Faislabad-2008 irrigated with industrial water in year 2 and the lowest was noticed in varieties Faislabad-2008 and Watan which were irrigated with ground water in year 2.

Evidence from results showed that the percent of chromium transfer from soil to root varied from 51.45 to 120.8% (Figure 7). The highest and lowest values were observed for variety Watan irrigated with industrial water in year 2 and variety Watan irrigated with ground water in year 1, respectively.

Shoot. Analysis of variance revealed that water source, year and water source×year had significant (p<0.05) effect on chromium concentration in shoot of wheat plants. Data showed that variety, variety×water source, variety×year and variety×water source×year had non-significant (p>0.05) effect on chromium concentration in shoot of various varieties of wheat plants (Table 3).

Chromium concentration in all types of wheat shoot samples ranged from 1.14 to 2.86 mg/kg (Figure 5). The highest 1.82 mg/kg chromium concentration in shoot of various varieties of wheat irrigated with various sources of water in year 1 was observed in variety Seher-2006 irrigated with industrial water and the lowest 1.15 mg/kg was observed in variety Watan irrigated with ground water. The minimum concentration of chromium 1.14 mg/kg in cropping year 2 was noticed in variety Watan irrigated with ground water and the maximum was observed for variety Punjab-2011 irrigated with industrial water.

Results for chromium transfer from root to shoot varied from 67.65 to 137.5% (Figure. 8). The maximum transfer was observed for variety Punjab-2011 irrigated with industrial water in year 2 and the lowest was noticed for variety Watan irrigated with ground water in year 1.

Grain. All sources had the significant (p<0.05) effect except for variety×year which showed non-significant (p>0.05) effect on chromium concentration in various varieties of wheat grains irrigated with different sources of water (Table 3).

Chromium concentration in all types of samples ranged from 0.78 to 1.48 mg/kg. The data showed that chromium was present in all the grain samples, but variety Seher-2006 irrigated with industrial water in year 2 had the highest concentration of chromium 1.48 mg/kg, while the lowest value of 0.78 mg/kg was recorded for variety Punjab-2011 irrigated with ground water in year 2 (Figure 6).

Results indicated that chromium transfer from shoot to grain ranged from 47.48 to 79.13% (Figure 9). The maximum and minimum transfer was observed for variety Watan irrigated with industrial water in year 2 and variety Watan irrigated with ground water in year 1.

Pollution Load Index. Pollution load index for chromium in all types of soil samples was ranged from 0.20 to 0.36 (Table. 4). Data for year 1 showed that the soil of the variety Faislabad-2008 irrigated with ground water and variety Galaxy-2013 irrigated with sewage water had the highest 0.33 Pollution load index for chromium and the variety Watan irrigated with industrial water in year 1 had the lowest 0.20. Variety Galaxy-2013 irrigated with sewage water had the highest 0.36 and the varieties Faislabad-2008 and Watan irrigated with industrial water had the lowest 0.20 PLI for chromium in year 2.

Bioaccumulation Factor. Bioaccumulation factor for chromium ranged from 0.40 to 1.56 (Table 4). The maximum value of BAF for chromium was noticed in variety Watan irrigated with industrial water in year 2 while the lowest was found in variety Faislabad-2008 irrigated with ground water in year 1.

Translocation Factor. Data indicated that TF for chromium ranged from 0.68-1.38. Translocation factor for chromium in all types of wheat shoot samples was noticed less than 1 but for all the varieties irrigated with industrial water in year 2, TF was more than 1. Variety Punjab-2011 irrigated with industrial water in year 2 had the highest 1.38 Translocation factor for chromium and the variety Watan irrigated with ground water in year 1 had the lowest 0.68 (Table 4).

Bioconcentration Factor. Highest BCF 0.74 for chromium was noticed in variety Watan irrigated with industrial water in year 2 and the minimum BCF 0.28 for chromium was noticed in variety Punjab-2011 irrigated with ground water in year 1 (Table. 4).

Enrichment Factor. The range of EF for chromium in all the samples was 1.11 to 2.92 (Table 4). Enrichment factor for chromium in five different types of varieties of wheat irrigated with different sources of water was observed more than 1. The highest EF for chromium was found in variety Watan irrigated with industrial water in year 2 while the lowest value of EF was noticed in variety Punjab-2011 irrigated with ground water in year 1.

Daily Intake of Metal. Daily intake of chromium ranged from 0.003 to 0.006 mg/kg/day (Table 4**)**. The minimum value was noticed for varieties Faislabad-2008 and Punjab-2011 irrigated with ground water in year 2 while the acceptable daily intake of chromium was observed for all the varieties irrigated

with industrial water in year 2 except for variety Galaxy-2013.

Health Risk Index. The range for HRI of chromium was 0.002 to 0.004 (Table 4). The minimum HRI for chromium was observed in all five varieties irrigated with ground water in year 2 but for variety Faislabad-2008 it is also observed for ground water irrigation in year 1. The highest was observed for in some industrial water irrigated varieties in both cropping years.

DISCUSSION

All types of water samples of two years were containing the chromium contents more than the concentration of chromium (0.03, 0.04 mg/l) in the ground and wastewater samples respectively, as reported by Alghobar and Suresha [21]. Chromium concentration in all the water samples was above than the maximum permissible value (0.1 mg/l) as recommended by WWF and USEPA [22]. Chromium is released in the excessive amount from the industries such as leather, electroplating, tanning and textile which are the main source of high chromium concentration in the wastewater. However, the leaching from rocks and topsoil are the natural sources of chromium entrance into the ground water reservoir [23]. Various industries produced the large amount of chromium which slowly leached down through the soil and became the part of ground water and the use of industrial wastewater for irrigation purpose might be the possible reason of higher chromium concentration in the water sources of current investigation.

Wang et al. [24] had suggested the higher concentration (54.95 mg/kg) of chromium in soil irrigated with sewage water, as compared to the chromium contents observed in the present research. Asdeo [25] reported the higher chromium concentration (18.24 mg/kg) in soil. In the present research, chromium values were found higher in all types of soil samples in contrast to the chromium concentration in soil samples irrigated with ground and sewage water (1.15, 1.59 mg/kg, respectively) as suggested by Ahmad et al. [26]. Concentration of chromium in the present work was much lower than the critical level (65 mg/kg) described by WHO [27]. Current chromium concentration in the soil was within the safe limits.

Yu et al. [28] had given the higher concentration (3.02 mg/kg) of chromium in roots while the range (0.02-1.02 mg/kg) given by Al-Othman et al. [29] was found lower than those values which were reported in the present work. Chromium value (1.23 mg/kg) in roots suggested by Xiao-Rui et al. [30] was lower than current findings.

Alrawiq et al. [31] suggested the lower chromium concentration (1.53 mg/kg) in shoots irrigated with sewage water than those given by present research. Heavy metals, such as Cr, Cd, Pb, As and Hg showed the synergistic effects which is between two or more metals, this might be the possible reason of higher chromium concentrations in the shoot [32].

In grain, the chromium concentration reported by Al-Othman et al. [29] was found lower (0.69 mg/kg). While the chromium concentrations were found higher in all types of samples in two cropping years in the current research as compared to the values (0.18, 0.49 mg/kg) suggested by Xiao-Rui et al. [30] and Wang et al. [24], respectively. It seemed that the ability of plants to accumulate heavy metals differ, it might be due to the difference in accumulation and translocation ability to the same heavy metal and it also observed that sewage sludge improved the chemical and physical characteristics of the soil [33, 34]. Chromium concentrations in the grains were within the permissible level (2.3 mg/kg) given by FAO/WHO [35].

The transfer of chromium from soil to root was lower as compared to the root to shoot, but its percentage was again decrease from shoot to grain transfer. The increase in the root to shoot transfer might be due to the combined effect of water and soil and in current investigation the chromium concentration in all types of water samples were found much higher. The soil organic matter results in the chelation of heavy metals, which increase the uptake ability of wheat for heavy metals which results in the severe health risks to human via the consumption of such grains [36].

The PLI value (1.84) investigated by Ahmad et al. [37] was also found higher. All the samples showed the higher Pollution load index for chromium in contrast to the values (0.014, 0.023) which were investigated by Khan et al. [38] in the ground and wastewater irrigated samples, respectively. The soil is categorized as contaminated when PLI>1 [39]. But in current research soil was not contaminated to the dangerous level.

The lower BAF value was reported by Hadif et al. [40] (0.01) in contrast to the current investigation. Alrawiq et al. [31] also suggested the lower BAF for chromium. Bio-accumulation factor varied for different wheat varieties and also differ in the ground and wastewater irrigated sites. This is known as one of the probable reasons to cause health risk in humans via grains consumption. Industrial water irrigated wheat samples in cropping year 2 showed the BAF for Cr>1, which indicated that continuous usage of wastewater increased the chromium concentration in soil [41]

The lower TF for chromium was reported by Hadif et al. [40] (0.5) and Neeratanaphan [41] (0.49) in contrast to the present study. Alrawiq et al. [31] also suggested the lower TF values (0.46, 0.39) for chromium in ground and wastewater samples, respectively. All the varieties irrigated with industrial water showed the TF for Cr>1, which indicated that

continuous use of wastewater increased the chromium concentration in soil.

The bioconcentration factor of chromium for all types of samples irrigated with different sources of water in two cropping years were found high in contrast to the findings (0.003) of Xiao-Rui et al. [33]. Chromium mostly remains in the roots of temperate trees and rarely move above into the aerial parts. Although in the present research, chromium was present in high amount in the wheat grains than the standard value (0.02) of chromium in grains suggested by WHO/FAO [35]

Enrichment factor was used to understand the influence of natural and anthropogenic sources in the accumulation of heavy metals in soils. Daily intake value (0.004 mg/kg/day) for chromium recommended by Bhatti et al. [42] was within the range of the present work. Wang et al. [24] reported the lower daily intake value (0.001 mg/kg/day) for chromium in contrast to the values given by present research. Khan et al. [2] had given the daily intake for chromium (0.0003, 0.0004 mg/kg/day) in the ground and wastewater grown samples respectively, which were found within the range of present study.

Bhatti et al. [42] suggested that the HRI for chromium was within the range (0.003-0.004) of present finding. Neeratanaphan [41] reported the much higher HRI value (0.30) for chromium. Chromium is not an essential element for plants. It is required by plants in small amount and its abundance can cause serious problems to the plant's physiology and the plants are exposed to various types of stress at the same time, in the same place where they are living [43]. In the present research, HRI for chromium was found less than 1 for all types of samples, which suggested no health risk to human.

CONCLUSION

The current findings suggested that the chromium concentration in all types of water samples exceeded the maximum permissible levels while in case of soil and grains it did not touch that limit. The daily intake of chromium was below than the maximum tolerable limit. And health risk index was also less than 1. Therefore, all types of grain samples of different varieties irrigated with various water sources were safe for consumption, with respect to the chromium concentration. However, variety Punjab-2011 irrigated with ground water in year 2 had the lowest chromium concentration. So, it is more suitable for consumption.

TABLE 1
Standard Concentrations (Mg/Kg) Of Chromium in Wheat Grain and Soil and Oral Reference Dose (Mg/Kg/Day)

Metal	Chromium
$Standard_{Grain}$	2.3[a]
$Standard_{Soil}$	9.07[b]
R_fD	9.07[c]

Sources: [a][44]; [b][35], [c][45]

TABLE 2
Analysis Of Variance Table For Chromium Concentration In Water

Source	Degree of freedom	Mean square
Water source	2	0.43***
Year	1	0.16***
Water source×Year	2	0.02*
Error	18	0.004

*, **, ***: Significant at 0.05, 0.01 and 0.001 levels

TABLE 3
Analysis of Variance for Chromium in Soils, Roots, Shoot and Grains of Various Varieties of Wheat Irrigated with Different Sources of Water in Two Cropping Years

Source	Degree of freedom	Mean square			
		Soil	Root	Shoot	Grains
Variety	4	1.63***	0.01*	0.04[ns]	0.007***
Water source	2	3.12***	2.53***	11.94***	2.04***
Year	1	1.35***	0.11***	5.26***	0.35***
Variety×Water source	8	0.18***	0.05***	0.01[ns]	0.02***
Variety×Year	4	0.02[ns]	0.01[ns]	0.02[ns]	0.0008[ns]
Water source×Year	2	0.02[ns]	0.55***	2.85**	0.25***
Variety×Water source×Year	8	0.14***	0.01[ns]	0.003[ns]	0.0006***
Error	90	0.03	0.01	0.45	0.001

*, **, ***: Significant at 0.05, 0.01 and 0.001 level, ns: Non-significant

TABLE 4
PLI. BAF. TF. BCF. EF. DIM. and HRI for Chromium in Two Cropping

Cropping	Irrigation Water	Wheat variety				
		Seher-2006	Punjab-2011	Faislabad-2008	Watan	Galaxy-2013
			PLI			
	Ground	0.27	0.30	0.33	0.25	0.29
Year 1	Sewage	0.27	0.31	0.32	0.25	0.33
	Industrial	0.21	0.25	0.23	0.20	0.30
	Ground	0.30	0.30	0.30	0.30	0.30
Year 2	Sewage	0.30	0.33	0.27	0.27	0.36
	Industrial	0.23	0.28	0.20	0.20	0.30
			BAF			
	Ground	0.49	0.46	0.40	0.51	0.46
Year 1	Sewage	0.57	0.55	0.51	0.63	0.48
	Industrial	0.96	0.75	0.87	0.95	0.64
	Ground	0.42	0.50	0.42	0.41	0.43
Year 2	Sewage	0.59	0.58	0.53	0.66	0.52
	Industrial	1.35	1.13	1.01	1.56	0.99
			TF			
	Ground	0.73	0.71	0.7	0.68	0.70
Year 1	Sewage	0.87	0.85	0.84	0.86	0.86
	Industrial	0.88	0.92	0.87	0.90	0.87
	Ground	0.73	0.89	0.82	0.80	0.83
Year 2	Sewage	0.91	0.90	0.88	0.89	0.89
	Industrial	1.23	1.38	1.22	1.29	1.23
			BCF			
	Ground	0.38	0.33	0.30	0.40	0.34
Year 1	Sewage	0.40	0.34	0.35	0.45	0.34
	Industrial	0.67	0.56	0.61	0.6	0.43
	Ground	0.31	0.28	0.29	0.32	0.31
Year 2	Sewage	0.42	0.38	0.38	0.48	0.37
	Industrial	0.71	0.58	0.53	0.74	0.50
			EF			
	Ground	1.49	1.30	1.20	1.59	1.34
Year 1	Sewage	1.57	1.35	1.37	1.78	1.33
	Industrial	2.64	2.19	2.39	2.37	1.68
	Ground	1.21	1.11	1.14	1.24	1.21
Year 2	Sewage	1.66	1.48	1.49	1.91	1.47
	Industrial	2.81	2.28	2.11	2.92	1.99
			HRI			
	Ground	0.003	0.003	0.002	0.003	0.003
Year 1	Sewage	0.003	0.003	0.003	0.002	0.002
	Industrial	0.004	0.004	0.003	0.003	0.003
	Ground	0.002	0.002	0.002	0.002	0.002
Year 2	Sewage	0.003	0.003	0.003	0.003	0.003
	Industrial	0.004	0.004	0.004	0.003	0.004
			DIM			
	Ground	0.004	0.004	0.004	0.004	0.004
Year 1	Sewage	0.004	0.004	0.004	0.004	0.004
	Industrial	0.005	0.005	0.005	0.005	0.005
	Ground	0.004	0.003	0.003	0.004	0.004
Year 2	Sewage	0.005	0.005	0.005	0.005	0.005
	Industrial	0.006	0.006	0.006	0.006	0.005

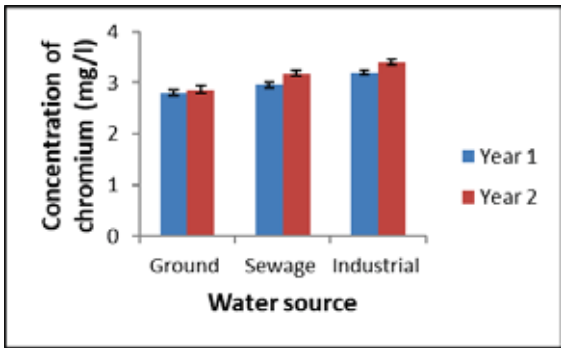

FIGURE 2
Concentration of Chromium in Different Water Sources in Two Cropping Years

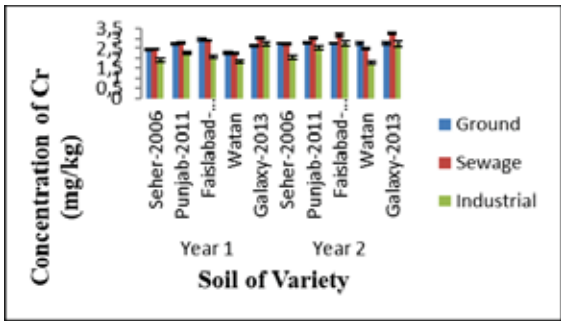

FIGURE 3
Concentration of Chromium in Soil Grown with Different Wheat Varieties with Three Different Sources of Water in Two Cropping Years

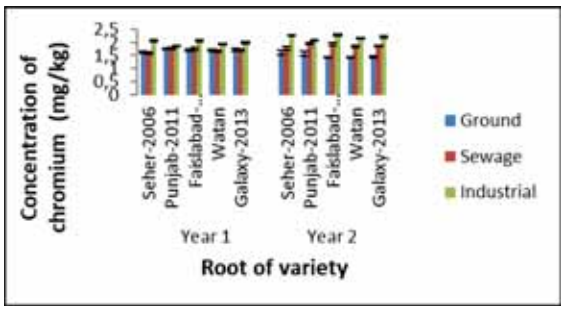

FIGURE 4
Concentration of Chromium in Roots of Different Wheat Varieties Irrigated with Different Sources of Water in Two Cropping Years

FIGURE 5
Concentration of Chromium in Wheat Shoot of Different Varieties Irrigated with Different Sources of Water in Two Cropping Years

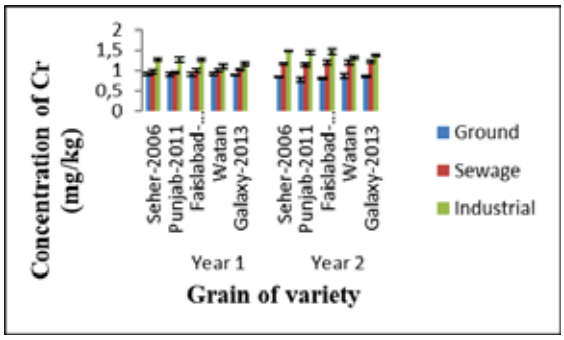

FIGURE 6
Concentration of Chromium in Different Varieties of Wheat Grains Irrigated with Different Sources of Water in Two Cropping Years

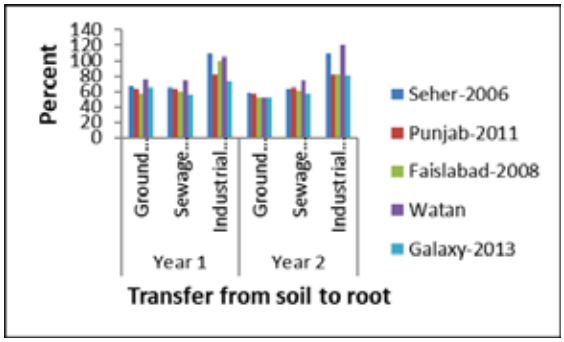

FIGURE 7
Percentage of Chromium Transfer From Soil to Root

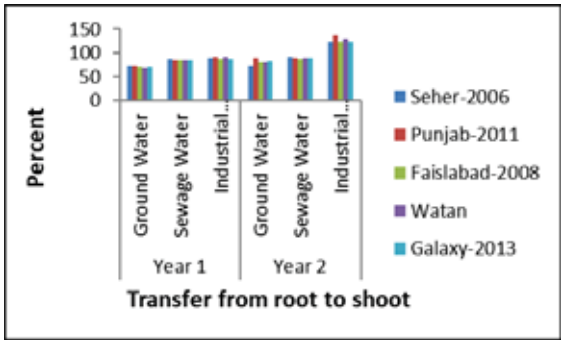

FIGURE 8
Percentage of Chromium Transfer from Root to Shoot

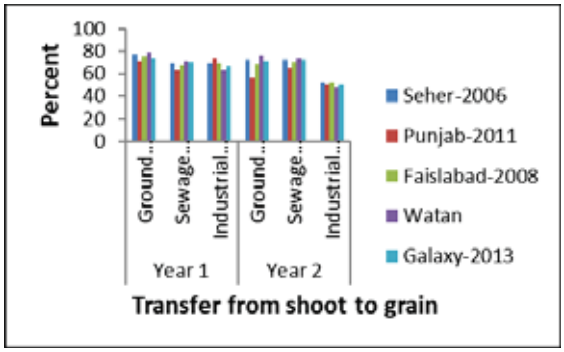

FIGURE 9
Percentage of Chromium Transfer from Shoot to Grain

REFERENCES

[1] Ahmad, K., Nawaz, K., Khan, Z.I., Nadeem, M., Wajid, K., Ashfaq, A., Munir, B., Memoona, H., Sana, M., Shaheen, F., Kokab, R., Rehman, S. U., Ullah, M.F., Mehmood, N., Muqadas, H., Aslam, Z., Shehzadi, M., Noorka, I.R., Bashir, H., Shad, H.A., Batool, F., Iqbal, S., Munir, M., sohail, M., Sher, M., Ullah, S., Ugulu, I. and Dogan, Y. (2018) Effect of Diverse Regimes of Irrigation on Metals Accumulation in Wheat Crop: An Assessment - Dire Need of the Day. Fresen. Environ. Bull. 27(2), 846-855.

[2] Khan, Z.I., Ugulu, I., Sahira, S., Ahmad, K., Ashfaq, A., Mehmood, N. and Dogan Y. (2018) Determination of Toxic Metals in Fruits of Abelmoschus Esculentus Grown in Contaminated Soils with Different Irrigation Sources by Spectroscopic Method. Int. J. Environ. Res. 12(3), 503-511.

[3] Khan, Z.I., Ahmad, K., Yasmeen, S., Akram, N.A., Ashraf, M. and Mehmood, N. (2017a) Potential Health Risk Assessment of Potato (Solanum Tuberosum L.) Grown on Metal Contaminated Soils in the Central Zone of Punjab, Pakistan. Chemosphere. 166, 157-162.

[4] OEHHA. (2000) Hexavalent Chromium (Soluble Compounds). Determination of Noncancer Chronic Reference Exposure Levels.

[5] Guertin, J. (2004) Toxicity and Health Effect of Chromium (All Oxidation States). 213.

[6] Ugulu, I., Unver, M.C. and Dogan, Y. (2016) Determination and Comparison of Heavy Metal Accumulation Level of Ficus Carica Bark and Leaf Samples in Artvin, Turkey. Oxidation Communications, Oxid Commun. 39(1-2), 765-775.

[7] Ongun, A.R. and Delibacak, S. (2018a) Successive Two Years Treated Sewage Sludge Applications: Effect on Total and Available Heavy Metal Concentration of Sandy Loam Soil. Fresen. Environ. Bull. 27(12A), 8779-8786.

[8] AFNOR (Association Francaise de Normalization). (1997) Water Quality and Analysis Methods.

[9] Rhue, R.D. and Kidder, G. (1983) Analytical Procedures Used by The IFAS Extension Soil Laboratory and the Interpretation of Results. Soil Sci. Dept., Univ. Florida, Gainesville.

[10] Aydin, M.E., Aydin, S., Beduk, F., Tor, Ali, Tekinay, A., Kolb, M. and Bahadir, M. (2015). Effects of Long-Term Irrigation with Untreated Municipal Wastewater on Soil Properties and Crop Quality. Environ. Sci. Pollut. Res. 22, 19203-19212.

[11] APHA (American Public Health Association). (2005) Standard Methods for the Examination of Water and Wastewater, American Public Health Association, Washington, DC.

[12] Allen, S., Grimshaw, H. and Rowland, A. (1986). Chemical Analysis. Blackwell Scientific Publications, Oxford. 285-344.

[13] Cui, S., Zhou, Q. and Chao, L. (2007). Potential Hyper-Accumulation of Pb, Zn, Cu and Cd in Endurant Plants Distributed in an Old Smeltery, Northeast China. Environ. Geol. 51, 1043-1048.

[14] Cui, Y.J., Zhu, Y.G., Zhai, R.H., Chen, D.Y., Huang, Y.Z., Qui, Y. and Liang, J.Z. (2004) Transfer of Metals from near a Smelter in Nanjing, China. Environ. Int. 30, 785-791.

[15] Buat-Menard, P. and Chesselet, R. (1979) Variable Influence of the Atmospheric Flux on the Trace Metal Chemistry of Oceanic Suspended Matter. Earth Planet Sci. Lett. 42, 398-411.

[16] Singh, R.P. and Agrawal, M. (2010) Variations in Heavy Metal Accumulation Growth and Yield of Rice Plants Grown at Different Sewage Sludge Amendments Rates. Ecotoxicol Environ Saf. 73, 632.

[17] Zeng, X., Wang, Z., Wang, J., Guo, J., Chen, X. and Zhuang, J. (2015) Health Risk Assessment of Heavy Metals via Dietary Intake of Wheat Grown in Tianjin Sewage Irrigation Area. Ecotoxicology. 24, 2115-2124.

[18] Sajjad, K., Farooq, R., Shahbaz, S., Khan, M.A. and Sadique, M. (2009) Health Risk Assessment of Heavy Metals for Population via Consumption of Vegetables. World. Appl. Sci. J. 6, 1602-1606.

[19] Liu, W.H., Zhao, J.Z., Ouyang, Z.Y., Soderlund, L. and Liu, G.H. (2005) Impacts of Sewage Irrigation on Heavy Metals Distribution and Contamination in Beijing, China. Environ. Int. 31, 805-812.

[20] Steel, R.G.D., Torrie, J.H. and Dicky, D.A. (2006) Principles and Procedures of Statistics. A Biometrical Approach. 3rd Edition of McGrave Hill Company, New York, USA.

[21] Alghobar, M.A. and Suresha, S. (2016) Effect of Wastewater Irrigation on Growth and Yield of Rice Crop and Uptake and Accumulation of Nutrient and Heavy Metals in Soil. Appl. Ecol. Environ. Sci. 4(3), 53-60.

[22] WWF. (2007) Report on National Surface Water Classification Criteria. Irrigation Water Quality Guidelines for Pakistan. February, 2007. Wastewater Forum Pakistan.

[23] Ahmad, K., Khan, Z.I., Kaukab, R., Wajid, K., Mehmood, N., Muqaddas, H., Abbas, T., Ullah, M.F., Elshikh, M.S., Sahli, A.A., El-Zaidy, M., Noorka, I.R., Mahpara, S., Shad, H.A. and Ayub, M. (2017) Health Risk Assessment of Toxic Heavy Metals in Wheat Crop Grown under Domestic Wastewater Irrigation. Fresen Environ Bull. 26(12), 7643-7650.

[24] Wang, Z., Zeng, X., Geng, M., Chen, Chunyi., Cai, J., Hou, Y. and Zhang, H. (2015) Health Risk of Heavy Metal Uptake by Crops Grown in a Sewage Irrigation Area in China. Pol. J. Environ. Stud. 24(3), 1379-1386.

[25] Asdeo, A. (2014). Toxic Metal Contamination of Staple Crops (Wheat And Millet) in Peri-urban Area of Western Rajasthan. Int. Ref. J. Eng. Sci. 3(4), 8-18.

[26] Khan Z.I., Ugulu, I., Sahira, S., Ahmad, K., Ashfaq, A., Mehmood, N. and Dogan Y. (2018b) Determination of Toxic Metals in Fruits of Abelmoschus Esculentus Grown in Contaminated Soils with Different Irrigation Sources by Spectroscopic Method. Int. J. Environ. Res. 12(3), 503-511.

[27] World Health Organization (WHO). (2000) Safety Evaluation of Certain Food Additives and Contaminants. International Program on Chemical Safety. WHO Food Additive Series. 52,1.

[28] Yu, X., Wang, Z., Lynn, A., Cai, J., Huangfu, Y., Geng, Y., Tang, J. and Zeng, X. (2016) Heavy Metals in Wheat Grown in Sewage Irrigation: A Distribution and Prediction Model. Pol. J. Environ. Stud. 25(1), 413-418.

[29] Al-Othman, Z.A., Ali, R., Al-Othman, A.M., Ali, J. and Habiba, M.A. (2013) Assessment of Toxic Metals in Wheat Crops Grown on Selected Soils, Irrigated by Different Water Sources. Arab. J. Chem. 9(2), 1555-1562.

[30] Xiao-Rui, W., Sheng-Lu, Z. and Shao-Hua, W. (2016) Accumulation of Heavy Metals in Different Parts of Wheat Plant from the Yangtze River Delta, China. Int. J. Agric. Biol. 18, 1242-1248.

[31] Alrawiq, N., Khairiah, J., Talib, M.L., Ismail, B.S. and Anizan. I. (2014) Accumulation and Translocation of Heavy Metals in Soil and Paddy Plant Samples Collected from Rice Fields Irrigated with Recycled and Non-Recycled Water in MADA Kedah, Malaysia. Int. J. Chemtech. Res. 6(4), 2347-2356.

[32] Khan, Z.I., Iqbal, S., Batool, F., Ahmad, K., Bashir, H., Noorka, I.R., Sher, M., Muneeb, A., Batool, A.I., Mahpara, S., Akhtar, M. and Mehmood, N. (2017) Evaluation of Heavy Metals Uptake by Wheat Growing in Sewage Irrigated Soil: Relationship with Heavy Metal in Soil and Wheat Grains. Fresen. Environ. Bull. 26(12), 7838-7848.

[33] Ongun, A.R. and Delibacak, S. (2018b) Effect of Successive Two Years Treated Sewage Sludge Applications on Corn And Second Crop Wheat Yield and Some Soil Properties of Sandy Clay Soil. 27(10), 6742-6750.

[34] Khan, Z.I., Ahmad, K., Rehman, S., Ashfaq, A., Mehmood, N., Ugulu, I. and Dogan, Y. (2019b) Effect of Sewage Water on Accumulation Of Metals in Soil and Wheat in Punjab, Pakistan. Pak. J. Anal. Environ. Chem. 20(1), 60-66.

[35] FAO/WHO. (2001) Codex Alimentarius Commission. Food Additive and Contaminants. Joint FAO/ WHO Food Standards Program. ALINORM 01/ 12A, 1-289.

[36] Borlu, H.O., Celiktas, V., Duzenli, S., Avci, M., Hossain, A. and Sabagh, A. E. (2019) A Growth, Physiology, and Biochemical Activity of Wheat (Triticum Aestivum L.) Seedlings is Affected by Lead Stress. Fresen. Environ. Bull. 28(7), 5122-5130.

[37] Ahmad, K., Khan, Z.I., Ashfaq, A., Ashraf, M. and Yasmin, S. (2014) Assessment of Heavy Metal and Metalloid Levels in Spinach (Spinacia Oleracea.) Grown in Wastewater Irrigated Agricultural Soil of Sargodha, Pakistan. Pak. J. Bot. 46(5), 1805-1810.

[38] Khan, M.U., Malik, R.N. and Muhammad, S. (2013) Human Health Risk from Heavy Metal via Food Crops Consumption with, Wastewater Irrigation Practices in Pakistan. Chemosphere, 93, 2230-2238

[39] Harikumar, P. S., Nasir, U. P. and Rahman, M. M. P. (2009). Distribution of Heavy Metals in the Core Sediments of a Tropical Wetland System. Int. J. Environ. Sci. Technol. 6(2), 225-232.

[40] Hadif, W. M., Rahim, S. A., Shahid, I., Bhuiyan, A. R. and Ibrahim, I. (2015). Heavy Metal Accumulation In Parts Of Paddy Oryza Sativa L. Grown In Paddy Field Adjacent To Ultrabasic Soil. AIP Conference Proceedings. 1-11.

[41] Akpinar, C. (2019) Effect of Zn and Cd Application On Wheat Growth And Mineral Nutrients Concentration. Fresen. Environ. Bull. 28(1), 410-415.

[42] Bhatti, S.S., Sambyal, V., Singh, J. and Nagpal, A.K. (2017) Analysis of Soil Characteristics of Different Land Uses and Metal Bioaccumulation in Wheat Grown around Rivers: Possible Human Health Risk Assessment. Environ. Dev. Sustain.19, 571-588.

[43] Turfan, N. (2018) Determination of Reactions of Cumhuriyet-75 and Selimiye-95 Wheat (Triticum Aestivum L.) Varieties Seddsto Salt, Heavy Metal and Lime Treatments. Fresen. Environ. Bull. 27(12B), 9962-9971.

[44] Singh, A., Sharma, R.K., Agrawal, M. and Marshall, F. M. (2010) Health Risk Assessment of Heavy Metals via Dietary Intake of Foodstuffs from the Wastewater Irrigated Site of A Dry Tropical Area of India. Food and Chem. Toxicol. 48, 611-619.

[45] USEPA (United States Environmental Protection Agency). (2010). Exposure Factors Handbook - General Factors. EPA/600/P-95/002Fa, vol. I. Office of Research and Development. National Center for Environmental Assessment. US Environmental Protection Agency. Washington, DC.

Received: **10.12.2019**
Accepted: **08.02.2020**

CORRESPONDING AUTHOR

Humayun Bashir
Department of Botany
University of Sargodha
Sargodha – Pakistan

e-mail: humayunuos@gmail.com

© by PSP Volume 29 – No. 05/2020 pages 3905-3913 Fresenius Environmental Bulletin

THE ROLE OF PROTECTIVE EFFECT OF ZINGERONE IN GENE REGULATION AGAINST GENOTOXIC EFFECT OF 2,4-D ISOOCTYLESTER HERBICIDE ON BARLEY SPECIES

Huseyin Bulut*

Erzincan Binali Yildirim University Vocational School of Health Services, 24100 Erzincan, Turkey

ABSTRACT

It has become increasingly important in the fight against pests that cause more than 50% of annual food production to disappear. Pesticides used against agricultural pests play an important role in increasing the yield. However, pesticides cause various problems such as deterioration of ecological balance, contamination of nutrients, teratogenic, mutagenic and carcinogenic effects in metabolisms, increase of environmental pollution depending on frequency of use. These substances, which have genotoxic effects, can change the structure or gene expression of DNA in a way that cannot be reversed. Different plant extracts and extracts were used differently in different organisms to determine the protective effects of natural antioxidants in order to reduce or prevent the effect of toxins. In our research, the protective effect of vanillylaceton against genotoxic effect caused by 2,4-D isooctylester herbicide was investigated in Aydanhanım, İnce 04 and Tarım 92 barley species. For this, 14.3.3 defense protein gene expression analysis, miRNA 156, miRNA 159 and miRNA 171 expression analyzes were performed. It has been found that the dose of 2,4-D isooctylester herbicide increases gene expression as the stress response in barley species, while vanillylaceton decreases stress level and thus gene expression. In addition, miRNA 156 and miRNA 159 gene regulation showed positive correlation with gene expression and miRNA 171 gene regulation showed negative correlation. Moreover, it was found that 2,4-D isooctylester herbicide showed genotoxic effect at least in İnce 04 and most in Aydanhanım species. Herbicides cause environmental pollution and genotoxic effects in non-target organisms. In the light of the data obtained from our study, vanillylacetone has a protective effect against herbicide stress.

KEYWORDS:
2,4-D Isooctylester, Barley species, Gene expression, Genotoxic effect, Herbicides, miRNA, Vanillylacetone

INTRODUCTION

Anthropogenic activities may play an important role in the disruption of the world ecological balance. For instance, the size of agricultural land sown in our country for the last 10 years has decreased from 39.122 thousand hectares to 37.817 thousand hectares. On the other hand, in the same period, the populations of Turkey increased from 71 million to 82 million [1]. With the effect of these factors, it is necessary to obtain more products from more areas [2, 3, 4, 5]. That these problems, along with those that have caused the disappearance of more than 50% of annual food production, have gained some importance from these reasons. Pesticides used against agricultural pests can play an important role in increasing the yield. In Turkey, the total pesticide used in 2016, with an increase of 28.2% compared to 50 054 tonnes in 2015, rose substantially. In our country, the amount of pesticide use in the last decade is given in Figure 1. It has a high utilization rate of 20% [6]. Herbicides are compounds used to prevent and destroy the growth of weeds and unwanted vegetation [7]. However, depending on the frequency of not using pesticides, the problem of the use of water and foodstuffs in the soil, acute and chronic poisoning, the chambers of ecological balance, adverse effects of non-target organisms being affected, pollution of nutrients, teratogenic, mutagenic and carcinogenic care in metabolisms, use of environmental pollution [8]. They have a genotoxic effect, these components that contain the structure or gene expression of DNA and do not involve recycling, they may change in some way [9, 10]. Therefore, a lot of study were conducted on the genotoxicity of herbicides in different organisms. There were genetic reasons for the exposure of 2,4-D and Dicamba at different dollars per year to the *Phaseolus vulgaris* plant [11], caused DNA damage [12], 2-Chlorophenol (2-CP) used in herbicide synthesis caused DNA damage in *Allium cepa* [13].

In previous studies of different plant extracts and extracts in different organisms to detect the protective effects of natural antioxidants, reducing or preventing the effect of toxins. For instance, template turmeric [14], black cumin [15], milk thistle

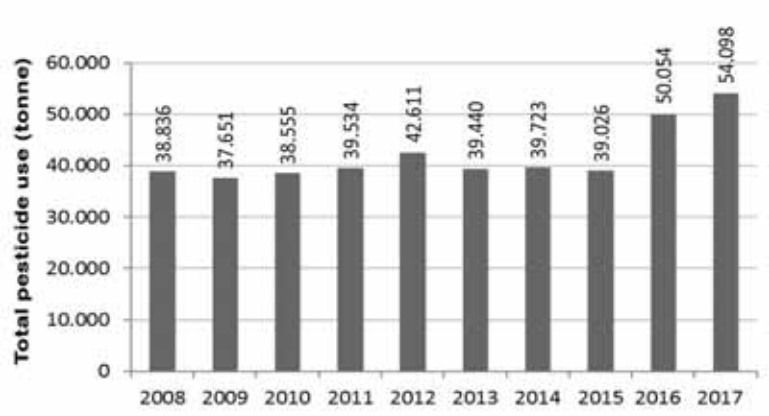

FIGURE 1
The amount of pesticide used in our country in the last decade.

[16], cinnamon [17], barberry [18] and ginger [19] antioxidant were analyzed.

Ginger features a very rich group with plant diversity and active compounds. Portrait of more than 60 active ingredients in ginger divided into volatile and non-volatile compounds in width. Ginger extracts and properties of gingerol, shagaol, zingerone and zerumbone in vivo and in vitro preclinical models of toxicity of different agents and the production of reactive oxygen species (ROS) has been specified in an efficient method [20, 21, 22, 23, 24].

Regulation of gene expression is a complex transcriptional process. Plants activate defense genes against stress-causing factors and increase gene regulation. MicroRNAs (miRNAs) are important regulators of the genetic expression of genetics of transcriptions in the recent times, as they play a broad role in the stress response of plants [25, 26]. In plants, miRNAs cause stress and play an important role in plant development and development and treatment as well [27, 28, 29].

Barley (*Hordeum vulgare* L.) ranks second after grain cultivation and production area in our country [1]. This will affect an important group of genotoxic, nutrient, chemical, chemical, lacquer, which can be observed in barley.

The protective effect of ginger extract Zingerone (Vanillylacetone) against the genotoxic effect of the 2,4-D isoctylester herbicide is likely to effect gene expression level and contribute to the development of the history of miRNAs.

MATERIALS AND METHODS

The seeds of Hordeum vulgare L obtained from Atatürk University Faculty of Agriculture were sterilized in 0.1% $HgCl_2$. Barley seeds of equal size were germinated in the petroleum with water only at 25 ° C. After the formation of shoots germinated seeds 0.1 ppm, 0.2 ppm, 0.3 ppm, 0.4 ppm and 0.5 ppm 2,4-D Isooctylester and 0.1 ppm, 0.2 ppm and 0.3 ppm zingeron was added to the experimental group. Seedlings that did not contain 2,4-D Isooctylester and zingerone and grown only with water were accepted as control group. All samples were grown in a growth chamber at 25 ° C (70% relative humidity). Leaves of barley seedlings were collected separately from experimental and control groups. The samples were then stored at -80 ° C for use.

mRNA isolation. After putting the roots and leaves of barley samples by liquid nitrogen in dust, RNA isolation was performed by Ribospin Plant 307-150 kit in accordance with the instructions of the manufacturer.

cDNA synthesis. The master mix 2 µl for the first step of cDNA synthesis from the RNA obtained was prepared by being completed with ultrapure water so as to be 1 µl primer, 1 µl dNTP up to a total volume of 14 µl and left for 5 min at 65 ºC. Then, the second master mix for the samples taken onto the ice was prepared in quantities as 2 µl 109 RTase reaction buffer, 2 µl 0.1 M DTT, 1 µl Hyper ScriptTM Reverse Transcriptase (200 µl) and 1 µl ZymAllTM RNase Inhibitor, and 6 µl hereof was added as per sample. The Samples were respectively incubated for 60 min at 55 ºC and 5 min at 85 ºC.

RT-PCR analysis. Primer Hv 14.3.3 for barley were designed for gene expression of the 14-3-3 protein family. β-actin has been used as the housekeeping gene. The details pertaining to the primers employed are provided in Table 1. The synthesized cDNAs, primers Ta14S1, Ta14S2 have been checked by using PCR analysis primer b-actin (GenBank ID: AB181991.1) has been used as reference. All real-time PCR samples have been executed in 3 repetitions. In RT-PCR analysis, cDNAs diluted at the rate of 1:200 have been used as templates. The RTPCR reaction components and the schedule belonging to reaction temperature cycle are given below. All reactions have been performed on the Bioneer Exicycler 96_ (Bioneer, South Korea). PCR

components and Amplification parameters are presented below.

10 µl of 2X SYBR master mix was prepared at the rates of 0.8 µl F (forward) (10 pm) primer, 0.8 µl R (reverse) (10 pm) primer, 2 µl ROX, 4 µl cDNA, and 2.4 µl ultrapure water and added to the loading wells. By loading 4 µl cDNA samples onto them, RT-PCR was carried out at 95 ºC for 10 min and at 95 ºC for 45 cycles in 15 s and at 60 ºC for 45 cycles in 1 min.

Data analysis. The threshold cycle values were used for assessing the gene expression levels obtained from RT-PCR results. Obtained from relative or comparative qualitative quantitation results of threshold cycle value, the $2^{-\Delta\Delta ct}$ value was used for calculating the gene expression levels [30]. For each of the samples, the mean of $2^{-\Delta\Delta ct}$ values of 10 samples taken from the same point was calculated. Representing the gene expression level, $2^{-\Delta\Delta ct}$ was computed using the formula below: $2^{-((a-b)-(c-d))}$; where a is Ct value obtained from the gene used for each of the samples; b, Ct value obtained from the gene used for control group; c, Ct value obtained from β-actin gene of each of the samples; d, Ct value obtained from β-actin gene of control group.

miRNA isolation. After putting the roots and leaves of barley samples by liquid nitrogen in dust, miRNA isolation was performed by GeneAll RiboEx and GeneAll Hybrid-R miRNA kits in accordance with the instructions of the manufacturer.

miRNA-cDNA synthesis. After miRNA isolation, miRNA-cDNA synthesis step was started. A specific "stem-loop primer" was designed for each miRNA to be investigated and these primers were used in cDNA synthesis. Stem-loop primers are considered to be highly reliable as they bind specifically to the miRNA sequence when performing cDNA synthesis from miRNA. miRNA-cDNA was synthesized using Atlas Bioscience A.T.TM cDNA Synthesis Kit with RNase inh.

PCR components and Amplification parameters are presented below;

10 µl of master mix was prepared at the rates of 2 µl 10X Reaction buffer, 2 µl Stem-loop primer (miRNA spesifik), 1 µl 20X dNTP mix, 1 µl Reverse transkriptaz, 0.5 µl RNase Inhibitor, 3.5 µl RNase free Water and 10 µl of miRNA sample and added to the loading wells.

The reaction was carried out at 25 ° C for 10 minutes, 37 ° C for 120 minutes, 85 ° C for 5 minutes and 4 ° C.

Real-time qPCR. Primers miRNA-156, miRNA-159 and miRNA-171 for barley were designed for gene regulation. Tubulin has been used as the housekeeping gene. The details pertaining to the primers employed are provided in Table 2.

After the miRNA-cDNA was obtained, the Real-Time qPCR step was started. For Real-Time qPCR, the Atlas Bioscience Inc. ™ 2X miRqGreen MasterMix (with ROX) kit was used.

Real-Time qPCR components and Amplification parameters are presented below.

20 µl of master mix was prepared at the rates of 10 µl A.B.T.™ 2X miRqGreen MasterMix (with ROX), 1 µl ROX Dye (20X), 1 µl miRNA Specific Forward Primer (5 µM)*, 1 µl miRNA Universal Reverse Primer (5 µM)*, 2 µl miRNA-cDNA Template, up to 20 µl RNase free Distilled Water and added to the loading wells.

The Real-Time qPCR reaction was performed on the Applied Biosystems ™ 7500 Fast Real-Time PCR instrument, respectively; Initial Denaturation 1 cycle for 300 sec at 95 ºC, denaturation 10-30 sec at 95 ºC for 25-40 cycles, 10-60 sec at anneal 55-68 C for 25-40 cycles and melting curve at 65-95 C for 2 -5 sec / cycle.

Calculation of relative quantitation. Quantitation of miRNA expressions snRNA U6 was used as reference and normalized to the control group. The ΔΔCt Method was used in the calculation of relative quantification.

TABLE 1
Primers used in RT-PCR for gene expression

PRIMER NAME	SEQUENCE 5'→3'	T.M. (ºC)
Hv14.3.3-Forward Primer	AGGTACGAGGAGATGGTTGAG	55
Hv14.3.3-Reverse Primer	CAGTGGAAGACGGAACAAGG	58
β-actin- Forward Primer	TTTGAAGAGTCGGTGAAGGG	52
β-actin- Reverse Primer	TTTCATACAGCAGGCAAGCA	50

TABLE 2
Primers used in RT-qPCR

miRNA PRIMER NAME	SEQUENCE 5'→3'
miR-156- Forward Primer	TGACAGAAGAGAGTGAGCACA
miR-159- Forward Primer	TTTGGATTGAAGGGAGCTCTG
miR-171- Forward Primer	TGATTGAGCCGTGCCAATATC
miRNA Universal Reverse Primer Tubulin	CGAGGAAGAAGACGGAAGAAT

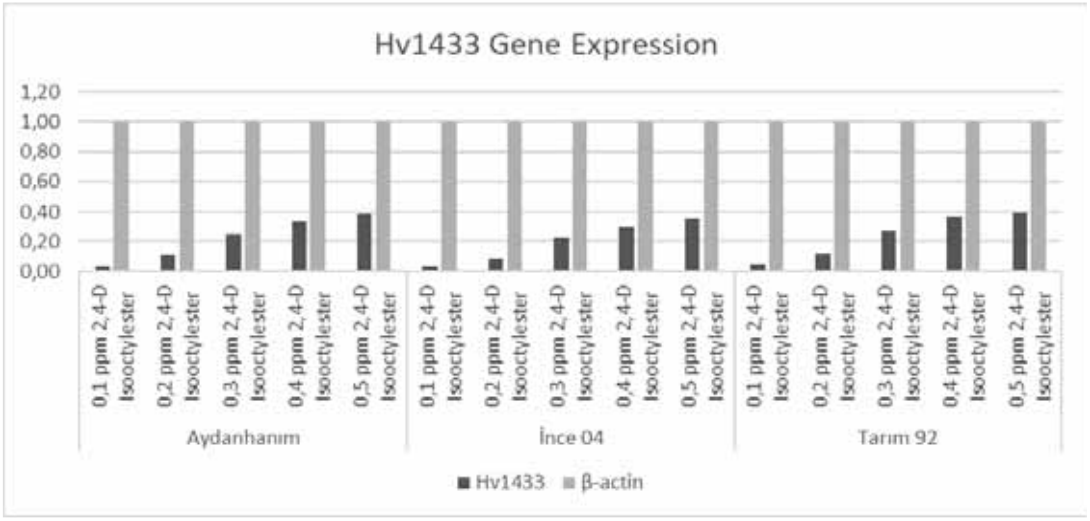

FIGURE 2
Gene expression levels of seedlings exposed to the herbicide.

RESULTS

Gene expression analysis results. In order to eliminate the margin of error in RT-PCR analysis results, the dimer formation was checked. In order to check the dimer formation of primers, the melting curve analysis was carried out. At the end of melting curve analysis, dimer formation in primers was mot observed. In RT-PCR, Hv14-3-3 and b-actin genes are used in both of our study and control groups. Threshold cycle (Ct) values were obtained for using in comparative analysis of samples. $2^{-\Delta\Delta ct}$, which is a parameter in evaluating the gene expression levels using Ct values was calculated.

The 14-3-3 gene family is a protein family that is regulated as a defense mechanism in case of stress. $2^{-\Delta\Delta ct}$ values, which is a significant expression in the quantitative analysis of gene expression amount, were calculated for all dose values of 2,4-D isooctylester and vanillylaceton in barley seedlings of Aydanhanım, İnce 04 and Tarım 92. In the barley samples germinated by 2,4-D Isooctylester herbicide, 14-3-3 gene expression level increased in direct proportion with the dose. The lowest gene expression level was obtained at a dose of 0.1 ppm, while the highest gene expression level was determined at a dose of 0.5 ppm. The highest Hv14-3-3 gene expression level was found in Tarım 92 while the lowest was found in İnce 04. The gene expression levels obtained only in different doses of 2,4-D Isooctylester herbicide of all three barley species samples are given in Figure 2.

In all three barley species examined, it was found that increasing level of 14-3-3 gene expression by 2,4-D isooctylester herbicide stress decreased due to the doses of vanillylaceton. 14-3-3 Decrease in gene expression level was detected at all doses. The highest decreases were obtained from the application of 0.3 ppm vanillylaceton. In Figure 3, 4 and 5, gene expression levels of Aydanhanım, İnce 04 and Tarım 92 species were given with 0.5 ppm 2,4-D Isooctylester in different doses of Vanillylacetone.

miRNA Analysis results. In plants, miRNAs largely regulate gene expression by targeting mRNAs by cleavage post-transcription; therefore, there may be an inverse relationship between a particular miRNA and gene expression. To examine the dynamic expression pattern of miRNAs under 2,4-D Isooctylester stress, real-time PCR was performed on samples and control groups of three barley species germinated by exposure to 2,4-D isooctylester herbicide with vanillylacetone. In barley samples exposed to different doses of 2,4-D Isooctylester and vanillylaceton, miRNA 156 regulation was found to increase at all doses. In barley where the 2,4-D isooctylester herbicide and vanillylaceton were applied at the same time, the highest level of miRNA 156 gene expression was observed in Tarım 92 and lowest level of miRNA 156 gene expression was observed in Aydanhanım. Changes in gene regulation have shown a positive correlation between vanillylacetone and miRNA 156. Figure 6 shows the regulation levels of miRNA 156 in Aydanhanım, İnce 04 and Tarım 92 samples exposed to 2,4-D Isooctylester and vanillylacetone.

2,4-D Isooctylester and vanillylaceton exposure showed positive correlation with miRNA 159 expression as well as miRNA 156. miRNA gene regulation was highest in Tarım 92. Tarım92 is followed by İnce 04 and Aydanhanım, respectively. Figure 7 shows the regulation levels of miRNA 159 in barley samples exposed to 2,4-D Isooctylester and vanillylacetone.

Unlike miRNA 156 and miRNA 159 expression values in all three barley, miRNA 171 expression level showed negative correlation to gene expression. The highest gene expression was detected in Aydanhanım, followed by İnce 04 and Tarım 92, respectively. Figure 8 shows miRNA 171 expression levels of all three species.

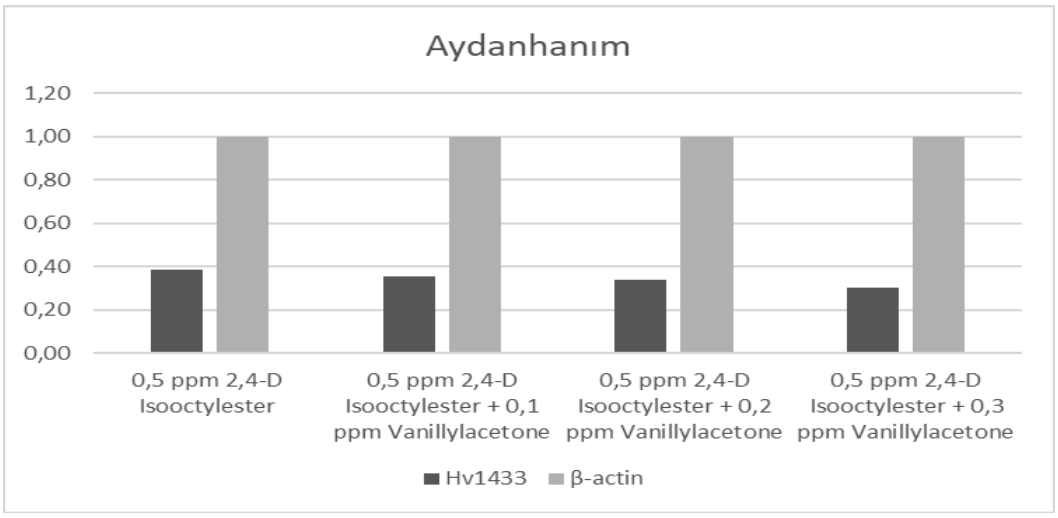

FIGURE 3
Aydanhanım gene expression level.

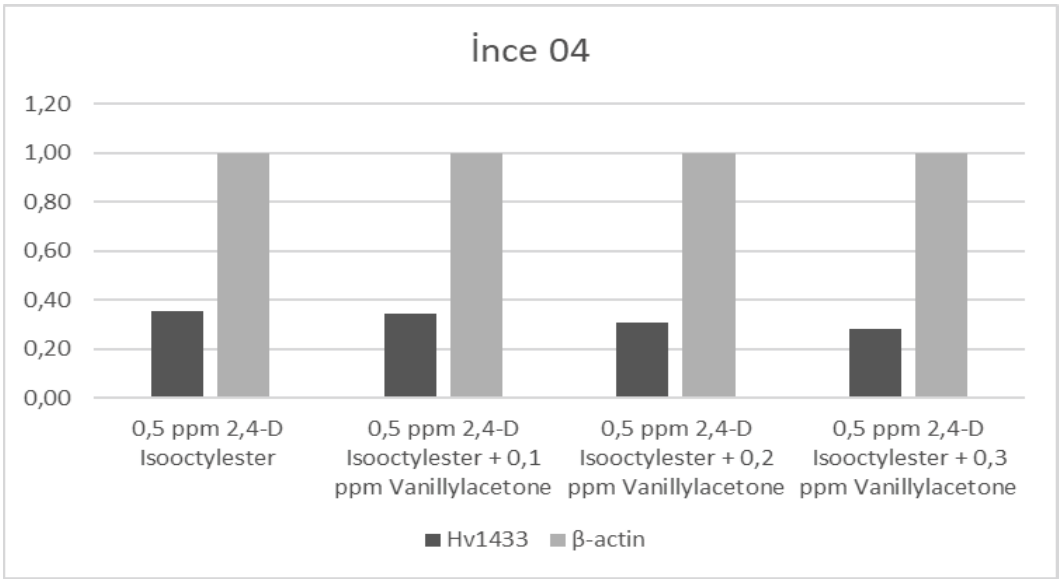

FIGURE 4
İnce 04 gene expression level.

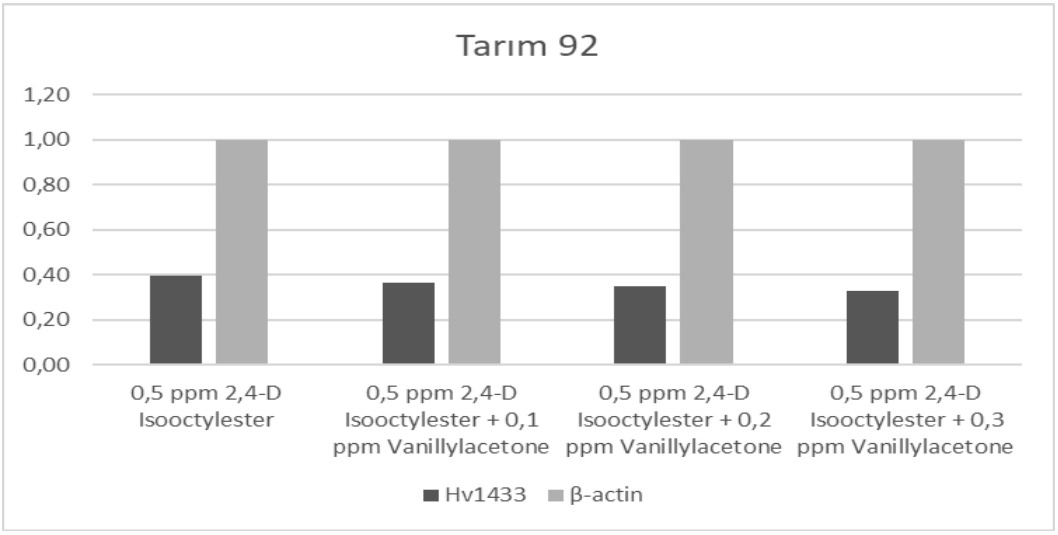

FIGURE 5
Tarım 92 gene expression level.

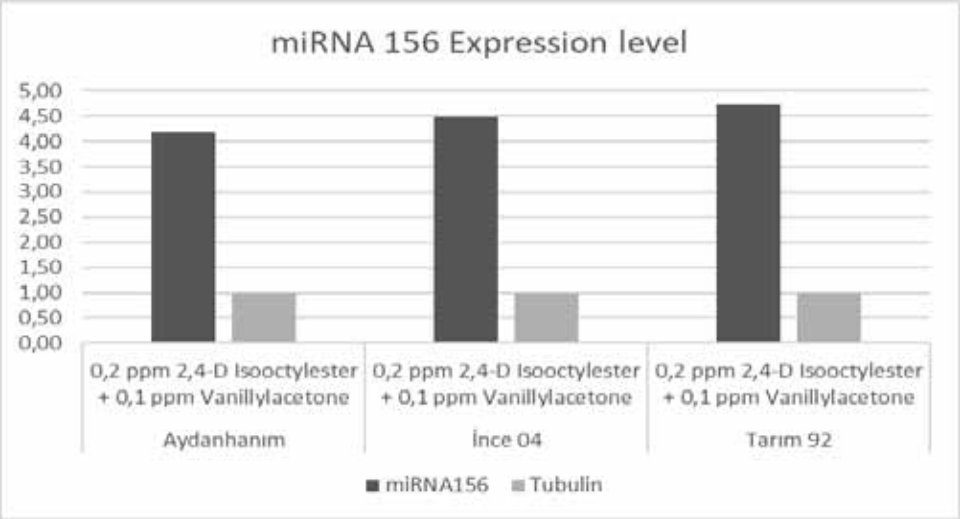

FIGURE 6
Regulation levels of miRNA 156.

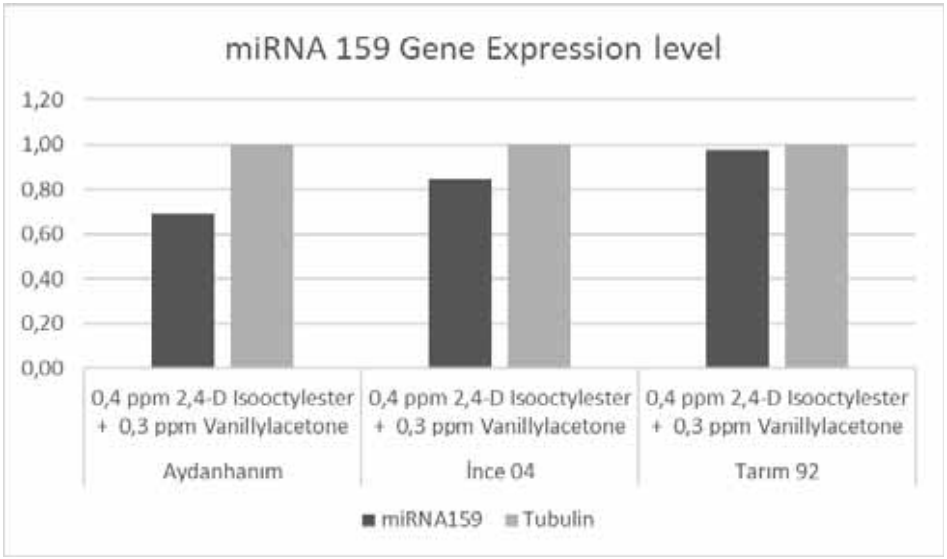

FIGURE 7
Regulation levels of miRNA 159.

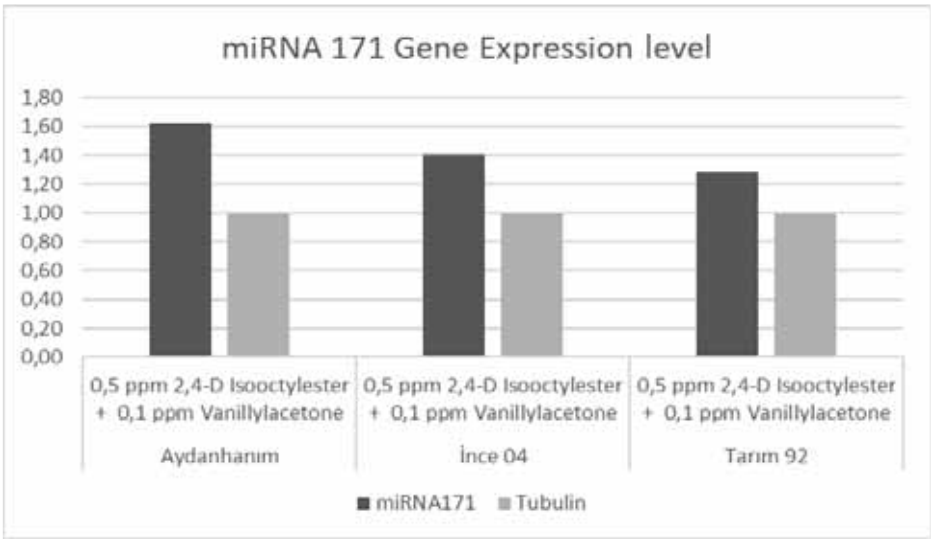

FIGURE 8
Regulation levels of miRNA 171.

DISCUSSION

Pesticides, which are frequently used in agriculture, are one of the important anthropogenic applications threatening ecological life. 2,4-D is a kind of phenoxy acid herbicide [31], are moderately stable chemicals and cause slowdown in the development of the products to which they are applied [32]. In addition, depending on the concentration of 2,4-D mutagenic and genotoxic effects have been expressed in different studies [33, 34].

Recently it has been found that miRNAs important factors in post-transcription of target mRNA in gene regulation after transcription. The discovery of the role of miRNAs as gene regulators has played an important role in understanding post-transcription gene regulation in plants. Recent findings argue that miRNAs may play a crucial role in responding to abiotic stresses in the regulation of plant genes at the post-transcriptional level [26, 27, 28, 35].

In plants, miRNAs greatly regulate gene expression by targeting mRNAs for cleavage. Thus, miRNAs generally negatively regulate the accumulation of mRNAs and display an inverse correlation expression pattern in the same plant cells. Increased evidence has shown that miRNAs may play a key role in regulating cellular adaptation mechanisms in stress-exposed plants [27, 36, 37, 38]. In our study, miRNA 156 and miRNA 159 regulation showed positive correlation with gene expression, while miRNA 171 showed negative correlation. Our results show that miRNAs in plants in the literature largely regulate gene expression by targeting mRNAs for cleavage, suggesting that there may be an inverse correlation between miRNA and its targets, and that this difference may be due to the regulation of the target by more than one miRNA [39]. In addition, the reduction of abiotic stress in the plant by Vanillylaceton decreased the level of defense gene expression 14-3-3. This reduction in expression level can be caused by increased regulation of miRNA 171. However, increasing doses of vanillylaceton were found to cause positive regulation at the expression level in miRNA 156 and miRNA 159. The data obtained from the study showed that there may be different correlations between miRNA and gene expression models. It was also found that vanillylaceton reduces the stress level caused by herbicide in barley samples. The results of our study support the statement that abiotic stress is a complex progression [39].

One of the findings obtained from our research is that 2,4-D isooctylester herbicide which has the least genotoxic effect on İnce 04. On the other hand, Tarım 92 is effected more than İnce 04 and Aydanhanım is effected at the highest level. Chosing this species when planting in areas exposed to toxic effects will be beneficial for product quality and efficiency. It can be stated that herbicides cause environmental pollution and genotoxic effects in non-target organisms.

Finally, even very low levels of herbicides have been found to be toxic to non-target organisms. Zingerone was found to have a protective effect against genotoxic agents. Further investigation of the regulatory functions of miRNAs will be effective in order to understand the plant defense reflex against herbicide-induced toxicity. However, the analysis of species, quantity, analysis of proteins etc., which are the main products of gene expression of genotoxic agents, will reveal the effects of abiotic stresses.

REFERENCES

[1] TSI-Turkish Statistical Institue (2019) Area and Production of Cereals and Other Crop Products Report. http://www.turkstat.gov.tr/mainstatistics/agriculture/ Area_and_Production_of_Cereals_and_Other_Crop_Products. Date of last Access: 07.12.2019.

[2] Rastogi, L., Dash, K., Ballal, A. (2017) Selective colorimetric/visual detection of Al3+ in ground water using ascorbic acid capped gold nanoparticles. Sensor. Actuat. B-Chem. 248, 124-132.

[3] Moreno-González, D., Pérez-Ortega, P., Gilbert-López, B., Molina-Díaz, A., García-Reyes, J.F., Fernández-Alba, A.R. (2017) Evaluation of nanoflow liquid chromatography high resolution mass spectrometry for pesticide residue analysis in food. J. Chromatogr. A. 1512, 78-87.

[4] Malarkodi, C., Rajeshkumar, S., Annadurai, G. (2017) Detection of environmentally hazardous pesticide in fruit and vegetable samples using gold nanoparticles. Food Control. 80, 11-18.

[5] Cheng, H., Marín-Sáez, J., Romero-González, R., Frenich, A.G. (2017) Simultaneous determination of atropine and scopolamine in buckwheat and related products using modified QuEChERS and liquid chromatography tandem mass spectrometry. Food Chem. 218, 173-180.

[6] EUM Environment and Urban Ministry (2019) Pesticide usage amounts report. https://environmentalindicators.csb.gov.tr/pesticide-use-i-86060. Date of last Access: 13.11.2019.

[7] Harrington, K.C., Ghanizadeh H. (2017) Herbicide application using wiper applicators - A review Crop Prot. 102, 380-390.

[8] Avcı, M.Ç. (2009) Investigation of resistance problems of phalaris brachystachys Link. (short spiked canarygrass) is problem weed of wheat fileds in Çukurova region against to some wheat herbicides. Çukurova University, Institute of Science, Master Thesis, Adana, Turkey (in Turkish)

[9] Vural, N. (1996) Toxicology, Metallic poisons. Publications of Ankara University Faculty of Pharmacy: 3. Ankara, 659 (Toksikoloji, Metalik zehirler. Ankara Üniversitesi Eczacılık Fakültesi Yayınları: 3. Ankara, 659- in Turkish).
[10] Bulut, H., Yildirim Doğan, N. (2017) Determination by molecular methods of genetic and epigenetic changes caused by heavy metals released from thermal power plants. Appl. Biol. Chem.
[11] Cenkci, S., Yildiz, M., Ciğerci, I.H., Bozdağ, A., Terzi, H., Terzi, E.S. (2010) Evaluation of 2,4-D and Dicamba genotoxicity in bean seedlings using comet and RAPD assays. Ecotox Environ. Safe. 73, 1558-1564.
[12] Taspinar, M.S., Aydin, M., Arslan, E., Yaprak, M., Agar, G. (2016) 5-Aminolevulinic acid improves DNA damage and DNA Methylation changes in deltamethrin-exposed Phaseolus vulgaris seedlings. Plant Physiol. Bioch. 118, 267-273.
[13] Küçük, D., Liman, R. (2018) Cytogenetic and genotoxic effects of 2-chlorophenol on *Allium cepa* L. root meristem cells. Environmental Science and Pollution Research. 25(36), 36117-36123.
[14] Hosseini, H., Hosseinzadeh, H. (2018) Antidotal or protective effects of Curcuma longa (turmeric) and its active ingredient, curcumin, against natural and chemical toxicities. A review. Biomed Pharmacother. 99, 411-421.
[15] Tavakkoli, A., Ahmadi, A., Razavi, B.M., Hosseinzadeh H. (2017) Black seed (*Nigella sativa*) and its constituent thymoquinone as an antidote or a protective agent against natural or chemical toxicities Iran. Iranian Journal of Pharmaceutical Research. 16, 2-23.
[16] Fanoudi, S., Alavi, M.S., Karimi, G., Hosseinzadeh H. (2018) Milk thistle (Silybum Marianum) as an antidote or a protective agent against natural or chemical toxicities. A review. Drug Chemster. Toxicology. 2018, 1-15.
[17] Dorri, M., Hashemitabar, S., Hosseinzadeh H. (2018) Cinnamon (*Cinnamomum zeylanicum*) as an antidote or a protective agent against natural or chemical toxicities. A review. Drug and Chemical Toxicology. 41(3), 338-351.
[18] Mohammadzadeh, N., Mehri, S., Hosseinzadeh H. (2017) *Berberis vulgaris* and its constituent berberine as antidotes and protective agents against natural or chemical toxicities. Iranian Journal of Basic Medical Sciences. 20(5), 538-551.
[19] Lee, J., Oh, S.W., Shin, S.W., Lee, K.W., Cho, J.Y., Lee J. (2018) Zingerone protects keratinocyte stem cells from UVB-induced damage. Chemico-Biological Interactions. 279, 27-33.
[20] Kim, M.K., Chung, S.W., Kim, D.H., Kim, J.M., Lee, E.K, Kim, J.Y., Ha, Y.M., Kim, Y.H., No, J.K., Chung, H.S., Park, K.Y., Rhee, S.H., Choi, J.S., Yu, B.P., Yokozawa, T., Kim, Y.J., Chung, H.Y. (2010) Modulation of age-related NF-kappaB activation by dietary zingerone via MAPK pathway. Exp Gerontol. 45, 419–26.
[21] Thongrakard, V., Rossella, C.F.T., Isidoro, C. (2014) Turmeric Toxicity in A431 Epidermoid Cancer Cells Associates with Autophagy Degradation of Anti-apoptotic and Anti-autophagic p53 Mutant. Phytotherapy Research. 28(12),1761-9. doi: 10.1002/ptr.5196.
[22] Kamel, B., Bourguignon, L., Marcos, M., Ducher, M., Goutelle, S. (2017) Is Trough Concentration of Vancomycin Predictive of the Area Under the Curve? A Clinical Study in Elderly Patients. Ther Drug Monit. 39(1), 83-87.
[23] Yang, P., Chen, Y., Wu, H., Fang, W., Liang, Q., Zheng, Y., Olsson, S., Zhang, D., Zhou, J., Wang, Z., Zheng, W. (2018) The 5-oxoprolinase is required for conidiation, sexual reproduction, virulence and deoxynivalenol production of Fusarium graminearum. Curr. Genet. 64(1), 285-301.
[24] Guahk, G.H., Keun, H.S., Hyuk, S.J., Chulhun, K., Chang, H.K., Yoon, B.K., Sun, Y.K. (2010) Zingiber officinale Protects HaCaT cells and C57BL/6 Mice from Ultraviolet B-Induced Inflammation. Journal of Medicinal Food. 13(3).
[25] Sunkar, R. (2010) MicroRNAs with macro-effects on plant stress responses. In: Seminars in Cell and Developmental Biology. Elsevier, 805–811.
[26] Budak, H., Kantar, M., Bulut, R., Akpinar, B.A. (2015) Stress responsive miRNAs and isomiRs in cereals. Plant Sci. 235(2015), 1-13.
[27] Zhao, X., Liu, X., Guo, C., Gu, J., Xiao, K. (2015) Identification and characterization of microRNAs from wheat (*Triticum aestivum* L.) under phosphorus deprivation. J. Plant Biochem. Biotechnol. 22, 113-123.
[28] Srivastava, S., Srivastava, A.K., Suprasanna, P., D'Souza, S.F. (2013) Identification and profiling of arsenic stress-induced microRNAs in Brassica juncea. J. Exp. Bot. 64, 303-315.
[29] Qiu, Z.B., Li, X.J., Zhao, Y.Y., Zhang, M.M., Wan, Y.L., Cao, D.C., Lu, S.F., Lin, J.X. (2015) Genome-wide analysis reveals dynamic changes in expression of microRNAs during vascular cambium development in Chinese fir. J. Exp. Bot. 66(2015), 3041-3054.
[30] Rao, X., Xuelin, H., Zhicheng, Z. and Xin, L. (2013) An improvement of the 2ˆ(–delta delta CT) method for quantitative real-time polymerase chain reaction data analysis. Biostat. Bioinforma Biomath. 3(3), 71–85.

[31] Gehring, C.A., Irving, H.R., Parish, R.W. (1990) Effects of auxin and abscisic acid on cytosolic calcium and pH in plant cells. Proc. Natl. Acad. Sci. USA, 87, 9645–9649.
[32] Donald, D.B., Syrgiannis, J., Hunter, F., Weiss, G. (1999) Agricultural pesticides threaten the ecological integrity of northern prairie wetlands. Sci. Total Environ. 231(2-3), 173-81.
[33] Pavlica, M., Papes, D. and Nagy, B. (1991) 2,4-Dichlorophenoxyacetic acid causes chromatin and chromosome abnormalities in plant cells and mutation in cultured mammalian cells. Mutat Res. 263, 77-81.
[34] Enan, M.R. (2009) Genotoxicity of the herbicide 2,4-Dichlorophenoxyacetic acid (2,4-D): higher plants as monitoring systems. JTFE. 25, 147-155.
[35] Ding, Y., Chen, Z., Zhu, C. (2011) Microarray-based analysis of cadmium-responsive microRNAs in rice (*Oryza sativa*) J. Exp. Bot. 62(2011), 3563-3573.
[36] Akpinar, B.A., Kantar, M., Budak, H. (2015) Root precursors of microRNAs in wild emmer and modern wheats show major differences in response to drought stress Funct. Integr. Genom. 15(2015), 587-598.
[37] Akdogan, G., Tufekci, E.D., Uranbey, S., Unver, T. (2016) miRNA-based drought regulation in wheat Funct. Integr. Genom. 16(3), 221-33. doi: 10.1007/s10142-015-0452-1.
[38] Liu, H.P., Able, A.J., Able, J.A. (2016) Water-deficit stress-responsive microRNAs and their targets in four durum wheat genotypes. Funct. Integr. Genom. 17(2-3), 237-251. doi: 10. 1007/s10142-016-0515-y.
[39] Khaksefidi, R.E., Mirlohi, S., Khalaji, F., Fakhari, Z., Shiran, B., Fallahi, H., Rafieim, F., Budak, H., Ebrahimie, E. (2015) Differential expression of seven conserved microRNAs in response to abiotic stress and their regulatory network in *Helianthus annuus*. Front. Plant Sci. 6, 741-754.

Received: **10.12.2019**
Accepted: **10.02.2020**

CORRESPONDING AUTHOR

Huseyin Bulut
Erzincan Binali Yıldırım University
Vocational School of Health Services,
24100 Erzincan – Turkey

e-mail: huseyinbulut@erzincan.edu.tr

© by PSP Volume 29 – No. 05/2020 pages 3914-3922 Fresenius Environmental Bulletin

BIOLOGICAL CONTROL OF TOMATO CORKY ROOT ROT CAUSED BY *PYRENOCHAETA LYCOPERSICI* USING *TRICHODERMA HARZIANUM* RIFAI RACE KRL-AG2

Aysegul Colak Ates*

Biological Control Research Institute, Department of Phytopathology, Adana, Turkey

ABSTRACT

The aim of this study was to determine the effect of *Trichoderma harzianum* Rifai race KRL-AG2 (TH) on the biological control of Corky root rot (*Pyrenochaeta lycopersici*, CRR) which caused significant yield losses in tomato cultivation. For this purpose, in concomitant inoculations with biological control agent alternative to chemical control with fungus (CRR + TH) and in 15 days squential inoculations (CRR+ 15 days after or before and singel or twice TH); It was found that using the biological preparation of TH once applications was not enough, but the incidence of the disease decreased significantly in two applications. In study, Money marker, Alice craig and H2274 tomato cultivars in the experiments on the highest % effect on *Pyrenochaeta lycopersici,* CRR + 15 days before the twice TH application, respectively 72.24-70.63-68.73%, while the lowest % effect was obtained 15,21-21,19-17,45%, with CRR + 15 days after TH applications. This study has revealed that the application of high amounts of biological preparation *Trichoderma harzianum* Rifai race KRL-AG2 would be an effective alternative to chemical control in order to prevent long-term diseases as symptoms become apparent, as in *Pyrenochaeta lycopersici* disease pathogen.

KEYWORDS:
Tomato, Corky root rot, Trichoderma, biological control

INTRODUCTION

World vegetable production is 1.71 billion tons. Vegetable production in Turkey increased by 1.8% in 2017 to 30 million 826 thousand tons of vegetable production in the world, China, India and is located after the United States. tomato production in Turkey increased by 1.2% in 2017, production is 12750.000 tons, the share of fruit-eaten vegetables are 40-45% [2]. Tomato production in Turkey constitutes approximately 65% of the fresh market production and 35% of the tomato paste production. Tomato (*Lycopersicon esculentum* Mill.) is one of the most widely produced, consumed and tradable agricultural products in the world. Tomato is one of the most important vegetables in human nutrition and it is one of the most important vegetables in the food industry because it has a wide range of uses such as frozen, canned, tomato paste, ketchup and pickles.

Plant diseases are a serious problem during tomato cultivation in our country and in the world. There are more than 200 diseases in tomatoes. Soil-borne fungal diseases are among the most important limiting factors of tomato cultivation which is so important economically [1,19,42]. Corky root rot, caused by *Pyrenochaeta lycopersici* (Schneider and Gerlach) in tomato, is a soil-borne fungal pathogen that causes diseases in different crops [25,29]. After the first report of the fungal disease in England in 1929, *P. lycopersici* has been reported from many countries; Germany, New Zealand, Lebanon, Massachusetts, Florida, California, Italy, Korea, Russia, Crete, Albania, Australia, Sweden, and tomatoes grown in Turkey has been reported in all areas [3,4,16,26,29,30,43,48,54,69]. The disease causes brown necrotic lesions on the roots of the tomato plant and limits the intake of water and nutrients. Tomato plant in time with wilt, early defoliation and weakening of the root system causes symptoms of the disease. *P. lycopersici* survives as microsclerotia for 5 and more years even in the absence of host plants in the soil [3,11,26]. Significant infections of the pathogen cause brown lesions in parts of the main and lateral roots that turn brown, swell and crack. The disease can cause 30-40% yield loss in tomato cultivation and damage up to 75% in the most pathogen intense areas. The fungal disease does not generally kill plants, but causes serious yield losses [3,68]. Diseased plants are stunted and slow to develop. *P. lycopersici* inoculum increases rapidly in cultivated soil with consecutive tomatoes or other sensitive crops. The pathogen primarily attacks tomatoes, but also infects the *Solanaceae* and *Cucurbitaceae* families, such as pepper, eggplant, cucumber, melon, squash, melon, tobacco as well as strawberry, lettuce and spinach plants [16,26,58].

Until today, in different tomato production in Turkey more pathogen detection, *P. lycopersici* isolates belonging to different production areas

there are few studies about the genetic variation [7,69,70]. In the study of determination of common plant pathogenic fungi in tomato cultivated areas in Ankara; P. lycopersici disease incidence was found to be 17.2% on average and found to be the highest in Ayaş (42.10%) and Beypazarı (1.22%) [52]. An important feature of the disease is that it is almost imperceptible until the appearance of obvious symptoms in the roots, with the exception of reduced fruit yield and excessive growth of the plant shoot. Up to the present, the lack of studies in the fight against the disease in our country, difficulties in early diagnosis of the disease, symptoms are seen after half of the growing period. In this context; symptoms such as *P. lyocersici* become evident after detection of long-time plant pathogens; in order to disease control, it is important to develop biological agents that survive in soil for a long time [26,57]. It is very difficult to control soil-borne diseases such as *P. lyocersici*. Because these pathogens produce various spores and similar structures that are capable of sustaining their existence in soil, plant residues mixed with soil and living root tissues for a long time. Factors such as the physical and chemical structure of the soil, other microorganisms in the rhizosphere, root secretions of host plants may make it difficult to control soil-borne pathogens. Chemical compounds known as fungicides are used in the control against plant diseases. Misuse of these fungicides; It poses risks in the control of plant diseases due to the development of resistance to pathogens against fungicides, decreasing their effectiveness through genetic changes in the population and creating undesirable results on non-target organisms [63]. In recent years, the chemicals used in the fight against plant diseases are being tried to be minimized due to the harm they cause to the environment and human health. A typical example is the prohibition of methyl bromide in the United States, which is an effective fumigant due to ozone depleting and bromine residues in water [28,39]. In parallel with the studies in the world, alternative approaches including organic and integrated agricultural systems have come to the forefront in our country in order to reduce the negative effects of chemical control. Biological control has become important as an alternative to chemical control in terms of environment and food safety. The use of microorganisms that act as biological control agents against plant pathogenic organisms helps to control the pathogen and disease suppression in a long term but sustainably effective manner, depending entirely on the areas where fungicides are used [8,13,17,20,55,64,67].

These useful microorganisms, which are widely used today, are effective in planting food and ground competition with pathogens that cause disease in the plant, producing antibiotics, hyperparasitism or by promoting resistance in the host plant. At least 30 different biological control preparations are available in the commercial formulation currently available for the control of plant diseases [18,46]. These include the most common fungal antagonists; *Trichoderma* spp., *Ampelomyces quisqualis*, *Candida oleophila*, *Gliocladium* spp. and *Coniothyrium minitans* [27,31,33,49,56]. *Trichoderma* genus is one of the most widely used biological control agents in the control against diseases caused by plant pathogenic fungi [40]. The high efficacy of *Trichoderma harzianum* strains against soil-borne diseases especially in tomato, has been accepted as the result of an antagonistic effect [10,17,32,61,64].The antagonistic fungus *Trichoderma* has been shown to inhibit the growth of *Pyrenochaeta lycopersici* in in vitro evaluations [32,35,36,53,57].

The aim of this study was to investigate the effect of *Trichoderma harzianum* race Rifai KRL-AG2 belonging to the genus *Thricoderma* which has a strong aggression against many soil-borne phytopathogenic fungi in the biological control of *P. lycopersici* disease which caused significant yield losses in tomato production.

MATERIALS AND METHODS

In the study, isolates of Pyrenochaeta lycopersici which caused Corky root rot disease in tomato were obtained from greenhouse tomatoes under cover in Mersin province (Figure 1). In order to determine the effectiveness of *Thricoderma hazianum* (*Trichoderma harzianum* Rifai race KRL-AG2 (T-22 Planter Box, $1x10^7$ cfu / g, Bioglobal) against CRR disease in tomato, the pots were established under the controlled conditions of Alata Horticultural Research Institute (ABKAE). Seedlings belonging to *P. lycopersici* disease susceptible Money maker and Alicia craig (obtained from ABKAE) and H2274 tomato varieties were used in the study.

FIGURE 1
***Pyrenochaeta lycopersici* region isolate in PDA medium**

The experiment design was established in CRR alone (positive control, CRR+), CRR+TH concomitant (CRR+TH), sequential inoculations of 15 days intervals before and after CRR pathogen application to the tomato plants as single and twice applications of TH preparation (CRR+ TH after 15 days / + TH after 15 days ve CRR+ TH before 15 days / + TH before 15 days). As a negative control (CRR-) plants received no pathogen application. In CRR and TH inoculations, the suspensions were homogeneously and meticulously applied to the root area of the plants. For this purpose, PDA medium was used for the spore suspension of CRR isolates. The CRR isolate was incubated at 25 ^{0}C for 7 days and after incubation, the spore concentration was adjusted to 10^7 conidia / ml in haemocytometer. In the experiment, FORL inoculation was inoculated by giving 50 ml spore suspension containing $1x10^7$ spores / ml to the roots of tomato seedlings for 3-4 weeks [19]. *Thricoderma harzianum* (TH) biological preparation was prepared at the recommended dosage (50 g / 100 l / T-22) and applied to the plant in 50 ml.

The experiment was established according to the randomized plot design. The experiment was established with 5 pots for each application and 3 plants in each pot. The pots are 30 x30 cm in size and in sterile soil: perlite: sand (1: 1: 1) mediums, with 16 hours light and 8 hours darkness, at 25 ± 26 ^{0}C and 60-70% under relative humidity was established in the ABKAE climate room. Experiment; 45 days after the treatments, the root browning and lesions of the plants were evaluated using the 0-4 scale and disease incidence (%) and disease index were evaluated [43]. Disease index of 0-4 were used on discoloration on the taproots; 0: healthy plants (no symptoms), 1: slight discoloration, 2: discolaration an done or two small lesions, 3: general discolaration and several lesions,4: general necrosis of the entire taproot. Çalışma sonucunda; the analyses of variance, mean values, differences between treatments were studied using Fisher's Least Significant Difference (LSD) test and Duncan's Multiple Range Lest. All analysis were tested at p: 0.05 level [23]. Istatistical analyzes were conducted using Statistic Analysis System Package (SAS İnstitute, Cary, NC, USA).

RESULTS

Trichoderma harzianum rifai race KRL AG2 (TH), one of the alternative biological agents for chemical control of Corky roort rot disease (*Pyrenochaeta lycopersici*), which causes significant economic losses in tomato cultivation, TH with concomitant inoculation and 15 days squential inoculation successively in order to determine the effectiveness of the application data are given in Table 1. When the table 1 was examined, it was found that % disease incidence was statistically significant ($P<0.05$) in the differences between the applications in pot trials of tomato varieties.

In the present study, it was found that the disease rate values in the presence of CRR in combination with TH and squential applications were earlier and more severe than in the case of TH and squential applications before CRR inoculation. *P. lyocersici* caused by Corky root rot disease in the treatment of tomato cultivars, the lowest disease incidence in TH applications CRR + 15 days + 15 days before TH application with 24.33% Money marker variety was obtained, followed by Alica craig 26.33% and 28.67% H2274 respectively. In the study, the highest disease incidence was obtained from CRR + 15 days after TH applications in H2274 cultivars with 75.67%, followed by Money marker and Alica craig tomato cultivars. In this study, it was found that *Trichoderma harzianum* rifai race KRL AG2 was significantly reduced the disease incidence of *P. lyocersici* when applied twice and 15 days before CRR inoculation (Table 1). As in our study, it was reported that successful results were obtained in two applications of biological preparations in the control against many soil-borne plant pathogens in different products [14,37].

In this study, it was found that CRR disease incidence decreased significantly in TH applications; ensuring long incubation time of antagonist fungus before plant exposure to pathogen, repeated applications, controlled climatic conditions and the use of different varieties may have influenced the variability in the disease incidence and % effect values among the three varieties. In addition, it has been reported that the success of biological preparations may vary according to soil type, species of biological agent, plant interactions and disease pathogen [12,57,60,65]. Sánchez-Téllez et al. [57] in their study for biological control of *Pyrenochaeta lycopersici*; the efficacy of alginate formulations of *Trichoderma harzianum* containing Th12.A.10.1 and ThF2-1, methyl bromide (60 g, m-2) and commercial biofungicide Trichonativa were investigated in tomato greenhouse. When the ThF2-1-containing formulation was administered immediately before planting, 15 days later, and a week before; reported that the level of root damage caused by *P. lycopersici* decreased from 1.6 to 0.2. In the study, it was reported that the detection of symptoms such as Corky root rot disease caused by *P. lycopersici* as a result of the persistence of high amount of specific Trichoderma strains in the soil is very important in the control against long-term diseases. In addition, it was stated that symptoms of Corky root rot disease were seen after half of the growing period [21]. Therefore, the strategy of applying the formulation containing ThF2-1 to soil 3 times; It has been reported that the presence of large amounts of *Trichoderma* strains in the soil for control of *P. lycopersici* may be sufficient for effec-

tive protection. These results are in parallel with our study.

In parallel to these findings, it has been reported by many researchers that some soil-borne plant pathogenic fungi in many crops have inhibitory effect on the development of fungus in the presence of *Trichoderma* species [50,71]. The potential of Trichoderma species to become a biological control agent has been known since the 1930s [32]. *Trichoderma harzianum* in this group is a widely used agent in biological control [24,40,45,59]. It is thought that antibiosis, mycoparasitism and fungus produced enzymes may play a role in the mechanisms of action of *T. harzianum* isolates on pathogens. It kills them in the form of mycoparasitism by feeding through the micelles of the pathogen fungus with enzymes secreted by some antogonist fungi. This is especially seen in Trichoderma spp. [47]. The success of Trichoderma isolates in biological control; high reproductive capacities, ability to survive under abiotic stress conditions, efficacy in nutrient uptake and use, potential to alter the rhizosphere environment, strong aggression against phytopathogenic fungi and plant growth and defense mechanisms are due to their effectiveness in controlling [5,9]. Monaco et al. [50] in their study; The metabolites produced by *T. harzianum* have been reported to have an inhibitory effect on the growth of pathogens. Trichoderma is able to convert phosphorus, manganese, copper and iron into a soluble form in soil. Thus, the roots can easily acquire these nutrients from the soil and the growth rate of the plant increases. As a result, many studies have been reported to reduce the disease rate of some pathogens by promoting vegetative and root development of plants in Thricoderma species treated plants [6,22,32,34,38,40].

In this study, antagonistic effect was observed in all TH inoculations; a higher % effect was detected in CRR+TH concomitant inoculation and 15 days squential inoculations than in control. In our study, when we look at the % effect of applications in the control against disease; the highest effect was obtained with CRR + 15 days + 15 days before TH applications in all tomato cultivars. The lowest % effect in CRR control was obtained from CRR + 15 days after TH applications in all tomato cultivars. The study showed promising results that could be used as an alternative in combating the disease according to the % effect control application of biopreparate TH concomitant inoculation and once-twice in 15 days squential inoculation. In this context; the highest % effect was obtained from Money marker tomato cultivar with 24.33% in CRR + 15 days + 15 days before TH application, followed by Alica craig with 26.33% and H2274 with 28.67%, respectively. The effect of biological agent applied on potted studies on the disease was slightly due to variability; as stated in Howel [40], it is concluded that biological control is affected by pathogen and host plant interaction and other micro-organisms in the soil microflora.

Our results showed that the application of *T. harzianum* before the CRR inoculum reached the level of damage to the plant increased the success in the struggle (Table 1). Hibar et al. [38] emphasized the need for alternative measures in the control against Fusarium crown and root rot (*Fusarium oxysp*orum f.sp. *radicis-lycoperisici*, FORL), one of the soil-borne diseases in greenhouse tomato cultivation in Tunisia. In their study, in order to suppress FORL disease, some bio-fungicides (*T. harzianun* strain T22 (RootShield Drench, BioWorks Inc. Geneva, NY), effective in in-vitro, climate chamber and greenhouse conditions, *T. harzianun* (Biocont-T WP and Biocont-T Gr, National Ammonia & amp; Chemical Industries, Amman), *Bacillus subtilis* strain QST 713 (Serenade, AgraQuest, Davis, CA), *B. pumilus* strain QST 2808 (Sonata, AgraQuest, Davis, CA), *Pythium oligandrrum* (Polyversum, Biopreparáty Ltd., Czech Republic) and natural microorganisms (Agralan Revive, Agralan Ltd., Swindon, UK) investigated their effectiveness. In in-vitro tests, all of the bio-fungicides inhibited FORL micellar growth by 50-73%. Climate chamber studies, one week prior to application to plants to pathogen was significantly effective bio-fungicide suspension. In addition, in cases where bio-fungicide and pathogen were given together, the disease incidence decreased significantly. This study has shown that the application of some bio-fungicides in pathogen control, especially before the pathogen reaches the level of attack inoculum, has been shown to increase success in the plant disease control. These results are in parallel with our study.

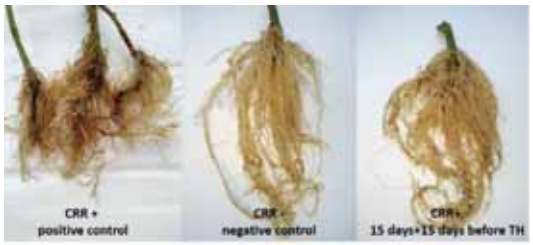

FIGURE 2
Image of the most effective *Trichoderma harzianum* applications for the control of corky root rot disease in tomato.

FIGURE 3
Brown areas and cracking symptoms of Corky root rot caused by *Pyrenochaeta lycopersici* in Money marker tomato roots.

TABLE 1
Corky root rot disease of TH applications in the control against the disease incidence and effect.

Treatments	H2274			Money marker			Alica craig		
	Diease incidence %	Effect %	Index (0-4)	Diease incidence %	Effect %	Index (0-4)	Diease incidence %	Effect %	Index (0-4)
CRR+TH	55,67 c	39,27	2,23	52.00 c	40,69	2,07	58,33 c	34,94	2,33
CRR+15 days after TH	75,67 d	17,45	2,97	74.33 d	15,21	2,97	70,67 d	21,19	2,83
CRR+15days+15days after TH	55,33 c	39,64	1,66	55.67 c	36,5	2,23	61,67 c	31,23	2,46
CRR+15days before TH	38,67 b	57,82	1,53	31.67 b	63,88	1,25	36,66 b	59,11	1,25
CRR+ 15 days+15 days before TH	28,67 a	68,73	0,85	24.33 a	72,24	0,97	26,33 a	70,63	1,05
CRR +	91,67 e	-	3,67	87.67 e	-	3,51	86,13 e	-	2,28
CRR -	-		-	-		-	-		-
Lsd 0.05	5,38			5.28			5,63		

CRR: Corky root rot, TH: *Trichoderma harzianum* rifai race KRL AG2, CR+: positive control (inoculated fungus), CRR-: negative control (non-inoculated fungus**),** Index: 0-4 scale for *P. lycopersici*

In the study, the biological preperate *Trichoderma harzianu*m antagonist fungus was given to the plant twice and single application before and after the CRR inoculum at 15 days intervals; especially in cases where the pathogen is applied twice, single and concomitant 15 days before the inoculum, the disease rate is 24.33-26.33-28.67%, 31.67-36-66.38.67% and 52-55.67-58%, respectively (Figure 2). It was determined that it decreased by 33% and 91,67-87,67-86,13% in the control (Figure 3). Hibar et al. [37] investigated the resistance mechanism of *Trichoderma harzianum* (3 isolates) and *Thricoderma viride* (1 isolate) antagonist fungi against soil-borne FORL disease, which caused significant damages in undergrowth tomato cultivation in Tunisia. In this study, the plant roots were divided into two pathogens and antagonists were applied to the same plant in separate pots. In the study, FORL inoculum was given one week before, one week after *Trichoderma* spp. antagonist fungus and in concomitant inoculation experiments; reported that the disease incidence decreased 10% and 13-18%, respectively, and 48% at the control, especially when the pathogen was administered one week before and inoculum together. These results are in parallel with our study.

Çolak and Biçici [17] in their study; for the integrated control of FORL in tomato cultivation, solarization, Metham sodium, compost, *Bacillus subtilis* QST-713 and *Trichoderma harzianum* alone or in different combinations were investigated. Among the biological agents, the most promising results in the control against soil-borne disease FORL were obtained from Basillus subtilis QST-713 and *Trichoderma harzianum*. Inbar et al. [41] greenhouse studies found that the effects of *Trichoderma harzianum* applications on White rot disease in lettuce decreased by 46 to 72% compared to control plants.

CONCLUSION

In tomato cultivation, Corky root rot caused by *Pyrenochaeta lycopersici*, one of the soil-borne pathogens, causes up to 75% crop loss in yield. Corky root rot disease is a soil-borne disease and its struggle is very difficult. It is known that the application of biological methods to control plant pathogens is safer for the environment than the use of pesticides. Bio-fungicides used in control soil-borne diseases in biological control methods may be partially sufficient to completely reduce the populations of plant disease pathogens. The complete eradication of the disease is only possible when the biological product remains in the soil for a long time. In this context, our study results; In the control against Corky root rot disease which caused significant yield losses in areas which are heavily contaminated as well as stunted and development in tomato cultivation, intensive pre-planting applications of *Trichoderma harzianum* can be used as an alternative to chemicals in disease control. In our study results; In biological preparations applied to soil twice before inoculation of CRR disease agent; *Trichoderma harzianum* persisted in the soil with *P. lycopersici* caused Corky root rot disease rate was 72.24-68.73% effect. These results suggest that, as in the case of CRR, the manifestation of disease symptoms in the plant is very important to prevent long-term diseases. In order to see the effect of Trichoderma harzianum as a biological control agent against Corky root rot disease; it was determined that using biological preparations once was not enough, but repeated treatments applied twice before planting significantly reduced the rate of the disease [15,57]. Soil-borne plant diseases can only be eradicated in the soil, but only when the disease pathogen concentration is low in the soil. However, plant pathogens can be used to provide a long-term and effective biological control, particularly in soil-

borne diseases such as *P. lycopersici*; crop rotation, use of resistant varieties, solarization (soil disinfection) and taking all cultural measures together are important. However, plant pathogens particularly in soil-borne diseases such as *P. lycopersici* can be used to provide a long-term and effective biological control with crop rotation, use of resistant varieties, solarization (soil disinfection) and taking all cultural measures together are important [62,66]. Therefore, it has been demonstrated that an integrated approach using multiple control measures can provide sustainable control of *P. lyocersici.* For such a strategy to be successful, it is important to select agricultural and crop management practices that reduce the accumulation of pathogen inoculum and the risk of disease spread [44,51].

ACKNOWLEDGEMENTS

The authors are so grateful to Alata Horticultural Research Institute, Mersin /Turkey for tomato seeds and climate room support.

REFERENCES

[1] Agrios, G.N. (2005) Plant Pathology. Fifth edition, Academic Press. New York, p. 633.

[2] Anonymous (2018). Crop production statistics TUİK, http://www.tuik.gov.tr/ PreTablo.do? alt_id=1001. (in Turkish)

[3] Aragona, M, Infantino, A., Papacchini, M. (2009) Developing a molecular method for screening the resistance to a pathogen of tomato to contribute to limit the use of toxic chemicals in soil. WIT Trans Ecol. Envir. 120,519-524.

[4] Aragona, M., Minio, A., Ferrarini, A., Valente, T.M., Bagnaresi, P., Orrù, L., Tononi, P., Zamperin, G., Infantino, A., Valè, G., Cattivelli, L., Delledonne, M. (2014) De novo genome assembly of the soil-borne fungus and tomato pathogen *Pyrenochaeta lycopersici.* BMC Genomics. 15, 313

[5] Aydın, H.M. (2015). Biological Control of Fungal Plant Disease with Trichoderma. Turk J. Agric. Research. 2, 135-148.

[6] Ayed, F., Daami-Remadi, M., Jabnoun-Khiareddine, H., El Mahjoub, M. (2006) Potato Vascular Fusarium wilt in Tunisia: Incidence and biocontrol by *Trichoderma* spp. Plant Pathology Journal. 5, 92-98.

[7] Bayraktar, H., Oksal, E. (2011) Molecular, physiological and pathogenic variability of *Pyrenochaeta lycopersici* associated with corky rot disease of tomato plants in Turkey. Phytoparasitica. 39, 165-174.

[8] Becker, J.O., Schwinn, F.J. (1993) Control of soil-borne pathogens with living bacteria and fungi, status and outlook. Pestic. Sci. 37, 355-363.

[9] Benitez, T., Rincon, A.M., Limon, M.C., Codon, A.C. (2004) Biocontrol mechanisms of *Trichoderma* strains. International Microbiology. 7 (4), 249-260.

[10] Besoain, X., Pérez, L., Araya, A., Lefever, L., Sanguinetti, M., Montealegre, J. (2007) New strains obtained af ter UV treatment and protoplast fusion of native *Trichoderma harzianum*: their biocontrol effect on *Pyrenochaeta lycopersici.* E- J. Biotechnol. 10, 604-617.

[11] Campbell, R.N., Hall, D.H., Schweers, V.H. (1982) Corky root of tomato in California caused by *Pyrenochaeta lycopersici* and control by soil fumigation. Plant Disease. 66, 657-661.

[12] Celar, F. (2002) Influence of root exudates of different plant seedlings on mycelial growth of antagonistic fungi *Trichoderma* spp. and *Gliocladium roseum*. Zb. Biotech. Fak. Univ. Ljublj. Kmet. 79-2, 343-348.

[13] Chet, I., Inbar, J. (1994) Biological control of fungal pathogens. Applied Biochemistry and Biotechnology. 48, 37-43.

[14] Chitrampalam, P., Cox, C.A., Turini, T.A., Pryor, B.M. (2010) Efficacy of *Coniothyrium minitans* on lettuce drop caused by *S. minor* in desert agroecosystem. Biological Control. 55, 92-96.

[15] Chitrampalam, P., Figuli, P.J., Matheron, M. E., Subbarao, K.V., Pryor, B.M. (2008) Biocontrol of Lettuce Drop Caused by *Sclerotinia sclerotiorum* and *S. minor* in Desert Agroecosystems Plant Disease. 92, 1625-1634.

[16] Clergeot, P.H., Schuler, H., Mørtz, E., Brus, M., Vintila, S., Ekengren, S. (2012) The corky root rot pathogen Pyrenochaeta lycopersici secretes a proteinaceous inducer of cell death affecting host plants differentially. Phytopathology. 102(9), 878–891.

[17] Çolak, A., Biçici, M. (2013) Integrated Disease Management of Fusarium Crown and Root Rot of Greenhouse–Grown Tomato in Eastern Mediterranean Region of Turkey. Journal of Agricultural Sciences. 19, 89-100.

[18] Çolak, A. (2007) Biocontrol Products For Use Against Tomato Diseases. Second International Symposium on Tomato Diseases, 8-12 October, Kuşadası-İzmir, Turkey. p.41

[19] Çolak, A.A., Dinçer, D., Ata, A. (2018) Determination of The Interaction Between Fusarium Crown - Root Rot Disease and Root-Knot Nematode on Tomato Genotypes. Journal Fresen. Environ. Bull. 27, 6785-6791.

[20] Cook, R.J. (1993) Making greater use of introduced microorganisms for biological control of plant pathogens. Annu. Rev. Phytopathology. 31, 53 -80.
[21] Crüger, G., Backhaus, G.F., Hommes, M., Smolka, S., Vetten, H.J. (2002) Pflanzenschutz in Gemüsebau. 4th ed. Ulmer. Stuttgart. Germany.
[22] Daami-Remadi, M., Hibar, K., Jabnoun-Khiareddine, H., Ayed, F., El Mahjoub, M. (2006) Effect of two *Trichoderma* species on severity of potato tuber dry rot caused by Tunisian *Fusarium* complex. International Journal of Agricultural Research. 1, 432-441.
[23] Duncan, D. (1955) Multiple range and multiple F-tests. Biometrics. 11, 1-42.
[24] Elad, Y., Barak, R., Chet, I. (1984) Parasitism of *Sclerotium rolfsii* sclerotia by *Trichoderma harzianum.* Soil. Bio. Biochem. 16, 381-386.
[25] Fiume, F., Fiume, G. (2003) Use of culture filtrates of Pyrenochaeta lycopersici in tests for selecting tolerant varieties of tomato. Journal of Plant Pathology. 85, 131-133.
[26] Fiume, G., Fiume, F. (2008) Biological Control of Corky root in Tomato. Comm. Appl. Biol. Sci, Gehent University. 73/2, 233-248.
[27] Fravel, D.R. (2000) Commercial Biocontrol Products Available for use Against Plant Pathogens, web: http://www.oardc.ohio-state.edu/apsbcc/productlist2005USA.htm
[28] Garibaldi, A. (1995) Soilborne pathogens in greenhouse crops and their control. Integrated Pest and Disease Management in Protected crops, 19-20 June, 1995, IAMZ, Zaragoza.
[29] Gerlach, W., Schneider, R. (1964) Nachweis eines Pyrenochaeta Stadiums bei Stammen des Korkwurzelerregers der Tomate. Phytopath Z. 50, 262–269.
[30] Grove, G.G., Campbell, R.N. (1987). Host range and survival in soil of *Pyrenochaeta lycopersici.* Plant Disease. 71, 806–809.
[31] Harman, G.E., Howell, C.R., Viterbo, A., Chet, I., Lorito, M. (2004a) Trichoderma species - Opportunistic, Avirulent Plant Symbionts. Nature Reviews. 2, 43-56.
[32] Harman, G.E. (2006) Overview of mechanisms and uses of *Trichoderma* spp. Phytopathology. 96, 190-194.
[33] Harman, G.E., Petzoldt, R., Comis, A., Chen, J. (2004b) Interactions between *Trichoderma harzianum* strain T22 and maize inbred line Mo17 and effects of this interaction on diseases caused by *Pythium ultimum* and *Colletotrichum graminicola*. Phytopathology. 94, 147-153.
[34] Harman, G.E., Kubicek, C.P. (1998) Trichoderma and Gliocladium, Vol.2, London.
[35] Harman, G.E., Lorito, M., Lynch, J.M. (2004c) Uses of *Trichoderma* spp. to remediate soil and water pollution. Adv. Appl. Microbiol. 56, 313-330.
[36] Hasna, M., Ögren, E., Persson, P., Märtensson, A., Rämert, B. (2009) Management of cork root disease of tomato in participation with organic tomato growers. Crop Protection. 28, 155-161.
[37] Hibar, K., Daami-Remadi, M., El Mahjoub, M. (2007) Induction of resistance in tomato plants against *Fusarium oxysporum* f. sp. *radicis-lycopersici* by *Trichoderma* spp. Tunisian Journal of Plant Protection. 2, 47-58.
[38] Hibar, K., Daami-Remadi, M., Khiareddine, H., El Mahjoub, M. (2005) Effet inhibiteur *in vitro* et *in vivo* du *Trichoderma harzianum* sur *Fusarium oxysporum* f. sp. *radicis-lycopersici*. Biotechnologie Agronomie Société et Environnement. 9, 163-171.
[39] Hoffman, G.M., Malkomes, H.P. (1974) Bromide residues in vegetable crops after soil fumigation with methyl bromide. Agric. Environ. 1, 321-328.
[40] Howell, C.R. (2003) Mechanisms Employed by Trichoderma Species in the Biological Control of Plant Diseases: The History and Evolution of Current Concepts. Plant Disease. 87, 1-10.
[41] Inbar, J., Menendez, A., Chet, I. (1996) Hyphal interaction between *Trichoderma harzianum* and *Sclerotinia sclerotiorum* and its role in biological control. Soil Biol. Biochem. 28, 757-763.
[42] Jones, J.B., Jones, J.P., Stall, R.E., Zitter, T.A. (1991) Compendium of Tomato Diseases. American Phytopathological Society, St. Paul, M.N., p:14-15.
[43] Kim, J.T., Park, I.H., Ryu, K.Y., Cheon, J. UK., Yu, S.H. (2003) Corky root of Tomato caused by *Pyrenochaeta lycopersici* in Korea. Plant Pathology Journal. 19, 181-183.
[44] Koike, S.T., Subbarao, K.V., Davis, R.M., Turini, T.A. (2003) Vegetable Disease Caused by Soil Borne Pathogens. University of California, Division of Agriculture and Natural Resources, Commercial Greenhouse Vegetable Handbook, Publication. 21575, 1-13.
[45] Kucuk, Ç., Kıvanç, M. (2004) In vitro antifungal activity of strains of *Trichoderma harzianum.* Turk J..Biol. 28, 111-115.
[46] Lumsden, R.D, Lewis, J.A., Fravel, D.R. (1995) Formulation and delivery of biocontrol agents for use against soil-borne plant pathogens (unpubl. rep. cited in National Research Council. Ecologically Based Pest Management: New Solutions for a New Century. Washington, DC: Natl. Acad. Press. 144 pp.
[47] Maloy, C.O. (1993) Plant Disease Control. Principles and Practices. Printed in the United States of America. 346 p.

[48] McGrath, D.M., Campbell, R.N. (1983) Improved methods for inducing sporulation of *Pyrenochaeta lycopersici*. Plant Disease. 67, 1245-1248.

[49] McSpadden, G.B.B., Fravel, D.R. (2002) Biological control of plant pathogens: Research, commercialization, and application in the USA. Online http://www.plantmanagementnetwork.org/pub/php/review/biocontrol

[50] Monaco, C., Sisterna, M., Perello, A., Dal Bello, G. (2004) Preliminary studies on biological control of the blackpoint complex of wheat in Argentina. World Journal of Microbiology and Biotechnology. 20 (3), 285-290.

[51] Munito, A., Gilardi, G., Pome A., Garibaldi, A., Gullino., M.L. (2000) Chemical and Physical Alternatives to Methyl Bromide For Soil Disinfestation: Results Against Soilborne Diseases of Protected Vegetable Crops. Journal of Plant Pathology. 82 (3), 179-186.

[52] Ozan, S., Maden, S. (2004) Root and crown rot and wilt of tomatoes caused by fungal diseases in Ankara province. Plant Protection Bulletin. 44(1-4), 105-120.

[53] Pérez, L.M., Besoaín, X., Reyes, M., Pardo, G., Montealegre, J. (2002) The expression of extracellular fungal cell Wall hydrolytic enzymes in different *Trichoderma harzianum* isolates correlates with their ability to control *Pyrenochaeta lycopersici*. Biol. Res. 35, 401-410.

[54] Punithalingam, E., Holliday, P. (1973) *Pyrenochaeta lycopersici*. CMI description of pathogenic fungi and bacteria, No. 398, Commonwealth Agricultural Bureaux, Kew, UK.

[55] Punja, Z.K., Utkhede**,** R. (2003) Using fungi and yeasts to manage vegetable crop diseases. Trends Biotechnol. 21, 400-407.

[56] Rodgers, P.B. (1993) Potential of biopesticides in agriculture. Pesticide Sci. 39, 117-29.

[57] Sánchez-Téllez, S., Herrera-Cid, R., Besoain-Canales, X., Luz M. Pérez-Roepke, L.M., Montealegre-Andrade, J.R. (2013) *In vitro* and *in vivo* inhibitory effect of solid and liquid *Trichoderma harzianum* formulations on biocontrol of *Pyrenochaeta lycopersici.* Interciencia. 38(06), 426-429.

[58] Shishkoff, N., Campbell, R.N. (1990) Survival of *Pyrenochaeta lycopersici* and influence of temperature and cultivar resistance on the development of corky root of tomato. Plant Disease. 74, 889-894.

[59] Sivan, A., Chet, I. (1986) Biological control of *Fusarium spp.* in cotton, wheat and muskmelon by *Trichoderma harzianum.* In Microbial Communities In Soil, Ed.by V. Jensensenetal, Elsevier Applied Science Publishers. 89-95.

[60] Smolinska, U., Kowalska, B. (2018) Biological control of the soil-borne fungal pathogen *Sclerotinia sclerotiorum*, a review. Journal of Plant Pathology. 100,1-12.

[61] Srivastava, R., Khalid, A., Singh, U.S., Sharma, A.K. (2010) Evaluation of arbuscular mycorrhizal fungus, fluorescent Pseudomonas and Trichoderma harzianum formulation against *Fusarium oxysporum* f.sp. *lycopersici* for the management of tomato wilt. Biological Control. 53,24-31.

[62] Subbaro, K.V. (1998) Progress toward integrated management of lettuce drop. Plant Dis. 82, 1068-1078.

[63] Tjamos, E.C., Papvizas, G.C., Cook, R.J. (1992) Biological Control of Plant Diseases: Progress and Challenges for the Future. Plenum Press, New York and London.

[64] Tunalı, B., Tosun, C., Maldar, B.M., Meyva, G., Kansu, B. (2018) The Determination of Their Efficiency Against Fusarium Root and Crown Rot Diseases of Some Antagonistic Trichoderma and Endophytic Acremonium Isolates. Turkish Journal of Agriculture - Food Science and Technology. 6(3), 266-272.

[65] Van Beneden, S., Leenknegt, I., Franca, S.C., Hofte, M. (2010) Improved control of lettuce drop caused by *Sclerotinia sclerotiorum* using Contans combined with lignin or a reduced fungicide application. Crop Prot. 29(2), 7.

[66] Villalta, O.N., Wite, D., Hunt, J., Stewart, A., Porter, I.J. (2012) Biological control of *Sclerotinia minor* on lettuce using *Trichoderma* and *Coniothyrium* species. Acta Horticulturae. 944, 51-58 pp.

[67] Weller, D.M., Raaijmakers, J.M., Mcspadden Gardener, B.B., Thomashow, L.S. (2002) Microbial populations responsible for specific soil suppressiveness to plant pathogens. Ann. Rev. Phytopath. 40, 309-348.

[68] Workneh, F., Van Bruggen, A.H.C., Drinkwater, L.E., Shennan, C. (1993) Variable associated with corky root and Phytophthora root rot of tomatoes in organic and conventional farms. Phytopathology. 83, 581-589.

[69] Yıldız, M., Yıldız, F., Delen, N. (1991) Root diseases in greenhouse tomatoes in Turkey, studies to determine the factors. VI. Turkey Phytopathology Congress İzmir, Turkey, pp. 183-186.

[70] Yücel, S. (1994) Survey studies on fungal diseases of covered vegetable areas in Mediterranean region. Plant Protection Bulletin. 34(1-2), 23-34.

[71] Yücel, S., Ay, T., Çolak A. (2009) Effect of *Trichoderma harzianum* rifai KRL AG2 to control root rot disease (*Rhizoctonia solani, Fusarium solani*) of cucumber in protected crops . Plant Protection Bulletin. 48(2),41-47.

Received: **11.12.2019**
Accepted: **19.02.2020**

CORRESPONDING AUTHOR

Aysegul Colak Ates
Biological Control Research Institute,
Department of Phytopathology,
01321, Adana -Turkey

e-mail: aysegulcolak@hotmail.com

© by PSP Volume 29 – No. 05/2020 pages 3923-3930 Fresenius Environmental Bulletin

SELECTION OF ROOF MATERIALS DEPENDING ON COSTS OF MATERIAL AND TOTAL HEAT REQUIREMENTS IN AGRICULTURAL STRUCTURE: CASE STUDY ON SILKWORM HOUSE

Serpil Gencoglan*

Department of Biosystem Engineering, Faculty of Agriculture, Kahramanmaras Sutcu Imam University, Kahramanmaras 46060, Turkey

ABSTRACT

The objective of this study is to select roof material for silkworm house using the costs of roof material and total heat requirements (THRC). For this aim, three different silkworm house of the same size were planned, one of which had flat reinforced concrete (RCC) and the other two had gable roof, in which uninsulated galvanized sheet metal (UGSM) and sandwich panel (SP) were used. The selection of roof materials was made according to the roof materials costs and THRC. With started breeding on 1st May, the THRCs for RCC, UGSM and SP house in the 5 larvae period of silkworm were 5483, 7429, 3925 W h^{-1} and their THRC were 74.12, 94.33 and 57.19$, respectively. The THRC of the SP house was found to be 22.83% and 39.37% less than RCC and UGSM. The costs of RCC, UGSM and SP roofs were calculated as 1172.79, 873.92 and 1470.44$, respectively. The cost of UGSM roof was determined to be 25.48% and 40.57% lower than that of RCC and SP. Although the SP roof cost was the highest among the roofs', SP's THRC was the lowest among them and no dew occurred in all larvae periods on the inside surface of SP roof and also provided the more stable environmental conditions in the house during the larvae periods. That is why, SP roof could be suggested to build silkworm house the growers.

KEYWORDS:
Roof material, Roof cost, Heat cost, Dew temperature, Silkworm

INTRODUCTION

Housing is one of the basic requirements of animals which not only protects them from extreme climatic conditions but also ensures comfort to its inhabitants [1]. Design of animal housing is complicated because many environmental factors affect the production and wellbeing of living organisms [2]. The designed animal houses are built to control living animals, provide security, create a suitable production environment, and regulate environmental conditions [3]. The roof is the main component of any animal house, which gives protection from natural elements and climatic conditions such as sun, rain, wind, heat, cold and provides an aesthetic appearance to the building whose construction and maintenance is expensive [4]. Housing design and the material used for the roof play an important role in the microclimate modification and reduction of radiant heat load inside the animal house [5] and reduce fuel consumption by minimizing heat losses and have good insulation properties [6].

The most commonly used roof materials include asbestos sheets, thatch, clay tiles, reinforced cement concrete, galvanized iron sheets, plastic sheets etc., which possess some merits as well as drawbacks. Ideal roof material should have high reflectivity, low conductivity, low under-surface emissivity besides being light, strong, durable, waterproof, good looking, free from the tendency to condense moisture inside and economical [7]. The roof cost takes a considerable portion of the total cost of house construction. It is approximately 10-20 percent of the total cost. The roof cost not only changes according to the type of roof material used but also according to the design of the roof [4].

Silkworm rearing, which is supported by the state, is a traditional agricultural branch for producers. It is important that the production tools are very simple, that the product can be obtained in a short time such as 35-40 days that migration from rural areas to urban can be prevented. It is also an ecological production branch that is compatible with the environment. Consumption of mulberry leaves only in silkworm production, the use of no additives and pesticides and no waste material to pollute the environment are important advantages of this branch of production [8].

The insect producing mulberry silk is a domesticated variety of silkworms. Silkworm is one of the most important insects which produces silk thread in the form of the cocoon by consuming mulberry leaves during the larvae period. As silkworms are poikilothermic (cold blooded) insects,

they cannot regulate their body temperature. Therefore, they were greatly influenced by environmental conditions. In order to provide these conditions for the silkworm, a separate rearing house is essential. It should designed to keep the micro-climate and environmental conditions suitable for the rapid and healthy growth of silkworms and also improves the cocoon stability, quality and higher cocoon productivity [9-10]. The required temperature and relative humidity (RH) for optimal growth of silkworm range from 23 °C to 28 °C and 70% to 85% respectively [11-13].

In China, both hard plastic sheets and bamboo or clay were used on a roof to build silkworm rearing houses in hot and mild climate regions [14]. On the contrary, in Thailand rearing houses were built by using inexpensive materials like corrugated metal sheets which reflect sunlight and maintain temperature fluctuation and proper ventilation [15].

Benchmin and Jolly [16] proved that successful cocoon crops could be raised reasonably in low-cost rearing houses (six different roofs and wall material) compared to RCC houses. Rearing of silkworms in RCC houses was recorded highest cocoon yield of 56.50 kg for 40.000 larvae compared to other rearing structures. It was also inferred that it was very difficult to maintain ideal temperature and RH in these structures during summer. Bharathi and Jayaramaiah [9] studied the 5 different rearing structures on cocoon productivity in mulberry silkworm. Thatched roof with the mud side wall and thatched roof with thatched side wall were good in maintaining the micro-climate, in turn had significantly influenced the economic characters compared to other structures evaluated for their suitability in silkworm rearing. Over 8 kg for 40.000 larvae of cocoon yield was more in thatched mud house compared to RCC.

The field investigation revealed that the cocoon yield was 40.97 kg in thatched mud house, 35.01 kg in tiled house and 33.02 kg in RCC building for 40.000 larvae. The larvae duration was prolonged by a day and a half in thatched structures [17]. In shoot feeding method, 99 silkworm farmers have obtained high efficiency from thatched roof, which followed by mud casting coupled with stones Wall. It has been found ideal for rearing houses for silkworms [18]. In the medium stone house satisfactory cocoon yield was recorded 68 kg. In the RCC house, cocoon yield was reduced to 55-64 kg, compared to that of stone house. It was concluded that the size of the stone house, number of tiers, number of ventilator and airuots have a beneficial effect on cocoon yield for 40.000 larvae [10].

In Turkey, silkworms are reared twice a year, one of which is spring rearing (April, May and June) and the other is autumn rearing (August and September). However, spring rearing is more common because of more advantageous in terms of fresh mulberry leaves and economy [19-20].

In the world, there are many studies on silkworm rearing houses roof material and wall material and their effect on cocoon yield. There is a lack of information on the selection of roof material using heat-moisture balance and dew point temperature for silkworm rearing houses. Thus, the aim of this study is to select roof materials for silkworm houses according to the roof materials costs and THRC.

MATERIALS AND METHODS

Three different silkworm houses of 20.000 capacities with the same size and natural ventilation were planned, one of which had RCC and the other two had gable roof, in which UGSM and SP were used. Collecting from the meteorological station at which Mediterranean climate is prevailed [21], long-term (1980-2016 years) the temperature and RH values in May were used to calculate HR. The most suitable starting date of the silkworm rearing, depending on the emergence of mulberry leaves, was determined as 1st May to calculate the HR [22]. The HR of the silkworms, which started to be reared on 1st May, was calculated by the heat-moisture balance method for 5 larvae periods. Rearing started on May 1 was called 1st May rearing. Total silkworm rearing period was 27 days.

Silkworm producers were given silkworm eggs in the boxes by the Kozabirlik Union, each box containing ten grams or 20.000 silkworm eggs. About 18.000 instars emerged from one box, and about 2.000 died when rearing bed was cleared of old mulberry leaves and fecal matter of silkworms. About 16.000 5th instar larvae were used for calculation of HR. Since silkworm is a poikilothermic insect, it does not release heat and moisture in its surroundings except for the 5th instar stage [19-23]. The 100 instars release about urine of 40 ml in the 5th instar stage and caused a RH and for 16.000 larvae, this value is about 6.400 g [24-25].

To calculate HR of the rearing house during 1st, 2nd, 3rd, 4th and 5th larvae period, optimum RH and temperature values were taken as 85%, 85%, 80%, 70% and 70%, and 28°C, 27°C, 26°C, 25°C and 24°C, respectively [11]. The larvae periods and durations used in the calculations, the amount of water vapor given to the surroundings by the silkworms, the inside and outside temperature, the RH values, the internal and external absolute humidity values of the silkworms in the houses were given in Table 1.

RCC, UGSM and SP roof materials were selected for the silkworm houses. At the planned rearing house, only the roof materials were changed but not the floor area, wall, door and window area. The house was 6 m long, 4 m wide and 2.7 m height [26]. In the house, there were three wooden windows with 1 m x 1.2 m size and with their total

area of 3.6 m^2 (its area was taken 15% of the house floor area), and one wooden door with 1.1 x 2.0 m size (area 2.2 m^2), and briquettes with 40x20x20 cm size, which were used on the walls. The walls were plastered 2 cm from the inside and 3 cm from the outside with lime mortar [3]. Total heat transfer coefficient (U) for RCC, door and wooden windows, given by Şahin and Ünal [27], were 3.07, 3.49 and 2.56 W $m^{-2}°C^{-1}$, respectively (Table 2). The height of the RCC was 10 cm (Figure 1-3). UGSM and SP were planned as gable roof, and their angle were 18° [28] and 10° [29]. UGSM's thickness was 0.5 mm, and its U value was 6.06 W m^{-2} $°C^{-1}$ [30]. SP was 5 cm thick with a density of 40-42 kg m^{-2} and its U was 0.022 W m^{-2} $°C^{-1}$ [31].

The probability of occurrence of temperature and RH values were calculated using the Weibull method in Eq. 1 [32]. Using this method, long term (1980-2016) monthly temperature and RH data in May were used. In the calculation, the temperature and RH was determined with the contingency of 80 percent.

$$F= (m/n+1)*100 \quad (1)$$

where; F: Cumulative probability (probability of values being greater than or equal to a value), m: Number of rows of values sorted from larger to smaller, n: Number of samples.

TABLE 1
Climate data used to provide indoor environmental conditions

Larvae Period	Instar Periods (day)	Water Vapor Production (ml/100 larvae)	Temperature (°C)			Absolute Humidity (g m^{-3})		
			Indoor (ti)	Outdoor (to)	Difference (ti-to)	Indoor (qi)	Outdoor (qo)	Difference (qi-qo)
Criteria used for the period started on 1st May								
1st	4	0	28	21.5	6.5	23.25	11.14	12.11
2nd	3	0	27	21.5	5.5	22.01	11.14	10.87
3rd	4	0	26	21.5	4.5	19.54	11.14	8.40
4th	6	0	25	21.5	3.5	16.08	11.14	4.94
5th	10	40	24	21.5	2.5	15.28	11.14	4.14

TABLE 2
Heat transfer coefficient and surface areas of structural members of the designed housings.

Structural Elements	Materials	Heat Transfer Coefficient (U) (W $m^{-2}°C^{-1}$)	Surface Areas of Structural Members (m^2)		
RCC	10 cm reinforced concrete	3.07	24.00		
UGSM	Uninsulated galvanized sheet metal (0.5 mm), angle of gable roof was selected as 18°	6.06	25.24		
SP	Polyurethane-insulated 3-5 trapezoidal galvanized sandwich panels, angle of gable roof was selected as 10°	0.022	24.37		
Door	1 (1.1×2.0 m) wood door	3.49	2.20		
Window	3 (1.0×1.2 m) wood frame	2.56	3.60		
Wall	40x20x20 cm briquette / inside 2cm and outside 3 cm plaster with lime	1.96	RCC 48.20	UGSM 51.94	SP 50.22

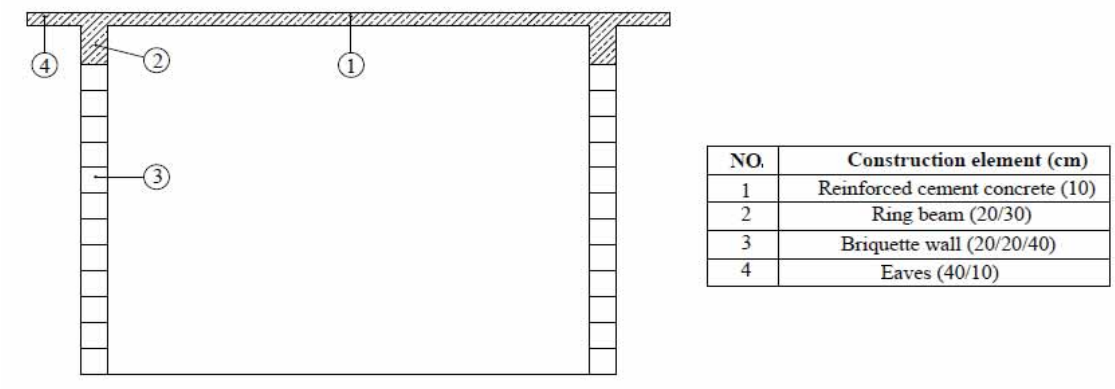

NO.	Construction element (cm)
1	Reinforced cement concrete (10)
2	Ring beam (20/30)
3	Briquette wall (20/20/40)
4	Eaves (40/10)

FIGURE 1
Cross section of reinforced cement concrete roof

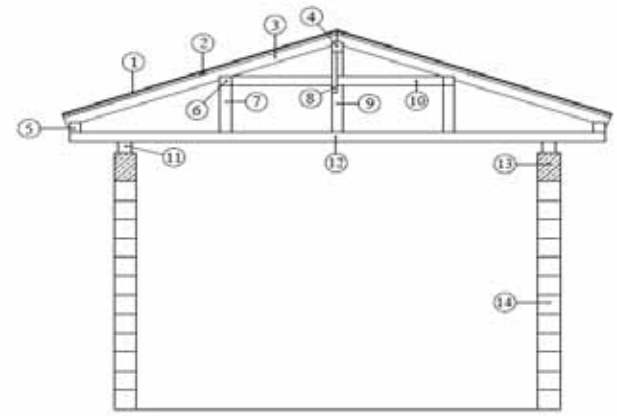

NO.	Construction element (cm)
1	Roof sheeting
2	Batten (3/5)
3	Rafter (5/10)
4	Ridge (10/10)
5	Ridge (10/10)
6	Ridge (10/10)
7	Stud(10/10)
8	Strut (5/10)
9	Stud (10/10)
10	Collar tie (2x5/10)
11	Beam (12/12)
12	Beam (10/10)
13	Ring beam (20/30)
14	Briquette wall (20/20/40)

FIGURE 2
Cross-section of uninsulated galvanized sheet metal and sandwich panel roof

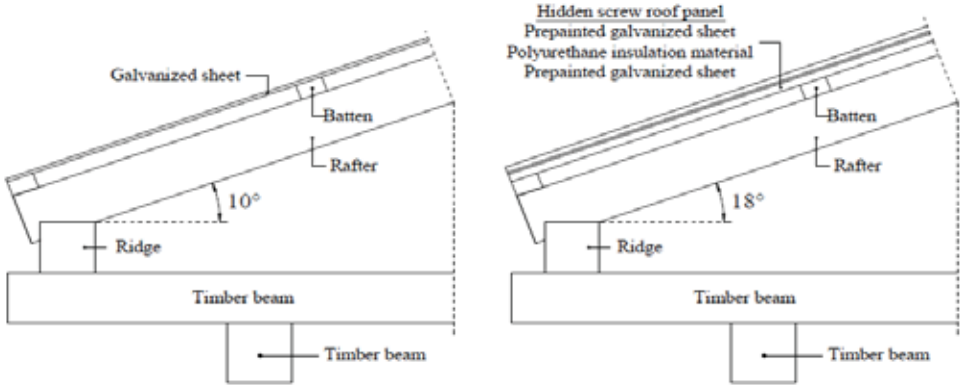

FIGURE 3
Roof details of uninsulated galvanized sheet metal and sandwich panel

Theoretical method was used to calculate the HR of three houses for the 1st, 2nd, 3rd, 4th and 5th instar stages [33]. Equations 2-7 were used to estimate heat-moisture balance.

$$Q_s = q_c + q_v \quad (2)$$

where; Q_s: Sensible heat released by the silkworm larvae to ambient (W), q_c: Total heat loss through structural members (roof, door, window, wall) (W), and q_v: Heat loss through ventilation (W).

The Q_s of silkworm in the 1-4. larvae period were taken equal to the heat lost (q_c) through the total structural elements. In the 5. larvae period, Q_s was equal to the sum of the heat lost (q_c) through the housing elements and the heat (q_v) lost by the ventilation.

Heat loss through the structural members (q_c) was calculated by using the following equation:

$$q_c = \sum U.\ A.\ \Delta t \quad (3)$$

where; $\sum U$: Total heat transfer coefficient of structural members (W m^{-2} $^oC^{-1}$), A: Surface area of structural members (m^2), Δt = ti – to, where ti is indoor and to is outdoor temperature (^oC).

U of structural member was calculated by using the following equation:

$$U = \frac{1}{\frac{1}{fi} + \sum_{i=1}^{n} \frac{di}{ki} + \frac{1}{fo}} \quad (4)$$

where; fi and fo: Surface heat transfer coefficient of inner and outer surfaces (W m^{-2} $^oC^{-1}$), d (m) and k (W m^{-1} $^oC^{-1}$) are, respectively, structural member thickness and heat transmission coefficient.

Heat loss through ventilation from the silkworm rearing house was calculated by the following equation:

$$q_v = 0.341 * Q * \Delta t \quad (5)$$

where; q_v: Heat loss through ventilation (W), 0.341 is the amount of heat required to increase temperature of 1 m^3 of air by 1 ^oC (W h m^{-3} $^oC^{-1}$), Q: Minimum air flow rate (m^3 h^{-1}).

Ventilation applied to control humidity should be based on moisture balance. The minimum air flow rate, Q, required to maintain the indoor moisture constant within the design criteria for the silkworm rearing house was calculated by the following equation [34-35]:

$$Q = \frac{\sum wa}{qi - qo} \quad (6)$$

where; $\sum wa$: Total amount of water vapor released by silkworm larvae (g h^{-1}), qi-qo: absolute humidity of indoor and outdoor air (g m^{-3}).

The internal surface temperatures of 3 roofs were calculated by the following equation, which were compared with the references dew point temperatures [36].

$$t_s = t_i - \frac{U}{f_i}(\Delta t) \quad (7)$$

where; t_s is the inside surface temperature of structural elements (ºC), f_i is inside surface heat transfer coefficient of roof material (W m^{-2} ºC^{-1}).

THR cost of the silkworm rearing house was calculated for May using by Equation 8.

$$THRC = \frac{\sum_{i=1}^{5}(Q_{s_i} x LP_i x 24)}{1000} xEUC \quad (8)$$

where; THRC is THR cost ($). Q_{si} is HR for per larvae periods (W h^{-1}). LP_i is larvae period (4,3,4,6,10 day). 24 is number of hours per day. EP was electricity price of 0.0938 $ per Kwh^{-1} in May 2019.

By Using Construction and Installation Unit Prices given by Anonymous [37] in 2019, roof material costs for RCC, UGSM and SP were calculated according to Anonymous [38]. The selection of roof materials was made according to costs of roof materials and THRC

RESULTS AND DISCUSSION

With 80% probability, analysis of long-term outdoor temperature and RH for May were predicted as 21.5 ºC and 58.7%. Based on these indoor and outdoor temperature and RH values, absolute humidity values were calculated as 15.28-23.25 g m^{-3} and 11.14 g m^{-3}, respectively (Table 1). Net wall and roof areas of houses with RCC, UGSM and SP were calculated as 48.2, 51.94 and 50.22 m^2, and 24.0, 25.24 and 24.34 m^2, respectively. The calculated U for wall and UGSM were 1.96 and 6.06 W m^{-2} °C^{-1}. U values of RCC, UGSM and SP were 3.07, 6.06 and 0.022 W m^{-2} °C^{-1}, respectively. According to Narwaria et al [7], one of the important features of an ideal roof is its low U value. Accordingly, in terms of U, SP can be said to be a more ideal roof material than others. The other two have higher U values which are inversely proportional to the material thickness (d) and is directly proportional to the heat transmission coefficient (k). In order to reduce the U, either the thickness of the material should be increased or the additional insulation material should be used.

The HR for the 5 larvae periods for the RCC, UGSM and SP were calculated as 1203, 1018, 833, 648 and 1781 W h^{-1}, 1765, 1494, 1222, 951 and 1997 W h^{-1}, and 753, 637, 521, 405 and 1608 W h^{-1}, respectively (Figure 4). As seen in the Figure 4, HR decreased from 1st to 4th larvae period and again increased in the 5th. The highest HR was determined in the 5th larvae period and the lowest in the 4th larvae period. The reason for being the highest HR was that the silkworm gave urine to the environment in the 5th larvae period. The cause of being the lowest HR was the decrease of the internal and external temperature difference in the 4th larvae period. In addition, according to the roof material, it was found to be the highest HR for UGSM and the lowest for SP roof material in the all 5 larvae periods. When the HR was compared in the all larvae periods, the SP's HR was 57.33-57.41% and 37.35-37.45% less than that of UGSM's and RCC's. And also in the 5th larvae period, the HR of SP was 19.47% and 9.71% less (Figure 4). THRs for RCC, UGSM and SP were found as 5483, 7429, and 3925 W h^{-1}. Using the Eq. 8, the THRC for RCC, UGSM and SP were calculated as 74.12, 94.33 and 57.19 $, respectively. As stated by Ergün and Kürklü [6], the THRC varied depending on the THR, which chanced depending on U of the roofs. In the UGSM roof with the highest U value, THRC was the highest and conversely, in the SP roof with the smallest U value, it was the lowest. When SP's THRC was compared with that of the RCC and UGSM, it was found to be lesser with 22.84 % and 39.37.

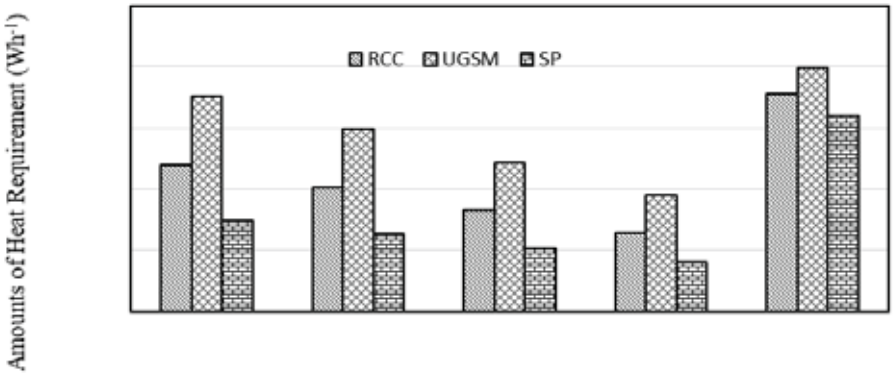

FIGURE 4
Heat requirements of silkworm larvae for different roof materials

The costs of RCC, UGSM and SP roofs constructed on reinforced concrete structure were calculated as 1172.79, 873.92 and 1470.44$, respectively (Table 3). The lower the U value of SP roof, the higher its cost. In this context, the costs of the roofs ranged from high to low as SP, RCC and UGSM depending on U value. The roof cost was the lowest in UGSM and the highest in SP when compared to the others. The cost of UGSM was determined to be 25.48% and 40.57% lower than that of RCC and SP. Roof cost, as is said by Perera and Fernando [4], is approximately 10-20 percent of the total cost and not only changes according to the type of roof material used but also according to the design of the roof.

TABLE 3
Costs of roof materials

Roof Materials	Roof Material Costs ($)
RCC	1172.79
UGSM	873.92
SP	1470.44

Calculations showed that there was no dew on the surface of the SP roof in all larvae periods. In the RCC and UGSM roofs, moisture condensation occurred only in the 1st, and in the 1st and 2nd larvae period. When U value of roof is lower like SP roof's U, dew point temperature gets higher and possibility of dew occurrence decreases (Gençoğlan et al 2019). According to this dew point results, the most suitable roof material was determined as SP. However, none roof materials possess all the desired properties [7]. In order to avoid moisture condensation on the structural materials, the calculated internal surface temperatures for different roof materials were given in Table 2. They should be equal to or above the referans dew point temperature (Table 4) by [36]. If there is a possibility of moisture condensation on the roof, the material used for roof materials must be replaced or the U of the same material should be reduced. Also, according to Pawar et al [26], silkworm rearing houses should be ventilated well.

Although the SP roof material cost (1470.44$) was the higher than the roof cost of RCC (1172.79$) and UGMS (873.92$), SP's THRC (57.19 $) was the lower than thats of RCC (74.12$) and UGMS (94.33$) and since low U (0.022 W m^{-2} $°C^{-1}$) of SP was, no dew accured in all larvae periods on the inside surface of SP roof. Also it can provide the more stable environmental conditions in the house with SP roof during the larvae periods [3-4]. In the more stable environmental conditions, the more the cocoon yield is harvested [17]. SP's THRC will pay off the roof cost of SP over the coming years. So, SP roof can be suggested to build a silkworm house to the silkworm growers.

TABLE 4
Dew point temperature of rearing house with different roof materials

Stages	Different Roof Materials: RCC	UGSM	SP	Dew point temperature
	Start of Rearing 1st of May			
1st	25.15	22.37	27.97	25.50
2nd	24.59	22.24	26.98	24.00
3rd	24.03	22.10	25.98	22.00
4th	23.46	21.97	24.99	21.00
5th	22.90	21.84	23.99	18.00

CONCLUSIONS

As a result, THRCs, roof material costs and dew were evaluated in the silkworm house with 3 roofing materials. SP roof has the important features such as providing a more stable environment, low THRC, no moisture condensation during all developmental periods of silkworm, possibility of higher yield. But it has higher cost. None roof materials possess all the desired properties [7]. Accordingly, SP roof can be preferred to build silkworm house.

REFERENCES

[1] Thomas, C.K., Sastry, N.S.R., Ravikiran, G. (2012) Dairy Bovine Production. 2nd revised edition, Kalyani Publisher, Ludhiana. pp. 125.
[2] ASHRAE. (2015) Environmental Control for Animals and Plants. Heating, Ventilating, and Air-Conditioning Applications. Atlanta.
[3] Olgun, M. (2016) Agricultural Structures. Ankara University, Faculty of Agriculture, Department of Agricultural Structures and Irrigation. Publication No: 1577, Course Book: 529, 450 p. (in Turkish).
[4] Perera, R.S. and Fernando, U.L.A.S.B. (2002) Cost modelling for roofing material selection. Built Environ. Sri Lanka. 3(1), 11-24.
[5] Badino, F. (2007) Helping cows to regulate body heat. Informative Agarino Supplemento. 62 (39), 18-21.
[6] Ergün, A. and Kürklü, G. (2008) Detail errors, results and correction studies in roof design and application. 4th Contemporary Materials and Technologies in National Roof & Facade Coverings" Symposium, İstanbul Technical University, Faculty of Architecture. Taşkışla, Istanbul. October 13-14, 2008. (in Turkish).
[7] Narwaria, U.S., Singh, M., Verma, K.K., Bharti, P.K. (2017) Amelioration of thermal stress using modified roof in dairy animals under tropics: A Review. J. Anim. Res. 7(5), 801-812.

[8] Sahan, Ü. (2011) Silkworm Textbook, Dora Publishing. Publication No: 15366, Bursa. (in Turkish).
[9] Bharathi, V.P. and Jayaramaiah, M. (2009) Impact of rearing houses on cocoon productivity in mulberry silkworm. Bull. Ind. Acad. Seri. 13(1), 49-53.
[10] Anusha, H.G. (2013) Studies on farmers practices of silkworm (*Bombyx mori* L.) rearing and in vivo Bacillus infection in zone–5 (Kolar and Chikkaballapur districts). M.Sc (Agri.) in Sericulture Thesis, pp:121. Department Of Serıculture University of Agricultural Sciences Gkvk, Bangalore.
[11] Rahmathulla, V.K. (2012) Management of climatic factors for successful silkworm (*Bombyx mori* L.) crop and higher silk production. Psyche. pp. 1-12.
[12] Devi, R. and Karuna, T. (2012) Silk worming rearing technology for the course of sericulture. (Accessed:5.6.2012) http://www.scribd.com/.../ Silkworm-Rearing.
[13] Bhaskar, R.N. and Anusha, H.G. (2015) Role of micro environment in the rearing house a boon for quality cocoon production in eastern dryzone of karnataka. Proceedings of the International Conference on Science Connecting Healty and Society Held at Colombo, Sri Lanka. 28-29 November 2015.
[14] Anonymous. (1980) China Sericulture. FAO. United Nations, Rome, pp. 42-43.
[15] Anonymous. (1993) Techniques in silkworm rearing in the tropics. United Nations, New York. 34-38.
[16] Benchmin, K.V. and Jolly, M.S. (1987) The principles of silkworm rearing, In Proc. Natn. Semin. Seric. Mahalingam, S. (Ed.) University of Madras. pp.63-108.
[17] Gangawar, S.K., Somasundram, P., Nataraja, N. (1993) Silkworm rearing performance under different rearing houses in Tamil Nadu. Indian Silk. 32(7), 37-38.
[18] Anonymous. (1982) Report of survey on crop production and cocoon loss: world bank project-A, UAS, Bangalore.
[19] Anonymous. (2018) Silkworm. Title change exam, technician course note. (Accessed: 11.7.2018) http://www.tarim.gov.tr /PERGEM /Link/124/Unvan-Degisikligi-Ders-Notlari ipekböcekciligi.pdf. (in Turkish).
[20] Anonymous. (2018) 2017 Silkworm report. T.C. Ministry of Customs and Trade. General Directorate of Cooperatives. (Accessed: 15.4.2018) http://www.ilikebugs.com/articles/ class_notes.pdf. (in Turkish).
[21] Anonymous. (2017) Climate data of Kahramanmaraş province. Meteorology Directorate (in Turkish).
[22] Gençoğlan, S. and Başpınar, A. (2016) Determination of the silkworm (Bombyxmori L.) Heat requirements in rearing room of village house for optimal environmental conditions. Pak. J. Zool. 48(2), 557-561.
[23] Wu, D.J. and Hou, R.F. (1993) Relationship between thermo tolerance and heat-stable esterase in the silkworm, Bombyxmori. Appl. Entolomol. Zool. 28(3), 371-377.
[24] Inal, Ş. (2000) Silkworm rearing. (Accessed: 17.11.2015) http://www.veteriner.selcuk.edu.tr/ veteriner/not_soru/ipek.htm. (in Turkish).
[25] Anonymous. (2018) Silkworm rearing press release.(Accessed:11.7.2018) http://ww.belekomahaber.com/ipekbocekciligi-yetistiriciligi-basin-aciklamasi/ (in Turkish).
[26] Pawar, A., Supekar, Y., Shinde, M., Pandhare, S., Nagare, P.S. (2017) Optimization in comfort conditions of silkworm rearing house. Int. J. Gen. Sci. Eng. Res. (IJGSER), ISSN 2455-510X. 3(2), 122-125
[27] Sahin, A. and Ünal, H.B. (2005) Building Material Knowledge. Ege University Publications. Faculty of Agriculture, Publication No: 568, page: 316. (in Turkish).
[28] Ekmekyapar, T. (1997) Agricultural Construction. Atatürk University, Faculty of Agriculture, Publication No: 151. page: 197. (in Turkish).
[29] Anonymous. (2016) Metal panel roof cover material feature. (Accessed: 1.8.2017) http://www.4emetal.com/teknik-bilgiler.html. (in Turkish).
[30] Öztürk, T. (2003) Agricultural Structures. Ondokuz Mayıs University, Faculty of Agriculture, Course Book: 49. Samsun. (in Turkish).
[31] Anonymous. (2019) Panelsan Catalog PDF. (Accessed: 25.9.2019) https://www.timas.net /2016/01/sandvic_cati_panelsan_katalog.pdf. (in Turkish).
[32] Gençoğlan, S., Başpınar, A., Gençoğlan, C. (2019) Determination of appropriate rearing period and roof covering material for silkworm rearing by heat requirement and dew point temperature. Mediterranean Agricultural Sciences. 32(1), 65-71.
[33] Lindley, J.A. and Whitaker, J.H. (1996) Agricultural Building and Structures. ASAE, USA.
[34] Albright, L.D. (1990) Steady-state energy and mass balances. Environment Control for Animals and Plants. Michigan-USA. pp. 143-320.
[35] Anonymous. (1994) ASAE Agricultural standards, ASAE, 41 st Edition. USA.
[36] Anonymous. (2018) dew point temperature at atmospheric pressure in degrees celsius. (Accessed:19.9.2019) http://www.nationalcompressedair.com/dat/files/pdf. (in Turkish).

[37] Anonymous. (2019) Environment and urbanization construction and installation unit prices for 2019. (Accessed: 28.8.2019) http://www.tesisat.org/insaat-ve-tesisat-birim-fiyatlari.html (in Turkish).
[38] Anonymous. (2019) Structure approximate cost calculation. (Accessed: 28.8.2019) http://www.istabul.imo.org.tr/resimler/dosya_ekler/ek.pdf. (in Turkish).

Received: **13.12.2019**
Accepted: **19.02.2020**

CORRESPONDING AUTHOR

Serpil Gencoglan
Department of Biosystem Engineering,
Faculty of Agriculture,
Kahramanmaras Sutçu Imam University,
Kahramanmaras 46060 – Turkey

e-mail: sgencoglan@ksu.edu.tr

© by PSP Volume 29 – No. 05/2020 pages 3931-3939 Fresenius Environmental Bulletin

CONTROL OF RESERVOIR ACCUMULATION BY SYNSEDIMENTARY FAULT IN SUNING OILFIELD, RAOYANG DEPRESSION, CHINA

Yi Li[1,*], Yuzong Cheng[2], Lan Zhang[2], Linlin Xie[2], Jing Chen[1], Shijing Zheng[1]

[1]Tianjin Zhengfang Science and Technology Development Co. Ltd., Tianjin 300270, China
[2]No. 3 Oil Recovery Plant of PetroChina Huabei Oilfield, Cangzhou 062450, China

ABSTRACT

The Suning Oilfield is located in the oil-producing trough in the eastern part of the Raoyang Sag. The main oil-bearing strata are the Es1 and Ed3 Member. The sedimentary faults are very developed and belong to tectonic-lithologic reservoirs. However, the current understanding of reservoir formation is still unclear: First, the formation of high-oil reservoirs is not ideal, and there are many failed wells for exploration; second, the low-lying down plates often obtain high-yield wells; and third, the faults in densely-drilled areas are prone to high yields. Based on a comprehensive study of geophysical, logging, geological and oil-producing production data, the following accumulation laws of the oilfield are found: the sedimentary fault can provide both oil and gas migration channels and control sand body deposition. Large faults with direct faults on the surface often have multiple fault activations, and there are many oil and gas losses in nearby reservoirs. The formation of the near-construction transition zone is the descending disk of the reverse normal fault. Because of its small hydrocarbon migration resistance and short distance, it is easier to accumulate. The sand body with dense faults is constructed, and the oil and gas supply is sufficient and easy to form. Directional wells with fault planes are more likely to drill high-yield reservoirs while wells far from faults have low success rates.

KEYWORDS:
Synsedimentary fault, transform fault zone, mantle, accumulation characteristics, Paleogene, Suning Oilfield

INTRODUCTION

Suning Oilfield is a relatively small oilfield in the area of Raoyang Sag in the Jizhong Depression. However, Ning 79X, Ning 2 and Ning 303 located in the Suning oilfield have been found in many high-production wells (the average daily oil production is greater than 10 tons). At present, the research on Suning Oilfield mainly focuses on the overall structural division [1], large-area fault evolution, deep buried hill structural transition zone [2], hydrocarbon accumulation [3-4], regional lithological oil and gas, and the distribution of Tibetan sedimentary facies [5]. The unclear understanding of the reservoir formation laws of Suning Oilfield makes some exploration phenomena unexplainable. For example, two exploration wells are less than 1km apart, and one well produces oil and the other produces water. The wells located in high structural positions have almost no oil production capacity while the adjacent structural low-wells have strong oil production capacity.

High-production wells are often associated with Cenozoic co-sedimentary faults, indicating that Cenozoic fault activity is closely related to hydrocarbon accumulation. Co-sedimentation faults are widely developed in petroleum-bearing basins, and their distribution and activities are closely related to hydrocarbon accumulation [6-9], the accumulation of oil-bearing basins. In addition, these faults affect the geological processes of oil and gas generation, migration, accumulation, and preservation [10-12]. It is of great significance to analyze the activity of the main syn-sedimentary faults in the oilfield and its influence on reservoir formation for the fine exploration and development of the old oilfield. The author analyzes the Cenozoic fault activity in Suning Oilfield using three-dimensional seismic data and drilling, logging, and test production data. On this basis, the author explores the controlling effect of fault activity on oil and gas accumulation which could provide a basis for further oil and gas exploration and development.

GEOLOGICAL BACKGROUND AND METHODS

The Raoyang Sag is located in the central and southern part of the Jizhong Depression in the Bohai Bay Basin. The Cenozoic strata have a tectonic pattern of east-west sub-zone characteristics [13-14]. Under the joint control of the Masi-Hejian-Liulu boundary faults on the east side, from east to west, it can be divided into buried main tectonic belts of eastern faults, eastern main depressions, central uplifts, western secondary depressions, and Yixian

Slope zone. Controlled by boundary fault segmentation activities and separated by internal structural transformation zones, three north-north eastward depressions, such as Masi, Hejian, and Raonan, have developed from north to south. Suning Oilfield is located in the middle of the Raoyang Sag. The fault and the inter-heavy depression controlled by the Dawangzhuang fault (Figure 1a).

The Suning Oilfield experienced 4 tectonic-sedimentary evolution stages during the Cenozoic [12, 14]: 1) The deposition period of the Kongdian Formation to the fourth member of Shahejie Formation (Ek-Es4). 2) Sedimentary period of Sha 3 Member to Sha 2 Member of the sedimentary period (Es3-Es2) 3) The first period of the Shahejie Formation-Dongying Formation (Es1-Ed) and 4) the stage of depression since the Neogene (N-Q). Since the Neogene, under the control of the overall thermal subsidence depression in the Bohai Bay Basin, the study area is characterized by stable subsidence, with weak or even stagnation (Figure 1b).

We collected the three-dimensional seismic data and drilling, logging, and test production data from the target area and then do the analysis.

RESULTS

Characteristics of vertical and horizontal fault development. (1) Vertical fault development. The study area can be clearly divided into two structural belts, namely the northern geomorphic structural belt and the southern transitional fault structural belt (Figure 2). The overall structural pattern is controlled by large sedimentary faults between rivers in the east. The overall trend of the stratum is gradually thickening from the northwest to the southeast. The overall structural pattern is high in the northwest and low in the southeast. The exploration wells are all located in the geomorphology with smaller sedimentary faults located in the middle of the structure. The faults in the geomorphology are mainly from the first member of the Shahejie Formation to the second member of the Donghe Formation. The fault activity in the eastern part of the period basically stopped, and the filling effect mainly occurred. The northern loquat is controlled by these syn-sedimentary faults and is divided into several small fault blocks.

The main survey line through the northern part of the study area (left in Figure 2) shows that the northern geomorphic structural belt is affected by multiple syn-sedimentation faults that trend towards the south-north direction. The main faults are from the Es1 to Ed3 sedimentary period, and the thickness of the strata is also obviously thicker from northwest to southeast.

The liaison line passing through the study area (right of Figure 2) shows that the southern transition fault structural belt is affected by two oppositely-synchronized syn-sedimentation faults that move towards the near southwest-northeast. The active period of the main faults is the sedimentary period of Es1 to Ed3. Therefore, due to the influence of co-sedimentary faults, the thickness of the strata gradually increases from southwest to north.

(2) Combination feature of fracture plane. The southern tectonic transition zone is mainly composed of two large faults (faults ⑤ and ⑥) running in the east-west direction and three regulatory faults sandwiched by the two large faults (Figure 3).

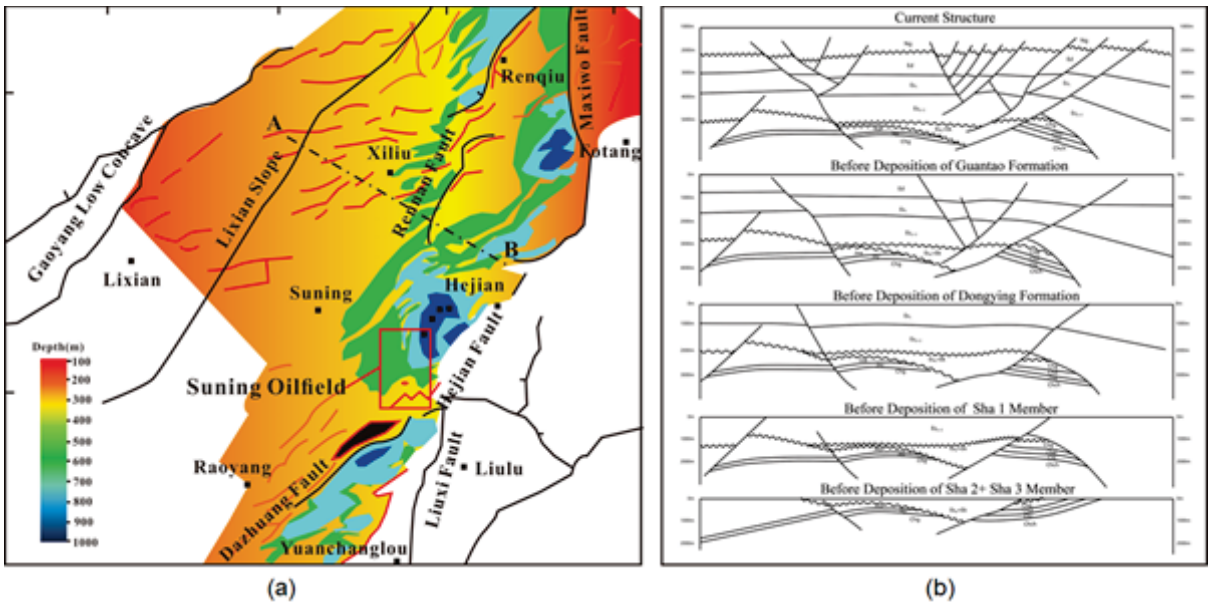

FIGURE 1
Information about the Suning Depression.
Notes: (a)Regional structural pattern of Suning Depression, (b) the evolution profile Suning Depression

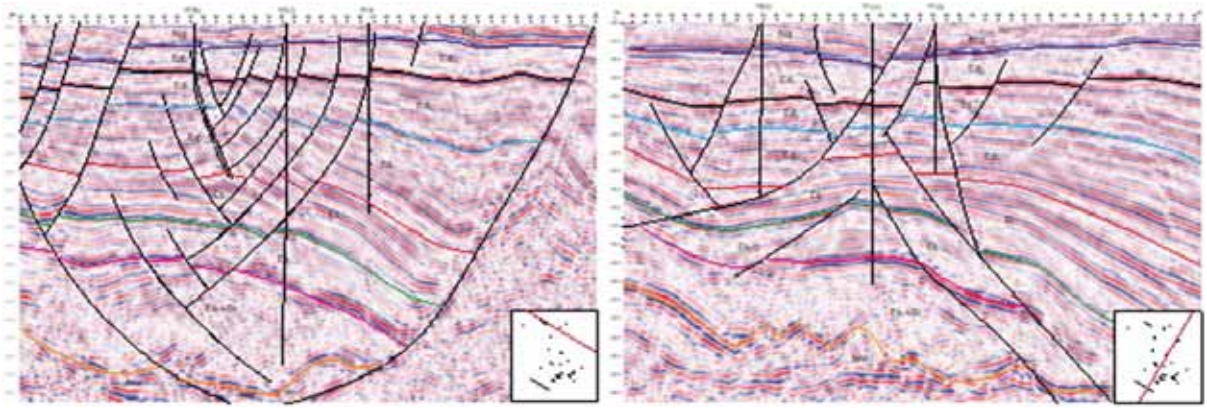

FIGURE 2
Seismic sections of the northern geomorphic (left) and southern structural transition zone (right) of the Suning Oilfield.

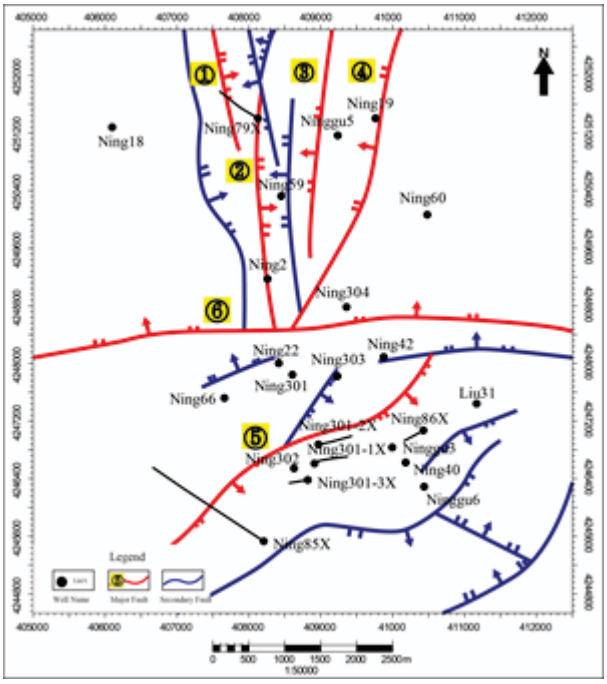

FIGURE 3
Bottom structure interpretation fault distribution map of the eastern third member of Suning Oilfield.

The fault ⑥ goes east-west, tends to the north, and extends 6km horizontally. The fault distance gradually increases from west to east. It divides the work into two regions with distinct structural features from north to south. The fault ⑤ goes southwest-northeast, tends to the southeast, and extends horizontally for 4km. The fault distance gradually increases and decreases from the southwest end to the northeast end. The apparent fault distance and horizontal fault distance reach the maximum near Ning 302 well. The three regulatory faults in the central uplift have shorter lateral extension distances, and the two regulatory faults in the north move closer to the east and west, which are the same as the major faults in the north and parallel. The southern regulatory faults run southwest-northeast. The central uplift zone is divided into east and west up and down.

The northern ridge area consists of eight faults that intersect near the north and south (Figure 3). Bounded by Well Ning59, the co-sedimentary faults to the west of this well tend to be east, and the faults to the east of this well have exactly the opposite tendency. The geomagnetism center is near Well Ning 59 and Ning 79x. The fault west of Well Ning59 goes to the north and south. The horizontal fault distance does not change sharply (less than 120m) and the vertical fault distance is small. However, the horizontal fault distances of the two large faults between Well Ning59 and Ning60 are smaller than those in the west. The faults (larger than 200m) gradually decrease from north to south. This geomorphological structure divides the target layer into six independent fault blocks from west to east. At present, each fault block is encountered by a well.

(3) Fault activity. The characteristics of fault activity are an important part of the analysis of petroliferous basins, and there are many research methods. The characteristic of the study area is that the floor reflection (T2) of the pavilion as the regional landmark layer is basically free of obvious faults. Therefore, the fault activity of this layer can be determined according to the vertical fault distance of other layers below the pavilion. The vertical fault distance is quantitatively characterized by measuring the time domain of T2 to T5 (sand bottom reflection in the sand) near the fault to characterize the activity intensity of the fault in a certain geological period. Select the time domain profiles of the main seismic lines for the structural transition zones in the north and the south, and then select the main faults that play a vital role in tectonic evolution and oil and gas accumulation. The fault distances at the isochronous stratigraphic interface and the Cenozoic fault activity characteristics in the study area are analyzed based on the strength of the fault distances at the interfaces in each time domain.

The comparison table of the vertical fault distances of the four main faults in the northern shoal area shows that the faults ① and ② tending to the east on the west side do not develop in the Shahejie fault, and the activity of the fault in the Es3 section is enhanced. The activity weakened until the Guantao fault ceased to be active. The faults ③ and ④ that tended to the west on the east side of the northern part of the ridge were always active during the sedimentary period from Shahejie to the Guantao Formation, and the fault distances of fault ④ in the same period are larger than faults ③. The fault reached the peak of growth fault activity in the Eds segment. After entered the Ed2 period, the fault activity gradually weakened, and there were still signs of activity until the Guantao period (Figure 4 left, Figure 5 left).

In the southern structural transition zone, two main faults controlling the structural transition zone were selected. According to the comparison table of vertical fault distances, the faults ⑥ tending to the north on the north side are violent in the Shahejie fault, and the vertical fault distance is large. The activity is the strongest in Es1 formation, and the activity of the fault entering the Es3 gradually weakens. The fault entering the Es2 becomes inactive, and the activity of the fault entering the Es1 weakens until the Guantao fault starts to work again. The fault⑤ activities during the deposition period of the Es3 were relatively intense, with the strongest activity at the upper and lower parts of the Es1, and the second-strongest activity in the middle of the Es3. The activity stopped at the Guantao fault (Figure 4 right, Figure 5 right).

Controlling effect of syn-sedimentation faults on reservoir formation. (1) Control of reservoir deposition. Co-sedimentation faults control the deposition by causing the migration of the deposition center, controlling the migration path of source debris after entering the depression, and controlling the spatial distribution of the deposition system due to the inheritance of fault activities [15]. The author extracted sand-land ratios from the logging data of the drilled wells in the Ed3 and Es1 sections of the sandstone as the plane distribution law and applied the 3D seismic data volume to extract the target ant body as the fault plane distribution law.

After superimposing the horizontal section of the ant body and the sandy land ratio according to the coordinates, the following rules can be found. Wells with a high sandy land ratio are often associated with faults and wells with a low sandy land ratio are often located in areas with less densely developed faults (Figure 6).

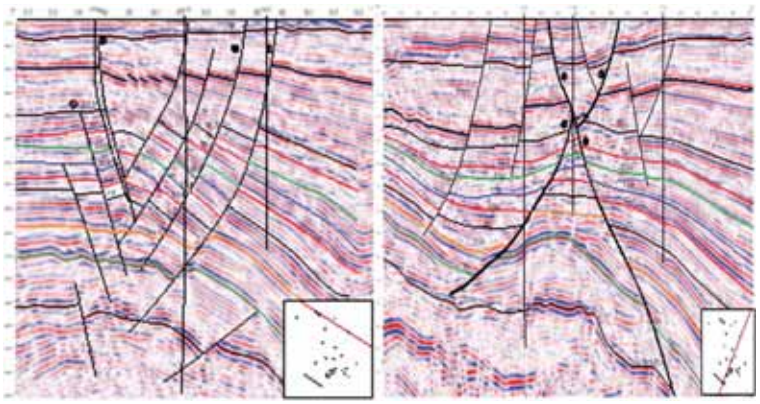

FIGURE 4
Interpretation of the structure of the main line through the northern part of the ridge (left) and the southern structural transition zone (right).

Notes: T2: Bottom of the Guantao Formation; T3_0: Bottom of the East 2nd Segment; T3_1: Bottom of the 1st Formation of the East 3rd Segment; T3_2: Bottom of the 2nd Formation of the East 3rd Segment; T3_3: Bottom of the 3rd Formation of the East 3rd Segment; T3_4: Bottom of the East 3rd Segment 5 The bottom of the sand group; T3: the bottom of the eastern third section; T4-1: the bottom of the upper section of Sha 1; T4: the bottom of the lower section of Sha 1; T5: the bottom of the second section of Sha 2.

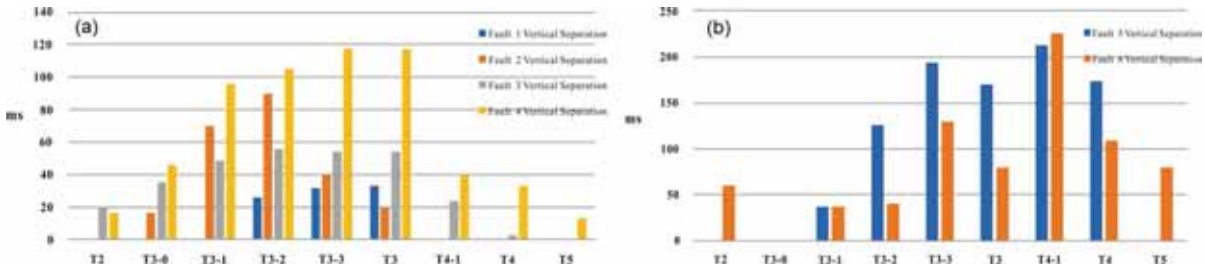

FIGURE 5

Statistical results of Paleogene mean vertical faults in the main faults of the Raoyang Sag oilfield.

Notes: (a) Comparison of vertical fault distance of northern graben, (b) Comparison of vertical fault distance in southern structural transition zone

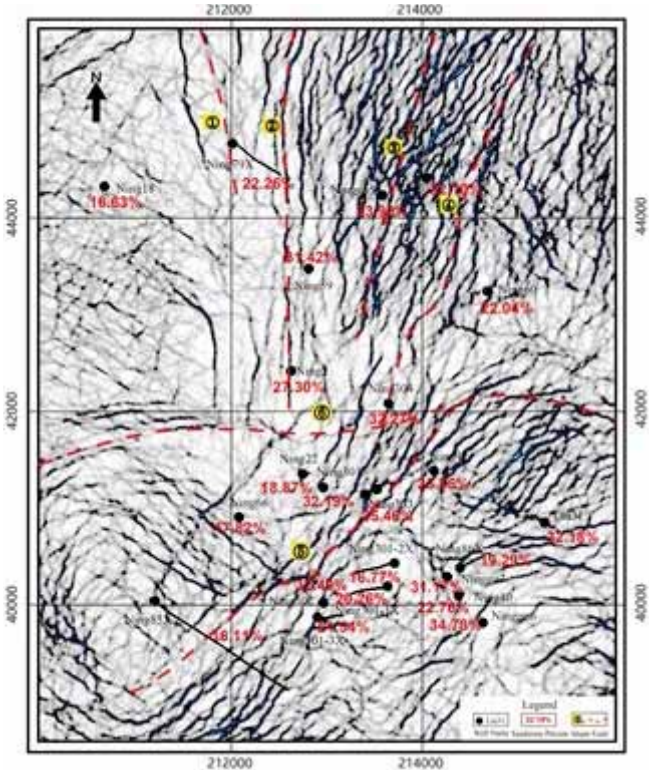

FIGURE 6

Overlapping map of ant body section and target sand ratio in Suning Oilfield.

For example, in the northwestern Ning 18 well, the sandy land ratio is 16.63%, and there is a lack of large faults in the vicinity. In the northern ravine area, the sandy land ratios in the densely populated areas are all greater than 30%, The flank of the sandy land gradually decreases toward the sides of the ridge, such as 22.79% in Well Ning 79X and 22.04% in Well Ning 60. The distribution ratio of sandy land ratio in the southern structural transition zone can also confirm this. The sandy land ratio of Wells Ning 66 and Ning 22 in the ascending plate is less than 20%, but due to the dense fractures in the nearby Well Ning 301, the sand to land ratio is as high as 32.19. %. The well Ning 302 in the descending plate is close to the fault, and the sand ratio is 32.49%. The sand to land ratio of wells Ning 301-1X, Ning 301-2X, and Ning 301-3X far from the fault is significantly reduced.

Further cross-well earthquakes and comprehensive sedimentary facies studies have found that the sand body distribution law of the Suning Oilfield conforms to the following model (Figure 7). The southern structural transition zone divides the study area into two sedimentary depressions: south low, middle high, and north low. The continuous activities of sedimentary faults ⑤ and ⑥ make the southern depression have enough space to accommodate, abundant sediment supply, and sand body development. In particular, the Late Es1and Early Ed3 periods with active co-sedimentary faults, the sand bodies in the study area are generally relatively developed, entering the Late Ed3 period, the syn-sedimentary faults are not active and the sand bodies are underdeveloped. The northern geomorphic area is the structure inside the northern sag of the structural transition zone. A set of homogeneous sedimentary faults (such as faults ①②③④) with opposite

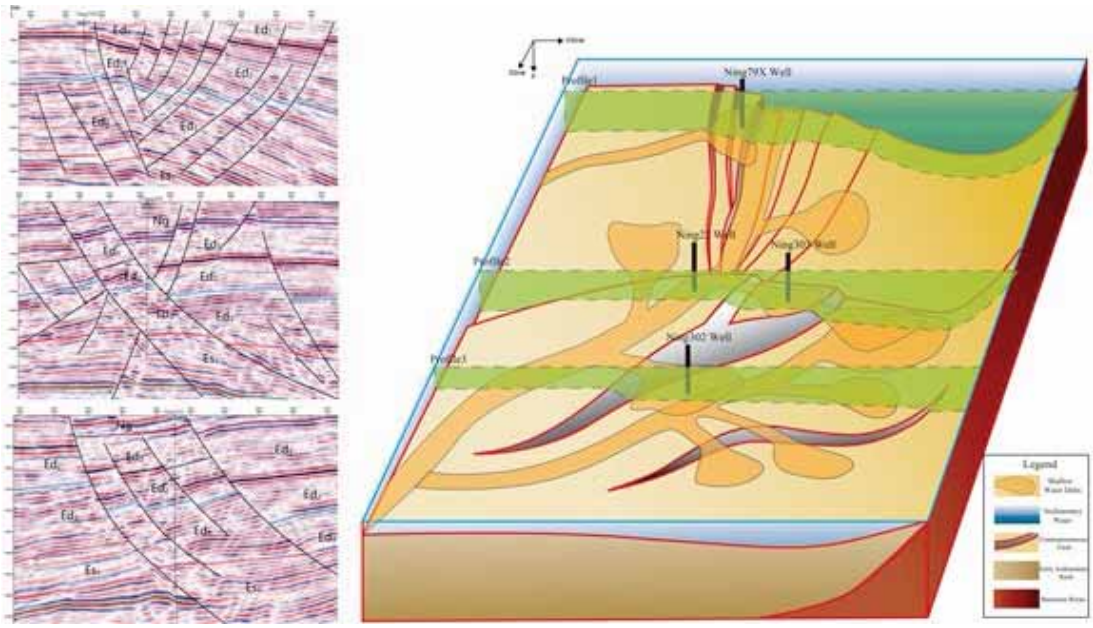

FIGURE 7
Sand body development model of co-sedimentary faults in Suning Oilfield.

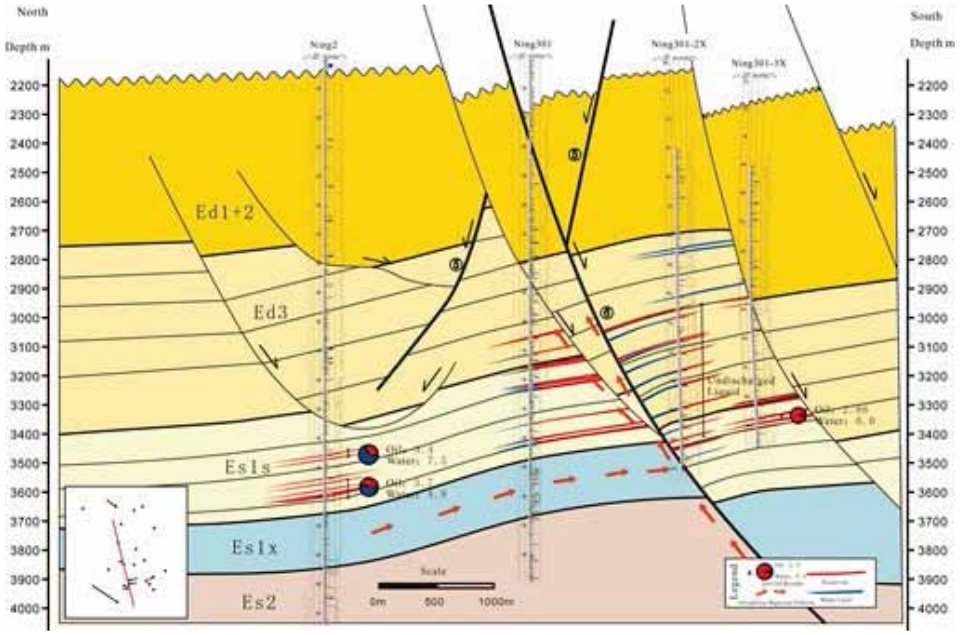

FIGURE 8
Accumulation model of Suning Oilfield.

tendencies in the north-south direction have formed a "lake bottom gorge" on the northern slop slope that facilitates sediment unloading. Because of the source from the southwest and the source from the northwest, so it is very easy to form a relatively high underwater diversion channel sediment along the" canyon ". At the same time, on the "canyon" slope, the northwest-oriented source was unloaded, forming a small shallow water delta.

(2) Oil and gas migration and accumulation. Reservoir types in the upper-Es1 and Ed3 in the study area are tectonic-lithologic reservoirs, and the source rocks are oil shale in the lower of Es1 and shale in the Es3. The accumulation section along the north-south direction of the work area (Figure 8) shows that the deep Es1 and Es3 oil sources are charged to the reservoirs of the sand groups from Es1 to Ed3 through deep faults (such as fault ⑥). Reservoirs from the upper Es1 to the lower Ed3 from the source fault are relatively developed, and the descending reservoirs (Ning 301-2X and Ning 301-3X) are more developed than the ascending ones. Affected by co-sedimentary faults, the favorable accumulation oil and gas zones are the descending plate of the co-sedimentary faults and the upper Es1 to Ed3. Affected by this law, Well Ning 2 is far from the co-sedimentation fault and is located on the fault

rising disk. Ning 301-3X is near the co-sedimentation fault and is located on the descending disk. The test result of the oil layer encountered by Well Ning 2 on Es1 is the oil-water layer, and the oil layer tested by Ning 301-3X on Es was pure oil layer.

The special reservoir accumulation law of Suning Oilfield is that the migration law of oil and gas from faults to fault blocks is that the descending plate of the reverse normal fault is easier to accumulate. The reverse normal fault is a special structure in which the tendency of the ascending stratum of the normal fault is the same as that of the descending disc, and the tendency of the fault plane is exactly the opposite. Oil and gas migration is mainly affected by buoyancy, so in the process of oil and gas migration, the falling plate of the reverse normal fault is the channel with the least resistance to oil and gas migration (Figure 9).

At the same time, the descending plate of the co-sedimentary fault is affected by the paleotopography, and the sediments are unloaded quickly, which is more likely to form continuous sand bodies than the ascending plate. In contrast, in the case of the ascending disk of the reverse normal fault, during the migration of oil and gas, the oil and gas must overcome the buoyancy resistance to enter the "upward irrigation" of the ascending disk to form reservoirs. For example, although the well Ning 22 in the upper plate of the structural transition zone is located in the high part of the structure, it is basically free of oil and has no oil and gas production. Instead, the well Ning 302, which descends the plate not far away, has oil production. The existence of the inverted normal fault structure is the reason why the ascending disk is not easy to accumulate, and the descending disk is more likely to accumulate.

(3) Oil and Gas Loss. Co-sedimentation faults can be used as paths for oil and gas migration if they cease to be active during hydrocarbon accumulation, otherwise they will form paths for oil and gas loss. Oil-free wells in the study area are basically located near large faults leading to the surface, such as Well Ning 304 (Figure 10). The faults of these two wells continue to be active after the formation of Guantao, so it can be judged that the development of large faults leading to the surface is a key factor that is not conducive to the later preservation of the reservoir. Therefore, the poor sealability of faults caused by the differential activation of the same sedimentary faults is the main reason for the exploration failure of Well Ning 304.

(4) Accumulation model and application examples. Inspired by the understanding of sedimentary control laws in the Suning Oilfield, the North China Oilfield changed its exploration thinking. In 2014, the Ning 78x well was drilled on the eastern side of the northern geological core ascending disk. Tectonic lithologic traps encountered two sets of reservoirs, with a daily output of 42.34 tons of pure oil, a daily oil output of 35.74 tons, respectively. The well has been producing 2.8 cubic meters of pure oil per day since it was put into production in 2014. The well Ning 78-2x, which was completed in 2018, is also located in the northern part of the area. It encountered 2 sets of oil layers, and the test oil produced 1.56 tons of oil per day and 0.67 cubic meters of water per day, and the other layer produced 3.6 tons of pure oil per day. The reservoir-forming potential of the Ed3 to Es1 Member near the synsedimentation fault in Suning Oilfield is well proved.

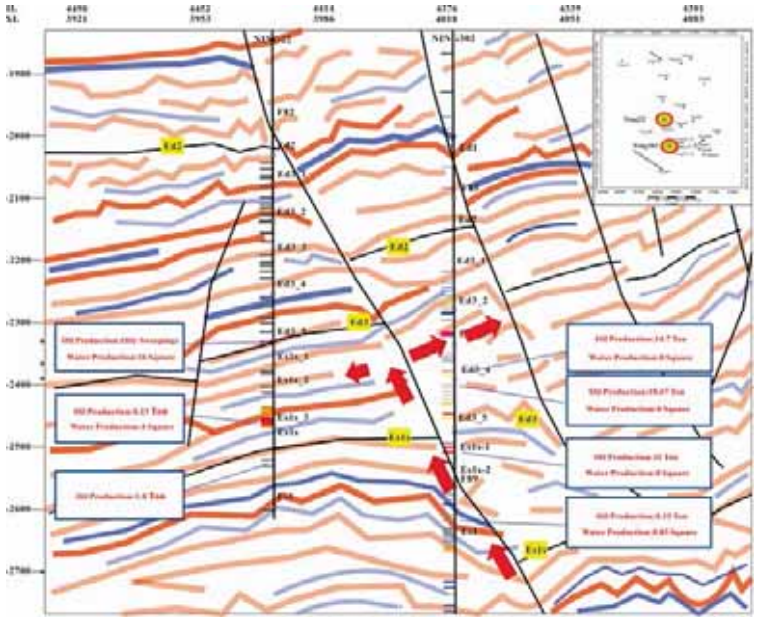

FIGURE 9
Oil and gas migration pattern of reverse normal fault.

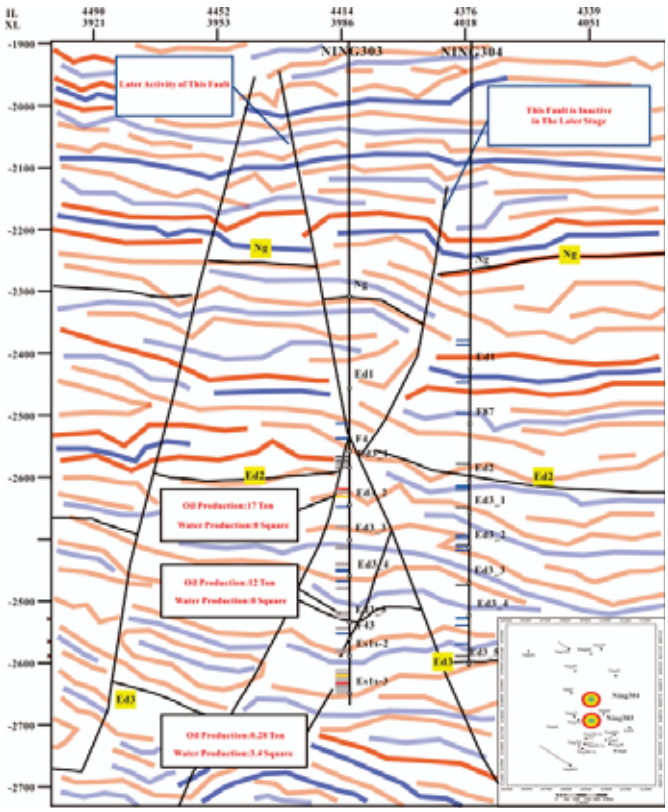

FIGURE 10
Seismic sections of wells Ning 304 and Ning 303.

CONCLUSIONS

(1) Co-sedimentation faults control the deposition of sand bodies, and reservoirs near the co-sedimentation faults are more developed. The faults are oil and gas migration channels and the sites where large faults develop are all potential sites.

(2) Co-sedimentary faults with faults reaching the surface are not conducive to the preservation of oil and gas due to later activation of faults. In the tectonic transition zone, the descending plate of the reverse normal fault is more likely to accumulate due to its low resistance to oil and gas migration and short distances. The sand body in the densely faulted part of the geomorphic structure belt is developed, and the oil and gas supply is sufficient, which is also a favorable location for accumulation.

(3) The guiding significance for the exploration and production of oilfields developed with the same sedimentary faults is that directional wells adjacent to fault planes are more likely to drill into high-yield reservoirs, and wells far from faults have low success rates.

ACKNOWLEDGEMENTS

This work was financially supported by the Major Science and Technology Project of CNPC, China (No. 2017E-1504-1).

REFERENCES

[1] Zou, J., Dai, J., Zhang, D., Wu, Y., Zhang, Y., Tian, B. (2014) Structural divisions of rift basin based on the intensity of tectonic activity: A case study from the Raoyang Sag. Acta Petrolei Sinica. 35(2), 294-302.

[2] Lao, H., Chen, Q., Wu, K. (2013) Tectonic characteristics and hydrocarbon accumulation rules of lateral buried hill transformation belt in the Raoyang Sag. Acta Geologica Sinica. 87(3), 415-423.

[3] Wu, K., Li, J., Lu, S., Cui, Y., Zang, M. (2010) Evolution types and hydrocarbon accumulation differences of buried hills in Raoyang Sag, Jizhong Depression. Marine Origin Petroleum Geology. 15(1), 27-34.

[4] Su, J., Zhang, S., Yang, H., Zhu, G., Zhang, B. (2010) Control of fault system to formation of effective carbonate reservoir and the rules of petroleum accumulation. Acta Petrolei Sinica. 31(2), 196-203.

[5] Zhao, X., Jin, F., Wang, Q., Bai, G. (2015) Buried- hill play, Jizhong Sub Basin, Bohai Bay Basin: A review and future prospectivity. AAPG Bulletin. 99(1), 1-26.

[6] Zeng, H., Zhao, X., Zhu, X., Jin, F., Dong, Y., Wang, Y., Zhu, M., Zheng, R. (2015) Seismic sedimentology characteristics of sub-clinoformal shallow-water meandering river delta: A case from the Suning area of Raoyang Sag in Jizhong Depression, Bohai Bay Basin, NE China. Petroleum Exploration and Development. 42(5), 566-576.
[7] Aydin, A. (2000) Fractures, faults, and hydrocarbon entrapment, migration and flow. Marine and Petroleum Geology. 17(7), 797-814.
[8] Sorkhabi, R., Tsuji, Y. (2005) Faults, fluid flow, and petroleum traps. Tulsa: The American Association of Petroleum Geologists. 1-31.
[9] Sun, T., Fu, G., Lü, Y., Zhao, R. (2012) A discussion on fault conduit fluid mechanism and fault conduit form. Geological Review. 58(6), 1081-1090.
[10] Zhang, S., Yang, M., Luo, X. (2015) Hydro carbonepisodic migration in fault zones: Insights from physical simulation experiments. Geological Review. 61(5), 1183-1191.
[11] Li, W., Liu, Z., Zhang, H., Ji, W., Lei, T. (2012) Control of fault on gas accumulation of Upper Paleozoic in Tabamiao Area of Ordos Basin. Journal of Earth Sciences and Environment. 34(4), 22-29.
[12] Fazli Khani, H., Back, S. (2015) The influence of pre-existing structure on the growth of syn-sedimentary normal faults in a deltaic setting, Niger Delta. Journal of Structural Geology. 73, 18-32.
[13] Lezzar, K., Tiercelin, J., Turdu, C. (2002) Control of normal fault interaction on the distribution of major Neogene sedimentary depocenters, Lake Tanganyika, East African rift. AAPG Bulletin. 86(6), 1027-1060.
[14] Ahaneku, C., Okoro, A., Odoh, B., Anomneze, D., Chima, K., Ejeke, C., Okoli, I. (2016) Sequence stratigraphy, structural framework and hydrocarbon migration of Ariki Field, Nigeria. Petroleum Exploration and Development. 43(1), 82-88.
[15] Zhang, Z., Wang, Y., Yun, J., Zhou, B., Zhang, Z., Zheng, M. (2009) Control of faults at different evolution stages on hydrocarbon accumulation in Tazhong Area, the Tarim Basin. Oil and Gas Geology. 30(3), 316-323+315.
[16] Zhao, W., Fang, J. (2007) Petroleum enrichment rules in lithologic and stratigraphic pools in different faulted basins: An example from the correlation of lithologic and stratigraphic pools in Jizhong Depression and in Erlian Basin. Petroleum Exploration and Development. 34(2), 129-134.
[17] Yang, M. (2009) Transfer structure and its relation to hydrocarbon exploration in Bohai Bay Basin. Acta Petrolei Sinica. 30(6), 816-823.
[18] Preto, N., Franceschi, M., Gattolin, G., Massironi, M., Riva, A., Gramigna, P., Bertoldi, L., Nardon, S. (2011) The latemar: A middle triassic polygonal fault-block platform controlled by synsedimentary tectonics. Sedimentary Geology. 234(1-4), 1-18.
[19] Hatem, E., Tribovillard, N., Averbuch, O., Vidier, D., Sansjofre, P., Birgel, D., Guillot, F. (2014) Oyster patch reefs as indicators of fossil hydrocarbon seeps induced by synsedimentary faults. Marine and Petroleum Geology. 55, 176-185.
[20] Hatem, E., Tribovillard, N., Averbuch, O., Sansjofre, P., Adatte, T., Guillot, F., Ader, M., Vidier, D. (2016) Early diagenetic formation of carbonates in a clastic-dominated ramp environment impacted by synsedimentary faulting-induced fluid seepage - evidence from the late Jurassic Boulonnais Basin (N France). Marine and Petroleum Geology. 72, 12-29.
[21] Yang, M., Liu, C., Yang, B., Zhao, H. (2002) Extensional structures of the Paleogene in the central Hebei basin, China. Geological Review. 48(1), 58-67.
[22] Sun, D., Liu, C., Yang, M., Du, J., Zhang, Y., Zhang, R. (2004) Study on complex extensional structures in the middle Jizhong depression in the Bohai Bay Basin. Geological Review. 50(5), 484-491.
[23] Wang, G., Gan, H., Zhao, Z., Chen, S., Zhao, Y. Liao, J., Li, X., Wu, L. (2018) Activity of Gaoliu fault and its control over sedimentation in the Nanpu Sag. Journal of Northeast Petroleum University. 42(02), 51-61+120.

Received: **21.12.2019**
Accepted: **16.02.2020**

CORRESPONDING AUTHOR

Yi Li
Tianjin Zhengfang Science and
Technology Development Co. Ltd.,
Tianjin 300270 – China

e-mail: 1270113343@qq.com

© by PSP Volume 29 – No. 05/2020 pages 3940-3951 Fresenius Environmental Bulletin

EVALUATION OF WATER HARVESTING TECHNIQUES ON SOIL PHYSIOCHEMICAL PROPERTIES IN THE JUNIPER PROCERA FOREST ECOSYSTEM, AL-SAUDA PARK, ASIR REGION, SAUDI ARABIA

Khalid A. Ibrahim[1,2], Essameldin I. Warrag[1,2], Sara A. M. Ebraheem[3], Muhammed A. Khan[4], Khaled F. Fawy[3], Ali A. Ateeg[3], Abubakr M. Idris[3,5,*]

[1]Prince Sultan Bin Abdulaziz Center for Environmental and Tourism Research and Studies
[2]Biology Department, College of Science, King Khalid University, Abha, Saudi Arabia
[3]Department of Chemistry, College of Science, King Khalid University, Abha, Saudi Arabia
[4]Department of Chemical Engineering, College of Engineering, King Khalid University, Abha, Saudi Arabia.
[5]Research Center for Advanced Materials Science (RCAMS), King Khalid University, Abha, Saudi Arabia

ABSTRACT

The Juniperus procera natural stands are an important part of the forest ecosystems in highlands across the world. Al-Sauda Park, Asir region, Saudi Arabia, which is one of the most interesting tourism area in the Arabian Gulf Countries, lies in the highest altitude in the Middle East. The dominant plant species in Al-Sauda Park is Juniperus procera, which has being threatened by dieback disease due to soil erosion by rainwater runoff. In this concern, seven water-harvesting techniques (WHTs) were applied in Al-Sauda Park. The effects of WHTs on 21 physiochemical properties of the soil at two depths (0–10 and 10–30 cm) were addressed. The WHTs include micro-catchment types (semicircular bunds (SCB) and square bunds (SB)) and terraces types (old terraces (OT), new terraces (NT) new terrace and plough (NTP), new terraces and mulch (NTM) and new terraces with both mulch and plough (NTMP)). The means of the levels of physiochemical properties were as follows: moisture content (MC) 0.30; bulk density (BD) 1.82 g/cm3; porosity 31.22%; organic matter (OM) content 3.10 mg/kg; pH 7.49; electrical conductivity (EC) 0.59 dS/m. The means of element contents (mg/kg) were as follows: N 96.05; P 16.75; K 27.20; Mg 88.63; Al 40.30; Ca 391.95; Cr 1.45; Mn 2.76; Fe 173.55; Co 0.09; Ni 0.21; Cu 0.50; Zn 0.42; Cd 0.007; Pb 0.15. Significant effects of WHTs on MC, BD, OM contents, EC, besides the contents of Al, Ca and almost all heavy metals were observed. OT and NTM addressed unpolluted to moderately polluted levels by heavy metals using the geoaccumulation index. Cluster analysis reported the following order of the pairs of soil depths in term of WHTs from nearer to farer: OT > NT > NTM > SB ≈ SCB > NTPM. The principal component analysis extracted the 21 examined parameter to five main components showing various significant inter-relationships.

KEYWORDS:
Heavy metals, physiochemical properties, micro-catchments, soil, terrace types, water-harvesting techniques

INTRODUCTION

Rainfall plays key roles in the growth and regeneration of forests through delivering essential nutrients, moisture and aeration to the roots of plants. Nevertheless, due to the rugged topography in highlands, rainfall exposes soil to serious erosion that put soil quality at risk. In another context, soil in highlands, particularly of rugged topography, could not sufficiently utilize rainfall water for irrigation and nutrition [1, 2]. Therefore, unless effective water catchment and soil conservation techniques are applied to highlands, soil nutrients are leached by rainfall and, simultaneously, water cannot be preserved in soil. Hence, soil conservation is important for the forest ecosystems in general, and for maintaining satisfactory physical, chemical and biological properties of forest soil in particular [3].

Water catchment is a method of capturing surface runoff and combating soil erosion from highlands followed by the collection in a surface reservoir or in a zone of cultivation area. This process have recorded improvement in soil fertility and increase in soil organic matter (OM) content [4]. Conservation tillage within terraced areas in agricultural highlands also improves soil quality, particularly aeration and fertility. Notably, conservation tillage enhances decomposition of OM by microorganisms and improves the physiochemical properties of soil [5, 6]. Furthermore, the addition of mulch and OM in terraced areas offers the benefits of enhancing the activities of microorganisms, increasing soil nutrients, improving soil physical properties and contributing to harvesting of rainwater [7].

In another context, Asir region, which is located in the southeastern part of Saudi Arabia, lies on a very high plateau with altitude rising 3000

MASL at Al-Sauda Park near Abha city. Asir region receives rainfall with an annual range of 300-500 mm [8, 9]. The Juniperus procera forest ecosystem in Asir region is dominant as it covers 95% of highlands higher than 1600 MASL. Water streams from rainfall in the highlands of Asir region, particularly in Al-Sauda Park, have resulted in soil erosion and nutrient transfer by leaching minerals and OM resulting in dieback disease as well as the decline of the Juniper natural stands. In this concern, water-harvesting techniques (WHTs) are important tools for the reduction of water runoff and improvement of the physicochemical properties of soil. Water harvesting is an old practice in the highlands of Asir region. During the last four decades, Junipers trees have being seriously affected by dieback disease as well as declining due to soil erosion and rapid flow of rainwater [10, 11].

On the other hand, farmers in Asir region had experienced traditional terraces against mountain slopes to harvest rainwater and to reduce soil erosion and silting [12]. The abandonment of experiencing terraces in the past decades due to changes in land use patterns has resulted in damaged and destroyed terraces [13, 14]. Juniper dieback and decline was linked with the destruction of terraces that increased water run-off and soil erosion [14].

Based on the aforementioned discussion, it has been proposed in the current study to apply different WHTs (micro-catchments and terraces types) for soil conservation of the Juniper procera forest ecosystem in Al-Sauda Park, Asir region, Saudi Arabia. In particular, the study addresses the levels of moisture content (MC), bulk density (BD), porosity, OM content, pH and electrical conductivity (EC) in soil at two depths, besides the contents of some major elements (N, P. K, Mg, Al and Ca) and some heavy metals (Cr, Mn, Fe, Co, Ni, Cu, Zn, cd and Pb). The study also demonstrates the effects of WHTs on soil physiochemical properties at two soil depths. Interrelationships between physiochemical parameters in the surface and the deep soils are investigated using multi-variate statistical analysis approaches, i.e. cluster analysis (CA) and principal component analysis (PCA).

MATERIALS AND METHODS

Study Area. The Junipers forest ecosystem lies in highlands in Al-Sauda Park (18° 17′ 59″ N/42° 21′ 47″ E), southwestern part of Asir region, Saudi Arabia (Figure 1). Alsouda Park is an interesting site for tourists. It is one of the most popular destinations in Saudi Arabia, which features green and mountainous landscape, wildlife and beauty. The temperature in summer do not exceed 15 °C. Alsouda Park is characterized by the richest plant density and diversity in Saudi Arabia [15]. The topography is undulating with valleys. The dominant soil types are loamy sand, sandy loam and loam [16].

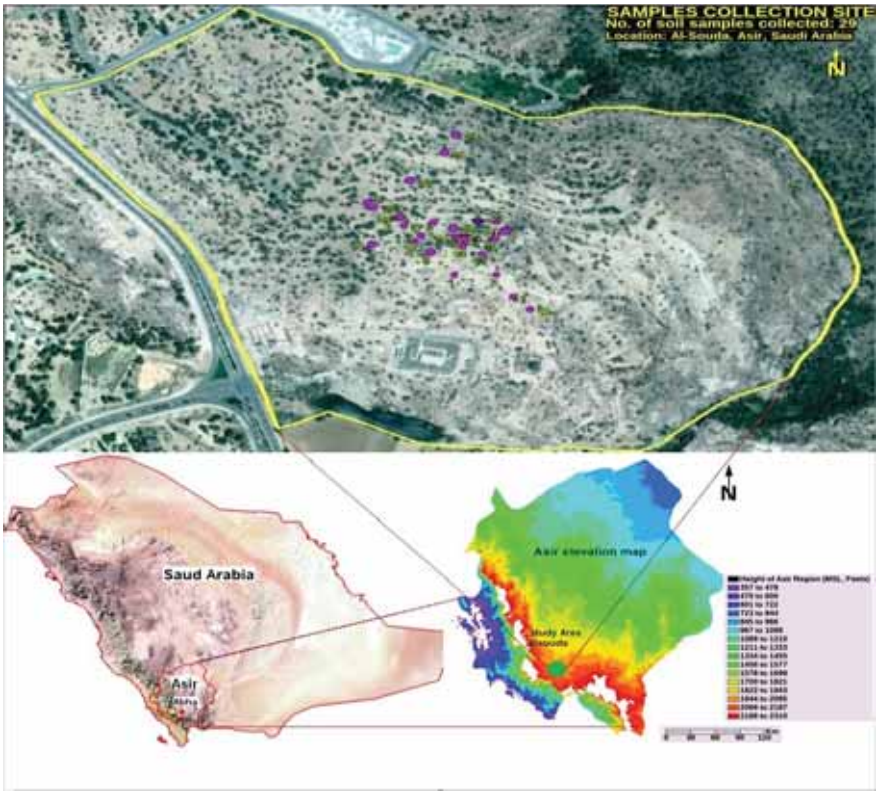

FIGURE 1
Soil samples locations at the Juniper procera forest ecosystem, Al-Sauda Park, Asir region, Saudi Arabia

Terrace Types. Five terrace types were carried out in the current study as follows: (i) old terraces (OT), which was considered a control type, were constructed against the mountain slopes with a channel for water runoff just above the ridge; (ii) new terraces (NT), which were carry out through building by rocks and stones against the slope of the mountain to receive surface runoff water descending from the top of highland; (iii) new terrace and plough (NTP), in which ploughed soil was within the terraced area; (iv) new terraces and mulch (NTM), in which mulch was added within the terraced area; (iv) new terraces with both mulch and plough processes (NTMP), i.e. a combination of mulch and ploughed soil [17].

Micro-Catchments. Two types of micro-catchments, i.e. semicircular bunds (SCB) and square bunds (SB), were constructed in Al-Sauda Park. The SCB type was constructed by raising soil around Juniper trees, with a radius range of 2.0–5.0 m and height range of 0.5–1.0 m, and an open end against the mountain slope to capture rainwater [18, 19]. The SB type was constructed with a dimension of 1.0 m × 1.0 m and a depth of 0.30 m using digger machine [17].

Soil Sample Collection. Fifty-eight sampling points along each transect were marked randomly in the micro-catchments and within the terrace types as shown in Figure 1. Two soil samples, 1.0 kg for each, were taken from each point at depths 0–10 cm and 10–30 cm. The samples were air dried and sieved at 2 mm for physiochemical analysis.

Analytical Methods of Soil for Physiochemical Properties. MC, BD and porosity were determined according to procedures demonstrated elsewhere [20]. The pH and EC were determined as described elsewhere [21]. OM content was determined by the potassium dichromate oxidation method [22]. Total N content was determined by the Kjeldahl method [23]. The available P content was determined by the Burriel-Hernando method [24]. The available Ca, Mg and K contents were extracted by 1 N ammonium acetate and measurement by atomic absorption and emission spectrophotometry [25]. The USEPA-3051 method was applied for soil treatment for the analysis of the rest of metals for total contents (Mg, Al, Ca, Cr, Mn, Fe, Co, Ni, Cu, Zn, cd and Pb). Inductively coupled plasma-optical emission spectrometer was used for the measurements [26-30].

Statistical Analysis. The physiochemical parameters of the surface and the deep soils were subjected to CA and PCA, as multi-variate statistical analysis methods. The analysis were carried out using SPSS software version 16.0 for Windows.

Assessment of Heavy Metal Levels Using Geochemical Indices. The contents of the examined heavy metals in soil samples at the two depths were geochemically assessed using the geoaccumulation index (Igeo), which was calculated using equation 1 [27-30]; where Ci is the concentration of a metal in a soil sample and CBackground is the concentration of the same element in a soil sample from the control area. An area far from any manmade activities in Al-Sauda Park was considered as a control area.

$$I_{geo} = \log_2\left(\frac{C_i}{1.5 \times C_{Background}}\right) \quad (1)$$

RESULTS AND DISCUSSION

Physiochemical Properties. The descriptive statistics of the major physiochemical parameters of the surface and the deep soils of the seven examined WHTs (n = 10) in Al-Sauda Park are shown in Table 1, while the typical levels of the major physiochemical parameters are depicted in Figure 2a-f. A wide range was observed in MC (0.07–0.74 %) with high relative standard deviation (RSD%, 71.14) indicating significant variation within WHTs and within the surface and the deep soil samples. However, the kurtosis of moisture content was < 1.0 suggesting insignificant tailing of distribution, while the skewness was almost 1.0 suggesting symmetrical distribution. Figure 2a shows that the highest soil moisture content was recorded in the deep soil of NTM and the surface soil of NTPM, while the lowest soil moisture content was recorded in both surface and deep soil of NT. In general, all WHTs demonstrated significant effect on MC compared to the control WHT, i.e. OT. A previous study in the Al-Sauda Park showed that different types of micro-catchments were effective in increasing soil MC [14]. a moisture content (%); b bulk density (g/cm3); c porosity (%); d organic carbon matter (%); e electrical conductivity (dS/m); f concentration (mg/kg)

Unlike MC, a narrow range of BD (1.67–198 g/cm3) with a limited standard deviation (SD, 0.11) was observed showing insignificant effect of WHTs on bulk density. Interestingly, the lowest BD (Figure 2b) was found in the deep soil of NTM and the surface soil of NTPM, while the highest BD was found in the surface soil of NTM and the deep soil of NTPM. On the other hand, a slight effect of WHTs on porosity might be observed since the RSD was 13.17%. The SCB showed the highest MC (Figure 2a), the highest porosity (Figure 2c) and the lowest BD (Figure 2b), whereas OT showed the lowest porosity (Figure 2c) and the highest BD (Figure 2b). In general, the levels of BD were all high, which is due to the sandy and rocky structure. The usual BD of soil of most coarse fragments structure was in the range of 2.2–3.0 g/cm3 [31]. Nevertheless, it was reported that BD > 1.6 g/cm3 tends to restrict root

TABLE 1
Descriptive statistics of physiochemical parameters of the surface and the deep soil samples of WHTs in the Juniper procera forest ecosystem, Al-Sauda Park, Asir region, Saudi Arabia

Parameter	Mst.[a]	BD[b]	Pors.[c]	OCM[d]	pH	EC[e]
Minimum	0.07	1.67	25.23	2.11	7.13	0.31
Maximum	0.74	1.98	37.00	4.79	7.64	1.28
Mean	0.30	1.82	31.22	3.10	7.49	0.59
Median	0.30	1.82	31.49	3.01	7.53	0.48
SD	0.22	0.11	4.11	0.89	0.14	0.27
RSD (%)	71.14	5.98	13.17	28.83	1.93	46.89
Kurtosis	0.56	-1.16	-1.16	-0.12	1.43	2.23
Skewness	1.04	0.27	-0.27	0.81	-1.22	1.63

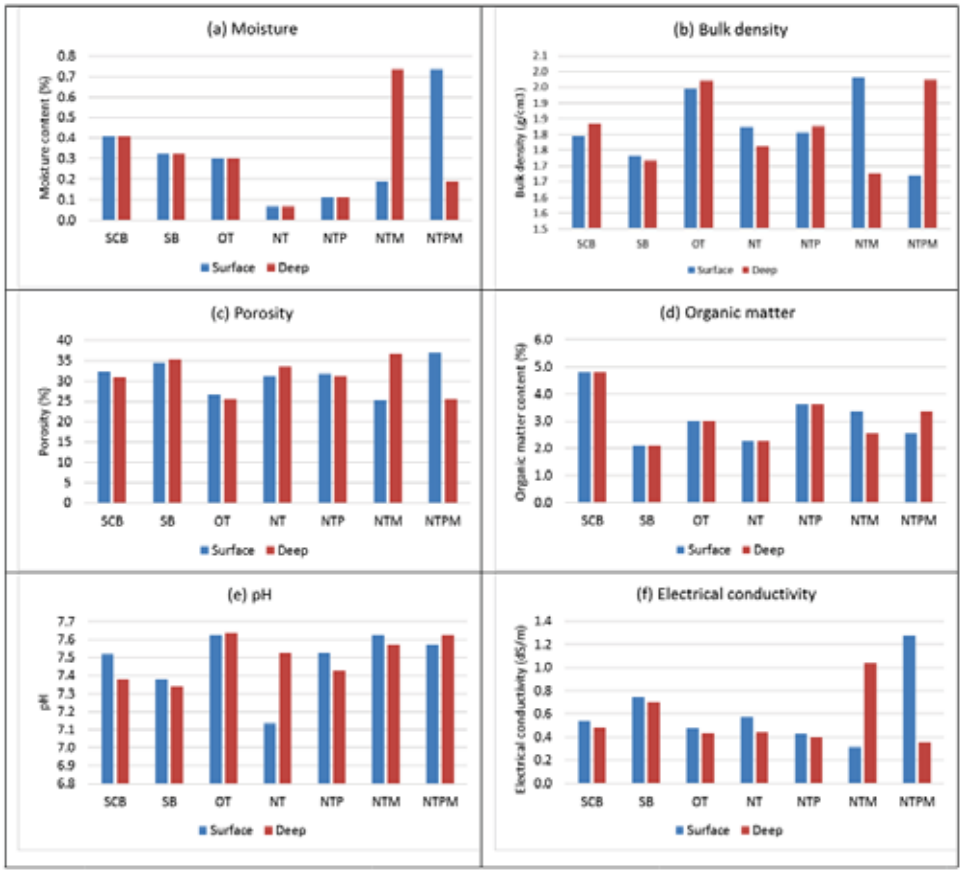

FIGURE 2
Physiochemical parameters of the surface and the deep soil samples of WHTs in the Juniper procera forest ecosystem, Al-Sauda Park, Asir region, Saudi Arabia

growth [32]. Accordingly, the most appropriate BD was obtained by NTM and NTPM, and to some extent bySB.

For OM content, the range of 3-6 % is recommended to obtain productive agricultural soil [4]. The control WHT, i.e. OT, maintained the minimum OM content (Figure 2d). Interestingly, SCB increased OM content from 3.0 % (as in soil of OT) to 4.7, while SB decreased OM content to 2.1 %. NT also decreased OM content to below the minimum recommended level, while NTP, NTM and NTPM recorded almost similar OM content to soil of OT.

Table 1 shows that the pH ranged from 7.13 to 7.64 demonstrating weakly alkaline soil, which in principle positively effect on the ease of utilization of nutrients in the soil to be ready for plantation that are absorbed through WHTs. In general, the usual ideal soil pH is in the range of 5.5-8.0. However, previous studies reported that at pH < 7, the mobility and leaching of heavy metals increased [27]. On the other hand, Similarly to MC (Figure 2a), the highest EC (Figure 2f) was recorded in the deep soil of NTM and the surface soil of NTPM, while the lowest EC was recorded in the surface soil of NTM and the deep soil of NTPM. Nevertheless, the limited range of pH indicates no significant effect of WHTs on soil pH.

Major Element Contents. Table 2 shows the descriptive statistics of major element contents (N, P, K, Mg, Al and Ca) in the surface and the deep soil

samples of WHTs (n = 10) in Al-Sauda Park. The typical elemental contents are depicted in Figure 3a-f. N, P and K are essential nutrients, which significantly affect the growth, functions and vigorousity of most plants [33]. Table 2 shows that N contents ranged from 87.20–108.75 mg/kg, which is categorized in the high level [33]. Nevertheless, P and K contents were in the range of 13.75–24.75 and 23.75–35.75 mg/kg, respectively, indicating low level [33]. Figure 2g-f shows that the highest levels of N, P and K were recorded in the surface soil of NTPM. The RSD of N, P and K contents were 6.15, 17.39 and 13.26 %, respectively, indicating insignificant variation in N contents in soils of different WHTs; and to some extent slight variation in P and K contents. In the same context, the kurtosis and skewness of N contents were < 1.0 suggesting symmetrical distribution with insignificant tailing. In contrast, the kurtosis and skewness of P and K contents indicate unsymmetrical distribution toward high values and significant tailing toward high values as well. It is recommended to support the growth of trees and shrubs in the Juniper ecosystem; an issue that enhances soil fertility through OM and hence improves the activity of microorganisms. This process results in releasing nutrients in soil and strength soil consistency from wind and water erosion [5, 6].

TABLE 2

Descriptive statistics of major element contents (mg/kg) in the surface and the deep soil samples of WHTs in the Juniper procera forest ecosystem, Al-Sauda Park, Asir region, Saudi Arabia

Parameter	N	P	K	Mg	Al	Ca
Minimum	87.20	13.75	23.75	79.20	7.34	370.25
Maximum	108.75	24.75	35.75	103.75	83.29	419.00
Mean	96.05	16.75	27.20	88.63	40.30	391.95
Median	96.35	16.13	25.88	87.60	29.42	388.75
SD	5.91	2.91	3.61	6.29	27.22	15.54
RSD (%)	6.15	17.39	13.26	7.10	67.54	3.96
Kurtosis	0.34	3.58	2.02	1.29	-1.44	-1.31
Skewness	0.42	1.71	1.67	0.92	0.36	0.21

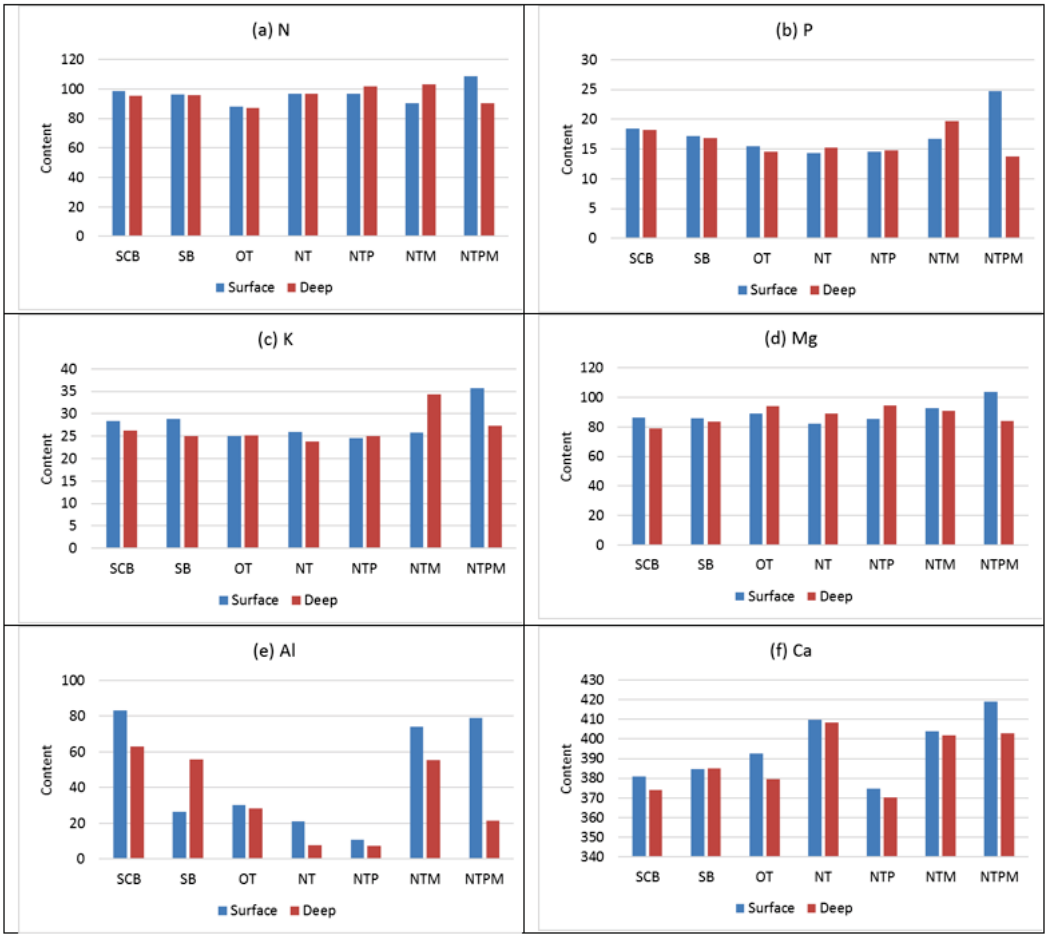

FIGURE 3

Major element contents in the surface and the deep soil samples of WHTs in the Juniper procera forest ecosystem, Al-Sauda Park, Asir region, Saudi Arabia

On the other hand, the RSD of Mg content did not reach 10% suggesting no considerable variation and hence there was no significant effect of WHTs on Mg contents in the surface and the deep soil samples. Al showed a wide range of contents (7.34–83.29 mg/kg). The mean and the median were 40.30 and 29.42 mg/kg, respectively, indicating significant difference in the distribution of Al contents in the surface and deep soil samples. The kurtosis of Al contents was -1.44 indicating significant tailing in the distribution toward low contents. Likewise, the kurtosis of Ca contents was -1.31 indicating significant tailing in the distribution toward low contents. The highest levels of Al (Figure 3e) were observed in surface soils of SCB, NTM and NTPM; whereas the lowest levels were observed in deep soil of NT and NTP. Figure 3e also shows that the variation of Al contents within the terrace types (OT, NT, NTP, NTM and NTMP) was higher than that within the micro-catchment types (SCB and SB). In this context, Al is not an essential element for plant and it could be toxic at pH below 6.0 [34]. Fortunately, the levels of Al in the soil samples were safe since the soil pH was in the range of 7.13–7.64.

Ca contents (Figure 3f) in the surface soil were higher, or almost similar, than that in the deep soil. The surface soil of NTPM recorded the highest Ca content followed by the surface soil of NT and the surface soil of NTM. In general, the effects of the terrace types (OT, NTP, NTM and NTMP, with the exception of NT) on Ca contents were almost higher than the effect of the micro-catchment types (SCB and SB) on Ca contents. This finding could be justified by the almost similar Ca contents in the soil of the micro-catchment types. Ca and Mg are essential nutrients for plant growing [35]. The soil of the current study area is rocky, which is rich in Ca and Mg contents that might obtained from weathering process. The levels of Ca and Mg in the current study were comparable to a previous study that was carried out in a similar environment and geological constructions [36].

Heavy Metal Contents. The descriptive statistics of heavy metals contents (Cr, Mn, Fe, Co, Ni, Cu, Zn, Cd, and Pb) in the surface and the deep soils of WHTs (n = 10) in the Juniperus procera forest ecosystem are compiled in Table 3. The mean and SD values of heavy metal contents (mg/kg) were as follows: Cr 1.45 ± 1.26; Mn 2.76 ± 1.50; Fe 173.55 ± 79.93; Co 0.09 ± 0.04; Ni 0.21 ± 0.08; Cu 0.50 ± 0.32; Zn 0.42 ± 0.19; Cd 0.007 ± 0.004; Pb 0.15 ± 0.16. Accordingly, the levels followed the following descending order: Fe > Mn > Cr > Cu > Zn > Ni > Pb > Co > Cd. This order is to far extent comparable with previous studies that were carried out in the same area [28, 29]. On the other hand, wide ranges were observed in all heavy metals irrespective WHTs and soil depths. With the exception of Cd, the mean values of the contents of all heavy metals differed from that of the median values. The RSD values, in general, ranged from 39.27 to 101.53%. These results suggest significant effect of WHTs on soil samples from the Juniperus procera forest ecosystem. The kurtosis values of the contents of Cr, Mn, Co, Ni and Zn were > +1.0 indicating significant tailing toward high levels. In contrast, Cd only recorded kurtosis of > -1.0 indicating significant tailing toward low contents. Fe, Cu and Pb recorded kurtosis values < 1.0 indicating insignificant tailing. The skewness values of Cr, Mn, Co, Ni, Zn and Pb were > +1.0 indicating asymmetrical distribution toward high contents, whereas the skewness values of Fe, Cu and Cd were < 1.0 indicating symmetrical distribution.

Figure 4a-i shows typical heavy metal contents in the surface and deep soils of WHTs in the Juniperus procera forest ecosystem. Almost similar heavy metal contents in the surface and the deep soil of OT was observed (Figure 4a-i). Nevertheless, the terrace type of NTP technique demonstrates lower or comparable metal contents (Cr, Mn, Fe, Cu, Cd and Pb) than OT. Notably, Figure 4a shows that Cr content in the surface soil of SB was 5-fold higher and that in the surface soil of NT was 3-fold higher compared to Cr content in the surface and the deep soil of OT. At any case, considering typical heavy metal contents in soil may be misleading in the term of environmental pollution assessment. Accordingly, Igeo was adopted to assess possible soil contamination by heavy metals [27-30, 37- 39].

TABLE 3
Descriptive statistics of trace element contents (mg/kg) in the surface and the deep soil samples of WHTs in the Juniper procera forest ecosystem, Al-Sauda Park, Asir region, Saudi Arabia

Parameter	Cr	Mn	Fe	Co	Ni	Cu	Zn	Cd	Pb
Minimum	0.29	1.17	87.38	0.05	0.13	0.05	0.23	0.002	0.03
Maximum	5.00	6.86	327.19	0.19	0.45	1.05	0.92	0.012	0.50
Mean	1.45	2.76	173.55	0.09	0.21	0.50	0.42	0.007	0.15
Median	0.94	2.19	141.25	0.08	0.19	0.62	0.35	0.008	0.06
SD	1.26	1.50	79.93	0.04	0.08	0.32	0.19	0.004	0.16
RSD (%)	87.11	54.48	46.05	41.68	39.27	65.00	44.63	52.334	101.53
Kurtosis	4.24	3.55	-0.72	1.88	4.70	-0.98	3.06	-1.242	0.06
Skewness	1.94	1.80	0.82	1.44	1.94	-0.32	1.72	-0.534	1.14

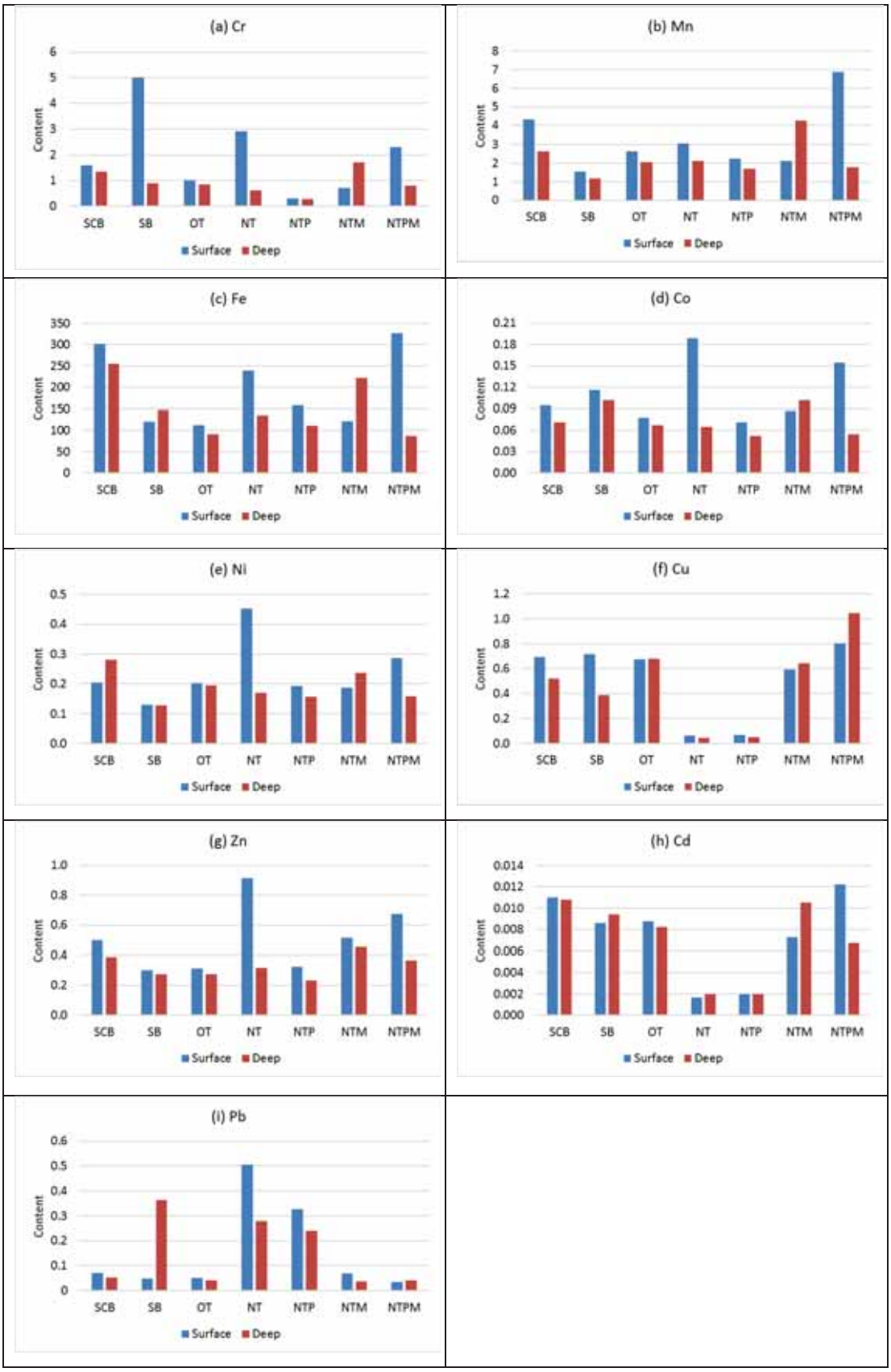

FIGURE 4
Heavy metal contents in the surface and the deep soil samples of WHTs in the Juniper procera forest ecosystem, Al-Sauda Park, Asir region, Saudi Arabia

TABLE 4
Geochemical indices of heavy metals in the surface and the deep soil samples of WHTs in the Juniper procera forest ecosystem, Al-Sauda Park, Asir region, Saudi Arabia

WHTs	Cr	Mn	Fe	Co	Ni	Cu	Zn	Cd	Pb
Surface soil									
OT	0.05	0.33	0.52	0.27	-0.79	0.55	-0.01	0.46	0.04
NTM	-0.47	0.02	0.64	0.44	-0.89	0.36	0.71	0.19	0.50
NTMP	1.25	1.71	2.06	1.27	-0.28	0.80	1.10	0.95	-0.51
NTP	-1.69	0.11	1.01	0.15	-0.85	-2.77	0.05	-1.67	2.74
NT	1.58	0.56	1.61	1.56	0.37	-2.89	1.54	-1.93	3.36
SCB	0.72	1.05	1.95	0.55	-0.76	0.58	0.67	0.79	0.54
SB	2.37	-0.45	0.62	0.85	-1.42	0.63	-0.07	0.44	-0.02
Deep soil									
OT	-0.17	0.54	0.44	0.24	0.52	0.41	0.50	0.45	-0.04
NTM	-0.27	0.32	0.37	-0.06	0.22	1.03	0.91	0.17	-0.01
NTMP	0.85	1.58	1.72	0.85	0.80	0.32	1.21	0.81	-0.15
NTP	-1.74	0.26	0.72	-0.12	0.21	-3.34	0.25	-1.58	2.52
NT	-0.60	0.58	1.00	0.20	0.33	-3.50	0.71	-1.58	2.74
SCB	0.51	0.90	1.92	0.33	1.04	0.02	0.99	0.85	0.32
SB	-0.11	-0.28	1.12	0.85	-0.09	-0.40	0.50	0.65	3.12

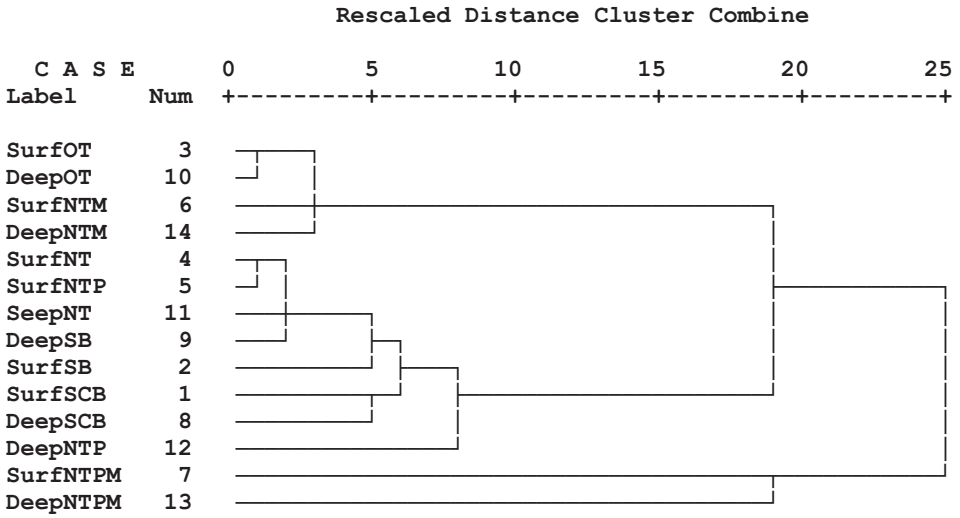

FIGURE 5
Dendrogram obtained from cluster analysis of physiochemical parameters in the surface and deep soil samples of WHTs in the Juniper procera forest ecosystem, Al-Sauda Park, Asir region, Saudi Arabia

I_{geo} for Assessment of Heavy Metal Contents. The Igeo values are compiled in Table 4. Muller [40] classified the hazardousness of heavy metals for the environment based on Igeo values into six categories as follows: (i) < 0: unpolluted; (ii) 0 – 1: unpolluted to moderately polluted; (iii) 1 – 2: moderately polluted; (iv) 2 – 3 moderately to strongly polluted; (v) 3 – 4 strongly polluted; 4 – 5 – strongly to extremely polluted; (vi) > 5: extremely polluted.

The terrace types of OT and NTM addressed Igeo values for all examined heavy metals in the range of -0.89–0.71 suggesting unpolluted to moderately polluted levels. In contrast, the terrace types of NTPM, NTP and NT addressed a wide range of Igeo values (-3.50–3.36). In these terrace types, the highest Igeo (3.36) was recorded for Pb in the surface soil of NT followed by Pb in deep soil of NT (2.74) suggesting moderately to strongly polluted level. In the micro-catchment techniques, all Igeo values were < 1.0 suggesting unpolluted to moderately polluted levels, with the exception of Cr (2.37) in the surface soil of SB, Fe (1.95) in the surface soil of SCB, Fe in the deep soil of SCB (1.92), Fe in the deep soil of SB (1.12) and Pb (3.12) in the deep soil of SB. In general, Igeo values for all metals in deep soil were less than those in surface soil. This result could be attributed to activities of traffic and domestic wastes particularly during tourism seasons. Previous studies in Asir region also recorded different levels of pollution by heavy metals using Igeo. Street dust in Asir region recorded moderately to strongly pollution levels by Cu, Zn and Pb [29].

Cluster Analysis. Figure 5 shows the dendrogram resulted from CA of all examined physiochemical parameters of the surface and deep soils of WHTs in the Juniper procera forest

ecosystem, Al-Sauda Park. The dendrogram demonstrates strong relationships between the surface and the deep soils of each WHT, with the exception of NTP. The order of the pair of soil depths in term of WHTs from nearer to farer was as follows: OT > NT > NTM > SB ≈ SCB > NTPM. This order indicates that the physiochemical parameters of surface and deep soils of OT were more similar than those of NT. In another context, irrespective of soil depths, the physiochemical parameters of NTPM greatly differed from OT, NT and NTM. Interestingly, the physiochemical parameters of the micro-catchment techniques (SB and SCB) are more similar to each other than the terrace techniques (OT, NT, NTM, NTP and NTPM). Principal component analysis. The PCA shows that five components, which represented 91.4% of the total loadings, were extracted from 21 components. The loadings of components in sequence were as follows: 41.8, 21.7, 11.2, 9. and 7.6. The component matrix is shown in Table 4, while the loadings are plotted in Figure 6. The first principal component was loaded by P, EC, K, Mn, MC, Fe, N, BD, porosity, Co, Al, Cd and Zn. This result indicate that those parameters were significantly related to each other in a proportional trend, with the exception of BD. The second principal component was loaded by Pb, pH, Cu, Cd and Ni indicating all parameters significantly related to each other. While pH, Cu and Cd were proportionally related, Pb, Zn and Ni were disproportionally related. The third principal component was loaded by BD, porosity, Zn and Ni, while the fourth component was loaded by Cr and Mg. In the same way, the pairs of BD/porosity, OM/Ca and Cr/Mg showed significant disproportional relationship since they were observed through the principal component-3, -4 and -5, respectively.

CONCLUSIONS

This manuscript reports the levels of 21 physiochemical parameters in the surface and the deep soil samples from seven areas experienced WHTs in the Juniper procera forest ecosystem, Al-Sauda Park, Asir region, Saudi Arabia. The main objective of the study was to assess the levels of the physiochemical parameters and to investigate the effects of WHTs on the physiochemical parameters of soil at surface and deep depths. From the results obtained in the current study, the following conclusions can be drawn:

TABLE 5
Extracted component matrix obtained from principal component analysis of the physiochemical parameters of the surface soil samples of WHTs in the Juniper procera forest ecosystem, Al-Sauda Park, Asir region, Saudi Arabia

Parameter	Component				
	1	2	3	4	5
P	**0.933**	0.228	-0.099	-0.082	0.078
EC	**0.931**	-0.042	-0.257	0.169	-0.068
K	**0.920**	0.207	-0.047	0.140	-0.007
Mn	**0.880**	0.084	0.206	-0.030	0.355
Moisture	**0.851**	0.421	-0.115	-0.063	-0.078
Fe	**0.811**	-0.179	0.213	-0.463	0.159
N	**0.753**	-0.289	-0.392	-0.144	0.312
BD	**-0.687**	0.373	**0.590**	0.135	0.047
Porosity	**0.687**	-0.373	**-0.590**	-0.135	-0.047
Co	**0.658**	-0.581	0.325	0.166	-0.209
Al	**0.653**	0.397	0.272	-0.334	-0.051
Pb	-0.261	**-0.898**	-0.075	-0.052	0.143
pH	-0.048	**0.845**	-0.015	0.301	0.354
Cu	0.329	**0.757**	0.262	0.179	-0.382
Cd	**0.616**	**0.632**	0.064	-0.184	-0.345
Zn	**0.543**	-0.486	**0.661**	0.062	0.096
Ni	0.391	**-0.547**	**0.640**	-0.097	0.128
OM	-0.169	0.399	0.270	**-0.785**	0.243
Ca	0.476	-0.167	0.349	**0.644**	0.149
Cr	0.488	-0.264	0.032	0.149	**-0.690**
Mg	0.408	0.307	-0.147	0.479	**0.539**

Bolded figures indicate significant loading (> 0.5)

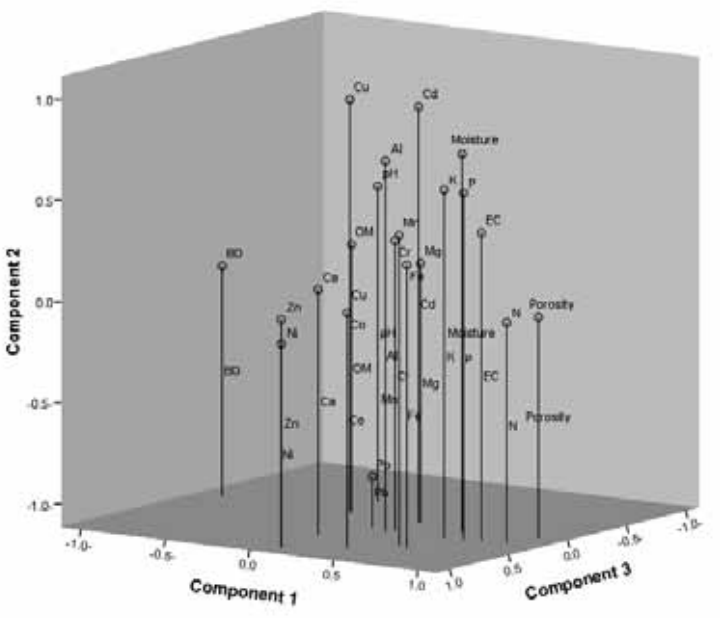

FIGURE 6
Principal component analysis chart of physiochemical parameters in the surface soil samples of WHTs in the Juniper procera forest ecosystem, Al-Sauda Park, Asir region, Saudi Arabia

- Significant effects of WHTs on soil BD were recorded. The most appropriate soil BD was obtained by NTM and NTPM, and to some extent by SB.
- The WHT of OT maintained the minimum OM content. The WHT of SCB increased OM content, while the WHT of SB decreased OM content. The WHT of NT also decreased OM content to below the minimum recommended level, while the WHTs of NTP, NTM and NTPM recorded almost similar OM content to soil of the WHT of OT.
- Limited range of soil pH was observed indicating no significant effect of WHTs.
- WHTs recorded insignificant effect on N contents, while slight variations in P and K contents in soils of different WHTs were observed. No significant effects of WHTs on Mg contents in surface and deep soils were observed. In general, the effects of the terrace types (OT, NTP, NTM and NTMP, with the exception of NT) on Ca contents were almost higher than the effect of the micro-catchment types (SCB and SB) on Ca contents.
- The terrace types of NTPM, NTP and NT addressed a wide range of Igeo values, which indicates unpolluted to strongly polluted levels. High levels of pollution by heavy metals were attributed to traffic and domestic activities.
- The dendrogram of CA representing all examined physiochemical parameters categorized WHTs into seven clusters. Each cluster was constructed from the same WHT of the surface and the deep soils. This result indicates that the effect of WHTs on physicochemical parameters was more than that of on soil depths.

ACKNOWLEDGEMENTS

The authors extend their appreciation to the Dean of Scientific Research at King Khalid University, Saudi Arabia for funding this work through the General Research Project under grant number (476 - 38).

REFERENCES

[1] Addis, H.K., Abera, A., Abebaw, L. (2020) Economic benefits of soil and water conservation measures at the sub-catchment scale in the northern Highlands of Ethiopia. Prog. Phys. Geog. In Press.
[2] Subhatu, A., Lemann, T., Hurni, K., Portner, B., Kassawmar, T., Zeleke, G., Hurni, H. (2017) Deposition of eroded soil on terraced croplands in Minchet catchment, Ethiopian Highlands. Intern. Soil and Wat. Conserv. Res. 5, 212-220.
[3] Chatanga, P., Sieben, E.J.J. (2019) Ecology of palustrine wetlands in Lesotho: Vegetation classification, description and environmental factors. Koedoe 61(1), a1574.
[4] Li, X.H., Yang J., Zhao, C.Y., Wang, B. (2014) Runoff and sediment from orchard terraces in southeastern China. Land Degrad. Dev. 25, 184-192.
[5] Gao, Y. Dang, X., Yu, Y., Li, Y., Liu, Y., Wang, J. (2016) Effects of Tillage Methods on Soil Carbon and Wind Erosion. Land Degrad. Dev. 27, 583-591.

[6] Lieskovský, J., Kenderessy, P. (2014) Modelling the effect of vegetation cover and different tillage practices on soil erosion in vineyards: A case study in vráble (Slovakia) using WATEM/SEDEM. Land Degrad. Dev. 25, 288-296.
[7] Kader, M.A., Senge, B.M., Moji, M.A., Ito, A. (2017) Recent advances in mulching materials and methods for modifying soil environment. Soil Till. Res. 168, 155-166.
[8] Asiri, H.F.M., Idris, A.M., Said, T.O., Sahlabji, T., Alghamdi, M.M., El-Zahhar, A.A., El Nemr, A. (2020) Monitoring and health risk assessment of some pesticides and organic pollutants in fruit and vegetables consumed in Asir region, Saudi Arabia. Fresen. Environ. Bull. 29(1), 615-625.
[9] El-Zahhar, A.A., Idris, A.M., Fawy, K.F., Arshad, M. (2020) SEM, SEM-EDX, μ-ATR-FTIR and XRD for urban street dust characterization. Intern. J. Environ. Anal. Chem. in press.
[10] El Atta, H.A. (2003) Decline of Juniperus procera in the Kingdom of Saudi Arabia. A report to the Ministry of Agriculture. Kingdom of Saudi Arabia.
[11] Barth, H.J., Strunk, H. (2000) The dieback phenomenon of Juniperus procera at the Al Souda family park. Report to Deutsche Forschungs Gemeinschaft (DFG), National Commission for Wildlife Conservation and Development (NCWCD), Riyadh.
[12] Gorashi, A. (2005) Sustainable Management of the Vegetal Cover in the Kingdom of Saudi Arabia. FAO Project Document.
[13] El Atta, H.A., Aref, I.M. (2010) Effect of terracing on rainwater harvesting and growth of Juniperus procera Hochst. ex Endlicher. Int. J. Environ. Sci. Tech.7, 59-66.
[14] El Atta, H.A., Aref, I.M., Alshahrani, T.A., Alazba, A., Ibrahim, K.A. (2013) Comparative efficiency of rainwater harvesting by some types of microcatchments. Intern. J. Plant, Anim. Environ. Sci. 3, 181-192.
[15] Vincent, P. (2008) Saudi Arabia: An Environmental Overview. Taylor and Francis, London.
[16] Mallick J. (2016) Geospatial-based soil variability and hydrological zones of Abha semi-arid mountainous watershed, Saudi Arabia. Arab J. Geosci. 9, 281.
[17] Mati, B.M. (2005) Overview of water and soil nutrient management under smallholder rainfed agriculture in East Africa. Working Paper 105. International Water Management Institute (IWMI), Colombo, Sri Lanka.
[18] FAO AGL (2000) Water Resources, Development and Management Services. Rome.
[19] Oweis, T., Prinz, D., Hachum, A. (2012) Rainwater harvesting for agriculture in the dry areas. CRC Press, Taylor and Francis Group, Leiden, 366 p.
[20] Sumner, E.M. (1999) Handbook of Soil Science. CRC Press, Boca Raton, Florida, USA.
[21] Mclean, E.O. (1982) Soil pH and Lime Requirement. In: Page, A.L., Ed., Methods of Soil Analysis. Part 2. Chemical and Microbiological Properties, American Society of Agronomy, Soil Science Society of America, Madison. 199-224.
[22] Nelson, D.W., Sommers, L.E. (1982) Total carbon, organic carbon, and organic matter. In: Page, A.L., Ed., Methods of Soil Analysis. Part 2. Chemical and microbiological properties. 2nd Edition, Agronomy Series No. 9, ASA SSSA, Madison.
[23] Bremner, J.M., Mulvaney, C.S. (1982) Methods of soil analysis, Part 2 Chemical and Microbiological Properties. 595-624.
[24] Díez, J.A. (1982) Consideraciones sobre la utilización de la técnica extractiva de Burriel-Hernando para la evaluación de fósforo asimilable en suelos. An. Edafol. Agrobiol, 41, 1345-1353.
[25] Knudsen, D., Peterson, G.A., Pratt, P.F. (1982) Lithium, Sodium and Potassium. In: American Society of Agronomy and Soil Science Society of America Journal, editor. Methods of Soil Analysis. Madison, I, 225-246.
[26] USEPA (US Environmental Protection Agency), 2007. Microwave assisted acid digestion of sediments, sludges, soils, and oils. Environmental Protection Agency, Washington, DC.
[27] Ashaiekh, M.A., Eltayeb, M.A.H., Ali, A.H., Ebrahim, A.M., Salih, I., Idris, A.M. (2019) Spatial distribution of total and bioavailable heavy metal contents in soil from agricultural, residential, and industrial areas in Sudan. Toxin Rev. 88(2), 93-105.
[28] Ali, I.H., Siddeeg, S.M., Idris, A.M., Brima, E.I., Ibrahim, K.A., Ebraheem, S.A.M. Arshad, M. (2020) Contamination and human health risk assessment of heavy metals in soil of a municipal solid waste dumpsite in Khamees-Mushait, Saudi Arabia, Toxin Rev. In Press.
[29] Idris, A.M., Alqahtani, F.M.S., Said, T.O., Fawy, K.F. (2020) Contamination level and risk assessment of heavy metal deposited in street dusts in Khamees-Mushait city, Saudi Arabia. Hum. Ecol. Risk Assess. In Press.
[30] Idris, A.M., Alnajjar, A.O., Alkhuraijid, T.S., Fawy, K.F. (2020) Long-term stability test of elements contents in new environmental certified reference material candidates using ICP OES and ICP-SFMS. Toxin Reviews, In Press.
[31] McKenzie, N., Coughlan, K., Cresswell, H. (2002) Soil physical measurement and interpretation for land evaluation. CSIRO Publishing: Collingwood, Victoria.
[32] McKenzie, N.J., Jacquier, D.J., Isbell, R.F., Brown, K.L. (2004) Australian soils and landscapes: an illustrated compendium. CSIRO Publishing: Collingwood, Victoria.

[33] Zhang, F., Niu, J., Zhang, W., Chen, X., Li, C., Yuan, L., Xie, J. (2010) Potassium nutrition of crops under varied regimes of nitrogen supply. Plant Soil 335(1-2), 21-34.
[34] Mládková, L., Borůvka, L., Drábek O. (2004) Distribution of aluminium among its mobilizable forms in soils of the Jizera Mountains region. Plant Soil Environ. 50(8), 346-351.
[35] Sillanpaa, M. (1982) Micronutrients and the nutrient status of SOUS: a global study. FAO Soils Bulletin No. 48, Rome.
[36] van Raij, B., Quaggio, J.A., da Silva, N.M. (1986) Extraction of phosphorus, potassium, calcium, and magnesium from soils by an ion-exchange resin procedure. Comm. Soil Sci. Plant Anal. 17(5), 547-566.
[37] Idris, A.M., Al-Tayeb, M.A.H., Potgieter-Vermaak, S.S., Van Greken, R., Potgieter, J.H. (2007). Assessment of heavy metals pollution in sediments harbours along the Red Sea coast, Microchem. J. 87(2), 104-112.
[38] Idris, A.M. (2008) Combining multivariate analysis and geochemical approaches for assessing heavy metal level in sediments from Sudanese harbors along the Red Sea coast. Microchem. J. 90(2), 159-63.
[39] Idris, A.M., Said, T.O., Brima, E.I., Sahlabji, T., Alghamdi, M.M., El-Zahhar, A.A., Arshad, M., El Nemr, A.M. (2019) Assessment of contents of selected heavy metals in street dust from Khamees-Mushait city, Saudi Arabia using multivariate statistical analysis, GIS mapping, geochemical indices and health risk. Fresen. Environ. Bull. 28(8), 6059-6069.
[40] Muller, G. (1981) The heavy metal pollution of the sediments of Neckars and its tributary: a stocktaking. Chemiker-Zeitung 105, 157-164.

Received: **28.12.2019**
Accepted: **27.02.2020**

CORRESPONDING AUTHOR

Abubakr M. Idris
Department of Chemistry,
College of Science,
King Khalid University,
Abha – Saudi Arabia

e-mail: abubakridris@hotmail.com

© by PSP Volume 29 – No. 05/2020 pages 3952-3960 Fresenius Environmental Bulletin

A NOVEL MODEL FOR PREDICTING THE BACTERIAL EFFECTS ON THE WELLBORE CORROSION IN SHALE GAS WELLS

Yuting Pan, Zhiquan Zhang*

Yangtze University, School of Petroleum Engineering, Hubei, Wuhan 430100, China

ABSTRACT

There are many factors affecting wellbore corrosion in shale gas wells, and the interactions between these factors are complex. Based on the analysis of sensitivity factors for different shale formations, the establishment of an applicable corrosion prediction model can effectively reduce maintenance costs and reduce environmental pollution during on-site production. In this paper, through the analysis of shale gas wellbore corrosion in the target block and data analysis, the main influencing factors of shale gas wellbore corrosion are clarified. Based on the De Warrd 95 model, the influence of bacterial content is considered. A new SPSS software nonlinear regression is used to establish a shale gas well borehole corrosion prediction model. The research results show that the average relative errors calculated by the new model are only 2.214% and 3.521%, respectively, indicating that the new model has good prediction accuracy, can meet the needs of field engineering technology, and has good value for popularization and application.

KEYWORDS:
Shale gas well, borehole corrosion, sensitivity factor, bacterial content, corrosion prediction model, environmental pollution

INTRODUCTION

Ground pipelines in a shale gas area have been severely perforated due to corrosion several times. In 2017, nearly 57 cases of tube steel defects were perforated. In January-April 2018, nearly 49 cases of ground transportation pipeline steel had multiple corroded perforations [1-3]. These corroded perforations are caused by the erosion and corrosion of the medium fluid, which brings economic losses. As the only channel for oil and gas outlets, corrosion failure of the production wellbore is one of the main causes of accidents.

Zhu et al. established a corrosion prediction model based on De Warrd model for Xushen Oilfield [4, 5]. Luo et al. established a corrosion prediction model for Fuling shale gas based on De Warrd model [6]. Aiming at the complex acidic corrosion environment of the Sulige gas field, Zhang et al. [7, 8] first analyzed the production data of the gas wells on the site (including pressure, temperature, gas production, and water production) and grasped the current status and technical problems of on-site wellbore corrosion. Then they analyzed in detail the properties of the produced water and natural gas components and the corrosion tendency of the Sulige gas field and combined the gas wells by the principal component analysis dimension reduction and system cluster analysis. After that, they carried out the wellbore corrosion detection test for each type of gas well and analyzed the corrosion degree and corrosion causes of various types of gas wells by using SEM, EDS, and XRD. After that, they analyzed the main control factors of various types of gas well borehole corrosion by ash correlation, and finally used the optimized corrected corrosion rate prediction model to predict the wellbore corrosion rate and the corrosion rules of different types of gas wells along the wellbore. Lu et al. [9] carried out a study on the effect of bacterial content on the corrosion rate of wellbore steels of two common shale gas well boreholes through dynamic corrosion assessment methods. The results show that the bacterial content increases in proportion to the corrosion of wellbore steels of two common shale gas well boreholes. The corrosion rate has an exponential relationship with the bacterial content. The main source of bacteria is carried through the fracturing fluid. It is recommended that bactericides should be added to the fracturing fluid to reduce the content of bacteria, thereby reducing the corrosion rate of the wellbore and surface pipes. Relevant scholars have recognized the effect of bacteria on wellbore corrosion, but no relevant research has been carried out on the influence rules and trends of bacteria on wellbore corrosion [10-13]. In general, most of the current studies consider the factors such as temperature and partial pressure of carbon dioxide in their basic model and compare the predicted results and the results from the laboratory tests and field tests, but the effects of bacterial corrosion were not considered for prediction.

The study area of this paper belongs to the high productivity gathering area of gas wells. Most of the pipelines have a short commissioning time and widely set up stations. The carbon dioxide content in

different regions is significantly different. The carbon dioxide does not contain gases such as hydrogen sulfide, and has a high concentration of mineralization, chloride ions and dissolved bicarbonate ions, and most of them are affected by bacterial corrosion [14-16]. Therefore, it is necessary to develop a corrosion prediction model considering the influence of bacterial content to provide a basis for the evaluation and development of safe production of shale gas [17].

MATERIALS AND METHODS

Analysis of corrosion sensitivity factors of shale gas wells. Based on the field data, the big data analysis of the corrosive factors of the produced gas and produced fluid in a typical area was carried out [18, 19]. This area is dominated by methane, and its content is generally greater than 98%. According to the wellbore pressure change range of the gas well, it ranges from 11.57MPa at the bottom of the well to 9.91MPa at the middle of the well to 7.64MPa at the wellhead. As the carbon dioxide concentration is 0.686%, the calculated corresponding carbon dioxide partial pressures are 0.0794 MPa, 0.0680 MPa, and 0.5240 MPa, respectively, which all exceed the maximum corrosion condition of 0.02 MPa. The pH value of the produced water from different gas gathering stations is mainly distributed between 6-7, with an average of 6.6. The produced water is mainly calcium chloride water, and the total salinity is mainly distributed between 24618.45 and 59014.38 mg/L. There is a certain amount of bicarbonate ions and a small amount of ferrous iron and oxygen. It shows that produced water has a certain weak acidity. The bicarbonate ion in the water sample indicates the presence of dissolved carbon dioxide in the water sample.

The bacterial content [20] in produced water from different gas gathering stations differs greatly. Data analysis was performed on the test results of the bacterial content of 45 samples. The correlation between the number of bacteria and the fracturing water source, gas volume, and water volume was not clear. From the sampling of three typical platforms, there were different levels of bacteria. The bacteria show a growth promoting effect, but it is impossible to determine which type of bacteria it is. At the same time, 16 samples were tested in the laboratory, which also showed that the growth of bacteria was still irregular. Therefore, the bacterial content (C_b) was taken as the influencing factor in the study.

Establishment of Wellbore Corrosion Prediction Model. Using the basic form of De Waard95 model [21, 22], a new corrosion rate prediction model was established after adding the effect of bacterial content on the corrosion rate. The model considers that the contact degree of the fluid medium with the wellbore wall surface is different under different flow conditions. The steel mold (N80) and the degree of immersion (non-immersion and full immersion) are discussed separately.

(1) Establishment of functional relationship. According to the related investigation of De Waard95 model and the study of the mechanism function relationship [23], it is necessary to consider the bacterial content (C_b) factor in this model. Combining the influence of bacterial content on the corrosion rate, the relationship between the logarithm of corrosion rate ($\lg V_r$) and bacterial content (C_b) was found to have a good logarithmic relationship. Therefore, when the new model is established, the bacterial content factor is increased according to the model relational equation, and the form of the model is changed to the equation (1) [24]:

$$\lg V_r = a + b/T + c\lg p_{CO_2} + d\lg C_b \quad (1)$$

Combining the independent kinetic model with the flow-dependent carbon dioxide mass transfer model, the relationship of the equation is shown in equation (2):

$$\frac{1}{V_{corr}} = \frac{1}{V_r} + \frac{1}{V_m} \quad (2)$$

Where V_m is the corrosion rate of the flow-dependent carbon dioxide mass transfer model, and the expression is:

$$V_m = 2.45^{\frac{U^{0.8}}{d^{0.2}}} p_{CO_2} \quad (3)$$

Among them, p_{CO2} is the partial pressure of carbon dioxide, and its value is equal to the product of system pressure p and carbon dioxide content, that is:

$$p_{CO_2} = p \cdot C_{CO_2} \quad (4)$$

Where p is the system pressure, MPa; C_{CO2} is carbon dioxide content (volume fraction), decimal.

Substituting equation (2) into equation (1) and transforming it. The transformed function relationship can be used to obtain the shale gas well borehole corrosion prediction model considering the influence of bacterial content, as shown in equation (5):

$$\lg \frac{V \cdot V_m}{V_m - V} = a + b\frac{1}{t} + c\lg p_{CO_2} + dC_b \quad (5)$$

Where C_b is bacteria content, 10^4 cells/mL.

Looking at the parts represented by the experimental data as a whole, the following functional form is further simplified:

$$y = a + bx_1 + cx_2 + dx_3 \quad (6)$$

Where $y = lg\frac{V \cdot V_m}{V_m - V}$; $x_1 = \frac{1}{T}$; $x_2 = lgpp_{CO_2}$ $x_3 = lgC_b$.

The equation is a typical three-variable linear equation. The shale gas well corrosion rate and influencing factor data can be used to obtain x_1, x_2, x_3, and y through corresponding function conversion.

The coefficients a, b, c, d can be calculated through the linear regression calculation by SPSS software.

(2) Model basic data. a) Experimental data of bacterial corrosion. We collect the produced water samples on different platforms or gas collection stations and perform the material bacterial corrosion experiments on the mixed water. The results are shown in Table 1. Although bactericides were added [25, 26], bacterial corrosion still existed. From the appearance of the experimental results, the appearance of the hanging piece appeared black when bacteria were present. Limited by the temperature and pressure and the influence of bacteria, the activity of the bacteria is weakened. When the bacterial content reached 11,000 cells/mL, the increase of the corrosion rate decreased sharply with the increase of the bacterial content.

According to the experimental results, it is shown that the bacterial content has a great influence on the corrosion rate. It is further concluded that bacterial corrosion is one of the main factors for the sensitivity of gas wells.

b) Influencing factor data. According to the analysis of shale gas well corrosion site data and the gas well corrosion mechanism, based on the N80 steel type, we consider the diversity of contact conditions between the medium fluid and the metal surface layer, the flow pattern is different and other complex factors [27]. The non-contact state is considered according to the non-immersion condition, and the contact state is considered according to the full immersion condition. The required nonlinear regression data is from the bottom of the well to the wellhead. As the depth of the well is gradually reduced, the temperature is gradually reduced to the wellhead (Table 2 and Table 3).

c) Determination of the relationship coefficient. The data used for regression calculation are shown in Table 4 and Table 5.

TABLE 1
Results of detection of bacteria content in water samples from different platforms or gas gathering stations

Sample name	Sampling time	Bacterial test（cells/mL）			Remark
		TGB	FB	SRB	/
1#	2019.01.06	6	0	2000	/
2#	2019.01.06	2.5	2.5	250	Bactericides Added
3#	2019.01.06	6	6	25000	/
4#	2019.01.06	2.5	2.5	700	Bactericides Added
5#	2019.01.06	130	2.5	250	Bactericides Added
6#	2019.01.06	.25	2.5	25	Bactericides Added

TABLE 2
Data of non-immersion corrosion rate of N80 gas wells in shale gas fields and influencing factors

Depth /m	Temperature /K	Pressure /MPa	p_{CO2} /MPa	Velocity /m/s	V_m /mm/a	C_b /10^4 /mL	Actual value V /mm/a
2657	362.05	11.57	0.079	2.457	0.696	0.750	0.166
2300	358.05	10.99	0.075	2.558	0.683	0.880	0.155
1500	341.15	9.91	0.068	2.703	0.643	2.200	0.106
1000	328.95	9.14	0.063	2.825	0.615	4.000	0.083
5	306.35	7.64	0.052	3.148	0.560	7.700	0.047

TABLE 3
Data of full immersion corrosion rate of N80 gas well in shale gas field and its influencing factors

Depth /m	Temperature /K	Pressure /MPa	p_{CO2} /MPa	Velocity /m/s	V_m /mm/a	C_b /10^4 /mL	Actual value V /mm/a
2657	362.05	11.57	0.079	2.457	0.696	0.750	0.413
2500	360.05	11.25	0.077	2.512	0.689	0.760	0.360
2300	352.85	10.59	0.073	2.616	0.670	1.350	0.232
1500	341.15	9.91	0.068	2.703	0.643	2.200	0.155

TABLE 4
Parameters required for N80 non-immersion regression

Depth/m	x_1	x_2	x_3	y
2657	0.00276	-1.10034	-0.12494	-0.66156
2300	0.00279	-1.12268	-0.05552	-0.69784
1500	0.00293	-1.16760	0.34242	-0.89651
1000	0.00304	-1.20273	0.60206	-1.01795
5	0.00326	-1.28058	0.88649	-1.28986

TABLE 5
Parameters required for N80 full immersion regression

Depth/m	x_1	x_2	x_3	y
2657	0.00276	-1.10034	-0.12494	0.00677
2500	0.00278	-1.11252	-0.11919	-0.12271
2300	0.00283	-1.13878	0.13033	-0.44986
1500	0.00293	-1.16760	0.34242	-0.68997

TABLE 6
Results of significance analysis of N80 non-immersion model

	Model	sum of squares	*df*	Mean square
1	Regression	4.421	4	1.105
	Residual	0.007	1	0.007
	Uncorrected total	4.428	5	/
	Corrected total	0.263	4	/

Note the fitting coefficient (R^2) is 0.973

TABLE 7
Results of significance analysis of N80 full immersion model

	Model	sum of squares	*df*	Mean square
2	Regression	0.714	4	0.179
	Residual	0.028	1	0.028
	Uncorrected total	0.742	5	
	Corrected total	0.306	4	

Note the fitting coefficient (R^2) of is 0.910

TABLE 8
List of regression coefficients of shale gas wellbore corrosion models

Model	Regression coefficients			
	a	b	c	d
N80 non-immersion	2.896	-1100	0.5	0.1
N80 full immersion	9.542	-3010	1.2	0.1

TABLE 9
Corrosion rate error table of shale gas well N80 non-immersion model

Depth/m	Actual value *V*/mm/a	Predicted value /mm/a	Error/%
2657	0.166	0.154	-7.404
2300	0.155	0.143	-7.824
1500	0.106	0.110	3.622
1000	0.083	0.088	5.880
5	0.047	0.052	9.580

The results of the significance analysis of the model after regression are shown in Table 6 and Table 7.

The regression coefficients under the influence of different steel types and different flow patterns are shown in Table 8.

It can be seen from the results that the regression coefficients of the models with different immersion levels are different, which indicates that it is correct to consider using fluid flow to separate the discussions when establishing the prediction model. The regression equation of shale gas wellbore corrosion prediction model considering bacterial corrosion is as follows:

N80 (non-immersion) model 1:

$$\lg V_r = 2.896 - \frac{1100}{T} + 0.5\lg p_{CO_2} + 0.1\lg(10^{-4} C_b) \quad (7)$$

N80 (full immersion) model 2:

$$\lg V_r = 9.542 - \frac{3010}{T} + 1.2\lg p_{CO_2} + 0.1\lg(10^{-4} C_b) \quad (8)$$

V_{rr} and V_m in different cases are calculated by the new model and substituted into Eq. (2), and the final corrosion rate V_{corr} can be obtained.

RESULTS

Model error analysis. The non-linear fitting module of SPSS software is used to fit a new corrosion prediction model that considers the effect of bacterial content on the corrosion rate. The experimental results under experimental conditions are predicted and the relative error analysis is performed. The error analysis results are shown in the Table 9, Table 10, Figure 1 and Figure 2. According to the error analysis results, the lowest error of the two models is 0.362% and the highest error is 16.782%.

TABLE 10
Corrosion rate error table of shale gas well N80 full immersion model

Depth/m	Actual value *V*/mm/a	Predicted value /mm/a	Error/%
2657	0.413	0.369	10.631
2500	0.360	0.343	4.646
2000	0.232	0.271	-16.782
1500	0.155	0.167	-7.522

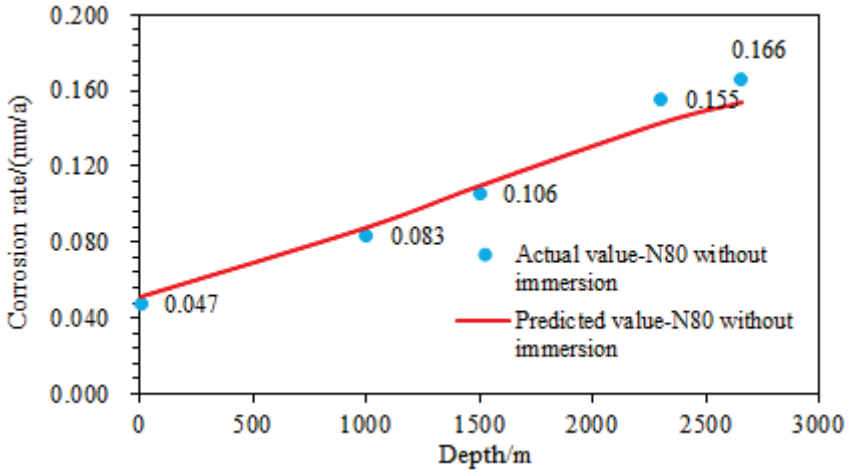

FIGURE 1
Comparison curve between the predicted value and experimental value of N80 non-immersion prediction model.

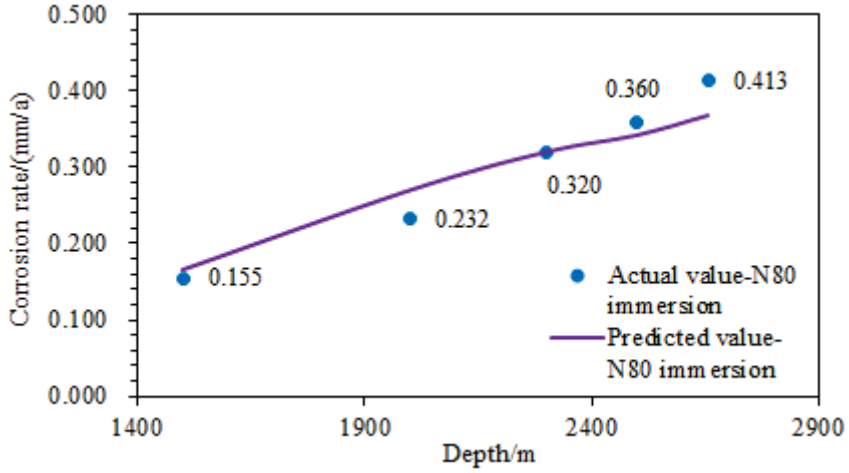

FIGURE 2
Comparison curve between the predicted value and experimental value of N80 full immersion prediction model.

From the results of the error analysis of the new model, it can be found that for the prediction of shale gas well borehole corrosion, different flow regimes should be analyzed separately to ensure the accuracy of the prediction. However, whether the new model can meet the conditions of other parameter changes needs to be further verified.

Model validation. During the production of shale gas wells, although the properties of the wellbore gas and produced fluids have not changed, as the gas and liquid flow from the bottom of the well to the wellhead, the wellbore environment, carbon dioxide partial pressure, and bacterial content will change, and there are still interrelationships and restraints between these factors [28-29]. The influence of a single factor on the corrosion rate cannot be considered during the experiment, and it cannot be considered when establishing a new prediction model. Therefore, when establishing a new prediction model, a set of experimental data is mainly used for non-linear regression. The corrosion prediction model after regression can effectively fit the experimental data of this group, but whether it can meet the results of other parameter changes is still a question. Therefore, the experimental results of other parameter changes were further used to verify the effective-

ness of the established shale gas well borehole corrosion prediction model and clarify the applicable conditions of the prediction model.

In order to further verify the reliability of the model, the parameter regression coefficients of the new prediction model were verified by selecting the experimental results of dynamic corrosion rate under the influence of different carbon dioxide concentrations and different bacterial contents.

(1) Verification of the effect of carbon dioxide concentration. The experimental results of the dynamic corrosion rate under different carbon dioxide concentrations and the prediction results of the new model are shown in Figure 3. It can be seen from the figure that the relative error of the model prediction under the condition that the pressure at the bottom of the wellbore is 11.57 MPa and the temperature is 88.9°C is as follows:

1) In the non-immersed state, the relative errors between the predicted values and the experimental values of the corrosion rate of N80 steel at carbon dioxide concentrations of 0.686%, 0.438%, and 0.218% are 0.593%, 1.276%, and 1.740%, respectively.

2) In the full immersed state, the relative error between the predicted value and the experimental value of the corrosion rate of N80 steel at carbon dioxide concentrations of 0.686%, 0.438%, and 0.218% was 6.133%, 2.453%, and 1.088%, respectively. The model has a good effect in predicting the influence of carbon dioxide concentration on the dynamic corrosion rate. The error of all models is 0.593%-6.133%, and the average error is 2.214%, which meets the engineering accuracy requirements.

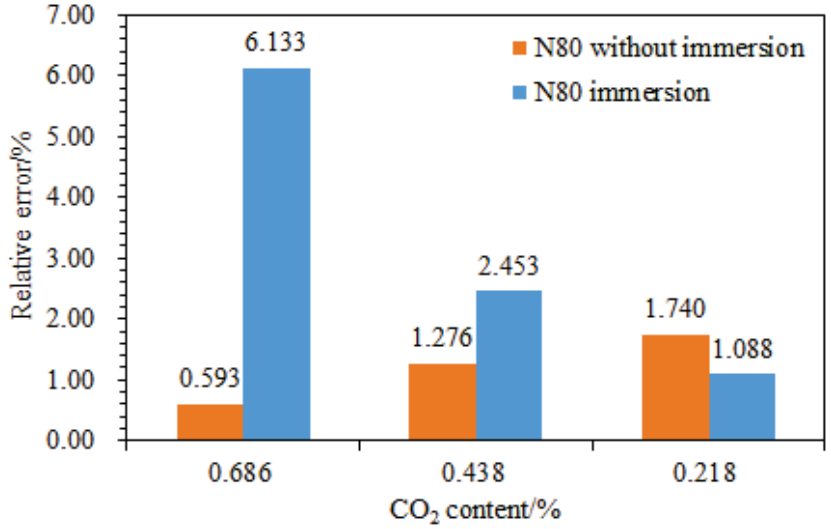

FIGURE 3
Comparison curve of predicted corrosion rate and experimental value for carbon dioxide concentration verification.

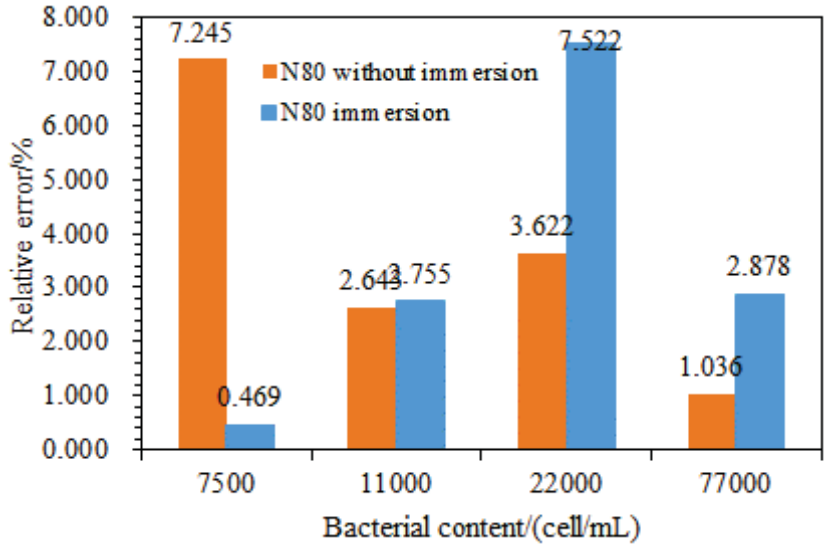

FIGURE 4
Comparison curve of predicted corrosion rate and experimental value for verification of bacterial content.

(2) Verification of the effect of bacterial content. The experimental results of the dynamic corrosion rate under different bacterial contents and the prediction results of the new model are shown in Figure 4. It can be seen from the figure that the relative error of the model prediction in the middle of the wellbore (9.91 MPa, 68 °C) is as follows:

1) In the non-immersed state, the relative errors between the predicted values of the corrosion rate of N80 steel under the conditions of 7500, 11000, 22000, and 77000 (cells /ml) and the experimental values were 7.2455%, 2.645%, 3.622%, and 1.036%, respectively, with an average error of 3.637%.

2) In the full immersed state, the relative errors between the predicted values of the corrosion rate of N80 steel under the conditions of 500, 11000, 22000, and 77000 (cells /ml) and the experimental values were 0.469%, 2.755%, 7.522%, and 2.877%, respectively, with the average error of 3.406%.

It shows that the new model is good in predicting the influence of bacterial content on the dynamic corrosion rate. The error of all models is 0.469%-7.522%, and the average error is 3.521%, which meets the engineering accuracy requirements.

In summary, the new prediction model is used to predict the corrosion rate under different carbon dioxide concentrations and different bacteria (SRB) content and compared with experimental values to verify that the relative errors of the new prediction model can meet the needs of the project. The prediction of wellbore corrosion of the target gas well has good adaptability. Since no experiments have been conducted on parameter changes such as high carbon dioxide concentration and high temperature and pressure, the extrapolation limits under the conditions of the prediction model fitting cannot be determined. The experimental conditions determine its applicable conditions: the well depth (using the temperature and pressure corresponding to different well depths) is <3000m, the carbon dioxide concentration is 0.2% -0.7%, and the bacterial content is <800,000 cells/mL. It can be extrapolated appropriately in actual use, and the new model still has good adaptability.

CONCLUSIONS

(1) Based on data such as the background of the shale gas wellbore area, the properties of the products, the fluid flow pattern, the bacterial corrosion experiment of the mixed water, and the dynamic corrosion test data, the potential corrosive factors of the shale gas wellbore materials include: carbon dioxide concentration, bacterial content, temperature, pressure, flow state, etc. Based on the N80 steel type, the liquid carried by the gas is in a full immersed or non-immersed state in contact with the wellbore, and the corrosion rate of the two is sequentially reduced.

(2) By carrying out the analysis of the corrosive factors of shale gas wellbore and the experiment of bacterial corrosion law, a corrosion rate prediction model that conforms to the wellbore corrosion law of shale gas well is established. Combined with the results of the bacterial corrosion rate experiment, additional considerations are added to the basic form of the De Warrd 95 model. The effect of bacterial content was analyzed, and error analysis and verification of the newly established shale gas well borehole corrosion prediction model were performed. The average relative error between the calculated results of the model and the experimental results was 6.832%. The model was calibrated based on the experimental results of the effects of different carbon dioxide concentrations and different bacterial contents on the corrosion rate. The average relative errors were 2.214% and 3.521%, respectively, which proved that the new model had better prediction accuracy and met the engineering requirements.

ACKNOWLEDGEMENTS

The authors would like to show sincere thanks to those who have offered experimental conditions for this work and all the authors of the references.

REFERENCES

[1] Zhang, W. (2018) Study on wellbore corrosion rule and influencing factors in Sulige gas field. Dissertation. Xi'an: Xi'an Shiyou University.

[2] Chen, X. (2017) Comparison and analysis of prediction methods for corrosion rate of gas wells containing CO_2. Natural Gas Technology. 11(5), 18-21.

[3] Wang, X. (2018) Corrosion Rules of P110 Casing for Carbon Dioxide Flooding of High Temperature and Salinity Reservoir. Corrosion and Protection. 39(9), 673-677.

[4] Zhu, J., Li, Y., Wang, Q. (2013) Establishment of prediction model of CO_2 corrosion in Xushen Gas Field. Oil-Gasfield Surface Engineering. 32(04), 16-17.

[5] Sun, Q. (2018) Prediction of CO_2 corrosion in gas well tubing and protection measures. Petro and Chemical Equipment. 21(3), 71-74.

[6] Luo, J. (2019) Study on wellbore corrosion mechanism of gas wells in Yanchang exploration area. Dissertation. Xi'an: Xi'an Shiyou University.

[7] Zhang, J. (2018) Study on wellbore corrosion law and treatment measures in Jing' an sour oil field. Dissertation. Xi'an: Xi'an Shiyou University.

[8] Li, F., Wang, Z., Liu, H., Shi, L. (2014) Corrosion of bacteria to pipeline and sterilization experiment. Oil-Gas field Surface Engineering. 33(9), 22-23.
[9] Lu, J. (2019) Experimental study on the corrosion of shale gas well bore by bacteria content. Chemical Engineering and Equipment. 11, 94-95.
[10] Luo, W. (2017) Simulation research and application of corrosion law in shale gas well casing. Dissertation. Chongqing: Chonqing University of Science and Technology.
[11] Choi, Y., Young, D., NesIc, S., Gray, L. (2013) Wellbore integrity and corrosion of carbon steel in co2 geologic storage environments: A literature review. International Journal of Greenhouse Gas Control. 16, S70-S77.
[12] Jamshidi, V., Davarnejad, R. (2019) Simulation of corrosion detection inside wellbore by x-ray backscatter radiography. Applied Radiation and Isotopes. 145, 116-119.
[13] Chilkoor, G., Shrestha, N., Soeder, D., Gadhamshetty, V. (2018) Corrosion and environmental impacts during the flowback water disposal associated with the BAKKEN shale. Corrosion Science: The Journal on Environmental Degradation of Materials and Its Control.133, 48-60.
[14] Tian, X., Gao, L., Li, D., Wen, N., Han, D., Wang, X., Wang, X. (2019) Reasons of Wellbore Corrosion in Yulin Gas Well. Corrosion and Protection. 40(5), 383-386+390.
[15] Yao, B., Guo, Y., Zeng, W., Zhang, J., Zeng, F., Zeng, D. (2019) Corrosion failure analysis of production tubing of an injection well in Tahe oilfield. Chemical Engineering of Oil and Gas. 48(4), 69-73.
[16] Xiang, L., Zhang, J., Liu, X., Wang, X., Li, D. (2019) Microbiological Influenced Corrosion and Microbiological Influenced Corrosion Inhibition-Overview and a Case Application in Oilfield Produced Water. Corrosion Science and Protection Technology. 31(1), 85-91.
[17] Anwar, I., Chojnicki, K., Bettin, G., Reda, M., Stormont, J. (2019) Characterization of wellbore casing corrosion product as a permeable porous medium. Journal of Petroleum Science and Engineering. 180, 982-993.
[18] Laumb, J., Glazewski, K., Hamling, J., Azenkeng, A., Watson, T. (2016) Wellbore corrosion and failure assessment for CO_2 EOR and storage: Two case studies in the Weyburn field. International Journal of Greenhouse Gas Control. 54, 479-489.
[19] Islam, A., Sun, A. (2016) Corrosion model of CO_2 injection based on non-isothermal wellbore hydraulics. International Journal of Greenhouse Gas Control. 54, 219-227.
[20] Zhang, R., Zhao, G., Shi, D., Li, L., Zhang, J., Cui, L., Pang, Y., Yuan, Z. (2019) Materials Protection. 52(11), 38-43.
[21] Ma, D., Wang, B., Wu, S. (2010) Research on Prediction of Carbon Dioxide Corrosion in Hydrocarbon Production Process. Journal of Southwest Petroleum University (Science and Technology Edition). 32(3), 137-140.
[22] Xu, B., Yuan, B., Wang, Y., Zhu, L. (2018) H_2S-CO_2 mixture corrosion-resistant Fe_2O_3-Amended wellbore cement for sour gas storage and production wells. Construction and Building Materials. 188, 161-169.
[23] Zeng, D., Chen, R., Zhang, Z., Shao, L., Li, G., Tian, G., Shi, T. (2012) Research on stress corrosion sensitivity of C110 casing in wellbore protection fluid. Energy Procedia. 16, 816-821.
[24] Yue, M., Wang, Y. (2018) Corrosion causes and protection measures of oil pipe and surface gathering pipeline in shale gas well. Drilling and Production Technology. 41(5), 125-127.
[25] Wang, J., Yuan, M. (2018) Effects of Setting Depth on Corrosion Behavior of Tubing. Materials Protection. 51(1), 105-108.
[26] Wan, L., Tang, T., Meng, Y. (2006) Corrosion Mechanism and Protection Measure of Wellbore of Oil Well in Changqing Oilfield. Chemical Engineering of Oil and Gas. 35(4), 311-313+325.
[27] Wu, D., Sun, H., Wu, D., Zhou, L., Tang, S., Liu, S. (2010) Influence factors of shaft corrosion in Tazhong-1 gas field in Tarim Basin. Global Geology. 29(2):352-356.
[28] Zhang, Z., Song, C., Dou, X., Yang, K., Ding, J. (2019) Study of the Patterns of Well Casing Corrosion by the CO_2 Huff-and-puff Process and the Maximum Number of Huff-and-puff Cycles. Journal of Southwest Petroleum University (Science and Technology Edition). 41(4), 135-143.
[29] Yuan, X., Xiao, J., Zhang, B., Wang, X., Zhu, Q., Cai, D., Wang, M. (2017) Study on wellbore corrosion control technology in sour gas wells. Chemical Engineering of Oil and Gas. 46(1), 76-78+82.

Received: **29.12.2019**
Accepted: **16.02.2020**

CORRESPONDING AUTHOR

Zhiquan Zhang,
Yangtze University,
School of Petroleum Engineering,
Hubei, Wuhan 430100 – China

e-mail: 3112987217@qq.com

© by PSP Volume 29 – No. 05/2020 pages 3961-3969 Fresenius Environmental Bulletin

EVALUATION OF *TY-2* GENE ABILITY FOR RESISTANCE TO THREE STRAINS OF TOMATO YELLOW LEAF CURL VIRUS-LIKE VIRUSES IN SEGREGATED POPULATIONS OF TOMATO

Mohamed S. Al-Saikhan[1], Adel A. Rezk[2,3,*], Tarek A. Shalaby[1,4]

[1]Department of Arid Land Agriculture (Horticulture Program), College of Agricultural and Food Science, King Faisal University, P.O 400 Al-Ahsa, 31982, , Saudi Arabia
[2]Department of Biotechnology, College of Agricultural and Food Science, King Faisal University, 31982, Al-Ahsa, Saudi Arabia
[3]Virus Research Department, Plant Pathology Research Institute, ARC, Giza 12619, Egypt
[4]Department of Horticulture, Faculty of Agriculture, Kafrelsheikh University, 33516, Kafr El-Sheikh, Egypt

ABSTRACT

The resistance to tomato yellow leaf curl disease was evaluated and analyzed in tomato plants of CLN2498E (source of resistance), Castle Rock, and their progenies F_1, F_2 and BC_1F_1 populations using a sequence tagged site marker, linked to *Ty-2* gene (T0302). Three viral strains (TYLCV-Has, TYLCV-IL and TYLCV-Pep) were used for segregation of resistance and disease evaluation for both parents and their progenies. Results showed that CLN2498E carried *Ty-2* gene marker but Castle Rock did not have this resistance gene. The F_2 and BC_1F_1 plants were segregated for *Ty-2* with ratio closed to 3:1 (X^2=0.86) and 1:1 (X^2=0.60), respectively. These ratios indicated that *Ty-2* gene was simply inherited into the F_2 and BC_1F_1. The phenotypic screening results showed that the resistance to infection was dependent on the type of viral strain. The line CLN2498E was resistant to TYLCV-Has and TYLCV-IL while Castle Rock was susceptible. The plants those have *Ty-2* gene homozygous (Ty-2/Ty-2) or heterozygous (Ty-2/ty2) were resistant to TYLCV-Has and TYLCV-IL while the plants did not carry *Ty-2* gene were susceptible for both strains. In contrast, all the plants were susceptible to TYLCV-Pep even if they were carrying the resistance gene (*Ty-2*).

KEYWORDS:
Molecular Marker, Plant breeding, Six populations, Tomato, *Ty-2* gene, TYLCV.

INTRODUCTION

Tomato (*Solanum lycopersicum* L.) is one of the most valuable vegetable crops worldwide. Its productivity could be improved through either using improved genotypes or applying good agricultural practices. Yield reduction of tomatoes results from a number of factors, including adverse weather conditions, cultural problems, insects and diseases. Low yield and viral diseases are the major limiting factors for good cultivation of tomato in many countries. Tomato yellow leaf curl virus (TYLCV), which is one of the most critical plant diseases, is transmitted by *Bemisia tabaci*. In addition, seeds could transmit it [1]. It is a devastating disease of tomato, seriously affecting the growth of infected tomato plants. Tomato yellow leaf curl virus has become a major limiting factor in tomato production in many tropical and subtropical production regions of the world [2]. Over the last decade, it is a major constraint to tomato production in Saudi Arabia. TYLCV is recorded as a major disease affecting tomato in different locations in Saudi Arabia [3, 4]. *Bemecia tabaci* biotype B spread through the spring and autumn period all over the Saudi Arabia [5]. Yield losses that caused by TYLCV are depended on the growing season and growth stage at which plants become infected [6, 7]. Although chemical control of the vector can limit whitefly and disease, resistance to the chemicals has been reported [8]. Much attention has focused on the transfer of resistant alleles from related wild species into the cultivated tomato. Resistance to TYLCV found in many wild tomato species [9, 10, 11]. Vidavski [12] showed that combining different resistance genes from two parents sometimes resulted in TYLCV resistance greater than that of either parent separately. Molecular markers can be used to produce lines with various combinations of alleles. The convenience of molecular markers that linked to these resistance genes help to accelerate the introgression resistance into the commercial cultivars [13]. These gene-based markers have been established for *Ty-1, Ty-2, Ty-3, Ty-4, Ty-5* and *Ty-6* genes by relative analysis of tomato accessions [9, 14, 15, 16, 17, 18, 19]. *Ty-2* gene is conceded one of the major sources of resistance to TYLCV that used in tomato breeding programs [15, 20]. This TYLCV resistance gene is derived from *Solanum habrochaites* [21]. *Ty-2* a dominant resistance gene introgressed from a *Sola-*

num habrochaites accession into tomato line H24, was maped to the short arm of chromocome 11[14]. *Ty-2* is linked to a region having two DNA markers, cLEN-11-F24 and C2_At1g07960 on chromosome 11[15]. Yamaguchi et al. [21] isolated An NB-LRR gene, TYNBS1 from Begomovirus-resistance locus *Ty-2* and they reported that TYNBS1 is a functional resistance gene and it is considered synonymous with *Ty-2*. The development of tomato genotypes with resistance to TYLCV is an important target for tomato breeding programs worldwide. It would be logical for breeders to focus on the simplest gene combinations that provide adequate resistance for given situations so that acceptable horticultural attributes can be realized along with the resistance. Resistance cultivars are among the cheapest and most environmentally safe ways to manage disease [22]. Therefore, the aim of this study was to evaluate the efficiency of *Ty-2* gene for resistant to some strains of TYLCV.

MATERIAL AND METHODS

Plant materials. The experiments were carried out at the Research and Training Station, King Faisal University in 2017 and 2018. The experiment was conducted with a comercial cultivar Castle Rock that has good fruit quality as female parent and an AVRDC line (CLN2498E) resistance to predominant begomoviruses as male parent. F_1 progeny was produced by crossing a susceptible cultivar (Castle Rock) and resistant line CLN 2498E. F_1 plants were self-pollinated to produce a segregation population of F_2 plants. F_1 plants were back crossed with Castle Rock cultivar to produced BC_1F_1.

Inoculation and disease resistance evaluation. The parents, F_1, F_2 and BC_1F_1 plants were grown under greenhouse conditions for exposing to whiteflies colonies *B. tabaci* biotype B were viruliferous to two strains of the virus; TYLCV-Has and TYLCV-Pep. TYLCV-Has under accession number KF435137 were isolated from Alhasa (East of Saudi Arabia) and characterized by [4] and TYLCV-Pep under accession number KF435136 were isolated from Jizan (South West of Saudi Arabia) [23]. In addition to TYLCV-IL as agrobacterium infectious clone (GV3101 pCAMBIA0390) of cells containing the TYLCV genome Israel strain were provided by Professor Douglas Maxwell (Wisconsin University, Madison, USA) consequently assessed for disease severity as described by Ji et al. [15]. In brief, seedlings at two to three leaves stage were exposed for two weeks to the viruliferous whiteflies with (TYLCV-Has) and (TYLCV-Pep) in two separated cages. Agro-infiltration using a 1-ml needleless syringe for the infectious clone of TYLCV-IL was performed on cotyledons of tomato seedlings at the two to three true leaf stage as described by Dong et al. [24]. After that, the plants were transplanted under greenhouse conditions. Four weeks after transplanting, the plants were first evaluated to disease severity of TYLCV and another two evaluations were carried out after six and eight weeks after transplanting. The disease rating scale was scored 0 to 4 as described by Scott et al. [25] as following; 0 = no symptoms, 1 = slight and light symptoms, 2 = moderate symptoms, 3 =severe symptoms over entire plant, and 4 = very severe symptoms and stunting over entire plant.

Resistant plants were selected according to its phenotypic characteristics. Furthermore, selected plants were evaluated for thier horticultural characterizations in a field experiment. The experiment was laid out in a randomized block design with three replications. Routine cultural practices, similar to those used in tomato commercial production was done as needed. The following data was recorded, plant height (cm), number of branches per plant, leaf number, chlorophyll content (SPAD), yield/plant, average fruit weight (g), and TSS% was measured with digital hand refractometer and presented as Brix. Plant from F_2 and BC_1F_1 progenies along with F_1 and both parents were genotyped using Ty-2 molecular marker (T0302).

DNA Extraction Polymerase Chain Reaction (PCR) analysis. Total genomic DNA was isolated from young leaves of plants 2 to 3 weeks after transplanting using PUREGENE® DNA Purification Kit (Gentra Systems, Inc., Minneapolis, MN) and DNA adjusted to approximately 10 ng/µl. PCR procedure was carried out using the primer pairs TG0302F/TG0302R [9] to identify a sequence tagged site (STS) marker linked with TY-2 locus in the six populations. PCR parameters were for 25-µl reactions containing 2.5 µl 2.5 mM $MgCl_2$, , 2.5 µl 10x buffer,2.5 µl 2.5 mM dNTPs, 0.5 units Dream Taq DNA polymerase (Thermo Fisher Scientific), 2.5 µl of 10 µM of each forward TG0302F: 5'TGGC TCATCCTGAAGCTGATAGCGC'3 and reverse TG0302R: 5' AGTGTACATCC TTGCCATTGACT'3 primers [9], at, 2.5 µl of 10 ng DNA extract and dd H_2O to final volume 25 µl. PCR cycles were 94 °C for 2 min, 35 cycles of 94°C for 30 sec, 55 °C for 1.5 min and 72 °C for 1min. These cycles were followed by 72 °C for 7 min, and then the reaction was held at 4 °C. PCR reactions were performed in the Gene Amp PCR System 9700 (Applied Biosystems). PCR products were separated on 2% agarose gel in 0.5 X TBE buffer, stained with ethidium bromide, and visualized under ultraviolet light to assess TY-2 gene marker. The PCR fragments were sequenced directly with Big Dye sequence kit and analyzed at Macrogen Inc. (Seoul, South Korea). The alignment analyses were performed using online BLAST service of the

National Center for Biotechnology Information (NCBI) (URL: https://blast.ncbi.nlm.nih.gov/Blast.cgi).

Statistical analysis. The data of horticultural characters were subjected to analysis of variance (ANOVA) using SAS general linear model analysis (SAS Institute, Cary, NC). Segrigation ratios were tested for goodnes-of-fit to theoritical ratio for the hypothesis and x^2 testes were performed on the segregating populations using numerical data.

RESULTS AND DISCUSSION

Inheritance of *Ty-2* and idintification of T0302 Marker. In order to screen the parents, F_1, F_2 and BC_1F_1 a sequnce tagged site (STS) marker (T0302) that linked to *Ty-2* gene was used. PCR products of resistant (CLN 2498E) and susceptible (Castle Rock) parents were amplified ~900 bp (Fig 1-A lanes 1 to 5) and ~800bp (Fig 1-A lanes 6 to 10) fragments, respectivily. Two bands (~800 and ~900 bp) were amplified for the F_1 plants as in Fig 1-B. These indicated that the F_1 plants carried Ty-2 locus with heterozygous (Ty/ty) allels. In addition, F_2 and BC_1F_1 plants were segregated Ty-2 locus. One hundred and twenty plants of F_2 were screened for T0302 marker and the results of screening are demonestrated in Fig 1-C and Table 1. The results showing 30 out of 120 plants showed only one band (~900 bp), 62 out 120 plants gave two bands (~800 and ~900 bp) and 28 out of 120 plants showed one band (~800 bp). These results demonstrated that the bands of ~900 bp were inhereted into the second generation and the segregation ratio was about 1:2:1 for (Ty/Ty, Ty/ty and ty/ty, respectivrely). Sixty plants of BC_1F_1 were screened and the results as in table 1 showed that 33 out of 60 plants were heterozygous and showed two bands (~800 and ~900 bp) while 27 out of 60 plants were suseplable and showed one band (~800 bp) (Fig 1-D). This indicated that the segregated ratio was near to 1:1 (X^2=0.6). The results indicated that the bands of ~900 bp were simply inherited into BC_1F_1. All the obtained results were confirmed by phenotypic screeening for the symptoms of virus infection. The nucleotide sequences from resistant and susceptible lines in addition to some of F_2 and BC_1F_1 were carried out and the obtained sequences were submitted in Genbank under accession numbers MK803281 and MK803282, respectively. The sequences of the T0302 for susceptible cultivar Castle Rock were different from the corresponding marker sequence from the resistant line CLN2498E. The alignment analyses demonstrated that the obtained sequences from resistant line (909 bp) were 100% identical with begomovirus-resistance Ty-2 locus derived from *Solanum habrochaites*. These results strongly supported that CLN2498E derived from *S. habrochaites* and had an introgression at Ty-2 locus. When the sequence of T0302 fragment of ty/ty (793 nt) were compared with T0302 fragment of Ty/Ty (909 nt), there were 50 SNPs and five indels (three indels of one nucleotide, one of 3 nt and one of 123 nt) were observed.

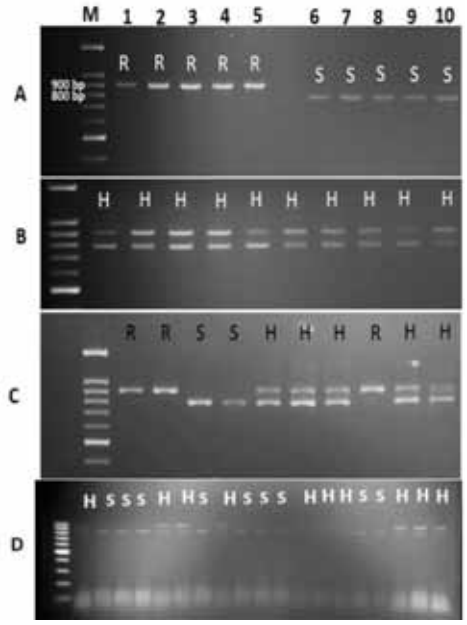

FIGURE 1
PCR fragments of Ty2 gene using TG0302F/TG0302R primers for the T0302 marker. A; PCR products from parents CLN2498E and Castle Rock, B; PCR from F1 and C; PCR products from F2. D; PCR product from BC1F1. R=resistant (Ty/Ty), S= suseptable (ty/ty) and H = heterozygous (Ty/ty).

TABLE 1
Molecular marker linked to *TY-2* gene analysis for both parents and their progeneies F_1, F_2 and BC_1F_1.

Populations	Number of plants	Number of observed plants			Expected ratio	Chi square X^2	P-value
		Resistance		Susceptible S (ty/ty)			
		R (Ty/Ty)	H (Ty/ty)				
Castle Rock	20	0	0	20	0:1	-	
CLN2498E	20	20	0	0	1:0	-	
F_1	20	0	20	0	1:0	-	
F_2	120	30	62	28	3:1	0.86	0.01
BC_1F_1	60	0	33	27	1:1	0.60	0.01

TABLE 2
Chi square (X^2) for the segregation of disease severity of *Tomato Yellow Leaf Curl Virus*(TYLCV-Has) resistance for diffrent populations Castle rock, CLN2498E, F_1, F_2 and BC_1F_1 progenies.

Populations	Total No of plants	Disease severty* TYLCV-Has					Expected ratio	Chi square (X^2)	P value
		0	1	2	3	4			
Castle Rock	125	0	0	10	40	75	0:1		
CLN2498E	109	92	17	0	0	0	1:0		
F_1	162	64	95	3	0	0	1:0		
F_2	306	123	98	19	14	52	3:1	1.25	0.01
BC_1F_1	187	43	49	14	32	49	1:1	0.048	0.01

*plants scored from 0 to 1 were concidered resistant and plant equal or greater than ≥2 were susceptable.

FIGURE 2
The disease Symptoms and rating scale of tomato (yellow) leaf curl disease on tomato plants. 0= Healthy and no symptoms, 1= very light symptoms, 2= moderate Symptoms, 3= severe symptoms and 4= very severe symptoms. From 2 to 4 considered susceptible and 0 to 1 considered resistant.

There are six TYLCV resistance or tolerant genes have been described *Ty-1, Ty-2, Ty-3, Ty-4, Ty-5* and *Ty-6* [9, 11, 15, 16, 27, 27]. Ty-2 is the (84 cM) and TG393 (103 cM) on the centromere and telomeric end of the chromosome, respectively, a distance of at least 19 cM [14]. Ty-2 was delimited to a smaller marker interval between TG36 and TG26 [9]. In the present study, we studied the inheritance of Ty-2 and idintified T0302 marker in the CLN2498E and Castle Rock as parents and their progenies F_1, F_2 and BC_1F_1. The primer set TG0302F/TG0302R effectivly detected the three genotypes Ty2/Ty2, Ty2/ty2 and ty2/ty2 and showed clear bands ~900 bp or ~800 bp for homozygous and ~900 & ~800 bp for heterozygous and no false positves were detected when 240 plants were evaluated. The amplified fragments were expected of TYLCV resistant and susceptible genotypes linked to the Ty-2 locus with primer TG0302F/TG0302R. These results demonstrated that the bands of ~900 and ~800bp were inhereted to the second generation and the segregation ratio was about 1:2:1 (Ty/Ty, Ty/ty and ty/ty, respectivrely) in case of F_2 and 1:1 (Ty/ty and ty/ty) in case of BC1F1.

Segregation of TYLCV resistance and disease evaluation. Three strains of TYLCV (TYLCV-Has, TYLCV-Pep and TYLCV-IL) were used to evaluate both parents and their progenies (F_1, F_2 and BC_1F_1). Evaluation of TYLCV disease severity for parents (Castle Rock and CLN2498E), F_1, F_2 and BC_1F_1 were carried out in the greenhouse by gene responsible for resistance in CLN2498E and was originally mapped to the long arm of chromosome 11 in a region spanning beyond TG36 inoculating with whiteflies from a colonies that were viruliferous for TYLCV-Has and TYLCV-Pep in addition infectious clone of TYLCV-IL. The disease severity were scored from 0 to 4 according to the symptom appearance on the plant as in figure (2). The results showed that there were differences in the resistance of the tested plants to those three strains of the virus. As in table (2) all CLN2498E plants showed resistant in the phenotypic screening for TYLCV-Has, however, all plants of Castle Rock showed severe symptoms, including foliar yellowing, severe stunting and leaf curling and scored equal or more than 2. F_1 plants showing mild symptoms (95 out of 162) and only three plants out of 162 showed moderate symptoms. While the rest of plants (64 out of 162) were with no symptoms (Table 2). Three hundreds and six of F_2 plants had a satisfactory appropriate to a 3:1 ratio (X^2=1.25, $p \leq 0.01$) of resistant to TYLCV-Has versus susceptible plants, supporting control of resistance by a single dominant gene (Table 2). All susceptible plants showed moderate to severe disease symptoms, including curling, stunting and foliar yellowing (Fig 2). No symptoms were observed on (123 out of 306) of the resistant plants. Ninety eight out of 306 of examined plants of F_2 displayed mild symptoms such as weak foliar yellowing and a little of curling with disease severity ratings of less than 2. BC_1F_1 plants were segregated in a ratio 92:95 (X^2=0.048).

They segregated for their reaction towered TYLCV-Has and 95 out of 187 plants of BC_1F_1 were showed moderate to severe symptoms and rating ≥ 2 whereas 92 out of 187 were showed very mild or no symptoms and rating less than 2. Almost same results obtained when the plants evaluated for resistance with TYLCV-IL. The results of disease severity of agro-infiltrated plant with infectious clone of TYLCV-IL are presented in Table 3. Most of the agro-infiltrated of Castle Rock plants (26 out of 28) showed sever symptoms of TYLCV and 2 out of 28 showed moderate symptoms with score 2. In contrast, all treated plants showed resistant to TYLCV-IL and there was no symptoms on the most of agro-infiltrated plant of CLN2498E (19 out of 22). Only three plant out of 22 showed very mild symptoms with score 1. Most of ago-infiltrated plants of F_1 (23 out of 25 plants) showed resistant to TYLCV-IL and scored from 0 to 1 and only 2 out of 25 scored 2 with moderate symptoms. Sixty of F_2 treated plants had segregated in ratio 3:1 (X^2=0.354, $p \leq 0.01$) of resistant to TYLCV-IL in competition with susceptible plants, whereas 26 plants showed no symptoms and 17 plants showed mild symptoms and scored from 0 to 1 while 17 plants showed moderate and sever symptoms of TYLCV and scored from 2 to 4. The infiltrated plants (56 plants) of BC_1F_1 with TYLCV-IL infectious clone had segregated to ratio near to 1:1 (X2=0.07, $p \leq 0.01$) resistance and susceptible whereas 29 plants scored from 0 to 1 and 27 plants scored ≥2. Eight weeks after exposing to viruliferous whiteflies the symptoms were developed from mild to moderate in a few plants. Even so, it still within the average of two or less and the molecular marker analysis for those plants demonstrated that they were homozygous for the introgression. Table (4) demonstrate the results of resistance evaluation for TYLCV-Pep and the results were quite different from the results obtained previously with other two viral strains. Most of treated plants (parents and their progenies) showed moderate to very severe typical symptoms of TYLCV and scored above or equal two. Only few plants (3 out of 78 in case of F_1 and 12 out of 165 in case of F_2) scored less than two. These results demonstrated that *Ty-2* gene is not effective against some strains of TYLCV.

In this study, we used three different strains of TYLCV to evaluate the resistance of TYLCV in the parents and threir progenies (F_1, F_2 and BC_1F_1). Two of them were isolated from the South West (TYLCV-Pep) and from the East (TYLCV-Has) of Saudi Arabia and both of them charachterized [23, 4], respectively. The third strain was TYLCV-IL isolated from Egypt and charachtrized and developed as infecius clone [28]. The results showed that there was a difference in the response of the tested plants to the resistance for the three isolates. The ratios of disease severity for the plants those are infected and evaluated with TYLCV-Has and TYLCV-IL were normal and as expected ratios. All plant of F_1 were resistance and the ratio was 3:1 resistance and susceptible for F_2 plants and was 1:1 for BC_1F_1 plants. These ratios is compatible with the ratios of presence of T0302 Marker in those plants and consistent with the previous obtained results [1, 15]. The results indicated that the analysis using the last rating eight monthes after exposure to whiteflies or agroinfiltration had the same interpretation of the resistance, i.e., an acceptable concordance to a 3:1 ratio of resistant versus susceptible of F_2 plants, as using the first rating. Plants either heterozygous or homozygous for line CLN2498E introgression carrying the *Ty-2* gene showed high levels of resistance to TYLCV-Has and TYLCV-IL, ranging from 0 to 1. The polymerase chain reaction using specific primers for TYLCV-Pep was used to confirm that these symptoms were due to viral infection. *Ty-2* gene is conseder one of the major sourse of resistance to TYLCV that using in many breeding programs but it is not effective againest some strains of TYLCV in some regions in the world as previously described [20]. Rezk [23] and Rezk and Alhudaib [4] were explained that TYLCV-Has and TYLCV-Pep are diffrent strains and separated in diffrent main clusters. TYLCV-Has were located in same main cluster with TYLCV-IL with idetity 94% while TYLCV-Pep located in another cluster with identity near to 90% [4]. This may explain the same respose of the treated plants to TYLCV-Has and TYLCV-IL and different respose of TYLCV-Pep. The phenotypic screening results that previously descibed suggested that the lines carry *Ty-2* gene were not resistant to TYLCV-Thailand strain whereas other lines does not carry *Ty-2* gene were resistant to TYLCV-Thailand strain [29]. Resistant based on *Ty-2* gene can be overcome by TYLCV related to tomato yellow leaf curl Sardinia virus (TYLCSV) [30], while breakdown of *Ty-2* mediated resistance has been recently demonstrated by an isolate of the TYLCV-Mild strain [31]. Our results indicated that there is a difference in the level of resistance of plants to different strains of the virus in Saudi Arabia. Despite they are carrying the resistance gene *Ty-2* but it has shown severe symptoms of viral infections when they are infected with TYLCV-Pep strain. It is important to pay attention as the breeding program takes several years and then the breeders discover that their products is sensitive to some viral strains. Therefore, the types of virus strains in the region should be investigated prior to breeding program for viral resistance. The obtained data indicated that the integration at least two resistance genes in one genotype is necessary to overcome multiple strains of this virus, especially that there are more than four strains of TYLCV in the Kingdom of Saudi Arabia.

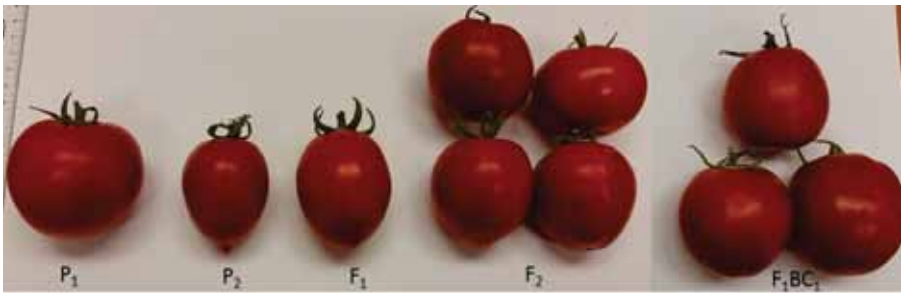

FIGURE 3
Fruits of both parents and their progenies

TABLE 3
Chi square (X^2) for the segregation of disease severity of *Tomato Yellow Leaf Curl Virus* (TYLCV-IL) resistance for diffrent populations Castle rock, CLN2498E, F_1, F_2 and BC_1F_1 progenies.

Populations	Total No of plants	Disease severty* TYLCV-IL					Expected ratio	Chi square (X^2)	P value
		0	1	2	3	4			
Castle Rock	28	0	0	4	11	13	0:1		
CLN2498E	22	19	3	0	0	0	1:0		
F_1	25	14	9	2	0	0	1:0		
F_2	60	26	17	3	3	11	3:1	0.354	0.01
BC_1F_1	56	15	14	6	7	14	1:1	0.07	0.01

*plants scored from 0 to 1 were concidered resistant and plant equal or greater than ≥2 were susceptable.

TABLE 4
Disease severity of *Tomato Yellow Leaf Curl Virus* (TYLCV-Pep) resistance for diffrent populations Castle rock, CLN2498E, F_1, F_2 and BC_1F_1 progenies.

Populations	Total No of plants	Disease severty* TYLCV-Pep				
		0	1	2	3	4
Castle Rock	98	0	0	2	27	69
CLN2498E	44	0	1	10	22	11
F_1	78	0	3	12	28	35
F_2	165	0	6	21	75	63
BC_1F_1	104	0	1	7	31	65

*plants scored from 0 to 1 were concidered resistant and plant equal or greater than ≥2 were susceptable.

TABLE 5
Means ± Standard Error (SE) for studied traits of different tomato populations.

Genotypes	Plant height cm	No of branches	No of leaves	SPAD	Fruit wt (g)	TSS %	Total yield Kg plant $^{-1}$
Castle Rock	140.2±4.1	6.1±0.13	60.2±2.3	32.3±3.2	129.2±5.4	5.3±0.09	4.8±0.02
CLN2498E	160.1±3.2	5.2±0.12	49.4±2.1	41.5±3.3	76.5±4.6	5.3±0.03	4.1±0.01
F_1	131.0±2.9	8.0±0.01	51.4±1.1	38.7±2.1	94.4±3.2	4.7±0.1	5.4±0.05
F_2	125.5±6.5	5.5±0.2	40.6±3.6	39.1±4.6	115.1±5.2	4.7±0.1	4.3±0.21
BC_1F_1	135.4±4.3	6.1±0.16	45.4±2.4	40.2±3.8	105.6±4.6	4.6±0.03	4.6±0.09

Field evaluation for vegetative growth, yield and fruit quality. Data in table (5) showed that wide differences among population means for all studied traits were noticed. F_1 mean was intermediate between both parents in all studied traits except the number of branches per plant. F_1 plants surpassed both parents for number of branches. Concerning this trait, Hegazi et al. [32] and Shalaby [33] mentioned that number of branches per plant inherited as incomplete dominance.

The susceptible parent (Castle Rock) surpassed all other populations in number of leaves and average fruit weight with 60.2 and 129.2g, respectively. Average plant height for F_2 and BC_1F_1 populations was 125.5 and 135.4 cm, respectively. The resistance parent (CLN2498E) surpassed other populations in plant height, and chlorophyll content (SPAD) but produced the lowest average fruit weight with 76.5g. The average fruit weight of F_1 was intermediate between both parents (Fig 3). While F_2 and F_1BC_1 plants gave fruits with an average weight heavier than F_1 plants. The quality characteristics of tomato fruits are very important because they affect the consumer purchase. Fruits of F_1 plants were intermediate between both parents in fruit weight. Shalaby [34] found no hybrid vigor was detected for average fruit weight, but heterosis over better parent was noticed for TSS content in his study. Regarding F_2 population, F_2 plants produced number of leaves less than other populations.

Concerning total yield, F_1 plants produced the highest yield per plant with 5.4 kg, while the parent CLN2498E produced the lowest one with 4.1 kg per plant. This result indicated that there is a hybrid vigor for this trait prior Shalaby [33] and Solieman et al. [35] reported that total fruit yield per plant was inherited by dominance or over dominance genes. In addition, F_2 and BC_1F_1 gave yield less than F_1. Regarding F_2, the means were greatly decreased compared to the F_1 means for plant height, number of branches per plant, total yield and TSS%. TSS content ranged from 4.1 for Line CLN2498E to 5.4 For F_1 fruits (Table 5).

Less yield from F_2 plants, this could be due to presence of inbreeding depression [36]. Significant differences between BC's population and other populations in most studied traits has been found [33]. We noticed from field evaluation that there were many plants that high degree of resistant with good yield. Therefore, selected resistant plants could be used in further tomato breeding programs or as new cultivar but after other cycles of selection to gather disease resistant and high yield and fruit quality. Ty genes are useful in Gulf Cooperation Council Countries and should be incorporated into local cultivar [37]. Disease resistance breeding must be conducted with selection for horticultural and fruit characters [22].

CONCLUSION

Ty-2 dominant gene is one of the important source of resistance to TYLCV in tomato breeding programs. Plants carrying this gene showed resistant to some strains of TYLCV and susceptible to others. Viral strains those are present in the region should be considered in breeding program which aims to use *Ty-2* gene as source of resistance. There are more than four strains of TYLCV are recorded in the Kingdom of Saudi Arabia so the integration at least two resistance genes in one genotype is necessary to overcome of diversity and multiplicity of this virus. Phenotypic screening indicated that there are differences in the level of plant resistance to different virus strains. Selected resistant plants from F_2 and BC_1F_1 that have high yield and fruit quality could be used as new cultivars or in further tomato breeding programs.

ACKNOWLEDGEMENT

The authors extend their appreciation to the Deanship of Scientific Research, King Faisal University, Saudi Arabia, for the financial support. (Grant no. 170014). The Authors wish to thank Research and Training Station in King Faisal University to help for conducting this study.

REFERENCES

[1] Kil, G.J., Kim, S., Lee, Y.J., Byun, H.S., Park, J., Seo, H., Kim, C.S., Shim, J.K., Lee, J.H., Kim, J.K., Lee, K.Y., Choi, H.S., Lee, S. (2016) Tomato yellow leaf curl virus (TYLV-IL): a seed-transmissible geminivirus in tomatoes. Sci. Rrp. 6, 19013.

[2] Lapidot, M., Friedmann, M. (2002): Breeding for resistance to whitefly-transmitted geminiviruses. Ann. Appl. Biol. 140, 109-127.

[3] Alhudaib, K.A., Alaraby, W., Rezk, A.A. (2014) Molecular Characterization of Tomato Yellow Leaf Curl Disease Associated Viruses in Saudi Arabia. International Journal of Virology. 10, 192-203.

[4] Rezk, A.A., Alhudaib, K.A. (2017): Genetic diversity of tomato yellow leaf curl- like viruses in Saudi Arabia. Journal of Plant Science. 12, 5-16.

[5] Alhudaib, K.A., Rezk, A.A., Abel-Banat, B.M., Soliman, A.M. (2014): Molecular identification of the biotype of whitefly (*Bemisia tabaci*) inhabiting the Eastern Region of Saudi Arabia. Journal of Biological Science. 14(8), 494-500.

[6] Polston, J.E., Anderson, P.K. (1997): The emergence of whitefly-transmitted geminiviruses in tomato in the western hemisphere. Plant Dis. 81, 1358-1369.

[7] Liu, J.F., Xiao, Q.M., Zhang, D.Y., Tang, Q.J. (2013): Research progress of Tomato yellow leaf curl virus. Chin. Agric. Sci. Bull. 13, 70-76.

[8] Schuster, D.J., Mann, R.S., Toapanta, M., Cordero, R., Thompson, S., Cyman, S., Shurtleff, A., Morris, R.F. (2010): Monitoring neonicotinoid resistance in biotype B of Bemisia tabaci in Florida. Pest. Management Sci. 66, 186-195.

[9] Hanson, P., Green, S.K., Kuo, G. (2006): Ty-2, a gene on chromosome 11 conditioning geminivirus resistance in tomato. Tomato Genet. Coop. 56, 17-18.

[10] Scott, J.W. (2007): Breeding for resistance to viral pathogens. In: Razdan M.K. and Mattoo A.K. (Eds.) Genetic improvement of Solanaceous crops. vol. 2 tomato (pp. 457-485). Enfield, Science Publishing.

[11] Ji, Y., Scott, J.W., Hanson, P., Graham, E., Maxwell, D.P. (2007): Sources of resistance, inheritance, and location of genetic loci conferring resistance to members of the tomato-infecting begomoviruses. In: H. Czosnek (Ed.), Tomato yellow leaf curl virus disease (pp. 343-362). The Netherlands, Springer.

[12] Vidavski, F.S. (2007): Exploitation of resistance genes found in wild tomato species to produce resistant cultivars; pile up of resistant genes. In: H. Czosnek (Ed.). Tomato yellow leaf curl virus disease: Management, molecular biology, breeding for resistance (pp. 363–372). The Netherlands, Dordrecht, Kluwer publisher.

[13] Yan, Z., Pérez-de-Castro, A., Díez, M.J., Hutton, S.F., Visser, R.G.F., Wolters, A.M.A., Bai, Y., Li, J. (2018): Resistance to Tomato Yellow Leaf Curl Virus in Tomato Germplasm. Front. Plant Sci. 9, 1198.

[14] Hanson, P.M., Bernacchi, D., Green, S., Tanksley, S.D., Muniyappa, V., Padmaja, A.S., Chen, H.M., Kuo, G., Fang, D., Chen, J.T. (2000) Mapping a wild tomato introgression Associated with Tomato yellow leaf curl virus resistance in a cultivated tomato line. J. Am. Soc. Hortic. Sci. 125, 15-20.

[15] Ji, Y., Scott, J.W., Schuster, D.J., Maxwell, D.P. (2009): Molecular Mapping of Ty-4, a new Tomato Yellow Leaf Curl Virus resistance locus on chromosome 3 of tomato. J. Amer. Soc. Hort. Sci. 134, 281-288.

[16] Anbinder, I., Reuveni, M., Azari, R., Paran, I., Nahon, S., Shlomo, H., Chen, L., Lapidot, M., Levin, I. (2009): Molecular dissection of Tomato leaf curl virus resistance in tomato line TY172 derived from *Solanum peruvianum*. Theor. Appl. Genet. 119, 519-530.

[17] Jung, J., Kim, H.J., Lee, J.M., Oh, C.S., Lee, H.J., Yeam, I. (2015): Gene-based molecular marker system for multiple disease resistances in tomato against tomato yellow leaf curl virus, late blight, and verticillium wilt. Euphytica. 205, 599-613.

[18] Lee, J.M., Oh, C.K., Yeam, I. (2015): Molecular markers for selecting diverse disease resistances in tomato breeding programs. Plant Breed Biotech. 3, 308-322.

[19] Gill, U., Scott, J.W., Shekasteband, R., Ogundiwin, E., Schuit, C., Francis, D.M., Sim, S., Smith, H., Hutton, S.F. (2019): Ty-6, a major begomovirus resistance gene on chromosome 10, is effective against Tomato yellow leaf curl virus and Tomato mottle virus. Theoretical and Applied Genetics. 132, 1543-1554.

[20] Mejı´a, L., Teni, R.E., Vidavski, F., Czosnek, H., Lapidot, M. Nakhla, M.K., Maxwell, D.P. (2005): Evaluation of tomato germplasm and selection of breeding lines for resistance to begomoviruses in Guatemala. Acta Hort. 695, 251-256.

[21] Yamaguchi, H., Ohnishi, J., Saito, A., Ohyama, A., Nunome, T., Miyatake, K., Fukuoka, H. (2018) An NB-LRR gene, TYNBS1, is responsible for resistance mediated by the Ty-2 Begomovirus resistance locus of tomato. Theoretical and Applied Genetics. 131, 1345-1362

[22] Hanssen, I.M., Lapidot, M., Thomma, B.J. (2016): Emerging viral disease of tomato crop. Mol. Plant Microbe Inter. 23, 539-548.

[23] Rezk, A.A. (2016): Molecular characterization of Tomato yellow leaf curl virus (TYLCV) infecting pepper and common bean. Int. J. Virol. (12), 1-9.

[24] Dong, P., Han, K., Siddique, M.I., Kwon, J., Zhao, M., Wang, F., Kang, B. (2016) Gene-Based Markers for the Tomato Yellow Leaf Curl Virus Resistance Gene Ty-3. Plant Breeding and Biotechnology. 4, 79-86.

[25] Scott, J.W., Stevens, M.R., Barten, J.H.M., Thome, C.R., Polston, J.E., Schuster, D.J., Serra, C.A. (1996): Introgression of resistance to whitefly-transmitted geminiviruses from Lycopersicon chilense to tomato. In: D. Gerling and R.T. Mayer (Eds.). Bemisia 1995: Taxonomy, biology, damage control, and management (pp. 357–367). UK, Intercept, Andover.

[26] Zamir, D., Ekstein-Michelson, I., Zakay, Y., Navot, N., Zeidan, M., Sarfatti, M., Eshed, Y., Harel, E., Pleban, T., Van-Oss, H., Kedar, N., Rabinowitch, H.D., Czosnek, H. (1994): Mapping and introgression of a tomato yellow leaf curl virus tolerance gene, Ty-1. Theor. Appl. Genet. 88, 141-146.

[27] Hutton S.F., Scott J.W. (2014): Ty-6, a major begomovirus resistance gene located on chromosome 10. Rept. Tomato Genet. Coop. 64, 14-18.

[28] Abhary, M.K., Anfoka, G.H., Nakhla, M.K., Maxwell, D.P. (2016): Post-transcriptional gene silencing in controlling viruses of the Tomato yellow leaf curl virus complex. Arch. Virol. 151, 2349-2363.

[29] Mohamed, S.A., Palchamy, K. (2012): Molecular marker screening for Ty-2 gene in two tomato genotypes (*Solanum lycopersicon* L.). Int J. Scientific and Technology Research. 1(4), 45-47.

[30] Barbieri, M., Acciarri, N., Sabatini, E., Sardo, L., Accotto, G.P., Pecchioni, N. (2010): Introgression of resistance to two Mediterranean virus species causing tomato yellow leaf curl into a valuable traditional tomato variety. J. Plant Pathol. 92, 485-493.

[31] Ohnishi, J., Yamaguchi, H., Saito, A. (2016): Analysis of the Mild strain of tomato yellow leaf curl virus, which overcomes Ty-2. Arch. Virol. 161, 2207- 2217.

[32] Hegazi, H.H., Hassan, H.M., Mousa, A.G., Wahb-Allah, M.A.E. (1995): Heterosis and heritability estimation for some characters of some tomato cultivars and their hybrid combinations. Alex. J. Agric. Res. 40(2), 265-276.

[33] Shalaby, T.A. (2013): Mode of gene action, heterosis and inbreeding depression for yield and its components in tomato (*Solanum lycopersicum* L.). Sci. Hortic. 164, 540-543.

[34] Shalaby, T.A. (2012) Line x tester analysis for combining ability and heterosis in tomato under late summer season conditions. J. Plant Production, Mansoura Univ. 3(11), 2857-2865.
[35] Solieman, T.H.I., El-Gabry, M.A.H., Abido, A.I. (2013) Heterosis, potence ratio and correlation of some important characters in tomato (*Solanum lycopersicum* L.). Sci. Hortic. 150, 25–30.
[36] Metwally, E.I., El-kassas, A.I., Abd El-moneim, A., Bayomy, K.E. (2003): Improving the quality of the Egyptian tomato cultivar "Edkawy". Egyp. J. Plant Breed. 7(1), 551-561.
[37] Alshihi, A.A., Hanson, P., Al-Sadi, A.M., Al-Yahyia, R.A., Briddon, R.W. (2018): Evaluation of tomato inbred lines for resistance to the tomato yellow leaf curl virus disease complex in Oman. Crop Protection. 110, 91-98.

Received: **30.12.2019**
Accepted: **13.02.2020**

CORRESPONDING AUTHOR

Adel A Rezk
Department of Biotechnology,
College of Agricultural and Food Science,
King Faisal University,
31982 Al-Ahsa – Saudi Arabia.

e-mail: arazk@kfu.edu.sa

© by PSP Volume 29 – No. 05/2020 pages 3970-3976 Fresenius Environmental Bulletin

DEVELOPMENT AND FIELD TRIAL OF AN NOVELENVIRONMENTALLY FRIENDLY NANO-SiO_2 PLUGGING AGENT

Ping Yi[1,2,*], Yongle Liao[3], Yungang Zhao[4], Xiliang Fan[1,2]

[1]Oil and Gas Technology Research Institute, PetroChina Changqing Oilfield Company, Xi'an 710018, China
[2]National Engineering Laboratory for exploration and development of low permeability oil and gas fields, Xi'an 710018, China
[3]The 5th Oil Production Plant of PetroChina Changqing Oilfield Company, Xi'an 710086, China
[4]The 8th Oil Production Plant of PetroChina Changqing Oilfield Company, Xi'an 710086, China

ABSTRACT

Ultra-low-permeability tight oil/gas reservoirs and shale gas reservoirs have small fracture sizes, reaching the nanometer level. The conventional water blocking agents have large sizes that cannot penetrate deep into the fractures in these reservoirs to effectively block water. With the increasing requirement of the environmental protection, water blocking agents must not only meet the requirements for entering the reservoir fractures and effectively perform water blocking operations, but also have environmental protection requirements such as non-toxicity, low heavy metal content, and protection of groundwater layers. Therefore, environmentally friendly paraffin wax emulsion was used as a reaction medium to prepare environmentally friendly nano-SiO_2 plugging agents, which solved the problems of conventional nano-SiO_2 plugging agents such as easy agglomeration, uneven particle size distribution, and environmentally unfriendly chemical modification. The experimental results show that the environmentally friendly nano-SiO_2 plugging agent is spherical, has a uniform particle size distribution, good dispersibility, and does not agglomerate. The median particle size is 66.91 nm. The environmentally friendly nano-SiO_2 plugging agent is non-toxic, has low fluorescence level, low oil content, and small heavy metal content. The ultra-low permeability pressure transmission experimental device was used to evaluate the plugging performance of environmentally friendly nano-SiO_2 plugging agent for low-permeability tight sandstone and shale rock samples. After plugging with 4% eco-friendly nano-SiO_2 plugging agent solution, the pressure transmission efficiency is only 10.5% and 7.5%, respectively. After the plugging, the permeability of the core is significantly reduced, and the plugging rate is larger than 95%. Field tests show that after adding environmentally friendly nano-SiO_2 plugging agent, the daily oil production increased from 1.1 t to 1.9 t, and the comprehensive water content decreased from 70.9% to 31.2%, achieving good economic benefits.

KEYWORDS:
Fracturing fracture, water blocking agent, nano-SiO_2, environmental protection, paraffin, plugging performance

INTRODUCTION

With the increase in the exploitation of resources such as oil and natural gas, the conventional oil and gas resources continue to decrease, while unconventional oil and gas resources such as shale gas and low-permeability tight oil and gas have gradually become the focus of exploration and development. Unconventional oil and gas resources play an important role in China [1-3]. China has large low-permeability tight oil and gas reserves and shale gas reserves. However, due to the geological characteristics of these kinds of reservoir, such as small pore throats, small degree of oil and gas extraction, and low oil and gas recovery rate, fracturing is adopted to improve the oil and gas recovery rate [4-5]. After fracturing the reservoir, fractures are generated to increase the degree of oil and gas migration. However, if the fracture is connected to the water layer, the water output will increase, the water content in the comprehensive recovery rate will be high, the degree of reservoir utilization will be low, and economic benefits cannot be guaranteed. Therefore, the oilfield uses a method of injecting water blocking agents to block fractured water layers, improve oil and gas recovery, and greatly improve economic benefits.

During the exploitation of unconventional oil and gas resources, low-permeability oil and gas reservoirs are densely cemented and usually have the characteristics of low porosity and low permeability. The micro-fractures and pore throat sizes of the reservoirs are usually nanometers. Shale gas resources usually exist in extremely small mud shales. Mud fractures and pore sizes of mud shales are usually between 5 and 100 nm [6-8], showing the nanoscale structure. The water blocking agent commonly used in oil fields to block water has a large particle size and cannot enter the depth of nano-scale structural reservoirs for efficient water blocking operations. Nanoparticles have outstanding advantages such as

small size effects, surface effects, and volume effects, and can enter the microfractures and pore throats of ultra-low permeability reservoirs to effectively block the water layer [9-12]. In addition, with the development of the economy, the environmental protection of oilfields has attracted more attention. Water blocking agents used in oil fields must not only meet the requirements for entering the reservoir fractures and effectively perform water blocking operations, but also have environmental protection requirements such as non-toxicity, low heavy metal content, and protection of groundwater layers [13-14].

Nano-SiO_2 has strong rigidity and high strength, which can be bridged and blocked in nanoscale micro-cracks. It is non-toxic, odorless, and pollution-free. The presence of hydrophilic hydroxyl groups on the surface of nano-SiO_2 results in its hydrophilic and oleophobic properties. The nano-SiO_2 is difficult to disperse in polymers or organic matter, and it is easy to agglomerate and lose nanometer scale. Scholars at home and abroad have chemically modified nano-SiO_2 to change its surface characteristics to achieve the function of easy dispersion, but the organic matter in the graft modification remains and the environmental protection performance is not good [15-16]. Studies have shown that paraffin emulsions are non-toxic, non-fluorescent, and easy to decompose. They have good environmental performance and meet the needs of field environmental protection [17-21]. Therefore, in this paper, environmentally friendly paraffin emulsion is used as an intermediate substance, and an environmentally friendly nano-SiO_2 plugging agent for plugging micro-fractured water layers is prepared by a precipitation method to meet the uniformity and other issues. The characteristics and the plugging performance evaluation of the prepared environmentally friendly nano-SiO_2 plugging agent are also evaluated.

MATERIALS AND METHODS

Materials and instruments. Paraffin emulsion, analytical grade, Quzhou County Teli Technology Co., Ltd. Sodium silicate, analytical grade, Shandong Kangmailin Chemical Technology Co., Ltd. Concentrated hydrochloric acid, analytical grade, Zhengzhou Longda Chemical Products Co., Ltd.

DC-B Muffle Furnace, Beijing Original Technology Co., Ltd.; Vacuum Dryer, Changzhou Drying Equipment Co., Ltd.; Microtrac Nano Particle Size Analyzer, Shandong Nakite Analytical Instrument Co., Ltd.; Scanning Electron Microscope, Hitachi, Japan; SQ Ultra-Low Permeability Pressure transmission experimental device, Jiangsu Youchuang Instrument Co., Ltd.

Preparation of environmentally friendly nano-SiO_2 plugging agent. A sodium silicate solution and a hydrochloric acid solution were prepared, wherein the concentration of the sodium silicate solution was 1 $mol \cdot L^{-1}$, and the concentration of the hydrochloric acid solution was 2 $mol \cdot L^{-1}$. Put 200 mL of paraffin emulsion into a three-necked flask, heat to 40 °C and start stirring at a speed of 150 r/min. While stirring, add 40 mL of sodium silicate solution and hydrochloric acid solution. After adding the two solutions, maintain the speed and temperature and stir for 20 min. After cooling to room temperature, a large amount of white precipitate was generated at the bottom of the three-necked flask. After decanting the upper transparent liquid, the white precipitate was centrifuged to obtain a white powder. The white powder was placed in a vacuum drying box and set at 60 °C for 36 hours. After drying, the dried white powder was taken out and placed in a muffle furnace at 850 °C for 1 hour. After taking out, it is cooled to room temperature and the environmentally friendly nano-SiO_2 plugging agent is prepared.

Characterization and performance evaluation. Scanning electron microscope was used to observe the morphology and particle size of environmentally friendly nano-SiO_2 plugging agent. The particle size and distribution of environmentally friendly nano-SiO_2 plugging agent were analyzed by using a nano-particle size analyzer. With reference to national environmental protection standards, the environmental performance of the prepared environmentally friendly nano-SiO_2 plugging agent was analyzed experimentally, including biological toxicity, fluorescence level, petroleum content evaluation, heavy metal content evaluation, etc. An SQ ultra-low permeability pressure transmission experimental device was used to evaluate the plugging performance of environmentally friendly nano-SiO_2 plugging agents for low-permeability tight sandstone and shale cores through pressure transfer efficiency and permeability changes before and after plugging.

RESULTS

Characterization. Scanning electron microscope was used to observe the morphology and particle size of environmentally friendly nano-SiO_2 plugging agent. Figure 1 is a scanning electron microscope photograph of the prepared environmentally friendly nano-SiO_2 plugging agent.

It can be seen from Figure 1 that the appearance of the environmentally friendly nano-SiO_2 plugging agent is regular spherical, the particle size distribution is uniform, and the particle size is between 40 and 80 nm. The environmentally friendly nano-SiO_2 plugging agent prepared by this method has good dispersibility and does not appear agglomeration.

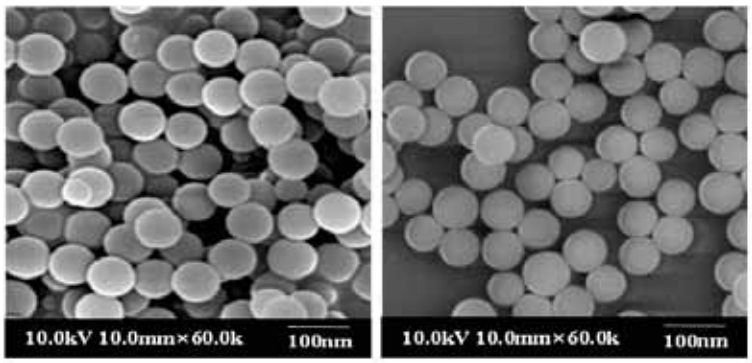

FIGURE 1
Scanning electron micrograph of the prepared environmentally friendly nano-SiO_2 plugging agent.

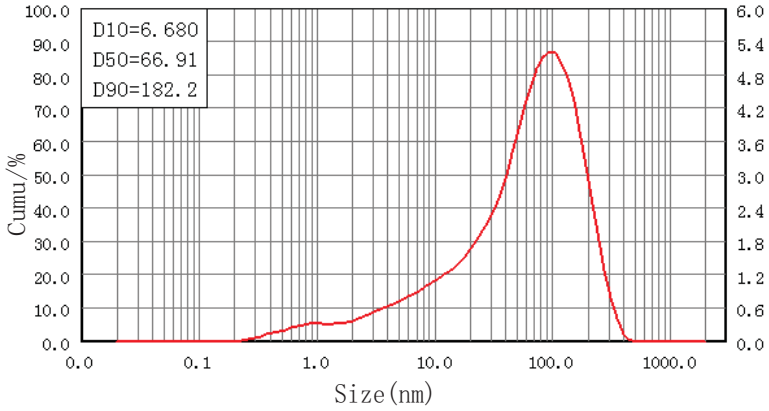

FIGURE 2
Particle size distribution curve of environmentally friendly nano-SiO_2 plugging agent.

An environmentally friendly nano-SiO_2 plugging agent prepared by a precipitation method, wherein a paraffin emulsion is a dispersion medium in the preparation system. The nano-SiO_2 formed in the paraffin emulsion is distributed in the paraffin emulsion and is in contact with the paraffin emulsion. Due to the strong surface effect of the nanoparticles, it has a high surface energy. It is combined with the paraffin emulsion through chemical and physical adsorption. The hydrophilic and oleophobic properties are changed to lipophilic properties, the surface energy is greatly reduced, and it is easy to disperse in organic matter or polymer systems. Therefore, the nano-SiO_2 prepared in the paraffin emulsion by the precipitation method can significantly optimize the surface properties between the nano-SiO_2 and the organic medium, improve its dispersibility in organic or polymer solutions, and help maintain the nanoscale [22-23].

The particle size and particle size distribution characteristics of the prepared environmentally friendly nano-SiO_2 plugging agent were tested using a nano-particle size analyzer. Figure 2 is a particle size distribution diagram of environmentally friendly nano-SiO_2 plugging agent. It can be seen from the figure that the prepared environmentally friendly nano-SiO_2 plugging agent has a unimodal distribution, good dispersibility, and a median particle size of 66.91 nm, which is consistent with the particle size observed by scanning electron microscope. The nano-scale particle size distribution of the nano-SiO_2 plugging agent can effectively block nano-cracks and pores in the formation.

Environmental Performance Evaluation. In recent years, the state has set higher standards for the environmental performance of oil field reagents. Therefore, referring to relevant national and industry standards for the evaluation of environmental performance of oil field reagents, the environmental performance of the prepared environmentally friendly nano-SiO_2 plugging agent has been tested and analyzed, including biological toxicity, fluorescence level, petroleum content, heavy metal content, etc. [24-25].

With reference to China National Petroleum Corporation's standard "Q/SY 111-2007 Oilfield Chemical Agents, Drilling Fluid Biological Toxicity Classification and Detection Method Luminous Bacteria Method", the biotoxicity of environmentally friendly nano-SiO_2 plugging agent was tested. The evaluation indicators are as follows: Luminous bacteria EC_{50} value <1 mg/L, judged to be highly toxic; EC_{50} value 1 ~ 100 mg/L, judged to be severely toxic; EC_{50} value 101 ~ 1000 mg/L, judged to be poisoned; EC_{50} value 1001 ~ 25000 mg/L, judged to be slightly toxic; EC_{50} value larger 25000 mg/L, judged to be non-toxic. Through laboratory experiments, the

biotoxicity EC_{50} value of the aqueous solution containing 4% environmentally friendly nano-SiO_2 plugging agent was tested at 67350 mg/L, and it was judged to be non-toxic. Therefore, the prepared environmentally friendly nano-SiO_2 plugging agent was not toxic to the surrounding environment influences. The ultraviolet light instrument showed that its fluorescence level is smaller than 3, indicating that this agent had no effect on logging.

With reference to the national standard "GB 4914-2008 Offshore Petroleum Exploration and Development Pollutant Emission Concentration Limits", using infrared spectrophotometry, the petroleum content of environmentally friendly nano-SiO_2 plugging agent was tested indoors. If the test result was less than 1%, the petroleum content meets environmental protection requirements. The oil content of the aqueous solution containing 4% environmentally friendly nano-SiO_2 plugging agent was determined to be 0.18%, which meets the requirements of the index. Therefore, the environmentally friendly nano-SiO_2 plugging agent prepared has low petroleum content and meets environmental protection requirements.

With reference to the national standard "GB 4284-1984 Control Standards for Pollutants in Agricultural Sludge", the emission of five heavy metals such as cadmium, mercury, lead, chromium and arsenic will cause pollution to the environment, so the five heavy metal emissions should be controlled [26]. The heavy metal content of environmentally friendly nano-SiO_2 plugging agent was tested according to relevant standards. Table 1 shows the evaluation indexes of heavy metal content and the test results of heavy metal content in environmentally friendly nano-SiO_2 plugging agent. According to the table results, compared to the maximum allowable content of wastewater, the content of five heavy metals in environmentally friendly nano-SiO_2 plugging agent is extremely low, which meets environmental protection requirements.

In summary, the prepared environmentally friendly nano-SiO_2 plugging agent is non-toxic, has a low fluorescence level, does not affect logging. In addition, the nano-SiO_2 plugging agent has a low oil content and extremely low contents of five heavy metals. Therefore, the prepared environmentally friendly nano-SiO_2 plugging agent belongs to the environment-friendly water plugging agent.

Evaluation of plugging performance. An ultra-low permeability pressure transmission experimental device was used to evaluate the plugging performance of nano-SiO_2 materials on low-permeability tight sandstone and shale samples. Core pillar size: 2.5cm in diameter and 5cm in length. The core post is placed vertically in the device, the upper end of the core is connected to the pressure inlet and the lower end of the core is connected to atmospheric pressure and connected to a pressure sensor. The upper pressure is adjusted to 4.0 MPa, and the lower pressure is initially 0 MPa. Rock samples with large porosity and good permeability will transmit the upper pressure to the lower pressure at a faster rate and higher down pressure. Therefore, the plugging performance of the plugging material is evaluated by testing the value of the down pressure. Through the ultra-low permeability pressure transmission experimental device, the core permeability can also be tested, and the plugging ability of the environmentally friendly nano-SiO_2 plugging agent can be judged by the permeability change.

The ultra-low-permeability tight sandstone samples from the HJ-18 block of Changqing Oilfield and the shale cores of the Longmaxi Formation in the Sichuan Basin were selected to conduct environmentally friendly nano-SiO_2 plugging agent plugging experiments. Figure 3 is a scanning electron microscope photograph of the tight sandstones of the Changqing Oilfield and the Longmaxi Formation shale of the Sichuan Basin. From Figure 3, it can be seen that the ultra-low permeability and tight sandstones of the Changqing Oilfield are densely cemented, with micropores (pore diameters of 40 to 200 nm) developed and poor connectivity. The microfractures, bedding and micropores of the Longmaxi Formation shale are developed with an opening of 50-400 nm. The micropores and microfractures of the selected rock samples are all nanometer-sized, which is suitable for the plugging experiments of environmentally friendly nano-SiO_2 plugging agents.

The simulated formation water and 4% environmentally friendly nano-SiO_2 plugging agent solution were used for plugging experiments. The plugging performance of the environmentally friendly nano-SiO_2 plugging agent was evaluated by testing the down pressure value and testing the core permeability before and after plugging.

It can be seen from Figure 4a that, for ultra-low permeability and tight sandstone cores, the simulated formation water pressure is 3.62 MPa after 24 hours of pressure transmission, and the pressure transmission efficiency is 90.5%. The environmentally friendly nano-SiO_2 plugging agent solution has a pressure of 0.42 MPa after 24 hours of pressure transmission, and the pressure transmission efficiency is only 10.5%. It can be known from Figure 4b that for the shale reservoir core, the pressure of the simulated formation water is 3.28 MPa after the pressure is transmitted for 24 hours, and the pressure transmission efficiency is 82%. The environmentally friendly nano-SiO_2 plugging agent solution has a pressure of 0.30 MPa after 24 hours of pressure transmission, and the pressure transmission efficiency is only 7.5%. It can be known from the results that after the environmentally friendly nano-SiO_2 plugging agent acts, the pressure transmission efficiency is low, the nano-silica particles enter the

TABLE 1
Contents of heavy metals in environmentally friendly nano-SiO_2 plugging agents.

Project	Cadmium	Mercury	Lead	Chromium	Arsenic
Permissible emissions /(mg/L)	< 0.1	< 0.05	< 1.0	< 1.5	< 0.5
4% environmental protection nano-SiO_2 blocking agent solution/(mg/L)	0.0016	0.000002	0.00072	0.00016	0.00007

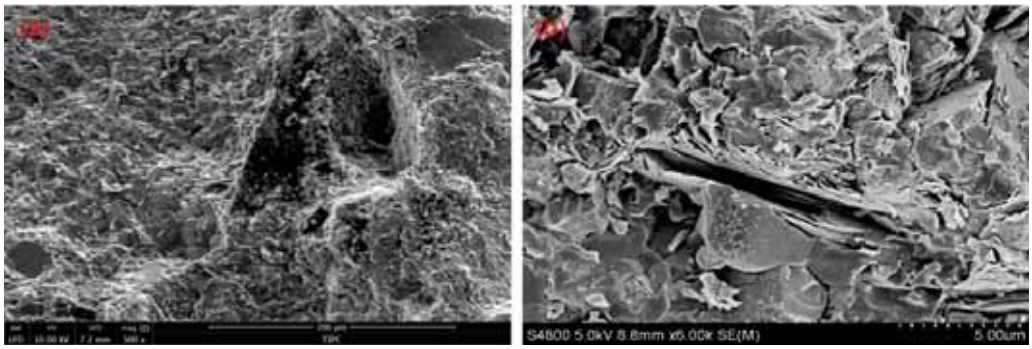

FIGURE 3
SEM photo of the core on site.
Notes: (a) Tight sandstone in Changqing Oilfield, (b) Longmaxi Formation shale in Sichuan Basin.

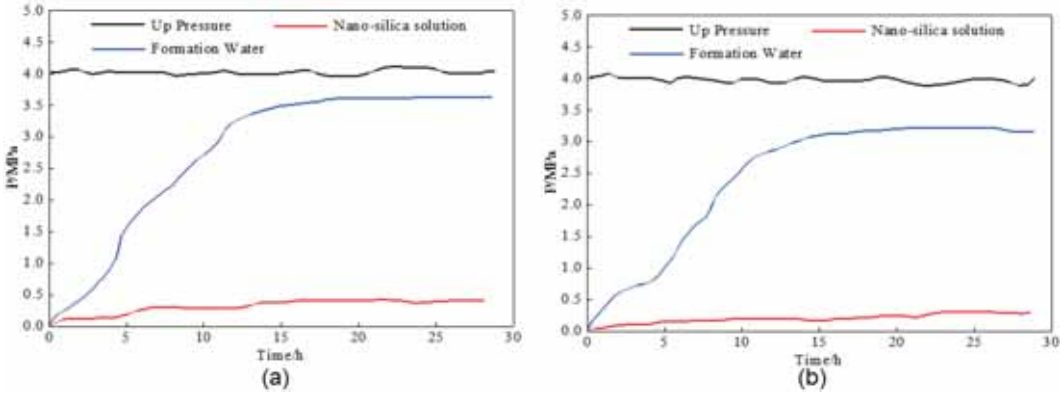

FIGURE 4
Pressure transmission experiment of environmentally friendly nano-SiO_2 plugging agent solution.
Notes: (a) Tight sandstone in Changqing Oilfield, (b) Longmaxi Formation shale in Sichuan Basin.

TABLE 2
Permeability changes before and after core plugging

Core	$K_0/10^{-3}$ μm^{-2}	$K/10^{-3}$ μm^{-2}	Plugging rate /%
Tight sandstone in Changqing Oilfield	0.053	0.0012	97.73
Longmaxi Formation shale in Sichuan Basin	3.2×10^{-4}	2.1×10^{-6}	99.34

Note: K_0 is the permeability before plugging and K is the permeability after plugging

nano-scale cracks and pores of the rock sample, and bridge plugging is performed to effectively plug the water layer.

From the results in Table 2, it can be seen that the core permeability is significantly reduced after plugging, and the plugging rate is> 95%, which proves that the environmentally friendly nano-SiO_2 plugging agent forms plugs in the micropores and microfractures in the core.

Field trial. With the deepening of mining, Chang 6 and Chang 8 reservoirs in Huanjiang Oilfield, Ordos Basin have encountered some production and development problems. For example, the water content of oil wells continues to increase. In this case, with the goal of stabilizing oil and controlling water, the reservoir water layer is effectively blocked. The oilfield reservoir has the characteristics of low porosity, ultra-low-ultra-low permeability. The particle size of conventional water blocking agents is too large, and it is impossible to enter the depth of microfracture formations for effective plugging. The environmental protection situation is grim. Therefore, using the environmentally friendly nano-SiO_2 plugging agent developed in this paper, in July 2018, the HJ-18 block of Huanjiang Oilfield was selected to carry out environmentally friendly nano-plugging agent water control technology mine test in

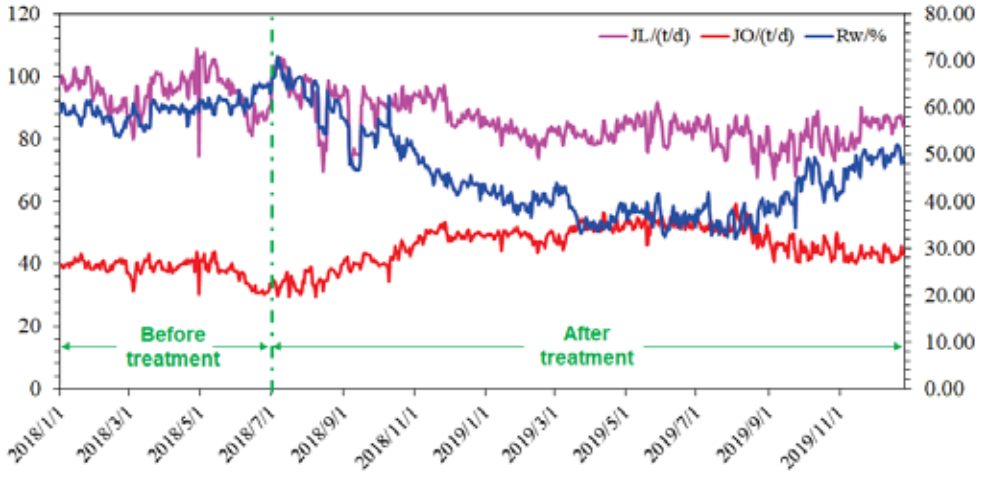

FIGURE 5
Analysis of water control test results of environmentally friendly nano-blocking agent.

Changqing Oilfield, including 4 well groups. The main parameters such as the daily liquid production volume (JL) and the daily oil production volume (JO) of the test well before and after the polymer water control test were calculated and compared to analyze the effect of the new environmentally friendly nano-blocking agent. Among them, the water content R_w is obtained according to formula (1):

$$R_w = \frac{JL - JO}{JO} \times 100\% \quad (1)$$

The test results are shown in Figure 5. From the test results, it can be seen that the average daily oil production of the test wells before construction was 1.1 t, the daily liquid production was 3.8 m^3, and the comprehensive water content reached 70.9%. After using the plugging agent, the daily oil production is 1.9 t, the daily liquid production is 2.7 m^3, and the comprehensive water content is reduced to 31.2%. The plugging effect is remarkable, and good economic benefits have been achieved.

CONCLUSIONS

(1) Using paraffin emulsion as the reaction medium, an environmentally friendly nano-SiO_2 plugging agent was prepared by a precipitation method. The shape of the environmentally friendly nano-SiO_2 plugging agent was spherical, with uniform particle size distribution, good dispersibility, non-agglomeration, and median particle size of 66.91 nm. The new plugging agent is an environmentally friendly nano-water blocking agent with low fluorescence level, low oil content and small heavy metal content.

(2) For low-permeability tight sandstone and shale rock samples, after using 4% environmentally friendly nano-SiO_2 plugging agent solution for plugging, the pressure transmission efficiency is only 10.5% and 7.5%, and the core permeability is significantly reduced after plugging. The plugging rate is larger than 95%. The environmentally friendly nano-SiO_2 plugging agent forms a bridge plugging in the nano-scale micro-pores and micro-cracks in the core.

(3) Field tests showed that after adding environmentally friendly nano-SiO_2 plugging agent, the daily oil production increased from 1.1 t to 1.9 t, and the comprehensive water content decreased from 70.9% to 31.2%. The plugging effect was significant and good economic benefits were achieved.

ACKNOWLEDGEMENTS

The authors would like to show sincere thanks to those techniques who have helped this research and all the authors of the references.

REFERENCES

[1] Chang, H., Liu, B., Crittenden, J., Vidic, R. (2019) Resource Recovery and Reuse for Hydraulic Fracturing Wastewater in Unconventional Shale Gas and Oil Extraction. Environmental Science and Technology. 53(23), 153-163.

[2] Auwalu, I., Mohammed, B., Mark, B., James, N. (2019) Prediction of casing critical buckling during shale gas hydraulic fracturing. Journal of Petroleum Science and Engineering. 35(2), 101-112.

[3] Ying, Z., Hao, Z., Ergun, K., Kuang, J., She, J. (2019) The forced imbibition model for fracturing fluid into gas shales. Journal of Petroleum Science and Engineering. 16(3), 179-192.

[4] Li, D. (2018) Investigation on plugging fractured water layer with nanoparticle in fracturing process. Dissertation. Chengdu: Chengdu University of Technology.

[5] Deville, J., Fritz, B., Jarrett, M. (2011) Development of Water-Based Drilling Fluids Customized for Shale Reservoirs. SPE Drilling and Completion. 26(4), 484-491.

[6] Jarvie, D., Hill, R., Ruble, T. (2007) Unconventional shale-gas systems: The Mississippian Barnett Shale of north-central Texas as one model for thermogenic shale-gas assessment. AAPG Bulletin. 91(4), 475-499.
[7] Bahattab, M., Donate, R., Garcia, P. (2011) Characterization of polyurethane adhesives containing nano-silicas of different particle size. International Journal of Adhesion and Adhesives. 31(2), 97-103.
[8] Zhang, Y., Li, G., Wu, D., Li X., Yu, Y., Luo, P., Chen, J., Dai, C., Wu, Y. (2019) Recent advances in emerging nano-materials based food sample pretreatment methods for food safety screening. Trends in Analytical Chemistry. 121, 115669.
[9] Yao, J., Huang, C., Liu, C., Yang, M. (2020) Upconversion luminescence nanomaterials: A versatile platform for imaging, sensing, and therapy. Talanta. 208.
[10] Chevron, I. (2018) Patent Issued for Hexadecene Synthetic Drilling Fluid with Improved Environmental Properties. Journal of Engineering. 12(5), 56-62.
[11] Pettersson, A. (2007) High-performance base fluids for environmentally adapted lubricants. Tribol Int. 40(4), 638-645.
[12] Cai, J., Chenevert, M., Sharma, M. (2012) Decreasing water invasion into Atoka shale using nonmodified silica nanoparticles. SPE Drilling and Completion. 27(01), 103-112.
[13] Qi, C., Zhi, Y., Tao, L. (2016) Preparation and analyses of nano SiO_2 plugging agent modified with silane coupling agent. Drilling Fluid and Completion Fluid. 33(4), 47-50.
[14] Yan, L., Sun, J., Ji, Y. (2014) Preparation and properties evaluation of silica nano plugging agent in drilling fluid. The 2014 National Conference on Drilling Completion Fluid Technology Communication, Beijing, China Petrochemical Press.
[15] Li, X., Hong, C., Pan, C. (2010) Preparation and characterization of hyperbranched polymer grafted mesoporous silica nanoparticles via self-condensing atom transfer radical vinyl polymerization. Polymer. 51(1), 92-99.
[16] Mao, H., Qiu, Z., Shen, Z. (2014) Synthesis and mechanism of hydrophobic associated polymer based nano-silica filtrate reducer. Acta Petrolei Sinica. 35(4), 771-778.
[17] Yan, J., Yu, C., Liang, C. (2018) Synthesis and evaluation of a nanophase wax emulsion plugging material. Drilling Fluid and Completion Fluid. 35(2), 73-77.
[18] Dai, L., Li, H., Su, X. (2012) Research and application on nano-prarffin emulsion. Drilling Fluid and Completion Fluid. 29(2), 5-7.
[19] Tadros, T., Zquierdo, P., Esquena, J., Solans, C. (2004) Formation and stability of nano-emulsions. Adv. Colloid Interface Sci. 108-109, 303-318.
[20] Pey, C., Maestro, A., Sole, I., Gonzalez, C., Solans, C., Gutierrez, J. (2006) Optimization of nano-emulsions prepared by low- energy emulsification methods at constant temperature using a factorial design study. Colloids and Surfaces A. 288, 144-150.
[21] Izquierdo, P., Esquena, J., Tadros, T., Dederern, C., Garcia, M., Azemar, N., Solans, C. (2002) Formation and Stability of Nano- Emulsions Prepared Using the Phase Inversion Temperature Method. Langmuir. 18, 26-30.
[22] Liu, Y., Qiu, Z., Zhong, H., Nie, Z., Li, J., Huang, W., Zhao, X. (2019) Bitumen Recovery from Crude Bitumen Samples from Halfaya Oilfield by Single and Composite Solvents-Process, Parameters, and Mechanism. Materials. 12(17), 2656.
[23] Liu, Y., Qiu, Z., Zhong, H., Nie, Z., Xing, X., Yan, F., Zhao, X., Bao, D. (2019) Experimental study on optimization of drilling fluid technology for bituminous formation. Fresen. Environ. Bull. 28, 5591-5598.
[24] Wu, D., Ju, Z. (2010) Synthesis of Nano-Alumina Hydroxide from Liquid Paraffin Microemulsion. Shandong Ceramics. 33(02), 8-10.
[25] Schaanning, M., Trannum, H., Xnevad, S., Carroll, J., Bakke, T. (2008) Effects of drill cuttings on biogeochemical fluxes and macrobenthos of marine sediments. Journal of Experimental Marine Biology and Ecology. 361(1), 49-57.
[26] Xing, X., Wang, J., Cao, Y., Shu, F., Xiang, X., Jiang, Z., Wang, B. (2018) Evaluation and Application of an Environmentally-Friendly Drilling Fluid Plugging Agent. Green Petroleum and Petrochemicals. 3(04), 52-55.

Received: **31.12.2019**
Accepted: **12.02.2020**

CORRESPONDING AUTHOR

Ping Yi
Oil and Gas Technology Research Institute,
PetroChina Changqing Oilfield Company,
Xi'an 710018 – China

e-mail: yip3_cq@petrochina.com.cn

© by PSP Volume 29 – No. 05/2020 pages 3977-3983 Fresenius Environmental Bulletin

DRIVING RISK PREDICTION TECHNOLOGY OF ECO-FRIENDLY VEHICLE BASED ON FUZZY COMPREHENSIVE EVALUATION MODEL

Jianren Liu*

School of Civil and Transportation Engineering, Qinghai Nationalities University, Xining 810007, China

ABSTRACT

Due to the vagueness of vehicle driving risk prediction, the traditional ecological environment-friendly vehicle driving risk prediction technology has poor accuracy in vehicle risk prediction. Therefore, an ecological environment-friendly type based on fuzzy comprehensive evaluation model is designed. This study, we analyzed the driving data, extracted the driving behavior characteristic parameters of the eco-friendly vehicle, and used the vehicle speed exceeding the speed limit, the average speed, the standard deviation of acceleration and the negative acceleration as the characteristic indicators of the driving risk prediction of the eco-friendly vehicle. Then we used the fuzzy comprehensive evaluation model to establish a predictive index matrix, calculate the index weight, and classify the vehicle driving risk. Finally, the index weight is combined with the vehicle driving risk classification result to obtain the ecological environment-friendly vehicle driving risk prediction. The experiment proved that the design of the eco-environment-friendly vehicle driving risk prediction technology based on the fuzzy comprehensive evaluation model is more accurate than the traditional technology and can accurately predict the vehicle driving risk.

KEYWORDS:
Fuzzy comprehensive evaluation model, eco-environment friendly, vehicle driving, risk prediction, weight

INTRODUCTION

The rapid development of the national economy is inseparable from various means of transportation. Vehicles, as one of the important ones, have important links with human social activities. Eco-environment-friendly vehicles are very important means of transportation, which are closely related to the various lives of human society [1-4]. As people pay more and more attention to the environmental protection, traditional fossil fuel vehicles are gradually turning to eco-friendly energy vehicles. Clean energy such as solar, hydrogen and other sustainable renewable energy sources have become the first choice for vehicle energy. While eco-friendly vehicles bring convenience to people, road traffic accidents have also increased. Improving the safety level of vehicle operation has become an urgent problem to be solved [5-7]. Eco-environment-friendly vehicle driving has great randomness, thus, the traditional risk prediction methods cannot obtain high-precision vehicle driving risk prediction results.

Therefore, an ecological environment-friendly vehicle driving risk prediction technology based on fuzzy comprehensive evaluation model is designed. The fuzzy comprehensive evaluation model refers to the overall evaluation of things or phenomena affected by a variety of fuzzy factors. Fuzzy refers to the unclear boundaries, the unclear intermediate functions, the exact meaning in quality, and the unclear wiring in quantity [8, 9]. It has better analysis performance on system safety and hazard. Therefore, it is applied to the driving risk prediction of eco-friendly vehicles to reduce the risk of driving. From the perspective of improving the accuracy of vehicle risk prediction, this study first analyzed driving data, extracted the driving behavior characteristic parameters of eco-friendly vehicles, and used the vehicle speed which exceeded the speed limit, the average speed, the standard deviation of acceleration, and negative acceleration as the indicators for driving risk prediction of ecological environment friendly vehicles. Then, the fuzzy comprehensive evaluation model is used to calculate the weight vector of each index, and the risk prediction index is graded [10-13]. The classification result is combined with the index weight to complete the prediction of the driving risk of eco-friendly vehicles. The experimental comparison results show that the technology designed in this study is more accurate than the traditional technology in vehicle driving risk prediction and has certain practical significance.

TABLE 1
Vehicle driving behavior characteristic parameters

Driving conditions	Driving speed	Driving acceleration
Speed limit	Average speed	Mean positive acceleration
Idle speed	Speed standard deviation	Standard deviation of positive acceleration
Cruise	Speed variance	Maximum positive acceleration
Travel distance	Sum of squares of vehicle speed	Acceleration mean
Kinetic energy	Maximum speed	Standard deviation of acceleration

BASIC PARAMETERS EXTRACTION AND METHODS

Extraction of characteristic parameters of driving behaviors of eco-friendly vehicles. There are different driving risks in the process of driving a vehicle. From the driving operation intention, it can be divided into various driving modes [1, 14-15], such as lane changing, straight driving, turning, etc. Each driving mode is the output of driving data. Therefore, we analyzed the driving data of eco-environment-friendly vehicles, and extracted the characteristic parameters related to vehicle driving behavior that involve vehicle driving risk. Table 1 is the main characteristic parameters of vehicle driving behavior.

Combining the driving attributes of eco-friendly vehicles and the main factors affecting the driving risk of the vehicle [16-18], the vehicle speed that exceeds the speed limit, the average speed, the standard deviation of acceleration, and the negative acceleration are used as the characteristic indicators for driving risk prediction of eco-friendly vehicles.

Vehicle speed is an important factor that causes vehicle driving safety. According to related research on vehicle running speed and road speed limit, when the speed is set to exceed 80% of the road speed limit, it is considered to have a driving risk tendency [19-21], and the speed exceeds the limit. The time ratio of speed is:

$$\eta=\frac{t_{180\%}}{t}\times 100\% \tag{1}$$

In formula (1), t represents the total time the vehicle travels, $t_{180\%}$ represents the cumulative time that the vehicle exceeds the speed limit, and η represents the proportion of time that the vehicle speed exceeds the speed limit value.

The average speed [22-24] is an important parameter index reflecting the driving behavior characteristics of the vehicle. The calculation formula is as follows:

$$\sigma=\sqrt{\sum_{i=1} a\left(d-b''\right)} \tag{2}$$

In formula (2), σ represents the standard deviation of the overall speed of the vehicle during driving, $\sum_{i=1} a$represents the total sample of vehicle speed in natural driving data, d represents the average value of the overall vehicle speed, and b'' represents the average value of the positive acceleration of the vehicle.

The driver's control of the accelerator pedal and other devices can be reflected by the acceleration value. This behavior directly affects the start and stop of the vehicle [25, 26], acceleration, deceleration, and ride comfort. Therefore, the acceleration standard deviation [8, 27] is used as a parameter index of driving behavior characteristics, as follows:

$$\overline{a}=\sqrt{\frac{1}{n}\sum n/o} \tag{3}$$

In formula (3), $\overline{a}$ represents the average acceleration of the vehicle during driving, $\frac{1}{n}$ represents the standard deviation of the overall acceleration, $\sum n$ represents the standard deviation of the positive price speed, o is the vehicle-mounted index parameter.

During the driving process of the vehicle, the driver will change the negative acceleration of the on-board parameter by controlling the pedal, and the speed could reflect the urgency of the vehicle braking [27, 28], expressed as:

$$c=\frac{q}{n}\left|v/h\right|*i \tag{4}$$

In formula (4), c represents the number of negative accelerations of the vehicle during driving, $\frac{q}{n}$ represents the average value of the overall negative acceleration of the vehicle, v , h represent the standard deviation, respectively, and i denotes hidden safety hazard parameter [29].

In summary, there are four extracted driving behavior characteristic parameters of eco-friendly vehicles. The rest are not selected because they are not closely related to the driving risk of the vehicle itself. The selected indicators are used as the basis for the prediction of driving risks of eco-friendly vehicles.

Realization of Eco-environment Friendly Vehicle Driving Risk Prediction. On the basis of the extraction of the characteristic parameters of the driving behavior of the eco-friendly vehicle, the driving risk prediction of the eco-friendly vehicle is completed. Due to the ambiguity of the selected characteristic parameters of driving behaviors of eco-environment-friendly vehicles [30-31], in order to make up for the deficiencies in the interpretation

of the main components of driving behavior parameters of vehicles, the fuzzy comprehensive evaluation model [32] is used. The evaluation model estimates the weights of the indicators selected above. The block diagram of the fuzzy comprehensive evaluation model is shown in Figure 1.

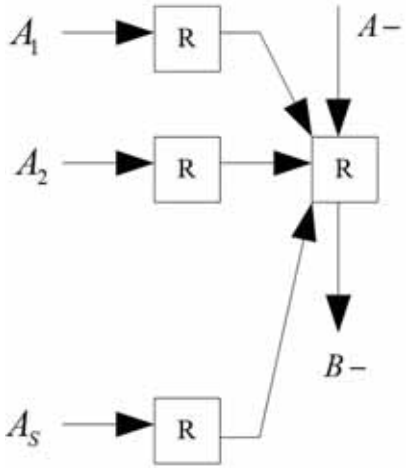

FIGURE 1
Fuzzy block diagram of fuzzy comprehensive evaluation.

The figure above shows a fuzzy block diagram of fuzzy comprehensive evaluation. This model is used as the core of the design to predict the driving risk of eco-friendly vehicles [33]. The steps are as follows:

Step 1: Use fuzzy comprehensive evaluation model to determine the weight of the risk index of eco-friendly vehicle risk prediction [16, 33], establish the prediction index matrix as the second index of the first vehicle risk prediction scheme, and obtain the following formula:

$$H = R^t\left(r_{ij}\right)/mn \tag{5}$$

In formula (5), R^t represents the degree of membership of the evaluation factor R to the evaluation index t, and mn represents the parameter of the prediction index.

Step 2: Calculate the weight vector of driving risk for eco-friendly vehicles [34], the calculation formula is:

$$\varepsilon_i = n - \sum_{i=1} f \tag{6}$$

In formula (6), ε_i represents the fuzzy composition operator, n represents the weight coefficient of each risk index, and $\sum_{i=1} f$ represents the degree of membership of the evaluation object to the evaluation level.

Step 3: The weight vectors of vehicle driving behavior characteristic parameters are linearly combined [35], and several comprehensive variables are extracted and processed to classify vehicle driving risk. The classification process is shown in Figure 2.

Step 3: According to the basic idea of the fuzzy comprehensive evaluation principle, the driving risk level of the vehicle is analyzed. If the indicator has no difference in the results of different risk prediction schemes, it means that the indicator has no effect or has a small effect on the risk prediction result, which can be ignored. Set its weight to 0. The deviation [36] between risk prediction results is defined as:

$$s_h = \sum_{i=1} v\left|r - r_k\right| \tag{7}$$

In formula (7), s_h represents the optimal weighting vector, $\sum_{i=1} v$ represents the total dispersion of the prediction result, r represents the calculation parameter of the total dispersion, and r_k represents the influence parameters of all indicators on the total dispersion of the prediction result.

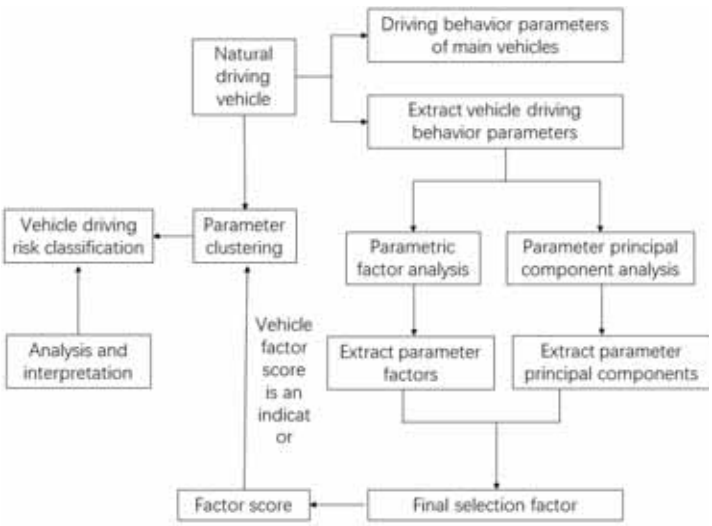

FIGURE 2
Vehicle driving risk classification process.

The vehicle driving risk prediction index weights obtained from the fuzzy comprehensive evaluation model are combined with the classification results to obtain the eco-environment-friendly vehicle driving risk prediction results.

RESULTS

In order to verify the effectiveness of the eco-environment-friendly vehicle driving risk prediction technology based on the fuzzy comprehensive evaluation model designed in this study, an experimental comparison was performed. The traditional prediction technology was compared with the designed technology in this study.

Experimental data. The historical risk data of one of the main lines in a city within ten days of a month was used as the experimental object. Using the number of collisions of eco-friendly vehicles in a city within 10 days of a month as the risk value, a graph of the number of collisions is generated to form a vehicle driving risk prediction dataset, as shown in Figure 3.

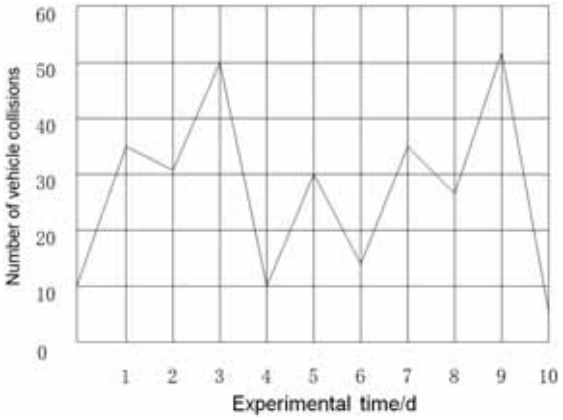

FIGURE 3
Actual number of vehicle collisions.

The figure above shows the curve of the actual number of collisions of vehicles on the experimental road within 10 days, which provides a basis for experimental comparison.

Experimental platform construction. We established an experimental platform based on Matlab 2017 and wrote a program to realize the vehicle driving risk prediction technology of fuzzy comprehensive evaluation model. The experimental platform built is shown in Figure 4.

It can be seen from the analysis of the above figure that the experimental platform uses the control terminal to control the experimental progress after inputting actual data, and outputs the final experimental results through the display. The data analysis software is used to analyze the number of vehicle collisions predicted by the two ecological environment-friendly vehicle driving risk prediction technologies [37-38]. The experimental values are compared with the actual values. A large difference from the actual values indicates that the prediction technology is ineffective, and the accuracy is low. Otherwise, the accuracy of risk prediction is high.

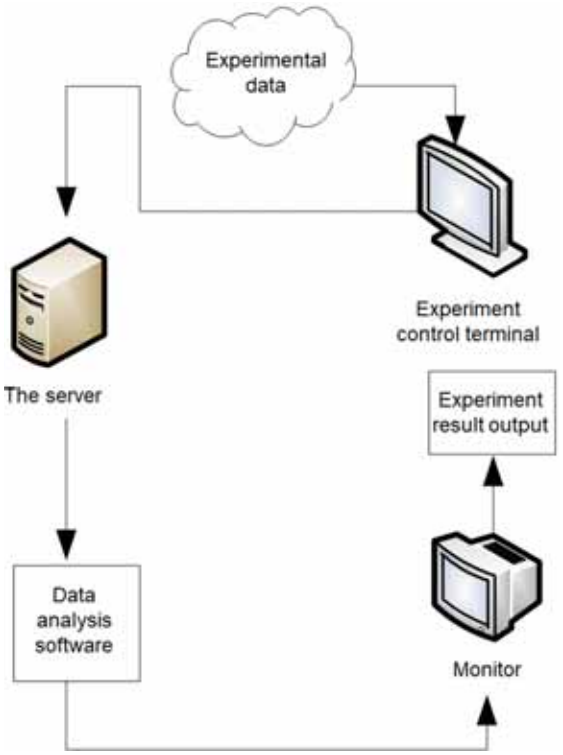

FIGURE 4
Experimental platform.

Discussion of experimental results. From the analysis of Figure 5, it can be known that the designed method in this study has a small difference from the actual value curve in the prediction of the number of collisions of the vehicle and is basically a fitted state. Only in the collision prediction on the 2nd and 4th days, it has a certain degree of difference with the actual value. However, the difference is small, which proves that the technical risk prediction accuracy of this method is high. However, the traditional driving risk prediction technology differs greatly from the actual value curve in the prediction of the number of vehicle collisions, and it also differs greatly from the prediction result of the method designed in this study. Therefore, through the above experiments, it can be known that the ecological environment-friendly vehicle risk prediction technology based on the fuzzy comprehensive evaluation model is more accurate than the traditional vehicle risk prediction technology. The risk prediction value of the designed technology is closer to the actual value, which improves the accuracy of driving risk prediction for eco-friendly vehicles.

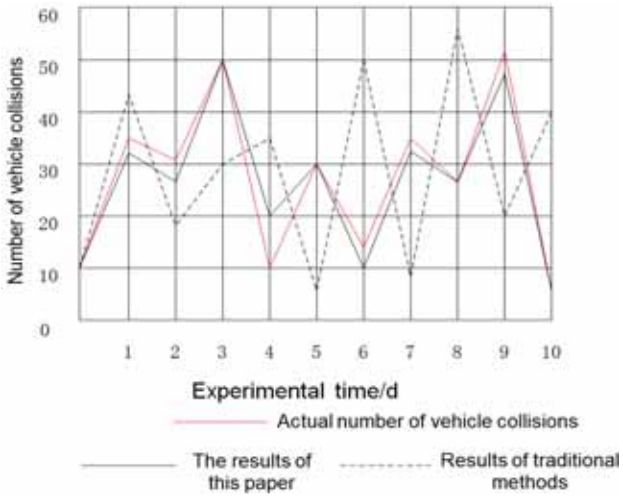

FIGURE 5
Experimental comparison results.

CONCLUSIONS

(1) By analyzing the shortcomings of traditional vehicle driving risk prediction technology in vehicle driving risk prediction, an ecological environment-friendly vehicle driving risk prediction technology based on fuzzy comprehensive evaluation model is designed.

(2) The design of the eco-environment-friendly vehicle driving risk prediction technology based on the fuzzy comprehensive evaluation model is more accurate than the traditional technology, and it can reasonably predict the vehicle driving risk. Eco-environment-friendly vehicle driving risk prediction can provide an important theoretical basis for objectively evaluating the degree of vehicle driving risk and risk control measures.

(3) Fuzzy comprehensive evaluation model provides a new forecast for vehicle risk prediction.

ACKNOWLEDGEMENTS

This work was financially supported by the Major Science and Technology Project in Qinghai Province, China (No. 2015-SF-A5).

REFERENCES

[1] Huang, L., Cui, W., Song, R., Wang, Y. (2018) Risk Prediction of the Freight Distribution in Dry Bulk Port Using Bayesian Network. Journal of Beijing Jiaotong University (Social Sciences Edition). 17(2), 118-130.

[2] Zhang, C., Qi, C., Yan, X., Shao, D., Zhang, M. (2018) Risk Analysis of Semitrailer Overtaking on Curved Sections Based on Dynamic Simulation. Journal of System Simulation. 30(4), 1439-1447.

[3] Hu, L., Li, L., Wang, M., She, T. (2017) Study on Braking Risk Threshold Value for Full-loaded Medium Trucks on Continuous Long and Steep Downhill Sections Based on Bench Test. Journal of Highway and Transportation Research and Development. 34(7), 135-144 + 152.

[4] Zhang, C., Wang, B., He, J., Xiang, D., Yilixiati, A. (2019) Traffic Risk Analysis of Ponding Sections on Freeways Based on Driving Dynamics. Journal of Transport Information and Safety. 37(5), 9-17.

[5] Bylykbashi, K., Qafzezi, E., Ikeda, M., Matsuo, K., Barolli, L. (2020) Fuzzy-based Driver Monitoring System (FDMS): Implementation of two intelligent FDMSs and a testbed for safe driving in VANETs. Future Generation Computer Systems. 105, 665-674.

[6] Abbasi, M., Taki, M., Rajabi, A., Li, L., Zhang, J. (2019) Coordinated operation of electric vehicle charging and wind power generation as a virtual power plant: A multi-stage risk constrained approach. Applied Energy. 239, 1294-1307.

[7] Jia, W., Wang, Y., Su, H., Liu, Y., Lin, S. (2019) Risk Evaluation of Rail Vehicles Based on Risk Network. Journal of Transportation Systems Engineering and Information Technology. 19(4), 143-148.

[8] Long, H., Hu, Y., Liu, B., Jin, X., Zhu, H. (2016) Fatigue Life Prediction for the Spot Welds of Body-in-white Based on Random Loadings. Automotive Engineering. 38(8), 1006-1010.

[9] Qin, Y., Liu, Z., Sui, Y. (2016) Compilation of the Driver's Risk Awareness Questionnaires Based on Risk Driving Scenarios. Journal of Wuhan University of Technology (Transportation Science and Engineering). 40(1), 1-5.

[10] Wu, Y., Jia, W., Li, L., Song, Z., Xu, C., Liu, F. (2019) Risk assessment of electric vehicle supply chain based on fuzzy synthetic evaluation. Energy. 182, 397-411.

[11] Sun, C., Xin, F. (2016) An Overview of the Conflict Indicators between Vehicles and Pedestrians. Journal of Transport Information and Safety. 34(2), 9-16+38.
[12] Peng, J., Fu, R., Guo, Y. (2015) Real-time prediction of lane-changing behaviors under naturalistic driving conditions. Journal of Harbin Institute of Technology. 47(9), 119-123.
[13] Zhou, K., Wu, W., Yao, W., Luo, X. (2015) Highway traffic safety assessment in foggy weather. Journal of Transport Science and Engineering. 1, 79-84.
[14] Sun, C., Nie, J. (2015) Efficiency Prediction of Automatic Braking System Based on Accident Form Research. Hunan Agricultural Machinery. 8, 51-52+57.
[15] Zhou, Y., Ravey, A., Marie-Cécile, P. (2019) A survey on driving prediction techniques for predictive energy management of plug-in hybrid electric vehicles. Journal of Power Sources. 412, 480-495.
[16] Mozaffari, L., Mozaffari, A., Azad, N. (2015) Vehicle speed prediction via a sliding-window time series analysis and an evolutionary least learning machine: A case study on San Francisco urban roads. Engineering Science and Technology, An International Journal. 18(2), 150-162.
[17] Sulaiman, N., Hannan, M., Mohamed, A., Ker, P., Majlan, E., Wan, D. (2018) Optimization of energy management system for fuel-cell hybrid electric vehicles: Issues and recommendations. Applied Energy. 228, 2061-2079.
[18] Elliott, D., Keen, W., Miao, L. (2019) Recent advances in connected and automated vehicles. Journal of Traffic and Transportation Engineering (English Edition). 6(2), 109-131.
[19] Zhang, S., Xiong, R. (2015) Adaptive energy management of a plug-in hybrid electric vehicle based on driving pattern recognition and dynamic programming. Applied Energy. 155, 68-78.
[20] Li, P. (2019) Application and practice of driving supervision platform in vehicle management institute. Manufacturing Automation. 41(11), 143-150.
[21] Rong, Y., Wen, H., Zhao, S. (2019) Study on Driving Risk Measurement for Two-lane Freeway Vehicle Group. Journal of Chongqing Jiaotong University (Natural Sciences). 38(9), 38(9), 95-100+121.
[22] Hu, L., Yang, J., He, Y., Meng, L., Luo, Z. (2019) Study on Vehicle Operational Risk Identification in Urban Traffic Congestion Based on Improved BP Neural Network. Journal of Highway and Transportation Research and Development. 36(10), 105-113.
[23] Fu, S. (2019) Safety Integrity Level Analysis of Urban Guided Transport Vehicle System. Urban Mass Transit. 22(10), 70-74.
[24] Ding, B., Song, Z. (2019) Analysis of Influencing Factors of Urban Intersections Risks Based on Traffic Conflict. Forest Engineering. 35(5), 98-105.
[25] Yuan, L., He, J., Zhang, X. (2019) Model for Un-signalized Intersection Risk Evaluation Based on Traffic Conflict Line Theory. Journal of Transportation Systems Engineering and Information Technology. 19(4), 172-178.
[26] Zheng, X., Yin, J., Chen, R., Lin, T., Li, S., Song, L. (2019) Environment Risk Assessment and Emergency Countermeasures of Dangerous Goods Transporting on Qinghai-Tibet Expressway. Bulletin of Soil and Water Conservation. 39(3), 270-275.
[27] Zhang, R., Ma, C., Xu, S., Li, W., Zhang, J. (2018) Compatibility matching of vehicle front-end when crashing between two cars with difference mass. Journal of Automotive Safety and Energy. 9(3), 295-302.
[28] Bocklisch, F., Bocklisch, S., Beggiato, M., Krems, J. (2017) Adaptive fuzzy pattern classification for the online detection of driver lane change intention. Neurocomputing. 262, 148-158.
[29] Nikabadi, M., Olfat, L., Jafarian, A., Khamene, H. (2013) Effect of necessary factors for deploying e-business models on business performance in automotive industry. International Journal of Asian Business and Information Management. 4(1), 44-56.
[30] Xydas, E., Marmaras, C., Cipcigan, L., Jenkins, N., Barker, M. (2016) A data-driven approach for characterising the charging demand of electric vehicles: A UK case study. Applied Energy. 162, 763-771.
[31] Wang, Y. (2017) Study on prediction method of vehicle lateral position at horizontal curve of two-lane highway. Communications Science and Technology Heilongjiang. 40(12), 14-16.
[32] Jia, W., Liu, Y., Wang, J., Bai, X. (2019) Application of LEC Method in Risk Assessment for Rolling Stock Maintenance. Urban Mass Transit. 22(6), 143-146.
[33] Deng, A. (2018) Analysis on Safety and Control Measures of Yuzhu Car Depot Test Line in Guangzhou Metro. Urban Mass Transit. 21(4), 66-68+74.
[34] Ren, Z. (2018) Safety analysis of lithium-ion batteries for explosion-proof vehicle in mine. Chinese Journal of Power Sources. 42(7), 1085-1088.
[35] Zhang, Y., Qin, Y., Du, Y., Gao, Z., Wei, X. (2016) Residual life prediction of rolling bearings on rail vehicles based on proportional hazard model. Journal of University of Jinan (Science and Technology). 30(5), 347-352.
[36] Wang, Q. (2016) Application of Copula Credibility Model in Ratemaking --Based on Auto Insurance Data. Insurance Studies. 1, 1.

[37] Wang, J., Wu, J., Li, Y. (2016) Concept, Principle and Modeling of Driving Risk Field Based on Driver-vehicle-road Interaction. China Journal of Highway and Transport. 29(1), 105-114.
[38] Zhang, L., Zhu, H., Wu, C., Zheng, A. (2015) Risk Estimation to Vehicles Collision at Intersection Based on ARMA Prediction Model. Journal of Transportation Systems Engineering and Information Technology. 15(5), 239-245.

Received: **03.01.2020**
Accepted: **11.02.2020**

CORRESPONDING AUTHOR

Jianren Liu
School of Civil and Transportation Engineering,
Qinghai Nationalities University,
Xining 810007 – China

e-mail: kanyi0580@163.com

© by PSP Volume 29 – No. 05/2020 pages 3984-3991 Fresenius Environmental Bulletin

DEVELOPMENT AND APPLICATION OF A NOVEL INTEGRATED TREATING EQUIPMENT FOR WASTE DRILLING FLUID

Jianxin Chen[1,*], Shuang Wu[2], Jiacui Luan[2], Hongtao Ming[1], Nanqing Liu[1], Dachao Liu[1], Zhenhua Lu[1]

[1]Drilling Fluids Technology Service Co., Bohai Drilling and Exploitation Co., PetroChina, Tianjin, 300280, China
[2]Drilling Technology Service Co., Bohai Drilling and Exploitation Co., PetroChina, Tianjin, 300280, China

ABSTRACT

With the development of petroleum industry, the environmental pollution caused by waste drilling fluid has begun to appear, which has caused different degrees of influence on the natural environment and human living environment. By using the newly developed integrated treatment equipment for waste drilling fluid while drilling, our company has achieved good environmental protection effects through a series of treatment processes such as waste drilling fluid collection, chemical pretreatment, pressure filtration, oxidation, sewage treatment and recycling after reaching the standard. In this paper, through the introduction of each part of the treatment device, the technical principle and characteristics of the equipment are described, and two key technologies are improved by combining the treatment process. The field test of the integrated treatment equipment in the well Zhang 27-34 shows that the solid phase and liquid phase treated by the integrated treatment equipment can reach the relevant environmental protection standards, and the equipment has a good application effect and prospect.

KEYWORDS:
Waste drilling fluid, environmental protection, processing equipment, field test, solid-liquid separation

INTRODUCTION

A favorable environment is the basic premise for human survival and development. With the development of social economy, environmental problems have become an unavoidable problem [1-4]. Protecting the environment, reducing environmental pollution, and curbing the trend of ecological degradation have become important tasks for government social management. In China, protecting the environment is a basic national policy [5-6]. It is particularly important to solve outstanding environmental problems and promote the coordinated development of the economy, society and the environment.

With the development of the petroleum industry, environmental pollution caused by drilling waste is becoming more and more serious [7]. Drilling pollutants are mainly contaminated by abandoned drilling fluids and wastewater. About 900, 000 cubic meters of waste drilling fluids are produced every year in China's drilling operations, and one third of them are directly discharged into the environment, causing pollution to different degrees to the natural environment and human living environment [8-10]. The impact of waste drilling fluid on the environment is also multifaceted, mainly manifested in [11-14]:

(1) Wide Pollution Area. Drilling fluid has the characteristics of fluidity, dispersibility and percolation, and it may spread the environmental pollution after discharge.

(2) Destroy Soil Structure and Affect Soil Quality. High pH value and high concentration of soluble salts and petroleum substances will affect the soil structure, making the land near the waste drilling fluid discharge area appear brown cracks, affecting the normal growth of plants.

(3) Befouling Water. Waste drilling fluid penetrates into the formation, or enters rivers and oceans with rainwater, will cause the COD_{Cr} value, chromaticity, suspended solids, petroleum, volatile phenols, sulfides and metal ions of the water body to exceed the relevant standards, affecting the normal life of aquatic organism and pollute underground water sources.

From the above analysis, it can be seen that the waste drilling fluid pollutes the environment, and the disposal of the waste drilling fluid is particularly important [15-16]. The existing processing methods are mainly sealing and burying the drilling fluid on site, or sealing and burying the solid phase after simple solid-liquid separation, and discharging the liquid phase. These methods also have potential damage to the environment [17]. Aiming at the problem of disposal of waste drilling fluid, this article has developed a set of integrated treatment equipment for waste drilling fluid while drilling, and carried out field application to verify the effect of the equipment.

MATERIALS AND METHODS

Experimental Apparatus. Composition and important components of integrated processing equipment for waste drilling fluids. The treatment equipment for waste drilling fluid is divided into two modules: solid waste treatment and sewage treatment [18-20]. The main equipment includes rock cuttings collection device, sewage destabilizing air flotation device, oxidation filtration device, drilling fluid destabilizing solid-liquid separation device, sewage coagulation pressure filter device and buffer storage device. Details are as follows:

(1) Cuttings Collection Device. The device is located at the exit of the sand guide tank of solid control equipment such as vibrating screen, centrifuge, sand remover, etc., The collected cuttings are introduced into the curing mixer through the conveyor belt, which is mixed with a variety of curing agents and processed before being transported and stacked. The processing capacity of the device can reach 20 m3/h.

(2) Drilling Fluid Destabilizing Solid-Liquid Separation Device. The waste drilling fluid processed by the cuttings collection device enters the drilling fluid destabilizing solid-liquid separation device. First, the waste drilling fluid is subjected to gel breaking treatment. The broken drilling fluid is subjected to solid-liquid separation by a centrifuge, and the liquid phase enters the sewage treatment process. The solid phase enters the curing agitator for curing treatment. The processing capacity of the device is 20m3/h.

(3) Sewage Destabilizing Air Flotation Device. A destabilizing agent is added to the liquid phase to separate the solid and the liquid, and micro-bubbles are injected into the liquid phase through a gas-dissolving pump. The adsorption and suspension of the micro-bubbles are used to separate the oil phase from the water phase to remove crude oil from the sewage. In the treated sewage, the petroleum content is ≤ 10mg/L, and the processing capacity of the device is 10m3/h.

(4) Sewage Coagulation Separation Device. The flocculant is added to the water phase after the oil-water separation, and the impurities and some harmful substances in the water phase are precipitated. The solid-liquid separation is performed by a hydraulic filter. After solidification, the separated solid phase is transferred to the storage site, and the water phase enters the oxidation filtration device. The device has a processing capacity of 20m3/h.

(5) Oxidation Filtration Device. An oxidant is added to the water phase to perform deep oxidation treatment on the sewage treated by the coagulation reaction. The oxidized water phase is treated by sand filtration, adsorption, membrane filtration and other processes to be discharged or reused after reaching the reuse standard. The processing capacity of the device is 20m3/h.

Features of the Equipment. This equipment combines the advantages of the existing waste drilling fluid processing equipment, and through series and process transformation, it refines each link of waste drilling fluid processing [21-24]. The main features of the equipment are as follows. (1) Wide range of use, both during and after drilling. (2) Save the floor area of wellsite sewage pond, reduce the workload of sewage pond construction. (3) Each part of the equipment adopts skid-mounted design, which is convenient for disassembly and assembly. (4) Good solid-liquid separation effect, better than other domestic solid-liquid separation equipment. (5) The waste does not fall to the ground, which can effectively avoid secondary pollution to the environment.

Methods. Process flow is as flows. The integrated treatment equipment for waste drilling fluid is combined with a cuttings transport system. Through the multi-stage treatment process of drilling fluid gel breaking and destabilization and solid-liquid separation, sewage destabilization and air flotation, efficient flocculation and oxidation of sewage, and fine filtration of sewage, the harmful chemical components in the liquid phase are gradually removed [25-27]. Properly handled, the liquid phase of waste drilling fluid is effectively used. The process flow diagram of this integrated processing equipment is shown in Figure 1.

RESULTS AND ANALYSIS

Waste Drilling Fluid Treatment Technology. Aiming at the problem of waste drilling fluid treatment, the integrated processing equipment combined with the corresponding technical processes, improved the solidification treatment technology and sewage treatment technology, greatly improved the treatment efficiency, and effectively promoted the development of waste drilling fluid treatment technology [28-30].

Curing Technology. Aiming at the cuttings and other wastes in the drilling fluid, combining the reaction mechanism of the hydrolysis and hydration reactions of the curing agent, the synergy of the curing agent and the clay, the ion exchange action of the curing agent and clay, and the reaction mechanism of stimulating the ion interaction of the curing agent and clay [24-25, 31]. The newly developed composite emulsifier is used to transform drilling waste into a high-strength solidified body with silicate gel

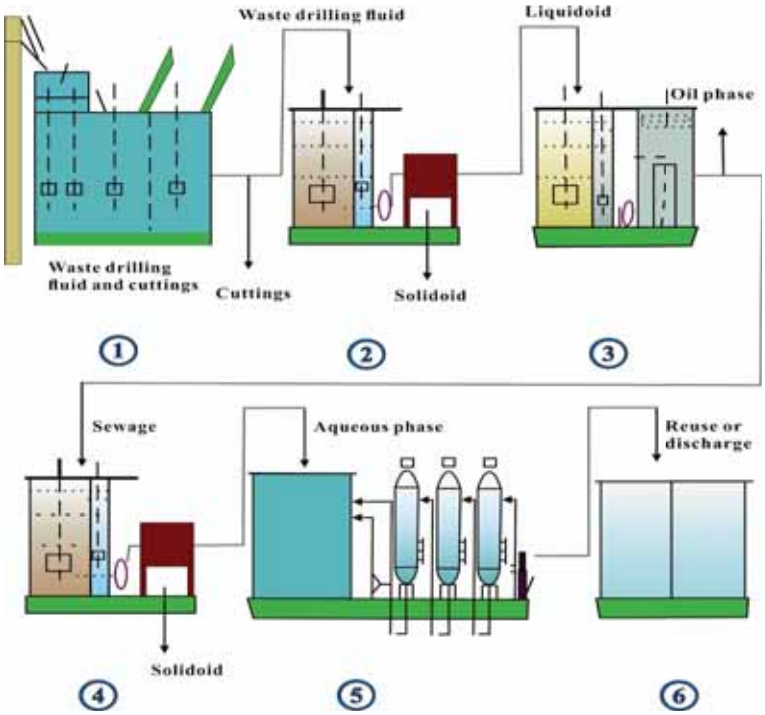

FIGURE 1
Process flow chart of waste drilling fluid integrated treatment equipment
Notes: ① Cuttings collection device ② Drilling fluid destabilizing liquid separation device ③ Sewage destabilizing air flotation device ④Sewage coagulation filter press device ⑤ Oxidation filter ⑥ Storage tank.

structure or ettringite structure. Composite emulsifiers include main consolidation agents, gel breakers, catalysts, coagulant aids, performance modifiers, and the like.

Wastewater Treatment Technology. The sewage treatment equipment is divided into 4 treatment tanks, with a daily treatment volume of 50-200m3. Purification of sewage through treatment processes such as destabilization, oil-water separation, coagulation, solid-liquid separation, oxidation, filtration. In the process of sewage destabilization, diatomite destabilizers with good environmental performance are introduced to destabilize the drilling waste fluid. The destabilized sewage is added to the environmental coagulant for coagulation, and the solid and liquid after coagulation are separated. Among them, the supernatant liquid enters the adjustment tank, and the preferred oxidant is added. In combination with micro-electrolysis technology, the sewage is deeply oxidized. Through sampling and testing, the water phase that meets the effluent standard is discharged. The water phase that meets the drilling fluid preparation standard is repeated used.

Waste Drilling Fluid Treatment Formula and Optimization. The waste drilling fluid integrated processing equipment was applied on-site at Zhang 27-34 well on Chenghai No.2 artificial island. According to the site conditions and treatment effects, the key treatment agent is selected indoors, and the treated water phase meets the national secondary discharge standard as an indicator to optimize the formula in each treatment link.

(1) Curing formula. There are many types of curing agents. For the drilling and completion fluid formula of well Zhang 27-34, through indoor optimization experiments, 3 curing agents are selected, which are the main curing agent XL-1, coagulant XL-2, and breaker XLA-1. Before and after curing, waste water is easily generated. Adding coagulants and oxidants to the waste enhances the environmental protection performance of the cured products (Table 1). The preferred coagulant is MLX-1 and the oxidant is ML-8. The formed curing treatment formula is: 0.6% -0.8% XL-1 + 0.1% XL-2 + 0.1%-0.2% XLA-1 + 0.5%-0.8% MLX- 1 + 0.1% -0.2% ML-8. For the

TABLE 1
Curing reagent

Curing agent	Dosage /(g·L-1)	Sewage treatment agent	Dosage /(g·L-1)
XL-1	6-8	MLX-1	5-8
XL-2	1	ML-8	1-2
XLA-1	1-2	/	/

solid waste solidified by the integrated treatment equipment, the Chinese national standard HJ557-2010 "Solid Waste Leaching Toxicity Leaching Method Horizontal Oscillation Method" was used to analyze the solid waste leachate [32]. The experimental results are shown in Table 2. The experimental results show that the solid waste of the drilling rig has reached the national level III emission standard after solidification treatment. (2) Optimization of liquid processing recipes. Well Zhang 27-34 uses organic salt drilling fluid. Based on previous laboratory experiments, a large amount of stabilizer treatment agent is used at one time, the economic benefit is low, and the stabilization effect is poor. The first used stabilization formula is like aluminum sulfate 0.5%, gel breaker 1%, polymer 0.001%. After the first stabilization, preliminary solid-liquid separation is performed, and the separated waste liquid phase is subjected to secondary stabilization. The formula is: sulfuric acid Aluminum 1% + SAL-1 0.5% + breaker 1%. After the stabilization, secondary solid-liquid separation is performed, and the separation liquid phase has a high chroma. The chroma is the main reference index, based on it, an oxidant is optimized, and the waste liquid phase is treated (Table 3).

It can be seen from the results of the preferred experiments that the oxidant No. 2 has the lowest chromaticity and the best treatment effect, and is preferably an oxidant for processing. The waste liquid after sample 2 treatment just reached the national secondary emission standard. In order to ensure the safety and environmental performance of the liquid phase, activated carbon adsorption method was used to adsorb and filter the treated liquid phase to improve the environmental performance of the treated liquid phase.

TABLE 2
Experimental results of solid waste leach analysis

Test Item	Method	Emission Standard	Testing Result
pH	Glass electrode method	6~9	8.72 mg/L
COD	Dichromate titration	≤150mg/L	310 mg/L
Petroleum	Infrared photometry	≤ 10.0 mg/L	2.0 mg/L
Animal and vegetable oil	Infrared photometry	≤ 15.0 mg/L	1.8 mg/L
Sulfide	Methylene blue spectrophotometry	≤ 1.0 mg/L	0.015 mg/L
Suspended solids	Weight method	≤ 150 mg/L	9 mg/L
Hrominance	Dilution multiple method	≤ 80 times	8 times
Ammonia nitrogen	Neutralization titration	≤ 25 mg/L	0.685 mg/L
Arsenic	Atomic fluorescence method	≤ 0.5 mg/L	0.01 mg/L
Copper	Atomic absorption spectrophotometry	≤ 1.0 mg/L	0.023 mg/L
Zinc	Atomic absorption spectrophotometry	≤ 5.0 mg/L	0.039 mg/L
Lead	Atomic absorption spectrophotometry	≤ 1.0 mg/L	0.038 mg/L
Cadmium	Atomic absorption spectrophotometry	≤ 0.1 mg/L	0.024 mg/L
Nickel	Atomic absorption spectrophotometry	≤ 1.0 mg/L	0.486 mg/L
Manganese	Atomic absorption spectrophotometry	≤ 5.0 mg/L	not detected

TABLE 3
Optimizing results of oxidizing agent

Sample	None	1	2	3	4	5
pH	6	9	9	8	8	9
Hrominance /time	50	15	10	20	50	30
COD_{Cr} /(mg·L^{-1})	6702	167	141	180	2569	146

TABLE 4
Performance of waste liquid before and after treatment

Sample	National levels	Filter Liquor	After Oxidation	After Filtering
Hrominance /time	≤80	50	10	0
COD_{Cr} /(mg·L^{-1})	≤150	6702	141	105

The performance evaluation results of the liquid phase after adsorption are as follows: chromaticity 0 times, turbidity 0FTU; COD_{Cr} 10^5 mg/L, far better than the national secondary emission standard (Table 4).
Combining formula optimization experiments, the preferred formula is as follows:
One-time stabilization: 0.5% aluminum sulfate + 1% breaker + 0.001% polymer;
Secondary breaking stability: aluminum sulfate 1% + SAL-1 0.5% + breaker 1%;
Sewage treatment: No.2 oxidant + activated carbon.

Field Test. The focus of Zhang 27-34 test is to verify the application effect of solid drilling fluid solid-liquid separation technology and liquid phase processing technology in the waste drilling fluid integrated processing equipment, and to explore the feasibility of related process equipment through the test results, and provide data support for the application of the whole equipment.

(1) Solid-Liquid Separation. The waste drilling fluid and cuttings in the drilling fluid pit are sent to the drilling fluid first-level stabilization device through the industrial pump to be uniformly stirred. Since different treatment agents are mixed and prone to self-flocculation, they need to be added in a reasonable order and time [33-35]. According to the treatment process, a breaker, a flocculant, and a regulator are added to the first-level destabilizing device of the drilling fluid, and the agitation is stopped after each substance is stirred. After stopping the stirring, turn on the centrifuge and the liquid supply pump to perform the first solid-liquid separation. The separated solid phase directly enters the solidification system, and the liquid enters the slurry secondary stabilization device for secondary stabilization. The principle of the second destabilization is similar to that of the first time. After the mixed liquid is evenly stirred, the hydrodynamic filter press is turned on to perform solid-liquid separation. Filtration device for further processing and the solid phase enters the curing system.

(2) Liquid Purification. The liquid phase separated by the filter press is untreated and cannot meet the discharge requirements, and must be further processed. The liquid phase is sent to the oxidation tank, and the oxidation treatment agent prepared in advance is added to perform 24 hours of static oxidation [36-38]. After the oxidation treatment is completed, the liquid phase. The phase enters the three-stage filter tank and is discharged after being absorbed and filtered to meet the discharge requirements.

(3) Waste solid-phase curing. Combined with the on-site operating conditions, the waste solid-phase solidification treatment is performed in the debris pit; different curing agents are evenly distributed in the waste solid phase in proportion and stirred at the same time until the mixture is uniform. After the stirring is completed, it is left for 12 hours to make the solid fully cured to meet emission requirements.
(4) Evaluation of field test results. The solid phase and liquid phase treated in the field test were tested in the laboratory. The test results are shown in Table 5.

According to the test results in Table 5, both the solid phase and liquid phase treated by the integrated drilling fluid processing equipment met relevant environmental protection standards and met the design requirements.

TABLE 5
On-site waste disposal test results

Test Item	Emission Standard	Oxidized Filtrate	Curing Leach
pH	6~9	8	8
COD	≤150mg/L	147 mg/L	290 mg/L
Petroleum	≤ 10.0 mg/L	0.1 mg/L	3.5mg/L
Animal and vegetable oil	≤ 20.0 mg/L	0.1 mg/L	2.0 mg/L
Sulfide	≤ 1.0 mg/L	0.025 mg/L	0.04 mg/L
Suspended solids	≤ 200 mg/L	26 mg/L	50 mg/L
Hrominance	≤ 80 times	——	5 times
Ammonia nitrogen	≤ 25 mg/L	13.3 mg/L	22.5mg/L
Arsenic	≤ 0.5 mg/L	0.013 mg/L	0.01 3mg/L
Copper	≤ 1.0 mg/L	0.194 mg/L	0.201mg/L
Zinc	≤ 5.0 mg/L	0.236 mg/L	0.260 mg/L
Lead	≤ 1.0 mg/L	0.826 mg/L	0.765 mg/L
Cadmium	≤ 0.1 mg/L	0.024 mg/L	0.024 mg/L
Nickel	≤ 1.0 mg/L	0.652 mg/L	0.567 mg/L
Manganese	≤ 2.0 mg/L	None	None

FIGURE 2

Field test diagram of waste drilling fluid integrated treatment equipment

Based on the results of field tests, the field application evaluation of the integrated device for environmentally-friendly disposal of waste drilling fluids is as follows (Figure 2). The average waste treatment capacity of the equipment is 20 m3/h. When the φ311mm drill bit is drilled at a speed of 20 m/h, the waste generation rate is about 15-20 m3/h. A set of equipment can meet the requirements of on-site processing while drilling. When a φ444mm drill bit is drilled at a speed of 25 m/h, the waste generation rate is about 30-40 m3/h. At this time, two sets of equipment need to be operated at the same time to meet the requirements of the site while drilling. The equipment technology is mature, the process is feasible, and the implementation effect is good. The entire device has a compact structure, can be disassembled, and is convenient for transfer, but it takes up a lot of space and needs to be optimized and upgraded. The treated wastewater meets the secondary requirements of the "National Integrated Wastewater Discharge Standard" and can be used as industrial water; the solid phase and leachate obtained after treatment meet the national tertiary discharge standard requirements. The overall process technology of this equipment is in the leading position in the industry.

CONCLUSIONS

The integrated processing equipment for waste drilling fluid includes rock cuttings collectiondevice, drilling fluid destabilizing liquid separation device, sewage destabilizing air flotation device, sewage coagulation separation device, and oxidation filtering device. The equipment has a wide range of applications, simple disassembly and assembly, and good treatment effect, which is superior to other domestic solid-liquid separation equipment and can effectively avoid secondary pollution to the environment;

(2) The integrated treatment equipment for waste drilling fluid improves the solidification treatment technology and sewage treatment technology, which greatly improves the treatment efficiency. The laboratory experiment optimized the curing treatment and the liquid phase treatment formula, and adopted the method of secondary destabilization to improve the processing efficiency and reduce the processing cost;

(3) The field test results show that the solid phase and liquid phase treated by the waste drilling fluid integrated treatment equipment meet the relevant environmental protection standards. The equipment has mature technology, feasible process, and is in the leading position in the industry. The equipment has a good application prospect.

ACKNOWLEDGEMENTS

The authors would like to show sincere thanks to those techniques who have helped to this work and all the authors of the references.

REFERENCES

[1] Zhao, X., Wang, F. (2004) Research Development of Waste Drilling Fluids Disposal. Drilling and Completion Fluid. 21(2), 45-50+66-67.

[2] Chen, L., Huang, M., Jiang, X., Li, H., Chen, Q., Zhang, M., Li, S. (2015) Pilot tests of microbe-soil combined treatment of waste drilling sludge. Natural Gas Industry. 35(2), 100-105.

[3] Zhang, Y., Hu, J., Xu, P., Zheng, X., Cao, J., Wang, Y. (2019) Development and Application of the Environmentally Friendly HL-FFQH Water Base Drilling Fluid. Drilling Fluid and Completion Fluid. 36(4), 437-441+448.

[4] Almeida, P., Araújo, O., Medeiros, J. (2017) Managing offshore drill cuttings waste for improved sustainability. Journal of Cleaner Production. 165, 143-156.

[5] Fang, J., Rooks, C., Krogness, C., Kutti, T., Hoffmann, F., Bannister, R. (2018) Impact of particulate sediment, bentonite and barite (oil-drilling waste) on net fluxes of oxygen and nitrogen in arctic-boreal sponges. Environmental Pollution. 238, 948-958.

[6] Mou, S., Dong, H., Ding, X., An, Q. (2012) Study on Treatment Technology of Drill Cuttings While Drilling. Oil Field Equipment. 41(07), 18-22.
[7] Yuan, Q. (2011) Study on Treatment of Drilling Wastewater. Tianjin: Tianjin University of Science and Technology (Dissertation).
[8] Li, W., Shu, F., Xiang, X., Hu, M., Xiao, J. (2009) Solid-liquid Separation of Waste Saturated Salt-water Drilling Fluid. Environmental Protection of Chemical Industry. 29(4), 344-347.
[9] Li, L., Liu, Q., Chen, Y., Yu, J. (2018) Resource utilization plan of waste drilling fluid in shale gas exploitation. Petro and Chemical Equipment. 21(10), 79-80.
[10] Sadiq, R., Husain, T., Veitch, B., Bose, N. (2004) Risk-based decision-making for drilling waste discharges using a fuzzy synthetic evaluation technique. Ocean Engineering. 31(16), 1929-1953.
[11] Yao, L., Neath, M., Jobson, A. (2015) Soil microbial response to waste potassium silicate drilling fluid. Journal of Environmental Sciences. 29, 189-198.
[12] Agwu, O., Akpabio, J. (2018) Using agro-waste materials as possible filter loss control agents in drilling muds: a review. Journal of Petroleum Science and Engineering. 163, 185-198.
[13] Khondaker, A. (2000) Modeling the fate of drilling waste in marine environment: an overview. Computers and Geosciences. 26(5), 531-540.
[14] Coday, B., Xu, P., Beaudry, E., Herron, J., Lampi, K., Hancock, N., Cath, T. (2014) The sweet spot of forward osmosis: treatment of produced water, drilling wastewater, and other complex and difficult liquid streams. Desalination. 333(1), 23-35.
[15] Wang, M. (2008) Environmental Problems of Disposal of Waste Drilling Fluid from Petroleum Drilling. Beijing: Petroleum Industry Press.
[16] Xu, L., Dong, H. (2014) Research on Depth Purification Technology of Waste Drilling Fluid. West-China Exploration Engineering. 26(02), 64-68.
[17] Du, F. (2011) Study on Risk Control Technology of Abandoned Drilling Cuttings. Qingdao: China University of Petroleum (East China) (Dissertation).
[18] Sorheim, R., Amundsen, C., Kristiansen, R., Paulsen, J. (2000) Oily Drill Cuttings From Waste to Resource. SPE-61273-MS.
[19] Tang, C., Wang, R., Xie, S. (2010) Research on Treatment Technologies of Waste Drilling Fluid. Corrosion and Protection in Petrochemical Industry. 27(2), 21-24.
[20] Shang, H., Zhai, Y., Wang, T., Zhang, W. (2018) Progress in Treatment of Oil-Contaminated Drill Cuttings. Journal of Wuhan Institute of Technology. 40(5), 473-478.
[21] Zhang, Y. (2007) Research of Waste Drilling Fluid Harmless Treatment Technology. Qingdao: China University of Petroleum (Dissertation).
[22] Yu, H. (2003) Study on Chemical Treatment of Abandoned Drilling Mud and Drilling Wastewater. Chengdu: Southwest Petroleum Institute (Dissertation).
[23] Ling, K., Guo, Z., Ye, H. (2017) Study on Post-treatment of Waste Drilling and Mud Wastewater. Heilongjiang Science. 8(20), 168-169.
[24] Liu, Y., Qiu, Z., Zhong, H., Nie, Z., Li, J., Huang, W., Zhao, X. (2019) Bitumen Recovery from Crude Bitumen Samples from Halfaya Oilfield by Single and Composite Solvents-Process, Parameters, and Mechanism. Materials. 12(17), 2656.
[25] Liu, Y., Qiu, Z., Nie, Z., Li, J., Zhong, H., Huang, W., Zhao, X. (2019) Numerical Simulation and Analysis of the Bitumen Intrusion Mechanism Based on Density Difference Between Bitumen and Drilling Fluid in Halfaya Oilfield, Iraq. Fresen. Environ. Bull. 28(11), 8275-8281.
[26] Xie, S., Deng, H., Wang, R., Liu, G., Xu, Y. (2008) A Review on Environmental Pollution Process Control Technology in Drilling. Environmental Protection of Oil and Gas Fields. 2, 38-40+61-62.
[27] Liu, X., Xie, S., Xu, Y., Ren, W., Zhang, M., Sun, J., Tong, K. (2019) Shale Gas Drilling Fluid Additives Environmental Performance VS Waste Pollution. Energy Conservation and Emission Reduction in Petroleum and Petrochemical Industry. 4, 53-59.
[28] Sui, D., Sun, Y., Sun, W., Sui, D. (2017) Development Status of Waste Drilling Fluid Treatment. Environmental Science and Management. 42(9), 117-121.
[29] Fan, F., Yang, B., Wu, M. (2018) Extraction Disposal of Oil Cuttings in Shale Gas Drilling. Drilling Fluid and Completion Fluid. 35(5), 78-82.
[30] Zhang, J., Li, Y., Jing, Y., Chen, G., Si, J., Zhang, J., Li, H. (2018) Research on Factors Affecting Cleaning Treatment of Waste Drilling Fluid in Chad. Advances in Fine Petrochemicals. 19(1), 1-4.
[31] He, T., Yang, R., Shu, C., Huang, M., Chen, L., Li, H., Jiang, X., Zhang, W. (2018) Summary of solid waste treatment methods in oil and gas exploration and drilling. Petrochemical Safety and Environmental Protection Technology. 34(6), 56-61.
[32] Lei, X., Mou, C., Tu,Z., Jiang, M., Xu, Z., Zhang, J., Hu, X. (2017) Development and Application of Integrated Drilling Solid Control and Environmental Protection Equipment. China Petroleum Machinery. 45(12), 28-31.

[33] Pereira, L., Sad, C., Da Silva, M., Corona, R., Dos Santos, F., Gonçalves, G., Castro, E., Filgueiras, P., Jr, L. (2019) Oil recovery from water-based drilling fluid waste. Fuel. 237, 335-343.
[34] Hájek, J. (2008) Computational fluid dynamic simulations in thermal waste treatment technology-design, optimization and troubleshooting. Energy. 33(6), 930-941.
[35] Wang, M., Zheng, Y. (2009) The Prospect of Waste Drilling Fluid Treatment Technology in China. Drilling and Completion Fluid. 26(6), 77-79.
[36] Huang, T., Lu, C., Wang, X., Chang, S., Xia, Y., Han, Y., Qin, X., Li, X. (2017) Application of no Landing Drilling Fluid Technology in Sulige Gas Field. Industrial Safety and Environmental Protection. 43(8), 99-102.
[37] Long, H., Wang, S., Li, X., Li, H., Shang, J. (2017) Study on solidification treatment of waste drilling fluid in Changqing Oilfield. Journal of Yangtze University (Natural Science Edition). 14(7), 50-52.
[38] Shang, H., Snape, C., Kingman, S., Robinson, J. (2006) Microwave treatment of oil-contaminated North Sea drill cuttings in a high power multimode cavity. Separation and Purification Technology. 49(1), 84-90.

Received: **04.01.2020**
Accepted: **29.02.2020**

CORRESPONDING AUTHOR

Jianxin Chen
Drilling Fluids Technology Service Co.,
Bohai Drilling and Exploitation Co.,
PetroChina, Tianjin, 300280 – China

e-mail: xiaoboshi100@163.com

© by PSP Volume 29 – No. 05/2020 pages 3992-3999 Fresenius Environmental Bulletin

QUANTITATIVE CHARACTERIZATION OF NANO-SCALE PORES IN SHALE RESERVOIRS OF WUFENG-LONGMAXI FORMATION BASED ON IMAGE PROCESSING

Difei Zhao[1,2], Yinghai Guo[1,*], Geoff Wang[3], Weiwei Jiao[4], Jing Liu[1], Yang Hui[1]

[1]School of Resources and Geosciences, China University of Mining and Technology, Xuzhou, Jiangsu 221116, China.
[2]Shandong Key Laboratory of Depositional Mineralization and Sedimentary mineral Shandong University of Science and Technology, Qingdao, Shandong 266590, China.
[3]School of Chemical Engineering, University of Queensland, Brisbane, Queensland 4072, Australia.
[4]Key Laboratory of Shale Gas Exploration, Ministry of Natural Resources (Chongqing Institute of Geology and Mineral Resources), Chongqing 401120, China

ABSTRACT

In this paper, we conducted image processing on FE-SEM images of representative shale samples from WX-1 well in the north-east Chongqing area. The structural parameters and proportions of major pore types were determined and analyzed following a workflow consisting of nano-scale images acquisition, image processing, pore-network evaluation and comprehensive analysis. We found four types of major reservoir space in matrix including organic matter pores (OM-Ps), clay mineral related pores (CM-Ps), brittleness mineral related pores (BM-Ps) and micro-fractures (MFs) with different pore size and morphological characteristics. OM-Ps are dominated by micro-meso pores, while mineral related pores have a wider pore size range. Pores on the mineralogical edge are the predominated contributor to the connectivity of pore network in shale matrix with wide spatial distribution and relative larger size in meso-macro pore scale. Vertical variation in pore structure, morphology and proportions are measured by parameters of plane porosity, average pore size, form factor, extensibility and eccentricity, indicating that the high-quality shale reservoirs of Wufeng to bottom Longmaxi formation are developed with the highest values of OM-Ps proportion (49%-68%) and form factor. A workflow was summarized to make pore-network characterization for shale matrix based on image processing, which is capable of making characterization of different types of pores and determining the quantification of pore proportions. Quantitative characterization method based on image processing was summarized to provide researchers with new approaches to make pore structure quantification and reservoir quantitative evaluation on nano-scale pores.

KEYWORDS:
Shale, image processing, nano-scale pores, quantitative characterization, Wufeng-Longmaxi formation, workflow

INTRODUCTION

Porosity and permeability are the key physical properties of shale reservoir [1-2]. For shale reservoirs that have experienced a long diagenetic evolution, the major factors affecting the physical properties are the structural characteristics, spatial distribution and connectivity of micro-reservoir space including pores and micro-fractures [3-5]. However, shale is a fine-grained sedimentary rock with complex material compositions and nanoscale pore size [6]. Its storage space in the matrix has significant micro-heterogeneity characteristics in pore types, size, spatial distribution and connectivity [7]. Systematic identification and quantitative characterization of micro reservoir space are the basis for in-depth understanding of shale pore-network system and its influence on the development of high quality shale reservoir.

In recent years, great progress has been made in the exploration and exploitation of shale gas resources in China [8-9]. Out of major shale gas bearing basins in China, the Sichuan basin is the predominant contributor to shale gas productivity [10]. The Longmaxi formation, with its underlying black shale layers from the Wufeng formation, formed the predominant shale gas bearing strata in the Sichuan basin [11].

In this paper, we study the structural characteristics of pores in shale reservoirs of the Wufeng formation and Longmaxi formation using samples of WX-1 well from Northeast Chongqing area. 8 samples were selected to make observations and obtain high resolution images using Field Emission Scanning Electron Microscopy (FE-SEM). Argon Ion Polishing method was used to prepare the sample surface and material compositions were deter-

mined using an Energy Dispersive Spectroscopy (EDS). Image processing was conducted using high resolution images of nano-sclae pores. The objectives of this study are to: (1) derive the structure and morphological characteristics of different types of pores in matrix; (2) make comparisons of different types of pores; (3) make comparisons of pore proportions between shale matrix of the Wufeng formation and the bottom, lower, middle and upper part of the Longmaxi formation.

MATERIALS AND METHODS

Experimental materials. As shown in FIGURE 1, WX-1 well is located in the north-east part of the Chongqing area. Eight representative shale samples of the Wufeng formation (O_{3w}) and Longmaxi formation (S_{11}) were selected and used in FE-SEM imaging and image processing (Table 1). As indicated by organic geochemical tests, selected shale samples have a TOC value ranging from 0.9%~3.3% with the maturity values ranging from 2.07% to 2.38%. The kerogen type of selected samples falls into Type I. The TOC content of the Longmaxi formation shale shows a decreasing trend from the bottom Longmaxi formation to the upper part. This trend in the Longmaxi formation can be widely observed in the Sichuan basin [13].

Nano-scale image acquisition and image processing. Representative samples of different part of the Longmaxi formation and Wufeng formation were polished by ion beam, forming a pseudo Gaussian area of about 2 mm^2 with high-quality surface (Figure 2). The polished surface was then imaged by Helios Nanolab 600i electronic double beam microscope and S-4700 field emission scanning electron microscope. Nano-scale images were obtained in a particular order to cover a certain micro area for image processing (Figure 2).

FE-SEM images were further automatically processed using Matlab and imageJ software after grid sorting and segmentation [14]. All pores in the FE-SEM images were identified and structure information was extracted, respectively. Image processing procedures can be found in reference [14]. Structural parameters, including pore area, perimeter, diameter, form factor and circular degree, were measured to provide a basis for comparison of different types of pores.

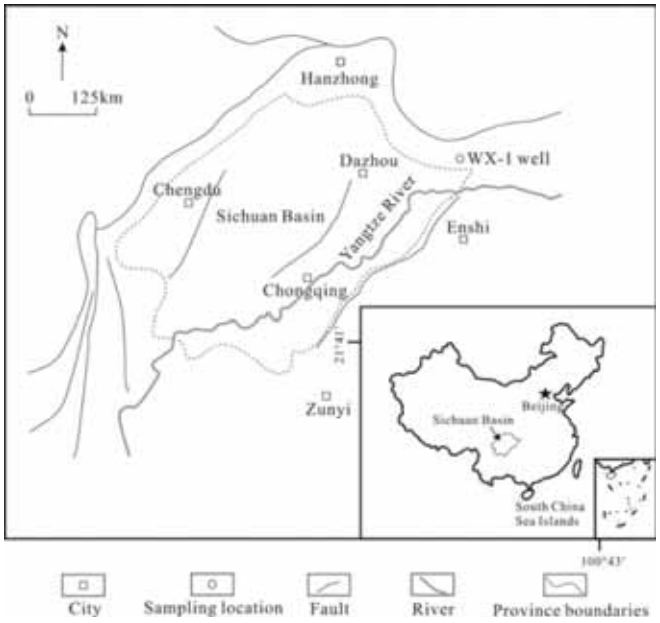

FIGURE 1
Research area and sampling locations(modified after [12])

TABLE 1
Information of representative shale samples

Sample ID	Formation	Sampling layer	TOC (%)	Maturity (%)	Kerogen type
W-1	Longmaxi Fr.	Upper part	0.9	2.5	Type I
W-2	Longmaxi Fr.	Upper part	1.1	-	Type I
W-4	Longmaxi Fr.	Middle part	1.4	2.4	Type I
W-6	Longmaxi Fr.	Lower part	2.1	2.7	Type I
W-7	Longmaxi Fr.	Bottom part	2.9	2.6	Type I
W-8	Longmaxi Fr.	Bottom part	3.3	2.8	-
W-9	Longmaxi Fr.	Bottom part	3.1	3.0	Type I
W-10	Wufeng Fr.		2.2	2.9	Type I

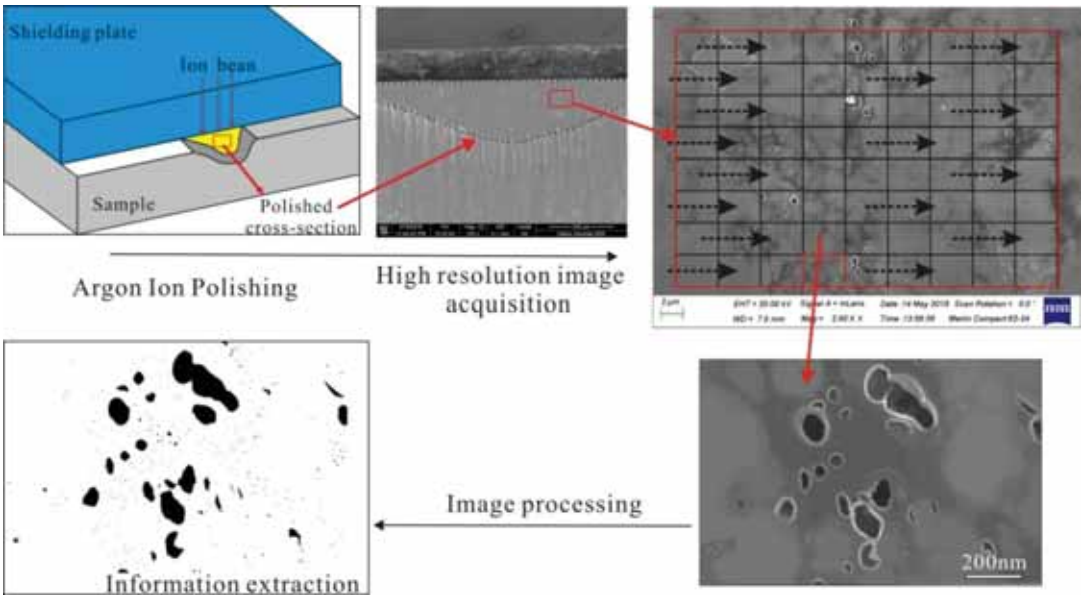

FIGURE 2
A step-wise method of high resolution FE-SEM imaging, image processing and information extraction

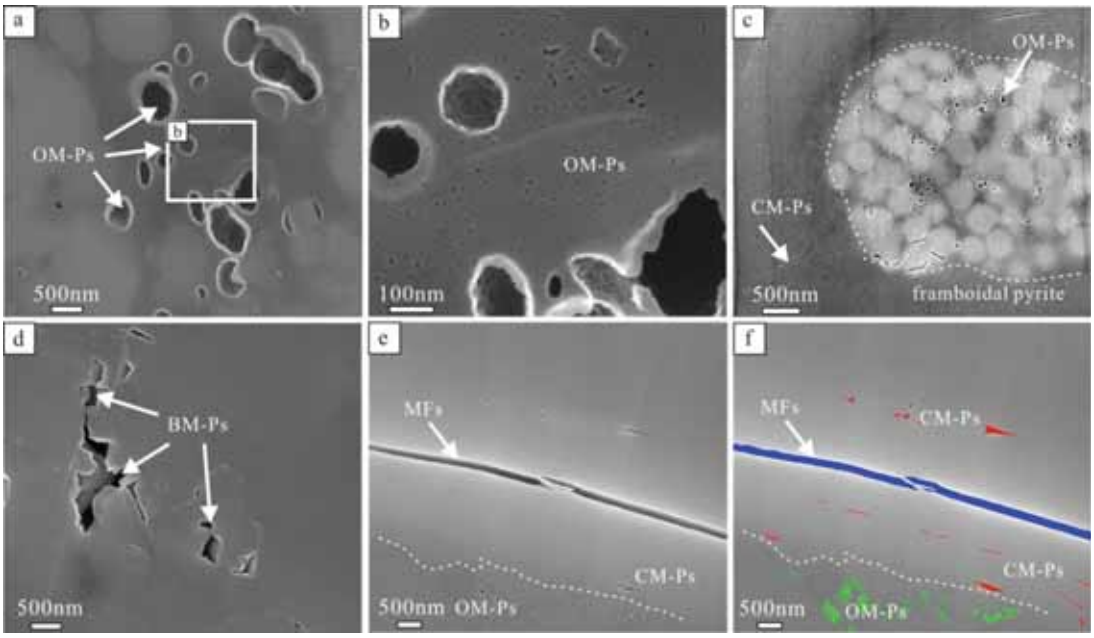

FIGURE 3
Major pore types in shale reservoirs of the Wufeng formation and Longmaxi formation

Different researchers report different methods to quantitatively characterize the pore structure in shale, however, the characterization of different types of pores and the quantification of pore proportion remains a challenge. Nano-scale image acquisition and image processing provides a possible solution to pore structure quantification and rich basic information for reservoir evaluation.

RESULTS

Pore types and structural characteristics. As shown in Figure 3, four major types of pores were identified in shale reservoirs of the Wufeng-Longmaxi formation, including organic matter pores (OM-Ps), clay mineral related pores (CM-Ps), brittleness mineral related pores (BM-Ps) and micro-fractures (MFs). Organic matter pores were developed in kerogen, solid bitumen and frambodial pyrite aggregate (Figure 3a-c). Most of OM-Ps were developed with a pore size range of smaller than 100nm, while a small proportion of OM-Ps has a significantly larger diameter (Figure 3a-b). OM-Ps in frambodial pyrite aggregate were developed within organic matter between pyrite microcrystals with a pore size range of 5nm-200nm. The pore size is limited by the surrounding microcrystals.

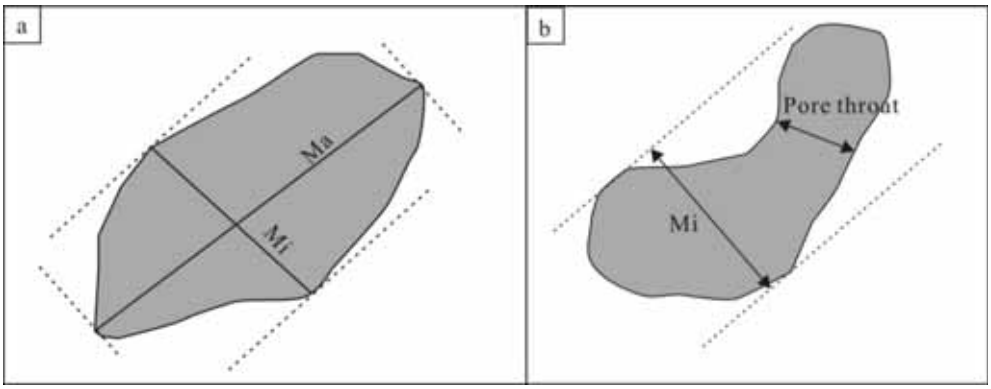

FIGURE 4
Pore-throat diameter, longest Fret diameter (Ma) and shortest Fret diameter (Mi)

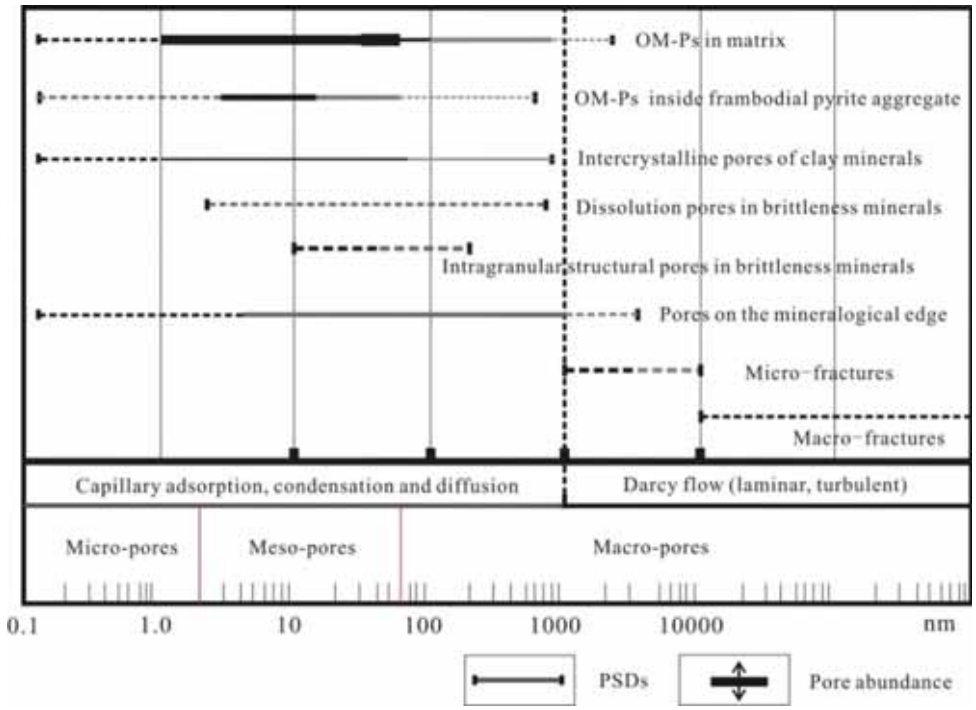

FIGURE 5
Pore size Distributions (PSDs) of major pore types based on image processing

Brittleness mineral related pores (BM-Ps) and clay mineral related pores (CM-Ps) can be subdivided into different types based on the related mineral type and spatial location of pores. Pores on the mineralogical edge were commonly developed around brittle minerals (Figure 3d). Besides, dissolution pores and intragranular structural pores can be observed in tested samples. According to FE-SEM images, CM-Ps in the Wufeng-Longmaxi formation are generally intergranular flaky pores and relatively closed (Figure 3e-f). Compared with pores, micro-fractures (MFs) in the shale matrix are developed with a larger size (a width of 10nm-500nm) and better connectivity (Figure 3e-f).

Pore size distributions (PSDs) based on image processing. Longest Fret diameter (Ma) and shortest Fret diameter (Mi) were obtained through image processing (Figure 4a). In this study, pore size was represented by Mi [15]. Note that pore-throat diameter is generally smaller than Mi (Figure 4b).

Pore size distributions of OM-Ps in matrix and inside frambodial pyrite aggregate, intercrystalline pores of clay minerals, dissolution pores and intragranular structural pores in brittleness minerals, pores on the mineralogical edge and micro-fractures were determined based on image processing and data analysis (Figure 5). OM-Ps in matrix and inside frambodial pyrite aggregate belong to micro-meso pores. Intercrystalline pores of clay minerals, dissolution pores and intragranular structural pores in brittleness minerals are significantly less developed compared with OM-Ps and distributed in the range of micro-meso-macro pores. Intragranular structural pores are developed inside brittleness minerals with poor connectivity. Pores on the mineralogical edge are mainly meso-macro pores. It is

notable that pores on the mineralogical edge might have a significant contribution to the connectivity of the pore network in shale matrix, because of their wide spatial distribution and relative larger pore size in meso-macro pore scale.

Pore Size Distributions (PSDs) of major pore types based on image processing builds a bridge between pore types, pore size and gas behavior (Figure 5). However, common experimental methods of shale pore characterization, such as high-pressure mercury porosimetry (MIP) and low-temperature nitrogen adsorption (LN_2GA), cannot be applied to achieve the special characterization of different types of pores. Thus, new approaches to improve pore characterization quantification degree and in-depth understanding of pore characteristics can be established through pore recognition and information extraction based on high resolution FE-SEM images.

Pore structure and morphology. Shale reservoir has significant micro heterogeneity characteristics. The proportion of different types of pores varies with depth, leading to the heterogeneity characteristics of reservoir physical properties in different stratigraphic position. Thus, the selection of favorable stratigraphic position in vertical direction provides important information for hydraulic fracturing of shale gas.

Structural evaluation parameters are detemained via image processing. Information of pore structure based on FE-SEM iamges, including plane porosity, average pore size (shortest Fret diameter), form factor, extensibility and eccentricity, are used to reflect the vertical variation of pore structure (Figure 6). As indicated in Figure 5, samples of W5, W6 and W7 from the bottom part of Longmaxi formation are deveploped with highest values of plane porosity and form factor, indicating that the development degree of pores in this interval is the highest part of the shale strata with dominant pore type of circular pores. The average pore diameter of the reservoir has a tendency upward, while the plane porosity and form factor show a decreasing trend. Note that sample W8 from Wufeng formation has similar average pore size with the bottom part of Longmaxi formation, but the plane porosity and form factor are relatively lower. Data volatility is significant of the extensibility and eccentricity parameters.

Vertical variation of organic and inorganic pores. Reservoir physical properties are not only affected by the development degree of pore-networks and morphology, but also by the type and proportion of organic/inorganic pores and micro-fractures. The proportion of different types of pores is determined by the ratio of organic/inorganic pore area and total pore area based on image processing:

$$R_{OM-Ps} = \frac{S_{OM-Ps}}{S_t} \quad (1)$$

$$R_{M-Ps} = R_{BM-Ps} + R_{CM-Ps} = \frac{S_{BM-P}}{S_t} + \frac{S_{CM-P}}{S_t} \quad (2)$$

$$R_{MFs} = \frac{S_{MFs}}{S_t} \quad (3)$$

In equation (1), (2) and (3), R_{OM-Ps} represents for the proportion of organic matter pores to pore system. R_{BM-Ps}, R_{CM-Ps} and R_{MFs} represent for the proportion of clay mineral related pores, brittleness mineral related pores and micro-fractures, respectively. S_{OM-Ps}, S_{BM-Ps}, S_{CM-Ps} and S_{MFs} represent for the calculated area of OM-Ps, BM-Ps, CM-Ps and MFs, respectively. S_t represents for the total calculated area of micro-reservoir space.

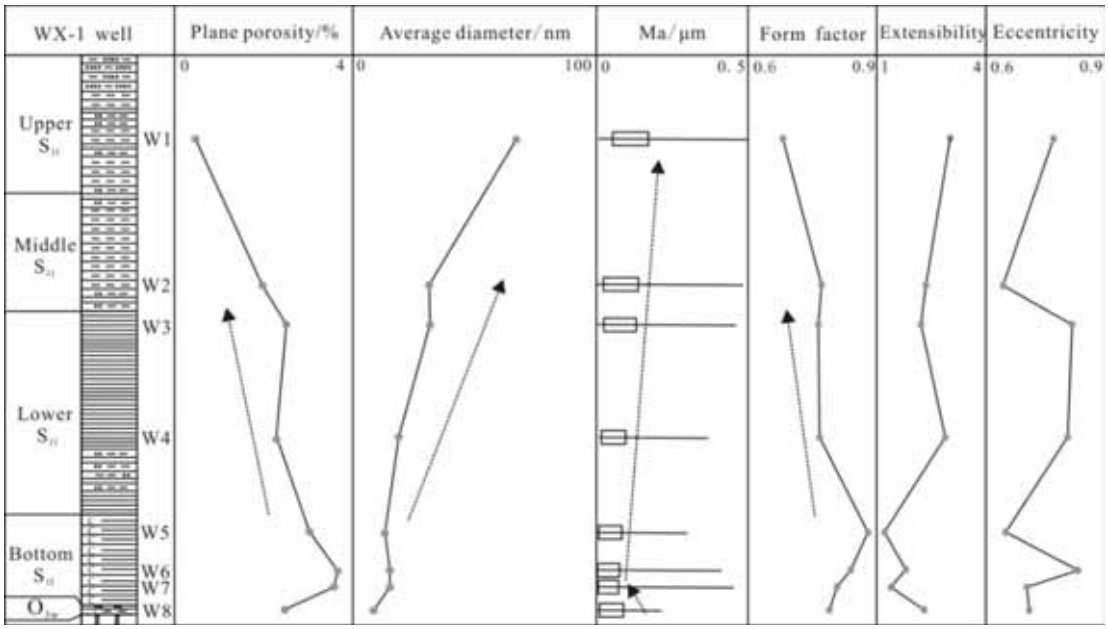

FIGURE 6
Longitudinal variation of numerical parameters based on image processing of WX-1 well

TABLE 1
Vertical variation of organic and inorganic pores

Sample ID	Formation	Sampling layer	TOC (%)	R_{OM-Ps}/%	R_{M-Ps}/%	R_{MFs}/%
W8	Longmaxi Fr.	Upper part	0.9	18	79	3
W7	Longmaxi Fr.	Upper part	1.1	24	73	4
W6	Longmaxi Fr.	Middle part	1.4	34	64	2
W5	Longmaxi Fr.	Lower part	2.1	39	60	1
W4	Longmaxi Fr.	Bottom part	2.9	63	35	2
W3	Longmaxi Fr.	Bottom part	3.3	68	31	1
W2	Longmaxi Fr.	Bottom part	3.1	58	40	2
W1	Wufeng Fr.		2.2	49	49	2

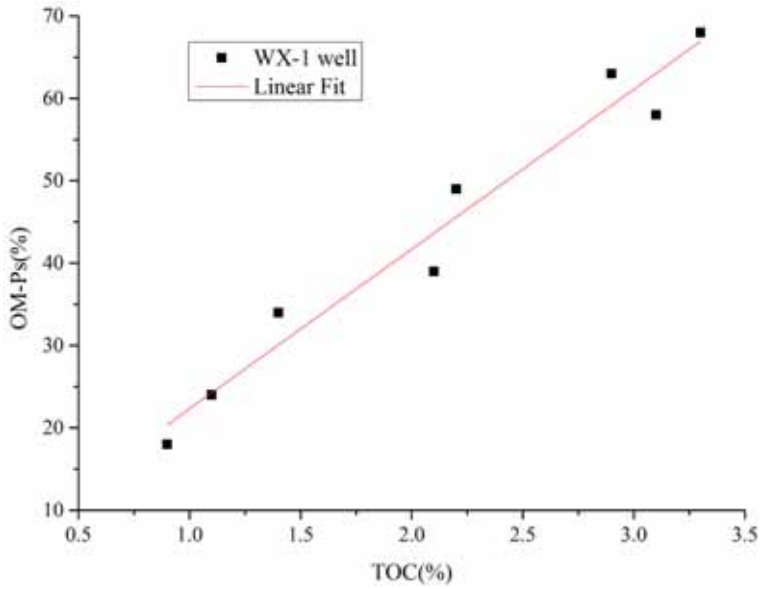

FIGURE 7
Relationship between TOC (%) and ratios of OM-Ps (%) in samples of WX-1 well

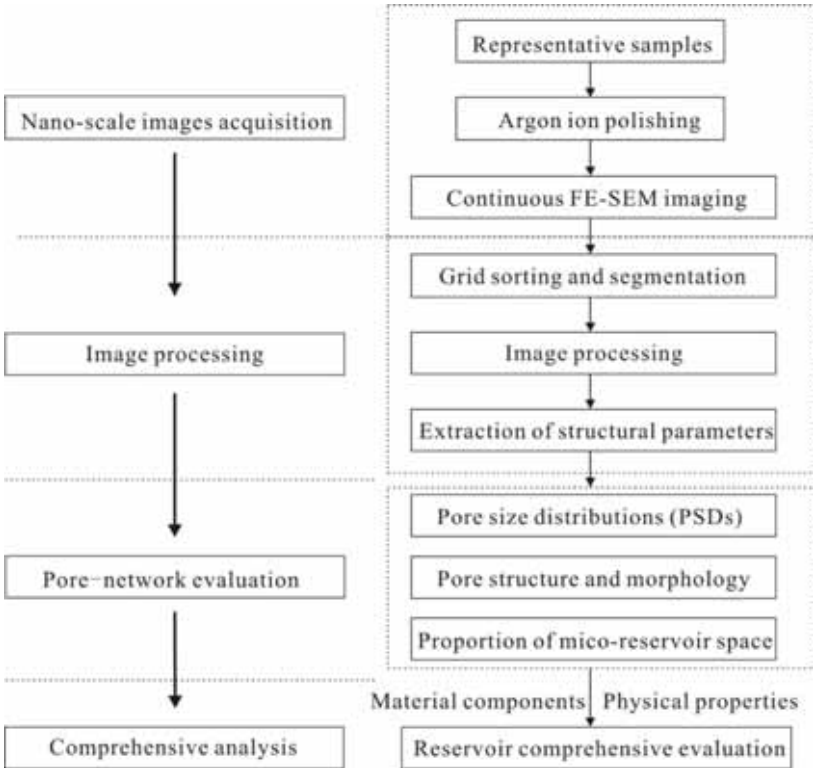

FIGURE 8
Workflow to make pore-network characterization based on image processing

The proportions of organic and inorganic pores are given in Table 1. Samples from the Wufeng formation and bottom Longmaxi formation have the highest values of R_{OM-Ps} and TOC content. Values of R_{OM-Ps} show a decreasing trend upward and a significant positive correlation with TOC content (Figure 7). It is notable that the values of R_{MFs} in shale matrix are lower in the Wufeng formation and bottom Longmaxi formation than the upper Longmaxi formation. Thus, shale reservoirs of the Wufeng formation and bottom Longmaxi formation have significantly better development degree of organic matter pores and lower proportion of micro-fractures, which is beneficial to gas storage potential and capacity.

Workflow to make pore-network characterization based on image processing. In this study, we conducted a series of experiments related to image processing to make pore structure quantification and reservoir quantitative evaluation. A workflow was summarized to make pore-network characterization for shale matrix based on image processing (Figure 8). The workflow consists of four major steps: nano-scale images acquisition, image processing, pore-network evaluation and comprehensive analysis. The workflow based on images is capable of making characterization of different types of pores and determining the quantification of pore proportions compared with previous pore system characterization methods [16]. Data of different pore structure parameters and proportions will provide vital information for reservoir evaluation with reservoir information of material components and physical properties, and is helpful to reveal the development mechanism of high quality shale reservoir.

CONCLUSIONS

(1) We found four types of major reservoir space in shale matrix. The pore size distribution and morphological characteristics of organic matter pores (OM-Ps), clay mineral related pores (CM-Ps), brittleness mineral related pores (BM-Ps) and micro-fractures (MFs) are measured using image processing, indicating OM-Ps are dominated by micro-meso pores, and mineral related pores have a wider pore size range.

(2) Vertical variation on pore structure, morphology and proportions can be measured by parameters of plane porosity, average pore size, form factor, extensibility and eccentricity. The high-quality shale reservoirs of Wufeng to bottom Longmaxi formation are developed with the highest values of OM-Ps proportion (49%-68%) and form factor.

(3) A workflow was summarized to make pore-network characterization for shale matrix based on image processing, which is capable of making characterization of different types of pores and determining the quantification of pore proportions.

ACKNOWLEDGEMENTS

The research is sponsored by the National Natural Science Foundation of China (No.41772130; No.41804106; No.41971335), the Shandong Key Labortory of Depositional Mineralization & Sedimentary Mineral (Shandong University of Science and Technology) (No.DMSMX2019002), the Natural Science Foundation of Jiangsu Province (No.BK20170274), the Project for performance incentive and guidance of scientific research institutions in Chongqing (No. cstc2019jxjl90001) and the Scientific Research Projects of Chongqing Shale Gas Company (No. CYS-FW-2019-0099). Author Difei Zhao also thanks to the China Scholarship Council (CSC) for providing the scholarship during visiting the University of Queensland and Yingxing Chen's suggestions (Huaiyin Normal University).

REFERENCES

[1] Bankole, S.A., Buckman, J., Stow, D., Lever, H. (2019) Automated Image Analysis of Mud and Mudrock Microstructure and Characteristics of Hemipelagic Sediments: IODP Expedition 339. Journal of Earth Science. 30(2), 407-421.

[2] Bohacs, K.M., Passey, Q.R., Rudnicki, M., Esch, W.L., Lazar, O.R. (2013) The Spectrum of Fine-Grained Reservoirs from 'Shale Gas' to 'Shale Oil'/Tight Liquids: Essential Attributes, Key Controls, Practical Characterization. IPTC 2013: International Petroleum Technology Conference.

[3] Shi, M., Yu, B., Xue, Z., Wu, J., Yuan Y. (2015) Pore characteristics of organic-rich shales with high thermal maturity: A case study of the Longmaxi gas shale reservoirs from well Yuye-1 in Southeastern Chongqing, China. Journal of Natural Gas Science and Engineering. 26(7), 948-959.

[4] Zhao, D., Guo, Y., Chong, X., Li, G., Wang, Y. (2019) Nuclear Magnetic Resonance Experiment Analysis of tight gas sandstone reservoir. Fresen.Environ. Bull. 28, 220-225.

[5] Li, F., Wang, M., Liu, S., Hao, Y. (2019) Pore characteristics and influencing factors of different types of shales. Marine and Petroleum Geology. 102, 391-401.

[6] Loucks, R.G., Reed, R.M., Ruppel, S.C., Hammes, U. (2012) Spectrum of pore types and networks in mudrocks and a descriptive classification for matrix-related mudrock pores. AAPG Bulletin. 96(6), 1071-1098.
[7] Zhao, D., Guo, Y., Zhu, Y., Wang, G., Chong, X., and Hu, X. (2018) Analysis of micro-scale heterogeneity characteristics in marine shale gas reservoir: Pore heterogeneity and its quantitative characterization. Journal of China University of Mining and Technology. 47(2), 296-307.
[8] Zhu, G., Gu, L., Su, J., Dai, J., Ding, W., Zhang, J., Song, L. (2012) Sedimentary association of alternated mudstones and tight sandstones in China's oil and gas bearing basins and its natural gas accumulation. Journal of Asian Earth Sciences. 50(5), 88-104.
[9] Tan, J., Horsfield, B., Fink, R., Krooss, B., Schulz, H.M., Rybacki, E., Zhang, J., Christopher, J.B., Ger van, G., Tocher, B.A. (2014) Shale gas potential of the major marine shale formations in the Upper Yangtze Platform, south China, Part III: Mineralogical, lithofacial, petrophysical, and rock mechanical properties. Energy & Fuels. 28(4), 2322-2342.
[10] Jiang, S., Tang, X., Long, S., McLennan, J., Jiang, Z., Jiang, Z., Xu, Z., Chen, L., Xu, G., Shi, X., He, Z. (2017) Reservoir quality, gas accumulation and completion quality assessment of Silurian Longmaxi marine shale gas play in the Sichuan Basin, China. Journal of Natural Gas Science and Engineering. 39(3), 203-215.
[11] Li, Y., Zhang, T., Ellis, G. S., and Shao, D. (2017). Depositional environment and organic matter accumulation of Upper Ordovician–Lower Silurian marine shale in the Upper Yangtze Platform, South China. Palaeogeography, Palaeoclimatology, Palaeoecology. 466(1), 252-264.
[12] Ji, W., Song, Y., Jiang, Z., Meng, M., Liu, Q., Gao, F. (2017) Micron-to nano-pore characteristics in the shale of Longmaxi Formation, southeast Sichuan Basin. Petroleum Research. 2(2), 156-168.
[13] Ran, B., Liu, S., Jansa, L., Sun, W., Yang, D., Ye, Y., Wang, S., Luo, C., Zhang, X., Zhang, C. (2015) Origin of the Upper Ordovician-lower Silurian cherts of the Yangtze block, South China, and their palaeogeographic significance. Journal of Asian Earth Sciences. 108(8), 1-17.
[14] Zhao, D., Guo, Y., Wang, G., and Mao, X. (2019). Characterizing nanoscale pores and its structure in coal: Experimental investigation. Energy Exploration & Exploitation. 37(4), 1-28.
[15] Jiao, K., Yao, S., Liu, C., Gao, Y., Wu, H., Li, M., Tang, Z. (2014) The characterization and quantitative analysis of nanopores in unconventional gas reservoirs utilizing FESEM–FIB and image processing: An example from the lower Silurian Longmaxi Shale, Upper Yangtze Region, China. International Journal of Coal Geology. 128(8), 1-11.
[16] Chen, S., Zhu, Y., Wang, H., Liu, H., Wei, W., Fang, J. (2011) Shale gas reservoir characterization: A typical case in the southern Sichuan Basin of China. Energy. 36(11), 6609-6616.

Received: **07.01.2020**
Accepted: **15.02.2020**

CORRESPONDING AUTHOR

Yinghai Guo
School of Resources and Geosciences,
China University of Mining and Technology,
Xuzhou, Jiangsu 221116, China.

e-mail: diffidiffi@126.com

© by PSP Volume 29 – No. 05/2020 pages 4000-4010 Fresenius Environmental Bulletin

CHARACTERISTICS OF SEDIMENTARY MICROFACIES DISTRIBUTION AND SEDIMENTARY MODEL OF PINGHU FORMATION FROM WELL P AREA IN A CERTAIN SAG, EAST CHINA SEA BASIN

Zhiyao Zhang[1], Changmin Zhang[1,*], Guowei Hou[2], Qinghai Xu[1], Wenjie Feng[1], Zhe Chen[1]

[1]School of Geosciences, Yangtze University, Wuhan 430100, China
[2]CNOOC China Limited, Shanghai Branch, Shanghai 200335, China

ABSTRACT

Based on the detailed observations and descriptions of the cores of 7 wells in the P well area of the western slope of a sag in the East China Sea Basin, this paper studies the sedimentary microfacies and sedimentary models of the Pinghu Formation by comprehensively using well logging analysis and seismic data. The results show that a set of sea-land transitional sedimentary systems developed in the Pinghu Formation in well P, mainly tidal-affected delta-tidal flat sediments and the sedimentary subfacies mainly include delta fronts, pre-deltas, and intertidal zones. Seven types of sedimentary microfacies have been further identified such as diverting channels, estuary sand bars, diverging bays, and tidal channels. Co-occurring faults have a significant effect on the plane distribution of sedimentary microfacies. When the fault distance is small, as the angle between the source and the fault direction increases, the underwater shunt channel will be diverted. When the fault distance is large, the underwater shunt channel will be deposited. The sediments only deposit in the lower part of the upper wall of the concomitant fault, and the advancement to the center of the basin is limited. Based on the analysis of the sedimentary system, a sedimentary model of the study area with tidal influence on the delta front is established. The identification of the sandstone and the prediction of favorable sand bodies have certain guiding significance.

KEYWORDS:
Pinghu Formation, sedimentary microfacies, East China Sea Basin, sedimentary model

INTRODUCTION

The East China Sea continental shelf basin is an important petroliferous basin in China. The Eocene Pinghu Formation is one of the main target intervals for oil and gas exploration in the sag. Predecessors have conducted in-depth research on the sequence stratigraphy, sedimentary system, structure, and reservoir of the Pinghu Formation [1-4]. In the study of sedimentary facies and sedimentary systems, some scholars believe that the sedimentary period of the Pinghu Formation is mainly the marine sedimentary environment, and the sedimentary facies such as deltas, tidal flats and confined bays affected by tidal development [5-11]. The terrestrial sedimentary environment mainly develops lake-marsh and delta sediments, and there is local transgression [12-16]. Previous researches mainly focused on large-area sedimentary systems, but less detailed analysis of small blocks. In order to further predict the favorable sand body distribution in the study area, it is urgent to conduct a detailed study of the sedimentary microfacies of the Pinghu Formation. This paper comprehensively studies the lithofacies types and sedimentary structural features of the Pinghu Formation in the P well area of a depression in the East China Sea shelf by comprehensively using core, logging, seismic, and analytical testing data. In addition, this paper analyzes the Pinghu Formation in combination with paleontology and ancient salinity features. Based on the types of sedimentary microfacies, combined with the seismic attribute map to analyze the planar distribution characteristics of sedimentary microfacies, the sedimentary model of the Pinghu Formation in this area is proposed. The research results have a certain guiding effect on the prediction of favorable sand bodies of the Pinghu Formation in the P well area.

GEOLOGICAL OVERVIEW AND METHODS

Geological profile of the study area. The East China Sea continental shelf basin is located on the eastern continental margin of the Eurasian plate with an area of about $2.6 \times 10^5 km^2$. It is separated from the Okinawa Trough by the Diaoyu Island uplift belt in the east, the Zhejiang-Fujian uplift in the west, and the Mesozoic and Cenozoic basin groups in Taiwan in the south, extending northward. To the vicinity of the Tsushima Strait, the general trend is northeastward. The depression is the largest secondary unit in

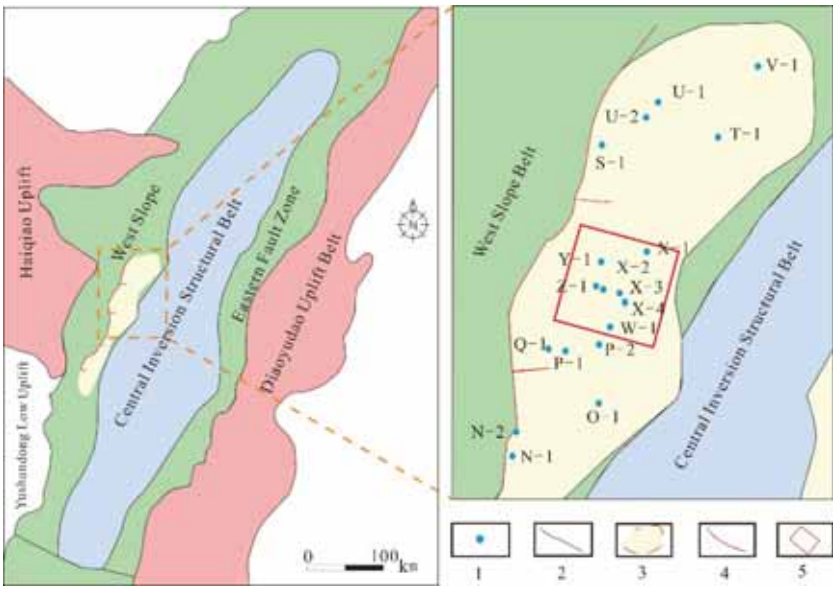

FIGURE 1
Well location of well X area in a certain sag
Notes: 1-Well location, 2-Secondary tectonic unit boundary, 3-Tectonic unit boundary, 4-Fault, 5-Study area.

the East China Sea shelf basin. It is located in the middle of the eastern Zhejiang depression belt in the East China Sea shelf basin and is distributed in a northeast direction. The length is 460km and the width is about 75- 130km, with an area of 5.9 × 10^4km^2. The depression is a large oil-bearing depression with a north-north-east trend. Its tectonic evolution has mainly experienced the Paleozoic fault depression stage-Late Eocene fault depression stage-Oligocene to Miocene depression Stage-Quaternary regional subsidence stage. It has the characteristics of east-west sub-zone and north-south sub-zone, and can be divided into western slope zone, central inversion tectonic zone and eastern fault zone [17-18] (Figure 1a).

Well P is located in the western slope of a sag (Figure 1b). From the bottom up, the Eocene Qijiang Formation, Wenzhou Formation, Baoshi Formation, Pinghu Formation, Oligocene Huagang Formation, Miocene Longjing Formation, Yuquan Formation. Heliulang Formation and Pliocene Sandan Formation (Figure 2). The entire Pinghu Formation is an interlayer of dark gray mudstone and light gray fine-coarse sandstone. The coal seam is developed and the thickness is 500-1500m. The Pinghu Formation can be divided into three third-order sequences (E2pSQ1-E2pSQ3 (lower Pinghu Formation-upper Pinghu Formation)) [19-20]. E2pSQ1 (the lower section of the Pinghu Formation) is a gray-dark mudstone and siltstone interlayers, interspersed with asphaltene coal. E2pSQ2 (the middle section of the Pinghu Formation) is composed of siltstone, argillaceous siltstone and coarse sandstone, mudstone Interlayer. The upper part of E2pSQ3 is mixed interlayer with siltstone, argillaceous siltstone and coarse sandstone, and mudstone while the lower part is coarse sandstone and gravel, coarse sandstone consists of muddy siltstone and silty siltstone.

Research method. This paper analyzes the log data and core data of seven wells in P well area. Using logging, seismic profile, sedimentary structure, lithofacies, cast body flakes, particle size analysis and other data, the sedimentary characteristics were analyzed, the sedimentary environment and sedimentary facies were identified, and finally the sediments in this area were established under the constraints of the seismic RMS plan.

RESULTS

Sedimentary characteristics. (1) Petrological features. The Pinghu Formation in the study area presents the characteristics of unequal-thick sand-mud interlayers with sand-land ratios less than 0.5. Statistics on the identification of 78 sandstone samples from the Pinghu Formation indicate that the sandstones of the Pinghu Formation are mainly feldspar sandstone and lithic feldspar sandstone, with a small amount of lithic sandstone and lithic quartz sandstone (Figure 3a). The quartz content is between 64% -81%, with an average of 68.9% and the feldspar content is between 7% -21%, with an average of 13.23%, mainly orthoclase and a small amount of plagioclase. Rock debris content is from 7% -20%, with an average of 17.78%, mainly magmatic rock and metamorphic rock cuttings, containing a small amount of sedimentary rock cuttings. The overall grain size is fine, and it is fine-medium sandstone, with pebbly medium coarse sandstone partially visible. Debris particles are mostly sub-circle-second angular, the particles are in a linear contact relationship and the particles are supported (Figures 3b, 3c).

The cumulative probability curve shows a four-segment feature of one roll, two jumps, and one suspension. The overall content of rolling is 30% -35%, the slope is high, and the classification is good. The overall suspension content is 5% -10% and the curve reflects the characteristics of the stable traction stream sediments (Figures 3d, 3e). Generally speaking, the sandstones of the Pinghu Formation in the study area are characterized by medium component maturity and high structural maturity.

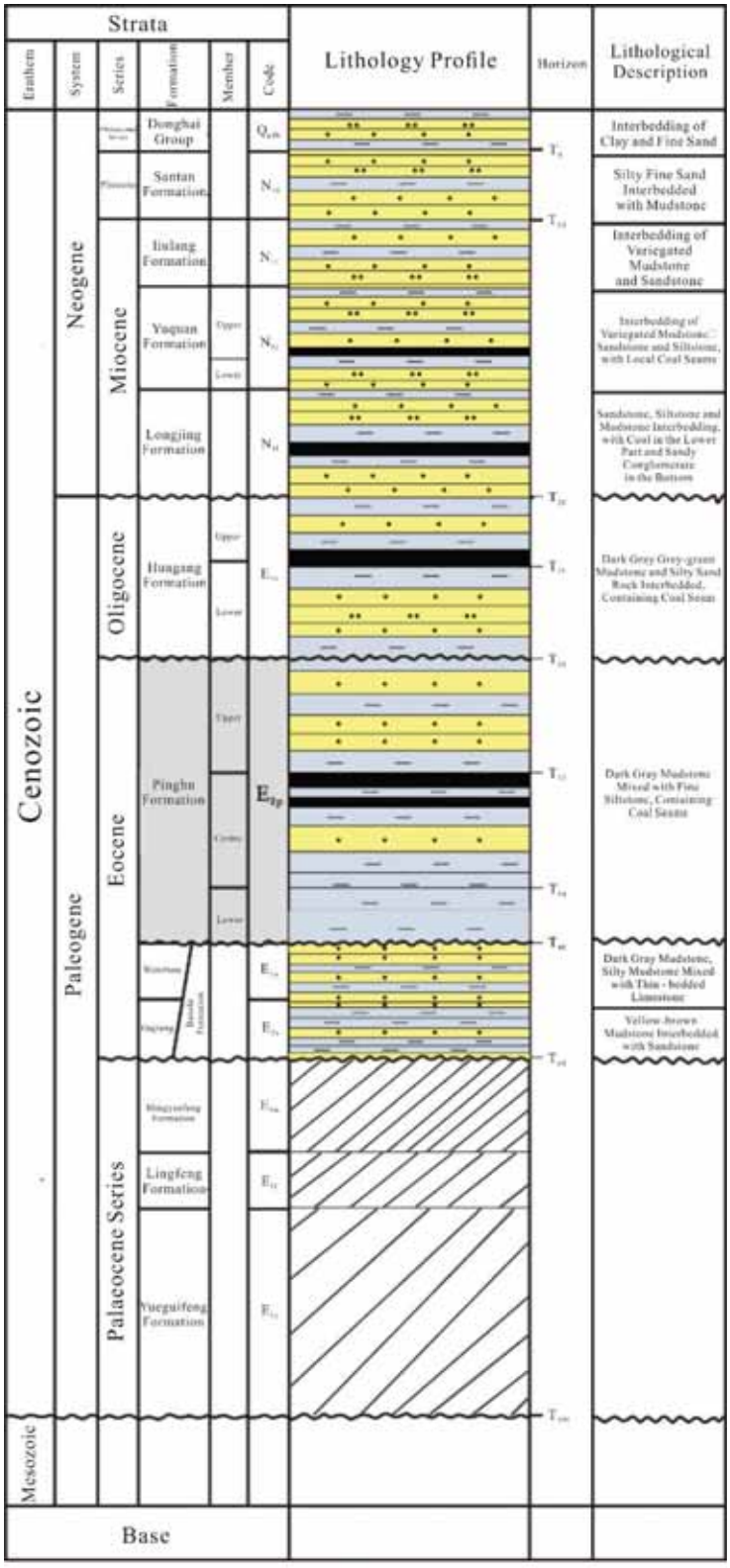

FIGURE 2
Integrated stratigraphy of well P area in a certain sag.

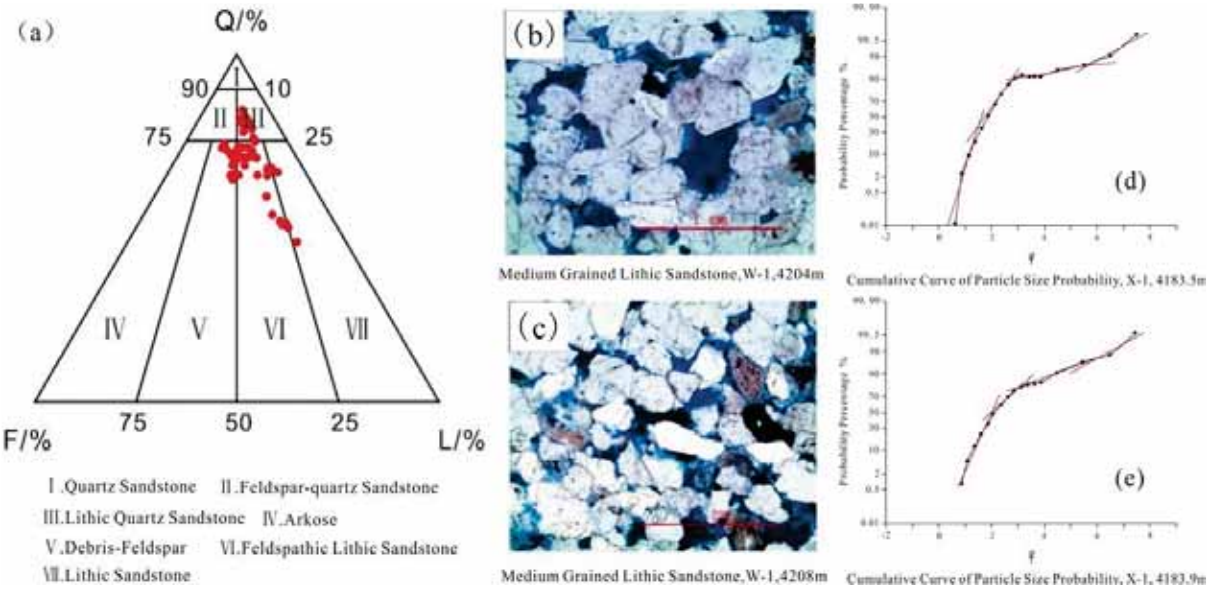

FIGURE 3
Petrological characteristics of Pinghu Formation in Well P Area.

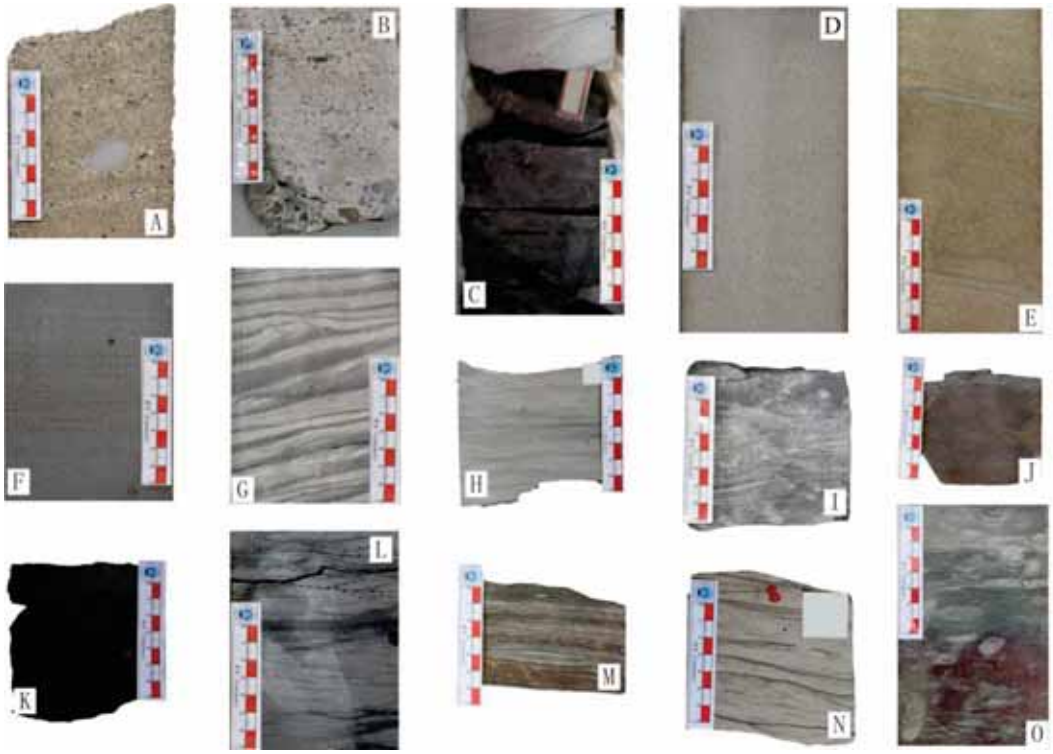

FIGURE 4
Typical sedimentary structure photographs in Well P Area.

Notes: A. Yellow-brown staggered layered gravelly coarse sandstone, the gravel is gray, white, and black, sub-circle-second angular, with obvious directivity, Well X-4, 4579.3m; B. Gray-brown parallel layered gravelly coarse sandstone, the gravel is gray, white, black, sub-circle-sub-angular, certain orientation, Well X-3, 4690.9m; C. Upper gray-white staggered layered fine sandstone, contact with lower gray mudstone scour, Well X-2, 4063.6 m; D. Gray-white massive fine sandstone without obvious sedimentary structure, Well X-4, 4566.4m; E. Gray-brown staggered fine-grained sandstone with a thickness of more than 10 cm and an inclination angle of about 20 °. Well X-2, 4562.05m; F. Gray-white parallel bedding fine sandstone, Well O-1, 4084.66m; G. Grey fine sandstone, developmental rhythm bedding, sand-mudstone interbed, well X-4, 4564.66m; H .Gray wave-shaped sand stratified fine sandstone, the stratum is herringbone, Well P-1, 3757m; I. Gray argillaceous siltstone, biological disturbance development, visible wormholes, biological lairs, well X-4, 4561.4m; J. Gray-brown blocky bedding mudstone, Well P-1, 3680.6m; K. Black blocky bedding carbonaceous mudstone, Well X-3, 4697.51m; L. Gray bidirectional staggered bedding rock, Well O-1, 4083.96m; M. Gray-black lenticular bedding silty mudstone, sandstone is lenticular in mudstone, Well P-1, 3345.7m; N. Gray veined bedding fine sandstone, mudstone is veined in sandstone, Well P-2, 3651.3m; O. Gray-brown mudstone, biological disturbance development, Well Y-1, 3494.9m.

Mudstone and siltstone in the study area are relatively developed, but because only sandstone is sampled, petrological characteristics of siltstone and mudstone will not be analyzed in this paper.

(2) Sedimentary structural features. The Pinghu Formation in the study area is rich in sedimentary structures. The staggered bedding (Figure 4A) and blocky bedding (Figure 4B) are common in coarse sandstones, reflecting strong hydrodynamic conditions. Among them, the staggered bedding angle is 5°-8°, the stratum thickness is 6-10cm, and gravel is occasionally found with diameter of 0.5-1.2cm, reflecting that the sediment deposition rate is relatively fast and generally occurs in river sediments.

Sedimentary structures such as scour structures (Figure 4C), block bedding (Figure 4D), staggered bedding (Figure 4E), parallel bedding (Figure 4F), and prosodic bedding (Figure 4G) are commonly developed in fine sandstone. Among them, the staggered bedding angle is 3°-6°, and the thickness of the strata is 10-15cm. The double clay layers are developed. The thickness of the parallel bedding strata is 5-8cm, and the separation is better. The rhythmic bedding performance is sandstone interlayer with thickness of 0.2-0.3cm. This type of sedimentary structure is generally formed by tidal effects or seasonal changes [21-22].

Sandstone bedding (Figure 4H), biologically disturbed structures (Figure 4I), and vein-like bedding (Figure 4N) are often developed in silty sandstones, which often represent weak hydrodynamic conditions. Sand texture layer is herringbone with layer thickness of 4-7cm. Vein bedding is characterized by the vein-like distribution of mudstone in sandstone. Mudstone thickness is less than 0.3cm, which is a kind of tidal bedding. This type of sedimentary structure is common in subtidal and intertidal zones.

Massive bedding (Figure 4J) and liquefaction deformed structures can be seen in the mudstone. Some mudstones have high carbon content (Figure 4K) and weak hydrodynamic conditions. Two-way staggered stratification (Figure 4L) and prosody stratification (Figure 4M) representing tidal action were also observed in the sediments of the Pinghu Formation. Biological boreholes and biologically disturbed structures were observed in dark powdery fine sandstone and mudstone (Figure 4O). Wormholes were mainly horizontal boreholes, which also reflected the shallow water and low-energy reducing environment during the sedimentary period of the Pinghu Formation.

Sedimentary microfacies. Based on the characteristics of petrology and sedimentary structure in the study area, and combined with previous studies, the tide-affected delta and tidal flat sedimentary facies were identified which can be divided into three types of sedimentary subfacies [23-25]: delta front, pre-delta, and intertidal zone. There are 7 types of sedimentary microfacies such as underwater diverted river channels, estuary sand dams, diverted bays, mat sands, pre-delta mud, tidal channels, and mud flats.

(1) The effects of tide on the delta sedimentary system. 1) Delta fronts. The subfacies consist of sedimentary microfacies such as underwater diverted river channels, estuary sand bars, diverted bays, and mat sands. The characteristics of each microfacies are as follows:

a) Underwater diverted river channels microfacies. In the delta front sediments, the underwater diversion channel is mainly composed of gray-off-white medium-coarse sandstone and gray pebbly medium-coarse sandstone. It has developed blocky bedding, staggered bedding, parallel bedding, and tidal bedding [26-27]. Clay layers are common, reflecting the presence of tidal effects during sedimentation. Due to the strong hydrodynamic conditions, scouring structures are common at the bottom of the river, and the migration of the river is not obvious. It appears as a multi-phase stacking feature in the vertical direction. The thickness of a single channel is 10-15m (Figure 5A).

b) Diverted bays microfacies. It is mainly composed of gray and dark gray mudstones and silt mudstones. The water body is quiet, mainly developing blocky bedding, biologically disturbed structures, and deformed structures. Occasionally, lenticular bedding and plant debris are visible. Due to the influence of tidal effects, sandy and silty bands develop, and the natural gamma curve appears as a toothed straight line (Figure 5B).

c) Microfacies of estuary sand bars. Estuary sand bars are mainly composed of gray-off-white medium-fine sandstones, and they develop blocky bedding, staggered bedding, parallel bedding, sand grain bedding, rhythm bedding, and tidal bedding. The natural gamma curve appears as a micro-toothed funnel (Figure 5C), reflecting an anti-granular order with a coarsening particle size.

d) Mat sand facies. Mat sands are formed by tidal and wave-reformed estuary sand dam sediments, and the lithology is mainly composed of gray-yellow silt fine sandstones and argillaceous siltstones. In the sedimentary structures such as stratification and parallel bedding, the natural gamma curve shows a finger pattern (Figure 5D), and generally does not exceed 2m. Due to the thin thickness of the mat sand, the vertical sequence is not obvious.

2) Sub delta delta. The pre-delta sedimentation is located at the far end of the delta sedimentary

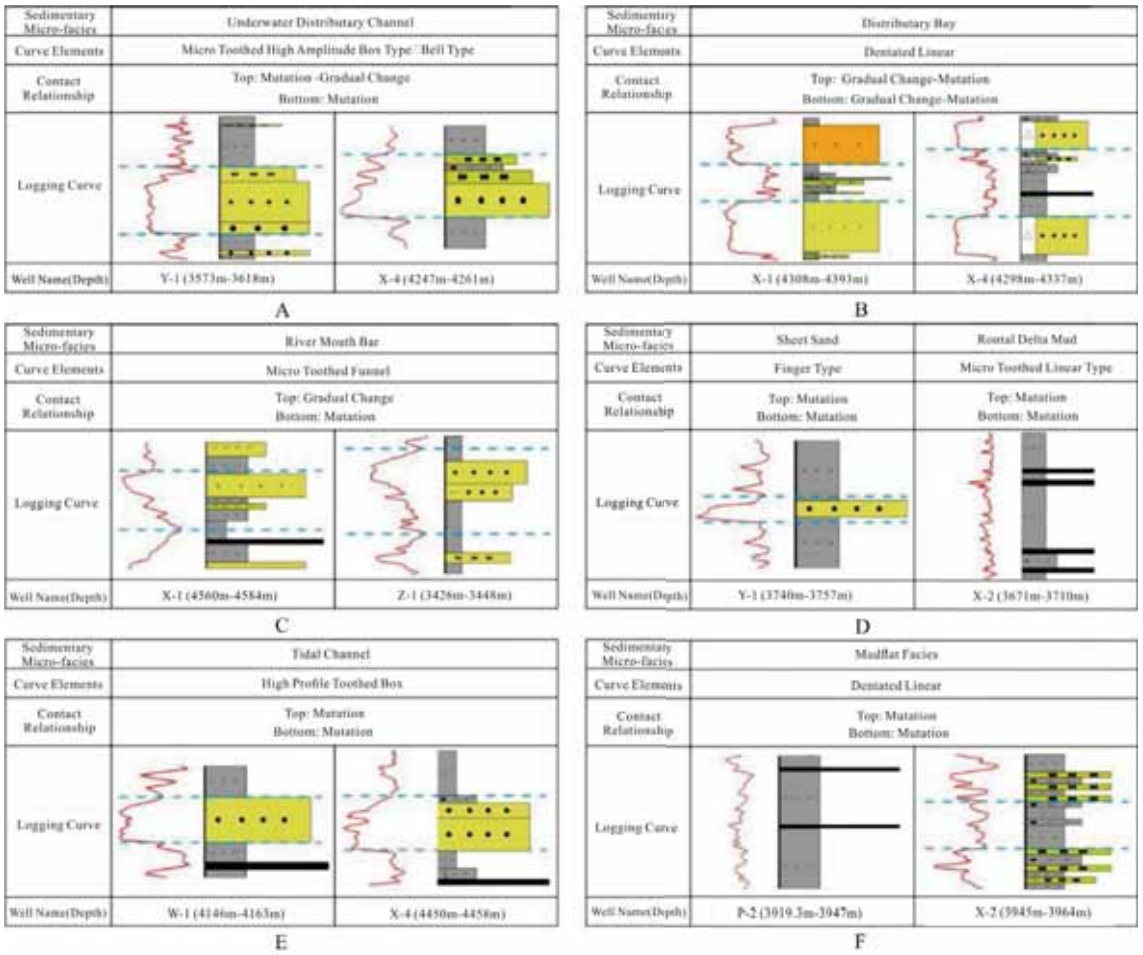

FIGURE 5
Logging Facies Characteristics of Pinghu Formation in Well P Area.

system. It is the deepest part of the water body in the sedimentary environment of the entire delta. The sedimentary water body is quiet and the lithology is mainly dark mudstone and silty mudstone. It has horizontal bedding and biological disturbance structures. The natural gamma curve appears as a straight line with large segments of microtoothing (Figure 5D).

(2) Tidal flat sedimentary system. The study area only identified tidal flat sediments at the bottom of individual well in Pinghu Formation and intertidal subfacies. The intertidal subfacies are further divided into two types of sedimentary microfacies: tidal channels and mud flats. The microfacies of the tidal channel are mainly yellow medium fine sandstone and yellow pebbly medium sandstone showing typical bidirectional staggered bedding, tidal bedding and other typical tidal sedimentation signs [28]. The natural gamma curve is mostly toothed box type (Figure 5E). Mud flats sedimentary rocks are mainly gray mudstone with horizontal bedding and wavy bedding. The natural gamma curve appears as a toothed straight line (Figure 5F).

Sedimentary microfacies distribution and deposition mode. (1) Vertical characteristics of sedimentary microfacies. Figure 6 reveals that the sedimentary facies changed from delta to delta and confined sea interactive sediments from northwest to southeast. The evolution of the facies sequence of the vertical sedimentary facies reflects three sea-level rises and falls in the Pinghu Formation during the sedimentary period.

E2pSQ1 (lower part of the Pinghu Formation) has a small sedimentary thickness during the deposition period, corresponding to the first sea level change. The sedimentary microfacies are mainly delta sediments. Delta fronts and pre-delta subfacies are developed. The northern sand bodies are relatively isolated, and the southern sand bodies are mutually isolated. E2pSQ2 (middle section of the Pinghu Formation) has a large sedimentary thickness during the deposition period, corresponding to the second sea level change. The overall sea level is higher than that of the upper section of the Pinghu Formation, and the lower sea level is lower. It is a delta deposition with delta fronts and pre-delta subfacies [29-30]. The underwater diversion channel is small in thickness and low in stacking. The central sea level is higher, which is a delta-limited sea sediment, and the tidal channel is not developed. The upper sea level is lower and the delta front and delta

subfacies are developed. The river channel is thick, and a thin layer of matting sand and estuary sand dam can be seen at the far end. E2pSQ3 (upper segment of the Pinghu Formation) has a small sedimentary thickness during the deposition period, corresponding to the third sea level change. The overall sea level is lower than that of the middle segment of the Pinghu Formation, and delta fronts and pre-delta subfacies are developed. The lower segment of the Pinghu Formation is similar. The sand bodies in the north are relatively isolated, and the sand bodies in the south are superimposed.

In addition, the seismic profile and plane RMS attribute maps reveal that the contemporaneous normal faults in the study area are more developed, showing a northeast-southwest distribution, and the fault tendency is northwest, which is opposite to the boundary fault tendency. There is a large difference in the sedimentary thickness of the two Panping Formations. For example, a large reverse congruent normal fault is developed between Wells Y-1 and X-4. Through the seismic profile measurement, the growth indices of the lower, middle, and upper faults of the Pinghu Formation are 1.03, 1.10, 1.20, respectively, reflecting that the fault has a certain effect on the sedimentation. During the E2pSQ1 (lower Pinghu Formation) deposition period, the fault distance is large. The river sediments are mainly deposited in the lower part of the upper plate, and it is difficult to cross the fault to the basin. The extent of the underwater shunt channel is limited while during the deposition period of E2pSQ2 (the middle section of the Pinghu Formation) and E2pSQ3 (the upper section of the Pinghu Formation), the fault distance is relatively small. After the underwater diversion channel sediment filled the lower part of the upper plate, it continued to deposit in the lower plate across the fault, and the underwater diversion channel sediment extended far.

(2) Planar distribution characteristics of sedimentary microfacies. On the plane, the Pinghu Formation in P well area mainly develops tidal influence delta front subfacies, which are distributed in the northwest-southeast direction, and are mainly composed of sedimentary microfacies of the submarine diversion channels and the diversion bay, mainly in the northeast-southwest direction [31]. Primary faults develop on the plate, tidal flats develop on both sides of the delta, and occasional tidal channel depositions occur. The fault growth index of the E2pSQ1 (lower Pinghu Formation) in the study area is between 1.06-1.34, and the fault activity is not strong. As the sediments advance toward the center of the basin, the area of the underwater diverging channel continues to increase, the bifurcation increases, and the estuary sediments often develop at the bifurcations and ends of river channels, and a small amount of tidal flat deposits develop in the eastern part of the study area. Occasionally, tidal water channels are connected to underwater diverted rivers (Figure 7A). E2pSQ2 (middle section of the Pinghu Formation) has a fault growth index ranging from 1.21-1.48, faults are relatively active. Due to the increase in the capacity of faults due to fault activity, the growth of the capacity is greater than the sedimentation rate (source supply). The sedimentation is mainly concentrated at low levels. The underwater diversion channel is widened, the bifurcation is reduced, and the estuary sand dam develops only at the end of the underwater diversion channel (Figure 7B). The fault growth index during the deposition period of E2pSQ3 (upper section of the Pinghu Formation) is between 1.1-1.45, fault activity is

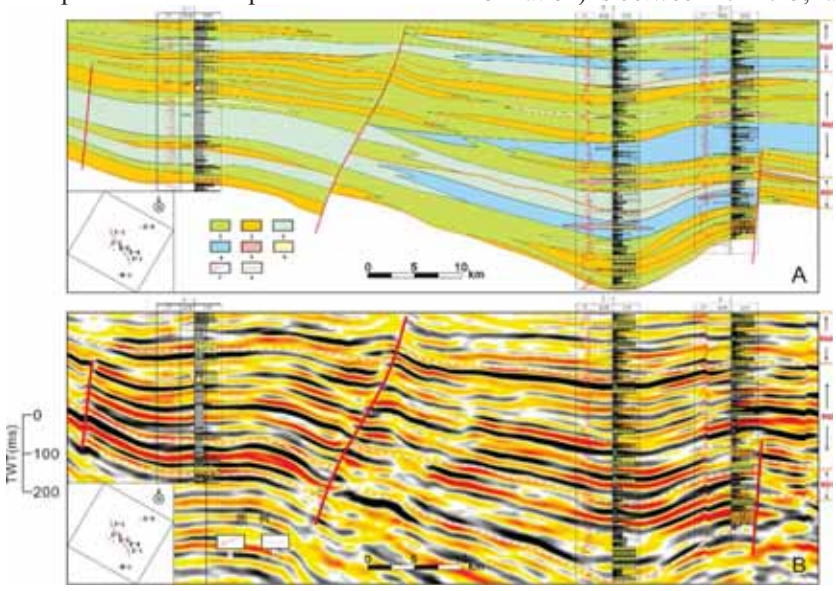

FIGURE 6
Well sections Characteristics of Pinghu Formation in Well P Area.
Notes: 1-Delta front, 2-Underwater distributary channel, 3- Prodelta, 4-Limited sea, 5-Mouth bar/ tidal bar, 6-Sand sheet, 7-Normal fault, 8-Sequence boundary.

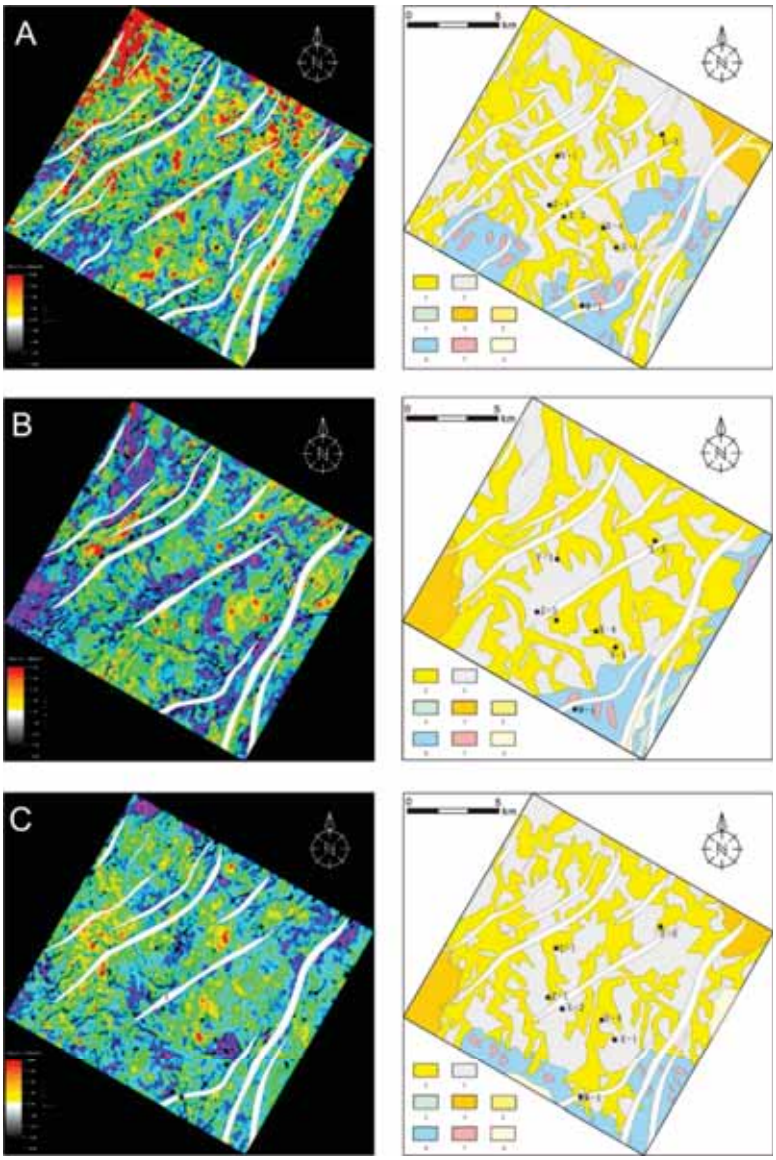

FIGURE 7
RMS Attribute and Sedimentary Facies Plane Distribution Characteristics of Pinghu Formation in Well P Area
Notes: 1-Underwater distributary channel, 2-Interdistributary, 3-Prodelta, 4-Mud flat, 5-Tidal channel, 6-Limited sea, 7-Mouth bar/tidal bar, 8-Sand sheet.

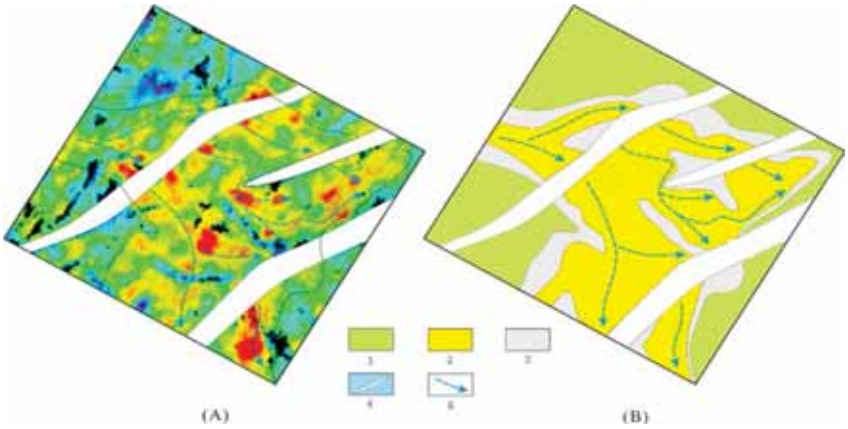

FIGURE 8
Patterns of Fault-Influenced Deposits in Well X Area.
Notes: 1-Delta front, 2-Underwater distributary channel, 3-Interdistributary, 4-Fault, 5-Direction of migration.

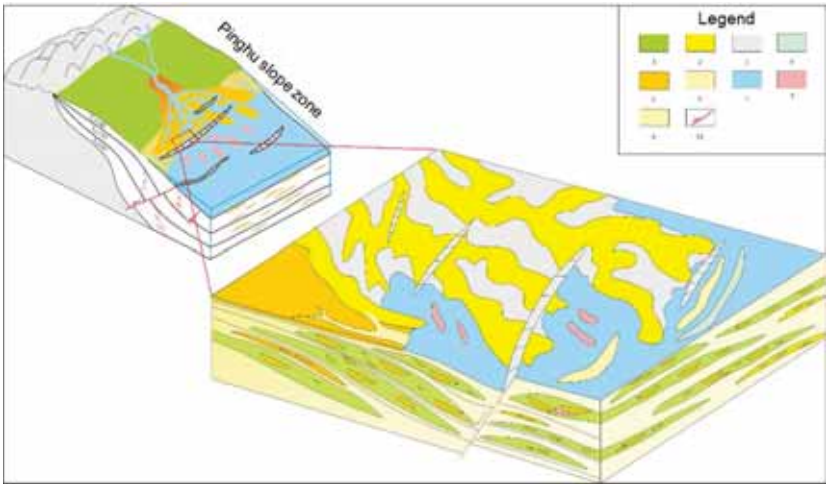

FIGURE 9
Sedimentary model of Pinghu Formation in P well area.
Notes: 1-Delta front, 2-Underwater distributary channel, 3-Interdistributary, 4-Prodelta, 5-Mud flat, 6-Tidal channel, 7-Limited sea, 8-Mouth bar/tidal bar, 9-Sand sheet, 10-Normal fault.

weakened, sediment supply is increased, channel divergence is increased, and estuary sands dam is developed. The tidal flat deposits only develop locally on both sides of the delta system (Figure 7C).

By analyzing the sedimentary microfacies and the plane distribution of the co-occurring faults in the study area, it is considered that the planar distribution of the sedimentary microfacies is affected by factors such as the angle between the source direction and the fault strike, and the fault distance [32]. As shown by the seismic attributes of the upper Pinghu Formation in the eastern part of the study area (Figure 8), when the fault distance is small, if the angle between the source direction and the fault strike is small, the underwater diversion channel may be diverted. When the fault distance is large, the sediments of the underflow diversion channel are deposited only on the lower part of the fault.

(3) Deposition mode. During the sedimentary period of the Pinghu Formation, the West Lake Sag was a confined sea (sedimentary environment), and the western sea reef uplift provided the source, forming delta deposition from west to east into the sea, and tidal flat deposits developed on both sides of the delta. Occasionally, tidal water channels, due to far distance to the source area, the thickness of the single sand body and the thickness of the continuous stacked sand bodies are small, the sediment size is fine, the mudstone thickness is large, and the terrain is relatively steep, which is conducive to the development of underwater diverted river channels in delta fronts with strong hydrodynamic conditions. Syngenetic faults have a significant effect on the distribution of sediments in the delta front of the study area. Underwater river channels may have diversions and other phenomena. The sediments are mainly distributed around the syngeneic faults and near the culmination point of faults, which may develop well reservoirs (Figure 9).

CONCLUSIONS

(1) A set of tidal-affected delta-tidal flat sedimentary systems is developed in the Pinghu Formation in well P area. The tidal influence delta can further identify the two sedimentary subfacies of the delta front and the pre-delta, including five types of sedimentary microfacies including underwater diverted channels, estuary sand bars, diverted bays, and mat sand. Sedimentary subfacies in the zone are divided into two types of sedimentary microfacies: tidal channels and mud flats.

(2) The planar distribution of the sedimentary microfacies is affected by the co-occurring faults. When the fault distance is small, as the angle between the source direction and the fault direction increases, the diversion channel will appear in the underwater diversion channel. When the fault distance is large, the sediments of the underflow diversion channel are deposited only in the lower part of the upper wall of the syngeneic fault.

(3) Based on the analysis of the sedimentary system, a sedimentary model of the delta front in the study area was established. The Pinghu Formation in the study area is strongly affected by tidal effects. Tidal flats are developed on both sides of the delta. Occasionally, tidal water channels are connected to the sub-diversion rivers. The sediment distribution is affected by the reverse syngeneic normal fault, which is mainly distributed on the epigenetic fault and near the fault tipping point.

ACKNOWLEDGEMENTS

This work was supported by the National Key Technology R & D Program of China (Grant No. 2016ZX05027-02-007).

REFERENCES

[1] Hou, G., Li, S., Qin, L., Cai, K., Li, J., He, M. (2019) Source-to-Sink system of Pinghu Formation in west slope belt of Xihu Sag, East China Sea basin. China Offshore Oil and Gas. 31(03), 29-39.

[2] Zhang, W., Hou, G., Xiao, X., Miao, Q., He, M., Shen, W. (2019) Genesis of low permeability reservoirs and main controlling factors of high quality reservoirs in Xihu sag, East China Sea basin. China Offshore Oil and Gas. 31(03), 40-49.

[3] Zhang, R., Wang, J., Ma, Y., Chen, G., Zeng, Q., Zhou, C. (2016) Sedimentary microfacies and palaeogeomorphology as well as their controls on gas accumulation within the deep-buried cretaceous in Kuqa Depression, Tarim Basin, China. Journal of Natural Gas Geoscience. 1(1), 45-59.

[4] Noori, H., Mehrabi, H., Rahimpour-Bonab, H., Faghih, A. (2019) Tectono-sedimentary controls on Lower Cretaceous carbonate platforms of the central Zagros, Iran: An example of rift-basin carbonate systems. Marine and Petroleum Geology. 110, 91-111.

[5] Esmeray-Senlet, S., Ozkan-Altiner, S., Altiner, D., Miller, K. (2015) Planktonic foraminiferal biostratigraphy, microfacies analysis, sequence stratigraphy, and sea-level changes across the cretaceous-paleogene boundary in the Haymana Basin, Central Anatolia, Turkey. Journal of Sedimentary Research. 85(5), 489-508.

[6] Yuan, J., Lu, Y., Li, Z. (2019) Physical Characteristics and Influencing Factors of Deep Reservoirs in Xihu Sag. Marine Oil and Gas. 31(03), 40-49.

[7] Zhang, P., Huang, C. (2018) Reservoir Characteristics and Influencing Factors of Pinghu Formation in the K Structure of Xihu Sag. Marine Oil and Gas. 38(02), 1-6+12.

[8] Gao, G., Ren, J., Yang, S., Xiang, B., Zhang, W. (2017) Characteristics and origin of solid bitumen in Glutenites: A case study from the Baikouquan Formation reservoirs of the Mahu Sag in the Junggar Basin, China. Energy and Fuels. 31(12), 13179-13189.

[9] Jiang, Y., Zhou, Q., Li, S., Zhang, X. (2016) Reconsideration of Pinghu Formation coal-bearing rock series sedimentary environment in Western slope of Xihu Depression. Coal Geology of China. 28 (8), 18-25.

[10] Wu, J., Wan, L., Zhang, L., Wang, Y., Zhao, Q., Li, K., Wang, S. (2017) Lithofacies types and sedimentary facies of Pinghu Formation in Xihu Depression. Lithologic Reservoirs. 29(1), 27-34.

[11] Zhao, H., Jiang, Y., Chang, Y., Li, S., Li, J. (2018) Study on sedimentary characteristics of the Pinghu Formation based on sedimentary facies markers in Xihu Sag, East China Sea Basin. Shanghai Land and Resources. 39(1), 88-92.]

[12] Fu, Z. (2014) The Study of sequence stratigraphy and Sedimentary characteristics of Pinghu Formationin in Xihu sag of East China Sea Basin. Dissertation. Chengdu: Chengdu University of Technology.

[13] Zhou, R. (2015) Sequence stratigraphy and sedimentary facies of the low porosity and low permeability reservoirs of Pinghu Formation-Huagang Formation, Xihu Sag. Dissertation. Chengdu: Chengdu University of Technology.

[14] Arriolabengoa, M., Iriarte, E., Aranburu, A., Yusta, I., Arnold, L., Demuro, M., Arrizabalaga, A. (2018) Reconstructing the sedimentary history of Lezetxiki II cave (Basque Country, northern Iberian Peninsula) using micromorphological analysis. Sedimentary Geology. 372, 96-111.

[15] Coskun Tunaboylu, B., Altiner, D., Isintek, I., Demirci, D. (2014) Foraminiferal biostratigraphy and sequence stratigraphy of Peritidal carbonates at the Triassic-Jurassic boundary (Karaburun Peninsula, western Turkey). Journal of Asian Earth Sciences. 90, 61-76.

[16] Mandurah, M., Aref, M. (2012) Lithostratigraphy and standard microfacies types of the Neogene carbonates of Rabigh and Ubhur areas, Red Sea coastal plain of Saudi Arabia. Arabian Journal of Geosciences. 5(6), 1317-1332.

[17] Wu, J. (2016) Discovery of Tidal Sand Ridges and Its Significance of Pinghu Formation in Xihu Depression. Acta Sedimentological Sinica. 5, 924-929.

[18] Su, A., Chen, H. (2015) Genesis and maturity identification of oil and gas in the Xihu sag, East China Sea Shelf Basin. Editorial Committee of Earth Science-Journal of China University of Geosciences. 6, 1072-1082.

[19] Zhong, Y., Zhou, L., Tan, X., Guo, R., Zhao, L., Li, F., Jin, Z., Chen, Y. (2018). Characteristics of depositional environment and evolution of Upper Cretaceous Mishrif Formation, Halfaya oilfield, Iraq based on sedimentary microfacies analysis. Journal of African Earth Sciences. 140, 151-168.

[20] Li, C., Zhang, Q., Meng, Q. (2002) Tertiary sequence and sedimentary environments of the Baoshi1well in the East China Sea. Marine Oil and Gas. 22(4), 14-23.

[21] Zhao, Y. (2003) Pool forming geology of Xihu depression in East China Sea. Marine Geology Letters. 19(5), 20-24.

[22] Zhu, Y., Zhou, J., Gu, S. (2012) Molecular geochemistry of Eocene Pinghu Formation coal-bearing source rocks in the Xihu Depression, East China Sea Shelf Basin. Acta Petrolei Sinica. 33(1), 32-39

[23] Xue, D., Hu, M., Deng, M. (2014) Sedimentary Facies Characteristics and Sandstone Body Prediction of the Upper Part of Pinghu. Science Technology and Engineering. 14(24), 40-47.

[24] Yin, S., Ye, J., Lei, C., Shan, C., Tian, Y., Liu, F. (2014) Geochemical characteristics of Pinghu crude oils in Pingbei area of Xihu Sag. Xinjiang Petroleum Geology. 35(5), 542-546.
[25] Mulayim, O. (2013) Microfacies analysis, depositional environments and sequence stratigraphy of the late cretaceous Karababa and Derdere formations in the Cemberlitas oil field, Adiyaman, southeastern Turkey. Dissertations and Theses – Gradworks. 153(2), 536-538.
[26] Emad, N., Abdullah, B., Abdullah, M., Ibrahim, B., Saleh, D. (2018) Relative sea-level changes and sedimentary facies development of the lowermost Cretaceous (Berriasian-Valanginian) cycles in the north of Ar Riyad City, Saudi Arabia. Journal of Asian Earth Sciences. 163, 163-176.
[27] Zhang, M., Zhong, Z., Xia, B., Sun, Z. (2005) Late Miocene tectonic inversion and hydrocarbon migration and accumulation in central and southern Xihu Sag, East China Sea. China Offshore Oil and Gas. 17(2), 73-79.
[28] Abbas, A., Zhu, H., Zeng, Z. (2018) Sedimentary facies analysis using sequence stratigraphy and seismic sedimentology in the Paleogene Pinghu Formation, Xihu Depression, East China Sea Shelf Basin. Marine and Petroleum Geology. 93, 287-297.
[29] Deng, H., Zheng, W. (2009) Depositional Characteristics of Offshore Tidal Deposits in the Lower Tertiary Zhuhai Formation, Huizhou Depression, Pearl River Mouth Basin. Geoscience. 23(05), 767-775.
[30] Shang, J., Xue, G., Yuan, L., Chen, J., Ye, M. (2019) Tidal flat facies division and dominant reservoir prediction of main oil group in Wenchang A oilfield. Petroleum Geology and Engineering. 33(05), 31-35.
[31] Hou, Y., Chen, A., Zhao, W., Dong, G., Yang, S., Xu, S., Gao, Z., Li, F., Liu, X., Zhang, X. (2018) Analysis on the depositional environment of Carboniferous Benxi Formation tidal-delta sand body complex, Ordos Basin, China. Journal of Chengdu University of Technology (Science and Technology Edition). 45(04), 393-401.
[32] He, H. (2015) Application of well -logging methods to studying sedimentary facies of xujiahe 2 member, Xinchang Gasfield, Western Sichuan Basin. Natural Gas Exploration and Development. 38(02), 38-42+5-6.

Received: **11.01.2020**
Accepted: **08.02.2020**

CORRESPONDING AUTHOR

Changmin Zhang
School of Geosciences,
Yangtze University,
Wuhan 430100 – China

e-mail: 2067293959@qq.com

RESEARCH ON A NOVEL PRESTACK AND POSTSTACK JOINT MATCHING METHODS OF P-WAVE AND S-WAVE USING IN OIL AND GAS PREDICTION

Qing Guo[1,2], Wei Li[1,*], Yijun Wang[1], Le Qu[2,3]

[1]Changqing Branch of Geophysical Research Institute, BGP, CNPC, Shaanxi, Xi'an 710021, China
[2]State Key Laboratory of Oil and Gas Reservoir Geology and Exploitation (Chengdu University of Technology), Sichuan, Chengdu 610059, China
[3]Post-Doctoral Contribution Center/College of Petroleum Engineering, Xi'an Shiyou University, Shaanxi, Xi'an 710065, China

ABSTRACT

The new multi-component seismic wave exploration technology can greatly improve the accuracy of seismic exploration. Aiming at the problem of P-wave and S-wave time matching, a joint method of P-wave and S-wave pre-stack and post-stack joint matching method is proposed. The simulation and the actual data of multi-wave seismic exploration in typical oilfields are used to match, and the matching results of curve waves and non-curvature waves are compared. The research results show that the matching results are consistent with known geological models and interpreted formation data. The correlation between P-wave data and S-wave data is significantly improved in the sense of curve waves. When the P-wave data contains noise, the matching advantage under the curve wave frame is even greater. Obviously, this technology is a key step of multi-wave exploration technology, and has important research value and application value.

KEYWORDS:
Multi-wave seismic wave exploration, P-wave and S-wave, post-stack joint inversion, seismic data matching, oil and gas prediction

INTRODUCTION

With the increasing requirements of the national economy for oil and gas exploration and development, petroleum exploration is becoming more and more difficult, and seismic exploration is becoming more refined. Multi-wave seismic exploration technology has developed rapidly with the collection of digital data and has brought significant economic benefits [1-2]. The key point of multi-wave seismic exploration technology is to combine the multi-wave data in order to reflect the huge advantages of multi-wave data. Therefore, it is necessary to accurately match the P-wave and S-wave data on a uniform time scale to accurately calculate the P-wave and S-wave velocity ratio, lithological properties such as Poisson's ratio and amplitude ratio [3-5]. The basic principle of P-wave and S-wave accurate time matching is based on the zero-shot offset profile time scale matching method. Zero-offset data requires less auxiliary information, which is straightforward and simple [6-8]. In the case of mathematically unsatisfactory matching, finding an accurate matching solution from a physical perspective is needed. Based on the pre-stack AVA constraint time-scale matching method, this paper establishes an accurate matching method for multi-wave amplitudes based on wave dynamics, compiles software, and tests the forward model and actual production data. The results meet the needs of reservoir monitoring and provide technical guarantee for the increase of oil and gas exploration reserves.

Basic theory and research methods. Because the P-wave velocity is greater than the S-wave velocity, the P-wave time value of the same stratum is small on the obtained seismic profile time axis. According to the Zoeppritz equation [9-10], it is also verified that the P-wave reflection coefficient and the converted S-wave reflection coefficient are significantly different. Therefore, the time axis of the converted S-wave needs to be compressed to match the P-wave time. This paper proposes the use of the initial value of the compression function using the depth domain calibration method, and joint calibration under the conditions of logging data and VSP data. The initial value is brought into the automatic comparison optimization program to obtain the optimal compression function value, and the converted shear wave profile is compressed.

Initial calibration of coherent and P-wave and S-wave coherent horizons. According to the Iverson formula [11-13], the velocity curve of S-wave logging is first equivalently converted to the layer velocity of the converted S-wave, and then converted to the reflection coefficient, which is convolved with the rake wavelet of about 15 Hz to obtain a composite record of the converted S-wave. The synthetic records of converted S-waves and seismic converted S-wave data are compared to calibrate each reflection horizon. Synthesizing the

two calibrations, the composite horizon can be used to calibrate the P-wave and converted S-wave reflection levels. From the initial calibration profile, the P-wave and S-wave velocity ratio of the formation of interest can already be calculated. The method is shown in Figure 1 [14-15]. The upper and lower interfaces A and B of the formation are determined on the P-wave profile, and the time difference read on the profile is recorded as T_{PP}. For the same formation, the time difference on the converted S-wave profile is T_{PS}, and the P-wave velocity and S-wave ratio of this formation can be calculated by the formula.

Using coherent volume calibration technology, horizon calibration is performed on the multi-wave seismic data in Luojia area of Shengli Oilfield, as shown in Figure 2.

In the figure, five important time points of the P-wave and the converted wave are selected. The time of the two is roughly corresponding, and then the respective coherent bodies are calculated. Then, the coherent bodies are compared and calibrated to determine the general time-correspondence relationship between the P-wave and S-wave sections. This is used as the initial value for subsequent matching calculations.

Correlation of P-wave and S-wave propagation time. Figure 3 is a schematic diagram of reflections of P- and S-waves [17-18]. P-wave source is incident from a point O and is reflected on a horizontal interface. At the same time, P-wave and S-wave are emitted at different reflection points and are received at the same receiving point R. It can be seen that the rays P-P are symmetrical and the rays P-S are asymmetric. The reflection point of P-P is the center point MP (M), and the reflection point of P-S is the transition point CP(C), not the center point of the gun line OR.

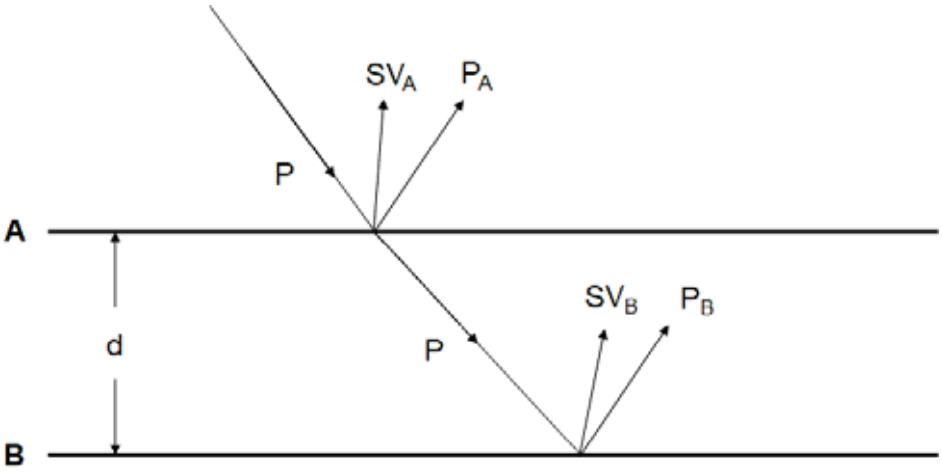

FIGURE 1
Calculating the P-wave and S-wave velocity ratio of a stratum based on the P-wave and S-wave profile time axis.

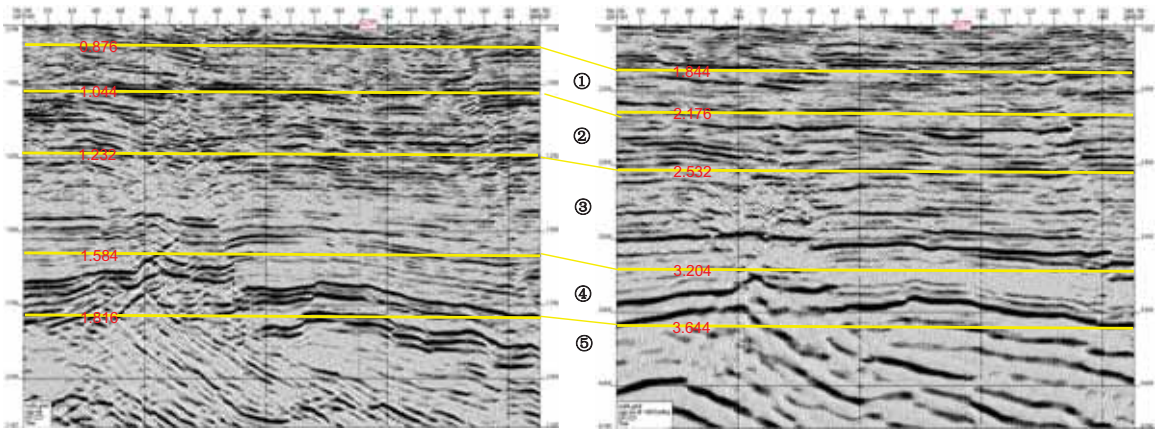

(a) P-wave profile (b) Converted wave profile

FIGURE 2
Overall section of P- and converted waves in Luojia multi-wave exploration.

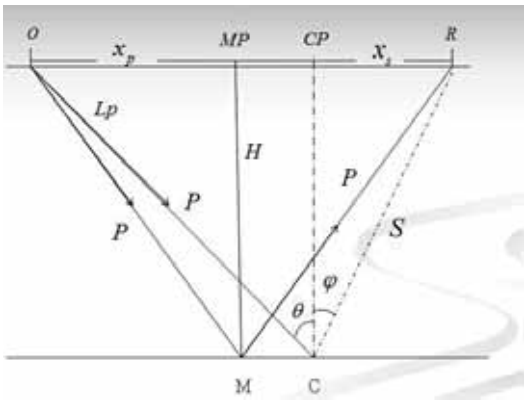

FIGURE 3
Geometry path of P-wave and S-wave.

According to Snell's law [13, 19]:

$$\frac{\sin\theta}{v_p}=\frac{\sin\varphi}{v_s}=p \tag{1}$$

$$v_p=\sqrt{\frac{K+4\mu/3}{\rho}} \tag{2}$$

$$v_s=\sqrt{\frac{\mu}{\rho}} \tag{3}$$

Where K is the bulk modulus; v_p is the P-wave velocity; v_s is the S-wave velocity; H is the depth; P is the P-wave ray; S is the S-wave ray; θ is the P-wave incident angle; φ is the exit angle of the shear wave; x_p is the offset of the P-wave; and x_s is the offset of the S-wave.

Let the function $P(t)$ representing the amplitude of the P-wave as a function of the P-wave travel time, and the function $C(\tau)$ representing the amplitude of the S-wave as a function of the S-wave travel time, then [20]:

$$P(t)\approx\alpha(t)C(\tau)=\alpha(t)C(\omega(t)) \tag{4}$$

Where $\alpha(t)$ represents the amplitude function, and the travel time relationship of P-wave and S-wave is established based on $\tau=\omega(t)$. If the expression of $\omega(t)$ can be found, then the problem is transformed into the calculation of the minimum of formula 5.

$$P(t)-\alpha(t)C(\omega(t)) \tag{5}$$

Most of the actual geological structures are layered structures. If the matching effect of the vertical and horizontal wave time scales of each layer is satisfactory, this method can also be applied to the measured seismic data [21-22]. The layered media model defined in this paper is shown in Figure 4.

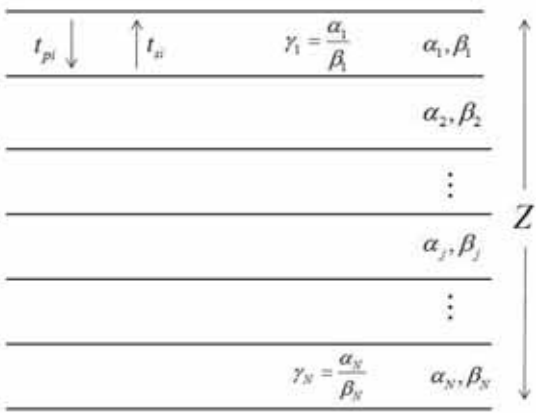

FIGURE 4
Layered geological model.

Let h_i be the layer thickness of the layer i, V_{2P} and V_{2s} be the root mean square velocity of the P-wave and S-wave from the surface to the n-layer geological horizon, α_i and β_i be the layer velocity of the P-wave at the i-layer geological horizon. γ_i is the P-wave and S-wave velocity ratio of the i-layer, then [23]:

$$V_{2p}{}^2=\frac{\sum_{i=1}^{n}\alpha_i{}^2\Delta t_i}{\sum_{i=1}^{n}\Delta t_i}=\frac{\sum_{i=1}^{n}\alpha_i h_i}{\sum_{i=1}^{n}\Delta t_i}=\frac{\sum_{i=1}^{n}\alpha_i h_i}{T_P} \tag{6}$$

In the formula, $\Delta t_i=\frac{h_i}{\alpha_i}$ is a single-layer and one-way P-wave travel, and $T_P=\sum_{i=1}^{n}\Delta t_i$ is a one-way P-wave to the n-layer normal incidence travel.

$$V_{2s}{}^2=\frac{\sum_{i=1}^{n}\beta_i h_i}{T_s} \tag{7}$$

In the equation, T_s is the S-wave travels to the normal incidence of the n-layer one-way.

Defining $\gamma=\frac{V_{2p}}{V_{2s}}$, then [24]:

$$\gamma^2=\frac{V_{2p}{}^2}{V_{2s}{}^2}=\frac{T_s\sum_{i=1}^{n}\alpha_i h_i}{T_P\sum_{i=1}^{n}\beta_i h_i} \tag{8}$$

Therefore:

$$V_{2p}{}^2T_P=\sum_{i=1}^{n}\alpha_i h_i \tag{9}$$

If $H_p=V_{2p}T_p$, then:

$$\gamma = \frac{H_S \sum_{i=1}^{n} \alpha_i h_i}{H_P \sum_{i=1}^{n} \beta_i h_i} \tag{10}$$

If $H_P = H_S$, then the above formula becomes:

$$\gamma = \frac{\sum_{i=1}^{n} \alpha_i h_i}{\sum_{i=1}^{n} \beta_i h_i} \tag{11}$$

Substituting it into the previous formula which brings:

$$\gamma^2 = \frac{T_s}{T_P}\gamma \tag{12}$$

Now defined $T_{Ps} = T_P + T_s$ as two-way converted wave travel, and $T_{pp} = T_P + T_p$ two-way P-wave travel, the above formula can be obtained by adding the numerator and denominator.

$$\frac{T_{ps}}{T_{pp}} = \frac{1+\gamma}{2} \tag{13}$$

The above formula shows that the relationship between the P-wave and converted wave travel time is only related to the velocity ratio, that is,

$$\omega(t) = \frac{1+\gamma}{2}t \tag{14}$$

If the speed ratio of each time window is accurately obtained, the S-wave time can be converted into the P-wave and S-wave domains according to the above formula to achieve the purpose of P-wave and S-wave matching.

P/S matching process based on simulated annealing algorithm. For automatic comparison of two sections, annealing simulation is a fast and effective algorithm. By giving an initial value, the optimization function can update this initial value and repeat it multiple times to get the result. Theoretically, the bridge that communicates the travel time of the P-wave is the wave speed ratio [25-26]. Let t be P-wave travel time, T be S-wave travel time, and γ be wave velocity ratio, then

$$T = \frac{1+\gamma}{2}t \tag{15}$$

Once γ values are obtained at all time points, the P-wave profile can be stretched to the S-wave profile. The value and quantity of γ to be estimated are our concern, and we want to achieve the best matching effect with the least value γ. An ideal choice is to match along key layers. For each key layer, find the corresponding best value, so as to stretch time by layer for time matching. The main idea of this section is to design a correlation function about γ and optimize the function. When it reaches the optimal value, it is regarded as the optimal speed ratio of the time window.

The specific steps of the simulated annealing method are: Take an hour window on the P-wave profile and find the corresponding time window on the S-wave profile according to the initial value.

Take n points in the P-wave time window and record them as $x_1, x_2, \cdots x_n$, and the corresponding amplitudes as $A_p^1, A_p^2, \cdots A_p^n$. Take the corresponding n points in the S-wave time window and record it as $y_1, y_2, \cdots y_n$ and the amplitude is $A_s^1, A_s^2, \cdots A_s^n$, then [27]:

$$y_i = \frac{1+\gamma}{2}x_i, \quad (i = 1, 2, \cdots n) \tag{16}$$

It can be seen that A_s^i is determined by γ.

Let $C = \sum_{i=1}^{n} A_p^i A_s^i$, C is a function about γ which is called a correlation function. Select an optimization method to numerically optimize the designed correlation function so that the value γ at the maximum value C is considered to be the best speed ratio γ of the time window. Find the optimal speed ratio γ for all time windows to stretch.

RESULTS AND DISCUSSION

Prestack and Poststack Matching Process of P- and S-waves based on Curvelet Transform. Curvelet transform can overcome the limitation of wavelet transform in removing random noise in two-dimensional signals. In addition, for the objective function with smooth singularity curve, curved edge transform can provide a more accurate and efficient representation (Figure 5).

It is precisely because of the above-mentioned good properties of curve wave transform that this project innovatively introduces curve wave transform into the problem of P-wave and S-wave matching. The specific steps of multi-scale horizon calibration based on curve wave transform are as follows: the P and S wave sections are decomposed into sections with different scales by curve wave transform [28]. Firstly, the simulated annealing method or the least square method is used to perform the P-and S-wave time scale on a larger scale and secondly match on a smaller scale based on the P- and S-wave matching results on a larger scale (Figure 6).

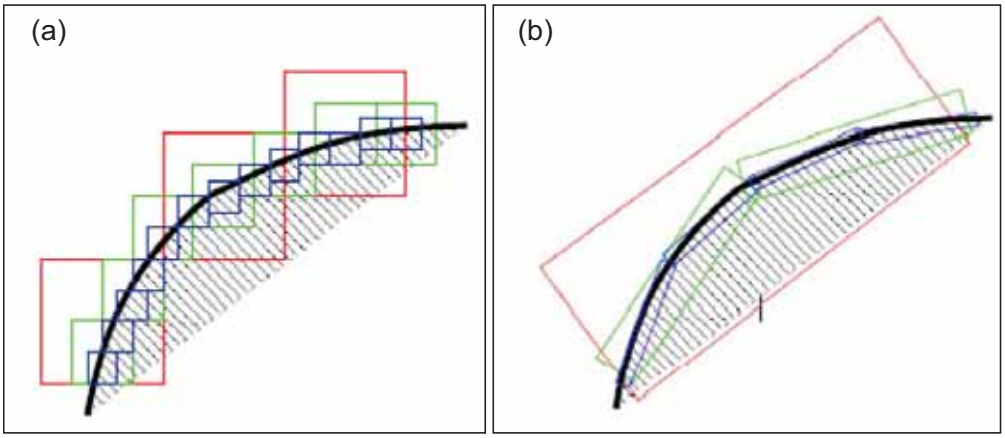

FIGURE 5
Comparison of image approximation by curve and wavelet.
Notes: (a) Approximation of curve by wavelet transform, (b) Approximation of curve by curved wave transformation

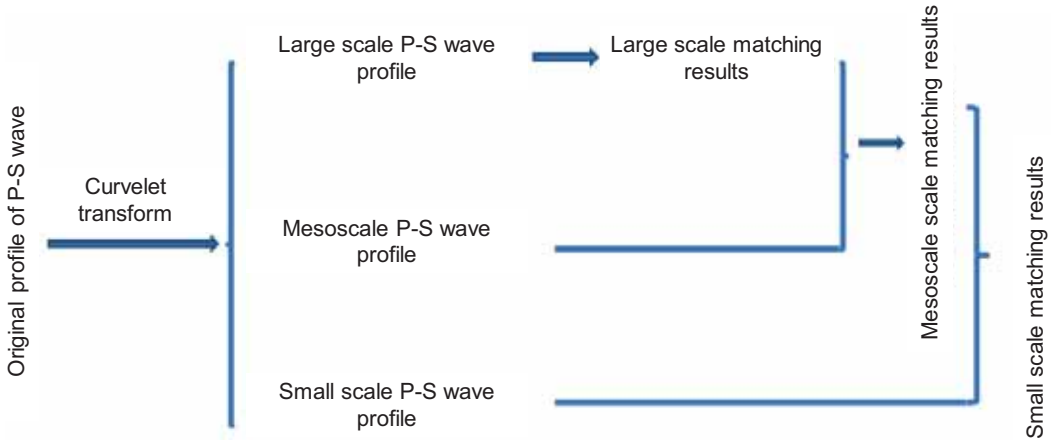

FIGURE 6
Flow chart of P-wave and S-wave matching based on curvelet transform.

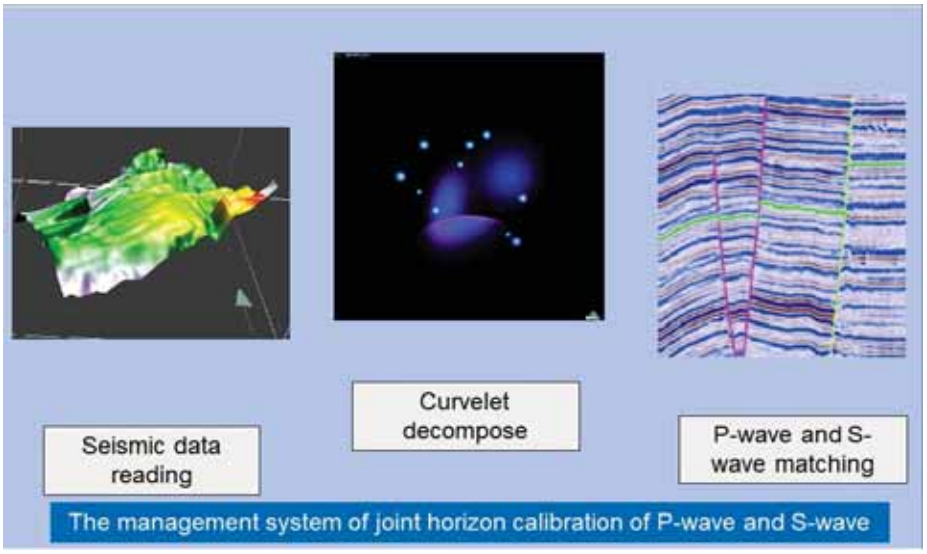

FIGURE 7
P-wave and S-wave matching software module interface.

Compilation and testing of matching software modules. According to the above-mentioned P-wave and S-wave matching theory and algorithm, a software module for P-wave and S-wave matching processing is compiled, and the interface is shown in Figure 7.

The matching software module realizes data reading of P-wave data. In the domain of curve wave transformation, multi-scale decomposition of P-wave seismic data is realized. For multi-scale P-wave and S-wave, according to the established model algorithm, the P-wave and S-wave velocity ratio is extracted, and the P-wave and S-wave e data is matched.

Field application. Aiming at the Luojia multi-wave seismic survey data of Shengli Oilfield, the application of P-wave and S-wave matching based on curvelet transform was carried out.

Figure 8 is the overall section of the P- and S-wave exploration data, and Figure 9 is a partial display of the hydrocarbon-bearing horizons. It can be seen that due to the inconsistency of the P-wave and S-wave propagation time, the same geological horizon has different propagation time on the P-wave and S-wave profile, which makes it impossible to directly interpret the earthquake. Therefore, it is necessary to match the P-wave and S-wave at the same time scale.

For the area near the oil-bearing layer of interest (medium-deep layer), that is, part of Figure 9, we conducted further quantitative analysis by comparing the maximum and average amplitudes of the P- and S-wave data to determine the feasibility of P- and S-wave matching. After calculation, we obtain the maximum and average amplitudes of the P-wave and S-wave. Although the magnitude difference between the P-wave and converted-wave data in terms of the maximum amplitude is not small, the average amplitude of the two is at the same amount Level.

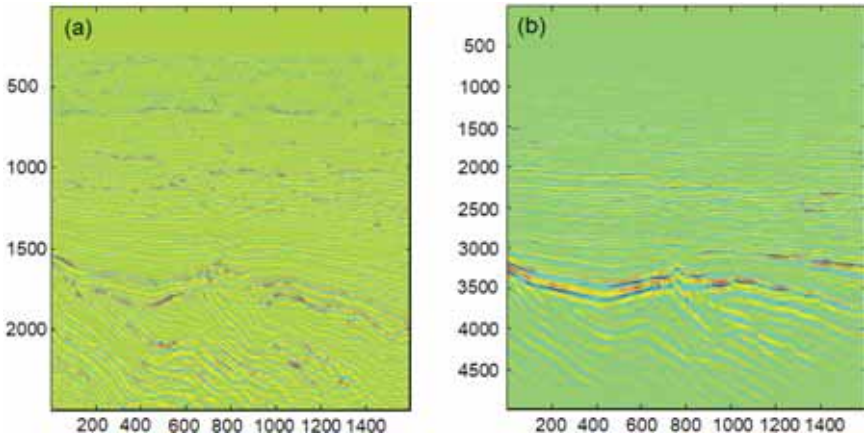

FIGURE 8
Overall section of multiwave exploration P-wave (left) and converted-wave (right) migration data in Luojia area.

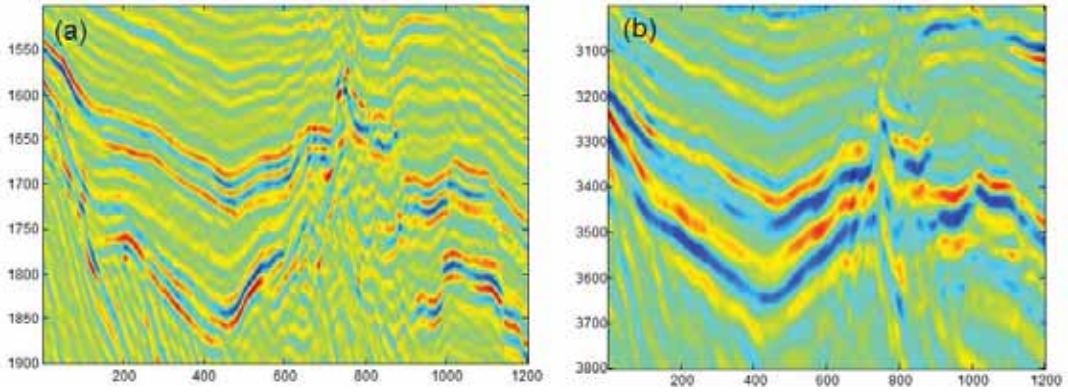

FIGURE 9
Partial display of fluid horizons in the P-wave (upper) and converted wave (lower) of Luojia.

TABLE 1
Statistics of amplitude of P-wave data in the Figure 9

/	P-wave	PS-wave
Maximum amplitude	3.7274×10^{4}	1.7805×10^{7}
Average amplitude	4.6756×10^{3}	7.8621×10^{3}

After the P-wave and converted wave data are subjected to a curved wave transformation and examined in a large-scale framework, it is found that after the P-wave and transformed wave data, the P-wave and converted wave data are at both the maximum amplitude value and the average amplitude value level. At the same magnitude, the absolute value is closer, showing that the feasibility of matching is significantly increased than that of non-curvature.

Figure 10 and Figure 11 show the matching results of large-scale and small-scale P-wave and S-wave under curved waves. The two profiles are connected around 600 channels to investigate the consistency of P-wave and S-wave horizons. It can be seen in the figure that the continuity of the two coincident axes is good, and the P- and S-wave horizons have a good corresponding relationship [29-30]. On a large scale, the structure of the seismic profile is clearer, which is beneficial to the matching of the P-wave and S-wave and the subsequent joint interpretation work. The horizon line information is added to verify the validity of the method. The horizons (T_2, Tr, es1di) known in the previous geological interpretation work were applied to large and small scale matching profiles. The results show that the P-wave and S-wave are well connected at 600 channels, and the validity of the matching is verified.

In-depth analysis of matching in the large-scale curved wave frame and small-scale matching, and comparing Figure 10 with Figure 11, it is found that on the large scale, the frequency of the P-wave data is closer to the frequency of the converted wave data, so that the two can be matched fast. At small scales, the frequency of P-wave data is higher than the frequency of converted-wave data. The correlation between the two is lower than at large scales.

TABLE 2
Statistical values of amplitude of P-wave and S-wave data after curve wave transformation

/	P-wave	PS-wave
FFT maximum coefficient	2.4380×10^6	9.0910×10^6
FFT average coefficient	1.5446×10^5	2.5795×10^5

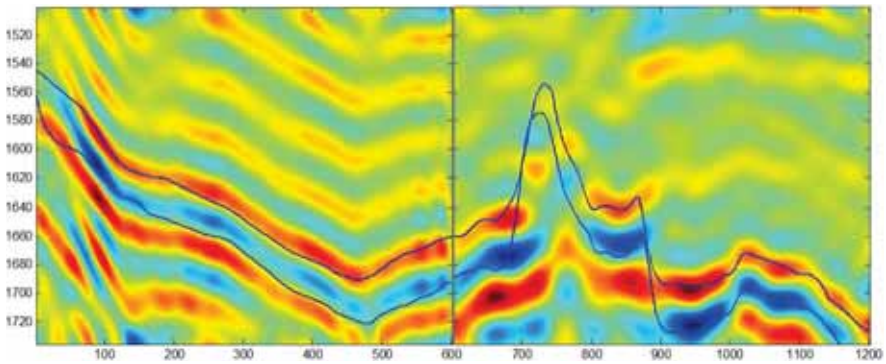

FIGURE 10
Matching results of P-wave and S-wave near the pesese1 and ppt2 formations on a large scale based on curvelet transform.

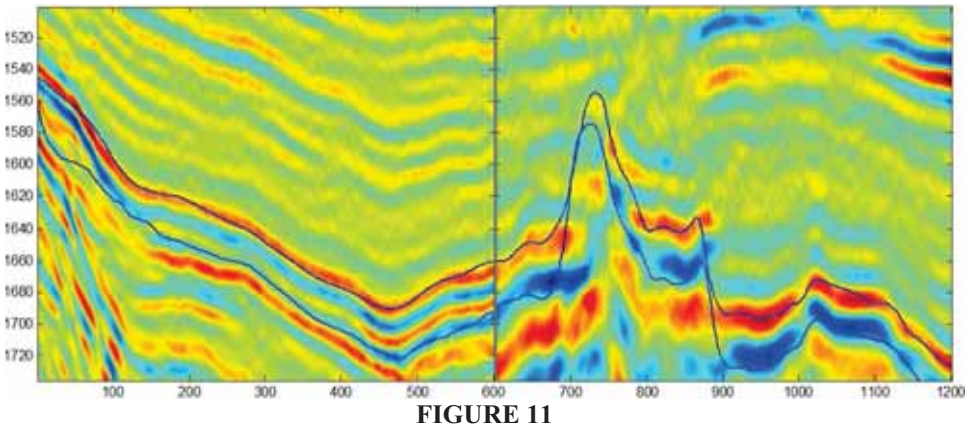

FIGURE 11
Matching results of P-wave and S-wave near the pesese1 and ppt2 formations on a small scale based on curvelet transform.

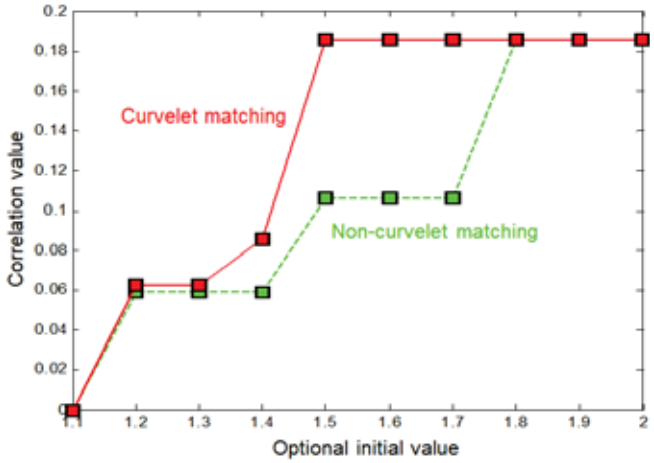

FIGURE 12
Correlation analysis between curved and non-curvature matching methods at different speed ratio initial values.

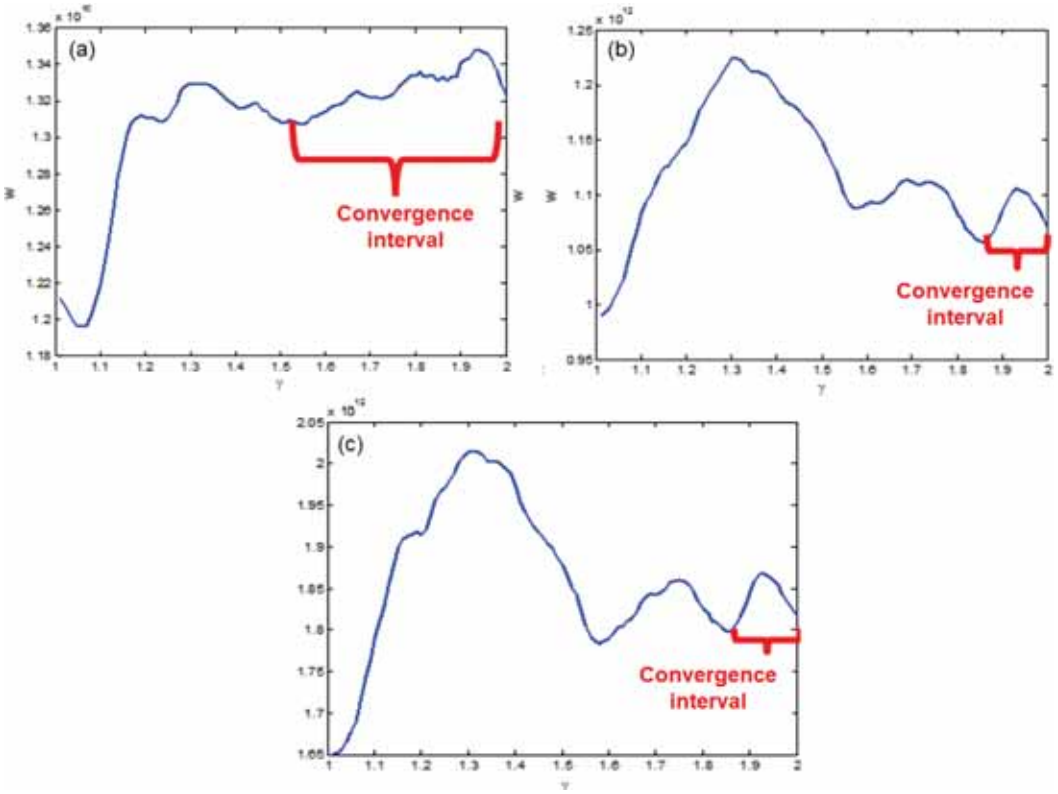

FIGURE 13
Multiscale convexity analysis.
Notes: Curve wave large scale (a) small scale (b) traditional method (c) objective function.

In order to further quantitatively examine the effects of P-wave and S-wave matching, we perform correlation analysis on the data after P-wave and S-wave matching, and the correlation value η is defined as follows:

$$\eta = \frac{\sum (X - \bar{X})(Y - \bar{Y})}{\sqrt{\sum (X - \bar{X})^2 \sum (Y - \bar{Y})^2}} \quad (17)$$

Where X and Y represent the P-wave and converted-wave data, respectively, $\bar{X}$ and $\bar{Y}$ represent the mathematical expectations of X and Y.

According to the definition of correlation value, we compare the effect of P-wave and S-wave matching in the sense of non-curvature and curve, as shown in Figure 12, the result shows that the correlation value of P-wave and S-wave matching in the sense of non-curvature is 10.46% while in the sense of curve wave, the correlation is 18.54%, an increase of 77.25%. And we set the initial velocity ratio of iterative optimization to different values to study the correlation of P-wave and S-wave pro-

files. The dependence of P-wave and S-wave matching based on the curvelet transform on the initial value is reduced, and the P-wave profile and S-wave correlation can be maintained well. This shows that the curvelet transform is of great significance to the problem of P-wave and S-wave matching.

In the multi-scale P-wave and S-wave matching problem, the convexity of the objective function is more obvious in the curved wave frame. As can be seen in Figure 13, at large scales, this method can not only effectively avoid local extreme values, but also expand the range of the convergence interval.

In order to further verify the validity of the curve-wave transform for the P-wave and S-wave matching methods, we added additional noise to the P-wave profile and then matched the profile with noise. Figure 14 shows the cross-sections of noise factors under non-curvature and curved waves. It can be seen that when there is a lot of noise, the cross-section structure without curve transformation has been blurred, but in the sense of curve, the basic structure of the section can still be reflected, indicating that the matching noise profile is not affected under curved waves.

Below we further verify the similarities and differences between the curve wave and non-curvature matching results at different noise levels. Here the degree of noise is defined as follows:

$$level = \frac{D_{noise} - D_{original}}{10000 \cdot R} \tag{18}$$

Where level represents the noise level, D_{noise} is the noisy data, $D_{original}$ is the original data, and R is a random (0, 1) matrix. Figure 15 shows the matching results. It can be seen that with the addition of a large amount of noise, the P-wave and S-wave matching based on curve waves are not sensitive to noise, and can still maintain high matching correlation values, indicating that the P-wave and S-wave matching shows good application prospects.

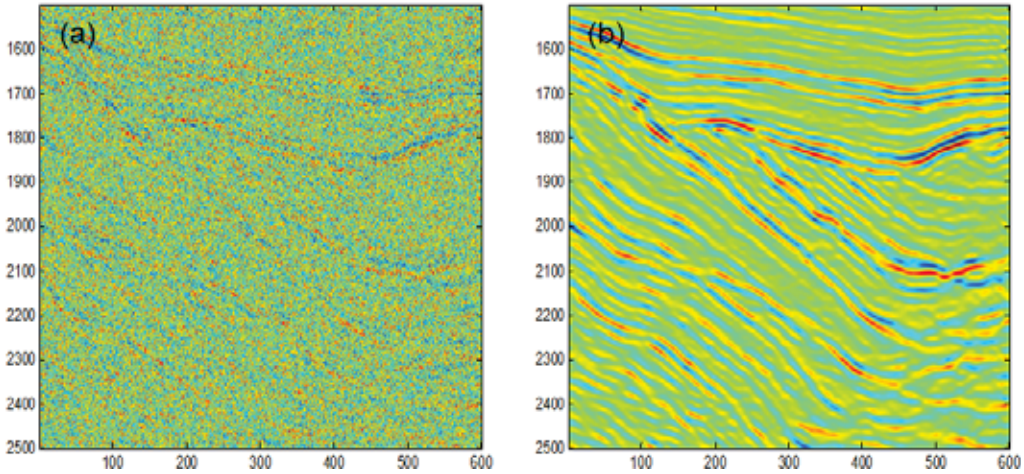

FIGURE 14

Sectional diagram of noise-free P waves under non-curvature (a) and under curve (b).

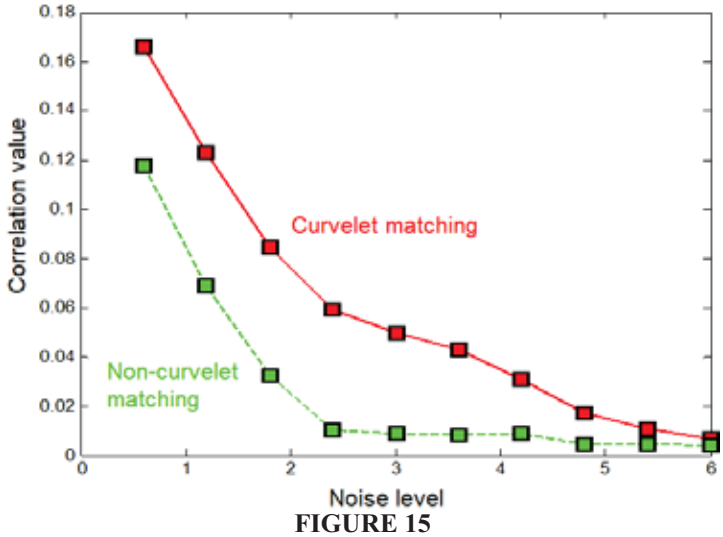

FIGURE 15

Correlation analysis of P-wave and S-wave in the case of noise.

CONCLUSIONS AND SUGGESTIONS

(1) Aiming at the problem of P-wave time matching, a P-wave and S-wave pre-stack and post-stack joint matching method based on curve wave transform is proposed, and a set of theory, algorithm and program module of P-wave and S-wave pre-stack and post-stack joint matching method are innovatively developed.

(2) The multi-wave forward modeling and the actual data of multi-wave seismic exploration in Shengli Oilfield were matched. The matching results were consistent with known geological models and interpreted formation data, which verified the validity of the method. The matching wave theory was used to reasonably explain the results of forward modeling.

(3) The matching results between curved and non-curved waves are compared, and the results show that the correlation between P-wave data and S-wave data is significantly improved in the sense of curve waves. When the P-wave data contains noise, the matching advantage under the curve wave frame is more obvious.

(4) The actual multiwave seismic exploration data of Shengli Oilfield were used for matching practice, and the forward data based on the unique geological characteristics of Shengli Oilfield were used to further verify the reliability and effectiveness of the matching technology.

ACKNOWLEDGEMENTS

This work was financially supported by the Open Fund (PLC20190702) of State Key Laboratory of Oil and Gas Reservoir Geology and Exploitation (Chengdu University of Technology) and the Natural Science Basic Research Plan in Shaanxi Province of China (2019JQ-407).

REFERENCES

[1] Lu, M., Wang, Y. (2009) Principles of seismic exploration (Third Edition). Qingdao: China University of Petroleum Press.

[2] Garotta, R., Marechal, P., and Magesan, M. (1985) Two-component acquisition as a routine procedure for recording P-waves and converted waves. Canadian Journal of Exploration Geophysics. 21, 40-53.

[3] Lawton, D., Bertram, M. (1993) Field tests of 3-component geophones. Canadian Journal of Exploration Geophysics. 29, 125-131.

[4] Li, Q., Wang, J. (2007) Difficulties and prospects of multiwave seismic exploration. Qingdao: China Ocean University Press.

[5] Stewart R., Gaiser J., Brown R., Lawton D. (2002) Converted-wave seismic exploration: Methods. Geophysics. 67, 1348-1363.

[6] Stewart R., Gaiser J., Brown R., Lawton D. (2003) Converted-wave seismic exploration: Applications. Geophysics. 68, 40-57.

[7] Liu, Y., Wei, X. (2003) Some problems and strategies in converted-wave seismic exploration. Progress in Exploration Geophysics. 26(4), 247-267.

[8] Zhang, L., Liu, Y. (2005) Overview of pre-stack time migration for converted wave. Progress in Geophysics. 20(4), 1134-1139.

[9] Ma, S., Tang, J. (2007) Application of pre-stack time migration in 3-D converted wave data processing. Petrochemical Industry Technology. 46(2), 174-180.

[10] Cui, B., Wang, W. (2010) Application of prestack time migration to seismic imaging of deep fault depression areas. Progress in Geophysics. 25(5), 1703-1708.

[11] Huang, Z., Qu, S., Wang, Y., Zhao, G., Wei, X., Xu, Y. (2010) 3D multi-component data processing technologies. Geophysical Prospecting for Petroleum. 49(2), 140-146.

[12] Samsonov, A. (2011) Longitudinal and transverse waves of the electric field. Journal of Communications Technology & Electronics. 56(11), 1324-1328.

[13] Sanditov, D., Mashanov, A., Darmaev, M. (2009) Propagation velocity of longitudinal and transverse acoustic waves and anharmonicity of lattice oscillations. Technical Physics. 54(9), 1398-1401.

[14] Sloan, F., Hanrahan, B. (2014) Cost offsets to medicare attributable to receipt of hip, knee, and shoulder arthroplasty. Arthritis Care & Research. 66(8), 1203-1212

[15] Katsuki, D., Gutierrez, M., Almrabat, A. (2019) Stress-dependent shear wave splitting and permeability in fractured porous rock. Journal of Rock Mechanics and Geotechnical Engineering. 11(01), 5-15.

[16] Mnatzaganian, G., Davidson, D., Hiller, J., Ryan, P. (2015) Propensity score matching and randomization. Journal of Clinical Epidemiology. 68(7), 760-768.

[17] Qian, Y., Zhao, J. (2015) Influence of PWHT on the residual stress in under-matching welded joint. Procedia Engineering. 130, 966-972.

[18] Lazar, A., Jin, L., Spurlock, C., Wu, K., Sim, A. (2017) Data quality challenges with missing values and mixed types in joint sequence analysis. 2017 IEEE International Conference on Big Data (Big Data). IEEE.

[19] Baev, A., Asadchaya, M. (2005) Specific features of excitation and propagation of longitudinal and transverse subsurface waves in solids: ii. effects of some boundary conditions on formation of acoustic fields. Russian Journal of Nondestructive Testing. 41(9), 577-585.
[20] Chapman, T., Berger, R., Cohen, B., Banks, J., Brunner, S. (2017) Longitudinal and transverse instability of ion acoustic waves. Physical Review Letters. 119(5), 055002.
[21] Danilov, V. (2010) On the calculation of characteristics of echo signals of transverse and longitudinal waves from reflectors with flat surfaces. Russian Journal of Nondestructive Testing. 46(1), 26-41.
[22] Han, Z., Li, D., Wang, H., Liu, X., Li, J., Geng, D., Zhang, Z. (2009) Broadband electromagnetic-wave absorption by FeCo/C nanocapsules. Applied Physics Letters. 95(2), 053115.
[23] Gaiotti, M., Ravina, E., Rizzo, C., Ungaro, A. (2018) Testing and simulation of a bolted and bonded joint between steel deck and composite side shell plating of a naval vessel. Engineering Structures. 172, 228-238
[24] Feng, F., Li, J., Mo, R. (2019) A mode-matching approach for ridge-guided wave investigation. Applied Mathematical Modelling. 75, 236-249.
[25] Liu, Z., Zhao, J., Wu, B., Zhang, Y., He, C. (2010) Configuration optimization of magnetostrictive transducers for longitudinal guided wave inspection in seven-wire steel strands. NDT and E International. 43(6), 484-492.
[26] Li, L., Luo, X., Wang, M., Kong, X., Zhou, H. (2010) 3D PP-PS joint inversion method and application in anisotropic medium. Oil Geophysical Prospecting. 45(1), 60-65.
[27] Guo, P., Zhang, S., Zhang, G., Zhong, Q. (2013) Research and application of joint inversion of prestack P & S wave. Oil Geophysical Prospecting. 48, 53-57.
[28] Yang, J., Wang, J., Peng, G., Ma, L., Xie, N. (2014) The Application of Multi-Wave and Multi-Component Joint Inversion of Seismic Data to S Oilfield in Tabei Uplift, Tarim Basin. Xinjiang Petroleum Geology. 35(3), 347-351.
[29] Huang, Y., Xu, T., Cheng, B., Gan, Q. (2010) Application of converted-wave poststack joint inversion in the Xujiahe Formation gas reservoir in the western Sichuan Basin. Natural Gas Industry. 30(4), 38-41.
[30] Leng, X., Du, Q., Meng, X. (2019) Reservoir fluid detection method based on joint PP-and PS-wave elastic impedance inversion. Fault-Block Oil and Gas Field. 36(3), 319-323+363.

Received: **11.01.2020**
Accepted: **19.02.2020**

CORRESPONDING AUTHOR

Wei Li
Changqing Branch of Geophysical Research Institute,
BGP, CNPC,
Shaanxi Xi'an 710021 – China

e-mail: guoqing2011@cnpc.com.cn

© by PSP Volume 29 – No. 05/2020 pages 4022-4039 Fresenius Environmental Bulletin

A STUDY ON THE RELATIONSHIP BETWEEN GEOTECHNICAL, MINERALOGICAL AND CHEMICAL PROPERTIES OF PLIOCENE CLAY SOILS IN ESKISEHIR

Hulya Erkoyun[1], Murat Turkoz[2,*], Bismillah Joyan[1]

[1]Department of Geological Engineering, Faculty of Engineering and Architecture, Eskisehir Osmangazi University, Turkey
[2]Department of Civil Engineering, Faculty of Engineering and Architecture, Eskisehir Osmangazi University, Turkey

ABSTRACT

Both geotechnical and mineralogical characteristics of the sixty five disturbed Pliocene core samples taken from Eskişehir province were examined in detail. In order to evaluate the mineralogical properties of soil samples, X-ray, differential thermal analysis-thermal gravimetric (DTA-TG), infrared spectroscopic (IR) and scanning electron microscopy (SEM) analyzes were performed. In the soil samples, the predominant clay mineral is smectite and a small amount of chlorite and illite are also observed based on the ideal DTA-TG and IR peaks and SEM analysis. The percentage of smectite, chlorite and illite positive correlated with liquid limit (LL), plastic limit (PL), plasticity index (PI) and clay activity (A). As the chemical composition of major oxides and geotechnical properties was evaluated together, it was determined that LL, PL and PI values with SiO_2 and Al_2O_3 content have a positive relationship and also the increase of Fe_2O_3, Na_2O and K_2O amounts result in increasing LL and clay's activity in Eskişehir soils. As a result of the study, it was evaluated that CaO content can be used as an alternative to A value in the evaluation of swelling potential.

KEYWORDS:
Eskişehir, Pliocene, clay mineralogy, geochemistry, geotechnical properties

INTRODUCTION

The mineralogical and geochemical properties of soil including clay minerals affect the engineering properties of cohesive soils [1-7]. Although mineralogical and chemical properties of soils are very important, most geotechnical studies are not taken into consideration [8].

Mineralogy of rocks affects geotechnical properties due to weathering, diagenesis and alteration [3]. The geotechnical behaviors of argillaceous rocks (swelling, slaking, fracturing and disintegration) give rise to serious civil engineering and geotechnical problems [3]. The percolation of absorbed water on the external surface of the clay minerals and increase of interlayer water give rise to swelling of montmorillonite and illite [6, 9].

The characteristics of the sediments from the drill holes in different districts of Eskişehir were examined using mineralogical, geochemical (chemical analyses of major and trace elements) and geotechnical (Atterberg limits, swelling, sieve and hydrometer analyses) analyses were conducted (Figure 1).

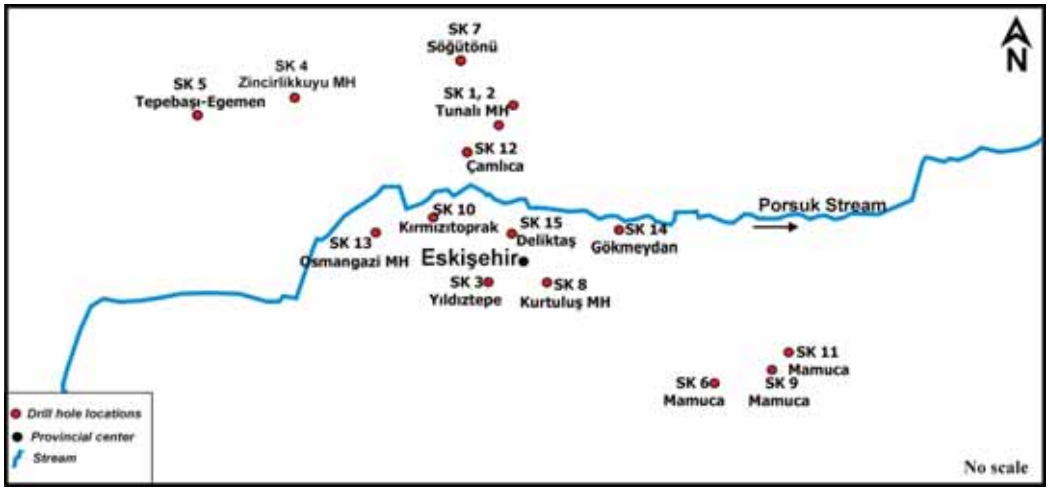

FIGURE 1
The location of drill holes in study area.

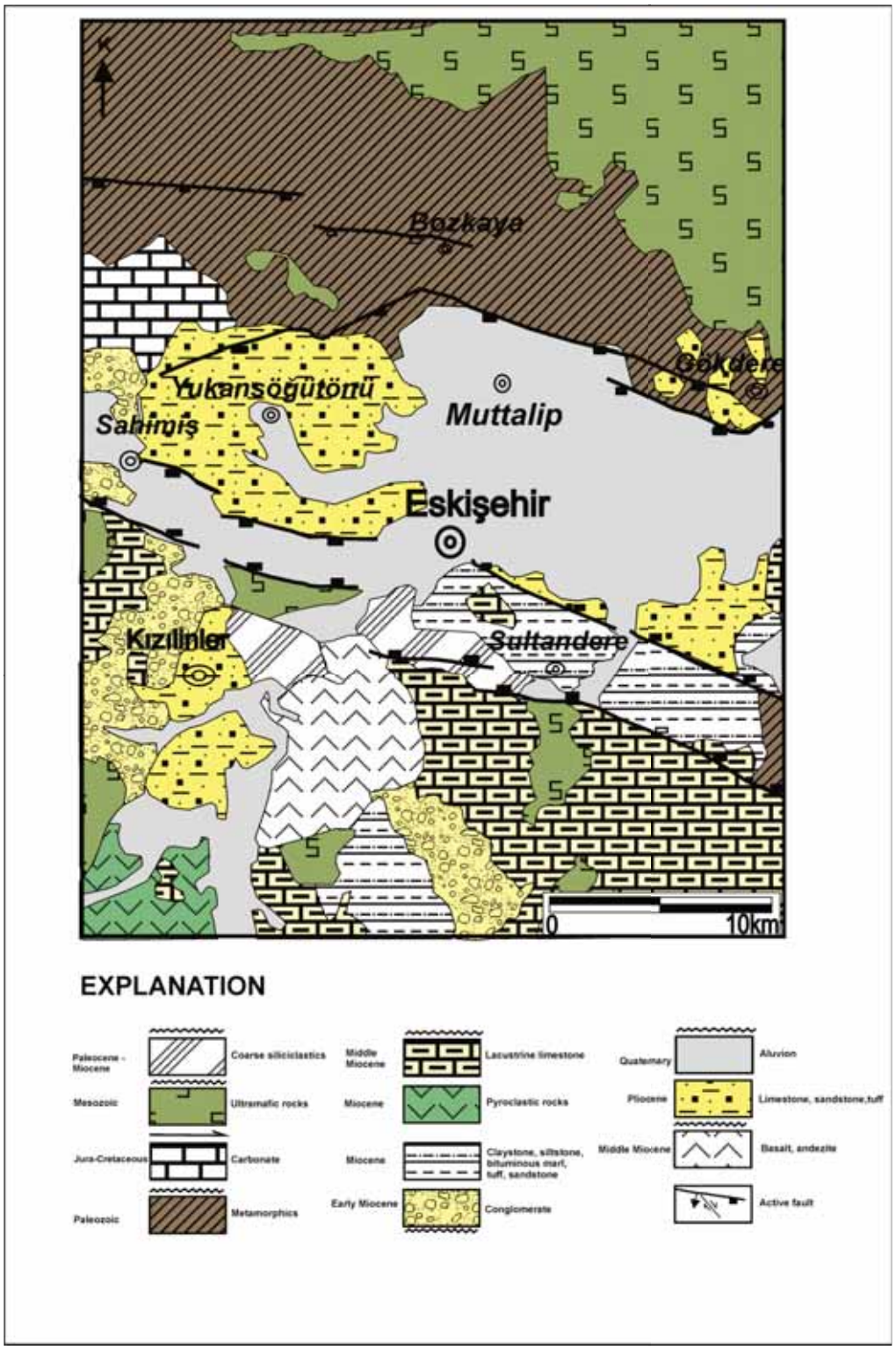

FIGURE 2
The geology of the study area [40-41] [16].

In previous studies conducted by [10-12], Eskişehir clays were evaluated in detail. The effects of mineralogical and chemical compositions on engineering parameters have not previously been studied in Eskişehir. The physical and mechanical behaviors of cohesive soils, such as swelling, shrinkage and strength properties are very important features that play major roles in civil engineering applications. In this study was investigated the geotechnical properties with the mineralogical and chemical compositions of the Pliocene sediments in Eskişehir. The relationships between clay mineral type and content and geotechnical parameters were demonstrated. In addition, the soils were classified based on clay mineral type.

GEOLOGICAL SETTING AND LITHOLOGICAL PROPERTIES

The study area consists of Paleozoic namely gneiss, schist, metagranite, marble, and amfibolite and Mesozoic serpentinized ophiolitic rocks that thrust-faulted overlain the metamorphics basement rock units [13-14] (Figure 2). The basement rocks are overlain unconformably by Paleocene-Miocene continental clastics, Miocene conglomerate, sandstone, claystone, siltstone, bituminous marl, tuff/tuffite, limestone, basalt, andesite, dolomite and gypsum. Miocene units are unconformably as low angle overlain by Pliocene red-grey conglomerate-sandstone, red-brown mudstone, green claystone, marl, gypsum, dolomite, dolomitic claystone, and limestone indicate fluvial and lacustrine sediments [15-16]. Quaternary travertine and alluvium are unconformably overlain by all units.

The drill holes (SK1, SK2, SK4, SK5, SK7, SK10, SK12, SK13, SK14, SK15) composed of from bottom to top dark brown gravel-clayey sand (2.00-10.00 m), dark brown gravel-silty sand (3.50-7.00), dark brown silty claystone and brown claystone (0.00-8.50 m) at the north-nortwest of the Eskişehir (Figure 3). The drill holes (SK3, SK6, SK8, SK9, SK11) consist of from bottom to top green claystone intercalated with marl (6.50-10.00 m), dark brown sandy-gravel (7.00-9.45 m), dark reddish claystone-siltstone (3.50-9.45 m), brown claystone intercalated with marl (2.50-6.50 m), light brown silty claystone (0.00-12.45 m) at the south-southeast of the Eskişehir.

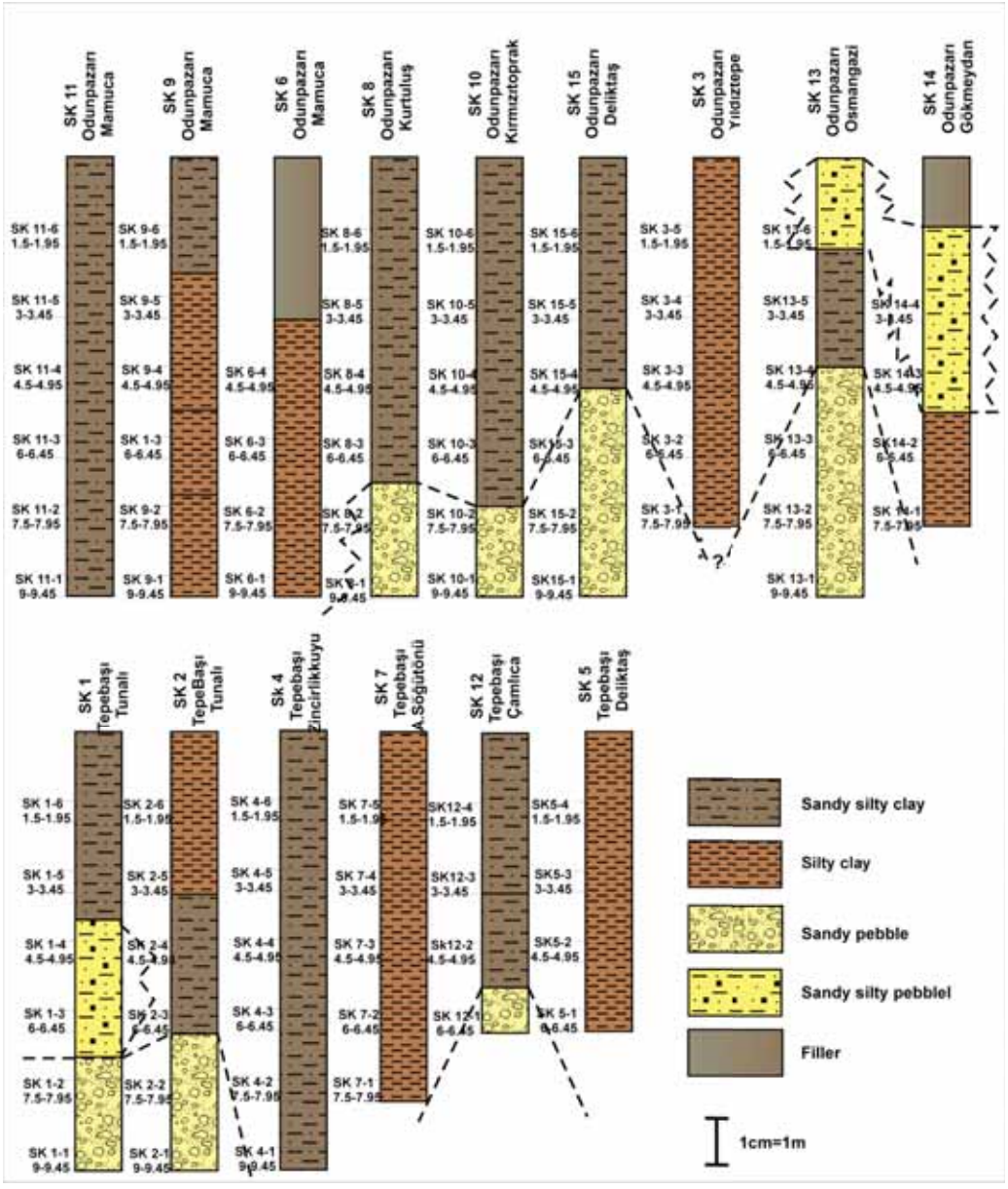

FIGURE 3
The lithology of drill holes in study area.

MATERIALS AND METHODS

Experimental studies were carried out in two stages: field and laboratory. Within the scope of field studies, drillings were opened in the field and samples were taken at certain levels. The 15 drillings were opened which approximately 10 m depth and separate location for obtaining the soil profile and sixty five disturbed core samples were collected from the field.

Standard tests were carried out to identify soil samples taken from the field. XRD analysis was performed using Rigaku Geigerflex model instrument. For the microstructure evaluation of the samples, SEM analyzes were performed using FESEM Zeiss Supra ™ 50 VP model equipment. Differential thermal-thermogravimetric (DTA-TG Rigaku TAS 100 E) and Infrared spectroscopic (IR) analyzes were performed in addition to XRD analysis for clay minerals.

Chemical analysis was performed on 18 silty-sandy-clayey whole-rock samples to determine the major and trace elements using inductively coupled plasma atomic emission spectroscopy (ICP-AES) and inductively coupled plasma mass spectrometry (ICP-MS).

RESULTS

Mineralogy. The clay-abundant drillhole samples consist of mostly smectite and decreasing chlorite, illite/mica and palygorskite, respectively in study area (Table 1; Figure 4). The non-clay minerals composed of calcite, dolomite, feldspar, quartz and amphibole. The concentration of smectite (10-65 %) exhibits differences to regions in silty clay and sandy- silty clayey soils of Eskişehir.

The sharp peaks at 14.07-16.54 Å, that swelling to 16.72-18.81 Å following ethylene-glycolation; the collapsed to 9.89-10.08 Å following heating at 550ºC demonstrate smectite (Figure 4). Chlorite was determined by a peaks at 13.91-14.2 Å, 7.07-7.11 Å, 3.53 Å, an absence of swelling ethylene-glycolation and palygorskite given at 10.51 Å. Illite/mica was demonstrated by characteristic peaks at 9.95-10.05 and 5.08 Å.

TABLE 1
Mineral composition of the samples from drillholes of Eskişehir

	Sme	Chl	Ill/Mca	Plg	Cal	Dol	Fsp	Qz	Amp
SK1-4	++	+	+		acc	acc	acc	+	acc
SK1-5	++	+	acc		acc	acc	acc	+	acc
SK2-6	++	+	+		+	acc	acc	+	acc
SK3-4	+++	acc	+		+		+	+	acc
SK4-2	+++	acc	acc		acc		acc	+	acc
SK4-4	+++	acc	acc		+		acc	+	acc
SK4-5	++	acc	+	+	+		acc	+	acc
SK6-1	+++	+	+		acc		+	+	
SK7-1	+	acc	+	acc	+	acc	acc	+	
SK7-2	++	+	acc	acc	+	acc	acc	+	
SK8-3	++++	+	acc		acc	acc	acc	+	acc
SK8-6	++++	+	+		acc	acc	acc	+	acc
SK9-3	++++					+	+	acc	
SK9-4	acc	acc			+	+++		acc	
SK9-8	+	acc	acc	acc	++	+	acc	+	
SK10-3	+++	+	acc	acc	+	acc	acc	+	acc
SK10-5	++	+	acc	+	acc	acc	acc	+	acc
SK11-1	+	acc	+	+	+		acc	+	acc
SK11-3	++		+	+	+		acc	+	
SK11-5	++	acc		+	+		acc	+	acc
SK12-1	+	acc	+	+	+		acc	+	
SK12-4	+	+	+	acc	+		acc	++	
SK13-5	++	+	acc	acc	+	acc	acc	+	acc
SK13-6	++	+	acc		acc	acc	+	+	acc
SK14-3	+	acc	+	+	+	+	acc	+	acc
SK15-4	++	+	+		acc	acc	+	+	acc

Sme: smectite, Chl: chlorite, Ilt/Mca: illite/mica, Plg: palygorskite, Cal: calcite, Dol: dolomite, Fsp: feldspar, Qz: quartz, acc: accessory, +: relative abundance of mineral (mineral name abbreviations after [42])

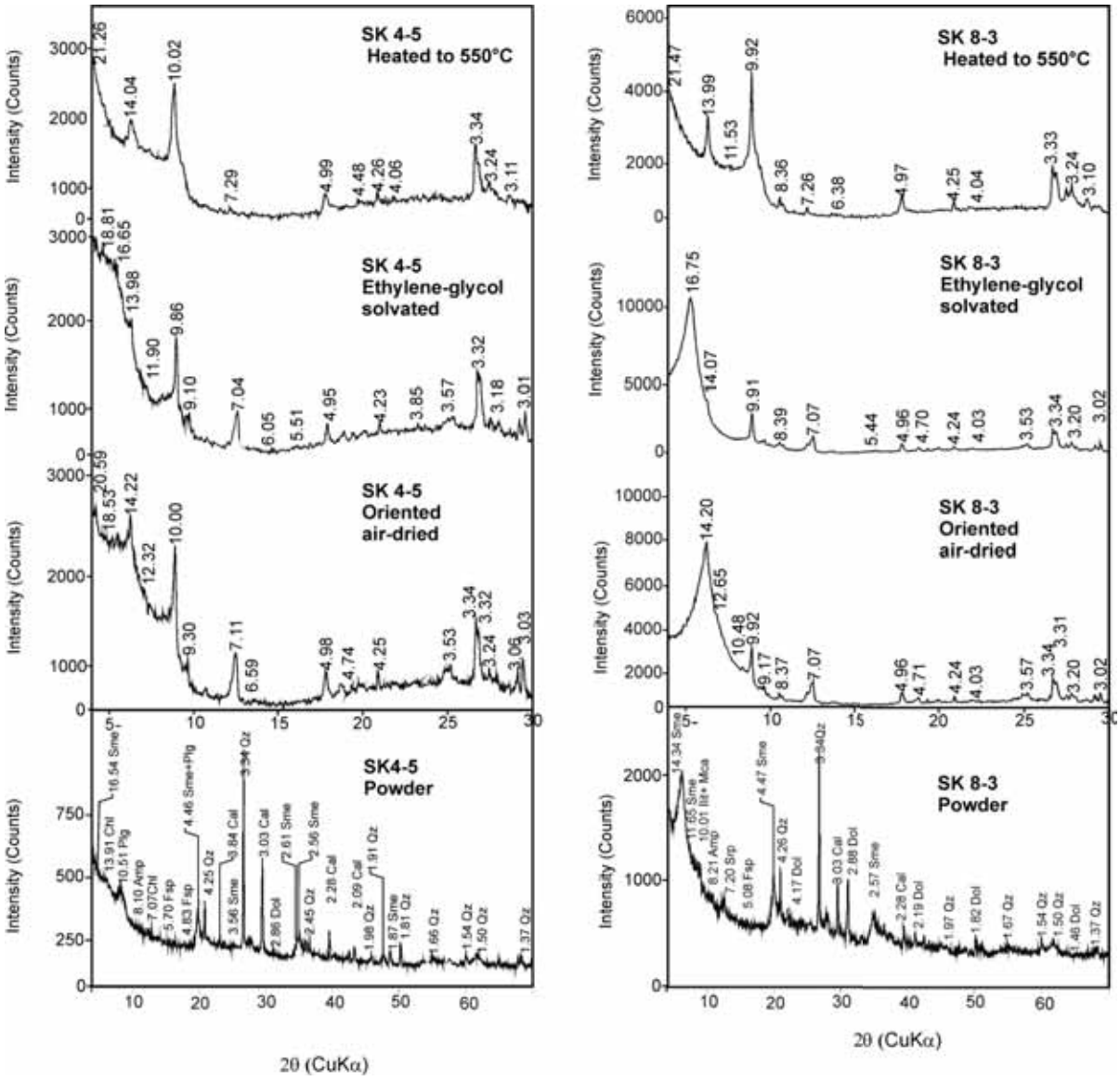

FIGURE 4
X-ray diffraction patterns for argillaceous samples.

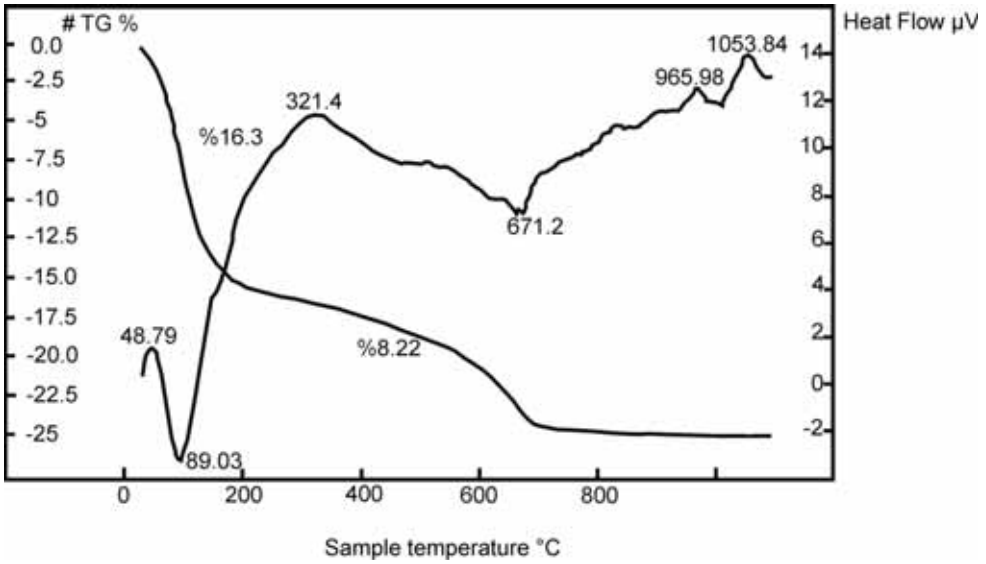

FIGURE 5
DTA-TG curves for the smectite sample (SK 9-3) from the drill holes.

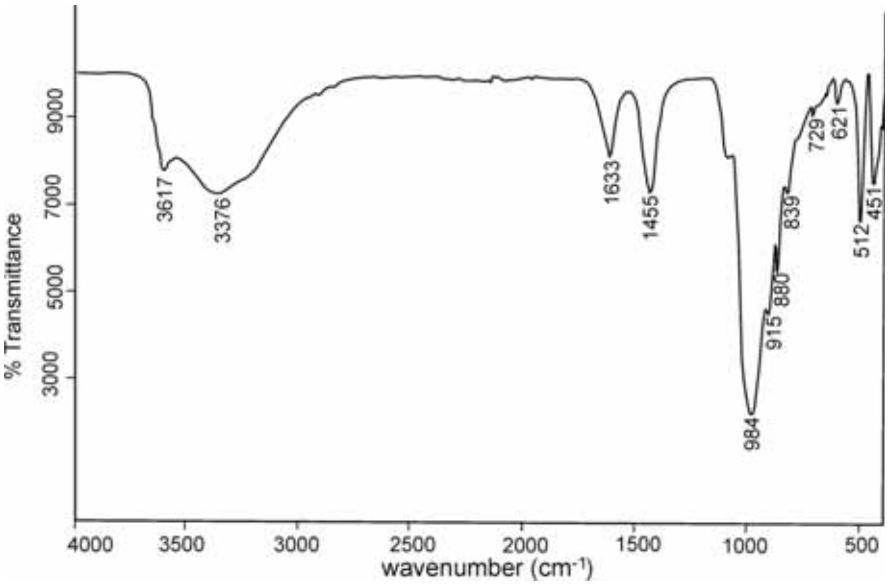

FIGURE 6
IR spectra for the for the smectite sample (SK 9-3) from the drill holes.

DTA-TG curves for the Eskişehir smectite (SK 9-3) exhibit that the endothermic peak at 89°C (total weight loss= 16.3%) match to smectite and show loss of absorbed moisture and interlayer free water (Figure 5; [17-18]). At about 671°C endothermic peak (total weight loss= 8.22%) exhibit dehydroxylation and occurrence of an amorphous meta-montmorillonite phase. The exothermic peak system between 965 and 1053°C solid phase showed that structural decomposition and crystallization of cordierite, mullite, Mg-spinel, quartz, cristobalite [18].

Smectite shows a narrow band at and 3617 cm^{-1} and a broad band at 3376 cm^{-1} identified as AlOHMg-stretching vibration and hygroscopic H_2O, respectively (Figure 6; [19-21]. In addition, the bending vibration of H_2O molecules occurs at 1633 cm^{-1} [19-20]. The bands at 915 cm^{-1} correspond to an (Al-Al-OH) bending vibration and 839 cm^{-1} to (Mg-OH-Al) due to partial substitution of octahedral Al by Mg [22-23]. The peaks at 512 and 451 cm^{-1} are typical in montmorillonite [22].

The SEM images indicate that smectite dominated in the Pliocene mudstones of Eskişehir. The smectite flakes had irregular outlines and such as cornflake and rose-like textures suggest detritic origin (Figure 7a, b; [24-25]). The smectite flakes were found between grains or coatings around relict feldspar and volcanic glass exhibit smectite occurred from feldspar and volcanic glass (Figure 7 c, d). Smectite occurred as porous associated with calcite (Figure 7e). Smectite flakes yielded Si, Al, Mg and less amount of Ca, indication montmorillonitic smectite (Figure 7f).

Chemical Composition. The chemical composition of cohesive soils (drill holes samples) include major oxides (CaO, Fe_2O_3, MgO, Al_2O_3, SiO_2, Na_2O, K_2O) and trace elements are presented in Table 2. The enrichment of smectite (SK 11-3, SK 9-3, SK 6-1, SK 8-3, SK 8-6, SK 3-4, SK 2-6, SK 4-2) in drill holes demonstrated that SiO_2 48.66-61.93 wt%, Al_2O_3 12.07-15.00 wt%, Fe_2O_3 1.5-6.95 wt%, MgO 1.73-6.76 wt% and K_2O 1.08-2.94 wt% values and suquare with XRD results. The high CaO (11.73-27.76 wt %) rather than other regions exhibit carbonaceous lithologies and the presence of calcite suggest that XRD datas.

Effect of Mineralogic and Chemical Composition on Geotechnical Properties. The chemical and mineralogical composition of clay soils has a great influence on physical and mechanical properties of cohesive soils [4]. Fine grained soils differ according to grain size distribution, types and amounts of various clay minerals and chemical composition. [8] stated that the chemical composition of the soil and water is highly effective on the swell potential and geotechnical properties of the soil. The Eskişehir cohesive soils, which are rich in clay fraction, smectite (montmorillonite) and lesser illite contents are very problematic according to engineering objects foundations, because they have low geotechnical properties and high compressibility. This is a similar senario to that reported for cohesive soils from Albania-Tirana [4].

Table 3 presents a summary of the geotechnical properties of the samples. The grain-size distributions are presented in Figure 8. On the basis of Unified Soil Classification System (USCS) soils are defined. The locations of the samples on the plasticity chart are shown in Figure9. The fine content of the soil (namely silt and clay) is between 52% and 94% and clay fraction percentages are between 16% and 37%. For the soil samples, the liquid limit (LL), plastic limit (PL) and plasticity index (PI) were in the range of 22-70%, 15-44% and 7-32%, respectively.

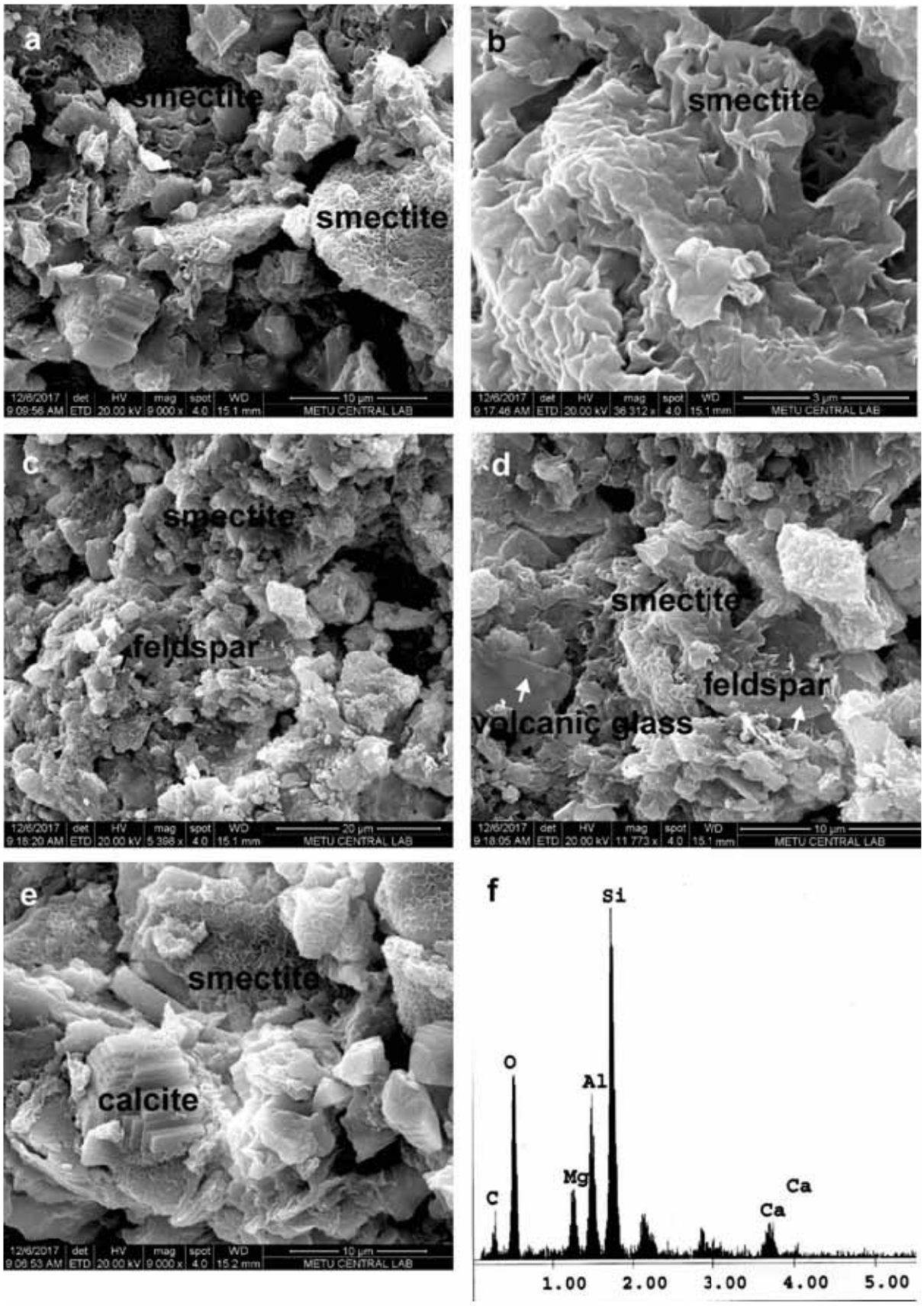

FIGURE 7

SEM images of a) smectite flakes enclosing calcite crystal, b) close-up view of smectite flake, c-d) smectite flakes associated with resorbed feldspar and devitrified volcanic glass, e) calcite crystal developed on the smectite flakes, f) EDS analysis of smectite samples.

TABLE 2
Major- (wt.%) and trace-element (ppm) compositions of drillholes samples in different regions from the study area (see Table 1 for the mineralogical compositions of the samples)

	Odunpazarı – Mamuca					Odunpazarı Kurtuluş		Odunpazarı KırmızıToprak		Odunpazarı Yıldıztepe
Major oxides (wt.%)	**SK 11-1**	**SK 11-3**	**SK 9-3**	**SK 9-8**	**SK 6-1**	**SK 8-3**	**SK 8-6**	**SK 10-3**	**SK 10-5**	**SK 3-4**
SiO_2	47.82	51.42	48.89	22.19	61.93	48.66	49.74	48.83	50.80	56.20
Al_2O_3	11.18	12.31	14.31	5.13	15.00	12.73	13.20	10.92	11.58	12.76
Fe_2O_3	5.01	5.49	1.50	2.27	4.62	6.95	6.81	5.93	6.36	3.54
MgO	3.04	3.45	6.76	7.46	1.89	6.73	6.05	7.01	7.28	1.73
CaO	11.33	7.44	4.56	27.76	2.55	4.71	4.30	7.19	4.81	8.80
Na_2O	0.40	0.45	0.42	0.15	1.16	0.51	0.52	0.72	0.62	1.25
K_2O	1.67	1.74	1.08	0.69	2.94	1.62	1.78	1.67	1.78	2.42
TiO_2	0.56	0.63	0.08	0.26	0.39	0.54	0.56	0.52	0.53	0.32
P_2O_5	0.03	0.05	0.02	0.03	0.06	0.06	0.07	0.07	0.07	0.06
MnO	0.13	0.12	0.10	0.05	0.09	0.09	0.09	0.11	0.09	0.16
Cr_2O_3	0.057	0.057	0.005	0.020	0.008	0.072	0.063	0.099	0.101	0.003
TOT/S	<0.02	<0.02	<0.02	<0.02	<0.02	<0.02	<0.02	<0.02	<0.02	<0.02
TOT/C	2.48	1.57	1.84	8.61	0.31	1.57	1.56	2.05	1.37	1.85
LOI	18.6	16.7	22.1	33.8	9.1	17.0	16.5	16.6	15.7	12.5
Total	99.85	99.85	99.82	99.79	99.82	99.79	99.80	99.79	99.79	99.84
Trace Elements (ppm)										
Ba	289	257	107	152	741	303	339	348	321	681
Be	1	1	3	<1	<1	3	1	4	2	2
Co	23.7	23.2	4.8	11.7	10.4	44.5	38.0	36.7	38.4	8.2
Cs	20.2	22.0	13.1	12.2	3.9	35.8	37.3	28.4	33.7	2.2
Ga	11.1	12.7	12.1	4.2	13.2	12.6	12.9	10.8	11.4	10.5
Hf	4.2	4.1	5.1	1.7	4.0	3.3	3.4	3.5	3.7	2.9
Nb	13.2	14.5	26.0	5.9	8.1	13.7	14.8	12.9	13.2	6.3
Rb	109.4	116.1	40.4	47.3	108.9	112.4	124.9	105.0	120.9	83.9
Sn	2	2	10	1	2	2	3	2	2	1
Sr	174.4	180.4	205.8	405.3	408.3	137.8	137.5	180.6	157.3	468.7
Ta	0.8	1.1	4.7	0.5	0.7	1.1	1.3	0.9	1.0	0.6
Th	11.8	13.1	43.6	5.8	14.5	12.3	13.6	11.9	12.8	9.6
U	1.7	1.9	2.0	3.8	3.5	1.9	1.8	2.2	2.0	4.1
V	76	79	30	42	83	101	103	87	87	80
W	1.7	1.6	0.7	1.7	1.6	2.1	2.4	2.1	2.1	4.7
Zr	157.2	153.7	108.3	64.9	147.8	111.3	112.6	126.9	133.5	115.8
Y	20.5	19.8	6.2	9.1	13.1	19.1	20.6	19.8	19.9	13.5
La	29.6	30.6	9.0	13.6	31.8	27.1	28.7	25.4	27.6	31.3
Ce	55.3	64.9	35.3	27.5	79.9	50.5	54.2	48.7	51.9	57.2
Pr	6.47	6.22	2.15	2.98	6.26	5.68	6.02	5.29	5.74	5.94
Nd	23.7	22.9	7.4	11.2	21.5	20.9	21.1	20.0	20.7	21.4
Sm	4.53	4.19	1.78	2.09	3.63	4.05	4.00	3.72	4.07	3.55
Eu	0.98	0.96	0.16	0.48	0.96	0.81	0.86	0.85	0.85	0.92
Gd	4.23	4.01	1.56	1.98	2.99	3.98	3.89	3.60	3.96	2.92
Tb	0.64	0.61	0.25	0.30	0.41	0.58	0.62	0.57	0.59	0.40
Dy	3.71	3.61	1.48	1.70	2.43	3.42	3.51	3.55	3.68	2.32
Ho	0.74	0.72	0.26	0.36	0.48	0.73	0.76	0.69	0.70	0.47
Er	2.14	2.13	0.77	1.01	1.41	2.02	2.18	2.08	2.05	1.36
Tm	0.29	0.31	0.11	1.14	0.22	0.30	0.30	0.29	0.28	0.19
Yb	1.89	1.93	0.86	0.89	1.51	1.90	2.03	1.89	1.86	1.41
Lu	0.31	0.30	0.13	0.13	0.25	0.31	0.30	0.30	0.29	0.20
Pb	21.1	21.4	38.1	9.2	68.5	24.2	24.8	20.4	23.6	37.6
Zn	45	49	24	25	166	58	62	49	58	83
Ni	217.7	197.0	129.5	81.9	28.0	522.4	471.7	451.3	532.8	16.2
Au (ppb)	1.8	<0.5	<0.5	2.1	1.6	18.7	8.6	2.5	1.9	6.1
Ag	<0.1	<0.1	<0.1	<0.1	<0.1	0.2	<0.1	<0.1	<0.1	<0.1
Mo	0.2	0.2	<0.1	0.4	2.2	0.2	0.2	0.4	0.2	1.8
Cu	26.1	27.3	34.1	14.1	116.2	36.6	36.3	28.6	31.2	68.0
As	8.3	7.0	0.8	4.9	5.0	21.1	18.0	14.4	12.4	4.3
Cd	0.2	0.1	<0.1	0.2	0.2	0.2	0.1	0.1	0.1	0.6
Sb	0.2	0.1	0.3	0.5	0.2	0.8	0.8	0.6	0.6	0.1
Bi	0.3	0.3	1.3	0.1	0.8	0.3	0.4	0.3	0.4	0.6
Hg	0.02	<0.01	<0.01	0.01	0.01	0.10	0.09	0.06	0.02	<0.01
Tl	0.5	0.4	0.7	0.2	0.3	0.8	0.8	0.6	0.6	0.2
Se	<0.5	<0.5	<0.5	<0.5	<0.5	<0.5	<0.5	<0.5	<0.5	<0.5

TABLE 2 (continued)

Odunpazarı-Osmangazi		Gökmeydan	Tepebaşı-Tunalı			Tepebaşı-Zincirlikkuyu		Tepebaşı-Çamlıca
Major oxides (wt.%)	**SK 13-6**	**SK 14-3**	**SK 1-4**	**SK 1-5**	**SK 2-6**	**SK 4-2**	**SK 4-4**	**SK 12-1**
SiO_2	51.07	34.24	52.32	50.07	49.26	60.15	47.55	62.11
Al_2O_3	9.89	6.05	10.87	10.53	12.07	12.69	11.28	6.04
Fe_2O_3	6.50	2.77	5.26	5.79	6.34	4.57	4.59	3.46
MgO	6.44	7.88	6.09	6.79	6.39	3.23	3.34	3.97
CaO	7.41	19.46	7.18	7.67	6.78	4.04	11.73	7.98
Na_2O	1.21	0.43	1.11	0.90	0.69	1.04	0.53	0.24
K_2O	1.86	1.06	1.75	1.59	1.79	2.08	1.70	1.06
TiO_2	0.43	0.33	0.51	0.53	0.57	0.50	0.49	0.27
P_2O_5	0.15	0.06	0.08	0.08	0.07	0.06	0.05	0.03
MnO	0.11	0.18	0.10	0.14	0.15	0.08	0.09	0.32
Cr_2O_3	0.172	0.089	0.115	0.097	0.079	0.115	0.076	0.016
TOT/S	0.07	<0.02	0.02	0.02	<0.02	<0.02	<0.02	<0.02
TOT/C	3.15	6.22	2.04	2.35	1.92	0.85	2.72	1.90
LOI	14.3	27.1	14.3	15.5	15.5	11.2	18.3	14.2
Total	99.64	99.73	99.81	99.80	99.80	99.84	99.86	99.90
Trace Elements (ppm)								
Ba	398	360	361	355	407	527	403	198
Be	3	<1	2	2	4	2	<1	<1
Co	31.4	17.2	29.2	41.1	41.4	26.4	23.8	18.1
Cs	17.9	13.8	21.5	23.9	28.1	23.1	26.2	15.8
Ga	9.1	5.2	9.8	9.9	12.2	12.0	10.5	5.8
Hf	3.3	3.7	4.0	3.3	3.5	5.3	4.0	2.0
Nb	11.6	8.0	12.6	12.1	13.9	17.2	16.3	8.2
Rb	91.6	67.7	94.1	87.4	105.1	113.1	109.3	69.5
Sn	745	2	2	2	2	3	2	1
Sr	189.9	698.0	171.8	164.3	165.2	193.7	170.4	64.6
Ta	1.0	0.6	1.1	1.0	1.1	1.6	1.3	0.7
Th	10.8	7.6	11.1	10.3	12.8	17.8	14.0	8.5
U	7.4	4.4	2.8	2.4	2.3	3.1	2.3	1.2
V	91	55	88	90	99	63	63	46
W	2.2	1.4	2.3	2.3	2.2	2.1	2.0	1.8
Zr	115.0	139.0	146.4	125.5	125.3	195.8	140.0	73.9
Y	17.7	14.3	20.8	19.5	21.1	19.6	18.8	8.1
La	23.7	21.8	25.9	24.8	28.4	35.9	29.2	18.6
Ce	42.5	39.0	47.9	47.6	54.4	61.8	56.4	40.7
Pr	4.78	4.48	5.42	5.24	5.98	6.82	5.90	3.34
Nd	17.3	16.6	19.7	18.8	22.5	24.1	21.3	11.3
Sm	3.28	3.05	3.86	3.79	3.96	4.33	3.93	1.71
Eu	0.72	0.64	0.84	0.82	0.89	0.89	0.80	0.35
Gd	3.26	2.81	3.86	3.77	4.07	4.03	3.69	1.56
Tb	0.52	0.41	0.60	0.58	0.16	0.60	0.57	0.23
Dy	3.05	2.60	3.57	3.41	3.98	3.61	3.40	1.34
Ho	0.61	0.52	0.75	0.70	0.72	0.67	0.69	0.29
Er	1.81	1.49	2.15	2.02	2.07	1.95	1.89	0.84
Tm	0.26	0.22	0.30	0.29	0.31	0.29	0.28	0.13
Yb	1.71	1.39	1.98	1.90	2.04	2.01	1.87	0.81
Lu	0.27	0.23	0.29	0.28	0.31	0.31	0.28	0.13
Pb	671.0	12.0	16.6	17.6	22.4	23.5	23.5	11.7
Zn	55	29	42	48	58	42	43	30
Ni	357.1	185.9	291.7	467.5	457.5	316.5	294.3	575.1
Au (ppb)	3.0	1.0	1.21	1.4	2.1	<0.5	0.7	3.4
Ag	<0.1	<0.1	<0.1	<0.1	<0.1	<0.1	<0.1	<0.1
Mo	1.7	0.2	0.3	0.4	0.4	0.2	0.2	0.8
Cu	42.3	17.2	28.5	30.0	31.8	18.5	26.0	16.3
As	25.2	9.4	10.2	11.4	22.9	5.5	8.3	6.8
Cd	0.2	<0.1	0.1	0.2	0.2	0.1	0.1	0.2
Sb	1.1	0.4	0.7	0.6	1.0	0.7	0.4	0.4
Bi	0.7	0.2	0.2	0.2	0.3	0.6	0.5	0.2
Hg	0.08	0.03	0.09	0.09	0.10	0.03	0.02	0.04
Tl	0.3	0.4	0.4	0.5	0.6	0.4	0.5	0.5
Se	<0.5	<0.5	<0.5	<0.5	<0.5	<0.5	<0.5	<0.5

Consistency limits are widely used for the identification and classification of cohesive soils as well as for the evaluation of mechanical properties. Both the type and amount of clay effect a soil's properties, and the Consistency limits represent both of these factors. The changes of plastic limit values are associated with the chemical and mineralogical composition. Montmorillonite and illite are known to have higher plastic limits, whereas kaolinite generally has lower values [9]. In this study, it was determined that the liquid limit and plastic limit values of the soils

containing montmorillonite and illite clay minerals were higher than the non-clay mineral (e.g. quartz, calcite and feldspar) samples similiar to reported by [26]. In addition, the medium-high liquid limit (22-70%) and low-medium plasticity (7-32%) indicate high compressibility [27]. The high plasticity index (26-32%) is related to the highest percentage of clay (24-38%), specially smectite content and exchangeable magnesium and potassium in the study area is similar reported by [28].

The percent of smectite increase with increased LL (r^2=0.44), PL (r^2=0.43), PI (r^2=0.37) and clay activity (A) (r^2=0.40) in the study area (Figure 10). As seen Figure 11, the percent of chlorite and illite exhibit negative correlation with LL (r^2=0.06, 0.06), PL (r^2=0.06, 0.04), PI (r^2=0.05, 0.06), A (r^2=0.002, 0.16). The lithologies of drill holes in Eskişehir region were changed based on depths that smectite was most abundant swelling clays at near of the surface in silty clay units, illite and chlorite were found at the middle of the depths similar to Kanada-Qubec marine sediments [29]. Furthermore, swelling clays were increased at the surface, shows that alteration is dominant with degradation [29]. Micromorphologically, the relationship between compact smectite flakes and altered feldspar and devitrified volcanic glass shard exhibit volcanogenic origin and dissolution of volcanic materials in mudstone by chemical weathering during early diagenesis with close hydrologic system in lacustrine environment under alkaline conditions [30-32] and resulted in increased concentration of Al_2O_3, Fe_2O_3 and MgO and precipitation of smectite [25]. The sharp XRD patterns, ideal DTA-TG and FT-IR peaks and chemical composition show montmorillonitic smectite in drill holes.

TABLE 3
Geotechnical properties of the soil samples used in the study

Sample Number	Gravel (%)	Sand (%)	Silt (%)	Clay (%)	LL (%)	PL (%)	PI (%)	Activity, A	Classification (USCS)
SK.1-4	6.0	24.0	48.0	22.0	49.0	30.0	19.0	0.86	ML
SK.1-5	4.0	43.0	35.0	18.0	53.0	31.0	22.0	1.22	MH
SK.2-4	9.0	32.0	42.0	17.0	46.0	25.0	21.0	1.24	CL
SK.3-4	7.0	27.5	39.5	26.0	57.0	33.0	24.0	0.92	MH
SK.4-2	0.0	31.0	53.0	16.0	70.0	44.0	26.0	1.63	MH
SK.4-4	0.0	14.0	61.0	25.0	45.0	24.0	21.0	0.84	CL
SK.8-3	0.0	30.0	38.0	32.0	68.0	36.0	32.0	1.00	MH
SK.9-8	0.0	21.0	60.0	19.0	22.0	15.0	7.0	0.37	CL
SK.10-5	0.0	48.0	24.0	28.0	63.0	32.0	31.0	1.11	CH
SK.11-1	0.0	6.0	70.0	24.0	42.0	26.0	16.0	0.67	CL
SK.11-3	0.0	13.0	50.0	37.0	55.0	29.0	26.0	0.70	CH
SK.12-1	7.0	30.0	28.0	35.0	59.0	32.0	27.0	0.77	CH
SK.13-6	8.0	22.0	47.0	23.0	50.0	27.0	23.0	1.00	CH
SK.14-3	0.0	31.0	46.0	23.0	30.0	20.0	10.0	0.43	CL

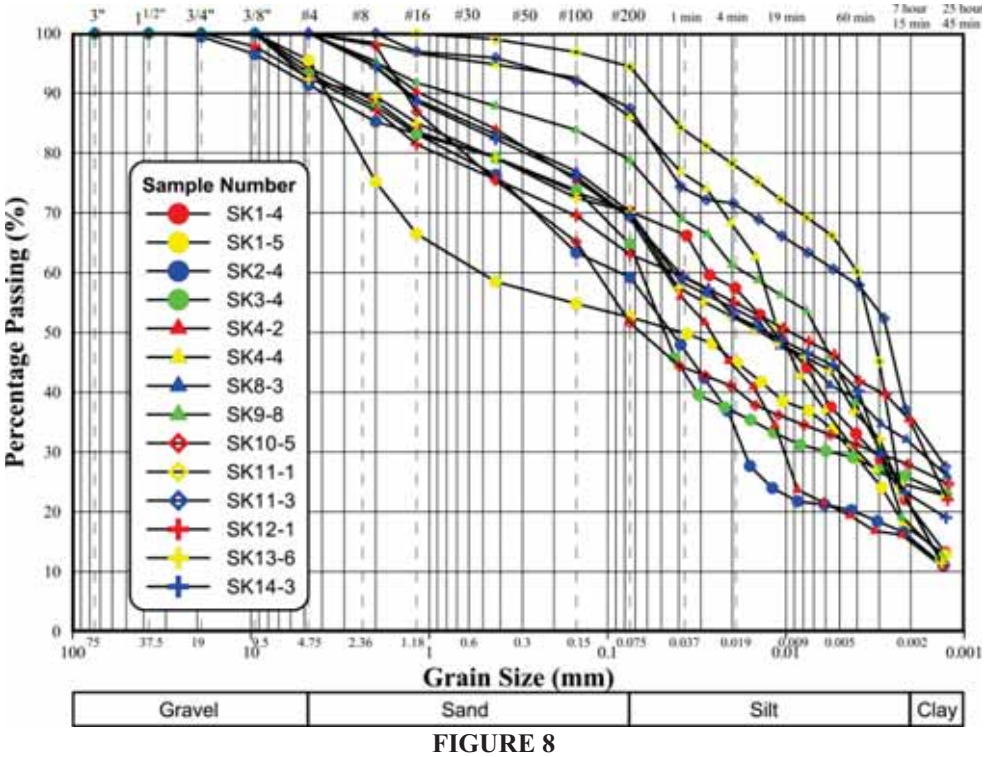

FIGURE 8
Grain-size distributions of the soil samples.

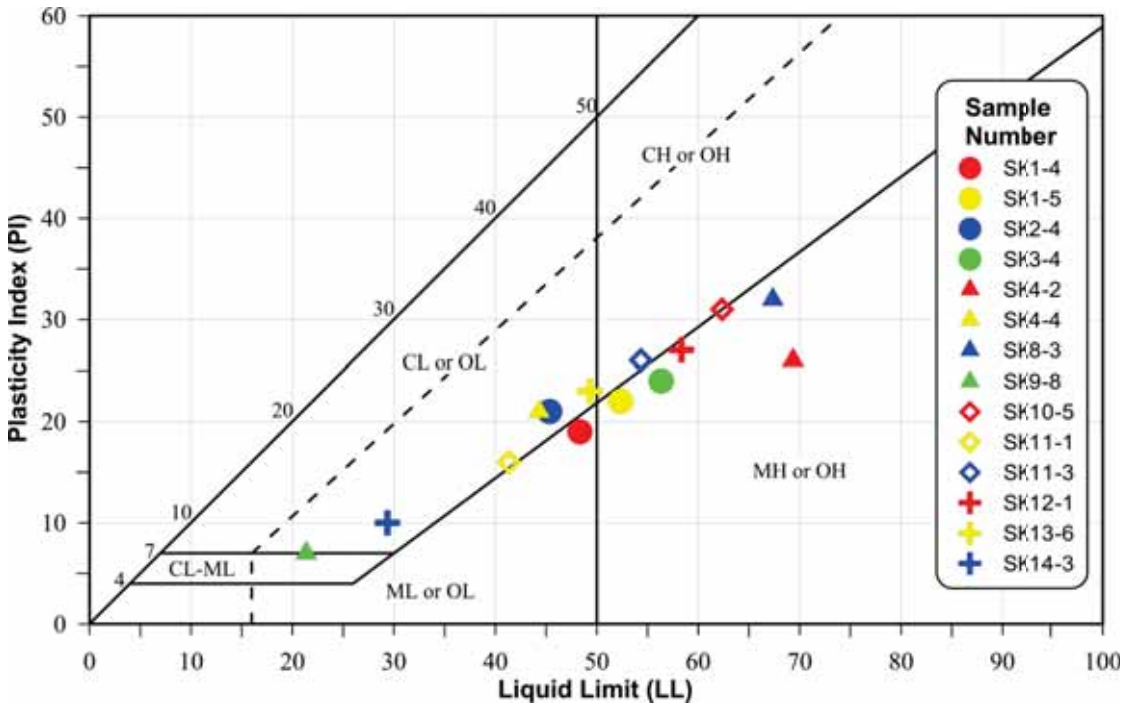

FIGURE 9
Samples on plasticity chart.

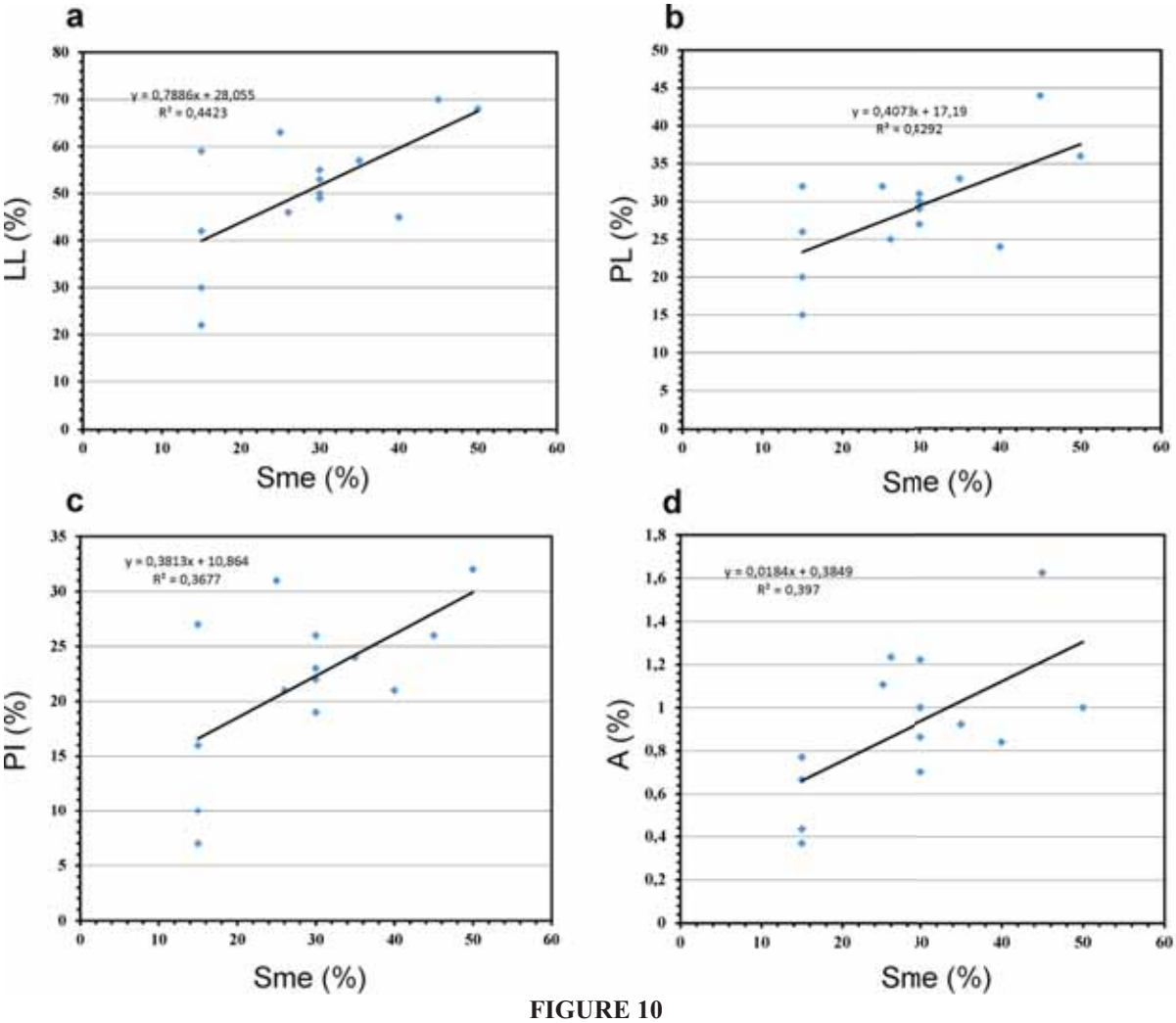

FIGURE 10
Associated between smectite and geotechnical properties. Sme: Smektit.

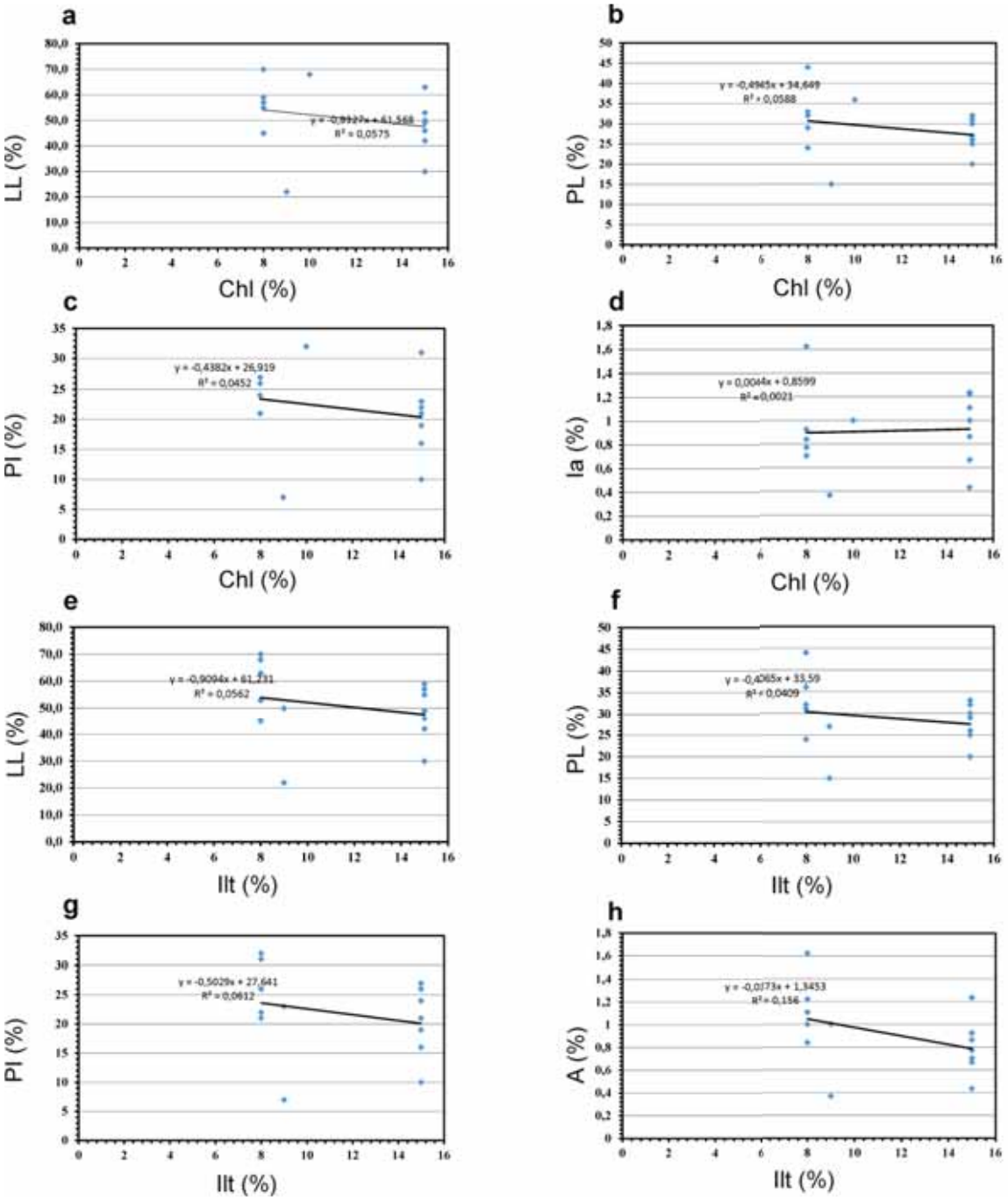

FIGURE 11
Associated between chlorite, illite and geotechnical properties. Chl: chlorite, Ilt: illite.

Information on the dominant clay type in the soil can be obtained from the activity value of the soil sample. A soil sample with a high activity value can be considered as a high swelling potential. Activity (A) of the samples used ranges from 0.37- 1.63 (SK9-8, SK4-2). As stated by [33] samples including SK9-8, SK11-1, SK11-3 and SK14-3 is considered as inactive (A < 0.75), as normally active (A = 0.75–1.25), for samples SK1-4, SK1-5, SK2-4, SK3-4, SK4-4, SK8-3, SK10-5, SK12-1 and SK13-6, and as active clays (A > 1.25) for sample SK4-2 (Table 3).

The data obtained from soil identification tests are also widely used to evaluate the swell potential of soils as a priority. According to the classification chart (Figure12) by [34] for the swell potential, it is seen that the samples have low (SK9-8 and SK14-3), medium and high expansion (SK8-3, SK10-5, SK11-3, SK12-1) potential. When the assessment is made according to the chart recommended by [35], samples have low and medium potential of swelling (Figure 13). Also, the swell potential chart developed by [36] demonstrated that two of the samples have low, four have medium, seven have high and one have very high swell potential (Figure 14).

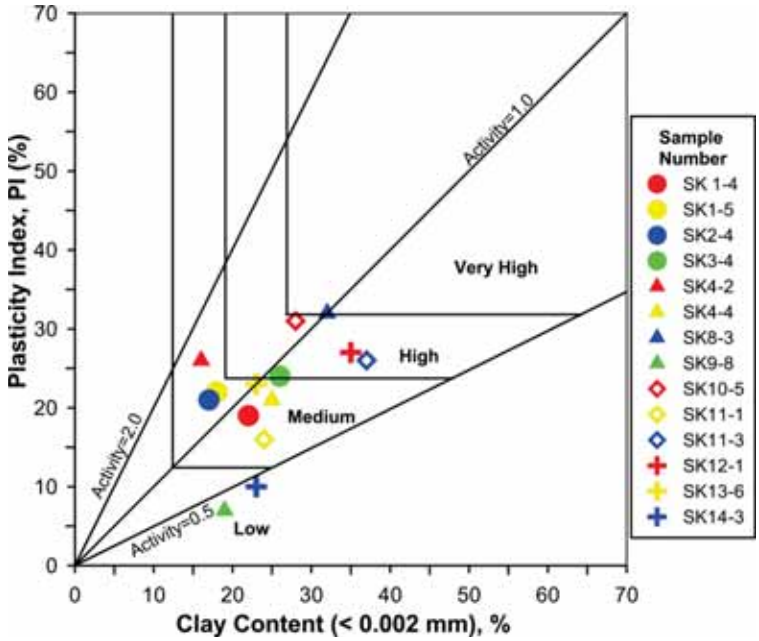

FIGURE 12
Classification chart, proposed by [34], used to estimate the swelling potential of soils.

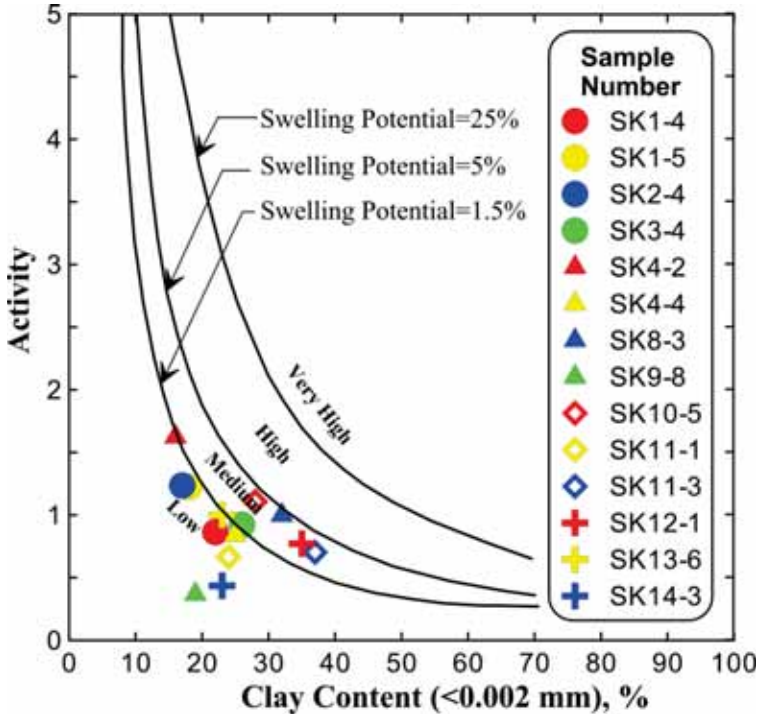

FIGURE 13
Swell potential chart developed by [35].

When the plasticity indices of the soil samples were taken into consideration, it could be determined that soils have low-high swelling potentials stated by [37]. The clays activity values "A" of the studied soils are generally normal but, some locations, the soils are characterized by high clay activity values, this means that the montmorillonite and illite clay minerals predominate in the Eskişehir clay soils. The swelling properties of sand+silt sample are reduced (<1.5%) by rising the non-clay minerals (quartz etc.) similar to that of marine clay in Egypt [3]. Damages in structures built on swelling soils have led researchers to work on the identification and classification of these soils. However, chemical properties of the soils were not taken into consideration in these studies which were established for the purpose of defining and classifying swelling soils. In many studies evaluating the swelling potential of clay soils [34, 38] activity variable was evaluated depending on the plasticity index. However, the charts suggested by [34, 38] used for evaluating of the swelling potential of soils were

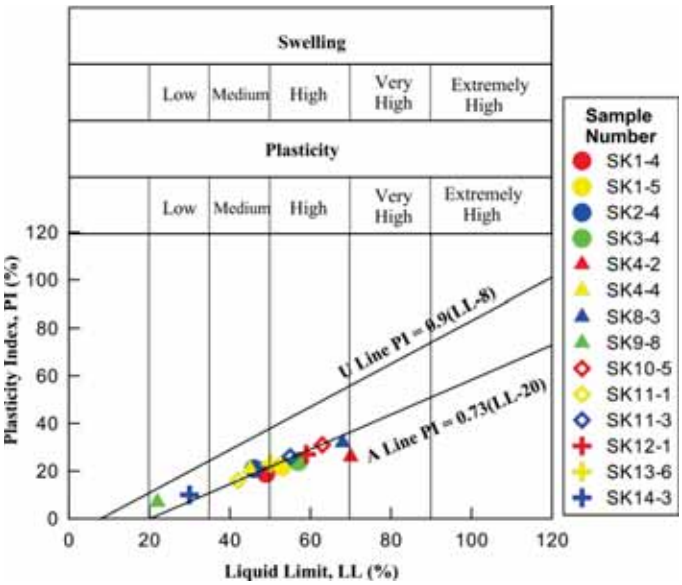

FIGURE 14
Swell potential chart developed by [36].

TABLE 4
Statistical summary of the major oxides of the samples

Major oxides (wt.%)	Value			
	Minimum	Maximum	Average	Std. Deviation
SiO_2	22.190	62.110	49.625	9.051
Al_2O_3	5.130	15.000	11.030	2.678
Fe_2O_3	1.500	6.950	4.876	1.566
MgO	1.730	7.880	5.307	1.987
CaO	2.550	27.760	8.650	5.941
Na_2O	0.150	1.250	0.686	0.335
K_2O	0.690	2.940	1.682	0.499
TiO_2	0.080	0.630	0.446	0.138
P_2O_5	0.020	0.150	0.061	0.028
MnO	0.050	0.320	0.122	0.057
Cr_2O_3	0.003	0.172	0.069	0.045

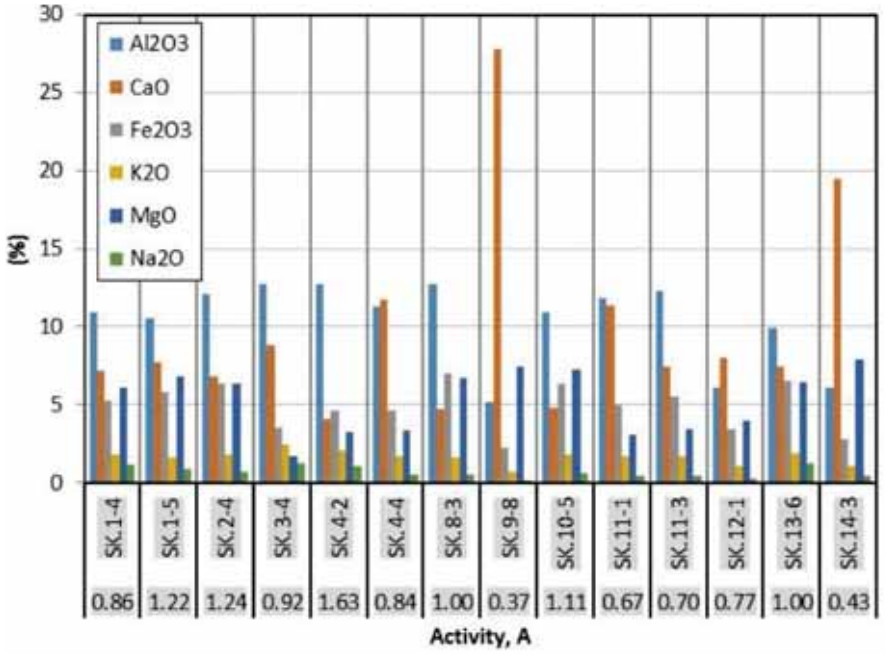

FIGURE 15
Relationship between Activity (A) and Major oxides.

TABLE 5
Correlation matrix for the properties of the samples

	Gravel	Sand	Fine	Silt	Clay	LL	PL	PI	A	Al_2O_3	CaO	Fe_2O_3	K_2O	MgO	Na_2O	SiO_2
Gravel	1															
Sand	.171	1														
Fine	-.450	-.957	1													
Silt	-.368	-.837	.867	1												
Clay	-.137	-.185	.208	-.307	1											
LL	.087	.368	-.359	-.518	.331	1										
PL	.050	.339	-.322	-.382	.135	.948	1									
PI	.114	.359	-.359	-.599	.490	.949	.798	1								
A	.234	.486	-.509	-.323	-.339	.745	.782	.632	1							
Al_2O_3	.015	-.069	.058	.050	.013	.634	.608	.594	.633	1						
CaO	-.292	-.288	.347	.453	-.226	-.902	-.828	-.883	-.772	-.738	1					
Fe_2O_3	.158	.204	-.232	-.271	.089	.560	.407	.654	.573	.670	-.753	1				
K_2O	.259	.036	-.109	-.074	-.063	.627	.632	.557	.658	.885	-.727	.496	1			
MgO	-.037	.501	-.443	-.300	-.258	-.340	-.393	-.253	-.145	-.459	.295	.165	-.533	1		
Na_2O	.504	.218	-.346	-.150	-.368	.401	.485	.277	.601	.526	-.518	.339	.786	-.179	1	
SiO_2	.399	.159	-.262	-.397	.279	.846	.824	.781	.659	.558	-.893	.414	.666	-.569	.487	1

LL = liquid limit (%), PL = plastic limit (%), PI = plasticity index (%), Silt (%), Clay (%), A = activity

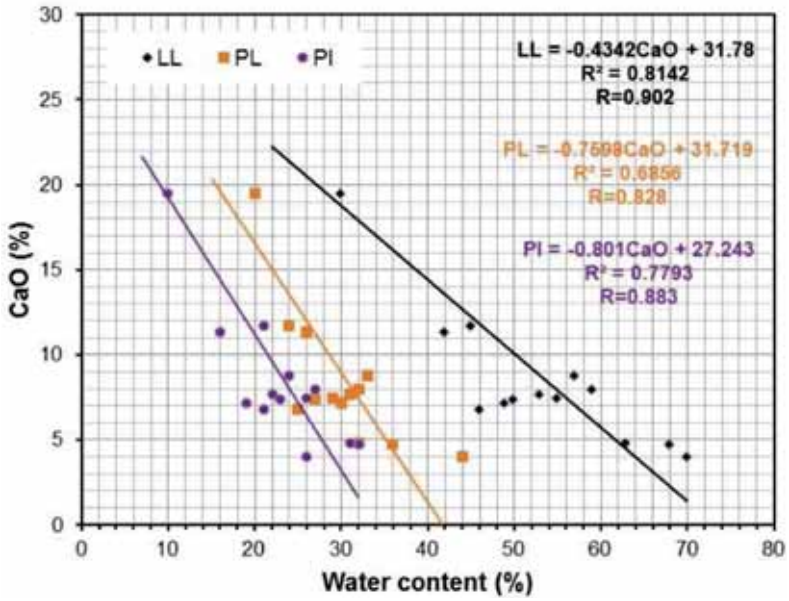

FIGURE 16
Relationship between Atterberg Limits and CaO.

different. The smectitic soil samples have more swelling due to in a sample having exchangeable Na^+ cation than in a sample with Ca^{2+} or Mg^{2+} cations and leaching of a salt from the clay pore fluid [8, 39].

The statistical evaluation of the major oxides of the 18 samples is shown in Table 4. It is seen that this table has high average values of SiO_2 (49.625%), Al_2O_3 (11.030%), CaO (8.65%), MgO (5.307%) and Fe_2O_3 (4.876%) respectively.

Figure 15 presents the relationship between activity and major oxides. Compared with other clay soil samples, it is seen that SK.9-8 and SK.14-3 samples having the highest CaO percentage have the lowest activity values. Therefore, it can be said that the CaO content of the sample on the activity value is more important than the other oxides.

The correlation matrix showing the level of the relationship between geotechnical and chemical properties of soil samples is given in Table 5. CaO content in the clay soils plays an important role and improves in geotechnical properties. The increment of CaO in soils is accompanied by a reduction in the LL, PL and PI in Table 5 and Figure16. SiO_2 and Al_2O_3 contents are much related to sand, silt and clay contents. Consequently therefore, it shows a positive correlation with LL (r^2=0.72 and 0.40), PL (r^2=0.68 and 0.37) and PI (r^2=0.61and 0.35) as shown in Figure17. CaO and Al_2O_3 variables have a positive and negative correlation on the activity of clay soil. In other words, the activity of the soil has decreased with the increasing percentage of CaO, whereas the activity value has increased with the increasing percentage of Al_2O_3. This situation has a similar effect on the liquid

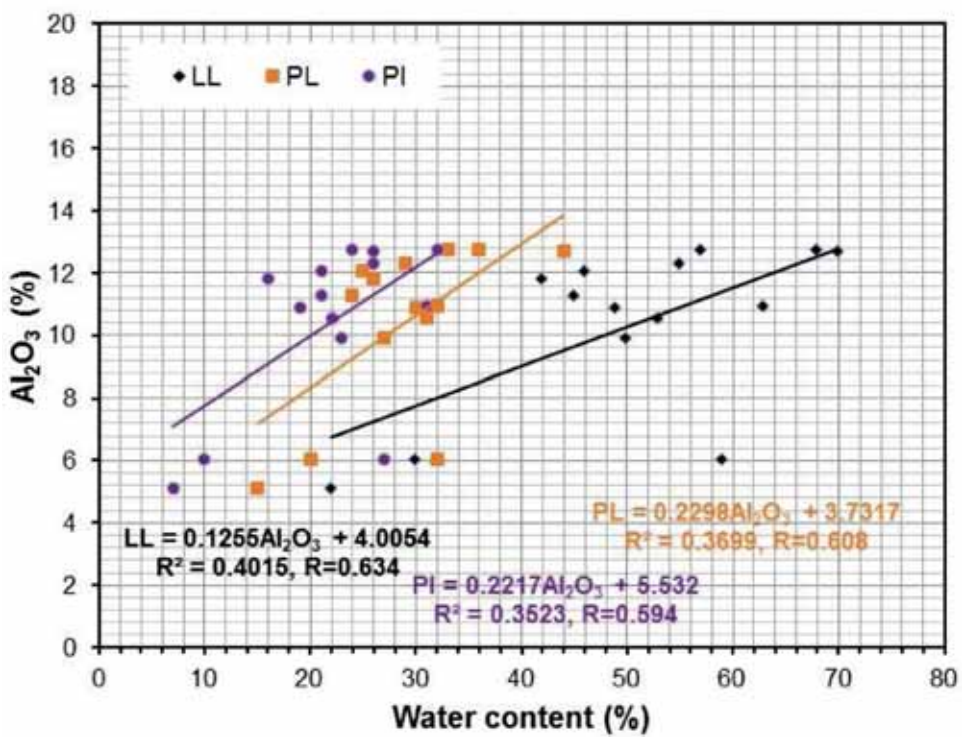

FIGURE 17
Relationship between Atterberg Limits and Al_2O_3.

limit, plastic limit and plasticity index values of the soils. SiO_2 is mainly from quartz in sand and silt fractions, and Al_2O_3 is from clay fraction and partly from feldspar minerals [3]. For this reason, LL, PL and PI values with SiO_2 and Al_2O_3 content have a positive relationship and similar situation has been observed in marine clays in Egypt [3]. The increase of Fe_2O_3, Na_2O and K_2O amounts give rise to increasing LL and clay's activity in Eskişehir soils similar to Tirana-Vora soils of Albania [4].

CONCLUSION

In this study, geotechnical properties, mineralogical and geochemical properties of Eskişehir soils were evaluated in detail. XRD, DTA-TG, FT-IR and SEM analyzes have shown that smectite type clay minerals with high swelling potential were formed in alkaline conditions with chemical weathering from feldspar and volcanic glass levels close to the surface of the soil. Such clay soils with low geotechnical properties and high compressibility can cause significant problems for engineering structures built on them. LL, PL and PI values increased due to increase in smectite content. Although the activity (A) value used in the primary assessment of swelling potential was positively correlated with Atterberg limits, it showed a negative correlation with the CaO content contained in the soil sample. In other words, the increase in CaO percentage of the soil sample was seen as a decrease in A value. It was evaluated that CaO content can be used as an alternative to A value in the evaluation of swelling potential. Also, the increase of Fe_2O_3, Na_2O and K_2O amounts result in increasing LL and clay's activity in Eskişehir soils.

ACKNOWLEDGEMENTS

This study has been supported in the scope of Eskisehir Osmangazi University, the Scientific Research Project No: 2016-1360, and consists of the third author's MSc study, supervised by the first and second authors.

REFERENCES

[1] Ohtsubo, M., Egashira, K., Kashima, K. (1995) Depositional and post-depositional geoche-mistry and its correlation with the geotechnical properties of marine clays in Arlake Bay, Japan. Geotechnique. 45(3), 509-523.
[2] Dananaj, I., Frankovska, J., Janotka, I. (2005) The influence of smectite content on microstructure and geotechnical properties of calcium and sodium bentonites. Applied Clay Science. 28(1-4), 223-232.
[3] Abd-Allah, A.M.A., Dawood, Y.H., Awad, S.A., Agila, W.A. (2009) Mineralogical and chemical compositions of shallow marine clays, East of Cairo, Egypt: A geotechnical perception. Journal of King Abdulaziz University Earth Sciences. 20(1), 141–166.

[4] Muceku, Y., Lazo, P. (2013) The chemical-mineralogical composition and their effect on physical and mechanical properties of cohesive soils in Tirana area, Albania. Fresen. Environ. Bull. 22, 3006-3015.
[5] Adebisi, N.O., Adeyemi, G.O., Oluwafemi, O.S., Songca, S.P. (2013) Important properties of clay content of lateritic soils for engineering project. Journal of Geography and Geology. 5(2), 99–115.
[6] Benac, Č., Oštrić, M., Jovančević, S.D. (2014) Geotechnical properties in relation to grain-size and mineral composition: The Grohovo landslide case study (Croatia). Geologica Croatica. 67(2), 127-136.
[7] Akgün, H., Türkmenoğlu, A.G, Kelam, A.A., Yousefi-Bavil, K., Öner, G., Koçkar, M.K. (2018) Assessment of the effect of mineralogy on the geotechnical parameters of clayey soils: A case study for the Orta Country, Çankırı, Turkey. Applied Clay Science. 164, 44-53.
[8] Mitchell, J.K. (1993) Fundamentals of Soil Behavior. 2nd ed. John Wiley, New York.
[9] Grim, R.E. (1962) Applied Clay Mineralogy. McGraw-Hill, New York.
[10] Türköz, M. (2006) Stabilization of swelling clays with lime admixture and an application to the Eskişehir-Meşelik clays. Journal of Engineering and Architecture Faculty of Eskisehir Osmangazi University. XIX, 75-88.
[11] Türköz, M., Savaş, H., Tosun, H. (2011) Stabilization of Problematic Clay Soils with Magnesium Chloride Solution. Journal of The Faculty of Engineering and Architecture of Gazi University. 26(1), 233-242.
[12] Orhan, A., Türköz, M., Tosun, H. (2013) Preliminary hazard assessment and site characterization of Meşelik campus area, Eskişehir-Turkey. Natural Hazards and Earth System Sciences. 13, 75-84.
[13] Kulaksız, S., (1981) Geology of north-west of Sivrihisar region. Bulletin for Earth Sciences. 8, 103-124.
[14] Gözler, M.Z., Cevher, F. (1987) 1/100.000 scale geological map of Eskişehir-J26.General Directorate of Mineral Research and Exploration (MTA), Ankara (in Turkish).
[15] Karakaş, Z., Varol, B. (2005) Clay mineralization in Neogene units around Babadat-Mülk region (Eskişehir-Sivrihisar) and their mineralogical and geochemical investigation. Ankara University Scientific Research Project Final Report. 67p (in Turkish).
[16] Kadir, S., Eren, M., Külah, T., Erkoyun, H., Huggett, J., Önalgil, N. (2018) Genesis of palygorskite and calcretes in Pliocene Eskişehir Basin, West central Anatolia, Turkey. Catena. 168, 62-78.
[17] Türkmenoğlu, A.G, Yavuz-Işık, N. (2008) Mineralogy, chemistry and potential utilization of clays from coal deposits in the Kütahya province, western Turkey. Applied Clay Science. 42, 63-73.
[18] Földvari, M. (2011) Handbook of Thermogravimetric System of Minerals and its use in Geological Practise. Occasional Papers of the Geological Institute of Hungary, 213.
[19] Farmer, V.C. (1974) Layer silicates. In: Farmer, V.C. (ed.) Infrared Spectra of Minerals. Mineralogical Society Monograph 4, London, 331-363.
[20] De Santiago Buey, C., Suarez Barrios, M., Garcia Romero, E., Doval Montoya, M. (2000) Mg-rich smectite 'Precursor' phase in the tagus basin, Spain. Clays and Clay Minerals, 48(3), 366-373.
[21] Zviagina, B.B., McCarty, D.G., Srodon, J., Drits, V.A. (2004) Interpretation of infrared spectra of diotahedral smectite in the reflection of OH-stretching vibration. Clays and Clay Minerals. 52(4), 399-410.
[22] Madejová, J., Kečkéš, J., Pálková, H., Komadel, P. (2002) Identification of components in smectite/kaolinite mixtures. Clay Minerals. 37(2), 377-388.
[23] Dudek, T., Cuadros, J., Huertas, J. (2007) Structure of mixed-layer kaolinite-smectite and smectite-to-kaolinite transformation mechanism from synthesis experiments. American Mineralogist. 92(1), 179-192.
[24] Erkoyun, H., Kadir, S., Külah, T., Huggett, J. (2017) Mineralogy, geochemistry and genesis of clays interlayered coal seams succession in the Neogene lacustrine Seyitömer coal deposit, Kütahya, western Turkey. International Journal of Coal Geology. 172, 112-133.
[25] Kadir, S., Külah, T., Önalgil, N., Erkoyun, H., Elliott, W.C. (2017) Mineralogy, geochemistry, and genesis of bentonites in Miocene volcanic-sedimentary units of the Ankara-Çankırı basin, central Anatolia, Turkey. Clays and Clay Minerals. 65, 64-91.
[26] Ohtsubo, M., Egashira, K., Tanaka, H., Mishima, O. (2002) Clay minerals and Geotechnical index properties of marine clays in East Asia. Marine Georesources and Geotechnology. 20, 223-235.
[27] Smith, G.N. (1978) Elements of soil mechanics for civil and mining engineers. 4th ed. Crosby Lockwood Staples (pub).
[28] Summa, V., Margiotta, S., Colaiacovo, R., Giannossi, M.L. (2015) The influence of the grain-size, mineralogical and geochemical composition on the Verdesca landslide. Natural Hazards and Earth System Sciences. 15, 135-146.

[29] Berry, R.W., Torrance, J.K. (1998) Mineralogy, grain-size distribution and geotechnical behavior of Champlain clay core samples, Quebec. Can Mineral. 36(6), 1625-1636.
[30] Deschamps, R., Kohler, E., Gasparrini, M., Durand, O., Euzen, T., Nader, F. (2012) Impact of mineralogy and diagenesis on reservoir quality of the Lower Cretaceous Upper Mannville Formation (Alberta, Canada). Oil and Gas Science Technology. 67, 31-58.
[31] Ekinci Şans, B., Esenli, F., Kadir, S., Elliott, W.C. (2015) Genesis of smectite in siliciclastics and pyroclastics of the Eocene İslambeyli Formation in the Lalapaşa region, NW Thrace, Turkey. Clay Minerals. 50, 459-483.
[32] Kadir, S., Aydoğan, M.S., Elitok, O., Helvacı, C. (2015) Composition and genesis of nickel-chrome-bearing nontronite and montmorillonite in lateritized ultramafic rocks in the Muratdağı region (Uşak, western Anatolia), Turkey. Clays and Clay Minerals. 63(3), 163-184.
[33] Skempton, A.W. (1953) The colloidal activity of clays. In*:* Proceedings 3rd International Soils Mechanics and Foundation Engineering. Switzerland, 57–61.
[34] Van der Merwe, D.H. (1964) The prediction of heave from the plasticity index and the percentage clay fraction of soils. Civil Engineering in South Africa. 6(6), 103-107.
[35] Seed, H.B., Woodward, R.J., Lungren, R. (1964) Clay mineralogical aspects of the Atterberg limits. Journal of Soil Mechanics and Foundation Division of ASCE. 90(SM4), 107-131.
[36] Daksanamurty, V., Raman, V. (1973) A simple method of identifying an Expansive Soil, Soils and Foundation. Japanese Society of Soil Mechanics and Foundation Engineering. 13(1), 97-104.
[37] Chen, F.H. (1975) Foundations on expansive soils. Elsevier, Amsterdam, Oxford, New York.
[38] Seed, H.B., Woodward, R.J., Lundgren, R. (1962) Prediction of swelling potential for compacted clays. Journal of the Soil Mechanics and Foundations Division (ASCE). 88(3), 53-87.
[39] Velde, B. (1995) Origin and Mineralogy of Clays, Clays and the Environment. Springer-Verlag, New York.
[40] Ocakoğlu, F. (2007) A revaluation of the Eskişehir fault zone as a recent extensional structure in NW Turkey. Journal of Asian Earth Sciences. 31(2), 91-103.
[41] Şengüler, İ. (2013) Geology and stratigraphy of the Eskişehir-Alpu coal basin. MTA (Doğal Kaynaklar ve Ekonomi Bülteni). National Research Economy Bulletin. 16, 89–93. (in Turkish).
[42] Whitney, D.L., Evans, B.W. (2010) Abbreviations for names of rock-forming minerals. American Mineralogist. 95, 185-187.

Received: **15.01.2020**
Accepted: **25.01.2020**

CORRESPONDING AUTHOR

Murat Turkoz
Department of Civil Engineering,
Faculty of Engineering and Architecture,
Eskisehir Osmangazi University,
Eskisehir – Turkey

e-mail: mturkoz@ogu.edu.tr

© by PSP Volume 29 – No. 05/2020 pages 4040-4048 Fresenius Environmental Bulletin

TECTONIC CONTROL OF LONG TERM EMISSION OF SHALE GAS FROM LONGMAXI FORMATION IN EAST CHONGQING AREA, CHINA

Haidong Chen, Dazhen Tang, Song Li*

School of Energy Resource, China University of Geosciences (Beijing), Beijing 434000, China

ABSTRACT

In order to explore the characteristics of oil and gas fugitives under the tectonic control effects of the Longmaxi Formation shale gas in East Chongqing area, organic geochemistry measurements were carried out. The results showed that the strong tectonic uplift that began in the late Himalayas in East Chongqing area as a whole had a destructive effect on the occurrence of shale gas in the Longmaxi Formation. The stagnation time of hydrocarbon generation in the Longmaxi Formation shale in East Chongqing area is about 115-142 Ma, and the earliest stratum uplift time starts from 145 Ma, and shows the characteristics of early southeast and late northwest. The Longmaxi Formation is a complex pore-fracture system composed of micro-fissures and pores. The pores and fissures developed in the shale form the formation space of shale gas. Reservoir overpressure coefficient has a negative correlation with structural complexity. Reservoirs in complex structural areas are mostly under-pressured or normal-pressured while the reservoir in simple structural areas are over-pressured. The vertical permeability of the Longmaxi Formation shale is lower than the lateral permeability. Macroscopically, the closer to the shale outcrop area, the smaller the overpressure coefficient of the reservoir.

KEYWORDS:
Shale gas, pore-fracture; structural control, history of hydrocarbon generation, Longmaxi Formation, East Chongqing

INTRODUCTION

Shale gas is an unconventional natural gas resource. It has certain common points with rich and integrated reservoirs of conventional natural gas resources, and also has obvious differences. In recent years, with the increasing difficulty of conventional oil and gas resources exploration and development, unconventional oil and gas resources, especially shale oil and gas resources, have been attracted attention [1-5]. The United States leads the world in the exploration and development of shale oil and gas resources, and has made major breakthroughs in related technologies which also laid a foundation for China's shale oil and gas exploration and development.

As the first batch of shale gas strategic survey pilot test area established in China, East Chongqing area has shown good prospects for shale gas exploration and development. Among them, the Wufeng Formation-Early Longmaxi Formation has black shales with large thickness, stable distribution, and high organic matter content which is regarded as a high-quality marine-rich organic shale, and has become the main stratum of shale gas exploration and development in China [6-8]. So far, several commercial gas fields such as Changning, Weiyuan, Zhaotong and Fuling gas fields have been developed successfully. Due to the high degree of thermal evolution of the main strata in the area and the strong tectonic effect in the later stage, it has brought certain difficulties to deep exploration and development. The research content covers the characteristics of tectonic movement, fracture development, pores, fracture classification, resource potential and sedimentary facies in this area [9-10]. However, there are few reports on the diagenetic structural background, redox and paleo-productivity conditions in this area. Marine source rocks are organic-rich intervals, and their development is obviously controlled by the sedimentary environment. The main controlling factors of shale organic matter enrichment and the establishment of organic matter deposition model fully reflect the important role of chemical elements in geological research. In addition, the differences in the combination of inorganic parameters such as chemical elements can reflect the influencing factors controlling the development of source rocks such as marine paleo-productivity, redox conditions, and paleo-productivity [11-13].

At present, there are two main types of factors affecting the selection of shale gas targets in China: "static" control factors and "dynamic" control factors. Static control factors include shale sedimentary facies, thickness, TOC, Ro, etc. Dynamic control factors include structural preservation conditions, burial depth, burial history, hydrocarbon generation history, etc. The research shows that there are two types of favorable targets or dessert areas in the ma-

rine area of southern China: "continuous" and "tectonic" [14-15]. The structure of East Chongqing area is complex and there are multiple stages of tectonic evolution, which belong to the "tectonic" favorable target area. A variety of tectonic styles develop in the East Chongqing area. Different tectonic features have significant control over shale gas enrichment and preservation conditions, and have a big impact on favorable areas.

GEOLOGICAL BACKGROUND AND METHODS

Study block geochemical characteristics. The distribution of gas-bearing layers of the Longmaxi Formation shale in the East Chongqing area is controlled by paleo-structures or paleogeomorphology (Figure 1).

Under the background of the entire Yangtze platform, the northeast-southwest depression zone is inherited and the terrain is relatively low-lying. Since the Late Ordovician Wufeng Period, the study area is located in a relatively deep-water shelf sedimentary environment [16]. The organic carbon-rich black silt mud shale of the Longmaxi Formation is generally deposited in the entire East Chongqing area. At the end of the Ludanian stage, the sea level began to decline. Therefore, the best source rocks are generally developed in the vesiculosus zone-cyphys zone at the bottom of the Longmaxi Formation, while the Ludanian stage in the depression zone has large sedimentary thickness and good source rock development. The terrain is relatively high, the time for maintaining deeper water as the sea level decreases is shorter, and the thickness of high-abundance source rocks is thin.

The TOC test results show that the overall TOC content in East Chongqing area is relatively high, generally greater than 2.0, and the TOC content in Shizhu and Tianba in Northeast Chongqing exceeds 3.0. The vertical TOC test shows that the TOC of the Longmaxi Formation has obvious changes [17-18]. The 30m black penstone shale section at the bottom of the Longmaxi Formation has a TOC content greater than 2.0% and a maximum of 4.77%. The TOC content of the upper segment is low with the value less than 1%. The top part is only 0.27% due to weathering and other effects. The evolution of the Longmaxi Formation in the middle and upper Yangtze region is relatively high, with the Ro value between 1.5% and 3.5%, which is generally in an overmature stage, and the kerogen type is mainly I-II1 (Table 1).

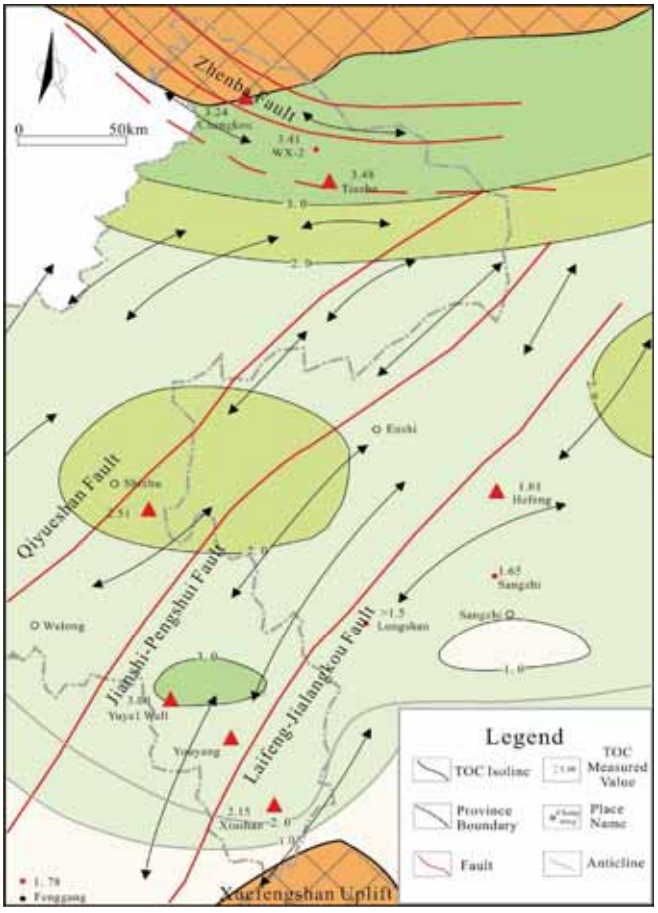

FIGURE 1
Structural distribution and TOC contour map of Longmaxi Formation in East Chongqing area.

TABLE 1
Organic geochemical characteristics of Longmaxi Formation in East Chongqing area

Type	Jiaoshiba	Qianjiang
Sedimentary environment	Deepwater shelf sedimentation	Shallow water shelf sedimentation
TOC (%)	2.54	2.51
R_o (%)	2.20～3.06	2.0～4.0
Kerogen type	I-II$_1$	Mainly type I, a small amount of type II1
Porosity (%)	2.78～7.08	2.37～8.71
Permeability (μm^2)	(0.0016～0.0713) ×10^{-3}	(0.0027～0.0712) ×10^{-3}
Clay content (%)	16.6～49.1	10～57, average 32.0
Brittle mineral content (%)	50.9～80.3	41～89, average 67.0
Gas content (m^3/t)	0.89～5.19	1.0～3.0, average 2.0

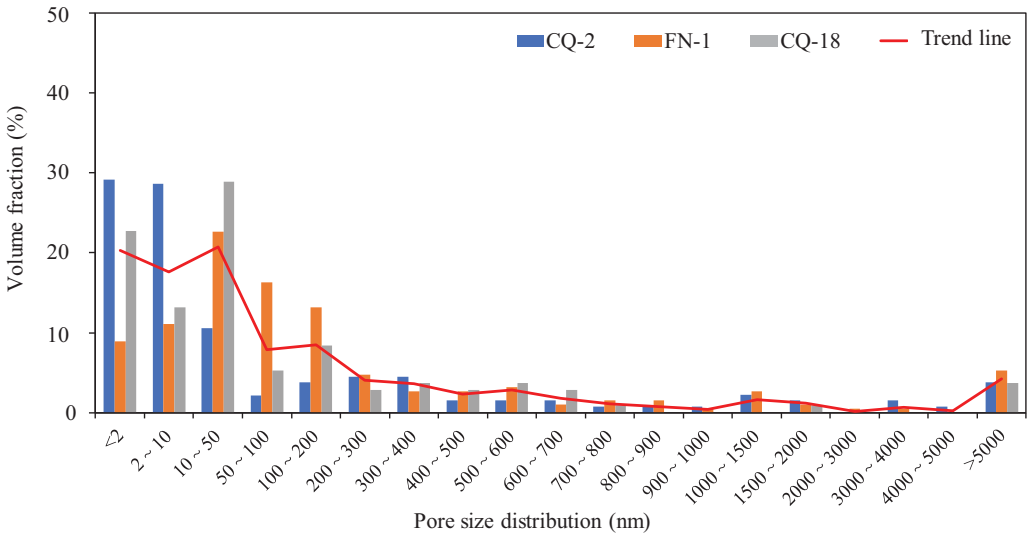

FIGURE 2
Comprehensive pore size distribution of Longmaxi Formation.

Research methods. This article aims at the unclear the structural characteristics of the Longmaxi Formation shale gas reservoirs during the exploration and development in East Chongqing area. In order to explore the characteristics of oil and gas fugitives of the Longmaxi Formation shale gas under the control of tectonic effects in the late stage, based on the analysis results of organic geochemical characteristics and micro-pore characteristics of typical rock samples, the relationship between tectonic evolution and hydrocarbon generation of shale gas was explored, and the coupling relationship between tectonic preservation and hydrocarbon generation history was analyzed [19-20]. Finally, the characteristics of oil and gas fugitives of the Longmaxi Formation shale gas under the control of tectonic action in the late period in East Chongqing area were revealed.

RESULTS

Micropore fracture. During the evolution of mud shale, complex micro-fractures and pores (including nano-pores) were formed due to tectonic, thermal and hydrocarbon generation-expulsion, which together constitute a complex pore-fissure system. The mud shale mesopore system is not only a storage space for natural gas, but also a percolation channel for natural gas [21]. The development degree of natural pore-fracture system and its transformability are of great significance to the evaluation of shale gas resources and industrial exploitation.

The mercury intrusion calculation results showed that the porosity of the Longmaxi Formation samples ranged from 1.6220% to 10.81169%, with an average of 5.906%. The pores with porosity greater than 4% accounts for 42.86% of the total (Figure 2). Through argon ion polishing scanning electron microscope experimental observation, it is found that the pore genesis types in the Longmaxi Formation shale reservoir are various, and the nanoscale pores are mainly organic pores, which is consistent with previous research conclusions. Observation of core samples by field emission scanning electron microscopy also found that the surface pores of the Longmaxi Formation shale are generally uneven, and the shale mercury pressure data and low-temperature nitrogen adsorption data also show that the pores have fractal characteristics (Figure 3).

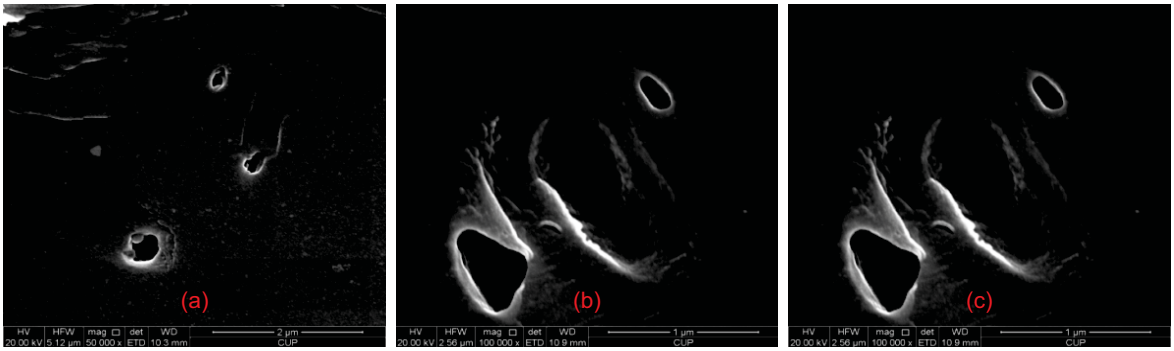

FIGURE 3
Organic matter pores and SEM images of the Longmaxi Formation shale.
Notes: (1)-(2) Samples are taken from Chongqing Pengshui section; (3) Samples are taken from Well WX2.

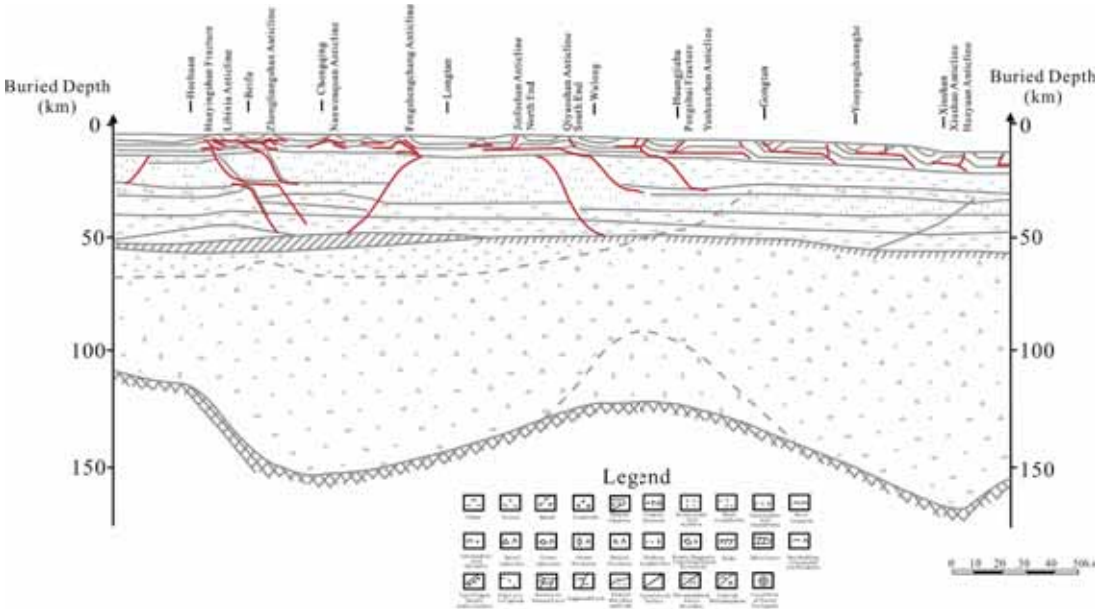

FIGURE 4
Comprehensive interpretation of geomagnetic cross section of Dazu-Xiushan magnetotellurics and earthquakes.

Tectonic evolution-hydrocarbon generation history coupling. (1) Late tectonic uplift. The main controlling fault in East Chongqing area is Qiyueshan fault, which belongs to the East Chongqing high-steep structural belt. The west of Qiyueshan is dominated by barrier folds, and the east structure is dominated by trough folds. The style gradually changes. The field geological survey results combined with the results of many researchers have shown that the Qiyueshan fault is a fault system consisting of three east-dipping faults and west-dipping faults of the caprock that recoil in the Cambrian system [22-23]. The tectonic deformation in the sedimentary caprocks on both sides is quite different. The aeromagnetic results show that the Qiyueshan fault is the boundary between the high positive anomaly area and the low positive and negative anomaly area. The crustal seismic sounding results show that there are obvious abrupt changes in layer velocity.

The results of stratigraphic basement research in East Chongqing area show that there are significant differences in the basement on both sides of the Qiyueshan fault, indicating that the fault was formed in the Jinning Period and is dominated by tensile properties (Figure 4). At this time, the Longmaxi Formation stratum has not yet been deposited. After that, the faults are mainly affected by the south-east Xuefeng intracontinental orogenic system and was activated again by the northwest-south eastward compression stress. The fault at this stage was a thrust fault. The Himalayan period was balanced and regulated by the Pengshui mantle and Moho uplift. In the sedimentary caprock including Longmaxi Formation east of Qiyueshan fault, a low-angle high-tension tensional normal fault is developed. The qualitative analysis results show that the difference in basement causes the shale gas in the east of Pengshui-Youyang area to be damaged. No favorable structural preservation conditions have been formed.

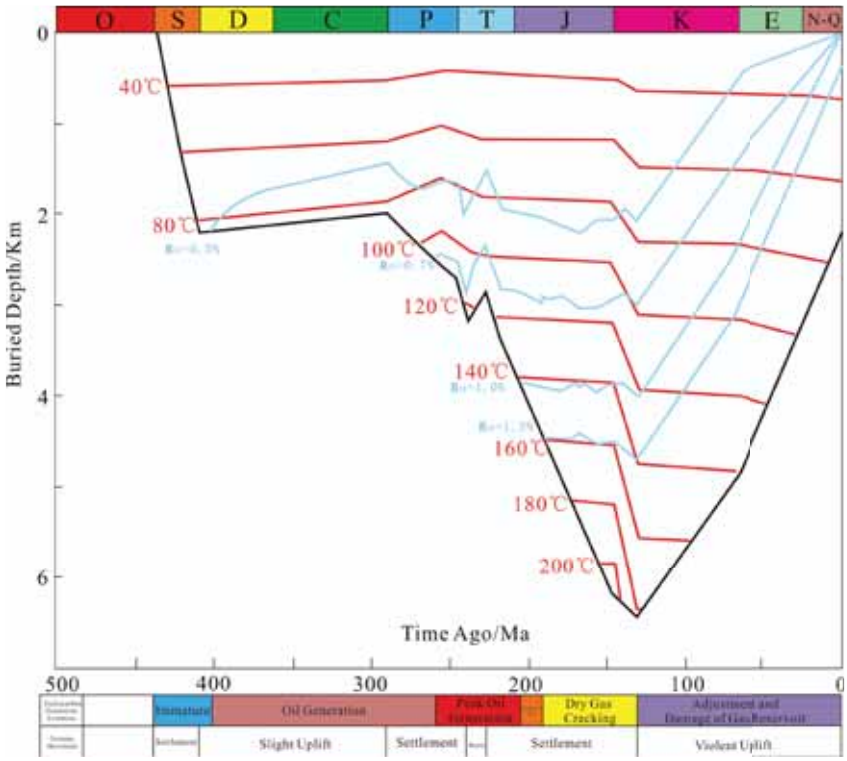

FIGURE 5
Hydrocarbon generation and structural evolution of Longmaxi Formation in Well PY1.

(2) History of shale gas generation. Affected by the Xuefeng orogenic belt on the southwest side, lifting occurred from about 154Ma in the southwestern area of the study area, and the northwestward lifting time gradually became later. The Lichuan reversal oblique lifting time was about 145Ma [12, 24]. The hydrocarbon generation simulation of wells JY-1 and PY1 using petromod simulation software shows that the main hydrocarbon generation time of the Longmaxi Formation in the two places is between 115-142Ma, and the combination of regional tectonic evolution shows that large-scale hydrocarbon generation process has ended during the uplifting process [25]. The strong tectonic uplift in the late period is mainly to control the differences in the structural preservation conditions of shale gas. The shale of the Longmaxi Formation of Qiyue Mountain has gradually weakened due to the lifting strength, and the overall performance gradually decreases from southeast to northwest, and the strength of structural deformation gradually weakens (Figure 5).

Tectonic preservation-hydrocarbon generation history coupling. The Himalayas in the East Chongqing area are bounded by the Qiyueshan fault, and the tectonic stress is characterized by "westward squeezing and eastward extension." The difference of gas preservation determines the difference of shale gas preservation in different tectonic belts in East Chongqing area.

(1) Overpressure characteristics of the Longmaxi Formation shale reservoir. The shale pores are mostly organic pores and clay mineral pores, which are plastic pores. The Longmaxi Formation shale bedding is relatively developed. The permeability test results of drilling core samples of the Longmaxi Formation show that the vertical permeability in the shale is higher than the lateral permeability [26]. Based on the drilling gas side results in the East Chongqing area, the contour of the overpressure coefficient of the Longmaxi Formation and the contour of the complexity of the East Chongqing structure (Figure 6) reflect the negative relationship between the present overpressure coefficient of the Longmaxi Formation and the complexity of the structure. Most of the regional reservoirs with high structural complexity coefficients are under-pressured or atmospheric pressure, and the regional reservoirs with low structural complexity coefficients are over pressured. In the northern and southern areas of the study area, the closer to the shale outcrop area, the smaller the overpressure coefficient of the reservoir, indicating that shale reservoirs close to the outcrop area cannot form effective surrounding rock trap conditions, which is not conducive to the occurrence of shale gas.

(2) Shale hydrocarbon generation and expulsion process and structural coupling and accumulation. Combining with the research on the hydrocarbon generation and evolution of marine shales in Xiahuayuan area of North China, similar to the geochemical indexes of marine shale in the

Longmaxi Formation, it can be seen that marine shales have a secondary hydrocarbon generation process, and the secondary hydrocarbon expulsion is much larger than amount of initial hydrocarbon expulsion [27-28]. Combined with the gas generation simulation curve (Figure 7), the marine shale Ro reached its peak for the first time at 0.8, and Ro reached its peak for the second time at 2.0. Combined with the study of shale burial history in East Chongqing area, the long-term continuous burial depth of shale in the area caused rapid rise of Ro, and the structure was stable during deep burial. According to the simulation results, when the maximum burial depth is reached, the simulated organic hydrocarbon expulsion per unit of shale gas in Well Jy1 is 0.102 mg, and the hydrocarbon generation rate is 0.44 mg/g, indicating that East Chongqing can form rich shale gas reservoirs.

After the maximum burial depth was reached, the formation was rapidly uplifted. At this time, the evolution of shale gas maturity stagnated, and Ro was at 2.65-3.3. At this time, the shale gas in the area was generally in an overpressure state, and the overpressure coefficient exceeded 2.0. As the overlying pressure continues to decrease and the cumulative increase in lateral pressure squeezes, the early generation of hydrocarbons tends to dissipate at the locations subject to strong tectonic effects. However, where the maximum buried structure is relatively weak, the hydrocarbons generated early can be easily preserved. In addition, coupled analysis of shale hydrocarbon generation simulation and burial history evolution curve shows that after large-scale uplift of marine shale gas in East Chongqing area, no secondary deep burial occurred in the formation, resulting in no further shale gas expulsion [29]. At this stage, the hydrocarbon content in the current state is directly controlled by the early hydrocarbon expulsion and the strength of the tectonic effect.

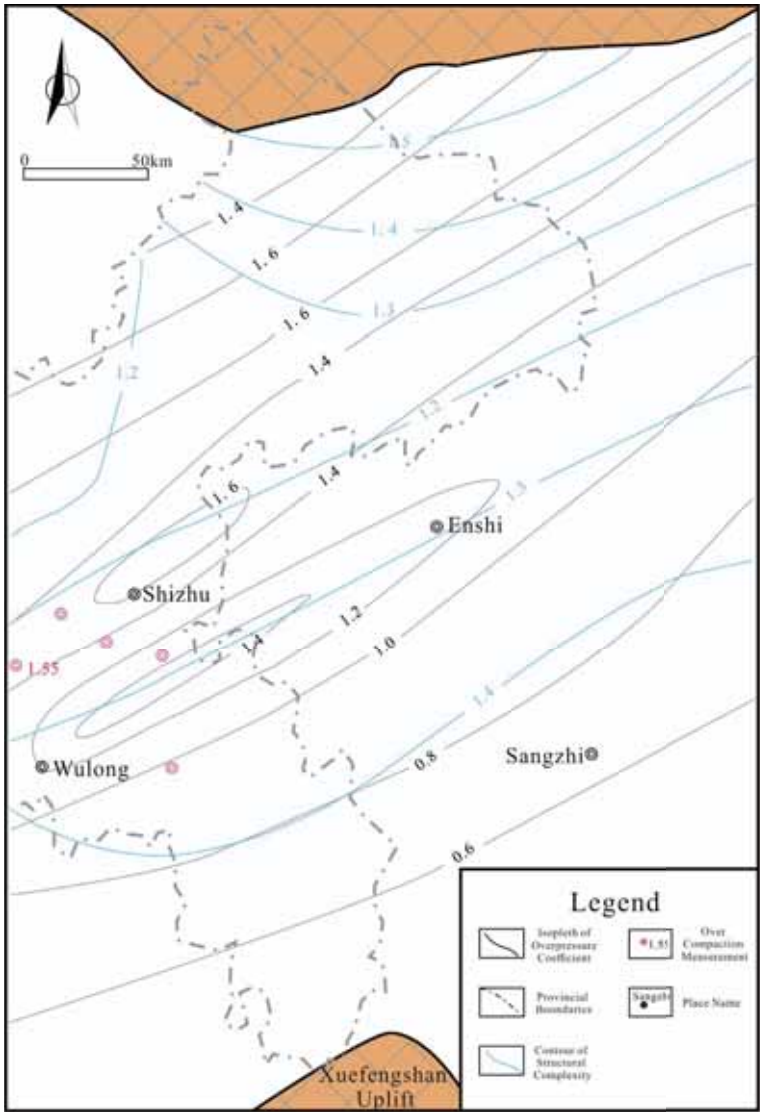

FIGURE 6
Overpressure coefficient of the Longmaxi Formation shale reservoir in East Chongqing area.

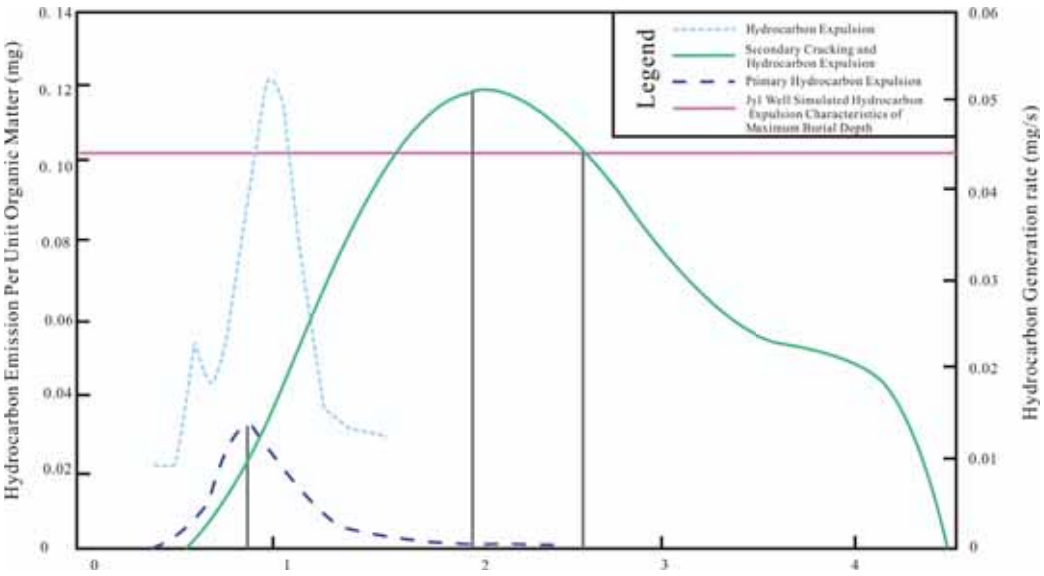

FIGURE 7
Simulated curves of hydrocarbon generation and expulsion and secondary cracking gas generation in marine shale.

During the burial of oil shale, due to the increasing burial depth, the temperature of oil shale is increasing, and the pore fissures in source rocks are increasing. The shale pore fissures in the current state can be divided into two categories: organic matter pyrolysis and tectonic genesis. How to distinguish the distribution ratio of different pore fissure types in oil shale, the fractal dimension of porosity, and explore the structural complexity of shale is still under research [30-31]. The mesoporous fissure development law can effectively represent the spatial change law of shale gas enrichment during tectonic evolution. The previous research shows that the migration rate of shale gas in the direction of the stratum is greater than that in the direction perpendicular to the stratum. The outcrop zone of the source rock and the fracture zone formed by the late tectonic action are the main channels for shale escape, which are controlled by the formation dip angle and uplift. There are many factors such as time, uplift rate, and shale physical properties. How to study the shale gas escape mechanism in this area needs further study.

CONCLUSIONS

(1) The strong tectonic uplift that began in the late Himalayan period in East Chongqing area as a whole has a destructive effect on the formation of the Longmaxi Formation shale gas. The stagnant hydrocarbon generation time of the Longmaxi Formation shale in the eastern area is about 115-142 Ma. It started at 145Ma and showed the characteristics of early southeast and late northwest. In addition, due to the action of Pengshui mantle and Mohoian uplift, the Himalayan period only formed tensile faults in the sedimentary caprocks to the east of the Qiyueshan fault or caused structural inversion of the early reverse faults. As a result, the shale gas in the area east of Pengshui-Liyang has suffered damage, and no favorable structural preservation conditions have been formed, which is also the reason for the poor gas bearing of exploration results under current conditions.

(2) The Longmaxi Formation is a complex pore-fracture system composed of micro-fissures and pores. The pores and fissures developed in the shale form the formation space of shale gas. Combined with the evolution of marine shale hydrocarbon generation, it is shown that there is a significant secondary hydrocarbon generation process in the marine shale of the Longmaxi Formation, and the secondary hydrocarbon expulsion is large.

(3) Reservoir overpressure coefficient has a negative correlation with structural complexity. Reservoirs in structurally complex areas are mostly under-pressured or atmospheric-pressured. Reservoirs in simple structural areas are over-pressured and some localized areas are under ultra-high pressure. The permeability characteristics of shale in different directions show that the vertical permeability of the Longmaxi Formation shale is lower than that of the lateral permeability. Macroscopically, the closer to the shale outcrop area, the smaller the overpressure coefficient of the reservoir.

ACKNOWLEDGEMENTS

This work was financially supported by the National Natural Science Foundation of China (41530314), the Key Project of the National Science & Technology (2016ZX05042-002), and the Fundamental Research Funds for the Central Universities.

REFERENCES

[1] Zou, C., Tao, S., Bai, B., Yang, Z., Zhu, R., Hou, L., Yuan, X., Zhang, G., Wu, Wu, S. (2015) Differences and Relations between Unconventional and Conventional Oil and Gas. China Petroleum Exploration. 20(1), 1-16.

[2] Zou, C., Yang, Z., Zhu, R., Zhang, G., Hou, L., Wu, S., Tao, S., Yuan, X., Dong, D., Wang, Y., Wang, L., Huang, J., Wang, S. (2015) Progress in China's Unconventional Oil and Gas Exploration and Development and Theoretical Technologies. Acta Geologica Sinica. 6, 979-1007.

[3] Li, Q., Ou, G., Wang,S., Zhang, M., Wu, D. (2019) Geochemical Characteristics of Fluid from Shale Gas Reservoir of Wufeng- Longmaxi Formations in the Southeastern Chongqing, China - A Case Study of Well YC2. Journal of Earth Sciences and Environment. 41(5), 529-540.

[4] Xiong, X., Wang, J., Xiong, G., Wang, Z., Men, Y., Zhou, X., Zhou, Y., Yang, X., Deng, Q. (2018) Shale Gas Geological Characteristics of Wufeng and Longmaxi Formations in Northeast Chongqing and Its Exploration Direction. Acta Geologica Sinica. 92(9), 1948-1958.

[5] Curtis, M., Sondergeld, C., Ambrose, R., Rai, C. (2012) Microstructural investigation of gas shales in two and three dimensions using nanometer-scale resolution imaging. AAPG Bulletin. 96(4), 665-677.

[6] Misch, D., Mendez-Martin, F., Hawranek, G. (2016) SEM and FIB-SEM investigations on potential gas shales in the Dniepr-Donets Basin (Ukraine): pore space evolution in organic matter during thermal maturation. IOP Conference Series: Materials Science and Engineering. IOP Publishing. 109(1), 012010.

[7] Chalmers, G., Bustin, R. (2007) The organic matter distribution and methane capacity of the Lower Cretaceous strata of Northeastern British Columbia, Canada. International Journal of Coal Geology. 70(1), 223-239.

[8] Jiao, W., Fang, G., Wang, S., Zhang, Z., Yu, C. (2019) Key control factor for the gas-bearing properties difference of lower Paleozoic shale in southeast Chongqing. Journal of China Coal Society. 44(6), 1786-1794.

[9] Zhai, G., Wang, S., He, W. (2012) Hotspot trend and enlightenment of global ten-year hydrocarbon exploration. Acta Petrolei Sinica. 33(z1), 14-19.

[10] Sun, L., Fang, C., Li, F., Zhu, R., Zhang, Y., Yuan, X., Jia, A., Gao, X., Su, L. (2015) Innovations and challenges of sedimentology in oil and gas exploration and development. Petroleum Exploration and Development. 42(2), 129-136.

[11] Fu, J., Xiu, X., Dan, W., Feng, S., Liang, X., Xin, H., You, Y. (2019) The geological characteristics and the progress on exploration and development of shale oil in Chang7 Member of Mesozoic Yanchang Formation, Ordos Basin. China Petroleum Exploration. 24(5), 601-614.

[12] Xiong, X., Wang, J., Yu, Q., Yang, Y., Xiong, G., Niu, B., Guo, X., Deng, Q. (2015) Element geochemistry inversion of the environment and background of organic-rich black shale formations: A case study of the Wufeng-Longmaxi black shale in the Tianba section in Northeastern Chongqing. Natural Gas Industry. 35(4), 25-32.

[13] Zhang, Q., Liang, F., Wang, H., Lei, Z., Qi, L. (2018) Elements geochemistry and paleo sedimentary significance: A case study of the Wufeng-Longmaxi shale in southeast Chongqing. Journal of China University of Mining and Technology. 47(2), 380-390.

[14] Yang, Y., Wang, J., Guo, X., Xiong, X. (2017) Mineralogical Characteristics and Petroleum Geological Significance of Wufeng-Longmaxi Formation Shale in the Tianba Area, Northeast of Chongqing. Acta Sedimentologica Sinica. 35(4), 772-780.

[15] Zhao, D., Guo, Y., Wang, G., Bai, W., Zeng, C., Jiao, W., Liu, J. (2020) Sedimentary characteristics of shales graptololite and its implications for high-quality shale gas reservoirs in the Wufeng-Longmaxi formation in southeast Chongqing. Journal of Henan Polytechnic University (Natural Science). 39(1), 26-36+46.

[16] Zhou, Z., Zhai, G., Shi, D., Wang, S., Guo, T., Liu, Y., Wang, H. (2019) Shale gas reservoir geology of the Upper Ordovician Wufeng Formation-Lower Silurian Longmaxi Formation in western Hubei and Northeastern Chongqing. Petroleum Geology & Experiment. 41(1), 1-9.

[17] Liang, M., Tan, X., Chen, X., Wang, J., Ran, T., Wang, P., Tan, D., Xue, W., Zeng, C. (2018) Sequence stratigraphy of Wufeng-Longmaxi Formation in the southeastern Chongqing area and its geological significance. Coal Geology & Exploration. 46(6), 40-51.

[18] Bustin, R., Bustin, A., Cui, X., Ross, D., Murthy Pathi, V. (2008) Impact of shale properties on pore structure and storage characteristics. SPE shale gas production conference. Society of Petroleum Engineers.

[19] Steuber, T., Veizer, J. (2002) Phanerozoic record of plate tectonic control of seawater chemistry and carbonate sedimentation. Geology. 30(12), 1123.

[20] Etiope, G., Drobniak, A., Schimmelmann, A. (2013) Natural seepage of shale gas and the origin of "eternal flames" in the northern Appalachian Basin, USA. Marine and Petroleum Geology. 43, 178-186.

[21] Jiao, F., Yao, S., Wu, H., Li, M., Tang, Z. (2014) Advances in Characterization of Pore System of Gas Shales. Geological Journal of China Universities. 3, 151-161.
[22] Chen, S., Zhu, Y., Wang, H., Liu, H., Wei, W., Fang, J. (2012) Structure characteristics and accumulation significance of nanopores in Longmaxi shale gas reservoir in the southern Sichuan Basin. Journal of China Coal Society. 37(3), 438-444.
[23] Yu, C., Zhou, X., Fang, G., Wang, S., Yu, Z. (2018) Adsorptivity of shale under the formation temperature and pressure: a case of Longmaxi Formation in Northeastern Chongqing. Lithologic Reservoirs. 30(6), 10-17.
[24] Jinag, S., Wang, S., Hong, K., Zhu, L., Hu, X. (2017) Accumulation conditions of Lower Paleozoic shale gas and its resources in Northeastern Chongqing. Lithologic Reservoirs. 29(5), 11-18.
[25] Zhao, W., Jing, T., Wu, B., Zhou, Y., Xiong, X. (2018) Controlling mechanism of faults on the preservation conditions of shale gas: A case study of Wufeng - Longmaxi Formations in Southeast Chongqing. Natural Gas Geoscience. 29(9), 1333-1344.
[26] Moore, J., Jacobson, A., Holmden, C., Craw, D. (2009) Ca isotopes reveal weak control of tectonic uplift on long-term climate change. Neues Jahrbuch für Mineralogie-Abhandlungen. 186(2), 195-200.
[27] Centner, T. (2016) Reducing pollution at five critical points of shale gas production: strategies and institutional responses. Energy Policy. 94, 40-46.
[28] Negi, B., Pandey, K., Sehgal, N. (2017) Renewables, shale gas and gas import- striking a balance for India. Energy Procedia. 105, 3720-3726.
[29] Hu, H. (2013) Porosity evolution of the organic-rich shale with thermal maturity increasing. Acta Petrolei Sinica. 34(5), 820-825.
[30] Wu, S., Zhu, R., Cui, J., Cui, J., Bai, B., Zhang, X., Jin, X., Zhu, D., You, J., Hu, H. (2015) Characteristics of lacustrine shale porosity evolution, Triassic Chang 7 Member, Ordos Basin, NW China. Petroleum Exploration and Development. 42(2), 167-176.
[31] Ju, B., Wu, D. (2016) Experimental study on the pore characteristics of shale rocks in Zhanhua depression. Journal of Petroleum Science and Engineering. 146, 121-128.

Received: **16.01.2020**
Accepted: **11.02.2020**

CORRESPONDING AUTHOR

Song Li
School of Energy resource,
China University of Geosciences (Beijing),
Beijing 434000 – China

e-mail: 1798145877@qq.com

© by PSP Volume 29 – No. 05/2020 pages 4049-4055 Fresenius Environmental Bulletin

NOTICE

ELEMENTAL ANALYSIS OF ECOLOGICAL ENTREPRENEURSHIP OF CHINESE NEW VENTURES-BASED ON THE PERSPECTIVE OF ENTREPRENEURIAL PROCESS

Liying Lei*

Commercial College, Hohai University, Nanjing, 211100, China

ABSTRACT

Based on the perspective of entrepreneurial process, this paper constructs eco-entrepreneurship elemental analysis framework of Chinese new ventures, which analyzes the types and characteristics of opportunities, resources, and team elements. By fuzzy set comparative analysis (FsQCA), it explores high environmental new venture performance with the structure of the ecological entrepreneurship elements. The results show that as follows. (1) Eco-entrepreneurial opportunities are divided into Pedunculated and intrapreneurship types; eco-entrepreneurial resources are divided into patchwork model and coupling model, and eco-entrepreneurship teams are divided into heterogeneous and homogeneous types. (2) For new ventures with high environmental performance, the structure of their ecological entrepreneurial elements is mainly divided into two categories. The first category mainly includes Pedunculated entrepreneurial opportunities, patchwork-type entrepreneurial resources, and homogeneous entrepreneurial teams. The second category mainly includes intrapreneurship entrepreneurial opportunities, coupling entrepreneurial resources, and heterogeneous entrepreneurial teams.

KEYWORDS:
New ventures, ecological entrepreneurial elements, environmental performance, entrepreneurial process

INTRODUCTION

Since the beginning of the 21st century, the "linear model died" in the industrial era, and the chain-based entrepreneurial model in the Internet era has completely deconstructed and reorganized the global industrial structure. How entrepreneurs can identify and develop entrepreneurial opportunities from a broader perspective, and practice entrepreneurial activities, scholars need to rethink entrepreneurial activities based on the system theory [1]. Since China's reform and opening up, the economy has continued to grow at a high speed. However, the rapid development of the economy has caused tremendous pressure on the ecological environment, which caused problems such as environmental pollution and ecological damage. Therefore, the Chinese government has called for "the development of ecological entrepreneurship and the creation of environmentally friendly new ventures". However, the results of eco-entrepreneurial practices of Chinese new ventures have shown two levels of differentiation. Some new ventures have generated high economic and social performance [2]. Some new ventures have fallen into a "start-up dilemma", facing the dual pressures of survival and the environment.

Most current research on entrepreneurial models focuses on the components of individual entrepreneurial ecosystems in isolation. Although each element contributes to the formation and development of the Silicon Valley entrepreneurial ecosystem, it does not fully support the sustainable development of the Silicon Valley entrepreneurial ecosystem [3]. There are complex interactions among these elements. In view of this, this paper analyzes the types of eco-entrepreneurship elements of new ventures based on the perspective of entrepreneurial process, and explores the entrepreneurial elemental structure of high environmental performance new ventures. The main structure of this paper is as follows. The first part introduces relevant theoretical analysis, such as entrepreneurial opportunities, entrepreneurial resources and so on. The second part constructs the variable measurement and performs the reliability and validity analysis. Based on this data analysis, the third part can be seen. Finally, a full-text research summary is made.

THEORETICAL ANALYSIS

Based on the process perspective, Timmons proposes that entrepreneurship is the process of balancing opportunities, resources, and teams. In view of this, this paper analyzes the eco-

entrepreneurship elements types of new ventures from the perspective of opportunities, resources, and team three-dimensionality.

Entrepreneurial opportunities. Opportunity is the core of entrepreneurial activities [3]. Eco-environmental entrepreneurship opportunities are mainly divided into pedunculated type and intrapreneurship. Pedunculated opportunities arise from the social demand for low-environmentally destructive economic activities [4]. New ventures with high entrepreneurial vigilance can timely discover external ecological entrepreneurial opportunities, which carry out entrepreneurial activities with low production energy consumption and low pollution emissions based on environmentally friendly orientation. Intrapreneurship opportunities come from innovations in production technology or business paradigms. New Venture with high technology or business model innovation can launch green products to break the existing market equilibrium, which can create green and low-carbon eco-environment opportunities.

Venture Resources. Resources are the foundation of entrepreneurial practice [5]. Ecological entrepreneurial resources are divided into two types: patchwork and coupling. Some new ventures lack resources are difficult to access external resources, so they can only piece together the resources at hand to implement eco-entrepreneurship. By patchwork resources, new ventures can not only reduce production and operation costs, but also tap the potential of resources to create higher environmental benefits. Some new ventures have certain market or technical resources, and therefore tend to couple similar resources to form resource advantages. With coupling resources, new ventures can efficiently develop green technologies or open up green markets.

Entrepreneurial team. The team is the leader of entrepreneurial behavior. According to the similarities and differences between team members' professional experience and knowledge background, the eco-entrepreneurship team mainly divided into heterogeneous teams and homogeneous teams. Some studies insist that heterogeneous entrepreneurial teams have multiple knowledge reserves [6], which can help new ventures improve existing technologies and products, thereby reducing waste of resources and reducing threats and impacts on the environment. Some studies believe that heterogeneous entrepreneurial teams have low goal consistency, and some entrepreneurs tend to pursue increased financial or investment dividends rather than generating environmental performance [7]. Relatively speaking, homogeneous entrepreneurial team can form a consistent ecological value, thereby promoting enterprises to focus resources on ecological entrepreneurship activities.

RESEARCH DESIGN

Questionnaire design and data collection (1) Questionnaire design. The questionnaire consists of two parts, the first part is the basic information of entrepreneurs and the type of entrepreneurship survey, which mainly includes gender, age, education, and so on. Among them, the measurement of entrepreneurial type mainly draws on the research of Schaltegger (2002) [8], and uses the item "Create environment-friendly new venture for the purpose of greening" to judge whether it belongs to ecological entrepreneurship. The second part is the measurement items of entrepreneurial opportunities, entrepreneurial resources, entrepreneurial teams and environmental performance, all measured by the Likert 7-level scale.

(2) Data recovery and sample characteristics. Questionnaire surveys were conducted in the three major entrepreneurial regions of Nanjing, Suzhou, and Wuxi in China. 550 questionnaires were distributed and 398 questionnaires were retrieved. The questionnaires with high deletion rate were excluded, and 376 valid questionnaires were obtained, with an effective rate of 68.4%. The main characteristics of the sample are shown in Table 1.

Ecological entrepreneurship system model. From the research literature of the current entrepreneurial ecosystem, the construction of the entrepreneurial ecosystem model further reveals the mechanism of action among the intrinsic elements. The model builds a model of a sustainable eco-entrepreneurship system that includes research universities, large corporations and informal networks, government agencies, professional services,

TABLE 1
Sample characteristics

Gender	NO. of questionnaires	Proportion	Age	NO. of questionnaires	Proportion
Male	294	78.19%	Under 30 years old	77	20.48%
Female	82	21.81%	30-40 years old	203	53.99%
			40 years old or older	96	25.53%
Business age			Education		
Less than 6 months	70	18.62%	College and below	23	6.12%
6 months to 18 months	122	32.45%	Bachelor	199	52.93%
18 months - 36 months	184	48.94%	Master level and above	154	40.96%

talent pool elements, and natural and cultural environments (see Figure 1). The entrepreneurial ecosystem is a circular system. The creation of some entrepreneurial activities will drive more ventures, which are new into the entrepreneurial ecosystem and realize the sustainable development of the entrepreneurial ecosystem. Governments should integrate them into a holistic system that considers how all system elements interact and drive the entrepreneurial ecosystem to grow. The model emphasizes that each ecosystem formed under specific conditions and environments, and the mechanism of interaction among system elements is highly complex and heterogeneous. However, these two models study the entrepreneurial ecosystem from a static perspective, ignoring the dynamic evolution of the origin, development, and self-sustainability of the entrepreneurial ecosystem.

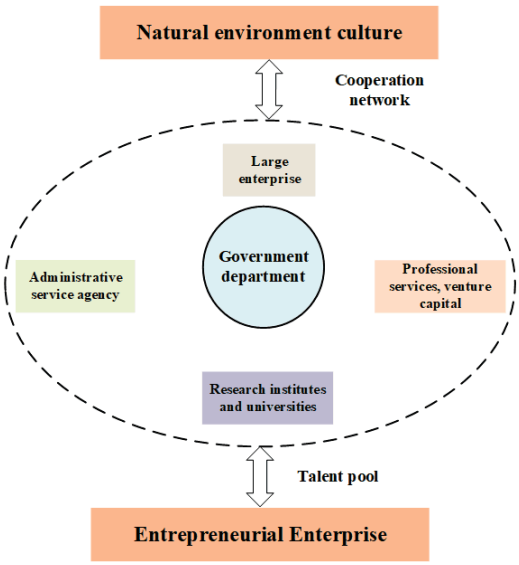

FIGURE 1
Eco-entrepreneurship system model

Variable Measurement and Reliability and Validity Analysis. (1) Variable measurement. In order to ensure the reliability and validity of the measurement items, this paper draws on the existing maturity scale and trims some items through semi-structured interviews. Among them, the entrepreneurial opportunity measurement mainly draws on the research of Korsgaard (2016) [7] and Suddaby (2015) [8]. The venture resource measurement mainly draws on the research of Baker and Nelson (2005) [9]. The survey item draws on the research of Linton (2017) [10]. The environmental performance measurement items mainly refer to the P1, P2, and P3 items in terms of energy conservation and emission reduction (see Table 2).

(2) Reliability and validity analysis. First, the Cronbach α coefficient and *CR* combined reliability coefficient are used to measure the consistency and combination reliability of entrepreneurial opportunities, entrepreneurial resources, entrepreneurial teams, and environmental performance variables. It can be seen from Table 2 that the two sets of coefficients corresponding to the four variables are all greater than 0.7, indicating that the consistency and the combined reliability of each variable are good. Secondly, the exploratory factor analysis and the average variation extraction (*AVE*) square root are used to measure the structural validity, discriminant validity and convergence validity of the questionnaire. It can be seen from Table 2 that in the entrepreneurial opportunity, entrepreneurial resources, entrepreneurial team and environmental performance variables. The load values of each factor are greater than 0.6, and the variance interpretation of each variable is higher than 70%, indicating that the structural validity is good. The AVE square root of each variable is greater than 0.5, which is higher than the correlation coefficient among the variables, indicating that the discriminant validity is good. It can be seen from Table 3 that the values X^2/df of each variable are all less than 5, the GFI values, *IFI,* and *CFI* values are all greater than 0.9, the NFI values are all greater than 0.8, and the RMSEA values are all less than 0.1, indicating that the convergence validity is good.

RESULTS

Analysis of the relationship between new urbanization and sustainable development. Opportunities, resources, and team elements in a new venture's eco-entrepreneurship interact. Therefore, this paper analyzes the eco-entrepreneurial element structure of high environmental performance start-up enterprises through fuzzy set qualitative comparison analysis (FsQCA). This is because the FsQCA method is based on set theory and is suitable for analyzing multi-element structures with interactive relationships.

Data analysis was performed using FsQCA3.0 software. First, the full membership, the intermediate point, and the complete non-affiliation anchor point is set, and the sample data converted into a fuzzy score set in the interval [0, 1]. Since the entrepreneurial opportunity, entrepreneurial resources, entrepreneurial team, and environmental performance variables are all based on the Likert seven-point scale, refer to the study of *Coduras* (2016) [11], 7 is set to the full membership point, 4 is set to the intersection, and 1 is set to the complete non-affiliation point. Secondly, the fuzzy score set is transformed into Boolean logic algebra, and the consistency threshold constructs the truth table. Referring to the research of Ragin (2006) [12], 0.75 is set as the consistency threshold, 1 is the case threshold, and 204 high environmental performance ecological entrepreneurship cases are formed. Finally, based on the intermediate solution of the calculation results, the eco-entrepreneurship

TABLE 2
Summary of reliability, validity and factor analysis of variables

Variable Dimension	factor	Item	PCA Factor load	Variance interpretation	CR combination Reliability coefficient	AVE Square root	Cronbach' sα Reliability coefficient
Business opportunity	Pedunculated	O1 enterprises search for eco-entrepreneurial opportunities discovered by market demand information	0.85				
	Intrapreneurship type	O2 business innovation technology or business model created by ecological entrepreneurship opportunities	0.869	77.51%	0.786	0.781	0.783
Venture resources	Patchwork	R1 companies put together the entrepreneurial resources formed by the resources at hand	0.815				
	Coupling type	R2 enterprise based on high-quality resources coupled with entrepreneurial resources	0.8	72.63%	0.805	0.79	0.795
Entrepreneurial team	Heterogeneous	T1 members Entrepreneurial team with different professional experience and knowledge background	0.874				
	Homogenous	T2 members Entrepreneurial team with small differences in professional experience and knowledge background	0.781	70.17%	0.798	0.765	0.754
Environmental performance	Energy saving	P1 reduces the consumption of non-renewable resources	0.889				
	Emission reduction	P2 reduces emissions of waste gas, waste residue and wastewater	0.891	80.33%	0.881	0.901	0.890
		P3 reduces the use of dangerous, toxic and hazardous materials	0.854				

TABLE 3
Summary of Fitting Indicators for Variables

Test indicator	X^2/df	GFI	NFI	IFI	CFI	RMSEA
Business opportunity	3.596	0.954	0.945	0.952	0.975	0.077
Venture resources	2.371	0.929	0.909	0.941	0.924	0.064
Entrepreneur	2.310	0.918	0.899	0.937	0.924	0.053
Environmental performance	2.360	0.910	0.819	0.921	0.932	0.052
Threshold	<5	>0.9	>0.8	>0.9	>0.9	<0.1

TABLE 4
Structure of eco-entrepreneurship elements of high environmental performance new ventures

Ecological entrepreneurship	Structure 1	2
Pedunculated opportunity	●	
Intrapreneurship opportunity		●
Patchwork resource	●	□
Coupling resource		●
Heterogeneous team		●
Homogeneous team	●	
Consistency	0.829	0.791
Coverage	0.181	0.192
Overall consistency		0.818
Overall coverage		0.362

element structure of the high environmental performance start-up enterprise is established (as shown in Table 4). In the table, symbol ● indicates the core entrepreneurial element [13].

According to Table 4, there are two main types of eco-entrepreneurship elements for new ventures with high environmental performance. In Structure 1, new ventures have pedunculated entrepreneurial opportunities, patchwork-type entrepre-

neurial resources, and homogeneous entrepreneurial teams. Among them, pedunculated entrepreneurial opportunities are the leading elements for such new ventures to carry out ecological entrepreneurial activities, which achieve higher environmental performance. Specifically, in the context of economic and social energy consumption and environmental pollution, the government and consumers are increasingly concerned about and support environmentally friendly economic activities, thus providing opportunities for ecological entrepreneurship. For example, the government promulgated policies and regulations to provide financial incentives and tax breaks for eco-entrepreneurial activities of new ventures, which provide market endorsements for eco-products and services of new ventures through government procurement. Under the constraints of resources, in order to grasp the opportunities of external entrepreneurship in a timely manner, new ventures tend to piece together the resources of entrepreneurship at hand and form a startup team with higher homogeneity. By patchwork-type entrepreneurial resources, new ventures can reduce resource time and financial acquisition costs on the one hand, which expands the scope and combination of resources on the other hand, thereby reducing resource consumption. By the formation of homogeneous entrepreneurial team, new ventures can build an entrepreneurial culture centered on ecological values, thereby enabling them to focus resources on developing eco-entrepreneurship projects and stick to the environmental bottom line when economic value conflicts with environmental values.

In Structure 2, new ventures have intrapreneurship entrepreneurial opportunities, coupling entrepreneurial resources, and heterogeneous entrepreneurial teams. Among them, coupling entrepreneurial resources are the basis for such new ventures to carry out ecological entrepreneurial activities and achieve higher environmental performance. Specifically, such new ventures adopt coupling resources to form market or technology advantages, launch green products, thereby changing the traditional market structure and technology paradigm, thereby creating opportunities for ecological entrepreneurship. Because of the innovative and leading nature of the opportunities for such new ventures, heterogeneous entrepreneurial teams are needed. This is because a team with higher heterogeneity can provide a multi-innovation perspective for enterprises, and on the other hand, it can provide enterprises with rich innovation resources based on their prior knowledge and network relationships.

DISCUSSION

Compared with other regions, the new-type urbanization in Yunnan Province has a general trend and its own characteristics. The new-type urbanization in Yunnan Province is similar to the Yangtze River Basin. The coupling level of new-type urbanization and the ecological environment shows a trend of rising first and then decreasing. Yunnan's new-type urbanization generally belongs to a state where the level of ecological environment development lags behind the new-type urbanization, which is similar to the development trend in the Northeast, but it is quite different from the pattern of the lagging cities in the Yangtze River Economic Belt. In addition, in terms of the factors that influence the coupling of new urbanization and the ecological environment, factors such as economic development level, technological innovation, and financial investment are more significant, which is more consistent with the Yangtze River Delta urban agglomeration. The impacts of urbanization and the Yangtze River Delta urban agglomeration are inconsistent, and there are differences in the upstream, middle, and lower reaches of the new urbanization in Yunnan Province. The main reason is that the overall economic strength and development level of new-type urbanization in Yunnan Province is far from that of the Yangtze River Delta city cluster. Within the new type of urbanization in Yunnan Province, the unbalanced development of related provinces in the downstream regions represented by Shandong and the western upstream regions is more prominent. In general, although the new-type urbanization in Yunnan Province has made considerable progress in economic and social development in recent years, and the level of urbanization has been continuously improved, due to the extensive development mode and heavy industrial structure, the pressure on the ecological environment has become increasingly serious. Yunnan's new urbanization strategy of ecological protection and high-quality development comes at the right time. The new urbanization of Yunnan Province urgently needs to change the development mode through the conversion of new and old kinetic energy, industrial structure adjustment and transformation and upgrading, and the cultivation of emerging industries to accelerate the promotion Coordinated development of industrialization, urbanization and ecological environment.

CONCLUSION

Based on the perspective of entrepreneurial process, this paper analyzes the types of eco-entrepreneurship elements of Chinese new ventures, which adopt the fuzzy set comparative analysis method (FsQCA) to analyze the eco-entrepreneurship elements of high environmental performance new ventures. The results show that: (1) Eco-entrepreneurial opportunities are divided into Pedunculated and intrapreneurship types, eco-

entrepreneurial resources are divided into patchwork and coupling, and eco-entrepreneurship teams are divided into heterogeneous and homogeneous types. (2) New environmental enterprises with high environmental performance have two main types of ecological entrepreneurial elements. The first category mainly includes pedunculated entrepreneurial opportunities, patchwork-type entrepreneurial resources, and homogeneous entrepreneurial teams, of which pedunculated entrepreneurial opportunities are the leading elements of eco-entrepreneurship activities. The other category mainly includes intrapreneurship entrepreneurial opportunities, coupling entrepreneurial resources, and heterogeneous entrepreneurial teams. The main innovations of the article are as follows. 1) From the perspective of entrepreneurial ability, explore the factors that generate high green entrepreneurial performance. Existing research rarely starts from the perspective of entrepreneurs. 2) Existing research on capabilities and performance mainly starts from a single latitude, and does not take into account the mutual influence of capabilities. Based on this, the existing research mainly uses the linear regression method, and this article innovatively uses the FsQCA research method. Coupling entrepreneurial resources are the basic elements of eco-entrepreneurship activities. New-type urbanization theory and empirical research are rich, but lack of research on new-type urbanization and sustainable development, and there are biases in the research area, and less research on the development of urbanization in less developed areas. This article studies the new urbanization and sustainable development of Yunnan Province, and analyzes its spatial-temporal coupling relationship, in order to provide scientific reference for promoting the urban and rural overall development of Yunnan Province.

REFERENCES

[1] Guo, Y.T., Wang, H.W., Nijkamp, P., Xu, J.G. (2015) Space-time indicators in interdependent urban- environmental systems: A study on the Huai River Basin in China. Habitat Internationa. 45, 135-146.

[2] Fang, C.L., Cui, X.G., Liang, L.W. (2019) Theoretical analysis of urbanization and eco-environment coupling coil and coupler control. Acta Geographica Sinica. 74(12), 2529-2546.

[3] Bai, X.M., Mcphearson, T., Cleugh, H., Tong, X., Zhu, T., Zhu, Y.G. (2016) Linking urbanization and the environment: Conceptual and empirical advances. Annual Review of Environment & Resources. 42(1), 215-240

[4] Arend, R.J. (2014) Promises, Premises. An Alternative View on the Effects of the Shane and Venkataraman 2000 AMR Note. Journal of Management Inquiry. 23(1), 38-50.

[5] Dean, T.J., Mcmullen, J.S. (2007) Toward a theory of sustainable entrepreneurship: Reducing environmental degradation through entrepreneurial action. Journal of Business Venturing. 22(1), 50-76.

[6] Ehnert, D. I. (2009). Theorising on Strategic HRM from a Sustainability Approach. Sustainable Human Resource Management. 1, Physica-Verlag GmbH & Co, Heidelberg, 110-120.

[7] Buyl, T., Boone, C., Hendriks, W., Matthyssens, P. (2011)Top Management Team Functional Diversity and Firm Performance: The Moderating Role of CEO Characteristics: TMT Functional Diversity and CEO Characteristics. Journal of Management Studies. 48(1), 151-177.

[8] Haleblian, J., Finkelstein, S. (1993) Top Management Team Size, CEO Dominance, and Firm Performance: The Moderating Roles of Environmental Turbulence and Discretion. Academy of Management Journal. 36(4), 844-863.

[9] Schaltegger, S.A (2009) Framework for Ecopreneurship: Leading Bioneers and Environmental Managers to Ecopreneurship. Social Science Electronic Publishing. 38(38), 45-58.

[10] Korsgaard, S., Berglund, H., Thrane, C., Blenker, P. (2016) A Tale of Two Kirzners: Time, Uncertainty, and the "Nature" of Opportunities. Entrepreneurship Theory & Practice. 40(4), 591-600.

[11] Suddaby, R., Bruton, G.D., Si, S.X. (2015) Entrepreneurship through a qualitative lens: Insights on the construction and/or discovery of entrepreneurial opportunity. Journal of Business Venturing. 30(1), 1-10.

[12] Baker, T., Nelson, R.E. (2005) Creating Something from Nothing: Resource Construction through Entrepreneurial Bricolage. Administrative Science Quarterly. 50(3), 329-366.

[13] Linton, G., Kask, J. (2017) Configurations of entrepreneurial orientation and competitive strategy for high performance. Journal of Business Research. 70(1), 168-176.

[14] Coduras, A., Clemente, J.A., Ruiz, J. (2016) A novel application of fuzzy-set qualitative comparative analysis to GEM data. Journal of Business Research. 69(4), 29-35.

[15] Ragin, C.C. (2006) Set Relations in Social Research: Evaluating Their Consistency and Coverage. Political Analysis. 14(3), 291-310.

[16] Brown, D.K. (2010) Redesigning Social Inquiry: Fuzzy Sets and Beyond by Charles C. Ragin. Social Forces. 88(4), 1936-1938.

Received: **12.10.2019**
Accepted: **19.02.2020**

CORRESPONDING AUTHOR

Liying Lei
Commercial College,
Hohai University,
Nanjing, 211100 – China

e-mail: leiliying_hhu@163.com

© by PSP Volume 29 – No. 05/2020 pages 4056-4061 Fresenius Environmental Bulletin

NOTICE

STUDY ON THE RELATIONSHIP BETWEEN FINANCIAL ECOLOGICAL ENVIRONMENT AND REGIONAL ECONOMIC DEVELOPMENT

Lan Liu*

Anhui Finance and Trade Vocational College, Hefei, 230601, China

ABSTRACT

The natural environmental degradation is specifically challenging in rapid urbanization areas where social economic development needs to swallow large amounts of resources and emit a great deal of pollutants (wastewater, solid wastes, and air pollutants). Coordinated development of social economic development and ecological environmental development is very necessary for sustainable urban development. In order to improve the comprehensive benefits, a sustainability evaluation method for multi-objective remanufacturing system synthesis based on economy and environment is proposed in this paper. Coordination assessment results based on the model show that Hefei shows a good coupling coordinated degrees, presenting harmonious relationship between advanced social economy and sound eco-environment. This study will provided a guidance for promoting sustainable development.

KEYWORDS:
Financial environment, Coordination assessment, Model,

INTRODUCTION

In recent decades, increasingly severe energy consumption and environmental pollution have attracted worldwide attention [1]. Fully realizing energy saving and low carbon of manufacturing industry and its products has become an inevitable trend in the development of manufacturing industry [2].

The climate change and related costs caused by the use of fossil fuels are worrying, and governments and enterprises are actively looking for countermeasures [3-5]. Seeking better clean energy as an alternative is a viable option [6,7]. Sustainable development has become a global consensus now. With technological progress and policy implementation, energy efficiency has been improved, which leads to lower energy consumption and environmental impact while achieving higher economic benefits [8,9]. In the early 1990s, the United States has established the National Center for Remanufacturing and Resource Recovery (NC3R), the Remanufacturing Institute (TRI) and other institutions. In 2000, the European Parliament and the Council of the European Union adopted the end-of-life Vehicle (ELV) Directive, which encouraged the reuse of scrap automobile parts. Waste Electrical and Electronic Equipment (WEEE) is a guiding policy and standard for the recycling and utilization of some electrical and electronic products [10]. The European Union already has legislation to regulate landfills for solid waste. In 2005, the Act of Recycling Scrap Vehicle was formally implemented in Japan. The act ensures the smooth progress of recycling and reusing of end-of-life vehicles in Japan.

The sustainable development of ecological environment and social economy has always been the focus of attention in the world [11-14]. The coordinated development of ecological environment and social economy was the common responsibility and pursuit of the international community. China, as the largest developing country in the world, has created the "miracle of China" at an average annual rate of 9.8% over 30 years of reform and opening up, but at the same time, "high investment, high pollution and high emissions" model has also led to a series of environmental problems. Environment pollution and ecological destroy gradually evolved into constraints of China's economic and social sustainable development of the outstanding obstacles [15-17].

It is urgent to develop clear information evaluation models to simulate the relationship between ecological environment and social economic development for management and decision-making basis. In summary, this study presents a method to model the dynamic interactions and future development of the urban system. Comparisons with existing results and policy recommendations are provided in this paper.

MATERIALS AND METHODS

Study area. A city with over 2200 years of history, Hefei was still a small city with a popula-

tion of only around 50,000 people in 1949 when the People's Republic of China was established. By the end of 2016, however, this city had grown into a metropolitan city with a permanent resident population of 7.87 million, covering a territorial area of 11,408 km2. Hefei's city proper has four administrative districts — Yaohai, Luyang, Shushan, and Baohe. The metropolitan region of Hefei also includes four additional counties (i.e., Feidong, Feixi, Changfeng, and Lujiang) and one county-level city (i.e., Chaohu). In 2014, the State Council positioned Hefei as a sub-center city of the Yangtze River Delta city-region, which meant that Hefei would be included, along with eastern coastal cities, such as Nanjing, Hangzhou, Suzhou, and Ningbo, in the Yangtze River Delta's national-level strategy pertinent to city-region coordination.

Evaluation of the coupling coordination degree. Assessment indicator system for the economy–environment system. Social and economic developments and environmental changes have similar stages of production, development, and maturity. The interrelationships between them can be described by growth curves. Therefore, the definition of social, economic and environmental coordinated development index is:

$$k = \frac{1}{1 + k\mathrm{e}^{-ds\ de}} \quad (1)$$

In the formula, d_S, d_e and k are the social, economic development and ecological environmental damage states under the identified evaluation criteria. The minimum value of dS, de, and k is 0.1, and the maximum value is 1. Therefore, from formula (1), when the social and economic development situation is small $d_S=d_e=0.1$), and the ecological environment function damage state is large, that is, the pollution is serious (k=1), the three coordinated development index kmin= 0.50; and when the social and economic development situation is large ($d_S=d_e=1$), the ecological environment function damage state is small, that is, when the pollution is light (k=0.1). The three coordinated development index kmax=0.97; and when $d_S=d_e=k=0.5$, k=0.72. By analyzing the k value when k, d_S, and d_e take certain values, the correspondence between the value range of k and the coordinated development evaluation result is:

RESULTS AND DISCUSSION

Coordinated relationship between social, ecological environment and economy. Urban ecological environment and its social economic development are interacted with one another widely. Improving the level of urban social economic development is beneficial to increasing the investment on improving the technology level of urban public pollution control infrastructures and other facilities. While raising technology level is useful for energy consumption reduction, cutting down pollution emissions, and urban environment improvement. The wonderful urban environment is in favor of improving the health situation of urban inhabitants and drawing population inflow which helps stimulate the economy and provide labor for social development. Moreover, good urban social development usually means beautiful landscape and complete facilities which beautifies urban natural environment; this helps to attract investment and promote the development of tourism industry Fig.1 -3 shows that the highest k value is 0.895, the smallest is 0.834, indicating it has good eco-environment development and has a bigger ecological carrying capacity or environmental capacity, meanwhile their industrial development is at the development stage. It has a good natural condition and has made great achievements in the construction of ecological civilization.

Fig. 4-6 show the spatial variation. It has the most harmonious relationship between social-economic subsystem and eco-environmental subsystem. Since 2015, Hefei has formulated and implemented "Hefei Blue Sky Plan ". According to the source analysis of PM2.5, it has focused on key areas such as reducing coal burning, reducing oil consumption by controlling vehicles, pollution control, emission reduction, and dust removal, and comprehensively promotes the scientific treatment of air pollution. In 2018, PM2.5 in air dropped by 25.4% compared with that of 2015. The total annual coal use in Hefei was reduced to less than 15 million tons.

TABLE 1
Evaluation results

k	(0.97, 0.85]	(0.85, 0.72]	(0.72, 0.60]	(0.60, 0.50]
Evaluation results	Coordinated development	Basic coordinated development	Weak coordinated development	Uncoordinated development

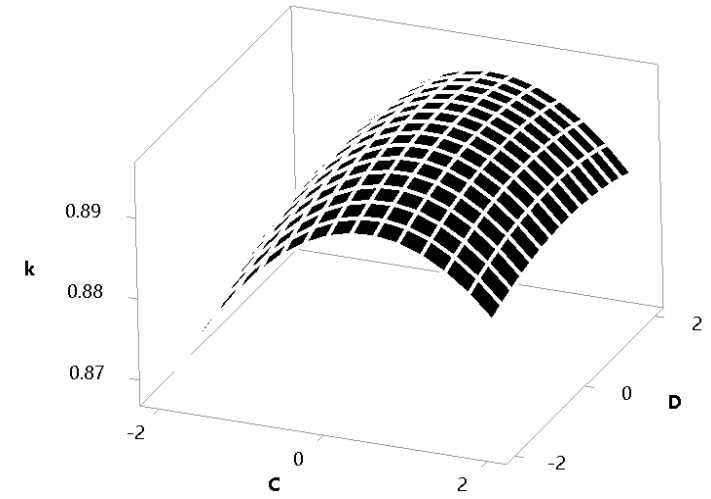

FIGURE 1
Surface Plot of k vs D, C

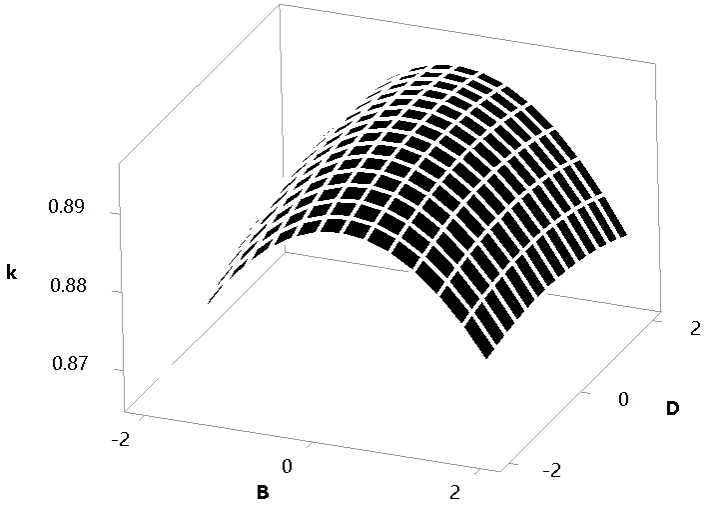

FIGURE 2
Surface Plot of k vs D, B

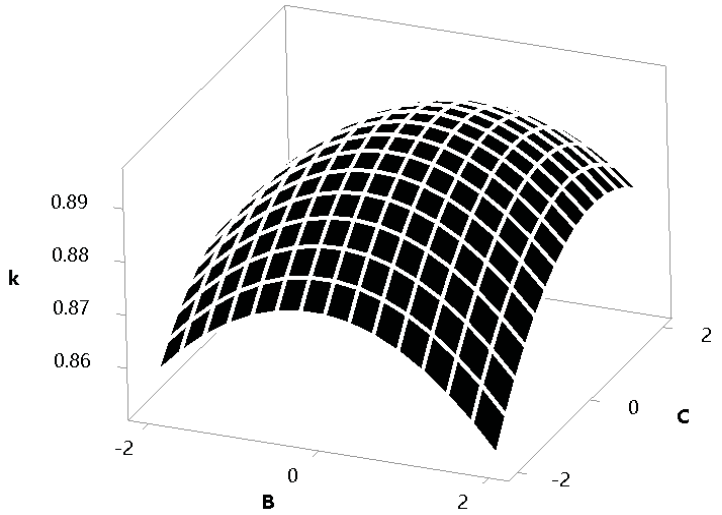

FIGURE 3
Surface Plot of k vs C, B

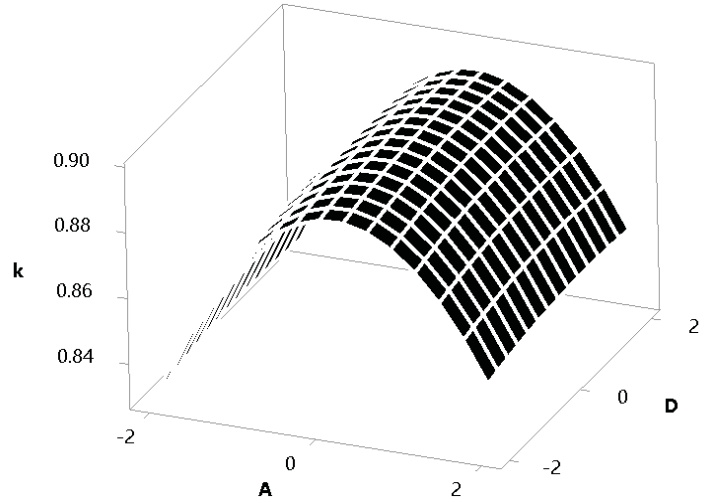

FIGURE 4
Surface Plot of k vs D, A

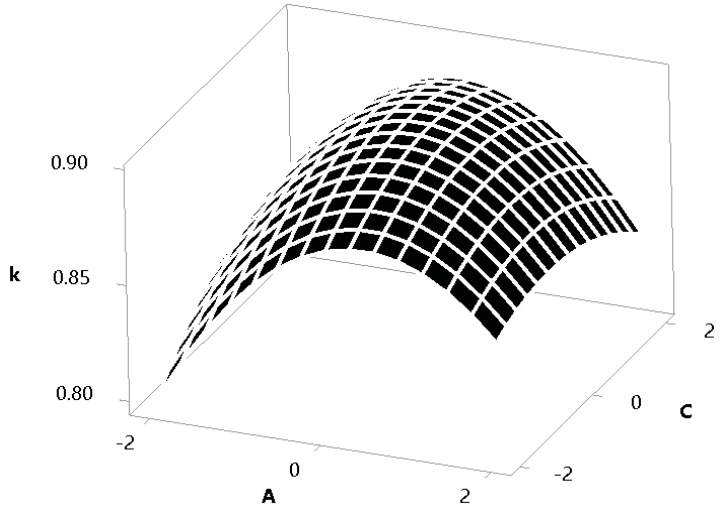

FIGURE 5
Surface Plot of k vs C, A

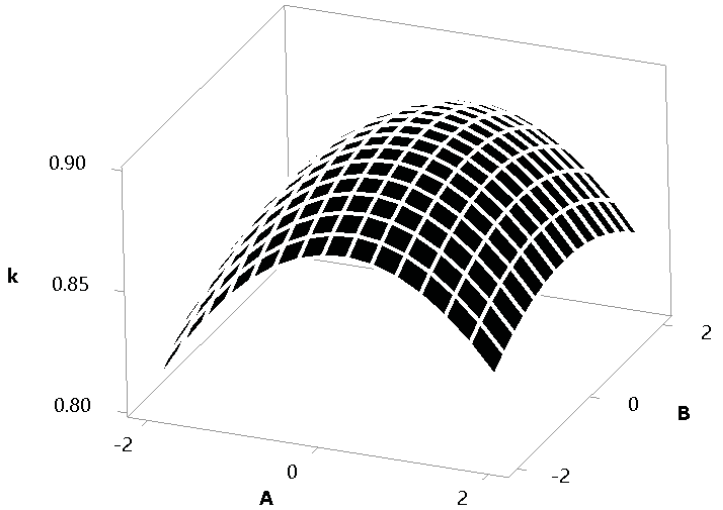

FIGURE 6
Surface Plot of k vs B, A

CONCLUSIONS

This study combines the method and theory to analyse and assess the simulated results of the economy–environment system in Hefei City. Coordination assessment results based on the model show that Hefei shows a good coupling coordinated degrees, presenting harmonious relationship between advanced social economy and sound eco-environment. This study will provided a guidance for promoting sustainable development.

Evaluation indicator system and coupling model used in our study lay particular emphasis on results and representation, and lack the in-depth exploration of process mechanism. The next step is to probe into the process mechanism of coupling by quantitatively analyzing the relationships among various systems.

REFERENCES

[1] Caliskan, H. (2015) Novel approaches to exergy and economy based enhanced environmental analyses for energy systems. Energy Convers. Manag. 89, 156-161.

[2] Spokas,, K.A., Cantrell, K.B., Novak, J.M., Archer, D.W., Ippolito, J.A., Collins, H.P., Boateng, A.A., Lima, I.M., Lamb, M.C., McAloon, A.J., Lentz, R.D., Nichols, K.A. (2012) Biochar: a synthesis of its agronomic impact beyond carbon sequestration. J. Environ. Qual. 41, 973-989.

[3] Mofijur, M., Atabani, A.E., Masjuki, H.H., Kalam, M.A., Masum, B.M. (2013) A study on the effects of promising edible and non-edible biodiesel feedstocks on engine performance and emissions production: a comparative evaluation. Renew. Sustain. Energy Rev. 23, 391-404.

[4] Yusuf, N.N.A.N., Kamarudin, S.K., Yaakub, Z. (2011) Overview on the current trends inbiodiesel production. Energy Convers. Manag. 52, 2741-2751.

[5] Cui, Y., Zhu, J., Meng, F. (2018) Techno-economic evaluation of multiple energy piles for a ground-coupled heat pump system. Energy Convers. Manag. 178 , 200-216.

[6] Maroušek, J. (2014) Biotechnological partition of the grass silage to streamline its complex energy utilization. Int. J. Green Energy. 11, 962-968.

[7] Maroušek, J., Stehel, V., Vochozka, M., Maroušková, A., Kolář, L. (2018) Postponing of the intracellular disintegration step improves efficiency of phytomass processing. J. Clean. Prod. 199, 173-176.

[8] Liu, C., Cai, W., Jia, S., Zhang, M. Guo, H., Hu, L., Jiang, Z. (2018) Emergy-based evaluation and improvement for sustainable manufacturing systems considering resource efficiency and environment performance. Energy Convers. Manag. 177, 176-189.

[9] Wang, H., Jiang, Z., Wang, Y., Zhang, H., Wang, Y. (2018) A two-stage optimization method for energy-saving flexible job-shop scheduling based on energy dynamic characterization. J. Clean. Prod. 188, 575-588.

[10] Yang, J., Lu, B., Xu, C. (2008) WEEE flow and mitigating measures in China. Waste Manag. 28, 1589-1597.

[11] Garry, S., Peter, N. (2016) The evolution of sustainable remediation in Australia and New Zealand: A storyline. J. Environ. Manage. 184 (15), 27-35

[12] Broman, G.I., Robèrt, K.H. (2017). A framework for strategic sustainable development. J. Cleaner Prod. 140, 17-31

[13] Jia, X., Foo, D.C.Y., Tan, R.R., Li, Z. (2017) Sustainable development paths for resource-constrained process industries. Resour. Conserv. Recycl, 119, 1-3.

[14] Siva, V., Gremyr, I., Bergquist, B., Garvare, R., Zobel, T., Isaksson, R.. (2016) The support of quality management to sustainable development: a literature review. J. Cleaner Prod. 138, 148-157.

[15] Boggia, A., Rocchi, L., Paolotti, L., Musotti, F., Greco, S. (2014) Assessing rural sustainable development potentialities using a dominance-based rough set approach. J. Environ. Manage. 144(1), 160-167.

[16] Wang, Q., Yuan, X., Cheng, X., Mu, R., Zuo, J. (2014) Coordinated development of energy, economy and environment subsystems-a case study. Ecol. Indic. 46 (6), 514-523.

[17] Yang, Z., Jing, S., Feng, D., Yu, L., Li, H. (2016) Vulnerability assessment of atmospheric environment driven by human impacts. Sci. Total Environ. 571 (15), 778-790.

Received: **19.10.2019**
Accepted: **23.01.2020**

CORRESPONDING AUTHOR

Lan Liu
Anhui Finance and Trade Vocational College,
Hefei 230601 – China

e-mail: gaoxing887qq@163.com

© by PSP Volume 29 – No. 05/2020 pages 4062-4075 Fresenius Environmental Bulletin

NOTICE

INCORPORATION OF INFORMATION: COMMUNICATION TECHNOLOGIES IN ECONOMIC AND ENVIRONMENTAL ESPIONAGE

Slobodan Neskovic[1], Anastazija Tanja Djelic[2], Ratomir Antonovic[3] , Mitar Lutovac[4], Sonja Ketin[5,*]

[1]University Business Academy in Novi Sad, Cvecarska 2, Novi Sad, Serbia
[2] Union Nikola Tesla University Belgrade, Faculty of Law, Security and Protection "Konstantin Veliki" of Nis, Serbia
[3]International University of Gorazde, Faculty of Law, Bosna and Herzegovina
[4]Faculty of management, Njegoseva 1a, Sremski Karlovci, Serbia
[5]Faculty of Maritime Academic Studies Belgrade, Bulevar Vojvode Misica 37, Belgrade, Serbia

ABSTRACT

Modern education must be of high quality and productive, that is, complementary to accelerated changes in everyday life. Innovation, the basis of which is human knowledge, is universally accepted as a key factor of growth and development in the globalized world. Information and communication technologies, on the one hand, have demolished spatial and temporal barriers, but have, on the other hand, increased integration and interdependence in the world. Many professions today depend on computer technology and technological awareness that have become key skills for professional success. The impacts of new technologies are increasing, both on a personal, corporate, national and global level. Therefore, every modern society has to invest as much of its resources into human and information and communication potential as education, skills, knowledge and business in the network have become key components of productivity of individuals and the economy as a whole. Evidence for this is many developed countries that have achieved their progress precisely thanks to investments in these areas as well as using knowledge and skills of their own human resources. Because of the easily accessible information that is at hand to all interested parties, there has been an expansion of economic espionage as an indispensable part of economic warfare.

KEYWORDS:
Information technologies, technological progress, economic espionage, incorporation, education, globalization, business

INTRODUCTION

Economic (somewhere used term industrial) and environmental spying is a collection of very delicate, planned and professionally performed activities to obtain confidential economic and environmental information for the benefit of business projects of your own company or the protection of the economic and environmental interests of your country. The objective of using economic and environmental espionage is to study competitive firms or countries, business projects and research new products, achieve a competitive position, conquer new markets, and compete in new jobs and "dominance" in the world market. The first spy tasks were predominantly military or war nature, which laid the foundations for the later expansion of this activity. When a company launches economic and environmental espionage activities, it has the ultimate goal of discovering the business secrets of another company. "The word secret (le secret), according to the French word Le Petit Robert, means - a set of knowledge and information that must be reserved for a narrow circle of individuals and which the mediator must not disclose. Within this term, the term "secret professional ou de fabrication" is defined as the narrow term, which means a recipe or one of the formulas (modes) of production that must be secret and known only by the manufacturer.

With this concept, a series of derivatives are connected, such as a secret agent, a secret police, a state secret. One of the types of business secrets is the production secret, which is nothing other than: the formula, scheme, invention or solution applied in the business, and the company that comes to this information can use them to improve the competitive advantage over companies from the same or similar activities who do not know them and do not use them. The business secret protects all production, commercial, financial, marketing and technical-technological advantages that the company has in relation to market competition. For this reason, in every company, employees are obliged to keep a business secret during the working relationship in the company, even after its termination. Business secret can only be disclosed at the justified request of the authorized persons and the com-

petent authorities and may be done by persons authorized by the company's general acts.

Today, in the 21st century, we live in a world marked by various changes and the effects of various phenomena on society and individuals in it, which are the result of the process of globalization. Globalization is a set of different processes that basically have the idea of developing and connecting the world. It can be seen from different angles, so it is often defined as a term, form and phenomenon that implies multiple and drastic changes in all dimensions of life. It has the ability to make changes and involve the whole world in those changes. In this process, one of the largest roles is information and communication technologies, which create a global network among people in different parts of the world. In the meantime, the transition of the focus of the activities of employees from the processing of materials to the processing of information has a major impact on the education process. In a globalized world, higher education has become the pillar of society and depends on its quality on the future of each country [1].

THE IMPORTANCE AND APPLICATION OF INFORMATION-COMMUNICATION TECHNOLOGY IN BUSINESS

Knowledge has always had a central role in the development of human society. Today it is precondition for the processes of innovation, the application of new ideas and the creation of goods. Progress in information and communication technologies has further strengthened the link between knowledge and overall development. Information and communication technologies are the infrastructure of the new Knowledge Economy and Environmental, is the Internet, i.e. Digital Economy. These technologies can significantly change, reorganize and fundamentally restructure existing working methods, processes and ways of doing business. Over the past few decades, we have witnessed a significant increase in the use of information and communication technologies that significantly affect all forms of human activity. The process of globalization and changes in the field of technology has significantly influenced the changing of today's world. The rapid development and application of information and communication technologies have led to a transformation from the industrial to the information age that has transformed almost all spheres of life. The advancement of these technologies has enabled the free movement of people, capital and the erosion of many borders. Networked computers, e-mail, internet, databases, electronic publications, electronic conferences, digital bookstores, on-line search engines, etc. are just some of the trends that affect everyday life and work.

Terms such as information society, internet economy, network, virtual environment, cyber space, etc. they entered everyday use. Under the influence of globalization, information and communication technologies are spreading rapidly in the world for several decades and "forced" to use the Internet in the realization of business as well as everyday activities. The notion of information and communication technologies is a common term for the study of assets, procedures and methods for managing, storing, processing, transmitting and presenting data and information. This definition indicates a strong link between information technologies and communication, both in technological and organizational terms.

Today's functioning takes place in the information society, so that successful life and business cannot be imagined without computers and other digital technologies. The number of Internet users in the world is constantly increasing, so everyone wants to capitalize on the great potential of the internet business. This conditioned the emergence and development of e-business as a new business activity. The development of information and communication technologies and the global, interdependent and integrated world market are crucial for the growth of business in a virtual environment. Society as a whole is faced with accelerated communication and constant increase of knowledge,

TABLE 1
Strategic potential of information-communication technologies in business

Innovation	ICT encourages innovation and the creation of a competitive advantage.
The structure of business processes	ICT transforms unstructured processes into routine.
Geographic spread	ICT makes it easy to transfer information that allows global visibility (365/7/24).
Automation	ICT business replaces / reduces the need for a large number of employees.
ICT ability	ICT capabilities enable the collection and processing of large amounts of information, which leads to overall business improvement.
Knowledge management	ICT knowledge management enables the creation of the so-called. "knowledge base" and their transfer in real time.
Control	ICT control facilitates the process of control, monitoring and reporting of the status of business activities through databases.
Organizational communication	ICT connects and facilitates communication between participants in the business process
Production cycle	ICT production cycle reduces the length of the production cycle, which ultimately reduces the costs of the overall business process

which leads to qualitative changes in working methods.

As can be seen from Table 1. Spatial and time constraints have been reduced or completely removed today. Business is based on new electronic information and communication technologies that create new forms of business organization. These technologies have created completely new ways of applying, using and transmitting information and their easy and fast storage. Today, information and communication technologies are the most dynamic factor in overall development. New information and communication technologies provide enormous opportunities for increasing the speed and quality of communications. This is of great importance in modern business, as it is quickly possible to get relevant information from the market. Today's world is the world of information. In this world, information is knowledge, power and capital. Information today is the most important factor in gaining advantage over competition and the basic argument of domination besides capital, labor and technology. The possession of information has become a strategic resource, so it is quite logical that the modern economy rests on the creation of information, their possession and exchange. Timely possession of important information gives priority over others. They are a powerful tool that enables the acquisition of a superior position, and in the decision-making process enable the making of quality decisions, easier navigation in the insecure world, and thus simpler achievement of goals [2].

In times of globalization and the ever-increasing and more frequent changes that occur on the market, all who want to succeed and survive have the task of adjusting to new changes. Today's circumstances require business organizations to perform as efficiently and effectively as possible. This can only be achieved by the implementation of information and communication technologies in the business process. Only in this way is today possible continuous, long-term and successful business. In times of frequent and sudden changes in trends in the world, it is necessary to constantly take care of upgrading existing information systems and the possibility of introducing new ones, which in time will lead to better results in business. The digital revolution has changed the way of production and sale of goods, providing services and transforming it almost all industrial branches. It also created a new business environment for business development that is based on the application and use of information and communication technologies. The emergence of the Internet economy has led to the development of electronic business, the essence of which is to exploit the benefits of new forms of communication. E-commerce in the broadest sense of the word represents the organization of business in the network environment, as well as the organization of business communication and care of it, while its narrower meaning can be related to conducting business on the Internet, or buying on this network [3,4].

This type of business has its roots in the seventies of the twentieth century, the emergence of an electronic transfer of cash that was taking place between banks through secure private networks. The term e-commerce was first used by an American company to name the business with the significant use of electronic technology. At the time, this term only concerned electronics business operations, whereas today this term is used to perform business processes using modern electronic technologies, based on the symbiosis of telecommunications and information technologies. In the eighties, two new forms of electronic business have been developed: electronic data interchange (EDI) and e-mail (e-mail). Both of these technologies have contributed to a significant reduction in the amount of paper in use and increased automation of business. Electronic data exchange enabled the sending and receiving of business documents in standard electronic form through secure private networks. Such a system has not been en masse due to high prices and additional investments (employee training, complex and inflexible software, etc.). Small and medium-sized enterprises could not afford it, so instead of private networks they used online value added services (VAN), which had programs that allow electronic data exchange.

In the nineties, the emergence of the World Wide Web (www) within the Internet, for the first time, made easy online work and easy and inexpensive publication and dissemination of information. Various forms of business are enabled, and only business has become significantly cheaper. The use of computers and networks was no longer the privilege of large and rich companies. E-commerce developed in two directions. The first was to allow companies to transfer money and information between themselves, faster and easier, was focused on their mutual cooperation. Another, more recent direction in focus has end users of products or services. Today, it is generally accepted the concept that treats electronic messaging (business transactions and information) in a trial which consists of: companies, public administration institutions and clients / consumers. In order to implement this type of work, a fast internet and developed information and telecommunication network is necessary. Additional conditions are the culture and habits of the users and the socio-economic and business environment that needs to be stable, without inflation and with regulated legislation.

From the point of view of communication, electronic commerce presents electronic delivery of information, products and services and electronic payment using computer and other communication networks. Speaking of its business aspect, it is the application of technology for the purpose of auto-

mating business transactions and business. From the point of view of services, e-commerce is a tool that reduces business costs while simultaneously increasing the quality and speed of service delivery. Or, in short, e-commerce implies the application of information and communication technologies that support all business activities. The purpose of e-commerce is to expand the market, increase the number of users and improve competitiveness. In its simplest form, electronic commerce enables you to earn more money while simultaneously saving costs and time by using information and communication technologies. More specifically, it enables achievement of goals by using cost-effective and affordable information and communication tools. It helps companies improve their products / services and gain access to customers outside the local market, increase their visibility for customers and partners, reduce marketing costs, compare products and prices, reduce costs associated with business transactions and communicate or operate without being on the local market the same location with consumers.

The rapid development of information and communication technologies triggered a revolution, both in everyday life and in business. Today, the use of these technologies in business processes is implied. The focus is increasingly on the information and content that these technologies can create which opens up new opportunities and encourages the creation of completely new content and services. The application of new technologies is no longer considered solely in terms of productivity, but also in relation to the creation of the so-called. Intangible benefits (such as customer satisfaction with a product or service). Almost all economic and non-commercial areas today rely heavily on these technologies that have become supportive of many business functions and have opened the door to innovations. With the help of information and communication technologies today, many jobs are being performed in many areas. Information and communication technologies have significantly affected the application of information systems, databases and computer networks, without which today's business is unthinkable. Although economic espionage is the notion of a newer date, other ideas, secrets and inventions in the field of production have been the subject of interest and theft for centuries. The first known activities in the field of international industrial espionage and systematic information collection are related to the earliest history. In addition to statesmen and famous conquerors, systems of this espionage have also been established by powerful families that have dominated societies for centuries. However, only the end of the Second World War and the phenomenon of economic globalization, that is, integration of the international economy, lead to the expansion of these activities.

In the past, the competition between countries and companies was sharper, the markets are more passive and customers are less demanding. Changes in the market were happening much slower (for example, Ford's T-brand model, which first appeared on the market in 1908, it was sold for 20 years in unchanged form, while today's cars are considered outdated today), jobs were made performed mainly at the local and national level, and business subjects knew almost all of their competitors. However, the time when an individual was a strategic company and when was able to track all the information and simultaneously understand the immediate environment, they passed. Companies today need to be organized on a much higher level, or in a global way. The reasons for this are, above all, in the external environment - because the company's operations today are global. Just two or three decades ago the information was direct and a businessman from any part of the world knew all of his competitors because they were mostly living in the same area. Today, thanks to the development of information-communication technologies, every job has a lot of direct competitors in every part of the planet, so everyone has to use business espionage. Otherwise, there will be no information about those who take their share of the world market.

Knowledge in today's business environment has become the most important potential of each company and the development of information technology has contributed to the whole global economy increasingly relying on intangible resources. The ultimate result of this is that a man (is his intellect) has become the center of a target of industrial espionage. In the (legal and illegal) research of competitive activities on the target, everything that brings profit is high: high technology, pharmaceutical industry, armaments industry, electronics, information technology, food industry, etc., and the activities of industrial espionage are directed, first of all, parts of national economies. This type of espionage is a collection of delicate, planned and professionally performed activities to obtain confidential information kept by competing companies in secrecy. "Economic, is industrial espionage in a modern international environment is an instrument for achieving the competitive advantage of companies, the advancement of the national economy and the realization of the national interests of each country. The use of legal and illegal means, which are very often incompatible with ethical norms of business, is aimed at eliminating competitors. Economic espionage is to get business secrets".

ECONOMIC AND ENVIRONMENTAL ESPIONAGE AND IMPLEMENTATION OF MODERN TECHNOLOGIES

The emergence a new phenomenon of economic and environmental globalization and the development of information and communication technologies have led to the emergence of economic information-based espionage. As the communication and information technology developed, so the espionage methods became more technologically advanced. This resulted in the need for highly educated human staff with specific knowledge to collect, analyze and implement the data collected. The concept of modern economic espionage is of military origin and was developed on the principles of military intelligence. Today, business is a kind of war, and the similarities between the military and business world are growing day by day. Both of them involve competition between enemies with different assets, motives and goals.

Information has always been the foundation of human action, behavior and relationship, but only by the development of science and technology, storage capabilities, rapid processing of a large number of data and communication capabilities, they demonstrate their true relevance and versatility of their uses and uses. "Modern times, channeled by the processes of globalization, are characterized by the acquisition of superiority in planetary exchanges, which is the result of not only military but also economic, technological and developmental supremacy over opponents. As once the weapon was the basic argument of domination, today it is information, as the fourth obligatory factor of production, next to capital, labor and technology. " [5,6]

Unlike all previous wars, when the priority is given to mass and weapons, today the struggle takes place through the use and use of communication-informatics-intelligent technologies. Only those who handle information can lead wars, because those who own them rule the planet. Although many are inclined to conclude that the use of communication-information technology has changed the course of warfare, that's not true. The nature of the war has not changed, what has changed is the way of waging war. Information technologies enable countries to do what they have always done, but considerably faster and more successful than before. Information warfare is actions taken to achieve information superiority through impact on other information, information-based processes, information systems and computer networks. On the other hand, information warfare includes actions of collecting and using information that are carried out both in times of peace and in times of war in order to influence opposing information and information systems. In contemporary society, the functioning of all sectors increasingly depends on information technologies and information infrastructures that represent the totality of connected computers and networks and the essential information that is being transmitted to them. Since business has become global, both the problems of storing and stealing information have become the issue of not just one company that competes with another, but also a way of economic warfare sponsored by national governments, all in order to gain advantage in the global market. Today, many countries, even those friendly ones, are leading economic wars against each other, in which economic espionage is used as the main weapon. The data obtained by this type of espionage are capital for anyone who obtains them, because it requires much less costs than is necessary for investing in the education, research and development sector, while following the technological development of others without the need of engaging a large number of experts and specialized professional cadres.

The phenomena of economics and information warfare have always been directly linked, which is particularly noticeable in contemporary international relations. Thus, for example, in the context of the economic competition in the world market, information and communications, which have always been an integral part of the strategy, tend to redefine the strategy through the concept of business intelligence, i.e. business espionage and / or business intelligence. Particularly important role of information is in the decision-making process in all areas of human activity, and so in the economic sphere. Decision makers know what their goal is and where to get, but they do not know how to reach the goal. And information is a guideline to achieving the goal; they are a key management resource. Without information and information systems, modern societies, states and the business world would not be able to provide support for their own processes. Information's that are most often targets of economic intelligence are strategic, financial, organizational, marketing, technical, technological and scientific. Primary targets include: access card codes, project information, pricing, market forecasts, various financial information, software, technology solutions, and more. Economic espionage is the totality of actions and procedures contained in the process, which is called the "intelligence cycle". It is a phenomenon that involves the complete treatment of information, from the acquisition, availability, transmission, evaluation, analysis and processing, so that it is completed as available to the holders of political activities and other actions at the national level. The stages of the intelligence cycle in the economic spy are:

1. Planning and managing economic espionage;
2. Collection of data and information;
3. Processing;
4. Analysis of all sources and production;

5. Dispensing;

In modern business conditions, it is more than obvious that, in order for a company to preserve its existence and also to improve its business, it must protect and secure its resources. Starting from the fact that the company is a part of the national economy or economy, it is clear that economic strength, strategic capacity control and security of strategic technologies are essential factors of sovereignty, national security and the concept of national interests of each country. Of course, practical work is conditioned by new scientific knowledge.

Protection of confidential data from espionage has become a necessity for every company that wants to survive and retain its supremacy in the global market. In order to achieve this, it is necessary to provide: physical security, IT security and risk management. Similarly, in order for a company to avoid becoming a victim of economic espionage, it must take the following steps:

1. Identification of business secrets - in order to protect business secrets, they must first be recognized and documented (if not documented, not protected).

2. Risk management - it is taking steps to avoid spying.

3. Training employees how to keep a business secret - keeping a business secret is of great importance for the stability of the company, and therefore for the stability of the state.

Contemporary intelligence and economic espionage for delivering information largely depend on data sources. The origin of information and data and the manner of their obtaining determine the legality and ethics, that is, the illegality and unethical nature of these activities.

Legal ways of accessing information

A large percentage of the necessary information in economic intelligence is obtained legally (even about 95%), and all the information received is carefully collected, sorted and analyzed. Legal methods of collecting information are:

- Internet - the easiest and most commonly used way of finding information. Anonymity when using the Internet is one of the reasons for its enormous exploitation when collecting confidential information.

- Search for employees - represents so-called. "Phantom interviews", where a person hired by a company is interviewing employees another company for alleged employment, and in fact, aims to extract data from employees.

- Joint venture and Mergers and acquisitions - when two firms join together, employees from both companies begin to consider they partners as result, relieve security related to important information related to the company and, therefore, facilitates access information and technology.

- Conferences, fairs, exhibitions, seminars - these events are a good place to get important information in direct contact, because experts often hire experts from governments or governments to collect information.

- Digging garbage can is a great source of information such as thrown documents, notes, and so on. That's why most companies waste sensitive paper. This form of information grabbing is completely legal because the rejected thing is not considered to be one of the properties

Illegal ways to access information

In this way, a small amount of intelligence comes to you (about 5%), but they carry a great deal of value - because they cannot be reached legally. They usually get them:

- Organized crime - (criminals do not hesitate to put pressure on business people by pressure and blackmail, and because of their power poses a serious threat to business and industry).

- Independent entrepreneurs (most often private detectives).

- Employees with the right of access - the so-called. Insiders are people who come from the same company or have access to sensitive information. They are trained professionals who are very confusing and tell the victim to give out information. As such, they represent a major security problem for companies.

- Infiltration among employees - this way represents a good way to espionage - with forged documents entering the subject of espionage.

- Employee recruitment - A mole or insider is recruited using a bribe, and once done, a specific type of information may be requested.

- Computer downturns - as computers are increasingly used to process and store data, more and more situations are "falling into" the company's systems for the illegal acquisition of information.

- Burglaries and thefts - represent a traditional way of accessing important data. They include: physical theft of documents, photographs or duplications of the requested document, etc. Often victims are not even aware that they have been stolen, which allows the competition to further monitor the development of the situation and further collect information.

- Electronic monitoring - is used more and more because the technique is progressing daily. Earlier, this technique was only available to intelligence services, and today, due to its affordable price, far more people are available.

SECURITY OF INFORMATION AND COMMUNICATIONS

Regardless of whether it operates in a traditional or electronic way, information security is always important for business systems. The main advantages of increased use of technology in business are improved quality of provision of goods and

services, higher profitability and efficiency, faster communication and cost reduction. In addition to the significant advantages, this form of business monitors and threatens the risks that are most often associated with the issue of security of communication and business through computer networks. In the traditional way of business, information protection is carried out mainly by physical means. In an electronic environment, access to information is different, so security is based on IT resources. Companies increasingly use new technologies for processing, storing and transmitting information. The new environment in which the information is located has become significantly larger. Information is increasingly available and can be accessed even from the furthest places, which creates room for increasing abuse.

Increasing the importance of information technologies and increasing dependence on them condition the necessity of investing in information security. The global spread of information and communication systems is associated with new and increased risks. Data stored and transmitted through information systems became the subject of threats and attacks. The application of modern technologies has caused new types of attacks and attackers. By introducing information and communication technologies, the spectrum of attacks is extended to the accuracy of information and the availability of information and services. The most common risks of communication via the Internet include malicious programs and deliberate or unintentional human activities. The most common risks that the information-communication system makes subject to different ways of manipulating and abusing are:

- Computer sabotage - means the destruction or damage of computers and other data processing devices within computer systems, deleting, changing and preventing the use of information contained in the memory of IT devices. The most common types of computer sabotage are those that act destructively to operational-information mechanisms and user programs, primarily those that have the function of data retention.

- Computer espionage - constitutes unlawful acquisition, disclosure, transfer or use of commercial and commercial secrets with the intention of causing economic loss to a person holding a secret and achieving an unlawful economic advantage. The perpetrators of computer espionage use various malicious programs and techniques in order to infiltrate into the computer network that targets them.

- Use of malicious programs - the use of harmful content programs is one of the most famous forms of a wide range of computer crime. Computer viruses are small programs that have the capability of self-replenishment and the sole aim of damaging the infected computer.

- Computer scams - represent the most widespread type of computer crime, which often causes significant harmful consequences. Computer fraudsters abuse cyber space and affect: anonymity, distance between parties and the current nature of transactions.

- Computer network abuses - crime related to this segment is a form of criminal behavior where services and data are stolen, damaging or destroying parts or entire networks and computer systems or obstructing the functions of their work.

- Identity theft - implies taking over someone's role on the Internet in order to obtain material or other benefits. This is the most drastic way of disrupting privacy because the perpetrator of this form of computer crime, after having come to the vital data for taking over someone's identity, represents in his name and performs various activities, leaving behind a material and non-material consequences.

- Abuse of payment cards - abuse and fraud by payment cards in the electronic banking sphere become a daily phenomenon. The perpetrators of these criminal activities inflict huge damage on banks and their clients.

Business operations with the help of information and communication technologies evidently carry with them a series of risks, which can be avoided using appropriate security measures and each company should have an appropriate security policy. Security services are generally a set of rules that apply to all security-related activities of the organization. In a concrete interpretation, security services are parts of the system that implement the activities of adequate protection if there are security threats and usually act upon the request. Every system that is based on information and communication technologies is exposed to potential threats by external malicious attackers.

In addition to the aforementioned, potential threats to an information system containing an e-commerce subsystem may be some of the following:

- Infiltration into the system - The attacker accesses the system and is able to modify files, reveals confidential information and uses system resources in an illegitimate manner. In general, infiltration is realized by an attacker representing an authorized user or by using weaknesses of the system.

- Supplant - The attacker leaves a program in the system that will allow him to ease attacks in the future. One type of implantation is the use of a "Trojan horse" which is basically unwanted software that is presented to the user as normal, but which during the execution reveals confidential information to the attacker.

- Change of data on the communication line - The attacker can change the information that is transmitted through the communication network. For example, he can deliberately change the finan-

cial details of a person during their transmission through a communication channel, or to present himself as an authorized server that requires confidential information from an authorized user.

- Hearing - The attacker can access confidential information (passwords for access to the system) by simply tapping the information flow in the communication network. Information obtained in this way can be used to facilitate other types of attacks.

- Exceeding authority - The person authorized to use the system uses it in an unauthorized manner. This is a type of threat that both internal attackers (so-called "insiders") and outsiders execute. Attackers from the inside can abuse the system to obtain various privileges, while outsiders can be placed into the system through orders with lesser authority. In this way, they allow the continuation of infiltration into the system using this approach for the unauthorized extension of user rights.

- Refusal of service - Due to frequent requests for execution of complex tasks issued by unauthorized system users, system services can become inaccessible to authorized users.

- Negation of the transaction - After the transaction has been executed, one of the parties may deny that the transaction occurred. Although this kind of event can occur due to an error, it always produces conflicts that cannot always be easily solved.

The availability, reliability and security of information and communication systems networks are gaining in importance. According to new types of attacks, new attacker profiles are being developed, and today's use of the Internet requires the use of security solutions that need to meet new security requirements. Therefore, many countries that use these technologies to a large extent adopt various documents that they want to improve the protection of their information assets. Confidentiality, integrity and availability are the three most common security requirements that are so-called. "Three pillars of security", and the increasing demands of e-commerce expand this model for two additional features, which are non-authenticity and authentication [7,8].

- Confidentiality implies that information is not available, nor is it available to those who are not authorized to receive it. Confidence becomes especially important when it comes to communication networks. Although for most organizations, trust in relevance only comes in third, after availability and integrity, for certain systems such as hospitals, banks, insurance companies, police, etc., confidentiality is of the utmost importance.

- Integrity means that data has not been altered or destroyed in an unauthorized manner. Integrity can be viewed from two perspectives: a.) Data integrity - is a feature that guarantees that data will not be changed in an unauthorized manner when accessing the archiving, processing or transfer process; and b.) System Integrity - means the quality that the system possesses while performing the required functionality in a flawless manner, protected from any unauthorized manipulation.

- Availability is a requirement to ensure that the system promptly and accurately responds to requests and that service will not be denied to authorize users. Availability means that data or other IT resources can be accessed without restrictions and can be freely used when necessary.

- Non-repudiation is a feature that the participants in the transaction cannot subsequently deny their participation in the transaction. In e-commerce, non-repudiation is essential in securing legitimate business transactions that must be recognized and incomprehensible by the parties involved.

- Authentication is the process of verifying the identity of users and entities. Identifying user data in some cases requires more than one authentication certificate. The authentication factor (PIN or password) is a secret or unique information associated with the user identifier, and is used to verify the identity of the user. Ensuring the authenticity of the sender's identity is achieved by using digital signatures and digital certificates. The purpose of the digital signature is to confirm the authenticity of the content of the message (proof that the message has not changed on the way from the sender to the recipient), as well as to ensure the guarantee of the identity of the sender of the message. The sender, using the application of certain cryptographic algorithms, first of all, from his message that is arbitrary length, creates a fixed-length record that completely reflects the content of the message. This practically means that any change in the content of the message leads to a signature change.

The most common attacks in e-commerce are related to: domain abuse, spamming, privacy, various data misconduct, online theft and fraud, unfair competition, intellectual property infringement, infringement of authenticity of e-commerce participants, as well as manipulation with electronic money. All of these defects negatively affect the creation of trust in the performance of the work through the Internet. Nevertheless, despite the aforementioned security problems, the overcoming of which in the future must definitely have to work even more, companies and countries in the virtual environment offer a wide range of benefits that are evident and have a significant positive impact on the growth, development and achievement of global competitiveness.

RESULTS

In the last few decades, the business has undergone significant changes. The introduction of information-communication technologies enabled

the automation of business and the emergence of the Internet opened the possibility for companies to abandon the traditional frameworks of the real environment and move some of their business into a virtual space. Many business systems today memorize and send information and data using available information and communication technologies. Illegal access to such information can cause significant losses or damages to other types of companies, as well as users of these electronic services. It is therefore of great importance to ensure the security of communications while transferring information from one system to another. In order to achieve business success, the aforementioned security measures for e-communication and security in computers should always be combined with measures that imply a traditional form of business (physical security, security of staff, administration, media, etc.).

Economic and environmental intelligence can be defined as a set of coordinated actions of research, processing and distribution, for the purpose of its exploitation, information useful to economic actors. These various actions are conducted legally with all guarantees of the necessary protection for the preservation of the heritage of the company, in the best conditions of quality, deadlines and prices. Useful information is the one that is required by different levels of decision making in an enterprise or a collective, in order to elaborate and establish a coherent strategy and necessary tactics in achieving the goals defined by the enterprise in order to improve its position in the competitive environment. These actions are regulated within the enterprise's framework in a continuous cycle, the generator of a common vision of the goals to be achieved.

On the basis of this activity, the strategy of acting and behavior of companies on the market is being prepared. Responsible behavior of modern management requires that its final decisions on business ventures be made on the basis of studious analyzes made after the obtained processed data of economic intelligence activity of their own specialized services or services of domestic and foreign specialized agencies. Every company with the ambition to win the market and stay on it should have a special, well-organized and equipped, its size-appropriate service for economic intelligence. For small companies or companies that do not have material and personnel resources to organize the permanent work of such a service, the only and necessary solution is precisely and deliberately ordering such information at different stages of processing for specialized and equipped agencies for economic intelligence. Collecting and analyzing public information in order to obtain an image of competitors, customers, markets or business branches of a company. In contrast to her dark sister - spies, CI (Competitive Intelligence), she is completely legal and ethical.

The motive with which a particular company moves into an industrial espionage is to get any information that will help the company to achieve the defined goals. The goal can be to conquer a new product or imitation, develop new technology, increase market share, increase competitive advantage, and so on. Companies go to such an extent that they deliberately enter the database of a competing company in order to inflict some damage on the business. They also use the take-over strategy of a well-performing company, and this strategy is completely hostile, and is used in a way to "rebuild" the management or majority shareholders to sell them. The economic spy is already altered and knows exactly places, is sources of spying. These can be:

• Formal documents (plans, reports, norms, job descriptions, technical documentation),

Sketches, which companies often ignore, in the sense that after drafting the formal document, the sketch becomes worthless. However, it is just becoming the target of economic spies,

• Various pieces of rejected paper, such as travel tickets, various accounts, from which some business moves or planned actions of a competitor can be foreseen. Internal correspondence (meeting minutes, decisions, solutions, newsletters, etc.) can be full of details about the company's business and future intentions);

• Various business associations, statistical institutes, patents and similar institutions, have certain information about the business of companies, and they can ruthlessly bring them closer to economic spies,

• Formal and informal forms of communication in companies can be a source of data for economic spies, especially where there is certain documentation as a trail, such as meeting minutes with the agenda and the like. Employees often recklessly talk about work in society, at lunch and in the visits, not thinking about who can hear it and abuses,

• Public information systems such as daily and weekly newspapers, newspapers, television, the Internet, etc. can also be a suitable source of espionage. Due to all this, in today's conditions of market economy and galloping competition, companies must face the risk, that is, they must understand the danger of economic espionage in order to take action to protect their important data from spying.

It is widely known that over 95% of the necessary information in economic intelligence can be obtained and obtained legally. There are several ways to get the information requested without using illegal means or methods: the internet is the easiest and most used way of finding information about economic entities. According to some surveys, between 1990 and 1995 there was an increase in economic intelligence activity of over 300%, and that is why, as the main culprit, the Internet and the information it provides is highlighted. The most

common way to obtain information is by e-mail, as well as through various inquiries. It is evident that IT staffing is relatively low when it comes to security on the Internet. Access to social networks such as Facebook, My space, Twitter or various chat rooms poses a huge risk to every company, as employees are inclined to speak highly confidential matters in full-time talks even to full strangers. The popularity of the Internet, as a way of obtaining confidential information, contributes to anonymity, which is much easier to accomplish on the Internet than in some other situations. The possibility of broadband Internet access from public places, such as libraries or Internet cafes, offers great opportunities for completely anonymous economic and intelligence work. Searching for employees is a common way of getting information.

Given that there is no intention of recruiting an interviewee, this method is very unethical, and in some situations it can also be considered a spyware activity. Joint ventures and mergers are another way of legally making important information. If A's employees work together with employees of firm B for a long time, they can be expected to eventually be considered partners, so they drop security protocols and allow them access to information and technologies. Also, another secure solution to get into possession of the required technology is buying or acquiring a company, but it's a rather expensive solution. Conferences, exhibitions, seminars and fairs represent a good place to get important information in direct contact. Due to their knowledge and expertise, participants are often engaged by companies or governments to obtain information. Direct visits have long been a valuable source of information from technology or manufacturing companies. Visitors are trained to come up with valuable information by deliberately entering into prohibited zones, by unauthorized photographing, or by asking questions beyond the permitted frameworks.

Although they represent only a small part of economic intelligence, data obtained in an illegal manner is often the most valuable, since they are so important that they cannot be reached by legal means. Organized crime has become a very common way to get information from companies. Business globalization has also allowed some new transnational forms of crime. Thus, criminals are not allowed to enter into the largest companies by pressure and blackmail of the largest people, and their power and power, which is often higher than the local authorities, poses a great threat to business and industry. Independent entrepreneurs include independent or poorly integrated persons in economic espionage. Basically, these are private detectives hired by companies to obtain information that the rental company considers potentially useful for themselves. Regardless of whom the information provider is. there are several ways in which companies or even foreign governments can obtain information. Employees (insiders) with the right approach are a major security problem for companies. According to some surveys, over 75% of economic espionage is done through insiders, people coming from the company itself or having access to sensitive data. Of course, there are a number of people who inadvertently give away secrets that they should not. Also, it is used to rent information from trained professionals, who indirectly and confidently confuse the victim and state that he or she would not normally. This is called social engineering, and although it is only a criminal offense, it can be an introduction to further criminal offenses.

Infiltration among employees represents a good method of spyware. Bearing in mind that in a large number of cases, without major difficulties, it can enter the subject of espionage using counterfeit false documents, this approach to the success rate of espionage has drastically increased. Employee recruitment is one of the most effective ways of espionage. Once an insider or a "mole" is recruited using a bribe or some other way, a specific type of information may be requested, not all of which is encountered. The information gatherer should not be focused on executive directors or researchers, but will do much more by recruiting lower staff such as answering machines, computer technicians or even maintenance staff. There are two advantages here: lower levels of employees are much less suspicious, and often have greater access to information and their price can be much lower, and the willingness to cooperate is much greater than, say, the general manager. This spyware is pretty easy, because a number of employees steal information for further sales, while others are dissatisfied with their attitude towards them and are created for this kind of cooperation.

Computer infections represent another, very common way to obtain information. As computers are increasingly used to process and store data, there is an increasing number of "downtimes" in corporate systems for the illegal acquisition of information. While a number of so-called hackers do this out of pure sports or hatred for globalization or multinational companies, there are also professionals who steal information for the sale on the black market. Both competing companies and intelligence services hire such professionals to break into other information systems. It is estimated that over 90% of companies were at least one victim of an information system intrusion, while direct losses only in 2002 amounted to over $ 170,000,000 due to theft of information.

The burglaries and theft are a traditional way to obtain intelligence. Although in most cases it is a matter of physical theft of documents, in which they are alienated, it may happen that the burglar only photographs or reproduces the requested document, so that the victim does not know that it is

stolen and normally continues to work on the project, which enables the competition to monitor the development further information. This method is usually associated with other methods of economic intelligence. With the advancement of technique, electronic monitoring is increasingly used, so it is possible, for example, to extract one vote between thousands of votes in the stadium or to intercept the victim's mobile phone. While earlier this equipment was the exclusivity of state intelligence, today it is possible to buy the best quality earmarking and surveillance equipment for a little money. As you can see a wide range of tools and techniques four accessing information. Traditional market games turn into real wars, and this goal justifies every asset, and each company must think primarily of its own security. Changes in political relations on the global stage result from the low-intensity low - intensity and totalitarian ideology of the new order, in order to create a number of dwarf states that will become a potential market for multinational corporations and cheap sources of labor and natural resources.

Unlike all previous wars, when priority is given to masses, weapons and national-patriotic feelings, today's struggle takes place in man's consciousness through mass media and similar intelligence-intelligent weapons. Redefining methods, techniques and special-purpose instruments meant building a sophisticated, super-corrosive information flow, with the task of informing public opinion, as a psychological basis for continuing military intervention or political pressure to change the ruling course. In doing so, sources of domination are hiding in technological superiority that gives the leading countries an undisputed position in the domain of information dissemination.

Only those who handle information can lead wars, because those who own them rule the planet. According to the results of a survey conducted for the needs of the European Parliament at the beginning of 2010, there were 134 satellite eavesdropping systems in the world. The only country that controls everything is America, which supplies nearly 70% of intelligence through the global intelligence-based Vortex (founded in 1947 with England) and the analysis of the largest spy organization En-Es-Ey. In Fort Midtown, Maryland, the headquarters of this mystical institution is located, which, employing 38,000 employees, represents the eyes and ears of the electronic intelligence agency. "Much has changed since we could deny that this agency exists, and I should add that there were presidents who did not even know about the existence of this institution, although its services and how they used it," said Robert Still, director this mammoth company ("Washington Post", December 11, 1999). Some analysts argue that this service is more effective than the CIA or Ef-Bi-Aj services, which somewhat justifies its involvement in all wars in the last few decades. There are also a large number of European collaborators on this plan, among which Britain is the largest, followed by Germany, France, Austria and Turkey. The supersonic system "Echelon" stationed in Gloucester, UK, controls the entire European space. The communications center in the Pacific is responsible for the Joachim's hospice center. The stations in Norway and Cyprus are under the direct control of NASA, and in order to calm down the world's public, they officially deal with "economic" and, more recently, the "anti-terrorist" espionage. The "Echelon" has 120 satellites and close to 1,320 powerful computer-dictionaries, allowing it to listen to all military-intelligence and political communications across Europe and the world.

Control is a term that will dominate the world in the future, which calls into question the freedom of every individual. The United States formed a special unit for the violent neutralization of foreign media, and specialists in the US Strategic Command General Staff, Offutt's overseas base in Omaha, have special responsibilities in the field of mass communication and propaganda. The system of preventive passenger control, established by the agreement of the European Commission and the US authorities through a computer, checks the identity of every citizen, marking it green (harmless), yellow (suspicious) and red (dangerous) color. In this sense, nothing has changed much since the time of Nazi Germany, only that citizens today are "marked" with invisible tapes, and special attention is paid to Muslims or persons originating from the Middle East. United States of America is in its files, the approval of their governments was introduced by 75 million Mexicans, 42 million Colombians, and 33 million Central Americans. Paranoia has not been spared even by American citizens, so a series of retrograde laws have been returned, which also call into question the privacy and freedom of human rights.

In the world of growing divisions and the difference in one we are the same - we are all consumers of different information. The media create a technological paradox - as many television programs, printed newspapers, magazines, radio stations, or the Internet - have less free time. Thus, the meaning of life becomes greed and satisfaction of ever wider needs, while the civilization relation to culture and the degree of satisfactory communicativeness disappears in the sea of growing hedonistic demands. Totalitarianism excludes freedom of expression, the development of critical thoughts and the contradiction of argumentation, while democracy rests on the media, so that the process of governance is open to the general public. The new civilization rests in the world of images, which often, in order to create an image, can be media-based lies. The basic and most important difference between the products of man (creator) and other

biological species is that man is the center of symbols that can frightfully interfere with the entire spiritual needs of spiritual needs. An intellectual, moral man of the new order, the future is the basis of thinking and choice of opinion, with respect to Montesy's thought: "Political freedom is not that everyone does what they want ... Freedom is the right to do what everyone permits."

Democratic structures cannot survive without free, economically independent media, and should not be fooled by the notion that creating a favorable political and economic climate is an easy job. Precise, accurate, applied and professional information develops positive values of a society, favors people who bring the common good. Without media there is no mass communication today, so, besides the classical understanding of their importance for the development of culture, education and preservation of national identity, we get the strategic dimension of the participants in the processes of democratic transformation of society. Instead of the former fourth, fifth or seventh force, journalism today becomes the first power, without which there is no social progress. More social and technological changes in the mid-millennium have given the media a new meaningful dimension, actively promoting them in the participants of dynamic global processes. The speed of decision-making, mobility of the population, with the expansion of individual and consumer values, change the traditional forms of communication, but also the relationship to information, whose value through mass media is increasingly instrumental zed.

Modern means of communication based on new technologies create a qualitatively new form of communication: multimedia that modifies the way of creating, distributing, disseminating and storing information.. The erosion and proliferation of electronic and digital messaging channels creates a new audience that will, by the flow of time, increasingly depend on the inflow of informative, entertaining or educational content. Intelligent engineering stands on knowledge and skills, whereby economic power is inextricably linked with politics. The power of knowledge and the power of conscience are the pillars of correct journalism, but under the pressure of the media to meet the demands of the market, journalists often come into conflict with their own ideals. Media society gets its own gladiators, new terrorists, which by abolishing spatial and temporal borders dictate desirable attitudes and public opinion. The digital economy is a challenge for the media, so only top-level knowledge of its structure can prevent manipulation. Thanks to technical inventions, the bandwidth of the media has increased, e.g. Fiber can simultaneously miss over one million television channels, 200 thousand times faster than copper pairs. In the near future, air signal transmission is envisaged, which in addition to the freedom of distribution also means huge data compression. In this way, users will gain a greater wealth of choice, of course, if they are able to fund it financially.

Such technologies are based on systems for digital broadcasting and images are not at all naïve, because they carry with them a number of important improvements, such as a single-frequency network of high definition television and multichannel broadcasting. The nature-to-technology scenario takes place with the help of information networks, which only increases the risk of conditioning opinions, needs, attitudes, value systems, forms of control, and so on. Collective behavior is directed towards the needs of media imperators, so you can provoke mass hysteria, hallucinations, rebellions, demonstrations, rumors, myths, as well as optimism, satisfaction, spectacle, legends, etc. New civilization nurtures new media that become the producers of millions of news by duplicating channels and content, they create depersonalized individuals subject to manipulation. New technologies create new sensibilities, above all the philosophy of Moody's, marvelous in efforts to unify ideas and value systems. Digital techniques change the character of standard communications, their shapes and sizes. Miniaturization of the equipment enables the technological connection of cameras, televisions, computers and telephones, at any time and from any place, to be included in information houses programs. Electronic equipment manufacturers already perfect the prototype of a liquid crystal television screen with special polarization of light so that when the camera in the network watches the picture, and while it is turned off, it is usually a mirror.

The user is offered a full range of options, for example, to use a portion of the screen for the mirror, and at the same time to watch the rest of the news. By connecting with the computer, two-way transmission of a surgical operation and an expert team is supervised, which monitors it from hundreds of kilometers of distance or the other end of the planet. Multimedia messaging deeply distorts psychological and psycho-social patterns, because technological change of the human environment is changing us. Conflicts, in a good way, arise from the abuse of the nature of the media, politics and public opinion, but less important is how much control mechanisms are covered. The new communication order is an open conceptual framework in which technologically advanced countries are preferred. The perception that the focus of influence is transferred to the media of local communities is only partly correct, because their reach is limited, which also means the power to the public's opinion. They facilitate persuasion and dialogue within smaller groups, but they are strategically insignificant on the broader plan, so resources need not be wasted on their development. The first institutions that made the transition to privatization were by no

means the media, both by their ownership and content. American capital largely aided independence in Poland, Hungary, the Czech Republic, Serbia and other communist countries, which was explained by the processes of democratization and defense of media independence.

Our public slowly understands the depth of media changes, so it is still blamed that journalists are "craftsmen" who do not need faculty education, especially if they are "talented." Between the notion of occupation and profession is the deep gap of misunderstanding. In the United States, the question of the need for their education is no longer being questioned, because it was realized in the meantime that new technologies, by changing the philosophy of the media and society, demand a higher level of knowledge. It is time to realize that knowledge in the wrong hands or heads is never useful.

CONCLUSION

Competitiveness of the economy on the global market requires a high level of competence and competence of the workforce, because modern technological processes are based on highly educated population. Even countries with significant natural resources cannot enter the global race today to provide further development without education and innovation for trained people. When it comes to the development and application of new technologies, development trends in the market economy countries show that education and creation of highly professional human resources are at the top of the priorities of national strategies and policies of economic, environmental and technological progress. Therefore, postmodern education must involve the development of highly educated personnel who can improve national development and respond adequately to the requirements of the modern environment. The development of higher education must be in correlation with the modern development of science and technology, which implies the education of human resources for specific needs and forms of technical-technology-communication-innovation technologies. All of the above points to the conclusion that education in the 21st century has to be focused on acquiring specific knowledge and skills.

New time called the digital eras and the age of knowledge, demands new forms of education. In these new and changing circumstances, education is tasked to increase human adaptability to the time that comes and to increase those skills that a person needs to make choices and adjust to change. This means that the future of man will depend on his education. Revolutionary advances in information and communication technologies have two simultaneous and complementary impacts on all countries. First, there are outstanding opportunities for accelerating social and economic development. Second, there is a growing need for higher education reform in order to take advantage of new opportunities and avoid falling international competitiveness. Finally, it can be concluded that the added value that is created today in the business process arises, first of all, from the knowledge, skills and skills of people employed in or working with it. Success and survival increasingly depend on the way people collect, organize and commercialize their know-how. Educated human potential is increasingly the basis on which all those who want to achieve high standards and achieve development in today's extremely competitive global environment must rely on[9,10].

The modern era, channeled by the processes of globalization, is characterized by the acquisition of superiority in the planetary exchanges, which is the result of economic, environmental, technological and developmental supremacy over competitors. As the weapon used to be the basic argument of domination, today it is information, as the fourth obligatory factor of production, besides capital, labor and technology. Information is the most important factor in gaining competitive advantage, and because of this, the most developed countries of the world use more and more of their intelligence resources to obtain carefully preserved industrial, production or financial information that will enable the state or the domestic company to better position in the global market. Since knowledge, ideas, innovations and technology are today governed by the world, companies and countries that own them have great advantages, but they are also at high risk of being subject to industrial espionage.

As an activity, economic and environmental espionage denotes activities aimed at revealing the business secrets of competing companies, with the aim of exploiting them and thereby gaining a better position on the market. Industrial espionage is also dealt with by business subjects and governments of states, and it represents an aspect of peaceful warfare between them. This type of espionage is a collection of delicate, planned and professionally performed activities to obtain confidential information kept by competing companies in secrecy. Victory and defeat in today's global market depends on the knowledge, skills, competence of business processes and the use of modern technologies. Extremely strong competition that exists in all markets and in all business activities, as well as a high degree of technology development, make it very difficult to take a good market position.

REFERENCES

[1] Antonijevic, R. (2010) Education for Knowledge Society - Prerequisites for European Integration, Faculty of Philosophy, Belgrade.

[2] Babic, Z., Matkovic, T., Sosix, V. (2006) Structural changes of higher education and labor market outcomes, Economic Trends and Economic Policy, Vol. 16, No. 108
[3] Bubanj, R (2007) New Models of Contemporary Educational Processes, Faculty of Philosophy, Nis, Serbia
[4] Kalakota, R., Robinson, M. (2002) E-Business 2.0, A Guide to Success, Mate, Zagreb
[5] Neskovic, S. (2006) Corporate Security, in: Security and Reforms in Serbia, Institute for Political Studies, Belgrade
[6] Neskovic, S. (2011) Economic spying in the modern international constellation: Economics - theory and practice, FIMEK no. 1, Novi Sad
[7] Epler, I., Andrejic, M., Milenkov, M., Sokolovic, V.(2017) Concept of logistics prevention development in a defence system, Military Technical Courier, 2017, vol. 65, No. 4, p. 1027-1043
[8] Neskovic, S.(2015) Business spying and compromising information systems, Proceedings of the 1st International Conference "Knowledge Management and Informatics" 28-31. January 2015, Novi Sad, Higher Technical School of Vocational Studies
[9] Neskovic, S., Ketin,S., Secerov,P., Djelic,A.T., Mirkovic, M.,Biocanin, R. (2018) International Politics and Ecology: Special Focus to the Protection of Air, Fresen. Environ. Bull. 27, 7545-7551
[10] Tomic,S., Bulajic, S., Radojevic, R.,Petrovic, D., Ketin S. (2019) The contribution of concentration of suspended particles-coal mine, Fresen. Environ. Bull. 28, 5764-5770

Received: **03.01.2020**
Accepted: **18.02.2020**

CORRESPONDING AUTHOR

Sonja Ketin
Faculty of Maritime Academic Studies Belgrade,
Bulevar Vojvode Misica 37,
Belgrade 11000 – Serbia

e-mail:ketin.sonja@gmail.com

AUTHOR INDEX

SUBJECT INDEX

FEB – GUIDE FOR AUTHORS

General

FEB accepts original papers, review articles, short communications, research abstracts from the entire sphere of environmental-chemistry,-biology,-microbiology,- technology, -biotechnology and-management, furthermore, about residue analysis/ and ecotoxicology of contaminants.

Acceptance or no acceptance of a contribution will be decided, as in the case of other scientific journals, by a board of reviewers. Papers are processed with the understanding that they have not been published before (except in form of an abstract or as a part of a published lecture, review or thesis);that they are not under consideration for publication elsewhere; that their publication has been approved by all co-authors, if any, as well as- tacitly or explicitly- by the responsible authorities at the institute where the work has been carried out and that, if accepted, it will not be published elsewhere in the same form, in either the same or another language, without the consent of the copyright holders.

Language

Papers must be written in English. Spelling may either follow American (Webster) or British (Oxford) usage but must be consistent. Authors who are less familiar with the English language should seek assistance from proficient colleagues in order to produce manuscripts that are grammatically and linguistically correct.

Size of manuscript

Review articles should not exceed 30 typewritten pages. In addition up to 5 figures may be included.

Original papers must not exceed 14 typewritten pages. In addition up to 5 figures may be included.

Short-Communications should be limited to 4 typewritten pages plus not more than 1 illustration.

Short descriptions of the authors, presentation of their groups and their research activities (with photo) should together not exceed I typewritten page. Short research abstracts should report in a few brief sentences (one-fourth to one page) particularly significant findings. Short articles by relative newcomers to the chemical innovation arena highlight the key elements of their Master and PhD-works in about I page.

Book Reviews are normally written in-house, but suggestions for books to review are welcome.

Preparation of manuscript

Dear authors,

FEB is available both as printed journal and as online journal on the web. You can now e-mail your manuscripts with an attached file. Save both time and money. To avoid any problems handling your text please follow the instructions given below:

When preparing your manuscripts have the formula K/SS (Keep It Simple and Stupid) in mind. Most word processing programs such as MS-Word offer a lot of features. Some of them can do serious harm to our layout. So please do not insert hyperlinks and/or automatic cross-references, tables of contents, references, footnotes, etc.

1. Please use the standard format features of your word processor (such as standard.dot for MS Word).
2. Please do not insert automatisms or secret link-ups between your text and your figures or tables. These features will drive our graphic department sometimes mad.
3. Please only use two fonts for text or tables "Times New Roman" and for graphical presentations "Arial".
4. Stylesheets, text, tables and graphics in shade of grey
5. Turn on the automatic language detection in English (American or British)
6. Please - check your files for viruses before you send them to us!!

Manuscripts should be uploaded on our website prt-parlar.de

Thank you very much!

STRUCTURE OF THE MANUSCRIPT

Title page: The first page of the manuscript should contain the following items in the sequence given: A concise title of the paper (no abbreviations). The names of all authors with at least one first name spelled out for every author. The names of Universities with Faculty, City and Country of all authors.

Abstracts: The second page of the manuscript should start with an abstract that summarizes briefly the contents of the paper (except short communications). Its length should not exceed 150-200 words. The abstract should be as informative as possible. An extended repetition of the paper's title is not considered to be an abstract.

Keywords: Below the Summary up to 6 key words have to be provided which will assist indexers in cross-indexing your article.

Introduction: This should define the problem and, if possible, the frame of existing knowledge. Please ensure that people not working in that particular field will be able to understand the intention. The word length of the introduction should be 150 to 300 words.

Materials and methods:
Please be as precise as possible to enable other scientists to repeat the work.

Results: Only material pertinent to the subject must be included. Data must not be repeated in figures and tables.

Acknowledgements: Acknowledgements of financial support, advice or other kind of assistance should be given at the end of the text under the heading "Acknowledgements". The names of funding organisations should be written in full.

References: Responsibility for the accuracy of references rests with the authors. References are to be limited in number to those absolutely necessary. References should appear in numerical order in brackets and in order of their citation in the text. They should be grouped at the end of the paper in numerical order of appearance. Abbreviated titles of periodicals are to be used according to Chemical or Biological Abstracts, but names of lesser known journals should be typed in full. References should be styled and punctuated according to the following examples:

ORIGINAL PAPERS:
l. Author, N.N. and Author, N.N. (Year) Full title of the article. Journal and Volume, first and last page.
BOOK OR PROCEEDING:
2. Author, N.N. and Author, N.N. (Year) Title of the contribution. In: Title of the book or proceeding. Volume (Edition of klitor-s, ed-s) Publisher, City, first and last page

DOCTORAL THESIS:
3. Author, N.N. (Year) Title of the thesis, University and Faculty, City

UNPUBLISHED WORK:
Papers that are unpublished but have been submitted to a journal may be cited with the journal's name followed by "in press". However, this practice is acceptable only if the author has at least received galley proofs of his paper. In all other cases reference must be made to “unpublished work" or "personal communication".

Discussion and Conclusion: This part should interpret the results in reference to the problem outlined in the introduction and of related observations by the author/s or others. Implications for further studies or application may be discussed. A conclusion should be added if results and discussion are combined.

Corresponding author: The name of the corresponding author with complete postal address

Reprints:
1 - 4 pp.: 200,- EURO + postage/handling
5 - 8 pp.: 250,- EURO + postage/ handling
More than 8pp: 350,- EURO +postage/ handling.
The prices are based upon the number of pages in our journal layout (not on the page numbers of the submitted manuscript).
Postage/ Handling: The current freight rate is Germany 10 €, Europe 18 €, International 30 €.
VAT: In certain circumstances (if no VAT registration number exists) we may be obliged to charge 7% VAT on sales to other EU member countries.MESAEP and SECOTOX members get a further discountof 20% (postage/ handling full).